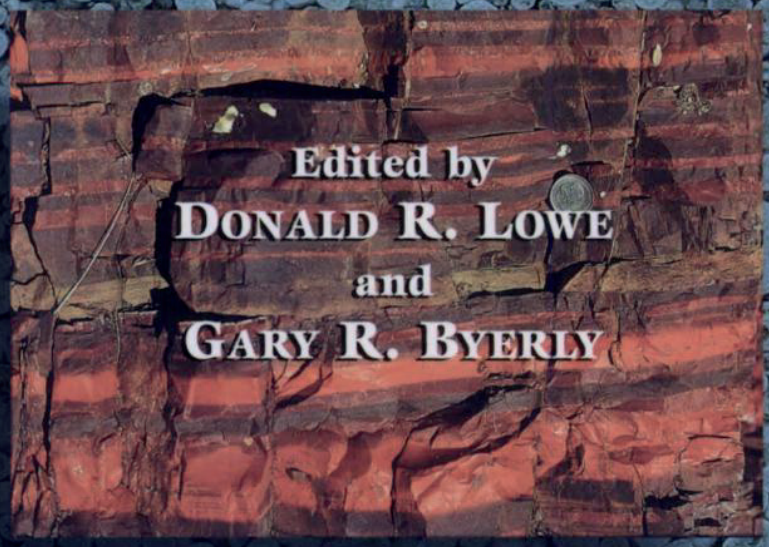
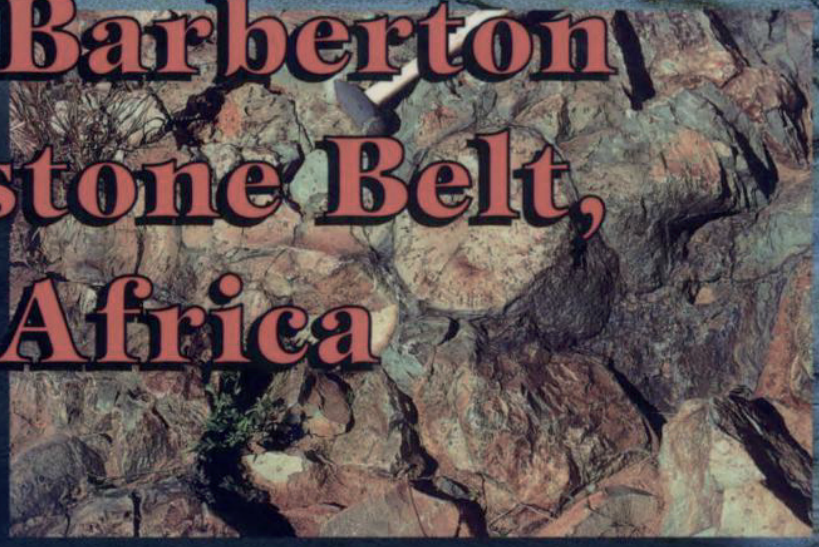


Edited by
DONALD R. LOWE
and
GARY R. BYERLY

Geologic Evolution of the Barberton Greenstone Belt, South Africa





Special Paper 329

Urheberrechtlich geschütztes Material

Copyright © 1999, The Geological Society of America, Inc. (GSA). All rights reserved. GSA grants permission to individual scientists to make unlimited photocopies of one or more items from this volume for noncommercial purposes advancing science or education, including classroom use. Permission is granted to individuals to make photocopies of any item in this volume for other noncommercial, nonprofit purposes provided that the appropriate fee ($0.25 per page) is paid directly to the Copyright Clearance Center, 222 Rosewood Drive, Danvers, MA 01923, USA, phone (978) 750-8400, http://www.copyright.com (include title and ISBN when paying). Written permission is required from GSA for all other forms of capture or reproduction of any item in the volume including, but not limited to, all types of electronic or digital scanning or other digital or manual transformation of articles or any portion thereof, such as abstracts, into computer-readable and/or transmittable form for personal or corporate use, either noncommercial or commercial, for-profit or otherwise. Send permission requests to GSA Copyrights.

Copyright is not claimed on any material prepared wholly by government employees within the scope of their employment.

Published by The Geological Society of America, Inc.
3300 Penrose Place, P.O. Box 9140, Boulder, Colorado 80301

Printed in U.S.A.

GSA Books Science Editor Abhijit Basu

Library of Congress Cataloging-in-Publication Data

Geologic evolution of the Barberton Greenstone Belt, South Africa /
edited by Donald R. Lowe and Gary R. Byerly
p. cm. -- (Special paper ; 329)
Includes bibliographical references and index
ISBN 0-8137-2329-9
1. Barberton Greenstone Belt (South Africa and Swaziland)
2. Greenstone belts--South Africa--Barberton Region. 3. Geology--South Africa--Barberton Region. I. Lowe, Donald R., 1942- .
II. Byerly, Gary R., 1948- . III. Series: Special papers (Geological Society of America) ; 329.
QE462.G77G45 1999 98-53073
556.82'6--dc21 CIP

Cover: Rocks typical of the Barberton Greenstone Belt. (Background photo—pale green rock) Accretionary lapilli, many showing nuclei, overlying a layer of rippled, current-deposited volcaniclastic ash and dust, Msauli Chert member of the Mendon Formation. Similar layers of accretionary lapilli, ash, and dust overlie komatiitic volcanic flow units throughout the Onverwacht Group and are inferred to have been composed originally of komatiitic pyroclastic debris. (Upper photo—banded bright red rock) Banded iron formation from the lower Mapepe Formation of the Fig Tree Group in the southeastern part of the Barberton Belt. Bright red layers are composed of jasper and darker maroon layers largely of hematite. (Lower photo—tan rock) Pillow basalts with well-developed radial pipe vesicles from the lower part of the Kromberg Formation in its type section along the Komati River. Photo by Donald R. Lowe.

10 9 8 7 6 5 4 3 2 1

Urheberrechtlich geschütztes Material

Geological Society of America
Special Paper 329
1999

Stratigraphy of the west-central part of the Barberton Greenstone Belt, South Africa

Donald R. Lowe
Department of Geological and Environmental Sciences, Stanford University, Stanford, California 94305
Gary R. Byerly
Department of Geology and Geophysics, Louisiana State University, Baton Rouge, Louisiana 70803

ABSTRACT

The Swaziland Supergroup in the Barberton Greenstone Belt (BGB) consists of a lower, predominantly volcanic sequence, the Onverwacht Group; a middle volcaniclastic and quartz-poor clastic succession, the Fig Tree Group; and an upper quartzose terrigenous unit, the Moodies Group. In classic sections in the Onverwacht anticline, the Onverwacht Group includes 8 to 10 km of komatiitic, basaltic, and dacitic volcanic rocks and thin, silicified sedimentary layers that have been subdivided, from base to top, into the Komati, Hooggenoeg, and Kromberg Formations, and a new unit, the Mendon Formation. The ages and stratigraphic relationships of the highly altered Sandspruit and Theespruit Formations in the anticline are not fully resolved, but the latter includes felsic volcanic components that are in part older than the Komati Formation and in part correlative with dacitic volcanic units at the top of the Hooggenoeg Formation. However, in the Steynsdorp anticline, rocks assigned to the Theespruit Formation lie stratigraphically below the Komati Formation and include the oldest dated stratigraphic units in the Swaziland Supergroup.

In the central part of the belt, north of the Granville Grove fault and south of the Inyoka fault, komatiitic volcanic rocks of the Onverwacht Group are younger than those of the Komati Formation and are here assigned to a new unit, the Mendon Formation. Exposed portions of the formation appear to young northward across a series of fault-bounded outcrop belts. North of the Inyoka fault, the Onverwacht Group includes a thick succession of komatiitic and basaltic volcanic rocks and tuffs, layered ultramafic intrusions, and thin cherty units. These rocks are here grouped into a new lithostratigraphic unit, the Weltevreden Formation. Age data suggest that the Weltevreden Formation is equivalent to at least the upper part of the Mendon Formation.

The overlying Fig Tree Group consists of interstratified terrigenous clastic units and dacitic to rhyodacitic volcaniclastic and volcanic rocks. South of the Inyoka fault, these strata appear to include two formation-level units: the Mapepe and Auber Villiers Formations. The Mapepe Formation includes as much as 700 m of shale, chert-grit sandstone, and chert-clast conglomerate interstratified with fine-grained felsic pyroclastic and volcaniclastic rocks. Chert, jasper, and barite make up a minor part of most sections. Deposition took place in alluvial, fan-delta, and shallow to perhaps moderately deep subaqueous environments. Dacitic tuffs have yielded single-crystal zircon ages of 3,252 ± 6, 3,243 ± 4, and 3,226 ± 4 Ma.

The Auber Villiers Formation includes 1,500 to 2,000 m of dacitic tuff; coarse vol-

Lowe, D. R., and Byerly, G. R., 1999, Stratigraphy of the west-central part of the Barberton Greenstone Belt, South Africa, *in* Lowe, D. R., and Byerly, G. R., eds., Geologic Evolution of the Barberton Greenstone Belt, South Africa: Boulder, Colorado, Geological Society of America Special Paper 329.

caniclastic sandstone, conglomerate, and breccia; and terrigenous chert-clast conglomerate, chert-grit sandstone, and shale. This sequence and the locally overlying Moodies strata form the hanging-wall succession above a thrust fault, named the 24-hour Camp fault. The footwall sequence includes rocks of the Mendon and Mapepe Formations. Volcanic breccia in the lower part of the exposed section of the Auber Villiers Formation has yielded a maximum age of 3,256 ± 4 Ma.

The northern facies of the Fig Tree Group, north of the Inyoka fault, includes nearly 1,500 m of strata comprising the Ulundi, Sheba, Belvue Road, and Schoongezicht Formations. The Ulundi Formation is a 20- to 50-m-thick unit of carbonaceous shale, ferruginous chert, and iron-rich sediments at the base of the Fig Tree Group. The overlying Sheba Formation includes between 500 and 1,000 m of predominantly fine- to medium-grained lithic graywacke. The Belvue Road Formation consists mainly of shale and thin, fine-grained turbiditic sandstone. Toward the top, it includes an increasing proportion of dacitic volcaniclastic rocks. Along the northeast end of the Stolzburg syncline, sedimentary rocks of the Belvue Road Formation are succeeded by serpentinized komatiitic volcanic rocks that have been included within the Belvue Road by previous workers. Extensive shearing and brecciation of the komatiitic volcanic rocks and overlying black and banded cherts suggest that the contact between the Belvue Road Formation and this komatiitic unit is a fault. This komatiitic unit is interpreted to be the upper part of the Weltevreden Formation (Onverwacht Group), which, along with overlying units, has been thrust over rocks of the Belvue Road Formation. The ultramafic rock and chert are overlain by nearly 450 m of turbiditic, plagioclase-rich sandstone and mudstone of the Schoongezicht Formation. Juvenile dacite-clast conglomerate near the top of the Schoongezicht Formation has yielded maximum single-crystal zircon of 3,226 ± 4 Ma.

The youngest rocks in the BGB are lithic, feldspathic, and quartzose sandstone, conglomerate, and siltstone of the Moodies Group. These strata reach about 3,500 m thick in the study area and include units correlative with the Clutha, Joe's Luck, and Baviaanskop Formations in the Eureka District. The wide development of conglomerate at the base of the Moodies and, in southern areas, of Moodies conglomerates resting with angular unconformity on rocks of the Onverwacht Group suggest that the base of the Moodies is an unconformity over much of the study area. Regionally, the Moodies Group and underlying Schoongezicht Formation are paraconformable but rest discordantly on older Fig Tree and Onverwacht units. This contact is thought to be a regional thrust fault that divides the northern sequences into footwall (Weltevreden, Ulundi, Sheba, and Belvue Road Formations) and hanging-wall (Weltevreden, Ulundi, and Schoongezicht Formations overlain by Moodies Group) sequences.

The Moodies Group appears to include two and possibly more distinct facies. Rocks north of the Inyoka fault comprise sections commonly exceeding 2,000 m thick that include microcline and clasts of potassic plutonic rock. South of the Inyoka fault, Moodies sections are generally less than 1,000 m thick and lack microcline and granitic detritus. Within the southern facies, individual northeast-trending outcrop belts are characterized by distinctive conglomerate-clast compositions. These facies contrasts suggest derivation of Moodies sediments from several different sources and either deposition in separate parts of a large basin, with incomplete mixing of detritus from different sources, or deposition in several small basins.

Although the stratigraphies of the Onverwacht, Fig Tree, and Moodies Groups north and south of the Inyoka fault are virtually identical, subtle but important petrologic differences suggest that they represent blocks that were separated until mid- to post-Moodies time. The present study emphasizes: (1) the diachronous nature of Onverwacht volcanic rocks across the study area, with a general younging trend from south to north; (2) the contrasting igneous facies between the classic formations of the Onverwacht Group in the south and the Weltevreden Formation in the north, with the Mendon Formation representing a transitional unit in the central part of the belt; (3) the stratigraphic complexity, widespread volcanic component, and predominantly

shallow-water character of Fig Tree rocks in southern facies and the more uniform, almost exclusively detrital, turbiditic aspect of northern facies Fig Tree units; (4) the existence of several major Fig Tree dacitic volcanic units, including the Auber Villiers (circa 3,260 Ma), Mapepe (3,243–3,225 Ma), and Schoongezicht (circa 3,226 Ma) Formations; and (5) the distinction between northern microcline- and granite-clast-bearing and southern, K-spar- and granite-clast-poor Moodies facies.

INTRODUCTION

The evolution of thought on the arrangement and correlation of supracrustal rocks in the Barberton Greenstone Belt has been reviewed by Hall (1918), Visser (1956), Viljoen, M. J., and Viljoen (1969a, b), Viljoen, R. P., and Viljoen (1969), and SACS (1980). The present discussion will focus on the stratigraphy in the west-central part of the belt (Fig. 1) based on recent work of others and the results of our studies over the last 20 years.

The volcanic-sedimentary succession making up the Barberton Greenstone Belt (BGB) has been assigned to the Swaziland Supergroup (Anhaeusser, 1975), the Barberton Sequence (SACS, 1980), and Jamestown Ophiolite Complex (de Wit et al., 1987a). Because of its priority and wide usage, the first of these names is retained here. Historically, the Swaziland Supergroup has included three major lithostratigraphic units (Figs. 2 and 3). From base upward, these are (1) the Onverwacht Group, composed largely of mafic and ultramafic volcanic rocks but including thin units of felsic pyroclastic and volcaniclastic rocks and chert; (2) the Fig Tree Group, a complex succession of graywacke, shale, chert, and siliceous fragmental volcanic rocks; and (3) the Moodies Group, composed largely of lithic, feldspathic, and quartzose sandstone, conglomerate, lesser amounts of siltstone and shale, and thin units of basalt, jasper, and magnetite-bearing shale.

Within the last 20 years geological, geochemical, petrologic, geochronological, paleobiological, and sedimentological studies have provided important details about development of the Barberton Belt and its relevance to the evolution of the early Earth. Many of these studies have contributed significantly to improving our knowledge of greenstone belt stratigraphy. Viljoen, M. J., and Viljoen (1969a, b) and Viljoen, R. P, and Viljoen (1969) subdivided rocks of the Onverwacht Group into six formations, which they mapped throughout much of the southern part of the greenstone belt. Their pioneering studies provide one of the most detailed and systematic accounts of greenstone belt stratigraphy and petrology available, even today. Reimer (1967) mapped the Stolzburg syncline and, with Condie et al. (1970), recognized three formations in the Fig Tree Group throughout the northern part of the belt. Studies of the Onverwacht Group by Viljoen, M. J., and Viljoen (1969a, b) and Viljoen, R. P., and Viljoen (1969) and the Fig Tree and Moodies Groups by Visser (1956), Reimer (1967), Anhaeusser (1969, 1973, 1975, 1976), Condie et al. (1970), Eriksson (1977a, b, 1978, 1980a, b), and Lamb (1984a, b) form the basis of most of our current understanding of greenstone belt stratigraphy.

Although these studies have provided essential details on the stratigraphy of selected regions, especially the widely separated Eureka District along the northern margin of the belt and the Komati River Valley in the south, stratigraphic relationships over much of the belt remain poorly resolved. In large part, this reflects both the paucity of distinctive marker beds and the lack of modern structural analysis within the main part of the greenstone belt. Ramsay (1963) pointed out that complex, polyphase deformation has affected Barberton rocks. De Wit (1982, 1983), Lamb (1984a, b), Lowe et al. (1985), de Wit et al. (1987b), Jackson et al. (1987), Lamb and Paris (1988), de Wit et al. (1992), de Ronde and de Wit (1994), Heubeck and Lowe (1994a, b), Lowe (1994b), and Lowe et al. (this volume, Chapter 2) have emphasized the existence of major thrust faults and fold nappes within the BGB that reflect major horizontal shortening of the belt and repeat major portions of the sequence. These authors differ, however, in their interpretation of which parts of the section are involved in this repetition. De Wit et al. (1992), de Ronde and de Wit (1994), and Lowe (1994b) have interpreted the Barberton Belt as an amalgamated belt, composed of a number of discrete blocks or terranes that have been assembled tectonically. De Wit (1982, 1983) and Paris (1985) discard previous stratigraphic classification within the southern part of the greenstone belt and reinterpret the entire 15-to-20-km-thick Onverwacht and Fig Tree succession of Viljoen, M. J., and Viljoen (1969a) as a relatively thin, 0.5- to-5-km-thick sequence repeated numerous times by faulting and folding.

Perhaps the key to evaluating the stratigraphy of and correlation within the BGB in the face of its complex structure, absence of fossils, and paucity of regional marker beds has come from recent age data provided by high-precision, single-crystal zircon geochronology. In particular, multiple ages throughout the Onverwacht and Fig Tree Groups in the Onverwacht anticline in the southern BGB (Armstrong et al., 1990; Kröner et al., 1991; Kamo and Davis, 1994; Byerly et al., 1996; Kröner et al., 1996) has finally established the existence of a coherent, younging-upward age arrangement of units for at least the Komati, Hooggenoeg, Kromberg, Mendon, and Mapepe Formations and has clearly indicated that the Theespruit Formation, although separated from overlying units in the Onverwacht anticline by the Komati fault, does indeed include components that are significantly older than rocks of the Komati Formation, as suggested 30 years ago by Viljoen, M. J., and Viljoen (1969a, b). Also, it has been clearly established that there are multiple generations of tonalite, trondhjemite, and grandiorite (TTG) intrusion around and beneath the greenstone belt that correlate with felsic volcanic events within the belt. A summary of age data from the Barberton Belt and surrounding areas is presented in Table 1 of Lowe (this volume, Chapter 12).

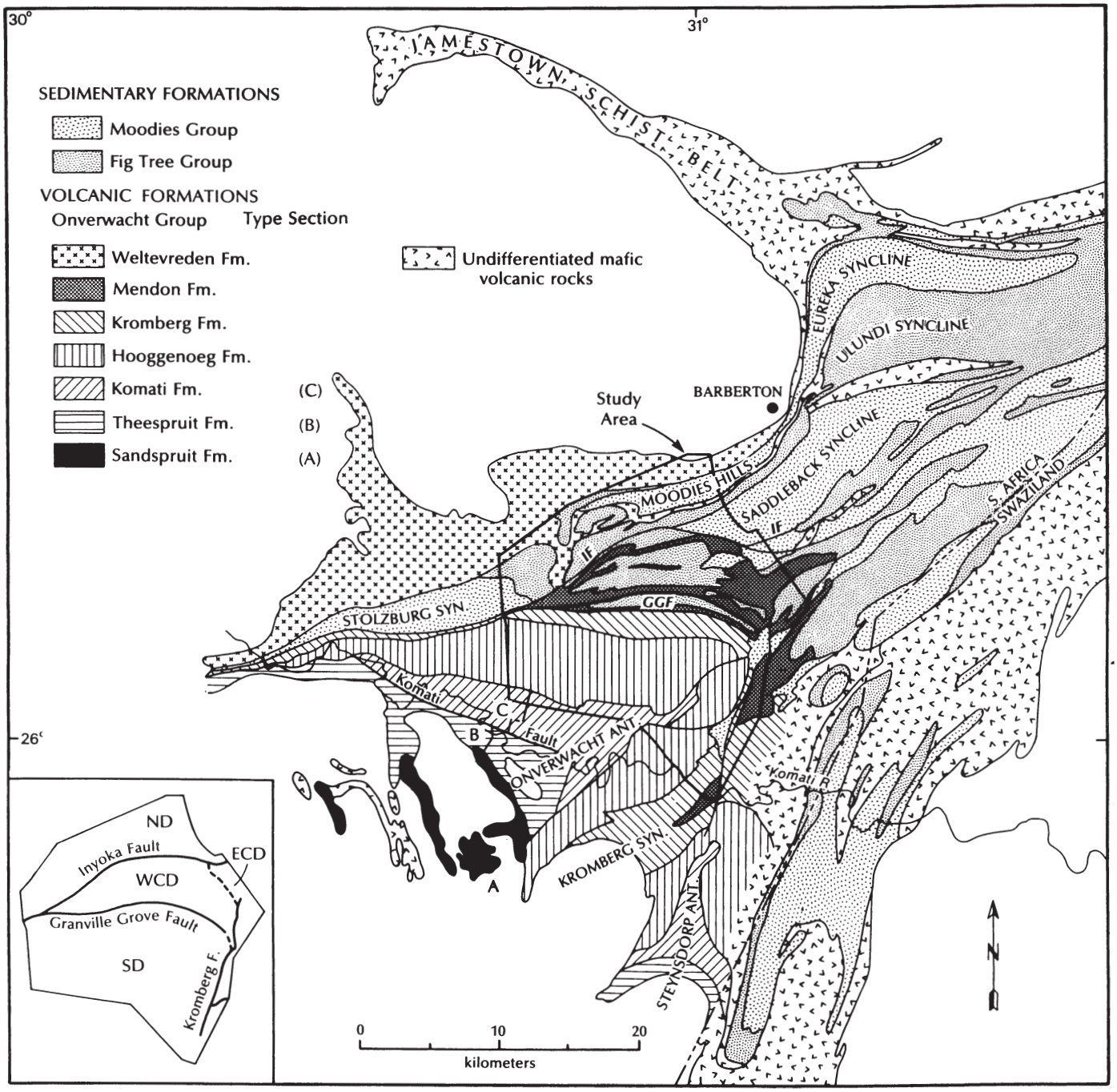


Figure 1. Generalized geologic map of the western half of the Barberton Greenstone Belt showing the location of the study area and type sections of the Sandspruit (A), Theespruit (B), and Komati Formations (C) of the Onverwacht Group. Geology outside of the study area modified from Anhaeusser et al. (1981). Symbols: IF, Inyoka fault; GGF, Granville Grove fault. Inset: Boundaries of the principal structural and stratigraphic domains in the study area (from Lowe et al., this volume, Chapter 2): Northern Domain (ND), West-Central Domain (WCD), East-Central Domain (ECD), and Southern (SD) Domain.

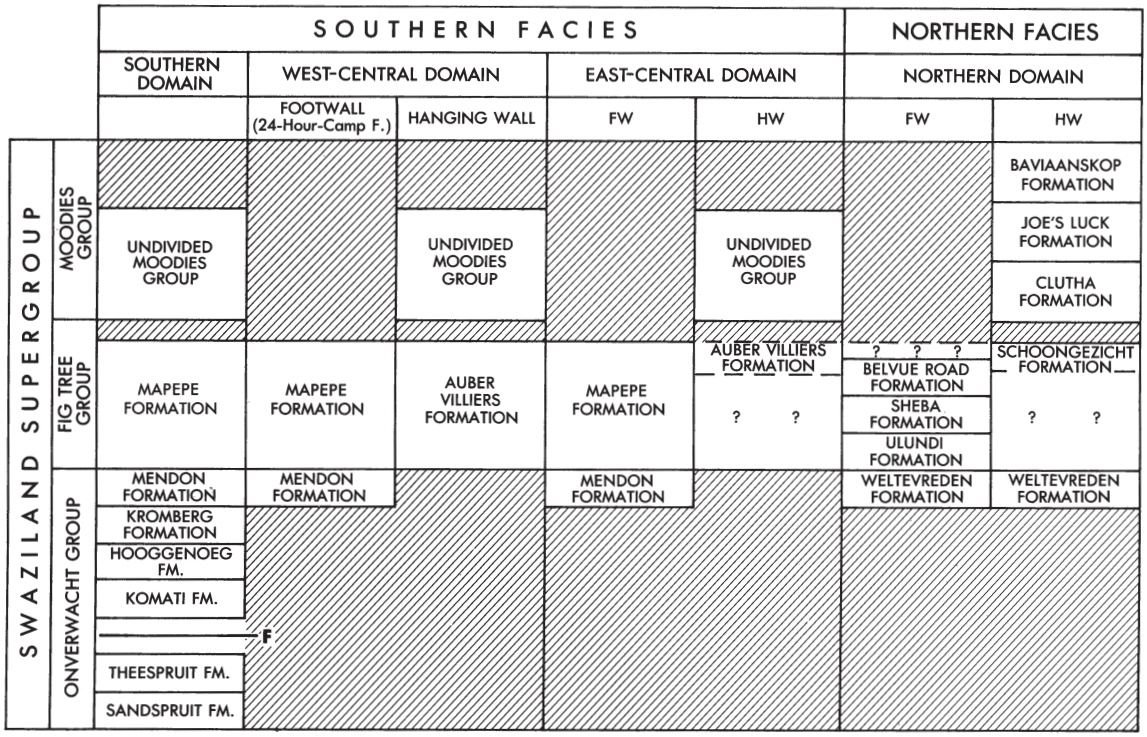


Figure 2. Present classification of rocks of the Swaziland Supergroup in the principal structural and stratigraphic domains of the Barberton Greenstone Belt. In all but the Southern Domain, rocks of the Swaziland Supergroup can be divided into a heavily deformed and faulted Onverwacht and Fig Tree succession and a less severely deformed Fig Tree and Moodies succession. These successions are separated by faults and/or unconformities and are termed hanging-wall (HW) and footwall (FW) sequences, respectively.

Lowe et al. (this volume, Chapter 2) subdivide the Barberton Greenstone Belt into four principal structural/stratigraphic blocks termed the (1) Southern, (2) West-Central, (3) East-Central, and (4) Northern Domains (Fig. 1). The Southern Domain (SD) includes a thick, largely intact succession from the Komati Formation of the Onverwacht Group through the Mapepe Formation of the Fig Tree Group (Figs. 2 and 3). The dominant structures are a series of large, tight to isoclinal folds with vertical to subvertical axes, including the Onverwacht anticline, Kromberg syncline, and Steynsdorp anticline (Fig. 1). On the west limb of the Onverwacht anticline, this domain is bounded on the north by the Granville Grove fault (Fig. 1). The West-Central Domain, developed between the Granville Grove and Inyoka faults on the west limb of the Onverwacht anticline, is made up of rocks of the Mendon Formation of the Onverwacht Group, the Mapepe and Auber Villiers Formations of the Fig Tree Group, and the Moodies Group. It consists of a tilted stack of fault-bounded structural sheets, now seen in cross section. The East-Central and Northern Domains are also made up of rocks of the uppermost Onverwacht Group and succeeding clastic units of the Fig Tree and Moodies Groups. They are dominated by tight, upright to overturned synclines in Moodies and Fig Tree strata that are commonly separated by narrow, sheared antiformal septa of Onverwacht rocks.

The following discussion addresses, first, the major modifications we propose to the stratigraphic classification of rocks within the Swaziland Supergroup (Figs. 2 and 3) and, secondly, the systematics of Barberton stratigraphy based in large part on a comparison of the stratigraphies of the individual domains. It will focus largely on a 300-square-km area (Figs. 1, 4, and 5) in the western part of the greenstone belt recently covered by our 1:6000- to 1:10,000-scale geologic mapping.

ONVERWACHT GROUP

Southern facies

The Onverwacht Group was named by Hall (1918) for outcrops of mafic volcanic rocks on farm Onverwacht 733 JT in the southern part of the Barberton Greenstone Belt. Viljoen, M. J., and Viljoen (1969a, b) and Viljoen, R. P., and Viljoen (1969) mapped the Onverwacht anticline, Kromberg syncline, and Steynsdorp anticline, estimating a thickness of more than 15,000 m. They subdivided the Onverwacht Group into six formations, including from base upward the Sandspruit, Theespruit, Komati, Hooggenoeg, Kromberg, and Swartkoppie Formations (Fig. 3).

The Swartkoppie or Zwartkoppie Formation was defined as

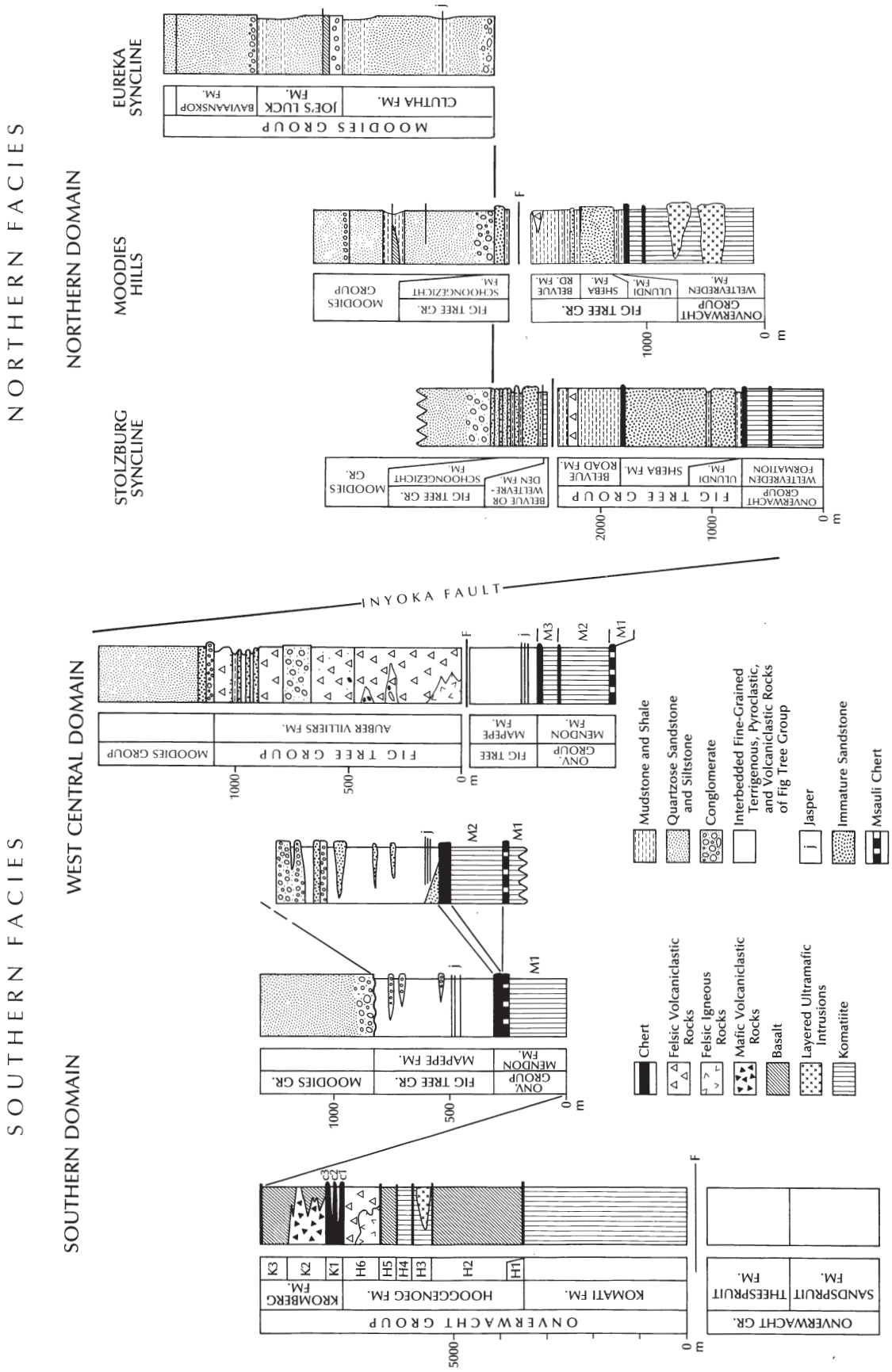


Figure 3. Stratigraphic sections of the Swaziland Supergroup in the principal structural and stratigraphic domains of the study area.

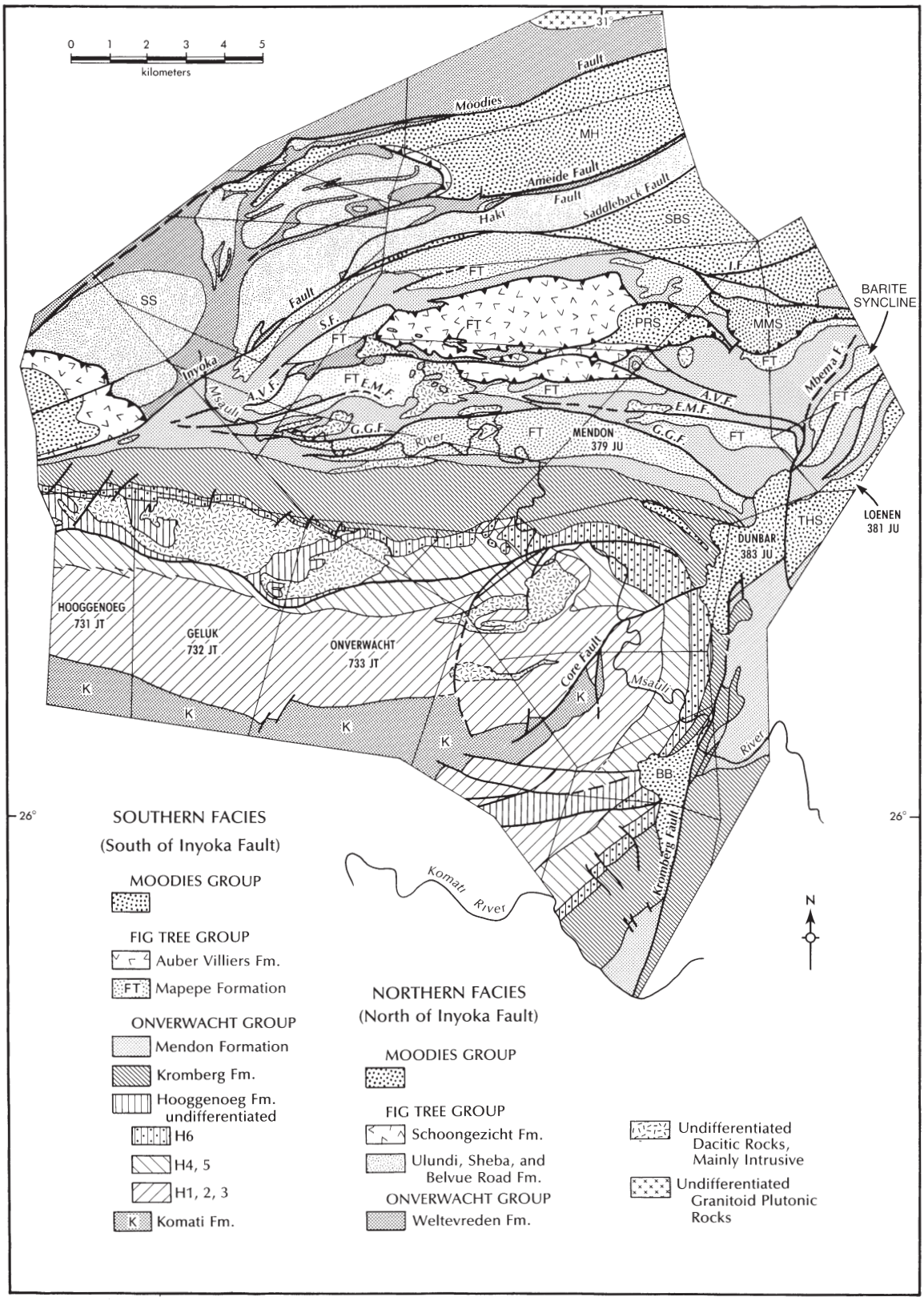


Figure 4. Geology of the study area. Symbols: MH, Moodies Hills Block; SS, Stolzburg syncline; SBS, Saddleback syncline; PRS, Powerline Road syncline; MMS, Maid-of-the-Mists syncline; THS, The Heights syncline; BB, Baviaanskloof Block; G.G.F., Granville Grove fault; A.V.F., Auber Villiers fault; and S.F., Schultzenhorst fault. The faults are named for local farms shown in Figure 5.

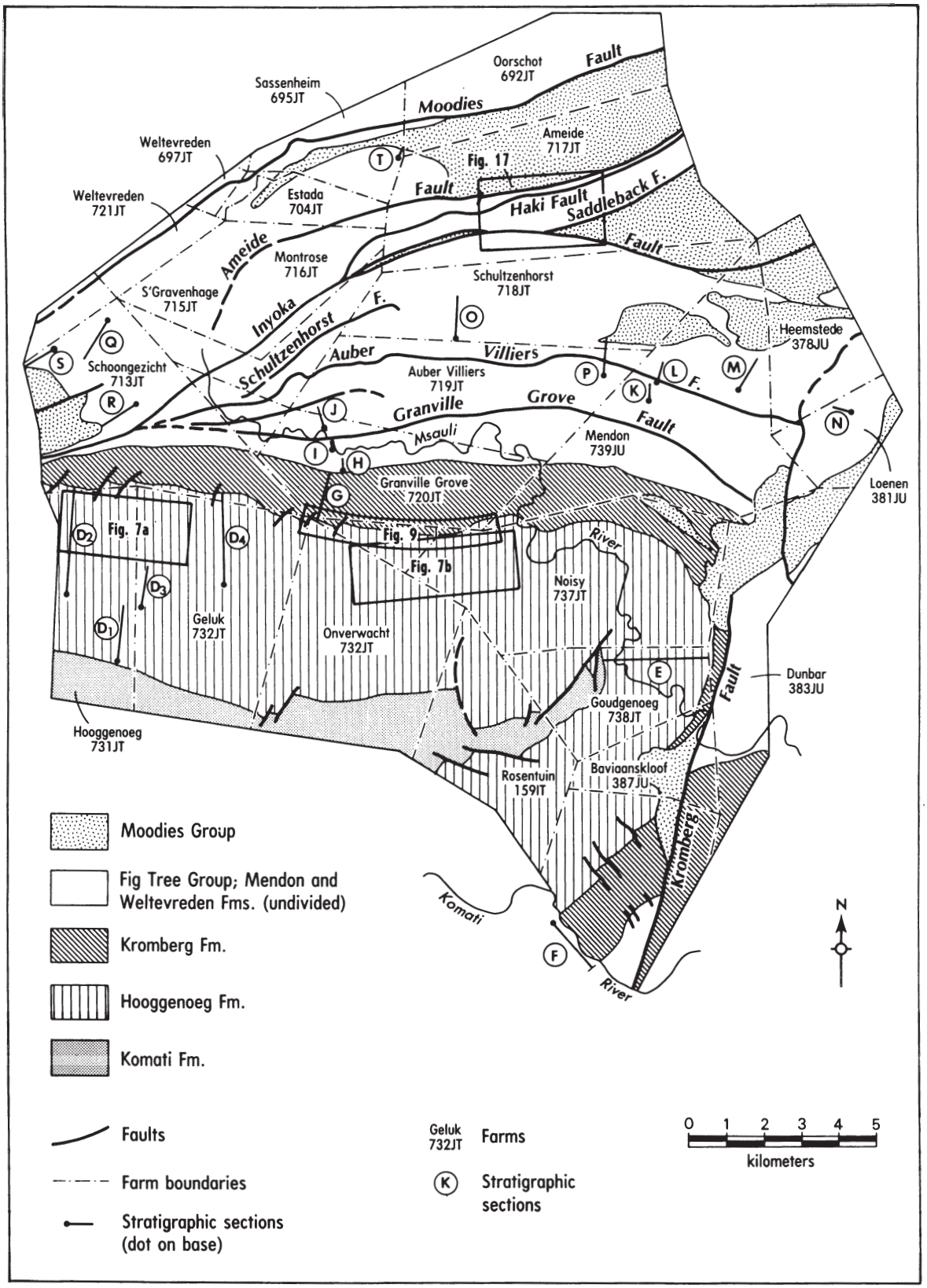


Figure 5. Location map of the study area showing farms, sections discussed in text, and locations of figures against major geologic features.

the uppermost unit of the Onverwacht Group by Viljoen, M. J., and Viljoen (1969a) and Viljoen, R. P., and Viljoen (1969). The formation grouped together a variety of stratigraphically problematic rocks, including cherts, heavily altered and sheared volcanic rocks, pyroclastic units, and ultramafic intrusive rocks, cropping out along the Swaziland border and at the east end of the Stolzberg syncline (Reimer, 1967). Our studies as well as those of Steyn (1965), Reimer (1967), Viljoen, R. P., and Viljoen (1969), and Paris (1985) have failed to establish either that these lithologies are part of a single, coherent stratigraphic succession or that they make up a mappable lithostratigraphic unit. In sections around the Onverwacht anticline, the Kromberg Formation of Viljoen, R. P., and Viljoen (1969) is succeeded directly by the Msauli Chert, regarded by previous investigators (Heinrichs, 1980; Stanistreet et al., 1981; Lowe et al., 1985; and others) as the basal unit of the Fig Tree Group. Our mapping has failed to disclose any Zwartkoppie rocks around the east end of the Stolzberg syncline (Fig. 4) and Reimer (personal communication, 1995) has indicated that rocks previously assigned to the Zwartkoppie Formation are actually structurally disturbed parts of other units. The Zwartkoppie Formation is not recognized in the present study.

The type sections and general distribution of the formations of the Onverwacht Group are shown in Figures 1 and 5.

Sandspruit and Theespruit Formations. The lowest formations of the Onverwacht Group, the Sandspruit and Theespruit Formations, are known mainly from the extreme southern part of the greenstone belt in the Onverwacht and Steynsdorp anticlines. The petrology of these units is summarized by Viljoen, M. J., and Viljoen (1969b). The Sandspruit Formation occurs mainly as xenolithic bodies isolated from the main part of the greenstone belt within tonalitic plutons (Fig. 1). It consists largely of massive, metamorphosed peridotitic and basaltic komatiite, now composed of alteration minerals including antigorite, chlorite, tremolite, and less commonly, magnetite. Thin, metamorphosed cherty sedimentary layers occur locally. Viljoen, M. J., and Viljoen (1969b) estimated the formation to be 2,134 m thick in its type section.

The Theespruit Formation in the Onverwacht anticline is made up largely of metamorphosed basalt, basaltic komatiite, and sericitic and aluminous rocks representing altered felsic volcanic and pyroclastic units. Altered felsic volcaniclastic units include coarse conglomerates and breccias, termed agglomerates by Viljoen, M. J., and Viljoen (1969b), and finer grained, generally schistose beds, some with cross-bedding (Viljoen, M. J., and Viljoen, 1969b; de Wit et al., 1983). These felsic units are commonly associated with thin beds of black and banded chert. Viljoen, M. J., and Viljoen (1969b) indicate a thickness of 1,890 m. Rocks of the Sandspruit and Theespruit Formations are widely metamorphosed to greenschist facies, and higher grade zones occur adjacent to intrusions. Schistose metamorphic fabrics and cleavage are well developed and cherty layers show a pronounced saccharoidal texture. All of the quartzites described by Viljoen, M. J., and Viljoen (1969b) are recrystallized cherts. The outcrops are cut by numerous faults and laced with minor felsic intrusive bodies.

The stratigraphic position of the Sandspruit and Theespruit Formations relative to other units in the Onverwacht Group in the Onverwacht anticline is not fully resolved. Although Viljoen, M. J., and Viljoen (1969b) regarded these units as the lowest formations in a more-or-less continuous sequence, they also recognized that they are in fault contact with "overlying" rocks. On the west limb of the Onverwacht anticline, the Komati fault separates extensively altered and sheared Theespruit rocks from relatively unstrained and less altered volcanic units of the Komati Formation. De Wit et al. (1983) suggested that the Theespruit Formation is a collection of structurally juxtaposed blocks, in part correlative with the less-deformed Hooggenoeg Formation. This interpretation is supported by the presence in the Theespruit Formation of dacitic clasts in a conglomerate that have yielded an age of 3,453 ± 6 Ma (Armstrong et al., 1990), the same age as dacitic volcanic units at the top of the Hooggenoeg Formation. However, the presence dacitic clasts and agglomerates with ages of 3,531 ± 10 Ma (Armstrong et al., 1990) and 3,511 ± 3 (Kröner et al., 1992) indicates that parts of the type Theespruit Formation are also older than the Komati Formation (Lowe, this volume, Chapter 12, Table 1). The present authors consider it likely that rocks in the Onverwacht anticline mapped as Theespruit and Sandspruit Formation by Viljoen, M. J., and Viljoen (1969b) include structurally juxtaposed and metamorphosed units older than and, in part, equivalent to the Komati and Hooggenoeg Formations. They represent the roof rocks to the 3,445 Ma TTG plutons in this area.

In the Steynsdorp anticline (Fig. 1), as much as several thousand meters of metamorphosed mafic and felsic volcanic rocks containing thin interbedded cherts underlie altered komatiites of the Komati Formation (Viljoen, M. J., and Viljoen, 1969b). These rocks form a heavily altered but largely intact pre–Komati Formation mafic and felsic sequence that was intruded by tonalitic plutons 3,502–3,511 Ma (Kamo and Davis, 1994; Kröner et al., 1996).

Komati Formation. The Komati Formation was defined by Viljoen, M. J., and Viljoen (1969a, b) to include peridotitic and basaltic komatiites underlying tholeiitic volcanic rocks of the Hooggenoeg Formation. The type section is located in the valley of the Komati River on the west limb of the Onverwacht anticline (Fig. 1), where the formation reaches 3,500 m thick. The unit crops out continuously along the west limb of the Onverwacht anticline and in the Steynsdorp anticline, but is faulted out on the east limb of the Onverwacht anticline. Komatiitic volcanic and intrusive rocks in the central and northern parts of the greenstone belt, previously considered to belong to the Komati Formation, are here reassigned to the Mendon and Weltevreden Formations, respectively.

The Komati Formation is distinguished by an immense thickness of komatiitic volcanic rocks (Viljoen, M. J., and Viljoen, 1969b; Williams and Furnell, 1979), many of which show pseudomorphed olivine or pyroxene spinifex textures and structuring typical of thin, rapidly extruded, low-viscosity ultramafic flows (Pyke et al., 1973; Viljoen et al., 1983). Although smaller intrusive bodies are widespread, large layered ultramafic intrusions, com-

mon in other komatiitic units, are absent in the Komati Formation. The formation is also striking because of the near absence of interflow sedimentary layers and of evidence of flow-top alteration and erosion. Evidently eruption rates were sufficiently high that little or no time elapsed between successive flows.

The Komati Formation is faulted at its base in the Onverwacht anticline, and overlain regionally by the Middle Marker, a thin cherty sedimentary unit at the base of the Hooggenoeg Formation (Viljoen, M. J., and Viljoen, 1969b; Lanier and Lowe, 1982). This contact is locally marked by felsic intrusive rocks and shearing and has been considered to represent an unconformity (Viljoen, R. P., and Viljoen, 1969). However, the Middle Marker is typical of cherts developed above komatiitic lavas throughout the Onverwacht Group (Lowe, this volume, Chapters 3 and 9) and is underlain by an alteration zone thought to have formed in part during early near-surface diagenesis and predeformation hydrothermal metasomatism (Lowe and Byerly, 1986b). Although the base of the Middle Marker may mark a minor hiatus in deposition, perhaps a surface of local erosion, and a locus of late shearing because of the extreme ductility contrasts between the underlying komatiitic and overlying massive basaltic volcanic sequences, the Komati and Hooggenoeg Formations appear to form a continuous, largely conformable stratigraphic succession, as suggested by Williams and Furnell (1979).

Hooggenoeg Formation. The Hooggenoeg Formation (Viljoen, R. P., and Viljoen, 1969) comprises a thick sequence of tholeiitic basalts, basaltic komatiites, felsic igneous rocks, and thin cherty units named for farm Hooggenoeg 731 JT in the southern part of the belt (Figs. 4 and 5). Viljoen, R. P., and Viljoen (1969) estimate a thickness of 4,847 m in the type section along the west limb of the Onverwacht anticline (section D1–D2, Fig. 5). However, this thickness includes the Buck Reef Chert, which in this report is included in the Kromberg Formation. The thickness of the formation in this area is about 3,900 m. Because of remoteness and access difficulties of the upper part of the type section, a supplementary section (section D1–D3–D4, Fig. 5) is here designated 2 to 5 km to the east (West Limb section, Fig. 6).

The upper parts of all sections of the Hooggenoeg Formation on the west limb of the Onverwacht anticline have been disturbed by shearing and intrusion (Fig. 4; Lowe et al., 1985; Lowe et al., this volume, Chapter 2). The stratigraphy is more coherent along most of the east limb, and a complete section of the formation, 2,900 m thick, is present immediately north of the Msauli River (Figs. 5 and 6). The upper, felsic part of the formation is well exposed along the Komati River (Viljoen, R. P., and Viljoen, 1969; Lowe and Knauth, 1977).

The Hooggenoeg Formation has long been characterized as showing well-developed mafic to felsic volcanic cyclicity (Viljoen, R. P., and Viljoen, 1969). Geochemical and petrologic studies, however, suggest that mafic to felsic cycles are absent and that only a single felsic volcanic unit is present at the top of the formation (Byerly et al., 1983). Apparent cycles lower in the formation reflect local alteration and silicification of the volcanic sequence (Byerly et al., 1983; Lowe and Byerly, 1984, 1986b).

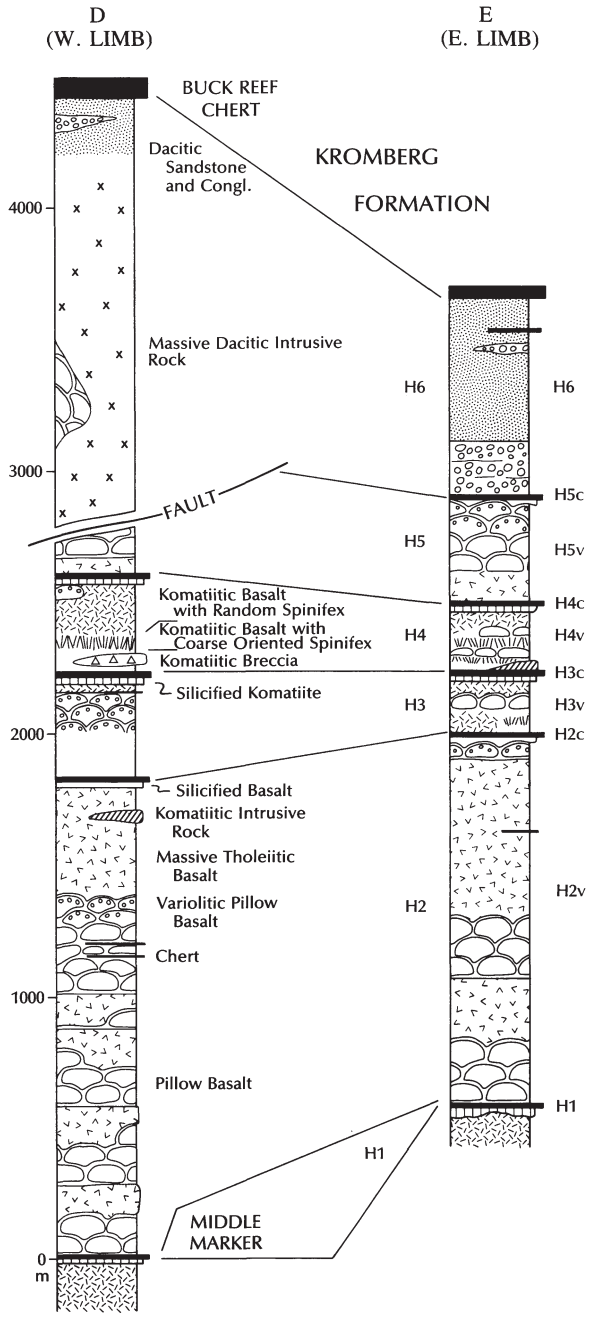


Figure 6. Stratigraphy of the Hooggenoeg Formation in and near its type section on the west limb of the Onverwacht anticline (left) and in a supplementary section on the east limb (right). Sections are located in Figure 5. The formation has been divided into six informal members, H1 through H6. With the exception of the Middle Marker (H1), each member includes a lower volcanic division (v) and a capping chert unit (c). The lowest spherule bed yet discovered in the Swaziland Supergroup, S1, occurs in H4c on both east and west limbs of the Onverwacht anticline.

The Hooggenoeg Formation is here divided into six informal members traceable throughout the Onverwacht anticline and Kromberg syncline (Figs. 3 and 6): H1, the Middle Marker; H2, massive and pillowed tholeiitic basalt capped by a thin unit of gray chert; H3 and H4, successive units of basaltic komatiite and basalt capped by thin units of silicified volcaniclastic debris; H5, basalt and variolitic basalt capped by a thin unit of gray chert and silicified volcaniclastic sediment; and H6, felsic volcanic and volcaniclastic rocks. Within individual members, the main volcanic units and capping cherts will be designated with "v" and "c" respectively (e.g., H2v and H2c).

H1: Middle Marker. The Middle Marker is a regionally extensive layer of silicified volcaniclastic debris and carbonaceous sediment averaging 4 to 5 m thick (Viljoen, R. P., and Viljoen, 1969; Lanier and Lowe, 1982). The original sediments consisted largely of volcaniclastic debris including airfall layers of very fine-grained komatiitic dust, ash, and volcanic accretionary lapilli and current-worked beds of sand- and fine-gravel-sized detritus. Nonvolcanogenic layers consist of black carbonaceous chert representing fine-grained biogenic particles deposited under low-energy conditions between current and fall events (Lanier and Lowe, 1982). Carbonate widely developed in the Middle Marker (Viljoen, R. P., and Viljoen, 1969; Hurley et al., 1972) is largely of diagenetic and metasomatic origin.

H2: Tholeiitic basalt. The Middle Marker is overlain directly and conformably by a thick sequence of tholeiitic basalt (H2v) capped by a thin unit of black chert (H2c), both assigned to member H2 of the Hooggenoeg Formation (Fig. 6). This subdivision is about 1,800 m thick on the west limb of the Onverwacht anticline and 1,200–1,400 m thick along the northern part of the east limb. It consists largely of alternating units of pillowed and massive tholeiitic basalt (Viljoen, R. P., and Viljoen, 1969). Individual pillowed and massive units range from several meters to nearly 500 m in thickness, although most are between 10 and 50 m thick, and show complex lateral and vertical interstratification and interfingering (Viljoen, R. P., and Viljoen, 1969, Fig. 4; Williams and Furnell, 1979). Pillows, which average between 0.5 and 1.5 m across, commonly show radial pipe vesicles around the outer edges and downward projections between underlying rounded pillow tops.

One or two thin, 0.5- to 2-m-thick layers of black and black-and-white banded chert are interbedded with pillowed volcanic rocks in the upper parts of many sections. The capping chert, H2c, consists largely of black and black-and-white banded chert and is 15 and 2.5 m thick in supplementary sections on the west and east limbs, respectively, of the Onverwacht anticline. This chert is underlain by a zone of highly silicified basalt as much as 10 m thick.

H3: Komatiitic and tholeiitic basalt. Member H3 of the Hooggenoeg Formation, about 380 m thick in the type section and 220 m thick in the supplementary section on the east limb (Fig. 6), is made up largely of pillowed tholeiitic basalt, variolitic pillow basalt, and massive spinifex-bearing basaltic komatiite (H3v). Although individual sections vary widely in the proportions of these rock types, there is generally a greater abundance of spinifex-bearing rocks at the top of the member and of pillowed tholeiitic units towards its base. One or two thin cherts layers less than 1 m thick are present locally in the upper part of the member.

Along the southern part of the east limb of the Onverwacht anticline, H3 includes a 150-m-thick, layered to massive ultramafic intrusion termed the Rosentuin Ultramafic Body (Viljoen, R. P., and Viljoen, 1969). This unit lies near the top of the volcanic member, H3v, and includes layers of serpentinized peridotite that locally contain large poikilitic pyroxene crystals enclosing olivine. Smaller ultramafic intrusions also containing olivine enclosed by poikilitic pyroxene are widely developed in H3 and H4 (Williams and Furnell, 1979).

The cap on member H3 is a distinctive layer of silicified volcaniclastic and carbonaceous sediment (H3c). Along the west limb of the Onverwacht anticline, this chert includes a basal zone as much as 15 m thick of massive, intensely silicified and metasomatically altered ash overlain by from 1 to 7 m of silicified airfall komatiitic dust, ash, and accretionary lapilli; current-deposited volcaniclastic debris; and carbonaceous black chert (Lowe, this volume, Chapter 3, Fig. 18). H3c is about 20 m thick along the east limb but lacks the massive basal ash. Sediment types and depositional styles closely resemble those of the Middle Marker (Lowe, this volume, Chapter 3) and the Msauli Chert (Lowe, this volume, Chapter 9).

H3c is underlain by a regionally traceable unit of metasomatically altered, spinifex-bearing komatiite containing Cr-bearing micas and stratiform, fibrous veinlets of silica and carbonate (Lowe and Byerly, 1986b).

H4: Basaltic komatiite and basalt. H3c is overlain by 250 to 350 m of volcanic rocks of H4v. The lower part of this member is generally komatiitic, and a regional zone, 10 to 20 m thick, of altered, coarse, vertical to subvertical pyroxene spinifex as much as 2 m high is present in all sections studied. Locally, coarse spinifex-bearing igneous units in this zone include thin caps of hyaloclastic breccia. Toward the middle and upper parts of the volcanic unit, thick massive flow rock containing fine, randomly oriented spinifex is interstratified with pillowed, spinifex-free basalt. The uppermost units generally consist of well-pillowed spinifex-free high-Mg basalt. Locally, intrusive sills and dikes of coarse, poikilitic komatiite are present near the base of the member.

The discontinuous chert cap (H4c), 0 to 3 m thick, is composed of silicified airfall and current-worked volcaniclastic sedimentary rock and carbonaceous chert. The unit includes a layer near the top, termed S1, containing spherules that appear to have formed as quenched liquid silicate droplets. This is the only spherule layer found to date in the Onverwacht Group. Others are present in the Fig Tree Group (Lowe and Byerly, 1986a; Lowe et al., 1989b). This chert is locally underlain by a zone of alteration and metasomatism that contains green, Cr-bearing micas and stratiform fibrous silica and carbonate veinlets (Lowe and Byerly, 1986b).

H5: Basalt. The uppermost part of the mafic volcanic sequence of the Hooggenoeg Formation is made up largely of pil-

lowed and massive high-Mg and tholeiitic basalt (H5v). This member is poorly preserved on the west limb of the Onverwacht anticline (Fig. 6) because of disruption within the Geluk shear zone at the top of the formation. It is well developed, however, along the eastern limb, where it averages about 390 m thick. Most of the rocks are pillowed basalts with pillows 0.5–1.5 m across, commonly with radial pipe vesicles and chilled selvages. Near the top of the section is a regionally developed unit of variolitic pillow basalt. The varioles are separated around the pillow margins but coalesce toward the interiors (Viljoen, M. J., and Viljoen, 1969b). This unit includes some of the largest varioles we have seen in the greenstone belt, locally reaching 3 cm in diameter.

Thin chert units are locally interbedded with the volcanic rocks. The volcanic sequence is capped by a layer of chert (H5c) from less than 1 to 2 m thick. It consists of a basal zone of massive black chert overlain by interbedded volcaniclastic sediments and black chert. The chert is underlain by a zone as much as 10 m thick of silicified basalt, locally cut by downward-extending black chert dikes.

H6: Felsic volcaniclastic and volcanic rocks. The uppermost member of the Hooggenoeg Formation, H6, is a complex association of felsic igneous and volcaniclastic rocks. On the central part of the west limb of the Onverwacht anticline, H6 consists largely of massive dacitic intrusive rock cut by numerous younger mafic and ultramafic intrusive bodies and overlain by a thin cover of volcaniclastic breccia, conglomerate, and sandstone (Figs. 4 and 7). This crudely stratiform dacitic intrusion, first noted by Viljoen, R. P., and Viljoen (1969) and Smith (1981), has been described and dated at 3,445 ± 4 Ma by de Wit et al. (1987a). It crops out for 9–10 km along strike, ranges from 1 to 2.5 km thick, and contains large, detached, rotated masses of basaltic and komatiitic volcanic rock of underlying Hooggenoeg members H4 and H5. Immediately underlying and peripheral to the intrusion is a zone of shearing and block rotation from a few tens to several hundreds of meters thick named the Geluk shear zone (Lowe et al., this volume, Chapter 2). It is made up largely of overturned blocks of Hooggenoeg members H3 to H5 and is sharply bounded below by undeformed rocks of members H4 and H5 (Fig. 7).

The intrusion and zone of overturned blocks are overlain and flanked by thick sequences of massive, coarse, volcaniclastic breccia and conglomerate containing sparse clasts of mafic and komatiitic volcanic rock (Fig. 7). These epiclastic units thin and fine away from the intrusion in both directions. On the far west limb of the Onverwacht anticline, H6 is represented by a sequence of fine-grained dacitic tuff less than 100 m thick. Along the east limb of the anticline, massive fan-delta and alluvial conglomerates more than 750 m thick in the supplementary section of the Hooggenoeg Formation (Fig. 6) grade southward into a section along the Komati River that includes about 10 m of oligomictic dacite-clast conglomerate and breccia overlain by 150 m of fining-upward dacitic debris-flow deposits, coarse-grained thick-bedded turbidites, and fine-grained, thin-bedded, silicified turbidites (Viljoen, R. P., and Viljoen, 1969; Lowe and Knauth, 1977). Paleocurrent indictors in the turbidites along the Komati River suggest general flow from north to south. The cherty turbidites at the top of the Komati River section have been correlated with the Buck Reef Chert on the west limb of the anticline (Viljoen, R. P., and Viljoen, 1969), but regional mapping indicates that these turbidites are a local facies of the felsic volcanic sequence in the type section of the Hooggenoeg Formation (Lowe et al., 1985).

The dacitic intrusion appears to have been emplaced beneath a roof of mafic volcanic rock of H4 and H5 and conglomerates of H6 that was no more than 200 m thick and which fractured and foundered into the silicic magma (Fig. 7). We have identified no evidence, such as foundered blocks of Buck Reef Chert, that overlying sedimentary units of the Kromberg Formation existed at the time of intrusion. Ages of 3,445 ± 6 Ma and 3,438 ± 12 Ma on volcaniclastic units laterally equivalent to the intrusion, of 3,445 ± 4 Ma on the intrusion itself (de Wit et al., 1987a), and of 3,416 ± 7 Ma on tuffs overlying the intrusion (Kröner et al., 1991) indicate that the intrusion is Hooggenoeg in age and was emplaced before deposition of overlying sedimentary units of H6 and the Buck Reef Chert. The intrusion probably formed a shallow silicic dome

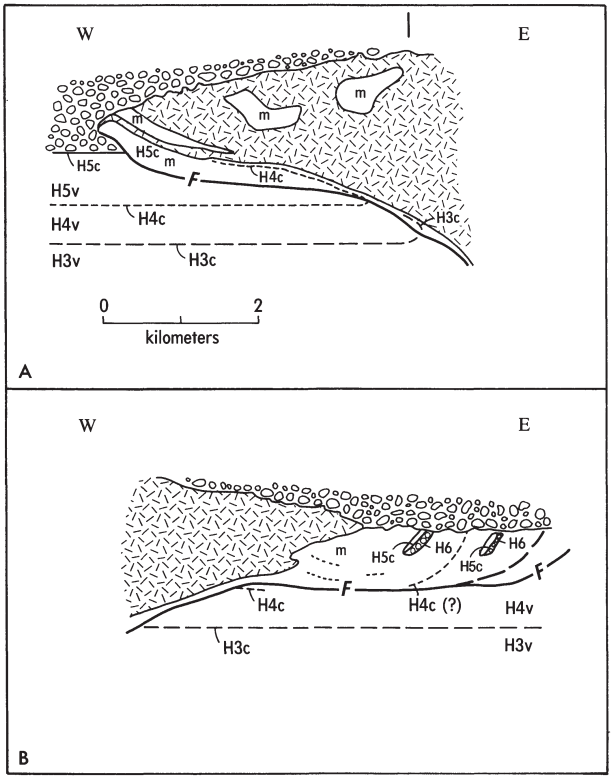


Figure 7. Schematic cross sections through the western (A) and eastern (B) ends of the large dacitic intrusive body in H6 along the west limb of the Onverwacht anticline. In both sections, rocks within the Geluk shear zone, which is bounded below by a sharp fault contact (F) and above by the intrusive body and flanking epiclastic dacite-clast breccia and conglomerate, are overturned and now young downward. All other rocks are in normal stratigraphic order. Symbols and patterns: (unpatterned) H3–H5 mafic volcanic units; (random line segments) dacitic intrusion; (blocky pattern) dacite-clast conglomerate and breccia; ("m") disturbed mafic volcanic units in the Geluk Shear Zone and intrusive body.

mantled by roof rock and its own chilled and fragmented debris that was subsequently eroded to form the flanking volcaniclastic aprons (Fig. 7). The intrusion may represent only the uppermost hypabyssal portion of a much larger body that was connected at depth to the 3,445-Ma-old tonalite-trondhjemite-granodiorite (TTG) suite bounding the southern margin of the BGB and upward to vents through which felsic extrusives of the Hooggenoeg Formation were erupted (de Wit et al., 1987a).

On the west limb of the Onverwacht anticline, a small dacitic intrusion extends upward into the overlying Buck Reef Chert, suggesting that minor Fig Tree–age dacitic intrusive rocks are also present locally in H6.

Kromberg Formation. Along the Komati River, silicified volcaniclastic turbidites at the top of the Hooggenoeg Formation are overlain by about 100 m of massive ultramafic rock marking the base of the type section of the Kromberg Formation (Viljoen, R. P., and Viljoen, 1969). Locally, this unit shows spinifex near the top and is clearly extrusive. In its type section (Fig. 5, section F), the Kromberg includes about 1,700 m of volcanic and sedimentary rocks representing three principal lithofacies: (1) massive and pillowed basalt and komatiite (Vennemann and Smith, this volume, Chapter 5), (2) mafic lapilli tuff and lapillistone, and (3) black and banded chert. The upper contact of the Kromberg Formation is here placed at the top of the Footbridge Chert, a newly named and regionally traceable unit of black and banded chert cropping out at the footbridge across the Komati River (5,700 ft. in section of Kromberg Formation, Fig. 11, Viljoen, R. P., and Viljoen, 1969). Viljoen, R. P., and Viljoen (1969) included in the Kromberg Formation an additional 300 m of basaltic and peridotitic komatiite above the Footbridge Chert. Based on regional stratigraphic relationships, we here include these komatiitic rocks in the Mendon Formation.

On the west limb of the Onverwacht anticline, felsic volcaniclastic strata of H6 are overlain with apparent conformity by basal cherts of the Kromberg Formation. A well-exposed section of the formation from 1,500 to 1,800 m thick is present on farm Granville Grove 720 JT (section G, Fig. 5). In this section (Fig. 8), the Kromberg can be divided into three informal members: K1, the Buck Reef Chert, K2, mafic lapilli tuff and lapillistone; and K3, tholeiitic basalt.

K1: Buck Reef Chert. On the west limb of the Onverwacht anticline and on the east limb north of the Msauli River, the basal member of the Kromberg Formation is a 150- to-350-m-thick unit of chert named the Buck Reef Chert by Hall (1918) in reference to the fact that it was a "reef" that lacked gold. This unit was mislabeled the Bucks Ridge Chert by Heinrichs (1980). The contact between silicified dacitic volcaniclastic sandstone at the top of H6 and the base of K1 is transitional, with thin beds of black chert, silicified wave-rippled carbonaceous sediment, and silicified evaporite occurring within the upper 5 to 50 m of the volcaniclastic section (Fisher Worrell, 1985; Lowe and Fisher Worrell, this volume, Chapter 7).

The Buck Reef Chert includes three and, in some sections, four subdivisions: (1) a basal division of silicified evaporite

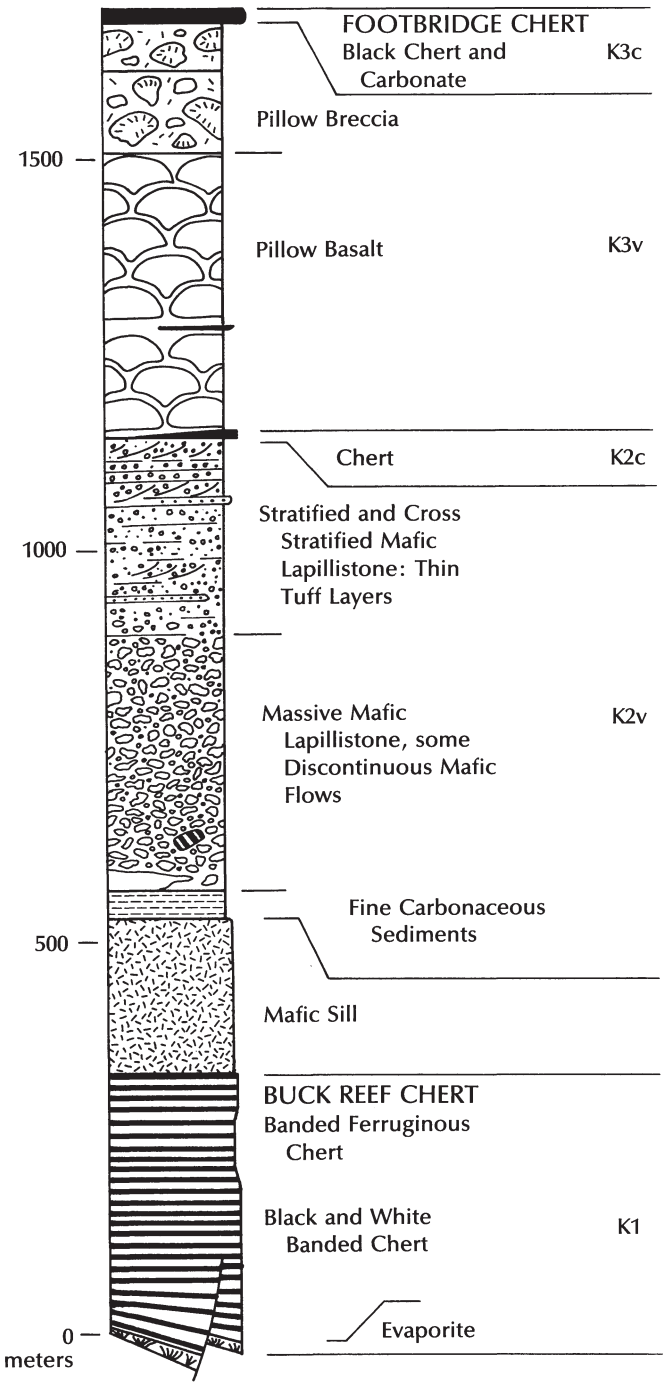


Figure 8. Stratigraphy of the Kromberg Formation along the west limb of the Onverwacht anticline (section G, Fig. 5). Details of the type section (section F, Fig. 5) are given by Viljoen, R. P., and Viljoen (1969, Fig. 9).

(Lowe and Fisher Worrell, this volume, Chapter 7), (2) a lower division of black-and-white banded chert, (3) a division of banded ferruginous chert, and (4) an upper division of black-and-white banded chert, present only locally on the west limb of the Onverwacht anticline (Fig. 8). The basal evaporite includes from 5 to 40 m of silicified, laminated and wave-rippled, shallow-water

sediments; silicified evaporite-solution collapse layers; conglomerate; and volcaniclastic debris (Fisher Worrell, 1985; Lowe and Fisher Worrell, this volume, Chapter 7).

On the central part of the west limb of the Onverwacht anticline, the evaporite and overlying black-and-white banded chert divisions are cut by a series of small, syndepositional normal faults (Figs. 8 and 9). Within the half grabens developed adjacent to these faults, the thickness of the basal evaporitic and overlying black-and-white bended chert divisions reach 200 m compared to 80–100 m in adjacent unfaulted areas. Deposition of the upper divisions of the Buck Reef Chert postdated faulting (Fig. 8).

In the hinge region of the Onverwacht anticline, the evaporitic and lower black-and-white banded chert divisions can be identified but the upper divisions are represented by a relatively uniform sequence of thinly layered banded ferruginous chert. Volcanic units are interstratified within the thinning chert sequence on the northern part of the east limb of the anticline and, south of the Msauli River, the equivalent section consists of three thin chert layers interbedded with thicker volcanic units (Viljoen, R. P., and Viljoen, 1969, Fig. 9, cherts at 750, 1,250 and 2,450 ft.). From base upward, these cherts are designated K1c1, K1c2, and K1c3 (Fig. 3). Interbedded volcanic rocks include massive and pillowed basalts, mafic pyroclastic layers, and komatiitic flow and intrusive units.

In all sections on the west limb, the Buck Reef Chert is cut by anastomosing dikes and sills of mafic and komatiitic igneous rock, some locally intruded along the syndepositional faults. Also on the west limb, the upper two divisions are the locus of extensive hydrothermal alteration. Broad areas have been enriched in iron with local formation of massive ironstone bodies as much as 100 m across (de Wit et al., 1982).

K2: Mafic lapilli tuff and lapillistone. On the west limb of the Onverwacht anticline, the middle part of the Kromberg Formation (Fig. 8) is made up largely of coarse, massive, heavily altered, mafic lapillistone and lapilli tuff (K2v; Ransom, 1987; Ransom et al., this volume, Chapter 6). In western sections, the basal 10–100 m consists of fine-grained tuff and fissile, nonsilicified, tuffaceous, carbonaceous shale containing local thin mafic flows. The overlying unit of coarse mafic lapillistone ranges from 300 to 1,000 m thick. The lower third to half consists largely of massive, unstratified 0.5- to 4-cm-sized lapilli containing accidental clasts of Buck Reef Chert, fine-grained mafic flow rock, and rare chunks of coarse-grained pyroxenite. Mafic flow units are widely interstratified within the fragmental sequence. The upper part of K2v is composed of stratified, generally finer grained lapilli and includes thin layers of altered silicified ash. The topmost 50–100 m consist of lapilli, generally less than 1 cm in diameter, showing abundant current structures, including large-scale cross-stratification (Fig. 8). Sparse chemical analyses (Ransom et al., this volume, Chapter 6), the chloritic alteration products, and the relatively high chrome content of the lapillistone, 1,450, 1,492, 2,060 ppm for three samples of carbonated lapillistone from the type section along the Komati River, suggests that the original debris was komatiitic in composition.

Near the central part of the west limb of the Onverwacht anticline, K2v reaches its maximum thickness of more than 1,000 m, and the lower half includes abundant large angular blocks of Buck Reef Chert. In this area, the upper 200–300 m of the Buck Reef Chert are missing over an outcrop distance of 1.5–2 km (Fig. 9). The vertical-sided depression left by removal of the chert is filled with mafic pyroclastic debris and mafic lavas, and the adjacent and underlying chert is cut by numerous dikes of similar intrusive rock. This area probably represents the site of a major phreatomagmatic explosion that marked the initiation of pyroclastic volcanism (Ransom et al., this volume, Chapter 6).

In the hinge region of the Onverwacht anticline, K2v is associated with an unusual assemblage of rocks including coarse quartzose sandstone, polymictic conglomerate, and breccia composed of angular plates of banded ferruginous chert in a quartzose matrix. Some of these rocks were regarded as a Kromberg-age submarine slide deposit by de Wit (1982) but all are actually part of a synclinal keel of Moodies strata that overlies and is partially infaulted into K2v.

The pyroclastic sequence is capped locally along the west limb by a thin unit of silicified ash and dust and black chert (K2c) showing abundant large-scale cross-stratification and other evidence of deposition in shallow water (Ransom et al., this volume, Chapter 6).

K2 is traceable around the hinge region of the Onverwacht anticline but is extensively faulted within the Kromberg fault zone along the east limb north of the Komati River. In the type section along the Komati River, the member includes only 75 m of mafic pyroclastic debris interbedded with basalt flows (Viljoen, R. P., and Viljoen, 1969, Fig. 9). Near the top, the volcaniclastic section shows well-developed current layering and large-scale cross-stratification (Viljoen, R. P., and Viljoen, 1969, Plate XIa).

K3: Basalt. On the west limb of the Onverwacht anticline, K2 is overlain by silicified pillow basalt (K3v) 500–600 m thick (Ransom, 1987). The upper part of the section includes thick units of pillow breccia. The formation is capped by the Footbridge Chert (K3c), which, on the west limb, consists of 15–25 m of black and black-and-white banded chert.

In the type section, the bulk of the Kromberg consists of massive and pillowed basalt (Viljoen, R. P., and Viljoen, 1969, Fig. 9) and interlayered komatiite (Vennemann and Smith, this volume, Chapter 5). Both the Buck Reef Chert and mafic lapillistone are represented largely by basaltic units and the upper 350 m of the formation is composed of interstratified pillow basalt, massive basalt, pillow breccia, thin komatiitic units, and highly altered tuffaceous material. A second unit of black chert, poorly silicified carbonaceous shale, and carbonate 14 m thick is present 60 m below the Footbridge Chert in the type section.

No felsic volcanic or volcaniclastic units have been identified in the Kromberg Formation, although many basalts show extensive postdepositional silicification (Ransom, 1987). Most of the lapillistone and other coarse-grained fragmental units have been extensively replaced by chlorite, tremolite, iron-rich dolomite, and ankerite.

The Kromberg Formation also crops out east of the Kromberg

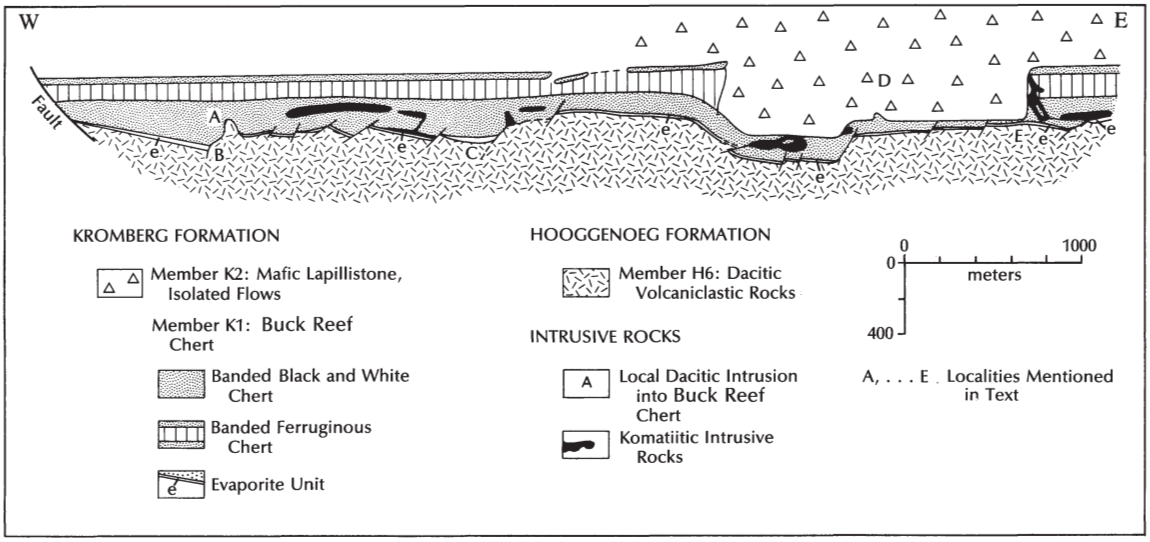


Figure 9. Detailed geologic cross section of the uppermost Hooggenoeg and lowest Kromberg Formations along part of the west limb of the Onverwacht anticline (Fig. 5). "A" is a small, Fig Tree–age dacitic intrusion into the Buck Reef Chert. Syndepositional normal faults (B to C), active during the initial stages of deposition of the Buck Reef Chert (K1), formed small basins that were sites of deposition of unusually thick sections of evaporitic deposits (e) at the base of K1 (Lowe and Fisher Worrell, this volume, Chapter 7). Following deposition of K1, as much as 300 m of chert was removed over a distance of about 1,300 m, probably by a major phreatomagmatic explosion (Ransom et al., this volume, Chapter 6), and the resulting excavation filled by komatiitic volcaniclastic debris and minor flow rocks of Kromberg Formation member K2 (D). The lack of faulting of evaporite unit at margin of excavation indicates that it was not produced by simple downfaulting of Buck Reef Chert (E).

fault between the Msauli and Komati Rivers (Fig. 4). This section consists largely of massive and pillowed basalt containing thin interstratified chert layers. Although we have not studied this sequence in detail, it appears to lack member K2 (lapilli tuff and lapillistone) and individual chert units cannot yet be correlated with those in the type section. It seems likely that the Kromberg fault separates facies of the Kromberg Formation that are grossly similar but differ in stratigraphic detail.

Mendon Formation. In the Southern Domain on both limbs of the Onverwacht anticline, the Footbridge Chert is overlain by massive komatiitic volcanic rocks (Byerly, this volume, Chapter 8). In the type section of the Kromberg Formation, these rocks were included in the Kromberg Formation by Viljoen, R. P., and Viljoen (1969), but regional mapping shows that they are part of a cyclic sequence of interbedded komatiitic volcanic rocks and cherts that overlies the predominantly basaltic Kromberg Formation and underlies sedimentary rocks of the Fig Tree Group. We assign these komatiites and cherts above the Footbridge Chert and below nonsilicified clastic units of the Fig Tree Group to the Mendon Formation (Fig. 10). The formation is named for farm Mendon 379 JU (Fig. 5).

Rocks of the Mendon Formation crop out throughout the central part of the Barberton Greenstone Belt (Figs. 1 and 4). The West-Central Domain is divided into a series of narrow structural blocks by a number of major bedding-parallel faults (Fig. 4). Faulting is commonly localized in serpentinized ultramafic rocks of the Mendon Formation, and each fault-bounded block includes rocks of the upper Mendon Formation and lower Fig Tree Group. In the Southern Domain the Mendon Formation consists of a single volcanic unit capped by the 20- to 35 m-thick Msauli Chert and an overlying succession 9–40 m thick of black, banded, and ferruginous cherts. The chert sequence is overlain conformably by Fig Tree strata (Fig. 10, section H). In the West-Central and East-Central Domains, the base of the Mendon Formation is not exposed. Correlation among structural belts suggests that the Mendon Formation includes increasingly younger volcanic-sedimentary cycles at the top in more northern parts of the WCD (Fig. 10).

Because of faulting and facies changes, it is impossible to designate a type section for the Mendon Formation that includes all volcanic-sedimentary cycles. A type section for the lowest cycle is on farm Granville Grove 720 JT from 25°55′10″ S., 30°55′56″ E. (base) to 25°55′03″ S., 30°55′57″E. (Figs. 5 and 10, section H). The type section for the Msauli Chert (Stanistreet et al., 1981) is at 25°54′50″ S., 30°55′52″ E. in this section (Fig. 5, section I). The second and third cycles are well exposed in section J on farm Mendon northward from 25°54′06″ S., 31°01′ E., and higher cycles occur in sections K and L (Figs. 5 and 10). The aggregate maximum thickness of the formation exceeds 1,000 m.

Correlation of the Mendon Formation among structural blocks is made possible by a series of distinctive marker units (Fig. 10). These include (1) the Msauli Chert (M1c) at the top of the lowest cycle; (2) a unit of silicified komatiitic ash containing

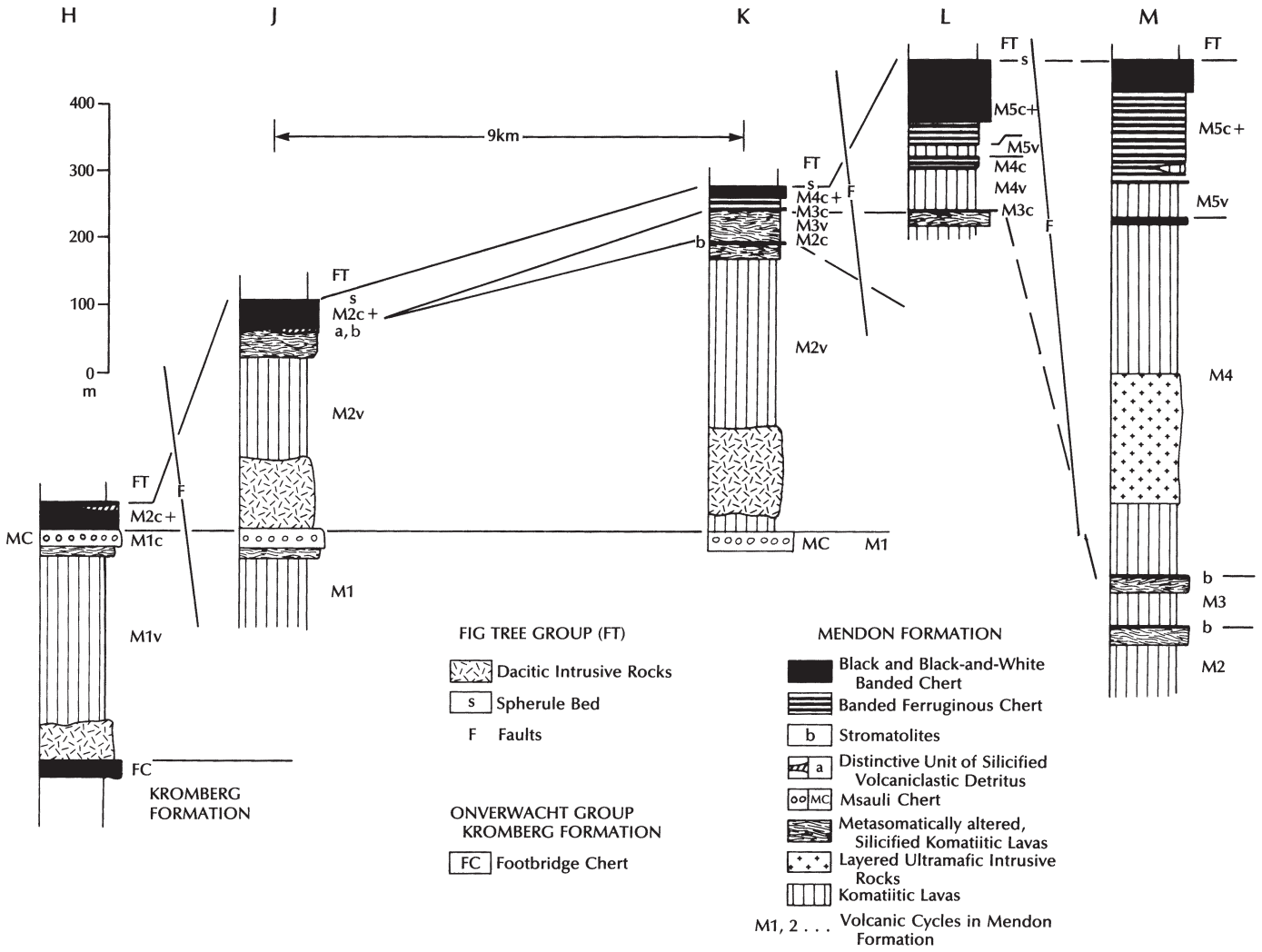


Figure 10. Stratigraphy and correlation of the Mendon Formation. Sections located in Figure 5.

distinctive, large, polygonal accretionary lapilli (Fig. 11A) at the top of the second volcanic cycle; (3) horizons of stromatolite-like structures (Byerly et al., 1986) at the tops of second and third volcanic cycles; and (4) a layer of spherules representing quenched liquid silicate droplets (Lowe and Byerly, 1986a) succeeded by barite and jasper units at the base of the overlying Fig Tree Group. Not all marker beds occur in all sections, but enough are usually present to permit correlation. In addition, M3v is everywhere a thin unit, generally less than 60 m thick. Individual volcanic members of the Mendon Formation can also be distinguished on the basis of trace element geochemistry, particularly their Al_2O_3/TiO_2 ratios (Byerly, this volume, Chapter 8). Some of the inferred south-to-north facies changes and correlations can also be verified locally by tracing beds within individual structural blocks.

M1: Lowest (first) cycle. The lowest volcanic-sedimentary cycle of the Mendon Formation is exposed in its entirety only along the northern edge of the Southern Domain (section H, Fig. 10), where it overlies rocks of the Kromberg Formation with apparent conformity. Along the central and eastern parts of the west limb of the Onverwacht anticline, this cycle consists of from 200 to 250 m of massive, serpentinized fine-grained peridotite locally showing thin spinifex-bearing zones at the top and base. The Al_2O_3/TiO_2 ratios are near 80, and other incompatible and immobile element ratios are distinctly nonchondritic and different from those of most other Barberton komatiites (Byerly, this volume, Chapter 8). The volcanic rocks are overlain by the 20- to 35-m-thick Msauli Chert. The ultramafic rocks crop out poorly except at the top of the unit where there is a regional, 10- to-50-m-thick zone of green, chrome-mica–rich, silicified komatiite showing abundant, bedding-parallel, fibrous, silica and carbonate crack-seal veins (Lowe and Byerly, 1986b). The local presence of spinifex textures in this unit and of detrital chrome-rich spinels and komatiite-grain sandstone beds in the basal part of the overlying Msauli Chert indicates that these komatiites were emplaced as lavas and subject to subaerial exposure and erosion prior to deposition of the Msauli Chert (Lowe and Byerly, 1986b).

The Msauli Chert (M1c) consists largely of silicified komati-

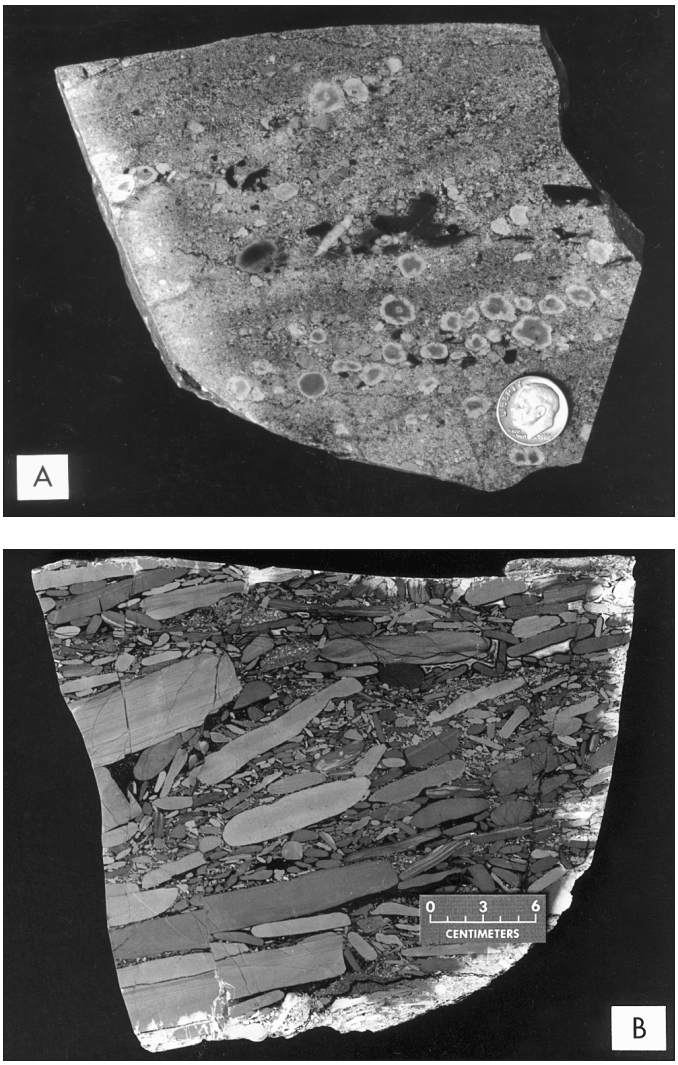


Figure 11. Marker units used in correlating member M2c of the Mendon Formation among fault-bounded blocks in the central BGB. A, Large, polygonal accretionary lapilli, here reworked and mixed with current-deposited coarse ash. The dark centers and light rims on the lapilli reflect post-depositional effects. B, Intraformational conglomerate composed of plates of silicified komatiitic volcaniclastic sediment ranging from fine dust to cross-laminated ash (top center). In addition, over wide areas, M2c includes distinctive structures interpreted to be either stromatolites (Byerly et al., 1986) or hot spring deposits (Lowe, 1994a).

itic pyroclastic debris interbedded with black, carbonaceous chert. Particularly characteristic are distinctive, regionally traceable beds of airfall and current-worked accretionary lapilli (Lowe and Knauth, 1977; Stanistreet et al., 1981; Heinrichs, 1984; Lowe, this volume, Chapter 9). The Msauli chert is overlain on the west limb by black, black-and-white banded, and banded ferruginous chert 9–40 m thick succeeded directly by clastic sediments of the Fig Tree Group (section H, Figs. 5 and 10).

The lowest cycle of the Mendon Formation is covered by Moodies strata on the northern part of the east limb of the Onverwacht anticline (Fig. 4), but is present east of the Kromberg fault immediately north of the Msauli River. It here consists of a thickened, structurally complex mass of serpentinized peridotitic komatiite, termed the Dunbar ultramafic body by Anhaeusser et al. (1981), overlain by the Msauli Chert. Along the Komati River, M1 includes about 300 m of komatiite overlain by the Msauli Chert, here 35 m thick.

M2: Second cycle. In the Southern Domain on the west limb of the Onverwacht anticline, black and banded chert overlying the Msauli Chert includes near the top a discontinuous unit, as much as 3 m thick, of pale greenish, silicified airfall and current-worked, komatiitic pyroclastic debris (Nocita, 1986; Fig. 10). At the base of this unit is a zone of ash containing distinctive, large, polygonal, concentrically zoned accretionary lapilli, some reaching 1 cm in diameter (Fig. 11A), and its top is widely marked by a unit of conglomerate composed of ellipsoidal to platy clasts of silicified, fine-grained komatiitic ash (Fig. 11B).

In the southernmost WCD, the Msauli Chert is overlain by about 2 m of black chert succeeded by 100–150 m of komatiitic flow rock, here assigned to M2v (sections J and K, Fig. 10). In western sections, M2v is composed largely of a single, thick unit of fine-grained peridotite. Upper portions of this section include thin units of spinifex-textured komatiite. Elsewhere, M2v includes a distinctive base of bladed olivine spinifex flow units, each about 5m thick, and overlying pyroxene spinifex flows with highly variable textures and structures, including pillows and pillow breccias. The Al_2O_3/TiO_2 ratio in M2v komatiites is generally about 10 (Byerly, this volume, Chapter 8).

At its top, M2v shows a 5- to 30-m-thick zone of greenish silicified and carbonated komatiite that contains silica pseudomorphs of pyroxene spinifex and cumulus textures (Lowe et al., 1985; Lowe and Byerly, 1986b; Duchac, 1986; Duchac and Hanor, 1987; Hanor and Duchac, 1990). The upper surface of this zone of silicification locally shows as much as 6 m of erosional relief (Figs. 5 and 10, section J). In one section, small pseudocolumnar stromatolite-like structures grew on the top of an erosional komatiite pinnacle and clasts derived by erosion of the structures are abundant in surrounding sediments (Byerly et al., 1986). The basal 2–5 m of strata of M2c locally consist of dust- and ash-sized komatiitic pyroclastic debris interbedded with black and banded chert. The ash contains large, polygonal, concentrically zoned accretionary lapilli. The distinctiveness of these lapilli leads us to correlate this pyroclastic horizon with that near the top of the black chert section above the Msauli Chert along the northern edge of the Southern Domain, immediately south of the Granville Grove fault. In section J (Fig. 10), this volcaniclastic zone is succeeded by 45 m of black chert capped spherule layer S2 marking the base of the Fig Tree Group.

In section K on farm Mendon 379 JU (Fig. 10), silicified komatiite at the top of M2v is overlain by 1–2 m of silicified stromatolite-like structures, banded chert, and fine volcaniclastic debris of M2c. This unit is succeeded by silicified komatiite of M3v. M2c contains thin layers of stromatolite-like structures, generally near its base or actually encrusting the surface of the underlying komatiitic volcanic rocks, in most sections. Lowe

(1992, 1994a) has recently suggested that these stromatolite-like structures may have formed through inorganic silica precipitation, perhaps around Archean hot springs.

M3: Third cycle. The third volcanic-sedimentary cycle in the Mendon Formation (M3) is exposed in section K and to the west, but not in more southerly sections. It consists of 46 m of silicified, spinifex-bearing komatiite in thin, highly altered flow units. The Al_2O_3/TiO_2 ratio of M2v is about 10. In section E, M2v is overlain by 20 m of banded ferruginous chert that is succeeded by as much as 14 m of black and black-and-white banded chert capped by spherule bed S2 at the base of the Fig Tree Group.

Higher cycles. Still higher cycles of the Mendon Formation occur in sections L and M (Fig. 10). The precise correlation between these sections is uncertain because of outcrop discontinuity, internal faulting, and a lack of unambiguous marker beds in section M. However, both sections consist of a basal sequence of altered komatiitic lavas overlain by banded ferruginous chert that is succeeded by black and black-and-white banded chert. This lithologic sequence is essentially identical to that of M3c in section E. In both sections, the banded ferruginous chert includes at least one interbedded unit of komatiite (Fig. 10), and komatiitic units above M3 lack zones of stratiform silica and carbonate veins at their tops. Because section L includes both banded ferruginous chert containing interbedded thin komatiitic units and spherule bed S2 succeeded by fine volcaniclastic strata of the Fig Tree Group, it appears to be transitional between sections K and M. Our interpretation is to correlate these sections as shown in Figure 10 and to suggest that the lower thin stromatolitic unit at the base of M is correlative with that at the top of M2c in sections K and L.

Correlation within the Mendon Formation thus suggests that mafic and ultramafic rocks in the central part of the greenstone belt are younger than any volcanic rocks in the Onverwacht Group in more southern areas. Recent dating likewise confirms the young age of Mendon volcanic rocks. A felsic tuff in M2c or M3c of the Mendon Formation has yielded an age of 3,298 ± 6 Ma (Byerly et al., 1996). The black and banded cherts capping the Mendon Formation probably represent a considerable interval of time, although of somewhat different duration in different areas, and probably constitute a greatly condensed stratigraphic section.

Northern facies

Weltevreden Formation. The oldest exposed rocks in the northern facies of the Swaziland Supergroup, north of the Inyoka fault, consist of a thick sequence of serpentinized komatiitic volcanic rocks, altered peridotitic layered intrusive rocks, serpentinized komatiitic tuff, and black and banded chert. These rocks occur in both thin structural slices and septa marking faults and anticlinal folds within the greenstone belt and a broad zone of ultramafic rocks lying along the northern margin of the belt (Figs. 1 and 4). They have previously been included within both the Onverwacht Group (Viljoen, M. J., and Viljoen, 1969a; Anhaeusser et al., 1981) and the Jamestown Series or Complex (Hall, 1918; Visser, 1956). The latter is an association of altered komatiitic and basaltic volcanic and intrusive rocks, tuffs, cherts, and sediments having a general type area in the Jamestown Schist Belt north and northeast of Barberton (Fig. 1). Although similar in lithology to both units, rocks included in the Weltevreden Formation cannot be traced continuously and unambiguously into the type area of either group. Available age data and across-belt correlation suggest that these rocks are younger than any part of the Onverwacht Group as defined by Viljoen, M. J., and Viljoen (1969 a, b) and Viljoen, R. P., and Viljoen (1969). We have reassigned these rocks to a new formation, the Weltevreden Formation, which is included in the Onverwacht Group.

The type area of the Weltevreden Formation (Fig. 12) is located on farms Weltevreden 712 JT, Weltevreden 697 JT, and Sassenheim 695 JT (Fig. 5). Its thickness is unknown because the base is nowhere exposed but at least several hundred and possibly several thousand meters of rock are present. The unit includes four principal primary lithologies: (1) komatiitic volcanic rocks, (2) layered ultramafic intrusive rocks, (3) komatiitic tuffs, and (4) black and banded chert.

Komatiitic and basaltic volcanic rocks. The Weltevreden Formation consists largely of heavily altered peridotitic and basaltic komatiite and lesser amounts of tholeiitic basalt (Wuth, 1980). Shearing and pervasive metasomatic alteration have obliterated most of the primary lithologies and structures, producing talc-carbonate, chlorite, and chlorite-amphibole schists (Wuth, 1980), but spinifex A-zone and cumulus B-zone komatiitic textures are preserved locally. Many ultramafic rocks have been serpentinized and, in some areas, replaced by brown-weathering iron-rich dolomite or ankerite. Some carbonated volcanic rocks in the frontal belt north of the Moodies fault have been regarded previously as carbonate sediments in the Moodies Group (e.g. Visser, 1956).

Intrusive rocks. The Weltevreden Formation includes a number of large, lenticular, layered ultramafic intrusive bodies. Along the northern margin of the belt, these include the Sawmill, Pioneer, and Emmenes intrusions (Wuth, 1980; Anhaeusser et al., 1981; Anhaeusser, 1985). Similar intrusions occur in the Jamestown Schist Belt, the Mendon Formation, and units H3 and H4 of the Hooggenoeg Formation (Viljoen, R. P., and Viljoen, 1969), but are absent in the Komati Formation. These intrusions are made up of alternating cyclic units of serpentinized dunite, peridotite, orthopyroxenite, clinopyroxenite, and gabbro (Wuth, 1980; Anhaeusser, 1985).

Komatiitic tuffs. Units of massive, very fine grained, tan to brownish-weathering, greenish gray talc showing well-developed layer-parallel and, locally, pencil cleavage occur throughout the Weltevreden Formation. These units have been interpreted as shear zones or possible tuffs (Wuth, 1980). In several areas, we have identified well-preserved cross-lamination and climbing-ripple cross-lamination in these units, indicating unambiguously that they represent altered komatiitic tuffs.

These tuffs evidently formed relatively weak horizons and served as the locus of intrusion of several of the large ultramafic intrusive complexes in the Weltevreden Formation. The Pioneer

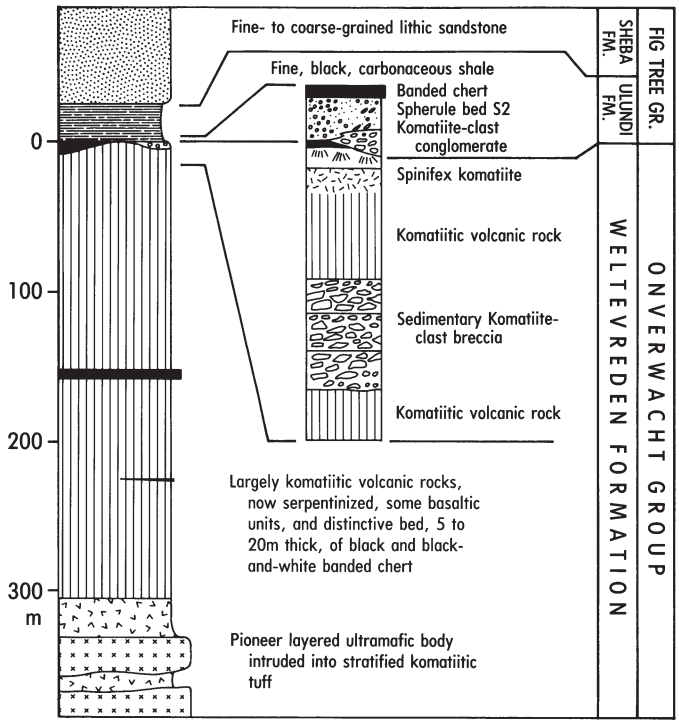


Figure 12. Stratigraphy of the type section of the Weltevreden Formation. Section is a composite of several sections north of the Moodies fault on farms Weltevreden 712 JT and 697 JT and Sassenheim 695 JT (Fig. 5).

layered intrusion immediately west of Barberton actually consists of several smaller sill-like differentiated ultramafic bodies overlain, underlain, and separated by altered komatiitic tuffs (Fig. 12).

Black and banded chert. Altered volcanic rocks at the top of the Weltevreden Formation are widely overlain by from less than 1 to 10 m of black chert. In part because of shearing at this contact, chert is commonly absent or present only as a series of isolated structural blocks. Overlying banded ferruginous chert is included in the Fig Tree Group.

A widespread unit of black and black-and-white banded chert, 5–20 m thick, occurs 100–200 m below the top of the formation in the Stolzburg syncline and throughout the ND west of the Moodies Hills (Fig. 12). Locally, this unit contains finely laminated layers of pale greenish chert that probably represent silicified komatiitic ash. In some localities in the western part of the ND this chert also includes an unusual layer of conglomerate made up of well-sorted, well-rounded clasts, 1–15 cm in diameter, composed of chert and silicified fine-grained volcanic or volcaniclastic rock. This chert unit has locally served as a locus of gold mineralization.

No sedimentary units were seen in the Weltevreden Formation showing evidence of deposition by turbidity currents, and there is an absence of banded iron formation, jasper, and other iron-rich sediments. The local presence of coarse komatiite-clast conglomerates in the upper part of the formation and of thick units of cross-laminated komatiitic tuff suggest shallow-water conditions of sedimentation. The black and banded cherts reflect sedimentation under quiet, subaqueous conditions. The environment of deposition during accumulation of the Weltevreden Formation was probably largely subaqueous but may have varied from shallow to moderately deep water.

The Weltevreden Formation bears a strong lithologic resemblance to the upper cycles of the Mendon Formation south of the Inyoka fault. Both consist largely of komatiitic volcanic rocks, include layered ultramafic intrusions, and are overlain directly by a spherule bed at the base of the Fig Tree Group. We, therefore, suggest that the Weltevreden Formation is correlative with the upper part of the Mendon Formation rather than with the lower komatiitic parts of the Onverwacht Group as suggested by previous investigators (Viljoen, M. J., and Viljoen, 1969a; Anhaeusser et al., 1981).

Onverwacht rocks in other areas

We have not systematically examined Onverwacht rocks outside of the present study area. However, germane to any understanding of greenstone belt evolution and Onverwacht stratigraphy are reported occurrences of quartzite, graywacke, shale, phyllite, and acid volcanic rocks near the base of the Onverwacht Group along the eastern margin of the belt in Swaziland (Hunter and Jones, 1969; Wilson, 1980). Quartzites in this sequence were dated by Kröner and Todt (1988) at about 3,457 ± 15 Ma and utilized by these authors to constrain the maximum age of Onverwacht volcanism.

We have examined these quartzites. They consist of medium- to coarse-grained black-and-white banded metaquartzite at least 100 m thick. Black carbonaceous bands, averaging 1–10 cm thick, alternate with white quartzite bands of comparable thickness. Breccias consisting of plates of white quartzite embedded within a matrix of black quartzite are common. Although fine layering is well preserved, cross-bedding or other evidence of current deposition is absent. This rock is closely associated with quartz-muscovite schists containing larger quartz grains and resembling altered quartz-phyric felsic volcanic rocks. The black-and-white banding, structuring, and lack of current features indicate to us that this unit represents thermally metamorphosed black-and-white banded chert. The close association with felsic volcanic rocks suggests that this unit may correlate with the Buck Reef Chert in the study area. Tiny, very sparse zircons dated by Kröner and Todt (1988) probably represent windblown material, in part derived from volcanic units approximately correlative with felsic volcanic units at the top of the Hooggenoeg Formation, H6. These rocks do not represent parts of an older, pre-Onverwacht or lower Onverwacht sedimentary sequence. Associated metamorphosed graywackes and shales, which we did not examine, probably belong to the Fig Tree Group.

Age

Pre-3.5-Ga ages. The age of the Onverwacht Group (Lowe, this volume, Chapter 12, Table 1) is becoming better constrained as new single-crystal zircon data become available (Kröner et al.,

1989, 1991, 1992, 1996; Armstrong et al., 1990; Kamo et al., 1990; Kamo and Davis, 1991, 1994; Byerly et al., 1993, 1996; de Ronde and de Wit, 1994). The oldest dated supracrustal rocks in the Barberton Belt are felsic metatuffs of the Theespruit Formation (Viljoen and Viljoen, 1969) in the Steynsdorp anticline (Fig. 1), dated at 3,544 ± 3 to 3,547 ± 3 Ma (Kröner et al., 1996). They are interbedded with and overlain by metabasalts and underlain by still older undated mafic to komatiitic metavolcanic rocks. This pre-3.50-Ga sequence is at least several kilometers thick and is in fault contact with but was probably intruded by the tonalitic Steynsdorp pluton dated 3,502 ± 2 to 3,511 ± 4 Ma (Kamo and Davis, 1994; Kröner et al., 1996). Felsic magmatism extended from at least 3,547 ± 3 to 3,502 ± 2 Ma. This sequence has been interpreted to have formed as a separate, older volcanic and plutonic block from that represented by the younger, Komati through Kromberg Formations (Lowe, 1994b; Kröner et al., 1996; Lowe, this volume, Chapter 12).

In the Onverwacht anticline, Armstrong et al. (1990) report ages of 3,538 ± 6 Ma on tonalitic gneiss fragments within areas mapped as Theespruit Formation by Viljoen, M. J., and Viljoen (1969a, b). These gneissic blocks occur along major faults (de Wit et al., 1983) and appear to be tectonically emplaced fragments from pre-3.5-Ga rocks, possibly part of the pre-3.5-Ga block exposed in the Steynsdorp anticline.

These TTG remnants indicate the presence of intrusive rocks and, thus, intruded, probably greenstone-type volcanic and sedimentary sequences in the Onverwacht anticline at least as old as 3,538 ± 6 Ma. The oldest xenocrysts, detrital zircons, and gneiss remnant ages are not far removed from Sm-Nd whole rock ages of 3.53–3.56 Ga on rocks of the Komati Formation (Hamilton et al., 1979, 1983; Jahn et al., 1982). We suggest that Onverwacht magmatism commenced before 3.5 Ga and possibly as early as 3.55 Ga. The oldest parts of the volcanic Onverwacht sequence have not been recognized in outcrop and have probably been largely destroyed or reworked during later magmatic and metamorphic events. Reported ~3.7-Ga zircon xenocrysts in small granodioritic bodies intrusive into the Komati Formation in the Steynsdorp anticline (Kröner et al., 1996) appear to be remnants of still older felsic volcanic or TTG units that have been destroyed or buried.

Post-3.5-Ga ages. Armstrong et al. (1990) report ages between 3,472 ± 5 Ma and 3,488 ± 5 Ma from thin cherty units in the lower part of the Onverwacht Group, including the Middle Marker. These represent the oldest reliable ages from the stratigraphically intact portions of the Swaziland Supergroup, although the detrital nature of the zircons makes these maximum age estimates for the stratigraphic units from which they were collected.

Attempts to date the lower parts of the stratigraphically intact Onverwacht Group by other techniques have yielded ambiguous results. Consistent ages of 3.40–3.46 Ga on rocks of the Komati Formation by Rb-Sr mineral (Jahn and Shih, 1974), Ar-Ar whole rock (López-Martínez et al., 1984), and common lead whole rock (Brevart et al., 1986) techniques almost certainly reflect metamorphic ages. There is an overlap between these ages and those of the felsic volcanic rocks of H6. Reliable and consistent single-crystal zircon ages between 3,456 ± 18 Ma and 3,438 ± 6 Ma, centering on about 3,445 Ma, have been obtained from felsic volcaniclastic rocks of H6. This episode of felsic volcanism is probably also reflected in the detrital zircons dated 3,457 ± 15 described from metacherts in Swaziland (Kröner and Todt, 1988). TTG plutons surrounding the southern part of the BGB have yielded similar single zircon ages, including ages of 3,448 ± 3 Ma on the Doornhook pluton (Kamo et al., 1990; Kamo and Davis, 1991), 3,448 ± 8 to 3,435 ± 7 Ma on the Theespruit pluton (Kröner et al., 1989, 1991; Kamo et al., 1990; Armstrong et al., 1990), and 3,445 ± 8 Ma on the Stolzburg pluton (Kröner et al., 1989, 1991). This age overlap, as well as petrologic similarities, indicate that the southern TTG suite and dacitic intrusive and extrusive units in H6 are comagmatic (Glikson and Jahn, 1985; de Wit et al, 1987b; Lowe et al., 1989a; Kröner et al., 1989, 1991; Armstrong et al., 1990). Published Rb-Sr, ^{40}Ar-^{39}Ar, and common lead ages on the Komati Formation probably reflect metamorphism associated with the circa 3,445 Ma magmatic event. Younger felsic volcanic and plutonic units in and surrounding the BGB have also yielded zircons, interpreted as xenocrysts, representing this 3,445-Ma magmatic event and sedimentary units have yielded detrital zircons between about 3,445 and 3,531 Ma (Kröner and Compston, 1988; Kröner et al., 1989, 1991; Armstrong et al., 1990).

The ages of the post–Hooggenoeg Formations of the Onverwacht Group have also been recently constrained by single zircon dating (Byerly et al., 1996). A thin tuff at the base of the Kromberg Formation has yielded an age of 3,416 ± 5 Ma (Kröner et al., 1991) and a tuffaceous band in the Footbridge Chert has been dated at 3,334 ± 3 Ma (Byerly et al., 1996). A felsic tuff associated with stromatolite-like structures in the Mendon Formation, probably in M2c or M3c, has provided an age of 3,298 ± 6 Ma (Byerly et al., 1996). Chauvel et al. (1987) have also report a Sm-Nd whole rock age of 3,317 ± 326 Ma on "Fig Tree" komatiites collected by Byerly from the upper part of the Mendon Formation. A Nd isochron age of 3,286 ± 29 Ma on komatiites of the Weltevreden Formation (Lahaye et al., 1995) indicates that this unit is perhaps the youngest major ultramafic volcanic sequence in the BGB and, at least in part, correlative with the youngest part of the Mendon Formation. The base of the Fig Tree Group appears to have a maximum local age of about 3,259 ± 4 Ma in the southern part of the BGB (Kröner et al., 1989, 1991; Armstrong et al., 1990; Byerly et al., 1996), although it may be significantly younger in the north.

FIG TREE GROUP

General stratigraphy

The Fig Tree Group was named by Van Eeden (1941) for outcrops along Fig Tree Creek in the Ulundi syncline (Fig. 1). The type section includes nearly 1,800 m of immature turbiditic sandstone, mudstone, and shale capped by 200 m of plagioclase-phyric lavas and fragmental volcanic rocks (Visser, 1956;

Anhaeusser, 1973; Condie et al., 1970). Thin cherty units make up a minor part of the section.

Reimer (1967) and Condie et al. (1970) divided Fig Tree rocks along the northeast side of the Stolzburg syncline and in the Ulundi syncline into three formations. From base upward, these include (1) the Sheba Formation, composed of turbiditic lithic sandstone and shale, having a type section in the Ulundi syncline; (2) the Belvue Road Formation, made up largely of shale, turbiditic siltstone and sandstone, chert, and, in the Stolzburg syncline, coarse volcaniclastic rocks near the top; and (3) the Schoongezicht Formation, composed of coarse felsic volcaniclastic sandstone, conglomerate, breccia, and interbedded mudstone and shale. The type sections of the Belvue Road and Schoongezicht Formations are on the northeast side of the Stolzburg syncline (Fig. 5). In addition, Reimer (1983) recognized the Ulundi Formation, a thin shale, chert, and iron-rich unit at the base of the Sheba Formation in northern areas.

These formations are broadly traceable throughout the Northern Domain. Most sections south of the Inyoka fault, however, show a very different association of lithologies. The stratigraphy of the southern facies has only recently been mapped and correlated on a regional basis (Heinrichs, 1980; Lowe and Nocita, this volume, Chapter 10; Lowe and Byerly, unpublished mapping). Problems in defining regionally useful stratigraphic subdivisions of southern facies rocks reflect both their structural and stratigraphic complexity.

Regionally, the Fig Tree and Moodies Groups include three major end-member clastic petrofacies: (1) greenstone-belt–derived clastic units dominated by quartz-poor, chert-grain sandstone and chert-clast conglomerate, (2) felsic autoclastic, pyroclastic, and current-worked volcaniclastic deposits, and (3) quartz-rich feldspathic to quartzose sandstone representing uplifted plutonic rocks. Petrofacies 1 and 2 are interstratified throughout southern facies Fig Tree sections, and all are interbedded near and above the Fig Tree–Moodies contact. The absence of an orderly petrologic succession compounds problems of defining and correlating lithostratigraphic units within the sedimentary portion of the Swaziland Supergroup.

Because of the lithologic contrasts between northern and southern facies of the Fig Tree Group, including contrasts in the petrology of felsic volcanic units (Byerly, personal communication, 1998), and the uncertain correlation of units that appear lithologically similar, we here assign separate formation names to all northern- and southern-facies Fig Tree rocks within the study area.

Southern facies

Heinrichs (1980) provides the most detailed discussion of southern-facies Fig Tree strata to date. Based on regional mapping and stratigraphic studies, he subdivided Fig Tree rocks in the southern part of the Barberton belt into four units of formation status. The lowest unit was an unnamed sequence of shale, sandstone, and chert with the Umsoli Oolite Member (= Msauli Chert) at its base. This is succeeded by an informally defined unit, the Ngwenya Formation, made up shale, sandstone, local conglomerate, fine-grained ferruginous strata, and a jasper and iron formation subdivision named the Manzimnyama Jaspilite Member (Heinrichs, 1980). The overlying Mapepe Formation is a sequence of shale, graywacke, conglomerate, and barite with an indicated thickness of 1,300 m. The uppermost Fig Tree unit is composed of coarse quartz- and feldspar-phyric dacitic breccias and finer grained tuff, which Heinrichs (1980) correlates with the Schoongezicht Formation of the northern facies.

The Msauli Chert is part of a thick succession of cyclic komatiitic volcanic rocks and cherts here assigned to the Mendon Formation of the Onverwacht Group. The Ngwenya Formation as defined by Heinrichs (1980) occurs only in the southern part of the study area and is represented mainly by fine-grained rocks below and including the Manzimnyama Jaspilite. Future studies in areas south and east may justify reinstating the Ngwenya Formation as a formal lithostratigraphic unit, but we cannot do so based on outcrops within the study area. We, therefore, assign the entire assemblage of interbedded terrigenous, fine-grained dacitic volcaniclastic, and iron-rich, cherty, and baritic units resting apparently conformably above the Onverwacht Group to the Mapepe Formation.

A large area in the West-Central Domain is underlain by a unit composed largely of massive dacitic tuff, coarse volcaniclastic sedimentary units, and chert-clast conglomerate. These rocks appear to represent the hanging-wall sequence to a thrust fault, named the 24-Hour Camp fault by Lowe et al. (this volume, Chapter 2). The foot-wall sequence includes rocks of the Mendon and Mapepe Formations. The hanging-wall rocks are here included in a separate stratigraphic unit, the Auber Villiers Formation.

Lamb (1984a, b), Paris (1985, 1986), and Lamb and Paris (1988) have proposed a modified nomenclature for post-Onverwacht rocks in southeastern parts of the belt. They subdivide the sedimentary section into two main lithostratigraphic units, to which they assign group status, although no formations are proposed. The Diepgezet Group, lower of the two, includes as much as 1,800 m of strata arranged in coarsening upward cycles. Each cycle is several hundred meters thick and composed of fine-grained rocks, including iron formation, ferruginous banded chert, siltstone, shale, and chert-grit turbidites, passing upward into coarse, massive chert-clast conglomerate. This unit is lithologically identical to and presumably correlative with the Ngwenya-Mapepe sequence of Heinrichs (1980) and the Mapepe Formation of this study. The overlying Malolotsha Group, as much as 3,200 m thick, includes a basal unit 100–1,800 m thick of coarse, predominantly chert-clast conglomerate and interbedded coarse-grained sandstone. The upper part consists largely of quartzites, immature quartzose sandstone, and conglomeratic quartzose sandstone. Local units of transitional character between the two groups are left unassigned. Rocks equivalent to the Schoongezicht and Auber Villiers Formations are apparently absent, and in most, but apparently not all, sections, the Malolotsha Group overlies the Diepgezet Group with angular unconformity. The upper, quartzose part of the Malolotsha Group can probably be correlated with the Moodies Group. The lower Malolotsha conglomerates cannot

yet be confidently correlated with rocks in the study area, although they most closely resemble conglomerates in the upper part of the Mapepe Formation.

Mapepe Formation. The stratigraphy of the Mapepe Formation within the study area is shown in Figures 13 and 14 and is discussed in detail by Lowe and Nocita (this volume, Chapter 10) and Nocita and Lowe (1990). The formation is named for and has its type section in Mapepe Valley, northeast of the study area (Heinrichs, 1980). A local and more accessible reference section (Fig. 5, section N; Fig. 13), 300 m thick, is located on farm Loenen 381 JU, at the eastern edge of the study area, from 25°54′43″ S., 31°03′42″ E. (base) to 25°54′30″ S., 31°03′30″ E. (top).

The lower contact of the Mapepe Formation is widely exposed because of structural repetition. It is apparently conformable and transitional and is drawn at the top of the continuous sequence of black and black-and-white banded cherts capping the Mendon Formation. Over much of the area, the lower 2 to 100 m of the Mapepe Formation includes an association of distinctive lithologic units that suggest correlation among sections in the Southern Domain and southern part of the WCD on the west limb of the Onverwacht anticline (Fig. 15, sections A, B, and C). From base upward, the complete section includes (1) a 20-cm to 2-m-thick layer of silicified coarse quartz-phyric dacitic ash; (2) spherule bed S2 (Lowe and Byerly, 1986a; Lowe et al., 1989b); (3) thin layers of sandy and bladed barite interbedded with fine-grained dacitic ash and mudstone of the Fig Tree Group; (4) the Manzimnyama Jaspilite Member and its equivalents; and, locally, (5) a bed of banded ferruginous chert and chert-clast breccia. The Manzimnyama Jaspilite is poorly developed in northern parts of the WCD and in the ECD in the study area. In these areas, such as section D, Figure 15, the lower few meters of the Mapepe Formation includes quartz-phyric tuff, S2, and baritic units, and a few thin jasper beds.

No unequivocal marker units have been identified in the middle and upper parts of the formation. Spherule beds S3 and S4 (Lowe et al., 1989b), and barite and jasper zones are present in the middle of the Mapepe Formation in the southeastern part of the WCD (Fig. 14) and in the Barite syncline in the ECD but have not been identified elsewhere. All terrigenous units are lenticular.

The stratigraphic top of the Mapepe Formation is nowhere exposed. Uppermost strata lie in the axial zones of synclines, are truncated by faults, or are overlain unconformably by younger formations.

The Fig Tree Group has long been regarded as representing the orogenic stage of greenstone belt evolution. This inference is

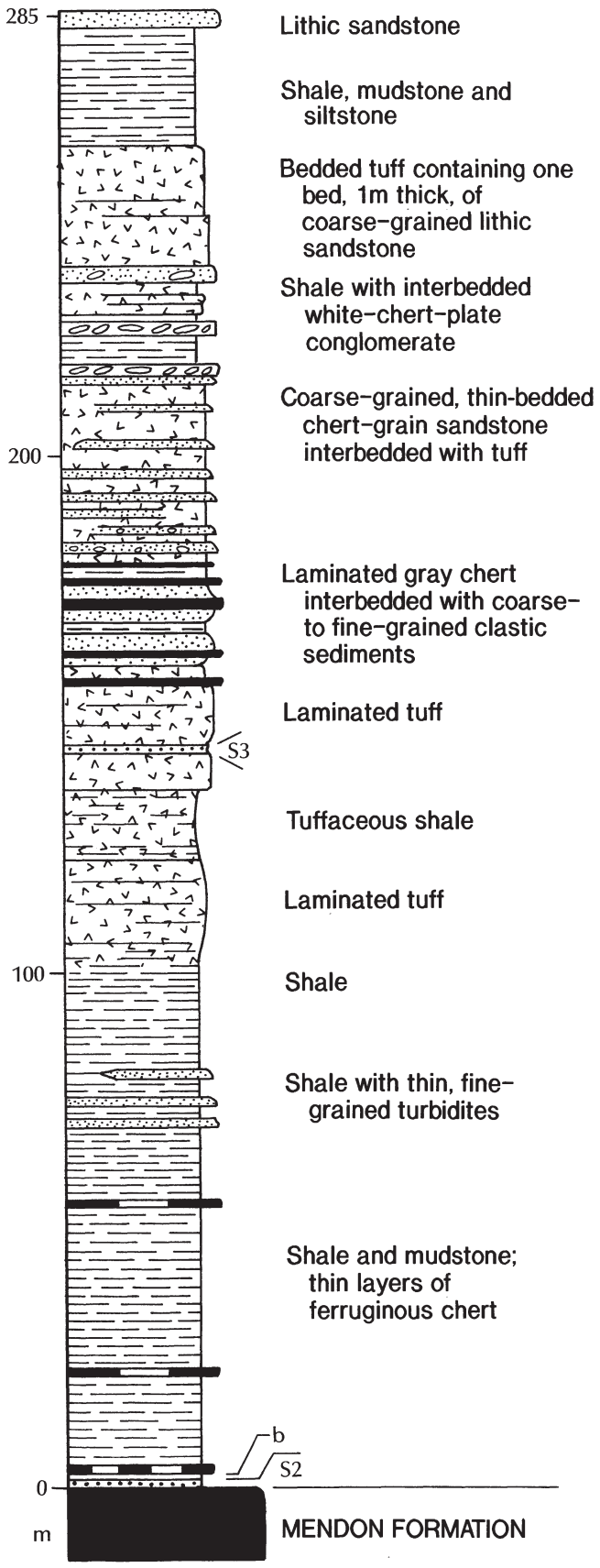


Figure 13 (right column). Stratigraphy of the reference section of the Mapepe Formation in the study area (section N, Fig. 5). A thin jasper unit, possibly equivalent to the Manzimnyama Jaspilite Member, is present immediately above the barite bed (b) near the base of the formation. S2 is the lowest of the three known spherule beds in the Fig Tree Group, S3 the middle, and S4 (not shown) the highest.

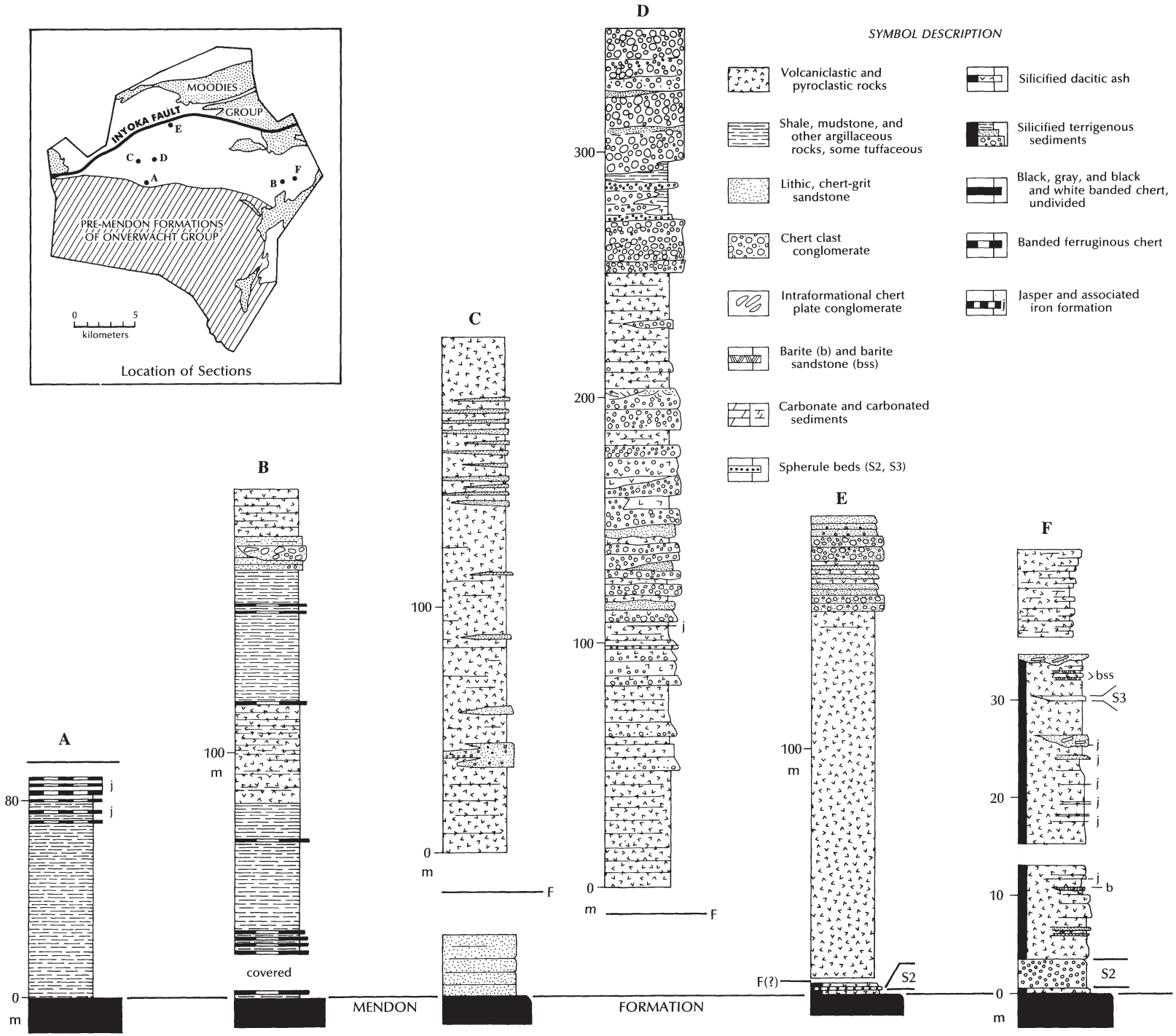


Figure 14. Sections of the Mapepe Formation within the study area. Jasper unit at the top of section A and base of B is the Manzimnyama Jaspilite Member of Heinrichs (1980).

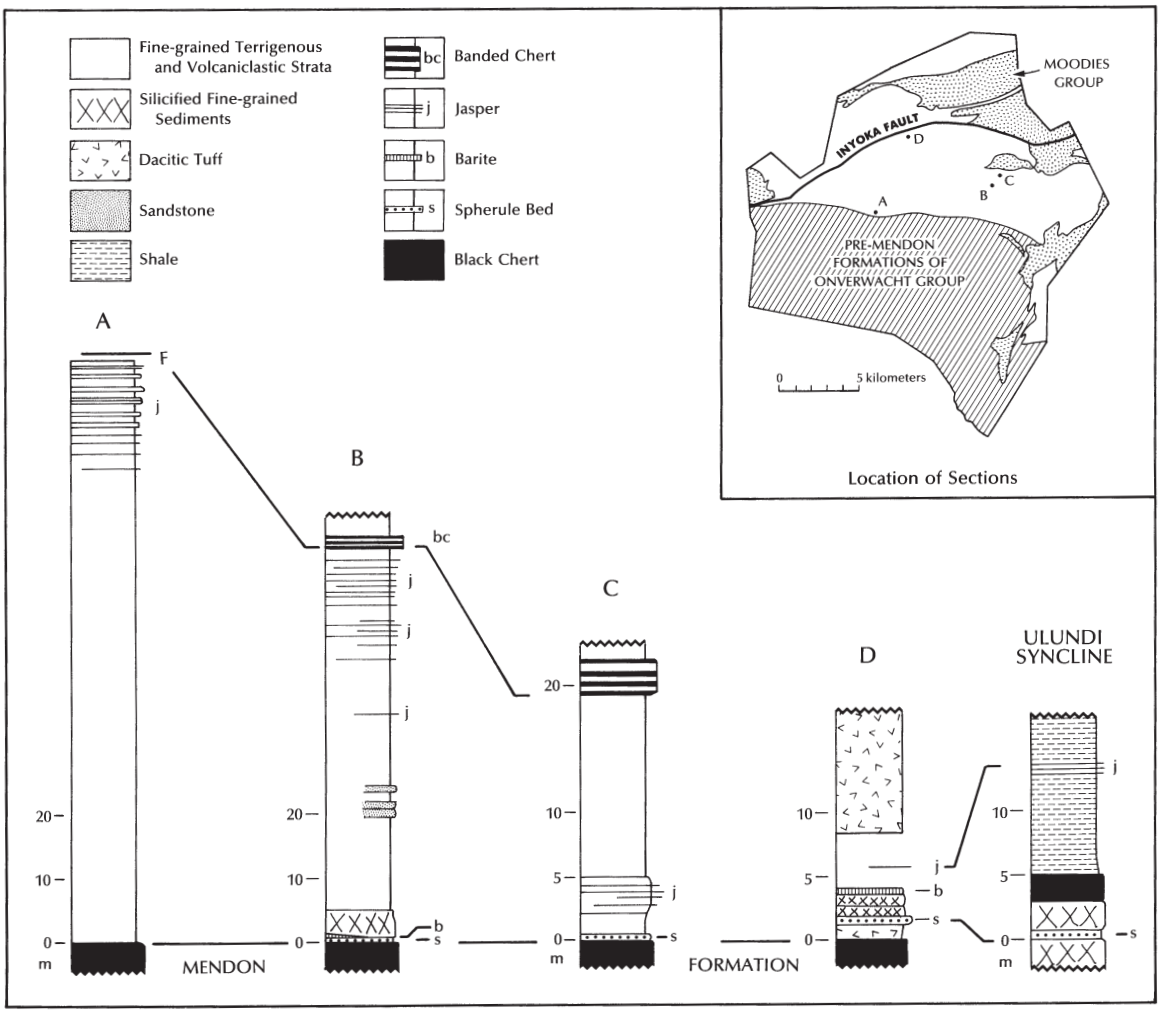


Figure 15. Correlation of marker units at the base of the Mapepe Formation of the Fig Tree Group within the study area. The column from the Ulundi syncline is from the southernmost end of that structure (Fig. 1).

supported by the abundance of terrigenous sediments in the Mapepe Formation, principally lenticular units of chert-grain sandstone and chert-pebble conglomerate. The bulk of this debris was derived by erosion of silicified units in the underlying Onverwacht Group (Nocita, 1989; Lowe and Nocita, this volume, Chapter 10). Quartz makes up less than 10% of most Mapepe sandstones and is mainly if not exclusively of volcanic origin. Detrital microcline and clasts of granitoid or metamorphic rocks were not identified during the present study.

Many thick units in the Mapepe Formation are composed of felsic tuff (Lowe and Nocita, this volume, Chapter 10). The rocks are tan, brown, or rust-red or "ferruginous" in outcrop, but in fresh exposures, most are light to medium gray. These units include sections of massive to well-layered tuff as much as 200 m thick, current-worked tuff, and mixed chert-grain and tuffaceous turbidites (Lowe and Nocita, this volume, Chapter 10). The finest, quiet-water deposits consist of rhythmically alternating bands of light gray, commonly iron-stained ash and white, translucent, or iron-stained chert from less than 1 mm to 10 cm thick.

Chert forms a minor component of most sections of the Mapepe Formation (Lowe, this volume, Chapter 3). The lower 5–20 m of clastic strata commonly include beds of gray or black chert representing silicified detrital sediment. A regional zone of jasper and iron-rich rocks from less than 1 to over 100 m thick, the Manzimnyama Jaspilite Member, is present in the lower part of the formation (Fig. 14). Sporadically developed cherts above the Manzimnyama Jaspilite are mostly silicified sand- and silt-sized terrigenous sediments, generally represented by black chert, or fine-grained tuffaceous beds, represented by medium to pale gray chert. In the eastern part of the study area, the west limb of the Barite syncline includes a condensed section of Mapepe strata, most of which is silicified (Fig. 14, section F). In both the Barite syncline and adjacent structural belts in the ECD, including the reference section (Fig. 13), shallow-water, orthochemical bank deposits in the upper part of the formation consist largely of silici-

fied ash and silicified carbonate, and include thin beds of jasper and translucent gray chert, possibly representing primary siliceous deposits. With the exception of iron-rich strata, silicification of Mapepe units is developed mainly in shallow-water sections.

At least two widespread barite horizons are present in the Mapepe Formation. One occurs immediately above spherule bed S2 at the base of the formation and another occurs 50–250 m above the base of the formation in eastern areas (Figs. 13 and 14). The latter is associated with the formation of local shallow-water banks during Mapepe time (Heinrichs and Reimer, 1977; Lowe and Nocita, this volume, Chapter 10). Other thin barite zones are developed locally, usually in association with fan deltas. These occurrences suggest that barite was a common sedimentary facies during Fig Tree deposition.

In the SD, ECD, and southeastern WCD, the Mapepe Formation was deposited in a variety of alluvial, fan-delta, and shallow-subaqueous depositional environments (Nocita and Lowe, 1990; Lowe and Nocita, this volume, Chapter 10). In the northwestern WCD, however, immediately south of the Inyoka fault, the formation is dominated by deep-water turbiditic units, including 100–200 m of fine tuffaceous strata overlain by several hundred meters of turbiditic chert-clast conglomerate, chert-grit sandstone, and mudstone. Facies relationships within the WCD suggest that the Mapepe basin deepened toward the north and west but that there was a major source of conglomeratic debris located west of the present western limits of the WCD. The Mapepe Formation resembles both the Belvue Road and Sheba Formations of Reimer (1967) and Condie et al. (1970). However, it includes a much higher proportion of tuffaceous material than either northern unit, is dominated by shallow-water and fan-delta deposits and lacks turbiditic layers in most southern sections, and contains thick layers of coarse pebble to cobble conglomerate. Turbiditic conglomerate and sandstone units in the Mapepe Formation along the northwestern edge of the WCD south of the Inyoka fault (Fig. 14, section E) may be correlative with northern-facies Fig Tree units, but petrologic contrasts, especially the abundance of tuff and absence of microcline in the Mapepe Formation and the paucity of tuff and presence of microcline in the Sheba Formation, suggest that they were derived from different source rocks and deposited in separate basins.

Available age data suggest that Mapepe strata in southern areas may span the entire interval from about 3,252 to 3,225 Ma. However, there are a number of marked lithologic breaks in many Mapepe sections, including a break between laminated dacitic tuff and the chert-clastic sequence at about 160 m and a break between the top of the fan delta-orthochemical bank sequence and overlying fine-grained tuffs at 245 m in the supplementary section (Fig. 13), that could mark unconformities.

Auber Villiers Formation. The hanging-wall sequence above the 24-Hour Camp fault includes 1,000–1,300 m of dacitic volcaniclastic and terrigenous sedimentary rocks that crop out across the WCD in two structural belts bounded by the Granville Grove and Auber Villiers, and Auber Villiers and Schultzenhorst faults (Fig. 4; see also detailed map of WCD, Fig. 10 in Lowe et al., this volume, Chapter 2). This unit is here named the Auber Villiers Formation for outcrops on farm Auber Villiers 719JT. The type section (Fig. 5, section O; Fig. 16) is exposed along forest roads on farm Schultzenhorst 718JT between 25°52′33″S., 30°58′15″E. (top) and 25°53′22″S., 30°58′26″E. (base). Neither the depositional top nor base of the formation is exposed in the type section. A well-exposed section also occurs on the south side of the Powerline Road syncline (section P, Fig. 5) between 25°53′50″S., 31°00′00″E. (base) and 25°3′23″S., 31°00′12″E. (top). The latter section is cut by the Auber Villiers fault, which repeats much of the formation. Grading in turbiditic units and cross-bedding indicate that Auber Villiers strata young to the north in both structural blocks.

In most outcrops, the Auber Villiers Formation consists of light tan to light gray weathering, massive, plagioclase-phyric dacitic rock. A pronounced, south-dipping fracture cleavage is present in many sections and widely obscures subtle stratification, which is also generally vertical to steeply south dipping. In the type section, the unit can be divided into three divisions (Fig. 16). The basal 350 m is composed of massive plagioclase-phyric dacitic rock. Stratification is rare, although the presence of breccias and conglomerates, some containing sparse clasts of altered komatiite; crude horizontal layering; and local cross-stratification suggest that much of this sequence represents volcaniclastic material. The middle 500 m consists of interbedded dacitic tuff, water-worked tuff containing pebbles of black chert, shale, and, near the top, coarse chert-pebble and cobble conglomerate. Turbiditic volcaniclastic layers interbedded with shale are present toward the middle of this sequence. A prominent quartz-rich ash-flow tuff overlies the uppermost coarse chert-clast conglomerate (Fig. 16). The upper part of the formation consists largely of massive tuff and current-worked, low-quartz, plagioclase-rich tuff and tuffaceous sandstone. Extensive faulting along the northern edge of the Auber Villers outcrop in the type section (Fig. 4) may repeat or cut out portions of the formation.

On the south side of the Powerline Road syncline (Fig. 5, section P), the formation includes about 500 m of strata. The lower two-thirds is composed of coarse, immature, dacite- and chert-clast conglomerate, dacitic breccia, and volcaniclastic sandstone. The uppermost 150–200 m consists largely of current-deposited volcaniclastic sandstone and, near the top, siltstone and tuffaceous shale. The uppermost siltstone is overlain by chert- and dacite-clast conglomerate that is taken as the base of the Moodies Group. Strata in both units appear parallel but the wide development of conglomerates at the base of the Moodies Group and evidence for at least local tectonism during early Moodies sedimentation (Lowe et al., this volume, Chapter 2) suggest that the contact is an unconformity.

Although we initially regarded this dacitic sequence as post-Mapepe in age and probably correlative with the Schoongezicht Formation of Reimer (1967) and Condie et al. (1970) north of the Inyoka fault (Heinrichs, 1969), available age data suggest that it may include rocks between 3,256 ± 4 Ma (Kröner et al., 1991) and 3,253 ± 3 Ma (Byerly et al., 1996). Also, dacitic rocks in the

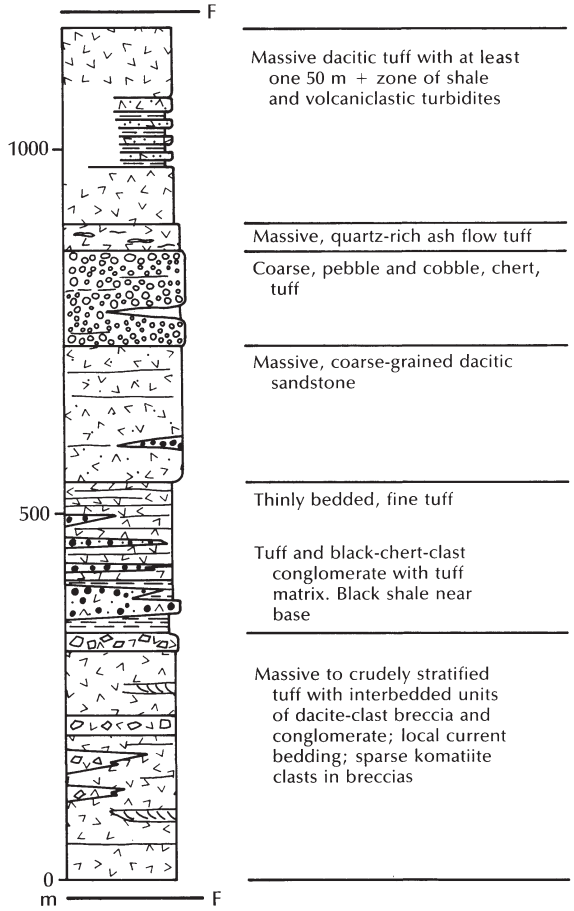


Figure 16. Stratigraphy of the type section of the Auber Villiers Formation (Section O, Fig. 5).

Auber Villiers Formation are quartz phyric whereas type Schoongezicht dacites lack quartz, and Byerly (unpublished) has noted significant geochemical differences between type Schoongezicht and Auber Villiers felsic rocks that indicate that they belong to different magmatic suites. Because of their structural isolation across the Inyoka fault, possible age difference, and petrologic distinctiveness, Fig Tree–age coarse-grained dacitic volcanic and volcaniclastic units south and north of the Inyoka fault are here included in separate units: the Auber Villiers and Schoongezicht Formations, respectively.

Northern facies

Within the study area, rocks of the northern facies crop out north of the Inyoka fault (Fig. 4), where they are repeated by tight isoclinal folds and faults. Northern-facies Fig Tree rocks include four main lithologic units (Figs. 2 and 3): (1) the Ulundi Formation, lowest subdivision of the Fig Tree Group, a thin unit of carbonaceous shale, thinly bedded chert, and iron-rich sediments overlying black cherts at the top of the Weltevreden Formation and underlying sandstones of the Sheba Formation; (2) the Sheba Formation, a thick sequence composed largely of medium- to fine-grained turbiditic, compositionally and texturally immature sandstone; (3) the Belvue Road Formation, consisting largely of fine-grained turbiditic siltstone and shale; and (4) the Schoongezicht Formation, composed mainly of plagioclase-rich volcaniclastic conglomerate, sandstone, and gray mudstone (Condie et al., 1970).

Ulundi Formation. Reimer (1983) assigned black carbonaceous shale, banded cherty units, and jasper and other iron-rich sediments at the base of the Sheba Formation to a new unit, the Ulundi Formation. This unit is identifiable in the Ulundi syncline, where the type section is located, in the Moodies Hills, and around the Stolzburg syncline. In the Stolzburg syncline, the Ulundi Formation consists of 25–30 m of fine-grained, brown-weathering, black, carbonaceous, noncherty shale with a spherule bed, probably S2, composed of current-worked spherules, chert chunks, and clasts of komatiite, at its base.

East of the Stolzburg syncline and west of the Moodies Hills, the Ulundi Formation is composed largely of thinly bedded banded ferruginous chert, but rarely jasper. It shows tight, small-scale folding and is greatly thickened in the hinge regions of some of the large synclines. Where least weathered, the ferruginous layers contain abundant partially oxidized rhombs of siderite. The primary sediments were probably fine oozes containing varying amounts of siderite, fine volcanic ash, clay, and organic matter. Ferruginous bands range from less than 1 to as much as 10 cm thick, but white bands seldom exceed 3 cm thick. The bands are generally continuous and even, but lenses of white chert are common. Many ferruginous bands are finely laminated but rhythmic microbanding was not seen. The white bands are generally structureless. Current structures and detrital sediments coarser than very fine sand or silt are absent, except within the spherule bed at the base. Thin layers of chert are present near the base and silty and sandy units, generally less than 10 cm thick, are developed throughout but are more common toward the top.

In the Ulundi syncline northeast of Barberton (Fig. 1), the unit varies from less than 1 to more than 50 m thick, although thinner sections may have been attenuated by shearing. It is made up of black, iron-rich shale, pyritic shale, and thin chert and jasper layers with some iron formation. The base is marked by a spherule bed, thought to be S2 of Lowe et al. (1989b), resting on black cherts of the Onverwacht Group and lacking evidence of current activity.

The Ulundi Formation was deposited under extremely quiet, deep-water conditions. Regionally, it becomes more iron rich and cherty and less shaly from the Stolzburg syncline in the southwest to the Ulundi syncline in the northeast. This facies transition and the accompanying changes in S2 suggest that the early Fig Tree basin deepened from southwest to northeast along the frontal part of the greenstone belt.

Sheba Formation. Throughout the northern facies, fine-grained rocks of the Ulundi Formation are succeeded directly by immature lithic sandstone of the Sheba Formation. The formation was named by Reimer (1967) and Condie et al. (1970) for exposures in the Sheba Hills in the Ulundi syncline. In the type sec-

tion, the Sheba Formation is about 2,000 m thick and composed mainly of coarse, immature turbiditic sandstone and thin interbedded units of siltstone and shale (Condie et al., 1970). In the study area, rocks assigned to the Sheba Formation consist largely of thick-bedded to massive, dark gray, fine- to coarse-grained immature turbiditic sandstone. Quartz generally makes up less than 20% of the rock. This sequence is complicated by faulting and folding but appears to be at least 500 m thick over most of the area and possibly 1,000 m thick in the Stolzburg syncline.

The top of the sandstone section is marked by a fining and thinning of the sandstone beds and the appearance of thicker interlayed mudstone units. A unit of banded ferruginous chert at the top of the Sheba Formation has locally been named the Haki Iron Formation (Philpot et al., 1988).

Belvue Road Formation. The Belvue Road Formation is developed in the central part of the study area north of the Inyoka fault and forms a broad belt around the east end of the Stolzburg syncline (Fig. 1). The type section is located at the northeastern end of the Stolzburg syncline (section Q, Fig. 5). The outcrop is poor because of heavy forestation. Where exposed along forest roads, the formation consists of deeply weathered, pale gray, brown, or pinkish shale, tuffaceous shale, and fine-grained sandstone and siltstone. The freshest exposures suggest that the bulk of the rock is dark gray to black carbonaceous shale. Interbedded units of fine- to coarse-grained immature turbiditic sandstone are generally less than 10 m thick. The basal 10–30 m of the formation widely consist of banded ferruginous chert, thinly bedded gray chert, and shale. The top of the formation was not seen in the central part of the area and structure is locally complex, but several hundred meters of strata are present. Condie et al. (1970) report a thickness of 600 m for the Belvue Road in its type section in the Stolzburg syncline, where it includes several 10s of meters of massive dacitic igneous rock near the top.

In the type section, the top of the Belvue Road of Condie et al. (1970) is a zone of serpentinized spinifex-bearing komatiite at least 100 m thick capped by 10–20 m of black and banded chert. This zone is structurally disturbed, and the chert occurs as a series of structurally isolated, rotated blocks. There is probably a fault between this komatiitic unit and the underlying Belvue Road Formation. Shearing along the contact is also suggested by the truncation of the Belvue Road and Sheba Formations as they are traced to the south and east until, at the eastern end of the syncline, Schoongezicht rocks are in contact with a thick sequence of serpentinites of the Weltevreden Formation and the intervening Sheba and Belvue Road Formations are absent (Fig. 4).

South of the western end of the Moodies Hills and north of the Inyoka fault, in a structural block isolated between the Saddleback and Haki faults (Fig. 4), the Fig Tree Group includes a thick sequence of graywackes, correlated with the Sheba Formation, overlain by a highly deformed sequence of banded ferruginous chert succeeded by interbedded shale and fine-grained sandstone (Fig. 17). This ferruginous chert has been termed the Haki Banded Iron Formation (BIF) by Philpot et al. (1988). We would correlate the Haki BIF in this area with ferruginous and black chert at the top of the Sheba Formation in the Stolzburg syncline. The overlying shaly strata resemble rocks of the Belvue Road Formation.

Schoongezicht Formation. Within the study area, the Schoongezicht Formation is exposed around the east and northeast end of the Stolzburg syncline and near the west end of the Moodies Hills (Fig. 4). The type section (Fig. 5, section R; Fig. 18, section E. Stolzburg syncline) is located on farm Schoongezicht 713 JT on the northeast side of the Stolzburg syncline from about 25°54′15″S., 30°52′40″E. (base) to 25°54′35″S, 30°52′00″E. (top). This section consists largely of thick-bedded, coarse-grained volcaniclastic turbidites and includes a thick capping sequence of interbedded coarse dacitic volcaniclastic sandstone and conglomerate. Sedimentation units are massive, commonly exceed 2 m thick, and are locally conglomeratic at the base. The conglomerate consists of relatively fresh plagioclase-phyric dacite clasts. Condie et al. (1970) report a thickness of about 450 m. We did not find the thick unit of crystal tuff noted by Condie et al. (1970) and Reimer (1975) near the top of the formation in this area.

The type section of the Schoongezicht Formation is now heavily forested and poorly exposed. A better exposed section (Fig. 5, section S; Fig. 18, section NE Stolzburg syncline) occurs about 2 km northwest of the type section along a firebreak from 25°53′30″S., 30°51′30″E. (base) to 25°53′50″S., 30°51′E. (top). This supplementary section consists of interbedded plagioclase-rich fine- to coarse-grained turbiditic sandstone and dark gray shale. The overall sandstone:shale ratio is probably between 1 and 2. Although some massive, thick-bedded turbidites are present, most are less than 1 m thick and many show flat and cross-lamination. Bouma sequences characterize some beds.

A second, previously unreported outcrop of Schoongezicht strata occurs beneath the Moodies Group at the west end of the Moodies Hills (Fig. 4). A well-exposed section (section T, Fig. 5; Fig. 18, section W. Moodies Hills) occurs along a forest firebreak from 25°50′47″S; 30°56′56″E. (base) to 25°50′42″S., 30°57′01″E. (top). The section includes about 150 m of strata including a basal zone composed largely of tan-weathering shale, a middle zone of interbedded shale and plagioclase-rich sandstone, a distinctive unit of laminated to banded chert, and a topmost zone of coarse, poorly sorted dacite-clast conglomerate, breccia, and sandstone. Stratification appears more-or-less parallel to that in the overlying Moodies chert-clast conglomerate and quartzose sandstones, although the disappearance to the northwest along strike of the upper dacitic conglomerate and breccias may reflect low-angle discordance.

The lower contact of the Schoongezicht Formation appears to be a regional surface of discordance that separates the underlying Fig Tree and Onverwacht rocks showing intense, small- as well as large-scale deformation from the overlying Schoongezicht and Moodies rocks characterized by large-scale structures. We suspect that this surface marks a fault rather than an unconformity (Lowe et al., this volume, Chapter 2), but the actual displacement, if any, is unknown. In the supplementary section at the northeast end of the Stolzburg syncline, the Schoongezicht rests on black

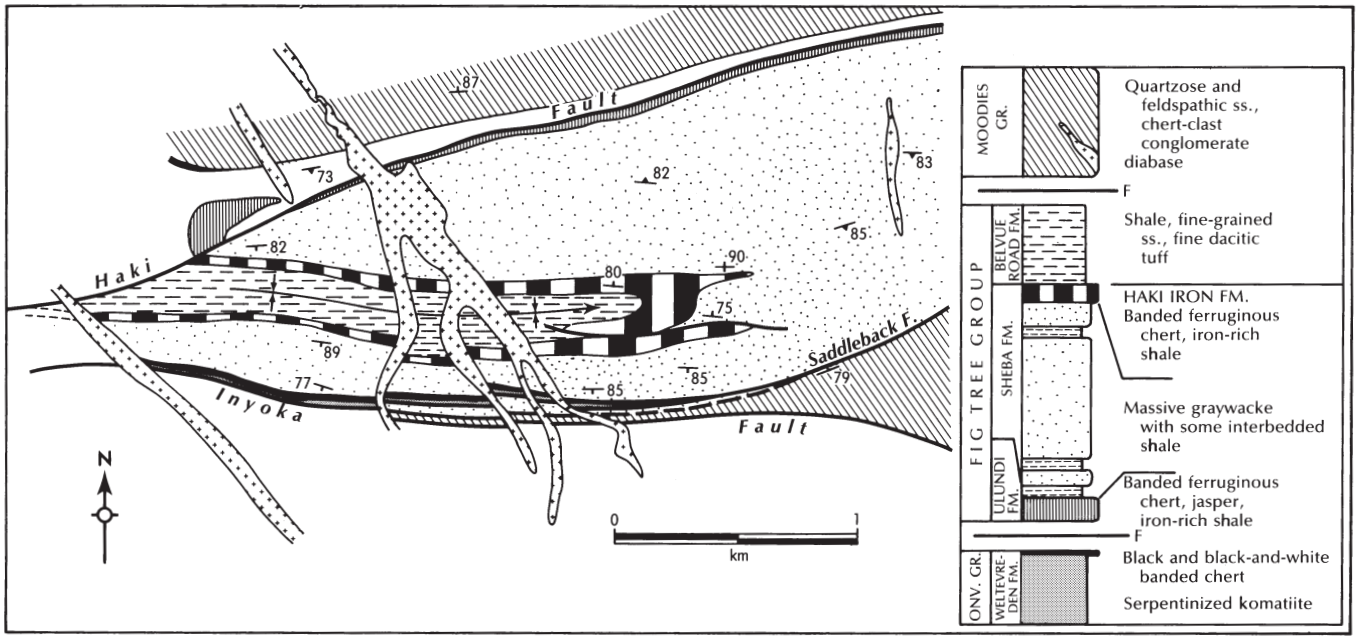


Figure 17. Geologic map and stratigraphy of rocks between the Haki and Inyoka faults south of the Moodies Hills Block.

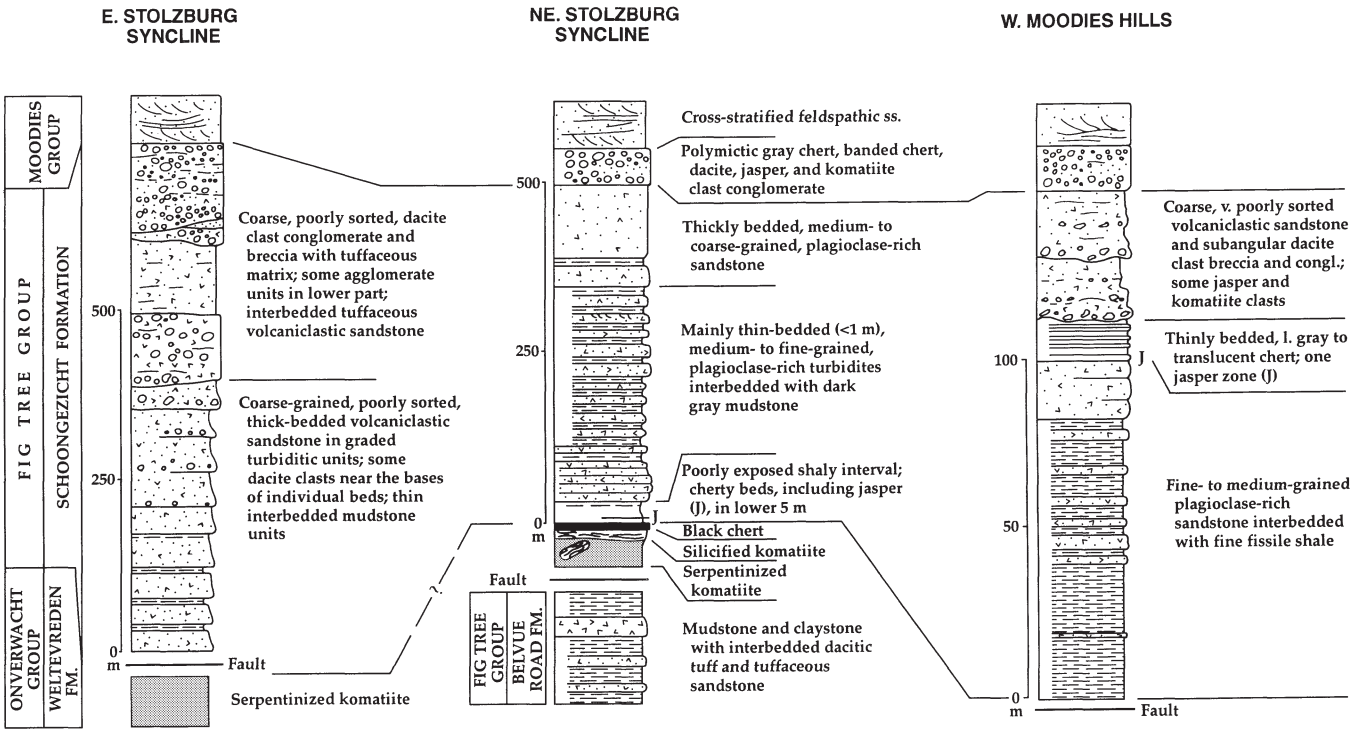


Figure 18. Stratigraphy of the Schoongezicht Formation in the study area. (Left) Type section (Section R, Fig. 5). (Middle) Supplementary section northwest of type section at east end of Stolzburg syncline (Section S, Fig. 5). (Right) Section at west end of Moodies Hills Block (Section T, Fig. 5).

chert overlying komatiite which Reimer (1975) and Condie et al. (1970) interpret as belonging to the upper part of the Belvue Road Formation. However, if this komatiite-chert sequence represents the Weltevreden Formation, or perhaps the Weltevreden and Ulundi Formations, then the Schoongezicht Formation may be in part or in total correlative with the Ulundi, Sheba, and Belvue Road Formations (Fig. 19).

At the west end of the Moodies Hills, steeply dipping, broadly folded Schoongezicht strata truncate strongly deformed Weltevreden, Belvue Road, and Sheba rocks with a sharp, angular contact. The lower sandy and shaly Schoongezicht strata also wedge out against this contact and lack conglomeratic debris or other evidence for an unconformity at this position. We suggest that this contact is also a fault or a faulted unconformity (Lowe et al., this volume, Chapter 2).

Poorly exposed dacitic volcanic rocks, probably belonging to the Schoongezicht Formation, also occur beneath basal Moodies conglomerate along the south limb of the Saddleback syncline immediately east of the study area.

It seems likely that throughout the study area north of the Inyoka fault, the Schoongezicht Formation and overlying Moodies strata rest with angular discordance on underlying, more heavily deformed Onverwacht and Fig Tree rocks (Lowe et al., this volume, Chapter 2). We consider it most likely that this contact is a regional thrust fault.

Age

A considerable number of single-zircon age dates are available from rocks of the Fig Tree Group (Kröner et al., 1989, 1991; Armstrong et al., 1990; Kamo and Davis, 1994; Byerly et al., 1996). Unfortunately, their interpretation is compromised by stratigraphic and structural complexities and because many rocks contain mixed age populations that include xenocrysts, magmatic zircons, and possibly severely disturbed zircons.

The age of the Mapepe Formation is reasonably well constrained. The oldest age yet measured on Mapepe rocks is 3,258 ± 3 Ma on a dacitic tuff in the basal 20 m of the formation just north of the Granville Grove fault (Byerly et al., 1996). A coarse quartz-phyric ash at the base of the formation 0.5 km south of the Inyoka fault (section E, Fig. 14) has yielded a maximum age of 3,243 ± 4 Ma (Kröner et al., 1991). The discrepancy between these ages suggests that the base of the Mapepe Formation is diachronous, possibly younging from south to north (Byerly et al., 1996). In the Barite syncline, a tuff sampled 0.5 km north of the reference section of the Mapepe Formation and thought to be equivalent to tuffs about 250 m above the base of the supplementary section (Fig. 13) yielded zircons indicating a maximum age of 3,227 ± 4 Ma (Kröner et al., 1991). These data suggest that the Mapepe Formation may range in age from about 3,253 ± 3 Ma to slightly younger than 3,227 ± 4 Ma.

A sample of dacitic breccia from the lower part of the type section of the Auber Villiers Formation yielded a complex assemblage of zircons, including xenocrysts as old as 3,522 ± 4 Ma, xenocrysts from the 3,445-Ma magmatic suite, xenocrysts 3,323 ± 4 Ma representing a post-Hooggenoeg Onverwacht magmatic episode, and zircons 3,256 ± 4 Ma that probably represent the crystallization age of the dacitic breccia (Kröner et al., 1991). A sample of tuffaceous sandstone from the uppermost Auber Villiers Formation immediately underlying the basal conglomerate of the Moodies Group on the south limb of the Powerline Road syncline has yielded an age of 3,253 ± 3 (Byerly et al., 1996).

A sample of quartz-rich dacitic tuff from farm Bien Venue 255 JU, part of a thick succession of coarse, silicic, quartz-phyric volcanic and volcaniclastic units in contact with the Moodies Group, yielded a zircon age of 3,259 ± 5 Ma (Kröner et al., 1991). This proximal felsic volcanic sequence may represent the basal part of the Schoongezicht Formation or it may be related to the Auber Villiers Formation, although it lies north of the Inyoka fault.

Fewer ages have been reported from rocks of the northern facies of the Fig Tree Group. No radiometric ages have been

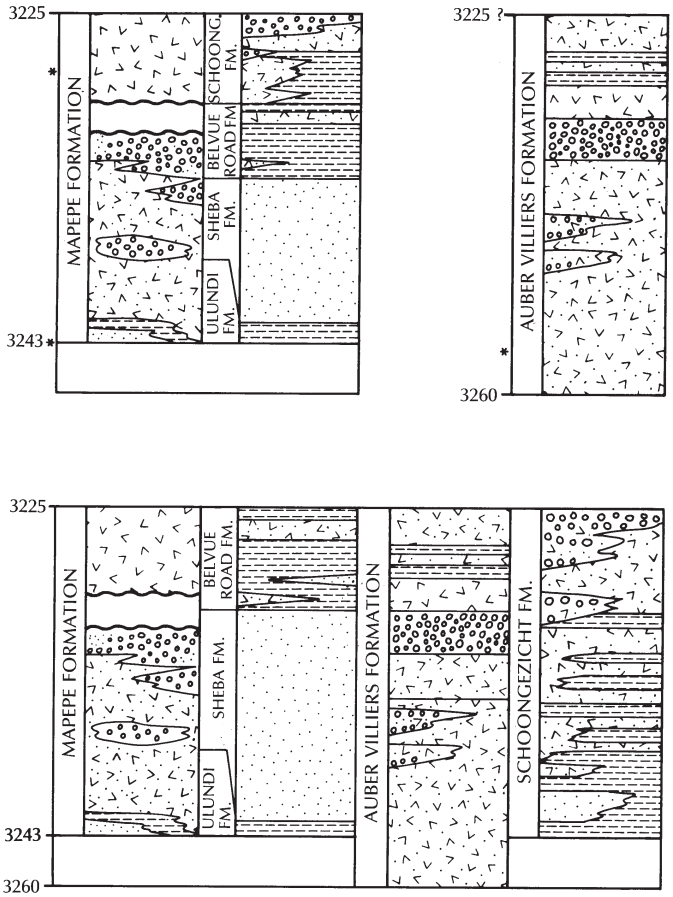


Figure 19. Summary of generalized age and stratigraphic relationships of formations of the Fig Tree Group. (Top) Possible relationships based on existing age data and assuming that the succession of Fig Tree formations at the east end of the Stolzburg syncline is not repeated by faulting (Reimer, 1975; Condie et al., 1970). (Bottom) Probable age relationships based on inference that Schoongezicht Formation in northern areas includes the age equivalents of at least the upper parts of the Belvue Road, Auber Villiers, and Mapepe Formations.

reported for rocks of the Ulundi, Sheba, or Belvue Road Formations. The presence of thin tuffs and, toward the top of the Belvue Road Formation, thicker dacitic volcanic units may reflect the early stages of Schoongezicht volcanism. However, it is also possible that dacitic volcaniclastic units in the upper part of the Belvue Road Formation are correlative with, rather than older than, those in the Schoongezicht.

The age of the Schoongezicht Formation is also unclear, although some radiometric data are available (Kröner et al., 1989, 1991; Armstrong et al., 1990). Zircons from fresh clasts of felsic volcanic rock in conglomerates near the top of the type section indicate a maximum age of 3,226 ± 6 Ma (Kröner et al., 1991). Armstrong et al. (1990) report detrital zircon ages as young as 3,163 ± 8 Ma from possible Schoongezicht or Moodies strata at the eastern end of the Stolzburg syncline. If representing unmodified detrital zircons and present in the Schoongezicht Formation, these zircons would indicate that the Schoongezicht Formation is younger than 3,163 Ma. However, other zircons from this assemblage show evidence of metamorphic origins and/or Pb loss (Armstrong et al., 1990) and the magmatic and depositional ages of the volcaniclastic material remain unclear. For the present, we regard the uniform 3,225 ± 6 ages from felsic clasts as providing the best estimate of the age of late Schoongezicht magmatism and the best maximum age for the overlying Moodies strata in the Stolzburg syncline. More recently, Kamo and Davis (1994) report ages of 3,226 ± 6 Ma and 3,222+10/–4 Ma on an ignimbrite in the Schoongezicht Formation and felsic porphyritic intrusive, respectively.

These results suggest that dacitic volcanism was more-or-less continuous within and around the Barberton Greenstone Belt from about 3,260 to 3,225 Ma. The youngest well-documented age for both the Mapepe and Schoongezicht Formations is about 3,225 Ma. Quite possibly, all four named Fig Tree units containing dacitic volcaniclastic rocks, the Mapepe, Auber Villiers, Belvue Road, and Schoongezicht Formations, are in large part coeval (Fig. 19). Until more precise age data is available, however, it is also possible that each records a somewhat different episode of felsic igneous activity.

MOODIES GROUP

The Moodies Group is the uppermost lithostratigraphic unit of the Swaziland Supergroup. It crops out in a series of structurally isolated blocks and erosional outliers (Fig. 4) including, in and near the study area, the Stolzburg syncline, Moodies Hills block, Eureka and Saddleback synclines, Powerline Road and Maid-of-the-Mists synclines, southern end of The Heights syncline, and Baviaanskloof block (Figs. 1 and 4).

The Moodies Group was named the Moodies Series by Kynaston (1906) for outcrops in the Moodies Hills, frontal mountains of the greenstone belt near Barberton, and originally included all rocks in the sedimentary part of the greenstone belt succession. Van Eeden (1941) and Visser (1956) subdivided the sedimentary section into the Moodies and Fig Tree Systems and Series, respectively. Viljoen, M. J., and Viljoen (1969a) renamed these the Moodies and Fig Tree Groups.

Anhaeusser (1969, 1976) divided the Moodies Group in the Eureka syncline into three formations, including from base upward the Clutha, Joe's Luck, and Baviaanskop Formations (Fig. 3). Each consists of a coarse basal unit of conglomeratic quartzose sandstone overlain by a thick section of finer grained quartzose sandstone, siltstone, and shale. The entire group totals about 3,140 m thick (Fig. 3). Eriksson (1977a, b; 1978) recognized five units in the Eureka and Saddleback synclines: MD1 (basal unit), MD2, MD3, MD4, and MD5. MD1 and MD2 correspond generally with the basal conglomerate-quartzite (MD1) and overlying sandstone, siltstone, and shale (MD2) of the Clutha Formation; MD3 and MD4 with the quartzite and shaly portions of the Joe's Luck Formation, respectively; and MD5 with the Baviaanskop Formation.

The principal units for regional correlation of Moodies strata north of the Inyoka fault are a zone of amygdaloidal basalt flows and an overlying layer of iron-rich shale and jaspilite that occur at the base of MD4 in the Eureka syncline (Eriksson, 1977a, b) or immediately above the basal part of the Joe's Luck Formation (Anhaeusser, 1973). Both are present in the Moodies Hills and the basalt occurs in the Saddleback syncline. These beds are absent south of the Inyoka fault.

Nearly 2,150 m of Moodies strata are present in the Moodies Hills block (Fig. 3), including units generally correlative with the Clutha and Joe's Luck Formations in the Eureka syncline. The Moodies Hills block is bordered on the north by the Moodies fault (Fig. 4), which brings Moodies strata on the south, striking at a low angle into the fault, into contact with ultramafic rocks of the Weltevreden Formation or, locally, sedimentary units of the Fig Tree Group north of the fault. Previously described Moodies carbonate units north of the fault (Visser, 1956, p. 78) are actually carbonated ultramafic rocks. We have identified no primary carbonate units in the Moodies Group within the study area.

Throughout the Barberton Greenstone Belt, the stratigraphic base of the Moodies Group is marked by pebble and cobble conglomerate. Although there has been considerable controversy regarding the definition of the Fig Tree and Moodies contact in southern areas (Lamb, 1984a, b; Lamb and Paris, 1988), we retain the term Moodies essentially as used by Visser (1956) to refer to quartz-rich (50%), predominantly arenaceous rocks at the top of the greenstone belt section. Where a well-defined conglomerate is present immediately below the first appearance of quartz-rich sandstone, it is considered to be the basal conglomerate of the Moodies Group. Otherwise, the Moodies–Fig Tree contact is drawn at the lowest occurrence of quartz-rich sandstone. In contrast to Moodies conglomerates, those in the Mapepe Formation interfinger with low-quartz (<10%) dacitic tuffs and volcaniclastic units.

In the Moodies Hills, Eureka syncline, Stolzburg syncline, and Saddleback syncline, all north of the Inyoka fault, the basal Moodies conglomerate includes clasts of chert, dacitic volcanic rocks, altered komatiite, sandstone, and jasper that were derived from immediately underlying Weltevreden and Fig Tree units.

Additionally, clasts of microcline-bearing plutonic rocks form a minor but distinctive component of the conglomerate on the north limb of the Eureka syncline but have no known pre-Moodies source (Visser, 1956; Reimer et al., 1985; Heubeck and Lowe, this volume, Chapter 11). Zircons from some of these clasts have yielded ages between 3,570 ± 6 Ma and 3,518 ± 11 Ma (Kröner and Compston, 1988). North of the Inyoka fault, Moodies sandstones also contain detrital microcline, also indicating the existence of potassic plutonic rocks (Hose, 1990; Heubeck and Lowe, this volume, Chapter 11).

Within the study area south of the Inyoka fault, there are four main outcrop areas of Moodies rocks: Powerline Road syncline (PRS), Maid-of-the-Mists syncline, The Heights syncline and outcrops west of the Kromberg fault on the northern part of the east limb of the Onverwacht anticline, and the Baviaanskloof block (Figs. 1 and 4). (1) The south limb of the Powerline Road syncline includes about 700 m of Moodies lithic-rich quartzose sandstone and conglomeratic sandstone grading downward into 100 m of low-quartz (<20%) sandstone. The base of the section is a 10- to 50-m-thick pebble and cobble conglomerate made up largely of clasts of banded ferruginous chert, black chert, dacitic volcanic rock, and volcaniclastic sandstone and siltstone. Facies and structural relationships (Lowe et al., this volume, Chapter 2, Fig. 18) suggest that much of the Moodies strata in the PRS were derived by uplift and erosion of Auber Villiers strata west of a fault, named the Two Springs fault by Lowe et al. (this volume, Chapter 2), active during lower Moodies time. Both the low-quartz sandstone overlying the basal conglomerate and higher, more quartzose sandstones contain units showing cross-sets as much as 4 m high.

Along the southern limb of the PRS, basal Moodies strata are subparallel to underlying mudstone and tuffaceous siltstone at the top of the Auber Villiers Formation. The contact is probably a paraconformity.

(2) Immediately east of the Powerline Road syncline, the Maid-of-the-Mists syncline includes at least 500 m of deformed quartz-rich Moodies sandstone. Conglomerate makes up a negligible part of the section. This sequence is characterized by very well sorted, fine- to medium-grained sandstone with enormous cross-sets, some as much as 9 m high. The bulk of the section appears to represent aeolian or tidal deposits. Along the north limb of the syncline, the Moodies is faulted along a branch of the Inyoka fault and intruded by mafic igneous rock. The western and southern contacts are irregular and show steeply dipping sandstone in contact with and crosscutting a melange of chert blocks and altered komatiite of the Mendon Formation and terrigenous chert-pebble conglomerate, sandstone, and shale of the Mapepe Formation. The lowest Moodies strata show no evidence of internal faulting but are quartz rich and lack a basal conglomerate. We regard this contact as a thrust fault correlative with the 24-Hour Camp fault (Lowe et al., this volume, Chapter 2).

(3) In The Heights syncline (Fig. 4), the Moodies includes several hundred meters of quartzose sandstone containing lenses and layers of conglomerate. In contrast to basal Moodies conglomerates in all other belts, those in The Heights syncline, for at least 30 km along strike to the northeast, are composed largely of dacitic volcanic clasts mixed with minor amounts of iron-rich ferruginous chert, basalt, and silicified komatiitic detritus. Black chert, black-and-white banded chert, and white chert make up less than 5% of the clast population.

Outcrops of Moodies strata on the east limb of the Onverwacht anticline (Lowe et al., this volume, Chapter 2, Fig. 9) represent the continuation of The Heights syncline across branches of the Kromberg fault. They extend from the hinge zone on the southern part of farm Mendon 379 JU, down the eastern limb through the northern edge of Dunbar 383 JU, and the eastern edge of Noisy 737 JU. Throughout this area, folded conglomerate at the base of the Moodies Group rests with marked angular discordance on rocks of the Hooggenoeg, Kromberg, Mendon, and lowermost Mapepe Formations. Although folds in Moodies and underlying Onverwacht rocks are disharmonic across the basal Moodies contact, basal Moodies strata are everywhere conglomeratic and closely reflect the compositions of immediately underlying Onverwacht units, indicating that the contact is an unconformity. In the Moodies outlier west of the main outcrop belt (Fig. 4), for instance, Moodies strata rest on banded ferruginous cherts of K1 and mafic lapillistone of K2. The basal Moodies is a breccia, 5–50 m thick, composed largely of clasts of banded ferruginous chert in a quartzose sandstone matrix. Breccia is overlain by dacite-clast conglomerate. Locally, where Moodies strata overlie cherts of the Mendon Formation, the conglomerates contain abundant black chert clasts. Over most of the area, however, the basal conglomerate is composed largely of dacite clasts, presumably derived from felsic volcanic rocks in H6, and contains little black chert, which is a minor component of Onverwacht units below the Kromberg Formation.

(4) On farm Baviaanskloof 387 JU on the eastern limb of the Onverwacht anticline (Fig. 4), faulted and tightly folded quartz-rich sandstones of the Moodies Group lie with angular unconformity on rocks of the Hooggenoeg and Kromberg Formations. The basal Moodies strata include a conglomerate 10–100 m thick that varies rapidly in composition from place to place and bed to bed. Locally, it contains as much as 80% clasts of silicified coarse dacitic feldspar- and quartz-rich porphyry. Other beds are composed exclusively of gray and black chert and subordinate altered ultramafic rocks. The block is truncated by the Kromberg fault on the east.

Although Moodies strata throughout the Barberton Belt have previously been regarded as part of a large, integrated depositional system deriving sediment from the uplifted Ancient Gneiss Complex and more local tonalitic, trondhjemitic, and granodioritic plutons (Eriksson, 1977a, 1978; Reimer et al., 1985; Jackson et al., 1987), the compositional differences of both conglomerates and sandstones within individual northeast-trending Moodies belts argue for more local sources and distribution systems (Fig. 20; and Heubeck and Lowe, this volume, Chapter 11). Perhaps the key belt is The Heights syncline, which is dominated by dacite-clast conglomerate throughout its length. To the northwest, two distinctive areas can be recognized. North of the Inyoka fault, basal Moodies conglomerates are dominated by black, white, and banded chert

varieties with small proportions of jasper, mafic volcanic rock, silicified komatiite, and distinctive microcline-bearing clasts. In the Powerline Road syncline, the conglomerate was derived from local uplifts of the Auber Villiers Formation and the underlying Mendon Formation and consists largely of clasts of banded ferruginous chert, dacite, and sandstone. Southeast of The Heights syncline, outcrops mapped as part of the Moodies Group along the Swaziland border (Fig. 4) are extremely conglomeratic and dominated by clasts of massive black chert. These rocks are interbedded with ferruginous sediments and chert-grain sandstones containing a low percentage of coarse detrital quartz (Heubeck and Lowe, this volume, Chapter 11). They are perhaps best regarded as correlative with the Fig Tree Group to the northwest (Heubeck and Lowe, this volume, Chapter 11). At least within the Powerline Road and The Heights syncline, transport was evidently from local uplifts in the southwest toward the northeast. Chert-rich conglomerates to the northwest must have been sourced in local uplifts or areas located farther to the north or northwest.

Age

The age of the Moodies Group has been reviewed by Heubeck and Lowe (1994a, b). Detrital grains and conglomerate clasts (Van Niekerk and Burger, 1978; Tegtmeyer and Kröner, 1987; Kröner and Compston, 1988) indicate that the source rocks ranged in age from older than 3.5 Ga to Fig Tree–age felsic volcanic units as young as 3,224 ± 6 Ma (Kröner and Todt, 1988). Kröner et al. (1991) obtained an age of 3,225 ± 3 Ma on felsic volcanic clasts in upper part of the Fig Tree Group and Kamo and Davis (1994) report ages of 3,226 ± 1 Ma and 3,222+10/–4 Ma from an ignimbrite and porphyritic intrusion, respectively, at the top of the Fig Tree. These represent maximum ages for the start of Moodies sedimentation and are consistent with interpretations that Moodies sedimentation began between about 3,225 and 3,222 Ma (Heubeck and Lowe, 1994a). Heubeck and Lowe (1994a) report an age of 3,207 ± 2 Ma on a felsic dike crosscutting Moodies strata locally, indicating that sedimentation began before about 3,207 Ma.

The Salisbury Kop pluton, composed of granodiorite and adamellite, crosscuts and metamorphoses Moodies rocks in the northeastern . Recent dates from single zircons suggest an intrusion age of about 3,109+10/–8 Ma (Kamo and Davis, 1994; Heubeck et al., 1993). In the southern part of the belt, the postkinematic Dalmein pluton crosscuts the Kromberg syncline that, several kilometers to the north, includes folded Moodies strata. This pluton has been dated at 3,216+2/–1 Ma (Kamo and Davis, 1994). In this area, at least, Moodies sedimentation was largely complete by about 3,216 Ma. Along the northern part of the belt, Layer (1986) has presented evidence that the Moodies Group was magnetically overprinted by the Kaap Valley pluton, dated by Ar-Ar hornblende at 3,214 ± 4 Ma (Layer et al., 1992).

These results suggest that Fig Tree sedimentation and volcanism ended about 3,224 ± 6 Ma and that Moodies sedimentation began between about 3,224 ± 6 and 3,207 ± 2 Ma. Moodies deposition and deformation was complete by 3,109+10/–8 Ma and probably by 3,214 ± 4 Ma. In view of the fact that Moodies strata were derived from a number of different sources and deposited within a number of separate sedimentary basins, it seems likely that both the beginning and end of sedimentation were diachronous across the greenstone belt.

DISCUSSION

The results of the present investigation suggest a number of significant revisions to previously proposed models of stratigraphic

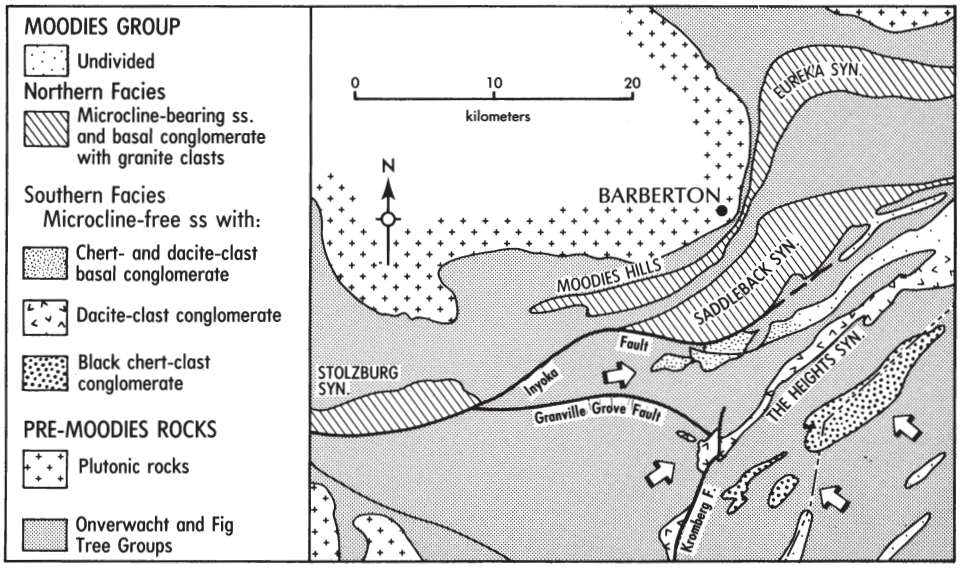


Figure 20. Compositional contrasts of conglomerates in the lower part of the Moodies Group in Moodies structural belts in the western part of the Barberton Greenstone Belt. Inferred transport directions (arrows) are based on contrasts in clast composition and clast coarsening trends.

classification and nomenclature in the west-central part of the Barberton Greenstone Belt. Exposed rocks of the Onverwacht Group are diachronous, younging from south to north across the belt. The oldest dated rocks in the BGB are 3,547 ± 3 Ma metamorphosed Theespruit Formation felsic schists in the Steynsdorp anticline. The stratigraphic positions of the Sandspruit and Theespruit Formations in the Onverwacht anticline and of all xenoliths, roof pendants, and supracrustal outliers detached from the main body of the belt remain problematic, although recent studies clearly indicate that they include rocks correlative with the upper part of the Onverwacht Group as well as components older than any part of the intact stratigraphic sequence (Armstrong et al., 1990). The Komati, Hooggenoeg, Kromberg, and Mendon Formations make up an overall intact stratigraphic sequence that, in the Southern Domain on the west limb of the Onverwacht anticline, totals at least 9,300 m thick.

In the central part of the greenstone belt, the Onverwacht Group is represented by a newly defined unit, the Mendon Formation, that includes the upper 200–300 m of the Kromberg Formation as defined by Viljoen, R. P., and Viljoen (1969) and overlying komatiite-chert cycles that may exceed 1,000 m thick. These higher cycles are developed mainly in the northern part of the West-Central Domain and are represented in the Southern Domain by a 30-m-thick section of black chert at the top of the Mendon Formation and possibly the basal part of the overlying Fig Tree clastic strata. Although the presence of a fall unit of spherules, S2, at the base of the Mapepe Formation of the Fig Tree Group provides a good basis for correlation among many structural blocks, its absence in the southernmost belts allows for the possibility that the top of the chert sequence capping the Mendon Formation is also diachronous. Moreover, contrasting ages of 3,252 ± 6 Ma and 3,243 ± 4 Ma on tuffs near the base of the Mapepe Formation in southern and northern parts of the WCD, respectively, suggest the possibility that the Onverwacht–Fig Tree contact youngs from south to north.

North of the Inyoka fault, the mafic and ultramafic volcanic suit has been assigned to the Weltevreden Formation of the Onverwacht Group. This unit is made up largely of komatiitic volcanic rocks containing interstratified basalts, layered ultramafic intrusions, komatiitic tuffs, and thin beds of black and banded chert. The Weltevreden Formation resembles the uppermost, northern volcanic cycles in the Mendon Formation whereas lower cycles of the Mendon are more similar to rocks and environments of the Kromberg and Hooggenoeg Formations. Available age data and lithologic similarities suggest that the Weltevreden Formation is correlative with or younger than the upper parts of the Mendon Formation.

The diachronous nature of mafic and ultramafic volcanism means that the composition of volcanic units cannot serve as a basis for stratigraphic correlation. Previously, komatiitic rocks in the central and northern parts of the belt were assigned to the lower formations of the Onverwacht Group (e.g., Anhaeusser et al., 1981) largely because of their resemblance to the Komati Formation, a correlation disputed by the present results. Similarly, layered komatiitic intrusions and associated komatiitic flows along the eastern part of the belt have been correlated with lower parts of the Onverwacht Group. Although we have not mapped systematically in this area, reconnaissance studies suggest that these units may also represent the Mendon Formation, not older Onverwacht units.

Correlation of rocks within the Mendon Formation also suggests that much of the time represented by the volcanic division of the Swaziland Supergroup resides in thin layers of black and banded chert deposited during intervals of local or regional volcanic quiescence and probably representing condensed sections. Because such cherts are widely developed in all volcanic formations, it may be expected that tracing them into regions where volcanism was more continuous may reveal substantial changes in stratigraphy and the appearance of major new volcanic units. Although many thin cherts are continuous and traceable over outcrop distances of many tens of kilometers, major facies changes in the Middle Marker (Lanier and Lowe, 1982), H2c, the Buck Reef Chert, and the cherts of the Mendon Formation clearly indicate that, on the scale of the greenstone belt as a whole, the cherts and associated volcanic members are lenticular, as demonstrated for individual flows (Williams and Furnell, 1979). Reliable correlations cannot be based only on the general similarity of chert units in widely separated outcrops or discrete structural belts.

Sedimentary rocks of the Fig Tree Group show a south-to-north change from shallow, platformal to deep-water facies. The Mapepe Formation in the southern part of the belt is dominated by lithologically complex, mainly shallow-water to subaerial terrigenous and volcaniclastic units. The depositional setting deepened toward the north across the WCD, and, immediately south of the Inyoka fault, the Mapepe Formation includes thick units of turbiditic chert-clast conglomerate and chert-grit sandstone. North of the Inyoka fault, northern-facies Fig Tree formations consist predominantly of turbiditic shale, mudstone, and lithic sandstone and conglomerate.

The abundant dacitic volcanic and volcaniclastic rocks in the Fig Tree Group are subdivided into four main formations: the Auber Villiers and Mapepe Formations south of the Inyoka fault and the Belvue Road and Schoongezicht Formations to the north. Mapping suggests that both south and north of the Inyoka fault, proximal Auber Villiers and Schoongezicht rocks and the overlying Moodies Group are thrust over more distal rocks of the Mapepe and Belvue Road Formations, respectively (Lowe et al., this volume, Chapter 2).

Although deformation affected portions of the greenstone belt toward the end of Hooggenoeg and beginning of Kromberg time, probably associated with major intrusive events, changes in tectonic and volcanic styles, and explosive phreatomagmatic volcanism, the principal deformational events occurred during and following deposition of the Mapepe Formation in pre-Moodies time and during and following deposition of the Moodies Group.

Although there are striking similarities in the stratigraphy, lithologies, and history of rocks of the Swaziland Supergroup south and north of the Inyoka fault, the following subtle compositional

and depositional differences suggest that these sequences were separated until post-Moodies time. (1) There are major lithologic and sedimentological contrasts in the Onverwacht Group across the Inyoka fault. (2) Fig Tree strata south of the Inyoka fault lack debris derived from plutonic rocks whereas microcline is a widespread constituent of the Sheba Formation north of the fault. (3) In addition to geochemical contrasts between Fig Tree dacitic units south and north of the Inyoka fault, the Mapepe and Auber Villiers Formations south of the fault are quartz-phyric units whereas the Schoongezicht Formation lacks quartz. (4) The Mapepe Formation south of the fault contains a high proportion of dacitic volcaniclastic material whereas sandstones and interbedded shales of the Sheba Formation contained little or no fresh dacitic debris. (5) Moodies strata north of the Inyoka fault contain abundant microcline and granitic clasts that are absent in Moodies units to the south. (6) Moodies sections north of the Inyoka fault are commonly thick, exceeding 2,000 m, and contain distinctive basaltic and jasper marker beds whereas most sections within the study area south of the fault are thinner, less than 1,000 m, and lack these marker units.

The obvious similarities but distinctive differences between northern and southern facies of the Swaziland Supergroup suggest that they may have been deposited in different parts of a single, large depositional basin. Clastic detritus in the Fig Tree and Moodies Groups north and south of the Inyoka fault were derived from grossly similar but, in detail, compositionally and geographically different sources. De Wit et al. (1992) have recently suggested that the Inyoka fault marks a major terrane boundary, but it is difficult to reconcile this interpretation with the overall similarity of these sequences in terms of lithologic succession, ages, and geologic evolution.

CONCLUSIONS

Stratigraphic analysis of the Swaziland Supergroup in the west-central part of the Barberton Greenstone Belt provides an improved basis for developing evolutionary models of this Early Archean orogenic terrane. Particularly important to such models are the strong contrasts in lithologies and depositional settings of northern and southern facies rocks throughout the supergroup, the diachronous nature of mafic and ultramafic volcanism within the belt, and the overlap of dacitic volcanism, deformation, and sedimentation during Fig Tree time.

REFERENCES CITED

Anhaeusser, C. R., 1969, The stratigraphy, structure, and gold mineralisation of the Jamestown and Sheba Hills areas of the Barberton Mountain Land [Ph.D. thesis]: Johannesburg, University of the Witwatersrand, 332 p.

Anhaeusser, C. R., 1973, The evolution of the early Precambrian crust of southern Africa: Royal Society of London Philosophical Transactions, series A, v. 273, p. 359–388.

Anhaeusser, C. R., 1975, The geological evolution of the primitive Earth: evidence from the Barberton Mountain Land: University of the Witwatersrand, Economic Geology Research Unit Information Circular 98, 22 p.

Anhaeusser, C. R., 1976, The geology of the Sheba Hills area of the Barberton Mountain Land, South Africa, with particular reference to the Eureka syncline: Geological Society of South Africa Transactions, v. 79, p. 253–280.

Anhaeusser, C. R., 1985, Archean layered ultramafic complexes in the Barberton Mountain Land, South Africa, *in* Ayres, L. D., Thurston, P. C., Card, K. D., and Weber, W., eds., Evolution of Archean supracrustal sequences: Geological Association of Canada Special Paper 28, p. 281–302.

Anhaeusser, C. R., Robb, L. J., and Viljoen, M. J., 1981, Provisional geological map of the Barberton Greenstone Belt and surrounding granitic terrane, eastern Transvaal and Swaziland: Geological Society of South Africa, scale 1:250,000.

Armstrong, R. A., Compston, W., de Wit, M. J., and Williams, I. S., 1990, The stratigraphy of the 3.5–3.2 Ga Barberton Greenstone Belt revisited: a single zircon ion microprobe study: Earth and Planetary Science Letters, v. 101, p. 90–106.

Brevart, O., Dupre, B., and Allegre, C. J., 1986, Lead-lead age of komatiitic lavas and limitations on the structure and evolution of the Precambrian mantle: Earth and Planetary Science Letters, v. 77, p. 293–302.

Byerly, G. R., Lowe, D. R., Nocita, B. W., and Ransom, B. L., 1983, Apparent volcanic cycles in the Archean Swaziland Supergroup, Barberton Mountain Land, South Africa: a result of non-magmatic processes: Lunar and Planetary Science Conference, 14th, Houston, Abstracts, pt. 1, p. 84–85.

Byerly, G. R., Lowe, D. R., and Walsh, M. M., 1986, Stromatolites from the 3,300–3,500-Myr Swaziland Supergroup, Barberton Mountain Land, South Africa: Nature, v. 319, p. 489–491.

Byerly, G. R., Kröner, A., Lowe, D. R., and Walsh, M. M., 1993, Sequential magmatic evolution of the early Archean Onverwacht Group: evidence from the upper formations: Eos (Transactions, American Geophysical Union), v. 74, p. 660.

Byerly, G. R., Kröner, A., Lowe, D. R., Todt, W., and Walsh, M. M., 1996, Prolonged magmatism and time constraints for sediment deposition in the early Archean Barberton greenstone belt: evidence from the Upper Onverwacht and Fig Tree Groups: Precambrian Research, v. 78, p. 125–138.

Chauvel, C., Arndt, N. T., Gruau, G., and Hofmann, A. W., 1987, Composition of the Archean mantle: evidence from Nd isotopes: TERRA Cognita, v. 7, p. 272.

Condie, K. C., Macke, J. E., and Reimer, T. O., 1970, Petrology and geochemistry of early Precambrian graywackes from the Fig Tree Group, South Africa: Geological Society of America Bulletin, v. 81, p. 2759–2776.

de Ronde, C. E. J., and de Wit, M. J., 1994, Tectonic history of the Barberton greenstone belt, South Africa: 490 million years of Archean crustal evolution: Tectonics, v. 13, p. 983–1005.

de Wit, M. J., 1982, Gliding and overthrust nappe tectonics in the Barberton Greenstone Belt: Journal of Structural Geology, v. 4, p. 117–136.

de Wit, M. J., 1983, Notes on a preliminary 1:25,000 geological map of the southern part of the Barberton Greenstone Belt, *in* Anhaeusser, C. R., ed., Contributions of the geology of the Barberton Mountain Land: Geological Society of South Africa Special Publication 9, p. 185–187.

de Wit, M. J., Hart, R., Martin, A., and Abbott, P., 1982, Archean abiogenic and probable biogenic structures associated with mineralized hydrothermal vent systems and regional metasomatism, with implications for greenstone belt studies: Economic Geology, v. 77, p. 1783–1801.

de Wit, M. J., Fripp, R. E. P., and Stanistreet, I. G., 1983, Tectonic and stratigraphic implications of new field observations along the southern part of the Barberton Greenstone Belt, *in* Anhaeusser, C. R., ed., Contributions to the geology of the Barberton Mountain Land: Geological Society of South Africa Special Publication 9, p. 21–29.

de Wit, M. J., Hart, R. A., and Hart, R. J., 1987a, The Jamestown Ophiolite Complex, Barberton mountain belt: a section through 3.5 Ga oceanic crust: Journal of African Earth Sciences, v. 6, p. 681–730.

de Wit, M. J., Armstrong, R. J., Hart, R. J., and Wilson, A. H., 1987b, Felsic igneous rocks within the 3.3 to 3.5 Ga Barberton Greenstone Belt: high crustal-level equivalents of the surrounding tonalite-trondhjemite terrain, emplaced during thrusting: Tectonics, v. 6, p. 529–549.

de Wit, M. J., Roering, C., Hart, R. J., Armstrong, R. A., de Ronde, C. E. J., Green, R. W. E., Tredoux, M., Peberdy, E., and Hart, R. A., 1992, Formation of an Archaean continent: Nature, v. 357, p. 553–562.

Duchac, K. C., 1986, Metasomatic alteration of a komatiitic sequence into chert [M.Sc. thesis]: Baton Rouge, Louisiana State University, 240 p.

Duchac, K. C., and Hanor, J. S., 1987, Origin and timing of the metasomatic sili-

cification of an Early Archean komatiite sequence, Barberton Mountain Land, South Africa: Precambrian Research, v. 37, p. 125–146.

Eriksson, K. A., 1977a, A paleoenvironmental analysis of the Archaean Moodies Group, Barberton Mountain Land, South Africa [Ph.D. thesis]: Johannesburg, University of the Witwatersrand, 155 p.

Eriksson, K. A., 1977b, Tidal deposits from the Archaean Moodies Group, Barberton Mountain Land, South Africa: Sedimentary Geology, v. 18, p. 257–281.

Eriksson, K. A., 1978, Alluvial and destructive beach facies from the Archaean Moodies Group, Barberton Mountain Land, South Africa and Swaziland, *in* Miall, A. D., ed., Fluvial sedimentology: Canadian Society of Petroleum Geologists Memoir 5, p. 287–311.

Eriksson, K. A., 1980a, Hydrodynamic and paleogeographic interpretation of turbidite deposits from the Archean Fig Tree Group of the Barberton Mountain Land, South Africa: Geological Society of America Bulletin, v. 91, p. 21–26.

Eriksson, K. A., 1980b, Transitional sedimentation styles in the Moodies and Fig Tree Groups, Barberton Mountain Land, South Africa: evidence favouring an Archaean continental margin: Precambrian Research, v. 12, p. 141–160.

Fisher Worrell, G. F., 1985, Sedimentology and mineralogy of silicified evaporites in the basal Kromberg Formation, South Africa [M.Sc. thesis]: Baton Rouge, Louisiana State University, 152 p.

Glikson, A. Y., and Jahn, B. M., 1985, REE and LIL elements, eastern Kaapvaal Shield, South Africa: evidence of crustal evolution by 3-stage melting, *in* Ayres, L. D., Thurston, P. C., Card, K. D., and Weber, W., eds., Evolution of Archean supracrustal sequences: Geological Association of Canada Special Paper 28, p. 303–324.

Hall, A. L., 1918, The geology of the Barberton gold mining district: Geological Survey of South Africa Memoir 9, 347 p.

Hamilton, P. J., Evensen, N. M., O'Nions, R. K., Smith, H. S., and Erlank, A. J., 1979, Sm-Nd dating of Onverwacht Group volcanics, southern Africa: Nature, v. 279, p. 298–300.

Hamilton, P. J., O'Nions, R. K., Bridgwater, D., and Nutman, A., 1983, Sm-Nd studies of Archean metasediments and metavolcanics from West Greenland and their implications for the Earth's early history: Earth and Planetary Science Letters, v. 62, p. 263–272.

Hanor, J. S., and Duchac, K., 1990, Isovolumetric silicification of Early Archean komatiites: geochemical mass balances and constraints on origin: Journal of Geology, v. 98, p. 863–877.

Heinrichs, T. K., 1969, Report on mapping carried out in search of chrysotile asbestos: Barberton, Unpublished report to Eastern Transvaal Consolidated Mines, Ltd., 5 p., 1 map.

Heinrichs, T. K., 1980, Lithostratigraphische Untersuchungen in der Fig Tree Gruppe des Barberton Greenstone Belt zwischen Umsoli und Lomati (Sudafrika): Gottinger Arbeiten zur Geologie und Palaontologie, v. 22, 118 p.

Heinrichs, T. K., 1984, The Umsoli Chert, turbidite testament for a major phreatoplinian event at the Onverwacht/Fig Tree transition (Swaziland Supergroup, Archaean, South Africa): Precambrian Research, v. 24, p. 237–283.

Heinrichs, T. K., and Reimer, T. O., 1977, A sedimentary barite deposit from the Archean Fig Tree Group of the Barberton Mountain Land (South Africa): Economic Geology, v. 72, p. 1426–1441.

Heubeck, C., and Lowe, D. R., 1994a, Depositional and tectonic setting of the Archean Moodies Group, Barberton Greenstone Belt, South Africa: Precambrian Research, v. 68, p. 257–290.

Heubeck, C., and Lowe, D. R., 1994b, Late syndepositional deformation and detachment tectonics in the Barberton Greenstone Belt, South Africa: Tectonics, v. 13, p. 1514–1536.

Heubeck, C., Wendt, J. I., Toulkeridis, T., Kröner, A., and Lowe, D. R., 1993, Timing of deformation of the Archaean Barberton Greenstone Belt, South Africa: constraints from zircon dating of the Salisbury Kop pluton : Journal of South African Geology, v. 96, p. 1–8.

Hose, L. D., 1990, The geology and stratigraphic evolution of the north-central part of the Early Archean Barberton Greenstone Belt, South Africa [Ph.D. dissertation]: Baton Rouge, Louisiana State University, 381 p.

Hunter, D. R., and Jones, D. H., 1969, Geological map of Swaziland: Sheet 2 Piggs Peak, 1st edition: Mbabane, Swaziland Geological Survey and Mines Department, scale 1:25,000.

Hurley, P. M., Pinson, W. H., Jr., Nagy, B., and Teska, T. M., 1972, Ancient age of the Middle Marker horizon, Onverwacht Group, Swaziland Sequence, South Africa: Earth and Planetary Science Letters, v. 14, p. 360–366.

Jackson, M. P. A., Eriksson, K. A., and Harris, C. W., 1987, Early Archean foredeep sedimentation related to crustal shortening: a reinterpretation of the Barberton Sequence, southern Africa: Tectonophysics, v. 136, p. 197–221.

Jahn, B. M., and Shih, C. Y., 1974, On the age of the Onverwacht Group, Swaziland Sequence, South Africa: Geochimica et Cosmochimica Acta, v. 38, p. 873–885.

Jahn, B. M., Gruau, G., and Glikson, A. Y., 1982, Komatiites of the Onverwacht Group, S. Africa: REE geochemistry, Sm/Nd age and mantle evolution: Contributions to Mineralogy and Petrology, v. 80, p. 25–40.

Kamo, S. L., and Davis, D. W., 1991, A review of geochronology from the Barberton Mountain Land, in Ashwal, L. D., ed., Two cratons and an orogen (Excursion guidebook and review articles for a field workshop): Johannesburg, Department of Geology, University of the Witwatersrand, IGCP Project 280, p. 59–68.

Kamo, S. L., and Davis, D. W., 1994, Reassessment of Archean crustal development in the Barberton Mountain Land, South Africa, based on U-Pb dating: Tectonics, v. 13, p. 167–192.

Kamo, S. L., Davis, D. W., and de Wit, M. J., 1990, U-Pb geochronology of Archean plutonism in the Barberton region, S. Africa: 800 Ma of crustal evolution: 7th International Congress on Geochemistry, Abstracts, Canberra, p. 53.

Kröner, A., and Compston, W., 1988, Ion microprobe ages of zircons from early Archaean granite pebbles and greywacke, Barberton greenstone belt, southern Africa: Precambrian Research, v. 38, p. 367–380.

Kröner, A., and Todt, W., 1988, Single zircon dating constraining the maximum age of the Barberton Greenstone Belt, southern Africa: Journal of Geophysical Research, v. 93, p. 15329–15337.

Kröner, A., Byerly, G. R., and Lowe, D. R., 1989, Precise single zircon evaporation ages documenting »200 Ma of Archean greenstone evolution in the Barberton Belt of South Africa: Eos (Transactions, American Geophysical Union), v. 70, p. 1404.

Kröner, A., Byerly, G. R., and Lowe, D. R., 1991, Chronology of early Archaean granite-greenstone evolution in the Barberton Mountain land, South Africa, based on precise dating by single zircon evaporation: Earth and Planetary Science Letters, v. 103, p. 41–54.

Kröner, A., Hegner, E., Byerly, G. R., and Lowe, D. R., 1992, Possible terrane identification in the Early Archean Barberton Greenstone Belt, South Africa, using single zircon geochronology: Eos (Transactions, American Geophysical Union), v. 73, p. 616.

Kröner, A., Hegner, E., Wendt, J. I., and Byerly, G. R., 1996, The oldest part of the Barberton granitoid-greenstone terrain, South Africa: evidence for crust formation between 3.5 and 3.7 Ga: Precambrian Research, v. 78, p. 105–124.

Kynaston, H., 1906, The geology of the Komatipoort coalfield: Geological Survey of the Transvaal Memoir 2, 55 p.

Lahaye, Y., Arndt, N., Byerly, G. R., Chauvel, C., Fourcade, S., and Gruau, G., 1995, The influence of alteration on the trace-element and Nd isotopic compositions of komatiites: Chemical Geology, v. 126, p. 43–64.

Lamb, S. H., 1984a, Geology of part of the Archaean Barberton Greenstone Belt, Swaziland [Ph.D. dissertation]: England, Cambridge University, 250 p.

Lamb, S. H., 1984b, Structures on the eastern margin of the Archaean Barberton Greenstone Belt, northwest Swaziland, *in* Kröner, A., and Greiling, A., eds., Precambrian tectonics illustrated: Stuttgart, E. Schweizerbart'sche Verlagsbuchhandlung, p. 19–39.

Lamb, S. H., and Paris, I., 1988, Post-Onverwacht Group stratigraphy in the SE part of Archaean Barberton Greenstone Belt: Journal of African Earth Sciences, v. 7, p. 285–306.

Lanier, W. P., and Lowe, D. R., 1982, Sedimentology of the Middle Marker (3.4 Ga), Onverwacht Group, Transvaal, South Africa: Precambrian Research, v. 18, p. 237–260.

Layer, P. W., 1986, Archean paleomagnetism of southern Africa [Ph.D. thesis]:

Stanford, California, Stanford University, 397 p.
Layer, P. W., Kröner, A., and York, D., 1992, Pre-3000 Ma thermal history of the Archean Kaap Valley pluton, South Africa: Geology, v. 20, p. 717–720.
López-Martínez, M., York, D., Hall, C. M., and Hanes, J. A., 1984, Oldest reliable $^{40}Ar/^{39}Ar$ ages for terrestrial rocks: Barberton Mountain komatiites: Nature, v. 307, p. 352–354.
Lowe, D. R., 1992, Probable non-biological origin of pre-3.2 Ga-old "stromatolites" in the Barberton and Pilbara Greenstone Belts: Geological Society of America Abstracts with Programs, v. 24, no. 7, p. A137.
Lowe, D. R., 1994a, The abiological origin of described stromatolites older than 3.2 Ga: Geology, v. 22, p. 387–390.
Lowe, D. R., 1994b, Accretionary history of the Archean Barberton Greenstone Belt (3.55–3.22 Ga), southern Africa: Geology, v. 22, p. 1099–1102.
Lowe, D. R., and Byerly, G. R., 1984, The formation of chrome-mica-bearing alteration zones in the Onverwacht Group, South Africa, by early Archean weathering: Geological Society of America Abstracts with Programs, v. 16, p. 579.
Lowe, D. R., and Byerly, G. R., 1986a, Early Archean silicate spherules of probable impact origin, South Africa and Western Australia: Geology, v. 14, p. 83–86.
Lowe, D. R., and Byerly, G. R., 1986b, Archean flow-top alteration zones formed initially in a low-temperature sulphate-rich environment: Nature, v. 324, p. 245–248.
Lowe, D. R., and Knauth, L. P., 1977, Sedimentology of the Onverwacht Group (3.4 billion years), Transvaal, South Africa, and its bearing on the characteristics and evolution of the early Earth: Journal of Geology, v. 85, p. 699–723.
Lowe, D. R., Byerly, G. R., Ransom, B. L., and Nocita, B. R., 1985, Stratigraphic and sedimentological evidence bearing on structural repetition in Early Archean rocks of the Barberton Greenstone Belt, South Africa: Precambrian Research, v. 27, p. 165–186.
Lowe, D. R., Byerly, G. R., and Kröner, A., 1989a, Relationship between episodic dacitic volcanism and tonalitic plutonism in the Archean Barberton Greenstone Belt (BGB), South Africa: Eos (Transactions, American Geophysical Union), v. 70, p. 1391.
Lowe, D. R., Byerly, G. R., Asaro, F., and Kyte, F., 1989b, Geological and geochemical record of 3400-million-year-old terrestrial meteorite impacts: Science, v. 245, p. 959–962.
Nocita, B. R., 1986, Sedimentology and stratigraphy of the Fig Tree Group, west limb of the Onverwacht anticline, Barberton Greenstone Belt, South Africa [Ph.D. dissertation]: Baton Rouge, Louisiana State University, 169 p.
Nocita, B. R., 1989, Sandstone petrology of the Archean Fig Tree Group, Barberton Greenstone Belt, South Africa: Tectonic implications: Geology, v. 17, p. 953–956.
Nocita, B. R., and Lowe, D. R., 1990, Fan-delta sequence in the Archean Fig Tree Group, Barberton Greenstone Belt, South Africa: Precambrian Research, v. 48, p. 375–393.
Paris, I. A., 1985, The geology of the farms Josefsdal, Dunbar and part of Diepgezet in the Barberton Greenstone Belt [Ph.D. thesis]: Johannesburg, University of the Witwatersrand, 239 p.
Paris, I. A., 1986, Polyphase thrust tectonics in the Barberton Greenstone Belt: Lunar and Planetary Institute Technical Report No. 86–10, 165 p.
Philpot, H. G., Tomkinson, M. J., von Aswegem, G. M., and Reid, K., 1988, Field trip to investigate stratigraphic and structural relationships in the area around Princeton Mine, Barberton Mountain Land, *in* Tregoning, T. D., Tomkinson, M. J., and Philpot, H. G., eds., Deformation and mineralization in the Archaean of Southern Africa: Barberton Mountain Land Branch, Geological Society of South Africa, Abstracts and Guidebook, p. 60–65.
Pyke, D. R., Naldrett, A. J., and Ecktrand, O. R., 1973, Archaean ultramafic flows in Munro Township, Ontario: Geological Society of America Bulletin, v. 84, p. 955–978.
Ramsay, J. G., 1963, Structural investigations in the Barberton Mountain Land, eastern Transvaal: Geological Society of South Africa Transactions, v. 66, p. 353–401.
Ransom, B. L., 1987, The paleoenvironmental, magmatic, and geologic history of the 3,500 Myr Kromberg Formation, west limb of the Onverwacht anticline, Barberton Greenstone Belt, South Africa [M.S. thesis]: Baton Rouge, Louisiana State University, 103 p.
Reimer, T. O., 1967, Die Geologie der Stolzburg Synklinale im Barberton Bergland (Transvaal-Sudafrika)[M.Sc. thesis]: Frankfurt, Goethe Universitat, 103 p.
Reimer, T. O., 1975, Untersuchungen uber Abtragung, Sedimentation und Diagenese im fruhen Prakambrium am Beispiel der Sheba-Formation (Sudafrika): Geologisches Jahrbuch, Reihe B, v. 17, 108 p.
Reimer, T. O., 1983, Pseudo-oolites in rocks of the Ulundi Formation, lower part of the Archaean Fig Tree Group (South Africa): Precambrian Research, v. 20, p. 375–390.
Reimer, T. O., Condie, K. C., Schneider, G., and Georgi, A., 1985, Petrography and geochemistry of granitoid and metamorphite pebbles from the early Archaean Moodies Group, Barberton Mountainland/South Africa: Precambrian Research, v. 29, p. 383–404.
SACS (South African Committee for Stratigraphy), 1980, Stratigraphy of South Africa: Part I: Lithostratigraphy of the Republic of South Africa, South West Africa/Namibia and the Republics of Bophuthatswana, Transkei, and Venda: Geological Survey of South Africa Handbook 8, 690 p.
Smith, A. J., 1981, The geology of the farms Hooggenoeg 731JT and Avontuur 721JT, southwest Barberton Greenstone Belt [B.Sc. thesis]: Johannesburg, University of the Witwatersrand.
Stanistreet, I. G., De Wit, M. J., and Fripp, R. E. P., 1981, Do graded units of accretionary spheroids in the Barberton greenstone belt indicate Archaean deep water environment?: Nature, v. 293, p. 280–284.
Steyn, M. V. R., 1965, Basal rocks of the Swaziland System in the Steynsdorp Valley and Fairview areas of the Barberton Mountain Land: Geological Society of South Africa, Symposium on the Geology of the Barberton Mountain Land, 37 p. (unpublished).
Tegtmeyer, A. R., and Kröner, A., 1987, U-Pb zircon ages bearing on the nature of Early Archaean greenstone belt evolution, Barberton Mountainland, southern Africa: Precambrian Research, v. 36, p. 1–20.
Van Eeden, O. R., 1941, Die geologie van die Shebarante en omstreke, distrik Barberton [Ph.D. thesis]: Stellenbosch, University of Stellenbosch.
Van Niekerk, C. B., and Burger, A. J., 1978, The age of the Moodies conglomerate boulders: Geological Society of South Africa Special Publication 4, p. 99–106.
Viljoen, M. J., and Viljoen, R. P., 1969a, An introduction to the geology of the Barberton granite-greenstone terrain: Geological Society of South Africa Special Publication 2, p. 9–28.
Viljoen, M. J., and Viljoen, R. P., 1969b, The geology and geochemistry of the lower ultramafic unit of the Onverwacht Group and a proposed new class of igneous rocks: Geological Society of South Africa Special Publication 2, p. 55–86.
Viljoen, M. J., Viljoen, R. P., Smith, H. S., and Erlank, A. J., 1983, Geological, textural and geochemical features of komatiitic flows from the Komati Formation, *in* Anhaeusser, C. R., ed., Contributions to the geology of the Barberton Mountain Land: Geological Society of South Africa Special Publication 9, p. 1–20.
Viljoen, R. P., and Viljoen, M. J., 1969, The geological and geochemical significance of the upper formations of the Onverwacht Group: Geological Society of South Africa Special Publication 2, p. 113–152.
Visser, D. J. L., 1956, The geology of the Barberton area: Geological Survey of South Africa Special Publication 15, 254 p.
Williams, D. A. C., and Furnell, R. G., 1979, A reassessment of part of the Barberton type area: Precambrian Research, v. 9, p. 325–347.
Wilson, A., 1980, Geological map of Swaziland: Sheet 2531CD and part of 2531CB, 2nd edition: Mbabane, Swaziland Geological Survey and Mines Department, scale 1:50,000.
Wuth, M., 1980, The geology and mineralization potential of the Oorschot-Weltevreden schist belt south-west of Barberton—Eastern Transvaal [M.Sc. thesis]: Johannesburg, University of the Witwatersrand, 185 p.

MANUSCRIPT ACCEPTED BY THE SOCIETY MARCH 26, 1998

Printed in U.S.A.

Geological Society of America
Special Paper 329
1999

Structural divisions and development of the west-central part of the Barberton Greenstone Belt

Donald R. Lowe
Department of Geological and Environmental Sciences, Stanford University, Stanford, California 94305
Gary R. Byerly
Department of Geology and Geophysics, Louisiana State University, Baton Rouge, Louisiana 70803
Christoph Heubeck*
Department of Geological and Environmental Sciences, Stanford University, Stanford, California 94305

ABSTRACT

The western part of the Barberton Greenstone Belt (BGB) is subdivided into four fault- and intrusion-bounded domains, termed the Southern, West-Central, East-Central, and Northern Domains, each having a distinctive stratigraphy and tectonic history. Their evolution is described in terms of five periods of deformation: D_1, deformation during accumulation of the upper part of the Onverwacht Group; D_2, late to post–Fig Tree deformation; D_3, early Moodies deformation; D_4, late Moodies to early post-Moodies deformation; and D_5, late post-Moodies deformation.

The Southern Domain (SD), including the southernmost parts of the BGB, is made up largely of volcanic rocks of the Onverwacht Group intruded by tonalite-trondhjemite-granodiorite (TTG) plutons at about 3,445 Ma. An initial period of faulting (D_1) accompanied or closely followed TTG intrusion. The large folds that form the framework of the SD, including the Onverwacht anticline and Kromberg syncline, formed initially during D_2, during and following Fig Tree sedimentation from about 3,260 to 3,226 Ma. Additional folding, tightening of D_2 folds, and thrust faulting occurred in post-Moodies time, during D_4 and D_5. The Komati fault appears to represent a folded thrust fault along which less metamorphosed, marginal parts of the Onverwacht volcanic platform were thrust onto the 3,445-Ma TTG intrusive complex and its roof rocks, probably during D_2.

The West-Central Domain (WCD) lies north of the SD, between the Granville Grove and Inyoka faults on the west limb of the Onverwacht anticline. It includes two stratigraphic assemblages separated by a folded D_4 thrust fault, here named the 24-Hour Camp fault (TCF). The footwall assemblage consists of subvertical rocks of the Mendon Formation (Onverwacht Group) and Mapepe Formation (Fig Tree Group) repeated by a series of faults that formed during D_2 as part of a south- to southeast-verging fold-and-thrust belt. The hanging-wall assemblage includes rocks of the Auber Villiers Formation (Fig Tree Group) and paraconformably overlying quartzose strata of the Moodies Group. Early Moodies sedimentation was locally accompanied by normal faulting (D_3). The TCF formed during early post-Moodies shortening (D_4) within a second south- to southeast-verging fold and thrust belt. D_5 involved

*Present address: Amoco, P.O. Box 3092, Houston, Texas 77253.

Lowe, D. R., Byerly, G. R., and Heubeck, C., 1999, Structural divisions and development of the west-central part of the Barberton Greenstone Belt, in Lowe, D. R., and Byerly, G. R., eds., Geologic Evolution of the Barberton Greenstone Belt, South Africa: Boulder, Colorado, Geological Society of America Special Paper 329.

regional northwest-directed thrusting (D_{5a}), fold tightening and rotation of planar structures to the vertical or subvertical (D_{5b}), and oblique shortening (D_{5c}).

The East-Central Domain (ECD) includes most of the southeastern part of the BGB southeast of the Mbema and Kromberg faults. It is dominated by a northwest-verging D_4 fold train of synclines in Moodies and Fig Tree rocks separated by and apparently in fault or unconformable contact with narrow faulted anticlines in Fig Tree and Onverwacht rocks. D_2 is reflected in folding and erosion along the trend of the Onverwacht anticline near the northwestern margin of the ECD and in clastic sedimentation in the Mapepe Formation to the southeast. The amount of deformation during D_2 and D_3 in the ECD is incompletely resolved.

The Northern Domain (ND) lies along the northern margin of the BGB, north of the Inyoka fault. It includes footwall and hanging-wall assemblages separated by a D_4 thrust fault. The footwall assemblage includes altered komatiites of the Onverwacht Group overlain by clastic deep-water Fig Tree formations. It is characterized by tight to isoclinal synclines in Fig Tree strata separated by narrow faulted anticlines of Onverwacht serpentinites. Initial deformation probably occurred during D_2. The hanging-wall assemblage includes, in stratigraphic order, sheared serpentinites and cherts at the top of the Weltevreden Formation (Onverwacht Group), conformably overlying rocks of the Schoongezicht Formation (Fig Tree Group), and paraconformably overlying clastic strata of the Moodies Group. Hanging-wall Fig Tree and Moodies strata were probably deposited in one or more basins formed in part during D_3 extension. The hanging wall was emplaced over the footwall during D_4, when the ND was part of a south- to southeast-verging fold-and-thrust belt. The large, asymmetric tight to isoclinal synclines that dominate hanging-wall structures formed during D_4. All previously formed folds were tightened and rotated during northwestward D_{5a} thrusting. The ND is divided by large D_{5c} strike-slip faults that formed during heterogeneous shortening of the sedimentary and volcanic sequence against the northern TTG plutons.

INTRODUCTION

Although the Barberton Greenstone Belt (BGB) has served as the basis of a number of models of greenstone-belt development and early crustal evolution, its overall structure and tectonic history remain conjectural. Until recently, structural investigations were focused on areas near its periphery and did not yield an integrated picture of the makeup and evolution of the belt as a whole. Ramsay (1963), Anhaeusser (1969, 1972, 1975, 1976, 1984), Gay (1969), and Fripp et al. (1980) outlined the late structural development of the Eureka and Ulundi synclines, the Jamestown Schist Belt, and adjacent areas in the northern part of the BGB. Lamb (1984a, b), Jackson and Robertson (1983), and Jackson et al. (1987) investigated areas along the southeastern margin of the belt. The structure of the central portion of the BGB, although partially mapped by a number of investigators (Heinrichs, 1980, and unpublished map, 1969; Reimer, unpublished map, 1980; de Wit, 1982, 1983; de Wit, et al., 1983, 1987a; Paris, 1985; Lowe et al., 1985; Nocita, 1986; Daneel, 1987; Ransom, 1987; Hose, 1990; de Ronde et al., 1991; Heubeck and Lowe, 1994a and b; and many others), remains controversial. While some investigators have emphasized the role of vertical movements in greenstone belt evolution, possibly related to the diapiric emplacement of surrounding batholiths (Anhaeusser, 1975, 1984), most recent workers have recognized thrust and nappe complexes and have interpreted the BGB as a zone of significant crustal shortening (Ramsay, 1963; de Wit, 1982, 1983; Jackson and Robertson, 1983; Lamb, 1984a, b; Lowe et al., 1985; Paris, 1985; de Wit et al., 1987a, b, 1992; de Ronde and de Wit, 1994; Lowe, 1994; Heubeck and Lowe, 1994b).

This report outlines the structural and tectonic implications of a program of geologic mapping and stratigraphic, sedimentological, and petrologic study in the western part of the BGB (Figs. 1 and 2) between 1977 and 1993. The BGB is divided into four structural and stratigraphic domains, here termed the Southern (SD), West-Central (WCD), East-Central (ECD), and Northern (ND) Domains (Fig. 1). The evolution of each domain and of the BGB as a whole is presented in terms of five intervals of deformation: (D_1) late Onverwacht deformation; (D_2) Fig Tree and early post–Fig Tree, pre-Moodies deformation; (D_3) early Moodies deformation, and (D_4 and D_5) late to post-Moodies deformation.

Because of the structural and stratigraphic complexity of the BGB, pervasive metasomatic alteration, lack of paleontological age control, and lack or paucity of high-precision zircon dating in many key areas, the structural and tectonic scenario outlined in this discussion is speculative. It represents our "best-guess" interpretation in many instances, and we endeavor to point out which arguments we consider particularly uncertain and the reasoning behind our choice of interpretations where there are several alternatives.

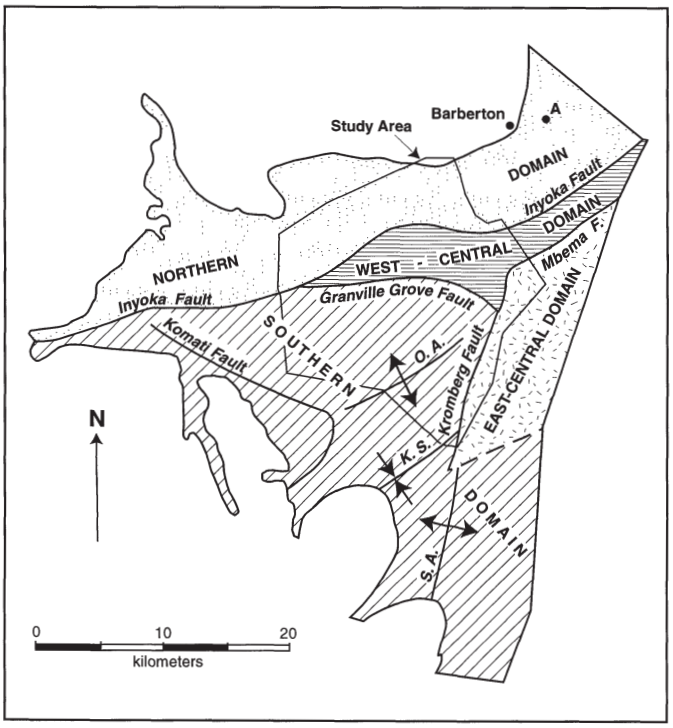


Figure 1. Generalized map of the southern part of the Barberton Greenstone Belt showing the locations of the structural domains and some of the large structural features discussed in the present paper. Symbols: O.A., Onverwacht anticline; K.S., Kromberg syncline; S. A., Steynsdorp anticline. Locality A marks the southern tip of the Ulundi syncline and the location of Figure 3.

SOUTHERN DOMAIN

Location and stratigraphy

The Southern Domain (SD; Fig. 1) includes areas along the southern and southeastern margins of the BGB underlain mainly by volcanic rocks of the Onverwacht Group. The supracrustal sequence forms a more-or-less continuous outcrop belt from the westernmost part of the Onverwacht anticline, around the Kromberg syncline, and through the Steynsdorp anticline (Fig. 1). In the Onverwacht anticline, Onverwacht rocks are intruded by tonalite-trondhjemite-granodiorite (TTG) rocks of the Badplaas, Stolzburg, Theespruit, Doornhoek, and related plutons (Anhaeusser et al., 1981), which have intrusion ages between 3,448 ± 4 and 3,437 ± 5 Ma (Armstrong et al., 1990; Kröner et al., 1991; Kamo and Davis, 1991, 1994). Comagmatic felsic volcanic units in the Hooggenoeg Formation range in age from 3,453 ± 6 (Armstrong et al., 1990) to 3,438 ± 6 Ma (Kröner and Todt, 1988). The entire magmatic episode probably lasted from about 3,457 to 3,437 Ma and is here referred to as the 3,445-Ma magmatic event.

The northern boundary of the SD is drawn at the Granville Grove fault and its eastern boundary along the Kromberg fault (Fig. 1). BGB rocks along the southeastern margin of the belt in Swaziland (Anhaeusser et al., 1981; Lamb, 1984a) may be correlative with those in the SD but were not investigated during the present study.

Stratigraphic integrity of the Southern Domain

Although Viljoen, M. J., and Viljoen (1969a, b) and Viljoen, R. P., and Viljoen (1969) regarded the Swaziland Supergroup as a continuous stratigraphic sequence, later studies have demonstrated that the classic sections around the Onverwacht anticline are cut by numerous faults (Williams and Furnell, 1979; de Wit, 1982, 1983; Lowe et al., 1985). In the Onverwacht anticline, the Sandspruit and Theespruit Formations are intruded by plutons of the 3,445-Ma TTG suite, are more highly metamorphosed than "overlying" units, and are isolated from them by the Komati fault (Viljoen, M. J., and Viljoen, 1969a, b; de Wit et al., 1983). The Theespruit Formation is a structural melange, cut by numerous large faults, and may include volcanic units as young as the Msauli Chert of the Mendon Formation (de Wit et al., 1983); dacitic volcanic rocks as young as 3,453 ± 6 Ma, equivalent to member H6 of the Hooggenoeg Formation (Armstrong et al., 1990); dacitic agglomerates with ages of 3,531 ± 10 Ma (Armstrong et al., 1990) and 3,511 ± 3 Ma (Kröner et al., 1992); and gneissic blocks as old as 3,538 ± 6 Ma (Armstrong et al., 1990; Kamo and Davis, 1994). It seems likely that the Komati fault is an important break within the stratigraphic sequence in the Onverwacht anticline along which the less metamorphosed Komati through Mendon succession has been juxtaposed with the partly correlative and partly older, metamorphosed and intruded Sandspruit and Theespruit rocks that formed the roof sequence to the 3,445-Ma TTG intrusive suite.

Although faults and folds locally disrupt, repeat, and remove portions of the Onverwacht and Fig Tree succession in the Southern Domain, strata of the Komati, Hooggenoeg, Kromberg, Mendon, and Mapepe Formations north of the Komati fault and south of the Granville Grove fault appear to form a continuous, largely intact stratigraphic sequence between 8 and 10 km thick (Lowe et al., 1985; Lowe and Byerly, this volume, Chapter 1). In contrast, de Wit (1982, 1983), de Wit et al. (1983, 1987a), Paris (1985), Armstrong et al. (1990), and de Ronde and de Wit (1994) have interpreted this sequence as a tectonic complex assembled by structural stacking and repetition of a section estimated to range from as little as 500 m (Paris, 1985) to 3 or 4 km thick (de Wit, 1982).

A number of observations argue against this interpretation (Lowe et al., 1985). An increasing number of high-precision single-zircon age dates demonstrate that units north of the Komati fault and south of the Granville Grove fault young progressively to the north (Armstrong et al., 1990; Kröner et al., 1991; Kamo and Davis, 1991, 1994; Byerly et al., 1993, 1996). Many of the specific interpretations of repetition within this succession and the suggested age equivalence of Onverwacht and Fig Tree units (de Wit, 1982; de Wit et al., 1983, 1987a) have been invalidated by these geochronological data. Available geochronological data indicate that these strata form a

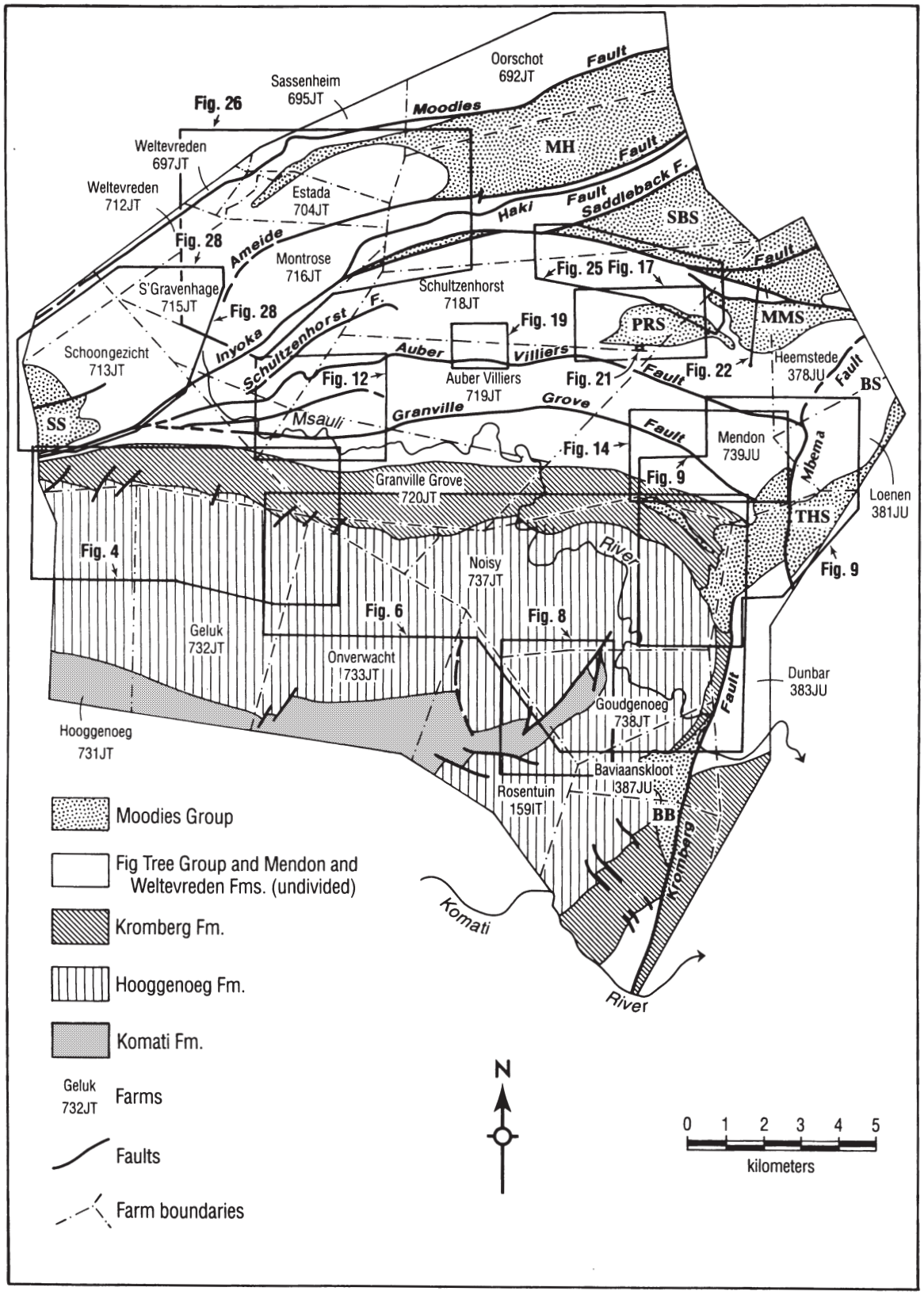


Figure 2. General geologic map of the study area and location map for the more detailed maps in this report. Symbols from south to north: BB, Baviaanskloof Block; THS, The Heights syncline; BS, Barite syncline; MMS, Maid-of-the-Mists syncline; PRS, Powerline Road syncline; SBS, Saddleback syncline; SS, Stolzburg syncline; MH, Moodies Hills.

younging-upward sequence and provide no indication of repetition or out-of-sequence stacking.

De Wit et al. (1987a) and de Ronde and de Wit (1994) interpret the Kromberg Formation in both the Onverwacht anticline and Kromberg syncline as an allochthonous sheet that is structurally juxtaposed against rocks of the Hooggenoeg Formation. The intervening bedding-parallel fault is drawn at the contact between our unit H6, felsic volcaniclastic strata at the top of the Hooggenoeg Formation, and K1, the Buck Reef Chert and its equivalents. Felsic volcanic rocks of H6 have yielded consistent single-crystal zircon ages between 3,456 ± 18 Ma and 3438 ± 6 Ma, centering on about 3,445 Ma (Kröner et al., 1991, 1992; Armstrong et al., 1990; Kamo and Davis, 1991, 1994). A thin tuff at the base of the Kromberg Formation on the west limb of the Onverwacht anticline has yielded an age of 3,416 ± 5 Ma (Kröner et al., 1991; Byerly et al., 1996) and a tuffaceous band in the Footbridge Chert, at the top of the formation along the Komati River, has been dated at 3,334 ± 3 Ma (Byerly et al., 1996). A felsic tuff in the Mendon Formation, probably in M2c or M3c, has provided an age of 3,298 ± 3 Ma (Byerly et al., 1996). These ages are consistent with this succession representing an intact stratigraphic sequence.

On the west limb of the Onverwacht anticline, the Buck Reef chert at the base of the Kromberg Formation contains detrital felsic volcaniclastic material eroded from the underlying H6 member of the Hooggenoeg Formation (Lowe and Fisher Worrell, this volume, Chapter 7), and normal faults associated with the formation of small, evaporite-filled extensional half grabens during deposition of the lowest part of the Buck Reef Chert cut both the underlying Hooggenoeg felsic volcaniclastic rocks and extend for 100–200 m upward into the overlying Buck Reef Chert before dying out (Lowe and Fisher Worrell, this volume, Chapter 7). In addition, mafic lapilli tuffs and lapillistones overlying the Buck Reef Chert contains abundant accidental blocks of the Buck Reef Chert. These features indicate that the uppermost, felsic volcanic member of the Hooggenoeg Formation and the lower members of the Kromberg Formation form a continuous, uninterrupted stratigraphic succession and are not juxtaposed across a regional bedding-parallel fault.

The thin, bedding-parallel zones mapped as syndepositional faults or glide planes by de Wit (1982, 1983) and characterized as quartz-carbonate-talc-fuchsite schist/gneiss zones (e.g., de Wit, 1983) and flaser-banded tectonites (de Wit, 1986) have also been interpreted to have formed through nontectonic silica, carbonate, and potash metasomatism of komatiitic volcanic rocks (Lowe et al., 1985; Lowe and Byerly, 1986; Duchac, 1986; Duchac and Hanor, 1987; Hanor and Duchac, 1990). Such zones are numerous throughout the volcanic portion of the Barberton Greenstone Belt and may include examples that are strictly of metasomatic origin, others that are of tectonic origin, and others where tectonic features have been superimposed on metasomatic features, or the reverse.

Many of the zones mapped by de Wit (1982, 1983, 1986) as faults or glide planes occur at the tops of komatiitic flow sequences, immediately below the capping cherts. Virtually every komatiitic flow sequence in the Onverwacht Group, including the Komati Formation below the Middle Marker (H1), komatiitic units in the Hooggenoeg Formation (H3 and H4), and komatiitic units M1, M2, M3, and M4 in the Mendon Formation, are topped by flow-top alteration units of this type immediately below the capping cherts. Zones of this type were studied by Lowe and Byerly (1986), Duchac (1986), Duchac and Hanor (1987), and Hanor and Duchac (1990) and interpreted to be of metasomatic, not tectonic origin. They are characterized by sets of crudely bedding parallel, anastomosing silica and carbonate veinlets, which give the rock its gneissic or schistose fabric.

The silica veinlets in these zones commonly show evidence of having formed early, at shallow depths, by an extensional crack-seal process unrelated to shearing (Lowe et al., 1985, Fig. 6b; Lowe and Byerly, 1986, Fig. 3a; Hanor and Duchac, 1990). Evidence for early, pretectonic vein formation is particularly well displayed in the ND along the frontal zone of the BGB in the southern part of the Ulundi syncline and in the Moodies Hills (Figs. 1 and 2). In these areas, silicified and veined komatiites are capped by 2 to 20 m of black and banded chert marking the top of the Onverwacht Group that include at the top a 20-cm-thick impact-produced spherule bed (Lowe et al., 1989a) succeeded by more than 1,000 m of ferruginous and clastic sedimentary rocks. Black chert dikes, formed by the downward flow of soft carbonaceous sediment containing loose spherules, extend from the chert into the underlying altered komatiites, truncating the silica veinlets (Fig. 3). The dikes lack ferruginous and clastic debris from the immediately overlying Fig Tree Group. These features suggest that the dikes formed shortly after spherule deposition and after veinlet formation in the komatiites but before the start of Fig Tree clastic sedimentation. The silica veinlets must thus have formed in the upper part of the komatiite flow sequence when there was less than 10 m of overlying soft sedimentary material and therefore cannot represent thrust faults or shear zones

Similar unsheared black chert dikes, lacking spherules, extend downward from chert layers and crosscut altered komatiite and silica veinlets at the top of the underlying komatiite flow sequence in the Mendon Formation in both the type locality of the Msauli Chert (Lowe, this volume, Chapter 9) and in the central part of the belt, near the localities studied by Duchac (1986), Duchac and Hanor (1987), and Hanor and Duchac (1990). These crosscutting chert dikes were sourced by soft-sediment layers that immediately overlay the altered komatiites and indicate that the silica veinlets which give these zones their characteristic gneissic texture formed within a few meters or 10s of meters of the sediment-water interface.

The cherts overlying the alteration zones also belong to a distinctive class of sedimentary units that contain abundant silicified fine komatiitic ash and dust. The Middle Marker, H1; cherts above the alteration zones at the tops of komatiitic units in the Hooggenoeg Formation, H3c and H4c; and cherts above komatiitic volcanic units in the Mendon Formation, including M1c (the Msauli Chert), M2c, and M3c, contain accretionary lapilli and volcaniclastic layers that have compositions indicating formation from

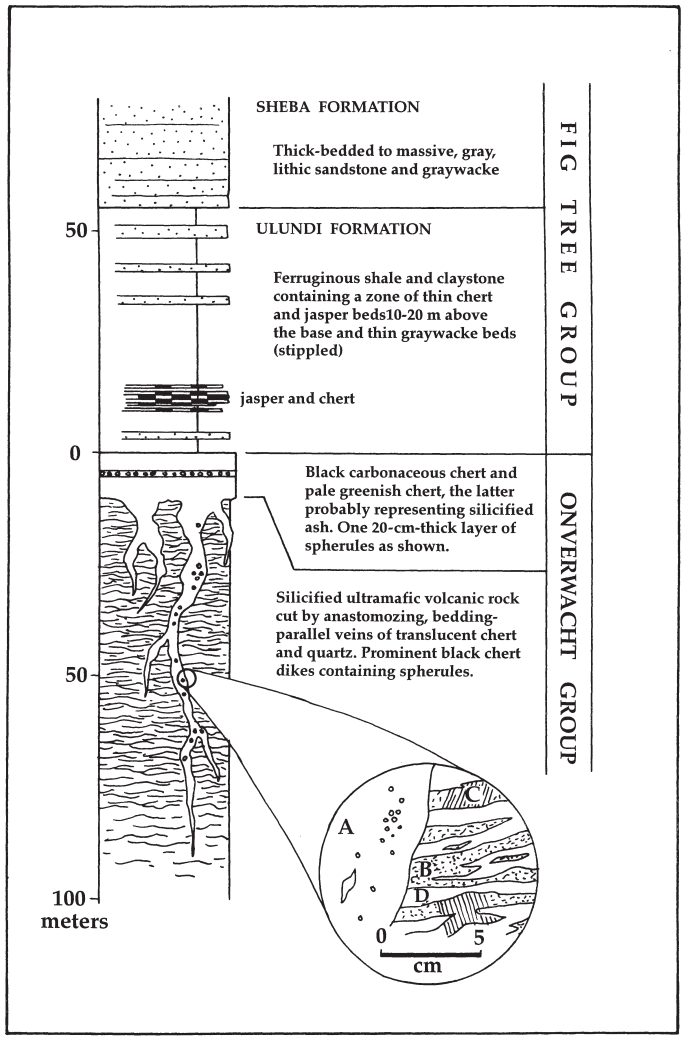


Figure 3. Sketch of black chert dikes containing isolated spherules from the Florence and Devon Mine at the southwestern tip of the Ulundi syncline (location A, Fig. 1). The dikes were formed by the downward injection of soft carbonaceous sediments and loose, unlithified spherules that were deposited on top of the ultramafic volcanic sequence and which are now represented by chert and spherule beds in the uppermost Onverwacht Group. Mud and sand, present in the overlying Fig Tree Group, are not present in the dikes. The dikes crosscut altered and veined komatiite that underlies the chert beds. These alteration zones have been widely interpreted to mark regional shear zones, but the stratigraphic relationships suggest that they formed before before lithification of the carbonaceous sediments and spherule beds and probably before deposition of the overlying Fig Tree clastic strata. Detailed sketch shows chert dike (A) crosscutting and truncating altered komatiite (B), some of which shows olivine spinifex (C), and anastomozing bedding-parallel chert/quartz veins (D).

komatiitic ash (Lowe, this volume, Chapters 3 and 9). Cherts overlying basaltic or felsic volcanic rocks generally lack such debris. It seems clear that the sediments represented by these cherts were deposited in the late stages of major komatiitic eruptions, in large part from volcaniclastic komatiitic debris. If the intervening alteration zones represent major thrust faults and glide planes, these faults are not only restricted to the upper few meters of komatiitic flow units, they have, in virtually every instance, fortuitously juxtaposed footwall komatiitic volcanic rocks and hanging-wall silicified komatiitic tuffs. It seems more likely that the komatiitic eruptive sequences were capped by late-stage fine komatiitic tuffs and biogenic sediments after lava effusion had ceased. Syndepositional and later metasomatic alteration was localized along this contact, both because of the exposure of the flow top to long-term interaction with seawater during deposition and because the cherts formed significant permeability barriers to subsurface fluid movement and would have thus served to localize alteration at flow tops after burial. The presence of dikes formed by the downward movement of soft-sediments into and through the underlying alteration zones confirms that the alteration zones formed in large part during the accumulation of the immediately overlying sediments. This interpretation is inconsistent with the scenario that these alteration zones formed as major faults.

There are many areas where these flow-top alteration zones, which now lie at the contacts of ductile serpentinites and brittle chert units, have been sites of later shearing and where later shear fabrics are superimposed on the original predeformation textures. In other areas, however, later shear fabrics and structures are absent, and altered komatiite between the veinlets shows unsheared primary magmatic features, including silicified spinifex and cumulus textures (Lowe et al., 1985, Fig. 6a; Paris et al., 1985, Fig. 7; Hanor and Duchac, 1990, Fig. 5). Where cut by later faults or in areas of widespread penetrative deformation, such as in the lower Hooggenoeg and Komati Formations on the east limb of the Onverwacht anticline, the metasomatic fabrics show overprinting by simple shear. Within such areas, all rocks show evidence of shearing, including both the silicified komatiites (de Wit, 1986, Figs. 1c and d) and surrounding sedimentary and less altered volcanic rocks.

There are areas where similar alteration zones containing silica and/or carbonate veinlets are developed at stratigraphic positions not coincident with the tops of komatiitic volcanic units. Along the Komati River, a thick zone of carbonate metasomatism occurs in the upper part of the Kromberg Formation (Viljoen, R. P., and Viljoen, 1969, Fig. XIb). The rock consists of anastomosing veins of chert separated by platy, tabular lenses of iron-rich carbonate containing patchy chlorite. Similar rocks are present at a number of positions in the Kromberg Formation within units of mafic lapillistone. Figure XIa of Viljoen, R. P., and Viljoen (1969) shows a very similar rock, but with more continuous silica and carbonate bands and with well-preserved cross-stratification. These units appear to have formed mainly by the silica and carbonate metasomatism of mafic lapilli tuffs and lapillistones, although the possibility that these more ductile units also served as the loci of shearing cannot be discounted.

The structural and stratigraphic relationships in this extremely complex terrain are likely to remain controversial until considerably more careful structural, stratigraphic, and geochronological work has been done. Based on our studies to date, we suggest that

the Komati, Hooggenoeg, Kromberg, and Mendon Formations of the Onverwacht Group and the Mapepe Formation of the Fig Tree Group on the west limb and in the hinge zone of the Onverwacht anticline form an intact, younging-upward stratigraphic sequence 8 to 10 km thick. Faults representing a number of deformational events can be recognized by the truncation and offset of lithologic units and by the development of localized shear zones, tectonic breccias, and truncated folds. Similarly, although faults occur within the sequence on the east limb of the Onverwacht anticline (west limb of the Kromberg syncline), we have found no evidence that the stratigraphic sequence above the Komati Formation is interrupted, truncated, attenuated, or repeated by major bedding parallel thrust faults as suggested by de Wit et al. (1987a) and de Ronde and de Wit (1994, Fig. 4). We have not investigated rocks below the Hooggenoeg Formation on the east limb of the Onverwacht anticline.

Structures and deformation in the Southern Domain

D_1: Onverwacht deformation. Accumulation of the Komati Formation and members H1–H5 of the Hooggenoeg Formation in the SD was marked by the quiet effusion of mafic and komatiitic lavas to form a large low-relief volcanic edifice (Lowe and Knauth, 1977; Lowe, 1980, 1982, this volume, Chapter 3). In contrast, dacitic magmatism represented by member H6 of the Hooggenoeg Formation and intrusion of comagmatic 3,445-Ma TTG plutons were accompanied by local and perhaps widespread deformation. On the west limb of the Onverwacht anticline, H6 consists largely of massive dacitic intrusive rock overlain by a thin cover of volcaniclastic conglomerate and sandstone (Figs. 4, 5, and 6). This intrusion/dome (Viljoen, M. J., and Viljoen, 1969b; Smith, 1981; de Wit et al., 1987b) crops out for 9–10 km along strike, reaches 2.5 km in thickness, and contains large, detached, rotated masses of basaltic and komatiitic volcanic rock of Hooggenoeg members H4 and H5. It is flanked by coarse volcaniclastic breccia and conglomerate derived by syn- and post-emplacement erosion of the intrusion/dome and its roof rocks. Exposed rocks appear to represent the edge of a shallow mushroom-shaped intrusive body and extrusive dome that may have been connected at depth to 3,445-Ma TTG plutons.

Immediately below and extending laterally from the intrusion is a crosscutting zone of shearing and block rotation up to several hundred meters thick, here named the Geluk Disturbed Zone (GDZ). The GDZ is made up largely of overturned slabs and blocks of Hooggenoeg members H3 to H5. The lower contact of the GDZ is a fault, the Geluk fault (GF), that sharply truncates strata in the underlying Onverwacht Group (Figs. 4, 5, and 6). It climbs gently up-section toward both eastern and western margins of the intrusion and extends beyond the intrusion to the east as a fault overlain structurally by a zone of rotated and overturned blocks (Figs. 5, 6, and 7). Although blocks in the GDZ are dislodged and rotated, their stratification shows systematic variations in attitude along the trace of the GF. After restoration of the regional subvertical bedding to the horizontal by simple rotation about regional strike, the primary dip of bedding within the rotated blocks changes progressively from southeast to south to southwest from west to east, suggesting that the GF may have formed as a south-dipping thrust or reverse fault (Fig. 5). Rocks as young as the flanking epiclastic units of H6 are involved in faulting, but nowhere have we seen faults of the GDZ cut rocks of the Kromberg Formation.

A number of small normal faults developed over the intrusive complex during deposition of the basal part of K1, the Buck Reef Chert (Lowe and Fisher Worrell, this volume, Chapter 7). These reflect local extension, perhaps related to cooling and subsidence of the underlying felsic intrusion. The faults die out upward within the Buck Reef Chert, indicating that faulting ceased during deposition of K1.

D_2: Fig Tree deformation. The structural framework of the SD was established by deformation between middle Fig Tree and early Moodies time. The dominant structures in the SD are the Onverwacht anticline and Kromberg syncline. Their fold axes generally plunge 80–90° to the northeast but are locally southwest plunging and the folds are downward facing. The Onverwacht anticline is a tight, upright to steeply inclined, parallel fold in which the west limb strikes roughly east-west and the east limb about N50–60°E. The Kromberg syncline is an isoclinal, upright to steeply inclined, similar fold. Within these two large folds, the Hooggenoeg and Kromberg Formations form a relatively competent, predominantly basaltic and dacitic, chert-bearing layer between incompetent komatiites and serpentinized komatiites of the Komati and Mendon Formations. Fold geometry suggests that these large folds formed, in part, as parallel single-layer buckle folds.

Several large faults cut the Onverwacht anticline in and adjacent to the hinge zone, including the Core fault (Figs. 6, 7, and 8). They show a distribution and sense of displacement suggesting that flexure in the hinge was accommodated in part by brittle fracture and block rotation (Fig. 7). These appear to be accommodation structures reflecting brittle deformation in response to shortening below and extension above the fold's neutral surface accompanied by hinge collapse.

Late fold tightening and hinge collapse caught hinge-thickened masses of serpentinite and komatiite of the Komati Formation in the Onverwacht anticline and of the Mendon Formation in the Kromberg syncline between more competent rocks of the Hooggenoeg-Kromberg layer. Locally, brittle extension in the outer arc of the hinge area appears to have allowed injection of the ultramafic rocks as dikes and sills into the adjacent more brittle layers (Fig. 8). In the Onverwacht anticline, the intrusions extend from the Komati Formation into the overlying lower Hooggenoeg Formation (Fig. 8) whereas in the Kromberg syncline they extend down-section from the Mendon Formation into the upper Kromberg Formation (de Wit et al., 1987a, Fig. 4; de Ronde and de Wit, 1994, Fig. 4). These features and the common development of crosscutting serpentinite bodies in tight or collapsed fold hinges are consistent with the interpretation that many of these intrusions are solid-state tectonic intrusions.

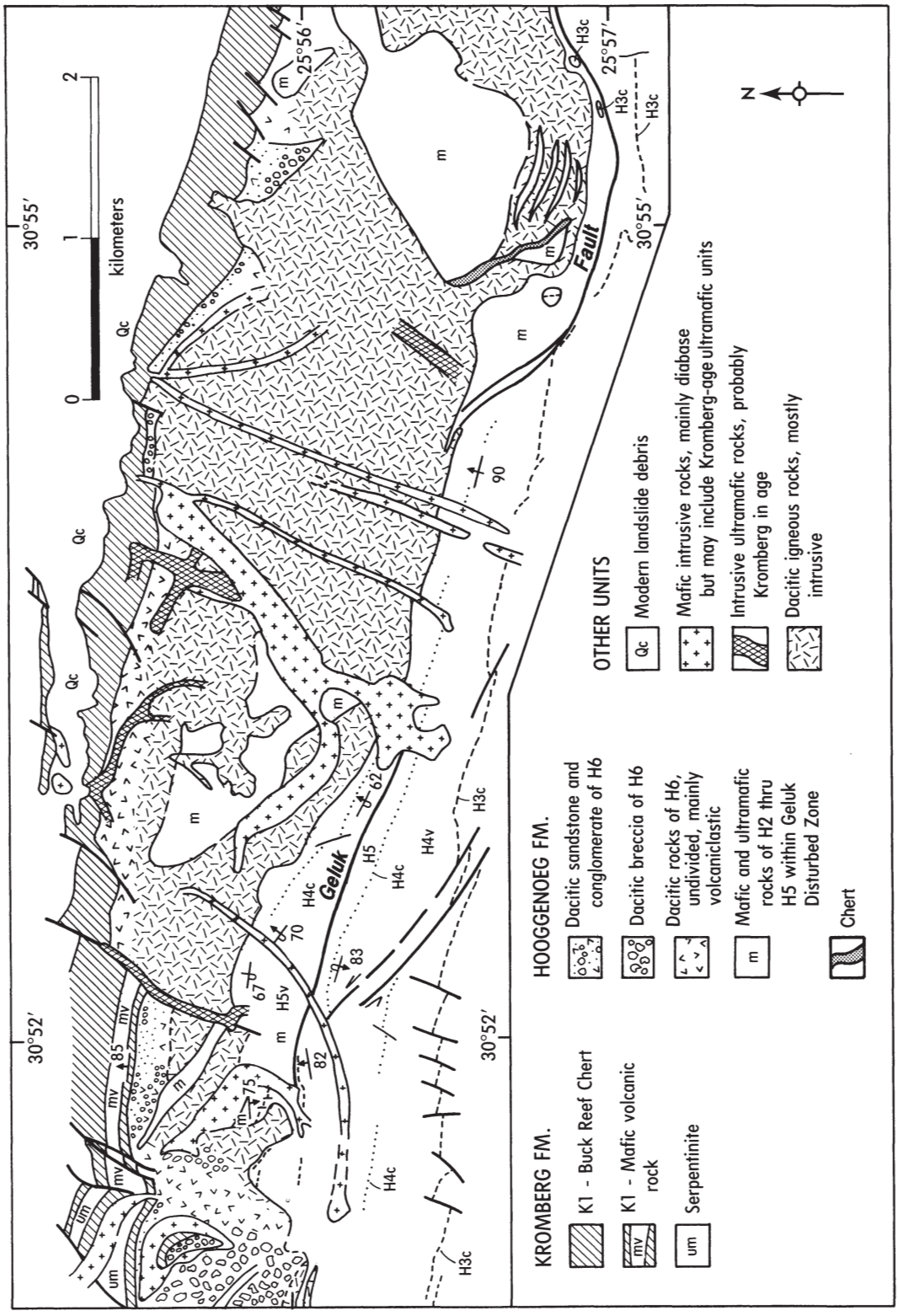


Figure 4. Geologic map of a part of the west limb of the Onverwacht anticline showing the western two-thirds of the felsic intrusion in H6 and its westward transition into breccia. The intrusion is composed of massive plagioclase-phyric intrusive rock and the sedimentary breccia is composed largely of clasts of the same rock. The breccia has been invaded and altered locally by the same intrusive material. The Geluk Disturbed Zone is bounded sharply at its base by the Geluk fault and overlain and truncated by the Buck Reef Chert.

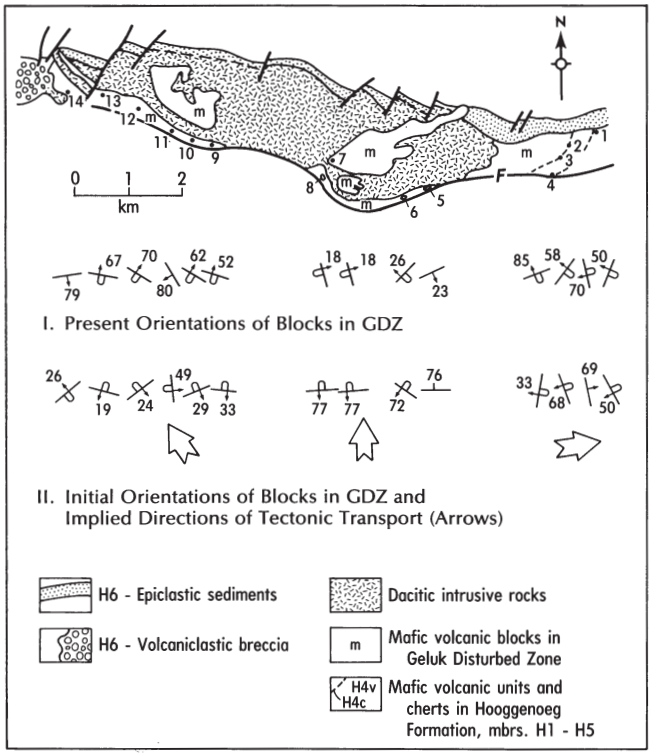


Figure 5. Geology of felsic hypabyssal intrusion in member H6 of the Hooggenoeg Formation, west limb of the Onverwacht anticline. Top: Map of shallow intrusion and surrounding units. F, Geluk fault. Present bedding attitudes of rotated blocks within Geluk Disturbed Zone below intrusion but above Geluk fault (I) are given immediately below numbered map localities for each block. Initial attitudes of rotated blocks (II) obtained by restoring bedding in Hooggenoeg Formation (N77°W, 85°N) to horizontal by simple rotation about strike. Corrections for plunge of Onverwacht anticline, which may not be required, would not alter the radial pattern of structural transport implied by block imbrication.

There are also igneous ultramafic intrusions in the Hooggenoeg Formation, including some in the hinge region of the Onverwacht anticline (de Wit et al., 1987a), but we have not been able to identify the gradational komatiite-to-gabbro-to-basalt relationships described by de Wit et al. (1987a). There are numerous komatiitic volcanic units in the upper part of the Hooggenoeg, the Kromberg, and the Mendon Formations (Lowe and Byerly, this volume, Chapter 1; Vennemann and Smith, this volume, Chapter 5; Byerly, this volume, Chapter 8) and komatiitic dikes and sills lower in the sequence may have served as parts of the feeder systems to these flow units.

The Onverwacht anticline began to form in middle to late Mapepe time (D_2). Lower Mapepe and Onverwacht rocks are parallel and apparently conformable along the west limb of the Onverwacht anticline, and both units are folded around its hinge. The presence of southerly derived clastic units in middle part of the Mapepe Formation along the northern edge of the SD and evidence of middle Mapepe uplift and erosion along the trend of the Onverwacht anticline in the ECD (Heinrichs and Reimer, 1977; Lowe and Nocita, this volume, Chapter 10) suggest that folding was initiated in middle Mapepe time (D_2), probably about 3,240 Ma. However, clastic debris in the Mapepe Formation around the Onverwacht anticline was derived by erosion of underlying parts of the greenstone sequence (Lowe and Nocita, this volume, Chapter 10) with little or no contribution from deep-level metagreenstone and intrusive rocks, which were apparently not exposed at this time.

Moodies Group conglomerates in the hinge zone of the anticline and in the Baviaanskloof Block (Figs. 2 and 9) overlie folded and faulted rocks of the Onverwacht and Fig Tree Groups with angular unconformity (Fig. 9). Traced northward along the east limb toward the hinge, Moodies strata in The Heights syncline (Fig. 9) truncate and rest unconformably on progressively younger units, from Hooggenoeg to Kromberg to Mendon and finally Mapepe Formation. Initial folding, plunge development, and faulting preceded deposition of the Moodies Group but followed deposition of at least the lower part of the Mapepe Formation. The angular discordance between Moodies and underlying units is variable but is as much as 90° in the hinge region (Fig. 9). Faults associated with hinge collapse are truncated by Moodies conglomerates on the east limb of the Onverwacht anticline, indicating that hinge collapse also largely preceded Moodies sedimentation. The age of folding of the Kromberg syncline, and probably of the Onverwacht anticline, is no younger than 3,216+2/–1 Ma, the age of the Dalmein pluton (Kamo and Davis, 1991; 1994), which truncates the fold south of the Komati River.

The Komati fault (Viljoen, M. J., and Viljoen, 1969a, b) lies within the SD south of the present study area (Fig. 1). It is folded around the Onverwacht anticline and appears to juxtapose supracrustal rocks at least as young as 3,445 Ma south of the fault with rocks of the Komati Formation that are probably older than 3,480 Ma (López-Martínez et al., 1984; Armstrong et al., 1990) north of the fault. The contrasting metamorphic grades and in part overlapping age relationships of the rock sequences across the Komati fault suggest that it may have formed initially as a D_2 (?) thrust fault along which the relatively unmetamorphosed portions of the greenstone sequence were thrust over the TTG complex and its metamorphosed greenstone-belt roof rocks. Later tectonism probably reactivated segments of the fault.

D_3: Moodies deformation. The sudden onset of Moodies sedimentation, dominated by deposition of coarse quartzose clastic debris, marks a profound change in the depositional and tectonic style in the BGB. Major new orogenic sediment source terranes formed that included not only uplifted portions of the greenstone sequence but also, apparently for the first time, deep-seated TTG plutonic rocks. In the SD, D_3 involved uplift and deep erosion of the 3,445-Ma TTG suite centered within the Onverwacht anticline. Although structural and age relationships are presently ambiguous, we would suggest that this uplift occurred initially through flexure along the flanks of the 3,445-Ma TTG block and finally by reactivation of the Komati fault with uplift of the central TTG block. Differential uplift of the central TTG complex, which underlay the southwestern portion of the earlier formed Onverwacht anticline, would have resulted

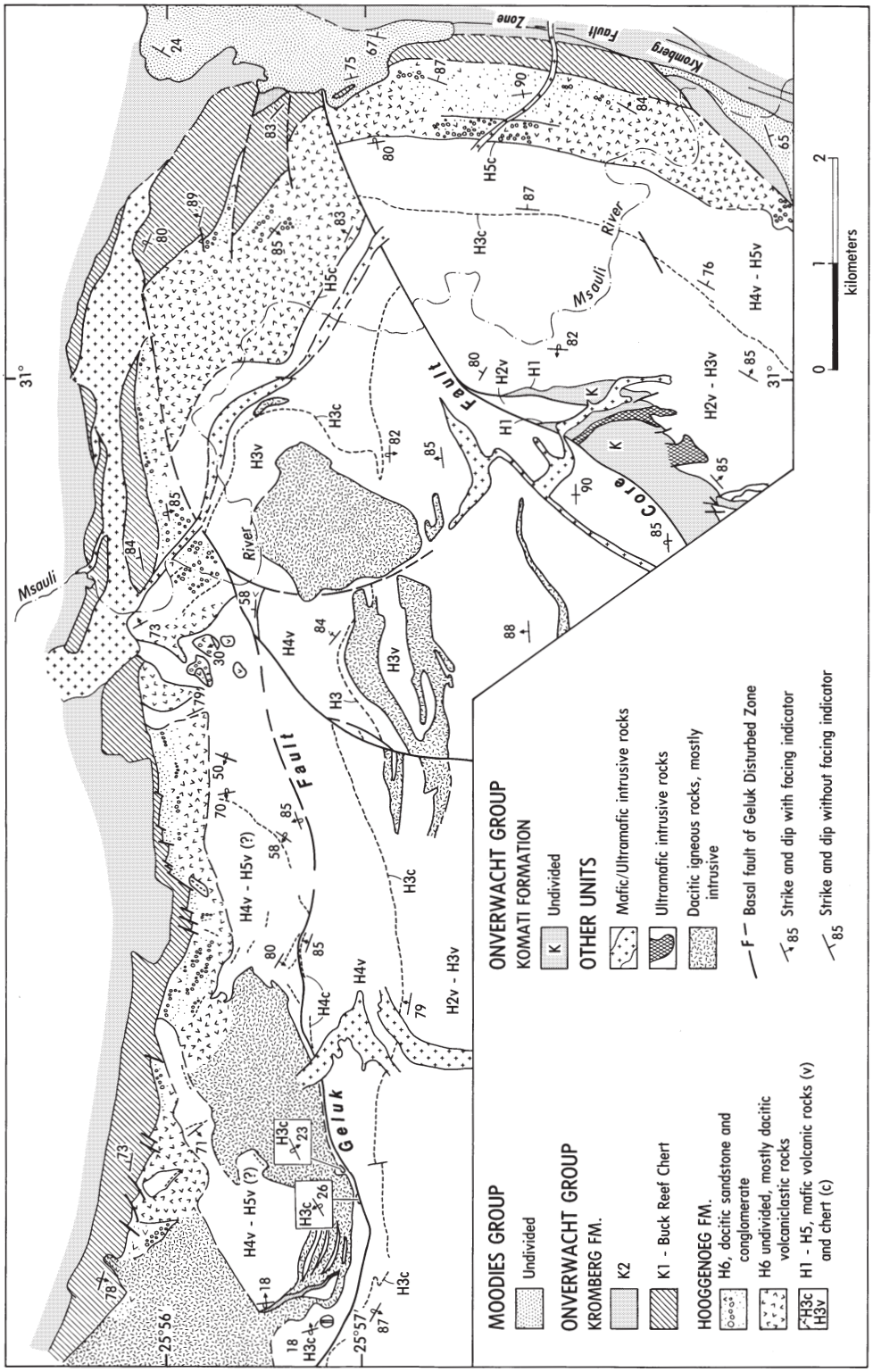


Figure 6. Geology of the central part of the hinge zone of the Onverwacht anticline. The eastern tip of the felsic intrusion in Figures 4 and 5 is at left side of figure. Dacitic intrusive rocks are H6 (3,445-Ma magmatic event) in age.

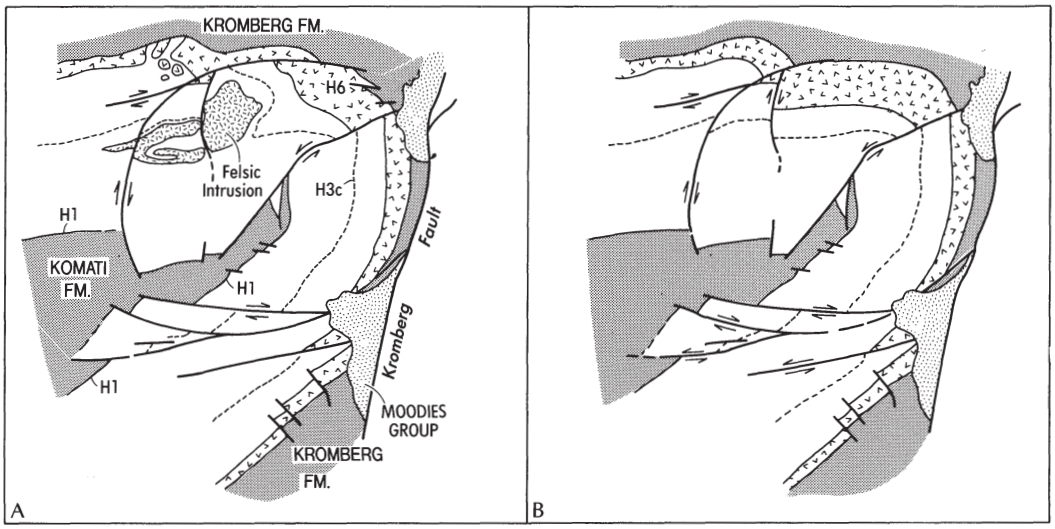


Figure 7. Simplified geologic maps of the hinge zone of the Onverwacht anticline. A, Present geology, simplified from Figure 6, including H6-age felsic intrusions in the lower and middle Hooggenoeg Formation. B, Geology after intrusions are removed. Results suggest that emplacement of shallow hypabyssal intrusions resulted in local faulting during D_1. Restored geology (B) shows faults associated with hinge collapse during D_2.

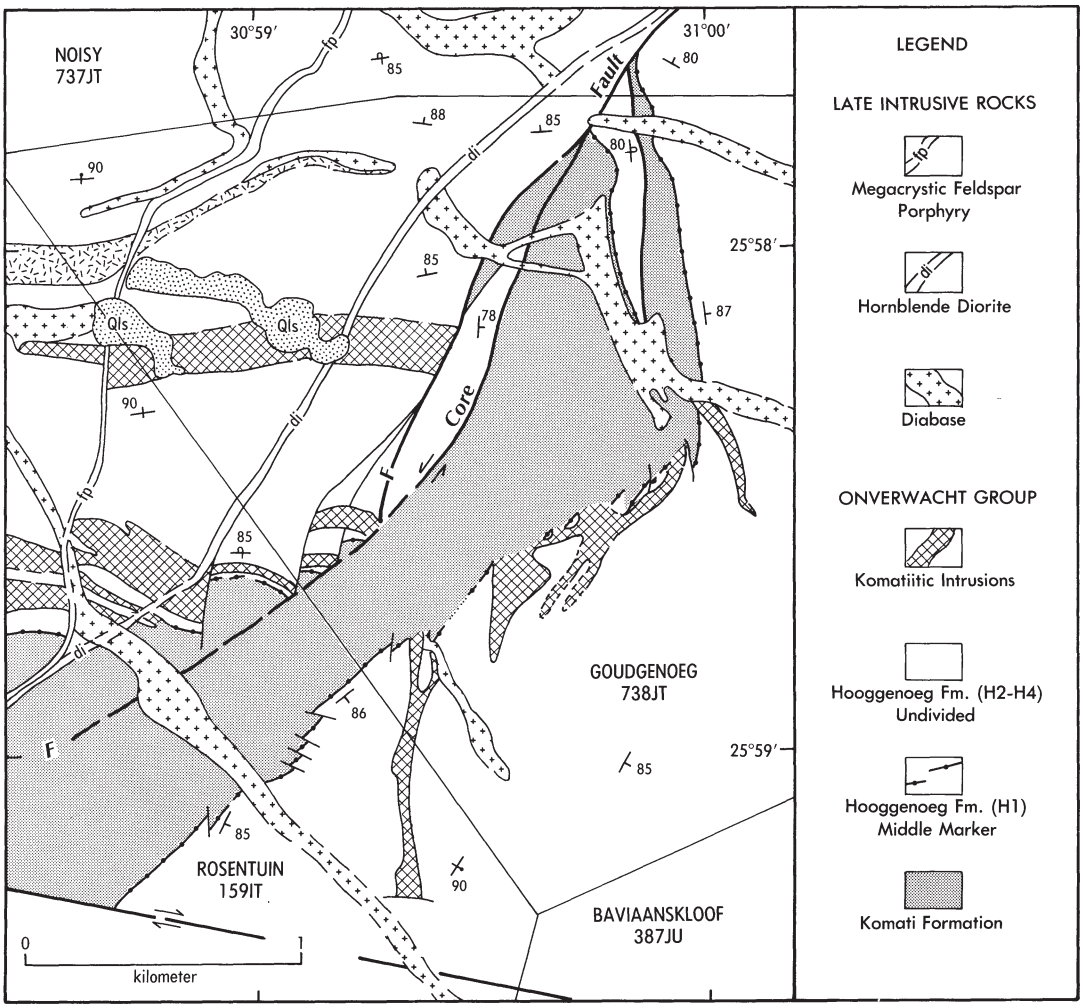


Figure 8. Geologic map of the southern part of the hinge zone of the Onverwacht anticline showing serpentinite intrusions into the Hooggenoeg Formation. Intrusions on the west side of the hinge zone appear to have formed during tightening and hinge collapse of the Onverwacht anticline during late D_{2b} and probably post-Moodies D_4 and D_5 deformation. Some or all appear to predate the latest faulting along the Core fault. At least some of those on the east appear to be igneous bodies (de Wit et al., 1987a), perhaps related to komatiitic volcanism in the Hooggenoeg, Kromberg, and Mendon Formations. Qls denotes localized modern landslide deposits.

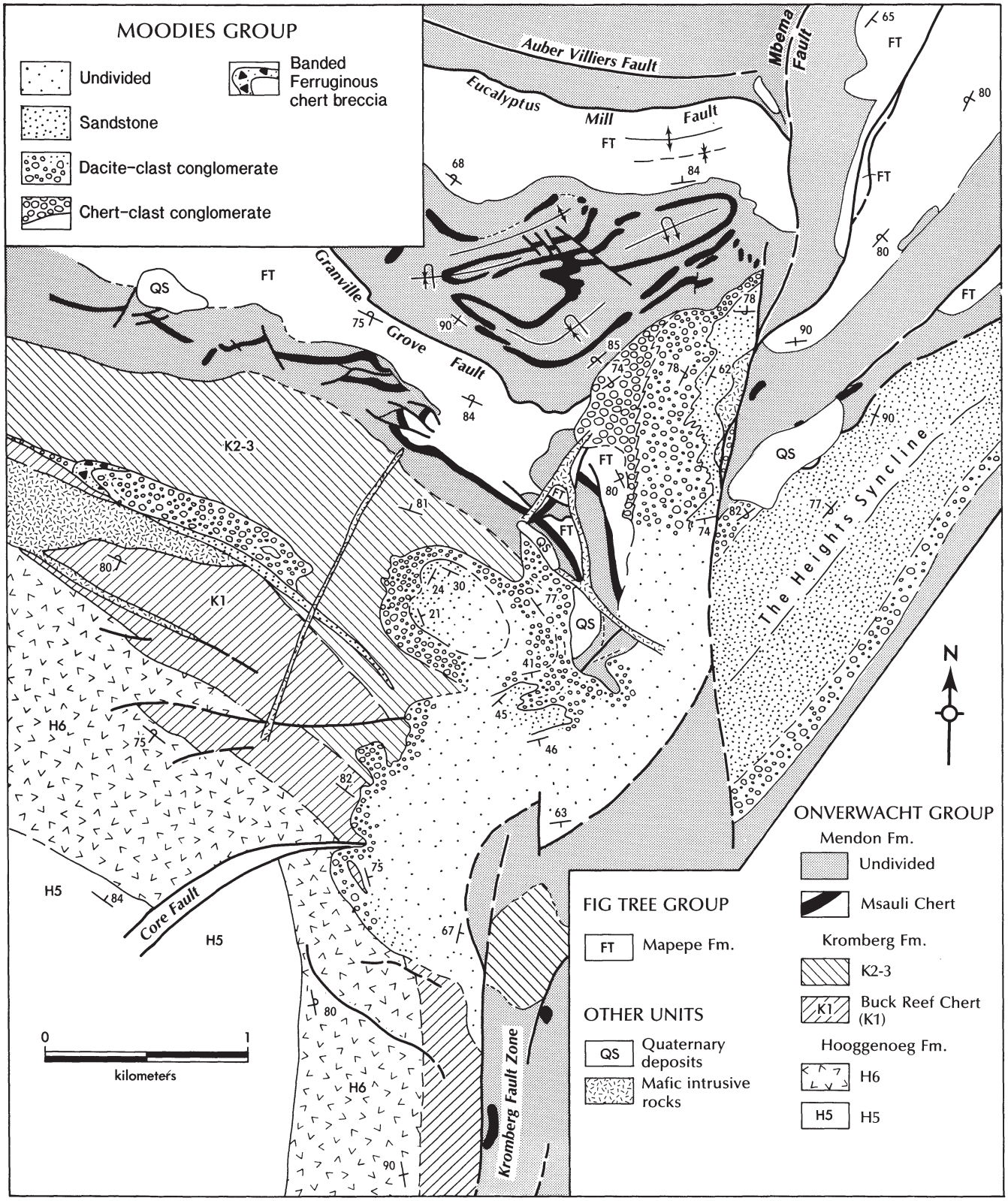


Figure 9. Geologic map of the northern part of the hinge zone of the Onverwacht anticline near the junction of the Southern Domain, East-Central Domain, and West-Central Domain. Rocks of the Moodies Group overlie older Fig Tree and Onverwacht units with angular unconformity but themselves show folding around the Onverwacht anticline. The pre-Moodies anticline was a more open, gently plunging D_2 fold.

in a steepening of the fold plunge where it crossed the northeastern margin of the uplifted block.

D_4 and D_5: Post-Moodies deformation. Moodies strata are only locally developed along the eastern margin of the SD, and it is therefore difficult to distinguish the effects of pre- and post-Moodies deformation. More complete accounts are given in sections on the ND and WCD. In the SD, Moodies strata are folded but not extensively faulted and generally show dips exceeding 45°. In the hinge and along the east limb of the Onverwacht anticline, Moodies rocks lie unconformably on folded and faulted Onverwacht and Fig Tree rocks. The angle of discordance is highly variable, ranging from nearly 90° in parts of the hinge region to 10–45° on the limbs of the anticline. However, the strike of Moodies strata generally parallels that of underlying Onverwacht and Fig Tree rocks. Moodies strata are thus folded around the Onverwacht anticline. These features suggest that the Onverwacht anticline was tightened significantly during post-Moodies shortening.

The Kromberg fault is a zone of closely spaced faults striking north to north-northeast along the eastern margin of the SD. North of the Komati River, it replaces the hinge of the Kromberg syncline (Fig. 1), separating east-younging rocks of the Hooggenoeg and Kromberg Formations west of the fault from west-younging units of the Kromberg and Mendon Formations east of the fault. Farther north, it truncates the east limb and possibly the hinge zone of the Onverwacht anticline (Fig. 9). The fault has not been traced beyond the southwestern edge of The Heights syncline (THS; Fig. 9). It seems likely that the Kromberg fault passes beneath Moodies strata in THS and is continuous or merges with the Mbema fault, which marks the boundary between the ECD and WCD northwest of the Barite syncline (Figs. 2 and 9). Moodies strata in the Baviaanskloof Block are cut by the Kromberg fault, however, so at least the southern part of the fault involved post-Moodies activity. Until the northern continuation of the Kromberg fault is traced with certainty, the amount of pre- versus post-Moodies displacement remains uncertain. It is also possible that Moodies strata in the Baviaanskloof Block are older than those in THS.

The sense and general magnitude of displacement along the southern segment of the Kromberg fault are indicated by offset of the Hooggenoeg-Kromberg and Kromberg-Mendon contacts on the east limb of the Kromberg syncline (Fig. 2; Viljoen, M. J., and Viljoen, 1969b), both of which indicate significant left-lateral slip. However, a fault more-or-less parallel to the Kromberg fault that displaces Moodies rocks near the southern end of THS (Fig. 9) shows only a small amount of right-lateral displacement. This fault is probably unrelated to the Kromberg fault.

WEST-CENTRAL DOMAIN

Location and stratigraphy

The West-Central Domain (WCD) lies between the Granville Grove and Inyoka faults in the western part of the study area and between the Inyoka and Mbema faults in the central part of the belt (Figs. 1 and 10). It lenses out to the west as the bounding faults merge. The WCD includes two contrasting stratigraphic and structural assemblages separated by a post-Moodies fault, here named the 24-hour Camp fault (TCF; Fig. 10). The footwall sequence dominates in western exposures and consists of serpentinized komatiites and cherts of the Mendon Formation overlain by terrigenous and volcaniclastic strata of the Mapepe Formation. These units are repeated in a series of east-west–trending structural slices bounded from south to north by the Granville Grove, Eucalyptus Mill, Auber Villiers, Schultzenhorst, and Inyoka faults (Figs. 2, 10, and 11). The stratigraphic thickness of rocks exposed in the footwall belts varies from 500 to 1,000 m. Most dip vertically to subvertically and young to the north. Extensive shearing within ultramafic layers makes thickness estimates within these units post-strain thickness, not original stratigraphic thickness.

The hanging-wall sequence of the TCF includes about 1,200 m of dacitic volcaniclastic rocks of the Auber Villiers Formation of the Fig Tree Group overlain paraconformably in the Powerline Road syncline (PRS) by the Moodies Group (Fig. 11).

Structures and deformation in the West-Central Domain

D_2: Fig Tree deformation: Footwall assemblage. Deformation during Fig Tree deposition (D_2) is reflected by lenticular detrital units in the Mapepe Formation (Lowe and Nocita, this volume, Chapter 10). Along the west limb of the Onverwacht anticline, a discontinuous unit of coarse, turbiditic, lithic graywacke as much as 100 m thick occurs at the base of the formation. The restriction of this unit to the structural belt immediately north of the Granville Grove fault suggests that it may reflect initial uplift south of the fault.

Also in the southern part of the WCD, the middle part of the Mapepe Formation includes chert-clast conglomerate and lithic sandstone derived from immediately underlying Mapepe and Onverwacht rocks and deposited in alluvial, fan-delta, shallow-water, and subaqueous environments (Nocita, 1986, 1989; Nocita and Lowe, 1990; Lowe and Nocita, this volume, Chapter 10). These detrital units appear to reflect faulting in the SD and southern WCD and folding along the trend of the Onverwacht anticline (Lowe and Nocita, this volume, Chapter 10). Conglomerates in the upper part of the Mapepe Formation are thickest and coarsest immediately south of the Inyoka fault and in the western part of the WCD immediately south of the Auber Villiers fault (Figs. 10 and 11) and include both fan-delta and deep-water facies. These units may be diachronous across the WCD. They appear to reflect faulting (D_{2a}) within and north of the WCD. Sedimentation occurred mainly on the southern sides of the faults, suggesting relative uplift of the northern blocks. Late Mapepe sedimentation may have occurred within piggyback basins in the sense of Ori and Friend (1984).

The oldest structures in the WCD are the large vertical to steeply dipping faults that divide the domain into structural blocks (Figs. 10, 11, and 12). From south to north, these include the Granville Grove, Eucalyptus Mill, Auber Villiers, Schultz-

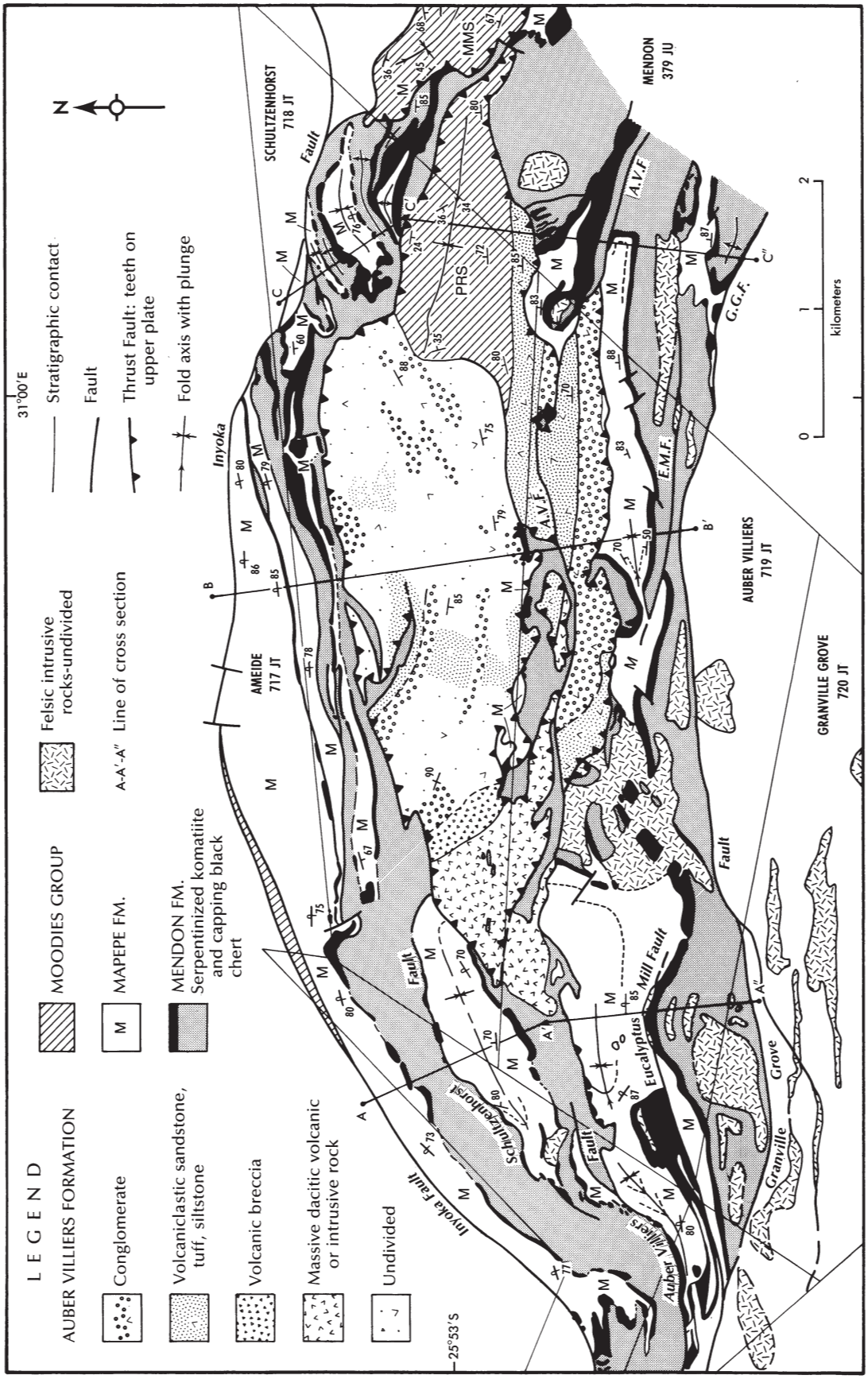


Figure 10. Geologic map of the western part of the West-Central Domain. Symbols: PRS, Powerline Road syncline; MMS, Maid-of-the-Mists syncline; E.M.F., Eucalyptus Mill fault; A.V.F., Auber Villiers fault; G.G.F., Granville Grove fault. Teeth shown on hanging wall of 24-Hour Camp fault. A-A″, B-B′, and C-C″ are lines of sections shown in Figure 11.

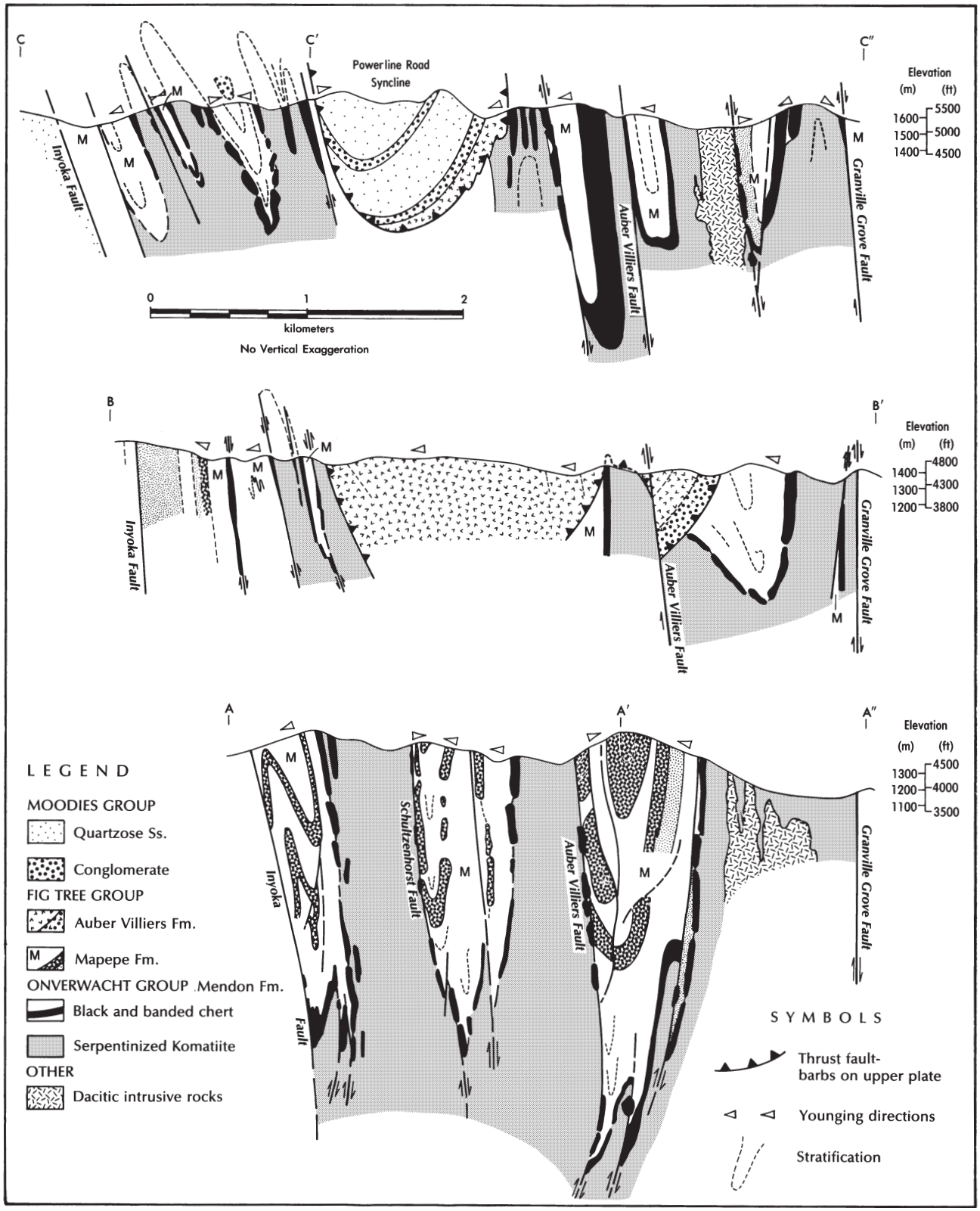


Figure 11. Cross sections of the West-Central Domain. See Figure 10 for lines of sections.

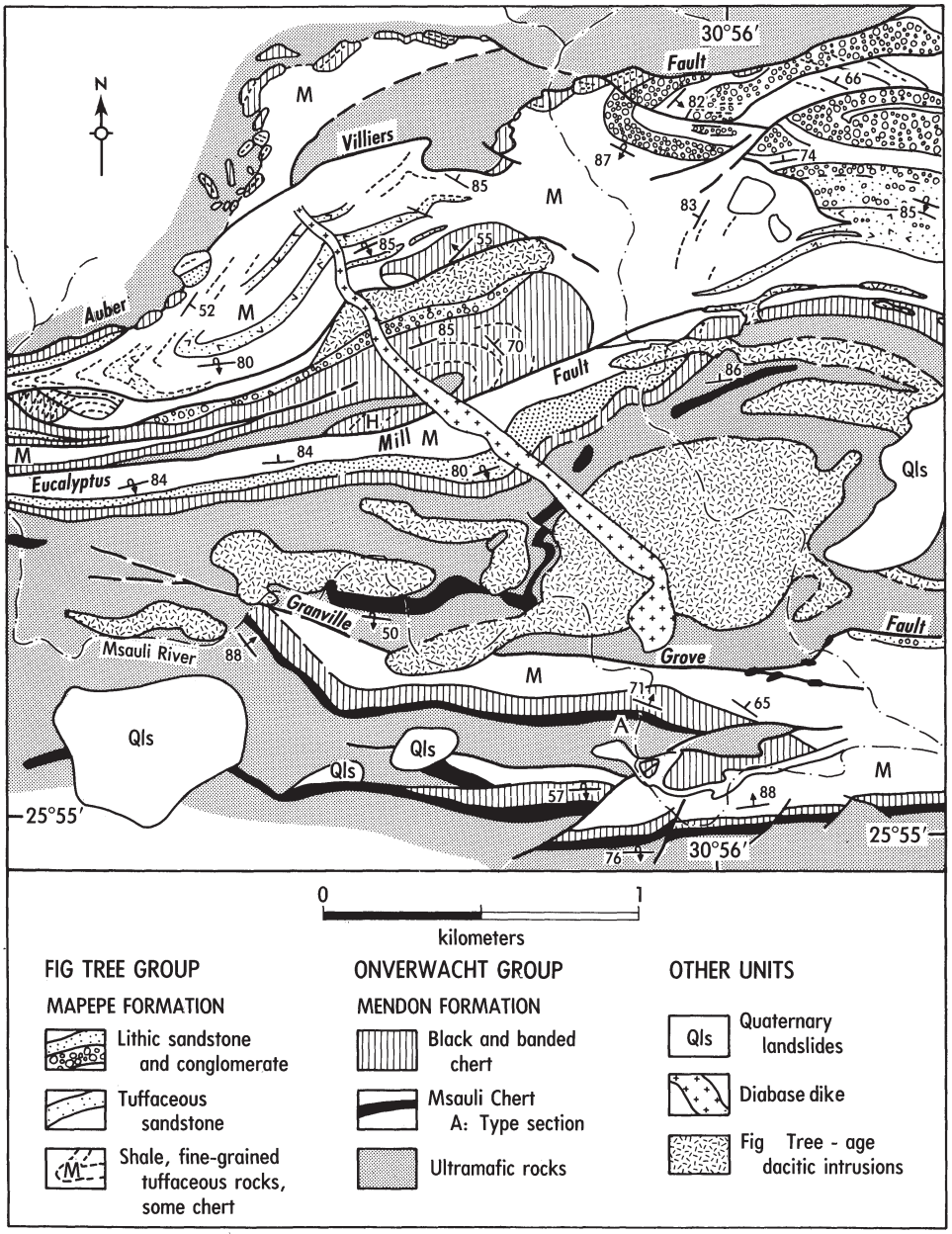


Figure 12. Geologic map of part of the western West-Central Domain and northern Southern Domain. Synclinal folds immediately south of the Auber Villiers fault and recumbent anticline and detached horse block (H) immediately north of the Eucalyptus Mill fault appear to represent drag structures related to D_2 movement on the adjacent faults. At the eastern edge of the figure, the Eucalyptus Mill fault hosts thin Fig Tree–age dacitic intrusions. Many unmapped faults lace through Mapepe strata between the Eucalyptus Mill and Auber Villiers faults. Locality A is the type section of the Msauli Chert.

enhorst, and Inyoka faults. Strata between the faults are folded into isoclinal, strongly asymmetric synclines with thick, stratigraphically complete southern limbs and heavily faulted, structurally attenuated and disrupted northern limbs (Fig. 11). These folds appear to have formed initially as drag folds or fault propagation folds related to shearing along the adjacent faults. Near the western end of the WCD, a small, rotated, recumbent, east-verging isoclinal anticline with an attenuated southern limb and a detached horse block is developed along the Eucalyptus Mill fault (Fig. 12). All of the faults merge with the Inyoka fault at the western end of the WCD.

These faults are zones of intense brittle deformation. They are marked by scaly serpentinite (Cowan, 1985) in ultramafic rocks. Competent units of chert, conglomerate, and sandstone are spread out along the fault traces as isolated, angular, rotated blocks. Numerous smaller branch faults lace through the adjacent sedi-

mentary sequences, especially in the hinges of the synclines (Fig. 11). The sense of slip along the major faults in the WCD can be estimated from the offset of units across the faults and the geometry of associated folds. The former is generally consistent along the faults and suggests right-lateral strike-slip movement, uplift of the northern blocks, or a combination of these in present coordinates.

Strain analysis based on the fault-related footwall folds is complicated because of later deformation. Although the general sense of displacement based on gross fold geometry is consistent with relative uplift of the northern blocks, more precise determination is complicated by the possibility of high shear strains in the folded rocks that could have rotated the fold hinges into the shear directions (e.g., Jackson et al., 1987). However, field observations suggest that strain has been taken up largely within the serpentinite layers and by brittle deformation along the faults. Altered micaceous lithic sand grains in unsilicified footwall Fig Tree graywackes, pebbles and cobbles in Fig Tree conglomerates, and cross-bedding and clasts in the associated volcaniclastic layers show little evidence of stretching or shear. While recognizing the possibility of undetected shear-related hinge rotation, we have estimated slip direction from fault-fold relationships, assuming that the intersections of the faults with the axial surfaces of the folds lie parallel to the y-axis of the strain ellipse (Moore, 1978). Because of later deformation, however, it was not possible to calculate with any accuracy the local orientation of the planes of the WCD faults. We have, therefore, approximated the above intersection and, hence, the y-axis of the strain ellipsoid by the axes of the drag folds.

Two structural corrections are required to restore the folds and faults to their initial orientation. (1) Fold plunges generally decrease from west to east (Fig. 13), reflecting post-Moodies (D_5) deformation. The westernmost folds are west-plunging antiformal synclines. Toward the east, plunges become vertical, then decrease to about 40–45°E in the easternmost synclines (Fig. 13). The fold axes are probably curved, flattening with depth toward the east. The folds were probably horizontal to gently plunging initially. We have restored them by rotating the more western folds about a horizontal, north-trending D_5 fold axis. (2) Bedding in the western WCD must then be restored to the horizontal by rotation about regional east-west strike. The results suggest that the folds were originally south- to southeast-verging recumbent synclines developed below low-angle thrust faults. The estimated sense of slip is consistent with that indicated by the offset of geologic units across the faults (Figs. 10 and 11) and with that implied by offset of units along minor faults common in the hinge zones of the folds (Fig. 11). The formation of the bounding faults as thrust faults is also consistent with observations of Lowe et al. (1985) that the Granville Grove fault was nearly horizontal when formed. These folds may have developed as fault-propagation folds during flat-ramp thrusting (Suppe and Medwedeff, 1984; Suppe, 1985).

Near the hinge of the Onverwacht anticline, a series of tight folds in the Msauli Chert and underlying and overlying altered komatiites of the Mendon Formation (Fig. 14; also see photograph of de Ronde and de Wit, 1994, Plate 1) has been interpreted as a refolded nappe showing at least three stages of deformation (de Wit, 1982; Lowe et al., 1985): F1, represented by fold axes plunging 30–60° to the northeast; F2, represented by axes that are horizontal or plunge gently to the northeast; and F3, by vertical

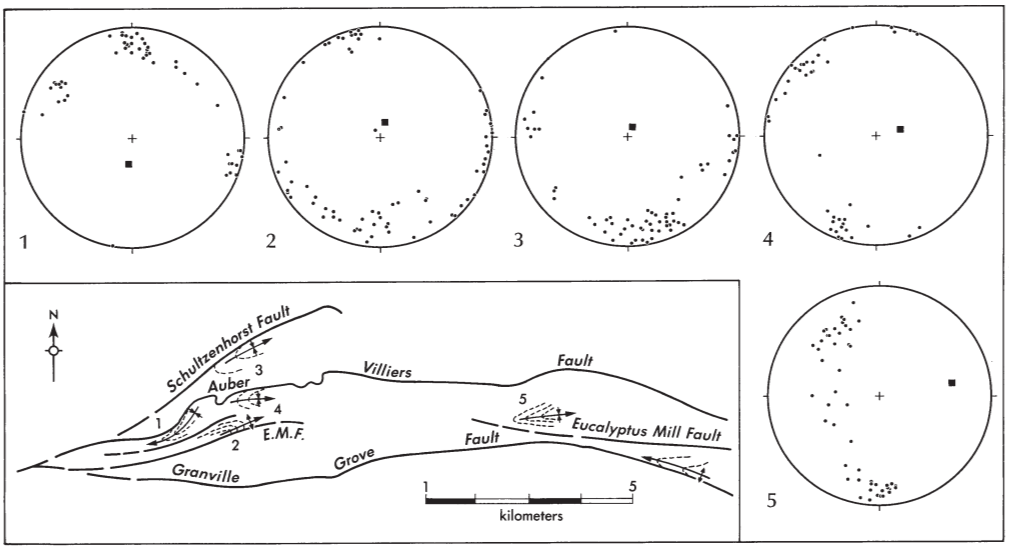


Figure 13. Equal-area, lower hemisphere stereograms of poles to bedding around D_{2a} drag folds developed adjacent to bounding faults in the western part of the West-Central Domain (WCD). Solid squares give plunges of fold axes. West-to-east sequence of folds shows progressive rotation of axes from overturned, west-plunging antiformal syncline (1) to vertically plunging folds (2 and 3) to eastward-plunging folds (3 and 4). Fold rotation reflects D_{5c} tilting of WCD and Northern Domain that must be removed before estimating directions of D_2 thrusting.

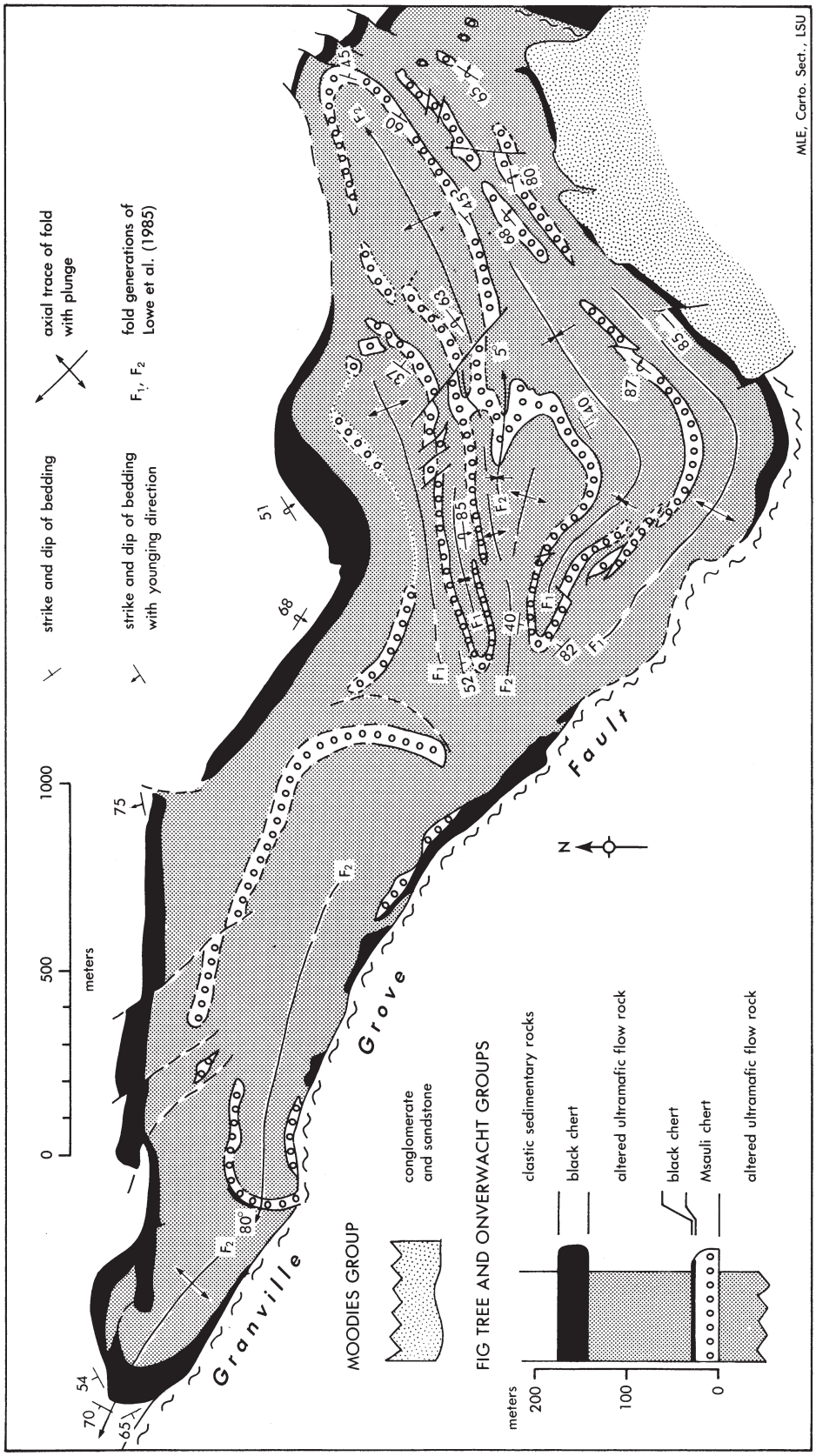


Figure 14. Geologic map of complex antiform between Eucalyptus Mill fault (slightly north of the area shown) and Granville Grove fault. The eastern part of this area is also shown in Figure 9. Tight folds in the hinge of the antiform are outlined by Msauli Chert. F_1 folds of Lowe et al. (1985) show east-plunging axes that shallow at depth to coincide with F_2. These are sheath folds formed during D_2 of the present study. These have been refolded around a nearly vertical axis, probably during D_5.

fold axes. We have attempted to test this hypothesis by careful measurement of paleocurrents in the Msauli Chert on several limbs of this fold complex. The use of paleocurrents within such a complex presumes no bulk differential plastic strain of the rocks. It is clear that throughout this fold complex, penetrative shear has been partitioned into the ultramafic rocks. The 20- to 25-m thick Msauli Chert contains literally dozens of graded layers of spherical air-fall volcanic accretionary lapilli (Lowe, this volume, Chapter 9). These layers are intact and can be traced continuously and the accretionary lapilli are spherical and unstrained (see photos in Lowe, this volume, Chapter 9). Microcrystalline sericitic mica in the recrystallized lapilli is randomly oriented. The strong and brittle chert layers appear to have been folded without major internal shearing within a matrix of shearing, weak, ductile serpentinite.

Along the west limb of the Onverwacht anticline, the Msauli Chert includes volcaniclastic layers deposited by currents flowing relatively uniformly toward the east and northeast (Heinrichs, 1984; Lowe, this volume, Chapter 9). These regional paleocurrents (Fig. 15-I) provide a general prefolding vector that can aid in unfolding the nappe structure. The observed paleocurrent patterns within the fold complex (Fig. 15-II) does not resemble that predicted by the three-stage fold model (Fig. 15-III). Unfolding about F1 axes yields paleoflow vectors that diverge from the future fold axis, which is unlikely given the present uniformity in bed thickness and composition around the folds. The most reasonable interpretation is that the fold axes are curved (Fig. 16), plunging steeply in most outcrops, where they were interpreted as F1 by de Wit (1982) and Lowe et al. (1985), but flattening to the northeast, where they were interpreted as F2. The folds are thus small, tight, doubly plunging folds in the hinge of a larger antiform between the Granville Grove fault on the south and the Eucalyptus Mill fault on the north (Fig. 14). When rotated about regional strike, this antiform appears to represent a large south- to southeast-verging recumbent fold nappe developed during shearing along enclosing thrust faults. The eastern portion of the nappe (Fig. 14) has been refolded about a subvertical axis from an initial east-west to a northeast-southwest strike during later deformation.

The timing of D_2 in the WCD is constrained by a suite of Fig Tree–age hypabyssal feldspar porphyry intrusions (Lowe et al., 1985; de Ronde et al., 1991). Most were emplaced into incompetent serpentinites at the top of the Mendon Formation, although many extend into the overlying Mapepe Formation. We have identified no intrusions that clearly cut across the bounding thrust faults in the WCD, but some appear to follow the thrust faults as zones of weakness (Lowe et al., 1985; de Ronde et al., 1991). The intrusions in the WCD have been dated from 3,240 ± 5 Ma (Kröner et al., 1991) to about 3,230 Ma (de Ronde et al., 1991). Thrust faulting probably occurred mainly in the latter part of this interval. In the hinge zone of the Onverwacht anticline, the Granville Grove fault passes beneath folded but relatively unfaulted rocks of the Moodies Group.

D_2: Fig Tree deformation: Hanging wall assemblage. The hanging wall of the TCF includes as much as 1,200 m of dacitic and terrigenous rocks of the Auber Villiers Formation overlain by as much as 700 m of sandstones of the Moodies Group (Figs. 10 and 11). Conglomerate in the middle of the Auber Villiers Formation, composed of clasts of black chert, banded chert, silicified komatiite, and dacite, probably reflects D_2 uplift of older Fig Tree and Onverwacht rocks, but we have identified no specific D_2 structures in the hanging wall.

D_3: Moodies deformation. In the Powerline Road syncline (PRS), local facies changes in the lower Moodies Group indicate that sedimentation was influenced by syndepositional faulting (Lowe and Byerly, this volume, Chapter 1). Along the west side of the PRS, basal Moodies strata terminate against the Two Springs fault (Figs. 17 and 18), which dies out about 200 m above the base of the Moodies Group. Conglomerates are thicker and coarser southeast of and adjacent to the fault and thin and fine to the east. These facies relationships and the abundance of dacitic volcaniclastic debris in the Moodies Group in the PRS suggest that sediments were derived from the upthrown side of the fault, which appears to have formed as a normal fault. Faulting ceased during Moodies deposition. The Two Springs fault appears confined to the hanging wall and predates formation of the TCF.

D_4: Late Moodies to early post-Moodies deformation. The 24-hour Camp fault (TCF) is one of the oldest post-Moodies structures in the BGB. It is well exposed around a number of structural windows in the western WCD. In the largest (Fig. 19), the lower plate includes faulted, vertical to subvertical rocks of the Mapepe and Mendon Formations. These are structurally overlain and truncated by overturned, south-dipping, north-younging dacitic tuffs and epiclastic rocks of the Auber Villiers Formation in the hanging wall (Figs. 19 and 20). The TCF is a zone of shearing and brecciation from less than a meter to more than 20 m thick. The fault breccia consists largely of angular clasts less than 10 cm in diameter of fine-grained purplish, pinkish, and rusty-weathering Mapepe tuff and shale in a fine comminuted matrix of the same materials. Minor clast types include chert, komatiite, and dacitic volcanic rock. Breccia dikes marking splay and accommodation faults extend as much as several meters into the footwall. The TCF has been tightly folded during later deformation (Fig. 20).

Another window in what we interpret as the TCF south of the PRS (Fig. 21) exposes vertical to overturned tuffaceous Auber Villiers strata thrust over folded cherts and silicified komatiites of the Mendon Formation and shales and sandstones of the Mapepe Formation. Breccia along the fault is composed largely of angular chert and Mapepe tuff fragments.

D_4 thrust faulting was accompanied or followed closely by folding to form the PRS, Maid-of-the-Mists syncline (MMS), and related synclines that constitute the framework of the WCD east of the study area. Both the PRS (Fig. 17 and 18) and MMS (Fig. 22) are tight to isoclinal, doubly plunging folds. Both exhibit thick, relatively unfaulted southern limbs and thinner, heavily faulted and structurally attenuated northern limbs. Footwall and hanging-wall strata along the southern limbs and in the hinges of both folds are truncated by the TCF. Although both folds are locally overturned to the north, their geometries and juxtaposition with Mendon ser-

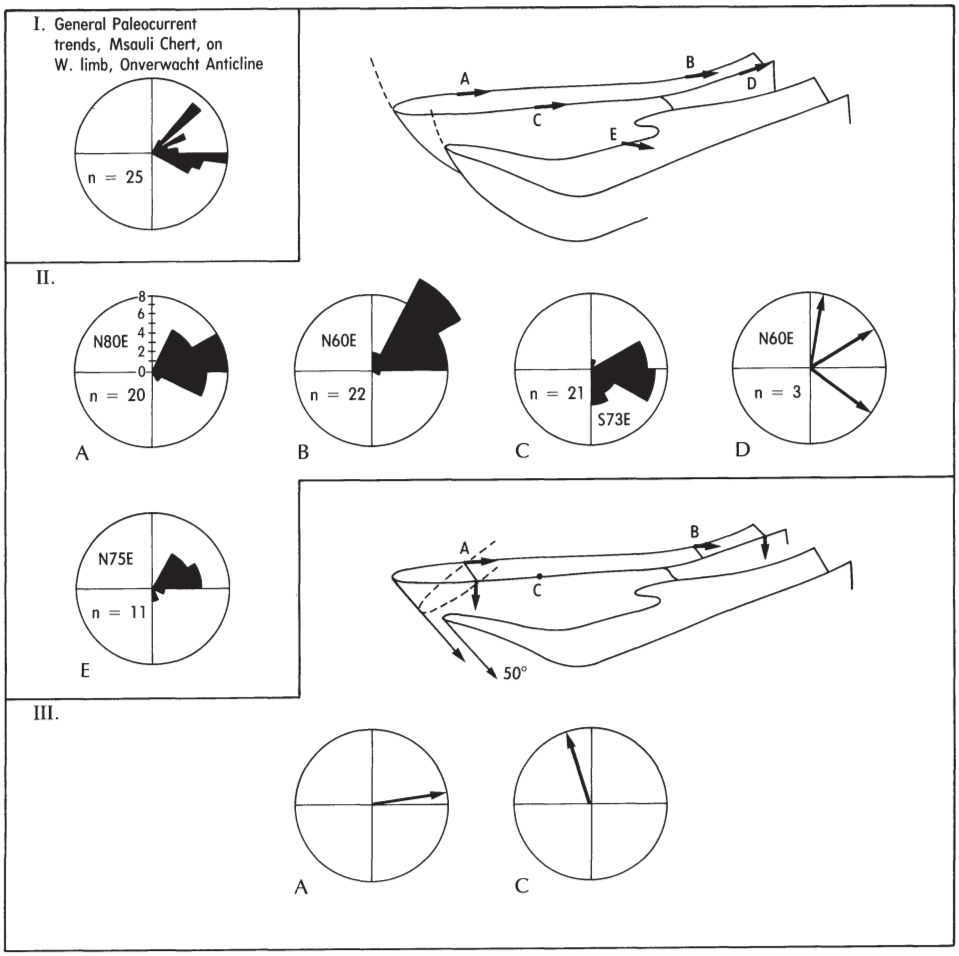


Figure 15. Paleocurrent analysis of the complex folds in the Msauli Chert within antiformal structure shown in Figure 14. I., Regional paleocurrent patterns in the Msauli Chert on the west limb of the Onverwacht anticline. II., Paleocurrents from a single horizon near the middle of the Msauli Chert on the limbs of the tight folds (Fig. 14). Paleocurrents have been restored by simple rotation about the strikes of the individual fold limbs. III., Expected outcrop (top sketch) and restored (bottom circles) paleocurrent directions at point (C) if they represent a regionally unidirectional flow, represented by paleocurrents at (A), folded around an isoclinal, steeply plunging cylindrical fold. The difference between the observed (II) and predicted (III) paleocurrents indicates that the folds are sheath folds rather than tilted or refolded cylindrical folds.

pentinites and chert blocks along their northern limbs suggest formation as south- to southeast-verging synclines during south- to southeast-directed thrust faulting. Their similarity in size, structure, and geometry suggest that they may be en echelon folds or parts of a single large refolded syncline in the hanging wall of the TCF.

D_5: Late post-Moodies deformation. In the WCD, D_5 structures are best distinguished in Moodies rocks along the eastern edge of the study area and farther east (Figs. 23 and 24). Moodies and post-Moodies deformation in this area has been studied recently by Heubeck (Heubeck and Lowe, 1994a and b, and this volume, Chapter 11). These Moodies strata occur in a train of tight to isoclinal synclines that are overturned to the north and show highly attenuated, faulted northern limbs (Fig. 24). These folds probably developed initially during D_4 as south-verging folds but were rotated to north-facing structures during D_5. Within the hinge zones, the quartzose Moodies sandstones are strongly recrystallized and thickened, commonly obliterating primary depositional features. Weak, spaced cleavage is locally developed in fine-grained beds. In some hinge zones, segments of sandstone beds have been imbricated in a chaotic fashion. Strain indicators are rare. Hinge zone shortening and limb extension were accommodated principally by tangential longitudinal strain, an interpretation consistent with the common presence of tension gashes in the outer arcs of the fold hinges and pressure solution in the inner arcs.

The synclines are separated by faults or northeast-striking belts of highly deformed Fig Tree and Onverwacht rocks replacing or representing narrow, commonly faulted anticlines. The

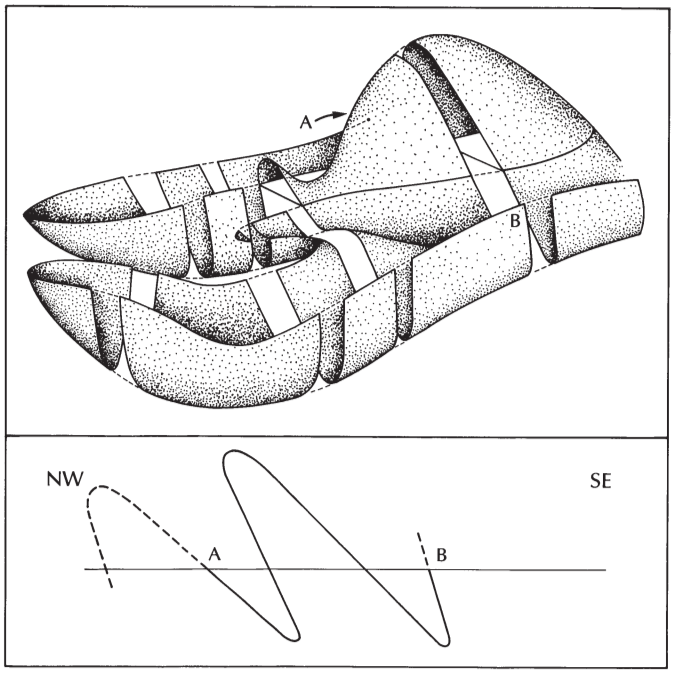


Figure 16. Simplified three-dimensional sketch (top) and cross section (bottom) of sheath folds shown in Figure 14. Plane shown is Msauli Chert.

faults dip steeply to the southeast. Most are linear zones of detached and rotated blocks and fault-bounded slivers of serpentinized ultramafic rock, chert, and altered Mapepe tuff and sandstone. Some bedding-parallel faults juxtapose Moodies rocks and can commonly be recognized only by changes in younging directions in the sandstones. A cross section of the Barberton Belt roughly along the line of the Barberton-Havelock Road (Fig. 24) illustrates the strong degree of similarity among D_5 synclines of the fold train in the WCD, ECD, and ND (Heubeck and Lowe, 1994a and b, and this volume, Chapter 11).

North of the PRS, a belt of tight, overturned, north-verging, doubly plunging folds occurs in Mendon and Mapepe rocks (Fig. 25). These folds mark a zone of intense shortening between the Inyoka fault and TCF that continues westward to the end of the WCD. West of the area shown in Figure 25, the Inyoka fault and TCF trend east-west, parallel to regional strike (Fig. 10). In that area, folds within the zone of intense shortening are long, narrow, north-verging faulted folds that appear to have been developed during D_2 or D_4 and tightened during D_5. The short, doubly plunging folds shown in Figure 25 are developed only in a zone of oblique right-lateral shortening where the bounding faults strike northwest, oblique to regional structure (Fig. 10). The northern part of this zone contains tight refolded D_2 or D_4 folds continuous with those farther west (Fig. 25). The change in the geometry of these folds suggests that there may have been right-lateral transpression late in development of the D_{5a} fold-and-thrust belt.

The formation of penetrative strain fabrics occurred during D_{5b}, concurrently with fold tightening. Cleavage is poorly developed in most parts of the study area, in part because it is parallel or subparallel to stratification in the isoclinally folded rocks and therefore difficult to distinguish from bedding in thinly bedded units. Massive rocks of the Auber Villiers Formation and Moodies Group display a crude, spaced vertical to steeply south-dipping cleavage. Auber Villiers tuffs in the hanging wall of the TCF show fracture cleavage that dips 55 to 85°S, subparallel to stratification and crosscutting the folded TCF.

Strike-slip faulting during D_{5c} is discussed more extensively in the section on the ND. Rocks in the westernmost part of the WCD were refolded about a subhorizontal axis during D_{5c} strike-slip movement on the Inyoka fault. This refolding is reflected in the overall eastward younging of rocks in the WCD and by the progressive westward increase in the plunge of drag fold axes adjacent to the large thrust faults.

Although the faults in the WCD formed as D_2 thrust faults, some and perhaps all were reactivated during D_5. The Auber Villiers and Schultzenhorst faults locally offset the Auber Villiers Formation and the TCF. The Auber Villiers fault widely shows evidence of late oblique faulting involving left-lateral strike-slip and relative upward movement of the northern block. Evidence includes (1) left-lateral drag folding of Mendon and Mapepe strata and left-lateral offset of the TCF south of the PRS along the Auber Villiers fault (Fig. 10), and (2) refolding and offset of the TCF across the Auber Villiers fault southwest of the PRS (Fig. 10).

EAST-CENTRAL DOMAIN

Location and stratigraphy

East of the SD and WCD, rocks of the upper Onverwacht, Fig Tree, and Moodies Groups crop out in northeast-striking belts that make up most of the southeastern part of the BGB (Figs. 2 and 23). This region is termed the East-Central Domain (ECD). It is sharply bounded to the southwest by the Kromberg fault (Fig. 2). The northwestern boundary is somewhat arbitrarily drawn at the Mbema fault; in the central part of the BGB (Figs. 23 and 24) the WCD and ECD are structurally and stratigraphically similar. Its southeastern limit lies outside of the study area. Heinrichs (1980) studied rocks over much of the ECD, including areas east and northeast of the present study area, and Paris (1985) mapped parts of the ECD east of the southern part of the present study area. The ECD is made up of folded and faulted rocks of the Mendon and Mapepe Formations, and the Moodies Group.

Structures and deformation in the East-Central Domain

D_2: Fig Tree deformation. Throughout the ECD, the Mapepe Formation includes, in addition to tuffaceous strata and the Manzimnyama Jaspilite Member (Heinrichs, 1980), thick units of shale, turbiditic lithic sandstone, and conglomerate reflecting uplift and erosion of older Fig Tree and Onverwacht rocks. These detrital units thin and fine progressively from southeast to the northwest, indicating uplift and erosion of greenstone

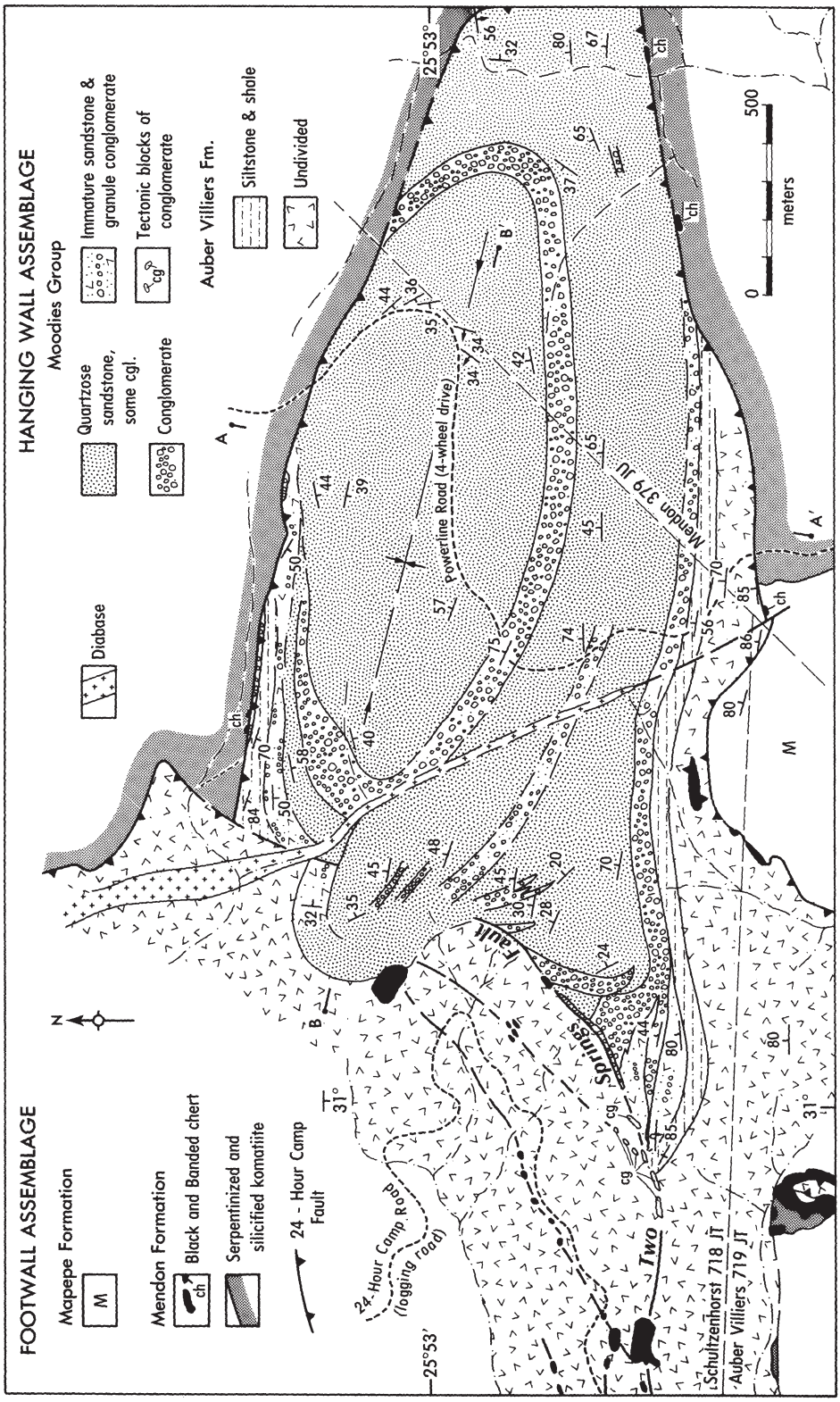


Figure 17. Geologic map of the Powerline Road syncline (PRS). The Two Springs fault along the west (left) side of the PRS was active, apparently as a normal fault, during deposition of the lower part of the Moodies Group but became inactive and was overlapped by strata in the upper part of the Moodies Group.

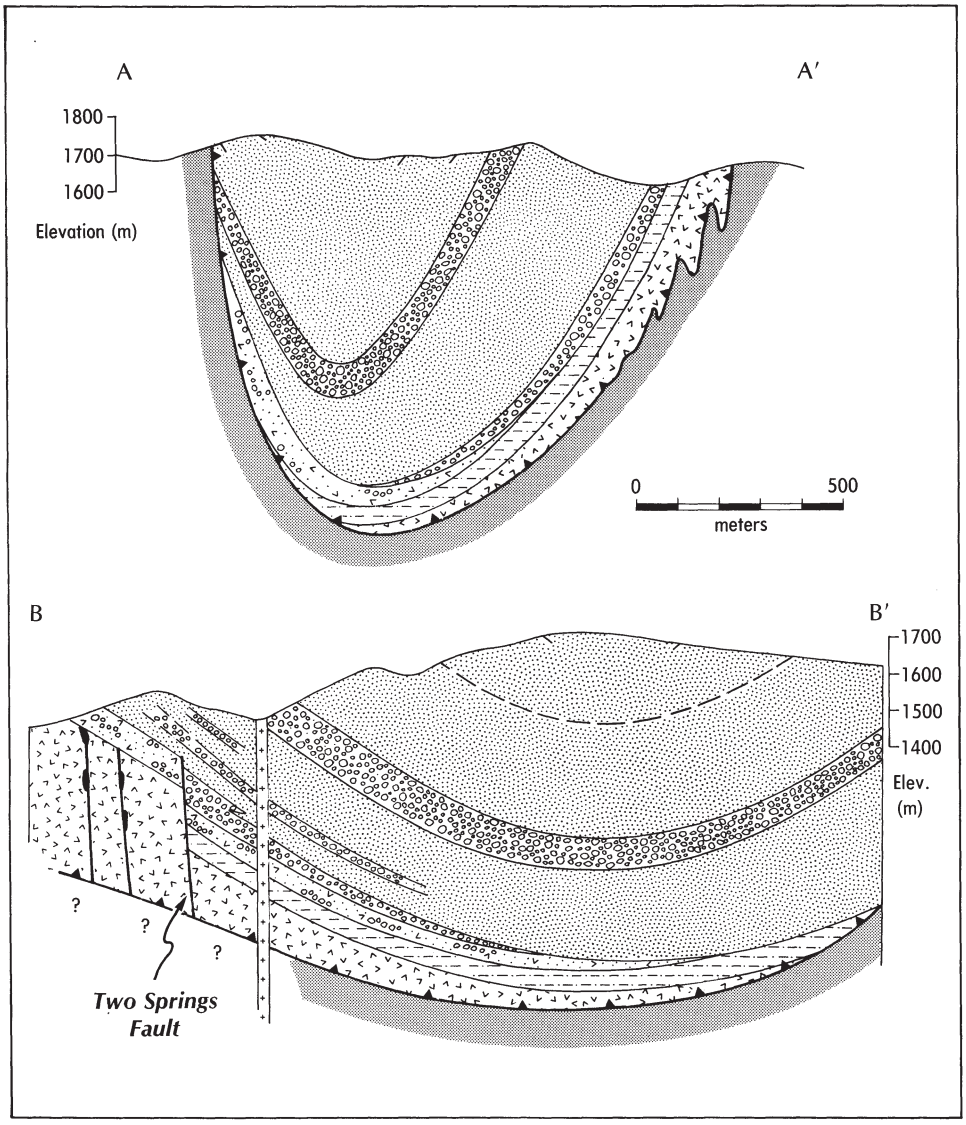


Figure 18. Cross sections of the Powerline Road syncline perpendicular (top) and parallel (bottom) to the fold axis. Lines of sections and definition of symbols shown in Figure 17. The progressive eastward thinning and decrease in abundance of conglomerates composed largely of dacitic clasts reflects erosion of Auber Villiers rocks west of the Two Springs fault and deposition of detritus on the east, downthrown side during early Moodies time.

rocks to the southeast. The western limb of the Barite syncline (Fig. 2) and areas along strike to the northeast, lying along the northwestern edge of the ECD, include a greatly condensed, heavily silicified section of Mapepe strata containing very localized lenticular units of shallow-water conglomerate, barite, jasper, and clastic debris derived in part by local erosion of komatiitic volcanic rocks (Heinrichs and Reimer, 1977; Lowe and Nocita, this volume, Chapter 10). This zone of uplift, erosion, and unusual sedimentation was termed the Proto-Inyoka Zone by Heinrichs and Reimer (1977). Its coincidence with the northeastward projection of the axial trace of the Onverwacht anticline (Fig. 2) suggests that the Proto-Inyoka Zone marks initial folding along the trend of the anticline.

We have found no unambiguous evidence for major pre-Moodies deformation within the ECD, although there is a strong discordance between a possible hanging wall sequence, that includes Moodies and paraconformably underlying Fig Tree tuffaceous strata, and footwall rocks, that include the Mapepe and conformably underlying Onverwacht rocks. We suspect that this discordance reflects the presence of an unconformity of upper Fig Tree age or a post-Moodies fault in the ECD like those in the other parts of the BGB.

D_5: Post-Moodies deformation. The structural framework of the ECD consists of a fold train of tight, overturned, north-verging anticlines and synclines in the Mendon and Mapepe Formations juxtaposed with The Heights syncline and part of the Emlembe

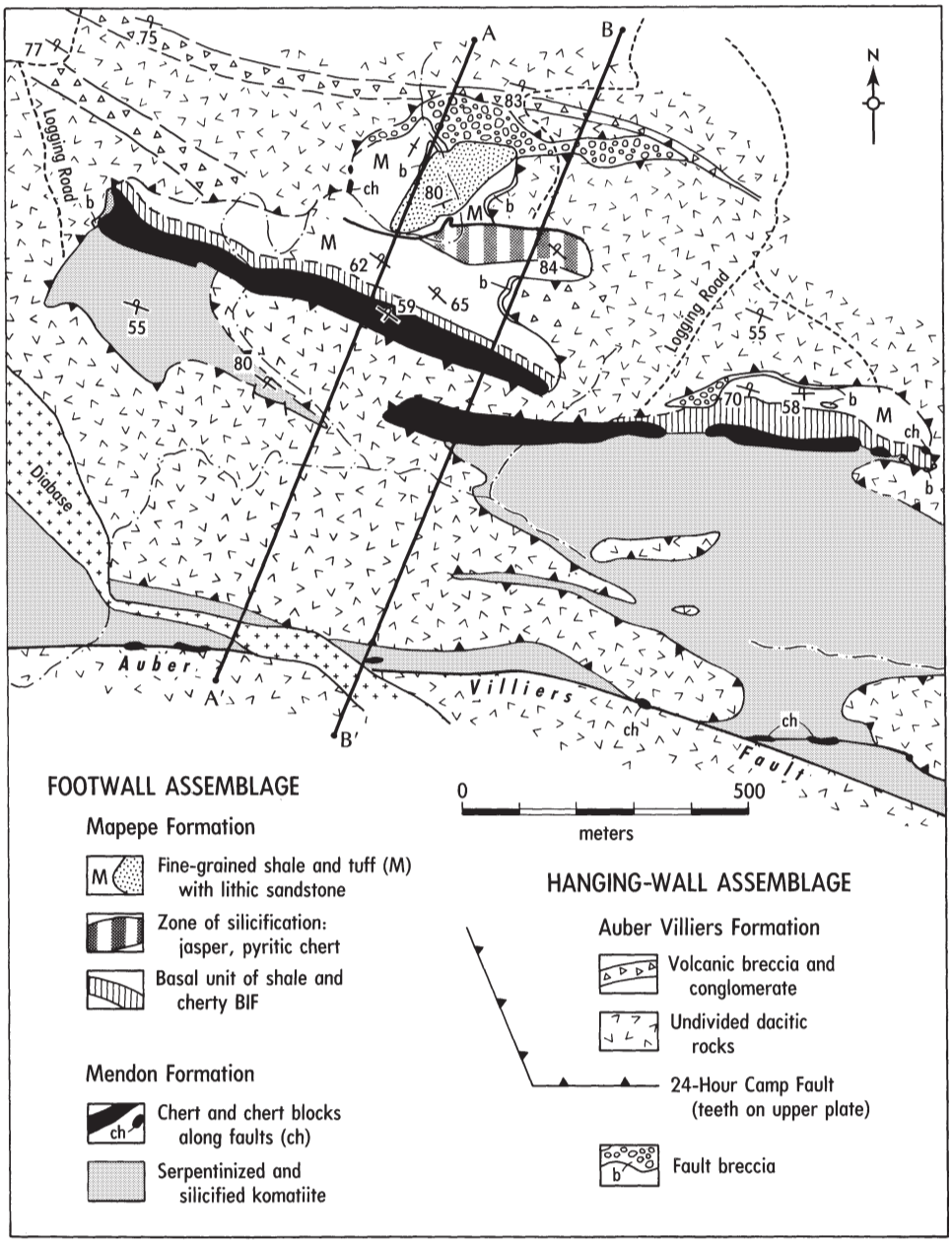


Figure 19. Geologic map of a window in the West-Central Domain exposing hanging-wall and footwall assemblages separated by the 24-Hour Camp fault. See Figure 2 for location of figure. BIF, banded iron formation.

belt made up of rocks of the upper Fig Tree and Moodies Groups (Fig. 24). Most folds plunge moderately to steeply to the northeast, but southwest plunges occur, and plunges often change along trend. Synclinal fold limbs are typically planar and hinge zones extremely tight. These folds are more complete than those in the WCD and lack features suggesting that they developed initially as southeast-verging structures. The principal deformation in the ECD appears to have involved northwest-verging D_5 folding.

The nature of the contact between the Mendon-Mapepe and overlying tuffaceous Fig Tree–Moodies assemblages is uncertain. Paris (1985) has mapped the contact east of the study area as a thrust fault. It could be an unconformity, but its overall similarity to the TCF in the WCD suggests that it, too, may indeed be a fault.

NORTHERN DOMAIN

Location and stratigraphy

The Northern Domain (ND) includes areas north of the Inyoka fault and south of the Kaap Valley pluton (Fig. 1). It is

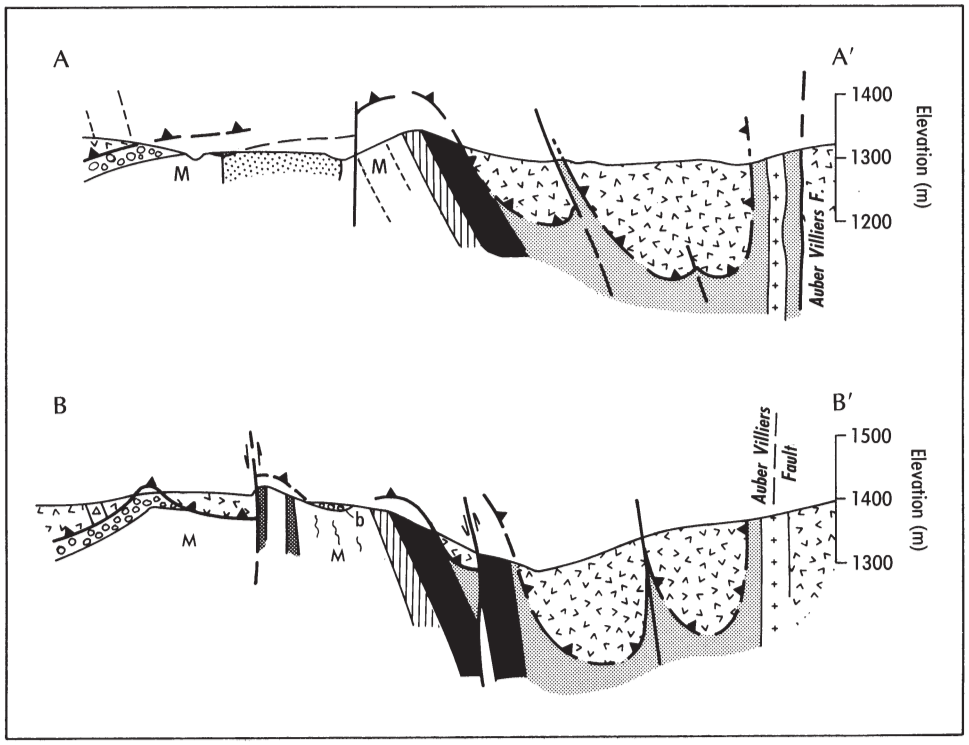


Figure 20. Cross sections of the structural window shown in Figure 19. Note that Auber Villiers rocks of hanging-wall assemblage young north and dip steeply to the south in both sections (extreme left). In lower diagram, Auber Villiers fault has been intruded by a late diabase dike. Symbols as in Figure 19.

made up of folded and faulted rocks of the northern facies of the Onverwacht, Fig Tree, and Moodies Groups (Figs. 26 and 27). Between the northern branch of the Moodies fault and the Kaap Valley pluton, the ND includes deformed, subvertical, south-younging komatiitic volcanic rocks, layered ultramafic intrusive units, and black cherts of the Weltevreden Formation (Wuth, 1980). Because these rocks lie north of the frontal faults of the BGB and lack many elements of classic BGB stratigraphy, they should probably be treated as a separate structural domain, but we have not mapped these units in sufficient detail to warrant discussing them separately here.

South of the Moodies fault (Figs. 26 and 28), ND rocks can be divided into two major assemblages separated by a regional fault or angular unconformity: (1) a footwall assemblage comprising the Weltevreden Formation overlain in sequence by the Ulundi, Sheba, and Belvue Road Formations of the Fig Tree Group; and (2) a hanging-wall assemblage that includes serpentinites and black and banded cherts of the Onverwacht Group succeeded in sequence by a thin unit of cherty and jasper-bearing strata resembling the Ulundi Formation, dacitic volcaniclastic strata of the Schoongezicht Formation, and quartzose sediments of the Moodies Group. The hanging-wall assemblage is completely developed only in the hinge zone of the Stolzburg syncline (Fig. 28).

The nature of the contact between the footwall and hanging-wall assemblages in the ND is poorly resolved. Available geochronological and stratigraphic evidence permits interpretation of the contact as either a fault, an unconformity, or a faulted unconformity. At the west end of the Moodies Hills (Fig. 26), the contact is a folded fault that truncates folds, faults, and stratification in the footwall and stratification in the hanging wall. In the Stolzburg syncline, bedding in the Ulundi, Sheba, Belvue Road, and Schoongezicht Formations, and Moodies Group appears subparallel and conformable (Fig. 28). However, the presence of serpentinized komatiite and chert between the Belvue Road and Schoongezicht Formations is anomalous. Moreover, a thin sequence of gray chert, banded ferruginous chert, and jasper below Schoongezicht sandstones and above black cherts capping the komatiites closely resembles the Ulundi Formation. Extensive brecciation and faulting marks the komatiite-chert unit, which disappears due to faulting in both directions (Fig. 28). Although the evidence is not conclusive, it seems likely that the base of the serpentinite is a folded, grossly bedding-parallel fault that partially duplicates stratigraphy.

Structures and deformation in the Northern Domain

D_2 and/or D_3: Post-Belvue Road, pre-Moodies deformation. The footwall sequence consists of faulted and tightly to isoclinally folded rocks of the Weltevreden, Ulundi, Sheba, and Belvue Road Formations (Figs. 26 and 27). More competent Sheba sandstones generally form broad synclines separated by

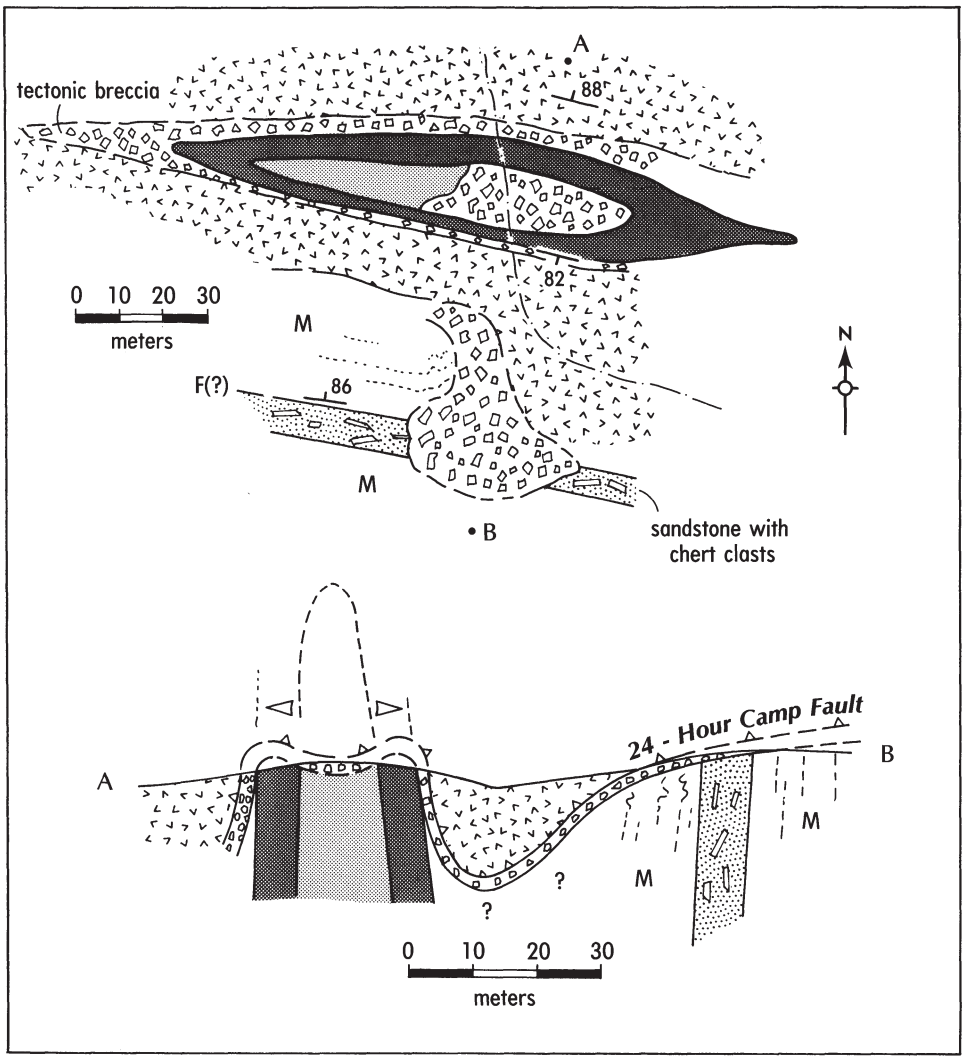


Figure 21. Geologic map and section through small structural window eroded through the 24-Hour Camp fault (TCF) south of the Powerline Road syncline (Fig. 2). Symbols as in Figure 19. Footwall cherts at the top of the Mendon Formation outline a tight, upright, doubly plunging anticline surrounding a core of silicified ultramafic rock that is truncated by the TCF. The TCF is defined by a zone of breccia composed of clasts of chert, Auber Villiers volcaniclastic rock, and Mapepe tuffaceous units that separates the footwall and hanging wall. It appears to dip steeply along the flanks of the anticline but the basal contact of the breccia is flat where it truncates the hinge of the anticline, possibly reflecting extreme hinge thickening of the breccia or the boxlike character of the fold.

narrow, tight to isoclinal, commonly faulted anticlines in less competent Onverwacht serpentinites and thinly layered shales and cherts of the Ulundi Formation. Cherts at the top of the Weltevreden Formation show brittle deformation and occur as detached, rotated blocks in serpentinite matrix along faulted fold limbs and in synclinal hinges. The anticlines are generally parallel folds with minor hinge thickening. The synclines, where complete, are isoclinal similar or Class 3 folds (Ramsay and Huber, 1987) showing enormous hinge thickening, especially of banded ferruginous cherts of the Ulundi Formation (Fig. 26), which also show abundant small-scale parasitic folds reflecting polyharmonic folding. Many of the larger folds are sheath folds, with axes generally plunging in excess of 50°. The axes of the parasitic folds plunge parallel to those of the regional folds.

Footwall fold geometry varies across the ND (Fig. 27). Synclines in the south are larger, more complete, and overturned to the north while those along the northern edge of the belt are narrower, more upright, and heavily faulted.

The continuity of sheared serpentinite around the hinges of the larger folds indicates that Weltevreden serpentinites underlie the entire ND (Figs. 26 and 27). Footwall folds formed initially as large, cuspate-lobate folds (Ramsay, 1963; Ramsay and Huber, 1987) during shortening of the interface between the

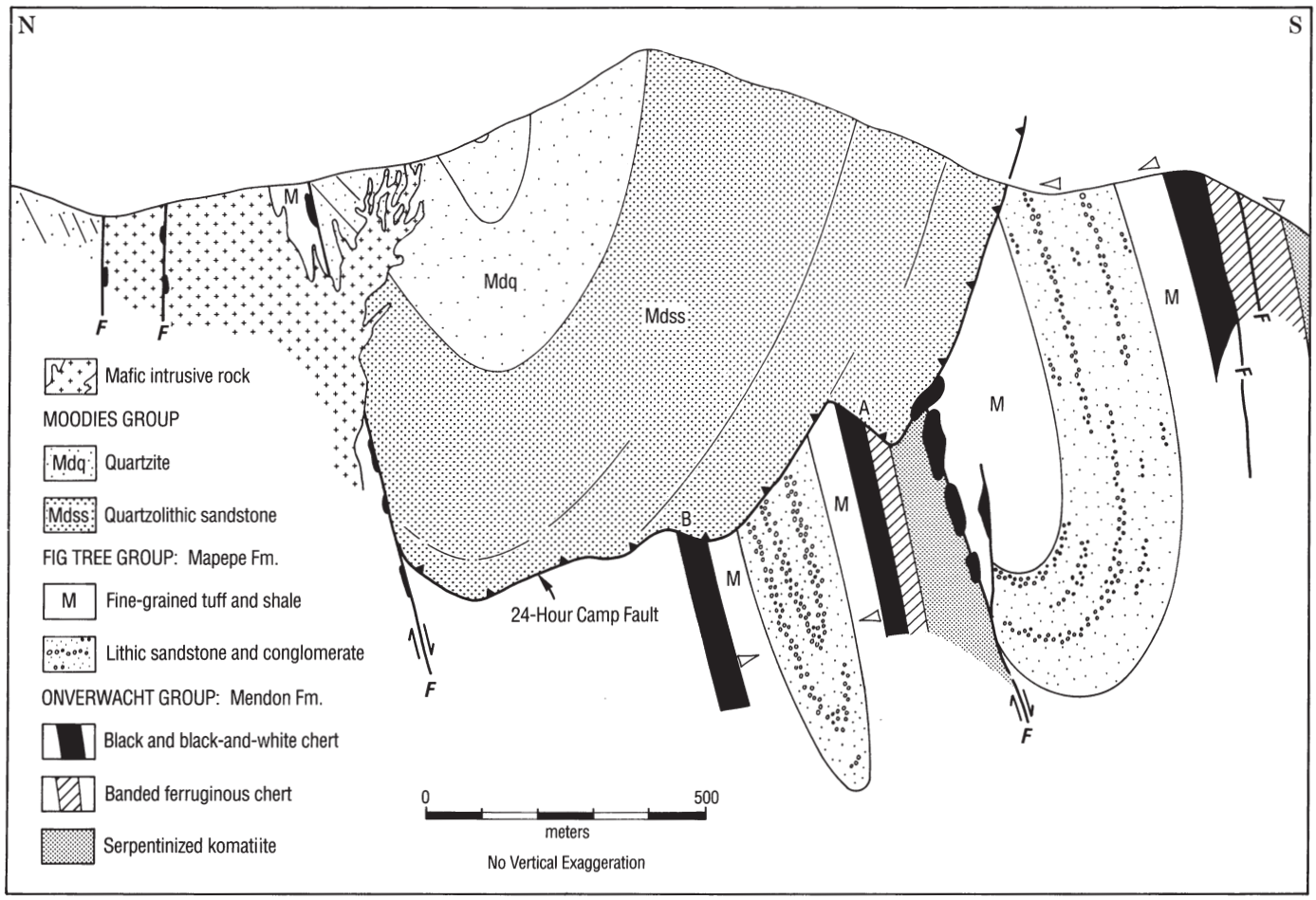
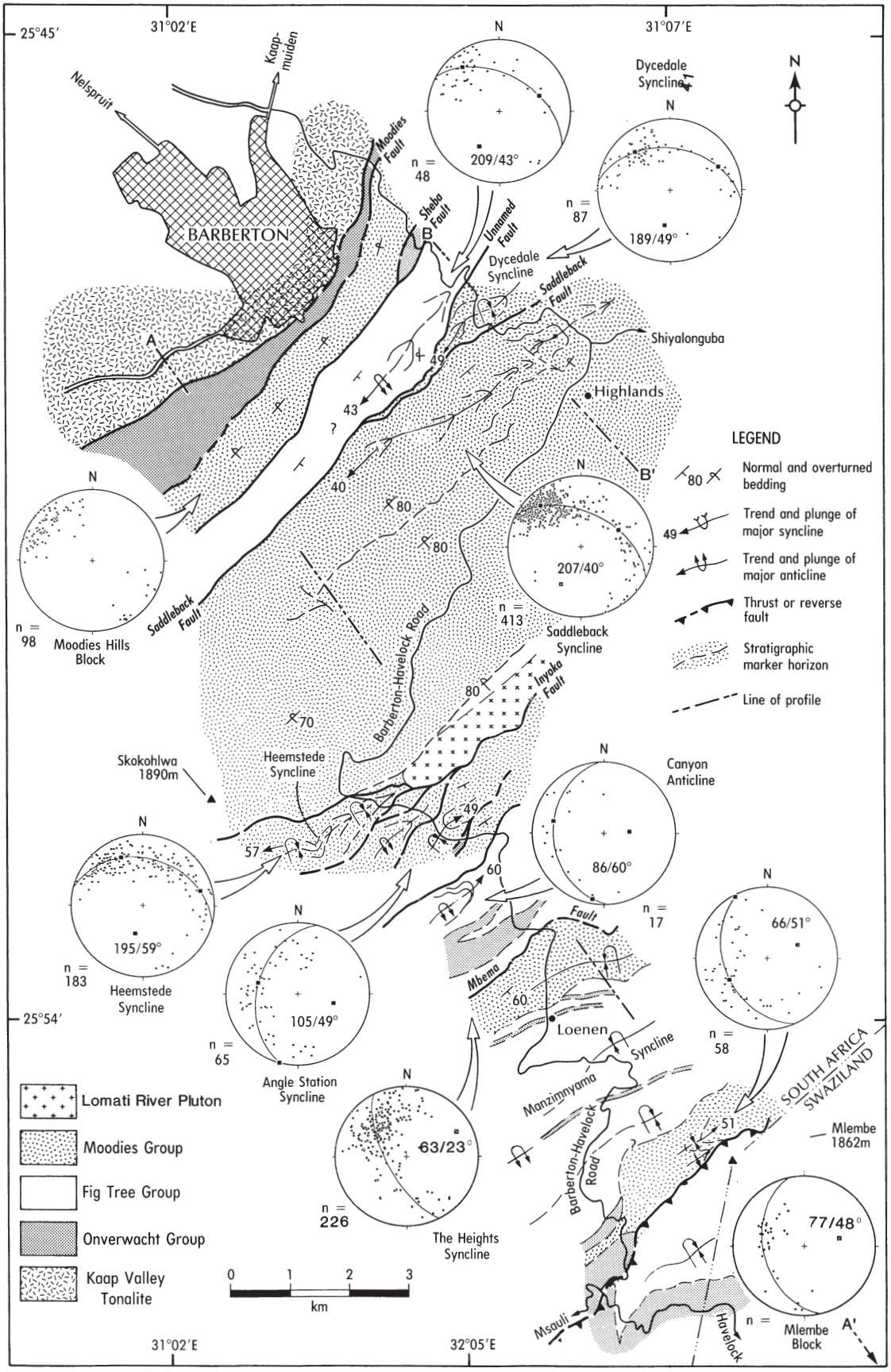


Figure 22. Cross section through the Maid-of-the-Mists syncline (MMS; See Fig. 2 for line of section). The MMS is a tight syncline in rocks of the Moodies Group that plunges at about 45 to 50° to the northeast, into the section. The D_4-D_5 syncline is bounded below by the folded, crudely bedding parallel D_4 24-Hour Camp fault. Folds in underlying Fig Tree and Onverwacht rocks were formed during D_2 and tightened and faulted during D_4-D_5. At A and B, the 24-Hour Camp fault (TCF) cuts up-section to the north in the hanging wall, suggesting possible northward tectonic transport, although regional relationships lead us to infer that the TCF formed by thrusting of Moodies and underlying rocks of the Auber Villiers Formation of the Fig Tree Group toward the south or southeast. Symbol F denotes steeply dipping faults. A D_4 thrust/reverse fault that truncates Moodies strata along the northern edge of the MMS is marked by displaced blocks of Onverwacht chert and silicified komatiite. The fault has an irregular surface trace and was probably deformed during D_{5a}. This fault is cut by a late mafic intrusion that invades into Moodies rocks on a centimetric scale and includes abundant, isolated grains of Moodies quartz. It is cut in turn by later D_{5c} (?) strike-slip faults near the left side of figure. These faults are branches of the Inyoka fault, which lies 200 m beyond the left margin of the figure.

competent clastic units of the Fig Tree Group and the incompetent serpentinites of the Onverwacht Group.

A number of features suggest that footwall rocks in the ND were deformed before emplacement of the hanging-wall assemblage. Footwall rocks show smaller and tighter map-scale folds, a greater abundance of small parasitic folds, and more closely spaced faults than the hanging-wall sequence. The truncation of footwall units and structures by hanging-wall strata at the west end of the Moodies Hills implies that the former were already deformed when the assemblages were juxtaposed during post-Moodies deformation. Although these contrasts could reflect decoupling and differential response of lower, incompetent and upper, competent portions of a single stratigraphic sequence in post-Moodies time, the development of separate footwall and hanging-wall synclines throughout the ND, as well as the WCD, and the lack of small-scale deformation and parasitic folding in incompetent mudstones and thinly interbedded mudstone and sandstone sequences of the Schoongezicht Formation in the hanging wall suggest that these units are less deformed than mechanically similar footwall units.


25°45′
31°02′E
31°07′E
Kaap-muiden
Nelspruit
Moodies Fault
BARBERTON
Sheba Fault
Unnamed Fault
Dycedale Syncline
Saddleback Fault
Shiyalonguba
Highlands
A
B
B′
49
43
40
80
70
?
N
209/43°
n = 48
189/49°
n = 87
207/40°
n = 413
Saddleback Syncline
n = 98
Moodies Hills Block
Barberton-Havelock Road
Inyoka Fault
Skokohlwa 1890m
Heemstede Syncline
57
60
Canyon Anticline
86/60°
n = 17
195/59°
n = 183
Heemstede Syncline
105/49°
n = 65
Angle Station Syncline
Fault
Mbema
Loenen Syncline
66/51°
n = 58
25°54′
63/23°
n = 226
The Heights Syncline
Manzimnyama
SOUTH AFRICA
SWAZILAND
Mlembe 1862m
51
77/48°
Msauli
Havelock
n =
Mlembe Block
A′
LEGEND
Normal and overturned bedding
Trend and plunge of major syncline
Trend and plunge of major anticline
Thrust or reverse fault
Stratigraphic marker horizon
Line of profile
Lomati River Pluton
Moodies Group
Fig Tree Group
Onverwacht Group
Kaap Valley Tonalite
0 1 2 3
km
31°02′E
32°05′E

Basal Moodies conglomerates contain abundant greenstone-derived debris as well as rare clasts of potassic plutonic rock. The provenance included Onverwacht komatiites and cherts and Fig Tree jasper, ferruginous chert, dacite, and sandstone, indicating widespread uplift, weathering, and erosion of older parts of the Swaziland Supergroup. The presence of granitic detritus also indicates uplift and exposure of deep-level plutons in early Moodies time. We feel that available data suggest that footwall strata in the ND were deformed prior to emplacement of the hanging-wall sequence.

D_4: Late Moodies to early post-Moodies deformation. Hanging-wall rocks in the ND occur mainly in large synclines that are in fault contact with surrounding footwall rocks. These include the Stolzburg and Saddleback synclines and the Moodies Hills Block. The Stolzburg syncline (Fig. 28) is a vertical to slightly antiformal, isoclinal syncline bounded by the Inyoka fault to the south and a branch of the Moodies fault to the north (Fig. 2; Reimer, 1967). The footwall Ulundi, Sheba, and Belvue Road Formations are restricted to the hinge of the syncline (Fig. 28) and show intense small-scale deformation associated with hinge thickening. Hanging-wall rocks show few small-scale folds and little hinge thickening. The apparent thinning of the Schoongezicht outcrop belt from hinge to limbs (Fig. 28) reflects progressive removal of the lower parts of the formation along the bounding faults.

Vertical to overturned, north-younging Moodies strata in the Moodies Hills Block represent the truncated southern limb of an originally much larger northeast-plunging syncline. This block of Moodies rocks continues to the northeast through a narrow belt of highly strained and attenuated Moodies rocks into the Eureka syncline (Anhaeusser, 1969a). Two smaller, more complete synclines in Moodies rocks are present along strike to the west and may represent parts of the same fold (Fig. 26). The Saddleback syncline is a large, tight, southwest-plunging syncline. Its southern limb is overturned to the north and the northern limb has been truncated and removed along the Saddleback fault except at the eastern end of the fold (Fig. 24). The southern limb includes the thickest continuous section of Moodies strata in the BGB, approximately 3,700 m thick. The basal conglomerate overlies a thin, discontinuous unit of dacitic volcanic or pyroclastic rocks, possibly representing the Schoongezicht Formation.

The northwest vergence of most synclines in the ND suggests overall northwest transport of the hanging-wall sequence. However, virtually all hanging-wall and many footwall synclines exhibit structurally attenuated or missing northern limbs and thick, relatively well preserved southern limbs. Similar relationships have been noted in the Eureka and Ulundi synclines to the northeast by Anhaeusser (1972). Although much of this attenuation may reflect truncation of the folds during late D_{5c} strike-slip faulting, the consistent localization of these faults along the northern limbs of large folds suggests that they might mark the location of pre-D_5 faults, possibly south-verging D_3 or D_4 thrust faults as in the WCD. Supporting this suggestion, Heubeck and Lowe (1992, this volume, Chapter 11) have described a progressive intraformational unconformity in the upper part of the Moodies Group in the Saddleback syncline indicating relative uplift of the block northwest of the Saddleback fault and the southeastward dispersal of Moodies debris eroded from the uplifted block.

The direction and magnitude of movement along the fault separating hanging-wall and footwall assemblages are uncertain. However, Schoongezicht volcanism was apparently cogenetic with TTG intrusive activity represented by the Kaap Valley and/or Nelshoogte plutons (de Wit et al., 1987b; Lowe et al., 1989b; Armstrong et al., 1990; Kröner et al., 1991). The coarse proximal character of Schoongezicht dacitic fragmental rocks would seem to place their depositional setting toward the northern margin of the belt, and similar proximal Fig Tree dacitic units are widely developed along the northern margin of the BGB outside of the study area. These relationships suggest that Schoongezicht strata are more closely related to rocks north of the BGB than to those to the south and that thrusting either involved little tectonic transport or a net transport from north to south.

D_5: Late post-Moodies deformation. Northwest-directed post-D_4 shortening resulted in rotation of bedding and older planar structures to vertical or subvertical dips and tightening and rotation of folds to form northwest-verging structures. Hanging-wall synclines are typically tight to isoclinal north-verging folds with axial planes that are either vertical or dip steeply to the east or southeast. All of these folds plunge moderately, either to the northeast or southwest, or both. Penetrative strain fabrics are developed locally; they are absent in resistant cherty units and are poorly developed in most Fig Tree shales and mudstones. Thick-bedded to massive sandstones of the Sheba Formation and Moodies Group commonly display vertical to south-dipping, more-or-less bedding parallel, spaced cleavage.

The ND also includes a number of major, late, subparallel faults that impose a distinctive regional fabric to the domain. These include, from south to north, the Inyoka, Saddleback, Haki, Ameide, and Moodies faults (Figs. 26 and 27). The Inyoka fault is a vertical to steeply south dipping curviplanar zone of brittle deformation marked, where well exposed, by a zone of shearing and subparallel faults less than 30 m wide. The Saddleback fault is nearly vertical and marked by a distinctive series of narrow, parallel bands including, from south to north, (1) a 5- to 20-m-thick band of resistant, intensely sheared, talcose, phyllitic cataclasite that appears to mark the fault trace; (2) a 0- to 10-m-thick band of ultramafic rock, and (3) a 0- to 5-m-thick unit of banded chert. At the western tip of the Saddleback syncline, the Saddleback and Inyoka faults parallel each other, separated by a septum of Moodies sandstone a few

Figure 23. Geologic map of a strip across the central part of the Barberton Greenstone Belt showing the structure of the East-Central Domain (ECD) and Northern Domain (ND). Map can be located by reference to the location of the cross sections (A–A′ and B–B′) in Figure 24. Rocks mapped as Moodies Group around Mlembe at the southern edge of the figure probably belong to the lower, Diepgezet Group of Lamb (1984a, b) and may be Fig Tree equivalents. Stereonets plot poles to bedding.

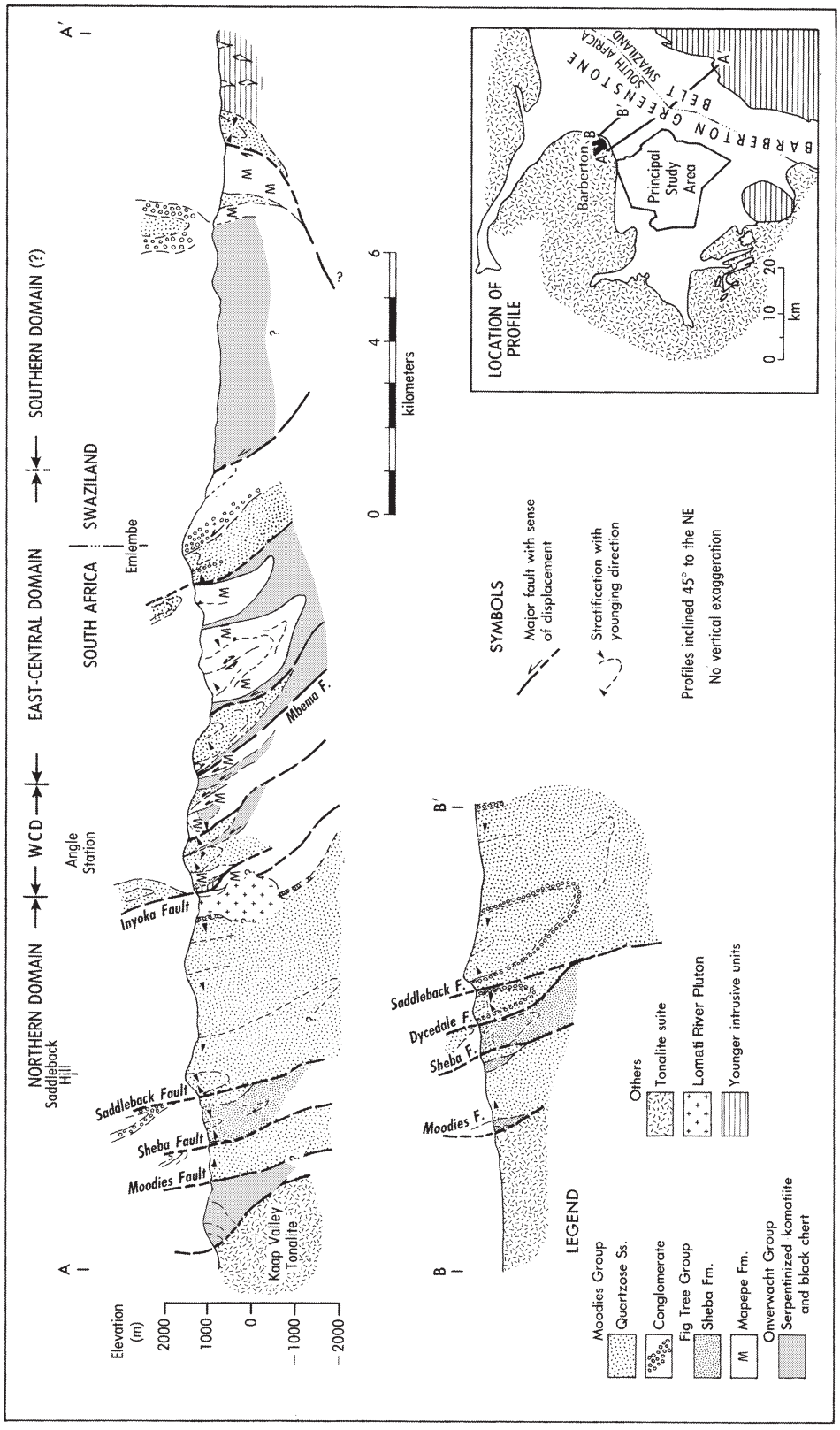


Figure 24. Cross sections of the central part of the Barberton Greenstone Belt in eastern South Africa and adjacent Swaziland.

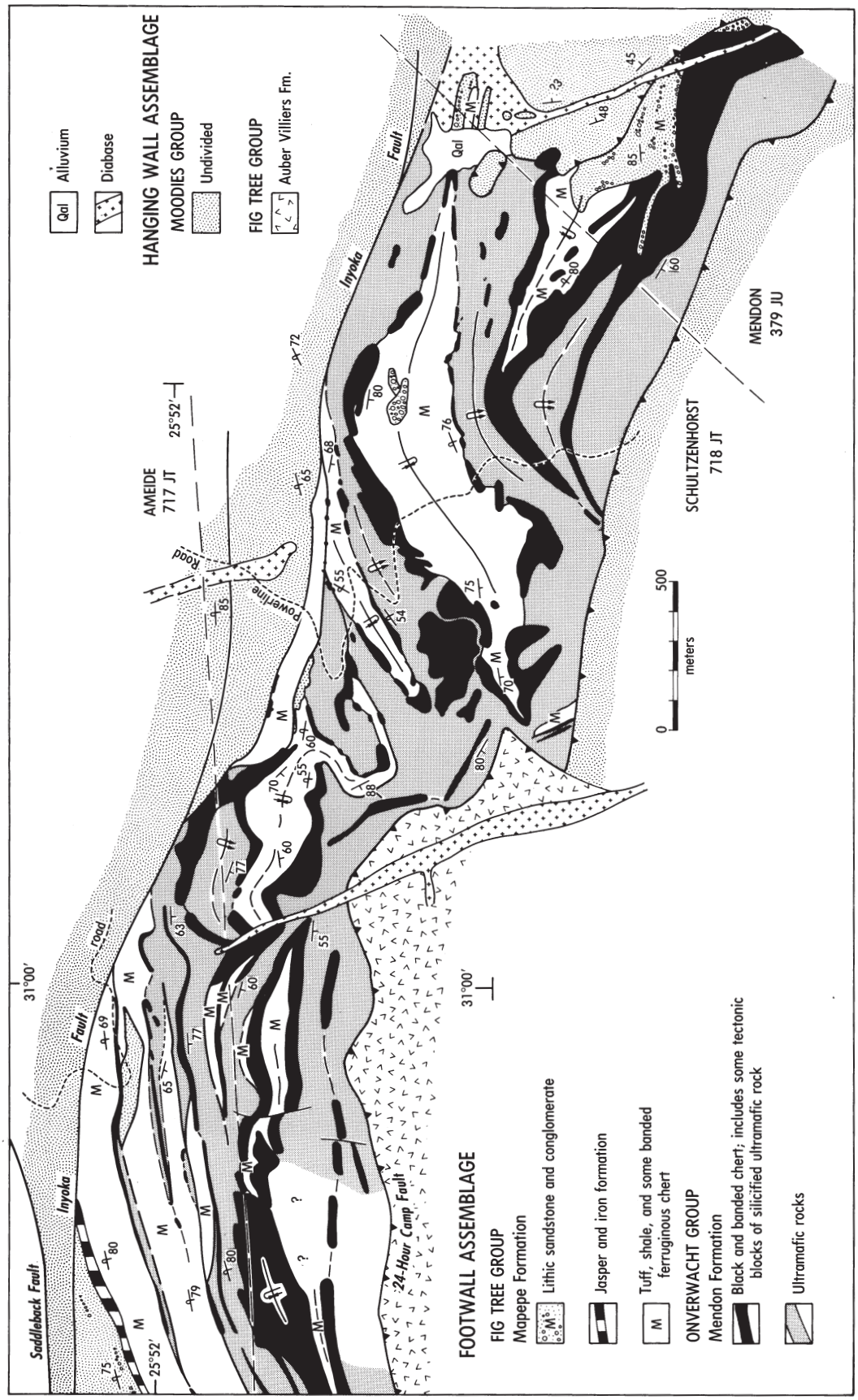


Figure 25. Geologic map of the northwest-trending zone of tight, overturned, doubly plunging folds developed in footwall rocks of the West-Central Domain between the 24-Hour Camp fault north of the Powerline Road syncline and the Inyoka fault south of the Saddleback syncline. The short-crested folds generally parallel regional fold and bedding trends and are oblique to the adjacent faults. In the northwestern part of the diagram, the bounding faults curve to an east-northeast trend, parallel to regional fold and bedding trends, and the intervening folds are long-crested with parallel limbs. Note that syncline in upper center of diagram has been refolded reflecting right-lateral slip on Inyoka fault.

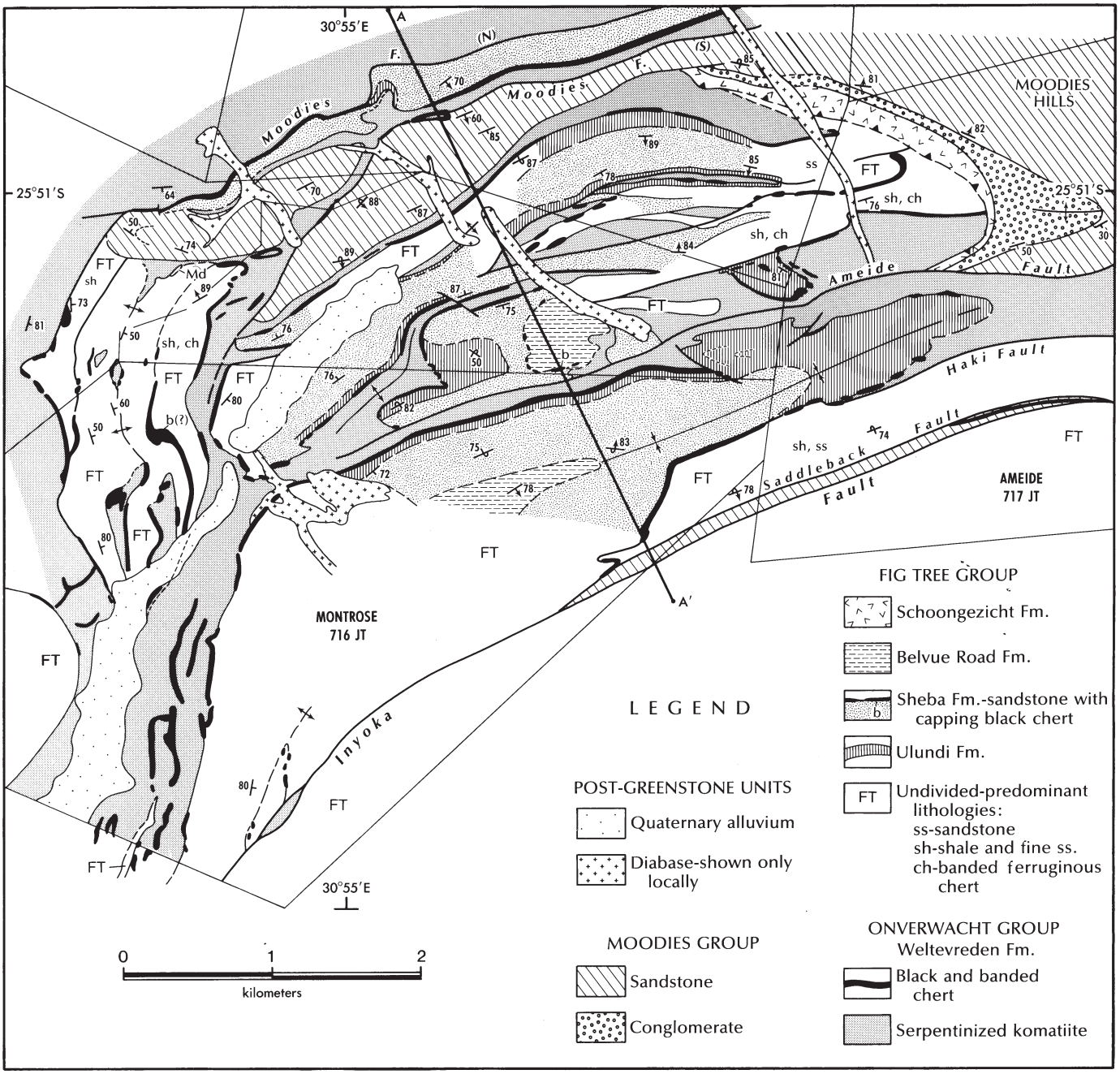


Figure 26. Geologic map of the Northern Domain (ND) between the Moodies Hills and the Stolzburg syncline. Location shown in Figure 2. Md indicates local tectonic blocks of sandstone of the Moodies Group.

meters to more than 100 m thick. The faults eventually merge in the western part of the study area (Figs. 1, 2, and 26).

The Haki and Ameide faults are vertical to subvertical faults occupying a narrow zone of serpentinite south of the Moodies Hills Block. Footwall Fig Tree strata between the Saddleback and Haki faults are more intensely sheared than in any other large Fig Tree block in the study area and show a strong, vertical to steeply south dipping cleavage. The Haki fault curves to the south and merges with the Saddleback fault in the central part of the study area (Fig. 26), and the Ameide fault passes westward into sheared ultramafic rocks, where it cannot be traced but appears to curve south and merge with the Inyoka fault.

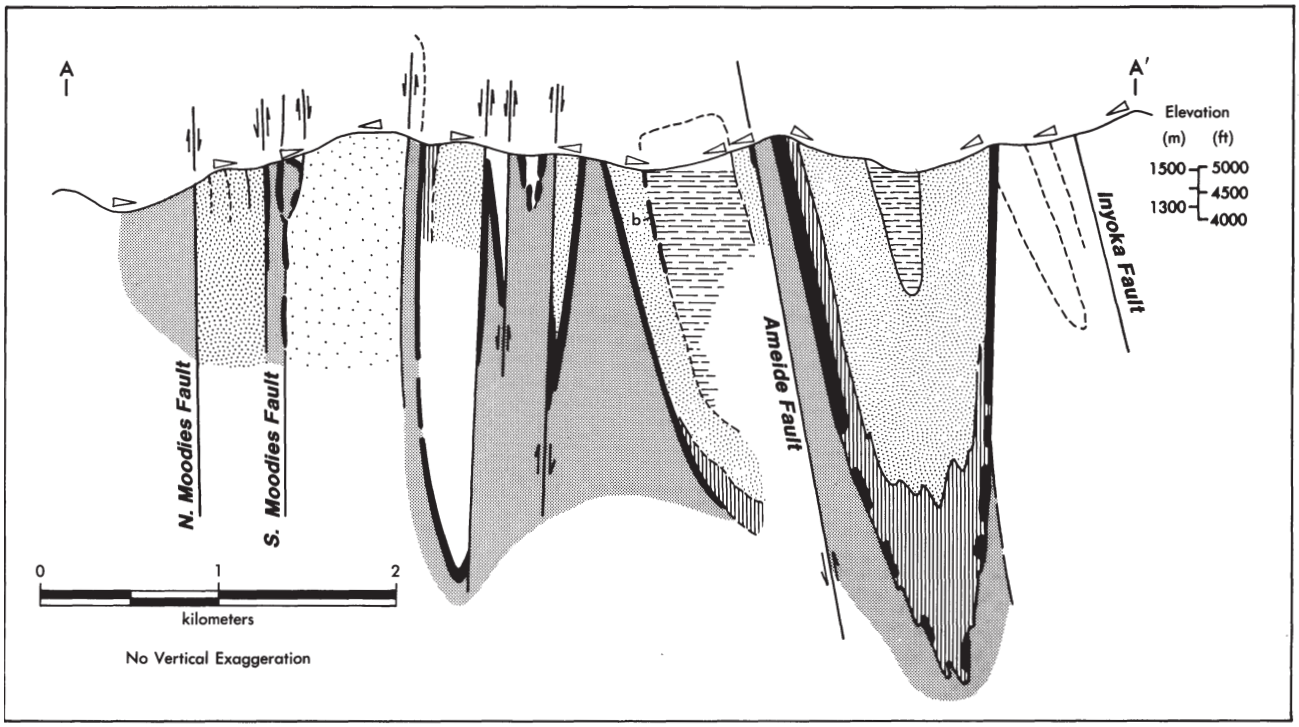


Figure 27. Cross section of the Northern Domain. Line of section and key to symbols shown in Figure 26.

The Moodies fault or fault zone is widely regarded as the frontal fault of the BGB, although additional major faults may be present in the belt of Weltevreden rocks north of the fault. Near the eastern edge of the study area, the Moodies fault appears to consist of a single fault that separates south-younging Weltevreden komatiites north of the fault from overturned, north-younging Moodies rocks in the Moodies Hills. To the west, the fault branches (Fig. 26). The northern branch appears to mark the northern limit of post-Onverwacht sedimentary rocks in the study area and to continue west to form the northern boundary of the Stolzburg syncline. The southern branch curves to the south and merges with the Inyoka fault.

Although these faults have been interpreted to have formed as north-verging thrust faults (Jackson et al., 1987), they show inconsistent slip relationships based on the offset of units across the faults (Fig. 27). Strain indicators suggest that they are, at least locally, zones of post-Moodies strike-slip movement (Hose, 1990). Some probably represent D_2 or D_4 thrust faults reactivated as D_5 oblique-slip to strike-slip faults.

The Stolzburg syncline appears to represent an example of D_5 escape tectonics. At the western end of the fold at the western tip of the BGB, Moodies rocks and adjacent parts of the Onverwacht and Fig Tree Groups form a thin, intensely deformed septum between the 3,445-Ma Badplaas and Stolzburg plutons to the south and the Nelshoogte pluton to the north (Fig. 29) that has yielded an age of 3,212 ± 2 Ma (York et al., 1989). The syncline widens and the intensity of penetrative strain decreases to the east (Reimer, 1967; de Wit et al., 1983). The present geometry of the syncline appears to reflect the eastward escape of Moodies and Fig Tree strata from between converging rigid plutonic blocks. The margins of the escaping body are bounded by and show shearing and truncation along the Inyoka and Moodies faults on the south and north, respectively. Along its eastern hinge, the escaping block of Moodies and Fig Tree strata plowed up an anomalous north-trending anticline of Weltevreden ultramafic rocks (Fig. 30) and folded previously active strike-slip faults. In both the ND and WCD immediately east of the north-trending anticline, rocks of the Fig Tree and Onverwacht Groups were tilted eastward, producing the observed west-to-east younging of outcropping rocks and decreasing plunges of D_2 drag folds in the WCD. This deformation may also have reactivated the WCD thrust faults as strike- or oblique-slip faults.

A number of later, minor, post-Moodies structural events have affected rocks of the ND, including tear faulting. These are not discussed here.

DISCUSSION

Cross-sections of the Barberton Greenstone Belt

Based on our overall geologic mapping and the preceding discussion, generalized cross sections of the BGB are presented in Figure 31 and a detailed cross section in Figure 32. These results suggest that the entire belt is floored at relative shallow depth by TTG intrusive rocks, largely in structural contact with the overlying greenstone units. This interpretation is consistent with inferences from geophys-

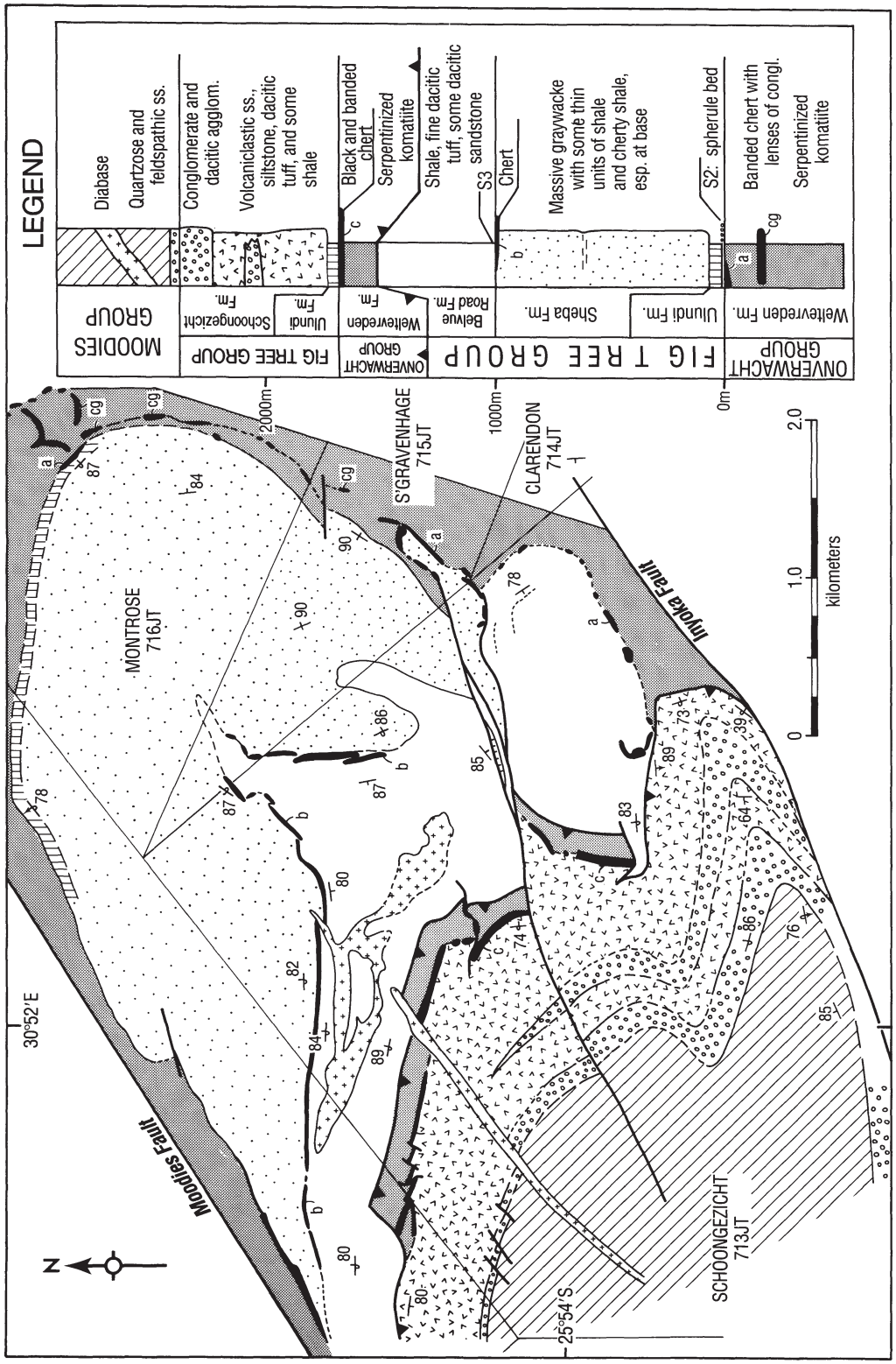


Figure 28. Geologic map of the hinge zone of the Stolzburg syncline. Contact between hanging-wall and footwall assemblages shown as a thrust fault with teeth on the upper plate. Location shown in Figure 2.

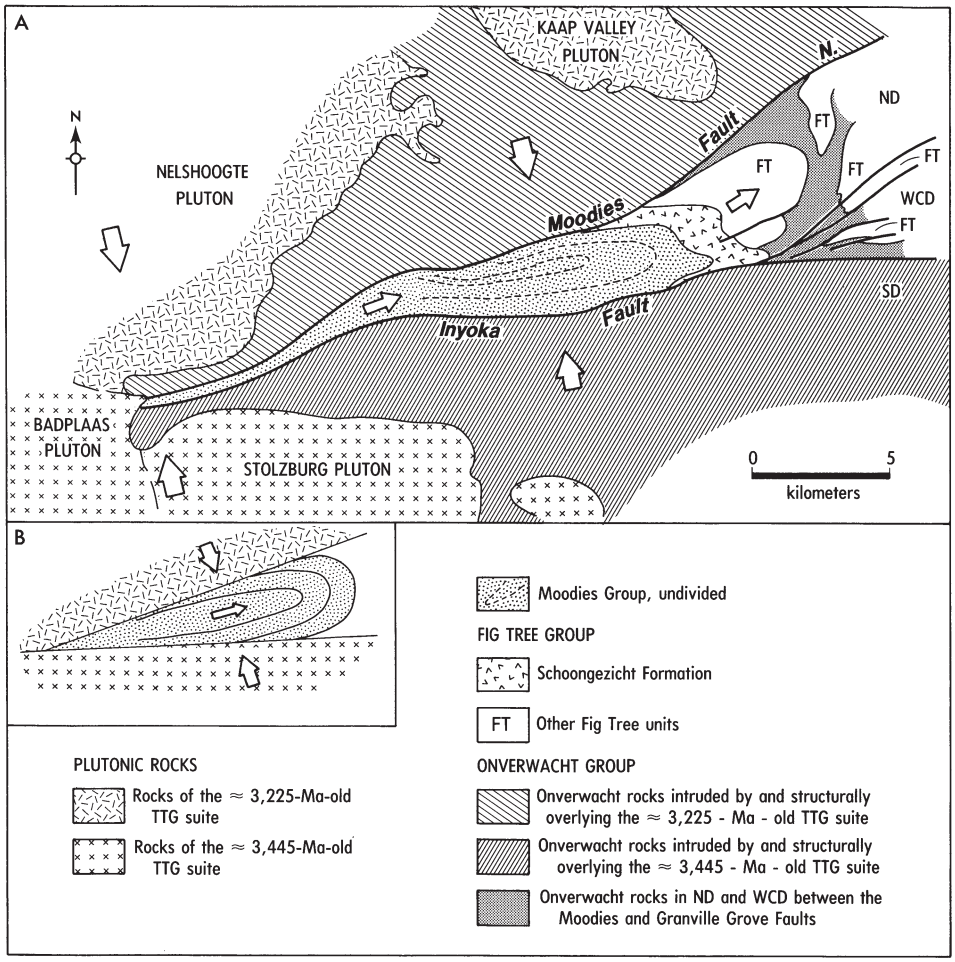


Figure 29. Generalized geologic map of the western tip of the Barberton Greenstone Belt showing the Stolzburg syncline and the inferred lateral escape of the Moodies and Fig Tree strata along bounding Moodies and Inyoka faults during D_5 heterogeneous shortening between northern and southern tonalite-trondhjemite-grandiorite (TTG) plutonic blocks. ND, Northern Domain; WCD, West-Central Domain.

ical surveys that the supracrustal sequence extends to depths of only 4 to 8 km (Darracott, 1975; de Beer et al., 1988). North of the Inyoka fault, the structural and intrusive basement is the 3,225-Ma TTG suite, mainly the Kaap Valley tonalite. There are no "basement" exposures south of the Inyoka fault in the central part of the BGB. We suggest that most of the southern part of the belt is underlain structurally by the 3,445-Ma TTG suite and possibly by a Fig Tree–aged TTG suite, 3,260–3,230 Ma, that does not crop out at the surface but is represented by volcaniclastic rocks in the lower parts of the Mapepe and Auber Villiers Formations in the WCD (Figs. 31 and 32).

Regional problems

This section focuses on two problems especially critical to resolving the structural makeup of the BGB: (1) the relationship between hanging-wall and footwall assemblages in the WCD, ECD, and ND; and (2) the relationship between sequences north and south of the Inyoka fault.

Relationship of hanging wall and footwall sequences. The supracrustal sequence throughout the western BGB can be divided into hanging-wall and footwall assemblages. The hanging wall includes Moodies and paraconformably underlying Schoongezicht or Auber Villiers strata; the footwall consists of the Mapepe Formation south of the Inyoka fault and the Ulundi, Sheba, and Belvue Road Formations north of the fault underlain by altered mafic to komatiitic rocks of the Onverwacht Group. Over much of the BGB, hanging-wall and footwall assemblages make up separate synclines, such as the Eureka and Saddleback synclines (hanging wall) and the Ulundi syncline (footwall). Adjacent hanging-wall and footwall synclines are usually parallel and separated by narrow belts of sheared serpentinite (Fig. 26). In a few areas, footwall strata and structures are truncated by hanging-wall units (Fig. 26). Nowhere do we know of a continuous, unfaulted stratigraphic succession that contains both assemblages, although the Stolzburg syncline section has been so interpreted (Reimer, 1967; Condie et al., 1970).

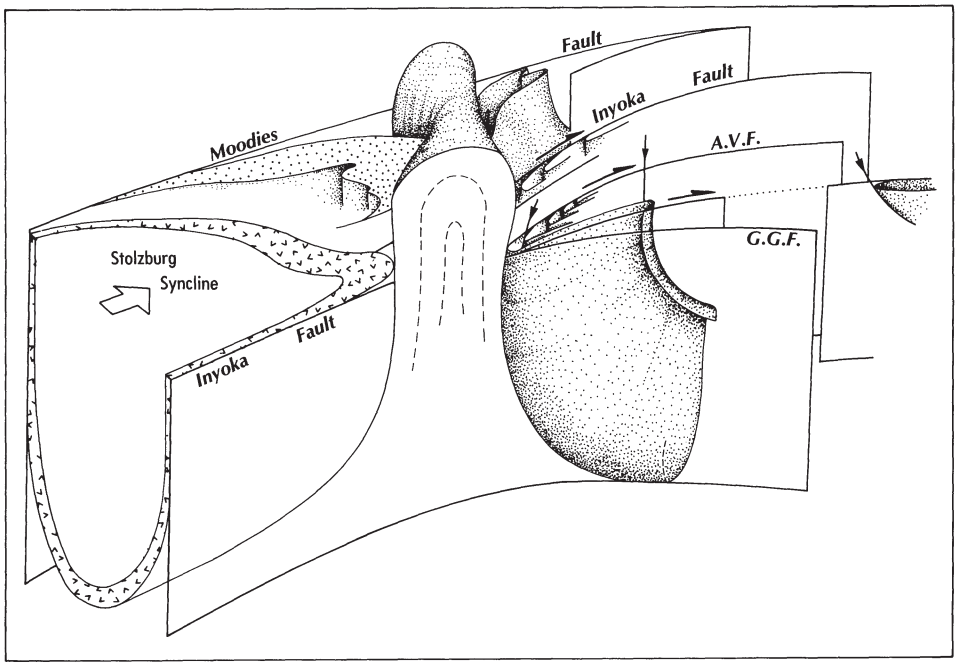


Figure 30. Three-dimensional sketch showing structures associated with the lateral escape of Moodies strata in the Stolzburg syncline. Escaping, steeply plunging Stolzburg syncline at left. Central sheared antiform represents ultramafic rock pushed up ahead of eastward-moving Moodies block. Upward movement of ultramafic rock has tilted and refolded Onverwacht and Fig Tree units and associated D_2 folds and faults to east. A.V.F., Auber Villiers fault; G.G.F., Granville Grove fault.

The contact between hanging-wall and footwall assemblages could be a fault, an unconformity, a faulted unconformity, or a regional surface of decoupling within an originally intact, although probably unconformable, stratigraphic succession. In the SD, changes in clast composition in the basal Moodies conglomerate parallel changes in composition of underlying, truncated Onverwacht rocks, suggesting that the contact there is an unconformity. In the ND and WCD, however, there is strong evidence that the contact is a fault with significant displacement. (1) Structural windows in the western WCD expose the contact, the 24-Hour Camp fault, which truncates both hanging-wall and footwall units and is marked by a zone of brecciation. Hanging-wall strata and structures are also truncated along the contact in the Powerline Road syncline, Maid-of-the-Mists syncline, and along the west side of the Moodies Hills Block (Figs. 2, 22, and 27). (2) The contact is not marked by a basal conglomerate. Conglomerate occurs along the contact only where it coincides with the base of the Moodies Group. Although the contact steeply truncates the Schoongezicht and Auber Villiers Formations in many areas, there are no facies changes in hanging-wall units toward the contact and no basal conglomerate that might be expected to mark an erosional unconformity. (3) Hanging-wall and footwall assemblages include strata that are in part of the same age. The hanging-wall Auber Villiers Formation in the WCD stratigraphically resembles the footwall Mapepe Formation and includes near its base rocks tentatively dated at 3,256 ± 4 Ma (Kröner et al., 1991). The base of the Mapepe Formation in the immediately underlying footwall assemblage includes tuffs dated at 3,243 ± 4 Ma (Kröner et al., 1991). In the Stolzburg syncline, the hanging-wall assemblage includes at its base units that are the lithologic and possibly the stratigraphic and age equivalents of the uppermost Onverwacht Group and overlying Ulundi Formation in the footwall.

In many areas, Schoongezicht or Auber Villiers rocks are absent in the hanging wall and the contact juxtaposes Moodies strata on older Fig Tree and Onverwacht rocks. Furthermore, we know of no sections where Moodies strata are present in the footwall. These features are perhaps more consistent with the contact being an unconformity or surface of decoupling within an originally continuous stratigraphic section. However, we suggest that the lower part of the hanging-wall sequence was deposited in a series of in-part extensional successor basins following D_2 and was thrust onto the adjacent older blocks during collapse of the basins during D_4 and D_5.

Relationship of rocks north and south of the Inyoka fault. It has long been recognized that there are distinct deep-water northern and shallow-water southern facies in the Fig Tree Group, separated by the Inyoka fault (Bell, 1967; Heinrichs, unpublished map, 1969; Reimer, 1975; Heinrichs and Reimer, 1977; Eriksson, 1980). The presence of turbiditic units in the Mapepe Formation immediately south of the Inyoka fault could indicate that southern and northern facies represent proximal and distal parts, respectively, of the same sedimentary

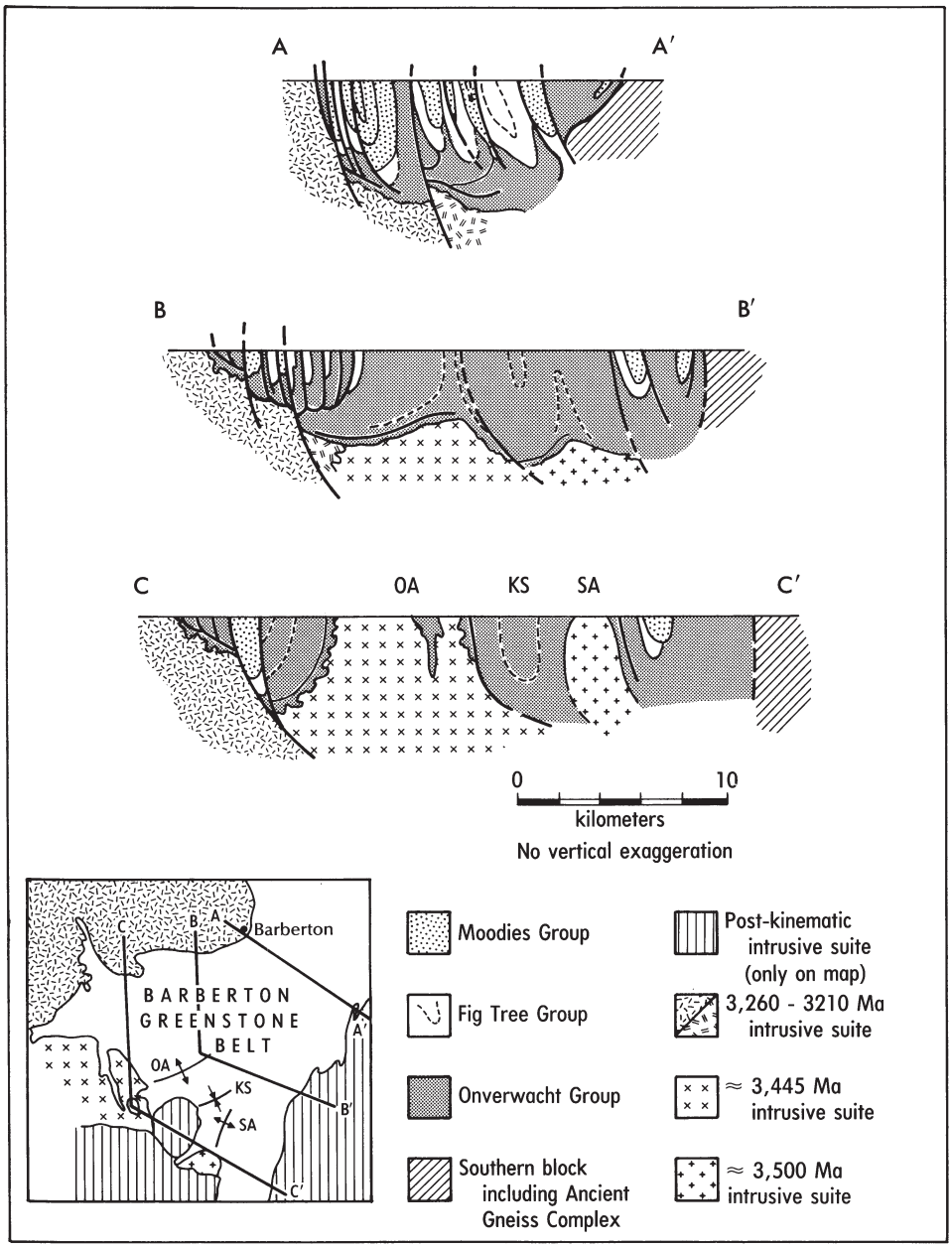


Figure 31. Generalized cross sections of the Barberton Greenstone Belt. OA, Onverwacht anticline; KS, Kromberg syncline; SA, Steynsdorp anticline.

sequence. There is also a remarkably similar structural architecture in the ND, WCD, and possibly ECD. Each includes hanging-wall and footwall assemblages separated by a fault. The intensity of deformation is greatest along the northern edges of both the ND and WCD, and kinematic indicators suggest relative uplift of blocks to the northwest. The overall stratigraphic, lithologic, and sedimentological similarity of these assemblages and their proximity across the Inyoka fault may indicate that they are parts of a single depositional basin bisected by the Inyoka fault.

However, Lowe and Byerly (this volume, Chapter 1), Heubeck and Lowe (this volume, Chapter 11), and Lowe and Nocita (this volume, Chapter 10) outline a number of important lithologic and sedimentological differences between southern and northern facies of the Fig Tree and Moodies Groups. Southern-facies Mapepe strata reflect active dacitic volcanism coupled with erosion of uplifted portions of the greenstone belt, but lack plutonic components, especially microcline. The northern-facies Sheba Formation, however, lacks evidence of concurrent dacitic volcanism and includes

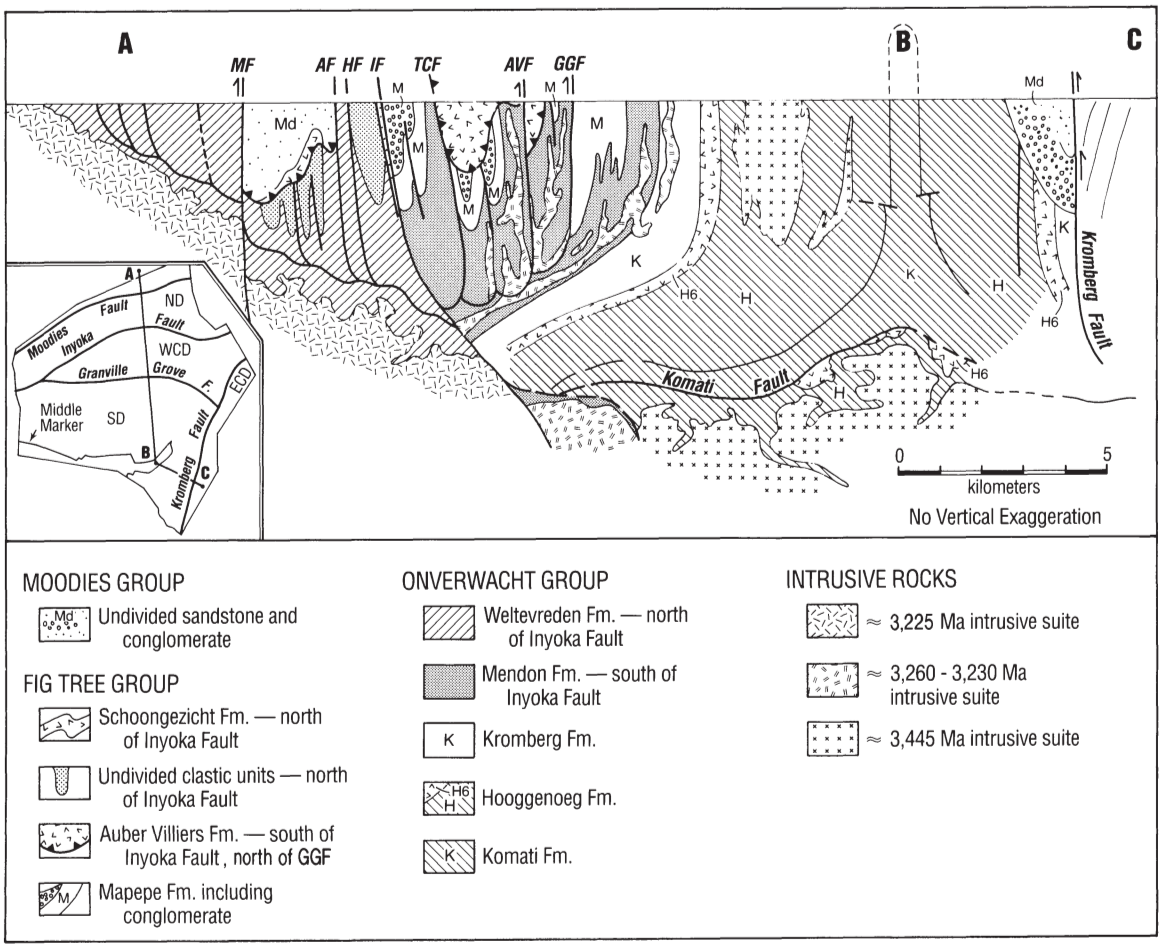


Figure 32. Detailed cross section of the Barberton Greenstone Belt.

common detrital microcline (Condie et al., 1970; Reimer, 1975). Byerly (unpublished data) has shown that hanging-wall Auber Villiers and Schoongezicht dacitic volcaniclastic rocks are geochemically dissimilar in detail and probably do not represent the same petrologic suite. Auber Villiers tuffs are quartz-phyric, vitric-rich, and probably mostly 3,260–3,230 Ma in age whereas Schoongezicht dacitic rocks lack quartz, are plagioclase-rich, and are probably mostly younger than 3,230 Ma. Moodies strata of both facies are generally similar, but north of the Inyoka fault, Moodies conglomerates contain clasts of plutonic rock and Moodies sandstones average 5 to 15% microcline (Hose, 1990; Heubeck and Lowe, this volume, Chapter 11). South of the Inyoka fault, Moodies rocks lack plutonic clasts and microcline (Hose, 1990; Heubeck and Lowe, this volume, Chapter 11).

The grossly similar stratigraphy, structure, lithology, and age of rocks on both sides of the Inyoka fault suggest that they represent parts of a single basinal sequence or separate but related basinal sequences. The contrasts suggest the latter.

History of deformation

D_1: Onverwacht deformation. The Komati and Hooggenoeg Formations of the Onverwacht Group in the SD accumulated as a large, complex shield volcano or volcanic platform (Fig. 33A). Metamorphism and deformation, D_1, accompanied emplacement of the 3,445-Ma TTG suite into this volcanic sequence (Fig. 33B). BGB rocks south of the Komati fault, which represent the roof sequence to the TTG plutons, were most heavily affected but age and structural details in this area are only beginning to emerge (de Wit et al., 1983; Armstrong et al., 1990; Kröner et al., 1996; Byerly et al., 1996). The volcanic sequence north of the fault, which accumulated more distally along the flank of the magmatic center, were less affected by intrusive activity, metamorphism, and deformation. The emplacement of hypabyssal felsic intrusions and an extrusive dome in H6 at 3,445 Ma along the west limb of the Onverwacht anticline was accompanied by faulting and overturning of immediately underlying volcanic units along the Geluk Disturbed Zone. This episode of magmatism, alteration, and deformation is also reflected in

$^{40}Ar/^{39}Ar$ ages of komatiites from the Komati Formation (López-Martínez et al., 1992).

Post-D_1, Pre-D_2 deformation. Lowe (1994, this volume, Chapter 12) has interpreted the Mendon Formation as having formed during an interval of extension and rifting. If so, this unnamed period of deformation is potentially represented by structures and fabrics within the BGB. Some of the large thrust faults within the WCD, across which the Mendon Formation shows progressive changes in stratigraphy, may represent later reactivated early normal faults associated with Mendon-age extension. To date, however, we have not labeled this as a separate interval of deformation. Tectonic quiescence seems to have prevailed between about 3,300 Ma and 3,260 Ma in the BGB (Fig. 33C).

D_2: Fig Tree deformation. All domains in the BGB record D_2 deformation in the form of clastic units within the Fig Tree Group representing uplift and erosion of older portions of the Swaziland Supergroup. Conglomerates in the middle and upper Mapepe Formation in the WCD mark uplift north of the Inyoka fault and along faults within the WCD. Thin, local conglomerate and sandstone units, attenuated sections, and intraformational unconformities in the Mapepe Formation along the trend of the Onverwacht anticline in the westernmost ECD reflect initial folding along the anticline, possibly as a foreland flexural bulge (Lowe and Nocita, this volume, Chapter 10) and/or as a ramp anticline (Fig. 33D). In the ECD, east of the study area, the Gelegela Grit (Heinrichs, 1980) records uplift of Fig Tree and Onverwacht rocks to the southeast. Although the details of late Mapepe deformation are poorly constrained, it appears that D_{2a} involved the formation of inward-facing fold-and-thrust belts along the northwestern and southeastern margins of the present BGB. These fold and thrust belts were separated by foreland basins that, during early Mapepe time, may have formed a single large basin but, by middle and late Mapepe time, were divided by uplift along the trend of the Onverwacht anticline and Proto-Inyoka Zone. The Onverwacht anticline and Proto-Inyoka Zone may have developed initially as a shared foreland bulge that later evolved into a ramp anticline or simply as a ramp anticline as thrusting propagated into the foreland basin.

Southward progradation of the northwestern fold-and-thrust belt during early D_{2b} emplaced off-platform rocks of the Mendon and Mapepe Formations over the unmetamorphosed portions of the older volcanic sequences (Komati through Mendon Formations) along the Granville Grove fault (Fig. 33E). D_2 was accompanied by the emplacement of a swarm of small hypabyssal plagioclase-phyric intrusions into serpentinites at the top of the Mendon Formation and Mapepe strata in the WCD and northern SD (Fig. 33E). During D_{2b}, in latest Mapepe and post-Mapepe time, the fold-and-thrust complex and structurally underlying relatively unmetamorphosed rocks of the older, pre-3,445-Ma platform sequence were thrust onto the central 3,445-Ma TTG intrusive block and its roof rocks along the Komati fault (Fig. 33E). Subsequent tightening of the Onverwacht anticline in late D_{2b} was probably associated with deformation along both northern and eastern margins of the 3,445-Ma TTG block. Compression of the flanking supracrustal sequences against this wedge-shaped TTG block resulted in oblique heterogeneous shortening, extreme hinge thickening of incompetent serpentinites, and eventual hinge collapse of the more competent Hooggenoeg and Kromberg Formations in the Onverwacht anticline.

The ND was also affected by D_2 but the kinematics of deformation have not been resolved.

Radiometric dating and stratigraphic relationships suggest that D_2 started in middle Fig Tree time, probably about 3,250–3,240 Ma. South-directed thrusting became general throughout the WCD during and following intrusion of shallow felsic plutons in the WCD, between 3,240 and 3,227 Ma. The upper limits of this deformation are poorly constrained, but the disappearance of coarse clastic debris in the uppermost tuffaceous rocks of the Mapepe Formation in the ECD suggests that local deformation ended by about 3,226 Ma.

D_3: Moodies deformation. The composition, wide distribution, and enormous thickness of Moodies strata imply large-scale relative uplift, exposure, and erosion of the TTG intrusive complexes and overlying and adjacent parts of the greenstone sequence and depression of the intervening areas, underlain mainly by deformed greenstone units. Clast and sandstone compositions suggest diverse source areas for Moodies strata and possibly deposition in a number of separate basins. If most Moodies rocks in the WCD and ND are allochthonous or parautochthonous, as we postulate, the principal basins may have been situated along the northwestern and southeastern margins of the BGB, adjacent to the hinterlands developed during D_2 and D_3. We suggest that D_3 may have involved extension or relaxation to form one or more successor basins (Tull and Groszos, 1990) on the D_2 orogen and along the junction of the northern 3,225-Ma TTG block and the greenstone terrane to the south (Fig. 33F).

D_4: Late-Moodies and early post-Moodies deformation. The synclinal fold train, narrow faulted anticlines, and subvertical dips characterizing much of the BGB originated in large part during post-Moodies deformation (Fig. 33G and H). Results of the present study suggest two separate stages of late Moodies and post-Moodies deformation: D_4 , during which a south- to southeast-verging fold-and-thrust belt developed in the WCD and ND, and D_5, involving extreme tightening within a northwest-directed fold belt and subsequent strike-slip faulting.

Among the major structures in the BGB are the TCF and similar inferred faults separating hanging- and footwall assemblages in the ND and ECD. The kinematics of this faulting are not resolved, and it is not even clear that these different faults formed at the same time. The simplest explanation is that these represent the sole thrusts of the thrust complex represented by faults separating individual synclines. This would imply that in the ND and parts of the WCD, thrusting was from northwest to southeast and the faults are D_4 structures (Fig. 33G). It would also imply, however, that in the ECD, where folds verge toward the northwest, a fault comparable to the TCF, if present, formed during northwest-verging deformation, perhaps during D_5. In the Powerline Road

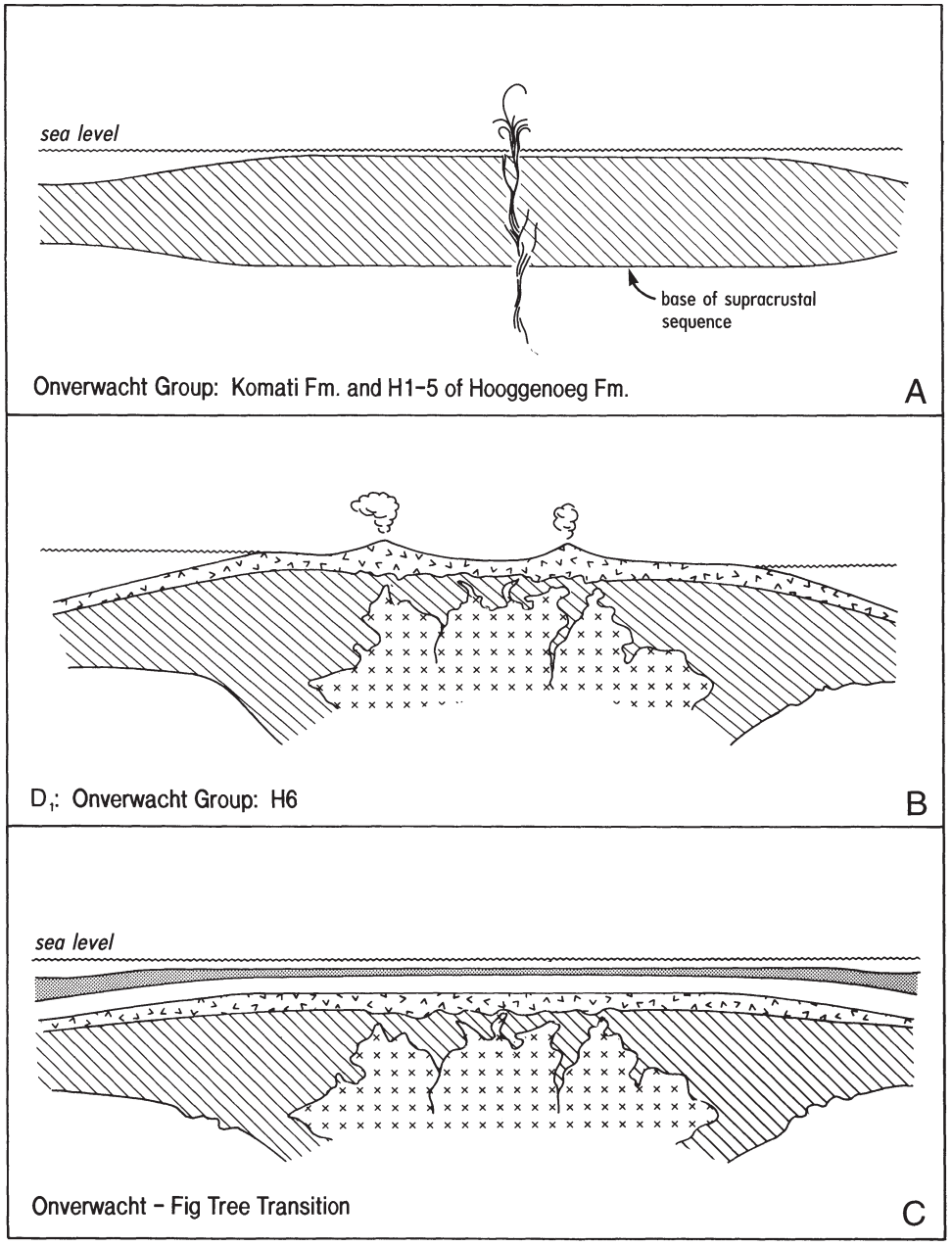
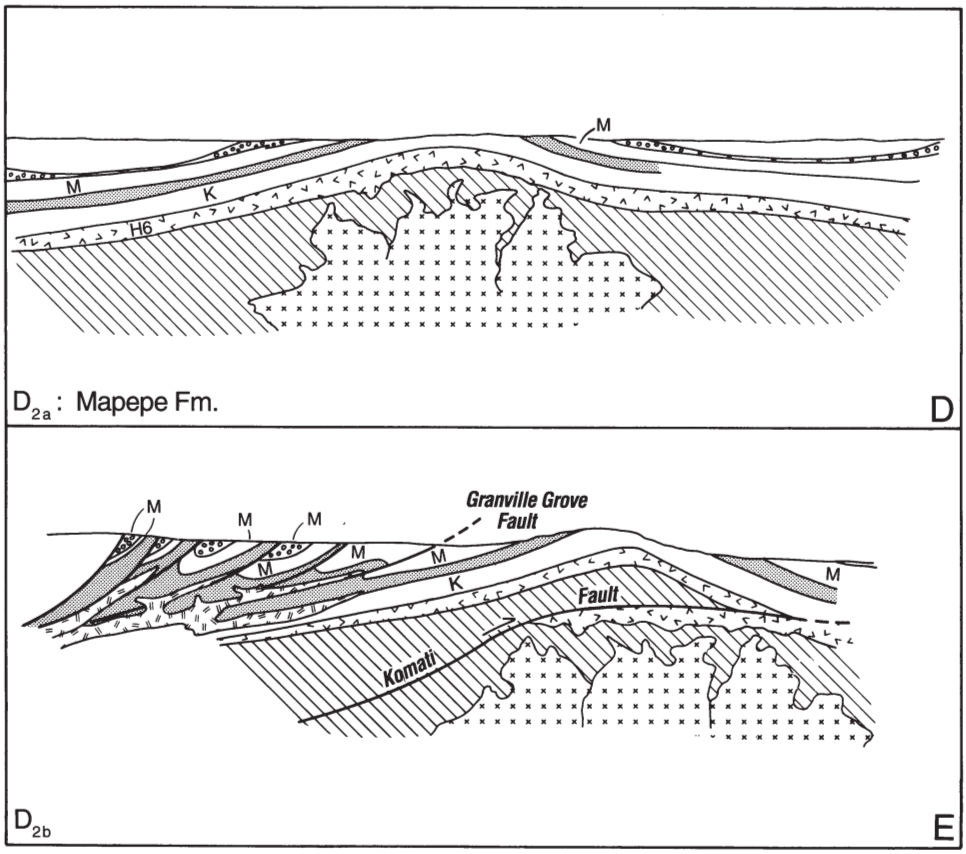


Figure 33 (above and next two pages). Geologic development of the west-central part of the Barberton Greenstone Belt (BGB). Symbols and orientation as in Figure 32. Northwest is to the left and southeast to the right in all figures. A, Volcanism and sedimentation from base of Komati Formation through member H5 of the Hooggenoeg Formation. B, Intrusion of 3,445-Ma tonalite-trondhjemite-grandiorite (TTG) suite into mafic volcanic sequence is accompanied by eruption of dacitic lavas and pyroclastic units at surface. Tectonism at this time (D_1) was associated with shallow emplacement of upper portions of TTG suite and subsidence/inflation during volcanism. C, Final stage of mafic volcanism is terminated by regional deposition of organic-rich siliceous sediments on magmatically quiescent, cooling, and subsiding platform immediately preceding Fig Tree deposition. D, During D_{2a} in middle Mapepe time, fully or partially facing foreland basins develop adjacent to fold and thrust belts (not shown) along the northwestern and southeastern margins of the BGB. These foreland basins formed around and were partially separated in the southwest by the 3,445-Ga TTG block. Northeast of the presently exposed TTG block, they were separated by the incipient Onverwacht anticline and its continuation, the Proto-Inyoka Zone, shown here. These uplifts may have been initiated as a shared foreland bulge or as a ramp anticline. Cherty clastic debris in the Mapepe Formation in the study area was derived from the north (left), and southeast (right), and locally from the incipient Onverwacht anticline and Proto-Inyoka Zone. E, D_{2a} deformation emplaces Mendon and Fig Tree units onto the marginal sequence of the older Onverwacht platform. Concurrent igneous activity along the northwestern margin of the fold-and-thrust belt is reflected in emplacement of shallow intrusions along thrust faults and into Mendon Formation. During D_{2b}, the younger fold-and-thrust complex and underlying platform-margin sequence was emplaced onto the central part of the older 3,445-Ma platform along the Komati fault. F, Following D_2, relaxation and regional extension form fault-bounded successor basins within which the lower part of the Moodies Group was deposited. G, Initial post-Moodies deformation (D_4) results in collapse of northern Moodies basins and southeastward thrusting of the basinal sequences onto older footwall units along 24-Hour Camp fault. H, Suturing of northern and southern TTG blocks during D_{5a} results in northwest-verging folding and thrust faulting, rotation of bedding and older faults and fold axial planes to vertical dips, folding of the 24-Hour Camp fault (TCF) and faulting of the TCF along reactivated D_4 faults, and tightening of Onverwacht anticline.



and Maid-of-the-Mists synclines (Figs. 18 and 22), the TCF appears to cut up-section to the north in the hanging wall, also suggesting northward tectonic transport or that the TCF here is a significantly out-of-sequence thrust fault. We are unable to resolve the kinematics of the TCF and related faults at the present time.

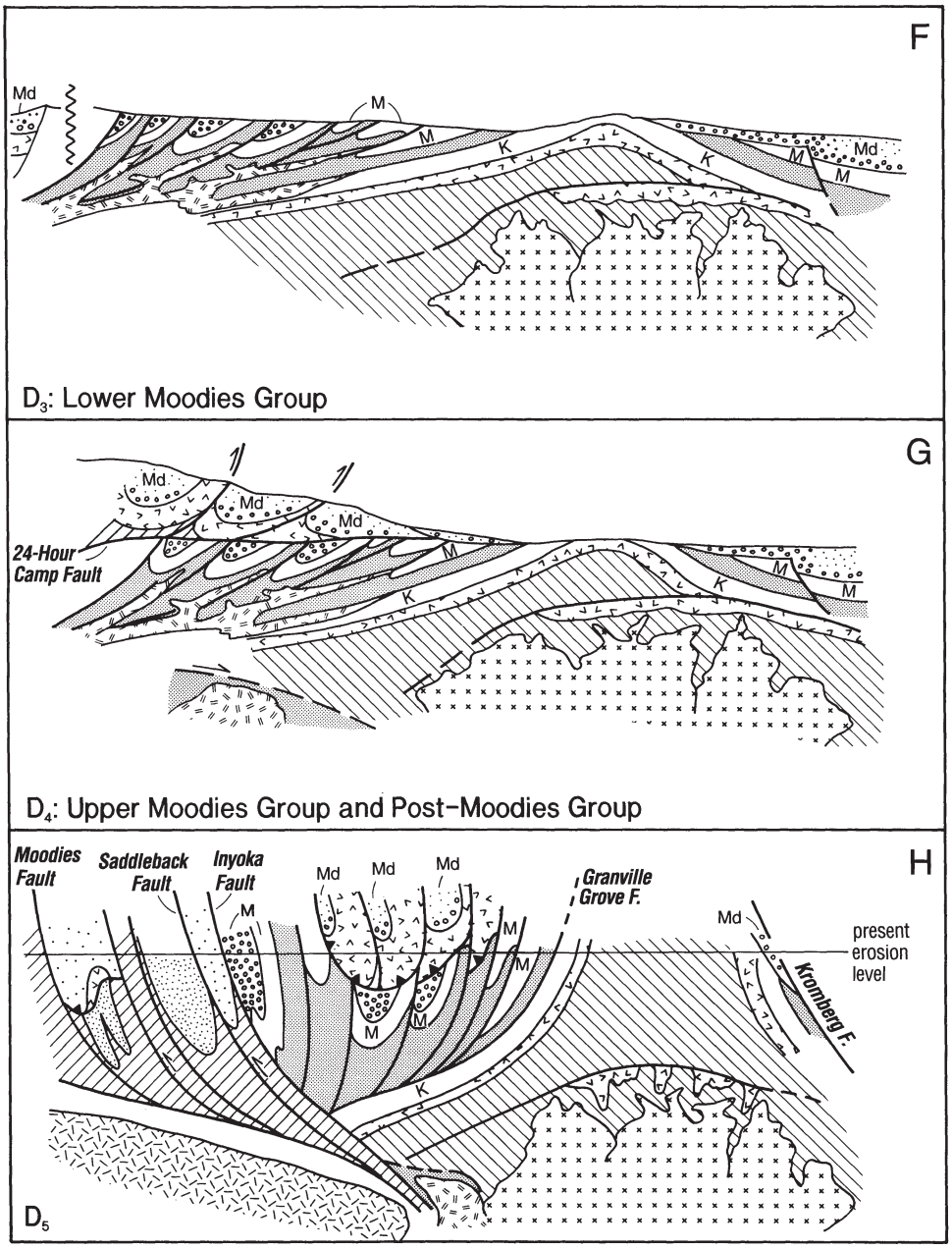
D_5: Late post-Moodies deformation. D_{5a} involved the formation of a regional northwest-verging fold belt (Ramsay, 1963; Anhaeusser, 1973; Jackson et al., 1987; Heubeck and Lowe, 1994a, b). Initially open D_4 folds and northwest-dipping thrust faults were rotated to subvertical or southeast-dipping orientations as the sequence was shortened between the rigid bounding TTG blocks. During fold rotation and tightening (D_{5b}), axial-plane cleavage developed across many of the earlier structures.

During final intense shortening, D_{5c}, the irregular shapes of the rigid plutonic blocks resulted in laterally heterogeneous strain distribution within the supracrustal sequence and the vertical and lateral escape of supracrustal rocks into zones of lower strain (Fig. 33H). Deformation was most intense along the northwestern margin of the greenstone sequence adjacent to the 3,225-Ma plutonic block. Fabrics produced during this deformation commonly include steeply plunging lineations, such as those defined by stretched conglomerate clasts (Ramsay, 1963; Gay, 1969). Also, the highly incompetent Mendon and Weltevreden serpentinites below the sedimentary sequence were widely squeezed upward into the cores of anticlines and along fault planes. Lateral escape is well displayed by the Stolzburg syncline.

Late D_{5c} refolded older structures around subvertical axes, gently refolding large synclines like the Eureka syncline. This deformation probably reflects molding of the sequence around the irregular boundaries of the bordering plutons.

It is possible that during D_4 or D_{5b} the largely unmetamorphosed Onverwacht and Fig Tree Groups making up the flanking portions of the 3,225-Ma TTG complex were thrust to the northwest over the central TTG-roof rock block along a fault analogous to the Komati fault. If it exists, this fault may coincide with the Moodies fault or lie within ultramafic rocks of the Weltevreden Formation north of the Moodies fault.

The depositional age of the Moodies Group is poorly constrained. It is younger than the 3,225-Ma age of the Schoongezicht Formation and probably older than the age of rutile possibly associated with mineralization northeast of Barberton dated at 3,084 ± 18 Ma (de Ronde et al., 1991). Folded and faulted Moodies rocks at the northeastern end of the BGB are intruded and metamorphosed by the 3,109-Ma Salisbury Kop pluton (Kamo and Davis, 1994; Heubeck et al., 1993). An indirect age locally is suggested by relationships in the Kromberg syncline. Moodies strata along the east limb of the Onverwacht anticline generally dip 10–40° less than underlying rocks of the Onverwacht Group, upon which they rest unconformably. The general parallelism of strikes and similarity of dip directions in Moodies and Onverwacht strata on the east limb suggest that late fold tightening in the Kromberg syncline followed deposition of the Moodies Group. The Dalmein



pluton is a post-kinematic pluton that truncates the south end of the isoclinal Kromberg syncline and has been dated at 3,216 +2/–1 Ma (Kamo and Davis, 1991, 1994). These relationships suggest that Moodies sedimentation and D_4 and D_5 in the Kromberg syncline may have occurred between 3,225 and 3,216 Ma.

Comparison to other deformational histories

Ramsay (1963) studied only post-Moodies deformation, but the sequence of post-Moodies events and their effects are generally the same as those outlined here. The first deformation event recognized by Ramsay (1963) corresponds to D_{5a} of the present study and the second to D_{5b}. His D_3 corresponds to the present D_{5c}. Ramsay noted that these might constitute part of a single orogeny as proposed here.

Comparison with structural scenarios of de Wit (1983) and de Wit et al. (1983, 1987a) are difficult because of our fundamentally different conclusions regarding stratigraphy and structure of the BGB. Because these authors considered Onverwacht and Fig Tree, and possibly Moodies, rocks to be facies of one another, virtually all deformation events, even those regarded as early and almost syndepositional, were considered to be post-Moodies in age. Hence, although de Wit et al. (1983) regarded the felsic intrusion in H6 along the west limb of the Onverwacht anticline as a

very shallow level dome that invaded its own surface rubble and may have been associated with the eruption of volcaniclastic units in H6, intrusion was considered to have occurred during post–Fig Tree thrusting (D_2 of de Wit et al., 1983). This structural scenario and the inferred age relationships are clearly contradicted by more recent dating, which demonstrates that Onverwacht and Fig Tree felsic magmatism were separated by about 200 m.y. (Armstrong et al., 1990; Kröner et al., 1991).

Overall, de Wit (1982, 1983) and de Wit et al. (1983, 1987a) recognized three periods of deformation in the BGB. The first, D_1, was thought to be an interval during which recumbent folds, inverted stratigraphy, nappes, olistostromes, and slides (faults) formed, mainly in rocks here included in the upper Onverwacht and Fig Tree Groups. Thrusting in the Onverwacht Group was accompanied by the formation of "quartz-carbonate-talc-fuchsite-schist/gneiss zones" marking decollement zones and low-angle faults. These zones have been discussed above and by Lowe and Byerly (1986), Duchac (1986), Duchac and Hanor (1987), and Hanor and Duchac (1990) and, in our opinion, represent horizons of flow-top metasomatic alteration unrelated to faulting. The bulk of the structures representing D_1 of de Wit (1982, 1983); and de Wit et al., (1987a) occur in the WCD and correspond to structures formed during D_2 of the present study.

D_2 of de Wit (1983) was regarded as the main interval of folding in the BGB. It involved horizontal shortening that produced upright, steeply plunging folds, such as the Stolzburg syncline; the major faults in the belt, including the Komati, Inyoka, and Moodies faults, and segments of the bounding faults in the WCD; the principal cleavage in the belt; and steeply plunging stretching lineation. These structures include features belonging to both D_2 and D_5 of the present study.

D_3 of de Wit (1983) resulted in the formation of crenulation cleavage and late faults and folds, including the Onverwacht anticline and Kromberg syncline. We regard these larger folds in the SD as D_2 structures, formed initially in late Fig Tree time, that were tightened during D_5.

Lamb (1984b) distinguished three stages of deformation, D_1, D_2, and D_3, in rocks in Swaziland along the extreme southeastern margin of the BGB. Stratigraphic contrasts between this area and the main BGB again make correlation of tectonic events difficult. However, the two major stratigraphic units recognized by Lamb (1984a, b), a lower Group B, the Diepgezet Group, and an upper Group A, the Malalotsha Group, generally correspond petrologically to the Fig Tree and Moodies Groups, respectively. D_1 of Lamb (1984b) affects rocks of the lower group more strongly than those of the upper group, and, in some areas, the two are separated by an angular unconformity, suggesting a general correspondence with D_2 or D_3 of the present study. Deformation was syndepositional with sedimentation of the upper group and characterized by the development of synsedimentary folds and a northwest-verging thrust belt. These structures were folded into north-trending, south-plunging synforms and antiforms (his D_2) and refolded by a later heterogeneous folding (his D_3). Lamb and Paris (1988) recognize two principal episodes of deformation, including D_2 and D_3 above as D_{2a} and D_{2b}. Precise correlation between these events and those of the present study is problematic, although it seems likely that most deformational events documented by Lamb (1984a, b) represent syn- or post-Moodies deformation.

The most recent analysis available (de Ronde and de Wit, 1994) outlines a tectonic history based largely on the stratigraphic and tectonic interpretations of de Wit (1982, 1983) and de Wit et al. (1983, 1987a). D_1 is interpreted as a shortening event involving thrust faulting and nappe formation that began as early as 3,445 ± 8 Ma (de Ronde and de Wit, 1994, p. 993) and affected rocks possibly as young as lower Fig Tree (about 3,260–3,240 Ma). The present study would indicate that most folds and faults interpreted by these authors as D_1 are Fig Tree and post–Fig Tree, pre-Moodies D_2 structures. These results correspond well with the interpretations of Kamo and Davis (1994) that the earliest well-documented regional deformation in the BGB is Fig Tree or post–Fig Tree in age. D_2 of de Ronde and de Wit (1994), dated at ~3,227 Ma, corresponds more-or-less to the latest stages of D_2 of the present study. Their D_3 and D_4 generally represent post-Moodies events and so correspond in timing to the present D_4 and D_5, although the specific structures and events may differ.

CONCLUSIONS

The structural development of the western part of the Barberton Greenstone Belt can be described in terms of at least five principal periods of deformation. The Onverwacht Group in the SD was deposited as an predominantly mafic to ultramafic volcanic sequence between about 3,550 and 3,445 Ma. Deformation (D_1) accompanied felsic volcanism and intrusion of the 3,445-Ma TTG suite in late Hooggenoeg time. Its identified effects, to date, are limited to faulting associated with the intrusion of hypabyssal felsic porphryries in the Onverwacht anticline. Minor extensional faulting occurred during deposition of the lower portions of the immediately overlying Kromberg Formation and additional major extension probably accompanied deposition of komatiites of the Mendon Formation.

D_2 involved initial shortening of the supracrustal sequence during Fig Tree time from about 3,250 to 3,226 Ma. During D_{2a}, facing foreland basins developed in the BGB, flanked by fold-and-thrust belts and separated by the early Onverwacht anticline, which may have formed as a shared foreland bulge. Deformation involved formation of a south- to southeast-verging fold-and-thrust belt in the WCD and ND within which rocks of the Mendon and Mapepe Formations were tectonically transported onto the marginal, unmetamorphosed parts of the older, 3,445-Ma platform sequence. The basal thrust was the Granville Grove fault. During D_{2b}, this fold-and-thrust complex was in turn transported southward onto the central part of the 3,445-Ma TTG and greenstone roof-rock complex. The basal thrust is the Komati fault. Late D_{2b} shortening along both sides of the 3,445-Ma TTG block was accompanied by hinge collapse in the Onverwacht

anticline and extreme hinge thickening, mostly of incompetent serpentinites of the Komati and Mendon Formations.

D_3 represents a period when the 3,445-Ma TTG suite, the Ancient Gneiss Complex, and possibly the younger 3,225-Ma northern TTG complex were uplifted and eroded to yield enormous quantities of quartz-rich Moodies clastic sediment. The locus of this uplift in the SD was probably the Komati fault and in the ND, the Moodies fault. It is possible that uplift during sedimentation of the lower part of the Moodies Group involved extension, with relative downdropping of the supracrustal sequence between the TTG blocks. Part of the lower Moodies Group may have accumulated in a number of separate successor basins to the D_2 orogen.

D_4 and D_5 were the principal deformational events in the BGB. During D_4, rocks in the WCD and ND were thrust to the south and southeast in response to shortening against the northern 3,225-Ma TTG block. D_4 may have commenced during deposition of the upper part of the Moodies Group. Regional shortening and formation of a northwest-verging fold-and-thrust belt occurred during D_{5a}. D_{5b} involved tightening of the D_{5b} folds; rotation of bedding, faults, and the axial planes of folds to vertical or subvertical dips; and development of axial-plane cleavage. D_{5c} involved heterogeneous shortening of the supracrustal sequence between the irregular bounding TTG blocks and the vertical and lateral escape of large blocks of supracrustal material. Strike-slip faulting, principally in the ND, accompanied the lateral escape of blocks, such as the Stolzburg syncline. Late D_{5c} involved refolding around vertical to subvertical axes as older structures were molded against the irregular TTG blocks.

The BGB is a compound belt made up of several TTG blocks and the intervening supracrustal sequences. Each block included a central rigid TTG core and overlying and surrounding metamorphosed and deformed Onverwacht rocks into which the plutons were emplaced. These complexes were flanked by distally thinning, unmetamorphosed parts of the Onverwacht volcanic succession. Late deformation records intense shortening and thickening of the incompetent supracrustal sequences between the rigid TTG blocks and finally amalgamation of the blocks themselves.

REFERENCES CITED

Anhaeusser, C. R., 1969, The stratigraphy, structure, and gold mineralisation of the Jamestown and Sheba Hills areas of the Barberton Mountain Land [Ph.D. thesis]: Johannesburg, University of the Witwatersrand, 332 p.

Anhaeusser, C. R., 1972, The geology of the Jamestown Hills area of the Barberton Mountain Land, South Africa: Geological Society of South Africa Transactions, v. 75, p. 225–263.

Anhaeusser, C. R., 1973, The evolution of the early Precambrian crust of southern Africa: Royal Society of London Philosophical Transactions, ser. A, v. 273, p. 359–388.

Anhaeusser, C. R., 1975, The geological evolution of the primitive Earth: evidence from the Barberton Mountain Land: University of the Witwatersrand, Economic Geology Research Unit Information Circular 98, 22 p.

Anhaeusser, C. R., 1976, The geology of the Sheba Hills area of the Barberton Mountain Land, South Africa, with particular reference to the Eureka syncline: Geological Society of South Africa Transactions, v. 79, p. 253–280.

Anhaeusser, C. R., 1984, Structural elements of Archaean granite-greenstone terranes as exemplified by the Barberton Mountain Land, southern Africa, *in* Kröner, A., and Greiling, R., eds., Precambrian tectonics illustrated: Stuttgart, Germany, E. Schweizerbart'sche Verlagsbuchhandlung, p. 57–78.

Anhaeusser, C. R., Robb, L. J., and Viljoen, M. J., 1981, Provisional geological map of the Barberton Greenstone Belt and surrounding granitic terrane, eastern Transvaal and Swaziland: Geological Society of South Africa, scale 1:250,000.

Armstrong, R. A., Compston, W., de Wit, M. J., and Williams, I. S., 1990, The stratigraphy of the 3.5–3.2 Ga Barberton Greenstone Belt revisited: a single zircon ion microprobe study: Earth and Planetary Science Letters, v. 101, p. 90–106.

Bell, M. C., 1967, The geology of the farm Heemstede 33 and portions of the farms Schultzenhorst 31 and Mendon 32 in the Barberton Mountain Land [M.Sc. thesis]: Durban, University of Natal, 115 p.

Byerly, G. R., Kröner, A., Lowe, D. R., and Walsh, M. M., 1993, Sequential magmatic evolution of the early Archean Onverwacht Group: evidence from the upper formations: Eos (Transactions, American Geophysical Union), v. 74, p. 660.

Byerly, G. R., Kröner, A., Lowe, D. R., Todt, W., and Walsh, M. M., 1996, Prolonged magmatism and time constraints for sediment deposition in the early Archean Barberton greenstone belt: evidence from the Upper Onverwacht and Fig Tree Groups: Precambrian Research, v. 78, p. 125–138.

Condie, K. C., Macke, J. E., and Reimer, T. O., 1970, Petrology and geochemistry of early Precambrian graywackes from the Fig Tree Group, South Africa: Geological Society of America Bulletin, v. 81, p. 2759–2776.

Cowan, D. S., 1985, Structural styles in Mesozoic and Cenozoic melanges in the western Cordillera of North America: Geological Society of America Bulletin, v. 96, p. 451–462.

Daneel, G. J., 1987, The structural controls of gold mineralization in the Moodies Hills which surround the Agnes Gold Mine, Barberton Greenstone Belt [M.Sc. thesis]: Durban, University of Natal, 128 p.

Darracott, B. W., 1975, The interpretation of the gravity-anomaly over the Barberton Mountain Land, South Africa: Geological Society of South Africa Transactions: v. 78, p. 123–128.

de Beer, J. H., Stettler, E. H., du Plessis, J. G., and Blume, J., 1988, The deep structure of the Barberton greenstone belt: a geophysical study: South African Journal of Geology, v. 91, p. 184–197.

de Ronde, C. E. J., and de Wit, M. J., 1994, Tectonic history of the Barberton greenstone belt, South Africa: 490 million years of Archean crustal evolution: Tectonics, v. 13, p. 983–1005.

de Ronde, C. E. J., Kamo, S., Davis, D. W., de Wit, M. J., and Spooner, E. T. C., 1991, Field, geochemical and U-Pb isotopic constraints from hypabyssal felsic intrusions within the Barberton greenstone belt, South Africa: Implications for tectonics and the timing of gold mineralization: Precambrian Research, v. 49, p. 261–280.

de Wit, M. J., 1982, Gliding and overthrust nappe tectonics in the Barberton Greenstone Belt: Journal of Structural Geology, v. 4, p. 117–136.

de Wit, M. J., 1983, Notes on a preliminary 1:25,000 geological map of the southern part of the Barberton Greenstone Belt, *in* Anhaeusser, C. R., ed., Contributions to the geology of the Barberton Mountain Land: Geological Society of South Africa Special Publication 9, p. 185–187.

de Wit, M. J., 1986, Extensional tectonics during the igneous emplacement of the mafic-ultramafic rocks of the Barberton Greenstone Belt: Lunar and Planetary Institute Technical Report No. 86-10, p. 84–85.

de Wit, M. J., Fripp, R. E. P., and Stanistreet, I. G., 1983, Tectonic and stratigraphic implications of new field observations along the southern part of the Barberton Greenstone Belt, *in* Anhaeusser, C. R., ed., Contributions to the geology of the Barberton Mountain Land: Geological Society of South Africa Special Publication 9, p. 21–29.

de Wit, M. J., Hart, R. A., and Hart, R. J., 1987a, The Jamestown Ophiolite Complex, Barberton mountain belt: a section through 3.5-Ga oceanic crust: Journal of African Earth Sciences, v. 6, p. 681–730.

de Wit, M. J., Armstrong, R. J., Hart, R. J., and Wilson, A. H., 1987b, Felsic

igneous rocks within the 3.3 to 3.5 Ga Barberton Greenstone Belt: high crustal-level equivalents of the surrounding tonalite-trondhjemite terrain, emplaced during thrusting: Tectonics, v. 6, p. 529–549.

de Wit, M. J., Roering, C., Hart, R. J., Armstrong, R. A., de Ronde, C. E. J., Green, R. W. E., Tredoux, M., Peberdy, E., and Hart, R. A., 1992, Formation of an Archaean continent: Nature, v. 357, p. 553–562.

Duchac, K. C., 1986, Metasomatic alteration of a komatiitic sequence into chert [M.Sc. thesis]: Baton Rouge, Louisiana State University, 240 p.

Duchac, K. C., and Hanor, J. S., 1987, Origin and timing of the metasomatic silicification of an Early Archean komatiite sequence, Barberton Mountain Land, South Africa: Precambrian Research, v. 37, p. 125–146.

Eriksson, K. A., 1980, Hydrodynamic and paleogeographic interpretation of turbidite deposits from the Archean Fig Tree Group of the Barberton Mountain Land, South Africa: Geological Society of America Bulletin, v. 91, p. 21–26.

Fripp, R. E. P., van Nierop, D. A., Callow, M. J., Lilly, P. A., and du Plessis, L. U., 1980, Deformation in part of the Archaean Kaapvaal Craton, South Africa: Precambrian Research, v. 13, p. 241–251.

Gay, N. C., 1969, The analysis of strain in the Barberton Mountain Land, eastern Transvaal, using deformed pebbles: Journal of Geology, v. 77, p. 377–396.

Hanor, J. S., and Duchac, K., 1990, Isovolumetric silicification of Early Archean komatiites: geochemical mass balances and constraints on origin: Journal of Geology, v. 98, p. 863–877.

Heinrichs, T. K., 1980, Lithostratigraphische Untersuchungen in der Fig Tree Gruppe des Barberton Greenstone Belt zwischen Umsoli und Lomati (Sudafrika) (Lithostratigraphic study in the Fig Tree Group of the Barberton Greenstone Belt between Umsoli and Lomati [South Africa]): Gottinger Arbeiten zur Geologie und Palaontologie, v. 22, 118 p.

Heinrichs, T. K., 1984, The Umsoli Chert, turbidite testament for a major phreatoplinian event at the Onverwacht/Fig Tree transition (Swaziland Supergroup, Archaean, South Africa): Precambrian Research, v. 24, p. 237–283.

Heinrichs, T. K., and Reimer, T. O., 1977, A sedimentary barite deposit from the Archean Fig Tree Group of the Barberton Mountain Land (South Africa): Economic Geology, v. 72, p. 1426–1441.

Heubeck, C., and Lowe, D. R., 1992, Petrographic evolution and provenance of the Archean Moodies Group, Barberton Greenstone Belt, South Africa: Geological Society of America, Abstracts with Programs, v. 24, p. A179.

Heubeck, C., and Lowe, D. R., 1994a, Depositional and tectonic setting of the Archean Moodies Group, Barberton Greenstone Belt, South Africa: Precambrian Research, v. 68, p. 257–290.

Heubeck, C., and Lowe, D. R., 1994b, Late syndepositional deformation and detachment tectonics in the Barberton Greenstone Belt, South Africa: Tectonics, v. 13, p. 1514–1536.

Heubeck, C., Wendt, J. I., Toulkeridis, T., Kröner, A., and Lowe, D. R., 1993, Timing of deformation of the Archaean Barberton Greenstone Belt, South Africa: constraints from zircon dating of the Salisbury Kop pluton : Journal of South African Geology, v. 96, p. 1–8.

Hose, L. D., 1990, The geology and stratigraphic evolution of the north-central part of the Early Archean Barberton Greenstone Belt, South Africa [Ph.D. dissertation]: Baton Rouge, Louisiana State University, 381 p.

Jackson, M. P. A., and Robertson, D. I., 1983, Regional implications of Early-Precambrian strains in the Onverwacht Group adjacent to the Lochiel granite, north-west Swaziland: Geological Society of South Africa Special Publication 9, p. 45–62.

Jackson, M. P. A., Eriksson, K. A., and Harris, C. W., 1987, Early Archean foredeep sedimentation related to crustal shortening: a reinterpretation of the Barberton Sequence, southern Africa: Tectonophysics, v. 136, p. 197–221.

Kamo, S., and Davis, D., 1991, A review of geochronology from the Barberton Mountain Land, *in* Ashwal, L. D., ed., Two cratons and an orogen: Excursion guidebook and review articles for a field workshop through selected Archaean terranes of Swaziland, South Africa, and Zimbabwe: International Geological Correlation Program (IGCP) Project 280, Johannesburg, University of the Witwatersrand, Department of Geology, p. 59–68.

Kamo, S. L., and Davis, D. W., 1994, Reassessment of Archean crustal development in the Barberton Mountain Land, South Africa, based on U-Pb dating: Tectonics, v. 13, p. 167–192.

Kröner, A., and Todt, W., 1988, Single zircon dating constraining the maximum age of the Barberton Greenstone Belt, southern Africa: Journal of Geophysical Research, v. 93, p. 15329–15337.

Kröner, A., Byerly, G. R., and Lowe, D. R., 1991, Chronology of early Archaean granite-greenstone evolution in the Barberton Mountain Land, South Africa, based on precise dating by single zircon evaporation: Earth and Planetary Science Letters, v. 103, p. 41–54.

Kröner, A., Hegner, E., Byerly, G. R., and Lowe, D. R., 1992, Possible terrane identification in the early Archean Barberton Greenstone Belt, South Africa, using single zircon geochronology: Eos (Transactions American Geophysical Union), v. 73, p. 616.

Kröner, A., Hegner, E., Wendt, J. I., and Byerly, G. R., 1996, The oldest part of the Barberton granitoid-greenstone terrain, South Africa: evidence for crust formation between 3.5 and 3.7 Ga: Precambrian Research, v. 78, p. 105–124.

Lamb, S. H., 1984a, Geology of part of the Archaean Barberton Greenstone Belt, Swaziland [Ph.D. dissertation]: Cambridge, Cambridge University, 250 p.

Lamb, S. H., 1984b, Structures on the eastern margin of the Archaean Barberton greenstone belt, northwest Swaziland, *in* Kröner, A., and Greiling, A., eds., Precambrian tectonics illustrated: Stuttgart, E. Schweizerbart'sche Verlagsbuchhandlung, p. 19–39.

Lamb, S. H., and Paris, I., 1988, Post-Onverwacht Group stratigraphy in the SE part of Archaean Barberton greenstone belt: Journal of African Earth Sciences, v. 7, p. 285–306.

López-Martínez, M., York, D., Hall, C. M., and Hanes, J. A., 1984, Oldest reliable $^{40}Ar/^{39}Ar$ ages for terrestrial rocks: Barberton Mountain komatiites: Nature, v. 307, p. 352–354.

López-Martínez, M., York, D., and Hanes, J. A., 1992, A $^{40}Ar/^{39}Ar$ geochronological study of komatiites and komatiitic basalts from the Lower Onverwacht volcanics: Barberton Mountain Land, South Africa: Precambrian Research, v. 57, p. 91–119.

Lowe, D. R., 1980, Archean sedimentation: Annual Review of the Earth and Planetary Sciences, v. 8, p. 145–167.

Lowe, D. R., 1982, Comparative sedimentology of the principal volcanic sequences of Archean greenstone belts in South Africa, Western Australia and Canada: implications for crustal evolution: Precambrian Research, v. 17, p. 1–29.

Lowe, D. R., 1994, Accretionary history of the Archean Barberton Greenstone Belt (3.55–3.22 Ga), southern Africa: Geology, v. 22, p. 1099–1102.

Lowe, D. R., and Byerly, G. R., 1986, Archean flow-top alteration zones formed initially in a low-temperature sulphate-rich environment: Nature, v. 324, p. 245–248.

Lowe, D. R., and Knauth, L. P., 1977, Sedimentology of the Onverwacht Group (3.4 billion years), Transvaal, South Africa, and its bearing on the characteristics and evolution of the early Earth: Journal of Geology, v. 85, p. 699–723.

Lowe, D. R., Byerly, G. R., Ransom, B. L., and Nocita, B. R., 1985, Stratigraphic and sedimentological evidence bearing on structural repetition in Early Archean rocks of the Barberton Greenstone Belt, South Africa: Precambrian Research, v. 27, p. 165–186.

Lowe, D. R., Byerly, G. R., Asaro, F., and Kyte, F., 1989a, Geological and geochemical record of 3400-million-year-old terrestrial meteorite impacts: Science, v. 245, p. 959–962.

Lowe, D. R., Byerly, G. R., and Kröner, A., 1989b, Relationship between episodic dacitic volcanism and tonalitic plutonism in the Archean Barberton Greenstone Belt (BGB), South Africa: Eos (Transactions, American Geophysical Union), v. 70, p. 1391.

Moore, J. C., 1978, Orientation of underthrusting during latest Cretaceous and earliest Tertiary time, Kodiak Island, Alaska: Geology, v. 6, p. 209–213.

Nocita, B. R., 1986, Sedimentology and stratigraphy of the Fig Tree Group, west limb of the Onverwacht anticline, Barberton Greenstone Belt, South Africa [Ph.D. dissertation]: Baton Rouge, Louisiana State University, 169 p.

Nocita, B. R., 1989, Sandstone petrology of the Archean Fig Tree Group, Barberton Greenstone Belt, South Africa: Tectonic implications: Geology,

v. 17, p. 953–956.
Nocita, B. R., and Lowe, D. R., 1990, Fan-delta sequence in the Archean Fig Tree Group, Barberton Greenstone Belt, South Africa: Precambrian Research, v. 48, p. 375–393.
Ori, G. G., and Friend, P. F., 1984, Sedimentary basins formed and carried piggyback on active thrust sheets: Geology, v. 12, p. 475–478.
Paris, I. A., 1985, The geology of the farms Josefsdal, Dunbar and part of Diepgezet in the Barberton greenstone belt [Ph.D. thesis]: Johannesburg, University of the Witwatersrand, 239 p.
Paris, I., Stanistreet, I. G., and Hughes, M. J., 1985, Cherts of the Barberton Greenstone Belt interpreted as products of submarine exhalative activity: Journal of Geology, v. 93, p. 111–129.
Ramsay, J. G., 1963, Structural investigations in the Barberton Mountain Land, eastern Transvaal: Geological Society of South Africa Transactions, v. 66, p. 353–401.
Ramsay, J. G., and Huber, M. I., 1987, The techniques of modern structural geology: Volume 2: folds and fractures: London, Academic Press, p. 309–700.
Ransom, B. L., 1987, The paleoenvironmental, magmatic, and geologic history of the 3,500 Myr Kromberg Formation, west limb of the Onverwacht anticline, Barberton Greenstone Belt, South Africa [M.Sc. thesis]: Baton Rouge, Louisiana State University, 103 p.
Reimer, T. O., 1967, Die Geologie der Stolzburg Synklinale im Barberton Bergland (Transvaal-Sudafrika) (The geology of the Soltzburg syncline in the Barberton Mountain Land [Transvaal, South Africa]) [M.Sc. thesis]: Frankfurt, Goethe Universitat, 103 p.
Reimer, T. O., 1975, Untersuchungen uber Abtragung, Sedimentation und Diagenese im fruhen Prakambrium am Beispiel der Sheba-Formation (Sudafrika) (Studies of denudation, sedimentation, and diagenesis in the early Precambrian with an example from the Sheba Formation [South Africa]): Geologisches Jahrbuch, Reihe B, v. 17, 108 p.
Smith, A. J., 1981, The geology of the farms Hooggenoeg 731JT and Avontuur 721JT, southwest Barberton Greenstone Belt [B.Sc. thesis]: Johannesburg, University of the Witwatersrand.
Suppe, J., 1985, Principles of structural geology: Inglewood Cliffs, New Jersey, Prentice-Hall, 537 p.
Suppe, J., and Medwedeff, D. A., 1984, Fault-propagation folding: Geological Society of America Abstracts with Programs, v. 16, p. 670.
Tull, J. F., and Groszos, M. S., 1990, Nested Paleozoic "successor" basins in the southern Appalachian Blue Ridge: Geology, v. 18, p. 1046–1049.
Viljoen, M. J., and Viljoen, R. P., 1969a, An introduction to the geology of the Barberton granite-greenstone terrain: Geological Society of South Africa Special Publication 2, p. 9–28.
Viljoen, M. J., and Viljoen, R. P., 1969b, The geology and geochemistry of the lower ultramafic unit of the Onverwacht Group and a proposed new class of igneous rocks: Geological Society of South Africa Special Publication 2, p. 55–86.
Viljoen, R. P., and Viljoen, M. J., 1969, The geological and geochemical significance of the upper formations of the Onverwacht Group: Geological Society of South Africa Special Publication 2, p. 113–152.
Williams, D. A. C., and Furnell, R. G., 1979, A reassessment of part of the Barberton type area: Precambrian Research, v. 9, p. 325–347.
Wuth, M., 1980, The geology and mineralization potential of the Oorschot-Weltevreden schist belt south-west of Barberton—Eastern Transvaal [M.Sc. thesis]: Johannesburg, University of the Witwatersrand, 185 p.
York, D., Layer, P. W., López-Martínez, M., and Kröner, A., 1989, Thermal histories from the Barberton greenstone belt, southern Africa: International Geological Congress Abstracts, Washington, D.C., p. 413.

MANUSCRIPT ACCEPTED BY THE SOCIETY MARCH 26, 1998

Geological Society of America
Special Paper 329
1999

Petrology and sedimentology of cherts and related silicified sedimentary rocks in the Swaziland Supergroup

Donald R. Lowe
Department of Geological and Environmental Sciences, Stanford University, Stanford, California 94305

ABSTRACT

Cherts and related silicified sediments occur mainly in volcanic portion of the Swaziland Supergroup, where they have formed by the silicification of virtually every primary sediment and igneous rock type, including (1) volcaniclastic and pyroclastic deposits, (2) terrigenous detrital layers, (3) biogenic sediments, and (4) orthochemical deposits. Many cherts formed by silicification of fine-grained volcaniclastic ash and dust. Coarser volcaniclastic units are commonly carbonated but rarely silicified to the point of being chert. Layers of pale greenish gray chert representing silicified komatiitic ash and dust are widespread in the Onverwacht Group. The rock is a mosaic of microquartz and sericite. Basaltic volcanic debris is uncommon, but mixtures of basaltic ash and other detrital and carbonaceous debris have locally been silicified to form black chert composed of microquartz, chlorite, iron oxides, and carbonaceous matter. Fine-grained felsic detritus, represented by pale to medium gray and bluish gray chert, is present in the Hooggenoeg (Onverwacht Group) and Mapepe (Fig Tree Group) Formations. The rock is composed largely of microquartz and sericite, and commonly includes quartz phenocrysts and sericite pseudomorphs after plagioclase. The various cherts formed by silicification of komatiitic, basaltic, and felsic detritus can be distinguished through a combination of petrographic, major and trace element, and rare earth element characteristics.

Cherts formed by the silicification of terrigenous conglomerate, sandstone, and shale occur locally in the Mapepe Formation. Silicified biogenic sediments included flat stromatolitic mats and detrital carbonaceous particles now contained within black and black-and-white banded chert. Silicified orthochemical deposits are represented by a major evaporitic unit in the Kromberg Formation, isolated diagenetic crystallites in many shallow-water volcaniclastic layers in the Onverwacht Group, and jasper, banded iron formation (BIF), silicified carbonate, and possibly primary precipitated silica in the Mapepe Formation. Banded ferruginous cherts were deposited as fine-grained mixtures of ash, clay, carbonaceous matter, siderite, and silica.

Cherts in the Onverwacht Group can be grouped into lithofacies representing two major depositional settings. Those in the southern facies of the Onverwacht Group, including the Hooggenoeg, Kromberg, and lower cycles of the Mendon Formation, constitute the platform or shallow-water association. They represent a diverse assemblage of predominantly shallow-water sediments that show an extremely close relationship between magma composition and depositional style. Komatiitic and felsic volcanism were accompanied by pyroclastic activity and sedimentation in shallow-water to subaerial environments whereas basaltic sequences accumulated with little pyroclastic activity under deeper, but still overall shallow-water conditions.

Lowe, D. R., 1999, Petrology and sedimentology of cherts and related silicified sedimentary rocks in the Swaziland Supergroup, *in* Lowe, D. R., and Byerly, G. R., eds., Geologic Evolution of the Barberton Greenstone Belt, South Africa: Boulder, Colorado, Geological Society of America Special Paper 329.

In central and northern parts of the greenstone belt, cherts in the Weltevreden and upper cycles of the Mendon Formation make up the basinal association. They include black, black-and-white banded, and banded ferruginous cherts representing a variety of fine-grained sediments deposited mainly under deep, quiet-water conditions. Banded ferruginous cherts are the proximal equivalents of komatiitic and basaltic flows whereas basinal black and black-and-white banded cherts accumulated distally during breaks in eruptive activity.

The results of this study emphasize the close relationships between volcanism and sedimentation, contrasts between shallow- and deep-water depositional facies, and the existence of environmental controls on silicification and its timing.

INTRODUCTION

Cherts and other intensively silicified sediments are characteristic components of early Archean greenstone belts. In the Barberton Greenstone Belt (BGB), they occur most abundantly in the predominantly volcanic part of the sequence, including the Onverwacht Group and locally the Mapepe Formation of the Fig Tree Group. Although once regarded as chemical precipitates, these cherts are now known to represent a wide variety of silicified volcaniclastic, biogenic, and nonsiliceous orthochemical deposits (Lowe and Knauth, 1977; Barley et al., 1979; Lowe, 1980, 1982; Buick and Barnes, 1984). Silicified volcanic rocks are also widely developed, especially in zones immediately underlying silicified sedimentary layers (Byerly et al., 1983; Paris et al., 1985; Lowe and Byerly, 1986; Duchac and Hanor, 1987; Hanor and Duchac, 1990).

With the recognition that most Archean cherts are not primary silica precipitates but silicified sediments having a wide range of original compositions and depositional styles, discussion of their formation has refocused to a considerable degree on the causes of silicification. Considerable controversy still surrounds the relative roles of (1) post-depositional silicification by recirculating hydrothermal fluids (e.g., de Wit et al., 1982; Barley, 1984; Buick and Barnes, 1984; Paris et al., 1985; Duchac and Hanor, 1987; Duchac, 1986; Lowe and Byerly, 1986; Hanor and Duchac, 1990), and (2) syndepositional silicification through low-temperature sediment-water interactions on the sea floor (Knauth and Lowe, 1978; Lowe and Byerly, 1986).

The present paper begins by reviewing the general distribution of cherts in the Swaziland Supergroup and their lithological and sedimentological characteristics. The initial approach will be to consider the observable products of silicification of the major primary sediment types. The principal sediment/chert assemblages will then be outlined and discussed in terms of their sedimentological implications. Finally, problems of timing and causes of silicification will be considered.

TERMINOLOGY

The term "chert" is used here for sedimentary rocks composed largely (generally >75%) of microcrystalline silica, most commonly chalcedony and/or microquartz (Folk and Weaver, 1952). The microquartz in most cherts is alpha quartz characterized by domains generally less than 35 microns across that in thin section under crossed nicols show ill-defined, changing boundaries and irregular extinction upon rotation of the stage. Most cherts in the Swaziland Supergroup are impure, made up of microcrystalline mosaics of microquartz and phyllosilicates (sericitic chert and chloritic chert); calcite, dolomite, and siderite (calcareous chert); oxidized siderite and iron oxide (ferruginous chert and jasper); or kerogen (carbonaceous chert). Banded cherts consist of interbedded layers of (1) nearly pure microquartz, from less than 0.1 to 10 cm thick, that generally are clear and translucent when fresh and weather to white, off-white, or, where they include iron impurities, pink, rust, or jasper/red color; and (2) black, carbonaceous chert (black-and-white banded chert); chert containing complex mixtures of fine-grained siderite, dolomite, ankerite, irox oxides, carbonaceous matter, ash, and clay (banded ferruginous chert); iron oxides (banded iron formation); and chert containing relatively pure ankerite or dolomite (banded chert-carbonate rock). The fracture in cherts is virtually always conchoidal and across, rather than around, silicified primary grains. Cherts in the Swaziland Supergroup generally contain greater than 85% SiO_2, although some sideritic layers in banded ferruginous cherts contain less than 50% silica.

In thin section, most cherts show no preferred orientation of microquartz domains and remain evenly illuminated as the stage is rotated under crossed nicols. Some, however, show aggregate or group polarization in which large irregular blocks of domains fade to extinction nearly simultaneously, a feature especially common in silicified evaporites in the sequence, or extinction sweeps across areas of the slide, commonly reflecting recrystallization of and optical orientation inheritance from fibrous quartz (chalcedony). Quartz made up of well-defined domains greater than 35 microns across is termed megaquartz.

DISTRIBUTION OF CHERT IN THE SWAZILAND SUPERGROUP

The distribution of chert in the Swaziland Supergroup is shown in Figures 1 and 2. Five general features of chert distribution are noteworthy.

(1) At least locally, virtually every sediment and igneous rock type has been silicified to form chert. Only quartz-rich sand-

stone and siltstone of the Moodies Group have not been altered to chert, but are widely cemented by syntaxial megaquartz overgrowths on primary detrital grains.

(2) Cherts representing silicified sediments are concentrated in the volcanic portions of the sequence. The 9,000-m-thick Onverwacht Group, from the Komati through the Kromberg Formations, contains nearly 1,800 m of sedimentary rock, including as much as 700 m of coarse dacitic sandstone and conglomerate in the Hooggenoeg Formation (H6) and 500–1,000 m of komatiitic lapillistone in the Kromberg Formation (K2v). Virtually all of the remaining 600 m of sedimentary rock is chert, including the 350-m-thick Buck Reef Chert (K1) at the base of the Kromberg Formation. The composite thickness of the Mendon Formation is about 1,000 m of which approximately 200 m is sediment, more than 90% of which is chert. Thin layers of black chert, black-and-white banded chert, and banded ferruginous chert are present in the upper 500 m of the Weltevreden Formation in the northern part of the BGB (Lowe and Byerly, this volume, Chapter 1). No sediments were observed in the Komati Formation in the study area.

The Mapepe Formation in its supplementary section (Lowe and Byerly, this volume, Chapter 1) is 300 m thick of which less than 10 m or 3% is chert. Laterally, in units interpreted to represent condensed sections, the formation includes as much as 60% chert. Chert makes up less than 1% of the other formations of the Fig Tree and Moodies Groups.

(3) Among volcaniclastic units, chert has widely developed by preferential silicification of fine-grained ash and dust. In the 700 m of predominantly coarse-grained dacitic sandstone and conglomerate in H6 and 1,200 m of dacitic fragmental rocks in the Auber Villiers Formation, some degree of silicification is not uncommon but cherts are rare. Most rocks contain less than 80% SiO_2 by weight. Fine-grained ash and dust in both H6 and locally in the Mapepe Formation, however, have been widely altered to chert, most containing greater than 85% SiO_2. The 500 m of coarse komatiitic lapillistone in K2 is extensively carbonated but only locally silicified whereas thin komatiitic ash and dust layers throughout the Onverwacht Group, including K2c, have been widely silicified to form impure chert containing more than 85% SiO_2 (Table 1).

Sandy turbidites composed of dacitic volcaniclastic debris in the upper part of H6 along the Komati River (Viljoen, R. P., and Viljoen, 1969; Lowe and Knauth, 1977) illustrate the widely developed relationships between silicification and sediment texture (Figs. 3A and 4). The coarse- to very coarse-grained bases, mostly Bouma T_a divisions, show extensive carbonation involving replacement of original grains by coarse ferroan dolomite. SiO_2 ranges from 50 to 65% (Table 1). The medium- to fine-grained T_b and lower T_c divisions are extensively silicified, but fracture is still largely around altered primary grains and microquartz makes up less than 50% of the rock. Total SiO_2 is generally between 70 and 80%. The turbidites are capped by medium gray chert representing thoroughly silicified fine-grained sand- to silt-sized debris of the upper T_c and T_d divisions. The rock fractures conchoidally across primary grains and contains 80 to 90% SiO_2. T_e is only locally developed and composed of fine, black, carbonaceous chert. Similar relationships between sediment texture and silicification and carbonation are seen in komatiitic volcaniclastic units (Fig. 3B).

(4) In sedimentary sequences, cherts are most abundant where the sedimentation rates of volcaniclastic and terrigenous sediment were low. Thick, rapidly deposited dacitic volcaniclastic sections in the Mapepe, Auber Villiers, and Schoongezicht Formations contain little chert whereas thin, probably condensed volcaniclastic sections in the Mapepe Formation contain abundant chert. Chert is nearly absent in terrigenous units deposited at high sedimentation rates, such as the Sheba, Belvue Road, and Schoongezicht Formations in the northern facies of the Fig Tree Group and in all formations of the Moodies Group.

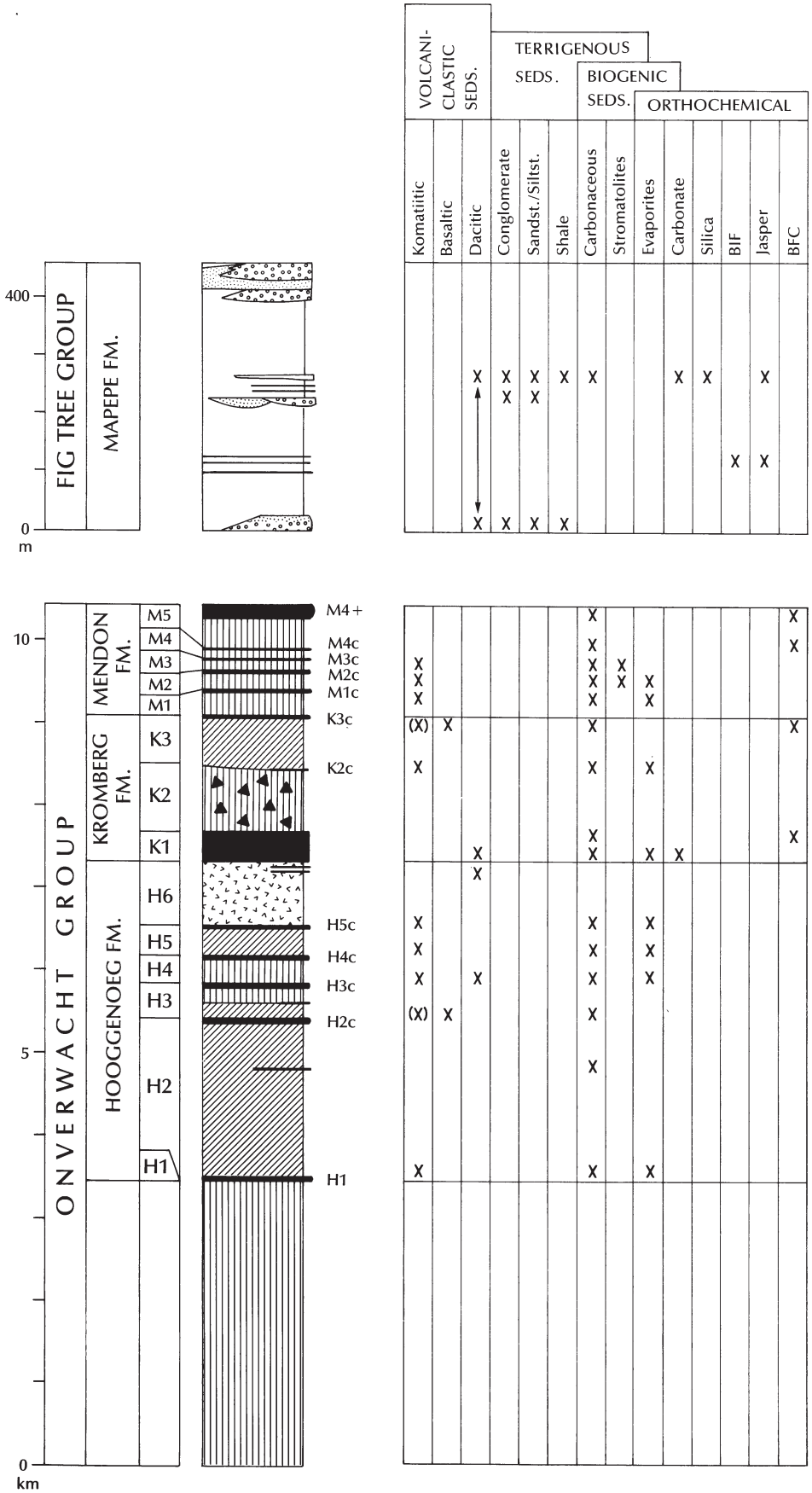
(5) Cherts representing silicified terrigenous and volcaniclastic sediments are preferentially developed in shallow-water sequences. Shallow-water, fan-delta-top units of lithic conglomerate and sandstone in the Mapape Formation are not uncommonly silicified to form black chert, but similar turbiditic units lower on the fan-delta fronts are poorly silicified and cherts representing silicified terrigenous units are lacking in thick turbiditic formations in northern facies of the Fig Tree Group. Komatiitic ash layers in the shallow-water southern facies of the Onverwacht Group are almost everywhere silicified to form greenish impure cherts but similar ash beds in the Weltevreden Formation, deposited in deeper water, remain unsilicified.

PRIMARY SEDIMENTS AND THE PRODUCTS OF SILICIFICATION: LITHOLOGY AND PETROLOGY

The following discussion outlines the characteristics of cherts formed by the silicification of the main types of primary sediments in the Swaziland Supergroup. Four major groups of primary sediments will be considered (Lowe, 1980, 1982; Buick and Barnes, 1984): (1) detrital volcaniclastic and pyroclastic deposits, (2) terrigenous sediments derived by weathering and erosion of older rocks, (3) biogenic sediments, and (4) deposits formed by direct chemical precipitation.

Volcaniclastic and pyroclastic deposits

Volcanism during accumulation of the Swaziland Supergroup was trimodal from the perspective of distinguishing the products of later silicification: (1) komatiitic, including peridotitic and basaltic komatiite and komatiitic basalt; (2) basaltic, including tholeiitic and some high-magnesium basalts; and (3) felsic, represented mainly by dacitic fragmental rocks. In the following discussion, stratigraphic units in the Onverwacht Group will be distinguished using the nomenclature system of Lowe and Byerly (this volume, Chapter 1). Formations are indicated by capital letters (H, Hooggenoeg Formation; K, Kromberg Formation; M, Mendon Formation), members by added numbers (e.g., H1, H2, H3), and volcanic and cherty sedimentary divisions by added small letters (e.g., H2v and H2c, respectively).


VOLCANI-CLASTIC SEDS.
TERRIGENOUS SEDS.
BIOGENIC SEDS.
ORTHOCHEMICAL
Komatiitic
Basaltic
Dacitic
Conglomerate
Sandst./Siltst.
Shale
Carbonaceous
Stromatolites
Evaporites
Carbonate
Silica
BIF
Jasper
BFC
FIG TREE GROUP
MAPEPE FM.
400
0
m
ONVERWACHT GROUP
MENDON FM.
KROMBERG FM.
HOOGGENOEG FM.
M5
M4
M3
M2
M1
K3
K2
K1
H6
H5
H4
H3
H2
H1
M4+
M4c
M3c
M2c
M1c
K3c
K2c
H5c
H4c
H3c
H2c
H1
10
5
0
km

Silicified komatiitic ash and dust. Silicified airfall and water-worked ash and dust representing pyroclastic eruptions of komatiitic basalt or basaltic komatiite occur throughout the Onverwacht Group (Figs. 1, 3B, 5, and 6) forming conspicuous layers in the Middle Marker (Viljoen, R. P., and Viljoen, 1969; Lanier and Lowe, 1982), H3c, H4c, H5c, K2c, the Msauli Chert (M1c), and parts of M2c. Beds range from a few centimeters to more than 15 m thick and were made up almost exclusively of ash- and dust-sized debris (Fig. 5A) and coarser accretionary grains (Fig. 5B). Locally, komatiitic lapillistone in K2v shows nearly complete silicification to form chert (Fig. 6A), although the bulk of this coarse-grained unit is pervasively carbonated.

The mineralogy and petrography of these volcaniclastic units have been discussed by Reimer (1975), Lowe and Knauth (1977, 1978), Stanistreet et al. (1981), Lanier and Lowe (1982), and Heinrichs (1980, 1984). In outcrop and slabs, the rocks consist mainly of pale green (5G7/2), very pale green (10G8/2), greenish gray (5G6/1), and medium bluish gray (5B5/1) fine-grained impure chert. In thin section, they are tightly intergrown micromosaics generally composed of more than 80% microquartz. Sericite, authigenic potash feldspar, ferroan dolomite, rutile, and opaque oxides are common trace constituents (Heinrichs, 1984). Locally, some clastic units contain fine detrital chrome spinels.

Relatively pure komatiitic dust is now represented by extremely fine-grained chert lacking relict primary textures or grain pseudomorphs. Pseudomorphs of primary particles occur in units originally composed of debris coarser than about 30 to 40 microns (Fig. 6B), and volcaniclastic textures in coarser ash layers are commonly exquisitely preserved (Lowe and Knauth, 1977, 1978; Lanier and Lowe, 1982; Heinrichs, 1984; Lowe, this volume, Chapter 9). Ash consisted largely of blocky, nonvesicular to slightly vesicular vitric debris, most less than 2 mm in diameter (Fig. 6B). Accretionary lapilli are widespread (Fig. 5B). Pseudomorphs after primary feldspar phenocrysts, microphenocrysts, and microlites, and primary megaquartz grains are absent.

The sediments show little evidence of compaction. Many ash units had depositional porosities exceeding 40%, now preserved by pore-filling authigenic silica. This pore-filling silica commonly shows relict fibrous quartz textures but is now composed of microquartz. Some units of accretionary grains may have included as much as 70–80% pore space because of the high intraparticle as well as interparticle porosity (Fig. 5B).

The primary composition of the volcaniclastic debris has proven elusive. Taken at face value, bulk chemical analyses (Table 2) suggest that these rocks represent silicic ash, and previous workers have concluded that most formed by the alteration of fine-grained felsic debris (Viljoen, R. P., and Viljoen, 1969; Anhaeusser, 1973; Lowe and Knauth, 1977; Lanier and Lowe, 1982; Heinrichs, 1984). Several features of these deposits, however, suggest that this interpretation is incorrect. (1) Every major

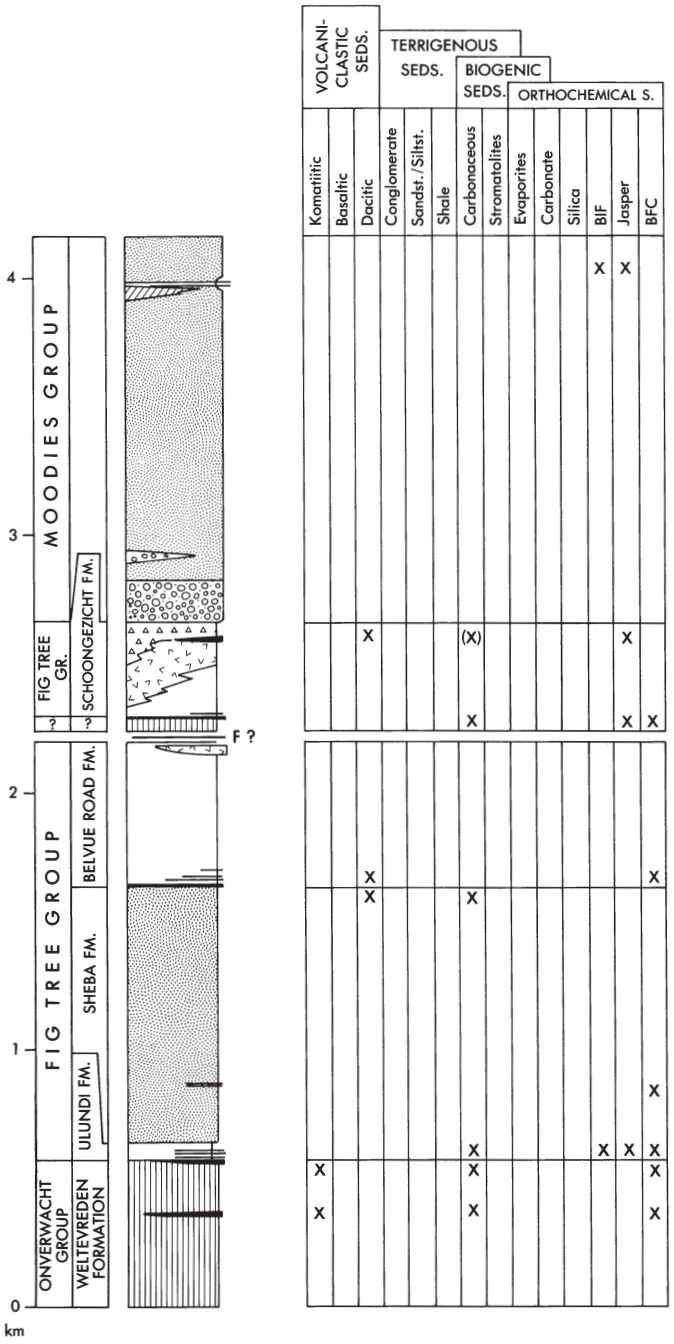


Figure 2. Generalized stratigraphy of the Barberton Greenstone Belt north of the Inyoka fault showing the distribution of chert and the nature of the primary sediments from which it formed. Key as in Figure 1.

Figure 1. Generalized stratigraphy of the Barberton Greenstone Belt south of the Inyoka fault showing the distribution of chert within the sequence and the nature of the primary sediments from which it formed (Xs). Key: komatiitic volcanic rocks (vertical rule); basaltic volcanic rocks (diagonal rule); komatiitic volcaniclastic rocks (solid triangles over vertical rule); dacitic volcaniclastic rocks in Onverwacht Group (random v's); interflow cherts in Onverwacht Group (black); fine dacitic and terrigenous sediments in Mapepe Formation (unpatterned); terrigenous sandstone (stippled) and conglomerate (circles). BIF, banded iron formation; BFC, banded ferruginous chert.

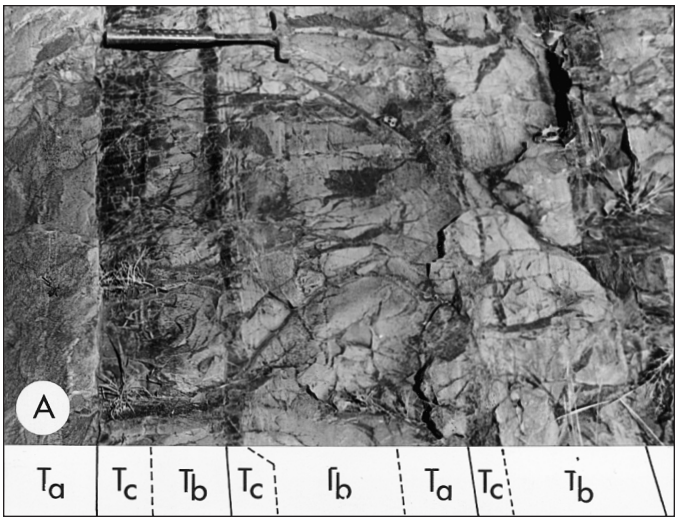
TABLE 1. COMPARISON OF THE MAJOR AND TRACE ELEMENT COMPOSITIONS OF COARSE-GRAINED, CARBONATED AND FINE-GRAINED SILICIFIED KOMATIITIC AND DACITIC VOLCANICLASTIC UNITS IN THE ONVERWACHT GROUP

	Major Elements (Wt%) Sample Numbers*				
	Komatiitic Rocks		Dacitic Rocks		
Oxide	SAF-23-187	SAF-10-12	SAF-23-179	SAF-23-183	SAF-23-181
SiO_2	53.98	90.20	66.09	76.63	90.52
Al_2O_3	2.84	6.33	9.71	13.38	4.93
Fe_2O_3	2.59	0.69	1.49	0.20	0.15
MgO	7.29	0.29	2.99	0.39	0.41
CaO	12.50	0.04	5.35	0.20	0.66
Na_2O	0.07	0.00	0.05	0.16	0.01
K_2O	0.79	2.17	5.77	8.26	3.01
TiO_2	0.05	0.25	0.36	0.67	0.22
MnO	0.31	0.01	0.20	0.00	0.01
P_2O_5	0.00	0.01	0.08	0.11	0.08
S	0.00	0.01	0.00	0.00	0.00
Total	80.42	100.00	92.09	100.00	100.00
	Trace Elements (ppm)				
Element					
Ba	25	188	77	90	53
Cr	1492	612	32	36	18
Zr	13	<10	83	111	59
Sr	16	<10	17	<10	<10
Rb	30	37	88	121	43
Y	<10	<10	<10	<10	<10
Ni	397	38	24	13	<10

Note: Analyses by Ron Hartree, Department of Geology, University of Ottawa, Ottawa, Canada.

*Sample descriptions:

SAF-23-187	Coarse-grained carbonated komatiitic lapillistone, member K2v, Kromberg Fm. Analysis not recalculated to 100%. Missing material is mostly CO_2, which was not determined separately.
SAF-10-12	Fine-grained, silicified komatiitic ash with accretionary lapilli, Msauli Chert (M1), Mendon Fm.
SAF-23-179	Coarse-grained carbonated dacitic sandstone, member H6, Hooggenoeg Fm. Not recalculated to 100%. Missing material is mostly CO_2.
SAF-23-183	Medium- to fine-grained silicified dacitic sandstone, member H6, Hooggenoeg Fm.
SAF-23-181	Fine-grained silicified dacitic sandstone, member H6, Hooggenoeg Fm.



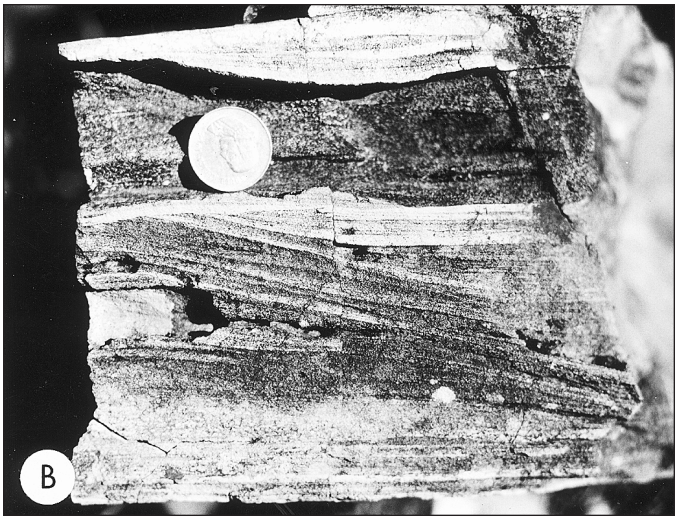


Figure 3. Silicified and carbonated tuffaceous sediments. A, Graded dacitic volcaniclastic turbidites from member H6 (member designations from Lowe and Byerly, this volume, Chapter 1) of the Hooggenoeg Formation along the Komati River on the east limb of the Onverwacht anticline. Major turbidites and Bouma divisions labeled. Coarse-grained T_a divisions are cemented and partially replaced by dark-brown-weathering iron-rich dolomite; medium-grained T_b divisions are partially silicified and light toned; and fine-grained T_c to T_d divisions have been altered to dark gray, nearly pure chert. B, Komatiitic ash from the Msauli Chert (M1c) slowing relationship between original texture (grain-size) and degree of silicification and carbonation. Medium- to coarse-grained, cross-stratified ash (dark) is heavily carbonated whereas fine-grained, cross-laminated ash (light) is silicified.

chert unit of this type caps komatiitic volcanic rocks, including the Middle Marker (Lanier and Lowe, 1982), H3c, H4c, the Msauli Chert (M1c), and M2c. Moreover, every komatiitic unit in the Onverwacht Group except the uppermost cycles of the Mendon Formation is capped locally and more commonly regionally by cherts of this type (Fig. 1).

(2) The silicified ash layers lack quartz phenocrysts and pseudomorphed magmatic feldspars (Fig. 6B). Both of these components are common and well preserved in unambiguous felsic volcaniclastic units in the Hooggenoeg and Mapepe Formations.

(3) Although bulk compositions of rocks throughout the Onverwacht Group have commonly been profoundly altered by metasomatism and many contrasting primary rock types now show remarkably similar major and trace element abundances, some immobile element ratios have survived alteration (Duchac and Hanor, 1987; Hanor and Duchac, 1990; Lahaye et al., 1995; Byerly, this volume, Chapter 8). Cherts representing silicified basaltic and komatiitic detritus can be distinguished from felsic ashes based on immobile element contents (Table 2) and ratios (Figs. 7 and 8). Most silicified komatiitic ashes show lower Al_2O_3 and Zr contents than silicified felsic units (Table 2). Al_2O_3 ranges from 6.3% to less than 1%, averaging 2.31% for 16 samples of komatiitic ash. In fresh komatiitic volcanic rocks, Al_2O_3 ranges from less than 5% by weight in peridotitic komatiites to 10 or 12% in komatiitic basalts (Viljoen, M. J., and Viljoen, 1969; Smith and Erlank, 1982; Byerly, this volume, Chapter 8).

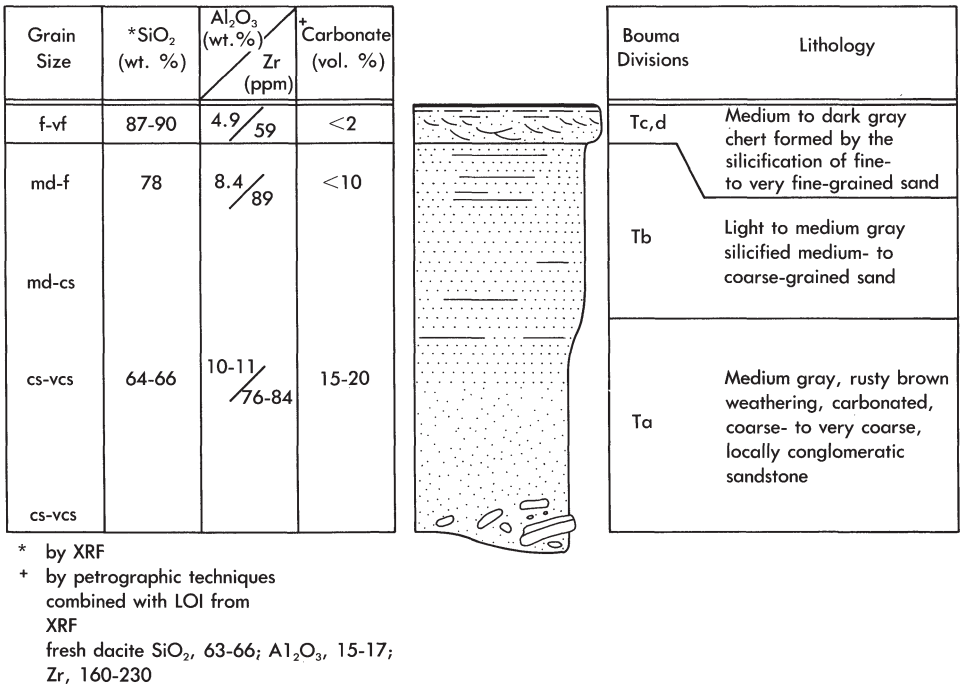


Figure 4. Relationships among sediment grain size, silicification, and carbonation in dacitic volcaniclastic turbidites in member H6.

Zr is below 40 ppm in all silicified komatiitic ashes, averaging 14 ppm in the same 16 samples. Silicified komatiites and basalts also show distinctly greater TiO_2/Zr and Cr/Zr ratios than silicified dacites in the Swaziland Supergroup (Table 3, Figs. 7 and 8). The low absolute abundances of Al_2O_3 and Zr in altered komatiitic ashes reflect both low primary rock abundances of these elements in komatiites and dilution factors related to the high initial porosities of the volcaniclastic sediments, which is now occupied largely by microquartz. Felsic volcaniclastic rocks experienced similar porosity-related dilution, but show Al_2O_3 values ranging from lows of about 4.5% to more than 15% and Zr contents are above 40 ppm (Table 4).

(4) Cherts representing silicified komatiitic ash show less fractionated REE distributions (Fig. 9), like those of associated komatiitic flows (Byerly, this volume, Chapter 8). In contrast, silicified dacitic ash is relatively depleted in the HREE (Fig. 9).

These compositional features and the ubiquitous occurrence of these fine silicified ash units in cherts capping komatiitic volcanic rock suggest that they represent fine-grained, silicified komatiitic ash and dust.

Basaltic detritus. Although the Swaziland Supergroup includes thick units of basalt, basaltic volcaniclastic sediments are difficult to identify with certainty. Most basalts in the Swaziland Supergroup are overlain by and interstratified with units of laminated black chert, such as H2c in the Hooggenoeg Formation and K3c, the Footbridge Chert, in the Kromberg Formation. These layers are composed largely of black, fine-grained carbonaceous chert. Intergrown iron-rich dolomite is widespread and locally makes up more than 50% of the rock. Fine intergrown chlorite occurs in most rocks. Bulk chemical analyses (Table 3) indicate the presence of alumina, iron, and magnesium compatible with the included phyllosilicate being chlorite. Iron contents are relatively high, suggesting the presence of iron oxides. The original sediments were probably mixtures of fine carbonaceous matter, clay, carbonate, iron oxides, and mafic ash and dust.

Dacitic volcaniclastic sediments. Dacitic volcanic, volcaniclastic, and pyroclastic rocks are present in member H6 of the Hooggenoeg Formation and throughout the Mapepe and Auber Villiers Formations in southern facies outcrops. The Schoongezicht and Belvue Road Formations in northern facies sections also include dacitic volcaniclastic debris, but much of this material was deposited by turbidity currents and mixed with other detrital constituents. It is locally silicified but not to the extent of being chert.

Chert is extensively developed only in fine-grained facies of the Hooggenoeg and Mapepe Formations, where silicification has affected both entire layers (Fig. 3A) and local patches within beds to form nodules (Fig. 10A). Turbidite T_c and T_d divisions in H6 along the Komati River on the east limb of the Onverwacht anticline consist of medium to dark gray chert (Figs. 3A and 10B; Viljoen, R. P., and Viljoen, 1969; Lowe and Knauth, 1977). The rock shows faint, current-produced flat and cross-laminations on weathered surfaces. In thin section, primary sand- and silt-sized volcaniclastic grains are texturally well preserved (Fig. 10B), but only grains of megaquartz also preserve their primary composition. Feldspar, showing crude microcline quadrille twinning and probably representing both recrystallized sanidine phe-

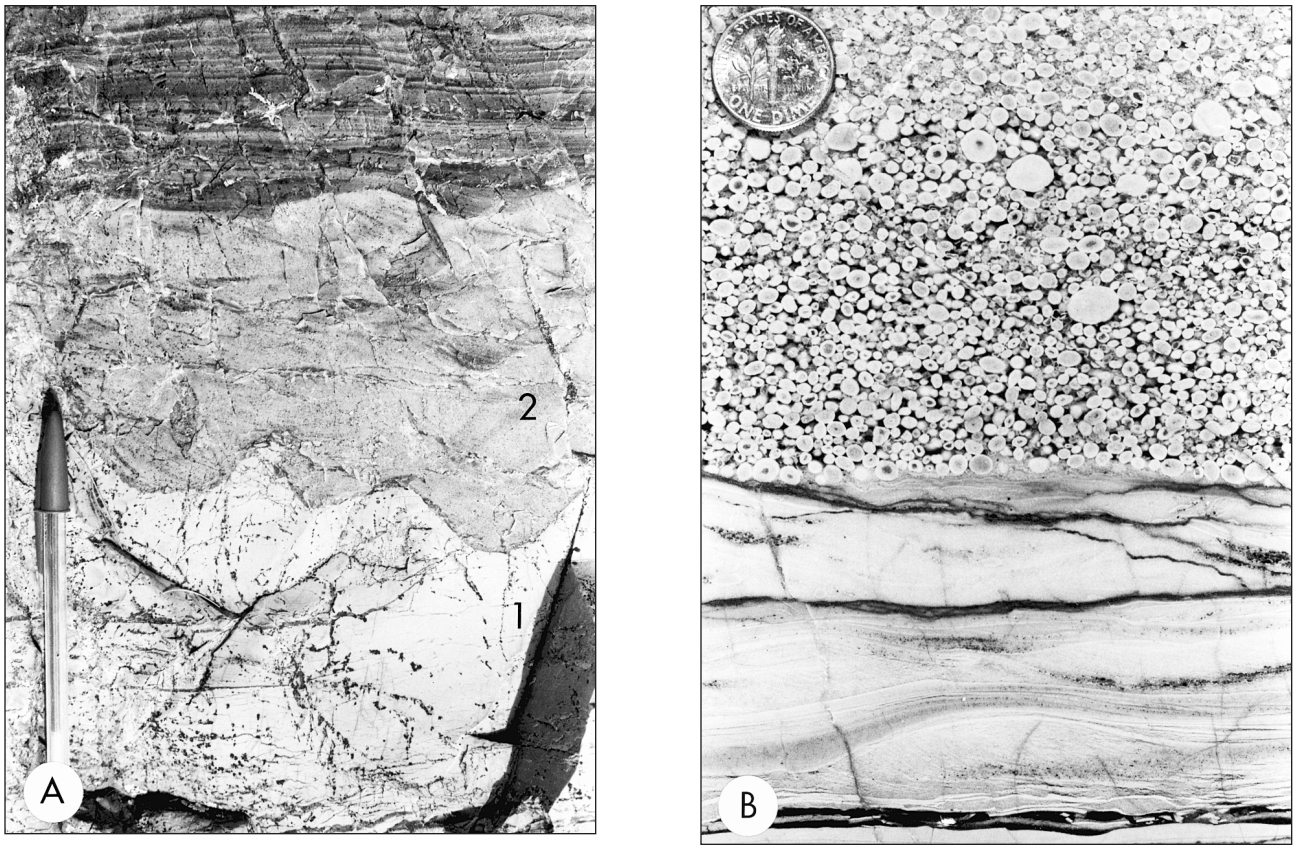


Figure 5. Cherts formed by the silicification of komatiitic volcaniclastic sediments in the Onverwacht Group. A, Silicified komatiitic ash and dust from H3c in the Hooggenoeg Formation. A layer of homogeneous, very fine-grained chert representing silicified komatiitic dust (1) is overlain along an erosive contact by slightly darker chert formed by silicification of current-deposited ash (2). The rippled surface of the ash is capped by black, carbonaceous chert containing thin ash laminations (light). B, Silicified accretionary lapilli in the Msauli Chert (M1). The lapilli show preservation of fine internal structuring, including concentric layering and nuclei. The lapilli layer is underlain by chert representing silicified, current-deposited komatiitic ash showing ripples and fine, laminated ash drapes.

nocrysts and authigenic grains, makes up from 10 to 20% of the rock. The remainder of the grains are heterogeneous micromosaics of microquartz and sericite, probably formed by the recrystallization of vitric particles.

The Mapepe Formation contains thick sections of felsic ash and, locally, chert units composed of silicified felsic ash and dust. In many sections, beds of pale yellowish gray weathering and light gray to medium gray chert representing silicified felsic ash underlie or overlie the spherule bed at the base of the formation (Lowe and Byerly, this volume, Chapter 1). Where the sediment originally consisted of massive, extremely fine-grained dust, the chert is now a structureless micromosaic of microquartz and sericite. Coarser silt- and sand-sized ash units show a clotted or patchy microquartz-sericite micromosaic (Fig. 10C), reflecting original grains and grain/cement contrasts in the original sediments. Volcanic quartz phenocrysts are well preserved (Fig. 10C), whereas plagioclase phenocrysts have been replaced by sericite and microquartz. Silicified felsic ash units commonly contain iron-rich dolomite and, locally, small amounts of patchy authigenic chlorite.

Thoroughly altered felsic ash layers consist largely of SiO_2, Al_2O_3, and K_2O (Table 4). Cr and Ni are generally low, commonly less than 100 ppm and 25 ppm, respectively, and Zr is above 40 ppm. Immobile element ratios (Figs. 7 and 8) provide a clear distinction between silicified dacitic, komatiitic, and basaltic ash. Mantle-normalized REE patterns are HREE depleted, like those of associated plagioclase-phyric dacitic breccias and coarser volcaniclastic sediments (Fig. 9).

Other volcaniclastic sediments. Upon weathering, some massive black cherts can be seen to have consisted of laminated or more rarely cross-laminated detrital sediments (Fig. 11). Most of these units lack detrital megaquartz and petrographically recognizable grains. They contain more than 95% SiO_2 and have yielded ambiguous results using trace-element ratios. They appear to represent silicified ash-bearing sediments, probably mixtures of ash, carbonaceous matter, and,

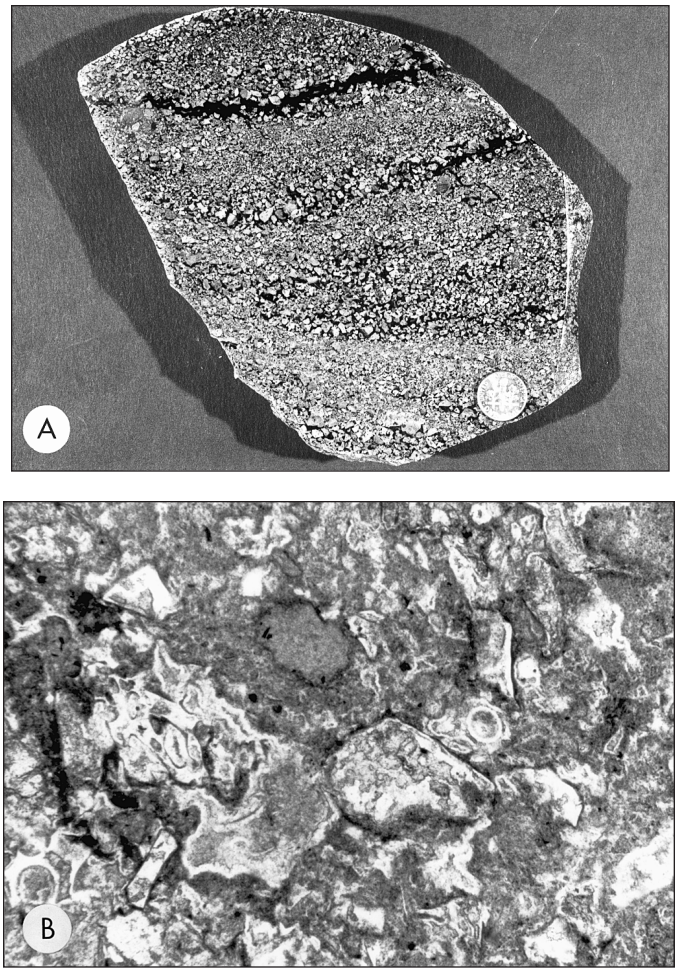


Figure 6. Cherts formed by the silicification of komatiitic volcaniclastic sediments in the Onverwacht Group. A, Silicified komatiitic lapillistone from K2v. The blocky lapilli (light) occur in well-sorted, normally graded, fall-deposited layers 4 to 6 cm thick. Cement between lapilli (dark) is pure, translucent silica. Over most of the outcrop of K2v, the lapillistone is heavily carbonated, not silicified. B, Typical angular, blocky, weakly to nonvesicular particles of silicified komatiitic ash in the Msauli Chert (M1c). See also Lowe, this volume, Chapter 9.

perhaps, orthochemical materials, but the original composition of the ash is uncertain.

Terrigenous sediments

Terrigenous sediments form during the weathering and erosion of older rocks. Within the Swaziland Supergroup, they range from cobble conglomerate through sandstone and siltstone to shale. All of these rock types locally but uncommonly show pervasive replacement by microquartz to form chert. Within the Onverwacht Group, terrigenous deposits are poorly represented but some black chert may represent silicified carbonaceous shale. The Mapepe Formation contains both unsilicified and silicified examples of all types of terrigenous deposits, including conglomerate (Fig. 12A), sandstone (Fig. 12B), siltstone, and, rarely, shale. Many units in the Moodies Group show extensive silicification, but generally involve the cementation of detrital materials by megaquartz, not microquartz.

Most terrigenous conglomerates in the Mapepe Formation are composed of chert clasts in a matrix of carbonated or poorly silicified lithic sandstone. Some conglomerates at the base of the formation are composed of chert clasts in fine, translucent, pore-filling chert cement and a number of conglomerates deposited in shallow water on fan-deltas in the middle of the unit include chert clasts in a matrix of immature but completely silicified sandstone (Fig. 12A). Chert-clast conglomerate interbedded with barite and jasper in shallow-water orthochemical bank sequences in the middle part of the Mapepe Formation (Lowe and Nocita, this volume, Chapter 10) shows nearly complete matrix replacement by microquartz, forming a dense, light gray to greenish rock in which the primary conglomeratic texture is well preserved (Lowe and Knauth, 1977, Fig. 18b). The depositional matrix in the original sediment was apparently carbonate (Lowe and Nocita, this volume, Chapter 10).

Completely silicified units of terrigenous sandstone and siltstone in the Mapepe Formation are composed of dense generally black chert, but grains and sedimentary structures are commonly visible on weathered surfaces (Fig. 12B; also, see Lowe and Knauth, 1977, Fig. 16a). Megaquartz grains, where present, are compositionally preserved but other primary minerals are preserved only as pseudomorphs. The compositions of cherts representing altered and unaltered lithic graywackes from the Fig Tree Group are shown in Table 5.

Terrigenous units of shale and mudstone are abundant in the Fig Tree Group and occur sparsely in the Moodies Group but nowhere have been silicified to form chert.

Biogenic sediments

Biogenic sediments are represented throughout the Onverwacht Group by black and black-and-white banded carbonaceous chert (Lowe and Knauth, 1977; Walsh, 1989, 1992; Walsh and Lowe, this volume, Chapter 4). Carbonaceous cherts are nearly pure mixtures of microquartz and opaque kerogen, although most contain traces of phyllosilicates and, where interbedded with volcaniclastic layers, admixed volcaniclastic materials. Ferroan dolomite, siderite, and iron oxides are common accessory constituents.

Lowe and Knauth (1977) and Walsh and Lowe (this volume, Chapter 4) illustrate four principal morphologic forms of carbonaceous matter in these cherts: (1) simple grains, (2) lobate composite particles, (3) flat stromatolitic mats, and (4) compressed wisps. The first three represent early cemented, largely uncompacted carbonaceous material and the latter compacted sediment (Walsh and Lowe, this volume, Chapter 4).

Massive and flat-laminated carbonaceous chert forms units from less than 1 cm to more than 50 m thick. It makes up thick, relatively homogeneous units in some parts of the sequence, including H2c, K3c, and forms chert caps in the upper cycles of

TABLE 2. MAJOR AND TRACE ELEMENT COMPOSITIONS OF SILICIFIED KOMATIITIC ASH AND SELECTED KOMATIITES FROM THE ONVERWACHT GROUP

	Major Elements (Wt%) Sample Numbers*						
Oxide	SAF-127-53	SAF-102-10	SAF-102-14	SAF-125-7	SAF-186-1	SAF-116-7	SA72-4
SiO_2	89.16	91.95	93.89	92.66	85.63	85.47	50.00
Al_2O_3	6.33	4.98	3.74	4.95	9.78	8.29	5.77
Fe_2O_3	1.50	0.40	0.31	0.31	0.91	1.82	11.95
MgO	0.74	0.68	0.49	0.27	0.52	1.07	22.06
CaO	0.09	0.00	0.03	0.05	0.01	0.18	9.26
Na_2O	0.15	0.00	0.01	0.34	0.08	0.05	0.00
K_2O	1.64	1.80	1.36	1.16	2.84	2.44	0.08
TiO_2	0.21	0.18	0.13	0.19	0.21	0.53	0.62
MnO	0.02	0.00	0.00	0.01	0.01	0.01	0.21
P_2O_5	0.10	0.00	0.02	0.01	0.00	0.12	0.06
S	0.06	0.01	0.02	0.05	0.01	0.02	NA
Total	100.00	100.00	100.00	100.00	100.00	100.00	100.00
	Trace Elements (ppm)						
Element							
Ba	167	219	218	86	146	100	<10
Cr	489	340	155	433	3777	2399	2244
Zr	<10	18	14	<10	<10	41	37
Sr	<10	<10	<10	<10	<10	<10	23
Rb	42	46	34	31	70	62	NA
Y	<10	<10	<10	<10	<10	21	14
Ni	82	68	63	15	153	188	376

Note: Analyses of samples except SA72-4 by Ron Hartree, Department of Geology, University of Ottawa, Ottawa, Canada. Analysis of SA72-4 by G. R. Byerly, Louisiana State University.

*Sample descriptions: All samples except SA72-5 have been metasomatically altered with the addition of SiO_2 and K_2O and depletion in Fe_2O_3, MgO, CaO, and Ma_2O.

SAF-127-53	Large accretionary lapilli, type section of Msauli Chert (M1), Mendon Fm.
SAF-102-10	Accretionary lapilli, Msauli Chert (M1), Mendon Fm.
SAF-102-14	Very fine-grained komatiitic ash, Msauli Chert (M1), Mendon Fm.
SAF-125-7	Fine-grained, current-deposited komatiitic ash, Middle marker (H1), Hooggenoeg Fm.
SAF-186-1	Coarse-grained, komatiitic sandstone, basal Msauli Chert (M1), Mendon Fm.
SAF-116-7	Spinifex-bearing komatiitic flow rock, member M2v, Mendon Fm.
SA72-4	Spinifex-bearing komatiite, Mendon Fm.

the Mendon Formation. In cycles M3 and M4 of the Mendon Formation, the main constituents are simple grains and wisps. Most layers show evidence of early compaction prior to silicification. In other units, such as H1, H3c, H4c, M1c, and M2c, carbonaceous chert occurs interbedded with volcaniclastic layers (Fig. 13A). These units consist mainly of simple grains, composite grains, and flat mats that were silicified before significant compaction had occurred.

Banded black-and-white chert is particularly well developed in the Buck Reef Chert (K1) at the base of the Kromberg Formation (Fig. 13B), where sections locally exceed 200 m thick. Lithification of the white bands occurred early and breccias formed by the intrastratal flowage of unlithified, hydroplastic carbonaceous sediment containing brittle, white chert plates are widespread (Fig. 13C). Black-and-white cherts also occur in thin chert units within H2v, as facies of massive black cherts in H2c and K3c, and in most chert units in the Mendon Formation. Carbonaceous matter in black-and-white banded cherts consists mainly of uncompacted simple and composite grains and flat mats (Fig. 13D). Compacted grains are virtually absent.

Silicified silt- and sand-sized carbonaceous grains also occur mixed with current-deposited detritus in many units of silicified fine-grained komatiitic and felsic ash (Fig. 5B) and terrigenous sediments (Fig. 12A, B). Large, now silicified carbonaceous rip-up clasts are also common in detrital units (Figs. 12A and 13A).

Carbonaceous cherts in both massive and black-and-white banded units consists of nearly pure silica, generally exceeding 98% by weight (Table 6, col. 1–3). Trace constituents include Al_2O_3, Fe_2O_3, MgO, and K_2O. Cr values are low, less than 100 ppm. TOC ranges from less than 0.5 mg/g to 14.3 mg/g (Walsh and Lowe, this volume, Chapter 4).

Orthochemical deposits

Many sedimentary layers in the Swaziland Supergroup are composed largely or in part of precipitated materials. These include (1) primary precipitated materials, pure or mixed with other primary sediments, that formed discrete sedimentary layers on the Archean sea floor; (2) early diagenetic precipitates that replace or cement primary sediments; and (3) primary sediments or early diagenetic materials that, during diagenesis, were redistributed, commonly by dissolution-reprecipitation reactions, to form new layers, nodules, or sedimentlike bodies.

Evaporites. Silicified crystallites possibly representing gyp-

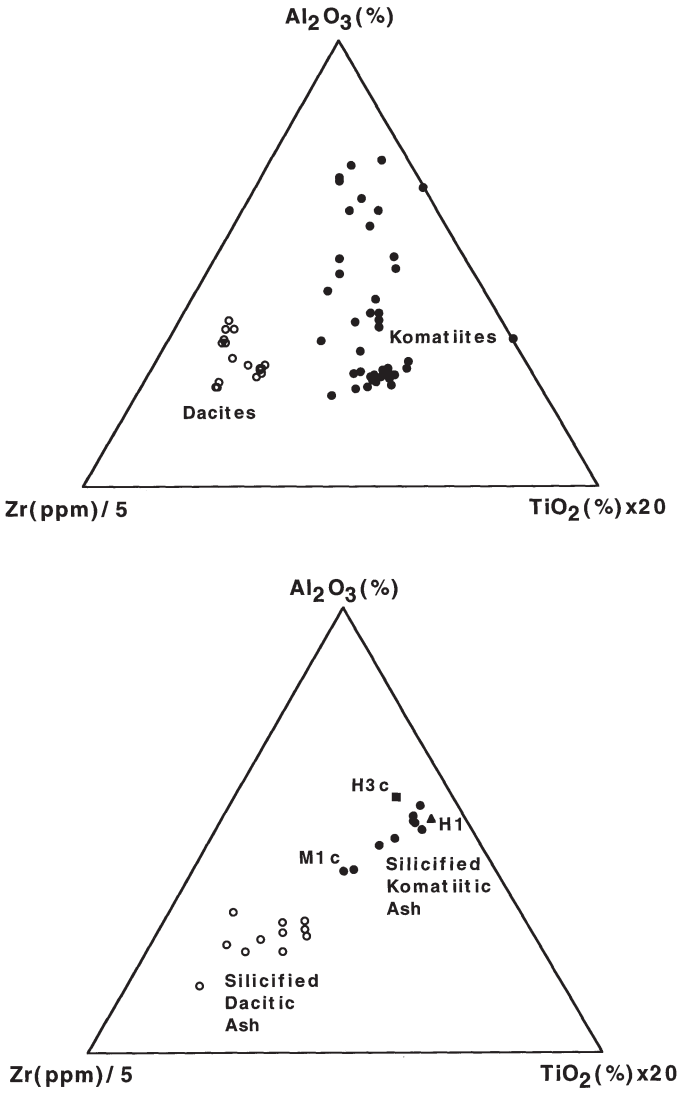


Figure 7. Triangular Al_2O_3-Zr-TiO_2 diagrams for, top, fresh dacites (open circles) and komatiites (solid circles) and, bottom, silicified dacitic (open circles) and komatiitic volcaniclastic sediments (solid figures) containing less than 95% SiO_2 by weight. Element ratios in rocks with more than 95% SiO_2 vary irregularly because of the low contents of the nonsilica components. Diagrams show separation of compositional fields for komatiitic and dacitic rock types. In bottom diagram, komatiitic ashes represent (1) the Mendon Formation, member M1c, the Msauli Chert (solid circles); (2) the Hooggenoeg Formation, member H1, the Middle Marker (solid triangle); and (3) the Hooggenoeg Formation, member H3c (solid square).

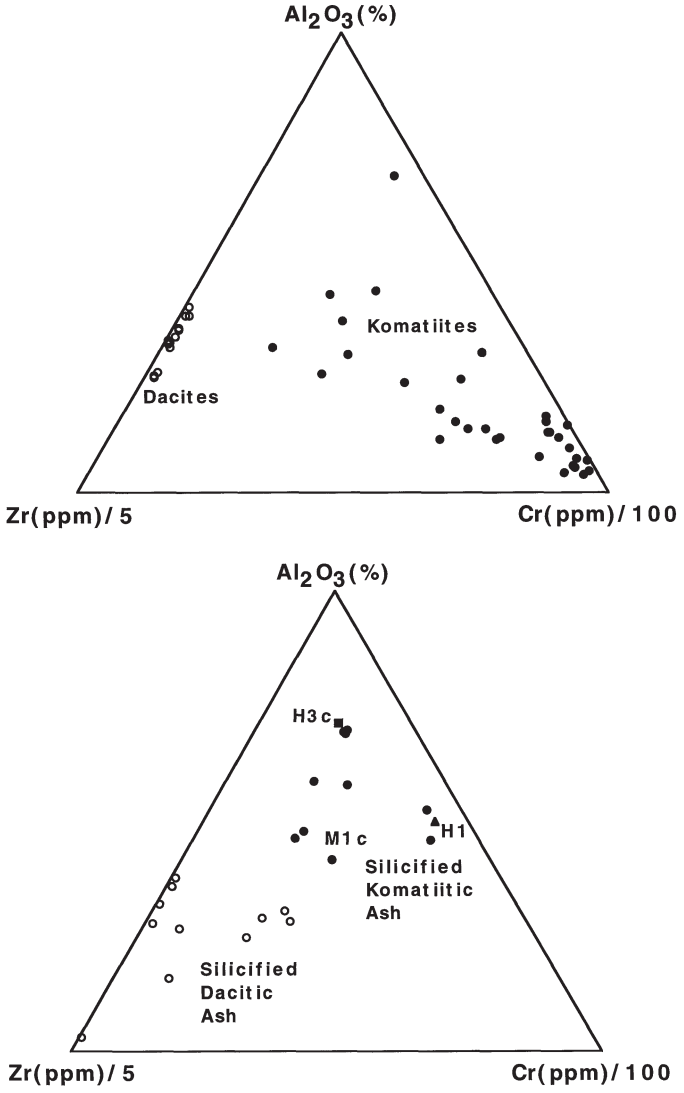


Figure 8. Triangular Al_2O_3-Zr-Cr diagrams for fresh dacites and komatiites (top) and silicified dacitic and komatiitic volcaniclastic sediments (bottom) containing less than 95% SiO_2 by weight. Symbols as in Figure 7.

sum are present in cherts throughout the Onverwacht Group and locally in silicified orthochemical bank deposits in the Mapepe Formation (Fig. 14). Most are small pseudohexagonal crystals (Fig. 14B) or stellate radiating crystal clusters that grew diagenetically in soft fine-grained komatiitic volcaniclastic sediments (Lowe and Knauth, 1977; Barley et al., 1979; Lanier and Lowe, 1982; Buick and Barnes, 1984). Some carbonaceous layers include microscopic pseudomorphs after lenticular gypsum (Fig. 14C), similar to that found in modern sediments and grown in the laboratory (Cody, 1979).

Layers as much as 1 m thick at the base of the Buck Reef Chert include large, vertical silica pseudomorphs after primary precipitative crystals (Fig. 14A), interpreted to have been nahcolite (sodium bicarbonate), and silicified evaporite solution collapse breccias (Lowe and Fisher Worrell, this volume, Chapter 7).

Carbonate. Carbonate is abundant in rocks of the Swaziland Supergroup, but, like silica, most has formed by the postdepositional cementation or replacement of primary sediments. Primary iron-rich dolomite or ankerite may be present locally in the Kromberg Formation (Lowe and Knauth, 1977) and dolomite forms units as much as several meters thick in orthochemical bank deposits in the middle part of the Mapepe

TABLE 3. MAJOR AND TRACE ELEMENT COMPOSITIONS OF BLACK CHERTS AND RELATED SEDIMENTARY ROCKS CONTAINING BASALTIC ASH

	Major Elements (Wt%) Sample Numbers*		
Oxides	SAF-23-221	SAF-23-118	SAF-23-219
SiO_2	96.36	94.91	67.49
Al_2O_3	1.49	1.51	9.86
Fe_2O_3	1.32	2.73	19.34
MgO	0.43	0.55	2.82
CaO	0.03	0.03	0.00
Na_2O	0.11	0.22	0.00
K_2O	0.21	0.00	0.00
TiO_2	0.04	0.04	0.37
MnO	0.00	0.01	0.09
P_2O_5	0.00	0.00	0.03
S	0.01	0.00	0.00
Total	100.00	100.00	100.00
	Trace Elements (ppm)		
Element			
Ba	<10	<10	<10
Cr	47	43	521
Zr	12	17	63
Sr	<10	<10	<10
Rb	<10	<10	<10
Y	<10	<10	44
Ni	74	77	286

Note: Analyses by Ron Hartree, Department of Geology, University of Ottawa, Ottawa, Canada.

*Sample descriptions:

SAF-23-221	Black chert replacing carbonated basaltic ash; Footbridge Chert (K3c), Kromberg Fm.
SAF-23-118	Laminated black chert containing altered basaltic ash; Footbridge Chert (K3c), Kromberg Fm.
SAF-23-219	Black, carbonaceous, chlorite-bearing sediment probably representing mixed basaltic and komatiitic ash, clay, iron oxides, and fine carbonaceous matter; Footbridge Chert (K3c), Kromberg Fm.

Formation (Lowe and Nocita, this volume, Chapter 10). All of these units contain disseminated microcrystalline silica, commonly 30 to 50% by volume.

Silica. The only sedimentary units considered by the present writer to represent primary sea-floor silica deposits occur locally in the Mapepe Formation (Fig. 15) as part of an orthochemical bank facies (Lowe and Nocita, this volume, Chapter 10). They are composed of pure, semitranslucent chert, and most were disrupted shortly after deposition to form contorted masses of plastically deformed sediment (Fig. 15A) or current-worked chert-plate conglomerates and breccias (Fig. 15B).

Possible primary silica deposits include nearly pure chert layers that occur within banded units throughout the Onverwacht and Fig Tree Groups (Fig. 16). These units include black-and-white banded chert, banded ferruginous chert, and banded iron formation. Each of these rock types is made up of couplets composed of alternating bands, generally less than 10 cm thick, of (1) nearly pure silica, and (2) carbonaceous, iron-rich, carbonate-rich, or detrital sediments (Fig. 16). The silica bands are composed of more than 99% silica (Table 6, col. 4) and almost certainly represent primary siliceous sediments, although, as will be discussed below, the banding itself may be largely diagenetic in origin.

Banded ferruginous chert. Banded ferruginous chert (BFC) consists of thin 0.1- to 10-cm-thick bands of white-weathering chert interlayed with fine-grained sediment that, in outcrop, com-

TABLE 4. MAJOR AND TRACE ELEMENT COMPOSITIONS OF DACITIC VOLCANICLASTIC AND VOLCANIC ROCKS, ONVERWACHT AND FIG TREE GROUPS

	Major Elements (Wt%) Sample Numbers*					
Oxide	AF-23-181	SAF-245-1	SAF-105-30	SAF-295-5	SAF-172-1	SA17-7
SiO_2	90.52	90.86	95.40	77.29	77.38	64.10
Al_2O_3	4.93	6.56	3.38	17.29	14.60	16.72
Fe_2O_3	0.15	0.38	0.55	0.65	1.98	5.22
MgO	0.41	0.11	0.00	0.26	0.60	1.98
CaO	0.66	0.01	0.03	0.01	0.05	2.63
Na_2O	0.01	0.00	0.00	0.14	0.15	6.26
K_2O	3.01	1.65	0.56	3.95	4.30	2.15
TiO_2	0.22	0.38	0.55	0.34	0.76	0.68
MnO	0.01	0.00	0.01	0.00	0.00	0.06
P_2O_5	0.08	0.03	0.01	0.07	0.15	0.20
S	0.00	0.02	0.01	0.00	0.03	NA
Total	100.00	100.00	100.00	100.00	100.00	100.00
	Trace Elements (ppm)					
Element						
Ba	53	5923	15440	18038	1086	400
Cr	18	538	89	46	1379	17
Zr	59	71	41	143	113	166
Sr	<10	<10	25	81	25	292
Rb	43	48	13	110	103	12
Y	<10	11	<10	12	22	15
Ni	<10	<10	<10	<10	82	24

Note: Analyses by Ron Hartree, Department of Geology, University of Ottawa, Ottawa, Canada.

*Sample descriptions:

SAF-23-181	Chert representing silicified dacitic volcaniclastic sandstone from H6, upper Hooggenoeg Fm., along Komati River
SAF-245-1	Silicified dacitic ash Mapepe Fm.
SAF-105-30	Chert representing heavily silicified, fine-grained dacitic ash, Mapepe Fm., in the Barite syncline.
SAF-295-2	Chert representing silicified quartz-phyric ash immediately below spherule bed S2 at the base of the Mapepe Fm.
SAF-172-1	Silicified dacitic ash, Mapepe Fm.
SA17-7	Fresh dacitic flow rock, Schoongezicht Fm.

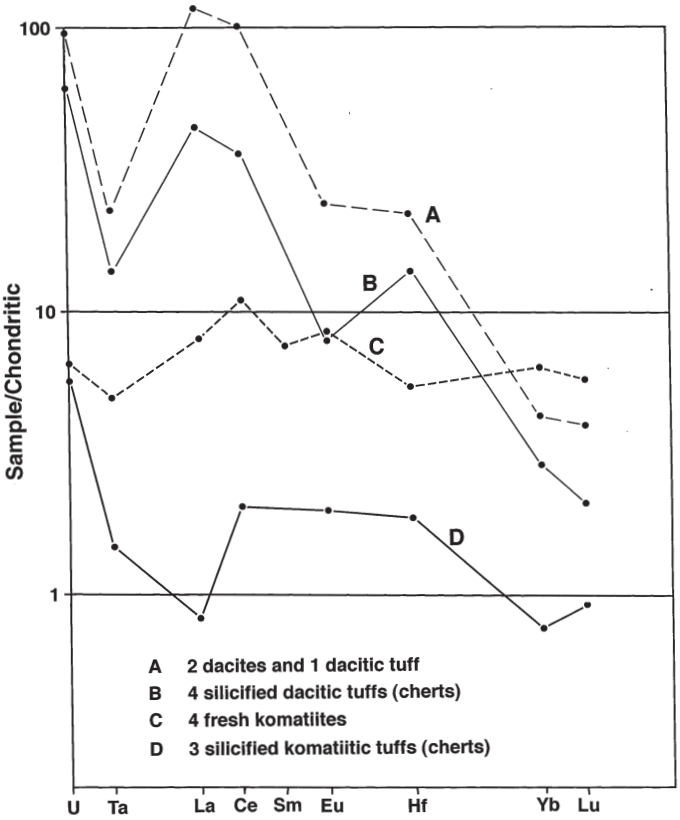


Figure 9. Chondrite-normalized rare earth element (REE) abundances in representative fresh volcanic and silicified volcaniclastic units in the Barberton Greenstone Belt. Relatively low REE abundances in silicified sediments compared to volcanic rocks probably reflect dilution by infilling of sediment pore space by low-REE silica cement.

monly weathers to a rusty brown, tan, pink, reddish, or ochre color (Fig. 16). Thick units of BFC are present at four main stratigraphic positions in the Swaziland Supergroup in the study area.

(1) Along the west limb, around the hinge, and on the northern part of the east limb of the Onverwacht anticline, the middle and upper parts of the Buck Reef Chert are made up largely of thinly layered BFC, locally reaching more than 100 m thick. On the east limb, this BFC is interstratified with basaltic and komatiitic flow units.

(2) BFC is widely developed in the upper cycles of the Mendon Formation. It locally occurs in thin units in the chert caps on cycles 1 and 2 in southern areas, where it appears to be laterally equivalent to the komatiitic flows of cycles M2v and M3v, respectively. BFC occurs in thick units in M3 and higher cycles, locally reaching thicknesses in excess of 100 m and containing interstratified komatiitic flows. Some thick komatiitic units in the upper cycles also include thin zones of BFC that have not been taken as cycle boundaries.

(3) From 20 to 50 m of BFC occurs locally in the Ulundi Formation in the northern part of the belt where it overlies black chert and komatiitic lavas of the Weltevreden Formation (Fig. 16A).

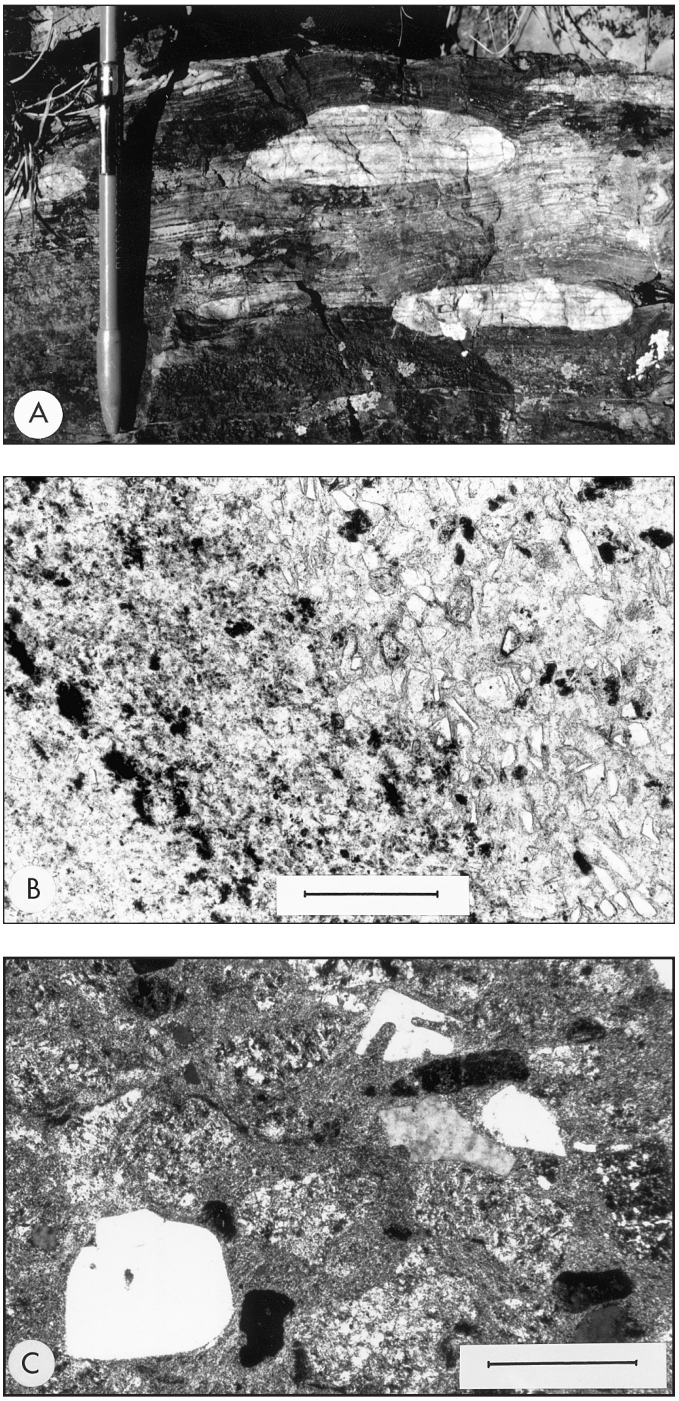


Figure 10. Cherts formed by the silicification of dacitic volcaniclastic units in the Onverwacht and Fig Tree Groups. A, Chert nodules formed by the local silicification of fine-grained, laminated dacitic tuff in the Mapepe Formation. B, Silicified fine-grained, current-deposited ash from upper part of a graded dacitic turbidite bed in H6 (see Fig. 3). Dark grains are admixed detrital carbonaceous matter. Plane light. Scale bar is 0.25 mm. C, Silicified quartz-phyric dacitic volcaniclastic sandstone from basal part of Mapepe Formation of Fig Tree Group. White grains are quartz phenocrysts; opaque grains are carbonaceous and ferruginous particles; mottled grains are chert-sericite micromosaics representing recrystallized vitric grains. Matrix is fine-grained quartz-sericite micromosaic formed by recrystallization of fine ash and dust. Crossed nicols. Scale bar is 0.5 mm.

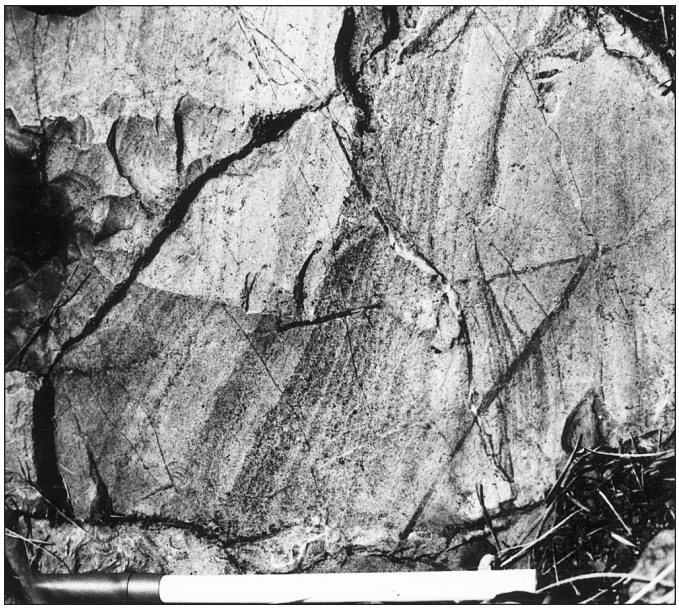


Figure 11. Black chert formed by silicification of fine-grained, flat-layered sediment. Similar units are common in black cherts of the Onverwacht Group, especially those capping upper cycles of the Mendon Formation. The primary sediments probably consisted of fine ash, carbonaceous matter, and possibly clay.

(4) Highly contorted, discontinuous units of BFC are present in the northern facies of the Fig Tree Group between the Sheba and Belvue Road Formations, where it has been termed the Haki Iron Formation (Philpot et al., 1988) and, locally, within the Sheba Formation.

Thin layers and patches of BFC also occur locally within many sections of black and black-and-white banded chert.

In most surface outcrops, BFC consists of white chert bands separated by massive layers of deeply weathered limonitic or goethitic material (Fig. 16B). In the least weathered surface rocks, the ferruginous bands consist of light tan to very light gray, fine-grained, finely laminated, earthy, porous, granular sediment that shows patchy intense iron staining (Fig. 16C). BFC in the Buck Reef Chert, Ulundi Formation, and Sheba Formation, seen in core and mine exposures, is composed of black, finely laminated, highly carbonaceous, partially silicified, granular sediment containing bands of semitranslucent chert. In thin section, the least weathered samples of BFC are composed of microquartz, siderite, small amounts of sericite, and carbonaceous matter. Finely crystalline, ash gray siderite, much weathered to a deep reddish color, constitutes from a few percent to more than 70% of the rock and accounts both for the intense weathering and high iron content of the near-surface rocks. The only structures seen in BFC are fine, even laminations and banding. Current structures and detrital particles coarser than silt and clay are absent. The original sediments were probably mixtures of fine, detrital organic matter, clay, fine fall-deposited pyroclastic ash and dust, precipitative siderite, and silica.

Outcrops of heavily weathered or hydrothermally altered BFC are commonly an intense rust color and bedding planes and joint surfaces are coated with ferric oxide and silica crusts as much as 1 cm thick. Many of these crusts show concentric iron-staining patterns that have been interpreted as fossil Archean mudpools by de Wit et al. (1982). However, the structures are developed on lower as well as upper bedding surfaces and locally on joint planes, lie entirely within the secondary iron oxide and silica crusts, are generally only 1 to 2 mm thick, and are commonly underlain and overlain by finely laminated, unmixed sediments. These features are inconsistent with an origin as hydrothermal springs or mudpools and are interpreted here as liesegang bands.

Jasper and iron formation. Jasper occurs in thin units of red-and-white banded chert at several levels in the Mapepe Formation, interlayed with iron-oxide bands in oxide facies banded iron formation in the lower part of the Mapepe Formation (Fig. 17),



Figure 12. Cherts formed by the silicification of terrigenous sediments in the Fig Tree Group. A, Silicified conglomeratic sandstone from the middle part of the Mapepe Formation. The clasts are composed of carbonaceous chert, silicified siltstone and sandstone, and jasper, all derived by erosion of the immediately underlying 10 to 20 m of Mapepe strata. B, Silicified cross-laminated sandstone from the Mapepe Formation. The original sediment was a mixture of volcaniclastic, lithic sedimentary, undifferentiated chert, and quartz grains. Black laminations contain carbonaceous matter.

TABLE 5. MAJOR AND TRACE ELEMENT COMPOSITIONS OF SILICIFIED AND UNSILICIFIED GRAYWACKES FROM THE FIG TREE GROUP

	Major Elements (Wt%) Sample Numbers*					
Oxide	SAF-234-1	SAF-115-5	SAF-229-4	SAF-229-3	SAF-296-4	SAF-288-6
SiO_2	96.32	90.66	86.88	64.68	67.23	71.72
Al_2O_3	1.93	3.33	5.12	14.39	12.86	8.10
Fe_2O_3	1.03	3.89	6.24	5.37	6.31	9.25
MgO	0.01	1.67	0.04	4.11	3.59	4.91
CaO	0.04	0.02	0.10	4.70	3.97	3.16
Na_2O	0.03	0.09	0.00	1.23	4.10	0.07
K_2O	0.49	0.13	1.32	4.68	1.25	1.98
TiO_2	0.13	0.17	0.23	0.57	0.45	0.46
MnO	0.01	0.00	0.03	0.24	0.18	0.28
P_2O_5	0.00	0.00	0.03	0.02	0.05	0.04
S	0.01	0.04	0.01	0.01	0.01	0.03
Total	100.00	100.00	100.00	100.00	100.00	100.00
	Trace Elements (ppm)					
Element						
Ba	2034	1421	7170	4088	419	403
Cr	254	253	548	385	381	659
Zr	22	48	34	122	125	86
Sr	<10	<10	<10	181	243	69
Rb	10	<10	30	161	50	61
Y	14	<10	12	15	19	17
Ni	<10	149	132	63	99	163

Note: Analyses by Ron Hartree, Department of Geology, University of Ottawa, Ottawa, Canada.

*Sample descriptions:

Southern Facies

SAF-234-1 Chert representing heavily silicified lithic graywacke, middle Mapepe Fm.

SAF-115-5 Chert representing silicified lithic graywacke, basal Mapepe Fm.

SAF-229-4 Partially silicified, coarse-grained lithic graywacke, middle Mapepe Fm., east limb of Barite syncline.

SAF-229-3 Lithic sandstone, upper Mapepe Fm., east limb of Barite syncline.

Northern Facies

SAF-296-4 Unsilicified lithic graywacke, lower Sheba Fm., southernmost Ulundi syncline.

SAF-288-6 Unsilicified lithic graywacke, lower Sheba Fm.

and interbedded with shale and magnetite-bearing shales in the Moodies Group. Silica layers in these rocks are essentially pure silica+iron-oxide mixtures (Table 6, cols. 5 and 6).

In the first of these occurrences (Table 6, col. 5), jasper occurs as part of a distinctive shallow-water orthochemical bank facies association that includes barite, carbonate, and, locally, pyritic chert (Lowe and Nocita, this volume, Chapter 10). The Mapepe BIF (Beukes, 1973) is a regionally extensive unit of banded oxide-facies iron formation (Table 6, col. 6) deposited under deep, quiet-water conditions (Beukes, 1973; Lowe and Nocita, this volume, Chapter 10). This unit is not clearly associated with any igneous rocks, and the regional controls on iron sedimentation are not known. Jasper layers and interbedded hematitic iron formation in the Moodies Group are associated with basaltic volcanic rocks and may be exhalites. They accumulated under quiet, subaqueous conditions.

LITHOFACIES

The preceding discussion has outlined the relationships between primary sediment types and the cherts produced by their silicification in the Swaziland Supergroup. Individual units of silicified sediments commonly include a variety of cherts representing more than one primary sediment type. These may be interbedded within individual sections or pass laterally into one another through facies changes.

In the Onverwacht Group, where cherts are most abundant, interflow sedimentary units are thin, and each generally includes a limited variety of cherts representing a limited range of precursor sediments deposited under a limited set of sedimentological conditions. These units essentially constitute individual lithofacies. In the Onverwacht Group, it is possible to classify cherty lithofacies in terms of three main variables: (1) style and composition of volcanism, (2) location of the depositional sites relative to volcanic centers (proximal versus distal), and (3) water depth (Table 6). In contrast, tectonism and local clastic depositional systems exerted a strong control on primary sediment types and later silicification in the Fig Tree Group.

Because of the extremely close relationship between volcanism and sedimentation, the following discussion will focus on lithofacies in the Onverwacht Group associated with the three main types of volcanic rocks: komatiites, basalts, and felsic volcanic units. Two major groups of lithofacies or lithofacies associations are recognized based on overall conditions of deposition. The platform or shallow-water association, comprising

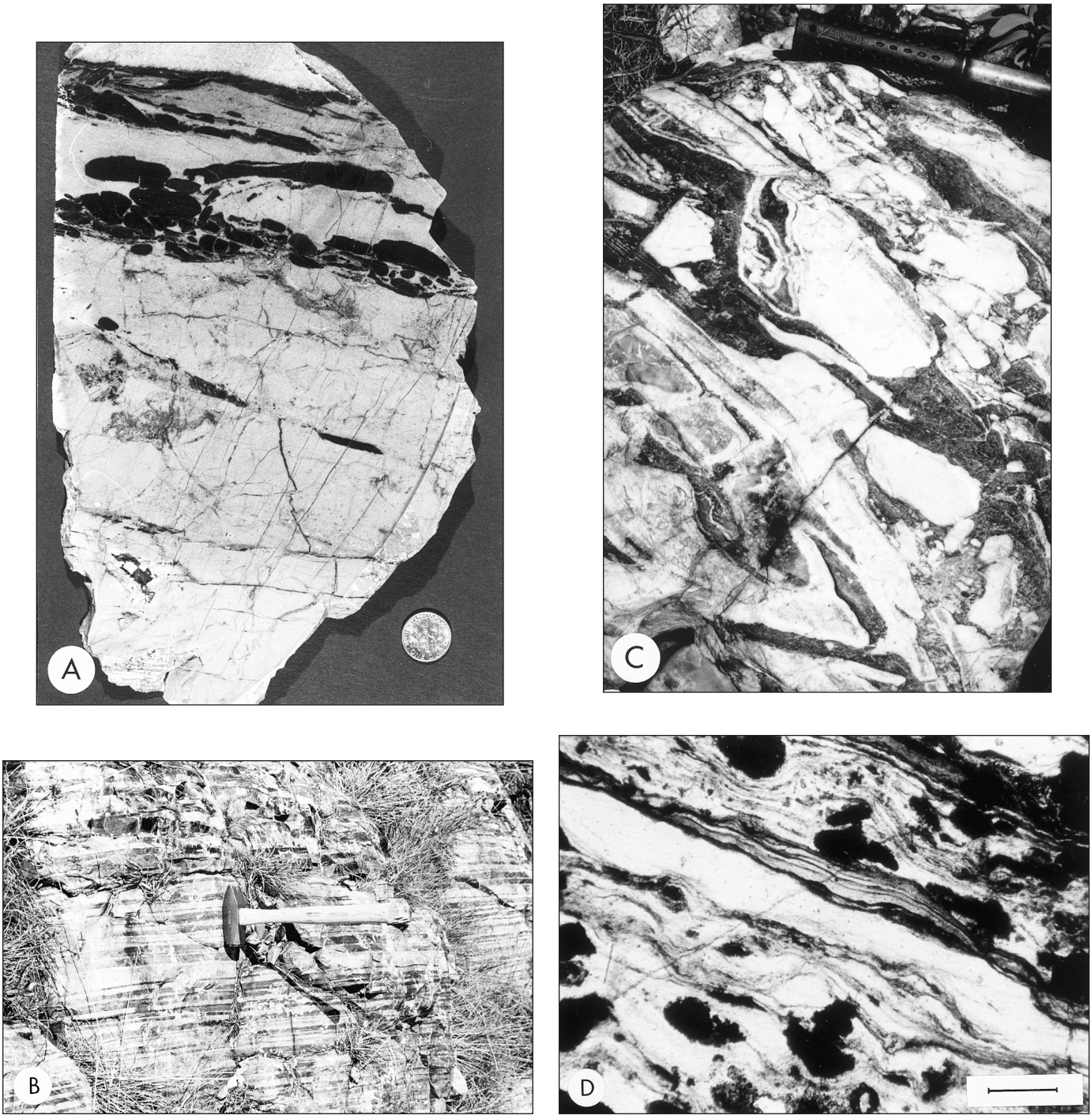


Figure 13. Chert formed by the silicification of biogenic sediments in the Onverwacht Group. A, Silicified carbonaceous mudstone and mudstone rip-up clasts interbedded with silicified cross-bedded komatiitic ash in the Msauli Chert. Carbonaceous clasts define large cross-set near middle of slab. The current-deposited ash overlies light-toned bed of extremely fine-grained silicified komatiitic dust. B, Black-and-white banded chert from K1, the Buck Reef Chert. The black layers contain both fine carbonaceous laminations, representing bacterial mats, and detrital carbonaceous grains. White layers are essentially pure silica. C, Early intraformational breccias in K1 formed by disruption of plastic to brittle white chert bands sandwiched between still fluid bands of soft, carbonaceous sediment. Buck Reef Chert (K1). D, Photomicrograph of fine, carbonaceous laminations, representing microbial mats, containing ripped-up carbonaceous grains. Note lack of compaction of particles and open, silica-filled pore spaces. From black-and-white banded chert in K1. Scale bar is 0.5 mm long.

TABLE 6. MAJOR AND TRACE ELEMENT COMPOSITIONS OF REPRESENTATIVE BIOGENIC AND ORTHOCHEMICAL CHERTS IN THE SWAZILAND SUPERGROUP

	Major Elements (Wt%) Sample Numbers*						
Oxide	SAF-23-195	SAF-36-57	SAF-115-3	SAF-23-196	SAF-179-1	SAF-296-3	SAF-127-X
SiO_2	99.56	99.27	98.97	99.41	95.56	85.16	66.80
Al_2O_3	0.17	0.48	0.68	0.11	0.08	0.01	0.11
Fe_2O_3	0.07	0.04	0.07	0.06	4.08	13.57	17.87
MgO	0.12	0.07	0.09	0.11	0.10	0.78	2.52
CaO	0.03	0.00	0.00	0.04	0.04	0.15	0.27
Na_2O	0.00	0.00	0.00	0.26	0.00	0.00	0.32
K_2O	0.04	0.12	0.14	0.01	0.00	0.00	0.02
TiO_2	0.00	0.01	0.03	0.00	0.00	0.00	0.00
MnO	0.00	0.00	0.00	0.00	0.03	0.17	0.62
P_2O_5	0.00	0.00	0.00	0.00	0.02	0.04	0.11
S	0.01	0.01	0.02	0.00	0.09	0.03	0.03
Total	100.00	100.00	100.00	100.00	100.00	100.00	100.00
	Trace Elements (ppm)						
Element							
Ba	17	10	93	<10	95	89	57
Cr	10	<10	41	<10	22	29	36
Zr	<10	30	17	14	<10	<10	<10
Sr	<10	<10	<10	<10	<10	<10	<10
Rb	<10	<10	<10	<10	<10	<10	<10
Y	<10	24	<10	<10	<10	<10	<10
Ni	23	19	38	22	<10	<10	<10

Note: Analyses by Ron Hartree, Department of Geology, University of Ottawa, Ottawa, Canada.

*Sample descriptions:

SAF-23-195	Black-and-white banded chert, member K1c2, Kromberg Fm., along Komati River.
SAF-36-57	Black chert, member H3c, Hooggenoeg Fm.
SAF-115-3	Black chert, Mapepe Fm.
SAF-23-196	White band in black-and-white banded chert, member K1c2, Kromberg Fm. along Komati River.
SAF-179-1	Pink, iron-bearing chert, middle Mapepe Fm.
SAF-296-3	Jasper, Ulundi Fm., Ulundi syncline.
SAF-127-X	Iron-rich ferruginous chert above Msauli Chert (M1) in its type section. Lateral equivalent of member M2v of Mendon Fm.

cherts in the Onverwacht Group up through the lower two or three cycles of the Mendon Formation, includes sediments deposited under predominantly shallow-water conditions. Many show evidence of deposition in current or wave active regimes and of in situ organic growth and biological activity. The basinal association includes cherts in the upper cycles of the Mendon and Weltevreden Formations and reflects deposition under mainly quiet, possibly deep-water conditions.

Platform association

Lithofacies associated with komatiitic volcanic rocks. Major komatiitic volcanic units from the Komati Formation through the lower cycles of the Mendon Formation are immediately overlain by silicified sedimentary units made up largely of two principal types of chert (Figs. 18 and 19): (1) silicified komatiitic pyroclastic and water-worked volcaniclastic detritus (Fig. 19A), and (2) black carbonaceous chert. Terrigenous debris is essentially absent. Units of this type include H1 the Middle Marker (Figs. 18 and 19A; and Lanier and Lowe, 1982), H3c (Fig. 19B), H4c, H5c, K2c, the Msauli Chert (M1c) (Lowe, this volume, Chapter 9), M2c, and, locally, parts of H2c (Fig. 16), K1c1 and K1c2, and M3c.

The sedimentology of these cherts has been discussed by Reimer (1975), Lowe and Knauth (1977, 1978), Heinrichs (1980, 1984), Stanistreet et al. (1981), Lanier and Lowe (1982), and Lowe (this volume, Chapter 9). The two main types of sedimentation units are (1) pyroclastic fall deposits, consisting mainly of graded beds of ash, dust, and accretionary lapilli (Fig. 5B) from 1 cm to over 2 m thick; and (2) deposits accumulating between fall events (Fig. 19; and Lowe, this volume, Chapter 9). Fall layers include massive or graded but otherwise structureless beds formed by the passive fall of ash and dust into quiet, standing water and graded ash and dust beds showing an internal succession of structures like the Bouma sequence, including T_a, T_b, T_c, and T_d (Lowe, this volume, Chapter 9). Although these layers have been interpreted to be deep-water turbidites (Stanistreet et al., 1981; Heinrichs, 1980, 1984), studies of the Msauli Chert (Lowe, 1988, and this volume, Chapter 9), Middle Marker (Lanier and Lowe, 1982), K2c (Ransom et al., this volume, Chapter 6). and H3c (Fig. 14) demonstrate that these turbidite-like units formed during pyroclastic falls into shallow water.

Interfall layers include two main types of deposits (Fig. 19): 2a, cross-laminated and cross-stratified ash, commonly containing rip-up clasts of black carbonaceous sediment, representing current-active intervals (Figs. 5A, 13A, and 19); and 2b,

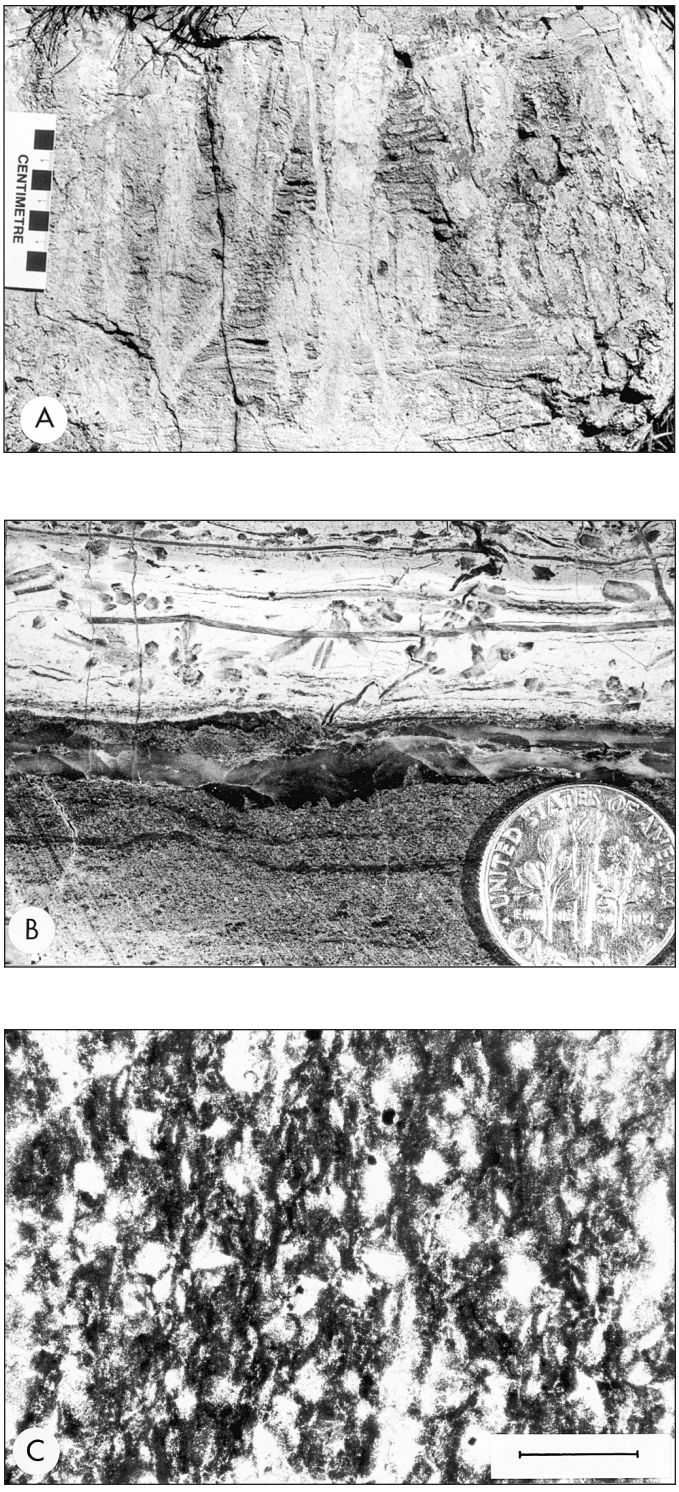


Figure 14. Cherts formed by the silicification of orthochemical sediments in the Onverwacht and Fig Tree Groups. A, Coarse, upward-radiating silicified evaporite crystals in silicified wave-rippled sediment from basal evaporitic unit of Buck Reef Chert (Lowe and Fisher Worrell, this volume, Chapter 7). B, Silica-pseudomorphs after diagenetic pseudo-hexagonal crystals and radiating crystal clusters, both resembling gypsum, in silicified komatiitic ash of H3c. C, Fine carbonaceous sediment from K1 containing minute silica pseudomorphs after lenticular gypsum. Scale bar is 0.2 mm.

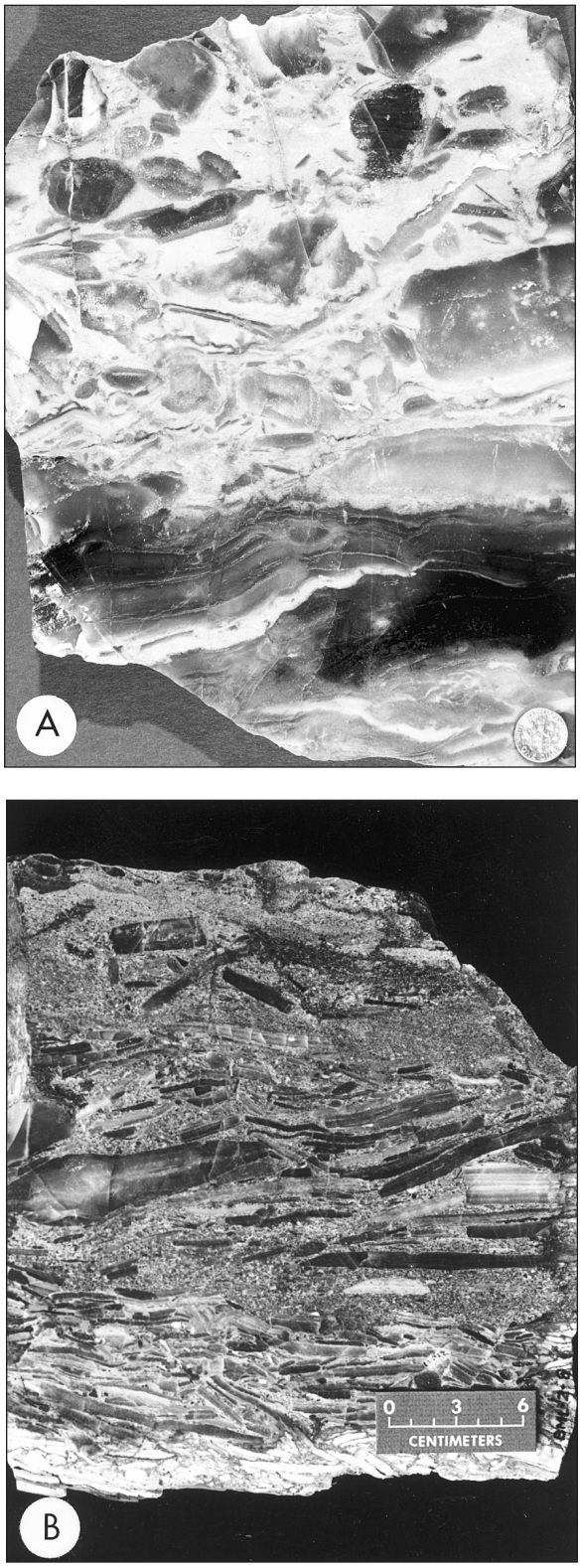
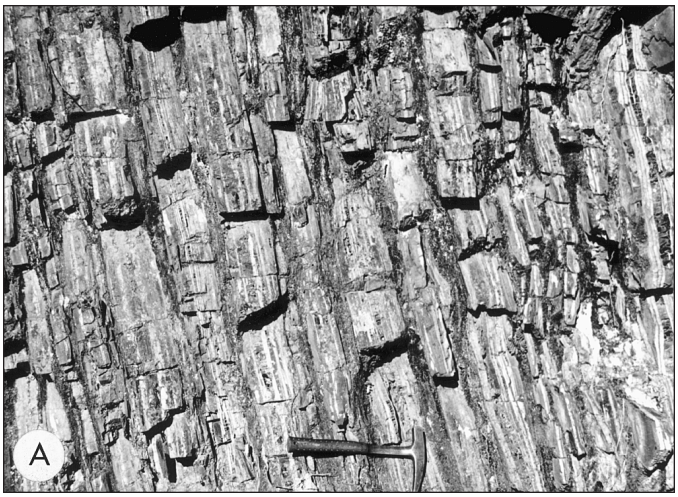
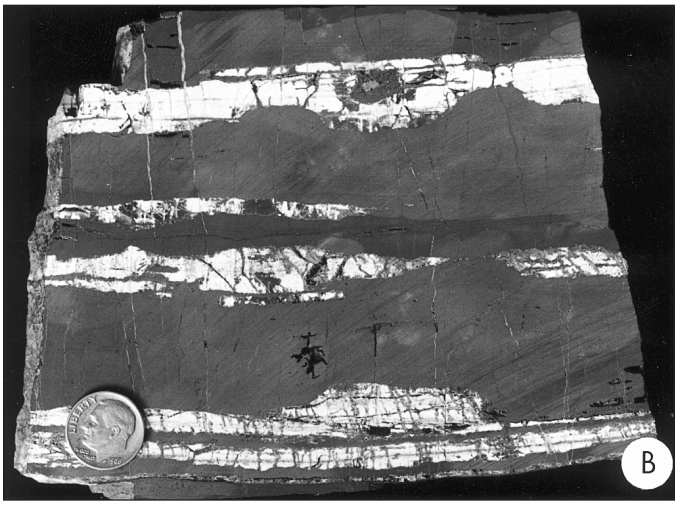


Figure 15. Possible primary silica sediments. A, Breccia-conglomerate composed of plastically deformed masses of nearly pure silica in matrix of barite-rich silicified carbonate. From orthochemical bank facies of Mapepe Formation (Lowe and Nocita, this volume, Chapter 10). B, Breccia composed of transported, rigid to plastically deformed plates of translucent silica in coarse-grained graywacke at base of Mapepe Formation. The chert plates may represent ripped-up primary silica deposits.





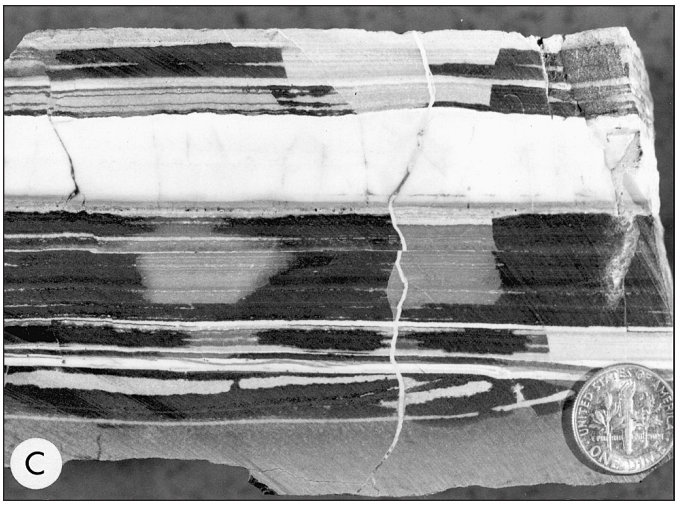


Figure 16 (left column and above). Banded ferruginous chert (BFC). A, Outcrop of BFC at base of Sheba Formation. The rock consists of silicified beds, 5–15 cm thick, made up of alternating bands of nearly pure silica (white) and oxidized sideritic, carbonaceous shale (dark), alternating with recessive nonsilicified units of carbonaceous, sideritic shale. B, Weathered BFC composed of irregular replacement bands of nearly pure silica alternating with deeply weathered, originally sideritic sediment. C, Relatively fresh BFC from Mapepe Formation showing white silica bands in finely laminated iron-stained sediment originally composed largely of fine ash, siderite, carbonaceous matter, and a minor amount of clay.

drapes, lenses, flazers, and thin layers of black carbonaceous chert formed during slack water periods (Fig. 19). Carbonaceous sediments included simple detrital grains and flat stromatolitic mats, but few wisps and little evidence of compaction (Walsh and Lowe, this volume, Chapter 4).

Silicified komatiitic dust layers widely show post-depositional brecciation (Lanier and Lowe, 1982; Stanistreet and Hughes, 1984; Lowe, 1986). Breccias consist of angular clasts of lithified volcaniclastic dust, most less than 10 cm across, and commonly display a gradation from (1) rocks in which discontinuous silica-filled fractures do not form a continuous fracture network (Fig. 20A), to (2) rocks in which dilational fractures are continuous but the individual clasts are only slightly displaced and their original interlocking character is apparent (Fig. 20B), to (3) rocks that are completely brecciated, the clasts rotated and displaced, and the relationships between adjacent clasts has been lost (Fig. 20C). The breccias are irregularly distributed, commonly grading over short distances, laterally and vertically, into unbrecciated or less brecciated rock.

Fractures between clasts are generally filled with clear microquartz, but near the upper contacts of some brecciated layers, loose black carbonaceous granules, volcaniclastic sand, and, more rarely, accretionary lapilli fell into the open fractures, indicating that brecciation began soon after deposition and that the cracks were partially infilled with loose sedimentary debris. The fine-grained pyroclastic dust forming the cracked layers probably settled and compacted slightly after deposition to form a stiff, cohesive sediment. Early cementation may have enhanced the brittle response of the sediment. Some of these sediments may have been brecciated during exposure and desiccation within intertidal and supratidal settings. Some could have been hydrofractured during sediment dewatering. It is also possible that much hydraulic fracturing resulted from boiling of interstitial water during deposition of the immediately overlying lavas, a process described by Mastin (1995) and Long (1989, as noted in Mastin, 1995). Locally, similar fracturing resulted from the displacive growth of early diagenetic crystals (Lanier and Lowe, 1982, Fig. 10). The absence of fragments of underlying rock in the breccias and of breccias intrusive into overlying units indicate that they were not formed by the upward flow of fluids with velocities sufficient to entrain even small particles.

Conglomerate composed entirely of clasts of fine-grained silicified komatiitic ash and dust occurs in lenticular units that locally cap massive or brecciated, fine-grained pyroclastic deposits (Fig. 20C, D). Most conglomerate units are less than 75 cm thick and show irregular, erosive bases and flat concordant tops. Internal stratification is crude to absent, the fabrics are generally clast sup-

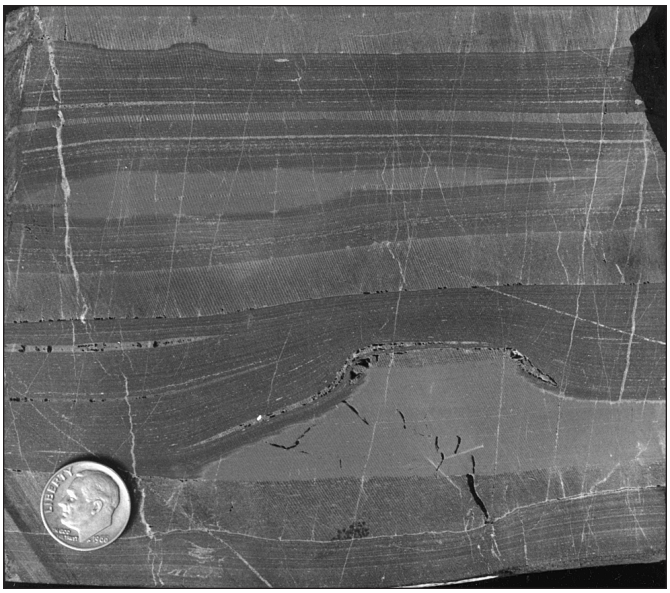


Figure 17. Banded iron formation from the Jasper Marker in the lower part of the Mapepe Formation. The rock consists of bands and lenses of jasper (lighter) alternating with laminated hematitic iron-formation (dark).

ported, and imbrication of larger clasts is common. Some conglomerates contain lenses of cross-laminated volcaniclastic sandstone. Most of these conglomerates formed by current erosion of fine-grained cohesive pyroclastic layers (Lowe, 1986). They are not discordant as suggested by Stanistreet and Hughes (1984) but commonly show erosive bases, do not form crosscutting dikelike bodies, and lack evidence for formation in hydrothermal conduits as proposed by Stanistreet and Hughes (1984).

The overall characteristics of the komatiitic ash–carbonaceous chert lithofacies are most like those of modern intertidal to shallow subtidal deposits (Lowe and Knauth, 1978; Lanier and Lowe, 1982; Lowe, this volume, Chapter 9). The regular alternation of current-active and quiet-water conditions during, as well as between, pyroclastic falls; the wide development of mud drapes, flazer and lenticular bedding, and local reactivation surfaces within ripples (Lowe, this volume, Chapter 9); the overall low energy but regionally extensive largely unchannelized currents; and local erosion of the fine-grained, cohesive or partially silicified volcaniclastic layers to form lenticular intraformational conglomeratic units resemble conditions prevailing on broad shallow shelves and intertidal flats. Unambiguous desiccation cracks were not noted in these units, but bedding-plane exposures are essentially absent. Small mudcracks may be present but difficult to identify in cross section. Some of the breccias may be desiccation breccias developed during long-term exposure. Isolated, sand-sized, pseudo-hexagonal, silicified gypsum crystallites and radiating crystal splays occur locally in many units of fine-grained silicified komatiitic dust.

Lithofacies associated with basaltic volcanic rocks. Thick basaltic units in the Onverwacht Group are commonly overlain by and interstratified with thin layers of chert (Figs. 21 and 22). Chert caps on predominantly basaltic sequences include H2c (Fig. 22), H5c, chert layers in the lower part of the type section of the Kromberg Formation along the Komati River (K1c2 and K1c3) that are the lateral equivalents of the Buck Reef Chert (K1) on the west limb of the Onverwacht anticline, and the Footbridge Chert (K3c). These cherts are composed mainly of black to dark gray chert, banded black-and-white chert, and/or banded chert-carbonate rock.

The petrology and structuring of cherts interbedded with basaltic volcanic rocks have been discussed by Viljoen, R. P., and Viljoen (1969), Lowe and Knauth (1977), and Walsh and Lowe (this volume, Chapter 4). H2c and K3c consist mainly of massive to laminated black chert and black-and-white banded chert lacking current structures, scour features, rip-up clasts, or other evidence of current activity (Fig. 21). Partial replacement by iron-rich dolomite is common and some layers may have included primary carbonate sediments (Fig. 21). Locally, noncherty sediments consist of laminated, highly carbonaceous iron-rich rock (Table 3, column 3) probably representing partially silicified mixtures of carbonaceous matter, iron formation, ash, and clays. The black cherts commonly contain simple and wispy carbonaceous grains and few mats or composite particles (Walsh and Lowe, this volume, Chapter 4). They appear to represent fine organic-rich muds deposited under quiet, low-energy, fully subaqueous conditions. There is little evidence of in situ biological activity and deposition probably took place well below local wave and storm base.

Traced laterally, many of these deeper water basalt-related cherts show transitions into shallow-water deposits (Fig. 22). On the west limb of the Onverwacht anticline, H2c consists mainly of massive to laminated black chert representing fine-grained sediments deposited in relatively deep, quiet water. Interbedded very fine-grained tuffs are primarily fall deposits. Local pumiceous deposits (Fig. 22) probably reflect the existence of nearby basaltic vents. Around the hinge of the anticline and along much of the northern east limb, H2c includes a high proportion of black-and-white banded chert. Immediately north of the Komati River, it is composed largely of silicified current-deposited and airfall ash and black chert of the shallow-water komatiitic lithofacies, although the underlying lavas are also pillow basalts (Fig. 22). Similar lateral facies changes occur in K3c. The common presence of broad facies changes in cherts associated with basaltic sequences suggests that, although they were deposited mainly under quiet, fully subaqueous conditions, overall water depths were not great. The lateral appearance of cherts representing silicified komatiitic ash and associated shallow-water lithofacies in H2c and K3c suggest that some komatiitic eruptions and pyroclastic activity were taking place elsewhere during intervals of largely basaltic volcanism in the BGB.

The tops of the basaltic units underlying cherts are zones of intense alteration and silicification as much as 20 m thick. Within these zones, the basalt has been metasomatically changed to a light gray microcrystalline aggregate of microquartz and sericite

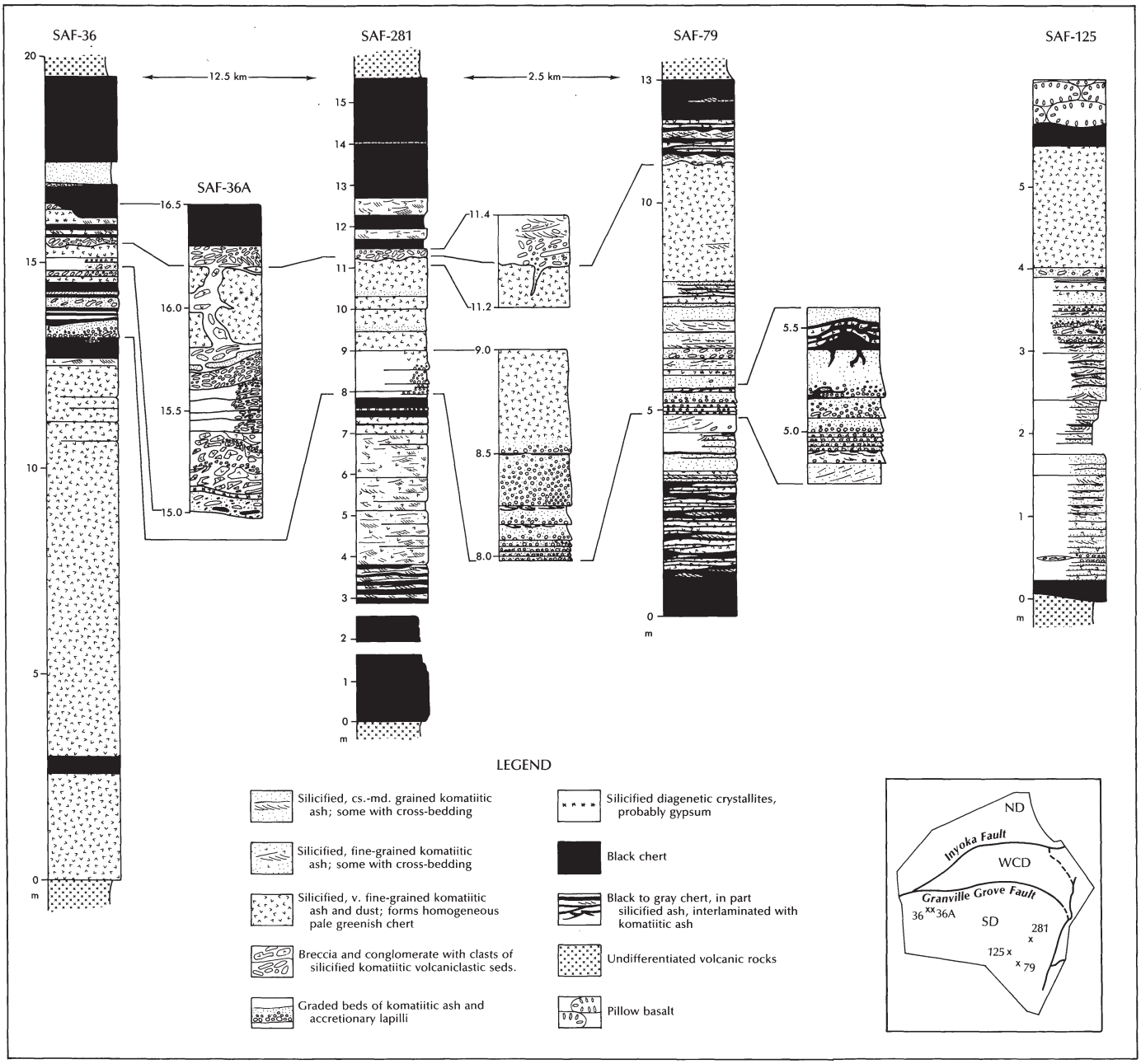


Figure 18. Stratigraphic sections of chert units above komatiitic volcanic sequences. Most units contain silicified komatiitic volcaniclastic sediments that include massive or, less commonly, current-structured silicified ash beds at the base grading upward to current-deposited ash and graded beds of fall-deposited accretionary lapilli and ash at the top. Associated carbonaceous sediments were deposited during intervals between episodes of pyroclastic activity. Sections SAF-36, SAF-36A, SAF-281, and SAF-79 from member H3c, middle Hooggenoeg Formation. Section SAF-125 from Middle Marker (H1).

with minor amounts of chlorite. The original rock has been depleted in MgO, CaO, and Fe_2O_3, and enriched in SiO_2 and K_2O (Byerly et al., 1983). These basaltic alteration zones lack stratiform silica and carbonate veinlets, evaporitic minerals, and other evidence of an early subaerial to shallow-water stage of alteration common in flow-top alteration zones in komatiitic sequences.

Lithofacies associated with felsic volcanic rocks. Only one relatively fresh felsic volcanic and volcaniclastic unit is present in the Onverwacht Group, that at the top of the Hooggenoeg Formation, H6. Older felsic units in the Theespruit Formation have been metamorphosed to quartz-sericite schists. H6 consists largely of massive silicified tuff and coarse volcaniclastic sediments deposited adjacent to an eruptive center.

Fine-grained felsic ash and dust was a minor component of

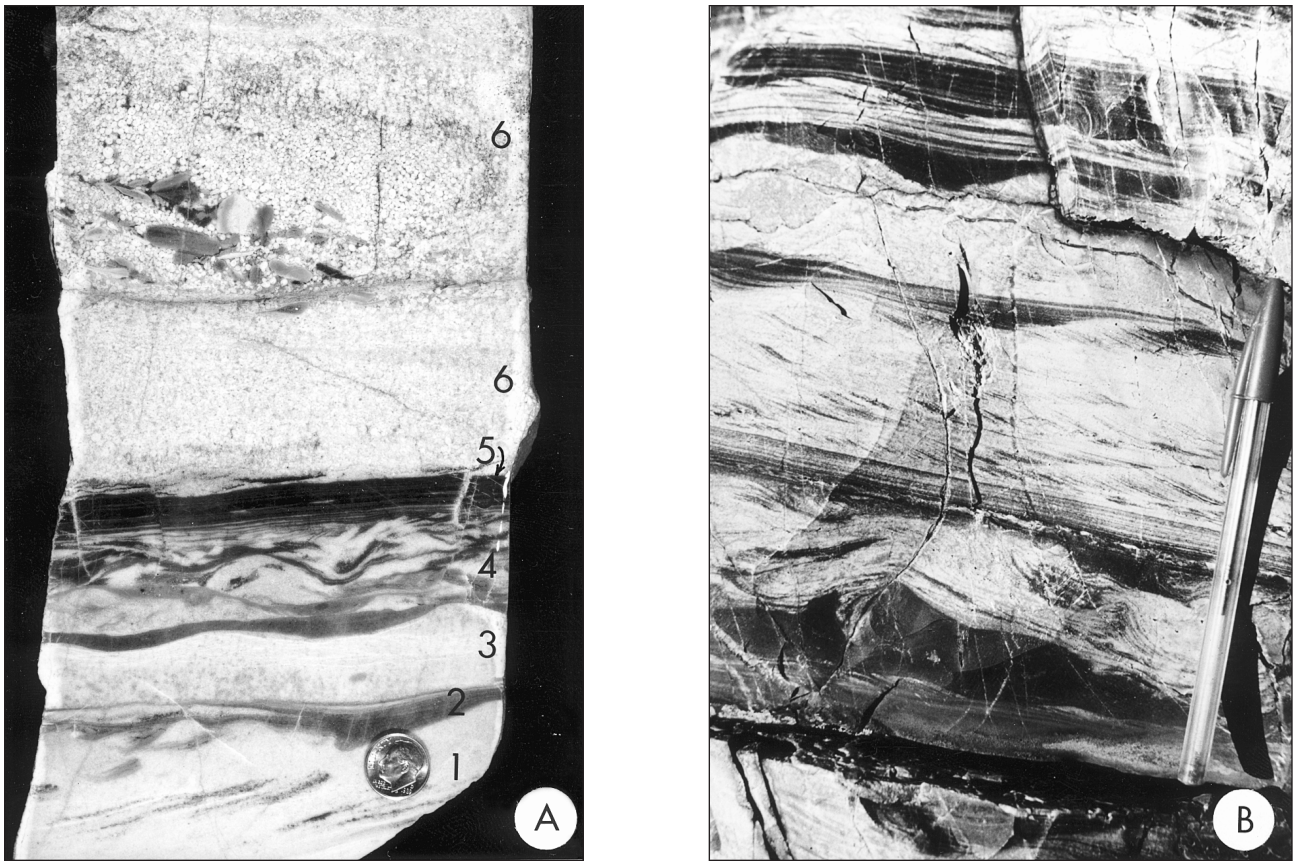


Figure 19. Typical sediment associations in cherts capping komatiitic volcanic sequences. A, Slab showing interbedded units of (1) silicified fine-grained, cross-laminated komatiitic ash containing detrital carbonaceous grains; (2) dark gray, silicified, very fine-grained komatiitic dust loaded and mixed into underlying sandstone; (3) fine-grained, rippled komatiitic ash; (4) rippled and cross-laminated komatiitic ash containing very fine-grained, tuffaceous drapes; (5) black, laminated, carbonaceous mudstone; and (6) coarse-grained, cross-bedded detrital layers containing abundant accretionary lapilli. The upper layer includes rip-up clasts of very fine-grained komatiitic chert. Middle Marker (H1). B, Thin beds of current-deposited komatiitic ash grading upward into layers of carbonaceous chert. The komatiitic ash shows flat lamination and climbing-ripple cross-lamination and contains dark detrital carbonaceous grains. This 1-m-thick sequence was deposited by cyclic currents of declining velocity, possibly turbidity currents, in a small, shallow, quiet-water area. It is impersistent and grades laterally across a distance of about 100 m into units like those in A. Member H3c of Hooggenoeg Formation.

these deposits and chert formed by the silicification of felsic detritus is only locally developed (Figs. 3A and 10B). It is, however, more extensive in the Mapepe Formation of the Fig Tree Group, where it consists of medium gray to bluish gray, commonly semitranslucent laminated chert (Lowe and Nocita, this volume, Chapter 10). Similar chert is abundant in distal turbiditic and pyroclastic fall deposits in the felsic Wyman and Panorama Formations of the early Archean Warrawoona Group, eastern Pilbara Block, Western Australia (Barley et al., 1979).

Felsic volcanism during deposition of H6 was followed by erosion and subsidence of the vent and surrounding sedimentary apron. On the west limb and northern part of the east limb of the Onverwacht anticline, the succession of cherts formed by the silicification of sediments deposited on this subsiding, initially subaerial volcaniclastic apron includes from base upward three main chert types: (1) silicified shallow-water and evaporitic sediments, (2) black-and-white banded chert, and (3) banded ferruginous chert. Initial deposits on the subsiding, eroded platform underlain by H6 included reworked dacitic volcaniclastic sands, evaporites, black carbonaceous muds, and wave-rippled, possibly carbonate detrital sediments deposited under very shallow water to subaerial conditions (Lowe and Fisher Worrell, this volume, Chapter 7). A remarkably similar sequence of shallow-water evaporitic and stromatolitic strata belonging to the Strelley Pool Chert overlies early Archean felsic volcanic and volcaniclastic rocks of the Panorama Formation in the Warrawoona Group, eastern Pilbara Block, Western Australia (Lowe, 1983). Overlying banded ferruginous cherts in the Buck Reef Chert reflect continued subsidence into quiet, deeper water and concurrent basaltic and komatiitic volcanism

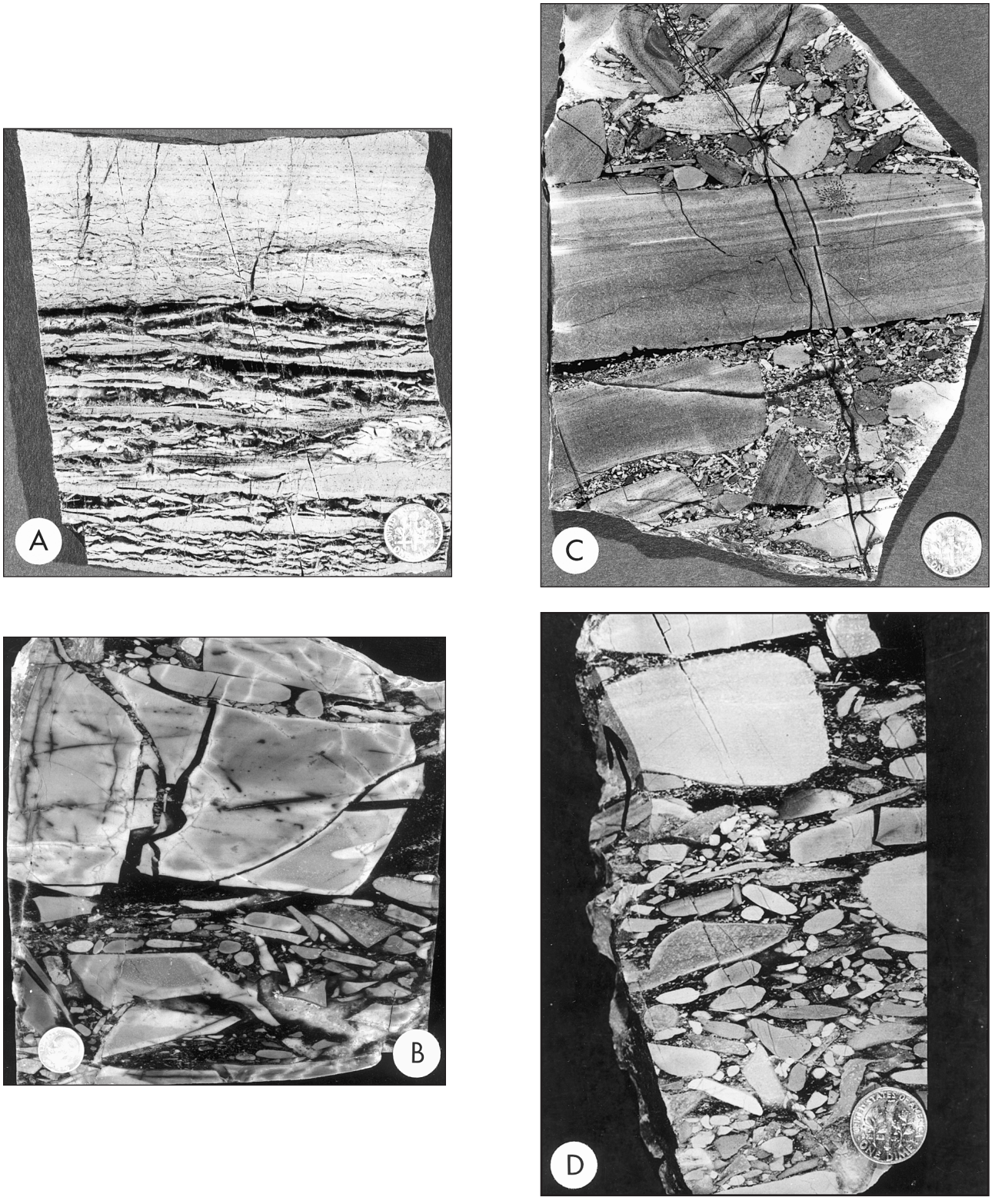


Figure 20. Breccias and conglomerates developed in cherts representing silicified komatiitic ash in Middle Marker (H1). A, Zebraic breccia formed by fracturing of laminated, very fine-grained komatiitic ash parallel to bedding with little displacement of breccia plates. Fractures are filled by translucent chert. Solid chert at top of slab shows development of incipient fractures. B, Blocky breccia formed by fracturing of very fine-grained komatiitic ash. Large clast shows internal fracturing with little displacement of pieces. Note rounding of some clasts, but overall lithologic homogeneity of clast population. C, Heterogeneous breccia showing a wide variety of clast types, all composed of fine- to very fine-grained komatiitic ash. Note bimodal grain size and silica-filled cavity beneath largest clast. D, Conglomerate composed of a variety of rounded clasts of fine-grained komatiitic ash in a matrix of carbonaceous chert.

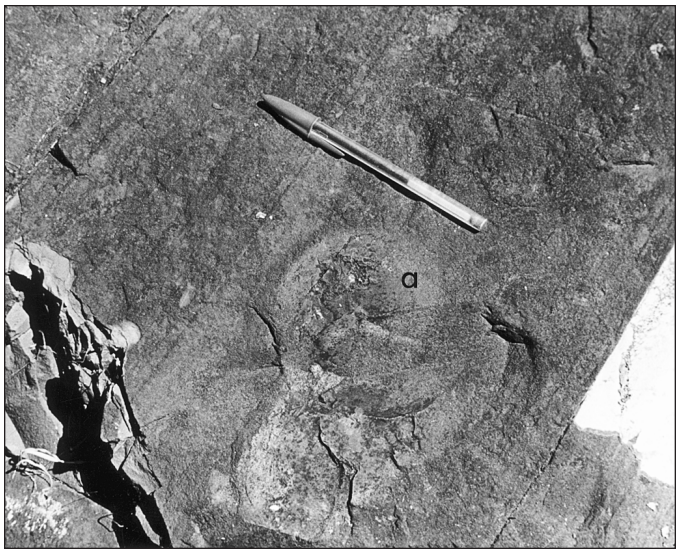


Figure 21. Laminated, deep-water, heavily carbonated and silicified, fine-grained carbonaceous sediment from Footbridge Chert (K3c) along Komati River. Round patches (a) are chert nodules lacking carbonate.

in areas represented by interbedded volcanic units on the east limb of the Onverwacht anticline.

Basinal association

Lithofacies associated with komatiitic and basaltic volcanic rocks. In the upper cycles of the Mendon Formation and locally in the Weltevreden Formation, komatiites and basalts are interbedded with three principal types of chert: (1) banded ferruginous chert, (2) black chert, and less commonly, (3) black-and-white banded chert. The carbonaceous units contain few flat matlike laminations and composite grains and lack evidence of current activity. Most were deposited under quiet, deep-water conditions as fine, clay-rich, organic and sideritic oozes.

Throughout the basinal facies and locally in the platformal facies, there is a close relationship between BFC deposition and subaqueous komatiitic and basaltic volcanism. Major BFC units are most commonly interbedded with or occur as proximal lateral equivalents of komatiitic flows whereas black and banded black-and-white cherts are developed in sections or parts of sections that do not include flow units (Fig. 23). This suggests that deposition of the precursor sediments of banded ferruginous cherts may have been directly influenced by volcanic processes and that the black and black-and-white banded cherts represent distal, nonvolcanogenic deposits (Fig. 24).

Lithofacies associated with felsic volcanic rocks. Deep-water felsic volcanic units have not been reported from the Barberton Greenstone Belt. Turbidites and debris-flow deposits in H6 on the east limb of the Onverwacht anticline (Lowe and Knauth, 1977) are local facies developed in close proximity to subaerial alluvial deposits and probably representing sedimentation at the toe of a fan delta.

In other Archean greenstone belts, deep-water silicified deposits are associated with felsic volcanic centers (see summary in Lowe, 1980, 1982). These consist largely of chemical deposits reflecting subaqueous hydrothermal springs and include sulfide, carbonate, and oxide facies iron formation.

DIAGENESIS

Some models of greenstone belt evolution relate silicification to the convective circulation of hot hydrothermal fluids, involving either subsurface metasomatism of rocks within the sequence or deposition of siliceous exhalites around hydrothermal vents (de Wit et al., 1982; Stanistreet and Hughes, 1984; Buick and Barnes, 1984; Paris et al., 1985; Duchac and Hanor, 1987; Hanor and Duchac, 1990). Although metasomatic alteration probably commenced shortly after deposition of the primary sediments in the Swaziland Supergroup and continued through burial and low-grade metamorphism, the collective properties of cherts within the sequence suggest that much silicification occurred early, probably within a few meters of the sediment-water interface, as a result of low-temperature, sediment/sea-water interaction. Although a detailed treatment of sediment diagenesis and metasomatism is beyond the scope of this paper, the following discussion outlines some of the main evidence relating to the timing and controls on silicification in the Swaziland Supergroup.

Styles of silicification

Six main genetic types of nondetrital silica can be recognized in sediments of the Swaziland Supergroup: (1) silica deposited directly as a relatively pure primary sediment to form discrete silica layers or laminations, (2) silica deposited as a primary sediment along with other nonsilica constituents, (3) secondary silica precipitated as an interstitial cement or cavity-filling material, (4) secondary silica mobilized and precipitated diagenetically along bedding planes to form new silica layers that were not present at the time of deposition (displacive silica), (5) secondary silica replacing primary grains and layers (replacive silica), and (6) late-stage silica veins.

Primary silica layers are rare and may be absent. The most probable candidates are thin bands of relatively pure chert in orthochemical bank facies of the Mapepe Formation (Lowe and Nocita, this volume, Chapter 10). Much silica in the Manzimnyama Jaspilite Member of the Mapepe Formation (Heinrichs, 1980) and most banded ferruginous cherts were probably deposited as fine, colloidal particles or sorbed layers associated with a background sedimentation of iron oxide, siderite, and fine detrital materials. Most silicified volcaniclastic and terrigenous rocks include silica cement between primary particles and replacement silica after primary particles. Primary soluble sediments, such as evaporites and carbonates, are widely replaced by silica or were dis-

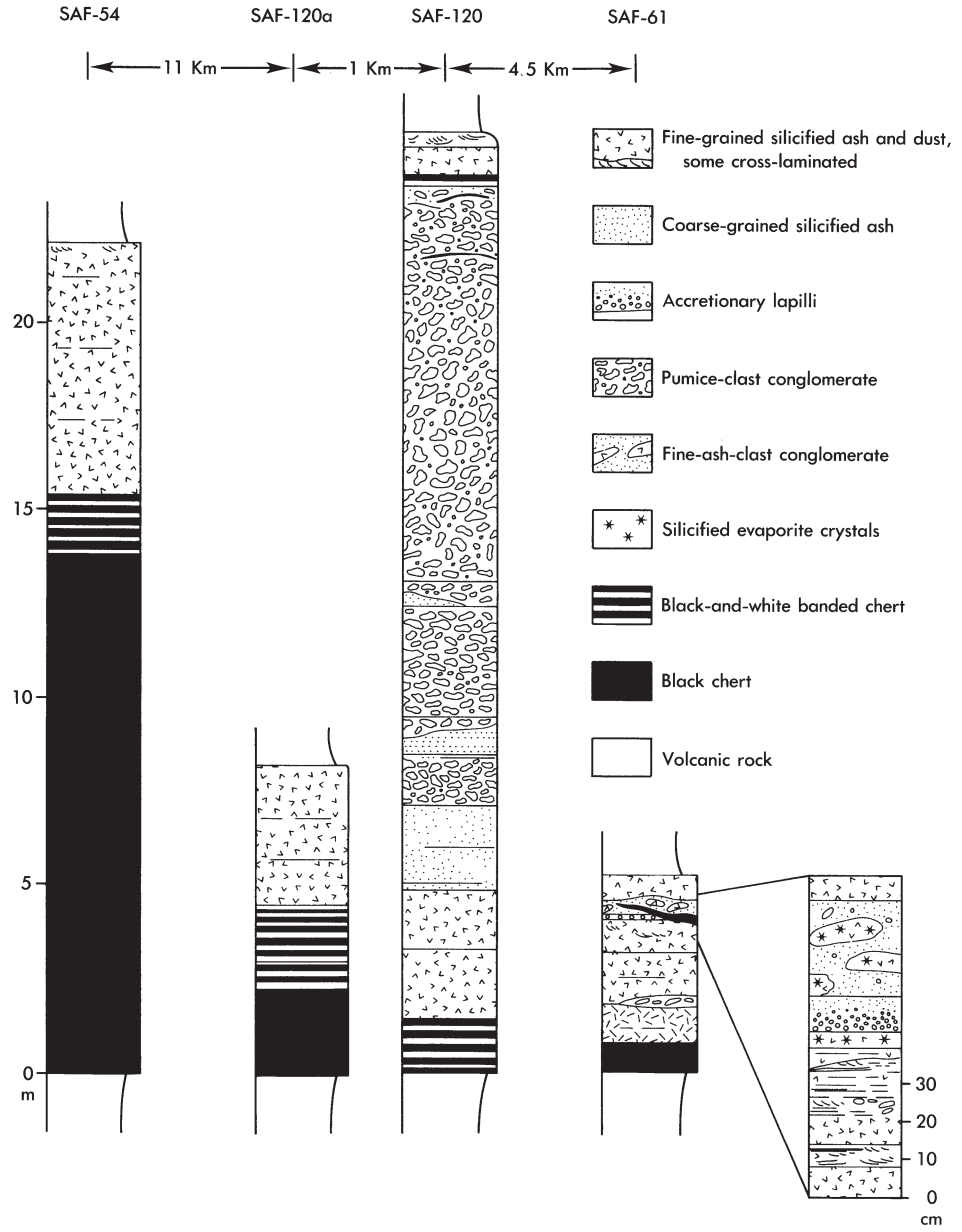


Figure 22. Sections of H2c on west and east limbs of Onverwacht anticline showing transition from predominantly deep-water, fine-grained carbonaceous chert on west limb to shallower water sections containing units of komatiitic accretionary lapilli and current-deposited ash on east limb. The underlying volcanics are basalts in both areas.

solved and the cavities infilled by silica. Virtually all units are cut by silica veins that commonly show concentric zonation indicating formation as cavity fill.

Origin of banding in banded cherts

Although the nearly pure silica bands in banded cherts represent candidates for primary silica precipitates or lithified gelatinous sediments, a number of features suggest circumstantially that, although the silica was probably deposited as a primary sediment, the silica bands may be post-depositional in origin. (1) The nearly pure white silica bands are everywhere less than about 10 cm thick. Alternating carbonaceous, iron-rich, and detrital sediment types are widely developed as nonbanded units as much as 10s of meters thick, but pure white or translucent chert is restricted to thin layers in banded sequences. If the silica bands were deposited as primary layers, they must reflect the development of a particular set of physico-chemical conditions within the local or regional deposystem. It seems unlikely that such conditions could have prevailed over enormous areas of the sea floor

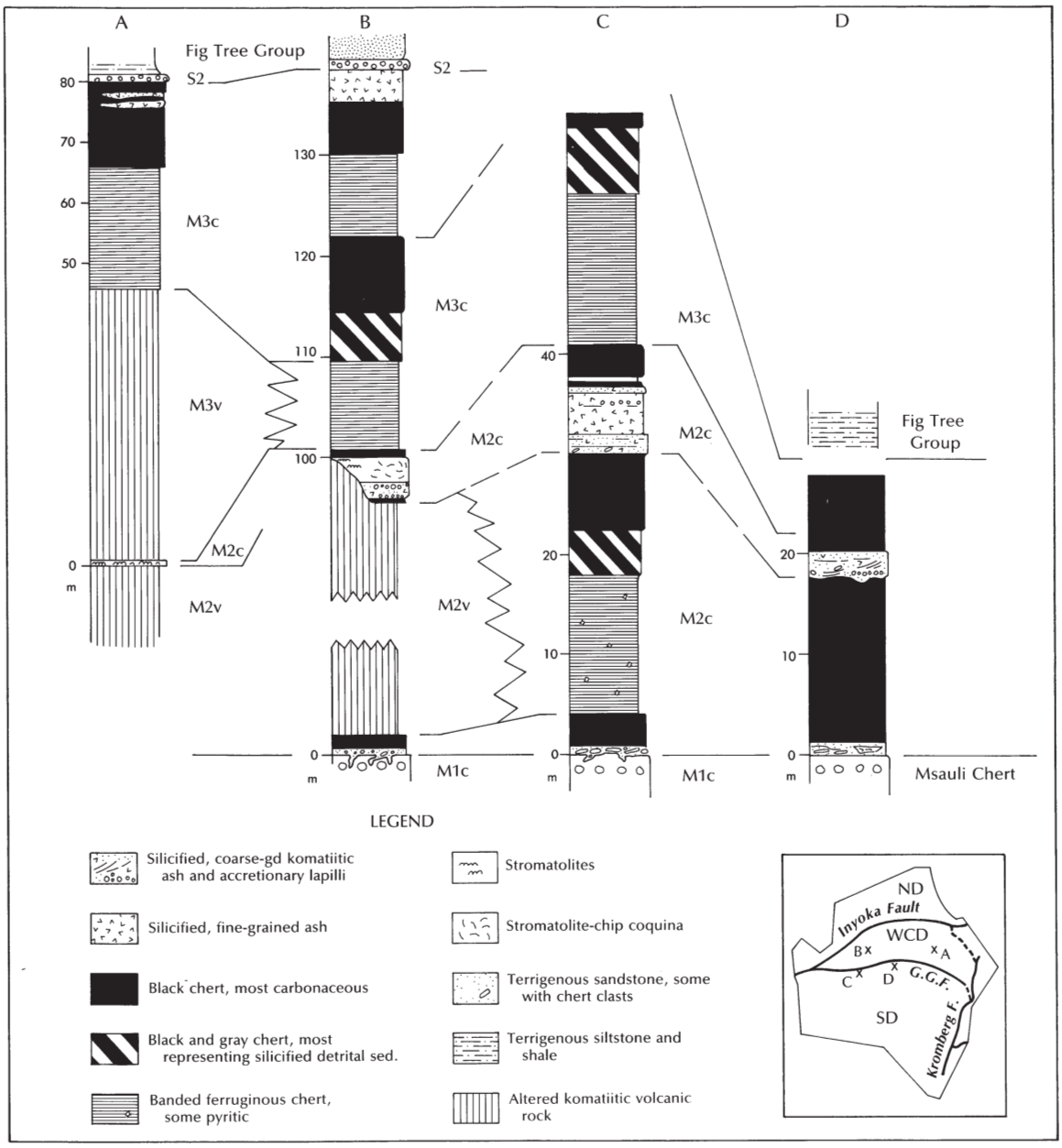


Figure 23. Stratigraphic sections through capping cherts of Mendon Formation, central part of west limb of Onverwacht Anticline, showing facies relationships between komatiitic flow units and banded ferruginous and carbonaceous cherts. Section A: 30°56′06″E., 25°55′00″S.; section B: 30°55′50.7″E., 25°54′47.6″S. (type section of Msauli Chert); section C: 30°55′33″E., 25°54′25″S.

as frequently as is required by the thousands of silica bands in these units without persisting long enough to deposit some layers exceeding 10 cm in thickness.

(2) With the exception of chemically precipitated constituents, such as iron oxide (jasper) and, locally, carbonate, the silica layers are essentially pure. Although silica occurs abundantly in the intervening bands, carbonaceous, volcaniclastic, and terrigenous detritus is not admixed within the silica bands. The absence in the silica bands of loose particles of associated constituents, which were present in the system during deposition, indicates either that silica was deposited so rapidly that foreign particles were totally excluded or that the silica layers formed after deposition by the diagenetic segregation of silica from originally nonbanded, more homogeneous sediments.

(3) Banding occurs in sediments representing enormously diverse depositional environments, from shallow to deep water, moderate to very low energy, biologically active to biologically inactive, and terrigenous, biologically, and orthochemically

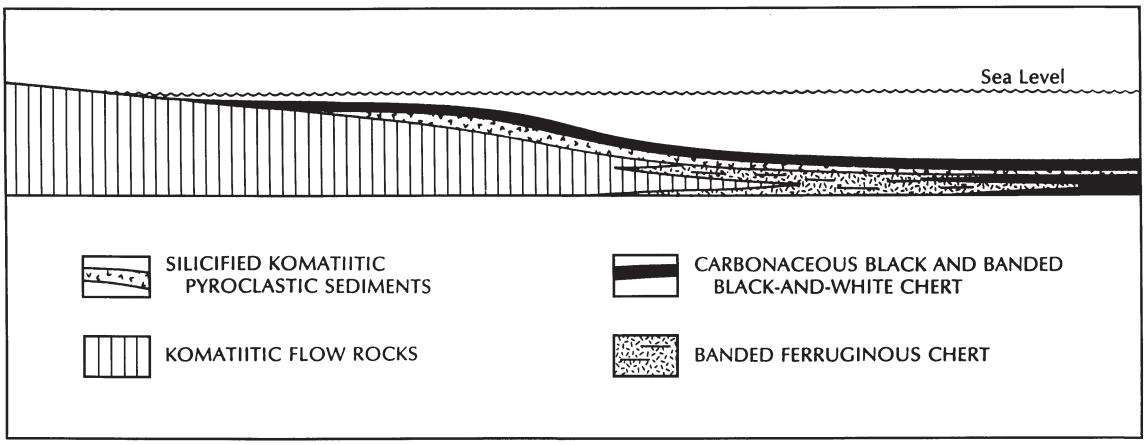


Figure 24. Interpreted facies relationships between banded ferruginous chert, black chert and black-and-white banded chert, and komatiitic extrusive units in the Onverwacht Group.

dominated. This distribution is wider than that of any other sediment type and appears incompatible with the existence of a particular combination of unstable, rapidly fluctuating environmental conditions in the water column.

It seems probable that the original sediments were more homogeneous mixtures of silica and carbonaceous, detrital, and/or orthochemical components and that banding developed as a self-organization phenomenon during early diagenesis, due in some instances to the selective silica replacement or cementation of certain sediment layers but in most units to the precipitation of silica to form entirely new diagenetic bands not present at the time of deposition. The diagenetic formation of similar chert-shale couplets in some younger bedded-chert sequences (Murray et al., 1992) and of the rhythmic banding in Precambrian banded iron formation (Merino, 1987) has also been suggested.

Timing of silicification

There are significant differences in the timing of silicification in the platform and basinal facies. The former show ubiquitous evidence of extremely early, nearly syndepositional silicification prior to sediment compaction whereas the latter were widely silicified after sediment compaction.

Platform association. Most platformal sediments show evidence of early silicification (Lowe and Knauth, 1977, 1978; Stanistreet and Hughes, 1984; Paris et al., 1985).

(1) Most pyroclastic, volcaniclastic, and carbonaceous layers were uncompacted at the time of silicification. Depositional porosities of 40 to 50% in pyroclastic units, resulting from the rapid accumulation of fall debris, were still present during silicification, and accretionary lapilli and fragile vitric grains show no evidence of crushing (Lowe, this volume, Chapter 9). Loose, puffy, composite carbonaceous particles routinely lack signs of flattening (Walsh and Lowe, this volume, Chapter 4).

(2) Pieces of chert are commonly reworked from identifiable beds into closely associated detrital or fragmental units. Unde-formed plates of white translucent chert are characteristic components of intrastratal flow breccias and intraformational detrital units in many black-and-white banded cherts. These breccias formed after silicification of the white bands but while the carbonaceous sediments were still soft and fluid (Lowe and Knauth, 1977, Fig. 8). Blocks of black-and-white banded chert from K1 occur abundantly as accidental debris in near-vent facies of the immediately overlying mafic lapillistone of K2v (Ransom, 1987; Ransom et al., this volume, Chapter 6) indicating silicification of K1 before the eruption of K2v. Blocks of carbonaceous chert and black-and-white banded chert, derived by erosion of cherts at the top of the Mendon Formation, are locally present in intraformational conglomerates at the base of the overlying Fig Tree Group. Conglomeratic fan-delta deposits in the middle part of the Mapepe Formation contain clasts of jasper and silicified sandstone derived by erosion of units 2–10 m lower in the section (Lowe and Nocita, this volume, Chapter 10). Orthochemical bank margin deposits in the middle Mapepe contain both rigid and plastically deformed clasts of penecontemporaneously deposited translucent chert eroded from the adjacent bank tops (Lowe and Nocita, this volume, Chapter 10). Conglomerates in the upper Mapepe Formation contain clasts of all chert types present in the underlying formations, including black chert, banded black-and-white chert, BFC, silicified komatiitic and dacitic ash, silicified komatiite, and chunks of coarse, druzy and chalcedonic cavity-fill quartz (Lowe and Nocita, this volume, Chapter 10).

(3) The first cement precipitated in open pore spaces of many sediments was chalcedony and, in a few units, fine microspherical ghosts adjacent to particle surfaces suggest the existence of early opal C-T lepispheres. There is an absence of phyllosilicate cements and no evidence of replaced zeolites that are common in younger volcaniclastic sequences.

Carbonaceous sediments remained unlithified longer than either interbedded pure silica layers or associated komatiitic volcaniclastic sediments. Their silicification was completed in most

cases, however, prior to compaction, probably within a few meters or tens of meters of the sediment-water interface.

Basinal facies. The basinal facies contains less cherts than the platform facies, both because it is dominated by thick unsilicified terrigenous sequences and because some sediment types that have experienced widespread silicification in a platformal setting are largely unsilicified in basinal sections. The Weltevreden Formation, for instance, contained many layers of komatiitic ash but virtually none is silicified. Many extremely carbonaceous mudstones in the Belvue Road and Ulundi Formations are black and carbon-rich where fresh, but not silicified. The main chert layers showing extensive silicification in basinal units are orthochemical deposits, such as BFC, and units of carbonaceous sediment interbedded with mafic and komatiitic volcanic rocks in the Onverwacht Group.

Early silicification

A number of features of cherts in the Onverwacht and lower Fig Tree Groups collectively suggest that much silicification occurred through low-temperature interaction between sea water and the upper portion of the volcanic and sedimentary sequence: (1) evidence outlined in the preceding section for extremely early silicification, at and within a few meters of the sea floor, during accumulation of the volcanic-sedimentary sequence; (2) the early silicification of sediments over enormous areas of the sea floor rather than in localized patches around possible hydrothermal conduits and vents; (3) the absence of recognizable siliceous sinter or travertine deposits, sulfide-rich exhalative units, or other local deposits that might have accumulated next to sea-floor hydrothermal vents ("Ironstone pods," interpreted as having formed during "sea-floor-related hydrothermal activity," de Ronde et al., 1994, have been described from the Barberton Belt. These are irregular masses of ironstone within an antiformal body of ultramafic rock brought up along a major fault zone: the eastern part of the Eucalyptus Mill fault of Lowe et al., this volume, Chapter 2. They truncate a variety of sedimentary and igneous units, are not stratiform, do not grade into surrounding sedimentary units, and were not clearly associated with sea-floor hydrothermal activity penecontemporaneous with sedimentation); (4) the widespread precipitation of disordered, low-temperature forms of silica, such as chalcedony and possibly opal C-T lepispheres, as pore-filling precompaction cements; and (5) the already-silicified layers apparently acted as permeability barriers to the later ascent of hydrothermal fluids (de Wit et al., 1982), which probably had to flow laterally to where the cherts ended or breach the cherty layers, forming silica veins.

Modern oceans are greatly undersaturated with respect to all forms of silica because of its utilization by marine organisms, principally diatoms, radiolarians, silicoflagellates, and sponges (Siever, 1962, 1992; Maliva et al., 1989). As a result, there has been little inorganic precipitation of Phanerozoic siliceous sediments except locally around hydrothermal vents. Most Phanerozoic siliceous deposits included biogenic opaline silica or volcanic ash. During burial, the highly soluble amorphous silica dissolves in undersaturated pore waters and reprecipitates as less soluble silica having a higher degree of structural order and/or a lower surface area (Williams et al., 1985). Virtually all Phanerozoic cherts, irrespective of geologic or tectonic setting, have formed in or closely associated with sediments containing abundant biogenic opal (Maliva et al., 1989).

It has been argued that, in the absence of silica-precipitating organisms, the silica content of early Precambrian oceans was regulated by inorganic reactions among dissolved silica, clays, zeolites, and organic matter (Siever, 1992). Glassy volcaniclastic particles might be added to this list. As a result, the Archean oceans probably contained higher levels of dissolved silica (Siever, 1962, 1992). Siever (1992) suggests that reactions between dissolved silica and inorganic minerals may have maintained silica concentrations at about 60 ppm in the Precambrian.

Siever (1992) also concluded that the modern diffusive flux of silica from interstitial waters in bottom sediments into the oceans would have been reversed in the Precambrian and involved the diffusion of silica from the oceans into the sedimentary pile. The result would have been early silica cementation by disordered silica phases in the uppermost levels of the sedimentary sequence. The results of the present study support this model of early diagenetic silicification as the principal mechanism for the formation of cherts in the Barberton Greenstone Belt.

Cherts in the Swaziland Supergroup are confined largely to the volcanic portions of the sequence, where it is possible to identify three principal primary sediments: (1) volcanic ash, (2) carbonaceous sediments, and (3) orthochemical deposits.

Volcaniclastic sediments. Although some Phanerozoic cherts have been interpreted to have formed by the alteration of volcanic ash (e.g., Gibson and Towe, 1971; Mattson and Passagno, 1971), most derived their silica from biogenic opal (Weaver and Wise, 1974). Exceptions may include some recrystallized and silicified, but not silica-enriched rhyolitic ashes (e.g., Hughes, 1976). Ash alteration in modern oceans favors the formation of clays and zeolites. However, in waters already saturated with respect to silica, silica release during the hydrolysis of volcanic glass would tend to supersaturate interstitial pore water with silica and promote direct silica precipitation. Many Onverwacht cherts represent altered, silicified komatiitic ash that would have been extremely labile and provided little alumina for the formation of clays. These cherts typically have silica contents above 90%. Cherts representing dacitic ash contain a consistently higher proportion of alumina and correspondingly lower silica contents. The abundance of sericite in silicified dacitic units suggests that their diagenesis involved the formation of an early generation of clay minerals.

The observed grain size control on the silicification of volcanic ash may have been related to the differential permeability and grain surface area of coarse- and fine-grained sediments. In coarser, permeable ash layers, hydrolysis would have proceeded slowly because of the low surface areas of the large grains, and rapid flushing by pore fluids would have removed the products

of hydrolysis and inhibited the development of silica-supersaturated pore fluids. Enhanced silicification of fine-grained ash could have resulted from the higher surface area of fine vitric particles and the lower permeabilities of fine-grained sediments, both promoting the development of supersaturated pore waters and silica precipitation.

Carbonaceous sediments. Carbonaceous matter interbedded with altering ash-rich sediments and irrigated with silica-saturated pore waters provides an ideal setting for rapid silica permineralization (Murata, 1940; Siever and Scott, 1963; Leo and Barghoorn, 1976; Stein, 1982). This setting is seldom encountered in modern marine sediments because of the silica undersaturation of modern ocean waters but has been commonly realized in ash-rich alluvial units, where the common product is petrified wood (Leo and Barghoorn, 1976). It may have been the norm in the Precambrian marine units, however, accounting for the pervasive early silicification of highly carbonaceous sediments in greenstone belts. Bonding of silica and organic molecules (Leo and Barghoorn, 1976) may have commenced at the sediment-water interface, producing loose, water-saturated sediments composed of silica-water-organic complexes. With shallow burial and dewatering, silica was released into already silica-saturated pore waters. Near-surface silica precipitation may have been enhanced by anerobic bacterial decomposition of organic matter, a process thought to cause polymerization and precipitation of dissolved silica (Zijlstra, 1987).

Orthochemical sediments. Evaporites and limestones are commonly silicified in modern environments where local, commonly biogenic sources of silica are available (e.g., Folk and Pittman, 1971; Siedlecka, 1972; Chowns and Elkins, 1974; McBride and Folk, 1977). Evaporites at the base of the Kromberg Formation and isolated gypsum crystallites, widely developed in many tuffaceous units in the Onverwacht Group, similarly show pervasive silica replacement (Lowe and Fisher Worrell, this volume, Chapter 7). In many cases, replacement proceeded on a molecule by molecule basis whereas in some coarse evaporite layers in the Kromberg Formation, wholesale evaporite dissolution preceded an episode of cavity-filling quartz precipitation (Fig. 15A).

Jasper is widely developed in iron-rich horizons in the Mapepe Formation, both in association with iron-formation facies near the base of the unit and at higher levels in the orthochemical bank facies (Lowe and Nocita, this volume, Chapter 10). The role of volcanism and exhalative processes (e.g., Hoffman, 1987) in forming the Mapepe iron formation is unknown.

Environmental controls. The contrasts in early silicification between shallow- and deep-water sequences may be related to a number of factors. (1) Deep-water sections generally include a smaller proportion of pyroclastic deposits than corresponding shallow-water sequences. Hence, sources of soluble amorphous silica were more restricted. (2) Many deep-water sediments, especially organic-rich layers, were complex mixtures of organic matter, clay, ash, and other components. A number of investigators have noted that the presence of certain impurities, particularly clays, can inhibit chert formation (Lancelot, 1973; Calvert, 1974; McBride and Folk, 1977), and it is possible that impure deep-water Barberton sediments were also less easily silicified than their clay-poor shallow-water equivalents. (3) Mixing zones between fresh and marine waters or sequences bathed in alternating fresh and marine pore waters are commonly sites of enhanced silica diagenesis and silicification (Folk and Pittman, 1971; Kolodny et al., 1980; Knauth, 1979, 1994). Although there is local evidence that meteoric waters influenced early diagenesis within the Onverwacht Group (Knauth and Lowe, 1978; Lowe and Fisher Worrell, this volume, Chapter 7), there is little direct evidence at present that early silicification was widely influenced by meteoric waters. However, the overall shallow-water site of deposition of the platformal facies and the probable alternating buildup of the sequence during komatiitic volcanism and subsidence during basaltic eruptions may have been accompanied by alternating flushing by meteoric and marine waters.

Late silicification

One or more late, post-compaction episodes of metasomatism has affected most rocks in the Onverwacht and Fig Tree Groups. The lower degree of alteration exhibited by Moodies rocks, including the wide preservation of detrital feldspars, suggests that this alteration was in part pre-Moodies in age and possibly related to igneous activity during the volcanic stage of greenstone belt development, perhaps including active hydrothermal circulation systems driven by magma bodies (de Wit et al., 1982). Late silicification and silica veining, carbonation, and potash metasomatism are evident in both deep- and shallow-water facies (Lowe and Byerly, 1986), in both altered sediments and associated altered volcanic rocks, and in volcanic units of all compositions. This stage of alteration shows no clear correlation with primary rock composition or environment of deposition.

CONCLUSIONS

Although present throughout the Swaziland Supergroup, cherts are preferentially developed in the volcanic portions of the sequence and particularly in association with komatiitic and mafic volcanic sections. The composition and distribution of cherty lithofacies emphasize the extremely close relationship between volcanism and sedimentation. In the shallow-water platform association, including cherts within the Onverwacht Group up through the lower cycles of the Mendon Formation, each major compositional variety of volcanic rock is associated with a distinctive and limited range of chert types. Komatiitic lavas are overlain by thin cherty units made up of silicified komatiitic ash and dust and carbonaceous sediments. Komatiitic debris was introduced largely by pyroclastic falls. There is abundant evidence of current activity, highly active biological systems, and local intrastratal sulfate precipitation. Deposition took place under shallow-water conditions. Underlying flow-top alteration zones show evidence of initial subaerial and shallow-

water development (Lowe and Byerly, 1986). Silicification began early, and volcaniclastic and carbonaceous grains show few compaction effects.

Basaltic units in the platform association are overlain by and interbedded with thin layers of carbonaceous chert containing little volcaniclastic or pyroclastic debris. In many sections, these units consist largely of massive and laminated black chert lacking current structures and evidence of in situ biological activity. These sediments accumulated under quiet, fully subaqueous conditions. There is little evidence for alteration of adjacent flow tops under near-surface conditions and extensive compaction commonly preceded silicification. Most of these chert layers, however, also show lateral transitions into banded black-and-white cherts and shallow-water units. Overall, water depths were probably less than a few hundred meters, even during deposition of the deeper water sections.

These contrasts between komatiitic and basaltic units are consistent throughout the platform association and indicate that volcanic style exerted a regional control on sedimentation. Komatiitic volcanism was associated with regional elevation of the volcanic surface, either through inflation or construction, at rates exceeding subsidence. It seems probable that many, if not most, platform komatiites represent subaerial flows. Basaltic volcanism was accompanied by regional subsidence, and capping and interflow sediments commonly reflect quiet, fully subaqueous conditions. Basaltic units are extensively pillowed and many interflow cherts delicately drape pillow surfaces.

Platform komatiitic volcanism was also accompanied by explosive pyroclastic activity that spread clouds of fine comminuted debris over wide areas (Lowe, this volume, Chapter 9; Ransom et al., this volume, Chapter 6). This activity may reflect the predominantly shallow-water sites of volcanism and access of sea water to reservoirs of komatiitic magma during late-stage volcanic activity (Lowe, this volume, Chapter 9). Basaltic eruptions involved little pyroclastic activity. Felsic volcanic units in the Onverwacht Group are restricted to the platform association. Felsic units in the Fig Tree Group include both platformal and basinal facies. Cherts associated with platformal felsic units represent both silicified fine-grained distally deposited felsic ash and dust accumulating during volcanism, best developed in the Mapepe Formation, and post-volcanism chert caps on felsic complexes, represented by the Buck Reef Chert. The former commonly reflect deposition under fully subaqueous but generally shallow-water conditions (Lowe and Nocita, this volume, Chapter 10) developed around but off of the high standing, subaerial to shallow-water felsic complexes and their flanking alluvial aprons. Subsidence of the complexes and aprons resulted in the deposition of a succession of nonvolcanogenic lithofacies reflecting progressively deeper water conditions: (1) evaporite and associated shallow-water to subaerial sediments, (2) banded black-and-white chert, and (3) BFC in the deepest water, probably influenced by laterally concurrent mafic volcanism.

The basinal association, developed mainly in the northern part of the greenstone belt, includes cherts in the upper cycles of the Mendon Formation and in the Weltevreden Formation. This association is dominated by fine-grained sedimentary rocks representing mixtures of fine tuffaceous, carbonaceous, calcareous, and siliceous sediments.

A comparison of the vertical and lateral relationships among cherts and volcanic rocks in the basinal and, locally, platform komatiitic sequences indicates that most or all units of banded ferruginous chert are either interstratified with or lateral equivalents of komatiitic or basaltic flows. They appear to represent proximal aprons of siliceous and sideritic sediments flanking and overlying flow sequences and may be analogous to carbonate facies iron formation in younger greenstone belts (Goodwin et al., 1985). These relationships suggest that BFC in the Fig Tree Group in northern part of the BGB may reflect relatively young mafic and ultramafic volcanism in surrounding areas.

Black cherts in the basinal association represent sediments that accumulated as distal deposits in areas far removed from the influence of active volcanism.

Early silicification appears to have commenced essentially at the sediment-water interface by the interaction of sea water that was saturated or nearly saturated with amorphous silica. Organic material was permineralized in much the same way as petrified wood has formed in younger sequences and soluble evaporites and orthochemical units were widely replaced by silica. Most of the banding in banded cherts throughout the Barberton sequence developed from more homogeneous sediments during early diagenesis.

Late-stage silicification probably involved hotter, deeper circulating hydrothermal fluids. Its effects were not selective but resulted in silica, carbonate, and potash metasomatism of igneous and sedimentary units in both deep- and shallow-water parts of the volcanic succession.

REFERENCES CITED

Anhaeusser, C. R., 1973, The evolution of the early Precambrian crust of southern Africa: Royal Society of London Philosophical Transactions, ser. A, v. 273, p. 359–388.

Barley, M. E., 1984, Volcanism and hydrothermal alteration, Warrawoona Group, East Pilbara, *in* Muhling, J. R., Groves, D. I., and Blake, T. S., eds., Archaean and Proterozoic basins of the Pilbara, Western Australia: Evolution and mineralisation potential: University of Western Australia Geology Department and Extension Service Publication 9, p. 54–67.

Barley, M. E., Dunlop, J. S. R., Glover, J. E., and Groves, D. I., 1979, Sedimentary evidence for an Archaean shallow-water volcanic-sedimentary facies, eastern Pilbara Block, Western Australia: Earth and Planetary Science Letters, v. 43, p. 74–84.

Beukes, N. J., 1973, Precambrian iron-formations of southern Africa: Economic Geology, v. 68, p. 960–1004.

Buick, R., and Barnes, K. R., 1984, Cherts in the Warrawoona Group: Early Archaean silicified sediments deposited in shallow-water environments, *in* Muhling, J. R., Groves, D. I., and Blake, T. S., eds., Archaean and Proterozoic basins of the Pilbara, Western Australia: Evolution and mineralisation potential: University of Western Australia Geology Department and University Extension Publication 9, p. 37–53.

Byerly, G. R., Lowe, D. R., Nocita, B. W., and Ransom, B. L., 1983, Apparent volcanic cycles in the Archean Swaziland Supergroup, Barberton Mountain Land, South Africa: a result of non-magmatic processes: Lunar and

Planetary Science Conference, 14th, Houston, Abstracts, pt. 1, p. 84–85.

Calvert, S. E., 1974, Deposition and diagenesis of silica in marine sediments, *in* Hsu, K. J., and Jenkyns, H. C., eds., Pelagic sediments: on land and under the sea: International Association of Sedimentologists Special Publication 1, p. 273–298.

Chowns, T. M., and Elkins, J. E., 1974, The origin of quartz geodes and cauliflower cherts through the silicification of anhydrite nodules: Journal of Sedimentary Petrology, v. 44, p. 885–903.

Cody, R. D., 1979, Lenticular gypsum: occurrences in nature, and experimental determinations of effects of soluble green plant material on its formation: Journal of Sedimentary Petrology, v. 49, p. 1015–1028.

de Ronde, C. E. J., de Wit, M. J., and Spooner, E. T. C., 1994, Early Archean (>3.2 Ga) Fe-oxide-rich, hydrothermal discharge vents in the Barberton greenstone belt, South Africa: Geological Society of America Bulletin, v. 106, p. 86–104.

de Wit, M. J., Hart, R., Martin, A., and Abbott, P., 1982, Archean abiogenic and probable biogenic structures associated with mineralized hydrothermal vent systems and regional metasomatism, with implications for greenstone belt studies: Economic Geology, v. 77, p. 1783–1801.

Duchac, K. C., 1986, Metasomatic alteration of a komatiitic sequence into chert [Masters thesis]: Baton Rouge, Louisiana State University, 240 p.

Duchac, K. C., and Hanor, J. S., 1987, Origin and timing of the metasomatic silicification of an early Archean komatiite sequence, Barberton Mountain Land, South Africa: Precambrian Research, v. 37, p. 125–146.

Folk, R. L., and Pittman, J. S., 1971, Length-slow chalcedony: a new testament for vanished evaporites: Journal of Sedimentary Petrology, v. 41, p. 107–113.

Folk, R. L., and Weaver, C. E., 1952, A study of the texture and composition of chert: American Journal of Science, v. 250, p. 498–510.

Gibson, T. G., and Towe, K. M., 1971, Eocene volcanism and the origin of Horizon A: Science, v. 172, p. 152–154.

Goodwin, A. M., Thode, H. G., Chou, C.-L., and Karkhansis, S. N., 1985, Chemostratigraphy and origin of the late Archean siderite-pyrite-rich Helen Iron Formation, Michipicoten belt, Canada: Canadian Journal of Earth Sciences, v. 22, p. 72–84.

Hanor, J. S., and Duchac, K., 1990, Isovolumetric silicification of Early Archean komatiites: geochemical mass balances and constraints on origin: Journal of Geology, v. 98, p. 863–877.

Heinrichs, T. K., 1980, Lithostratigraphische Untersuchungen in der Fig Tree Gruppe des Barberton Greenstone Belt zwischen Umsoli und Lomati (Sudafrika) (Lithostratigraphic study in the Fig Tree Group of the Barberton Greenstone Belt between Umsoli and Lomati (South Africa)): Gottinger Arbeiten zur Geologie und Palaontologie, v. 22, 118 p.

Heinrichs, T. K., 1984, The Umsoli Chert, turbidite testament for a major phreatoplinian event at the Onverwacht/Fig Tree transition (Swaziland Supergroup, Archaean, South Africa): Precambrian Research, v. 24, p. 237–283.

Hoffman, P. F., 1987, Early Proterozoic foredeeps, foredeep magmatism, and Superior type iron-formations of the Canadian Shield, *in* Kröner, A., ed., Proterozoic lithospheric evolution: American Geophysical Union and Geological Society of America, Geodynamics Series, v. 17, p. 85–98.

Hughes, C. J., 1976, Volcanogenic cherts in the late Precambrian Conception Group, Avalon Peninsula, Newfoundland: Canadian Journal of Earth Sciences, v. 13, p. 512–519.

Knauth, L. P., 1979, A model for the origin of chert in limestone: Geology, v. 7, p. 274–277.

Knauth, L. P., 1994, Petrogenesis of chert, *in* Heaney, P. J., Prewitt, C. T., and Gibbs, G. V., eds., Silica: physical behavior, geochemistry, and materials applications: Mineralogical Society of America Reviews in Mineralogy, v. 29, p. 231–258.

Knauth, L. P., and Lowe, D. R., 1978, Oxygen isotope geochemistry of cherts from the Onverwacht Group (3.4 billion years), Transvaal, South Africa, with implications for secular variations in the isotopic composition of cherts: Earth and Planetary Science Letters, v. 41, p. 209–222.

Kolodny, Y., Taraboulos, A., and Frieslander, U., 1980, Participation of fresh water in chert diagenesis: evidence from oxygen isotopes and boron-track mapping: Sedimentology, v. 27, p. 305–316.

Lahaye, Y., Arndt, N., Byerly, G. R., Chauvel, C., Fourcade, S., and Gruau, G., 1995, The influence of alteration on the trace-element and Nd isotopic compositions of komatiites: Chemical Geology, v. 126, p. 43–64.

Lancelot, Y., 1973, Chert and silica diagenesis in sediments from the central Pacific, *in* Winterer, E. L., Ewing, J. I., et al., eds., Initial reports of the Deep Sea Drilling Project, Volume 17: Washington, D.C., U.S. Government Printing Office, p. 377–405

Lanier, W. P., and Lowe, D. R., 1982, Sedimentology of the Middle Marker (3.4 Ga), Onverwacht Group, Transvaal, South Africa: Precambrian Research, v. 18, p. 237–260.

Leo, R. F., and Barghoorn, E. S., 1976, Silicification of wood: Harvard University, Botanical Museum Leaflets, v. 25, no. 1, 47 p.

Lowe, D. R., 1980, Archean sedimentation: Annual Review of the Earth and Planetary Sciences, v. 8, p. 145–167.

Lowe, D. R., 1982, Comparative sedimentology of the principal volcanic sequences of Archean greenstone belts in South Africa, Western Australia and Canada: implications for crustal evolution: Precambrian Research, v. 17, p. 1–29.

Lowe, D. R., 1983, Restricted shallow-water sedimentation of 3.4 Byr-old stromatolitic and evaporitic strata of the Strelley Pool Chert, Pilbara Block, Western Australia: Precambrian Research, v. 19, p. 239–283.

Lowe, D. R., 1986, Comment on "Pseudoconglomerate and a re-examination of some paleoenvironmental controversies": Geology, v. 14, p. 632–633.

Lowe, D. R., 1988, Suspended-load fallout rate as an independent variable in the analysis of current structures: Sedimentology, v. 35, p. 765–776.

Lowe, D. R., and Byerly, G. R., 1986, Archean flow-top alteration zones formed initially in a low-temperature sulphate-rich environment: Nature, v. 324, p. 245–248.

Lowe, D. R., and Knauth, L. P., 1977, Sedimentology of the Onverwacht Group (3.4 billion years), Transvaal, South Africa, and its bearing on the characteristics and evolution of the early Earth: Journal of Geology, v. 85, p. 699–723.

Lowe, D. R., and Knauth, L. P., 1978, The oldest marine carbonate ooids reinterpreted as volcanic accretionary lapilli, Onverwacht Group, South Africa: Journal of Sedimentary Petrology, v. 48, p. 709–722.

Maliva, R. G., Knoll, A. H., and Siever, R., 1989, Secular change in chert distribution: A reflection of evolving biological participation in the silica cycle: Palaios, v. 4, p. 519–532.

Mastin, L. G., 1995, Thermodynamics of gas and steam-blast eruptions: Bulletin of Volcanology, v. 57, p. 85–98

Mattson, P. H., and Passagno, E. A., 1971, Caribbean Eocene volcanism and the extent of Horizon A: Science, v. 174, p. 138–139.

McBride, E. F., and Folk, R. L., 1977, The Caballos Novaculite revisited: Part II; Chert and shale members and synthesis: Journal of Sedimentary Petrology, v. 47, p. 1261–1286.

Merino, E., 1987, Textures of low-temperature self-organization, *in* Rodriguez-Clemente, R., and Tardy, Y., eds., Geochemistry and mineral formation in the Earth's surface: Madrid, Cons. Sup. Investigaciones Cientificas (Spain) and Centre National Researche Scientifique (France), p. 597–610.

Murata, K. J., 1940, Volcanic ash as a source for silica for the silicification of wood: American Journal of Science, v. 238, p. 586–596.

Murray, R. W., Jones, D. L., and Buchholtz ten Brink, M. R., 1992, Diagenetic formation of bedded chert: Evidence from chemistry of the chert-shale couplet: Geology, v. 20, p. 271–274.

Paris, I., Stanistreet, I. G., and Hughes, M. J., 1985, Cherts of the Barberton Greenstone Belt interpreted as products of submarine exhalative activity: Journal of Geology, v. 93, p. 111–129.

Philpot, H. G., Tomkinson, M. J., von Aswegem, G. M., and Reid, K., 1988, Field trip to investigate stratigraphic and structural relationships in the area around Princeton Mine, Barberton Mountain Land, *in* Tregoning, T. D., Tomkinson, M. J., and Philpot, H. G., eds., Deformation and mineralization in the Archaean of South Africa: Barberton Mountain Land Branch,

Geological Society of South Africa, Abstracts and Guidebook, p. 60–65.
Ransom, B. L., 1987, The paleoenvironmental, magmatic, and geologic history of the 3,500 Myr Kromberg Formation, west limb of the Onverwacht anticline, Barberton Greenstone Belt, South Africa [M.S. thesis]: Baton Rouge, Louisiana State University, 103 p.
Reimer, T. O., 1975, Untersuchungen uber Abtragung, Sedimentation und Diagenese im fruhen Prakambrium am Beispiel der Sheba-Formation (Sudafrika) (Studies of denudation, sedimentation, and diagenesis in the early Precambrian with an example from the Sheba Formation (South Africa)): Geologisches Jahrbuch, Reihe B, v. 17, 108 p.
Siedlecka, A., 1972, Length-slow chalcedony and relicts of sulphates—Evidence of evaporitic environments in the upper Carboniferous and Permian beds of Bear Island, Svalbard: Journal of Sedimentary Petrology, v. 42, p. 812–816.
Siever, R., 1962, Silica solubility, 0–200°C., and the diagenesis of siliceous sediments: Journal of Geology, v. 70, p. 127–150.
Siever, R., 1992, The silica cycle in the Precambrian: Geochimica et Cosmochimica Acta, v. 56, p. 3265–3272.
Siever, R., and Scott, R. A., 1963, Organic geochemistry of silica, *in* Breger, I., ed., Organic geochemistry: New York, Pergamon Press, p. 579–595.
Smith, H. S., and Erlank, A. J., 1982, Geochemistry and petrogenesis of komatiites from the Barberton greenstone belt, South Africa, *in* Arndt, N. T., and Nisbet, E. G., eds., Komatiites: London, Allen & Unwin, p. 347–398.
Stanistreet, I. G., and Hughes, M. J., 1984, Pseudoconglomerate and a re-examination of some palaeoenvironmental controversies: Geology, v. 12, p. 717–719.
Stanistreet, I. G., De Wit, M. J., and Fripp, R. E. P., 1981, Do graded units of accretionary spheroids in the Barberton Greenstone Belt indicate Archaean deep water environment?: Nature, v. 293, p. 280–284.
Stein, C. L., 1982, Silica recrystallization in petrified wood: Journal of Sedimentary Petrology, v. 52, p. 1277–1282.
Viljoen, M. J., and Viljoen, R. P., 1969, The geology and geochemistry of the lower ultramafic unit of the Onverwacht Group and a proposed new class of igneous rocks: Geological Society of South Africa Special Publication 2, p. 55–86.
Viljoen, R. P., and Viljoen, M. J., 1969, The geological and geochemical significance of the upper formations of the Onverwacht Group: Geological Society of South Africa Special Publication 2, p. 113–152.
Walsh, M. M., 1989, Carbonaceous cherts of the Swaziland Supergroup, Barberton Mountain Land, Southern Africa [Ph.D. dissertation]: Baton Rouge, Louisiana State University, 199 p.
Walsh, M., 1992, Microfossils and possible microfossils from the Early Archean Onverwacht Group, Barberton Mountain Land, South Africa: Precambrian Research, v. 54, p. 271–293.
Weaver, F. M., and Wise, S. W., 1974, Opaline sediments of the southeastern coastal plain and Horizon A: biogenic origin: Science, v. 184, p. 899–901.
Williams, L. A., Parks, G. A., and Crerar, D. A., 1985, Silica diagenesis, I. Solubility controls: Journal of Sedimentary Petrology, v. 55, p. 301–311.
Zijlstra, H. J. P., 1987, Early diagenetic silica precipitation, in relation to redox boundaries and bacterial metabolism, in Late Cretaceous chalk of the Maastrichtian type locality: Geologie en Mijnbouw, v. 66, p. 343–355.

MANUSCRIPT ACCEPTED BY THE SOCIETY MARCH 26, 1998

Geological Society of America
Special Paper 329
1999

Modes of accumulation of carbonaceous matter in the early Archean: A petrographic and geochemical study of the carbonaceous cherts of the Swaziland Supergroup

Maud M. Walsh*
Department of Geology and Geophysics, Louisiana State University, Baton Rouge, Louisiana 70803
Donald R. Lowe
Department of Geological and Environmental Sciences, Stanford University, Stanford, California 94305

ABSTRACT

Three main types of carbonaceous chert occur in the Swaziland Supergroup, Barberton Greenstone Belt, South Africa: black-and-white banded chert, massive black chert, and laminated black chert. These cherts are composed of six main morphological types of carbonaceous matter: carbonaceous laminations, simple grains, composite grains, wisps, diffuse carbonaceous matter, and crystalline carbonaceous matter. The black bands in black-and-white banded cherts are generally composed of well-preserved fine carbonaceous laminations, representing the remains of microbial mats, interbedded with layers of simple and composite carbonaceous grains. Massive black cherts contain a large proportion of lithic grains as well as carbonaceous detritus, but lack matlike laminations. Laminated black cherts are also accumulations of detrital lithic and carbonaceous matter, but are commonly finer grained than massive black cherts and contain a high proportion of carbonaceous wisps.

Comparison of the aspect ratios of carbonaceous grains among the various chert types suggests that the original sediments were silicified at different times relative to compaction. Black-and-white banded chert and to a lesser extent massive black chert contain round or lobate carbonaceous grains and were silicified before sediment compaction. Laminated cherts are dominated by wispy grains, indicating that compaction largely preceded silicification.

The relationship between grain shape and total organic carbon (TOC) indicates that TOC in carbonaceous cherts is a function of both primary carbon content and the amount of prelithification sediment compaction. In general, laminated cherts show the greatest presilicification sediment compaction and the highest TOC contents. Carbon isotope values indicate that all of the carbonaceous matter probably had a biological origin.

Most cherts in the Hooggenoeg, Kromberg, and lower cycles of the Mendon Formations contain carbonaceous matter deposited in shallow water as both loose detritus and microbial mats. During periods of explosive volcanism, volcaniclastic

*Present address: Institute for Environmental Studies, Louisiana State University, Baton Rouge, Louisiana 70803.

Walsh, M. M., and Lowe, D. R., 1999, Modes of accumulation of carbonaceous matter in the early Archean: A petrographic and geochemical study of the carbonaceous cherts of the Swaziland Supergroup, *in* Lowe, D. R., and Byerly, G. R., eds., Geologic Evolution of the Barberton Greenstone Belt, South Africa: Boulder, Colorado, Geological Society of America Special Paper 329.

debris was locally mixed with accumulating carbonaceous matter. These shallow-water sediments were generally lithified soon after deposition, probably through the interaction of the uppermost sea-floor sediment layers and sea water. During deposition of basaltic sequences, detrital carbonaceous matter accumulated in deeper water along with fine volcanic ash. Cherts in the upper part of the Mendon Formation represent deep-water sediments that rarely contain mat accumulations. Carbonaceous matter was preserved mainly as fine detritus mixed with lithic grains deposited under low-energy conditions. Lithification and silicification occurred after sediment compaction, probably well below the sea-floor. The abundance of in situ bacterial mats and composite grains in shallow-water deposits and their paucity in deep-water carbonaceous cherts is consistent with the interpretation that some early Archean organisms were photosynthetic, with much primary production occurring in the photic zone.

INTRODUCTION

Carbonaceous cherts of the 3.2- to 3.5-Ga Swaziland Supergroup have yielded microfossils and stromatolites that are among the oldest on Earth (Knoll and Barghoorn, 1977; Walsh and Lowe, 1985; Byerly et al., 1986; Walsh, 1989, 1992). Fossils are, however, rare even in the most carbonaceous cherts. Of more than 400 samples examined during this study, only 9 contained fossils or possible fossils. Even cherts that lack microfossils, however, contain carbonaceous particles and depositional or diagenetic textures that provide information on the composition and sedimentation of the primary deposits and important clues regarding the distribution and paleoecology of early life forms and their role in sedimentation. This paper presents the results of an integrated field, petrographic, and geochemical study of the composition, sedimentation, and diagenesis of carbonaceous cherts in the upper part of the Onverwacht Group in the Barberton Greenstone Belt.

The Barberton Greenstone Belt is located in the eastern part of the Kaapvaal Craton, South Africa. The predominantly volcanic supracrustal sequence making up the belt, the Swaziland Supergroup, is intensely deformed and in many areas supracrustal rocks have undergone extensive early metasomatic alteration and greenschist facies metamorphism. Near plutons, more highly metamorphosed facies are developed (Viljoen and Viljoen, 1969). The principal large-scale structures are northeast-trending folds with steeply dipping to vertical axes (Viljoen and Viljoen, 1969) and a complex of faults representing several generations of deformation (Lowe et al., this volume, Chapter 2).

The Swaziland Supergroup includes three major lithostratigraphic subdivisions: the Onverwacht, Fig Tree, and Moodies Groups (Fig. 1). The age of the Onverwacht Group has recently been revised. Sm-Nd whole rock ages of approximately 3,550 Ma for volcanic rocks of the Komati and Hooggenoeg Formations are now regarded as too old (Kröner et al., 1991). More precise single zircon evaporation ages at 3,445 ± 4 Ma have been determined for the felsic volcanics of the uppermost Hooggenoeg Formation (Kröner et al., 1991). The lowermost Kromberg chert has been dated at 3,416 ± 4 Ma (Kröner et al., 1991; Byerly et al., 1996) and the upper chert of the Kromberg Formation has been recently dated at 3,334 ± 3 Ma (Byerly et al., 1996). The uppermost dated unit of the Onverwacht Group is a chert within the Mendon Formation dated at 3,298 ± 3 Ma. Ages for the overlying Fig Tree Group range from 3,258 ± 3 Ma to 3,225 ± 3 Ma (Kröner et al., 1991; Byerly et al., 1996).

The present study is based on carbonaceous cherts collected from both the Onverwacht and Fig Tree Groups in the southern part of the Barberton Greenstone Belt. Onverwacht samples were collected from both the west limb of the Onverwacht anticline and the east limb along the Komati River. Fig Tree samples were also collected from the northern part of the greenstone belt in the Ulundi syncline (see Lowe and Byerly, this volume, Chapter 1, Fig. 1).

METHODS

Petrography

Approximately 400 thin sections were examined during this study. The morphological types of carbonaceous matter and their abundances in each thin section were tabulated for 166 thin sections. The percentages of carbonaceous and noncarbonaceous grain types were estimated to the nearest 5% using the visual chart of Terry and Chilingar (1955). An estimate of packing was made based on percentage of thin section area occupied by carbonaceous or lithic particles as opposed to chert matrix.

The results were categorized by both chert type and stratigraphic position. Analysis of variance was employed to relate particle types to chert types. Chi-squared analysis of 2 × 2 contingency tables was used to test the significance of apparent associations between particle types. Overall percentages of carbonaceous and noncarbonaceous particle types for individual chert units were obtained by calculating the average composition of each chert type within the stratigraphic unit and then weighing the average compositions based on relative thicknesses of each chert type in the individual unit.

Twenty-seven of the samples that were analyzed for TOC and sixteen of those that were analyzed for bulk rock composition were examined petrographically to determine aspect ratios of the carbonaceous grains. The aspect ratio, a measure of grain

flatness, is defined as the ratio a/b, where a is the longest dimension and b is the longest dimension normal to a.

Chemical analyses

Eighteen carbonaceous chert samples were analyzed at the University of Cape Town by X-ray fluorescence for major and trace elements using the methods described by Willis et al. (1971, 1972) and by combustion-gas chromatography for C. Fifty samples were analyzed for total organic carbon (TOC) and $\delta^{13}C$ in the laboratory of Dr. J. M. Hayes of Indiana University using the techniques outlined in Wedeking et al. (1983).

Analysis of variance was used to determine whether banded, massive, and laminated cherts are chemically distinguishable. Pearson matrix correlation was used to test for relationships between any of the elements or between any elements and percentage of particle types. A confidence level of 95% was set for statistical significance. Regression analysis was employed to describe correlations between elements and between elements and aspect ratios.

TYPES OF CARBONACEOUS CHERT

Chert units representing silicified sediments and varying from a few meters to more than 350 m thick cap many of the volcanic flows and volcaniclastic deposits in the upper part of the Onverwacht Group (Fig. 1). They include silicified volcaniclastic units, biogenic deposits, and orthochemical sediments (Lowe and Knauth, 1977; Lowe, 1982; Lowe, this volume, Chapter 3). Carbonaceous cherts are widely developed in these interflow sedimentary units. Their black or dark gray color is imparted by the presence of kerogen formed by the degradation of organic matter (Hayes et al., 1983). These cherts are distinct from black or gray cherts representing silicified volcanic rock, sandstone, or tuff that are colored by finely disseminated oxide or sulfide minerals.

Three main types of carbonaceous chert are distinguishable in both outcrop and hand specimen: black-and-white banded chert, massive black chert, and laminated black chert.

Black-and-white banded chert

Black-and-white banded chert consists of alternating bands of black carbonaceous chert and virtually pure microcrystalline quartz that range in thickness from a few millimeters to about 5 cm. On weathered surfaces the pure chert bands are light gray to off-white in color and the carbonaceous bands a flat or glossy black (Fig. 2A), whereas in fresh samples the pure chert bands are translucent, so that the carbonaceous and noncarbonaceous bands both appear glossy black. The white bands appear to have lithified before the more fluid black layers and commonly form breccias made up of elongate white chert clasts in a matrix of black chert (Lowe and Knauth, 1977; Lowe, this volume, Chapter 3). The white bands are generally composed of homogeneous microquartz, although in some cases the lower or upper few millimeters consist of more coarsely crystalline microquartz or fine megaquartz. The black carbonaceous bands range from massive to streaky, and many show well-developed lamination. A few contain concentric layering and appear to represent cavity fill units. They commonly contain trace amounts of gray, brown-weathering dolomite or siderite and stylolites parallel to bedding.

Massive black chert

Massive, structureless, glossy to dull black chert (Fig. 2B) forms layers from a few millimeters to about l m thick that are commonly interbedded with or cap units of volcaniclastic siltstone and sandstone, pyroclastic ash, or accretionary lapilli in the Onverwacht Group. The thickest unit of massive black chert observed during the present study is a 12-m-thick bed in the Mendon Formation.

Laminated black chert

Laminated black chert resembles massive black chert in outcrop appearance and distribution. Weathering of laminated chert units, however, reveals 1- to 3-mm-thick black laminations separated by light gray laminations less than 1 mm thick (Fig. 2C). Units of laminated black chert range from a few millimeters to more than 13 m thick.

PETROGRAPHY OF THE CARBONACEOUS CHERTS

Composition

Chert is composed primarily of microcrystalline quartz or microquartz (Folk and Weaver, 1952), a form of quartz characterized by equant crystal domains less than 35 μm across. Many units of carbonaceous chert in the Onverwacht Group are massive micromosaics of microquartz, carbonaceous matter, and accessory minerals. Others, however, represent coarse detrital sediments composed of a variety of carbonaceous, mineral, and lithic grains. The most common lithic grains are varieties of chert distinguishable from the surrounding matrix by size differences in the microquartz domains or the abundance of impurities. These include grains of carbonaceous chert and sericitic chert, the latter probably representing silicified volcanic and volcaniclastic rock. Carbonate, phyllosilicates, pyrite, and hematite are accessory constituents of many carbonaceous cherts. Fine pyrite and other opaque minerals resemble finely dispersed opaque carbonaceous matter, but are distinguishable petrographically by their crystal form and reflectance.

Four main petrographic varieties of carbonaceous matter can be recognized: (1) fine carbonaceous laminations, (2) simple grains, (3) lobate composite grains, and (4) elongate wisps. There are two less common types: (5) cloudy, diffuse carbonaceous matter; and (6) crystalline carbonaceous material.

Fine carbonaceous laminations. Carbonaceous laminations are 1–20 μm thick, more-or-less planar concentrations of car-

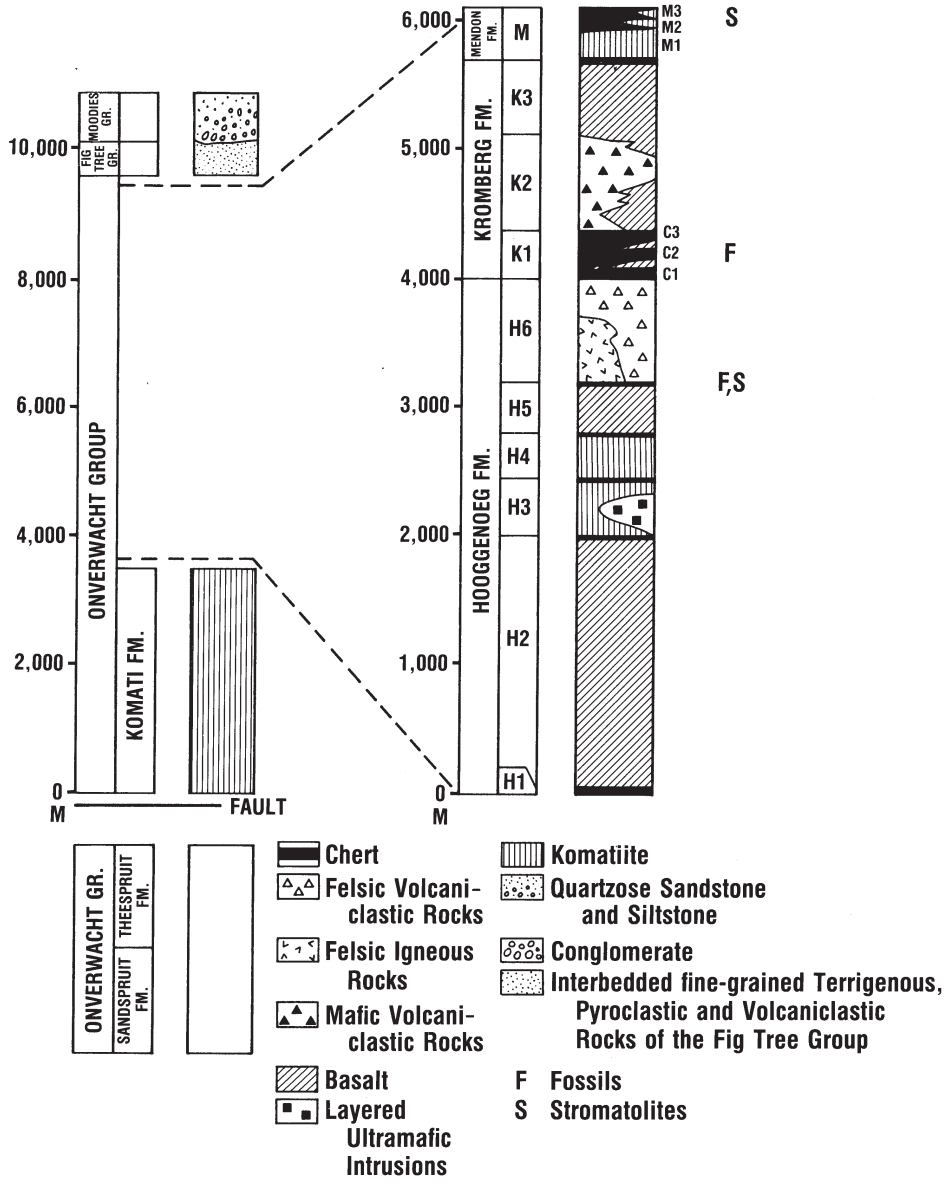


Figure 1. Generalized stratigraphic column of the Swaziland Supergroup in the Onverwacht anticline. Modified from Lowe and Byerly (this volume, Chapter 1).

bonaceous matter separated by 10–25 μm thick layers of pure microquartz (Fig. 3). On the micron scale the laminations are commonly discontinuous, but on a larger scale many can be traced across sample surfaces several centimeters wide. They are wavy or crinkly on a small scale, with maximum relief of a few millimeters. The carbonaceous laminations are commonly grouped into layers 0.5–5 cm thick separated by bands of white noncarbonaceous chert in black-and-white banded cherts, or by detrital layers. The laminations are commonly buckled or broken and in some cases are folded over on themselves or fragmented (Figs. 3C, D).

Carbonaceous laminations resemble modern microbial mats whose millimeter-scale couplets of alternating organic-rich and organic-poor sediments result from the trapping of sediment by the sticky mats or the precipitation of minerals, especially $CaCO_3$, on the mat surface followed by upward migration of the organisms to colonize the new surface. Modern mats are inhabited by a variety of microorganisms, but the constructing organisms are generally interwoven filamentous photosynthetic bacteria or cyanobacteria (Monty, 1967; Golubic, 1973; Golubic and Focke, 1978; Horodyski et al., 1977; Margulis et al., 1983). Filamentous and spheroidal microfossils have been found associated with fine carbonaceous laminations in cherts from the Hooggenoeg and Kromberg Formations (Walsh and Lowe, 1985; Walsh, 1992). The thickness of the individual laminae, usually only a few microns, is much less than in a typical modern

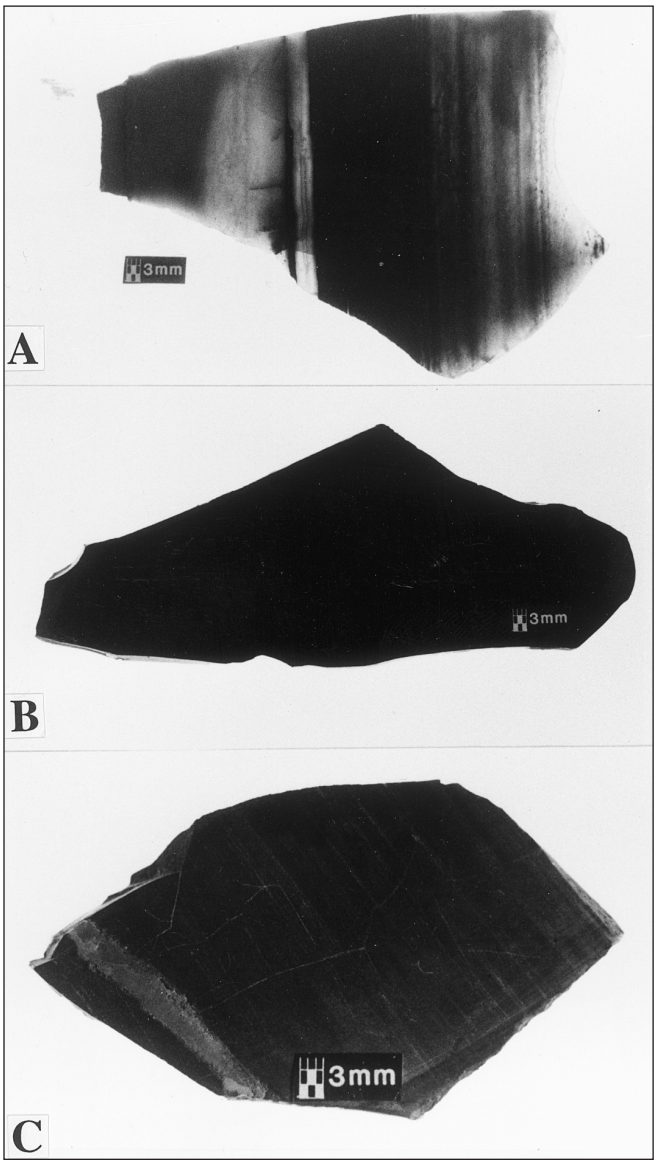


Figure 2. Photographs of the three major carbonaceous chert types: A, Black-and-white banded chert; B, massive black chert; C, laminated black chert.

cyanobacterial mat, in which laminations are commonly tens to a few hundreds of microns thick (Golubic, 1973; Monty, 1976). The thinner laminae may reflect the size of constructing organisms, but might also result from compaction of the organic-rich layers. The overall similarity of the fine carbonaceous laminations to modern microbial mats and the presence of bacteria or cyanobacterialike microstructures in some samples argue strongly for their interpretation as fossil microbial mats.

Some of the earliest described microbial mats were from shallow-water environments, where the constructing organisms were photosynthetic (Monty, 1967; Golubic, 1973; Golubic and Focke, 1978; Horodyski et al., 1977; Margulis et al., 1983), but microbial mats have also been discovered in a number of deep marine environments (Soutar and Crill, 1977), including hydrothermal vents (Jannasch, 1984), areas of coastal upwelling (Gallardo, 1977; Williams and Reimers, 1983), and natural petroleum seeps (Roberts et al., 1989). Williams and Reimers (1982) found that deep-water microbial mats could only be distinguished from shallow-water mats by the organisms within them, not by any features of the mats themselves. The fossils associated with the fine carbonaceous laminations in the cherts examined during this study cannot be definitively identified as cyanobacterial, and therefore photosynthetic, so the question of whether the mat-constructing communities were photosynthetic or chemosynthetic has not been resolved (Walsh, 1992). Some features of the mats, such as fragments of rolled-up mat (Fig. 3C, D) are similar to features found in environments where there is periodic exposure and desiccation (Davies, 1970), but such roll-up structures have also been described from preserved deep-water microbial mats (Klein et al., 1987; Simonson et al., 1993; Sumner, 1997), so by themselves these features do not indicate a particular environment. As will be discussed later, it is the characteristics of surrounding sedimentary layers that provide evidence of a shallow-water origin for the microbial mats.

Simple grains. The most common carbonaceous particles are simple carbonaceous grains. These are irregularly shaped, internally unstructured kerogen grains that range in size from less than 5 μm to more than 750 μm (Fig. 4) and typically have ragged, rather than well-defined edges. Microquartz surrounds and permeates the grains. Simple grains occur in more than 75% of the samples examined. The bulk of the simple grains represent detrital, current-worked, or possibly hemipelagic particles.

The density of the simple carbonaceous grains was estimated by comparing the sizes of lithic and carbonaceous grains in a current-deposited layer, where they might be expected to exhibit approximate hydraulic equivalence. In a sample from H5c in the upper part of the Hooggenoeg Formation (Lowe and Byerly, this volume, Chapter 1), fine- and medium-grained carbonaceous particles averaging 0.24 mm in diameter are mixed with very fine-grained lithic detritus, averaging 0.11 mm in diameter. An approximate density of the carbonaceous particles was calculated using Stokes law of settling:

$$w = (\rho_p - \rho_f) g d^2 / 18\mu$$

where

w = grain settling velocity (cm/sec),
$(\rho_p - \rho_f)$ = density difference between the particle and the fluid (g/cm^3),
g = acceleration due to gravity = 980 cm/sec^2,
d = particle diameter (cm), and
μ = fluid viscosity (~0.01 poise for water at 20°C).

The settling velocity of the lithic grains was set equal to the settling velocity of the carbonaceous grains. The density of the lithic grains was assumed to be that of quartz, 2.65 g/cm^3, and the

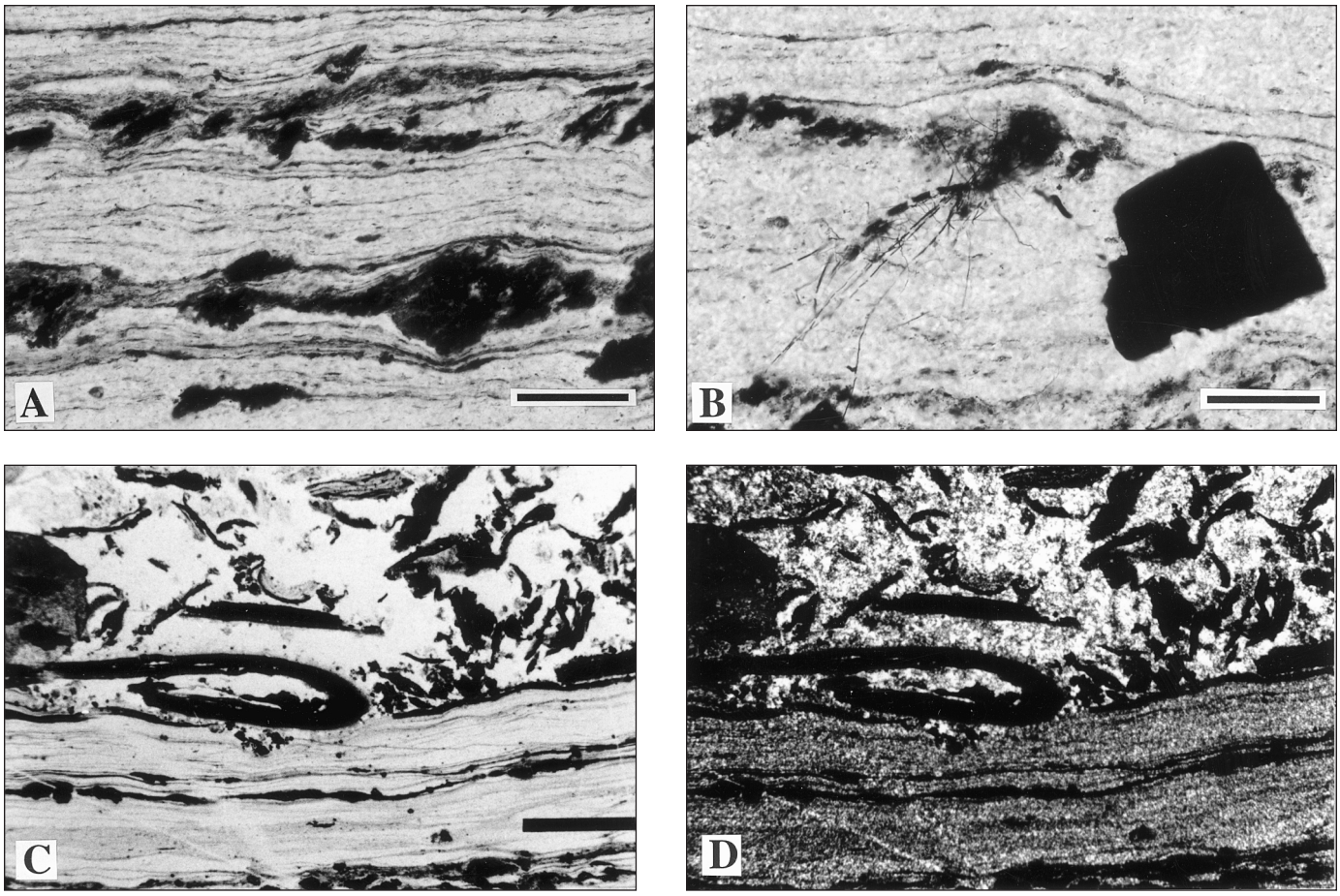


Figure 3. Photomicrographs of matlike laminations. A, Fine carbonaceous laminations with scattered simple and composite grains in fossiliferous sample. Scale bar equals 200 μm. B, Threadlike filamentous fossils in same sample. Scale bar equals 100 μm. C, Matlike laminations folded over on themselves and loose detrital fragments of carbonaceous laminations. Plane light. Scale bar equals 1 mm. D, Same in crossed nicols.

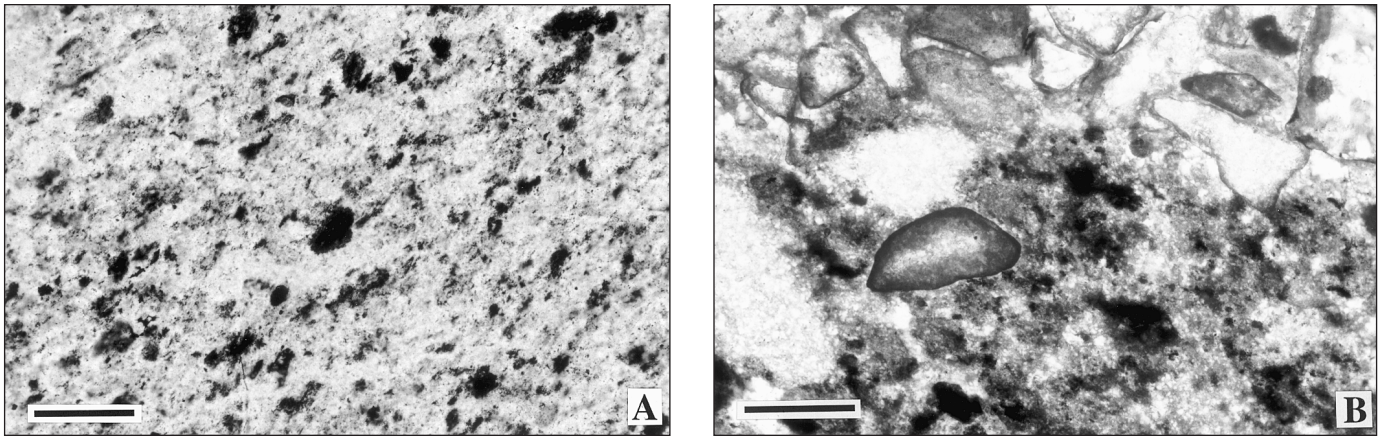


Figure 4. Photomicrographs of simple carbonaceous grains. A, Layer of simple grains that overlies matlike laminations in fossiliferous sample. Scale bar equals 200 μm. B, Simple grains mixed with lithic grains. Scale bar equals 200 μm.

density of the water approximately that of normal seawater, 1.02 g/cm^3. The density of the simple carbonaceous grains was calculated as approximately 1.36 g/cm^3, a density similar to that of modern kerogen (Huc, 1980). This behavior contrasts with that of the lobate composite grains, discussed below.

Lobate composite grains. Lobate, usually more-or-less equant clumps of kerogen that are made up of smaller, commonly rounded carbonaceous particles are here termed composite grains (Fig. 5). They range from about 100 μm to more than 1,000 μm in diameter. Individual component carbonaceous particles, ranging from 25 to 100 μm in diameter, are commonly surrounded and cemented by botryoidal, coarsely crystalline microquartz that, in rare cases, shows relict fibrous texture. Isolated flakes of sericite are common within the particles.

Composite grains are most common in bands of carbonaceous laminations and in detrital layers composed of mixtures of simple and composite grains. Layers composed largely or exclusively of composite grains, which are rare, occur in both black-and-white banded chert and thin massive black chert interbedded with silicified ash and sandstone layers. In some beds, composite grains are mixed with sand-sized lithic grains. In others, composite grains are so loosely packed within pure translucent chert that there are few grain-grain contacts.

The association of composite grains and microbial mat layers in black-and-white banded cherts suggests that composite grains may be similar to globular colonies of cyanobacteria, so-called "algal lumps," that occur in intertidal sediments on Andros Island, Bahamas (Monty, 1967), to organic aggregates held together by gelatinous secretions of inhabiting bacteria and algae (Riley, 1970), or to the flocculent material found near modern submarine hydrothermal vents, which commonly contains filamentous sheathlike material as well as rod and vibriod cells (Wirsen et al., 1993; Juniper et al., 1995). The fine sericite grains in many of the composite particles indicate that clay minerals, which could have facilitated aggradation of carbonaceous matter (Sheldon et al., 1967; Krank, 1980), were once present. Some composite grains may have been coated with silica, contributing to the early lithification and relative resistance to compaction of these sediments. Unlike simple carbonaceous grains, composite grains are typically associated with lithic grains of approximately the same size, indicating that the density of the composite grains was similar to that of the lithic grains, possibly because they were already coated and internally cemented at the time of deposition. A modern analogy may be the flocculent material found in the vicinity of the Juan de Fuca hydrothermal vents which contains cells uniformly coated with iron and silica and has been interpreted to represent microbial cells that inhabited the subseafloor hydrothermal system and were coated with mineral precipitates as they made contact with cooling fluids (Juniper et al., 1995).

Carbonaceous wisps. Carbonaceous wisps are particles with aspect ratios of five or greater, generally with their longest axes subparallel to bedding (Fig. 6). The largest wisps are 50 μm thick and 500–1,000 μm long. The smallest recognizable wisps are less than 10 μm thick and 50–100 μm long. Cherts in which wisps are the dominant carbonaceous particles typically show tightly packed carbonaceous matter and contain abundant fine-grained volcaniclastic sand, silt, and mica (sericite, biotite or chlorite), which probably originated as volcanic ash. The close packing of the grains, their orientation parallel to bedding, and the presence of abundant noncarbonaceous, rigid detritus indicate that the shape of the wisps is due to compaction and suggest that the wisps were originally simple carbonaceous grains. Compaction flattening is also suggested by packing differences between grain types. In both black-and-white banded and massive black cherts, simple and composite grains are commonly equidimensional and loosely packed; where the grains are elongate, they are more closely packed than in adjacent layers with equant grains. Another explanation for the flattened nature of the grains is suggested by the work of Lewan (1987), which demonstrates that increased thermal stress transforms amorphous kerogen masses in shales to a viscous bitumen that spreads along the bedding fabric of the shale and may eventually form a bitumen network. The flattened nature of the carbonaceous wisps may, therefore, be the result of thermal maturation of the organic matter and resultant redistribution along bedding planes.

Cloudy, diffuse carbonaceous matter. Carbonaceous matter is present in some cherts as indistinct, faint, cloudy background or irregular patches that are not resolvable into individual grains. Cloudy patches of carbonaceous matter are most abundant in cherts made up of closely packed simple carbonaceous grains, but, even here, are a minor component of carbonaceous cherts. In a few cases, the faint cloudy carbonaceous matter is evenly disseminated within a chert matrix (Fig. 7). This material is interpreted as extremely fine detrital or degraded carbonaceous matter.

Crystalline carbonaceous material. All samples from the Theespruit Formation and some from the Fig Tree Formation in the northern part of the greenstone belt contain fine, shiny, black crystalline carbonaceous matter in a matrix of fine megaquartz (Fig. 8A). One of these samples was examined by scanning electron microscope. It contains tabular hexagonal crystals that are probably graphite dispersed within the quartz matrix (Fig. 8B). These samples have been affected by thermal metamorphism during intrusion of nearby tonalitic plutons. Recrystallization has converted original kerogen to graphite and largely obliterated the original sedimentary fabric.

Petrographic differences among chert types

The three types of carbonaceous chert, black-and-white banded chert, massive black chert, and laminated black chert, are characterized by different but overlapping populations of carbonaceous material (Fig. 9). Black-and-white banded cherts are composed largely of fine carbonaceous laminations, composite grains, and simple detrital grains. Most matlike laminations occur in black-and-white banded chert. In the carbonaceous bands, layers of matlike laminations commonly alternate with layers of simple carbonaceous grains or a mixture of carbonaceous grains and elongate, coarse sand-sized grains of carbonaceous chert.

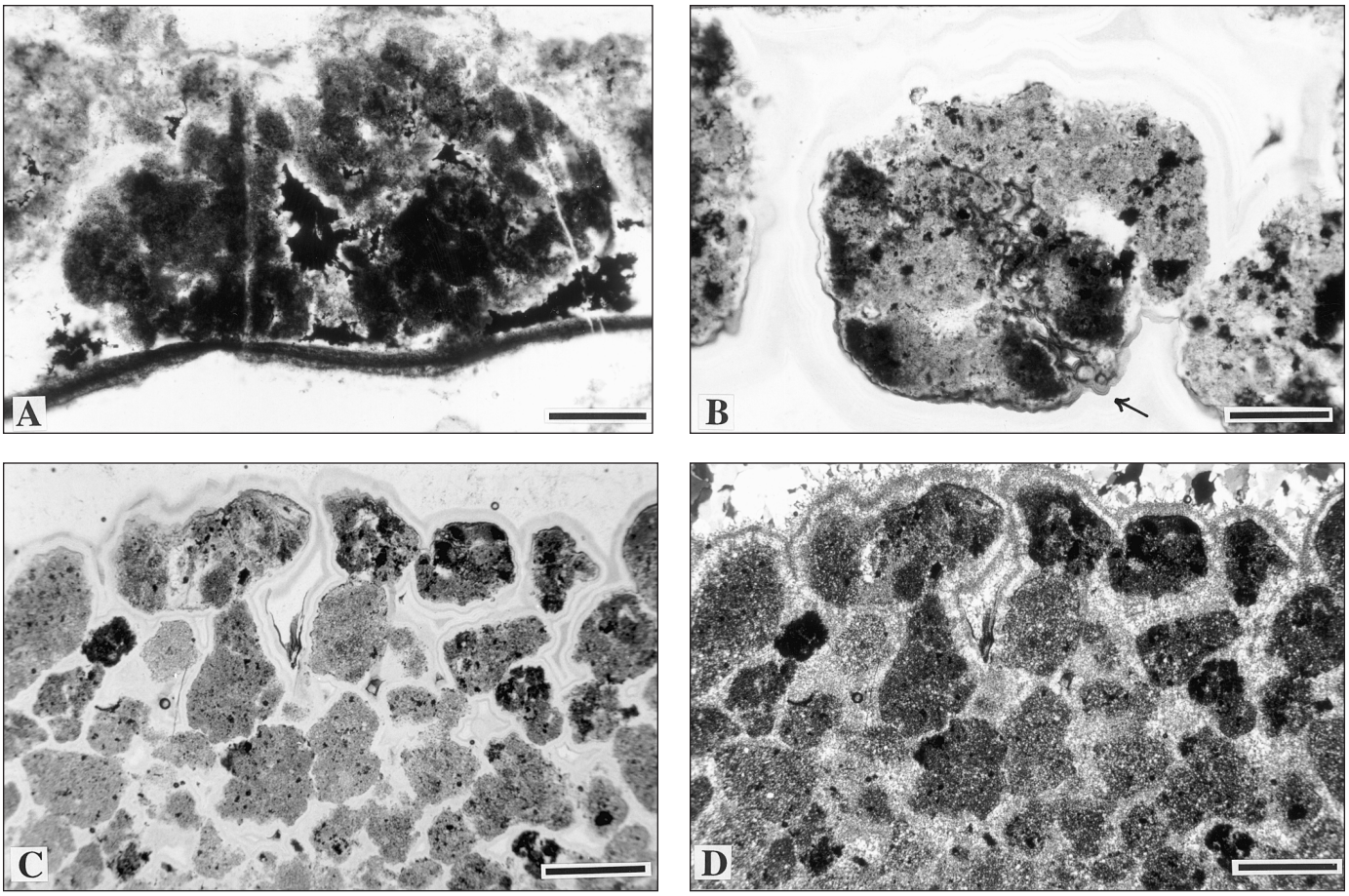


Figure 5. Photomicrographs of composite carbonaceous grains. A, Composite grain in black-and-white banded chert. Scale bar equals 200 μm. B, Composite grain with internal and external finely laminated botryoidal silica cement (arrow). Scale bar equals 200 μm. C, Layer of composite grains with botryoidal coating of silica cement. Plane light. Scale bar equals 1 mm. D, Same with crossed nicols.

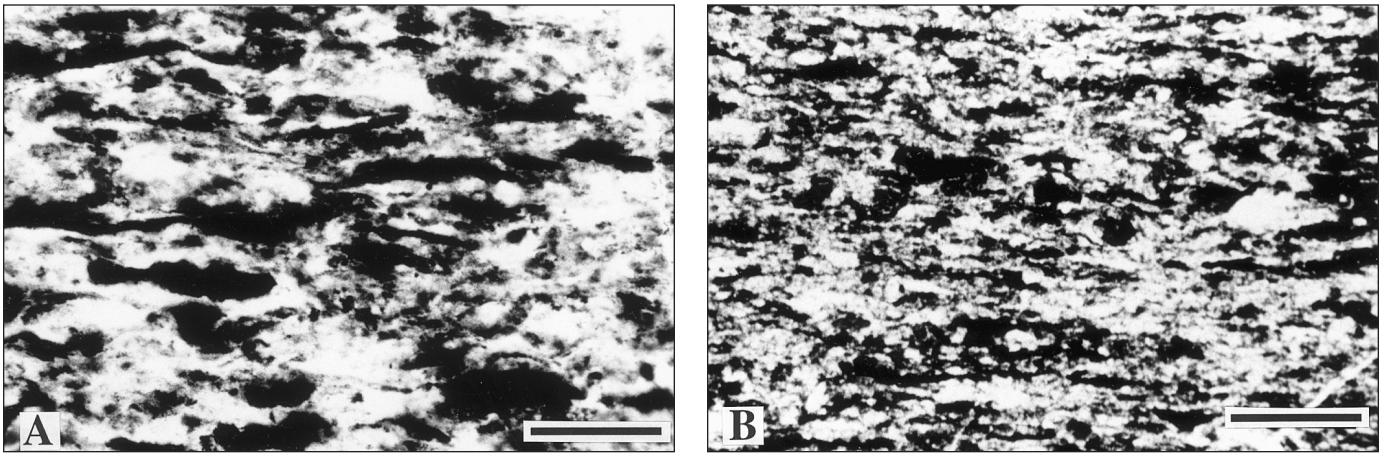


Figure 6. Photomicrographs of carbonaceous wisps. A, Partially flattened wisps in massive black chert. Scale bar equals 200 μm. B, Carbonaceous wisps in laminated black chert. Scale bar equals 1 mm.

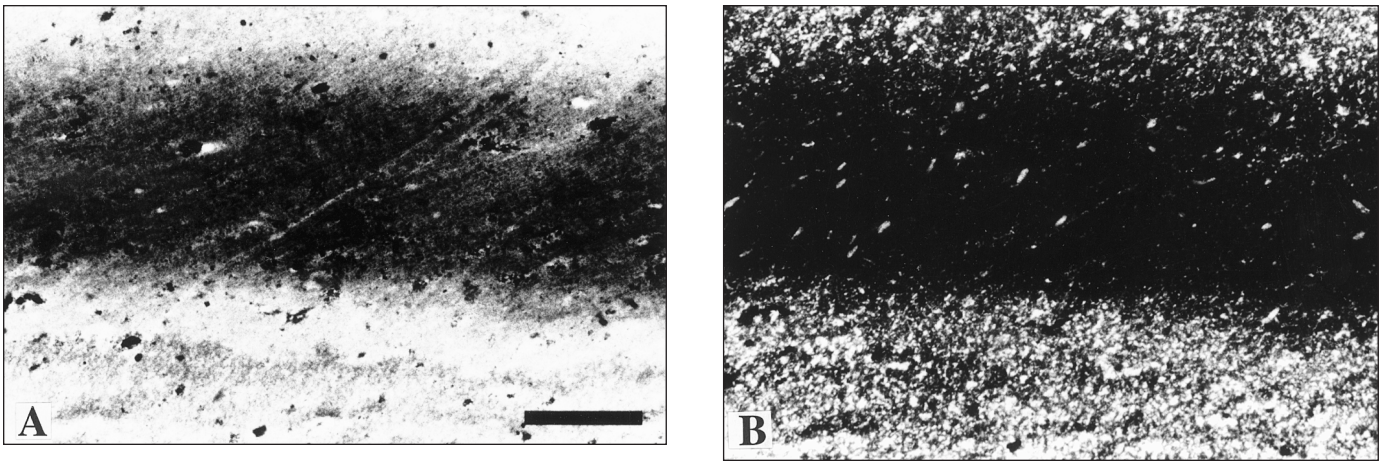


Figure 7. Photomicrographs of cloudy carbonaceous matter. A, Layer of very fine grained cloudy carbonaceous matter. This sample also contains microfossils, although not within this field of view. Scale bar equals 200 μm. B, Same with crossed nicols. Fine scattered tourmaline grains appear as elongate white grains within dark carbonaceous matter.

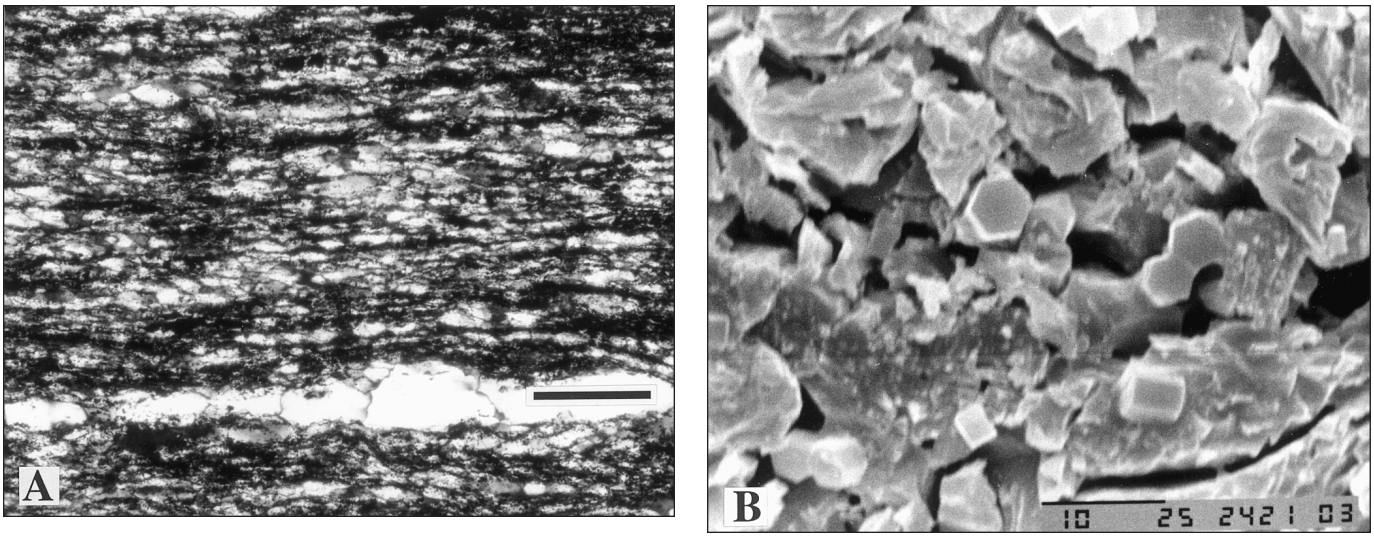


Figure 8. Photomicrographs of crystalline carbonaceous matter. A, Photomicrograph of sample composed largely of megaquartz and carbonaceous matter, much of which is finely crystalline graphite. The presence of abundant nondetrital megaquartz grains and graphite indicates that it represents an originally cherty sedimentary rock that has been recrystallized during thermal alteration. Scale bar equals 200 μm. B, SEM photograph of same sample showing hexagonal habit of crystalline carbonaceous matter (graphite). Scale bar equals 10 μm.

Scattered composite grains draped by matlike laminations are common. Many black bands consist of a single detrital layer of simple carbonaceous grains underlain by a layer of matlike laminations, each about 0.5 to 1 cm thick. In such layers, the simple grains are closely packed and range in size from less than 50 μm to approximately 350 μm.

Most massive black cherts are dominated by simple detrital grains. Simple grains may occur to the exclusion of other particles or mixed with lithic detritus, composite carbonaceous grains, or carbonaceous wisps. Laminated black cherts are composed mainly of simple carbonaceous grains and wisps, but commonly include silt-sized terrigenous clastic grains. Matlike laminations and composite grains are rare.

Analysis of variance of the abundance of carbonaceous matter type by chert type confirms the significance of these general observations (Table 1). Black-and-white banded cherts have more matlike laminations than massive and laminated cherts. Laminated cherts contain fewer composite grains than massive and banded black cherts. The three chert types all differ in the abundance of carbonaceous wisps and grain packing.

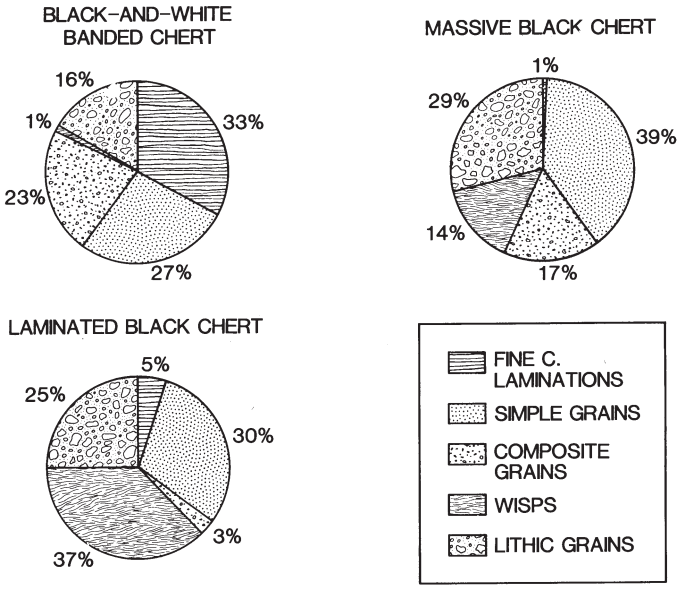


Figure 9. Pie charts illustrating the mean populations of petrographic types of carbonaceous matter in the three chert types. Based on 162 samples.

Certain particle associations are also preferentially developed. Of the ten possible binary combinations of particle types, chi-square analysis of compositional data shows that three are significantly developed at the 95% level of confidence. Matlike laminations and composite carbonaceous grains show a strong positive association. There is a also positive association between wisps and terrigenous detritus. Wisps and composite grains show a negative association.

SEDIMENTOLOGY

Black-and-white banded chert

The thinness and lateral continuity of individual laminations and layers within the banded black-and-white cherts suggest deposition under low-energy conditions. The presence of coarse sand-sized intraclasts as well as ripped up, folded, and locally transported fragments of matlike laminations indicates that the sediments were frequently affected by low-level wave or current activity. The paucity of very fine carbonaceous and noncarbonaceous detritus, including shale layers, also suggests winnowing by currents or waves. Where coarse-grained noncarbonaceous detrital beds are also present, such as in unit K1c2 along the Komati River and in the Mendon Formation, cross-bedding is well-developed. The widespread evidence of low-level, nonsurging current activity, as well as the suggestion of local exposure and desiccation (Lowe and Knauth, 1977; Worrell, 1985; Lowe and Fisher Worrell, this volume, Chapter 7) argue for shallow-water deposition. The extremely loose packing of grains in most black-and-white banded cherts argues for early silicification of the sediments.

Massive black chert

Massive black cherts are mixtures of simple carbonaceous grains, lithic grains, and less commonly, composite grains. The lack of carbonaceous laminations suggests that they did not form through the buildup of microbial mats. The predominance of simple carbonaceous grains and lithic grains as well as the common association of massive black cherts with volcaniclastic units suggest that units of massive black chert represent strictly detrital accumulations. Layers of massive black chert interbedded with black-and-white banded chert probably represent flood or storm deposits. Massive layers of particulate carbonaceous detritus have been observed on the surface of modern bacterial mats in Laguna Figueroa, Baja California, after extensive floods (Margulis et al., 1983). Thicker massive black chert units in the Mendon Formation, which have no association with matlike deposits, may represent quiet water accumulations of pelagic or hemipelagic carbonaceous matter that settled through the water column.

Laminated black chert

Despite its overt similarity to massive black chert in lithologic association and abundance of lithic debris, laminated black chert is petrographically and chemically distinct. Most laminated black chert contains chlorite and sericite, which probably originated as volcanic ash. Size sorting of grains and flat- and cross-laminations in some laminated cherts containing sand-sized lithic grains indicates that the original sediments of at least some laminated chert were current deposited. Finer grained laminated chert containing a high proportion of micaceous particles was probably deposited by weak currents or by suspension sedimentation.

The predominance of flattened particles, which correlates with high TOC relative to other chert types, suggests that the sediments underwent considerable compaction and that silicification was late.

DISTRIBUTION OF CHERT AND CARBONACEOUS-MATTER TYPES

Black-and-white banded chert is common in the Hooggenoeg Formation and makes up more than 90% of the carbonaceous chert in the Kromberg Formation by virtue of the 150- to 350-m-thick Buck Reef Chert (K1) on the west limb of the Onverwacht anticline. On the east limb of the Onverwacht anticline, the Buck Reef Chert is represented by three thin chert units, K1c1, K1c2, and K1c3, separated by basaltic and komatiitic volcanic rocks (Lowe and Byerly, this volume, Chapter 1). The lowest, K1c1, is made up largely of black-and-white banded chert with interlayered carbonate bands. The middle chert unit, K1c2, is also composed mainly of black-and-white banded chert that contains flat- and cross-laminated carbonate layers, possibly representing carbonated volcanic ash. K1c3 also consists of black-and-white banded chert. Most of its primary features have been obscured by

TABLE 1. MEAN PERCENTAGES OF PARTICLE TYPES AND PACKING DENSITIES IN THE THREE CARBONACEOUS CHERT TYPES

Chert type	Matlike laminations	Simple grains	Composite grains	Wisps	Lithics	Packing*
Black-and-white banded	29†	25	21	1†	14	39†
Massive black	1	33	14	12†	24	55†
Laminated black	5	26	3	34†	23	69†

Note: Based on 152 samples.
S*Estimates of packing are based on percentage of thin section area occupied by carbonaceous or lithic particles as opposed to chert matrix.
†Chert is significantly different than other chert types at the 95% confidence level.

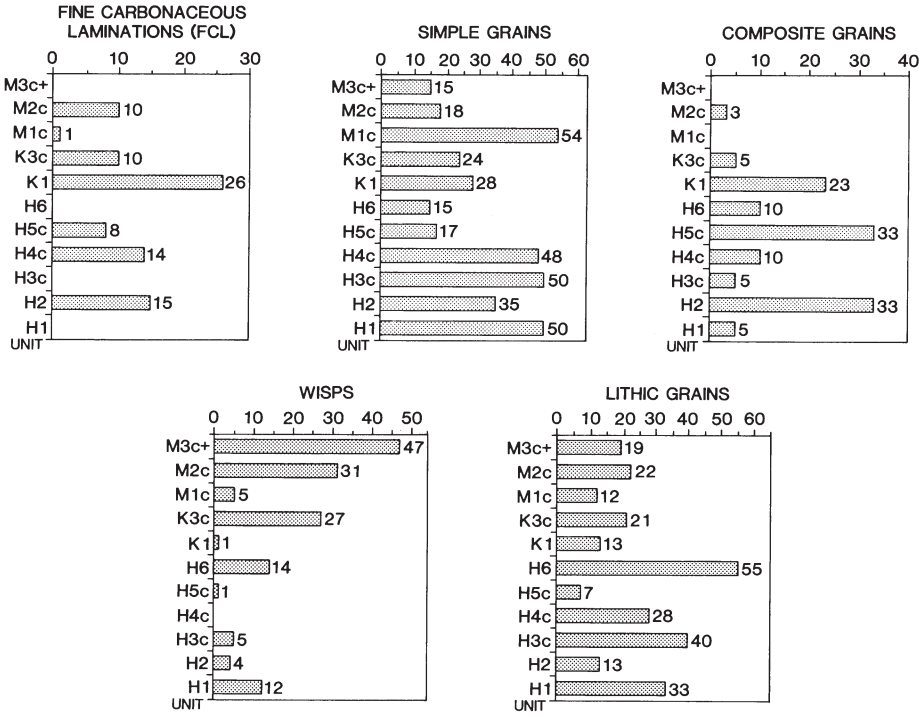


Figure 10. Charts showing stratigraphic distribution of petrographic types of carbonaceous matter and lithic grains. Horizontal axes indicate overall percentages for each chert unit. Unit designations follow those of Lowe and Byerly (this volume, Chapter 1).

later mineralization, and it hosts gold at the Sheba Gold Mine, just south of the Komati River.

Massive black chert is a subordinate chert type in all three formations of the upper Onverwacht Group, but it is more common in the Hooggenoeg and Mendon Formations than in the Kromberg Formation. It is associated with laminated black chert and, less commonly, black-and-white banded chert in volcaniclastic-dominated interflow chert units in the Hooggenoeg Formation. In the Kromberg Formation, layers of massive black chert 0.5 to 1 m thick are present at the base of the black-and-white banded chert of K1.

Laminated black chert predominates in the upper cycles of the Mendon Formation and in the Fig Tree Group in the northern part of the greenstone belt. Layers of laminated black chert as much as several tens of centimeters thick occur within thicker layers of massive black chert beds. The Footbridge Chert (K3c)

of the Kromberg Formation (Lowe and Byerly, this volume, Chapter 1) is among the thickest units of laminated black chert. In the upper cycles of the Mendon Formation, laminated black chert layers as much as 13 m thick directly overlie silicified komatiite flows.

The relative abundances of carbonaceous particle types in the different chert units of the Swaziland Supergroup, when related to tectonic setting and sedimentary environment of the units, allow some conclusions to be drawn about the mode of accumulation of the carbonaceous deposits. The overall percentages of particle types in the carbonaceous cherts throughout the stratigraphic section are shown in Figure 10. Composite grains and matlike laminations are common in most units of the Hooggenoeg and lower Kromberg Formations. The abundance of both, especially composite grains, is much lower in K3c and in the Mendon Formation. Wisps, on the other hand, are minor components of the carbonaceous cherts of the Hooggenoeg and lower Kromberg, but are abundant in K3c and in the upper cycles of the Mendon Formation. Lithic grain and simple carbonaceous grain abundances vary by chert unit, but exhibit no upsection trends.

TECTONIC AND ENVIRONMENTAL ASSOCIATIONS

The type of carbonaceous deposits shows a strong dependence on environmental setting. The depositional settings for the cherts of the Onverwacht Group are of two major types: platformal and basinal (Lowe, this volume, Chapter 3). The platform deposits of the Hooggenoeg, Kromberg, and lower cycles of the Mendon Formation were deposited either in shallow-water and subaerial environments, where they tend to be associated with komatiitic or dacitic volcanic units, or under quiet, slightly deeper water conditions associated with basaltic volcanism (Lowe, this volume, Chapter 3). The upper cycles of the Mendon Formation represent fine-grained basinal sediments deposited predominantly in deep, quiet water.

The relative influence of microbial and detrital sedimentation on deposition of carbonaceous sediments in each of the chert units can be estimated by comparing the abundance of matlike laminations and composite particles to that of detrital carbonaceous and lithic grains (Fig. 11). The upper Hooggenoeg chert H5c and the K1 cherts, both on the east and west limbs of the Onverwacht anticline, show the most influence by microbial activity. Hooggenoeg units that are dominated by volcaniclastic sediments, such as H1, H3c, and H6, include carbonaceous cherts that are composed almost exclusively of detrital material. Facies changes in K3c are apparent in the dominance of lithic and detrital grains, mainly wisps, in the east and the presence of fine carbonaceous laminations and composite grains in the west. As discussed by Lowe (this volume, Chapter 3) the contrast is probably due to a facies change eastward from shallow to deeper water deposits. The basinal deposits of the upper Mendon Formation (Lowe, this volume, Chapter 3) are dominated by carbonaceous detritus made up almost exclusively of simple grains and wisps.

Samples from the Fig Tree Group in the Ulundi syncline are plotted as a group on the ternary diagrams. Collected from various chert bars in the northern part of the greenstone belt, they seem to represent a mixture of environments that are dominated by detrital sedimentation, although some samples collected from the vicinity of the Daylight Mine, a locality described by Schopf and Barghoorn (1967), contain matlike laminations.

A comparison of the abundances of the three carbonaceous grain types illustrates the contrast in extent of compaction of the chert units (Fig. 12). The platformal sediments of the Hooggenoeg, Kromberg and lower Mendon Formations, dominated by matlike laminations, composite grains, and simple grains, show little overall compaction before lithification/silicification. The carbonaceous cherts of the eastern facies of K3c, which are relatively deeper water deposits, the basinal deposits of the Mendon Formation above M1c, and the Fig Tree of the northern Mountain Land are dominated by wisps, which indicate extensive presilicification compaction of the sediments.

CHEMICAL COMPOSITION OF THE CARBONACEOUS CHERTS

Two selected suites of carbonaceous cherts were analyzed both to characterize the general range of the compositions of Swaziland carbonaceous cherts, which have generally not been treated in detail in previous geochemical studies of Swaziland sedimentary rocks (Dungworth and Schwartz, 1974; Moore et al., 1974; Reimer and Kröner, 1979), and to determine if different chert types exhibit distinctive geochemical signatures.

Silica dominates all samples, ranging from 94.47 to 99.40%

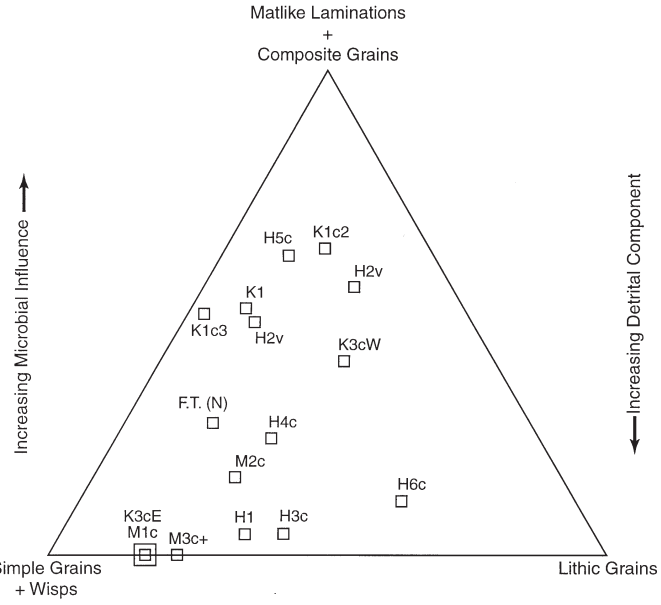


Figure 11. Ternary plot assessing stratigraphic variations in the amount of microbial influence on local sedimentation. Matlike laminations and composite grains, indicating the existence of local benthic microbial communities, versus simple grains and wisps, which are thought to represent mainly transported detrital particles.

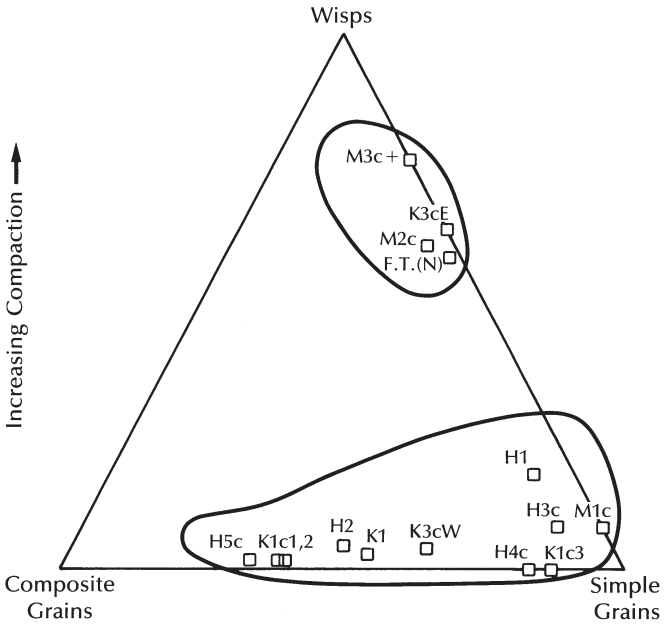


Figure 12. Ternary plot assessing the relationship between stratigraphy and degree of compaction. Simple and composite grains are largely uncompacted prior to silicification whereas wisps, found mainly in the upper parts of the Onverwacht and overlying Fig Tree Groups, have been heavily flattened by compaction before silicification.

by weight (Table 2). FeO and/or Fe_2O_3 are the only other oxides present as more than 1% in any sample, ranging from 0.46 to 3.06%. With the exception of laminated black chert, most carbonaceous cherts in the Swaziland Supergroup contain little alumina. The low levels of alumina in carbonaceous cherts, compared to other chert types in the Swaziland Supergroup (Lowe, this volume, Chapter 3) indicate that the primary sediments contained only small amounts of aluminosilicate material, such as volcaniclastic debris and clays, at the time of deposition.

Measured TOC contents of carbonaceous cherts range from 0.10 to 14.6 mg C/g of rock and δ^{13} C from –16.5 to –40.8‰ (Table 3). These values show the same range as those reported previously from the Swaziland Supergroup (Oehler et al., 1972; Moore et al., 1974; Schidlowski et al., 1983) and from other early Precambrian carbonaceous sediments (Awramik et al., 1983; Schidlowski et al., 1983; Robert, 1988). Laminated black cherts show significantly higher TOC contents than either black-and-white banded or massive cherts.

The carbon isotopic composition of most samples of carbonaceous chert, and all Kromberg samples, falls between –24 and –35‰ δ^{13}C. These results are consistent with biological production of the organic matter, even if post-depositional effects of alteration and metamorphism are considered (Schidlowski et al., 1983; Galimov, 1985; Robert, 1988).

Oehler et al. (1972) noted anomalously heavy carbon in the Theespruit Formation, which they attributed to prebiotic carbon production. However, no upsection shifts in carbon isotope values were noted in samples analyzed during this study. One of the two Theespruit samples has a relatively heavy δ^{13}C value (–19.8‰), but δ^{13}C from the second falls in the same range as samples higher in the section. Other workers (McKirdy and Powell, 1974; Hayes et al., 1983) suggest that heavy carbon values in Theespruit rocks reflect metamorphism. Our observations support this view. Samples from the Theespruit Formation examined during this study contain graphite, observed by scanning electron microscope (SEM; Fig. 8b), and are extensively recrystallized, unlike samples from the upper formations of the Onverwacht Group.

The extent of thermal alteration of carbonaceous matter can be estimated using H/C ratios of kerogen, as thermal alteration results in dehydrogenation of the kerogen. The H values reported in Table 2 are from whole-rock analyses rather than extracted kerogen analyses and therefore represent the maximum H that could be in the carbonaceous matter. The extremely low H values for all of the cherts are consistent with reported values for H/C ratios of kerogen in Archean carbonaceous cherts and, along with the black color of the carbonaceous matter, indicate extensive thermal alteration (McKirdy and Powell, 1974; Hayes et al., 1983).

Compositional differences among chert types may be due in part to the relative timing of cementation, probably by silica, and sediment compaction. In sediments where early silicification occurred, silica filled the pore spaces, minimizing compaction, and maintaining close to original carbon per volume values. There is a positive correlation between grain aspect ratio, a measure of the degree of prelithification compaction, and TOC: the flatter the carbonaceous grains, the higher the measured TOC content (Table 4 and Fig. 13). This relation indicates that the TOC content of the cherts is a function not only of the original carbon content of the sediments and postdepositional carbon loss, but also the amount of presilicification sediment compaction. In general, black-and-white banded cherts were the least compacted and laminated black cherts the most compacted prior to cementation. Massive black cherts also show a positive relationship between grain aspect ratio and Al_2O_3 (Fig. 14), indicating that in this chert group, Al concentration positively correlates with the extent of precementation sediment compaction. The carbonaceous cherts as a group, however, show no similar trend, indicating that differences in Al_2O_3 between massive and black-and-white banded cherts reflect original chemical differences, probably the presence of volcaniclastic debris and/or clays in the massive cherts.

DISCUSSION

The results of this study provide a basis for examination of carbonaceous cherts in other Archean terranes by allowing some prediction of the petrographic and chemical characteristics of the cherts based on outcrop characteristics. Black-and-white banded cherts are generally well preserved, extensively silicified accumulations of fine carbonaceous laminations, interpreted as remains of microbial mats, interbedded with layers of simple or composite carbonaceous grains. They are the most promising targets in the

TABLE 2. MAJOR ELEMENT (WT. %) AND TRACE ELEMENT (PPM) COMPOSITIONS OF AND ASPECT RATIOS OF CARBONACEOUS PARTICLES IN CARBONACEOUS CHERTS OF THE SWAZILAND SUPERGROUP

Sample	MW 37-6	MW 37-7a	MW 37-7b	MW 41-2	MW 45-3b	MW 45-7	MW 48-5	MW-48-12	MW 55-2b
Chert Type	Banded	Banded	Banded	Banded	Banded	Banded	Banded	Banded	Banded
SiO2	99.40	94.48	98.91	97.60	97.28	95.68	99.21	98.90	98.68
Al2O3	0.08	0.07	0.10	0.08	0.00	0.10	0.05	0.06	0.00
Fe2O3	0.56	3.54	0.81	1.03	1.08	3.96	0.69	0.50	0.60
MgO	0.13	0.24	0.12	0.22	0.28	0.11	0.17	0.01	0.17
CaO	0.00	0.02	0.01	0.02	0.44	0.01	0.04	0.00	0.41
Na2O	0.00	0.00	0.00	0.00	0.00	0.00	0.00	0.00	0.00
K2O	0.03	0.01	0.04	0.03	0.03	0.04	0.03	0.03	0.06
TiO2	0.00	0.01	0.01	0.01	0.00	0.01	0.00	0.02	0.00
P2O5	0.08	0.02	0.04	0.02	0.03	0.07	0.05	0.02	0.01
MnO	0.00	0.00	0.00	0.00	0.00	0.00	0.00	0.00	0.00
Total	100.28	98.39	100.04	99.01	99.14	99.98	100.24	99.54	99.93
S	0.00	94.45	11.17	623.18	1144.77	246.62	196.24	115.63	307.03
Zn	2.02	3.09	2.83	2.21	5.64	4.75	47.08	13.07	12.74
Cu	0.00	4.91	0.48	3.23	6.13	4.52	9.12	17.29	11.01
Ni	7.29	30.22	11.02	8.01	37.46	22.11	34.72	39.37	10.16
C (inorg)	0.07	0.24	0.09	0.02	0.29	0.11	0.06	0.07	0.12
C(org)	0.03	0.39	0.14	0.10	0.02	0.11	0.14	0.05	0.05
H	0.01	0.03	0.02	0.00	0.00	0.02	0.00	0.00	0.00
N	0.00	0.00	0.00	0.00	0.00	0.00	0.00	0.00	0.00
Mean aspect ratio	1.30	2.17	1.41	1.12	1.35	1.89		1.61	1.54

Sample	MW 62-1a	MW 63-2b	MW 37-1	MW 37-5	MW 43-1	MW 48-1	MW 55-3	MW-59-8	MW 48-9
Chert Type	Banded	Banded	Massive	Massive	Massive	Massive	Massive	Laminated	Sandst.
SiO2	99.40	99.08	98.76	97.97	99.02	98.27	95.69	96.88	97.99
Al2O3	0.01	0.05	0.16	0.25	0.26	0.21	0.28	0.33	0.85
Fe2O3	0.46	1.01	0.49	1.02	0.49	0.87	1.52	2.00	0.63
MgO	0.02	0.13	0.14	0.03	0.12	0.15	0.24	0.15	0.18
CaO	0.01	0.01	0.02	0.02	0.02	0.03	0.95	0.00	0.09
Na2O	0.00	0.00	0.00	0.00	0.00	0.00	0.00	0.00	0.00
K2O	0.04	0.03	0.03	0.08	0.06	0.10	0.03	0.07	0.30
TiO2	0.06	0.01	0.00	0.01	0.01	0.02	0.01	0.02	0.03
P2O5	0.05	0.02	0.05	0.00	0.02	0.00	0.03	0.02	0.05
MnO	0.00	0.00	0.00	0.00	0.00	0.00	0.00	0.00	0.00
Total	100.05	100.34	99.65	99.38	100.00	99.65	98.75	99.47	100.12
S	0.00	18.15	104.57	61.12	63.53	400.66	1645.45	9330.53	56.41
Zn	3.38	2.68	0.00	4.40	1.11	366.56	100.20	226.46	13.26
Cu	1.66	7.38	0.00	4.25	4.20	45.67	29.78	20.02	14.33
Ni	1.07	7.58	2.72	53.69	15.29	44.31	70.90	233.19	8.49
C (inorg)	0.11	0.10	0.05	0.07	0.04	0.10	0.28	0.04	0.07
C(org)	0.03	0.08	0.02	0.28	0.07	0.18	0.21	0.09	0.00
H	0.00	0.01	0.01	0.02	0.01	0.01	0.02	0.02	0.02
N	0.00	0.00	0.00	0.00	0.00	0.00	0.00	0.00	0.00
Mean aspect ratio	1.11	1.61	1.02	1.61	1.37	1.23	1.37		1.67

Note: Aspect ratio is the longest dimension of a grain in thin section ("a" intercept) divided by the longest grain dimension perpendicular to "a."

search for preserved microfossils. Massive black cherts contain a large proportion of lithic grains as well as carbonaceous detritus, but lack matlike laminations. Laminated black cherts are also detrital accumulations of both lithic and carbonaceous matter, but are commonly finer grained and were more compacted prior to cementation than massive black cherts and subsequently have higher TOC values than the other chert types, whose TOC is diluted by the presence of silica in pore spaces.

Petrographic evidence, in particular the aspect ratios of carbonaceous grains, suggests that the precursor sediments of the various chert types were silicified at different times relative to sediment compaction. Black-and-white banded chert and, to a lesser extent, massive black chert contain round or lobate carbonaceous grains. The virtually uncompacted state of the carbonaceous matter, including delicate, lobate carbonaceous particles, indicates that cementation, probably silicification, took place at or within a few centimeters of the sediment-water interface. This evidence of early silicification of sediments prior to burial must be considered in discussions of methods of silicification of the Swaziland rocks (de Wit et al., 1982; Paris et al., 1985; Lowe and Byerly, 1986; Duchac and Hanor, 1987), particularly those models that invoke subsurface silicification by hydrothermal fluids. We would sug-

TABLE 3. TOTAL ORGANIC CARBON (TOC), CARBON ISOTOPIC VALUES, AND ASPECT RATIOS OF CARBONACEOUS PARTICLES IN CARBONACEOUS CHERTS OF THE SWAZILAND SUPERGROUP

Sample	MW24-1	MW24-2	MW13-1	MW36-54	SAF-36-57	MW52-10	MW52-11a	MW52-11b	MW21-3	MW21-4
Unit	Th	Th	H3c	H3c	H3c	H2	H2	H2	K1c3	K1c3
Type	L	ND	M	ND	ND	L	ND	ND	B	M
TOC	9.10	3.30	0.46	2.90	2.00	2.30	4.30	6.00	0.36	1.08
C13	-31.2	-19.8	-38.5	-32.2	-31.7	-36.3	-28.4	-36.3	-32.6	-30.2
Ave. asp. ratio	ND	ND	ND	ND	ND	1.89	ND	ND	1.18	1.37

Sample	MW11-2	MW11-6	MW12-1	MW9-6	MW19-5	MW19-6	SAF-23-218	SAF-23-219	SAF-23-221	SAF-23-223
Unit	K1	K1	K1	K3c	K3c	K3c	K3c	K3c	K3c	K3c
Type	M	B	B	B	L	L	L	L	ND	ND
TOC	1.12	0.53	1.29	1.77	1.47	1.29	4.10	4.10	3.70	2.40
C13	-31.9	-29.9	-33.1	-30.7	-27.5	-27	-25.8	-28.4	-24.7	-24.1
Ave. asp. ratio	1.19	1.30	1.25	1.32	1.75	2.22	7.14	ND	ND	ND

Sample	SAF-23-188	SAF-23-195	SAF-23-199	SAF-23-204	MW25-4	MW25-6	MW25-13	MW25-15	MW25-16	MW29-3
Unit	K1c1	K1c2	K1c2	K1c2	M	M	M	M	M	M
Type	ND	ND	ND	ND	B	M	ND	L	L	M
TOC	14.60	1.38	6.90	2.30	0.46	1.32	1.90	1.85	3.38	0.63
C13	-33.6	-34.5	-33.9	-27.7	-28.9	-32.1	-23.8	-26.9	-22.9	-28.8
Ave. asp. ratio	ND	ND	ND	ND	1.11	1.33	ND	7.69	10.00	2.13

Sample	MW29-4	MW141-10	MW8-3	MW8-7	MW14-1	MW26-1	MW30-4	MW32-1a	MW1-2	MW4-6
Unit	M	M	M1c	M1c	M1c	M2c	M2c	M2c	M2c	F.T
Type	M	M	M	L	M	M	B	L	M	ND
TOC	0.28	1.20	0.65	2.21	1.40	0.38	0.72	1.26	1.21	0.81
C13	-30.5	-35.8	-24.4	-32.5	-30.8	-32.4	-33.9	-22.4	-40.8	-33.6
Ave. asp. ratio	2.04	2.22	1.11	2.94	1.20	1.16	1.09	ND	2.94	ND

Sample	MW5-2	MW5-3	MW6-7	MW6-9	MW7-3	MW7-21	SAF-59-16	SAF-16-11	SAF-102-12	SAF-102-13
Unit	F.T.	F.T.	M2c	M2c	M2c	M2c	K1c1	F.T.	M1	M1
Type	B	B	M	L	M	M	ND	ND	ND	ND
TOC	0.15	0.48	1.91	4.33	1.02	2.94	2.10	1.00	2.30	0.94
C13	-26	-30.3	-30	-30	-16.7	-32.4	-28.5	-32	-26.6	-25.5
Ave. asp. ratio	ND	1.28	3.13	3.57	ND	3.70	ND	ND	ND	ND

Note: Aspect ratio is the longest dimension of a grain in thin section ("a" intercept) divided by the longest grain dimension perpendicular to "a." ND = not detected.
Types: M = massive black chert; B = black-and-white banded chert; L = laminated black chert. Units designations follow those of Lowe and Byerly (this volume, Chapter 1).

TABLE 4. AVERAGE TOTAL ORGANIC CARBON (TOC) AND CARBONACEOUS GRAIN ASPECT RATIOS FOR THE THREE MAIN TYPES OF CARBONACEOUS CHERT

Chert type	TOC (mgC/g rock)	Aspect ratio*
Black-and-white banded	0.72	1.18
Massive black	1.11	1.54
Laminated black	3.22†	3.13†

*Aspect ratio of a grain in thin section is the ratio of longest diameter of the grain (the "a" intercept) to the longest diameter perpendicular to "a."
†Statistically significant diffference from other types.

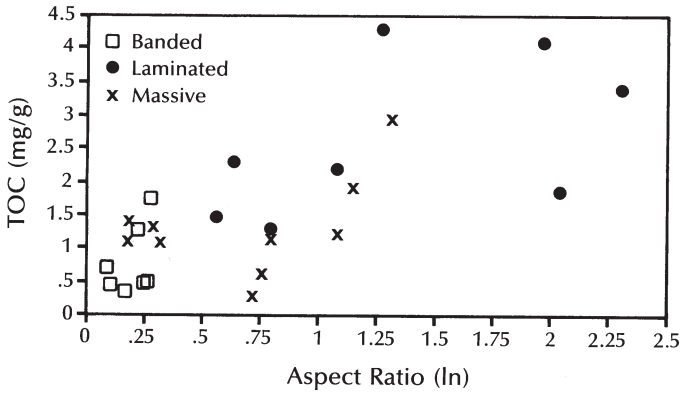


Figure 13. Relationship between aspect ratios of carbonaceous grains and total organic carbon (TOC) values in cherts of the Swaziland Supergroup. The results suggest that TOC content of cherts is directly related to the amount of presilicification compaction of the carbonaceous sediment.

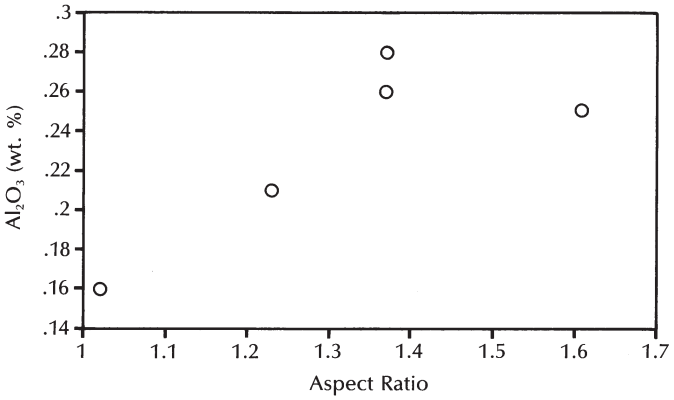


Figure 14. Relationship between carbonaceous grain aspect ratio and Al_2O_3 content of massive black cherts. The results suggest that measured Al_2O_3 contents of cherts can be related to the amount of presilicification sediment compaction, probably because widely divided clay and volcaniclastic grains are concentrated at the expense of pore space and fluid during compaction.

gest that much of the silica in these units was either deposited along with the carbonaceous sediments, perhaps loosely bonded to the carbonaceous particles, or was precipitated from seawater within the uppermost layers of sediment.

The relationship between grain shape and TOC indicates that TOC in carbonaceous cherts is a function of both primary carbon content and the amount of prelithification sediment compaction. In cases where early cementation occurred, silica filled the pore spaces, replacing the air and water, so that compaction was minimized and close to original gross TOC content per unit volume (grams of organic C/cc) may have been maintained. In sediments where early cementation did not occur, water and air were expelled and compaction concentrated organic matter relative to volume of remaining sediment.

The results of this study also emphasize the abundance of in situ microbial mats and composite particles in shallow water and their paucity in deep-water deposits. These relationships reinforce the interpretation that early Archean bacteria included photoautotrophs that would probably have been restricted to the photic zone, either as benthic bacterial communities in shallow water or planktic organisms in more open marine environments. Deeper water accumulations appear to represent carbonaceous detritus that was transported to the sites of deposition by currents or settled to the bottom through the overlying water column.

CONCLUSIONS

During deposition of most cherts in the Hooggenoeg Formation, Kromberg Formation, and lower cycles of the Mendon Formation, carbonaceous matter accumulated in shallow water both as loose detritus and as microbial mats. Microbial layers, preserved as fine carbonaceous laminations in black-and-white banded cherts, formed during periods of low clastic influx in areas of overall weak but common wave and current activity. Periods of explosive volcanism and associated deposition of pyroclastic and volcaniclastic material restricted growth of microbial mats and are represented by interbedded silicified tuffaceous units. Carbonaceous matter accumulated as detritus in the form of simple grains mixed with volcaniclastic grains. Hooggenoeg and lower Kromberg sediments were generally lithified soon after deposition.

During deposition of some Kromberg sediments, detrital carbonaceous matter collected in deeper water where fine volcanic ash also settled slowly into the sediments. Mendon sediments represent both shallow- and deep-water deposition, with both platformal and basinal sediments preserved (Lowe, this volume, Chapter 3). Mat accumulations were very rare. Carbonaceous matter was preserved almost exclusively as detritus mixed with lithic grains deposited under extremely low energy conditions. During late Kromberg and Mendon time carbonaceous sediments generally were compacted before silicification occurred.

ACKNOWLEDGMENTS

Dr. John Hayes, Woods Hole Oceanographic Institution, performed the total organic carbon and carbon isotope analyses. The Departments of Geology and Geochemistry at the University of Cape Town provided assistance and instrumentation for chemical analyses. A. H. Knoll and D. J. DesMarais reviewed the paper, providing numerous helpful comments. In addition to NSF and NASA support listed in the Forward to this volume, this research was supported by a National Science Foundation Graduate Fellowship, an ARCO Foundation Fellowship, and a Chevron scholarship to MMW.

REFERENCES CITED

Awramik, S. M., Schopf, J. W., and Walter, M. R., 1983, Filamentous fossil bacteria from the Archean of western Australia: Precambrian Research, v. 20, p. 357–374.

Byerly, G. R., Lowe, D. R., and Walsh, M. M., 1986, Stromatolites from the 3,300–3,500 Myr Swaziland Supergroup, Barberton Mountain Land, South Africa: Nature, v. 319, p. 489–491.

Byerly, G. R., Kröner, A., Lowe, D. R., Todt, W., and Walsh, M. M., 1996, Prolonged magmatism and time constraints for sediment deposition in the early Archean Barberton greenstone belt: evidence from the Upper Onverwacht and Fig Tree Groups: Precambrian Research, v. 78, p. 125–138.

Davies, G. R., 1970, Algal-laminated sediments, Gladstone Embayment, Shark Bay, Western Australia: American Association of Petroleum Geologists Memoir 13, p. 169–205.

deWit, M. J., Hart, R., Martin, A., and Abbott, P., 1982, Archean abiogenic and probable biogenic structures associated with mineralized hydrothermal vent systems and regional metasomatism with implications for greenstone belt studies: Economic Geology, v. 77, p. 1783–1802.

Duchac, K. C., and Hanor, J. S., 1987, Origin and timing of the metasomatic silicification of an Early Archean komatiite sequence, Barberton Mountain Land, South Africa: Precambrian Research, v. 37, p. 125–146.

Dungworth, G., and Schwartz, A., 1974, Organic matter and trace elements in Precambrian rocks from South Africa: Chemical Geology, v. 14, p. 167–172.

Folk, R. L., and Weaver, C. E., 1952, A study of the texture and composition of chert: American Journal of Science, v. 250, p. 498–510.

Galimov, E. M., 1985, The biological fractionation of isotopes, translated by Vitaliano, D. B., Meinschein, W. G., translation ed.: New York, Academic

Press, p. 225–252.
Gallardo, V. A., 1977, Large benthic microbial communities in sulfide biota under Peru–Chile subsurface counter current: Nature, v. 268, p. 331–332.
Golubic, S., 1973, The relationship between blue-green algae and carbonate deposits, *in* Carr, N. G., and Whitton, B. A., eds., The biology of blue-green algae: London, Blackwell Publications, p. 434–472.
Golubic, S., and Focke, J. W., 1978, *Phormidium hendersonii* Howe: identity and significance of a modern stromatolite building microorganism: Journal of Sedimentary Petrology, v. 48, p. 751–764.
Hayes, J. M., Kaplan, I. R., and Wedeking, K. W., 1983, Precambrian organic geochemistry, preservation of the record, *in* Schopf, J. W., ed., Earth's earliest biosphere: its origin and evolution: Princeton, Princeton University Press, p. 93–133.
Horodyski, R. J., Bloeser, B., and Vonder Haar, S. P., 1977, Laminated algal mats from a coastal lagoon, Laguna Mormona, Baja California, Mexico: Journal of Sedimentary Petrology, v. 47, p. 680–696.
Huc, A. Y., 1980, Origin and formation of organic matter in recent sediments and its relation to kerogen, *in* Durand, B., ed., Kerogen: insoluble organic matter from sedimentary rocks: Paris, Editions Technip, p. 445–474.
Jannasch, H. W., 1984, Chemosynthetic microbial mats of deep-sea hydrothermal vents, *in* Cohen, Y., Castenholz, R. W., and Halvorson, H. O., eds., Microbial mats: Stromatolites: New York, A. R. Liss, p. 121–131.
Juniper, S. K., Martinequ, P., Sarrazin, J., and Gelinas, Y., 1995, Microbial-mineral floc associated with nascent hydrothermal activity on CoAxial Segment, Juan de Fuca Ridge: Geophysical Research Letters, v. 22, p. 179–182.
Klein, C., Beukes, N. J., and Schopf, J. W., 1987, Filamentous microfossils in the Early Proterozoic Transvaal Supergroup: their morphology, significance, and paleoenvironmental setting: Precambrian Research, v. 36, p. 81–94.
Knoll, A. H., and Barghoorn, E. S., 1977, Archean microfossils showing cell division from the Swaziland System of South Africa: Science, v. 198, p. 396–398.
Krank, K., 1980, Experiments on the significance of flocculation on the settling of fine-grained sediments in still water: Canadian Journal of Earth Sciences, v. 17, p. 1517–1526.
Kröner, A., Byerly, G. R., and Lowe, D. R., 1991, Chronology of Early Archean granite-greenstone evolution in the Barberton Mountain Land, South Africa, based on precise dating by single zircon evaporation: Earth and Planetary Science Letters, v. 103, p. 41–54.
Lewan, M. D., 1987, Petrographic study of primary petroleum migration in the Woodford Shale and related rock units, *in* Doligez, B., ed., Migration of hydrocarbons in sedimentary basins, 2nd Institute Francais de Petrole Exploration Research Conference, Carcans, France, June 15–10, 1987: Paris, Editions Technip, Collection Colloques et Seminaires, p. 113–130.
Lowe, D. R., 1982, Comparative sedimentology of the principal volcanic sequences of Archean greenstone belts in South Africa, Western Australia, and Canada: implications for crustal evolution: Precambrian Research, v. 17, p. 1–29.
Lowe, D. R., and Byerly, G. R., 1986, Archaean flow-top alteration zones formed initially in a low-temperature sulphate-rich environment: Nature, v. 324, p. 245–248.
Lowe, D. R., and Knauth, L. P., 1977, Sedimentology of the Onverwacht Group (3.4 by), Transvaal, South Africa, and its bearing on the characteristics and evolution of the early Earth: Journal of Geology, v. 85, p. 699–723.
Margulis, L., Barghoorn, E. S., Ashendorf, D., Banerjee, S., Chase, D., Francis, S., Giovannoni, S., and Stolz, J., 1983, The microbial community in the layered sediments at Laguna Fugueroa, Baja California, Mexico: does it have Precambrian analogues?: Precambrian Research, v. 11, p. 93–123.
McKirdy, D. M., and Powell, T. G., 1974, Metamorphic alteration of carbon isotopic composition in ancient sedimentary organic matter: new evidence from Australia and South Africa: Geology, v. 2, p. 591–595.
Monty, C. L. V., 1967, Distribution and structure of Recent Stromatolitic algal mats, eastern Andros Island, Bahamas: Annals de la Société Géologique de Belgique, v. 90, p. 55–100.
Monty, C. L. V., 1976, The origin and development of cryptalgal fabrics, *in* Walter, M. R., ed., Stromatolites: Amsterdam, Elsevier, p. 193–249.
Moore, C. B., Lewis, C. F., and Kvenvolden, K. A., 1974, Carbon and sulfur in the Swaziland sequence: Precambrian Research, v. 1, p. 49–54.
Oehler, D. Z., Schopf, J. W., and Kvenvolden, K. A., 1972, Carbon-isotopic studies of organic matter in Precambrian rocks: Science, v. 175, p. 1246–1248.
Paris, I., Stanistreet, I. G., and Hughes, M. J., 1985, Cherts of the Barberton Greenstone Belt interpreted as products of submarine exhalative activity: Journal of Geology, v. 93, p. 111–129.
Reimer, T. O., and Kröner, A., 1979, Note on the nickel and chromium content of cherts from the Archean Swaziland Supergroup (South Africa): Chemical Geology, v. 27, p. 171–175.
Riley, G. A., 1970, Particulate organic matter in sea water: Advances in Marine Biology, v. 8, p. 1–118.
Robert, F., 1988, Carbon and oxygen isotope variations in Precambrian cherts: Geochimica et Cosmochimica Acta, v. 52, p. 1473–1478.
Roberts, H. H., Sassen, R., Carney, R., and Aharon, P., 1989, Carbonate buildups on the continental slope of central Louisiana: Offshore Technology Conference, Houston, Texas, May 1–4, 1989, p. 655–662.
Schidlowski, M., Hayes, J. M., and Kaplan, I. R., 1983, Isotopic inferences of ancient biochemistries: carbon, sulfur, hydrogen and nitrogen, *in* Schopf, J. W., ed., Earth's earliest biosphere: its origin and evolution: Princeton, Princeton University Press, p. 149–186.
Schopf, J. W., and Barghoorn, E. S., 1967, Alga-like fossils from the Early Precambrian of South Africa: Science, v. 156, p. 508–512.
Sheldon, R. W., Evelyn, T. P. T., and Parson, T. R., 1967, On the occurrence and formation of small particles in sea water: Limnology and Oceanography, v. 12, p. 367–375.
Simonson, B. M., Schubel, K. A., and Hassler, S. W., 1993, Carbonate sedimentology of the Early Precambrian Hamersley Group of Western Australia: Precambrian Research, v. 60, p. 287–335.
Soutar, A., and Crill, P. A., 1977, Sedimentation and climatic patterns in the Santa Barbara Basin during the 19th and 20th centuries: Geological Society of America Bulletin, v. 88, p. 1161–1172.
Sumner, D. Y., 1997, Late Archean calcite-microbe interactions: Two morphologically distinct microbial communities that affected calcite nucleation differently: Palaios, v. 12, p. 300–316.
Terry, R. D., and Chilingar, G. V., 1955, Summary of "Concerning some additional aid in studying sedimentary formations by M. S. Shvetsov": Journal of Sedimentary Petrology, v. 25, p. 229–234.
Viljoen, M. J., and Viljoen, R. P., 1969, An introduction to the geology of the Barberton granite-greenstone terrain: Geological Society of South Africa Special Publication 2, p. 9–28.
Walsh, M. M., 1989, Carbonaceous cherts of the Swaziland Supergroup, Barberton Mountain Land, Southern Africa [Ph.D. thesis]: Baton Rouge, Louisiana State University, 199 p.
Walsh, M., 1992, Microfossils and possible microfossils from the Early Archean Onverwacht Group, Barberton Mountain Land, South Africa: Precambrian Research, v. 54, p. 271–293.
Walsh, M. M., and Lowe, D. R., 1985, Filamentous microfossils from the 3,500-Myr-old Onverwacht Group, Barberton Mountain Land, South Africa: Nature, v. 314, p. 530–532.
Wedeking, K. W., Hayes, J. M., and Matzigkeit, U., 1983, Procedures of organic geochemical analysis, *in* Schopf, J. W., ed., Earth's earliest biosphere: its origin and evolution: Princeton, Princeton University Press, p. 428–442.
Williams, L. A., and Reimers, C., 1982, Recognizing organic mats in deep water environments: Geological Society of America Abstracts with Programs, v. 14, p. 647.
Williams, L. A., and Reimers, C., 1983, Role of bacterial mats in oxygen-deficient marine basins and coastal upwelling regimes: preliminary

report: Geology, v. 11, p. 267–269.

Willis, J. P., Ahrens, L. H., Danchin, R. B., Erlank, A. J., Gurney, J. J., Hofmeyer, P. K., McCarthy, T. S., and Orren, M. J., 1971, Some interelement relationships between lunar rocks and fines and stony meteorites, *in* Levinson, A. A., ed., Proceedings, Lunar Science Conference, 2nd, Houston, Texas: Cambridge, Massachusetts, MIT Press, v. 2, p. 1123.

Willis, J. P., Erlank, A. J., Gurney, J. J., Theil, R. H., and Ahrens, L. H., 1972, Major, minor and trace element data for some Apollo 11, 12, 14, and 15 samples, *in* Heymann, D., ed., Proceedings, Lunar Science Conference, 3rd, Houston, Texas: Cambridge, Massachusetts, MIT Press, v. 2, p. 1269.

Wirsen, C. O., Jannasch, H. W., and Molyneaux, S. J., 1993, Chemosynthetic microbial activity at Mid-Atlantic Ridge hydrothermal vent sites: Journal of Geophysical Research, B6, v. 98, p. 9693–9703.

Worrell, G. F., 1985, Sedimentology and mineralogy of silicified evaporites in the basal Kromberg Formation, South Africa [M.S. thesis]: Baton Rouge, Louisiana State University, 152 p.

MANUSCRIPT ACCEPTED BY THE SOCIETY MARCH 26, 1998

Geological Society of America
Special Paper 329
1999

Geochemistry of mafic and ultramafic rocks in the type section of the Kromberg Formation, Barberton Greenstone Belt, South Africa

T. W. Vennemann* and H. S. Smith
Department of Geochemistry, University of Cape Town, Cape Town, South Africa

ABSTRACT

On the basis of their petrography and geochemistry, igneous rocks in the type section of the Kromberg Formation along the Komati River can be divided into tholeiitic and komatiitic groups. The tholeiitic group includes massive and pillowed volcanic units and intrusive rocks of similar major and trace element composition. All of the rocks now consist of a typical greenschist-facies mineral assemblage of actinolite-tremolite, chlorite, albite, and quartz with only some relict primary pyroxene. Chemical variation within the noncumulate tholeiites is consistent with pyroxene, plagioclase, and minor olivine (with/without chromite) separation and, in the more evolved lavas, additional titano-magnetite separation. Cumulate rocks represent partial accumulation of pyroxene and olivine only. Rocks of the komatiitic group are generally massive and coarse grained with an alteration mineral assemblage similar to that of the tholeiites, except for higher proportions of actinolite-tremolite, chlorite, serpentine, and opaque minerals, but no feldspar. Compositional variation within the komatiitic group can be accounted for by separation of olivine and chromite. Large variations in the amount of Cr and Ni content relative to the major elements of the coarse-grained komatiites are consistent with partial accumulation of olivine and chromite.

The interlayering of the tholeiitic and komatiitic rocks in the type section of the Kromberg Formation suggests a genetic relationship between the two groups. Our proposed model involves high-pressure partial melting of a chondritic-type mantle to derive a parental magma of komatiitic composition. Olivine and minor chromite and clinopyroxene fractionation in a transient magma chamber results in the formation of tholeiitic melts. Subsequent extraction of melts from this chamber produces an igneous sequence similar to that of the Kromberg Formation.

INTRODUCTION

The Barberton Greenstone Belt (BGB), one of the best-documented greenstone belts in the world, is made up of metavolcanic and metasedimentary rocks between 3.55 and about 3.2 Ga (Brevart et al., 1986; Armstrong et al., 1990; Kröner et al., 1991; Kamo and Davis, 1994). Because of its extreme age and the excellent preservation, the BGB has been the focus of a number of studies aimed at interpreting the origin and possible tectonic setting of ancient greenstone belts. In addition, it contains some of the oldest preserved materials tapped from the Earth's mantle, and is therefore of interest as a window into Archean mantle compositions and mantle-crust evolutionary processes (Anhaeusser, 1973; Sun and Nesbitt, 1977; Smith and Erlank, 1982).

The environment of formation of greenstone belt volcanic rocks has been the subject of considerable study and speculation. For example, some authors (Anhaeusser, 1973) have suggested

*Present address: Institut für Mineralogie, Petrologie, und Geochemie, Universität Tübingen, Wilhelmstr. 56, D-72074 Tübingen, Germany.

Vennemann, T. W., and Smith, H. S., 1999, Geochemistry of mafic and ultramafic rocks in the Kromberg Formation in its type section, Barberton Greenstone Belt, South Africa, *in* Lowe, D. R., and Byerly, G. R., eds., Geologic Evolution of the Barberton Greenstone Belt, South Africa: Boulder, Colorado, Geological Society of America Special Paper 329.

that greenstone belts were formed in oceanic or island arc–like settings, while others (Hunter, 1974) have suggested that they formed through rifting of older continental crust. It has been suggested that the BGB represents obducted oceanic crust (Hoffman et al., 1986; de Wit et al., 1987). More recently, many investigators have interpreted the komatiitic volcanic rocks in Archean greenstone belts as having formed in association with hot spots and mantle plumes (Storey et al., 1991; Arndt, 1994) and the felsic volcanic units as representing subduction-related volcanic arcs (Card, 1990; de Ronde and de Wit, 1994). However, structural complexities (de Wit, 1982; Lowe et al., 1985; de Ronde and de Wit, 1994; Lowe et al., this volume, Chapter 2) and controversies regarding the nature of granite-greenstone contacts (Anhaeusser, 1973) significantly complicate interpretations of the setting and evolution of magmatism in the BGB.

Previous work on the volcanic rocks of the BGB has focused largely on komatiites in the lower part of the stratigraphic sequence (Smith et al., 1980; Smith and Erlank, 1982; Jahn et al., 1982; Gruau et al., 1990). Far less attention has been paid to both komatiites and tholeiitic volcanic rocks in the upper part of the Onverwacht Group. In addition, little emphasis has been placed on the relationship between the tholeiitic and komatiitic rocks, which are commonly found in close spatial and stratigraphic association in the upper formations of the Onverwacht Group. It is the aim of this study (i) to determine the petrogenetic relationship between the mafic and ultramafic rocks found closely associated in space in the Kromberg Formation of the BGB, and (ii) to determine possible constraints that can be placed on the chemical composition of the source to the parental melts of the tholeiitic and komatiitic rocks.

GEOLOGIC SETTING

Rocks of the BGB collectively constitute the Swaziland Supergroup, which is subdivided from base to top into the Onverwacht, Fig Tree, and Moodies Groups. In the southern part of the BGB, the Onverwacht Group has been subdivided into six formations (Viljoen and Viljoen, 1969a, b; Williams and Furnell, 1979; Lowe and Byerly, this volume). The Sandspruit and Theespruit Formations are metamorphosed and structurally isolated from the other formations in most areas. The overlying sequence, 8–10 km thick and interpreted to be stratigraphically intact by Lowe and Byerly (this volume, Chapter 1), includes from base to top ultramafic volcanic rocks of the Komati Formation, basaltic and felsic volcanic rocks of the Hooggenoeg Formation, basaltic and komatiitic volcanic rocks of the Kromberg Formation, and komatiites of the Mendon Formation. In addition to flow rocks, layered sills and dikes are found throughout the Onverwacht Group and some are reported to be closely associated in space and time with the extrusive rocks (Viljoen, M. J., and Viljoen, 1969a, b; Viljoen, R. P., and Viljoen, 1969). This chapter focuses on the rocks of the Kromberg Formation in the upper part of the Onverwacht Group.

Figure 1 summarizes the stratigraphy of the Kromberg Formation in the type section along the Komati River as defined by Viljoen, M. J., and Viljoen (1969a). De Wit (1982) has argued that large-scale horizontal translations in the form of fold and thrust nappes along glide planes have drastically affected the stratigraphy of the Onverwacht Group in the southern part of the BGB. Lowe and Byerly (this volume, Chapter 1) review the stratigraphic interpretations in the BGB and suggest that the type sections of the Komati and higher formations of the Onverwacht Group are largely intact. Recent age determinations from the Onverwacht and Fig Tree Groups support this interpretation (Armstrong et al., 1990; Kröner et al., 1991, Byerly et al., 1996).

FIELD RELATIONSHIPS AND PETROGRAPHY

The Kromberg Formation is confined to the southern parts of the BGB. Some of the best exposures are found in the Komati River gorge, along the west limb of the Kromberg syncline, where the type section for this formation has been established (Fig. 1; Viljoen, M. J., and Viljoen, 1969a; Viljoen, R. P., and Viljoen, 1969). Massive tholeiitic volcanic units that range in thickness from barely a meter to as much as 70 m are most abundant in the Kromberg Formation. Some massive units appear to grade upward into thinner pillowed zones. The basaltic pillows vary in size from 0.6 × 0.5 m to 2 × 1 m and commonly have well-defined chill margins. The presence of pillows, pillow breccias, and volcaniclastic breccias suggest subaqueous deposition. The massive and pillowed basalt varieties are similar in mineralogy. They consist of a fine- to medium-grained, equigranular assemblage of actinolite and albite with less abundant chlorite, epidote, sphene, quartz, and carbonate. The tholeiitic rocks vary from fine-grained assemblages consisting solely of alteration minerals with random orientations (i.e., originally aphyric rocks) to coarser grained assemblages with pseudomorphs after subophitic pyroxene with occasional relict coarse-grained clinopyroxene (i.e., porphyritic rocks). Quartz and carbonate commonly occur in vesicles, voids, and fractures and are interpreted to have crystallized during alteration of these rocks prior to, or accompanying, low-grade greenschist-facies metamorphism.

A few tholeiitic units could be positively identified as intrusive because of their chilled upper and lower contacts with neighboring units. As their strike is parallel to that of the extrusive units, they could represent sills. While the texture of these commonly thin units is coarser grained in the central parts, their modal mineralogy and also bulk chemical composition is similar to that of the extrusive tholeiites.

Altered ultramafic units in the Kromberg Formation include higher proportions of clinopyroxene and actinolite, the latter commonly as pseudomorphs after larger pyroxene grains. Fibrous chlorite and serpentine are found as pseudomorphs after stubby, equant grains of pyroxene and/or olivine. Small amounts of sphene, albite, and altered chromite are also present within the matrix. Ultramafic units are generally massive and only rarely can chilled margins be recognized. The coarse-grained texture of most of the ultramafic rocks suggests porphyritic precursors. No

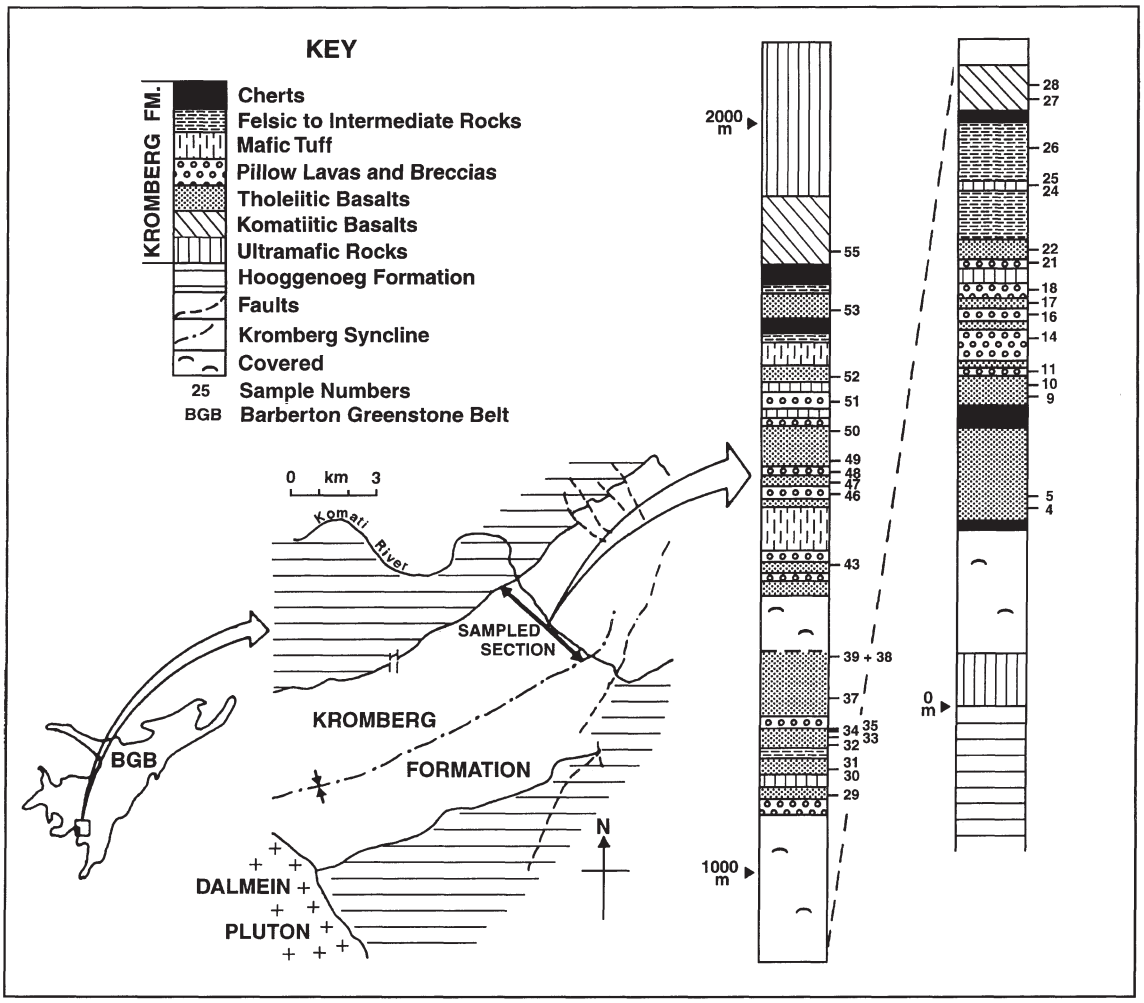


Figure 1. Sketch map showing the location of the type section of the Kromberg Formation along the Komati River in the southern part of the Barberton Greenstone Belt. Sample localities are shown in a schematic stratigraphic column on the west limb of the Kromberg syncline (after Viljoen and Viljoen, 1969b). Samples GH100 to GH103 were sampled elsewhere in the Kromberg Formation.

spinifex textures were observed and many units cannot be assigned an intrusive or extrusive origin.

Minor lithologies include acid to intermediate rocks and cherts and chert-carbonate rocks. The former have also been interpreted to be products of the metasomatic alteration of basalts (Byerly et al., 1983; Smith et al., 1984) and are characterized by a gray-green color and a massive, fine-grained texture. The dark brown, weathered chert-carbonate rocks have textural features that are consistent with a sedimentary origin (Lowe and Knauth, 1977; Lowe, this volume, Chapter 3).

The apparent random stacking of basalts and komatiites in the Kromberg Formation argues against a cyclicity in volcanic events as originally described by Viljoen, M. J., and Viljoen (1969a). Furthermore, there is no apparent increase in the amount of tholeiitic or acid rocks relative to ultramafic rocks with increasing height in the type section (Fig. 1).

SAMPLE SELECTION AND ANALYTICAL TECHNIQUES

A total of 59 whole-rock samples were collected from the type section of the Kromberg Formation for chemical analysis and thin-section studies (Fig. 1). Sample selection in the field was based on the criterion that rocks should not show veining or large cavities. After removal of weathered surfaces, at least 500 g to 1 kg of material had to be available for sample preparation. Subsequent selection for chemical analysis was based on the following criteria:

1. Wherever possible igneous textures should be recognizable, with secondary phases restricted to pseudomorphs after igneous minerals.

2. Samples should not contain monomineralic aggregates of secondary minerals.

3. Samples should have no veins or cavities and should have as little carbonate as possible (<5%).

Analysis of the rocks are given in Table 1. All analysis were obtained by X-ray fluorescence (Phillips PW 1400 and Siemens SRS 100) at the University of Cape Town and analytical methods were those described in Willis et al. (1972). Average absolute errors were as follows: SiO_2 0.23%, TiO_2 0.02%, Al_2O_3 0.14%, Fe_2O_3 0.08%, MnO 0.008%, MgO 0.10%, CaO 0.05%, Na_2O 0.10%, K_2O 0.03%, P_2O_5 0.01%; Nb, Zr, Y, Rb, Zn, and Cu all about 0.7 ppm (parts per million), Sr and Sc about 0.8 ppm, Ni and Co about 1.5 ppm, V 1.9 ppm, Ba 2.45 ppm, and Cr 3 ppm. Total iron was determined as Fe_2O_3 and the Mg# was calculated assuming a Fe_2O_3/FeO ratio of 0.15. H_2O^- and LOI (loss on ignition) were determined by heating the samples at 110°C and 1,000°C overnight and determining weight loss after each heating period.

The only remnant mineral that could be analyzed by electron microprobe was clinopyroxene. Analysis were performed at the University of Cape Town using a Cameca Camebax microprobe set at a 15 kV accelerating potential, a beam current of 0.3–0.5 mA and a beam size of 1–10 μm. Matrix corrections were carried out using ZAF correction procedures. Representative analysis are given in Table 2.

RESULTS

Clinopyroxene mineralogy

Remnant clinopyroxenes from tholeiitic rocks (GH04, GH21, GH100), cumulates (GH28, GH103), and komatiites

TABLE 1. MAJOR (WT%) AND TRACE ELEMENT (PPM) DATA AND INTERELEMENT RATIOS FOR ROCKS FROM THE KROMBERG FORMATION

	Tholeiites									
	GH04	GH05	GH09	GH10	GH11	GH14	GH16	GH17	GH18	GH21
SiO_2	50.73	51.71	53.86	55.65	62.31	60.89	57.34	51.21	53.98	50.06
TiO_2	1.47	1.43	1.61	1.67	1.56	1.41	1.40	1.31	1.05	3.21
Al_2O_3	14.75	14.39	15.24	15.35	14.30	14.27	15.50	15.58	16.06	13.90
Fe_2O_3	15.50	14.65	13.72	12.98	7.72	9.50	10.08	13.46	8.38	9.30
MnO	0.20	0.18	0.17	0.17	0.16	0.15	0.18	0.20	0.17	0.15
MgO	6.10	5.49	5.37	6.59	2.84	4.14	4.05	4.66	6.98	9.77
CaO	8.86	9.12	7.42	4.85	5.75	5.43	6.67	9.32	6.34	10.16
Na_2O	2.14	2.66	2.28	1.94	3.20	3.77	4.21	3.83	2.03	2.82
K_2O	0.08	0.20	0.16	0.61	1.97	0.28	0.40	0.28	4.94	0.37
P_2O_5	0.17	0.17	0.17	0.91	0.19	0.16	0.17	0.15	0.07	0.26
Total	100.00	100.00	100.00	100.00	100.00	100.00	100.00	100.00	100.00	100.00
H_2O-	0.06	0.10	0.08	0.08	0.18	0.06	0.09	0.05	0.07	0.09
LOI	2.72	2.34	3.40	4.90	4.81	3.22	2.20	2.06	3.54	2.84
Orig. Total	99.81	100.03	100.27	99.82	99.48	99.26	99.11	100.38	100.00	99.84
Nb	3.6	3.5	3.2	3.9	5.0	4.9	3.6	4.9	3.8	8.1
Zr	95	100	110	128	113	105	102	92	76	157
Y	36	37	33	38	36	32	31	29	16	40
Sr	137	141	186	98	130	68	80	106	94	73
Rb	2.1	4.6	3.6	16	40	5.7	6.4	5.2	81	5.7
Ba	11	33	25	64	127	36	22	23	333	59
Sc	37	37	27	25	25	33	31	34	40	32
Zn	127	117	131	98	146	95	98	87	93	70
Cu	131	168	200	109	179	156	3.6	84	6.2	233
Ni	133	116	83	76	110	43	51	66	158	216
Co	65	56	47	44	57	39	39	50	73	60
Cr	139	118	129	104	95	12	13	46	369	351
V	393	401	329	338	335	348	344	340	342	315
CaO/Al_2O_3	0.601	0.634	0.487	0.316	0.402	0.380	0.430	0.598	0.395	0.731
Al_2O_3/TiO_2	10.1	10.1	9.5	9.2	9.2	10.1	11.0	11.9	15.3	4.3
MgO/TiO_2	4.16	3.85	3.33	3.94	1.82	2.94	2.89	3.56	6.64	3.04
CaO/TiO_2	6.05	6.40	4.60	2.90	3.69	3.84	4.75	7.11	6.03	3.16
TiO_2/P_2O_5	8.83	8.48	9.51	8.91	8.01	8.74	8.49	9.00	14.67	12.30
Ti/Nb	24.5	24.4	29.8	25.5	18.6	17.3	23.2	15.9	16.8	23.9
Ti/Zr	92.3	85.5	87.7	78.3	83.0	80.9	82.2	84.9	82.8	122.3
Ti/Y	242	232	294	263	257	267	271	270	384	485
Ti/V	22.4	21.3	29.3	29.7	27.9	24.3	24.5	23.1	18.4	61.0
Ti/Sc	240	234	359	401	369	258	267	232	158	595
V/Zr	4.13	4.01	2.99	2.64	2.98	3.33	3.36	3.68	4.50	2.00
Sc/Zr	0.385	0.366	0.245	0.196	0.225	0.314	0.308	0.366	0.524	0.205
Zr/Nb	26.5	28.5	33.9	32.6	22.4	21.4	28.2	18.7	20.3	19.5
Zr/Y	2.62	2.71	3.35	3.36	3.10	3.30	3.30	3.18	4.63	3.96
Nb/Y	0.099	0.095	0.099	0.103	0.139	0.154	0.117	0.170	0.228	0.203
Mg#	46.9	45.7	46.8	53.3	45.3	49.5	47.5	43.8	65.2	70.2

(GH20, GH25) range in composition from subcalcic augite to endiopside. This range is similar to that of Munro Township clinopyroxenes (Arndt et al., 1977), except for a wider range in FeO contents and somewhat lower Al_2O_3 contents in the Kromberg pyroxenes. The observed range in clinopyroxene compositions is compatible with crystallization from a magma of basaltic composition.

Chemical alteration

The Barberton rocks have been subjected to greenschist-facies metamorphism (Viljoen, R. P., and Viljoen, 1969), surface weathering, and perhaps seawater alteration and hydrothermal metasomatism (Smith et al., 1984; Duchac and Hanor, 1987; Hanor and Duchac, 1990). It is difficult to assess the chemical changes resulting from metamorphism and alteration. Most studies of effects of alteration on the geochemistry of basalts (Hart et al., 1974; Condie et al., 1977; Donelly et al., 1980; MacGeehan and MacLean, 1980; Smith et al., 1984) conclude that concentrations of some or all of the elements such as K, Na, Sr, Rb, Zn, Cu, and Ba may have been significantly changed while elements such as Zr, Ti, Y, Nb, and P tend to be rather immobile (Pearce and Cann, 1973), and their relative concentrations in the altered rocks reflect those at the time of crystallization. The immobility of these elements in rocks of the Kromberg Formation is suggested by a comparison of their relative con-

TABLE 1. MAJOR (WT%) AND TRACE ELEMENT (PPM) DATA AND INTERELEMENT RATIOS FOR ROCKS FROM THE KROMBERG FORMATION

	Tholeiites									
	GH04	GH05	GH09	GH10	GH11	GH14	GH16	GH17	GH18	GH21
SiO_2	50.73	51.71	53.86	55.65	62.31	60.89	57.34	51.21	53.98	50.06
TiO_2	1.47	1.43	1.61	1.67	1.56	1.41	1.40	1.31	1.05	3.21
Al_2O_3	14.75	14.39	15.24	15.35	14.30	14.27	15.50	15.58	16.06	13.90
Fe_2O_3	15.50	14.65	13.72	12.98	7.72	9.50	10.08	13.46	8.38	9.30
MnO	0.20	0.18	0.17	0.17	0.16	0.15	0.18	0.20	0.17	0.15
MgO	6.10	5.49	5.37	6.59	2.84	4.14	4.05	4.66	6.98	9.77
CaO	8.86	9.12	7.42	4.85	5.75	5.43	6.67	9.32	6.34	10.16
Na_2O	2.14	2.66	2.28	1.94	3.20	3.77	4.21	3.83	2.03	2.82
K_2O	0.08	0.20	0.16	0.61	1.97	0.28	0.40	0.28	4.94	0.37
P_2O_5	0.17	0.17	0.17	0.91	0.19	0.16	0.17	0.15	0.07	0.26
Total	100.00	100.00	100.00	100.00	100.00	100.00	100.00	100.00	100.00	100.00
H_2O-	0.06	0.10	0.08	0.08	0.18	0.06	0.09	0.05	0.07	0.09
LOI	2.72	2.34	3.40	4.90	4.81	3.22	2.20	2.06	3.54	2.84
Orig. Total	99.81	100.03	100.27	99.82	99.48	99.26	99.11	100.38	100.00	99.84
Nb	3.6	3.5	3.2	3.9	5.0	4.9	3.6	4.9	3.8	8.1
Zr	95	100	110	128	113	105	102	92	76	157
Y	36	37	33	38	36	32	31	29	16	40
Sr	137	141	186	98	130	68	80	106	94	73
Rb	2.1	4.6	3.6	16	40	5.7	6.4	5.2	81	5.7
Ba	11	33	25	64	127	36	22	23	333	59
Sc	37	37	27	25	25	33	31	34	40	32
Zn	127	117	131	98	146	95	98	87	93	70
Cu	131	168	200	109	179	156	3.6	84	6.2	233
Ni	133	116	83	76	110	43	51	66	158	216
Co	65	56	47	44	57	39	39	50	73	60
Cr	139	118	129	104	95	12	13	46	369	351
V	393	401	329	338	335	348	344	340	342	315
CaO/Al_2O_3	0.601	0.634	0.487	0.316	0.402	0.380	0.430	0.598	0.395	0.731
Al_2O_3/TiO_2	10.1	10.1	9.5	9.2	9.2	10.1	11.0	11.9	15.3	4.3
MgO/TiO_2	4.16	3.85	3.33	3.94	1.82	2.94	2.89	3.56	6.64	3.04
CaO/TiO_2	6.05	6.40	4.60	2.90	3.69	3.84	4.75	7.11	6.03	3.16
TiO_2/P_2O_5	8.83	8.48	9.51	8.91	8.01	8.74	8.49	9.00	14.67	12.30
Ti/Nb	24.5	24.4	29.8	25.5	18.6	17.3	23.2	15.9	16.8	23.9
Ti/Zr	92.3	85.5	87.7	78.3	83.0	80.9	82.2	84.9	82.8	122.3
Ti/Y	242	232	294	263	257	267	271	270	384	485
Ti/V	22.4	21.3	29.3	29.7	27.9	24.3	24.5	23.1	18.4	61.0
Ti/Sc	240	234	359	401	369	258	267	232	158	595
V/Zr	4.13	4.01	2.99	2.64	2.98	3.33	3.36	3.68	4.50	2.00
Sc/Zr	0.385	0.366	0.245	0.196	0.225	0.314	0.308	0.366	0.524	0.205
Zr/Nb	26.5	28.5	33.9	32.6	22.4	21.4	28.2	18.7	20.3	19.5
Zr/Y	2.62	2.71	3.35	3.36	3.10	3.30	3.30	3.18	4.63	3.96
Nb/Y	0.099	0.095	0.099	0.103	0.139	0.154	0.117	0.170	0.228	0.203
Mg#	46.9	45.7	46.8	53.3	45.3	49.5	47.5	43.8	65.2	70.2

centrations in Kromberg rocks to those in unaltered Archean tholeiites and more recent basalts (Arndt et al., 1977; Nisbet et al., 1977; Jolly, 1980; Erlank and Reid, 1974). In addition, when plotting Kromberg tholeiites in the Ti-Y-Zr diagram of Pearce and Cann (1973), little scatter is displayed (Fig. 2), and incompatible element plots (Figs. 3 and 4) show consistent, well-defined trends. Furthermore, a careful choice of rocks having low carbonate contents (Hynes, 1980) can minimize the effects, if any, of carbonate alteration on Ti, Y, Zr, Nb, and P. The immobile elements Ti, P, Zr, Y, and Nb can therefore be used to estimate the mobility of other elements by plotting immobile-element abundances against those of other major and trace elements. For most elements the trends obtained are consistent with igneous fractionation trends. For some elements, such as Si, Fe, Na, K, Rb, Ba, Zn, and Cu, there is a large scatter about the trends. Hence these elements are considered to have been mobile (Condie et al., 1977; Smith et al., 1984; Lécuyer et al., 1994), and they are not used in the petrogenetic modeling.

If mobile element concentrations depart significantly from magmatic values, then absolute immobile element abundances are likely to vary significantly from original magmatic values through either dilution or concentration effects. For such rocks, it is necessary to use ratios of the immobile elements to infer petrogenetic relationships. Although high field strength elements (HFSE) and rare earth elements (REE) generally appear to be immobile during alteration in komatiitic as well as basaltic rocks, some recent studies suggest that this is not always the case (Gruau et al., 1990, 1992; Lécuyer et al., 1994; Lahaye et al., 1995).

TABLE 1. MAJOR (WT%) AND TRACE ELEMENT (PPM) DATA AND INTERELEMENT RATIOS FOR ROCKS FROM THE KROMBERG FORMATION (CONTINUED, p. 3)

	Tholeiites					Komatiites				
	GH46	GH47	GH48	GH49	GH50	GH24	GH25	GH33	GH34	GH35
SiO_2	58.95	53.62	50.31	52.12	54.00	50.07	48.10	48.80	46.19	46.82
TiO_2	1.58	1.11	1.10	1.21	1.15	0.45	0.50	0.48	0.68	0.52
Al_2O_3	15.75	13.47	13.31	14.72	14.87	5.72	6.54	6.91	8.86	8.07
Fe_2O_3	11.63	12.66	12.91	14.55	14.16	12.15	12.79	13.77	13.70	13.47
MnO	0.15	0.20	0.22	0.20	0.19	0.18	0.14	0.25	0.24	0.22
MgO	4.58	7.46	9.53	6.26	3.57	21.93	22.40	20.51	22.67	23.01
CaO	2.83	9.11	9.14	7.26	8.54	9.44	9.47	9.20	7.58	7.82
Na_2O	3.82	1.82	0.09	3.25	2.07	<0.02	<0.02	0.02	<0.02	<0.02
K_2O	0.55	0.42	3.26	0.29	1.32	0.00	0.00	0.00	0.00	0.00
P_2O_5	0.16	0.13	0.13	0.14	0.13	0.06	0.06	0.06	0.08	0.07
SubTotal	100.00	100.00	100.00	100.00	100.00	100.00	100.00	100.00	100.00	100.00
H_2O-	0.15	0.11	0.08	0.05	0.05	0.11	0.32	0.08	0.08	0.17
LOI	4.13	5.98	2.72	2.24	5.14	4.95	5.00	4.69	5.98	6.14
TOTAL	99.47	99.79	100.28	99.50	99.67	99.35	99.73	99.92	100.01	100.00
Nb	4.7	4.2	2.6	3.3	4.0	<2.0	<2.0	2.2	<2.0	<2.0
Zr	118	94	93	88	90	28	27	34	51	36
Y	28	29	30	29	28	8.8	9.7	13	19	14
Sr	44	135	182	158	285	1.8	4.0	8.7	6.1	11
Rb	7.5	9.6	74	6.2	28	<1.8	<1.8	<1.8	<1.8	<1.7
Ba	63	43	333	19	121	13	7.5	46	32	56
Sc	35	44	44	37	31	29	26	28	38	34
Zn	126	91	92	105	111	73	59	88	95	89
Cu	135	95	82	65	69	31	256	67	36	59
Ni	103	158	180	75	38	1925	1672	892	713	1240
Co	59	68	64	64	66	129	150	101	93	112
Cr	18	270	307	40	9.7	4625	4685	2465	1962	3226
V	363	294	300	300	292	162	182	163	229	188
CaO/Al_2O_3	0.180	0.677	0.687	0.494	0.574	1.649	1.448	1.332	0.855	0.969
Al_2O_3/TiO_2	10.0	12.1	12.1	12.2	12.9	12.7	13.0	14.4	12.9	15.7
MgO/TiO_2	2.90	6.70	8.66	5.18	3.11	48.76	44.42	42.80	33.11	44.63
CaO/TiO_2	1.79	8.19	8.31	6.00	7.43	20.99	18.78	19.20	11.07	15.16
TiO_2/P_2O_5	9.57	8.34	8.18	8.91	8.76	7.44	8.81	7.86	8.35	7.92
Ti/Nb	20.3	16.0	25.6	22.2	17.2	<13.4	<15.3	12.9	<20.4	<15.8
Ti/Zr	80.4	71.2	70.9	82.5	76.8	98	113.6	84.5	81.1	86
Ti/Y	336	230	223	247	242	308	312	218	215	214
Ti/V	26.0	22.7	22.0	24.1	23.6	16.6	16.6	17.7	17.9	16.4
Ti/Sc	271	151	149	197	223	92	117	101	107	91
V/Zr	3.09	3.14	3.23	3.42	3.25	5.90	6.85	4.79	4.52	5.24
Sc/Zr	0.297	0.473	0.476	0.418	0.345	1.061	0.972	0.837	0.757	0.944
Zr/Nb	25.3	22.5	36.1	26.9	22.4	<13.7	<13.5	15.3	<25.1	<18.4
Zr/Y	4.17	3.23	3.15	3.00	3.16	3.14	2.75	2.58	2.65	2.49
Nb/Y	0.165	0.143	0.087	0.112	0.141	<0.229	<0.204	0.169	<0.105	<0.135
Mg#	46.9	57.0	62.4	49.2	36.2	80.2	79.7	77.0	78.8	79.3

Geochemical classification of Kromberg igneous rocks

As Archean greenstone belt lithologies are almost invariably altered, the classification of tholeiitic and komatiitic suites of rocks is based largely on chemical criteria. Diagnostic chemical features of rocks from the komatiitic series include (i) MgO > 18% (Arndt and Nesbitt, 1982) and (ii) TiO_2 < 1% (Jahn et al., 1980). In addition, the diagram devised by Jensen (1976) clearly separates rocks belonging to komatiitic and tholeiitic series (Fig. 5). Inspection of the chemical data for rocks of the Kromberg Formation (Table 1 and Figs. 5, 6, 7, and 8) indicates the existence of komatiitic and tholeiitic volcanic suites and their cumulates.

Komatiitic rocks

Komatiitic rocks analyzed in this study exhibit a small compositional range for most of the major elements (Fig. 6). However, the restricted range in the MgO content (19.8–23.1% volatile free) is in sharp contrast to the compositional range of Cr, Ni (1,960–4,685 ppm and 713–1,925 ppm, respectively; Fig. 7), Co, and Sc, all of which are generally compatible elements in mafic-ultramafic systems. These large compositional ranges of the compatible elements also contrast to the more restricted ranges of Zr (Fig. 8) and Y content.

In Table 3 some average interelement ratios of the Kromberg komatiites and tholeiites are compared to those of chondrites and MORB. Interelement ratios may assist in the

TABLE 1. MAJOR (WT%) AND TRACE ELEMENT (PPM) DATA AND INTERELEMENT RATIOS FOR ROCKS FROM THE KROMBERG FORMATION (CONTINUED, p. 4)

	Komatiites		Cumulates				Evolved Tholeiites		
	GH51	GH52	GH27	GH28	GH103	GH55	GH43	GH53	GH26
SiO_2	49.79	48.95	52.18	51.37	53.05	54.35	66.13	60.89	62.76
TiO_2	0.50	0.63	0.36	0.56	0.78	0.43	1.45	1.70	0.34
Al_2O_3	6.74	6.70	3.37	5.79	10.67	4.70	13.63	12.46	19.08
Fe_2O_3	14.06	13.06	13.29	16.31	12.87	12.15	8.99	11.43	3.56
MnO	0.22	0.22	0.27	0.28	0.19	0.22	0.09	0.18	0.11
MgO	19.87	21.31	15.09	10.92	9.78	14.34	3.73	4.25	2.76
CaO	8.75	9.03	15.02	13.28	10.43	12.30	1.34	5.88	7.34
Na_2O	<0.02	0.03	0.36	1.40	1.77	1.44	3.61	2.66	1.47
K_2O	0.00	0.00	0.01	0.03	0.37	0.02	0.73	0.01	2.52
P_2O_5	0.07	0.07	0.05	0.06	0.09	0.05	0.30	0.54	0.06
SubTotal	100.00	100.00	100.00	100.00	100.00	100.00	100.00	100.00	100.00
H_2O-	0.11	0.10	0.07	0.08	0.09	0.08	0.07	0.09	0.15
LOI	4.54	4.94	1.62	1.01	1.87	1.10	2.41	4.51	8.59
TOTAL	99.93	99.91	100.65	100.54	100.10	100.12	99.28	99.97	100.57
Nb	2.2	2.5	<2.1	<2.1	<2.0	<2.0	9.8	17	1.7
Zr	43	41	18	28	57	26	227	295	25
Y	14	14	9.7	14	21	10.0	42	86	18
Sr	4.9	8.5	13	57	113	30	27	145	75
Rb	<1.8	<1.8	<1.9	<1.9	9.0	<1.8	9.6	<1.7	82
Ba	4.2	27	32	37	37	11	63	6.2	226
Sc	31	30	45	51	46	38	22	19	58
Zn	85	86	97	105	79	89	153	92	69
Cu	17	116	119	130	158	12	56	12	25
Ni	1199	1655	336	196	143	275	26	<1.9	162
Co	122	118	85	90	72	75	33	31	62
Cr	4191	3248	659	75	285	980	<1.9	<2.2	717
V	188	186	178	294	273	170	97	132	258
CaO/Al_2O_3	1.298	1.347	4.458	2.295	0.978	2.615	0.098	0.472	0.385
Al_2O_3/TiO_2	13.4	10.6	9.4	10.3	13.7	10.9	9.4	7.3	56.3
MgO/TiO_2	39.60	33.70	41.94	19.36	12.55	33.23	2.57	2.50	8.16
CaO/TiO_2	17.43	14.27	41.75	23.54	13.38	28.49	0.92	3.45	21.67
TiO_2/P_2O_5	7.24	8.95	7.91	9.67	9.11	8.21	4.89	3.13	5.36
Ti/Nb	13.8	15.0	<10.3	<15.8	<23.8	<12.9	8.9	6.0	11.7
Ti/Zr	70.3	91.5	118.4	123.0	81.7	100.7	38.2	34.6	80.3
Ti/Y	216	265	223	250	219	260	208	119	111
Ti/V	16.0	20.4	12.1	11.5	17.1	15.3	89.8	77.1	7.9
Ti/Sc	97	126	48	66	101	67	398	545	35
V/Zr	4.39	4.49	9.75	10.69	4.77	6.60	0.43	0.45	10.19
Sc/Zr	0.724	0.726	2.483	1.856	0.809	1.497	0.096	0.063	2.305
Zr/Nb	19.7	16.4	<8.7	<12.8	<29.1	<12.8	23.3	17.5	14.6
Zr/Y	3.08	2.89	1.89	2.04	2.67	2.58	5.44	3.44	1.38
Nb/Y	0.156	0.177	<0.218	<0.158	<0.092	<0.201	0.234	0.197	0.095
Mg#	76.1	78.6	71.8	60.1	63.1	72.6	48.2	45.6	63.5

TABLE 2. AVERAGE ELECTRON MICROPROBE ANALYSES OF CLINOPYROXENES FROM SOME IGNEOUS ROCKS OF THE KROMBERG FORMATION

	GH04	GH21	GH100	GH20	GH25	GH28	GH103
Number	1	5	5	5	3	5	4
SiO_2	52.14	52.30	51.24	52.57	53.21	51.76	52.01
TiO_2	0.28	0.23	0.60	0.71	0.23	0.24	0.37
Al_2O_3	1.59	1.69	1.94	2.05	1.90	1.33	1.77
Cr_2O_3	0.62	0.53	0.05	0.90	0.88	ND	0.11
FeO	5.90	6.37	12.30	5.25	5.48	11.98	9.77
MnO	0.27	0.22	0.25	0.19	0.18	0.26	0.23
MgO	16.86	16.76	14.66	17.80	17.54	15.23	16.01
CaO	21.34	21.02	19.07	20.66	20.13	18.36	19.05
Na_2O	0.21	0.15	0.23	0.24	0.17	0.19	0.16
Total	99.21	99.29	100.34	100.37	99.72	99.35	99.48
Cation Proportions Calculated on the Basis of 6 Oxygens							
Si	1.936	1.940	1.923	1.921	1.949	1.953	1.943
Ti	0.008	0.007	0.017	0.020	0.006	0.007	0.011
Al	0.070	0.074	0.086	0.089	0.082	0.060	0.047
Cr	0.018	0.016	0.001	0.026	0.026	ND	0.003
Fe	0.183	0.198	0.386	0.161	0.168	0.378	0.306
Mn	0.008	0.007	0.008	0.006	0.005	0.009	0.008
Mg	0.933	0.927	0.820	0.960	0.957	0.856	0.891
Ca	0.849	0.835	0.767	0.810	0.790	0.743	0.763
Na	0.015	0.013	0.016	0.017	0.012	0.014	0.011
Sum	4.020	4.017	4.024	4.010	3.995	4.020	3.983

Notes: GH04, GH21, GH100 are tholeiitic rocks; GH20, GH25 are komatiitic rocks; GH28, GH103 are cumulates.

recognition of komatiites formed by the crystallization of high-Mg magmas and also provide a means of interpreting subtle differences in source compositions that may exist during the production of these magmas (Nesbitt and Sun, 1976; Sun and Nesbitt, 1977; Jahn et al., 1982; Smith and Erlank, 1982). Thus, close to chondritic Ti/Zr, Zr/Nb, and Zr/Y ratios of ultramafic rocks have been taken to suggest crystallization of these rocks from melts produced by large amounts of partial melting of a "chondritic-type" Archean mantle (Nesbitt and Sun, 1976). CaO/Al_2O_3, Al_2O_3/TiO_2, and CaO/TiO_2 ratios that are respectively higher, lower, and similar to those of chondrites are typical for a large group of komatiites from the underlying Komati Formation (Smith and Erlank, 1982). This depletion in Al relative to Ca and Ti, in rocks representative of primary melt compositions, has been interpreted to be the result of high-temperature melting of primitive mantle composition with garnet as a residual phase (Gruau et al., 1990).

Of the komatiites analyzed in this study, only sample GH34 is considered representative of liquid compositions, while all the other komatiites have textures consistent with originally porphyritic rocks. GH34 has close to chondritic CaO/Al_2O_3, TiO_2/P_2O_5 ratios, but lower CaO/TiO_2, Al_2O_3/TiO_2, Ti/Zr, and Ti/Y with higher Zr/Y ratios relative to those for chondrites. In part, these interelement ratios are unlike those for the komatiites from the Komati Formation (Smith and Erlank, 1982), implying a different petrogenesis for the Kromberg rocks. It is interesting to note the similarity in all interelement ratios, except for those involving Y and Sc, between the komatiite GH34 and the low-fractionated tholeiite end members (T1; Table 3).

Tholeiites and associated rocks

Inspection of the major and trace element variation diagrams (Figs. 2–8) allows recognition of several distinct end members, which are described below:

Tholeiites. Considering the range in MgO and SiO_2 compositions (3.6–9.8% MgO and 50.0–55.7% SiO_2), the massive

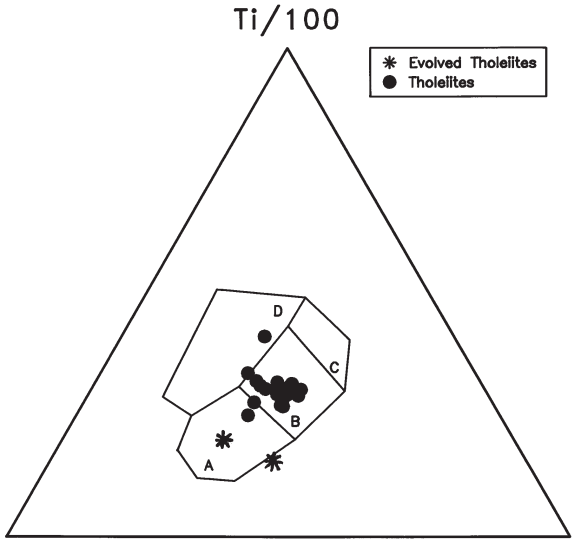


Figure 2. Zr-Ti/100-Y*3 diagram for the Kromberg tholeiites (after Pearce and Cann, 1973). A, low K-tholeiites; B, ocean flood basalts; C, calc-alkaline basalts; D, continental basalts.

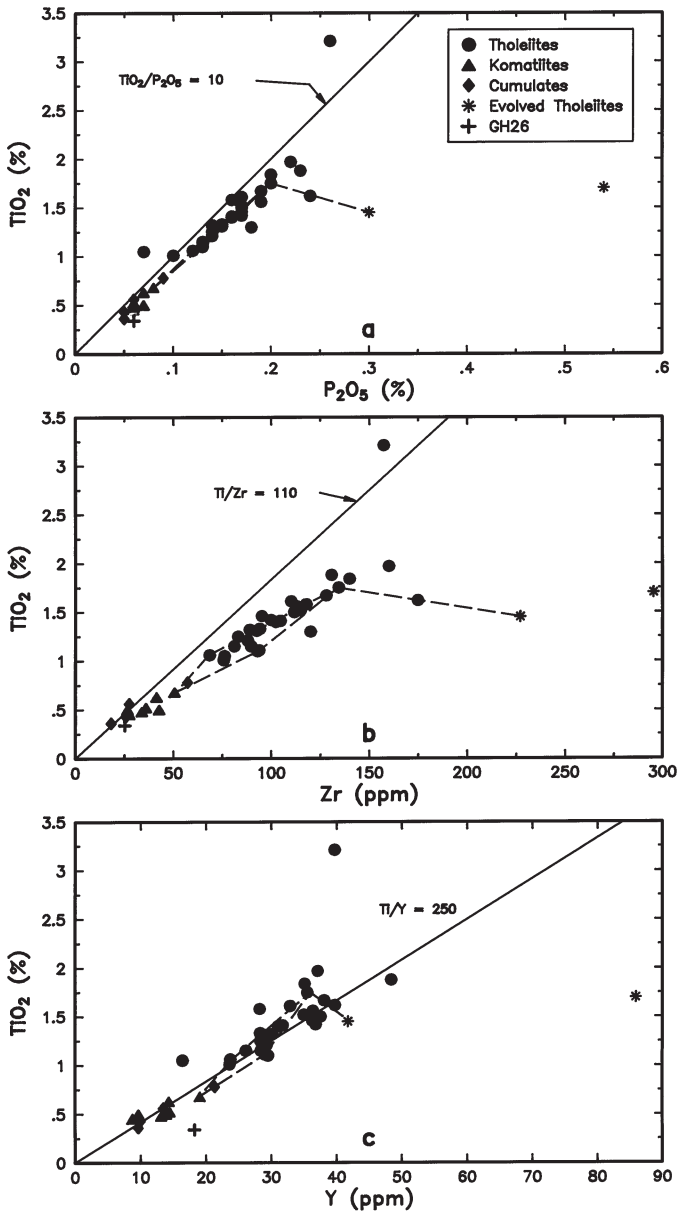


Figure 3. TiO_2 variation with P_2O_5 (a), Zr (b), and Y (c) for volcanic rocks of the Kromberg Formation. Rocks representative of melt compositions are joined by dashed lines. Chondritic-incompatible interelement ratios are indicated by the solid lines.

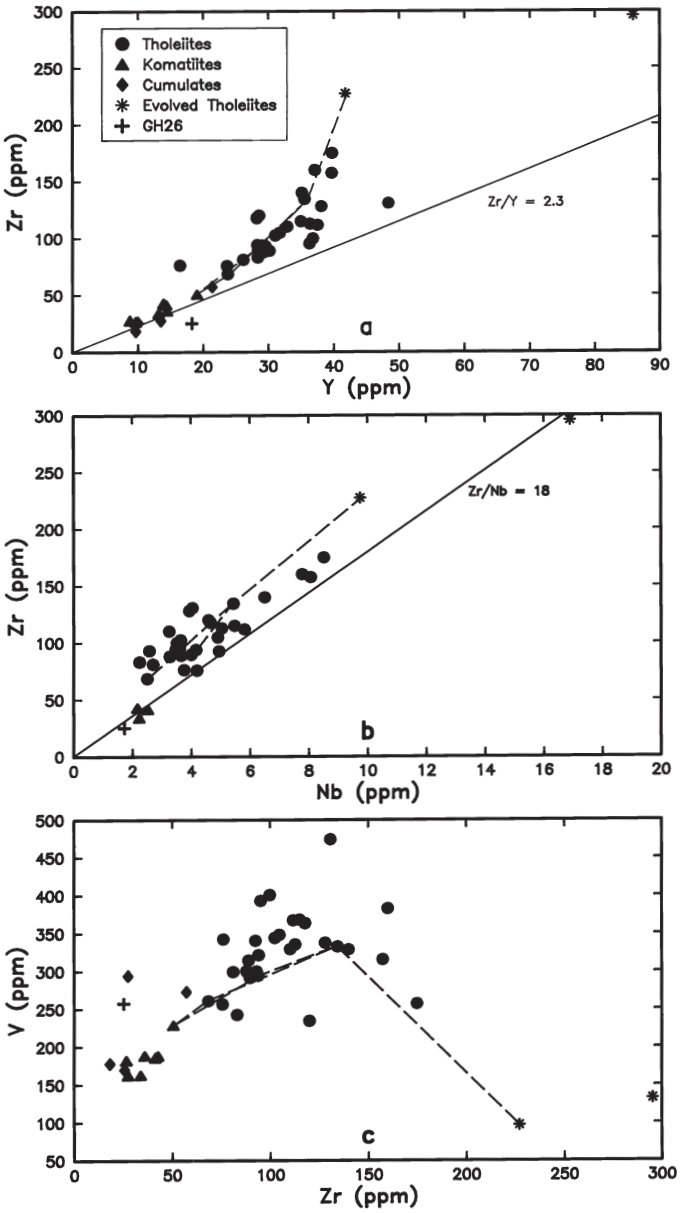


Figure 4. Zr variation with Y (a), Nb (b), and V (c) for volcanic rocks of the Kromberg Formation. Rocks representative of melt compositions are joined by dashed lines. Chondritic-incompatible interelement ratios are indicated by the solid lines in a and b.

rocks in this study correspond to basaltic or gabbroic compositions. The samples analyzed from pillowed units or pillow breccias (GH11, 14, 16, 18, 46, 48) generally have somewhat higher SiO_2, Na_2O, and K_2O and lower FeO, MgO, and CaO content compared to the massive rocks (Fig. 1 and Table 1). This difference in composition may be related to a combination of crystal fractionation and alteration processes. Both of these processes presumably contributed to the scatter shown by the rocks in major element variation diagrams (Fig. 6). In terms of trace elements, Figure 7 illustrates that the Ni and Cr content varies systematically with MgO content, both Ni and Cr decreasing exponentially with decreasing MgO content. Systematic variations also exist for immobile elements such as Ti, P, Zr, Y, and Nb (Figs. 3 and 4). Interelement ratios of TiO_2/P_2O_5, Ti/Y, and, for the low-fractionated tholeiitic end members, Zr/Y and Ti/Zr are similar to those for the komatiitic rocks of the Kromberg Formation (Table 3, and Figs. 3 and 4).

The overall major and trace element chemistry of the Kromberg tholeiites compares well with that for tholeiites or basalts in other greenstone belts (Condie and Harrison, 1976; Nesbitt and Sun, 1976; Arndt et al., 1977; Nisbet et al., 1977; Jolly, 1980; Barley et al., 1984), except for somewhat higher con-

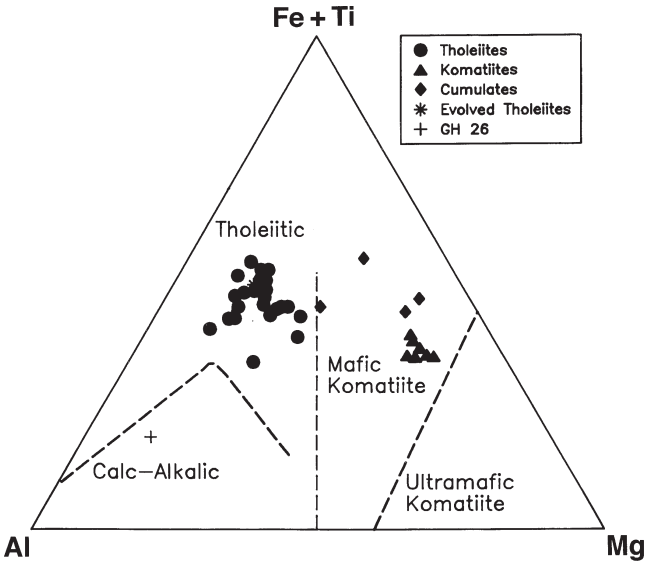


Figure 5. (Fe+Ti)-Al-Mg cation plot for volcanic rocks of the Kromberg Formation. Field boundaries adapted from Jensen (1976).

centrations of SiO_2, K_2O, Na_2O, and Rb in the Kromberg rocks. This characteristic enrichment is considered to be the result of postdepositional metasomatism (Condie et al., 1977; Smith et al., 1984; Duchac and Hanor, 1987) and is reflected by the SiO_2, Na_2O, K_2O, and Rb-rich nature of the samples analyzed from the pillow units and pillow breccias (Fig. 1 and Table 1). The SiO_2 enrichment results in the majority of the Kromberg tholeiites being quartz-normative, whereas only 6 out of 25 tholeiites are olivine normative.

Tholeiitic cumulates. The cumulate nature of some of the rocks is suggested by their texture, mineralogy, and geochemistry (Table 1, Figs. 6, 7 and 8). Relative to the tholeiites, these rocks are characterized by low Al_2O_3, TiO_2, P_2O_5, and Zr, but higher CaO, MgO, Cr, Ni, and Sc. Figures 6 and 7 leave little doubt that these rocks formed largely as partial cumulates of clinopyroxene derived from the tholeiites. In addition to clinopyroxene, partial but minor accumulation of a magnesian phase poor in CaO is suggested from a comparison of the clinopyroxene chemistry measured in the cumulates (Table 2; GH28) to the chemistry of the most magnesian cumulate rocks (GH27 and GH55). Such a CaO-poor but MgO-rich phase could well have been olivine or orthopyroxene. The relatively high Cr content in clinopyroxenes of the tholeiitic rocks (Table 2) makes it unnecessary to invoke chromite accumulation during their formation.

Evolved tholeiites. The highly evolved end members of the tholeiitic suite include samples GH43 and GH53. These rocks are quartz normative and have high Nb, Zr, and Y concentrations, but low concentrations of compatibles such as Cr, Ni, Co, Sc, and V (Table 1; Figs. 3, 4, and 8). Also characteristic are slightly lower TiO_2 content compared to tholeiites of similar Mg# (Fig. 6). Despite these differences in trace element content, samples GH43 and GH53 plot in close association with the tholeiitic suite rocks in several major element variation diagrams (Figs. 5 and 6). These samples are, therefore, interpreted to have crystallized from highly evolved tholeiitic magmas, rather than representing a separate calc-alkaline basaltic magma series (Condie and Harrison, 1976; Jolly, 1980; Barley et al., 1984).

Sample GH26. This was collected from an outcrop that is classified, according to Viljoen, M. J., and Viljoen (1969a), as an acid to intermediate rock. This relatively light colored rock shows a fine-grained assemblage of quartz, albite, and sphene with only minor actinolite. It has high SiO_2, Al_2O_3, K, Rb, and Ba and low Fe_2O_3 (total), MgO, TiO_2, Nb, and Zr. In contrast to its low MgO content, it has a fairly high content of Cr, Ni, Co, V, and Sc, which is not readily explained by alteration alone. It is possible that this sample was derived from a magma distinctly different from that of the other rocks considered in this study. This sample will not be discussed further.

DISCUSSION

The interbedding and lateral interfingering of komatiites and tholeiitic or komatiitic basalts has led to a number of different conclusions regarding the petrogenesis of these mixed volcanic suites. Arth et al. (1977), Arndt (1977), and Green (1981) suggest sequential mantle melting models. According to these authors, first-generation komatiitic magmas would require about 50–80% partial melting of the mantle source. The low viscosities of magnesian melts and their low densities relative to the source rocks would inhibit their accumulation and one-stage separation in large quantities. Thus, low-degree melts of basaltic or picritic compositions would separate first, leaving a peridotitic residue containing a small amount of trapped liquid. Subsequent melting of the residue would produce komatiite magmas.

An alternative model has been proposed by Nisbet and Chinner (1981) for interlayered komatiite and komatiitic basalt. In this model, the basalts are derived from komatiite magmas by high-level fractionation within a transient magma chamber. Owing to their lower density (Huppert and Sparks, 1981), only the basalts will be erupted. If a new pulse of komatiite melt enters a preexisting magma chamber, rapid thermal exchange occurs between the new high-density magma pulse and the evolved earlier melts. This thermal exchange is not accompanied by chemical exchange because of the low diffusivity of the major components (Huppert and Sparks, 1981). Komatiite magmas can only be erupted if no magma chamber exists, that is, during periods of higher regional stress. The resultant erupted sequence of rocks will therefore include some minor unfractionated parental melts, with a predominance of more evolved basaltic rocks (Nisbet and Chinner, 1981). However, from detailed analysis of komatiites, komatiitic basalts, and tholeiites in Munro Township, Canada, Arndt and Nesbitt (1982, 1984) conclude that these rocks were derived from separate magma types, each derived from distinctive mantle sources or from the same source under different partial melting or high-pressure fractionation conditions. Similarly, Jahn et al. (1980) concluded

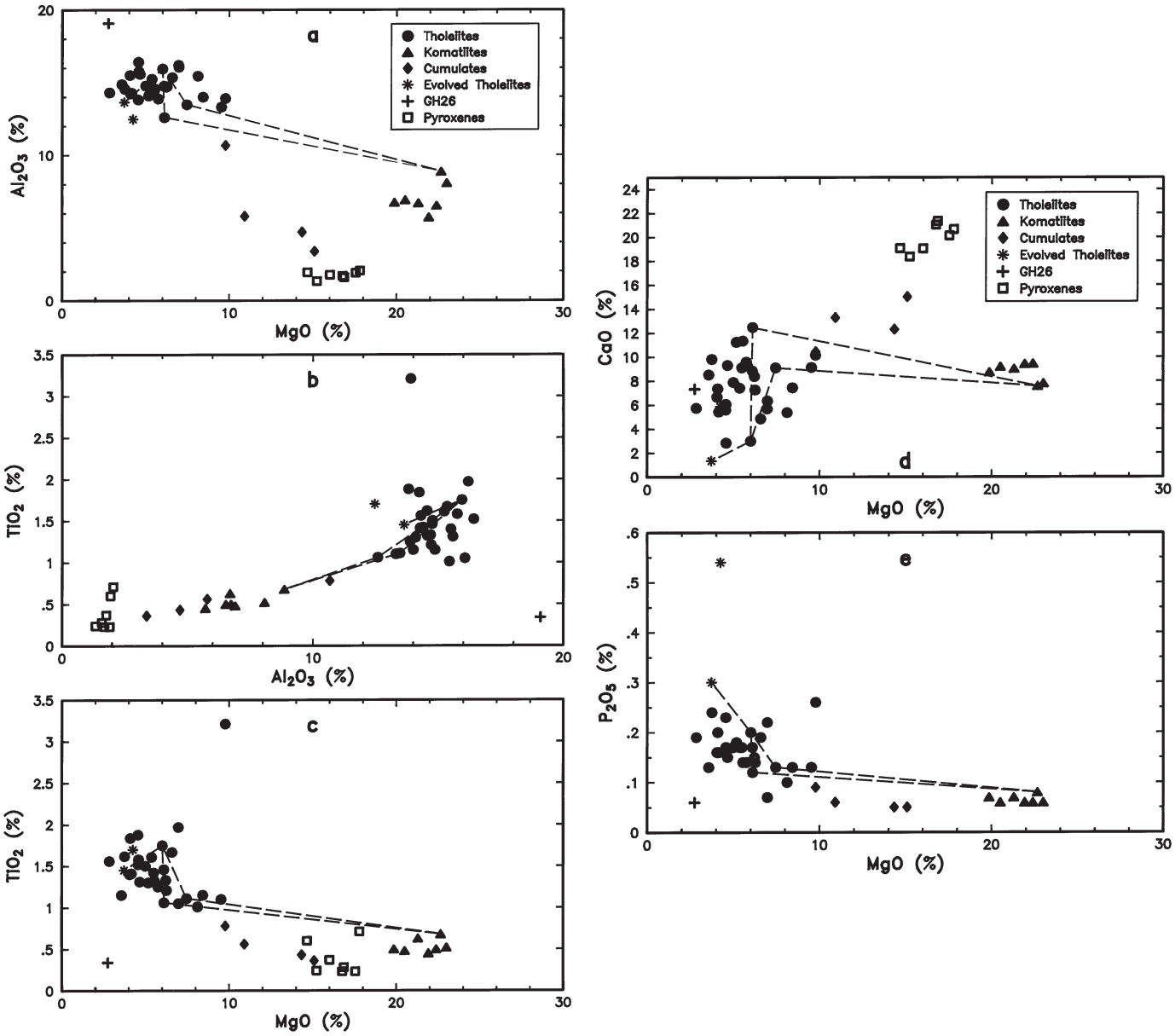


Figure 6. Major element variation diagrams for volcanic rocks of the Kromberg Formation. Rocks representative of melt compositions are joined by dashed lines.

that the komatiitic and tholeiitic series in Finnish greenstone belts do not have a clear genetic relationship.

The close spatial association between the rocks of komatiitic and tholeiitic compositions in the type section of the Kromberg Formation suggest that they were derived from either (1) two separate parental magmas that used the same plumbing system but may or may not have had compositionally similar sources, or (2) a single parental magma source and the two series are related to each other by crystal fractionation processes.

In evaluating these two alternatives, all calculations using trace element models for crystallization are based on the Rayleigh fractionation law ($C_1/C_o = F^{(D-1)}$), while for partial melting the equation of Shaw (1970; $C_1/C_o = 1/[D+F(1-D)]$) is used. D is the bulk mineral/liquid distribution coefficient for the fractionating phase, F is the fraction of liquid in the system, C_1 and C_o represent the element concentrations in the liquid and in the original source (magma or mantle source, respectively). Distribution coefficients were selected from the literature (Irving and Frey, 1978; Hart and Davis, 1978; Pearce and Norry, 1979; Le Roex, 1980; Shervais, 1982) and are summarized in Table 4.

A fundamental assumption upon which models of fractional crystallization are based is that the trends in variation diagrams (Figs. 3 to 8) represent a liquid line of descent. Porphyritic lavas are phenocryst enriched and thus their bulk compositions can fall

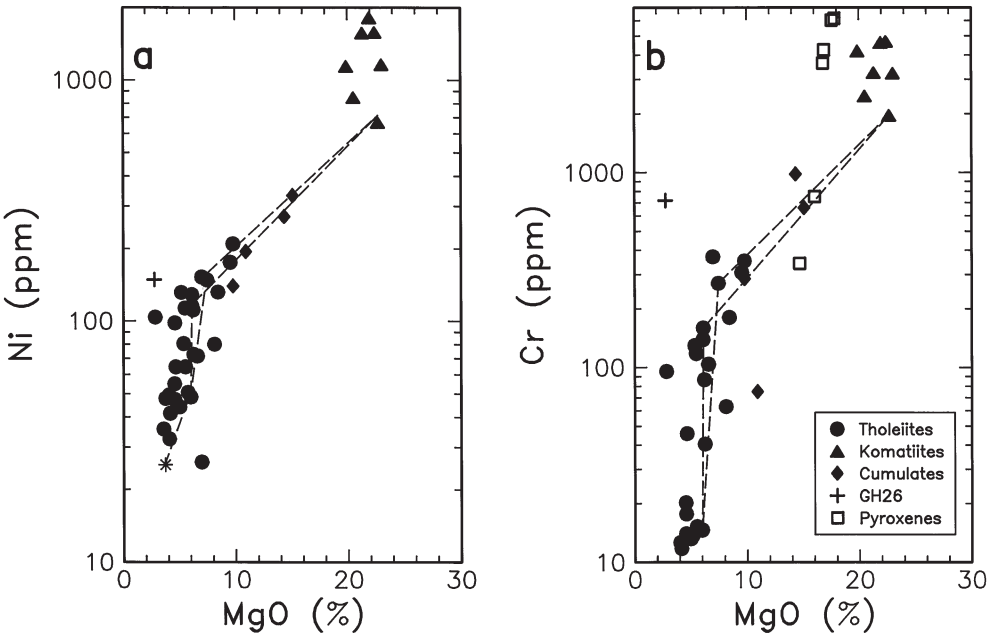


Figure 7. Ni (a) and Cr (b) variation with MgO for volcanic rocks of the Kromberg Formation. Rocks representative of melt compositions are joined by dashed lines.

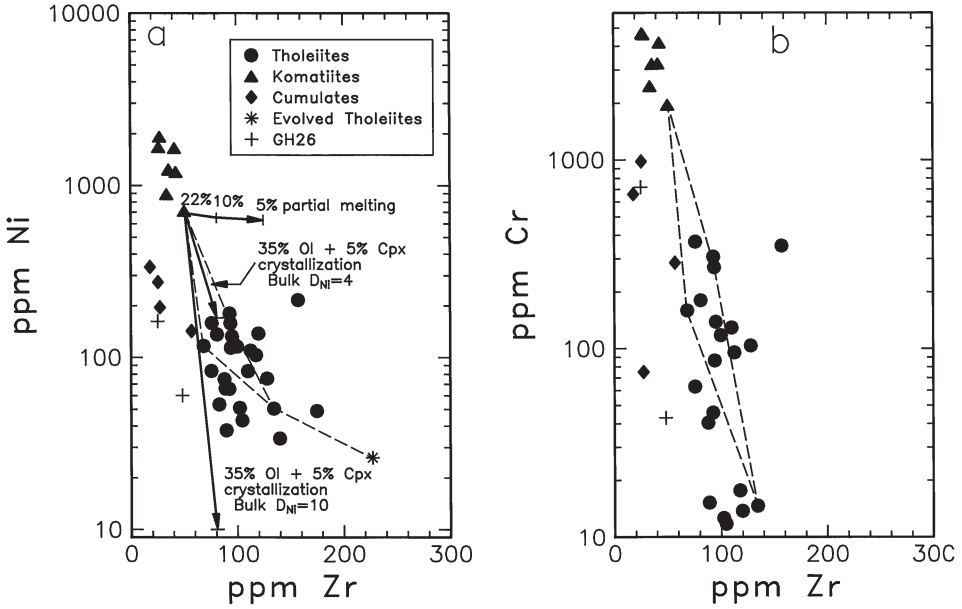


Figure 8. Variation of Ni (a) and Cr (b) with Zr for volcanic rocks of the Kromberg Formation. Rocks representative of melt compositions are joined by dashed lines. In 8a the variations of Ni and Zr for 40% crystallization of a liquid such as GH34 are shown for different bulk D_{Ni} values (solid arrows). Bulk D_{Ni} of 10 = linear mean between 5 and 17 for D_{Ni} in olivine, D_{Ni} in clinopyroxene of 1.5. Bulk D_{Ni} of 4 = D_{Ni} in olivine of 4.7 and D_{Ni} in clinopyroxene of 1.5. Also shown are the Ni and Zr variations for different degrees of partial melting (~horizontal solid arrow). See text for further discussion.

TABLE 3. AVERAGE INTERELEMENT RATIOS OF CHONDRITES, MORB, AND VOLCANIC ROCKS FROM THE KROMBERG FORMATION

	K*	T1†	T2§	Chondrite #	MORB**
CaO/Al_2O_3	0.86	0.83	0.19	0.82	0.8
Al_2O_3/TiO_2	12.9	12.0	9.1	20.4	20
CaO/TiO_2	11.0	10.0	1.7	17	17
TiO_2/P_2O_5	8.35	8.46	8.8	10	9
Ti/Zr	81	82	78	110	110
Ti/Y	215	248	295	256	NA
Ti/V	17.9	23.5	31.5	10	22
Ti/Sc	107	169	344	78	110
V/Zr	4.5	3.4	2.5	11-13	6
Sc/Zr	0.76	0.48	0.23	1.4	1
Zr/Y	2.7	3.1	3.8	2.3	3.2

* Komatiite GH34; chill zone sample.

† T1: Low fractionated basalt, average of samples GH30 and GH47; aphyric, high-Mg end members.

§ T2: High fractionated basalt, GH102; aphyric, low-Mg end member.

from Sun and Nesbitt (1977).

** from Nesbitt and Sun (1976).

TABLE 4. DISTRIBUTION COEFFICIENTS OF SELECTED TRACE ELEMENTS USED IN DISCUSSION

Element	cpx	olv	plg	mgt	opx	gar
Nb	0.2	0.01	0.01	1.0	0.01	0.1
P	0.01	0.01	0.01	0.01	0.01	0.01
Zr	0.01-0.1	0.01	0.01	0.2	0.01	0.2
Ti	0.25	0.03	0.03	15-20	0.06	0.03
Y	0.5-1.2	0.01	0.03	0.5	0.01	2-3.2
V	0.7-1.5	0.09	0.04	5-100	0.25	0.3
Sc	1.2-3.2	0.14	0.01	0.7-6	0.40	6
Cr	4.7-11.4	0.8	0.03	38	2-6	6
Ni	1.4-4.4	a	0.03	10	2-5	0.5

a = 124/MgO-0.9 (Hart and Davis, 1978).
cpx = clinopyroxene; olv = olivine; plg = plagioclase; mgt = magnetite; opx = orthopyroxene; gar = garnet.

off the liquid line of descent. Therefore, rocks chosen for the petrogenetic modeling are phenocryst free, or free of coarse-grained pseudomorphs after phenocryst phases, and are end members to the trends. In view of the possible mobility of SiO_2, Fe_2O_3, Na_2O, and K_2O, and the accompanying dilution effects on the other oxides, the choice of rocks as well as the bulk of the following discussion are based on trace elements that are reported to be stable during alteration processes, including Ti, Zr, Y, P, Ni, Cr, and Sc. Rocks considered to be representative are GH34 (chill zone sample to GH35) for the komatiites, GH30 (chill zone sample of an intrusive unit) and GH47 (fine-grained massive rock) as low-fractionated tholeiitic end members, GH102 (fine-grained massive rock) as a somewhat more fractionated end member, and GH43 (fine-grained massive rock) for the "evolved tholeiites." For the purpose of the following discussion, these rocks have been joined by lines in the major and trace element variation diagrams (Figs. 3, 4, and 6–8).

Relationship between the rocks of tholeiitic and komatiitic composition in the Kromberg Formation

Studies in both natural and experimental systems of komatiitic rocks indicate that the near-liquidus phase crystallizing from MgO-rich (~20 wt%) melts is olivine but that this is joined at lower temperatures (and therefore lower MgO contents) by clinopyroxene and chromite (Smith et al., 1980; Arndt, 1986). A reasonable mechanism for deriving tholeiitic rocks such as GH30 or GH47 (T1 = average of GH30 and GH47) from a rock of komatiitic composition such as GH34 could be crystal fractionation involving just these phases. The presence of clinopyroxene as a fractionating phase is confirmed by thin section and microprobe analyses in all rock types (Table 2). There is also evidence for chromite, which is now altered Ti-magnetite (with ~30 to 50 wt% Cr_2O_3). Olivine may also be assumed to have been present in the komatiites as they contain serpentine and chlorite pseudomorphs after olivine.

Taking the lines joining GH34 and GH30 or GH47 in Figure 6 to represent rough estimates of igneous fractionation lines, it becomes apparent that major element variations are consistent with a fractionation assemblage predominated by olivine, with lesser amounts of clinopyroxene. Simple mass balance calculations for MgO and CaO suggest fractionation of about 35% olivine (with an assumed MgO = 50 wt%) and about 5% clinopyroxene (see Table 2). Ni variations with MgO are also consistent with the above fractionating assemblage, provided a D_{Ni} in olivine of 5 (for MgO ~22%, Table 4) and a D_{Ni} in pyroxene of 1.5 are used. However, the D_{Ni} in olivine is considered to increase with decreasing MgO content (Hart and Davis, 1978). Using, as a minimum estimate to the Ni content in the fractionated liquid, a D_{Ni} in olivine of about 17 (for MgO ~7%), then only about 10% olivine fractionation is required. Thus, if D varies with MgO according to the equation of Hart and Davis (1978), then between 10 and 40% crystallization is required by the Ni variation between GH34 and T1. The discrepancy between the Ni and MgO results could be related to the following:

a. D_{Ni} in olivine is overestimated by the equation of Hart and Davis (1978; c.f. Smith et al., 1980),

b. the given MgO or Ni concentrations of GH34 and/or GH30, GH47 are not representative of melt compositions, or

c. the komatiites and tholeiites are related to each other by partial melting processes.

When the equation of Smith et al. (1980) is used to calculate D^{Ni} in olivine (D_{Ni} in olivine = 111.33/MgO – 1.71), between 54 and 13% crystallization is required for the Ni, comparing more favorably with the 40% crystallization as required by MgO content. Since Ni is a compatible element during crystallization of mafic-ultramafic melts, the Ni concentrations in the residual liquids are very sensitive to changes in the D_{Ni} values (Fig. 8a; Arth, 1976). In view of the variations in published D_{Ni} values (Smith et al., 1980), the agreement between the amounts of crystallization as independently predicted by variations in MgO and Ni content are considered good.

Samples GH34, GH30, and GH47 have textures consistent with aphyric precursors. Possible nonrepresentative melt compositions could have been imposed on these rocks during alteration processes. Silicification of, for example, GH30 or GH47 could lead to a systematic dilution of other oxides, such as MgO, in these rocks. The result would be an overestimation in the amount

of crystallization of olivine needed to lower the MgO from about 22% to about 7%. However, independent estimates from incompatible elements such as Zr, Ti, P, and from Y are in good agreement with 40% crystallization as predicted by MgO variations. Preferential Ni mobility during alteration is considered unlikely by, amongst others, Condie et al. (1977) and Smith et al. (1980).

During partial melting relatively large differences in the amount of partial melting result in only small variations of compatible element concentrations (Ni, Cr) but in large differences of incompatible elements (Arth, 1976). The relative behavior of Ni with respect to that of Zr during melting is illustrated in Figure 8a. Assuming source mineral modes similar to those of common garnet lherzolites (i.e., olivine/orthopyroxene/clinopyroxene/garnet proportions of 64/25/5/6; Mathias et al., 1970) and a bulk distribution coefficient for Ni of 3.3 (Ds are 3.8/3/1.5/0.5 respectively), then sample GH34 can be derived from a mantle source containing 11 ppm Zr and 2,000 ppm Ni (Sun and Nesbitt, 1977; Nixon et al., 1981) by about 22% partial melting. The Ni and Zr contents obtained by lower degrees of partial melting are shown in Figure 8a. It is clear that samples GH30 and GH47 (~138 ppm Ni; T1) cannot be related to sample GH34 (713 ppm Ni) by different degrees of partial melting of the same source. Indeed, Figure 8a suggests that the variations of Ni and Zr for both the rocks of tholeiitic and of komatiitic composition are indicative of crystal fractionation rather than partial melting processes. Similarly, the Cr versus Zr variations (Fig. 8b) of Kromberg rocks imply processes of crystal fractionation. However, even when using high D_{Cr} values for both olivine and clinopyroxene, the calculated Cr contents in the residual liquid left after crystallization of 35% olivine and 5% clinopyroxene from a liquid such as GH34, is still considerably higher than that for T1. Thus, a small amount of chromite crystallization (~1–2%) is also required.

Another argument in favor of a crystal fractionation relationship between the komatiite GH34 and the tholeiites GH30, GH47 is given by the low Mg numbers of the latter samples. According to Kesson (1973), only noncumulate rocks with Mg# of 67 or higher are representative of primary magmas in equilibrium with mantle olivine. The Mg# of 57.0 for the low fractionated tholeiites thus suggests that, if these rocks truly represent melt compositions, then these melts must have undergone crystal fractionation subsequent to the separation of the parental melt from a mantle source. In addition, the similarity in all interelement ratios, except for those involving Y or Sc, between the komatiite GH34 and the low fractionated tholeiite T1 (Table 3) is consistent with a fractionation involving predominantly olivine. Differences in the interelement ratios involving Y and Sc between the komatiite and T1 are explained by additional minor clinopyroxene fractionation, since these elements are compatible in clinopyroxene (Table 4).

As an extension to the above relationship, the rocks of komatiitic composition in the Kromberg Formation may represent partial cumulates of olivine, clinopyroxene, and lesser chromite. This interpretation is in good agreement with their coarse-grained textures and is also reflected by their compatible-incompatible element relations (Fig. 8), as well as by their interelement ratios (Table 1). Furthermore, it may explain the high Cr and Ni contents of these rocks relative to other komatiitic rocks (Arndt et al., 1977; Nisbet et al., 1977; Jahn et al., 1980; Smith and Erlank, 1982).

Fractionation within the tholeiitic series

GH30 and GH47 (T1) to GH102. Melt evolution from GH30 and GH47 to GH102 by crystal fractionation requires that clinopyroxene was a major fractionating phase, with lesser amounts of plagioclase (clinopyroxene/plagioclase ~7/5; assuming plagioclase of $An_{60–70}$; e.g., Jolly, 1980). Both of these phases are consistent with thin section evidence from the porphyritic rocks. A comparison of the chemical composition of the cumulate rocks to that of the clinopyroxenes (Table 2), suggests that an additional low-CaO, high-MgO phase, such as olivine or orthopyroxene, may also have been present in the partial cumulates. Thus, in addition to clinopyroxene and plagioclase, minor olivine or orthopyroxene fractionation is also possible.

For the incompatible trace elements of Nb, Zr, P, and Ti, the concentrations in GH102 relative to those of T1 predict F values close to 0.58, that is, approximately 25% clinopyroxene and 17% plagioclase crystallization. Such a crystallization assemblage is also in agreement with the change in concentrations observed for Y, Sc, and V in these rocks, assuming D_{Cpx} values for these elements of 0.7, 2.5, and 0.9, respectively. For Ni and Cr, however, the D_{Cpx} values must be maximized ($D_{Ni} = 4$, $D_{Cr} = 11.4$) in order to obtain a reasonable agreement between the theoretical values of C_1 and those observed in GH102, suggesting the possibility of minor olivine and chromite crystallization (~1–2%) accompanying clinopyroxene and plagioclase.

In contrast to the above suggested crystallization assemblage of clinopyroxene and plagioclase with minor amounts of olivine and chromite, the tholeiitic partial cumulates tend to fall along a clinopyroxene (with minor olivine) control line (Fig. 6). The absence of plagioclase as a cumulate phase in these rocks is in disagreement with the above proposed fractionation assemblage. One possible explanation for this disagreement is that early clinopyroxene and olivine fractionation was followed by a stage of plagioclase fractionation. In this case the partial cumulates must have been formed during the early fractionation stage. The preferred alternative interpretation is the coeval precipitation of clinopyroxene, plagioclase, and minor olivine but with the plagioclase crystals removed by flotation, leaving behind partial cumulates of clinopyroxene and minor olivine (Bottinga and Weill, 1970; Cox and Mitchell, 1988).

GH102 to GH43. If the so-called "evolved rocks," such as GH43, were derived from a magma composition such as GH102 by further fractionation, then Figures 3 and 4c would indicate the fractionation of titano-magnetite in addition to clinopyroxene and plagioclase (Fig. 6). Involvement of such an additional phase is in agreement with the presence of altered oxides and sphene in some phenocryst-rich, more evolved members of the tholeiite

group. Incompatible elements such as Zr and P suggest a further 37% crystallization in order to derive GH43 from GH102. Assuming that Ti-magnetite crystallizes and that it is the major phase for the observed Ti reduction, then a D_{bulk} of 1.4 is required for 37% crystallization. This corresponds to about 7–9% of titano-magnetite, given D_{Ti} in titano-magnetite of between 20 and 15, respectively (Table 4). Similarly one can estimate the amount of clinopyroxene in addition to ~7% Ti-magnetite from the Sc data. Using D_{Sc} in clinopyroxene of 3 and D_{Sc} in Ti-magnetite of 6 then, for a fractionation of 37%, 42% clinopyroxene is obtained. The rest of the crystallization assemblage is assumed to be made up of plagioclase. Additional trace element information for V, Ni, and Y appears to be in good agreement with such a crystallization assemblage.

Possible constraints on melting models

Field and textural evidence for sample GH34 indicates that this sample represents chill zone material to the coarse-grained massive rock GH35. In the previous discussion, GH34 was therefore assumed to represent melt compositions. It is not known, however, whether this melt actually represents a primary melt composition, that is, a melt that has remained unaffected by crystal fractionation subsequent to its separation from the source. If GH34 has experienced crystal fractionation, then such fractionation was presumably olivine dominated (see above; Arndt, 1986). As long as the amount of olivine fractionation is relatively small (~10–20%), the relative concentrations of elements incompatible in olivine (expressed by the interelement ratios; Table 3) will not be affected. Fractionation of significantly more than 20% olivine is unlikely as it would imply a primary melt with >30% MgO.

In the previous section it was suggested that the Zr content in GH34 required about 22% partial melting, assuming melting of a chondritic-type mantle source (Sun and Nesbitt, 1977). For P, Ti, and V, about 26% partial melting of the same source is required. These estimates are considerably lower than the 50–80% melting suggested by Arndt (1977) for komatiitic melts derived from "undepleted" (i.e., chondritic) mantle sources. However, viscosity considerations led Arndt (1977) to suggest that komatiitic melts are derived from a "depleted" mantle, that is, a mantle source from which a previous melt has been removed. In this case, the second-stage komatiitic melt will only form a relatively small amount of melt, yet this liquid will be high in MgO, Ni, and Cr, with a relatively low incompatible element content as commonly observed for komatiites (Arndt et al., 1977; Nisbet et al., 1977; Jahn et al., 1980; Smith and Erlank, 1982). For GH34, this sequential melting model may be discounted on the basis of interelement ratios. Assuming an initial chondritic source to melting, the first-stage liquid would leave a residue that is depleted in the highly incompatible elements such as Zr and P. As the bulk D values for Zr and P are lower than those for Ti, the lower than chondritic TiO_2/P_2O_5 and Ti/Zr ratios of GH34 would argue against the derivation of GH34 from a depleted source. Similar arguments can be used for the lower than chondritic Al_2O_3/TiO_2 and CaO/TiO_2 ratios where Ti would almost certainly be more incompatible than Ca or Al.

The relatively high concentration of incompatible elements in GH34 compared to other komatiitic rocks (Jahn et al., 1980; Arndt and Nesbitt, 1984; Smith and Erlank, 1982) results in the relatively low estimated amount of partial melting required for GH34. This difference in amount of melting needed for GH34 relative to other komatiitic rocks may be explained if (1) GH34 is not representative of melt compositions, or (2) the melts were derived from distinct sources, or via different source melting conditions (e.g., pressure). If the fine-grained aphyric texture of GH34 relative to GH35 is a function of postemplacement alteration, then by analogy to the other komatiitic rocks in this study, GH34 may also represent a partial cumulate of olivine (with lesser clinopyroxene, chromite; see above). However, a simple chemical comparison between GH34 and GH35, particularly in trace elements considered to be resistant to alteration processes, such as Ti, P, Zr, Y, Ni, and Cr (Pearce and Cann, 1973; Condie et al., 1977; Smith et al., 1984), suggests that GH34 may well represent chill zone material to the phenocryst-enriched host rock GH35. Thus possibility 1 above is considered unlikely.

It is generally accepted that the bulk mantle has a garnet lherzolitic mineral assemblage and a composition similar to that of chondrites (O'Hara et al., 1975; Hawkesworth and O'Nions, 1977; Sun and Nesbitt, 1977). Table 3 lists the interelement ratios of elements largely incompatible in olivine for GH34 (and T1) and for a chondritic-type mantle. Of all the ratios shown only the CaO/Al_2O_3 ratio of GH34 is nonchondritic. Given the distribution coefficients (Table 4), the interelement ratios of GH34 (and of T1) are generally consistent with residual garnet and clinopyroxene in the source to partial melting. This is consistent with relatively small amounts of partial melting (<30%) for the parental melts to the Kromberg rocks (O'Hara et al., 1975; Mysen and Kushiro, 1977). If this parental melt is komatiitic in composition, then the relatively high incompatible element content of this melt, as suggested by a comparison of GH34 with other komatiites, may indicate melt derivation from a source enriched in incompatibles, garnet, and clinopyroxene relative to a more depleted source proposed for other komatiites (Arndt, 1977). Alternatively, it may suggest that the komatiitic parental melt to the Kromberg rocks was derived at high pressures from a garnet lherzolitic source (O'Hara et al., 1975; Mysen and Kushiro, 1977; Takahashi and Scarfe, 1985; Xie and Kerrich, 1994).

If all the Kromberg "komatiites" are considered to be of a cumulate origin, then a melt with a lower MgO content relative to GH34 may have been parental to the tholeiitic rocks. Partial accumulation of olivine (+ minor chromite and clinopyroxene) crystallizing from this melt can account for the composition of komatiitic rocks, leaving a residual melt of similar composition to T1. Interelement ratios of T1 will still require residual garnet and clinopyroxene in the source to the parental melt. No high-pressure partial melting is necessary in this case (Takahashi and Scarfe, 1985).

CONCLUSIONS

Based on chemical compositions, the rocks of the Kromberg Formation can be divided into tholeiitic and komatiitic suites. Simple chemical modeling suggests, however, that these two suites are related to each other by olivine plus minor clinopyroxene and chromite fractionation, in agreement with their close spatial association observed in the field. The preferred genetic model is similar to that proposed by Nisbet and Chinner (1981) for komatiite-komatiitic basalt associations. In the model for the Kromberg rocks, the parental, komatiitic melt is derived by high-pressure melting of a chondritic-type mantle (Takahashi and Scarfe, 1985). This melt feeds a large magma chamber, within which fractionation results in the formation of a lower density tholeiitic liquid (Huppert and Sparks, 1981) and partial olivine and chromite cumulates. Erupted volcanic rocks would be dominated by tholeiitic compositions or of fractionated derivatives thereof, with lesser amounts of higher density volcanic rocks of komatiitic composition (Nisbet and Chinner, 1981; Huppert and Sparks, 1981). Field evidence for the Kromberg Formation rocks showing interlayering of predominantly tholeiitic with subordinate komatiitic volcanic rocks is consistent with this model of magma genesis.

ACKNOWLEDGMENTS

This work was carried out as an Honours project at the Department of Geochemistry, University of Cape Town, and G. Conway and R. King are thanked for their assistance with the sampling, sample preparation, and analyses. T. W. V. would also like to acknowledge the financial support of the Council for Scientific and Industrial Research of South Africa. Drs. C. Harris, G. Ryder, G. Byerly, and, in particular, G. Gruau are thanked for their comments on earlier drafts of this work.

REFERENCES CITED

Anhaeusser, C. R., 1973, The evolution of early Precambrian crust of southern Africa: Royal Society London Philosophical Transactions, v. 273, p. 359–388.

Armstrong, R. A., Compston, W., de Wit, M. J., and Williams, I. S., 1990, The stratigraphy of the 3.5–3.2 Ga Barberton Greenstone Belt revisited: a single zircon ion microprobe study: Earth and Planetary Science Letters, v. 101, p. 90–106.

Arndt, N. T., 1977, Ultrabasic magmas and high-degree melting of the mantle: Contributions to Mineralogy and Petrology, v. 64, p. 201–221.

Arndt, N. T., 1986, Differentiation of komatiite flows: Journal of Petrology, v. 27, p. 279–301.

Arndt, N. T., 1994, Archean komatiites, *in* Condie, K. C., ed., Archean crustal evolution: Amsterdam, Elsevier, p. 11–44

Arndt, N. T., and Nesbitt, R. W., 1982, Geochemistry of Munro Township basalts, *in* Arndt, N. T., and Nisbet, E. G., eds., Komatiites: London, George, Allen and Unwin, p. 309–323.

Arndt, N. T., and Nesbitt, R. W., 1984, Magma mixing in komatiitic lavas from Munro Township, Ontario, *in* Kröner, A., Hanson, G. N., and Goodwin, A. M., eds., Archean geochemistry: Berlin, Springer Verlag, p. 99–114.

Arndt, N. T., Naldrett, A. J., and Pyke, D. R., 1977, Komatiitic and iron-rich tholeiitic lavas of Munro Township, northeast Ontario: Journal of Petrology, v. 18, p. 319–369.

Arth, J. G., 1976, Behaviour of trace elements during magmatic processes—a summary of theoretical models and their application: U.S. Geological Survey Journal of Research, v. 4, p. 41–47.

Arth, J. G., Arndt, N. T., and Naldrett, A. J., 1977, Genesis of Archean komatiites from Munro Township, Ontario: trace element evidence: Geology, v. 5, p. 590–596.

Barley, M. E., Sylvester, G. C., Groves, D. I., 1984, Archean calc-alkaline volcanism in the Pilbara Block, Australia: Precambrian Research, v. 24, p. 285–319.

Bottinga, Y., and Weill, D. F., 1970, Densities of liquid silicate systems calculated from partial molar volumes of oxide components: American Journal of Science, v. 269, p. 169–182.

Brevart, O., Dupre, B., and Allegre, C. J., 1986, Lead-lead age of komatiitic lavas and limitations on the structure and evolution of the Precambrian mantle: Earth and Planetary Science Letters, v. 77, p. 293–302.

Byerly, G. R., Lowe, D. R., Nocita, B. W., and Ransom, B. L., 1983, Apparent volcanic cycles in the Archean Swaziland Supergroup, Barberton Mountain Land, South Africa: a result of non-magmatic processes: 14th Lunar and Planetary Science Conference, Houston, Abstracts, pt. 1, p. 84–85.

Byerly, G. R., Kröner, A., Lowe, D. R., Todt, W., and Walsh, M. M., 1996, Prolonged magmatism and time constraints for sediment deposition in the Early Archean Barberton Greenstone Belt: evidence from the Upper Onverwacht and Fig Tree Groups: Precambrian Research, v. 78, p. 125–138.

Card, K. D., 1990, A review of the Superior Province of the Canadian Shield, a product of Archean accretion: Precambrian Research, v. 48, p. 99–156.

Condie, K. C., and Harrison, N. M., 1976, Geochemistry of the Archean Bulawayan Group, Midlands Greenstone belt, Rhodesia: Precambrian Research, v. 3, p. 253–267.

Condie, K. C., Viljoen, M. J., and Kable, E. J. D., 1977, Effects of alteration on element distribution in Archean tholeiites from the Barberton area: Contributions to Mineralogy and Petrology, v. 64, p. 75–89.

Cox, K. G., and Mitchell, C., 1988, Importance of crystal settling in the differentiation of Deccan Trap basaltic magmas: Nature, v. 333, p. 447–449.

de Ronde, C. E. J., and De Wit, M. J., 1994, Tectonic history of the Barberton Greenstone Belt, South Africa: 490 million years of Archean crustal evolution: Tectonics, v. 13, p. 983–1005.

de Wit, M. J., 1982, Gliding and overthrust nappe tectonics in the Barberton Greenstone Belt: Journal of Structural Geology, v. 4, p. 117–136.

de Wit, M. J., Hart, R. A., and Hart, R. J., 1987, The Jamestown Ophiolite Complex, Barberton mountain belt: a section through 3.5 Ga oceanic crust: Journal of African Earth Sciences, v. 6, p. 681–730.

Donelly, T. W., Thompson, G., and Salisbury, M. H., 1980, Chemistry of altered basalts at site 417: Deep Sea Drilling Project Leg 51 Initial Reports, v. 51/53, p. 1319–1330.

Duchac, K. C., and Hanor, J. S., 1987, Origin and timing of the metasomatic silicification of an Early Archean komatiite sequence, Barberton Mountain Land, South Africa: Precambrian Research, v. 37, p. 125–146.

Erlank, A. J., and Reid, D. L., 1974, Geochemistry, mineralogy and petrology of basalts: Deep Sea Drilling Project Leg 25, p. 543–551.

Green, D. H., 1981, Petrogenesis of Archean ultramafic magmas and implications for Archean tectonics, *in* Kröner, A., ed., Precambrian plate tectonics: Amsterdam, Elsevier, p. 469–491.

Gruau, G., Chauvel, C., Arndt, N. T., and Cornichet, J., 1990, Al-depletion in komatiites and garnet fractionation in the Early Archean mantle: Hf isotopic constraints: Geochimica et Cosmochimica Acta, v. 54, p. 3095–3101.

Gruau, G., Tourpin, S., Fourcade, S., and Blais, S., 1992, Loss of isotopic (Nd, O) and chemical (REE) memory during metamorphism of komatiites: new evidence from eastern Finland: Contributions to Mineralogy and Petrology, v. 112, p. 66–82.

Hanor, J. S., and Duchac, K., 1990, Isovolumetric silicification of Early Archean komatiites: geochemical mass balances and constraints on origin: Journal of Geology, v. 98, p. 863–877.

Hart, S. R., and Davis, K. E., 1978, Nickel partitioning between olivine and melt:

Earth and Planetary Science Letters, v. 40, p. 203–219.
Hart, S. R., Erlank, A. J., and Kable, E. J. D., 1974, Seafloor basalt alteration: Contributions to Mineralogy and Petrology, v. 44, p. 219–230.
Hawkesworth, C. J., and O'Nions, R. K., 1977, Petrogenesis of some Archean volcanic rocks from southern Africa: Journal of Petrology, v. 18, p. 487–520.
Hoffman, S. E., Wilson, M., and Stakes, D. S., 1986, Inferred oxygen isotope profile of Archean oceanic crust, Onverwacht Group, South Africa: Nature, v. 321, p. 55–58.
Hunter, D. R., 1974, Crustal development in the Kaapvaal Craton: Precambrian Research, v. 4, p. 259–294.
Huppert, H. E., and Sparks, R. S. J., 1981, The fluid dynamics of a basaltic magma chamber replenished by an influx of hot dense ultrabasic magma: Contributions to Mineralogy and Petrology, v. 75, p. 279–289.
Hynes, A., 1980, Carbonitization and mobility of Ti, Y and Zr in the Ascot Formation metabasalts, Quebec: Contributions to Mineralogy and Petrology, v. 75, p. 79–87.
Irving, A. J., and Frey, F. A., 1978, A review on trace element distribution in rocks: Geochimica et Cosmochimica Acta, v. 42, p. 771–787.
Jahn, B. M., Auvray, B., Blais, S., Capedevila, R., Cornichet, J., Vidal, F., and Hameurt, J., 1980, Trace element geochemistry and petrogenesis of Finnish greenstone belts: Journal of Petrology, v. 21, p. 411–441.
Jahn, B. M., Gruau, G., and Glikson, A. J., 1982, Komatiites of the Onverwacht Group, S. Africa: REE Geochemistry, Sm/Nd age and mantle evolution: Contributions to Mineralogy and Petrology, v. 80, p. 25–37.
Jensen, L. S., 1976, A new cation plot for classifying sub-alkalic volcanic rocks: Ontario Division of Mines Miscellaneous Paper 66, 22 p.
Jolly, W. T., 1980, Development and degradation of Archean lavas, Abitibi area, in the light of major element geochemistry: Journal of Petrology, v. 21, p. 323–363.
Kamo, S. L., and Davis, D. W., 1994, Reassessment of Archean crustal development in the Barberton Mountain Land, South Africa, based on U-Pb dating: Tectonics, v. 13, p. 167–192.
Kesson, S. E., 1973, The primary geochemistry of the Monaro alkaline volcanics, S.E. Australia: Contributions to Mineralogy and Petrology, v. 42, p. 93–108.
Kröner, A., Byerly, G. R., and Lowe, D. R., 1991, Chronology of Early Archean granite-greenstone evolution in the Barberton Mountain Land, South Africa, based on precise dating by single zircon evaporation: Earth and Planetary Science Letters, v. 103, p. 41–54.
Lahaye, Y., Arndt, N., Byerly, G. R., Chauvel, C., Fourcade, S., and Gruau, G., 1995, The influence of alteration on the trace-element and Nd isotopic compositions of komatiites: Chemical Geology, v. 126, p. 43–64.
Lécuyer, C., Gruau, G., Anhaeusser, C. R., and Fourcade, S., 1994, The origin of fluids and the effects of metamorphism on the primary chemical compositions of Barberton komatiites: New evidence from geochemical (REE) and isotopic (Nd, O, H, $^{39}Ar/^{40}Ar$) data: Geochemica et Cosmochemica Acta, v. 58, p. 969–984.
Le Roex, A. P., 1980, Geochemistry and mineralogy of selected Atlantic Ocean basalts [Ph.D. thesis]: Cape Town, University of Cape Town, 166 p.
Lowe, D. R., and Knauth, L. P., 1977, Sedimentology of the Onverwacht Group (3.4 billion years), Transvaal, South Africa, and its bearing on the characteristics and evolution of the early earth: Journal of Geology, v. 85, p. 699–723.
Lowe, D. R., Byerly, G. R., Ransom, B. L., and Nocita, B. R., 1985, Stratigraphic and sedimentological evidence bearing on structural repetition in Early Archean rocks of the Barberton Greenstone Belt, South Africa: Precambrian Research, v. 27, p. 165–186.
MacGeehan, P., and MacLean, W., 1980, An Archean sub-seafloor geothermal system, "calc-alkali" trends and massive sulfide genesis: Nature, v. 286, p. 767–771.
Mathias, M., Siebert, J. C., and Rickwood, P. C., 1970, Some aspects of ultramafic xenoliths: Contributions to Mineralogy and Petrology, v. 26, p. 75–86.
Mysen, B. O., and Kushiro, I., 1977, Compositional variations of coexisting phases with degree of melting of peridotite in the upper mantle: American Mineralogist, v. 62, p. 843–865.
Nesbitt, R. W., and Sun, S. S., 1976, Geochemistry of Archean spinifex-textured peridotites and magnesian and low magnesian tholeiites: Earth and Planetary Science Letters, v. 31, p. 433–453.
Nisbet, E. G., and Chinner, G. A., 1981, Controls on the eruption of mafic-ultramafic lavas, Ruth Well Ni-Cu prospect, west Pilbara: Economic Geology, v. 76, p. 1729–1735.
Nisbet, E. G., Bickle, M. J., and Martin, A., 1977, The mafic and ultramafic lavas of the Belingwe Greenstone Belt, Rhodesia: Journal of Petrology, v. 18, p. 521–566.
Nixon, P. H., Rogers, N. W., and Gibson, I. C., 1981, Depleted and fertile mantle xenoliths from southern Africa: Annual Review of Earth and Planetary Sciences, v. 9, p. 285–322.
O'Hara, M. J., Saunders, M. J., and Mercy, E. L. P., 1975, Garnet-peridotite, primary ultrabasic magma and eclogite; interpretation of upper mantle processes in kimberlite: Physics and Chemistry of the Earth, v. 9, p. 571–604.
Pearce, J. A., and Cann, J. R., 1973, Tectonic setting of basic volcanic rocks determined using trace element analysis: Earth and Planetary Science Letters, v. 5, p. 361–376.
Pearce, J. A., and Norry, M. J., 1979, Petrogenetic implications of Ti, Zr, Y, Nb variations in volcanic rocks: Contributions to Mineralogy and Petrology, v. 69, p. 33–47.
Shaw, D. M., 1970, Trace element fractionation during anatexis: Geochimica et Cosmochimica Acta, v. 34, p. 237–243.
Shervais, J. W., 1982, Ti-V plots and petrogenesis of modern ophiolitic lavas: Earth and Planetary Science Letters, v. 59, p. 101–118.
Smith, H. S., and Erlank, A. J., 1982, Geochemistry and petrogenesis of komatiites from the Barberton Greenstone Belt, *in* Arndt, N. T., and Nisbet, E. G., eds., Komatiites: George, London, Allen and Unwin, p. 348–398.
Smith, H. S., Erlank, A. J., and Duncan, A. R., 1980, Geochemistry of some ultramafic komatiite lava flows from the Barberton Mountain Land, South Africa: Precambrian Research, v. 11, p. 399–415.
Smith, H. S., O'Neil, J. R., and Erlank, A. J., 1984, Oxygen isotope compositions of minerals and rocks and chemical alteration patterns in pillow lavas from Barberton, *in* Kröner, A., ed., Archean geochemistry: New York, Springer Verlag, p. 115–137.
Storey, M., Mahoney, J. J., Kroenke, L. W., and Saunders, A. D., 1991, Are oceanic plateaus sites of komatiite formation?: Geology, v. 19, p. 376–379.
Sun, S. S., and Nesbitt, R. W., 1977, Chemical heterogeneity of the Archean mantle, composition of the earth and mantle evolution: Earth and Planetary Science Letters, v. 35, p. 429–448.
Takahashi, E., and Scarfe, C. M., 1985, Melting of peridotite to 14 Gpa and the genesis of komatiite: Nature, v. 315, p. 566–568.
Viljoen, M. J., and Viljoen, R. P., 1969a, The geology and geochemistry of the upper formations: Geological Society of South Africa Special Publication 2, p. 113–153.
Viljoen, M. J., and Viljoen, R. P., 1969b, Introduction to the geology of the Barberton Greenstone Belt: Geological Society of South Africa Special Publication 2, p. 9–28.
Viljoen, R. P., and Viljoen, M. J., 1969, The effects of metamorphism and serpentinization on the volcanic and associated rocks of the Barberton region: Geological Society of South Africa Special Publication 2, p. 29–54.
Williams, D. A. C., and Furnell, R. G., 1979, Reassessment of part of the Barberton type area: Precambrian Research, v. 9, p. 325–347.
Willis, J. P., Erlank, A. J., Gurney, J. J., Theil, R. H., and Ahrens, L. H., 1972, Major, minor and trace element data for some Apollo 11, 12, 14 and 15 samples, *in* Heymann, L. D., ed., Proceedings, Third Lunar Science Conference, v. 2: Cambridge, Massachusetts, MIT Press, p. 1269–1273.
Xie, Q., and Kerrich, R., 1994, Silicate-perovskite and majorite signature komatiites from the Archean Abitibi Greenstone Belt: Implications for early mantle differentiation and stratification: Journal of Geophysical Research, v. 99, p. 15799–15812.

MANUSCRIPT ACCEPTED BY THE SOCIETY MARCH 26, 1998

Printed in U.S.A.

Geological Society of America
Special Paper 329
1999

Subaqueous to subaerial Archean ultramafic phreatomagmatic volcanism, Kromberg Formation, Barberton Greenstone Belt, South Africa

Barbara Ransom
Scripps Institution of Oceanography, University of California at San Diego, La Jolla, California 92093-0220
Gary R. Byerly
Department of Geology and Geophysics, Louisiana State University, Baton Rouge, Louisiana 70803
Donald R. Lowe
Department of Geological and Environmental Sciences, Stanford University, Stanford, California 94305

ABSTRACT

Thick mafic and ultramafic volcanic sequences that characterize Archean greenstone belts are made up largely of massive and pillowed flow rocks; corresponding pyroclastic rocks are less common. Widespread mafic volcaniclastic deposits of the middle member of the Kromberg Formation (K2) in the Barberton Greenstone Belt are an exception. Their outcrops in the Onverwacht anticline and the adjoining Kromberg syncline expose a well-preserved tephra blanket more than 30 km in extent and as much as 1 km thick. On the west limb of the Onverwacht anticline, where the tephra sheet is thickest, it includes from base upward: 0–100 m of fine-grained tuff (division K2v-a); 300–1,000 m of massive to current-structured lapillistone and lapilli tuff (K2v-b); and a thin capping chert composed of silicified, commonly current-worked ash and dust (K2c). The mineralogy and composition of all rocks have been changed by early low-temperature alteration and later metamorphism. However, relict mineralogy, pyroclast textures, and trace-element chemistry suggest that the pyroclastic debris of K2v-b were derived from mafic to ultramafic magmas.

The thickest section of pyroclastic debris on the west limb of the Onverwacht anticline represents the fill of a phreatomagmatic explosion crater formed by the removal of as much as 300 m of the underlying Buck Reef Chert. The lower part of the 1,000-m-thick fill consists largely of coarse lapillistone containing accidental blocks of Buck Reef Chert. This debris was deposited mainly by coarse subaqueous sediment flows but may include pyroclastic fall deposits, both deriving material from a subaqueous eruption column. Initial water depth is estimated to have been 700 m or less. Shoaling of the vent and the eventual transition to subaerial eruptions are suggested by upward transitions in the volcaniclastic pile into shallow-water, current-structured lapilli tuff deposits in the upper part of the sequence. The chert cap, K2c, is composed of fine-grained silicified ash and accretionary lapilli deposited under very shallow water to subaerial conditions.

Ransom, B., Byerly, G. R., and Lowe, D. R., 1999, Subaqueous to subaerial Archean ultramafic phreatomagmatic volcanism, Kromberg Formation, Barberton Greenstone Belt, South Africa, *in* Lowe, D. R., and Byerly, G. R., eds., Geologic Evolution of the Barberton Greenstone Belt, South Africa: Boulder, Colorado, Geological Society of America Special Paper 329.

INTRODUCTION

A crucial step in understanding the evolution of the early Earth lies in unraveling the lithologic and chemical successions within Archean greenstone belts. Determining the conditions under which these thick mafic, ultramafic, and felsic volcanic sequences formed is an essential step in reconstructing early tectonic regimes, surface environments, and the formative processes of the oldest continental crust. Whereas thick sequences of massive lavas commonly provide relatively little information about the eruption environment, interbedded pyroclastic and volcaniclastic units often contain abundant information on the processes and conditions of eruption and deposition. In this regard, Sylvester et al. (1997) have recently reviewed the styles and products of volcanism in greenstone belts and suggest that volcaniclastic materials may be more important than previously considered. Thick mafic pyroclastic deposits are locally well developed in the Kromberg Formation of the Onverwacht Group in the Barberton Greenstone Belt but, to date, have been described only briefly (Viljoen, R. P., and Viljoen, 1969a). In the present paper, we report the results of a study of the origin and paleoenvironmental significance of mafic pyroclastic rocks in the Kromberg Formation on the west limb of the Onverwacht anticline.

GEOLOGIC SETTING

General stratigraphy

The 3,500- to 3,200-Ma supracrustal rocks of the Barberton Greenstone Belt, South Africa, form a 12- to 15-km-thick volcanic and sedimentary sequence that includes the Onverwacht Group, a predominantly mafic and ultramafic volcanic unit, and overlying felsic volcaniclastic and terrigenous sedimentary rocks of the Fig Tree and Moodies Groups. In classic sections in the southern part of the Barberton Greenstone Belt (Fig. 1), the 10- to 11-km-thick Onverwacht Group is made up largely of komatiitic and basaltic flow rocks of the Komati, Hooggenoeg, Kromberg, and Mendon Formations (Viljoen, M. J., and Viljoen, 1969; Viljoen, R. P., and Viljoen, 1969a; Williams and Furnell, 1979; Lowe and Byerly, this volume, Chapter 1). Although felsic pyroclastic and volcaniclastic units occur widely within both the Onverwacht and the overlying Fig Tree Groups (Viljoen, M. J., and Viljoen, 1969; Viljoen, R. P., and Viljoen, 1969a; Lowe and Byerly, this volume, Chapter 1), mafic and ultramafic fragmental units are less common. The Kromberg Formation is a mixed basaltic and komatiitic unit (Viljoen, R. P., and Viljoen, 1969a; Vennemann and Smith, this volume, Chapter 5) about 1.7 km thick and is unusual in containing thick laterally extensive deposits of coarse mafic tephra (Fig. 2). Byerly et al. (1996) have obtained single zircon evaporation ages from tuffs at the base (3,416 ± 5 Ma) and top (3,334 ± 3 Ma) of the Kromberg Formation.

Structural setting

Mafic pyroclastic rocks of the Kromberg Formation are thickest in the central part of the west limb of the Onverwacht anticline (Fig. 1) where they strike nearly east-west. The beds are steeply dipping to slightly overturned to the north (Fig. 3). Although there is minor faulting, the Kromberg stratigraphy appears to be intact (Lowe et al., 1985; Ransom, 1987; Lowe and

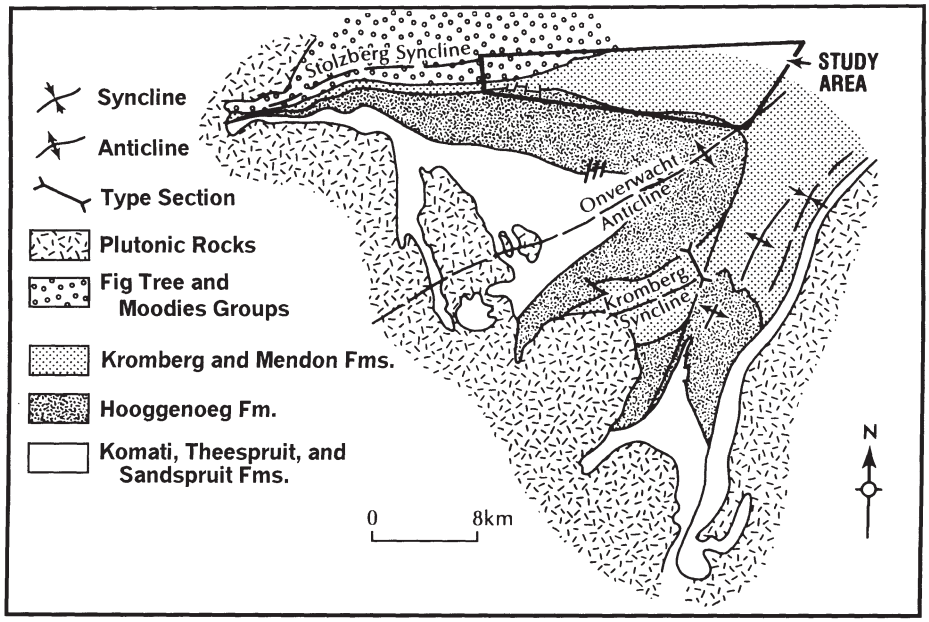


Figure 1. General geology of the southwestern part of the Barberton Greenstone Belt showing the location of the study area on the west limb of the Onverwacht anticline (modified from Lowe and Byerly, this volume, Chapter 1). The type section of the Kromberg Formation is shown on the north limb of the Kromberg syncline.

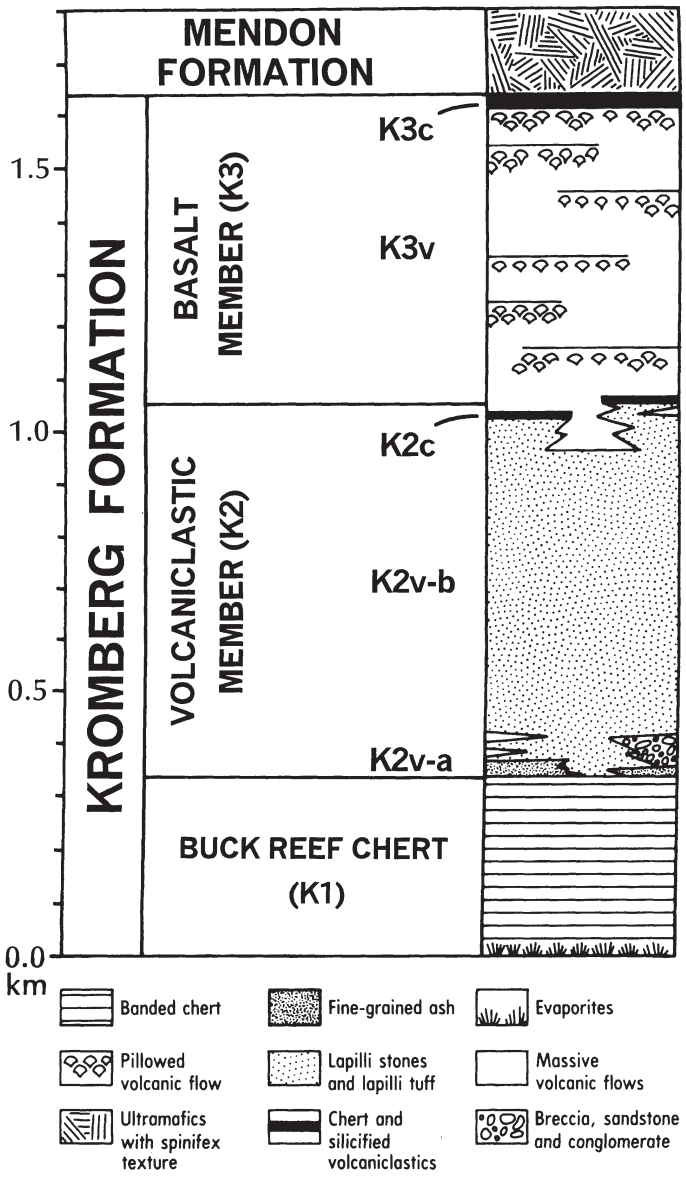


Figure 2. Generalized stratigraphic section of the Kromberg Formation in the study area on the west limb of the Onverwacht anticline.

Byerly, this volume, Chapter 1). Isoclinal folding and southward-younging units in the Kromberg Formation have been reported from this area by de Wit (1982, 1983). However, abundant sedimentary structures occur throughout the section, including cross-lamination, cross-stratification, scour features, load structures, graded beds, pillow lavas, and geopetally filled vesicles. These structures show unambiguously that the formation youngs uniformly toward the north (Ransom, 1987).

Cleavage is generally absent or poorly developed in the cherts, volcanic flow rocks, and silicified volcaniclastic rocks over much of the west limb of the Onverwacht anticline, including rocks of the Kromberg Formation. Unsilicified volcaniclastic deposits, however, commonly display weak foliation oriented parallel or subparallel to bedding; and local pods show moderate to strong cleavage. Pervasive cleavage is developed in rocks of the Kromberg Formation immediately adjacent to the Inyoko fault in the western part of the study area. The strong foliation in this area probably developed during movement along the fault because the cleavage strikes parallel to and rapidly decreases in intensity away from the fault.

Metamorphism, alteration, and replacement

Greenschist facies alteration has affected most of the mafic volcanic and volcaniclastic rocks in the study area, producing a mineral assemblage of chlorite, tremolite, serpentine, talc, epidote, chert (microquartz), carbonate, sericite, tourmaline, rutile, and magnetite. Nevertheless, metasomatism was not complete and, in places, relict magmatic minerals such as chrome spinel, olivine, and pyroxene remain. In earlier studies, this alteration was attributed to regional metamorphism accompanying intrusion of surrounding Archean tonalitic plutons (Anhaeusser et al., 1969; Viljoen, R. P., and Viljoen, 1969b; Hunter, 1974). However, similar greenschist-grade mineral assemblages are also common in hydrothermally altered mafic volcanic rocks (Hekinian, 1968; Spooner and Fyfe, 1973; Humphris and Thompson, 1978; Seyfried and Bischoff, 1979; Dimroth and Lichtblau, 1979; Quinby-Hunt et al., 1986). Much of the low-grade alteration exhibited by rocks in the Onverwacht anticline has more recently been interpreted to represent early low-temperature hydrothermal alteration of Archean age (de Wit et al., 1982; Smith et al., 1984; Duchac and Hanor, 1987; Hanor and Duchac, 1990). Much of the alteration to fine-grained chlorite, tremolite, and serpentine minerals has occurred without shearing, and primary textures and structures as small as 0.05 cm across are commonly well preserved.

Coarse-grained volcaniclastic rocks in the Kromberg Formation commonly show cementation and replacement by carbonate, including dolomite, siderite, ankerite, and calcite. In areas of extensive replacement, intergrown secondary carbonate grains crosscut original grain boundaries and obliterate most primary textures less than 1–3 mm in size. Locally, zones within the volcaniclastic member of the Kromberg Formation consist almost completely of secondary carbonate. These have been mapped and interpreted by de Wit et al. (1982) as primary carbonate sediments. However, the layering and sedimentary structures in these carbonate-rich zones can be traced along strike into less altered coarse-grained mafic volcaniclastic rocks with identical layering and bedforms, indicating that the carbonate is of replacement rather than primary origin (Ransom, 1987).

In the Onverwacht Group as a whole, fine-grained volcaniclastic ash and dust are widely silicified, forming thin resistant, laterally continuous chert beds interbedded with volcanic flows (Viljoen, M. J., and Viljoen, 1969; Viljoen, R. P., and Viljoen, 1969a; Lowe and Knauth, 1977; Stanistreet et al., 1981; de Wit, 1982; de Wit et al., 1982; Paris et al., 1985; Ransom, 1987; Lowe, this volume, Chapter 3). The isovolumetric replacement

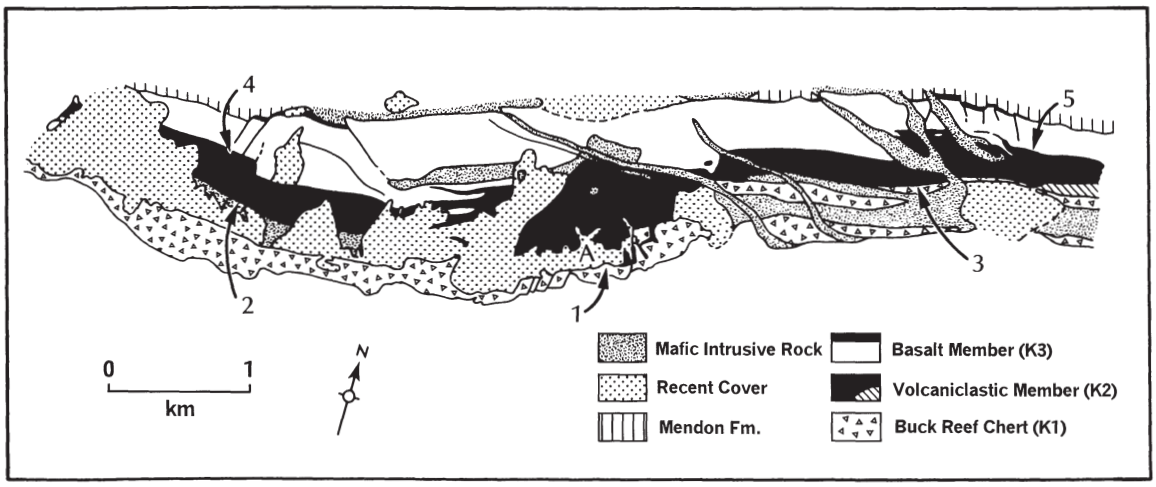


Figure 3. Generalized geologic map of the Kromberg Formation and adjacent units in the study area. Numbers indicate locations of sections and features shown in following figures. The 1.7-km-wide crater, within which the upper 200–300 m of the Buck Reef Chert is missing, is centered on locality A. Many faults, including ones that offset the Buck Reef Chert and volcaniclastic member of the Kromberg Formation, are not shown.

of original volcaniclastic grains by microcrystalline quartz and the preservation and accumulation of fine opaque oxides, vacuoles, and dust along grain boundaries and crystal defects have resulted in the excellent preservation of primary textures, structures, and grain outlines. These features have yielded key information on the nature of the original rocks and on the physical processes of deposition (Lowe and Knauth, 1977; Lowe, this volume, Chapters 3, 9).

STRATIGRAPHY AND FACIES

The stratigraphy of the Kromberg Formation on the west limb of the Onverwacht anticline (Fig. 2) has been described in detail by Ransom (1987). Member and division names used here are those of Lowe and Byerly (this volume, Chapter 1). In the study area, K1, the basal member of the formation, includes 150–400 m of chert and other silicified sediments that are collectively called the Buck Reef Chert. This unit is equivalent to a series of thin chert layers, interbedded basaltic and komatiitic volcanic rocks, and at least one layer of mafic lapillistone in the type section of the Kromberg Formation along the Komati River, 18 km to the southeast (Viljoen, R. P., and Viljoen, 1969a; Lowe and Byerly, this volume, Chapter 1). The middle volcaniclastic member of the Kromberg Formation (K2) is composed largely of mafic pyroclastic deposits 400–1,100 m thick. Toward the east and southeast, intercalated volcanic flows become increasingly abundant and, in the type section along the Komati River, pyroclastic rocks are subordinate to flow rocks. In the study area, the contact between the Buck Reef Chert (K1) and the mafic volcaniclastic member (K2) is commonly covered or intruded by mafic and ultramafic dikes and sills. Where intact, however, the contact is concordant and appears conformable. The uppermost member of the Kromberg Formation (K3) consists of 300–500 m of mafic volcanic flows and pillow breccias (K3v) that appear to be conformable on and locally interfinger with the underlying mafic volcaniclastic member. These volcanic flows are capped by the Footbridge Chert (K3c), the uppermost unit in the Kromberg Formation (Lowe and Byerly, this volume, Chapter 1).

Volcaniclastic member (K2)

On the west limb of the Onverwacht anticline, the volcaniclastic member of the Kromberg Formation (K2) includes three subdivisions (Figs. 4 and 5): (1) a basal tuffaceous division (K2v-a), (2) the main lapillistone and lapilli-tuff division (K2v-b), and (3) the capping chert (K2c). These deposits reach a maximum thickness of about 1,100 m in the central part of the study area, where the present outcrop cuts across the periphery of an Archean explosion crater. The section thins to 300–400 m thick at the eastern and western boundaries of the study area (Fig. 6).

Lithologic names used here for volcaniclastic rocks are taken from Fisher and Schmincke (1984). Tephra range in size from lapilli (2–64 mm) to ash (<2 mm). However, large blocks and bombs (>64 mm) are also present. Pyroclastic deposits composed of lapilli and <25% ash are termed lapillistones; those with 25–75% ash are called lapilli tuffs. Tuffs contain >75% ash. Juvenile material is defined as debris that originated as magmatic liquid related to the volcanic event responsible for the deposit (i.e., pyroclasts, bombs, or volcanic flows) and accidental material designates blocks derived either from subvolcanic basement rocks or the fragmentation of volcanic rock from prior eruptions.

Basal tuffaceous division (K2v-a). The basal division of the volcaniclastic member is composed largely of fine-grained tuff (Fig. 4) that is generally unsilicified and deeply weathered. The

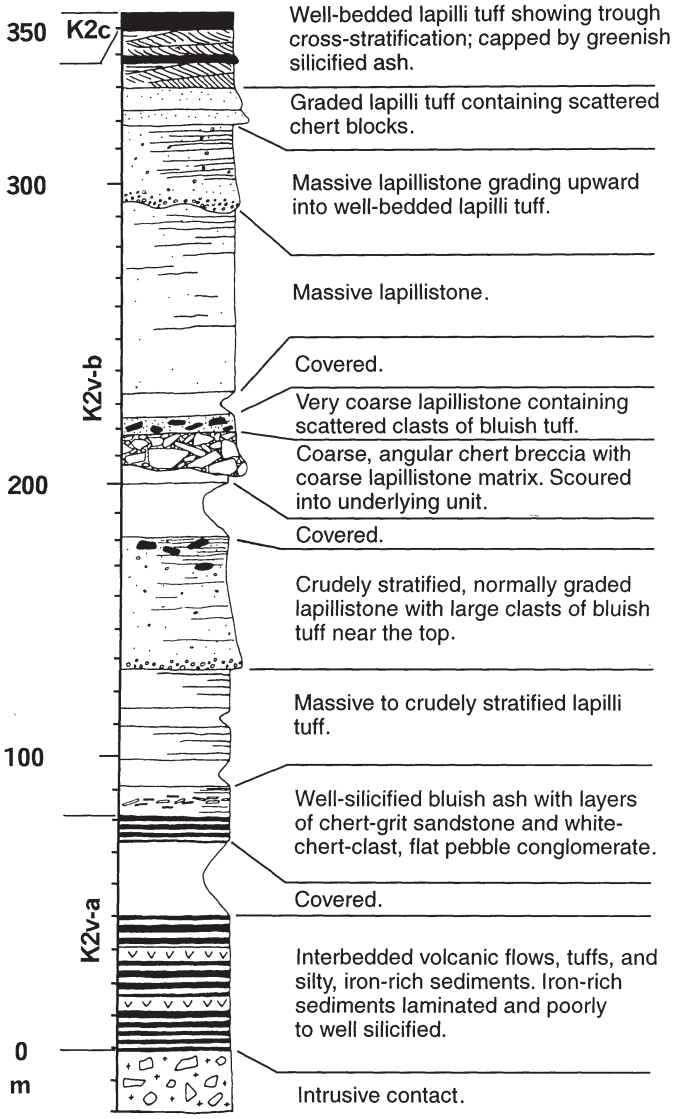


Figure 4. Measured stratigraphic section (Fig. 3, location 2) of the volcaniclastic member of the Kromberg Formation in the western part of the study area showing subdivisions discussed in text.

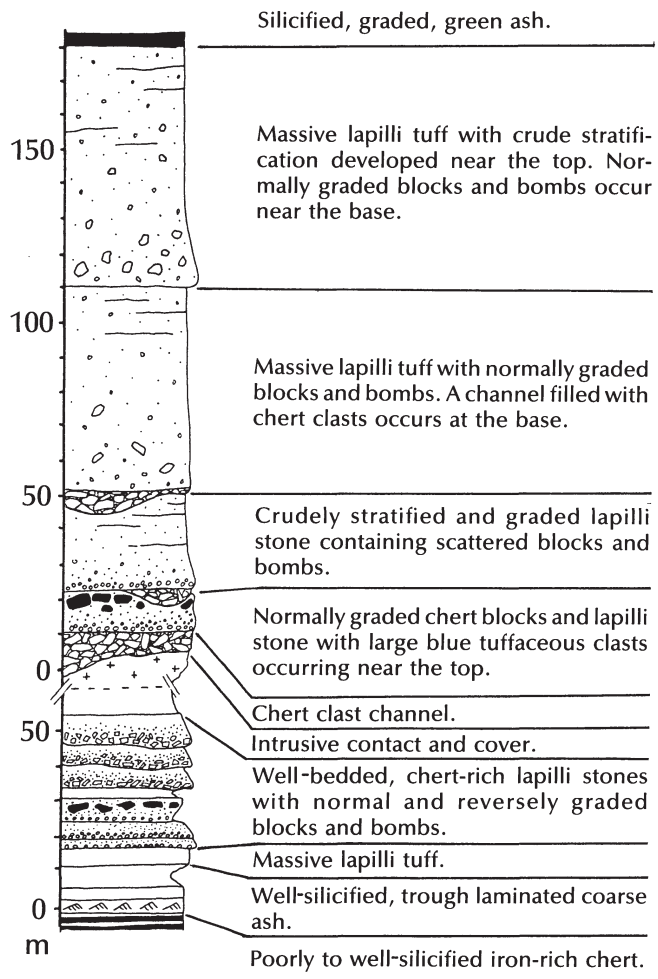


Figure 5. Measured stratigraphic section (Fig. 3, location 3) of the volcaniclastic member of the Kromberg Formation in the eastern part of the study area. A break in the section due to the intrusion of a later diabase dike occurs ~50 m above the base. The section is continued again above the dike, with the thickness beginning at zero meters.

thickness of this division reaches 100 m in the western part of the study area (Fig. 4), where it is composed mainly of massive to flat-laminated tuff containing 3- to 4-cm-thick layers of white chert. Near the base of the unit, these sediments interfinger with thin, badly weathered mafic lava flows, some of which are vesicular. The division thins and coarsens to the east. It is less than 10 m thick in the central part of the study area and contains stringers of coarse to medium-grained, cross-stratified chert-grain sandstone and coarse ash (Fig. 5). The chert grains in these clastic units resemble cherts in the underlying Buck Reef Chert.

At the top of the division is a distinctive marker bed, 1–8 m thick, composed of well-indurated, blue-gray- to green-gray-weathering tuff that, in places, contains coarse-grained, chert-rich, lithic sandstone; large rectangular white chert clasts; and flat-pebble conglomerate (Fig. 4). This blue-gray tuff forms a distinctive marker layer between K2v-a and overlying coarse lapilli deposits of K2v-b. Although generally persistent along strike, the basal tuffaceous division is absent within the explosion crater (Fig. 6).

Lapillistone and lapilli-tuff division (K2v-b). The basal tuffaceous division is overlain by 300 to nearly 1,000 m of coarse lapillistone and lapilli tuff containing occasional small mafic flows and fine-grained mafic dikes. The lapillistone division reaches its maximum thickness in the center of the study area (Fig. 6) and thins irregularly to both the east and west. The lower half of K2v-b consists mainly of coarse, thick-bedded, grain-supported, normally graded, massive or crudely stratified lapillistone containing abundant blocks of accidental material (Figs. 4, 5, and 7). Identifiable sedimentation units are as much as 70 m thick, with stratification developed only in their upper parts. Most beds are massive or show normal size grading (Figs. 4, 5, 7, and

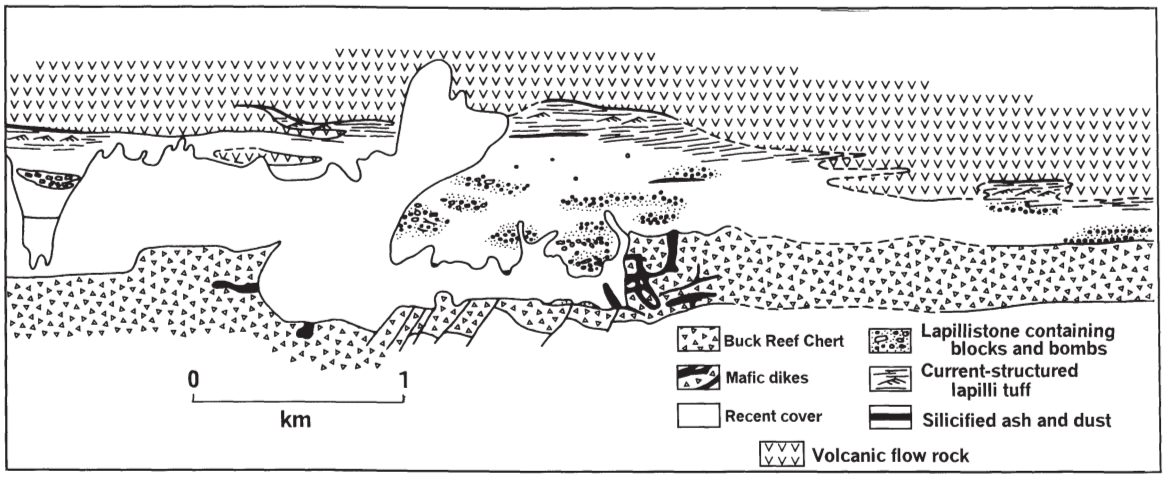


Figure 6. Generalized map of the Kromberg Formation in the vicinity of the crater (locality A, Fig. 3). Blocks and bombs in the lapillistone and lapilli tuff division (K2v-b) are concentrated within and adjacent to the crater in the underlying Buck Reef Chert. Fine-grained olivine-phyric dikes (black) at the base of the division invade the Buck Reef Chert below and adjacent to the crater.

8A), although a few are inversely graded. Inversely graded zones, only a few centimeters thick, are present at the bases of some normally graded beds. Within individual beds, accidental blocks of chert commonly show normal size grading (Figs. 4, 5, and 7). However, large, low-density blocks of bluish tuff from the top of K2v-a are commonly concentrated toward the tops of normally graded beds (Figs. 4 and 5). Within the crater, the massive and crudely stratified lapillistone units comprise a section about 500–600 m thick (Fig. 6).

The middle and upper parts of K2v-b show a gradual upward transition from poorly stratified lapillistone to current-worked, well-stratified lapilli tuff at the top of the section (Fig. 4). Layering becomes prominent in the upper half of the unit. Evidence for penecontemporaneous slumping and downslope flowage, including chaotic, contorted, and disrupted volcaniclastic strata, occurs locally near the middle of the unit (Fig. 4). Lapilli tuffs are common in the upper third of K2v-b in beds a few centimeters to a meter thick that commonly show normal grading. Well-developed large-scale cross-stratification from 0.5 to 1.5 m high is present in the upper 50–100 m of K2v-b (Figs. 8B and 9).

Most lapilli in K2v-b are 0.5–1 cm in diameter, reaching a maximum diameter of about 2 cm. Tephra clots greater that 5 cm in diameter, composed of lapilli welded together by aphanitic material, occur throughout the deposit. Lapilli in the lower part of the division tend to be the coarsest, and overall the division fines upward. Lapilli in the top of the division are generally less than 0.5 cm across. The lapilli of K2v-b appear to represent a monogenetic assemblage of pyroclasts. Texturally, the best preserved pyroclasts are in layers that have been silicified. Silicified deposits show little or no compaction and excellent preservation of pyroclast shapes, packing, and internal structuring, including pseudomorphic replacement of olivine phenocrysts by silica (Fig. 10A). Units that have not been silicified and lack carbonate show tightly packed lapilli that have been completely altered to Mg- and Fe-bearing silicate minerals and oxides (Fig. 10B). In such units, lapilli shapes have commonly been modified by compaction and, in many places, internal structures have largely been lost.

Most of the juvenile pyroclasts in the volcaniclastic member are Type I and II pyroclasts of Wohletz (1983) and, based on preserved textures, were originally largely glassy or aphanitic. Type I pyroclasts are blocky with smooth surfaces that cut across large vesicles (Fig. 10C). Type II are elongate to equant, irregular in shape, and have rounded, lumpy surfaces (Fig. 10D, E, and F). Many Type II pyroclasts are coated, commonly with several thin outer layers of material that was originally glassy or aphanitic, which enclose centers that originally included olivine phenocrysts and other pieces of tephra (Fig. 10D). These appear to represent armored lapilli (Fisher and Schmincke, 1984). In finer grained layers, many armored lapilli consisted of coated olivine grains. Within both Type I and II lapilli, some pyroclasts have dark, fine-grained quenched rims showing swirled and streaked laminations defined by opaque oxide grains (Fig. 11); these tephra always possess partially rounded to subspherical forms. In thin section, the lapilli include two main types: dark lapilli containing abundant opaque oxide grains (Fig. 10B, D, and F) and oxide-poor lapilli consisting primarily of chlorite (Fig. 10B and E). Both lapilli types exhibit similar shapes, commonly contain fine vesicles, and show replaced olivine phenocrysts. Common constituents of andesitic and dacitic eruptions, such as ragged pyroclastic grains with plagioclase microlite pseudomorphs or plagioclase and quartz crystal fragments (Fisher and Schmincke, 1984), were not observed.

Small, widely spaced circular structures, now filled with microquartz showing a radial structure, carbonate, or axiolitic chlorite (Figs. 10C and F and 11), indicate that many lapilli were weakly vesicular. Commonly, 30–60% of the lapilli in a given sample show vesicles, and, in most, vesicles constitute

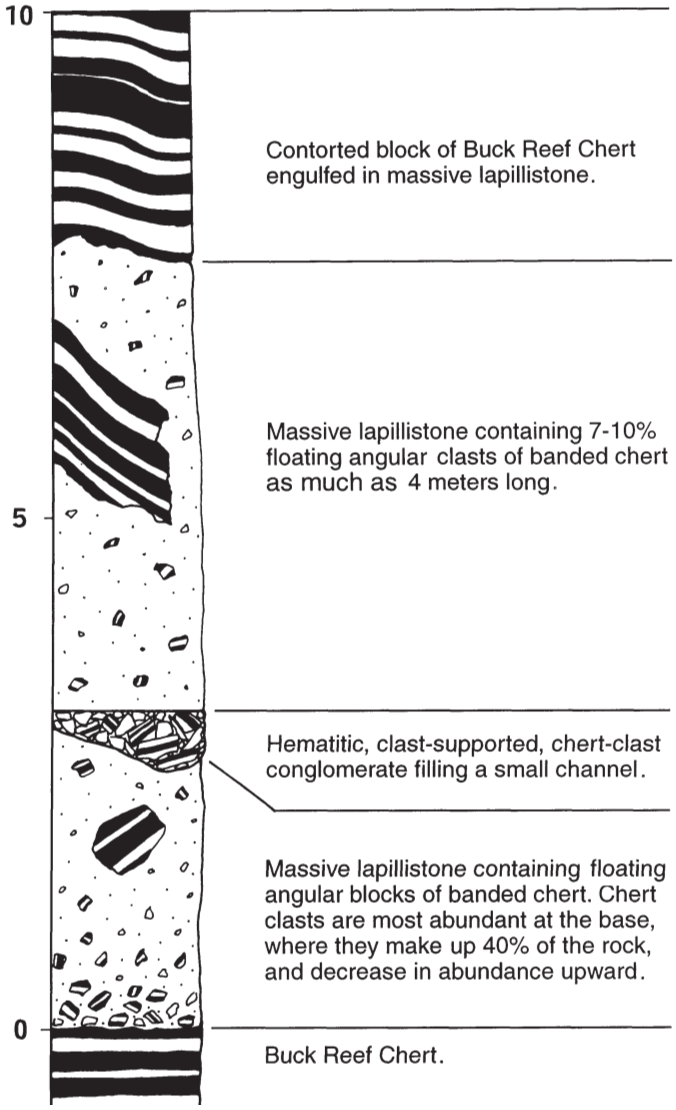


Figure 7. Measured stratigraphic section (Fig. 3, location 1) through the lowest 10 m of the volcaniclastic deposits inside the crater in the Buck Reef Chert. The basal tuffaceous division (K2v-a) is absent within the crater and deposits of the lapillistone and lapilli tuff division (K2v-b) rest directly on the Buck Reef Chert.

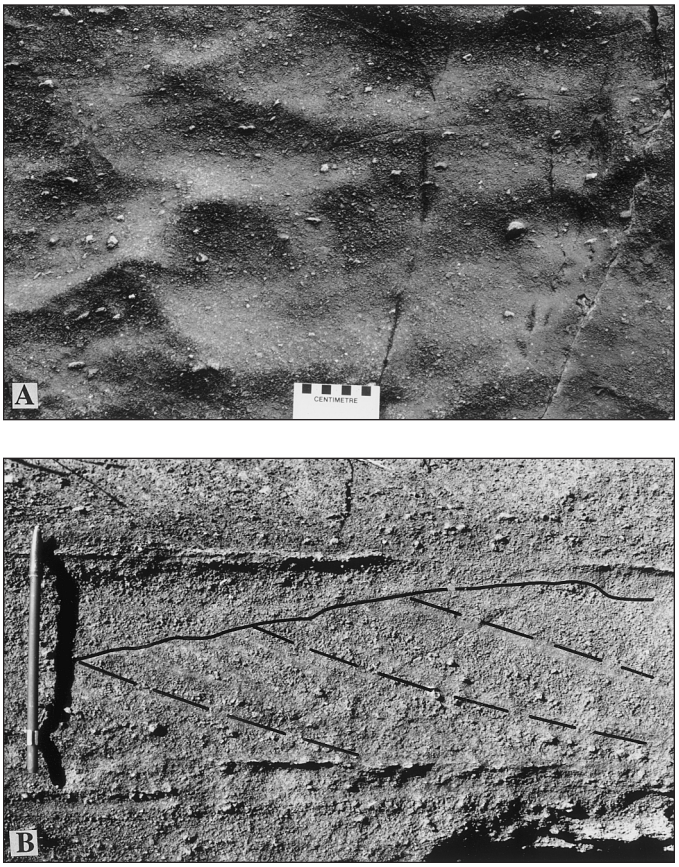


Figure 8. Outcrop photographs of the lapillistone and lapilli tuff division. A, Massive lapillistone containing randomly distributed larger tephra and accidental clasts in a matrix of material that is mostly 0.5–2 mm in size. B, Cross-stratified lapilli tuff from the upper part of the K2v-b division. Cross-sets (dashed), about 20 cm thick, dip uniformly to the right (east). The top of the lower set has been cut by a small scour filled by massive lapilli. The base of this scour is shown as a solid line.

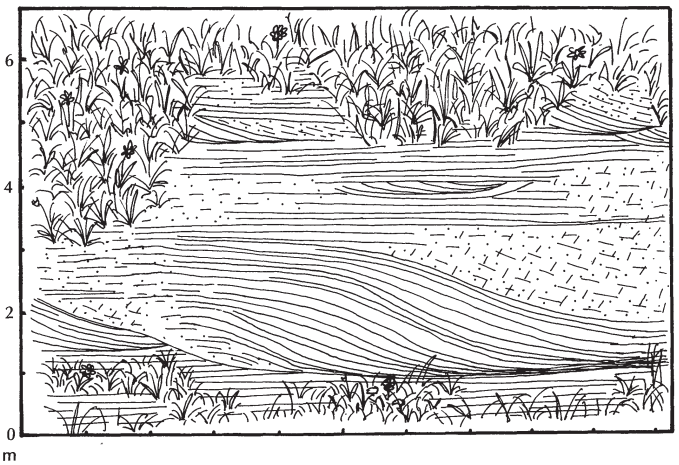


Figure 9. Sketch of well-preserved dune cross-stratification 1.5 m high in lapilli tuff at the top of the lapillistone and lapilli tuff division (K2v-b). Stratification is defined by alternating laminations of coarse lapilli (0.3–0.5 cm) and fine ash.

less than 20 volume% of individual lapilli. Virtually all vesicles are less than 0.2 mm in diameter and most are less than 0.1 mm.

Accidental material in K2v-b is mainly sedimentary ejecta, dominated by clasts of Buck Reef Chert, but chunks of stratified ferruginous tuff and bluish tuff that appear to have been derived from the basal tuffaceous division (K2v-a) also occur. Sedimentary blocks are equidimensional to tabular in shape. Accidental igneous blocks are rounded and include rare coarse-grained pyroxenite and dunite. Accidental blocks, with the exception of pieces of Buck Reef Chert, have a maximum cross section of 0.5 × 1.5 m; those of Buck Reef Chert reach sizes 15 m long and 3 or 4 m wide at the base of the section (Fig. 7). Smaller acci-

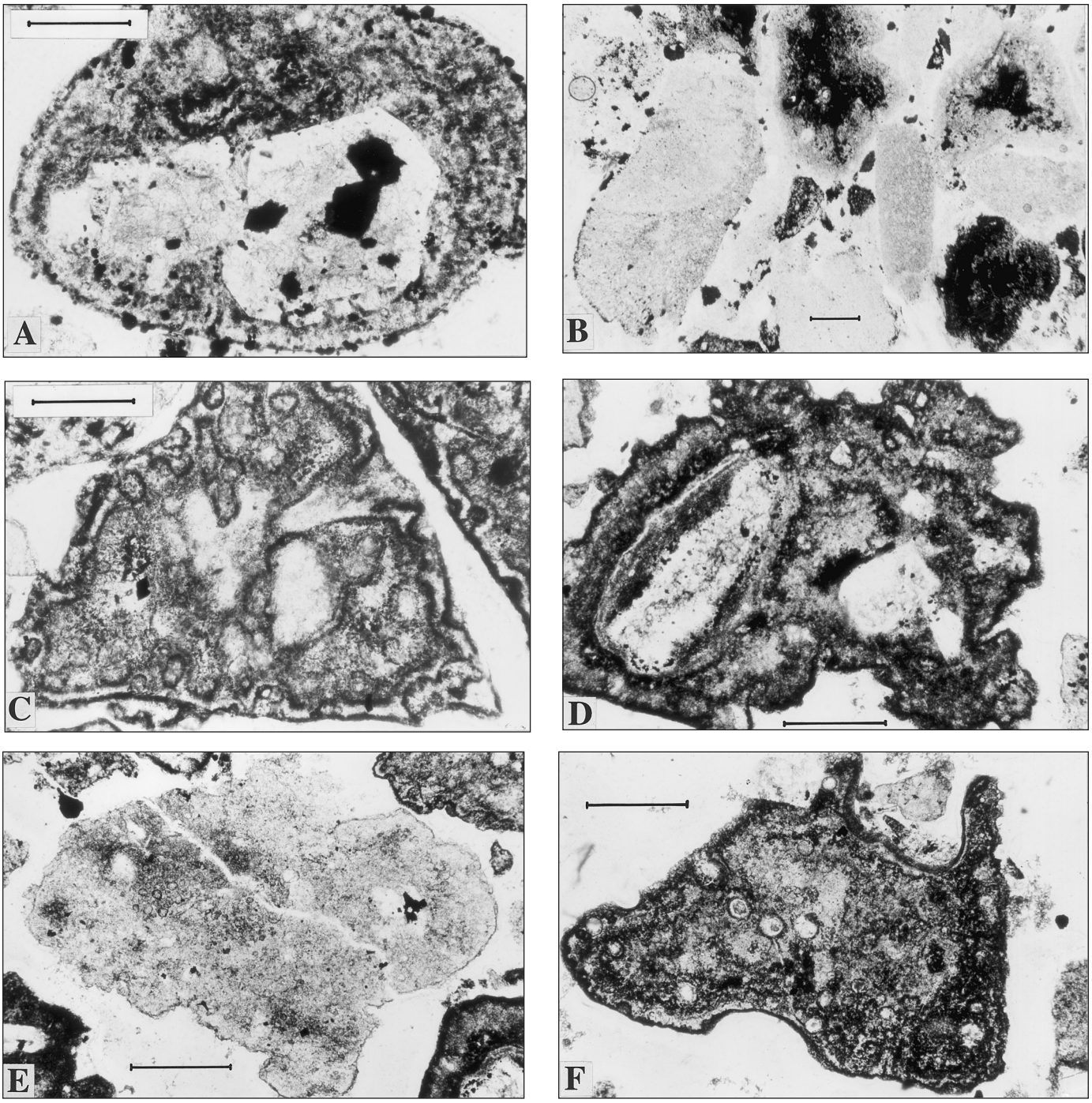


Figure 10. Lapilli types. Scale bars in all photos are 0.5 mm long. A, Rounded lapillus containing chrome spinel-bearing (black squares) in olivine phenocrysts (clear) replaced by quartz. B, Mixed oxide-rich (dark) and oxide-poor (light) lapilli. This sample has not been silicified and both lapilli types are composed largely of chlorite, tremolite, and serpentine. C, Type I lapillus of Wohletz (1983) showing straight to curved sides that truncate small vesicles. The interior of the lapillus appears to contain angular phenocryst remanents (clear), now replaced by quartz. D, Lumpy Type II, oxide-rich armored lapillus that includes olivine phenocryst pseudomorph (clear, right) and unidentified larger clast (left) collectively coated by heterogeneous glassy layers. E, Type II, oxide-poor, chlorite-rich lapillus. F, Oxide-rich lapillus containing numerous small vesicles and portions of several larger vesicles.

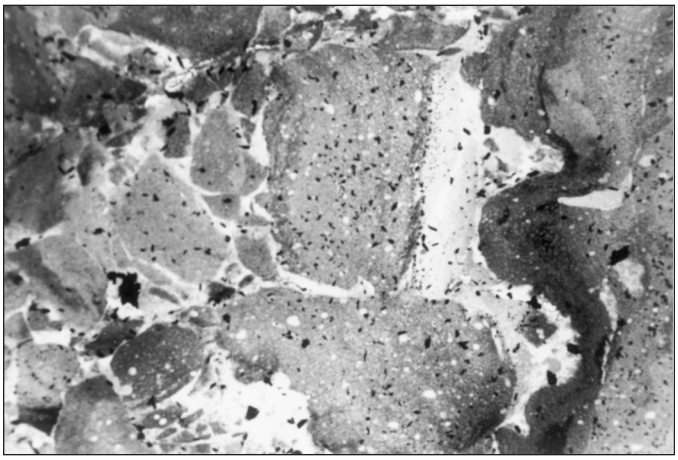


Figure 11. Photomicrograph of large lapilli, some showing partial dark, fine-grained, quench rims. Present mineralogy is chlorite, iron and titanium oxides, and microquartz. Note small rounded vesicles and the rounded, lobate shapes of the lapilli. Plane light. Photograph is approximately 2 mm across.

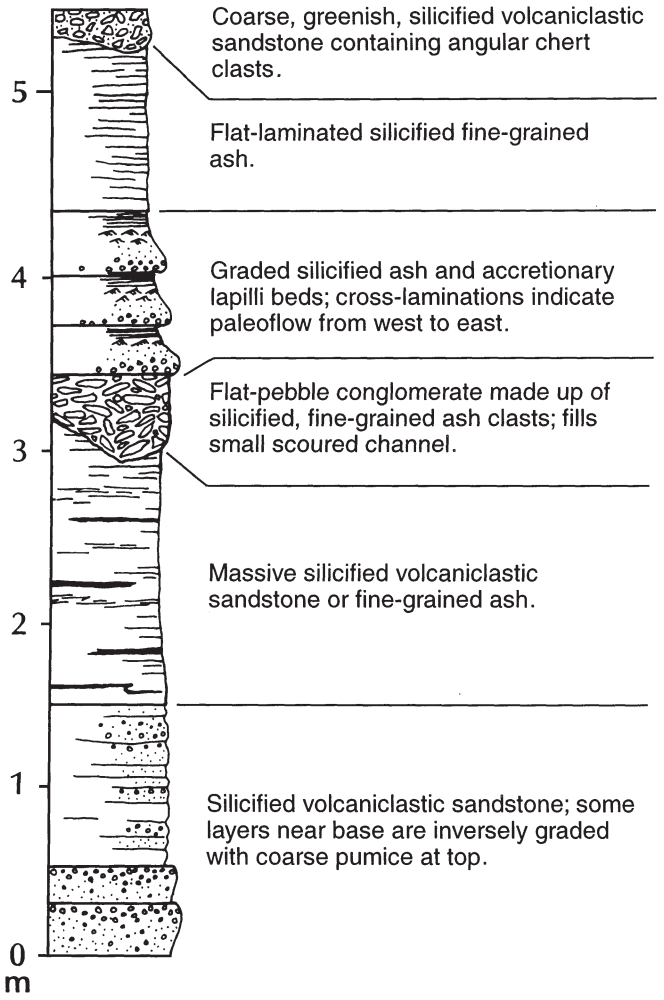


Figure 12. Measured stratigraphic section of the capping chert, K2c, in the western part of the study area (Fig. 3, location 4). Note the presence of channels filled with intraformational conglomerate, inversely graded beds near the base, and the abundance of current structures.

dental fragments (<5.0 cm across) are almost exclusively chert. Rounded igneous clasts, possibly bombs, are composed of fine-grained mafic volcanic rock. Although scattered throughout the lapilli division, accidental components tend to be concentrated in the lower third of the deposit. Blocks and bombs are also most abundant in the central part of the study area, in and adjacent to the crater in the Buck Reef Chert (Fig. 6).

Olivine-phyric mafic dikes in which the olivine has been altered and locally replaced by microquartz are common in the lowest part of the lapillistone sequence within the crater and lace extensively through the Buck Reef Chert below and adjacent to the crater (Fig. 6). Such dikes are absent in the upper part of the division within the crater and were not seen outside of the crater.

Capping chert (K2c). The upper division of the volcaniclastic member heralds the cessation of coarse-grained, mafic pyroclastic volcanism on the west limb of the Onverwacht anticline. It is as much as 8 m thick and crops out as a distinctive resistant chert marker. Much of K2c is composed of massive or faintly laminated, fine-grained, pale greenish to bluish silicified ash (Figs. 12 and 13). This ash is overlain by pumiceous layers, accretionary-lapilli-bearing tuffs, intraformational flat pebble conglomerate, and coarse-grained current-structured to massive volcaniclastic sandstone. Accretionary lapilli occur in graded accretionary lapilli and ash beds that are commonly current structured at the top. K2c is well bedded and shows rapid facies changes. Current structures are common and uniformly indicate flow from west to east. Member K2c is absent in only a few areas where mafic pillowed volcanic rocks of K3v rest directly on pyroclastic rocks of K2v.

The capping chert has been altered to a fine micromosaic of quartz, sericite, green phyllosilicates, and oxides; but textural features as small as 20–40 microns across are well preserved (Fig. 14). Petrographic analysis of pseudomorphs indicate that the original clastic material included vitric grains, microlitic pyroclasts, pumice, prong-shaped shards, and accretionary lapilli. Some grains show internal features such as small vesicles, silicified olivine phenocrysts, and possible pilotaxitic textures (Fig. 14).

DISCUSSION

Composition of the original magma

Volcanic rocks in the type section of the Kromberg Formation are primarily basalts and komatiites (Viljoen, R. P., and Viljoen, 1969a; Vennemann and Smith, this volume, Chapter 5). On the west limb of the Onverwacht anticline, volcanic flows in the basal tuffaceous division (K2v-a) and at the top of the lapillistone and lapilli tuff division (K2v-b) have intersertal and intergranular textures similar to those of basalts and more mafic

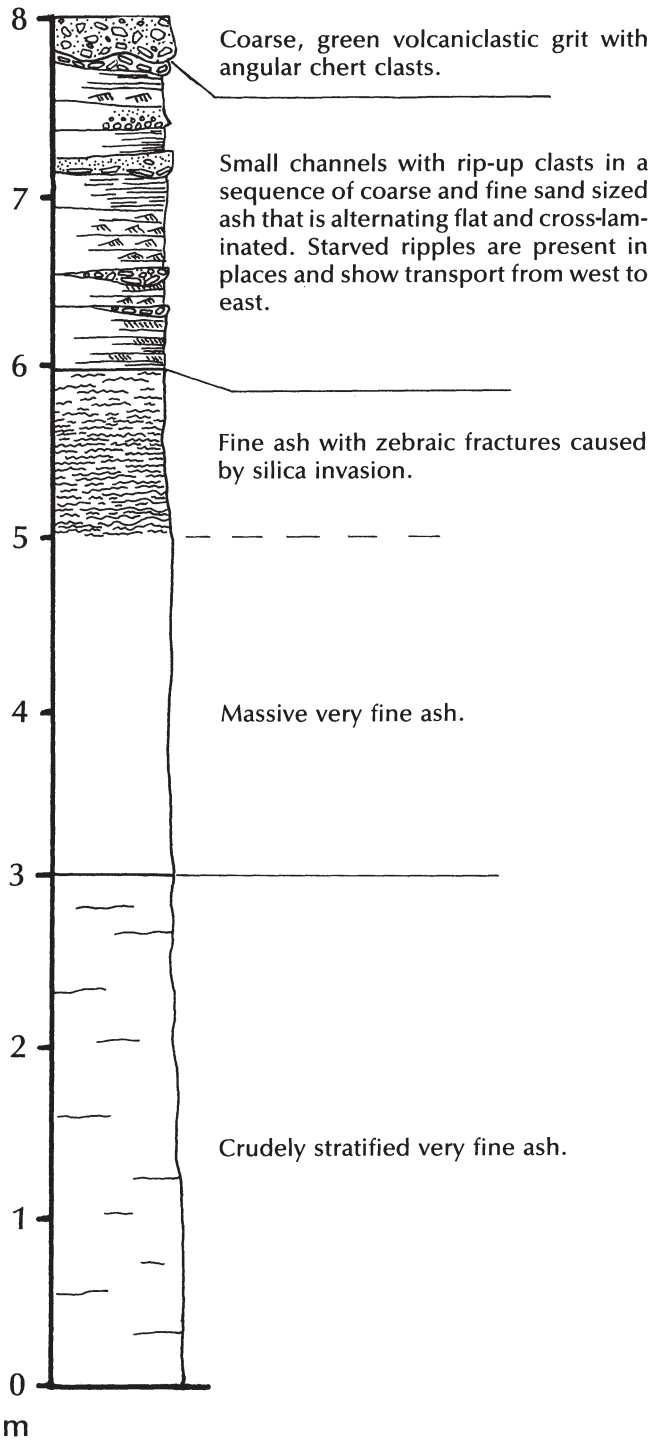


Figure 13. Measured stratigraphic section of K2c in the eastern part of the study area (Fig. 3, location 5). Note the abundance of current structures in the upper part of the unit and presence of intraformational conglomerate.

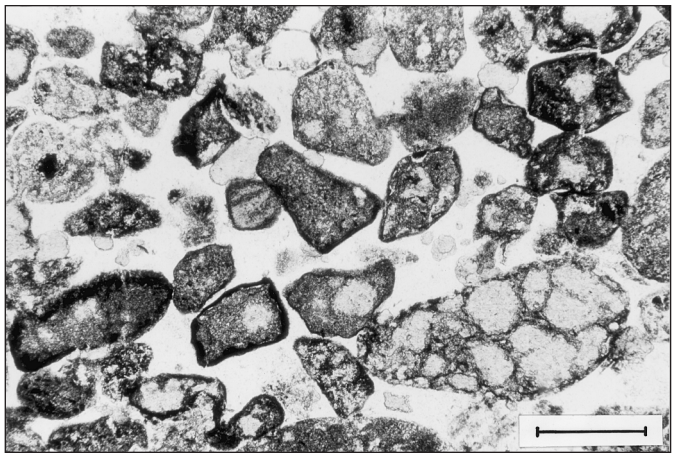


Figure 14. Photomicrographs of volcaniclastic sand grains in K2c. Scale bar is 0.5 mm long.

rocks. These lava flows are similar to those in the overlying basalt member (K3v), which chemical data show to be mainly tholeiitic basalts (Byerly, unpublished).

Pyroclasts in the volcaniclastic division of the Kromberg Formation are composed largely of Fe- and Mg-rich alteration products such as chlorite, tremolite, and talc, like many altered mafic and ultramafic flow rocks in the Onverwacht Group. Where primary textures are well preserved, lapilli from the volcaniclastic division commonly contain microquartz pseudomorphs of olivine and pyroxene phenocrysts suggesting original mafic magma compositions. Tephra Types I and II of Wohletz (1983), which predominate throughout K2v-b, are also suggestive of mafic liquids. Overall, pyroclasts in the Kromberg Formation are similar in shape and texture to basaltic and ultramafic pyroclasts described by Heiken (1972), Stolz and Nesbitt (1981), and Echeverria and Aitken (1986). Absent from the Kromberg Formation in the study area are coarse fragmental breccias characteristic of felsic volcanic sequences, such as H6 at the top of the Hooggenoeg Formation (Viljoen, R. P., and Viljoen, 1969a).

Geochemistry. Major and trace element compositions (Table 1) were determined for a large juvenile block from the lapillistones and for a mafic dike containing altered olivine phenocrysts that cuts the base of the lapillistone and lapilli tuff division in the vicinity of the crater in the Buck Reef Chert. The dike is 10- to 20-cm-thick and may represent either a comagmatic liquid that was injected into its overlying pyroclastic pile or a rootless dike (Fuller, 1931) associated with a K2v-b lava flow. Both samples represent magmas that were probably coeval with volcanism in division K2v-b. For chemical analysis, only relatively unweathered samples that contained little or no secondary carbonate were selected. Thus, no samples of lapillistone and lapilli tuff were analyzed. An analysis of a sample of carbonated lapillistone from the type section of the Kromberg Formation is given by Lowe (this volume, Chapter 3, Table 1). All three samples were analyzed by XRF at the University of Ottawa in Canada.

TABLE 1. MAJOR ELEMENT (WT. %) AND TRACE ELEMENT (PPM) CHEMISTRY OF ROCKS FROM THE VOLCANICLASTIC MEMBER (K1) OF THE KROMBERG FORMATION ON THE WEST LIMB OF THE ONVERWACHT ANTICLINE

Oxides	Sa62-1*	Sa62-2*
SiO2	52.91	50.80
Al2O3	6.96	5.91
FeO	13.01	12.38
MgO	15.20	20.35
CaO	8.80	8.45
Na2O	1.98	1.12
K2O	0.04	0.05
TiO2	0.86	0.72
P2O5	0.00	0.00
MnO	0.25	0.22
TOTAL	100.01	100.00
LOI	3.32	3.25
Ba	57	54
Cr	1631	1365
Zr	44	71
Sr	50	24
Y	17	20
Nb	0	4
Zn	50	29
Ni	296	928
V	337	171
Al/Ti	7.1	7.3
Ti/Zr	1117.0	60.8
V/Zr	7.7	2.4
Ti/V	15.3	25.5

*Sample descriptions:
Sa62-1 Comagmatic mafic dike in volcaniclastic member.
Sa62-2 Volcanic bomb.

Data in Table 1 show that the rocks analyzed have high Mg, Cr, and Ni contents as well as Al_2O_3/TiO_2 ratios above 7. This chemistry is similar to that of many komatiites in the Komati and Mendon Formations (Viljoen, M. J., and Viljoen, 1969; Smith and Erlank, 1982; Smith et al., 1984; Byerly, this volume, Chapter 8). The high concentration of immobile trace elements, such as Cr, V, and/or Y, at constant Zr, Ti, or Al indicates that these rocks were originally mafic to ultramafic in composition (Byerly et al., 1983; Smith et al., 1984; Duchac and Hanor, 1987; Hanor and Duchac, 1990; Lahaye et al., 1995). Although these rocks have high SiO_2 and Na_2O contents, similar to those of felsic rocks, it is likely that these reflect later metasomatic alteration and silicification.

Texturally, the silicified ash of K2c closely resembles other silicified ash layers that directly overlie komatiitic volcanic units throughout the Onverwacht Group (Lowe, this volume, Chapter 3). These units include the Middle Marker (Lanier and Lowe, 1982), cherts H3c and H4c in the Hooggenoeg Formation (Lowe and Byerly, this volume, Chapter 1), and the Msauli Chert (Lowe and Knauth, 1978; Stanistreet et al., 1981; Lowe, this volume, Chapter 9). Chemical analyses of these units suggest that they formed by the silicification of komatiitic ash (Lowe, this volume, Chapter 3).

On the basis of these compositional and textural features, we infer the parental magma of the pyroclastic debris in the volcaniclastic member of the Kromberg Formation to have been mafic to ultramafic in composition, possibly basaltic komatiite.

Early explosive activity and crater formation

The thickness trends and facies of the volcaniclastic member suggest that sections on the central part of the west limb of the Onverwacht anticline were located close to a volcanic center. Geologic mapping indicates that this area exposes a cross section of an explosion crater and the overlying, highly modified tuff cone. This crater (Fig. 6) is characterized by (1) a zone about 1.7 km wide along strike over which the upper two-thirds to half of the Buck Reef chert has been removed by explosive activity; (2) the thickest section of the volcaniclastic member, about 1,000 m; (3) the most abundant and largest accumulation of volcanic bombs and accidental blocks of Buck Reef Chert; and (4) the presence of abundant, small, anastomozing, olivine-rich mafic dikes that cut the lower part of the volcaniclastic member and the adjacent Buck Reef Chert along and below the margins of the crater.

The western wall of the crater is covered by modern slope debris. The eastern wall is well exposed and originally formed a vertical face 250–300 m high. The evaporite member marking the base of the Buck Reef Chert (Lowe and Fisher Worrell, this volume, Chapter 7) passes continuously below this wall from a section where it is overlain by less than 50 m of chert beneath the crater floor to a section 100 m to the north where the evaporites are overlain by more than 300 m of chert. In addition, the Buck Reef Chert in the vicinity of the crater shows several small normal faults that cut steeply across bedding, offsetting the evaporite member. Some of these faults intersect the floor of the crater where they end without offsetting the upper surface of the Buck Reef Chert or the overlying lapilli deposits (Fig. 6). These features indicate that faulting predated formation of the crater and deposition of the lapilli. Similar small normal faults, a few kilometers to the west, have been shown to have formed during deposition of the lowest part of the Buck Reef Chert (Lowe and Fisher Worrell, this volume, Chapter 7).

The lowest 100–200 m of K2v-b inside the crater are largely covered by recent colluvium, but exposures on and near the crater floor are present. These outcrops consist of massive lapillistone, coarse breccia containing blocks of Buck Reef Chert as much as 15 m across, flow rock, and mafic intrusive rocks (Fig. 7). The Buck Reef Chert adjacent to the 250- to 300-m-high eastern crater wall is shattered and cut by numerous olivine-phyric dikes and sills. The emplacement of these intrusions appears to have coincided with the eruption and deposition of the Kromberg lapilli section as evidenced by (1) dikes within the lower part of the lapillistone section that contain isolated lapilli, and (2) the great abundance of similar dikes and sills in the Buck Reef Chert immediately below and adjacent to the crater.

It seems most likely that this crater formed by the removal of the upper 250–300 m of Buck Reef Chert, as a result of one or

more violent, hydromagmatic explosions that marked the initiation of coarse pyroclastic volcanism in the Kromberg Formation on the west limb of the Onverwacht anticline. The large volume of accidental material ejected during this explosive phase suggests that it may have been a "gas eruption" in the sense of Mastin (1995). Such explosions are characterized by high explosivity of short duration, typically ejecting a relatively small amount of material. Gas eruptions occur mainly in systems where the escape of magmatic gases is blocked. It seems likely that the 350- to 400-m-thick, impermeable Buck Reef Chert could have provided a substantial barrier to upward magma migration and volatile escape. It is noteworthy that several large stratiform mafic intrusions occur within the Buck Reef Chert immediately east of the crater locality (Fig. 3). The age of these intrusions is constrained only to being younger than the Buck Reef Chert, but similar intrusions are absent above it. These may be intrusive equivalents of K2v-b that never completely vented to the surface.

The volcanic and sedimentary rocks below the Buck Reef Chert were probably water saturated. The Buck Reef Chert itself, at that time, was probably composed mainly of opaline silica, which commonly contains 5–10% water, and other water-saturated sediments. These units would have provided considerable water to magmas trapped below the chert. During emplacement of the magmas that fed the Kromberg pyroclastic eruptions, both volatiles and magmas may have been trapped beneath and within the Buck Reef Chert until brittle fracturing through the chert occurred. The resulting pressure release, perhaps accompanied by sea-water flooding, could have triggered a gas eruption and explosive stripping of the upper part of the chert and the overlying basal tuffaceous division (K2v-a).

Moore (1985) has outlined a mechanism by which Surtseyan eruptions, during continuous-uprush explosions, can quarry several hundred meters into the deep volcanic pile and underlying sedimentary deposits. In the Kromberg Formation, accidental blocks of Buck Reef Chert are most abundant and largest near the base of the crater fill, and the lapillistones containing these ejecta are clearly horizontally stratified. These features suggest that excavation of the crater and formation of large accidental blocks accompanied the early stages of pyroclastic volcanism.

The small amount of dike rock in the crater fill suggests that the exposed section does not intersect the crater center but represents a slice across the crater periphery.

Formation of the pyroclasts

More than 95% of the juvenile debris in the lapillistone and lapilli tuff division are monogenetic and reworked pyroclasts. The abundance of Type I and II pyroclasts of Wohletz (1983) suggests that hydromagmatic fragmentation was the primary mechanism of pyroclast formation (Carlisle, 1963; Heiken, 1972; Wohletz, 1983). The absence of pumice and overall low vesicularity of the pyroclasts indicate that rapid vesiculation was not a major factor in the fragmentation process; and the paucity of volcanic flows within the lapilli deposits indicates that cooling-contraction granulation (Kokelaar, 1986) along the margins of such flows also played a minor role in forming pyroclasts.

The most likely mechanism for the complete fragmentation of a magma to form Type I and II pyroclasts is contact-surface steam explosivity (Kokelaar, 1986), also called fuel-coolant interactions (Sheridan and Wohletz, 1983). In magmatic fuel-coolant interactions, fragmentation results from mechanical shocking, produced as steam films and bubbles form, grow, and collapse along the magma/water interface. The optimal water:melt mixing ratio for highly explosive fuel-coolant interactions involving basaltic magmas is in the range 0.1–0.3. Explosion products in experimental systems near this optimum mixture are always fine ash less than 50 microns in size (Sheridan and Wohletz, 1983). Larger particles (1–10 mm) are formed under less explosive conditions at lower or higher water:magma ratios. Although it is possible that some fine ash was transported completely outside of the area represented by the Kromberg outcrops, there is little evidence in the lower part of K2v-b that a substantial amount of fine hydroexplosive material was formed. The shapes and sizes of the Kromberg pyroclasts in the study area suggest water:magma ratios outside the optimal range for highly explosive fuel-coolant interactions. As a result, eruptions following the initial explosions that formed the crater were probably of relatively low explosivity. Such eruptions were probably responsible for the formation of the lapillistone sequence.

Many subaqueous pyroclastic eruptions involve periodic, short-lived explosive jetting; but where there is a balance between the rate of magma eruption and the inflow of water, large eruptions can produce continuous uprush columns (Kokelaar, 1983). When fully subaqueous, uprush columns can form steam-filled cupolas or water exclusion zones (Kokelaar, 1983, 1986; White, 1996). An abundance of armored lapilli, such as occur in the Kromberg lapillistones and lapilli tuffs, suggests the existence of a subaqueous steam-filled cupola during eruption of K2v-b (Fig. 16).

Environments and processes of deposition

Basal tuff division (K2v-a). In western exposures, K2v-a is composed largely of fine-grained laminated tuff indicating deposition in a quiet, low-energy, subaqueous setting, below storm wave base, probably at water depths in excess of 100 m. The presence of coarser, cross-stratified layers and thinner sections toward the east suggests deposition under shallower, but still largely quiet and subaqueous conditions, perhaps within storm wave base.

Lapillistone and lapilli-tuff division (K2v-b). The volcaniclastic debris in K2v-b were deposited by at least three mechanisms of sedimentation: (1) sediment gravity flows, (2) pyroclastic falls, and (3) current-related traction transport. The characteristics of these processes are outlined below.

The lower part of K2v-b is dominated by thick, grain-supported lapillistone beds that lack current structures; appear massive or show normal size grading, commonly of both juvenile and accidental debris; locally include thin basal inversely

graded layers; and show density grading by the presence of large "floating clasts" of comparatively low density K2v-a tuff at their tops (Figs. 4 and 5). These features suggest that the debris were size and density sorted within dense sediment flows. The basal inversely graded layers probably represent traction carpets, which develop as collision-dominated laminar bed-load layers at the bases of turbidity currents (Lowe, 1979, 1982). Normal grading of lapilli and accidental chert clasts in the overlying parts of many beds indicates differential grain settling and suggests that, for the most part, the flows were not strongly cohesive and were, therefore, not actual debris flows. The flows were probably high-density turbidity currents (Lowe, 1982), powered by eruption column collapse. Some more massive or poorly sorted lapilli beds, especially those containing a fine tuffaceous matrix, may have been deposited by debris flows.

Some of the thick, grain-supported, largely ash-free, massive or normally graded lapilli beds in the lower part of member K2v-b, especially inside the crater, may have been deposited from subaqueous pyroclastic falls. Fall deposits can be difficult to distinguish from sediment-flow deposits. The monogenetic character of the debris, the low ash content, and the random to normally graded distribution of larger clasts are common to both deposit types (Cashman and Fiske, 1991; Lirer and Vinci, 1991; Lirer et al., 1996).

Tephra in the upper 30–100 m of K2v-b on the west limb of the Onverwacht anticline and in many Kromberg units elsewhere were deposited as traction or bed-load material by energetic currents (Ransom, 1987). Preserved structures include well-developed layering, flat-stratification, large-scale cross-stratification (Fig. 9; Viljoen, M. J., and Viljoen, 1969, Plate XIa), and cross-lamination.

Although it is often difficult to distinguish between rapidly deposited, coarse-grained subaerial and subaqueous pyroclastic deposits, a number of features make it clear that the lapillistone and lapilli tuff division in the study area was deposited subaqueously. (1) The deposits largely lack the fine stratification and thin, complex layering characteristic of subaerial near-vent pyroclastic fall and surge deposits (Heiken, 1971; Walker, 1981; Fisher and Schmincke, 1984). (2) Current structures, common in both subaerial and shallow-water pyroclastic deposits (Sigvaldason, 1968; Fisher and Schmincke, 1984) are absent in all but the uppermost part of the volcaniclastic member. (3) Thick, dense sediment flows redistributed much or most of the debris in the lower part of the member. Although debris flows can occur in both subaerial and subaqueous depositional settings, turbidity currents are restricted to subaqueous settings. In addition, studies of phreatomagmatic volcanic deposits in the Oregon Cascades and Japan (Fiske and Matsuda, 1964) have shown that the collapse of subaqueous eruption columns commonly results in the deposition of thick, grain-supported, subaqueous sediment-flow sequences. (4) Angle-of-repose, or similar steep depositional slopes, common in subaerial pyroclastic settings are absent in the Kromberg Formation. The redistribution of tephra by subaqueous sediment flows would have formed depositional slopes like those in submarine settings, which are commonly less than a degree. (5) Accretionary lapilli, a common product of subaerial phreatomagmatic eruptions (Moore and Peck, 1962; Fisher and Schmincke, 1984; Gilbert and Lane, 1994) and common in subaerially erupted mafic and ultramafic tuffs throughout the Onverwacht Group (Lowe and Knauth, 1978; Lowe, this volume, Chapters 3 and 9), including K2c, are absent in K2v-b.

The overall sequence in K2v-b in the crater area shows an upward transition from a basal unit dominated by subaqueous fall and sediment flow deposits through a transitional zone characterized by crude flat layering to an upper division showing well-developed large-scale cross-stratification and other high-energy current structures (Fig. 9). This succession indicates a gradual shoaling upward from a deep subaqueous, sediment-flow-dominated setting to shallow-water current- and/or wave-active conditions.

A number of stratigraphic and sedimentological features suggest that the lapillistone and lapilli-tuff division in the study area was deposited over a relatively short period of time during one, or a series of closely spaced volcanic events. Lapilli throughout the section are remarkably homogeneous, both texturally and compositionally. There is also a gradual transition between the basal, massive sediment-flow- and fall-dominated division of K2v-b and the overlying well-stratified, current-deposited lapilli tuffs as well as a smooth upward decrease in the number and size of accidental clasts. Neither the lapilli deposits nor the sparse interfingering mafic volcanic flows show any evidence of prolonged depositional breaks such as weathering horizons or rinds, erosional breaks or scour surfaces, fine-grained suspension, or biogenic deposits.

It is probable, therefore, that the lapilli deposits of K2v-b accumulated rapidly, perhaps over an interval of a few months to a few years, as is common in monogenetic pyroclastic eruptions. Therefore, because the uppermost part of K2v-b and all of K2c are shallow-water deposits, the thicknesses of the volcaniclastic member provides an estimate of the water depth. The sea floor before the beginning of the eruption would have been at the top of the basal tuff division, K2v-a. Removal of K2v-a and 300 m of underlying Buck Reef Chert would have abruptly increased water depths in the immediate vicinity of the volcanic vent by about 300 m. The thickness of the massive lapillistone deposited above the crater floor within the crater is approximately 500–600 m. Above the massive lapillistone is about 300–400 m of crudely stratified tuff and lapillistone, and the top 50–100 m of K2v-b shows abundant current structures. Overlying the stratified lapilli tuffs is the capping chert (K2c), which everywhere shows abundant features indicating deposition under very shallow water to emergent conditions. The basal 300 m of K2v-b represents crater fill. The thickness of the overlying lapillistone and lapilli tuff section suggests an initial eruption depth of about 600–700 m. Only 4 km to the west (Lowe and Byerly, this volume, Chapter 1, Fig. 8), K2v-b is about 600 m thick below K2c, also suggesting a maximum water depth at the start of the accumulation of K2v-b of 600 m. This calculation assumes no subsi-

dence or magma-chamber deflation during eruption and, hence, provides a probable maximum estimate of water depth. If there was substantial deflation of a magma chamber located within or immediately beneath the Buck Reef Chert as the eruption proceeded, the initial eruption water-depth could have been substantially less, perhaps closer to the 500–400 m depth at which vesiculation becomes a common mechanism of pyroclast formation in sea-floor basaltic eruptions today (Oehmig and Wallrabeadams, 1993; Lackschewitz et al., 1994).

Pyroclastic volcanism at water depths of 600–700 m would have formed a substantial subaqueous eruption column (Sheridan and Wohletz, 1983; Cashman and Fiske, 1991). Winnowing and removal of fines by currents within this water column would have produced proximal deposits consisting of coarse-grained, well-sorted, grain-supported pyroclasts (Fiske and Matsuda, 1964; Cashman and Fiske, 1991; White, 1996), like those characterizing the lower part of K2v-b. Subaqueous column collapse could also have fed laterally moving turbidity currents and debris flows, analogous to subaerial base surges, that would have carried most of the coarse debris away from the vent where it would have been deposited as an apron of surge deposits having a surface slope of a few degrees or less (Figs. 15 and 16).

At the top of K2v-b, the orientation, abundance, and size of cross-stratification indicates that these sediments were deposited and reworked by strong, persistent, eastward-flowing currents. The uniform current directions across the study area indicate that these layers were not deposited by base surges or other eruption-related currents or flows. Because the vent must have been topographically higher than its surrounding pyroclastic apron, it is probable that these shallow-water deposits reflect the existence of a subaerial vent. The uppermost part of the current-structured sequence may reflect the erosion and reworking of subaerially exposed parts of the pyroclastic cone within an energetic shallow-water environment after volcanism had ceased.

Capping chert (K2v-c). The transition from the uppermost current-structured lapilli tuffs to the capping chert marks the transition from the accumulation of coarse sediment under energetic shallow-water conditions to the deposition of very fine-grained ash under less energetic but perhaps even shallower water conditions. It also reflects the termination of coarse pyroclastic volcanism and possibly the complete erosion of subaerial portions of the pyroclastic vent.

Sections of the capping chert vary rapidly in thickness and facies along strike (Figs. 12 and 13) and show widespread evidence for deposition under shallow-water conditions. Graded layers of accretionary lapilli and ash show an association of structures indicating deposition of airfall debris into shallow, flowing water (Lowe, this volume, Chapter 9). Units of intraformational conglomerate, commonly lenticular and filling small erosional channels, are present in most sections (Figs. 12 and 13). Other ash layers show abundant cross-lamination and flat current lamination. Layers of fine pumiceous debris, some inversely graded, probably indicate density stratification characteristic of airfall deposits. This collection of features is common to a family of silicified ash layers that directly overlie komatiitic and other mafic volcanic units throughout the Onverwacht Group (Lowe, this volume, Chapter 3), including the Middle Marker (Lanier and Lowe, 1982), cherts in the middle part of the Hooggenoeg Formation (H3c and H4c), and the Msauli Chert (Lowe and Knauth, 1978; Stanistreet et al., 1981; Lowe, this volume, Chapter 9). These layers everywhere show evidence for deposition under shallow water to intermittently exposed conditions (Lanier and Lowe, 1982; Lowe, this volume, Chapters 3 and 9). Common to most units of this type, but rare in K2c, are layers containing black carbonaceous material representing bacterial mats. The absence of mat layers in K2c suggests that little time ensued between airfall events and current reworking during its accumulation.

CONCLUSIONS

With the exception of a relatively thin basal tuff (K2v-a) and a fine silicified ash cap (K2c), the bulk of the Kromberg volcaniclastic member consists of coarse-grained, lapilli-sized pyroclastic debris deposited rapidly from subaqueous to subaerial phreatomagmatic eruptions (Figs. 15 and 16). Thickness trends in the volcaniclastic member; the distribution of blocks, bombs, and mafic pyroclasts; and the presence of a crater excavated into the underlying Buck Reef Chert indicate that a major center of explosive phreatomagmatic volcanism during Kromberg time is exposed on the west limb of the Onverwacht anticline. The regional distribution of pyroclastic rocks in the Kromberg Formation in the southern part of the Barberton Greenstone Belt indicates the existence of many other similar centers of pyroclastic volcanism during this stage of formation of the Onverwacht Group. Initial magmatic activity along the west limb of the Onverwacht anticline probably occurred in water no more than about 700 m deep as a result of a major hydromagmatic explosion that in one area removed the upper 300 m of the Buck Reef Chert and the overlying K2v-a division of the Kromberg volcaniclastic member. The resulting crater was then rapidly filled with backfalling explosion debris, newly generated pyroclastic materials, and liquid melt in the form of dikes and flows. Subsequent pyroclastic volcanism involved the formation of a steam-filled cupola or water exclusion zone at the base of a subaqueous eruption column. The fall of debris out of the eruption column produced both direct fall deposits and large subaqueous sediment flows that distributed materials around the vent as a gently sloping pyroclastic apron. Aggradation of the pyroclastic pile resulted in shoaling and eventual subaerial exposure of the vent. The top of the member records erosion of the subaerial part of the pyroclastic cone and sedimentation in energetic shallow-water systems. Overall, water depths during formation of these volcaniclastic deposits were shallow, less than 700 m and during late stages of eruption commonly less than 100 m.

The volcanic rocks of the Kromberg Formation are altered to greenschist-facies mineral assemblages. Nevertheless, relict textures and the distribution of the relatively immobile elements,

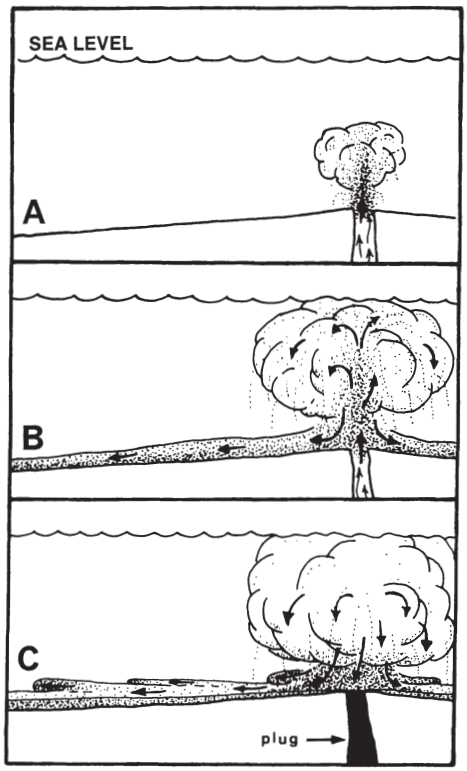


Figure 15. Sketch showing a subaqueous phreatomagmatic volcanic eruption and the generation of subsequent pyroclastic flows (modified from Fiske and Matsuda, 1964). A, Early stages of eruption. B, Climax of eruption; large subaqueous pyroclastic flows move down the sides of the accumulating pile of debris. C, Late stages of eruption. This style of eruption and sedimentation characterized the early stages of deposition of the lapillistone and lapilli tuff division (K2v-b).

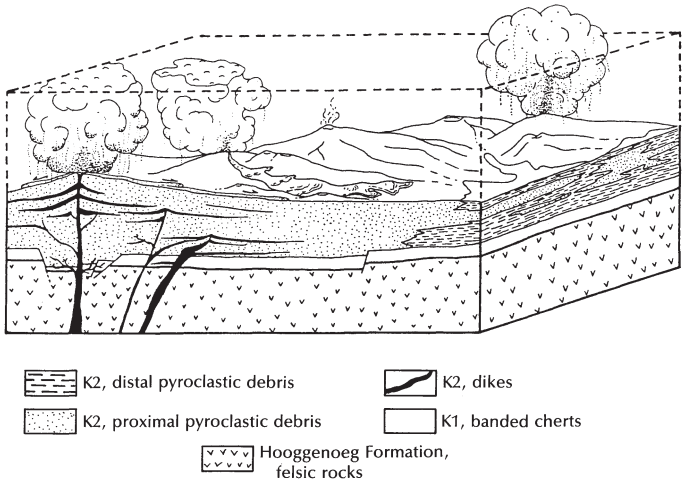


Figure 16. Schematic paleogeographic reconstruction of the Kromberg Formation on the west limb of the Onverwacht anticline during the deposition of the coarse lapilli deposits of the K2v-b division. Pyroclastic aprons, deposited on low slopes, were built by subaqueous phreatomagmatic eruptions that shallowed over time. Aggradation of the volcanic pile beyond what is shown here resulted in well-stratified lapilli-tuff deposition and eventual formation of subaerial eruption columns and shallow-water reworking of the pyroclastic debris.

such as Al, Ti, Zr, Cr, and V, provide compelling evidence that the initial rocks were mafic to ultramafic in composition. Chemical data suggests that the pyroclastic rocks of K2v-b were probably basaltic komatiites, with MgO contents of 15–25%.

Komatiitic volcaniclastic rocks in the Kromberg Formation are remarkably similar to komatiitic pyroclastic units described by Shaefer and Morton (1991) from the Late Archean Superior Province, Canada, and by Saverikko (1985) from the Late Archean of Finland. In each of these areas, the pyroclastic sequences are dominated by lapillistones and lapilli tuffs, with only a minor component of ash and dust. Similarities of these deposits indicate that explosive phreatomagmatic activity may have characterized many komatiitic eruptions.

REFERENCES CITED

Anhaeusser, C. R., Mason, R., Viljoen, M. J., and Viljoen, R. P., 1969, A reappraisal of some aspects of Precambrian Shield geology: Geological Society of America Bulletin, v. 80, p. 2175–2200.

Byerly, G. R., Lowe, D. R., Nocita, B. W., and Ransom, B. L., 1983, Apparent volcanic cycles in the Archean Swaziland Supergroup, Barberton Mountain Land, South Africa: a result of non-magmatic processes: Lunar and Planetary Science Conference, 14th, Houston, Abstracts, pt. 1, p. 84–85.

Byerly, G. R., Kröner, A., Lowe, D. R., Todt, W., and Walsh, M. M., 1996, Prolonged magmatism and time constraints for sediment deposition in the Early Archean Barberton Greenstone Belt: evidence from the Upper Onverwacht and Fig Tree Groups: Precambrian Research, v. 78, p. 125–138.

Carlisle, D., 1963, Pillow breccias and their aquagene tuffs, Quadra Island, British Columbia: Journal of Geology, v. 70, p. 48–71.

Cashman, K. V., and Fiske, R. S., 1991, Fallout of pyroclastic debris from submarine volcanic eruptions: Science, v. 253, p. 275–280.

de Wit, M. J., 1982, Gliding and overthrust nappe tectonics in the Barberton Greenstone Belt: Journal of Structural Geology, v. 4, p. 117–136.

de Wit, M. J., 1983, Notes on a preliminary 1:25,000 geological map of the southern part of the Barberton Greenstone Belt, *in* Anhaeusser, C. R., ed., Contributions to the geology of the Barberton Mountain Land: Geological Society of South Africa Special Publication 9, p. 185–187, plus map, scale 1:25,000.

de Wit, M. J., Hart, R., Martin, A., and Abbott, P., 1982, Archean abiogenic and probable biogenic structures associated with mineralized hydrothermal vent systems and regional metasomatism, with implications for greenstone belt studies: Economic Geology, v. 77, p. 1783–1801.

Dimroth, E., and Lichtblau, A. P., 1979, Metamorphic evolution of Archean hyaloclastites, Noranda area, Quebec, Canada. Part I: Comparison of Archean and Cenozoic sea-floor metamorphism: Canadian Journal of Earth Sciences, v. 16, p. 1315–1340.

Duchac, K. C., and Hanor, J. S., 1987, Origin and timing of the metasomatic silicification of an Early Archean komatiite sequence, Barberton Mountain Land, South Africa: Precambrian Research, v. 37, p. 125–146.

Echeverria, L. M., and Aitken, B. G., 1986, Pyroclastic rocks: Another manifestation of ultramafic volcanism on Gorgona Island, Columbia: Contributions to Mineralogy and Petrology, v. 92, p. 428–436.

Fisher, R. V., and Schmincke, H. -U., 1984, Pyroclastic rocks: Berlin, Springer-Verlag, 472 p.

Fiske, R. S., and Matsuda, T., 1964, Submarine equivalents of ash flows in the Tokiwa Formation, Japan: American Journal of Science, v. 262, p. 76–106.

Fuller, R. E., 1931, The aqueous chilling of basaltic lava on the Columbia River Plateau: American Journal of Science, v. 221, p. 281–300.

Gilbert, J. S., and Lane, S. J., 1994, The origin of accretionary lapilli: Bulletin of Volcanology, v. 56, p. 398–411.

Hanor, J. S., and Duchac, K., 1990, Isovolumetric silicification of Early Archean

komatiites: geochemical mass balances and constraints on origin: Journal of Geology, v. 98, p. 863–877.
Heiken, G. H., 1971, Tuff rings: Examples from the Fort Rock–Christmas Lake Valley Basin, South-central Oregon: Journal of Geophysical Research, v. 76, p. 5615–5626.
Heiken, G. H., 1972, Morphology and petrography of volcanic ashes: Geological Society of America Bulletin, v. 83, p. 1961–1988.
Hekinian, R., 1968, Rocks from the mid-oceanic ridge in the Indian Ocean: Deep Sea Research, v. 15, p. 195–213.
Humphris, S. E., and Thompson, G., 1978, Hydrothermal alteration of oceanic basalts by seawater: Geochimica et Cosmochimica Acta, v. 42, p. 107–125.
Hunter, D. R., 1974, Crustal development of the Kaapvaal Craton, I. The Archean: Precambrian Research, v. 1, p. 259–294.
Kokelaar, P., 1983, The mechanisms of Surtseyan volcanism: Journal of the Geological Society of London, v. 140, p. 939–944.
Kokelaar, P., 1986, Magma-water interactions in subaqueous and emergent basaltic volcanism: Bulletin of Volcanology, v. 48, p. 275–289.
Lackschewitz, K. S., Dehn, J., and Wallrabeadams, H. J., 1994, Volcaniclastic sediments from mid-oceanic Kolbeinsey Ridge, north of Iceland—evidence for submarine volcanic fragmentation processes: Geology, v. 22, p. 975–978.
Lahaye, Y., Arndt, N., Byerly, G. R., Chauvel, C., Fourcade, S., and Gruau, G., 1995, The influence of alteration on the trace-element and Nd isotopic compositions of komatiites: Chemical Geology, v. 126, p. 43–64.
Lanier, W. P., and Lowe, D. R., 1982, Sedimentology of the Middle Marker (3.4 Ga), Onverwacht Group, Transvaal, South Africa: Precambrian Research, v. 18, p. 237–260.
Lirer, L., and Vinci, A., 1991, Grain-size distributions of pyroclastic deposits: Sedimentology, v. 38, p. 1075–1083.
Lirer, L., Sheridan, M., and Vinci, A., 1996, Deconvolution of pyroclastic grain-size spectra for interpretation of transport mechanisms: An application to the AD 79 Vesuvio deposits: Sedimentology, v. 43, p. 913–926.
Lowe, D. R., 1979, Sediment gravity flows: Their classification and some problems of application to natural flows and deposits: Society of Economic Paleontologists and Mineralogists Special Publication 27, p. 75–82.
Lowe, D. R., 1982, Sediment gravity flows: II. Depositional models with special reference to the deposits of high-density turbidity currents: Journal of Sedimentary Petrology, v. 52, p. 279–297.
Lowe, D. R., and Knauth, L. P., 1977, Sedimentology of the Onverwacht Group (3.4 billion years), Transvaal, South Africa, and its bearing on the characteristics and evolution of the early Earth: Journal of Geology, v. 85, p. 699–723.
Lowe, D. R., and Knauth, L. P., 1978, The oldest marine carbonate ooids reinterpreted as volcanic accretionary lapilli, Onverwacht Group, South Africa: Journal of Sedimentary Petrology, v. 48, p. 709–722.
Lowe, D. R., Byerly, G. R., Ransom, B. L., and Nocita, B. R., 1985, Stratigraphic and sedimentological evidence bearing on structural repetition in Early Archean rocks of the Barberton Greenstone Belt, South Africa: Precambrian Research, v. 27, p. 165–186.
Mastin, L. G., 1995, Thermodynamics of gas and steam-blast eruptions: Bulletin of Volcanology, v. 57, p. 85–98.
Moore, J. G., 1985, Structure and eruptive mechanisms at Surtsey volcano, Iceland: Geological Magazine, v. 122, p. 649–661.
Moore, J. G., and Peck, D. L., 1962, Accretionary lapilli in volcanic rocks of the western continental United States: Journal of Geology, v. 70, p. 182–193.
Oehmig, R., and Wallrabeadams, H. J., 1993, Hydrodynamic properties and grain-size characteristics of volcaniclastic deposits on the Mid-Atlantic Ridge north of Iceland (Kolbeinsey Ridge): Journal of Sedimentary Petrology, v. 63, p. 140–151.
Paris, I., Stanistreet, I. G., and Hughes, M. J., 1985, Cherts of the Barberton Greenstone Belt interpreted as products of submarine exhalative activity: Journal of Geology, v. 93, p. 111–129.
Quinby-Hunt, M. S., Wilde, P., Corrigan, D., Dengler, A. T., and Normark, W. R., 1986, Very recent analogs of volcanogenic Archean sequences: Geology, v. 14, p. 48–51.
Ransom, B., 1987, The paleoenvironmental, magmatic, and geologic history of the ~3,500 Myr Kromberg Formation, west limb of the Onverwacht anticline, Barberton Greenstone Belt, South Africa [M.S. thesis]: Baton Rouge, Louisiana, Louisiana State University, 79 p.
Saverikko, M., 1985, The pyroclastic komatiite complex at Sattasvaara in northern Finland: Geological Society of Finland Bulletin, v. 57, p. 55–87.
Schaefer, S. J., and Morton, P., 1991, Two komatiitic pyroclastic units, Superior Province, northwestern Ontario: their geology, petrography, and correlation: Canadian Journal of Earth Sciences, v. 28, p. 1455–1470.
Seyfried, W. E., and Bischoff, J. L., 1979, Low temperature basalt alteration by seawater: An experimental study at 70 and 150 degrees C.: Geochimica et Cosmochimica Acta, v. 43, p. 1937–1947.
Sheridan, M. F., and Wohletz, K. H., 1983, Hydrovolcanism: basic considerations and review: Journal of Volcanology and Geothermal Research, v. 17, p. 1–29.
Sigvaldason, G. E., 1968, Structure and products of subaquatic volcanoes in Iceland: Contributions to Mineralogy and Petrology, v. 18, p. 1–16.
Smith, H. S., and Erlank, A. J., 1982, Geochemistry and petrogenesis of komatiites from the Barberton Greenstone Belt, South Africa, *in* Arndt, N. T., and Nisbet, E. G., eds., Komatiites: London, Allen and Unwin, p. 347–397.
Smith, H. S., O'Neil, J. R., and Erlank, A. J., 1984, Oxygen isotope compositions of minerals and rocks and chemical alteration patterns in pillow lavas from Barberton, *in* Kröner, A., ed., Archean geochemistry: New York, Springer Verlag, p. 115–137.
Spooner, E. T. C., and Fyfe, W. S., 1973, Sub-seafloor metamorphism, heat, and mass transfer: Contributions to Mineralogy and Petrology, v. 42, p. 287–304.
Stanistreet, I. G., de Wit, M. J., and Fripp, R. E. P., 1981, Do graded units of accretionary spheroids in the Barberton Greenstone Belt indicate Archaean deep water environment?: Nature, v. 293, p. 280–284.
Stolz, G. W., and Nesbitt, R. W., 1981, The komatiite nickel sulfide association of Scotia: A petrochemical investigation of the ore environment: Economic Geology, v. 76, p. 1480–1502.
Sylvester, P. J., Harper, G. D., Byerly, G. R., and Thurston, P. C., 1997, Volcanic aspects, *in* de Wit, M. J., and Ashwal, L. D., eds., Greenstone belts: Oxford, United Kingdom, Oxford University Press, p. 55–90.
Viljoen, M. J., and Viljoen, R. P., 1969, An introduction to the geology of the Barberton Granite–Greenstone terrain: Geological Society of South Africa Special Publication 2, p. 9–28.
Viljoen, R. P., and Viljoen, M. J., 1969a, The geological and geochemical significance of the upper formations of the Onverwacht Group: Geological Society of South Africa Special Publication 2, p. 113–152.
Viljoen, R. P., and Viljoen, M. J., 1969b, The effects of metamorphism and serpentinization on the volcanic and associated rocks of the Barberton region: Geological Society of South Africa Special Publication 2, p. 29–54.
Walker, G. P. L., 1981, Generation and dispersal of fine ash and dust by volcanic eruptions: Journal of Volcanological and Geothermal Research, v. 11, p. 81–92.
White, J. D. L., 1996, Pre-emergent construction of a lacustrine basaltic volcano, Pahuant Butte, Utah: Bulletin of Volcanology, v. 58, p. 249–262.
Williams, D. A. C., and Furnell, R. G., 1979, Reassessment of part of the Barberton type area, South Africa: Precambrian Research, v. 9, p. 325–347.
Wohletz, K. H., 1983, Mechanisms of hydrovolcanic pyroclast formation: grain-size, scanning electron microscopy, and experimental studies: Journal of Volcanology and Geothermal Research, v. 17, p. 31–63.

MANUSCRIPT ACCEPTED BY THE SOCIETY MARCH 26, 1998

Geological Society of America
Special Paper 329
1999

Sedimentology, mineralogy, and implications of silicified evaporites in the Kromberg Formation, Barberton Greenstone Belt, South Africa

Donald R. Lowe
Department of Geological and Environmental Sciences, Stanford University, Stanford, California 94305
Gail Fisher Worrell*
Department of Geology and Geophysics, Louisiana State University, Baton Rouge, Louisiana 70803

ABSTRACT

The Kromberg Formation, near the top of the predominantly volcanic Onverwacht Group in the Barberton Greenstone Belt, South Africa, is composed largely of altered mafic and ultramafic volcanic and volcaniclastic rocks. Its lowest member, the Buck Reef Chert, is a thick sequence of cherty sedimentary rocks marked locally at its base by a unit, 5–40 m thick, of silicified evaporite. The evaporitic section and immediately underlying rocks of the Hooggenoeg Formation are here divided into seven lithofacies. The uppermost 50 to 100 m of the Hooggenoeg Formation consists of dacitic volcaniclastic rocks (lithofacies 1) that record sedimentation on a braided floodplain or sand flat. Laminated and wave-rippled chert (lithofacies 2) and silicified evaporite (lithofacies 3) are interbedded with and overlie these volcaniclastic strata. They represent sedimentation in marginal hypersaline salinas and low-energy coastal lagoons developed on and fringing the volcaniclastic sand flat. Units of cavity-fill megaquartz and brecciated rocks (lithofacies 4) toward the top of the evaporitic section formed by evaporite solution and collapse during subaerial exposure. Overlying polymictic conglomerate (lithofacies 5), generally less than 6 m thick, reflects local uplift and erosion of immediately underlying units. Black chert (lithofacies 6) and volcaniclastic rocks (lithofacies 7) in the upper part of the evaporite unit were deposited during regional submergence and a transition into quieter, possibly deeper water. Available evidence suggests that these waters were marine. Thickness and facies trends indicate that the thickest evaporitic sections accumulated in local fault-bounded basins formed by contemporaneous extensional faulting. This extension was localized and may have been related to cooling of a large body of dacitic magma lying a few hundred meters below the top of the Hooggenoeg vocaniclastic sequence.

Beds of evaporite include at least five types of silicified evaporite crystals: (1) large, pseudohexagonal prismatic crystals as much as 20 cm long that increase in diameter upward; (2) small isolated microscopic pseudohexagonal crystals; (3) small, tapering-upward prismatic crystals as much as 5 cm long; (4) small acicular crystallites forming halos around type 1 crystals; and (5) tightly packed, subvertical crystal aggregates within which individual crystals cannot be distinguished.

*Present address: 3206 Meredith, Austin, Texas 78703.

Lowe, D. R., and Fisher Worrell, G., 1999, Sedimentology, mineralogy, and implications of silicified evaporites in the Kromberg Formation, Barberton Greenstone Belt, South Africa, *in* Lowe, D. R., and Byerly, G. R., eds., Geologic Evolution of the Barberton Greenstone Belt, South Africa: Boulder, Colorado, Geological Society of America Special Paper 329.

Measurement of interfacial angles between prism and pinacoid faces on types 1 and 2 crystals show four interfacial angles of about 63° and two of about 53°. The morphologies and interfacial angles of these crystals correspond to those of nahcolite, $NaHCO_3$. Other precipitative minerals were probably present, but have not been identified with certainty. There is no clear evidence for the presence of gypsum. The existence of nahcolite as a primary evaporitic mineral in hypersaline marine coastal settings supports inferences that the early Archean oceans had elevated bicarbonate levels and that the Archean atmosphere was richer in CO_2 than during later geologic time. Removal of calcium by the precipitation of aragonite under more open marine conditions could have made nahcolite, not halite, the next mineral to precipitate from bicarbonate-enriched seawater under moderately evaporitic conditions.

INTRODUCTION

Evaporites are common in Phanerozoic sedimentary sequences, and deposits interpreted to be recrystallized or replaced evaporites are also widely distributed in Precambrian rocks. Recent studies have shown that evaporitic deposits were important components of Archean greenstone belt sequences in the Barberton Mountain Land, South Africa (Lowe and Knauth, 1977; Lowe, 1980, 1982; Fisher Worrell, 1985), the Pilbara Block, Western Australia (Dunlop, 1978; Dunlop and Groves, 1978; Lambert et al., 1978; Barley et al., 1979; Dunlop et al., 1979; Groves et al., 1981; Lowe, 1983; Boulter and Glover, 1986; Buick and Dunlop, 1990), and the Belingwe Belt, Zimbabwe (Martin et al., 1980). These units represent shallow-water sediments deposited during periods of volcanic quiescence that separated intervals of komatiitic, basaltic, and/or felsic volcanism. Associated sedimentary rocks are mainly cherts representing a variety of volcaniclastic, biogenic, and orthochemical sediments (Lowe and Knauth, 1977; Barley et al., 1979; Lowe, 1980, 1982).

Evidence for Archean evaporites comes largely from layers of well-preserved pseudomorphs after what appear to have been primary precipitated crystals and crystal splays. Original evaporite minerals are widely replaced by microcrystalline quartz (chert) and megaquartz (Lowe and Knauth, 1977; Lowe, 1982, 1983), barite (Dunlop, 1978), or calcite (Martin et al., 1980). The primary minerals are interpreted to have been gypsum (Dunlop, 1978; Lambert et al., 1978; Barley et al., 1979; Dunlop et al., 1979; Martin et al., 1980; Lowe, 1983; Fisher Worrell, 1985) or carbonate, including aragonite (Martin et al., 1980), based on general crystal morphology and the overall similarity of crystal habits and depositional settings to those of Phanerozoic evaporites.

The existence of Archean evaporites has important implications for studies of the early terrestrial ocean, atmosphere, and sedimentary systems. Evaporite mineralogies and precipitation sequence would set significant constraints on the composition of waters from which they were deposited and the conditions of sedimentation (Holland, 1984; Grotzinger and Kasting, 1993). Early Archean evaporite deposits are commonly associated with fossil organic material such as bacterial mats and stromatolites (Dunlop, 1978; Walter et al., 1980; Martin et al., 1980; Lowe, 1983). The sedimentology of these associations may help us to understand better the environments within which organisms lived and evolved on the early Earth.

This report describes early Archean evaporite-bearing sedimentary rocks in the upper part of the predominantly volcanic Onverwacht Group in the southern part of the Barberton Greenstone Belt, South Africa. It addresses the compositions and facies of the evaporite-bearing rocks, environments of deposition, and primary mineralogy.

STRATIGRAPHY

The Swaziland Supergroup consists of a lower volcanic succession, the Onverwacht Group, and an upper mainly clastic sequence, the Fig Tree and Moodies Groups (Anhaeusser, 1973; Viljoen and Viljoen, 1969; Lowe and Byerly, this volume, Chapter 1). In the southern part of the Barberton Greenstone Belt, rocks of the Onverwacht Group crop out in a series of large folds including the Onverwacht anticline, Kromberg syncline, and Steynsdorp anticline (Fig. 1). On the west limb of the Onverwacht anticline (Figs. 1 and 2), the Komati, Hooggenoeg, Kromberg, and Mendon Formations form a continuous, vertical to slightly overturned, north-younging sequence 8–9 km thick (Viljoen and Viljoen, 1969; Williams and Furnell, 1979; Lowe et al., 1985; Lowe and Byerly, this volume, Chapter 1). The Hooggenoeg Formation is made up largely of tholeiitic and basaltic komatiitic volcanic rocks containing thin, interflow sedimentary units of silicified ash and black carbonaceous chert (Lowe, this volume, Chapter 3).

The top of the Hooggenoeg Formation is a 150-m to 2-km-thick unit of felsic volcaniclastic and intrusive rock, termed member H6 of the Hooggenoeg Formation (Lowe and Byerly, this volume, Chapter 1). On the west limb of the Onverwacht anticline, H6 includes a large homogeneous dacitic igneous body or bodies about 10 km long and as much as 2 km thick in outcrop (Fig. 2) that is mantled and flanked by brecciated volcanic rock. This complex has been collectively interpreted to be a large lava dome formed in latest Hooggenoeg time (Lowe et al., this volume, Chapter 2). Felsic volcaniclastic rocks are succeeded by 250–400 m of banded chert of the Buck Reef

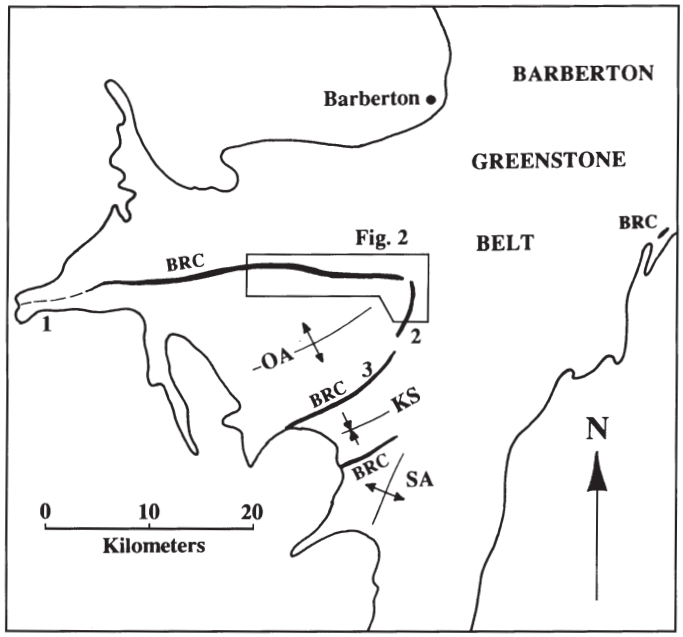


Figure 1. Map of the southern part of the Barberton Greenstone Belt showing outcrops of the Buck Reef Chert member of the Kromberg Formation (BRC) and area of evaporites at the base of the BRC. Principal large folds include the Onverwacht anticline (OA), Kromberg syncline (KS), and Steynsdorp anticline (SA). The Buck Reef Chert, if present, has not been mapped on the east limb of the Steynsdorp anticline. Numbers refer to localities discussed in the text.

Chert, basal member of the Kromberg Formation (Fig. 3). Lenses and beds of silicified evaporite are interbedded with felsic sandstone in the top 10 m of the Hooggenoeg Formation and make up much of the basal 50 m of the overlying Buck Reef Chert for about 17 km along strike on the west limb and around the hinge zone of the Onverwacht anticline (Fig. 2). The mineralogy, sedimentology, and implications of these evaporitic units and the associated beds are the subject of this report.

LITHOFACIES AND SEDIMENTATION

Fisher Worrell (1985) divided evaporitic rocks at the base of the Buck Reef Chert and the immediately underlying part of H6 into seven lithofacies (Fig. 4).

Lithofacies 1: Felsic volcaniclastic rocks (H6)

Description. The uppermost 10 m of H6 consist largely of coarse- to very coarse-grained volcaniclastic sandstone containing lenses of pebble and cobble conglomerate. Medium- to very coarse-grained, light gray weathering, crudely stratified, commonly pebbly sandstone predominates (Fig. 5). Most beds are massive, but flat-lamination is common and rare cross-stratification is present in some fine- to medium-grained units.

The rocks have been extensively silicified. Primary framework grains have been largely replaced by mosaics of microquartz (chert), sericite, and, rarely, chlorite. The only remaining unaltered primary minerals are megaquartz phenocrysts and zircons. Accessory alteration minerals, making up less than 1%

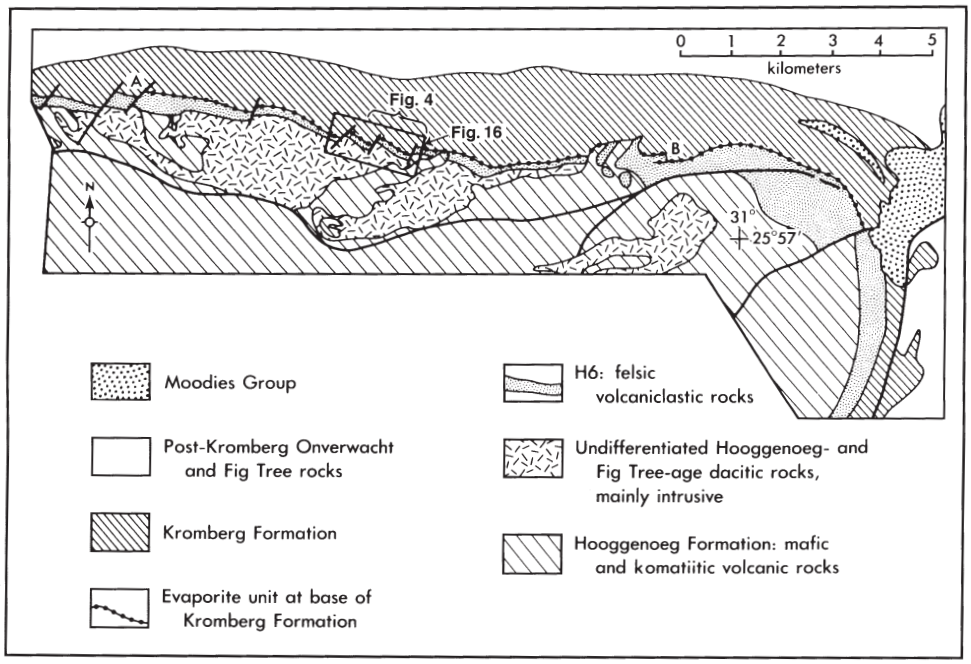


Figure 2. Map of part of the west limb and hinge zone of the Onverwacht anticline showing the distribution of evaporitic strata at the base of the Kromberg Formation. Letters A and B refer to sections shown in Figure 17.

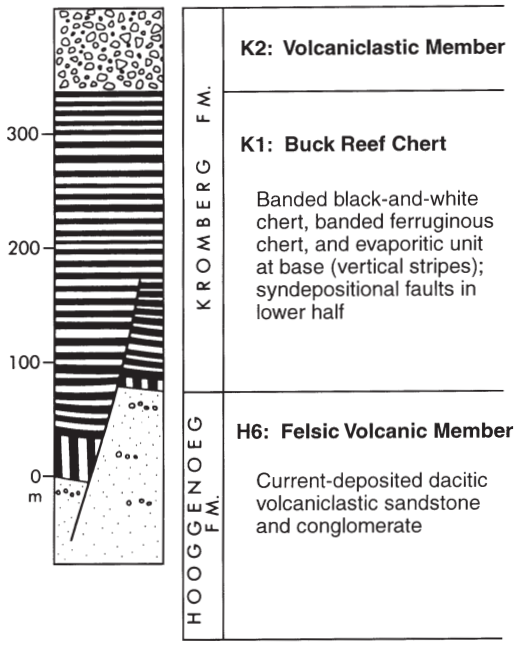


Figure 3. General stratigraphic section of the uppermost Hooggenoeg and lower Kromberg Formations on the central part of the west limb of the Onverwacht anticline showing the stratigraphic setting of the evaporitic member of the Buck Reef Chert.

of the rock, include pyrite, hematite, and, locally, rutile, and dolomite. Blocky micromosaics of sericite, chlorite, and minor chert are probably pseudomorphs after plagioclase feldspar because of their common lath shapes (Fig. 6). Primary, subrounded to euhedral beta quartz phenocrysts are clear and inclusion free. Many have straight edges, 90° and 120° interfacial angles, and corrosion embayments. The original sandy sediments were composed largely of vitric volcaniclastic grains. Shards or pumiceous textures were not recognized. Framework grain textures and shapes, the common presence of volcanic quartz, and chemical analysis (Viljoen and Viljoen, 1969, Table IV, p. 147) indicate that the volcaniclastic debris was dacitic in composition.

Volcaniclastic sandstone of lithofacies 1 locally includes interstratified lenses as much as 1 m thick of pebble and cobble conglomerate. These show erosive bases, grade upward into sandstone, and generally form upward-fining layers (Fig. 5). The clasts are composed largely of dacitic volcanic rock and felsic volcaniclastic sedimentary rock, but locally there are pebbles and cobbles of wave-rippled chert like that in the interbedded and overlying silicified evaporite. The matrix is felsic volcaniclastic sandstone.

Sedimentation. The textures and structuring of the felsic sandstone and conglomerate indicate that the bulk of the debris was current deposited. The coarse grain size and lack of argillaceous layers, and, near the top, the presence of interbedded

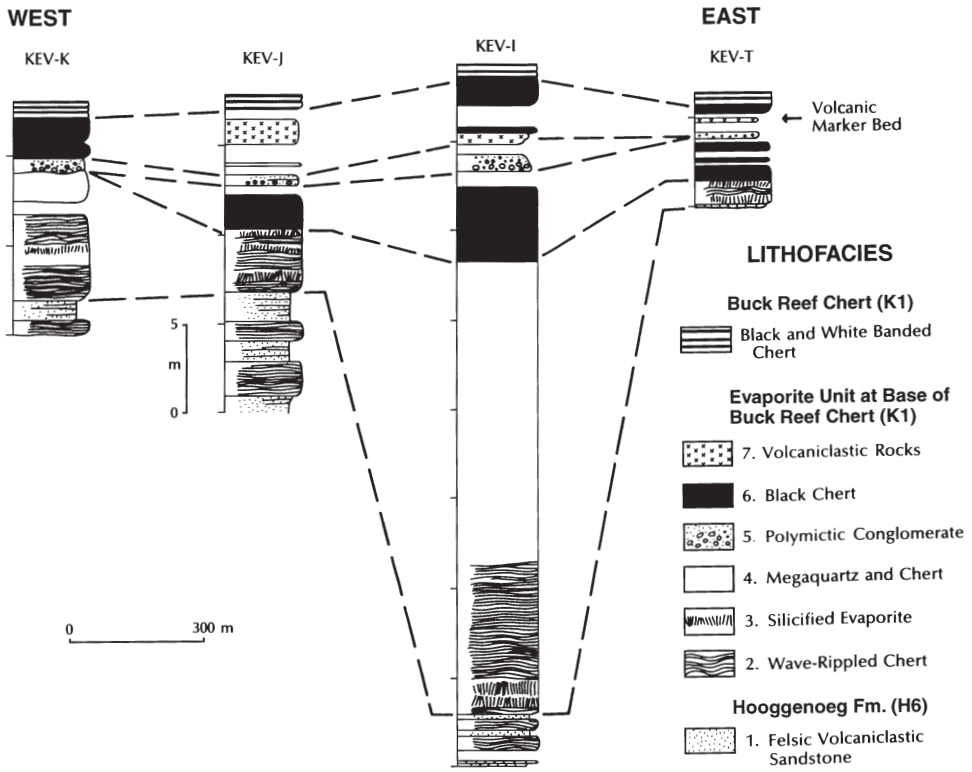


Figure 4. Sequencing and correlation of lithofacies 1–7 of the Buck Reef evaporitic section on the west limb of the Onverwacht anticline (see Fig. 2 for location). Sections KEV-I and KEV-T are separated by a syndepositional normal fault, downdropped on the western side.

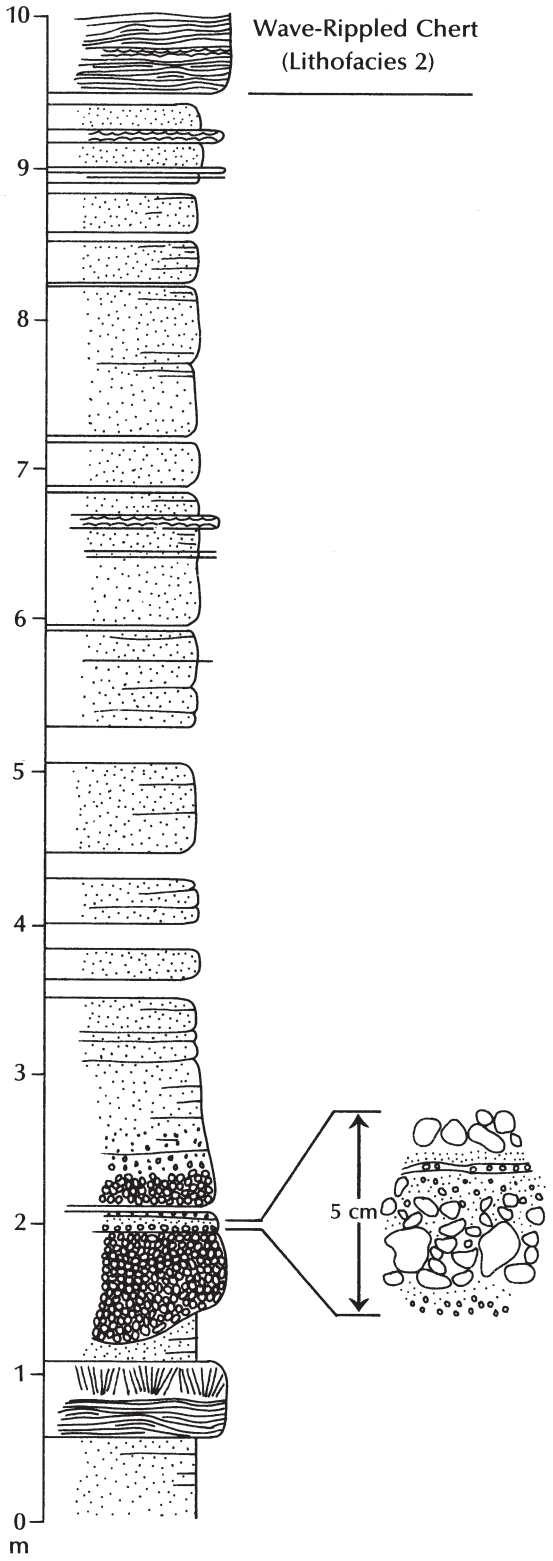


Figure 5. Stratigraphic section of dacitic volcaniclastic rocks of lithofacies 1, member H6 of the Hooggenoeg Formation, about 2 km east of locality A (Fig. 2).

evaporitic and wave-rippled strata suggest deposition in a subaerial to shallow-marine coastal system, such as a braided floodplain (McKee et al., 1967; Tunbridge, 1981), sand flat (Hardie et al., 1978), or, less likely, wave- or tide-dominated coastal environment (Clifton et al., 1971; Klein, 1971). Large-scale cross-stratification, common in coarse-grained wave- or tide-dominated coastal systems, is rare in lithofacies 1, whereas crude horizontal layering, common in braided floodplain settings, is abundant. The lenticular, clast-supported conglomerate appears to represent the fill of shallow channels.

The homogeneity of lithofacies 1 sandstones, the dominance of vitric volcaniclastic debris, and the preservation of euhedral quartz and feldspar phenocrysts indicate that there was neither long-term reworking nor long-distance transport of the detritus. The main source of debris was apparently the immediately underlying felsic volcanic sequence of H6. Lithofacies 1 at the top of H6 is interpreted to represent the closing stages of the erosion of and volcaniclastic sedimentation on and around the H6 felsic volcanic complex. The overlying evaporite and Buck Reef Chert reflect regional submergence and mantling of the volcanic and volcaniclastic units by fine marine sediments.

Lithofacies 2: Laminated and wave-rippled chert

Description. Beds of laminated and wave-rippled chert from 10 cm to 6 m thick directly overlie and are interbedded with the uppermost layers of volcaniclastic sandstone of the Hooggenoeg Formation throughout the study area. This facies makes up the bulk of the evaporite member. The most common rock type consists of thinly, and commonly rhythmically interlaminated black to dark gray and light-gray- to white-weathering chert (Figs. 7 and 8). Light and dark layers commonly alternate

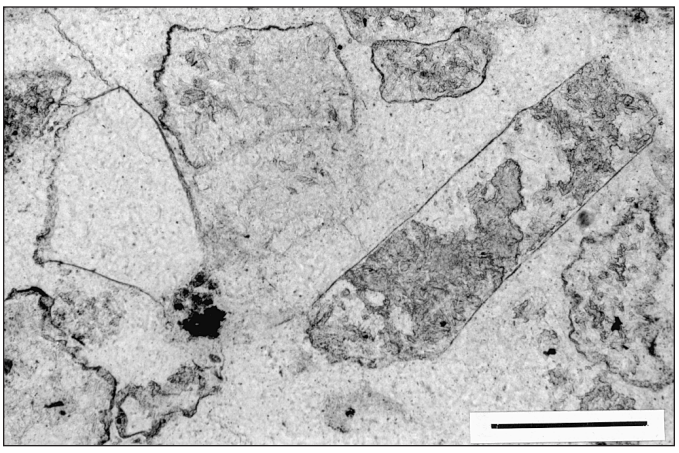


Figure 6. Photomicrograph of silicified dacitic volcaniclastic sandstone of lithofacies 1. Lath-shaped grain probably represents plagioclase now replaced by intergrown sericite (dark) and microcrystalline quartz. Translucent grain at left is megaquartz, probably part of a quartz phenocryst. Remainder of grains are altered vitric particles composed of intergrown sericite and microquartz. Cement between the grains is chert. Scale bar is 0.25 mm long.

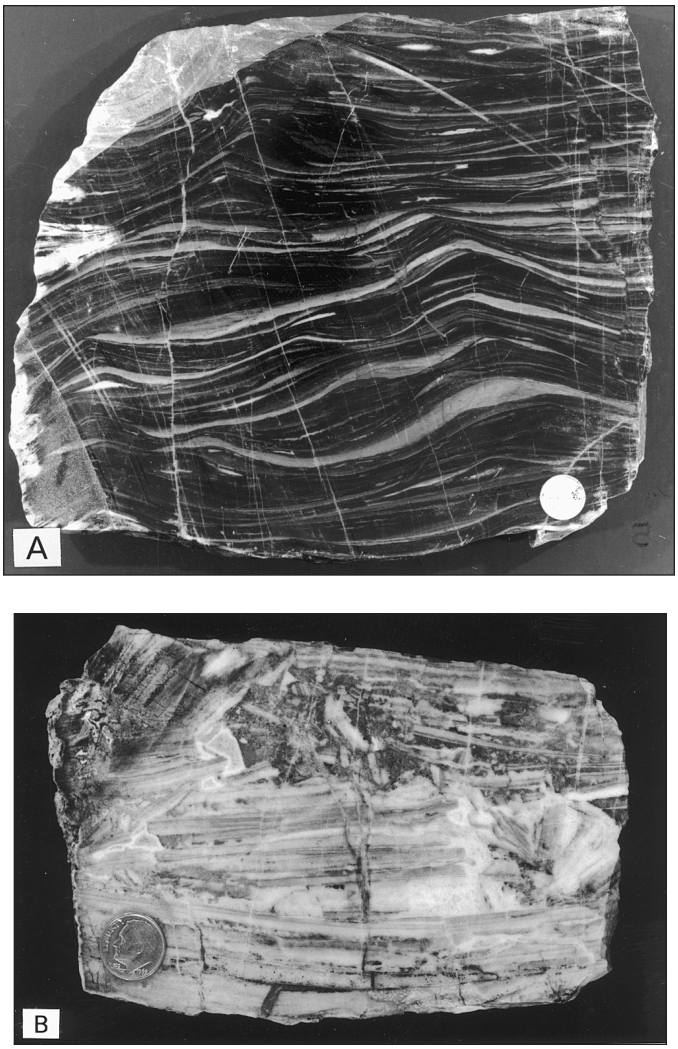


Figure 7. Rocks of lithofacies 2. A, Silicified wave-rippled sediment showing light laminations that probably represent mixed evaporitic sediment and ash and dark laminations rich in carbonaceous matter. B, Thin solution-collapse breccia within lithofacies 2. The slightly displaced plates of laminated sediments of lithofacies 2 are now separated by cavity-filling druzy megaquartz.

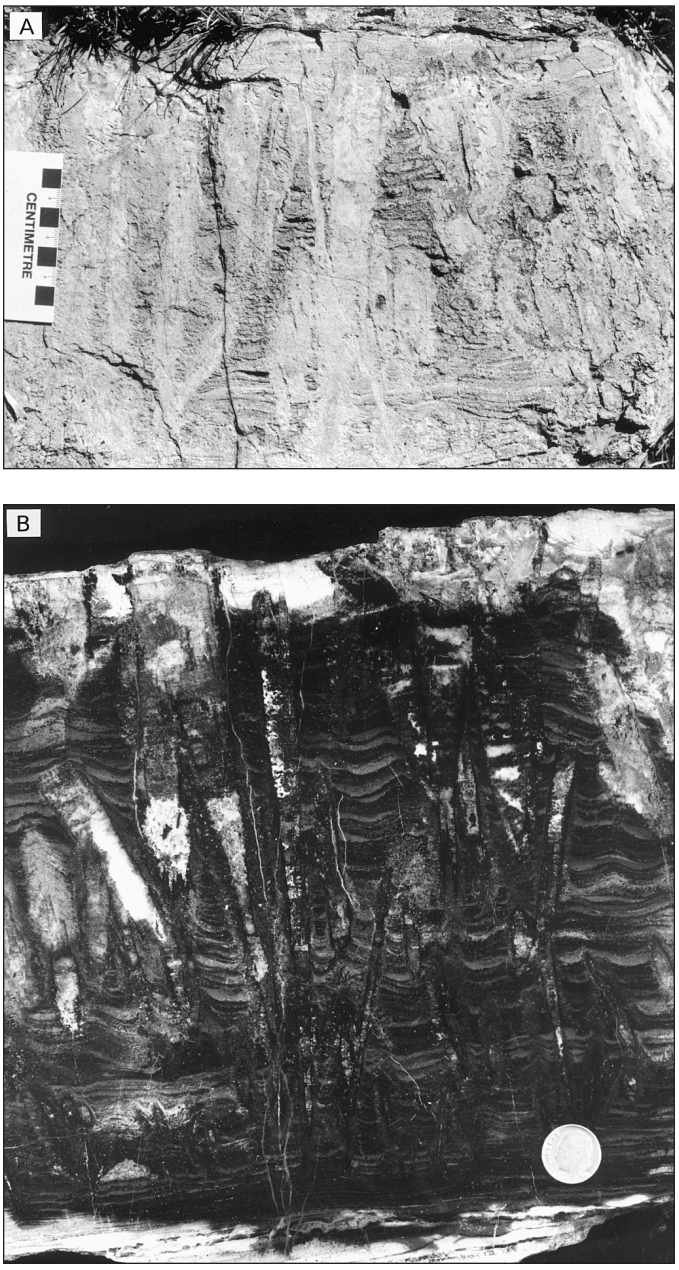


Figure 8. Evaporitic units of lithofacies 3. A, Outcrop view of large, upward-radiating type 1 silicified crystals cutting across laminated and wave-rippled sediments of lithofacies 2. B, Slab of type 1 crystals cutting across rhythmically alternating light-dark couplets of lithofacies 2. The type 1 upward-radiating crystals have been largely dissolved and the cavities infilled by precipitative megaquartz (light) or loose sedimentary debris. Some show partial replacement by microquartz and contain faint internal lamination perpendicular to the growth direction of the crystals and flat, bedding-parallel terminations, especially near or along the top of the bed, similar to structures reported from selenite crystals growing in association with covering organic mats (Lo Cicero and Catalano, 1976; Vai and Ricci Lucchi, 1977). Many type 1 crystals also show fringes of dark, type 4 crystallites.

to form distinctive couplets (Figs. 7 and 8). A third type of lamination is composed of translucent chert.

The light-gray- to white-weathering laminations, from less than 1 mm to about 2 cm thick, are composed of very fine-grained, generally structureless chert that contains a small amount (<1%) of disseminated sericite. Isolated silt- to sand-sized detrital carbonaceous particles are common and authigenic dolomite is locally present. The presence of sericite suggests that the original sediment included a small amount of clay or volcanic dust. The bulk of the sediment, however, was nonaluminous, probably fine-grained orthochemical sediment. Mixing of isolated carbonaceous grains within these laminations suggests that the original sediment was composed of fine, loose, granular particles.

The dark gray to black chert laminations are from 1 mm to about 5 cm thick (Figs. 7 and 8). They consist of carbonaceous chert containing trace amounts of sericite, dolomite, and, rarely, chlorite. The carbonaceous matter is largely detrital and includes fine silt- to sand-sized, irregular to well-rounded simple grains and some sand-sized lobate composite grains (Walsh and Lowe, this volume, Chapter 4). The primary sediment consisted largely of fine orthochemical material but included variable amounts of admixed carbonaceous matter and traces of clay or volcaniclastic debris.

Laminations of translucent chert typically show flat bases but irregular tops characterized by crystal terminations and lack included carbonaceous matter. These laminations represent layers of silicified bottom cements or crystalline precipitates.

Although many units of lithofacies 2 are dominated by flat, even, light-dark lamination couplets, other beds show symmetric cross-lamination (Fig. 7A) with amplitudes of as much as 2 cm and wave-lengths of 6–15 cm. This cross-lamination displays many characteristics of wave-ripple lamination (de Raaf et al., 1977) including (1) scooping and undulatory lower set boundaries resulting from the irregular migrational behavior of wave ripples; (2) off-shooting and draping laminations, where the inclined foreset laminations generally pass the trough and ascend onto the adjacent ripple; (3) swollen lenslike sets; and (4) chevron structures consisting of oppositely dipping lamination and less often concordant lamination (Fig. 7A). Ripple crests are generally strongly peaked.

Intraformational breccia composed of angular, platy, white or gray chert clasts forms units as much as 25 cm thick in lithofacies 2 (Fig. 7B). Spaces between clasts are filled either by cavity-filling quartz or a matrix of carbonaceous chert, silicified volcaniclastic debris, and/or silicified orthochemical sediment. In some samples (Fig. 7B), the breccia clasts are only slightly moved. The laminated chert below the breccia in Figure 7B shows 0.5–1.5 cm long vertical cracks infilled with detrital sediment that appear to represent desiccation or dissolution cracks.

Lithofacies 2 serves as the principal host for the main evaporite units of lithofacies 3. These units are distinguished by the presence of vertical to subvertical crystals crosscutting laminated sediments of lithofacies 2.

Sedimentation. The association of sediments and sedimentary structures in lithofacies 2 reflects deposition of fine, largely orthochemical, carbonaceous, and minor volcaniclastic sediments in quiet to gently wave-agitated subaqueous environments. Both light and dark layers appear to represent fine granular sediments. The general absence of current structures and even thickness of the laminations suggest that the primary sediment was probably precipitated within the water column. The carbonaceous laminations record periods of increased biological productivity, increased influx of particulate carbonaceous matter, or reduced precipitative sedimentation.

The local interbedding of coarse-grained felsic sandstone and conglomerate of lithofacies 1 with the laminated chert of lithofacies 2 probably records a coastal braid plain–sandflat system grading into an extremely low energy, protected subaqueous environment. The thinness, commonly less than 50 cm thick, and lateral impersistence of individual units of lithofacies 2 toward the base of the evaporite sequence suggest deposition in small coastal ponds or salinas, perhaps similar to those described by Gunatilaka and Shearman (1988). Wave-formed ripples with small wave lengths indicate shallow water, probably less than 1 m deep (Evans, 1942). The occurrence of probable solution and desiccation breccias suggests that sediments were at times exposed subaerially.

The abundance of light-dark lamination couplets in lithofacies 2 (Fig. 7) indicates the cyclic alternation of depositional conditions within the coastal lagoons and brine ponds. Where the dark laminations are highly carbonaceous, the couplets commonly consist of sharp-based light laminations grading upward into sharp-topped carbonaceous laminations (Fig. 8B). In other beds, the light laminations alternate with clear chert that has replaced thin layers of evaporite crystals, some with included carbonaceous grains or discrete carbonaceous laminations. These couplets indicate the development of more extreme hypersalinity and the direct precipitation of bottom cements. The couplets record cyclic changes in sedimentation that probably correlate with changes in water chemistry. The evaporitic setting suggests that these changes may have involved shifts from low salinity (dark carbonaceous laminations) to intermediate salinity (light laminations), and from intermediate salinity (light laminations) to high salinity (crystal layer) conditions. The regularity of couplets dominated by precipitative phases could suggest that individual lamination types represent seasonal layers and that the couplets may be annual deposits or varves. However, Hardie et al. (1978) have emphasized that not all cyclic varvelike layering in evaporite deposits represent varves, and there is no firm evidence for annual cyclicity in lithofacies 2.

Lithofacies 3: Silicified coarsely-crystalline evaporite

Description. Coarsely crystalline evaporites (lithofacies 3) originally consisted mainly of laminated sediments of lithofacies 2 crosscut by vertical to subvertical crystals. Layers of crystalline evaporite range from less than 1 cm to as much as 2 m thick and are interbedded with units of lithofacies 2 that lack evaporite crystals, or, toward the top of the section, with units of black chert of lithofacies 6. Many crystalline evaporite layers cannot be correlated between sections only 60–100 m apart.

Evaporite crystals show three forms of preservation. (a) The most poorly preserved crystals were completely dissolved prior to silicification and neither internal structure nor crystal outlines are well preserved. They are now represented by masses of cavity-filling megaquartz, chert, or chert after concentrically layered chalcedony. Crystal boundaries are typically defined by concentrations of dark material, mainly fine carbonaceous matter. (b) Many crystals were dissolved prior to silicification but the surrounding sediments remained intact, and the crystal molds were subsequently filled with cavity-filling quartz. These

show well-developed crystal outlines but lack internal structuring. Both types (a) and (b) crystals were also commonly partially infilled by sedimentary debris after dissolution. (c) The best preserved crystals suffered little or no dissolution prior to silicification, and the external morphology and internal features can be well preserved. These crystals generally consist of fine microquartz containing a variety of fine fluid inclusions.

The chert replacing evaporitic crystals is characteristically somewhat coarser than that replacing surrounding laminated sediments. It commonly shows quartz domains greater than 50 microns in diameter with sharp but wandering boundaries as the stage is rotated under crossed nicols, and group polarization in which the domains over large areas, as much as several millimeters across, come to full illumination and go through extinction together.

Five principal crystal habits can be recognized in lithofacies 3: (1) large, individual prismatic crystals as much as 20 cm long that increase in diameter upward, (2) small isolated microscopic crystals having the same crystal shapes as type 1 crystals, (3) small, tapering-upward prismatic crystals as much as 5 cm long, (4) small acicular crystallites forming halos around type 1 crystals, and (5) tightly packed, subvertical crystal aggregates within which individual crystals shapes cannot be distinguished. A sixth habit, individual lens-shaped crystals, similar to those described by Buick and Dunlop (1990, Fig. 10c) may be present, but most examples of this morphology are oblique sections of type 1 crystals.

Type 1 crystals are the most distinctive evaporite crystals in the Buck Reef evaporite (Figs. 8–12). They occur as individual crystals and small clusters of vertical to subvertical crystals that are separated by and crosscut intervening laminated sediments of lithofacies 2 (Fig. 8). They were prismatic crystals, more-or-less equant and pseudohexagonal in cross section (Fig. 9), that grew vertically or nearly so within lithofacies 2 (Fig. 8). The geometry of type 1 crystals is shown in Figure 10. Most begin from thin laminations of translucent chert representing evaporitic crusts. Individual crystals increase in diameter upward. Those in Figure 8 are as large as about 15 cm long and are 1–2 mm in diameter near the base to 1–3 cm at the top (Fig. 10). At their bases, type 1 crystals typically began growth as single, isolated crystals coated by radiating type 4 crystals (Fig. 10). Upward, many crystals persisted as single, prismatic individuals, but others grew together and were collectively coated by crusts of radiating type 3 crystals, forming aggregates of two, three, or even four crystals (Figs. 10 and 11). Type 1 crystals reach a maximum observed height of about 20 cm and width of 5 cm. Upper terminations are poorly preserved and rarely seen in slabs. Where they are preserved, they are either ragged or flat (Fig. 8B). Most large type 1 crystals are truncated along irregular surfaces at the tops of beds.

Many type 1 crystals exhibit faint internal laminations, defined by trains of inclusions and impurities, that are flat and perpendicular to the growth direction of the crystals (Figs. 8B and 12). These laminations could mark growth or dissolution surfaces. Dissolution surfaces in many evaporites (Lo Cicero and Catalano, 1976; Vai and Ricci Lucchi, 1977) form when the hypersaline brines are diluted by the influx of less saline waters, resulting in dissolution of crystal apices. The decrease in salinity is commonly accompanied by the growth of bacterial mats (Schreiber and Kinsman, 1975; Schreiber, 1978; Warren, 1982, 1983; Peryt, 1996).

Some steeply inclined type 1 crystals appear to have broken near their bases and fallen against adjacent crystals (Fig. 12).

Type 2 crystals are microscopic, silicified, subvertical prismatic crystals that occur below and in the lower parts of beds of type 1 crystals (Fig. 13). They range as large as 5 mm in length. The crystals are clear and lack inclusions and coatings of radiating type 4 crystals. They are defined by concentrations of opaque carbonaceous matter that coated the crystals at some

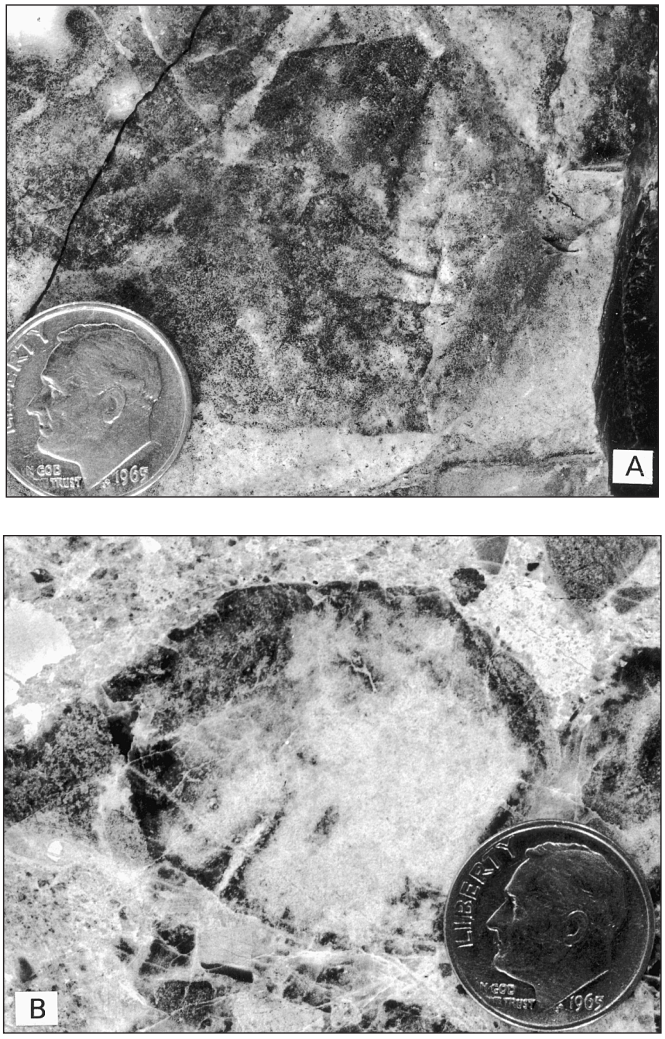


Figure 9. Cross sections of type 1 silicified crystals illustrating their pseudohexagonal form in sections perpendicular to the growth direction. A, A crystal that has been completely replaced by microquartz. B, A crystal that was partially dissolved and the cavity infilled by coarsely crystalline quartz (light).

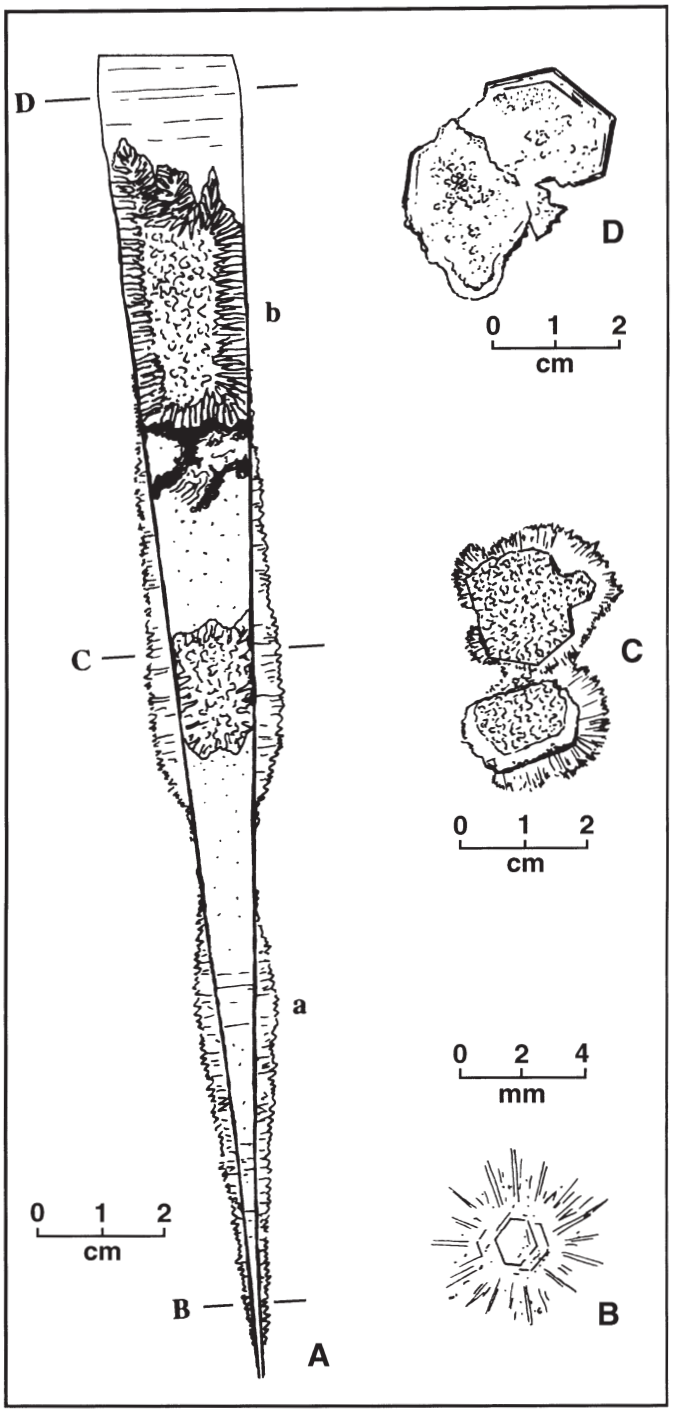


Figure 10. General sketch showing main features of type 1 crystals (A). Most are elongate, prismatic, pseudohexagonal crystals, equant in cross section (B–D) that increase in size upward and show overgrowths, commonly nonuniformly developed, of fine acicular type 4 crystallites (a). Portions of the crystals have been dissolved and the cavities partially filled by druzy quartz (b). Sections B, C, and D are cut perpendicular to direction of elongation (growth) at indicated locations along the large crystal.

point in their development. The presence of multiple carbonaceous layers in some crystals indicates several alternating episodes of crystal growth and organic coating.

Type 3 crystals are small vertical to subvertical crystals, generally less than 4 cm in height, that show tapering-upward outlines (Fig. 14). They occur in the lower parts of individual layers of coarsely crystalline evaporite, where they grew upward from laminations of translucent chert representing silicified evaporite crusts in lithofacies 2. Type 3 crystals tend to be tightly packed initially, forming nearly solid crystal layers, but upward, individual crystals develop preferentially, separated by laminated sediments of lithofacies 2. Where terminations are preserved, they are usually pointed or ragged. Type 2 crystals typically show little or no evidence of dissolution and thus contain few or no quartz-filled vugs. No clear cross sections of type 3 crystals have been identified. In cut slabs, they appear to be equant and pseudohexagonal in cross section and lack coatings of type 4 crystals.

Type 4 crystals form dark rims or halos of silicified fine acicular crystallites coating type 1 crystals (Figs. 8, 12, 15). They range from thin crusts to crystals about 3 mm long and 0.25 mm wide. The crusts are not uniformly developed along the lengths of the type 1 crystals, but tend to be absent near the tops in some beds and to be missing in certain zones in others (Fig. 10).

Type 5 crystals cannot actually be distinguished as a separate crystal type. They form tabular layers as much as 15 cm thick composed of tightly packed, vertical to subvertical crystals with little or no intervening sediment. The crystals show differential solution effects and some coatings and infillings of carbonaceous matter that help to define crystal boundaries. No crystallographic or morphological information is available on type 5 crystals. Most have been extensively dissolved and the cavities infilled by druzy quartz.

Sedimentation. A number of features suggest that type 1, 2, and 3 crystals represent primary precipitates and grew more-or-less concurrently with deposition of the associated detrital sediments. (1) Well-developed crystal morphologies, vertical growth habit, and the paucity detrital inclusions suggest that the crystals grew into water rather than within the sediment. (2) Laminated sediments of lithofacies 2 show compaction effects adjacent to the crystals but lack major disruption that would have resulted if the crystals had grown diagenetically within and displaced significant volumes of laminated sediment. (3) A few toppled type 1 crystals indicate that they were free-standing columns when growing (Fig. 12). These features suggest that type 1 crystals formed forests of long, prismatic crystals growing on the sediment bottom. Type 2 crystals have the same cross sections as type 1 crystals and appear to represent small early formed type 1 crystals that failed to grow into larger crystals, perhaps because they were buried by fine granular sediments. Type 3 crystals formed crystal crusts as much as 4–5 cm thick that were commonly buried by the accumulation of overlying lithofacies 2 sediments.

The halo crystal overgrowths (type 4) could have been precipitated within the water column or diagenetically from con-

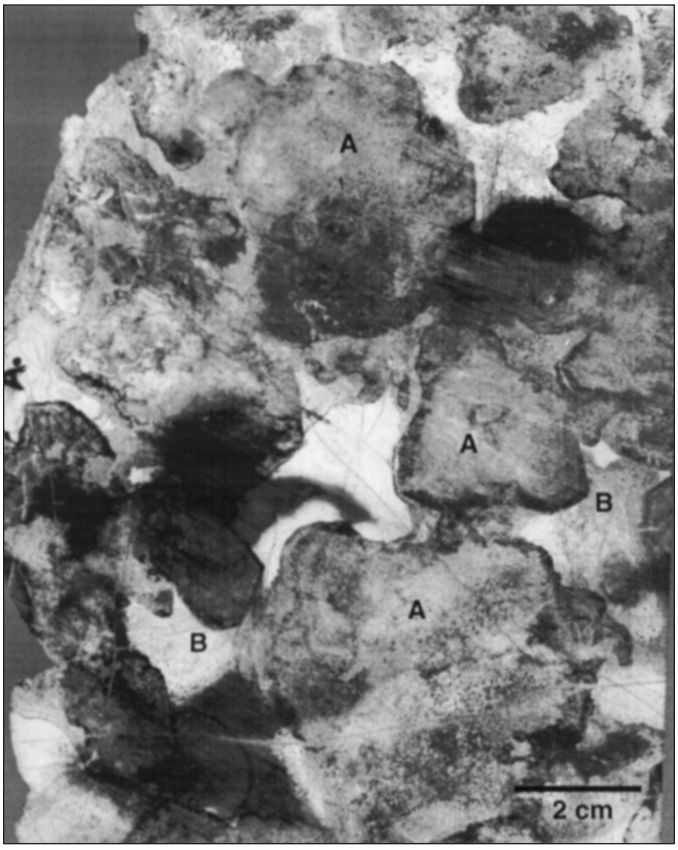


Figure 11. Horizontal slab of complex assemblage of type 1 crystals. This slab was one of several used to measure the interfacial angles on type 1 crystals. Light areas are laminated sediment fill between crystals. Dark equant patches (A) are cross sections of clusters of type 1 crystals. Crystal faces and interfacial angles are locally well preserved (B) and show the aggregate nature of many of the crystal clusters.



Figure 12. Photo of inclined type 1 crystal from Figure 8B. The crystal has been broken off at the base (not shown) and is leaning against an adjacent type 1 crystal. The lower part of the crystal was dissolved and the cavity filled by coarse quartz. The upper third was replaced by microquartz and shows fine, flat laminations perpendicular to the growth direction of the crystal. The crystal also has a flat termination. The adjacent crystal, which is cut obliquely to the long axis, shows a halo of type 4 crystallites.

centrated pore waters after sediment deposition. However, they form very tight, compact crusts on type 1 crystals and show well-formed radiating crystallites. The presence of surface coatings of finely divided opaque carbonaceous particles suggest that type 4 crystal halos were themselves coated at times by bacterial mats. These features suggest to us that they precipitated within the water column rather than diagenetically. In the upper parts of type 1 crystals, some type 4 crystal halos show concentric layering and lack well-defined crystal terminations, suggesting several episodes of crystal growth and partial dissolution.

The evaporites were deposited in an overall low energy environment as indicated by (1) their interbedding and interlamination with fine, graded couplets of lithofacies 2; (2) the abundance of low-density carbonaceous sediments; (3) the absence of coarse clastic sediments; (4) the lack of scour around large crystals; and (5) the paucity of intraclast conglomerate and breccia. However, the detrital character of most of the laminated sediments between type 1 crystals and the common presence of wave-ripples suggests that low-level wave activity commonly deposited and reworked lithofacies 2 sediments. Physical evidence for exposure is largely absent within crystal layers, but the presence of growth or dissolution breaks within crystals suggests that their upward growth occurred in increments, perhaps related to changing water-body chemistry, with intervals of subaqueous crystal growth alternating with intervals of nongrowth or partial dissolution.

Many individual evaporite beds from 20 to 50 cm thick form thin shoaling upward cycles (Figs. 8B and 14). The lower parts of such beds show fine flat-laminated sediment of lithofacies 2 (Fig. 14). Laminations are commonly 1 mm or less thick and lack wave and current structures. A few centimeters above the base, thin evaporitic laminations or thin layers of type 3 crystals are present within light-dark couplets. Upward, thicker, light-dark couplets dominate, commonly 1–5 mm thick, and thin layers of type 1 crystals are interbedded with the dark, carbonaceous and light layer couplets. In the upper parts of such units,

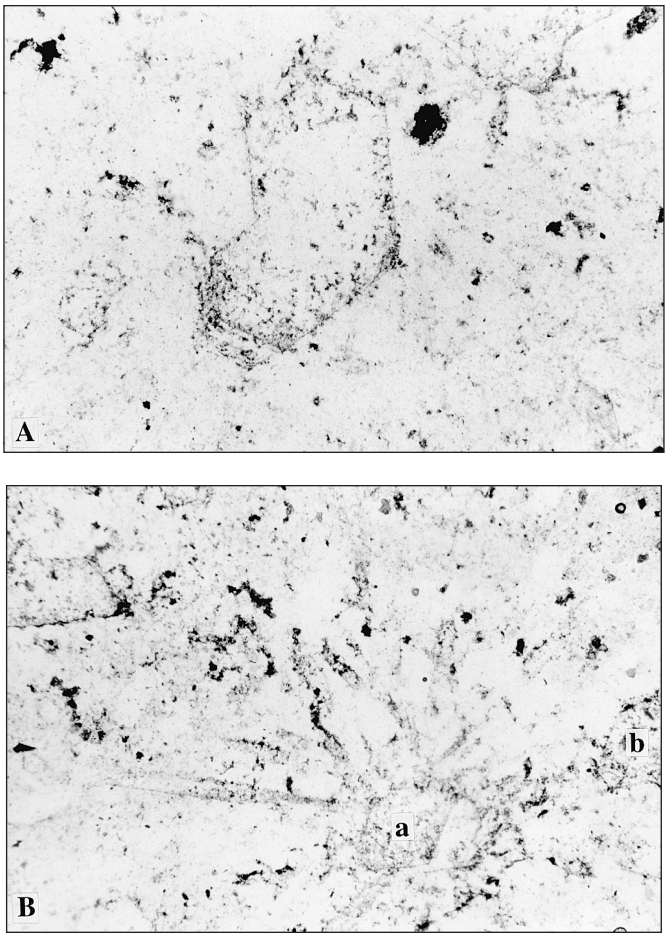


Figure 13. A, Photomicrograph of type 2 crystal cut parallel to stratification and perpendicular to growth and elongation direction. Crystal faces are defined by concentrations of opaque organic matter. B, Photomicrograph of type 1 crystal near its base (a). Pseudohexagonal type 1 crystal is surrounded by a halo of radiating type 4 crystals. Several small intergrown type 2 crystals at far right (b).



Figure 14. Type 3 silicified crystals in lithofacies 3. Small, sharply terminated crystals crosscut flat, evenly layered light-dark couplets of lithofacies 2. Most of crystals taper upward.

lithofacies 2 commonly includes relatively thick couplets (to 1 cm) and wave-ripple cross-lamination, and the crystals are predominantly of type 1 with or without halos of type 4. Blunt terminations and dissolution surfaces are common, especially near and at the bed tops. These features suggest fully subaqueous, very quiet water sedimentation and evaporite precipitation in the lower parts of the units and gently wave active conditions toward their tops. The large evaporite crystals are terminated at the tops of the evaporite beds by flat, bedding-parallel solution terminations, even on inclined crystals.

The lateral impersistence and thinness of most coarse-crystal layers is consistent with the interpretation that lithofacies 3 layers represent sedimentation in and the filling of small, shallow, protected coastal salinas or ponds.

Lithofacies 4: Megaquartz and chert

Description. Lithofacies 4 is a complex, only locally developed association of gray, pink, and white megaquartz and chert



Figure 15. Obliquely cut type 1 silicified crystal showing dark halo of type 4 crystallites.

in units ranging from several centimeters to 17 m thick. These rocks include (1) rotated blocks of wave-rippled chert and silicified evaporite; (2) concentric, botryoidal, and stalactitic cavity-fill silica between the blocks; (3) massive black chert; and (4) heterogenous megaquartz and chert that represent mainly cavity-fill material.

Rocks of lithofacies 4 contain abundant silica representing the fill of cavities left by evaporite solution and spaces between rotated and disrupted sedimentary blocks. Concentrically layered botryoidal masses of silica commonly coat the upper and lower surfaces of or entirely envelope rotated blocks of layered or wave-rippled chert. The fill of individual cavities generally contains outer layers of chalcedony, recrystallized to microquartz, passing inward to late-stage coarse megaquartz fill. In some cavities, concentric silica layers are well developed mainly on the undersides of blocks, where they show stalactitic projections. In one case, a unit of stalactitic cavity-filling silica can be traced laterally over about 10 m into an intact silicified evaporite bed.

In some cavities, precipitative infilling was arrested by the introduction of oozy sediment now represented by massive black carbonaceous chert.

Formation. Lithofacies 4 records an interval of evaporite dissolution and collapse followed by a period of precipitation and infilling of solution cavities. Intense corrosion and dissolution resulted in collapse and the formation of breccias, now cemented by megaquartz and chert. Botryoidal cavity fill probably precipitated under fully saturated, phreatic-zone conditions because it forms continuous, isopachous coats around blocks and within cavities. Stalactitic fill indicates precipitation in gas-filled cavities, probably in the vadose zone (Esteban and Klappa, 1983). The absence of conglomerate clasts of lithofacies 5 within the collapse breccias indicates that solution and brecciation occurred before deposition of lithofacies 5. The presence of massive black-chert fill in some cavities suggests that exposure, solution, and cavity infilling was arrested as a result of submergence and deposition of fine-grained carbonaceous sediments.

Lithofacies 5: Polymictic conglomerate

Description. Polymictic conglomerate of lithofacies 5 (Fig. 3) locally overlies both evaporitic and solution-collapse rocks of lithofacies 3 and 4 and black chert of lithofacies 6 (Fig. 4). It crops out discontinuously throughout the study area and ranges from less than 1 to 6 m thick. The conglomerate contains thin, 1- to 10-cm-thick, interbedded layers of wave-rippled chert, megaquartz and chert, and black chert.

The conglomerate is composed of pebble- and cobble-sized, angular to subrounded, predominantly intraformational clasts of sedimentary rock. It is clast-supported and poorly sorted with a continuous grain-size spectrum from pebble- and cobble-sized clasts to the medium-grained sandstone matrix. The lithic clasts consist primarily of black chert, wave-rippled chert, and translucent chert with lesser amounts of silicified evaporite, felsic volcanic rock fragments, and felsic arenite. The matrix is made up of the same chert types as the clasts, but includes a greater percentage of reworked felsic detritus and a small amount of ultramafic to mafic debris and volcanic quartz. The ultramafic to mafic grains show relict spinifex textures, chrome-bearing spinels, and silica pseudomorphs after olivine. Pumicelike grains are found locally. Pore spaces are filled with microquartz. Conglomerate beds are massive to normally graded. Sedimentation units range in thickness from approximately 20 cm to 1 m. Clast imbrication is present in some beds and most beds show slight basal scour.

Interbedded sandstone is medium- to very coarse-grained and composed of the same grain types as the conglomerate, but the sandstone appears to contain a higher percentage of felsic rock fragments. Most of the sandstone is massive, but flat laminations and cross-laminations are present in some sections.

Sedimentation. The conglomerate was deposited rapidly by energetic flows or floods of debris into local, quiet, low-energy environments represented by black chert of lithofacies 6. The debris was eroded from already lithified felsic sandstone, wave-rippled chert, silicified evaporite, and black chert, probably from uplifts associated with the formation of local half-grabens during and following evaporite sedimentation (Fisher Worrell, 1985). There is no evidence for a major tectonic event or regional interval of erosion at this time.

Lithofacies 6: Black chert

Description. Black chert (lithofacies 6) makes up most of the upper parts of the evaporite-member sections (Fig. 4). It is succeeded by black-and-white banded chert making up the overlying 200–400 m of the Buck Reef Chert (Fig. 3). Lithofacies 6 is composed of massive and finely laminated black chert in units ranging from 5 cm to 4 m thick. The black chert is made up of carbonaceous detrital grains and sparse fine-sand-sized volcaniclastic detritus containing trace amounts of fine authigenic pyrite and carbonate. Flat-pebble conglomerate, made up of platy black chert intraclasts in a detrital carbonaceous matrix, forms layers 2–3 cm thick in some sections.

Sedimentation. The abundance of loose, low-density carbonaceous material in lithofacies 6 indicates deposition under predominantly low-energy conditions. The lack of evaporites and paucity of current-produced features suggests deposition under more open, subaqueous conditions than underlying sediments. This unit is transitional into the overlying black-and-white banded Buck Reef Chert. Thin, flat-pebble conglomerate layers indicate erosion of early lithified or cohesive layers, probably during storms.

Lithofacies 7: Upper volcaniclastic rocks

Description. Beds as much as 5.4 m thick of green to greenish gray silicified volcaniclastic detritus are interbedded with black chert of lithofacies 6 near the top of the evaporite

section (Fig. 4). These rocks are now composed of intergrown microquartz, sericite, chlorite, and minor pyrite. The primary, silt- to coarse-sand-sized volcaniclastic detritus included both lithic and vitric components. Vitric material included shards that can be recognized by their distinct angular shapes and curved bubble walls. Volcaniclastic debris forms flat-laminated, cross-laminated, and normally graded beds. Flat laminations, 1–8 mm thick, are composed of sand-sized to very fine-grained volcaniclastic debris. Lenticular bedding and wave-ripple cross-lamination occur in some layers.

This facies also includes graded beds of accretionary lapilli resembling those described from other parts of the sequence by Lowe and Knauth (1978) and Lowe (this volume, Chapters 3, 9). Normally graded accretionary lapilli beds range from a few millimeters to 10 cm in thickness and the accretionary lapilli from 0.5 to 5 mm in diameter, averaging 1–2 mm. Most beds include a basal zone of accretionary lapilli grading upward into a mixture of vitric debris, broken accretionary lapilli, and a few whole accretionary lapilli. The accretionary lapilli locally form cross-laminated beds.

The volcaniclastic division may be correlative with a unit of mafic or komatiitic lapillistone and tuff, including accretionary lapilli, that underlies the lowest chert in the Kromberg Formation in the type section along the Komati River on the east limb of the Onverwacht anticline (Klcl of Lowe and Byerly, this volume, Chapter 1; chert at 750 m in section of Kromberg by Viljoen and Viljoen, 1969, Fig. 9).

In several sections, thin volcaniclastic layers in lithofacies 5 contain isolated, randomly oriented, silicified, pseudohexagonal crystals 2–5 mm long. These are similar to evaporite crystals hosted by very fine-grained silicified komatiitic ash layers in the Middle Marker at the base of the Hooggenoeg Formation (Lanier and Lowe, 1982) and by fine-grained, possibly orthochemical deposits in the 3.5-Ga-old Warrawoona Group, Western Australia (Lambert et al., 1978, Fig. 2; Buick and Dunlop, 1990, Fig. 8). All have been interpreted to represent silicified diagenetic gypsum.

Sedimentation. Lithofacies 7 consists of airfall volcanic ash, dust, and accretionary lapilli deposited in a generally low-energy subaqueous environment. Low-energy currents and waves reworked some of the volcanic material into rippled and flat-laminated layers, but large-scale current structures, scour, and other indicators of high-energy conditions are lacking. Graded accretionary lapilli beds appear to represent fall deposition of pyroclastic debris into low-energy, shallow-water environments with little subsequent current reworking. Local higher energy events, possibly storms, ripped-up cohesive or early lithified layers forming local intraformational conglomerates.

DEPOSITIONAL SETTING

The evaporite unit is between 5 and 10 m thick over most of its outcrop area but locally reaches 40 m thick. Mapping along the central part of the west limb of the Onverwacht anticline shows the existence of at least three syndepositional half-grabens within which the thickest evaporite sections occur (Fig. 16). The half-grabens range from 1.0 to 1.5 km across, include evaporite sections 38–40 m thick, and are bounded sharply on their eastern sides by normal faults. The lower half of the overlying black-and-white banded chert also shows thickness variations related to syndepositional faulting along these faults. It averages about 100–125 m in thickness over most of the area but is as much as 200 m thick within the half-grabens. The normal faults die out within the lower half of the Buck Reef Chert. The megaquartz and chert evaporite-solution unit (lithofacies 4) and polymictic conglomerate (lithofacies 5) are thin or absent between the half-grabens and reach their greatest thicknesses in the half-grabens (Fig. 16). These features indicate that, at least locally, extension during accumulation of the evaporite unit and overlying banded chert formed local half-grabens that served as small basins for the accumulation of relatively thick evaporite units. The greater number of evaporite beds and greater stratigraphic complexity of evaporite sections in the half-grabens suggests that the evaporitic ponds were commonly confined to them. The adjacent uplifts served as sources of debris for local intraformational conglomerate of lithofacies 5.

The zone of evaporite sedimentation on the west limb of the Onverwacht anticline is coincident in lateral extent with a thick, shallow-level dacitic intrusive body and adjacent units of coarse dacitic breccia, collectively interpreted to represent a large dacitic dome and flanking debris apron, that make up much of the underlying felsic volcanic unit, H6, in this area (Lowe et al., this volume, Chapter 2). Normal faulting during and following the deposition of the Buck Reef evaporite may have occurred in response to cooling and subsidence of this felsic lava dome. Away from the center of felsic activity, H6 is represented by thinner, distal, more fully subaqueous volcaniclastic deposits, and evaporites are rare to absent at the base of the Kromberg Formation. The westernmost sections examined (Fig. 17) consist entirely of black chert of lithofacies 6 and interbedded volcaniclastic rocks of lithofacies 7. These sections are similar in thickness, from 8 to 16 m, to the evaporite-bearing sections farther east. However, they differ in the absence of

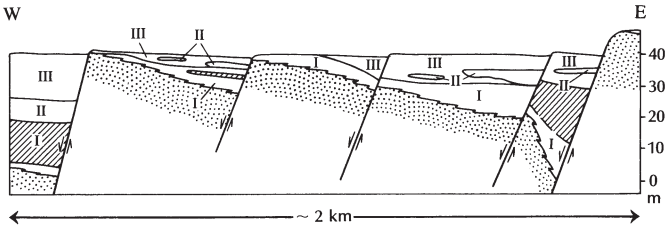


Figure 16. Cross section perpendicular to stratification of small evaporite-filled basins formed by syndepositional normal faulting on the west limb of the Onverwacht anticline during accumulation of the uppermost volcaniclastic strata of H6 (Hooggenoeg Formation) and the basal, evaporitic unit of the Kromberg Formation. Section located on Figure 2. Roman numerals refer to packages of sediment that can be correlated across the area.

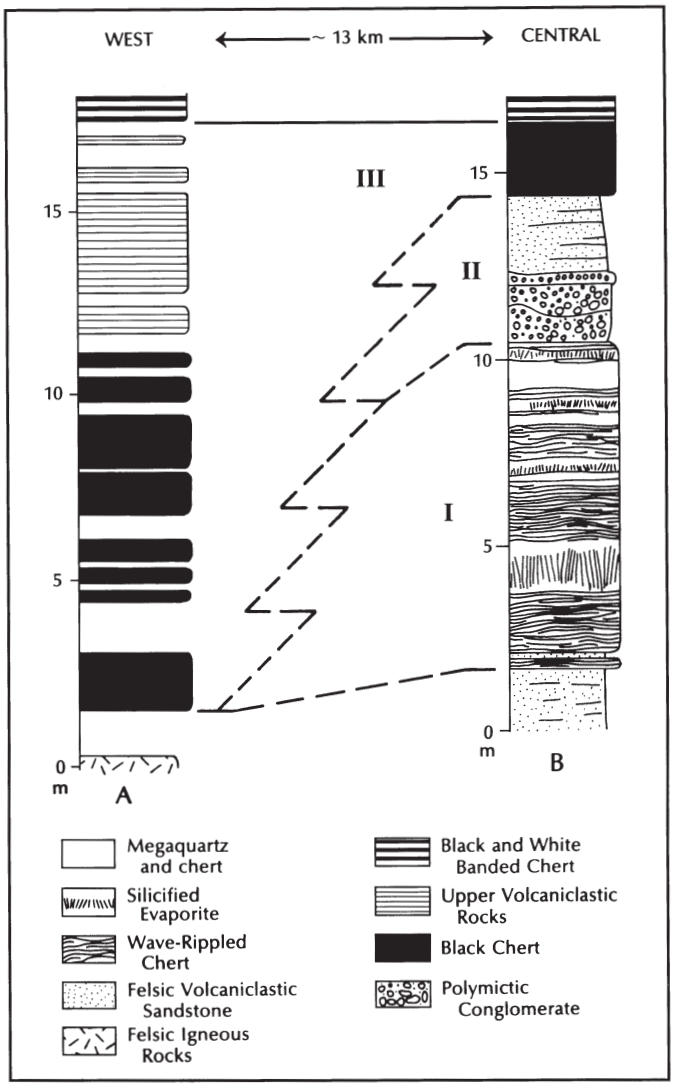


Figure 17. Facies changes within the evaporite member of the Buck Reef Chert along the west limb of the Onverwacht anticline. Roman numerals refer to sediment packages that can be correlated across the area (see Fig. 16). The locations of the measured sections are shown in Figure 2.

wave-formed sedimentary structures, evaporites, evidence for exposure, and coarse clastic deposits, recording instead quiet-water sedimentation with little if any reworking of debris by waves or currents. The lack of evaporites and features indicative of exposure suggest deposition under less restricted conditions and possibly in somewhat deeper water.

Along the east limb of the Onverwacht anticline (Fig. 1, locality 2), sections correlative with the silicified evaporite sequence range from 10 to 50 m thick. They are composed of complexly interstratified felsic volcaniclastic sandstone, wave- and current-rippled chert, thin units of black and banded chert, and near the top, fresh volcaniclastic debris including accretionary lapilli. Silicified evaporites were not seen. Deposition appears to have taken place on an alluvial fringe and under wave- and current-active, shallow-water but nonevaporitic conditions.

EVAPORITE MINERALOGY

Primary evaporite minerals in the evaporite member of the Buck Reef Chert have been modified by dissolution and replacement, but primary textures and crystal shapes are commonly well preserved. In the absence of primary minerals, the most reliable indicators of original mineralogy are crystal morphology and habit. Lambert et al. (1978) used interfacial angle measurements on baritized evaporites in the early Archean Warrawoona Group, Western Australia, to infer that the primary sediment was gypsum. Where primary crystal forms are imperfectly preserved, original mineralogy can sometimes be deduced from the frequency, distribution, and arrangement of interfacial angles measured on many individual crystals. In addition, the more general crystal habits, crystal associations, and inferred sedimentology can be used to estimate primary mineralogy in silicified evaporites.

Types 1 and 2 crystals

Samples of evaporite showing well-preserved type 1 crystal pseudomorphs were cut into slabs, 5–15 mm thick, parallel to bedding and perpendicular to crystal growth direction. Slabs with well-preserved crystal outlines (Fig. 11) were scanned directly into a Power Macintosh 8500/180 computer using a Apple Color OneScanner 600/27 and Adobe Photoshop 3.0. Enlarged sections of each slab were enhanced in color, brightness, and contrast to provide maximum resolution of the crystal faces. Adjacent crystal faces and the included interfacial angles were marked directly on the screen. The scanned slab surfaces were then printed and the marked interfacial angles measured directly to 1°.

No crystals were sufficiently well preserved that all 6 interfacial angles could be measured, although on several, 4 angles between 5 crystal faces were preserved. In many cases, only a single angle between 2 faces was measured. A total of 200 interfacial angle measurements were made in this way (Fig. 18).

In addition, thin sections were cut parallel to bedding from most slabs. Those from near the bases of the crystals show cross sections of both type 1 and type 2 crystals, commonly with all faces well preserved. The crystal boundaries are defined by concentrations of diffuse opaque particles, probably carbonaceous matter. Using a rotating stage with degree measurements, angles between crystal faces were measured, with emphasis on crystals where all crystal faces were present to insure closure. A total of 144 interfacial angles were measured petrographically, all but a dozen or so on type 2 crystals.

In both slabs and thin sections, corners between crystal faces commonly show rounding by solution, and most faces exhibit steps, dislocations, and solution effects. The angle measurements were strongly affected by difficulties in clearly defining crystal faces. In general, the measured angles have an error of from ±2°, where the faces were well preserved, to as much as ±10° between poorly preserved faces.

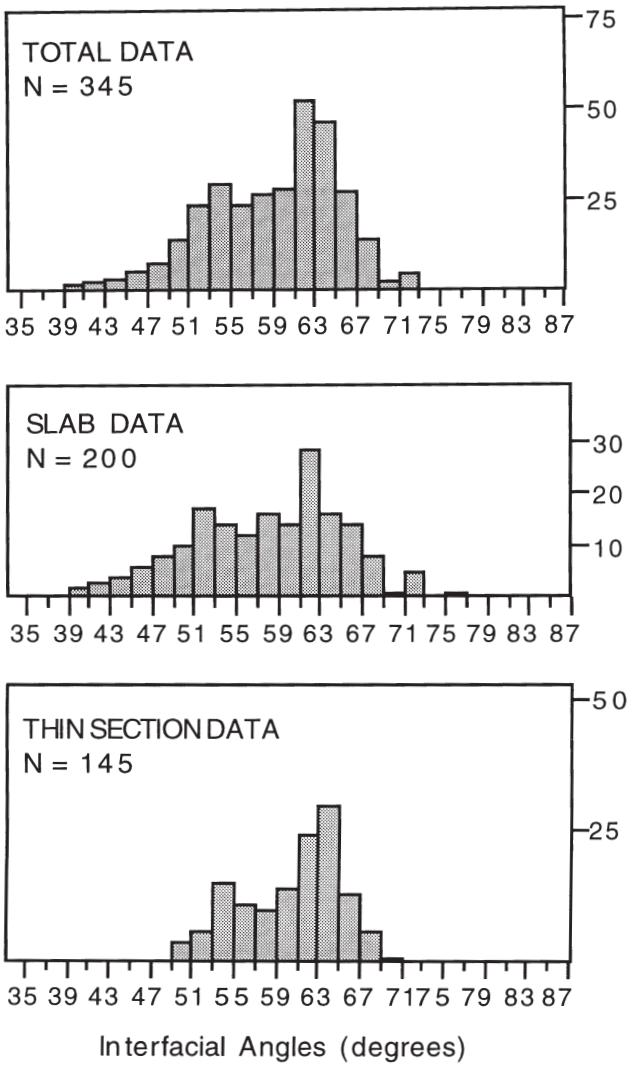


Figure 18. Measured interfacial angles between prism and pinacoid facies of types 1 and 2 silicified crystals on slabs (type 1) and in thin sections (type 2). Slabs and thin sections were cut perpendicular to the growth (elongation) direction of the crystals.

The measured interfacial angles display a wide range of values but show a clear bimodal distribution (Fig. 18). The smaller mode lies between 51 and 55°, with a modal value of about 53°, and the larger mode is between 60 and 64°, with a modal value of about 63° (Fig. 18). These results suggest that type 1 and type 2 crystals are pseudohexagonal prismatic crystals with four angles between pinacoid and prism faces of about 63° and two angles between prism faces of about 53°. Measurements on individual crystals also show a regular arrangement of interfacial angles. As can be seen for crystals in Figure 9, the angles tend to be arranged with two adjacent angles of about 63° separated by single angles of 53°.

Fisher Worrell (1985) reported the results of a previous study in which interfacial angles on type 1 crystals were measured directly from a set of slabs without enlargement. She concluded that type 1 crystals included four interfacial angles of about 50–58° and two of 66–70° and interpreted the primary mineral to have been gypsum. We have subsequently concluded that many of the faces measured were not single, flat faces but rather faces that had been extensively modified by dissolution. In the present study, computer enlargement and enhancement of the slabs permitted recognition and elimination of poorly preserved crystal faces and angles.

A variety of common and not-so-common evaporitic minerals exhibit pseudohexagonal prismatic morphologies (Table 1). Both gypsum and aragonite are pseudohexagonal prismatic minerals that have been described as primary precipitates in Archean sedimentary sequences. Gypsum contains four interfacial angles between the pinacoid (010) and prism (110) form faces of 55.75° and two between the prism (110) forms of 68.50°. In aragonite, which has been widely described as a primary marine precipitate from Late Archean and Paleoproterozoic sedimentary sequences (Grotzinger, 1989, 1993), the pinacoid (010) to prism (110) interfacial angle is 58.10°, and the interfacial angle between the prism (110) forms is 63.80°. Both gypsum and aragonite, however, have four smaller pinacoid-to-prism angles and two larger, prism-to-prism angles, whereas type 1 crystals show four larger, pinacoid-to-prism interfacial angles and two smaller, prism-to-prism angles. In addition, the unusual morphology of type 1 crystals, which grew as individual, vertical, nearly equant crystals, is unlike the generally bladed, twinned selenite crystals characteristic of coarser evaporitic gypsum and the fibrous radiating aragonite fans common in younger Archean and Paleoproterozoic carbonate units (Grotzinger, 1989, 1993).

Based on interfacial angle measurements, we conclude that silicified type 1 and type 2 evaporite crystals most closely resemble nahcolite, sodium bicarbonate ($NaHCO_3$). Nahcolite is monoclinic and prismatic and shows four pinacoid (010) to prism (110) interfacial angles of 63.2° and two angles between prism faces of 53.6°.

Type 3 crystals

No well-preserved type 3 crystals were sectioned for measurement of interfacial angles. These crystals are developed mainly in laminated lithofacies 2 sediments that lack wave ripples. They narrow, show tapering-upward shapes with sharp to ragged terminations (Fig. 14). Type 3 crystals precipitated under somewhat quieter and possibly somewhat less saline, more fully subaqueous conditions than type 1. The paucity of quartz-filled cavities within type 3 crystals suggests that they may have been less easily dissolved than type 1 crystals. Their general crystal form is similar to that of some bottom-nucleated selenite crystals in Messinian evaporites (Lo Cicero and Catalano, 1976, Fig. 7a, p. 73), although the Messinian splays are commonly much larger than those described here. Type 3 crystals and crystal layers also resemble some submarine aragonite fans reported by Grotzinger and Reed (1983, Fig. 1C, D), and

TABLE 1. INTERFACIAL ANGLES BETWEEN PRISM AND PINACOID FACES ON COMMON PRISMATIC PSEUDOHEXAGONAL SEDIMENTARY MINERALS

Group	Mineral	Crystal system	Pinacoid face	Prism face	Prism to pinacoid interfacial angle	Prism to prism interfacial angle
SULFATES	Barite $BaSO_4$	Orthorhombic	(001)	(011) (101)	52.72 38.86	74.56 102.28
	Celestite $SrSO_4$	Orthorhombic	(001)	(001)	52.05	75.90
	Gypsum $CaSO_4 \cdot 2H_2O$	Monoclinic	(010)	(120) (011)*	55.75 69.33	68.50 41.34
	Mirabilite $Na_2SO_4 \cdot 10H_2O$	Monoclinic	(010)	(110)	49.98	80.04
CARBONATES	Aragonite $CaCO_3$	Orthorhombic	(010)	(110) (011)*	58.10 54.22	63.80 71.56
	Strontianite $SrCO_3$	Orthorhombic	(010)	(110)	58.66	62.68
BICARBONATES	Nahcolite $NaHCO_3$	Monoclinic	(010)	(110)	53.6	63.2
BORATES	Borax $Na_2B_4O_5(OH)_4 \cdot 8H_2O$	Monoclinic	(010)	(110)	43.50	93.00

*Rare prismatic forms.

the general morphology, inferred depositional conditions, and contrasts with type 1 crystals suggest to us that type 3 crystals may have been carbonate.

Type 4 crystals

Type 4 crystals were precipitated as halo overgrowths around type 1 crystals. Their habit and occurrence resemble those of syntaxial diagenetic rim cements surrounding some gypsum crystals in Messinian evaporites (Vai and Ricci Lucchi, 1977, Fig. 7b), diagenetic anhydrite found surrounding some gypsum crystals in recent sediments of the Persian Gulf (Warren, personal communication, 1987), and acicular aragonite rim cements. However, without more details on crystal morphology, the primary mineralogy of type 4 crystals cannot be determined.

Type 5 crystals

Tightly packed type 5 crystals yielded no clear crystal forms. Their original mineralogy remains unknown.

DISCUSSION

Sedimentary evolution

The Buck Reef Chert accumulated above a thick succession of felsic volcanic rocks and volcaniclastic sediments following volcanism and erosion of the exposed parts of the volcanic complex. Erosion and gradual subsidence of the felsic center and flanking sedimentary apron provided a low relief surface upon which cherty and evaporitic sediments of the basal Kromberg Formation were deposited. Coarse-grained sandstone and conglomerate of lithofacies 1 at the top of the Hooggenoeg Formation reflect deposition of volcaniclastic debris in a low-gradient alluvial system, probably a braided floodplain or sand flat, deriving virtually all of its sediment by erosion of dacitic volcanic rocks.

Laminated and wave-rippled chert of lithofacies 2, commonly interbedded with layers of volcaniclastic debris, widely characterizes shallow-water, wave-active environments at the transition from subaerial to subaqueous conditions at the Hooggenoeg-Kromberg contact. Silicified evaporites of lithofacies 3 overlie and are interbedded with the uppermost layers of volcaniclastic sandstone of lithofacies 1 only along the central part of the west limb and hinge zone of the Onverwacht anticline. They record the local formation of small, restricted bodies of water along the distal edge of the alluvial fringe and in protected, restricted parts of the wave-active shallow-water zone. The development of evaporites at the regional transition from alluvial volcaniclastic sedimentation to the deposition of fine carbonaceous sediments under fully subaqueous conditions, represented by the overlying Buck Reef Chert, suggests that the restricted water bodies were salinas or coastal lagoons, probably isolated from more open waters by coastal sand bodies. These restricted water bodies were maintained by ground-water exchange and/or narrow connections to open water and possibly by occasional flooding by terrestrial runoff. They may have had a setting like Solar Lake and similar marginal ponds along the

Red Sea and Gulf of Aqaba (Friedman et al., 1973; Aharon et al., 1977) and Marion Lake and coastal salinas in South Australia (Warren, 1982).

Some features in the evaporite sequence are similar to Recent tidal flat deposits of the Trucial Coast, but evidence for the development of sabkhas, such as diagenetic anhydrite nodules, enterolithic folds, and surfaces marking prolonged subaerial exposure (Butler, 1969; Kinsman, 1969; Shearman, 1978), are absent. Sabkhas are also best preserved in progradational sequences (Kinsman, 1969; Patterson and Kinsman, 1981), whereas the upper Hooggenoeg to lower Kromberg section reflects submergence and overall deepening-upward conditions.

This deepening-upward trend led to the deposition of fine black carbonaceous sediments over most of the area following deposition of more restricted lithofacies 2 and 3. Regional subsidence was interrupted locally on the west limb of the Onverwacht anticline by an interval of subaerial exposure during which lithofacies 4 (solution collapse breccia) formed and 5 (conglomerate) was deposited. Megaquartz and chert of lithofacies 4 record an interval of exposure and leaching of the evaporites. The presence of stalactitic growths on the undersides of some solution-collapse blocks suggests that this occurred at least in part in the vadose zone. Black chert of lithofacies 6, volcaniclastic rocks of lithofacies 7, and the overlying black-and-white banded chert reflect renewed regional submergence and an upward transition into quieter, deeper water.

Marine or lacustrine setting of sedimentation

The significance of the Buck Reef evaporites depends in large part on the nature of the water body from which and within which they were precipitated. This water body could have been (a) the Archean ocean or a coastal water body, the chemistry of which was controlled by exchange with the ocean; (b) a large Archean lake supplied with water and dissolved materials by terrestrial runoff; or (3) a water body nourished by hydrothermal discharge. Several factors lead us to suggest that this water body was the ocean or coastal ponds connected to and/or exchanging water with the ocean:

(1) The Buck Reef Chert is a regional sedimentary unit, present in every part of the greenstone belt where sedimentary rocks deposited during the interval 3,438–3,416 Ma are known. It crops out in the southern part of the belt around the Onverwacht anticline, Kromberg syncline, and Steynsdorp anticline, where it is as much as 400 m thick (Fig. 1). It is present nearly 50 km to the northeast (Fig. 1) in northwestern Swaziland (sample locality of samples AGC 208 and 225 of Kröner and Todt, 1988), where it includes at least 100 m of recrystallized banded chert in contact with felsic metavolcaniclastic rocks. There is no evidence of boundaries, shores, or limits to this unit or to the body of water within which it was deposited.

(2) The water body was completely removed from sources of clastic debris throughout most of its existence. Chemical analyses of white and carbonaceous cherts in the Buck Reef Chert show 95–99% SiO_2 and a negligible amount of alumina (Lowe, this volume, Chapter 3). There is no evidence for the existence of clastic sediment sources fringing the water body locally or regionally.

(3) The area of evaporite sedimentation on the west limb of the Onverwacht anticline was located on a topographically high area. Uppermost Hooggenoeg (H6) strata in this area were deposited in a terrestrial setting. Laterally on the east limb of the Onverwacht anticline along the Komati River (locality 3, Fig. 1), these same strata consist of thick subaqueous debris-flow deposits and turbidites (Lowe and Knauth, 1977). On the far west end of the west limb (locality 1, Fig. 1), H6 is represented by fine, massive ash. Evaporite sedimentation occurred on the eroded remanents of a high-standing felsic volcanic complex. Whereas large volcanic islands are widely developed in oceans, they are less likely to grow, erode, and accumulated a terrestrial sedimentary cover entirely within lakes.

(4) The volcanic succession represented by the Hooggenoeg and Kromberg Formations totals 4–6 km thick. It is characterized throughout by units of pillowed volcanic rock and thin, subaqueously deposited cherty sedimentary units. The persistence of subaqueous environments of volcanism and sedimentation in areas dominated by the rapid effusion of thick sequences of mafic and ultramafic volcanic rocks is more likely to characterize marine settings than lakes.

(5) Ephemeral and perennial saline lakes derive their salts by weathering of surrounding subaerially outcropping rocks. This weathering and the influx of salts by runoff from surrounding land areas lead to the deposition of not only extensive sand flats but also dry mud flats and mud and clay layers within the lakes themselves (Hardie et al., 1978). The Buck Reef evaporite lacked mud layers. The saline ponds developed in areas of coarse sand deposition without accompanying mud sedimentation or any evidence for the existence of transitional silty and muddy environments. This type of setting most likely reflects deposition in partially restricted bodies of marine water isolated by coastal sand bodies.

(6) Terrestrial salinas, playas, and saline lakes, especially as small as those in which the Buck Reef evaporite was deposited, typically show fluctuating water levels and frequent drying, desiccation, mud cracking, and other features associated with exposure. These facies are lacking or rare in the Buck Reef evaporite. The small evaporite ponds existed for extended periods, probably years, characterized by fine, cyclic, couplet sedimentation (lithofacies 2) and type 1 and 2 evaporite crystal growth. There are only a few layers showing desiccation cracks, rip-up clasts, solution breccias, disturbed couplets, or other evidence of exposure during the accumulation of lithofacies 2 and none in the small brine ponds within which lithofacies 3 was deposited.

The Buck Reef Chert evaporite member crops out more-or-less continuously for only 10–15 km along the west limb and hinge zone of the Onverwacht anticline. Facies relationships indicate that the shallow-water surface upon which the evaporite accumulated passed laterally into deeper water to the west and east.

The overlying Buck Reef Chert is a regional deposit that includes as much as 400 m of silicified subaqueous sediments. The scale of this and other sedimentary units in the Barberton sequence make it unlikely that they represent ephemeral volcanic lakes. It is the abundance of evidence for the long-term persistence of widespread subaqueous settings for both volcanism and sedimentation that provides the strongest circumstantial evidence for sedimentation within marine and marginal marine rather than lacustrine environments.

An argument could be made that the setting of evaporite sedimentation, above a large felsic dome that may have been in the late stages of cooling and collapse, would have been ideal for the influx of hydrothermal fluids. Such fluids could have made their way up the small syndepositional normal faults developed over the felsic intrusion. We cannot unequivocally rule out a hydrothermal contribution to the water bodies, but have been unable to locate any tufas, spring mounds, or other deposits that are common around hydrothermal discharge sites. The evaporite layers are not massive precipitative crusts but mainly reflect the slow upward growth of type 1 crystals and the simultaneous deposition of fine laminated granular sediments. We consider it likely that the preceding felsic volcanic regime controlled the depositional setting by forming a local topographic high upon which a low-gradient, coarse-grained alluvial and coastal system developed that in turn localized evaporite deposition during submergence.

Early Archean ocean and atmosphere

Although surface waters in the modern oceans are supersaturated with respect to calcium carbonate (Li et al., 1969), biological precipitation maintains dissolved carbonate levels sufficiently low that, because of kinetics, neither calcite nor aragonite are normal open-marine precipitates. Also, in modern marine systems bicarbonate is the limiting component in calcite and aragonite deposition. That is,

$$[HCO_3^-] < 2[Ca^{+2}].$$

When seawater is concentrated through evaporation in restricted embayments and lagoons, the concentrations of calcium, remaining after exhaustion of dissolved bicarbonate, and sulfate commonly increase until gypsum ($CaSO_4$) is precipitated. With increasing evaporative concentration, halite (NaCl) and potassium salts are deposited.

In the Late Archean and Paleoproterozoic, dissolved carbonate and bicarbonate were not biologically limited and aragonite has been interpreted to have been a widespread precipitative sediment under shallow-water, open-marine, nonevaporitic conditions (Grotzinger, 1989, 1993; Grotzinger and Kasting, 1993). Grotzinger (1989) and Grotzinger and Kasting (1993) have further argued that, during the Archean and Paleoproterozoic, calcium was the component limiting carbonate sedimentation under normal marine conditions, implying that:

$$[HCO_3^-] > 2[Ca^{+2}].$$

Archean marine surface waters under evaporitic conditions may thus have been largely depleted in calcium, suppressing aragonite, calcite, and gypsum as evaporitic sediments (Grotzinger and Kasting, 1993). The evaporative concentration of seawater would rather have seen increasing concentrations of bicarbonate and sodium. Archean coastal salinas, hypersaline lagoons, and brine ponds may have thus had sodium carbonate and bicarbonate minerals as normal evaporative precipitates. The presence of nahcolite as a marine evaporite mineral 3,438–3,416 m.y. ago provides direct evidence that this scenario may be correct and that Archean oceans may have contained significantly higher levels of bicarbonate than their modern equivalents. Today, nahcolite occurs mainly in the deposits of alkaline lakes, such as Searles Lake, California, where it has formed by the diagenetic alteration of trona, $Na_2CO_3 \cdot NaHCO_3 \cdot 2H_2O$ (Foshag, 1940; Eugster, 1966). Nahcolite has also been reported from crusts lining cuniculi, confined conduits that transported hot spring waters to Roman baths (Bannister, 1929). Nahcolite is not a primary evaporitic mineral under normal surface conditions today because it readily alters to trona through the reaction

$$3NaHCO_3 + H_2O = Na_2CO_3 \cdot NaHCO_3 \cdot 2H_2O + CO_2.$$

This reaction is halted or reversed and nahcolite becomes a stable solid phase in equilibrium with solution and gas phases if the level of CO_2 in the gas phase is sufficiently high, substantially above that in the present atmosphere. The results of experiments by Eugster (1966) in the system sodium carbonate+sodium bicarbonate+solution+gas at 1 bar and solubility product calculations for the sodium carbonate and bicarbonate minerals by Monnin and Schott (1984) suggest that the minimum level of atmospheric CO_2 at which nahcolite is in equilibrium with liquid and gas phases is a direct function of temperature (Fig. 19). At temperatures of 30, 50, and 60°C the corresponding minimum CO_2 levels are about 2,900, 9,500, and 20,000 ppm, respectively. With a present atmospheric CO_2 level (PAL) of about 300 ppm, these CO_2 levels represent roughly 10, 32, and 67 times PAL, respectively. These represent general *minimum* CO_2 levels in the gas phase at 1 bar for nahcolite to exist as an equilibrium phase; the actual atmospheric CO_2 levels could have been substantially higher. These estimates may be somewhat modified by the presence of other dissolved species, but are probably within the general range of values to be expected (Eugster, 1966; Monnin and Schott, 1984).

In addition to the evaporites described here, pre-3.0-Ga Archean evaporites have also been reported from the 3.5 to 3.3 Ga Warrawoona Group, Eastern Pilbara Block, Western Australia (Dunlop, 1978; Groves et al., 1981; Lowe, 1983; Buick and Dunlop, 1990). In the North Pole area (Dunlop, 1978), evaporites in the lower part of the Warrawoona group include barite pseudomorphs after layers of primary crystals interpreted to have been gypsum and a complex association of facies thought to include silicified carbonate and gypsiferous

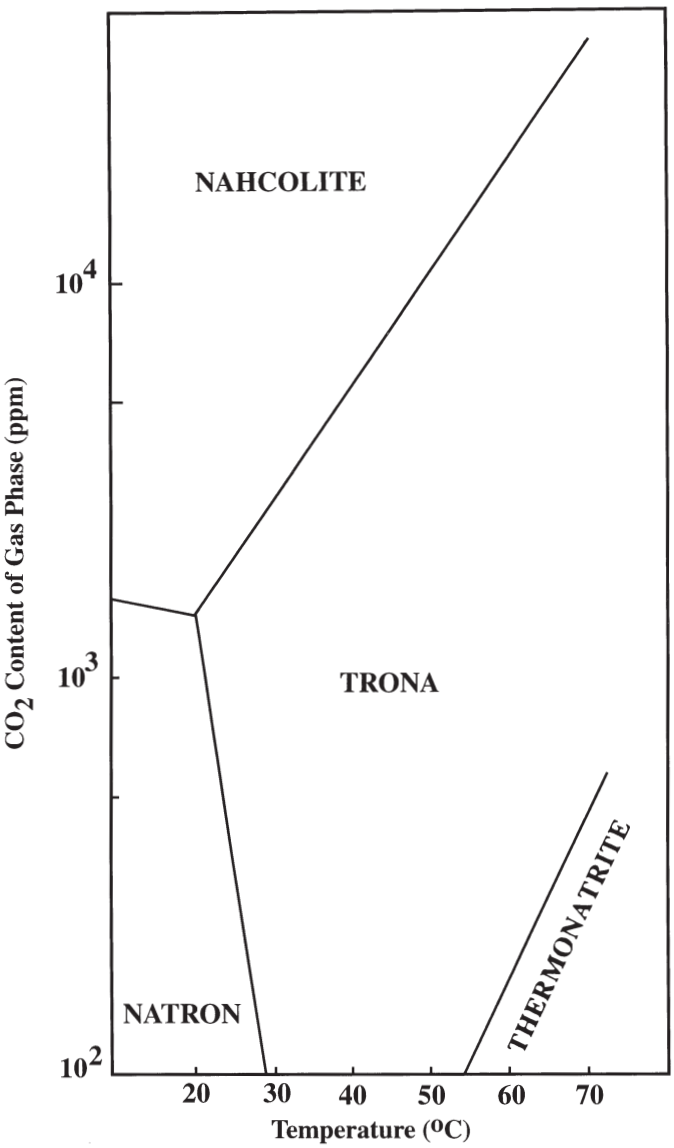


Figure 19. Mineral stability fields in system sodium carbonate + sodium bicarbonate + solution + gas. Modified from Eugster (1966).

sands, silts, and muds. These sediments, which crop out over a much larger area than the Buck Reef Chert evaporites, show evidence of having been deposited in a restricted marine body of water within a range of supratidal to shallow subtidal settings (Groves et al., 1981; Buick and Dunlop, 1990). The Strelley Pool Chert near the top of the Warrawoona Group (Lowe, 1983) contains silicified carbonate; beds as much as several meters thick of large, radiating silicified crystals interpreted to have been gypsum; isolated silicified gypsum crystallites; and, locally, silicified anhydrite crystallites. This unit crops out regionally over distances spanning at least 120 km.

Although previous studies have suggested the presence of silicified gypsum in the Buck Reef evaporite (Fisher Worrell, 1985), the present study has found no unambiguous evidence for its former existence. We consider that the presence of gypsum as a primary evaporitic mineral in the North Pole and Strelley Pool Cherts in the Warrawoona Group, Pilbara Block, Western Australia, needs to be more systematically evaluated, including the collection of more detailed crystallographic data than is now available. Available crystallographic data (Lambert et al., 1978), although sparse, and the general crystal morphologies (Groves et al., 1981; Buick and Dunlop, 1990) provide substantial evidence that gypsum may have been a primary evaporitic mineral during deposition of the North Pole Chert.

Grotzinger and Kasting (1993, p. 238) dismiss possible primary Archean gypsum occurrences as reflecting the existence of local "land-derived calcium-rich waters from the erosion of highly basaltic surrounding source rocks." This may be true, but without a more careful analysis, it is equally possible that the enormous span of time represented by the preserved Archean record saw many fluctuations in the bicarbonate levels of the oceans and corresponding changes in their calcium:bicarbonate ratios and, hence, the minerals that would have precipitated out of seawater with evaporation. Such fluctuations could have been driven by changes in atmospheric CO_2 levels, the rate of HCO_3^- production by weathering, or the rate of HCO_3^- utilization through sea-floor alteration and sedimentation. The Late Archean and Paleoproterozoic were intervals when enormous new blocks of continental crust were formed (Lowe, 1992). The weathering of these newly formed crustal blocks effectively transferred large amounts of carbon dioxide from the Late Archean atmosphere to the oceans as bicarbonate (Lowe, 1994). It may thus be expected that the latest Archean and Paleoproterozoic oceans contained exceptionally high levels of dissolved bicarbonate and that the sediments deposited on continental blocks at that particular time include thick sequences of marine precipitative carbonate. This conclusion is clearly substantiated by the available geologic record of carbonate sedimentation (Grotzinger and Reed, 1983; Grotzinger, 1993; Grotzinger and Kasting, 1993; Sumner and Grotzinger, 1996; Sumner, 1997). The areal extent of large continental blocks may have been significantly less before 3.0 Ga (Lowe, 1992, 1994), so the rate at which atmospheric CO_2 was being transferred by weathering of continental crust to oceanic bicarbonate may have been less and the degree of oceanic oversaturation with bicarbonate may have been lower than after 2.7 Ga. It is noteworthy that pre-3.0-Ga shallow-marine sedimentary sequences, represented mainly by widely developed shallow-water sediments in the Barberton and Pilbara greenstone belts, contain only minor primary carbonate sediments and, to date, no reported occurrences of marine precipitative aragonite. We feel that the Archean may have seen fluctuations in ocean composition and geochemistry greater than any other interval of Earth history as a consequence of the major changes in crustal inventory that took place between 3.5 and 2.5 Ga.

If not a common marine sediment, there is considerable evidence that gypsum may have been a common diagenetic component of early Archean greenstone sequences. Silicified

microcrystallites reported by Lowe and Knauth (1977) from black carbonaceous bands in the black-and-white banded Buck Reef Chert bear a strong resemblance in morphology and depositional setting to lenticular gypsum precipitated experimentally in carbonaceous muds (Cody, 1979). Similarly, small isolated silicified crystals and radiating crystal splays (Lowe, this volume, Chapter 3, Fig. 14B) are present in many fine-grained silicified mafic and ultramafic ash unit in the Onverwacht and Fig Tree Groups (Lowe and Knauth, 1977; Lanier and Lowe, 1982; Fisher Worrell, 1985; Lowe et al., 1985; Lowe, this volume, Chapter 3) and are widely developed in similar units in the Warrawoona Group (Buick and Dunlop, 1990). These closely resemble radiating gypsum clusters crystallized experimentally in bentonitic muds (Cody, 1976). Both of these modern experimental and Archean crystal types formed diagenetically and it is probable that the calcium required for diagenetic gypsum precipitation in the Archean was added to interstitial waters during alteration of the interbedded thick sequences of mafic and ultramafic volcanic and volcaniclastic rocks. In the case of the radiating crystal clusters, calcium was probably derived locally by alteration of the enclosing mafic ash. The absence of gypsum as an evaporitic sediment in the Onverwacht Group but wide development of diagenetic gypsum in volcanic ash units reinforces the inference that calcium was the limiting component and that normal early Archean marine waters contained little calcium.

One important aspect of these and other potential Archean gypsum occurrences lies in their implications regarding the sulfate content of Archean oceans. The presence of some level of dissolved sulfate could be expected in the Archean oceans because of the presence of reduced volcanic sulfur sinks for biologically and photochemically produced O_2. The actual concentrations of dissolved sulfate in the Archean oceans and the role of sulfate sedimentation on the early Earth remain poorly resolved. However, the wide development of sedimentary and early diagenetic barite and probable wide presence of early diagenetic gypsum suggest to the present author that dissolved sulfate was a normal and possibly abundant component of Archean seawater.

CONCLUSIONS

Although evaporitic units constitute a volumetrically minor part of the thick, predominantly volcanic Onverwacht and Warrawoona Groups, they make up a significant proportion of the thin sedimentary layers between volcanic flow units. Terrigenous clastic sediments are rare in these largely volcanic sequences (Lowe and Knauth, 1977; Barley et al., 1979; Lowe, 1980, 1982). If the volcaniclastic components are subtracted from the total sediment thickness, only precipitated layers, including the evaporites, and carbonaceous biogenic sediments remain. In fact, evaporite layers probably constitute a greater proportion of the nonvolcanic portions of these early Archean greenstone belt sequences than they do in analogous greenstone-type sequences of Proterozoic and Phanerozoic age.

Silicified evaporites 3,438–3,416 m.y. old at the base of the Kromberg Formation in the Barberton Greenstone Belt, South Africa, were deposited during regional subsidence following a period of felsic volcanism. They are localized at the transition from a subaerial, volcaniclastic sedimentary regime to a subaqueous, predominantly orthochemical and biogenic marine depositional system. Felsic volcaniclastic sandstones of the Hooggenoeg Formation (lithofacies 1) at the base of the evaporitic section were deposited on a braided coastal floodplain or sand flat. The interbedded and overlying evaporitic units record deposition in a range of shallow subaqueous to exposed coastal environments. Lithofacies 2, 3, and 4 reflect deposition of evaporites in local restricted salinas, brine ponds, and coastal lagoons. Polymictic conglomerate of lithofacies 5 was deposited during an interval of local uplift, block faulting, and erosion. Lithofacies 6 and 7 record regional subsidence and deposition of carbonaceous and distal pyroclastic airfall material, respectively, in a quiet, subaqueous environment.

No primary evaporite minerals have been recovered to date from the Buck Reef evaporite. Although mineralogical determinations based on the morphology of silicified, often poorly preserved pseudomorphs after original evaporite crystals are less reliable than those based on preserved primary mineralogies, the morphologies of crystals in this 3,438- to 3,416-Ma evaporite sequence suggest that nahcolite ($NaHCO_3$), sodium bicarbonate, was an major evaporitic mineral that precipitated subaqueously in quiet to gently wave active shallow brine ponds. These ponds were probably recharged by marine-water inflow through bordering porous sand bodies. Other evaporitic minerals could have been present but have not yet been identified.

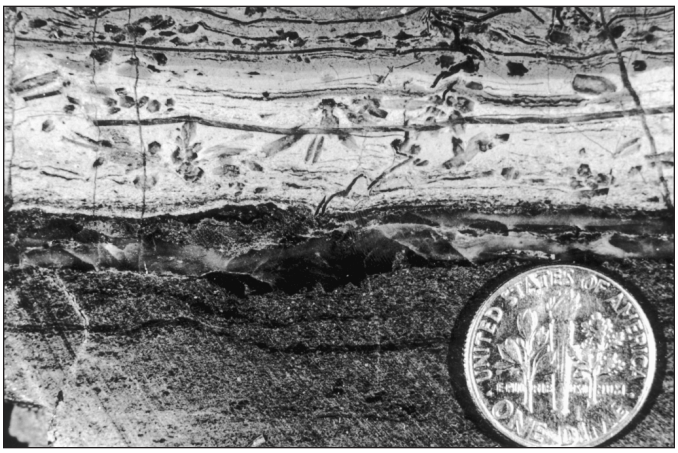


Figure 20. Small silica pseudomorphs after diagenetic pseudohexagonal crystals and radiating crystal clusters in a silicified basaltic komatitic ash, Unit H3c, Hooggenoeg Formation. The general morphology of these crystals suggests that they may represent gypsum. If Archean sea water was depleted in calcium, these and similar occurrences may have formed diagenetically where calcium was derived through sea-floor alteration of glassy volcanic ash.

The presence of sodium bicarbonate as an evaporitic mineral in the Archean is consistent with previous inferences that the early atmosphere contained much higher CO_2 levels than the modern atmosphere. At inferred surface temperatures of 30–60°C (Knauth and Lowe, 1978; Ohmoto and Felder, 1987), minimum CO_2 levels implied by nahcolite stability would have been about 10–67 PAL, respectively.

Available evidence suggests that the water bodies in which the evaporites formed were marine or actively exchanging water with the marine environment. If so, the presence of nahcolite supports the inference that calcium was commonly depleted in Archean marine surface waters by carbonate deposition (Grotzinger and Kasting, 1993). The present results suggest that the resulting bicarbonate-rich waters, when concentrated by evaporation, yielded sodium bicarbonate as the next mineral in the evaporite sequence.

REFERENCES CITED

Aharon, P., Kolodny, Y., and Sass, E., 1977, Recent hot brine dolomitization in the "Solar Lake," Gulf of Elat, isotopic, chemical, and mineralogical study: Journal of Geology, v. 85, p. 27–48.

Anhaeusser, C. R., 1973, The evolution of the early Precambrian crust of southern Africa: Royal Society of London Philosophical Transactions, ser. A, v. 273, p. 359–388.

Bannister, F. A., 1929, The so-called 'thermokalite' and the existence of sodium bicarbonate as a mineral: Mineralogical Magazine, v. 22, p. 53–64.

Barley, M. E., Dunlop, J. S. R., Glover, J. E., and Groves, D. I., 1979, Sedimentary evidence for an Archaean shallow-water volcanic-sedimentary facies, Eastern Pilbara Block, Western Australia: Earth and Planetary Science Letters, v. 43, p. 74–84.

Boulter, C. A., and Glover, J. E., 1986, Chert with relict hopper moulds from Rocklea Dome, Pilbara Craton, Western Australia: An Archean halite-bearing evaporite: Geology, v. 14, p. 128–131.

Buick, R., and Dunlop, J. S. R., 1990, Evaporitic sediments of Early Archaean age from the Warrawoona Group, North Pole, Western Australia: Sedimentology, v. 37, p. 247–277.

Butler, G. P., 1969, Modern evaporite deposition and geochemistry of coexisting brines, the Sabkha, Trucial Coast, Arabian Gulf: Journal of Sedimentary Petrology, v. 39, p. 70–89.

Clifton, H. E., Hunter, R. E., and Phillips, R. L., 1971, Depositional structures and processes in the non-barred high-energy nearshore: Journal of Sedimentary Petrology, v. 41, p. 651–670.

Cody, R. D., 1976, Growth and early diagenetic changes in artificial gypsum crystals grown within bentonitic muds and gels: Geological Society of America Bulletin, v. 87, p. 1163–1168.

Cody, R. D., 1979, Lenticular gypsum: occurrences in nature, and experimental determination of effects of soluble green plant material on its formation: Journal of Sedimentary Petrology, v. 49, p. 1015–1028.

de Raaf, J. F. M., Boersma, J. R., and Van Gelder, A., 1977, Wave-generated structures and sequences from a shallow marine succession, Lower Carboniferous, County Cork, Ireland: Sedimentology, v. 24, p. 451–483.

Dunlop, J. S. R., 1978, Shallow-water sedimentation at North Pole, Pilbara, Western Australia, *in* Glover, J. E., and Groves, D. I., eds., Archaean cherty metasediments: University of Western Australia Geology Department and Extension Service Publication 2, p. 30–38.

Dunlop, J. S. R., and Groves, D. I., 1978, Archaean evaporitic sulphates from the North Pole barite deposits, Pilbara Block, Western Australia: Geological Society of America Abstracts with Programs, v. 10, p. 393.

Dunlop, J. S. R., Groves, D. I., and Buick, R., 1979, Evidence for Archaean evaporites: Open Earth, v. 6, p. 15–16.

Esteban, M., and Klappa, C. F., 1983, Subaerial exposure, *in* Scholle, P. A., Bebout, D. G., and Moore, C. H., eds., Carbonate depositional environments: American Association of Petroleum Geologists Memoir 33, p. 1–96.

Eugster, H. P., 1966, Sodium carbonate-bicarbonate minerals as indicators of P_{CO2}: Journal of Geophysical Research, v. 71, p. 3369–3378.

Evans, O. F., 1942, The relation between the size of wave-formed ripple marks, depth of water, and the size of the generating waves: Journal of Sedimentary Petrology, v. 12, p. 43–70.

Fisher Worrell, G., 1985, Sedimentology and mineralogy of silicified evaporites in the basal Kromberg Formation, South Africa [Masters thesis]: Baton Rouge, Louisiana State University, 152 p.

Foshag, W. F., 1940, Sodium bicarbonate (nahcolite) from Searles Lake, California: American Mineralogist, v. 25, p. 769–778.

Friedman, G. M., Amiel, A. J., Braun, M., and Miller, D. S., 1973, Generation of carbonate particles and laminates in algal mats—example from sea-marginal hypersaline pool, Gulf of Aqaba, Red Sea: American Association of Petroleum Geologists Bulletin, v. 57, p. 541–557.

Grotzinger, J. P., 1989, Facies and evolution of Precambrian carbonate depositional systems: emergence of the modern platform archetype, *in* Crevello, P. D., Wilson, J. L., Sarg, J. F., and Read, J. R., eds., Controls on carbonate platform and basin development: Society of Economic Paleontologists and Mineralogists Special Publication 44, p. 79–106.

Grotzinger, J. P., 1993, New views of old carbonate sediments: Geotimes, v. 38, p. 12–15.

Grotzinger, J. P., and Kasting, J. F., 1993, New constraints on Precambrian ocean composition: Journal of Geology, v. 101, p. 235–243.

Grotzinger, J. P., and Reed, J. F., 1983, Evidence for primary aragonite precipitation, lower Proterozoic (1.9 Ga) Rocknest dolomite, Wopmay orogen, northwest Canada: Geology, v. 11, p. 710–713.

Groves, D. I., Dunlop, J. S. R., and Buick, R., 1981, An early habitat of life: Scientific American, v. 245, p. 64–73.

Gunatilaka, H. A., and Shearman, D. J., 1988, Gypsum-carbonate laminites in a recent sabkha, Kuwait: Carbonates and Evaporites, v. 3, p. 67–73.

Hardie, L. A., Smoot, J. P., and Eugster, H. P., 1978, Saline lakes and their deposits: a sedimentological approach, *in* Matter, A., and Tucker, M. E., eds., Modern and ancient lake sediments: International Association of Sedimentologists Special Publication 2, p. 7–41.

Holland, H. D., 1984, The chemical evolution of the atmosphere and oceans: Princeton, New Jersey, Princeton University Press, 582 p.

Kinsman, D. J. J., 1969, Modes of formation, sedimentary associations, and diagnostic features of shallow-water and supratidal evaporites: American Association of Petroleum Geologists Bulletin, v. 53, p. 830–840.

Klein, G. D., 1971, A sedimentary model for determining paleotidal range: Geological Society of America Bulletin, v. 82, p. 2585–2592.

Knauth, L. P., and Lowe, D. R., 1978, Oxygen isotope geochemistry of cherts from the Onverwacht Group (3.4 billion years), Transvaal, South Africa, with implications for secular variations in the isotopic composition of cherts: Earth and Planetary Science Letters, v. 41, p. 209–222.

Kröner, A., and Todt, W., 1988, Single zircon dating constraining the maximum age of the Barberton Greenstone Belt, southern Africa: Journal of Geophysical Research, v. 93, p. 15329–15337.

Lambert, I. B., Donnelly, T. H., Dunlop, J. S. R., and Groves, D. I., 1978, Stable isotopic compositions of early Archaean sulphate deposits of probable evaporitic and volcanogenic origins: Nature, v. 276, p. 808–811.

Lanier, W. P., and Lowe, D. R., 1982, Sedimentology of the Middle Marker (3.4 Ga), Onverwacht Group, Transvaal, South Africa: Precambrian Research, v. 18, p. 237–260.

Li, T. H., Takahashi, T., and Broecker, W. S., 1969, The degree of saturation of $CaCO_3$ in the oceans: Journal of Geophysical Research, v. 74, p. 5507–5525.

Lo Cicero, G., and Catalano, R., 1976, Facies and petrography of some Messinian evaporites of the Ciminna Basin (Sicily), *in* Catalano, R., Ruggieri, G., and Sprovieri, R., eds., Messinian evaporites in the Mediterranean: Memorie della Societa Geologica Italiana, v. 16, p. 63–81.

Lowe, D. R., 1980, Archean sedimentation: Annual Review of Earth and Plan-

etary Sciences, v. 8, p. 145–167.
Lowe, D. R., 1982, Comparative sedimentology of the principal volcanic sequences of Archean greenstone belts in South Africa, Western Australia, and Canada: implications for crustal evolution: Precambrian Research, v. 17, p. 1–29.
Lowe, D. R., 1983, Restricted shallow-water sedimentation of 3.4 Byr-old stromatolitic and evaporitic strata of the Strelley Pool Chert, Pilbara Block, Western Australia: Precambrian Research, v. 19, p. 239–283.
Lowe, D. R., 1992, Major events in the geological development of the Precambrian Earth, *in* Schopf, J. W., and Klein, C., eds., The Proterozoic biosphere: Cambridge, Cambridge University Press, p. 67–76.
Lowe, D. R., 1994, Early environments: Constraints and opportunities for early evolution, *in* Bengtson, S., ed., Early life on Earth: Nobel Symposium No. 84, Columbia University Press, p. 24–35.
Lowe, D. R., and Knauth, L. P., 1977, Sedimentology of the Onverwacht Group (3.4 billion years), Transvaal, South Africa, and its bearing on the characteristics and evolution of the early Earth: Journal of Geology, v. 85, p. 699–723.
Lowe, D. R., and Knauth, L. P., 1978, The oldest marine carbonate ooids reinterpreted as volcanic accretionary lapilli, Onverwacht Group, South Africa: Journal of Sedimentary Petrology, v. 48, p. 709–722.
Lowe, D. R., Byerly, G. R., Ransom, B. L., and Nocita, B. R., 1985, Stratigraphic and sedimentological evidence bearing on structural repetition in Early Archean rocks of the Barberton Greenstone Belt, South Africa: Precambrian Research, v. 27, p. 165–186.
Martin, A., Nisbet, E. G., and Bickle, M. J., 1980, Archaean stromatolites of the Belingwe Greenstone Belt, Zimbabwe (Rhodesia): Precambrian Research, v. 13, p. 337–362.
McKee, E. D., Crosby, E. J., and Berryhill, H. L., Jr., 1967, Flood deposits, Bijou Creek, Colorado, June 1965: Journal of Sedimentary Petrology, v. 37, p. 829–851.
Monnin, C., and Schott, J., 1984, Determination of the solubility products of sodium carbonate minerals and an application to trona deposition in Lake Magadi (Kenya): Gochimica et Cosmochimica Acta, v. 48, p. 571–581.
Ohmoto, H., and Felder, R. P., 1987, Bacterial activity in the warmer, sulphate-bearing, Archaean oceans: Nature, v. 328, p. 244–246.
Patterson, R. J., and Kinsman, D. J. J., 1981, Hydrologic framework of a sabkha along Arabian Gulf: American Association of Petroleum Geologists Bulletin, v. 65, p. 1457–1475.
Peryt, T. M., 1996, Sedimentology of Badenian (middle Miocene) gypsum in eastern Galicia, Podolia and Bukovina (West Ukarine): Sedimentology, v. 43, p. 571–588.
Schreiber, B. C., 1978, Environments of subaqueous gypsum deposition, *in* Dean, W. E., and Schreiber, B. C., eds., Marine evaporites: Society of Economic Paleontologists and Mineralogists Short Course No. 4, Lecture Notes, p. 43–73.
Schreiber, B. C., and Kinsman, D. J. J., 1975, New observations on the Pleistocene evaporites of Montallegro, Sicily and a modern analog: Journal of Sedimentary Petrology, v. 45, p. 469–479.
Shearman, D. J., 1978, Evaporites of coastal sabkhas, *in* Dean, W. E., and Schreiber, B. C., eds., Marine evaporites: Society of Economic Paleontologists and Mineralogists Short Course No. 4, Lecture Notes, p. 6–42.
Sumner, D. Y., 1997, Late Archean calcite-microbe interactions: Two morphologically distinct microbial communities that affected calcite nucleation differently: Palaios, v. 12, p. 300–316.
Sumner, D. Y., and Grotzinger, J. P., 1996, Herringbone calcite: petrography and environmental significance: Journal of Sedimentary Research, v. 66, p. 419–429.
Tunbridge, I. P., 1981, Sandy high-energy flood sedimentation—some criteria for recognition, with an example from the Devonian of S.W. England: Sedimentary Geology, v. 28, p. 79–96.
Vai, G. B., and Ricci Lucchi, F., 1977, Algal crusts, autochthonous and clastic gypsum in a cannibalistic evaporite basin: a case history from the Messinian of Northern Apennines: Sedimentology, v. 24, p. 211–244.
Viljoen, R. P., and Viljoen, M. J., 1969, The geological and geochemical significance of the upper formations of the Onverwacht Group: Geological Society of South Africa Special Publication 2, p. 113–152.
Walter, M. R., Buick, R., and Dunlop, J. S. R., 1980, Stromatolites 3,400–3,500 Myr old from the North Pole area, Western Australia: Nature, v. 284, p. 443–445.
Warren, J. K., 1982, The hydrological setting, occurrence and significance of gypsum in late Quaternary salt lakes in South Australia: Sedimentology, v. 29, p. 609–637.
Warren, J. K., 1983, On the significance of evaporite lamination, *in* Schreiber, B. C., ed., Proceedings, International Symposium on Salt, 6th, Toronto, v. 1, p. 161–170.
Williams, D. A. C., and Furnell, R. G., 1979, A reassessment of part of the Barberton type area: Precambrian Research, v. 9, p. 325–347.

MANUSCRIPT ACCEPTED BY THE SOCIETY MARCH 26, 1998

Geological Society of America
Special Paper 329
1999

Komatiites of the Mendon Formation: Late-stage ultramafic volcanism in the Barberton Greenstone Belt

Gary R. Byerly
Department of Geology and Geophysics, Louisiana State University, Baton Rouge, Louisiana 70803

ABSTRACT

The Mendon Formation is a newly defined stratigraphic unit composed of interbedded komatiitic lavas and cherty metasedimentary rocks at the top of the Onverwacht Group in the Barberton Greenstone Belt. It lies conformably on a chert at the top of the underlying Kromberg Formation that has been dated at 3,334 ± 3 Ma and beneath the conformably overlying basal Fig Tree Group dated at 3,259 ± 3 Ma. A chert within the Mendon Formation has yielded an age of 3,298 ± 3 Ma. Although rocks of the Mendon Formation crop out in a structurally complex portion of the Barberton Greenstone Belt, several key marker beds and distinctive geochemical traits of individual flows can be used to develop a coherent stratigraphy for the unit. The formation consists of a number of thick komatiitic flow units separated by thin, widely traceable layers of chert representing silicified tuffs, carbonaceous sediments, and chemical deposits.

The freshest Mendon komatiites contain relict igneous clinopyroxene and chrome-spinel. Olivine and glass have been completely altered to chlorite and plagioclase to albite. Micron-scale details of original igneous textures are commonly preserved in even the most altered samples where fine-grained quartz and sericite replaced original igneous minerals soon after deposition. Individual stratigraphic subunits of the Mendon Formation contain sets of flows with distinctive chemical compositions. The variation within each subunit is primarily due to olivine fractionation. Two major compositional groups of komatiites are recognized. Al-depleted komatiites have Al_2O_3/TiO_2 ratios near 10, and other magmatically incompatible and metasomatically immobile element ratios that are distinctly nonchondritic, though similar to komatiites found lower in the Onverwacht Group. Al-enriched komatiites have Al_2O_3/TiO_2 ratios greater than 30, and other incompatible and immobile element ratios distinctly non-chondritic and dissimilar to those of the Al-depleted komatiites. Al-enriched komatiites have been found only rarely in other portions of the Barberton sequence. Al-undepleted komatiites, with nearly chondritic incompatible element ratios are not found in the Mendon Formation, though they are found in the correlative Weltevreden Formation.

A preferred mechanism for the formation of both Al-depleted and Al-enriched komatiites in the Mendon Formation requires two stages of melting during the ascent of deeply sourced plumes. At depths between 450 and 650 km majoritic garnet is removed yielding melts with Al-depleted komatiite composition. Continued melting of these plumes would yield Al-enriched komatiite compositions.

Byerly, G. R., 1999, Komatiites of the Mendon Formation: Late-stage ultramafic volcanism in the Barberton Greenstone Belt, *in* Lowe, D. R., and Byerly, G. R., eds., Geologic Evolution of the Barberton Greenstone Belt, South Africa: Boulder, Colorado, Geological Society of America Special Paper 329.

INTRODUCTION

The Barberton Greenstone Belt (BGB) is perhaps the most studied sequence of early Archean rocks on Earth. From it has come the important work in the 1960s (Viljoen, M. J., and Viljoen, 1969a, b; Viljoen, R. P., and Viljoen, 1969) that demonstrated the existence of extrusive ultramafic rocks—the komatiites. Indeed, because of fairly good exposure and a large amount of work in the region by South African and international scientists, the BGB has often been used as a model for all Archean greenstone belts.

The stratigraphic distribution of ultramafic volcanic flow rocks in the BGB is complex. The coherent sequence more than 12 km thick in the southern portion of the belt includes the Komati Formation, a unit composed largely of komatiitic volcanic rocks (Viljoen, M. J., and Viljoen, 1969a); the overlying Hooggenoeg Formation (Viljoen, R. P., and Viljoen, 1969), which is dominantly basaltic but includes minor ultramafic and felsic lavas; and the overlying Kromberg Formation (Viljoen, R. P., and Viljoen, 1969; Vennemann and Smith, this volume, Chapter 5) that is dominantly basaltic with minor ultramafic rocks. The Mendon Formation rests conformably on the Kromberg Formation but is more complex in outcrop because of repetition by faulting and lateral facies changes of both lavas and interbedded sedimentary units. The Fig Tree Group appears to lie conformably on top of the Mendon Formation. This interpretation of the geology of the central BGB (Lowe and Byerly, this volume, Chapter 1) is in sharp contrast to the views of some workers, who have suggested that the Barberton sequence is, in fact, a sequence of lavas and sedimentary rocks at most a few kilometers thick repeated by isoclinal folds and low-angle faults (de Wit, 1982; de Wit et al., 1987). De Wit et al. (1987) have also interpreted the komatiites of the Komati Formation as sheeted dikes with spinifex margins. Our work (Lowe and Byerly, this volume, Chapter 1), while recognizing the structural complexity of the BGB, conforms generally with earlier interpretations (e.g., Viljoen, M. J., and Viljoen, 1969a, b; Viljoen, R. P., and Viljoen, 1969) of the stratigraphic arrangement and thickness of units in the Barberton Greenstone Belt.

Both field relationships (Byerly and Lowe, 1985) and isotopic age determinations indicate that the Mendon Formation is a separate unit that is considerably younger than the Komati Formation. A Sm-Nd date of 3,310 ± 150 Ma on komatiites of the Mendon Formation (Chauvel et al., 1987) has a large error, but is significantly younger than a Sm-Nd date for the Komati Formation of 3,540 ± 30 Ma (Hamilton et al., 1979). Both of these Sm-Nd dates are considered to be maximum ages because of the common problem of contamination of komatiitic rocks by assimilation of even small amounts of older crustal rocks (Arndt and Jenner, 1986; Gruau et al., 1990b). Recent high-precision, single-crystal zircon dating has substantially clarified age relationships within the Barberton sequence. The oldest portions of the BGB are at least 3,550 Ma (Kröner et al., 1996), a thin tuff in the type section of the Komati Formation has yielded an age of 3,472 ± 5 Ma (Kamo and Davis, 1994), the top of the Hooggenoeg Formation has been dated at 3,445 ± 3 Ma (Kröner et al., 1991), the base of the Kromberg Formation at 3,416 ± 5 Ma, and the top of the Kromberg Formation at 3,334 ± 3 Ma (Byerly et al., 1996). The age of the Mendon Formation is constrained by an age obtained from a thin cherty metasedimentary unit 300 m above the base of the formation, which yields an age of 3,298 ± 3 Ma (Byerly et al., 1996), and by the date of 3,334 ± 3 Ma on the top of the Kromberg Formation and of 3,258 ± 3 Ma on overlying rocks at the base of the Fig Tree Group (Byerly et al., 1996). Hence, although long mapped as part of the lower Onverwacht Group, equivalent to the Komati Formation (e.g., Anhaeusser et al., 1981), rocks of the Mendon Formation are younger than all but the upper sedimentary units of the Barberton sequence. Lowe and Byerly (this volume, Chapter 1) have further grouped a thick section of ultramafic volcanic and intrusive rocks and thin interbedded sedimentary layers into a new unit, the Weltevreden Formation, which they correlate with the more generally shallow marine sediments and komatiites of the Mendon Formation to the south. It, too, appears to lie conformably beneath the basal rocks of the Fig Tree Group and has yielded a Sm-Nd age on komatiites and komatiitic basalts of 3,286 ± 29 Ma (Lahaye et al., 1995).

The geology, petrology, and geochemistry of komatiites of the Mendon Formation have not been previously studied because they lie in a structurally complicated part of the greenstone belt and sufficient control has not been available to discriminate these rocks from those in the classic sections of the Komati Formation to the south. This paper will examine the field relationships, flow characteristics, major- and trace-element compositions, and, briefly, the nature of the alteration of the komatiitic volcanic rocks of the Mendon Formation. The Mendon komatiites will also be compared to other komatiites in the Barberton sequence, and models for petrogenesis will be discussed.

STRATIGRAPHIC POSITION AND LATERAL FACIES CORRELATIONS

The main outcrop area of the Mendon Formation is in the south-central portion of the BGB on the west limb of the Onverwacht anticline (Fig. 1). The complex outcrop distribution of the Mendon Formation is primarily due to fault repetition of parts of the unit and the overlying Fig Tree Group. Several episodes of folding and late Fig Tree dacitic intrusion have further added to the complexity of the outcrop distribution (Lowe and Byerly, this volume, Chapter 1; Lowe et al., this volume, Chapter 2). Key sample locations are also shown in Figure 1.

The stratigraphic nomenclature used here is that presented by Lowe and Byerly (this volume, Chapter 1) and is shown in Figure 2. Regionally the uppermost unit in the Kromberg Formation is a thin black and black-and-white banded chert, the Footbridge Chert (FC), that overlies pillow basalts. Rocks of the overlying Mendon Formation can be divided into a number of regionally traceable cycles of komatiitic volcanism separated by thin chert layers marking intervals of volcanic quiescence. From the lowest to the highest, these cycles are termed M1, M2, M3, etc., the included volcanic units M1v, M2v, M3v, etc., and the

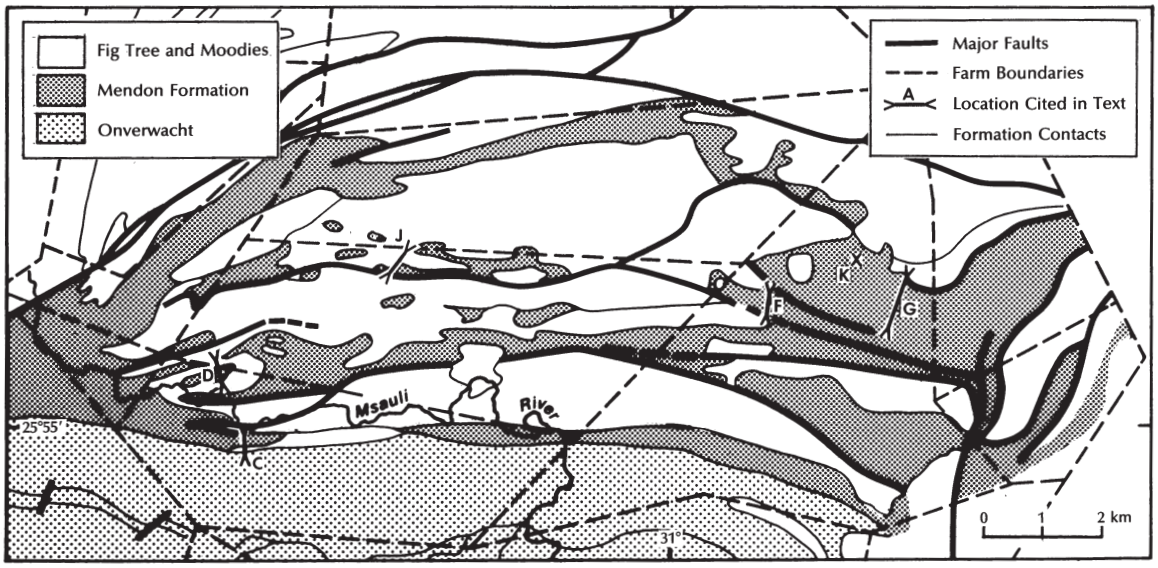


Figure 1. Map of west limb of Onverwacht anticline showing distribution of rocks of the Mendon Formation. Major faults separate structural belts that repeat sections of the Mendon Formation but differ in stratigraphy, relative proportions of sediments and lavas, and depositional setting. Letters designate locations of measured sections cited in text.

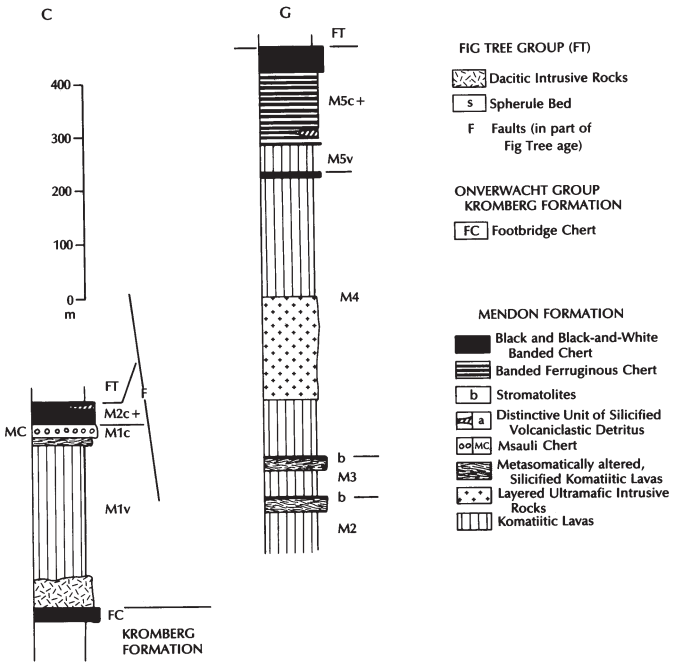


Figure 2. Generalized stratigraphic sections of Mendon Formation from location C, lowest structural belt, and location G, fourth structural belt (Fig. 1). Details of stratigraphic variation in the Mendon Formation are given in Lowe and Byerly (this volume, Chapter 1). In higher structural belts the Mendon Formation becomes thicker and contains at least five separate subunits designated M1 to M5. Each subunit is composed of a lower volcanic sequence and upper sedimentary sequence.

capping chert layers M1c, M2c, M3c, etc. (Lowe and Byerly, this volume, Chapter 1). The basal volcanic unit of the Mendon Formation, M1v, is dominated by massive fine-grained peridotitic komatiite that in places is more than 200 m in thickness. In some sections a 10-m-thick series of thin olivine spinifex-textured flows is developed with or without a cross-bedded lapilli tuff layer at the top of the thick peridotite section. In one section a 20-m-thick series of spinifex-textured flows is also present at the base. This thick unit is most likely a thick ponded komatiitic flow rather than a sill. Prior to, or during, deposition of the overlying Msauli Chert, M1c, this lava flow was weathered and subsequently hydrothermally altered to a depth of nearly 50 m in places like the Little Msauli Gorge (Lowe and Byerly, 1986), the type section of the Msauli Chert (Stanistreet et al., 1981). This alteration zone is composed of highly silicified and carbonated rocks that commonly preserve original igneous textures, but have highly modified compositions (e.g., Duchac and Hanor, 1987; Hanor and Duchac, 1990). The Msauli Chert itself is composed of fine-grained ash and accretionary lapilli (Lowe and Knauth, 1978; Stanistreet et al., 1981; Lowe, this volume, Chapters 3 and 9) of probable komatiitic composition (Lowe, this volume, Chapters 3 and 9). Similar thin komatiitic pyroclastic units occur in M2c and M3c, stratigraphically higher in the Mendon Formation. Units overlying the Msauli Chert are highly variable from section to section. In southernmost sections of the Mendon Formation on the west limb of the Onverwacht anticline, the Msauli Chert is overlain by black cherts at the top of the formation that are succeeded directly by clastic units of the Fig Tree Group (Lowe and Byerly, this volume, Chapter 1; section C in Fig. 2). To the north, across a series of intervening faults, lower cycles disappear or are not exposed and progressively higher vol-

canic and sedimentary cycles appear at the top of the sequence below rocks of the Fig Tree Group (Fig. 2, section G).

M2v is also composed exclusively of komatiitic lava flows of highly variable thickness. In section D (Fig. 1) as much as 150 m of komatiite is present with no sedimentary interbeds. The lower portion of the section is composed of a single, thick flow of fine-grained peridotitic komatiite. Upper portions of this section are represented by thin spinifex-textured flows or spinifex zones within a single flow. The uppermost flows are highly silicified and overlain by M2c, composed of black chert and interbedded silicified komatiitic pyroclastic rock. Figure 3 illustrates the stratigraphic distribution of komatiitic lavas in a section of M2v near the northern boundary of Farm Auber Villiers. This section of lavas, section J in Figure 1, is at least 200 m thick with no sedimentary interbeds. It has a distinctive base of bladed olivine spinifex flows, each about 5 m in thickness. Their local preservation and resistance to weathering may in part be due to silicification associated with a nearby crosscutting diabase dike. The upper three quarters of the section is made up of pyroxene-spinifex flows with highly variable textures and structures including pillows and pillow breccias, massive flows, and coarse acicular pyroxene spinifex units. The good exposure in this part of the section may also be due to silicification related to a nearby felsic dike. The section is underlain by silicified komatiitic ash of the Msauli Chert (M1c) and capped by a thin silicified komatiite flow overlain by chert of M2c.

Figure 4 shows a stratigraphic section of part of M2v from location F (Fig. 1). In this section, M2v is at least 100 m in aggregate thickness, including a poorly exposed base of serpentinized komatiite, 60 m of silicified komatiite, and a thin sedimentary chert, M2c. It is overlain by a serpentinized komatiite of M3v. At least six flow units are recognized in the upper silicified portion of M2v, where primary textures are especially well preserved. Individual flows are characterized by very fine grained tops with quench textures, including variolites, but only rarely vesicles. Fine random spinifex at the flow tops gives way downward to coarse oriented spinifex layers that are easily traced tens of meters along strike. Platy spinifex layers are present in some locations and are underlain by fine cumulate layers at the bases of the flows. A distinctive layer of large vesicles is present at about the 50 m mark in this section. The vesicles range in size to about 5 mm and account for as much as 10% by volume of the rock. Most were geopedally filled by late interstitial melt, which itself developed a microspinifex texture with fine chrome spinels settling to the bottoms of vesicles. Similar vesicular zones have been found in other sections of the Mendon Formation but are a minor lithologic component. The alteration zone at the top of M2v was studied by Duchac and Hanor (1987) and Hanor and Duchac (1990).

Komatiites of M3v are poorly exposed except in a few sections where they are highly silicified. One such is section G (Fig. 1), where about 50 m of thin, highly altered lava flows with spinifex-texture lie between M2c and M3c. Individual flow units range from 1 to 5 m in thickness. A similar sequence of M3v flows is developed at the top of Section F. The chert M3c contains several subcentimeter thick tuff layers that yielded zircons with an age of 3,298 ± 3 Ma (Byerly et al., 1996).

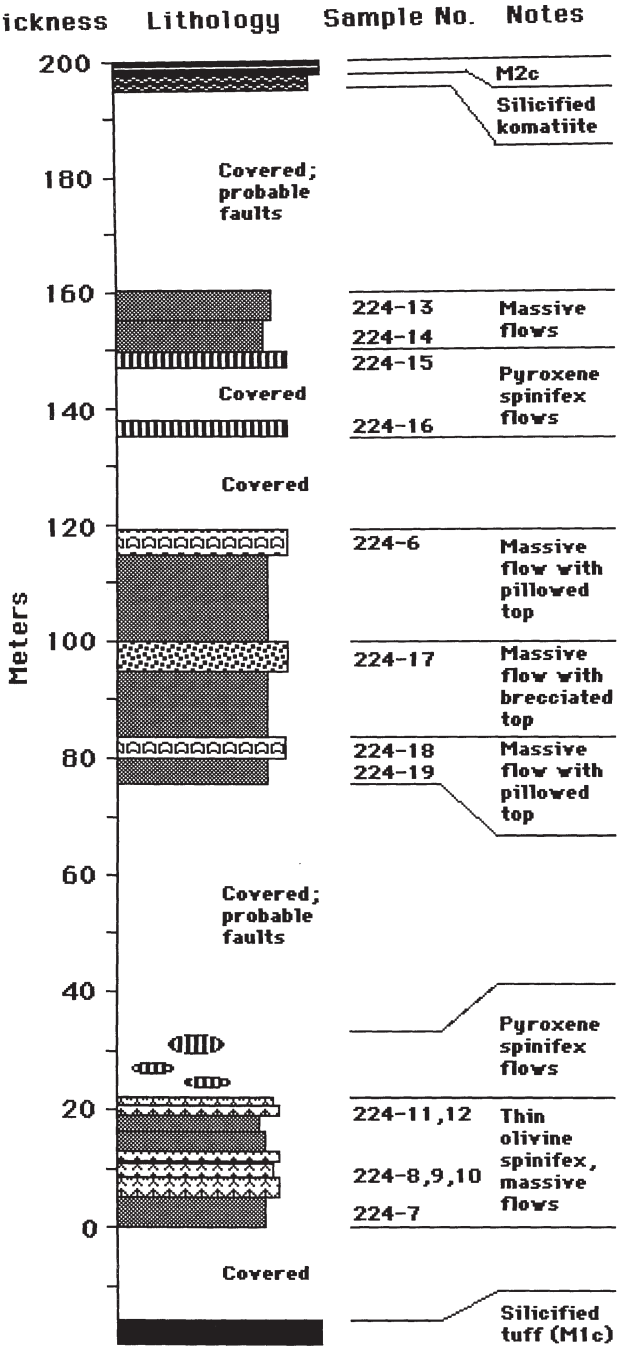


Figure 3. Stratigraphic section of M2 on the northern part of Farm Auber Villiers (location J, Fig. 1). More than 200 m of lavas are present with no exposed interbedded sedimentary units. Thin olivine spinifex-bearing, high-MgO flows occur at the base of the unit. The upper 75% of the unit consists of massive and pyroxene spinifex, low-MgO flows. M2v is underlain by the Msauli Chert (M1c) at this location.

M4v is recognized in only a few locations, including the area near Section G where a thickness of as much as 500 m may be

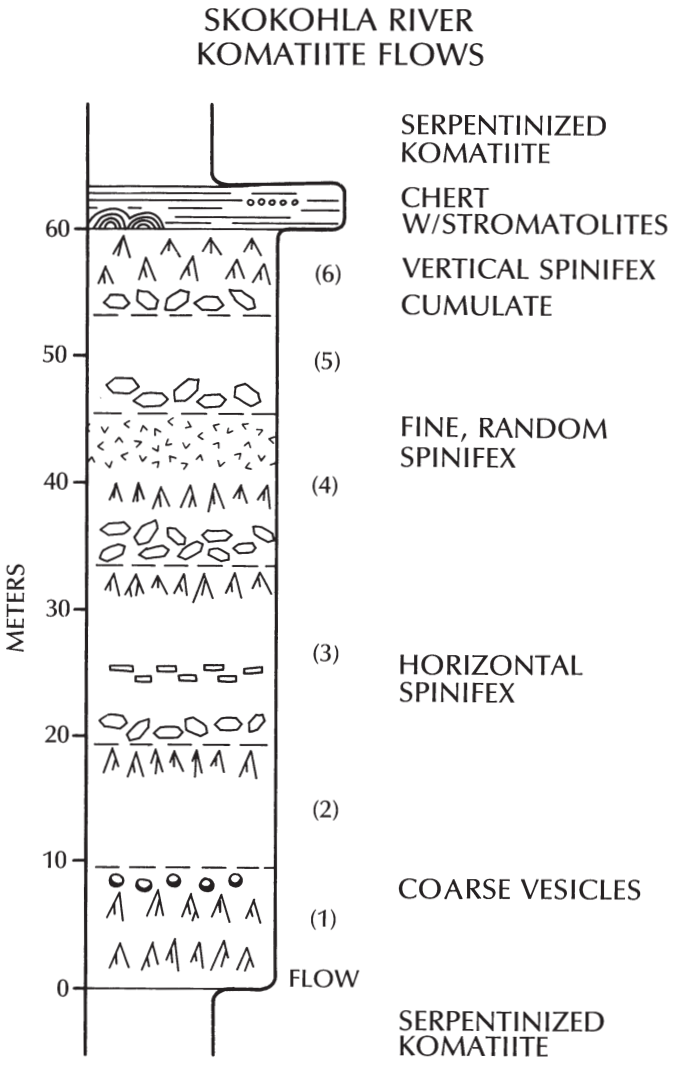


Figure 4. The Skokohla River section of the upper part of M2v (location F, Fig. 1). The top of M2v at this locality includes at least six flows in a section of silicified lavas about 60 m thick. M2v is overlain by chert unit M2c that is conformably succeeded by M3v.

present. Section G is near the hinge of a major fold and the intersection of several large faults, and the total thickness of M4v may thus be somewhat exaggerated. At Location K (Fig. 1) a minimum thickness of 125 m of M4v komatiites is present. The lower 90 m is represented by a single thick komatiitic flow with cumulate layering near the base, though it is generally a fine-grained peridotite. Individual cumulate layers vary in color, grain size, and boldness of outcrop. The pyroxene-rich layers are lighter in color, coarser grained, and more resistant to weathering and erosion. Intervals of about 25 m above and 20 m below the flow are covered. In several other nearby localities the lower 10 m of this unit is represented by several highly altered, spinifex-textured lava flows. The upper 35 m of M4v contains a sequence of pillowed to massive komatiitic lava flows with abundant random to oriented pyroxene spinifex zones. Pillows are typically as much as 1 m in height and 3 m in width. This is the only place in the Mendon Formation where the komatiites are variolitic. Varioles occur in isolation, as much as 3 cm in diameter, or in aggregates that make up the bulk of some pillow interiors. The varioles are typically more bleached in appearance than the enclosing host rock.

The uppermost unit of the Mendon Formation, M5, is composed primarily of a thick sequence of cherts. Figure 5 illustrates the textural variation within a very thin komatiitic lava flow in M5. This 60-cm-thick flow is an isolated flow within banded ferruginous cherts at the top of the formation. Typical komatiitic textures are developed from top to base. The upper two-thirds of the flow shows random to oriented olivine spinifex and the lower third of the flow is predominantly cumulate olivine. As with most flows closely associated with sedimentary rocks, this unit is completely silicified, resulting in lithology now composed of quartz, sericite, and chromite.

The Msauli Chert, M1c, shows abundant evidence for deposition in shallow water (Lowe and Knauth, 1978; Lowe, this volume, Chapter 9). M2c also shows evidence for a shallow depositional setting. It contain structures interpreted to be stromatolites and debris from desiccated and eroded stromatolites (Byerly et al., 1986). These features have also been interpreted to represent possible hot spring deposits (Lowe, 1994a). M2c also contains thin layers of fine ash and accretionary lapilli of apparent komatiitic composition, including a distinctive regional marker bed with large, polygonal accretionary lapilli (Lowe and Byerly, this volume, Chapter 1). The silicified ash layers in M2c also show abundant current structures, including cross- and flat laminations, and rapid facies changes along the outcrop. M3c is less clearly shallow water in origin and M4c and the sediments in M5 consist mainly of finely laminated ferruginous rocks showing little evidence for current activity, no accretionary lapilli, and no in situ carbonaceous mat layers. These chert layers probably accumulated in deeper, quiet water (Lowe and Byerly, this volume, Chapter 1; Lowe, this volume, Chapter 3).

The tops of the lava flows are invariably extensively altered beneath the chert caps. Where the lavas are thicker and contain no sedimentary interlayers, the flow tops are relatively unaltered. Models for the development of these flow-top alteration zones have been presented by Lowe and Byerly (1986), Duchac and Hanor (1987), and Hanor and Duchac (1990). De Wit (1982) has interpreted them as regional bedding-parallel thrust faults. Their origin is also discussed by Lowe et al. (this volume, Chapter 2).

PETROGRAPHIC CHARACTERISTICS OF THE KOMATIITIC ROCKS

The lavas of the Mendon Formation display many of the characteristics common to komatiites elsewhere in the Barberton sequence and in other Archean greenstone belts. In some flows this includes the hallmark of komatiitic lavas, the development of coarse spinifex layers in the upper portions of the flows. Both olivine and clinopyroxene spinifex layers are common, though usually not interlayered. Other types of flow structures are also common, including thick complexly layered flows that have often been

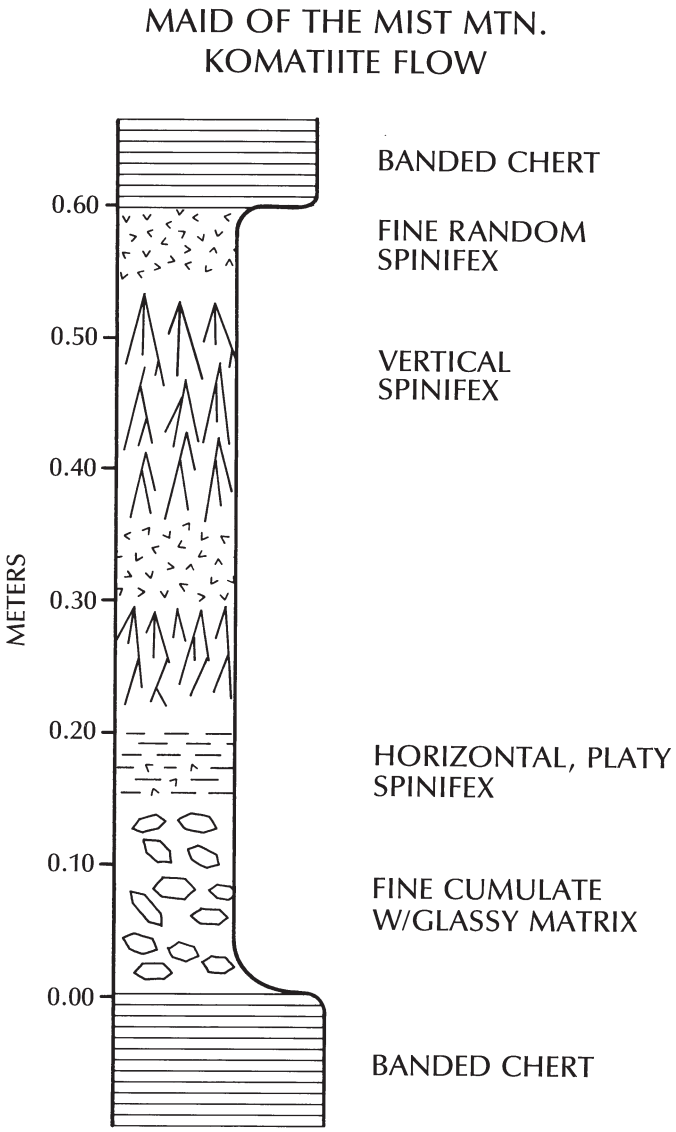


Figure 5. Mendon lavas display typical textures and structures of komatiites. This 60-cm-thick flow is an isolated subunit of M5.

regarded as sills (Viljoen, M. J., and Viljoen, 1969a; Anhaeusser, 1985; de Wit et al., 1987). Outcrops within the sequences of lavas are generally poor except where flow-top alteration has silicified the original lavas to a more chemically and mechanically resistant lithology. Units greater than 200 m thick have been mapped as komatiite with no clear indication of internal boundaries. In the best exposed sections it is clear that some individual flows must exceed 100 m in thickness. Most exposures reveal lava flows a few meters thick and, in rare cases, less than 50 cm thick. The komatiites may be classified into four lithologic groups.

Coarse-grained cumulates

Coarse-grained cumulate layers are common throughout the greenstone belt. They are often mineralogically layered and commonly develop a characteristic poikilitic texture. They are usually, but not always, associated with fine-grained komatiites and in many places show evidence for an extrusive origin, including altered tops beneath sedimentary rocks, and fine, quench groundmass textures. Anhaeusser (1985) has reviewed the geology and petrology of thick layered mafic and ultramafic bodies of the Barberton Greenstone Belt. Arndt et al. (1977) have suggested that similar bodies from the late Archean of Canada are massive flows that did not develop characteristic spinifex textures because they did not pond. Layering is defined in all of these Archean ultramafic bodies by variable proportions of olivine, pyroxene, and groundmass. In the Mendon bodies olivine, typically equant grains less than 2 mm across, is always replaced by serpentine. Augite and less commonly orthopyroxene are in places unaltered, occurring as either fine groundmass quench crystals or as large, as much as 1 cm, poikilocrysts in the coarsest rocks. Large chrome spinels, as much as 0.1 mm in diameter, are common to all komatiitic rocks of the Mendon Formation. Very fine secondary magnetite, which outlines original, magmatic crystal boundaries, produces the dark color of these rocks and also preserves fine textural details down to the micron scale. In the Weltevreden Formation along the northern edge of the belt, which may correlate with the Mendon Formation, very thick layered units of komatiitic composition are interbedded with minor komatiitic lavas and sedimentary rocks. As mentioned earlier, most workers have interpreted these as sills, but they were likely contemporaneous with volcanism, and may in fact be very thick ponded lava flows.

Olivine spinifex and fine olivine cumulates

Olivine-spinifex rocks are invariably very dark gray, dense, and completely altered to serpentine and magnetite, much like those elsewhere in the BGB (e.g., Viljoen, M. J., and Viljoen, 1969a). Pseudomorphs after olivine spinifex show tabular to bladed magmatic crystals. The olivine spinifex most commonly occurs as thin (0.1 mm wide) parallel serpentine pseudomorphs in places as much as a meter in length. Fine, plumose groundmass pyroxenes are in places fresh and surrounded by chlorite, which replaced original interstitial glass. Chromite is less common than in other lithologies and where present commonly forms fine dendritic crystals in the spinifex layers, and small, as much as 50 micron, euhedra in the basal cumulate layers. Olivines in the basal layers occur as equant euhedra pseudomorphed by serpentine and ranging in size to about 0.3 mm.

Pyroxene-spinifex and fine pyroxene cumulates

These rocks are usually altered to green, actinolite-rich, lithologies quite distinct from the olivine-rich rocks. The pyroxenes generally occur as coarse to fine acicular crystals, as much as 0.2 mm wide, that form layers as much as 50 cm thick. In some samples the random pyroxene spinifex shows a complex tabular-plumose habit with crystal lengths of several millimeters,

widths as much as 1 mm, and shortest dimension as much as about 0.2 mm. The crystals are elongate along the c-axis, tabular on the (010) pinacoid, but with distinctive subcrystals radiating out in places almost to become parallel to the a-axis of the host crystal. Under crossed-nicols, crystals viewed with b-axis nearly normal to the stage display complex radiating extinctions and the coarsest examples of plumose texture. Crystals viewed with the a-axis normal to the stage commonly have a linearly segmented character, with adjacent segments in different crystallographic orientation but alternate segments crystallographically coherent. In basal cumulate layers the pyroxenes occur as equant euhedra as much as about 0.2 mm in size in a very fine groundmass of quenched crystallites and chlorite after glass. In thicker flows, where groundmass minerals are coarser grained, late-stage plagioclase can be seen. Distinctly zoned pyroxenes have altered cores that may reflect original pigeonite with augite overgrowths. Chromites are fresh and abundant in this lithology. In random spinifex layers the rocks are commonly mottled in appearance, in places grading into a lithology commonly described as variolitic. These textures appear to be produced by variable proportions of phenocrysts and groundmass. In places the lighter colored phenocryst-poor portions of the rock have filled vesicles or cracks that formed after the lava was crystalline enough to be rigid, about 50%, but still above the solidus temperature. Chromites that settled to the bottom of some of these late-stage segregations provide consistent geopedal up directions.

Komatiitic ash

The Msauli Chert and M2c contain texturally well preserved volcanic ash (Lowe, this volume, Chapters 3 and 9). In outcrop these ashes are dense, thoroughly silicified, buff to pale green rocks that are in places interlayered with carbonaceous cherts. Textures in the coarser grained ash are beautifully preserved by silicification. They commonly include accretionary lapilli and easily recognized shards of glass pseudomorphed by fine-grained quartz and sericite (Lowe and Knauth, 1977, 1978; Lowe, this volume, Chapters 3 and 9). These glasses were virtually aphyric; only rarely have chromites been found, or silica pseudomorphs after fine olivine microphenocrysts. In some samples subequant glass shards are as much as 400 microns across. The larger shards are typically blocky to tabular and smaller shards more cuspate. In the larger shards vesicle density is not greater than about 10%, with nearly spherical vesicles as much as 150 microns in diameter. A minor but distinctive shard type has abundant fine, parallel vesicles similar to those in Pele's hair. Lowe (this volume, Chapters 3 and 9) has presented evidence that the ashes were komatiitic in composition.

METAMORPHISM AND ALTERATION

Metamorphic mineral assemblages in these magnesian lavas are consistent throughout the central portion of the Barberton Greenstone Belt where the Mendon Formation has been defined. Rocks once olivine rich are now typically serpentine + chlorite + magnetite ± talc ± actinolite ± magnesite. The low-MgO komatiites are now actinolite + chlorite + albite + magnetite ± sphene ± epidote. Fresh, magmatic chromite, augite, and less commonly orthopyroxene, are occasionally preserved in these rocks. Minor potassium-rich rocks found at the tops of altered flows contain primary chromite and quartz + sericite + rutile ± chlorite ± magnesite ± tourmaline, but do not contain biotite. All these points indicate metamorphism no greater than the lower portion of "lower greenschist grade" and temperatures slightly above 300 °C. Chlorite and amphibole geothermometry also confirm these metamorphic conditions (Xie et al., 1997). Most workers agree that most of the features present in BGB rocks likely reflect subseafloor metamorphism and metasomatism that was probably very early, perhaps nearly contemporaneous with volcanism (de Wit et al., 1982; Smith et al., 1984; López-Martínez et al., 1984; Paris et al., 1985). Later metamorphic overprinting associated with dacitic magmatism of Fig Tree age may have developed locally near some of the larger intrusives into the Mendon Formation, but the Mendon Formation is generally unaffected by contact metamorphic zones, which are more commonly developed near the margins of the greenstone belt.

GEOCHEMISTRY

Komatiitic volcanic rocks

Komatiites of the Mendon Formation display a broad spectrum of compositional variation related to igneous fractionation and secondary alteration processes. In many samples all primary silicates have been hydrated to amphiboles and chlorites. Despite the pervasive hydration of these rocks, much of the major and minor element variation seems to be consistent with shallow-level igneous fractionation. An exception to this is a group of Mendon komatiites that display extreme metasomatic alteration to quartz-sericite lithologies. The alteration of some of the Mendon komatiites presents a major problem in understanding their magmatic petrogenesis. This alteration (Lowe and Byerly, 1986; Duchac and Hanor, 1987; Hanor and Duchac, 1990) is characterized by replacement of primary minerals by fine-grained quartz and sericite, but often with remarkable preservation of original textures. SiO_2 and K_2O have been added to these rocks; and FeO, MgO, CaO, and Na_2O removed. Al_2O_3 and TiO_2 are variable, but Al_2O_3/TiO_2 is constant within a single flow or sequence of flows. Variable Al_2O_3 and TiO_2 at a nearly constant Al_2O_3/TiO_2 is partly due to olivine fractionation but also to two distinctive alteration processes. The altered rocks in places developed stylolites that have concentrated sericite and rutile; elsewhere quartz fills veins, diluting the other rock components. In these altered rocks the ratios of the relatively immobile elements, including Al, Ti, Cr, V, Zr, Y, and Sc, are nearly constant and probably reflect original magmatic ratios. In the silicified rocks that retain well-preserved spinifex textures and no veins or stylolites, these immobile elements are in concentrations that are also typical of magmatic values. Because these altered komatiites rep-

resent important end-components of volcanic episodes, they have been carefully studied and compared to the less abundant, relatively fresh komatiites of the Mendon Formation.

Analyses of Mendon komatiites are reported in Table 1A and 1B. Table 1C includes analyses of the highly silicified samples. The sample lithology has also been included in the tables because of the substantial variation in composition that is found in komatiitic lava flows as a function of position and cooling sequence—parameters that are easily related to lithologic variation within the flows (Arndt, 1986; Kinzler and Grove, 1985). The samples are arranged by stratigraphic unit in the tables. Analyses were performed by two techniques, as indicated in the table: (1) inductively coupled plasma emission spectroscopy (ICP) analyses were done at Louisiana State University using metaborate fusion and nitric acid digestion; (2) X-ray fluorescence spectroscopy (XRF) analyses were done at University of Cape Town using glass discs for major elements and pressed pellets for trace elements. Six Mendon samples were analyzed by both techniques and the results were quite compatible. Results for Na, Ba, and Sr were better using ICP and those for P, Zr, and Y were better using XRF. The only distinct analytical bias was for Zr, about 20% higher by ICP compared to XRF analyses. The major elements have been normalized to 100% dry weight and all iron reported as FeO.

The overall compositional variation in the Mendon Formation komatiites is seen in the MgO variation diagrams (Fig. 6a). In general, three compositional groups can be recognized: (1) coarse-grained olivine cumulates with MgO contents greater than 28%, (2) fine-grained olivine spinifex with MgO values mostly between 22 and 28%, and (3) fine-grained pyroxene spinifex with MgO values mostly between 16 and 18% MgO. The group of analyses with MgO near zero represents rocks that have been extensively altered. Major element variation in fresh Mendon Formation komatiites seems to reflect the dominant effects of crystal fractionation from 28 to 10% MgO, and accumulation in lavas where MgO is greater than 28%. This is best illustrated in the MgO-TiO_2 variation diagram, though there is a distinct gap between the high MgO and low MgO komatiitic

TABLE 1A. MAJOR AND TRACE ELEMENT COMPOSITIONS OF KOMATIITIC ROCKS FROM THE NORTH AUBER VILLIERS SECTION OF THE MENDON FORMATION

Sample	SA224-6	SA224-7	SA224-8	SA224-9	SA224-10	SA224-11	SA224-12	SA224-13	SA224-14	SA224-15	SA224-16	SA224-18	SA224-19
Lith.	random pyx spin	oriented ol spin	random ol spin	fine ol B-zone	oriented ol spin	random ol spin	oriented ol spin	random pyx spin	oriented pyx spin	oriented pyx spin	random pyx spin	random pyx spin	random pyx spin
Unit	M2v	M2v	M2v	M2v	M2v	M2v	M2v	M2v	M2v	M2v	M2v	M2v	M2v
Tech.	icp	icp	icp	icp	icp	icp	icp	icp	icp	icp	icp	icp	icp
SiO_2	48.16	47.08	47.28	48.44	48.98	48.14	49.87	47.83	50.00	52.45	52.65	48.64	49.60
Al_2O_3	8.52	4.72	4.36	3.71	4.01	3.98	4.34	7.06	6.68	6.88	6.51	8.11	7.80
FeO	13.58	13.38	12.00	11.20	10.87	13.16	12.76	12.70	12.60	11.95	11.21	14.06	13.14
MgO	16.61	26.44	28.28	28.59	26.02	26.71	25.51	20.92	18.05	15.55	13.52	17.27	15.23
MnO	0.21	0.19	0.19	0.17	0.20	0.20	0.19	0.19	0.20	0.22	0.21	0.23	0.22
CaO	10.69	7.20	6.96	6.98	8.99	6.57	6.07	9.62	10.84	10.33	12.81	9.76	11.04
TiO_2	0.81	0.50	0.45	0.38	0.40	0.44	0.43	0.66	0.65	0.72	0.63	0.76	0.78
P_2O_5	0.07	0.03	0.02	0.02	0.00	0.00	0.00	0.03	0.00	0.02	0.00	0.05	0.00
Na_2O	1.25	0.42	0.45	0.40	0.52	0.81	0.81	0.83	0.97	1.71	2.30	1.12	1.98
K_2O	0.09	0.04	0.02	0.11	0.02	0.00	0.01	0.15	0.00	0.17	0.16	0.00	0.21
Ba	20	10	9	19	18	11	12	22	45	19	32	13	22
Co	76	81	95	81	55	80	103	59	48	58	45	66	38
Cr	1881	2199	2153	1748	1474	1777	1809	1224	1514	1086	819	1484	956
Cu	87	40	135	10	52	38	29	57	99	25	17	87	73
Ni	505	1099	1510	1486	689	775	715	412	263	260	203	419	186
Sc	32	24	22	21	18	20	20	25	27	31	27	28	29
Sr	39	63	81	90	88	57	49	24	50	236	97	37	59
V	227	140	133	110	104	114	119	152	164	190	162	180	169
Y	17	11	10	21	9	7	8	13	17	16	12	14	13
Zn	107	95	97	85	81	96	88	80	74	81	58	96	89
Zr	55	44	36	46	47	39	38	60	66	64	46	67	59

Note: Major element compositions in wt%; trace element compositions in ppm. The major elements normalized to 100% dry weight and all iron reported as FeO.

rocks. In the MgO-Al_2O_3 variation diagram most of the cumulate rocks define a parallel but distinctly higher Al_2O_3 variation trend. These rocks are from M1v and M4v-l, which seem always to have very high Al_2O_3. A slight variation in MgO at constant Al or Ti may reflect some mobility of MgO during alteration of these rocks. Similarly Ca and Fe show more variation than expected in such closely associated lavas, and were likely mobilized during interaction with seawater. The cumulate rocks are especially low in CaO. This is in part due to an abundance of orthopyroxene in some samples, but even those samples with as much as 50% trapped melt, as seen in a fine, quench-textured groundmass, display similarly low CaO contents. Smith and Erlank (1982) consider that in even the freshest komatiites of the Komati Formation CaO has been mobilized. Arndt et al. (1977) and Arndt and Jenner (1986) argue that CaO loss in Mg-rich komatiites is ubiquitous. FeO displays a variation that could represent either mixtures of olivine-orthopyroxene or olivine-melt. Na shows the most extreme variation, with the high MgO komatiites having values too low (less than 0.2 wt.%) to represent igneous liquids, whereas the low MgO komatiites have reasonable values (about 2 wt.%). The low MgO komatiitic rocks have plagioclase in the groundmass, which may have stabilized Na, though albitization of the plagioclase may have added some Na to the rocks. Potassium shows no consistent variation that might be attributed to magmatic processes and would be expected to be easily mobilized in these rocks. Phosphorus is near the lower limit of detection for the ICP analytical technique used, yet when individual stratigraphic units or even particular sections are split out of the data set, fairly consistent values are recognized that likely reflect original magmatic compositions. Such altered komatiitic rocks typically have remarkably preserved pseudomorphs of quartz after olivine, with magmatic chromite inclusions, and groundmass of quartz and sericite.

Trace elements are plotted on MgO variation diagrams in Figure 6b. Two compatible elements, Ni and Cr, and two incompatible elements, Sc and V, generally reflect olivine-liquid fractionation and accumulation. Individual sequences of flows have distinctive compositions that apparently reflect a component of variation in addition to that imparted by the olivine-liquid fractionation. The M1v and M4v-l samples are well above the

TABLE 1B. MAJOR AND TRACE ELEMENT COMPOSITIONS OF KOMATIITIC ROCKS FROM THE MENDON FORMATION OUTSIDE THE NORTH AUBER VILLIERS SECTION

Sample	SA 4-3	SA70-4	SA78-15	SA72-1	SA72-2	SA72-3	SA72-4	SA72-5	SA72-6	SA72-7	SA73-1	SA73-2
Lithology	coarse ol cum	coarse ol cum	coarse ol cum	ol-px B zone	ol-px B zone	ol-px B zone	random pyx spin	oriented pyx spin	ol-px B zone	ol-px B zone	coarse ol cum	coarse ol cum
Unit	M1v	M1v	M1v	M2v	M2v	M2v	M2v	M2v	M2v	M2v	M2v	M2v
Tech.	icp	icp	icp	icp	icp	xrf	xrf	xrf	icp	icp	xrf	xrf
SiO_2	49.14	46.14	46.60	52.43	52.12	52.21	50.08	49.66	52.18	50.35	45.99	41.62
Al_2O_3	6.16	4.35	5.38	4.72	3.55	4.30	5.78	6.29	4.52	5.64	1.82	2.56
FeO	6.88	8.37	7.34	12.05	9.90	11.25	11.81	11.87	11.55	12.99	9.34	11.60
MgO	37.36	40.70	38.88	22.97	25.43	23.49	22.09	22.21	23.23	22.63	39.73	34.28
MnO	0.04	0.09	0.10	0.18	0.17	0.18	0.21	0.20	0.18	0.20	0.12	0.24
CaO	0.09	0.10	1.30	6.83	7.57	8.09	9.27	9.05	7.47	7.14	2.76	9.39
TiO_2	0.07	0.05	0.06	0.44	0.36	0.40	0.62	0.62	0.43	0.45	0.17	0.23
P_2O_5	0.08	0.03	0.10	0.05	0.01	0.04	0.06	0.05	0.05	0.02	0.02	0.02
Na_2O	0.20	0.21	0.24	0.33	0.88	0.00	0.00	0.00	0.39	0.59	0.00	0.00
K_2O	0.00	0.00	0.00	0.00	0.00	0.03	0.08	0.05	0.00	0.00	0.04	0.03
Ba	12	110	12	107	98	13	10	8	25	26	15	6
Co	77	71	81	75	200	149	80	84	69	69	148	116
Cr	2825	2885	2691	2363	1967	2510	2244	1951	2137	2536	1077	2532
Cu	33	0	18	67	51	53	31	89	41	131	25	12
Ni	1701	4450	1731	1611	1524	1629	376	396	1240	1407	2810	2532
Sc	22	17	18	18	20	26	34	31	17	20	10	12
Sr	3	2	8	29	35	25	22	26	23	26	62	192
V	113	64	96	156	121	149	201	199	146	160	42	53
Y	7	40	4	7	6	9	14	13	9	15	3	6
Zn	57	61	77	92	76	79	92	84	64	81	58	44
Zr	5	5	6	48	0	24	36	37	24	36	11	14

Note: Major element compositions in wt%; trace element compositions in ppm. The major elements normalized to 100% dry weight and all iron reported as FeO.

MgO-Sc trend observed in most of the other komatiitic rocks of the Mendon Formation. Incompatible element ratios (Fig. 6c) in most Mendon Formation komatiites are consistent with those found in the dominant Al-depleted lavas of the lower Onverwacht (Smith and Erlank, 1982). These are distinctly non-chondritic, with Ti/Sc 25% high and Ti/V 150% high. The komatiitic rocks of M1v and M4v-l are distinct, with Ti/Sc 75% low and Ti/V about 25% low. Though the general variation within individual sequences seems to be related to olivine-liquid fractionation, the extreme variations in incompatible element ratios between sequences must reflect source composition or process differences. These will be discussed in the next section.

In Figure 6c Al_2O_3 is plotted against TiO_2 for all Mendon Formation komatiitic rocks, including the cumulate and altered lithologies. Several units have distinctive and unusually high Al_2O_3/TiO_2 ratios. Most Barberton komatiites have an Al_2O_3/TiO_2 near 10, as do komatiitic rocks from Mendon units M2v, M3v, and the upper flows of M4v (M4v-u). The single flow unit sampled from M5 has an Al_2O_3/TiO_2 of about 35. Though there is a substantial spread in values, all the komatiitic rocks of the lower portion of M4v (M4v-l) have Al_2O_3/TiO_2 of about 50. The most extreme values are Al_2O_3/TiO_2 of 80 for the komatiitic rocks of M1v.

Chrome-spinels

Chrome-spinels are commonly the only magmatic phase preserved in the Mendon komatiites. Spinel zoning trends in most Mendon komatiites display little variation in chromium, but major variation in magnesium and iron from core to rim. The outer margins often have a discrete overgrowth of magnetite. The cores of these spinels seem to have unmodified magmatic compositions while the magnetite overgrowths are probably of low-grade metamorphic origin. Compositional zoning in the outer margins of the grains is probably magmatic but less certainly so. Table 2 contains examples of the range of spinel composition in the Mendon komatiites along with an example from an Al-undepleted komatiite of the Hooggenoeg Formation.

Barberton komatiitic spinels are unlike those found in modern abyssal basalts (MORB) but rather more like the unusual spinels found in the basalts of oceanic platforms, the boninites of island arcs, or the rare "ultramafic" lavas of some ophiolites

TABLE 1B. MAJOR AND TRACE ELEMENT COMPOSITIONS OF KOMATIITIC ROCKS FROM THE MENDON FORMATION OUTSIDE THE NORTH AUBER VILLIERS SECTION (CONTINUED, p. 2)

Sample	SA115-1	SA115-9	SA48-1	SA87-1	SA87-2	SA105-1	SA105-2	SA106-1	SA106-2	SA106-3	SA106-4
Lithology	random pyx spin	random pyx spin	coarse ol cum	coarse ol cum	coarse ol cum	coarse ol cum	coarse ol cum	coarse ol cum	coarse. ol-pyx cum	coarse. ol-pyx cum	coarse ol cum
Unit	M3v	M3v	M4v-l	M4v-l	M4v-l	M4v-l	M4v-l	M4v-l	M4v-l	M4v-l	M4v-l
Tech.	xrf	icp	icp	icp	icp	icp	icp	xrf	xrf	icp	icp
SiO_2	56.97	54.84	42.30	42.08	48.97	45.87	44.23	45.40	48.49	50.93	45.97
Al_2O_3	9.20	9.12	2.52	2.04	3.97	3.62	3.04	2.62	6.46	5.91	3.27
FeO	10.72	12.52	7.78	7.31	8.82	8.58	7.36	8.51	7.89	8.11	8.18
MgO	10.61	9.97	46.78	48.22	37.54	41.31	44.74	43.10	36.19	34.08	42.08
MnO	0.19	0.17	0.12	0.03	0.08	0.14	0.10	0.11	0.15	0.15	0.07
CaO	9.47	10.38	0.10	0.10	0.21	0.09	0.09	0.07	0.56	0.35	0.09
TiO_2	0.80	0.80	0.06	0.06	0.09	0.10	0.13	0.12	0.11	0.10	0.07
P_2O_5	0.10	0.12	0.09	0.05	0.03	0.07	0.05	0.04	0.04	0.09	0.03
Na_2O	1.85	2.08	0.25	0.16	0.32	0.24	0.27	0.00	0.03	0.29	0.25
K_2O	0.06	0.00	0.00	0.00	0.00	0.00	0.00	0.02	0.09	0.00	0.00
Ba	8	12	3	16	12	1	0	13	27	2	11
Co	86	74	105	106	65	111	89	99	88	89	117
Cr	797	745	5038	4685	4527	5401	4279	4633	3831	5010	5500
Cu	101	86	18	22	9	54	6	0	0	77	13
Ni	186	140	2087	2427	1441	2307	1738	2107	1469	1623	2296
Sc	33	31	2	13	18	13	12	13	21	21	14
Sr	85	71	0	6	3	1	0	4	5	0	2
V	188	198	62	67	66	86	69	58	74	111	82
Y	16	22	9	12	6	5	7	6	5	8	4
Zn	68	85	85	60	52	65	48	36	38	71	58
Zr	48	37	6	7	5	10	8	15	9	6	3

(Cameron and Nisbet, 1982; Dick and Bullen, 1984). Figure 7 displays the variation in Cr# and Fe# for modern volcanic rocks, after Dick and Bullen (1984), and for Mendon komatiites. The groupings for Barberton lavas are based on Al_2O_3/TiO_2 ratios discussed in other sections of the paper.

Because Cr is favored in solid phases and Al in liquids during partial melting, a first-order interpretation would be that all rocks with high Cr# spinels formed by unusually high degrees of partial melting. Dick and Bullen (1984) have reviewed both the natural variation in chrome-spinels and the experimental studies. Cr# changes dramatically with variation in degree of partial melting while Fe# changes little. Conversely, during fractional crystallization Fe# changes radically while Cr# changes only slightly. Indeed, for low-Al melts the spinel Cr# may remain nearly constant with increasing Fe# (Irvine, 1967). In more typical compositions of MORB the zoning in single spinels may be extreme and show either increases or decreases in Cr# with slight to moderate increases in Fe#.

Irvine (1967) considered Si/Al of the rock to be the most important control on the Cr# of the spinel. Sigurdsson and Schilling (1976) have demonstrated a close correlation between rock and spinel aluminium contents. Barberton Al-depleted komatiites have high rock Si/Al and Cr-rich (Al-poor) spinels, whereas Al-enriched komatiites have low Si/Al rocks and have relatively Cr-poor (Al-rich) spinels. Al-undepleted komatiites have chondritic Al and intermediate Al in the spinels.

TABLE 1B. MAJOR AND TRACE ELEMENT COMPOSITIONS OF KOMATIITIC ROCKS FROM THE MENDON FORMATION OUTSIDE THE NORTH AUBER VILLIERS SECTION (CONTINUED, p. 3)

Sample	SA107-1	SA107-5	SA107-6	SA107-7	SA107-8	SA162-6
Lithology	random pyx spin	random pyx spin	random pyx spin	random pyx spin	random pyx spin	random pyx spin
Unit	M4v-u	M4v-u	M4v-u	M4v-u	M4v-u	M4v-u
Tech.	xrf	icp	icp	icp	icp	icp
SiO_2	52.46	52.93	51.07	53.03	48.66	56.59
Al_2O_3	7.17	7.43	8.04	7.14	6.74	7.97
FeO	12.42	12.05	15.19	13.79	15.84	10.22
MgO	16.36	12.22	12.82	12.83	15.24	10.13
MnO	0.23	0.17	0.21	0.18	0.22	0.16
CaO	9.39	11.21	9.69	9.60	11.30	10.20
TiO_2	0.69	0.68	0.74	0.73	0.66	0.69
P_2O_5	0.08	0.09	0.13	0.12	0.11	0.12
Na_2O	1.11	3.22	1.97	2.41	1.23	3.92
K_2O	0.08	0.00	0.14	0.15	0.00	0.00
Ba	17	18	111	240	25	33
Co	70	71	77	66	99	70
Cr	1486	1196	1170	1143	2232	1065
Cu	92	58	106	52	74	68
Ni	289	186	197	194	636	170
Sc	34	33	36	36	34	34
Sr	25	37	49	63	19	33
V	197	196	242	234	219	214
Y	16	21	21	21	25	22
Zn	101	66	110	95	115	97
Zr	48	33	41	40	38	40

Pyroxenes

Clinopyroxene (cpx) is the most commonly preserved igneous silicate in komatiitic rocks of the Barberton Greenstone Belt. Less often orthopyroxene (opx) may be preserved in coarser grained cumulate zones of thick flows or shallow sills. Examples of pyroxene compositions from these rocks are presented in Table 3. In Barberton komatiitic rocks the clinopyroxene is typically composed of cores near Mg# 85 and outer margins zoned to about Mg# 55. Figure 8 displays the oxide variation in a typical highly zoned clinopyroxene. Minor element zoning is also consistent with changing magmatic composition and/or supercooling. The Cr_2O_3 is near 0.50 wt.% in core interiors but continuously drops to below 0.05 wt.% well before the outer margin zoning begins. All other elements examined are nearly constant within the cores but highly variable within the outer margins. The most significant minor element variations are with Al_2O_3 and TiO_2. As seen in Figure 9 these elements show as much as a four-fold enrichment within the outer margins of clinopyroxene. Extreme compositions include Al_2O_3 making as much as 13% and TiO_2 making as much as 1.5%. Apparent cpx/rock and opx/rock distribution coefficients for Al_2O_3/TiO_2 are near 0.5, similar to previously published values. Such extreme Al_2O_3 values require substantial supercooling that results in the complete suppression of plagioclase crystallization (Kinzler and Grove, 1985).

The Al_2O_3/TiO_2 within individual clinopyroxenes is nearly constant, but highly variable between komatiitic rocks from differing stratigraphic units and primary magma types. Komatiitic rocks with Al_2O_3/TiO_2 near 10, typical of most Barberton and many early Archean komatiites, have clinopyroxene with Al_2O_3/TiO_2 near 5; komatiitic rocks with Al_2O_3/TiO_2 near 25, typical of many late Archean komatiites and near the chondritic ratio, have clinopyroxene with Al_2O_3/TiO_2 near 15; and the unusual komatiitic rocks with Al_2O_3/TiO_2 greater than 50 have clinopyroxene with Al_2O_3/TiO_2 greater than 25. Orthopyroxene, which is less commonly preserved in the Barberton rocks and for which less data are available, shows the same relationships. These data, along with cpx/rock and opx/rock distribution coefficients are summarized in Table 4.

These observations are consistent with the interpretations of variations in primary komatiitic magmas based on

distinctive Al/Ti, Sc/Ti, Sc/V, and other trace element ratios in the bulk rocks and the Al/Cr ratios in coexisting spinels discussed in the previous sections. Three distinctive magma types are required for petrogenesis of Barberton komatiites. The extreme variations in Al_2O_3/TiO_2 found in these Barberton komatiites are not due to post-emplacement alteration since both oxides and silicates seem to be in equilibrium with bulk rock compositions. The compositional characteristics of these three magma types are displayed in Table 5.

PETROGENESIS

Three broad areas regarding the genesis of Mendon Formation komatiitic rocks will be discussed in this section: (1) near-surface, post-eruptive alteration; (2) shallow-level fractionation; and (3) mantle source variations and contamination.

Alteration

Arndt et al. (1989) have observed that some komatiitic rock suites lose their original chemical signatures of magmatic processes during near-surface alteration, and Herzberg (1992) dismissed Barberton komatiites with elevated Al_2O_3/TiO_2 from consideration in his models for komatiitic petrogenesis because of assumed alteration. Some Barberton komatiites have certainly been altered. However, much important information about the Earth's early mantle is lost when alteration is presumed to account for otherwise unexplained compositional variation. In this study the komatiites with unusual rock compositions have magmatic pyroxenes and spinels with correspondingly unusual yet predictable compositions. The present author concludes that the Barberton komatiitic magmas acquired their unusual compositional traits prior to crystallization of their magmatic pyroxenes and spinels and not through posteruption alteration.

TABLE 1C. MAJOR AND TRACE ELEMENT COMPOSITIONS OF SILICIFIED KOMATIITIC ROCKS FROM THE MENDON FORMATION

Sample	SA70-1	SA70-2	SA163-1	SA163-2	SA163-3	SA163-4	SA163-5	SA162-4	SA162-2
Lithology	fine ol cum	oriented ol spin	random spin	random spin	random spin	random spin	random spin	oriented spin	oriented spin
Unit	M1v	M1v	M3v	M3v	M3v	M4v-l	M4v-l	M5v	M5v
Tech	icp	icp	icp	icp	icp	icp	icp	icp	icp
SiO_2	92.29	73.07	86.73	87.93	86.96	95.06	87.47	71.85	78.11
Al_2O_3	5.47	20.10	7.93	7.23	7.97	2.91	8.14	18.81	14.46
FeO	0.66	0.70	0.93	1.29	0.95	0.64	0.86	1.37	1.32
MgO	0.14	0.68	0.62	0.43	0.62	0.15	0.64	1.17	0.74
MnO	0.01	0.01	0.01	0.01	0.01	0.01	0.01	0.01	0.01
CaO	0.09	0.10	0.09	0.09	0.09	0.10	0.09	0.09	0.08
TiO_2	0.07	0.24	0.57	0.53	0.57	0.07	0.18	0.55	0.41
P_2O_5	0.00	0.08	0.07	0.08	0.08	0.06	0.08	0.15	0.14
Na_2O	0.15	0.44	0.08	0.10	0.11	0.10	0.06	0.13	0.09
K_2O	1.12	4.57	2.97	2.32	2.65	0.88	2.47	5.86	4.63
Ba	80	197	324	78	126	50	52	74	69
Co	43	59	26	39	37	17	29	31	20
Cr	2968	5495	3227	3209	2060	2062	1297	4633	2563
Cu	24	28	21	104	80	30	30	26	18
Ni	162	347	152	277	164	185	98	125	104
Sc	7	48	31	24	27	9	39	48	32
Sr	12	28	15	7	14	0	2	8	9
V	90	277	233	205	226	55	132	292	255
Y	49	8	32	15	20	12	36	104	26
Zn	35	24	30	34	28	28	23	32	20
Zr	6	8	19	21	23	8	13	91	77

Note: Major element compositions in wt%; trace element compositions in ppm. The major elements normalized to 100% dry weight and all iron reported as FeO.

Shallow-level fractionation

Each stratigraphic subunit of the Mendon Formation has distinctive compositional and mineralogical traits: Al_2O_3/TiO_2 in rocks and pyroxenes, incompatible trace element ratios, and Cr# in spinels. Within each subunit, however, much of the major and trace element variation can be interpreted in terms of simple partial melting, leaving a mantle residue of olivine or olivine and majoritic garnet, followed by lower pressure olivine fractionation. Least squares modeling of low-pressure fractionation is not well constrained for these rocks because of the variation in SiO_2, CaO, Na_2O, and K_2O produced during pervasive late alteration. The best results indicate that fractionation of melts containing 26–16% MgO could be achieved by about 35% removal of olivine. These figures are consistent with values obtained from trace element models of vanadium, scandium, and zirconium variation as well. In spite of a fairly large sample population several small but distinct compositional gaps exist as shown in Figure 6a: at 30% MgO and 0.30% TiO_2, and at 20% MgO and 0.60% TiO_2, and the high and low MgO rocks are not interbedded but rather occur in discrete sequences. Neither of these observations is consistent with a simple, shallow-level fractionation process, which might result in complex layered flows or a sequence of flows displaying nearly continuous compositional variation between end members. Thick olivine-rich cumulates at the base of M1, M2, and M4, however, are clear evidence for this type of shallow fractionation.

Mantle source variations

A variety of mantle and deep crustal processes have been proposed to account for the compositional variations in Al_2O_3/TiO_2 among komatiites, like those exhibited by subunits of the Mendon Formation. These include crustal contamination, mantle metasomatism, pyroxene fractionation, and majoritic garnet fractionation.

Crustal contamination. Assimilation of crustal rocks with highly fractionated incompatible elements has been suggested as an explanation for some komatiitic compositions (Cattell et al., 1984; Arndt and Jenner, 1986). Because of the very high temperatures of komatiitic lavas this could take place in the lower crust or on the surface (Huppert et al., 1984). Geologic evidence, specifically the correlation of high Al_2O_3/TiO_2 komatiites with the presence of sedimentary interbeds and the presence of volumetrically large flows, suggests the possibility of some degree of crustal contamination. The relatively constant Al_2O_3/TiO_2 along strike within single flows of the Mendon Formation suggests that if contamination took place it was more likely in the subvolcanic environment. However, a number of serious objections to this model can be raised. (1) The most probable high Al_2O_3/TiO_2 lithologies available to contaminate rising komatiite magmas in the near-surface environment, granites and dacites, have Al_2O_3/TiO_2 values no greater than 40, making contamination to produce komatiites with Al_2O_3/TiO_2 over 80 impossible. (2) The very high Al/Sc and Zr/Al of dacitic rocks in the BGB also make them unlikely contaminants for komatiites of the Mendon Formation. (3) There are no significant pelitic metasedimentary rocks within the Onverwacht or surrounding pre–Fig Tree units.

Mantle metasomatism. A possible mechanism for the petrogenesis of Al-enriched komatiites is one similar to the models invoked for modern volcanic rocks with similar compositional traits. Sun and Nesbitt (1978) were early advocates of models for low-Ti basalt petrogenesis that required hydrous remelting of previously depleted mantle, a process that might occur at either intra-arc spreading centers or at incipient magmatic arcs. Metasomatic introduction of water and large-ion lithophile elements, such as light rare earth elements (LREE), Zr, and alkalis, to a depleted mantle has been suggested for the source of modern volcanic rocks with extreme variations in Al_2O_3/TiO_2, like those of the upper sections of the Troodos Complex (Taylor and Nesbitt, 1988) or the boninites of western Pacific subduction zones (Hickey and Frey, 1982). At Troodos, Al_2O_3/TiO_2 remains constant within limited groups of flows but ranges from 20 to over 65 for the entire Troodos Complex. Boninites have Al_2O_3/TiO_2 ratios as much as 130. In both instances, heavy rare earth element (HREE) enrichment and low, but highly variable Ti/Zr is observed and attributed to variable degrees of melting, at least in part due to variable metasomatism of the local mantle, with progressive melt extraction. This should result in systematic enrichment of the less incompatible elements so that chondritic normalized HREE>LREE and Sc>Ti>Zr. Variable LREE and Zr are, however, a consequence of variable degrees of metasomatism and not simply the degree of melting. At Troodos the Al_2O_3/TiO_2 does seem to change systematically with stratigraphic height, suggesting remelting of a progressively more depleted source with time. Although individual stratigraphic units in the Mendon Formation have distinctive Al_2O_3/TiO_2, there is no obvious temporal variation within this formation or the Barberton sequence as a whole.

The spinifex-textured basalts of the 2.7-Ga Negri Greenstone Belt (Sun, 1984) are unusual in a number of respects. The Al_2O_3/TiO_2 is greater that 40, Ti/Zr is well below chondritic, and HREE are slightly enriched relative to Gd. They are also distinctive in their relatively high silica contents. Sun (1984) likened their petrogenesis to that responsible for modern boninites—hydration and possibly metasomatism of previously melted mantle within subduction zones. However, Barley (1986) and Sun et al. (1989) suggest that these variations are due to crustal contamination.

Pyroxene fractionation. Although pyroxene is an important phenocryst phase in some Barberton komatiitic rocks, shallow-level pyroxene fractionation does not seem to have produced major compositional changes in these rocks. As noted above, compositional variation within flow sequences is primarily due to olivine fractionation. Pyroxenes may be important high-pressure phases as suggested by the work of Herzburg (1992). He suggests that Barberton komatiitic liquids (Al-depleted) may result from high pressure melting at a pseudoinvariant point multiply saturated with olivine, garnet, and clinopyroxene. Though

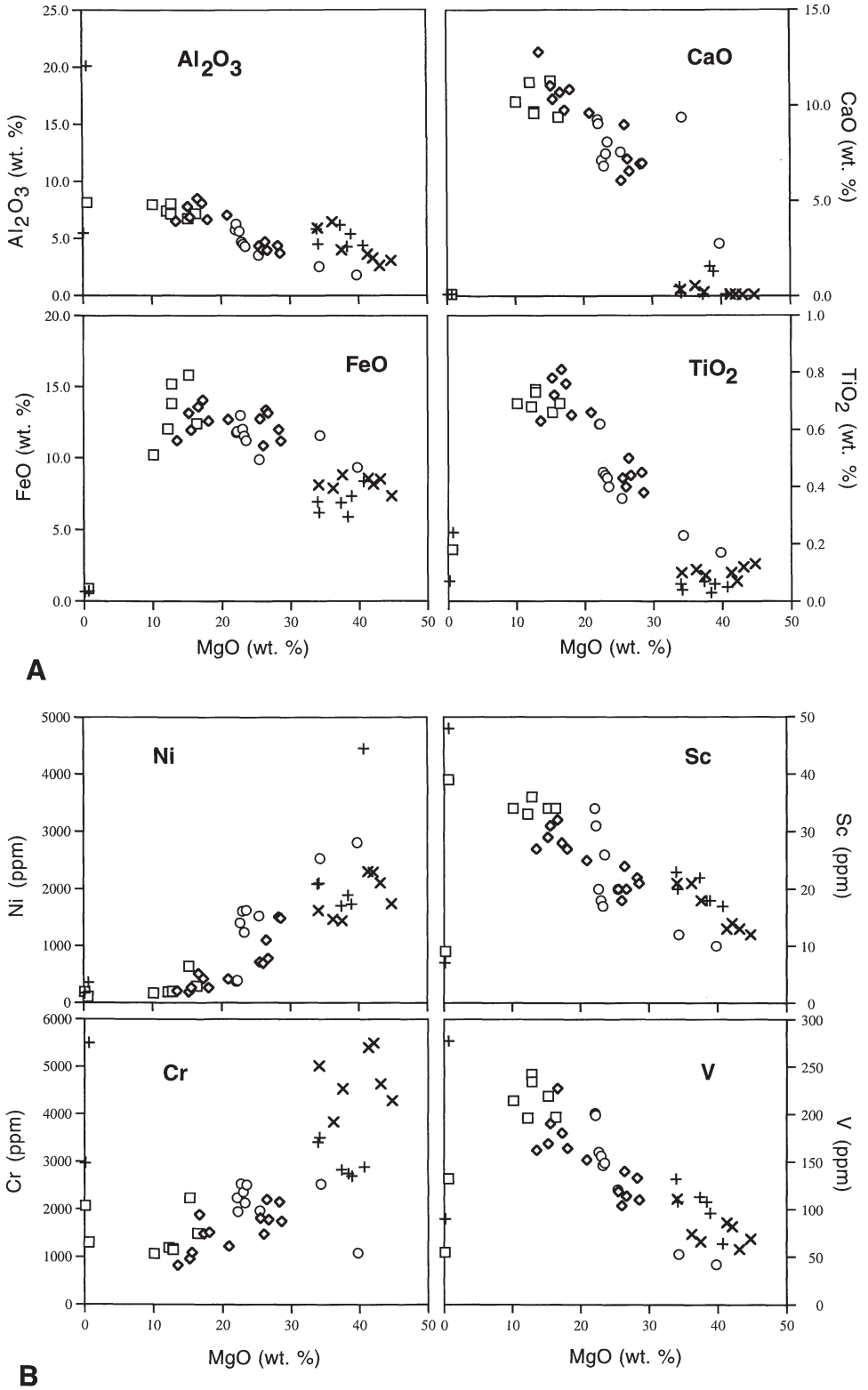
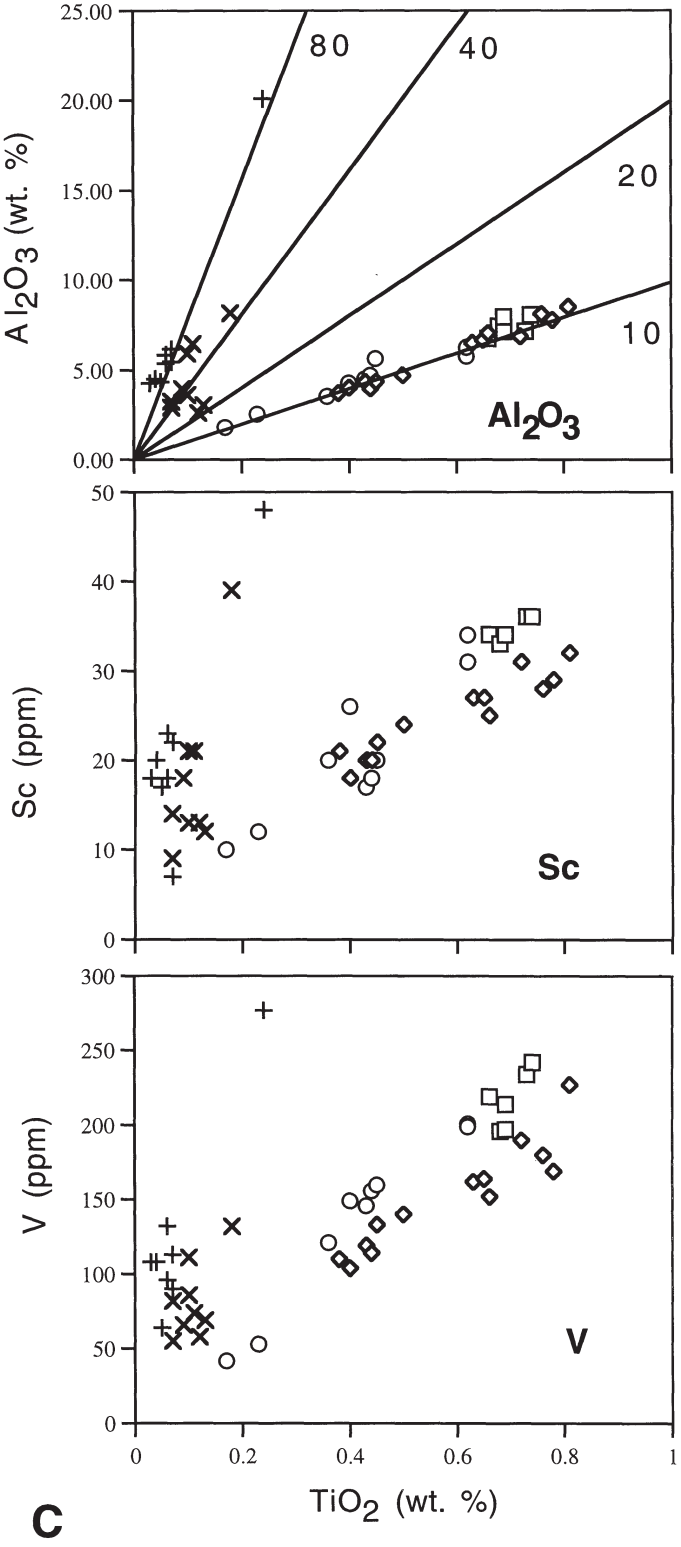


Figure 6 (this and facing page). a, Major element variation diagrams are for komatiitic rocks of the Mendon Formation. Symbols indicate stratigraphic unit: pluses are M1v; crosses are lower flows of M4v; circles are M2v, except for the northern Farm Auber Villiers section, which are represented by diamonds; and the upper flows of M4v are represented by open squares. b, Trace element variation diagrams of two compatible elements, Ni and Cr, and two incompatible elements, Sc and V, for komatiitic rocks of the Mendon Formation. Symbols as in a. c, Incompatible and immobile element ratios, Al_2O_3/TiO_2, Sc/TiO_2, and V/TiO_2, in all Mendon Formation komatiites define two distinct groups of lavas, one consistent with those found in the dominant Al-depleted lavas (Smith and Erlank, 1982) and one like the rare Al-enriched lavas (Jahn et al., 1982; Gruau et al., 1990a) of the lower part of the Onverwacht Group. Lines in upper diagram identify specific Al_2O_3/TiO_2 ratios.



some effect of pyroxene fractionation may be preserved in Barberton komatiites, it does not have the ability to affect Al_2O_3/TiO_2 as greatly as does garnet, and conversely has too great an effect on Al/Sc when it is a major fractionating phase.

Garnet fractionation. In order to characterize the complex fractionation or source variation that distinguishes individual Mendon komatiitic members, the composition of komatiites from each was normalized to 26% MgO. This was done by interpolating or extrapolating along the olivine control lines to a value of 26% MgO for each of the elements Zr, Ti, Sc, Al, and V. These elements were selected because, for individual stratigraphic units, they formed generally coherent trends with respect to MgO and with respect to each other. For comparative purposes these data are plotted normalized to chondritic abundances in Figure 10. Elements are arranged by apparent compatibility relative to the dominant Al-depleted komatiites of the Barberton Greenstone Belt.

The compositional patterns shown in Figure 10 confirm two widely held views regarding komatiite petrogenesis: (1) Al-undepleted komatiites have nearly chondritic proportions of these elements and are likely products of melting that leaves a residue of olivine, and (2) Al-depleted komatiites have highly fractionated incompatible element ratios suggestive of a residue that includes substantial majoritic garnet.

Al-enriched komatiites from M1v and M4v-l display a very unusual fractionation (Fig. 10). Sc, Al, and to a lesser extent V are enriched, whereas Ti and to a lesser degree Zr are depleted compared to either Al-undepleted or Al-depleted komatiites. This variation is generally consistent with an excess component of garnet in the source prior to partial melting. The simplest hypothesis invokes enrichment of garnet in an initially chondritic mantle source (see Xie and Kerrich, 1994; Lahaye et al., 1995). This could have taken place early in Earth history via crystallization of a global magma ocean and mineralogical stratification of the upper mantle into a lower garnet enriched layer and upper garnet depleted layer, or garnet redistribution could have occurred immediately prior to, or during, partial melting (see Gruau et al., 1990a).

The komatiites of Gorgona Island (Echeverria, 1982) have typical Al_2O_3/TiO_2 ratios of about 20, but a separate upper sequence of picritic lavas and komatiitic tuffs have Al_2O_3/TiO_2 ratios of about 50; extreme LREE depletion, about 0.5 chondritic; and moderate HREE depletion, 6 times chondritic, compared to the underlying komatiites (Echeverria and Aitken, 1986). Here there is no suggestion of LREE metasomatism, though remelting of a previously depleted mantle source is the preferred petrogenetic model (Echeverria and Aitken, 1986). Arndt et al. (1997) suggest that complex melting processes in a deep-seated and very hot mantle plume may have produced these variations.

In a recent study of komatiites from the Mendon and Weltevreden Formations, Lahaye et al. (1995) suggest a number of aspects of the petrogenesis of Barberton komatiites. Several samples they examined required as much as 20% assimilation of continental crustal material to account for anomalously high Th values. One pyroxene separate from the Mendon Formation also had an initial e_{Nd} of +0.5 consistent with contamination by older conti-

TABLE 2. COMPOSITIONS OF CHROME-SPINELS FROM KOMATIITES OF THE MENDON (M) AND HOOGGENOEG (H) FORMATIONS

Sample	SA70-2	SA224-14	SA224-19	SA163-5	SA106-1	SA106-1	SA106-2	SA106-2	SAI0-II	SAI0-II
Unit	M1	M2	M2	M3	M4	M4	M4	M4	H3	H3
Chem	T?	T2	T2	T?	T3	T3	T3	T3	T1	T1
Al_2O_3	12.71	5.35	6.73	12.03	12.67	13.19	16.05	20.13	8.81	9.34
Cr_2O_3	58.26	61.20	58.29	56.20	50.90	43.96	43.20	41.36	60.43	57.57
TiO_2	0.04	0.39	0.43	0.12	0.25	2.76	0.41	0.42	0.16	0.18
Fe_2O_3	2.70	5.80	6.70	3.67	9.04	13.76	9.63	10.33	4.99	5.28
FeO	8.70	13.59	15.65	10.59	15.96	15.30	14.92	14.09	13.62	17.05
MnO	0.15	0.24	0.32	0.12	0.22	0.20	0.22	0.22	0.22	0.26
MgO	16.65	12.06	10.96	14.60	11.74	12.40	12.67	13.58	13.00	10.71
Total	99.21	98.63	99.08	97.33	100.78	101.57	97.10	100.13	101.23	100.39
Normalized to 3 cations										
Al	0.471	0.213	0.267	0.461	0.480	0.495	0.675	0.735	0.335	0.362
Cr	1.449	1.632	1.551	1.445	1.294	1.106	1.083	1.013	1.541	1.498
Ti	0.001	0.010	0.011	0.003	0.006	0.066	0.010	0.010	0.004	0.004
Fe^{+3}	0.078	0.145	0.171	0.090	0.219	0.333	0.233	0.242	0.121	0.135
Fe^{+2}	0.215	0.387	0.441	0.289	0.431	0.407	0.395	0.367	0.369	0.467
Mn	0.004	0.007	0.009	0.003	0.006	0.005	0.006	0.006	0.006	0.007
Mg	0.781	0.606	0.550	0.708	0.563	0.588	0.599	0.627	0.625	0.526
Cr#	0.755	0.885	0.853	0.758	0.729	0.691	0.616	0.579	0.821	0.805
Fe#	0.216	0.390	0.445	0.290	0.434	0.409	0.398	0.369	0.371	0.471
$Fe^{+3}/Fe(total)$	0.267	0.273	0.279	0.238	0.337	0.451	0.370	0.397	0.246	0.224

Note: Major element compositions in wt%.

nental crust. Older units of differentiated crust have been reported within and around the Barberton Greenstone Belt (Armstrong et al., 1990; Kröner et al., 1996) and very old zircon xenocrysts are found in the overlying Fig Tree volcanic units (Byerly et al., 1996). However, the main petrogenetic process required to account for HFSE and REE variations in the dominant Al-depleted komatiites is fractionation at very high pressures of as much as 40% majoritic garnet from a chondritic source (Lahaye et al., 1995).

These observations and interpretations are consistent with those originally proposed for all three types of Barberton komatiites by Jahn et al. (1982). Gruau et al. (1990a, b) also use Sm-Nd and Lu-Hf isotopes to infer that the majoritic garnet fractionation was a part of the melting process rather than an artifact of mantle heterogeneity due to fractionation within an early terrestrial magma ocean. Ohtani et al. (1989) have now experimentally determined the distribution coefficients between majoritic garnet and melt. They also conclude that the three komatiite types can be attributed to differing depths of partial melting and prior melting history of mantle plumes. Al-undepleted komatiites are likely the products of melting shallower than 200 km, yielding a residue of olivine only. Al-depleted komatiites are likely produced by partial melting between 450 and 650 km leaving a residue of majoritic garnet in the source. Al-enriched komatiites are then generated during the ascent and further melting of the garnet-enriched portions of plumes that had earlier yielded the Al-depleted melts.

COMPARISON TO OTHER KOMATIITES

Komatiites and komatiitic basalts occur throughout the Onverwacht Group. Table 6 is a compilation of data from the literature on volcanic compositional types in the Barberton Greenstone Belt. Three distinctive compositional types of komatiitic rocks are recognized: Al-undepleted, where Al_2O_3/TiO_2 = 15–30; Al-depleted, where Al_2O_3/TiO_2 <15; and Al-enriched, where Al_2O_3/TiO_2 >30 (see Gruau et al., 1990a, for additional discussion). Basaltic rocks have not been subdivided, though Smith and Erlank (1982) have recognized a similar coherent variation in Al_2O_3/TiO_2 of basaltic rocks from the Komati Formation. Moodies Group volcanic rocks are exclusively tholeiitic in composition. Felsic volcanic rocks of the Onverwacht and Fig Tree Groups are calc-alkaline, generally dacite to rhyodacite, but calc-alkaline basalts and andesites are absent from the Barberton Greenstone Belt.

The lowest stratigraphic unit in the coherent block of the

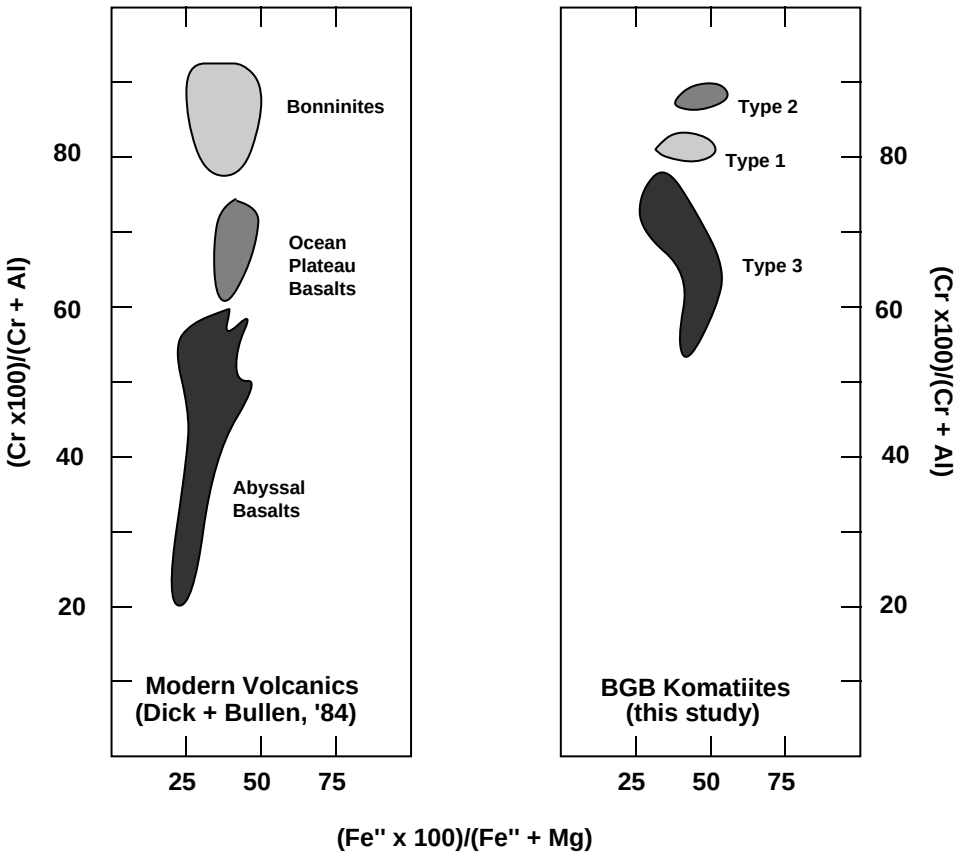


Figure 7. All Barberton komatiites contain very chrome rich spinels. They are unlike those in modern abyssal basalts (MORB) but rather more like the unusual spinels found in the basalts of oceanic platforms or the boninites of island arcs. Al-depleted komatiites (Type 2) have Al-poor spinels whereas Al-enriched komatiites (Type 3) have relatively Al-rich spinels. Al-undepleted komatiites (Type 1) have chondritic Al and intermediate Al contents in the spinels.

southern BGB is the Komati Formation, which is composed of Al-depleted and minor Al-undepleted lavas (Smith et al., 1980; Smith and Erlank, 1982). A single example of Al-enriched lava is reported (Jahn et al., 1982). Units H3 and H4 of the Hooggenoeg Formation (stratigraphic units of Lowe and Byerly, this volume, Chapter 1) are exclusively Al-undepleted komatiitic lavas (Williams and Furnell, 1979; Byerly, unpublished data). The Kromberg Formation contains minor Al-depleted and rare Al-undepleted komatiitic lavas interbedded with tholeiites throughout (Vennemann and Smith, this volume, Chapter 5; Ransom et al., this volume, Chapter 6). Stratigraphic units of uncertain stratigraphic relationships include the Theespruit Formation in the Onverwacht anticline (Viljoen, M. J., and Viljoen, 1969b; Lowe and Byerly, this volume, Chapter 1) with abundant Al-depleted komatiites and a two Al-enriched komatiitic basalts (Jahn et al., 1982); the Sandspruit Formation with abundant Al-depleted komatiites (Viljoen, M. J., and Viljoen, 1969b; Jahn et al., 1982); the Weltevreden Formation with abundant Al-undepleted komatiite and minor Al-depleted and Al-enriched komatiite (Anhaeusser, 1985; Byerly, unpublished data); the Schapenburg Schist Belt, with abundant Al-depleted komatiites and komatiitic basalts (Anhaeusser, 1983); and the Jamestown Schist Belt, with four known examples of Al-depleted komatiite (Anhaeusser, 1972).

Several of the Onverwacht formations are quite distinctive based on major element analyses cited above. Figure 11 displays the variation of Al_2O_3 and TiO_2 for komatiites and komatiitic basalts from all formations of the BGB. The Sandspruit Formation has very low Al_2O_3/TiO_2 of 8. These compositions do not overlap with any other Barberton komatiites. It is possible that in some way the higher grade of metamorphism typically found in the Sandspruit might affect the Al_2O_3/TiO_2, but Schapenburg rocks and some Theespruit rocks are metamorphosed to similar higher grade mineralogies without an apparent decrease in Al_2O_3/TiO_2. The Hooggenoeg Formation basaltic komatiites produce a distinct trend at moderately high Al_2O_3/TiO_2 of 25. Other Al-undepleted komatiites and komatiitic basalts have Al_2O_3/TiO_2 close to 16. Although individual stratigraphic units have distinctive Al_2O_3/TiO_2 values, there is no obvious temporal variation within the Barberton sequence. These distinctive compositions may ultimately be useful in correlating stratigraphic units at the member and formation level in structurally complex portions of the Barberton Greenstone Belt.

TABLE 3. MICROPROBE ANALYSES OF KOMATIITIC PYROXENES, BARBERTON GREENSTONE BELT

	Clinopyroxenes								Orthopyroxenes				
	SA107-5c	SA107-5i	SA107-5r	SA355-1c	SA355-1i	SA355-1r	SA345-8c	SA345-8r	SA256-8	SA78-4	SA345-8c	SA345-8i	SA345-8r
SiO_2	51.83	48.78	45.88	52.83	50.65	45.72	48.39	45.34	56.04	54.14	55.46	52.22	51.68
Al_2O_3	1.53	3.16	6.22	1.48	3.54	7.55	8.60	13.21	0.76	1.37	2.18	6.58	6.93
FeO	7.91	14.35	17.65	7.12	11.41	15.26	6.53	6.29	7.58	13.04	5.81	7.75	8.92
MgO	16.79	13.63	10.22	18.57	15.65	11.26	16.36	13.42	33.49	28.44	36.75	31.40	28.66
CaO	20.32	18.42	19.24	18.50	17.48	18.67	18.58	19.73	1.09	1.84	0.55	1.75	3.21
Na_2O	0.24	0.26	0.26	0.15	0.16	0.21	0.08	0.08	0.07	0.03	0.04	0.01	0.00
TiO_2	0.26	0.64	1.43	0.10	0.35	0.69	0.25	0.52	0.05	0.27	0.05	0.12	0.13
Cr_2O_3	0.50	0.05	0.00	0.48	0.02	0.02	0.01	0.02	0.50	0.43	0.25	0.11	0.09
Total	99.38	99.29	100.90	99.23	99.26	99.38	98.80	98.61	99.58	99.56	101.00	99.94	99.62
Al/Ti	5.88	4.94	4.35	14.80	10.11	10.94	34.40	25.40	15.20	5.07	43.60	54.83	53.31
Normalized to 4 cations													
Si	1.9176	1.8479	1.7411	1.9425	1.8931	1.7398	1.7816	1.6811	1.9501	1.9398	1.8713	1.8109	1.8189
Al	0.0667	0.1411	0.2782	0.0641	0.1560	0.3386	0.3732	0.5773	0.0312	0.0579	0.0867	0.2690	0.2875
Fe^{+2}	0.2017	0.3825	0.4716	0.1979	0.3321	0.4070	0.1735	0.1767	0.1921	0.3718	0.0806	0.1744	0.2299
Fe^{+3}	0.0431	0.0721	0.0886	0.0210	0.0246	0.0786	0.0275	0.0184	0.0285	0.0189	0.0833	0.0504	0.0327
Mg	0.9263	0.7699	0.5783	1.0181	0.8722	0.6389	0.8981	0.7419	1.7377	1.5194	1.8489	1.6236	1.5040
Ca	0.8056	0.7477	0.7823	0.7289	0.7001	0.7612	0.7330	0.7838	0.0406	0.0706	0.0199	0.0650	0.1211
Na	0.0172	0.0191	0.0191	0.0107	0.0116	0.0155	0.0057	0.0058	0.0047	0.0021	0.0026	0.0007	0.0000
Ti	0.0072	0.0182	0.0408	0.0028	0.0098	0.0197	0.0069	0.0145	0.0013	0.0073	0.0010	0.0031	0.0034
Cr	0.0146	0.0015	0.0000	0.0140	0.0006	0.0006	0.0003	0.0006	0.0138	0.0122	0.0067	0.0030	0.0025
Mg#	0.82	0.67	0.55	0.84	0.72	0.61	0.84	0.81	0.90	0.80	0.96	0.90	0.87
Wo	0.42	0.39	0.43	0.37	0.37	0.42	0.41	0.46	0.02	0.04	0.01	0.03	0.07
En	0.48	0.41	0.32	0.52	0.46	0.35	0.50	0.44	0.88	0.77	0.95	0.87	0.81
Fs	0.10	0.20	0.26	0.10	0.17	0.23	0.10	0.10	0.10	0.19	0.04	0.09	0.12

SIGNIFICANCE FOR GREENSTONE BELT TECTONIC SETTING

It is clear from its complex geology, prolonged history, and multiple magmatic and tectonic stages that the Barberton Greenstone Belt did not evolve within a single tectonic setting (de Ronde and de Wit, 1994; Lowe, 1994b, and this volume, Chapter 12). It represents an amalgamated geologic province that grew over at least 350 m.y. (Lowe, 1994b; Byerly et al., 1996; Kröner et al., 1996) through multiple cycles of mafic and ultramafic volcanism, such as those represented by the Komati, Mendon, and Weltevreden Formations, separated by major periods of felsic volcanism and tonalite, trondhjemite, granodiorite (TTG) plutonism, probably within subduction-related magmatic arcs.

Over the past 10–15 years, studies of komatiite petrogenesis have generally concluded that the high temperatures implied by the high degree of partial melting of the mantle represented by komatiites are most likely to have existed several hundred kilometers down within the Archean mantle and that the most likely sites for such melting and for bringing the resulting melts to the surface was within mantle plumes (Storey et al., 1991; Xie et al., 1993; Arndt, 1994; Arndt et al., 1996). The results of the present study suggest that the chemical and physical petrogenesis of komatiites in the Mendon Formation is consistent with this interpretation. Ohtani et al. (1989) have suggested that the three types of komatiites observed in studies of the BGB, Al-depleted, Al-undepleted, and Al-enriched, can all be generated by magmatic evolution at various depths within mantle plumes. Lowe et al. (this volume, Chapter 2) and Lowe (this volume, Chapter 12) have suggested that the Mendon Formation was deposited during an interval of extension of older greenstone and TTG crust. It seems likely, based on the results of the present study, that this extension may have resulted from or been associated with the formation of a mantle plume beneath the older crustal block.

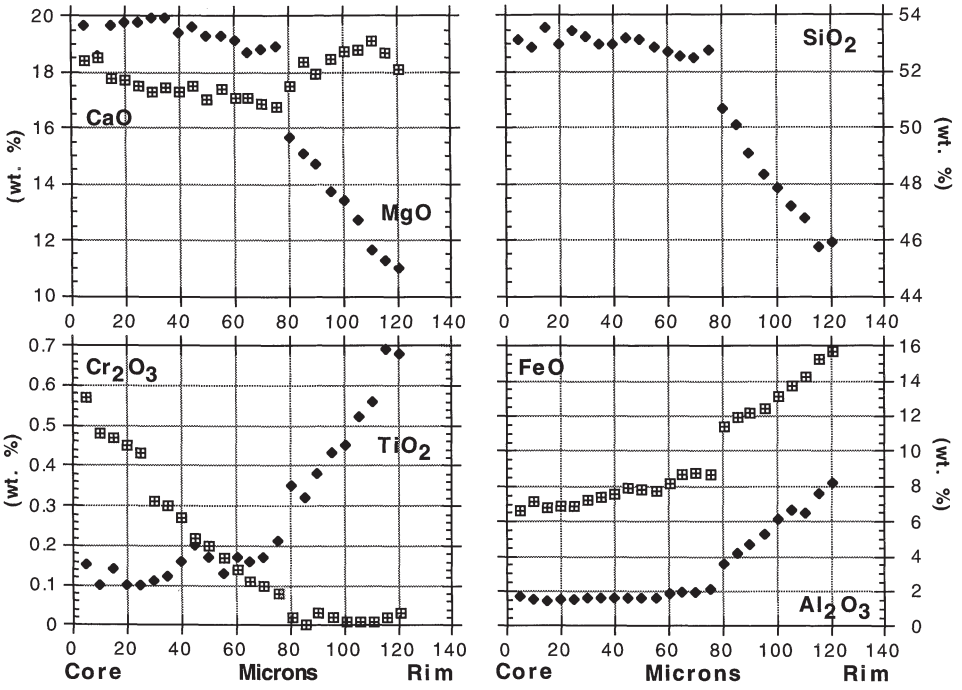


Figure 8. Compositional variation in a complexly zoned pyroxene from spinifex-textured portion of komatiitic flow (sample SA355, Weltevreden Formation). The core of the pyroxene is nearly homogeneous except for decreasing Cr_2O_3. A compositional discontinuity at 80 microns is followed by abrupt increases in FeO, Al_2O_3, and TiO_2 and decreases in SiO_2 and MgO. Such compositional zoning is typical in Barberton komatiitic pyroxenes.

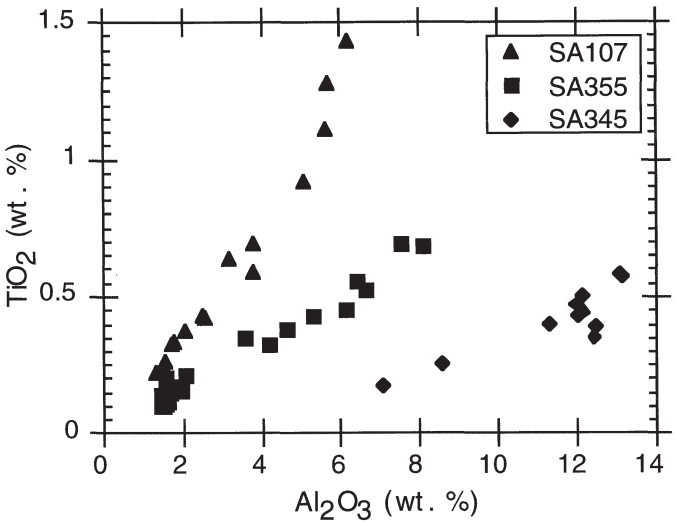


Figure 9. Though many Barberton komatiitic pyroxenes are complexly zoned to extreme compositions, they still preserve nearly constant Al_2O_3/TiO_2 ratios that are characteristic of the rock's magma type. Aluminium undepleted komatiites are represented by SA355, Al-depleted komatiites are represented by SA107, and Al-enriched komatiites are represented by SA345.

TABLE 4. AL_2O_3/TIO_2 IN KOMATIITIC ROCKS AND PYROXENES FROM THE BARBERTON GREENSTONE BELT

Sample	rock	cpx	K	opx	K
SA300-9	5.0	3.6	0.72		
SA343-1	6.0	2.4	0.40		
SA78-8	7.0	3.2	0.46		
SA107-8	10.0	6.6	0.66		
SA1-22	11.0	6.5	0.59		
SA6-4	11.0	5.9	0.54		
SA107-5	11.0	5.8	0.53		
SA78-4	12.0	3.1	0.26	3.6	0.30
SA107-3	13.0	5.7	0.44		
SA355-1	24.0	12.0	0.50		
SA212-8	27.0	18.0	0.67		
SA256-8	32.0	15.0	0.47	16.0	0.50
SA345-8	88.0	27.0	0.31	60.0	0.68
Average K			0.50		0.49

TABLE 5. THREE MAGMA TYPES FROM THE BARBERTON GREENSTONE BELT

Magma type	Rock (Al/Ti)	Cpx (Al/Ti)	Opx (Al/Ti)	Spinel (Cr/Al)	Chondritic Al_2O_3
Type 1	20-30	12-18	16	80-85	"Undepleted"
Type 2	5-15	3-6	4	85-90	"Depleted"
Type 3	40-90	27	60	50-75	"Enriched"

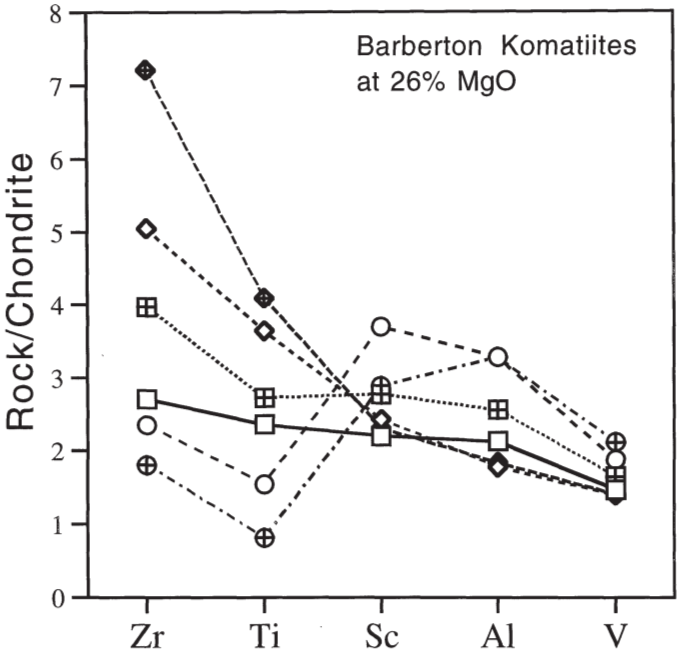


Figure 10. Compositions of six well-characterized komatiitic units in the Mendon Formation are interpolated to 26% MgO and normalized to 1.5 times the chondritic values of Anders and Ebihara (1982). Elements are arranged by apparent compatibility relative to residual garnet in the source as seen in the common Al-depleted komatiites. Petrogenesis of Barberton Al-undepleted komatiites (Komati Formation, Smith and Erlank, 1982, open squares; Weltevreden Formation, Byerly, unpublished data, filled squares); Al-depleted komatiites (Komati Formation, Smith and Erlank, 1982, open diamonds; Mendon Formation, this study, filled diamonds), and Al-enriched komatiites (Mendon Formation, M4v-l this study, open circles; M1v, filled circles) requires extreme high pressure fractionation to account for the variation seen in this group of elements. Al-undepleted komatiites have the most nearly flat pattern, reflecting a relatively simple petrogenesis from a chondritic source and only olivine in the source melt residue. Al-depleted komatiites are also highly enriched in Zr and Ti, requiring very high pressure melting with residual garnet in the source. Al-enriched komatiites are unusually enriched in Sc and Al, perhaps reflecting multistage melting of a previously depleted source that included residual garnet.

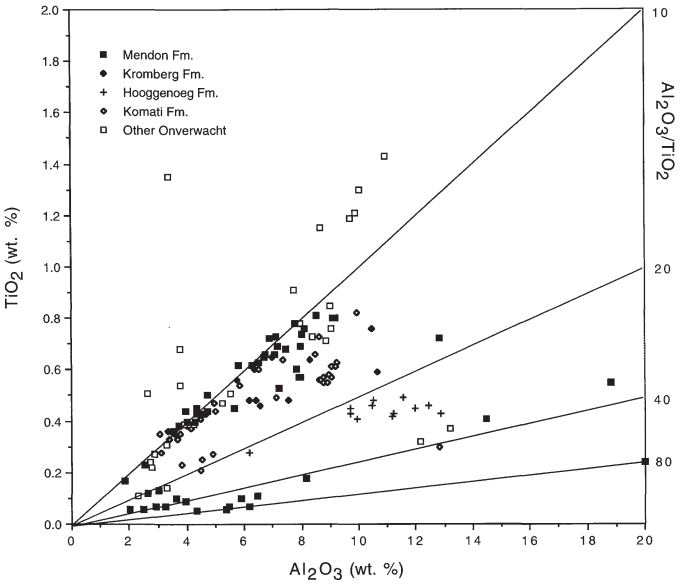


Figure 11. Komatiitic rocks from several formations of the Barberton Greenstone Belt (BGB) have very distinctive Al_2O_3/TiO_2 ratios. Most of the Mendon Formation komatiites have ratios near 10, the most common value for komatiites of the BGB. All samples with values at about 8 are from the Sandspruit Formation (Viljoen, M. J., and Viljoen, 1969b). Hooggenoeg Formation komatiites have distinctively higher values, near 25. Four Al-enriched komatiites with Al_2O_3/TiO_2 greater that 30 are from the Mendon, Komati, and Theespruit Formations. No temporal changes in Al_2O_3/TiO_2 are recognized in spite of distinctive signatures for some of the stratigraphic units.

CONCLUSIONS

A revised stratigraphy for the central part of the Barberton Greenstone Belt recognizes a new formation at the top of the Onverwacht Group, the Mendon Formation, that is composed of interbedded sedimentary rocks and komatiitic lavas (Lowe and Byerly, this volume, Chapter 1). These rocks have for many years been interpreted as lower Onverwacht units faulted into place against rocks of the upper part of the greenstone belt sequence. Indeed many faults do occur in this part of the greenstone belt, but radiometric ages have now constrained the ages of these komatiitic units to less than 3,334 ± 3 Ma, far younger than the ~3,450- to 3,500-Ma rocks of the Komati Formation.

Alteration of some of the Mendon komatiites presents a major problem to interpreting their magmatic petrogenesis. The alteration is characterized by replacement of primary minerals by fine-grained quartz and sericite, which commonly preserves original textures. SiO_2 and K_2O have been added to these rocks and FeO, MgO, CaO, and Na_2O removed. Ratios of the relatively immobile elements, including Al, Ti, Cr, V, Zr, Y, and Sc, are nearly constant within single flow units and sequences of flows, however, and probably reflect original magmatic ratios.

Much of the major and trace element variation found in the Mendon Formation komatiites can be interpreted in terms of simple partial melting, leaving a mantle residue of olivine and majoritic garnet, followed by lower pressure olivine fractionation. The maximum range of fractional crystallization is about 50% to include the komatiitic rocks with MgO as low as 10–12%. Incompatible, immobile element ratios in most Mendon Formation komatiites are consistent with those found in the Al-depleted lavas that are predominant in the Komati Formation lower in the Onverwacht Group (Smith and Erlank, 1982). These values are distinctly nonchondritic and nearly unique to early Archean greenstone belts. Al, V, and, to a lesser extent, Sc are especially depleted in these lavas as seen in their nonchondritic ratios with other incompatible elements.

Two komatiitic units within the Mendon Formation have unusual compositional variations, including very high Al_2O_3/TiO_2, that are similar to the rare Al-enriched komatiites found elsewhere in Barberton and other greenstone belts. These are likely products of multistage melting of mantle material enriched in a majoritic garnet component.

Chrome-spinels are commonly the only magmatic phase preserved in the Barberton komatiites, and all Barberton komatiites contain very chrome rich spinels. The cores of these spinels seem to have unmodified magmatic compositions whereas magnetite overgrowths are probably of low-grade metamorphism. Barberton komatiitic spinels are unlike those in modern abyssal basalts (MORB) but resemble the unusual spinels found in the basalts of oceanic platforms, the boninites of island arcs, or the rare "ultramafic" lavas of some ophiolite sequences (Cameron and Nisbet, 1982; Dick and Bullen, 1984). Barberton Al-depleted komatiites have high rock Si/Al and Cr-rich (Al-poor) spinels whereas Al-enriched komatiites have low Si/Al rocks and have relatively Cr-poor (Al-rich) spinels. Pyroxenes are less commonly preserved in Mendon komatiites, but display similar compositional relationships to the host komatiitic rocks: Al-depleted komatiitic rocks have pyroxenes with very low alumina contents, and Al-enriched komatiitic rocks have pyroxenes with very high alumina contents compared to the pyroxenes found in Al-undepleted komatiitic rocks.

Rock and mineral compositions from the Mendon Formation and correlative komatiite volcanic rocks in the Weltevreden Formation define three distinct magma types. A relatively minor magma type displays nearly chondritic elemental ratios, including Al_2O_3/TiO_2 (about 20). These are likely the products of extreme melting events that leave a residue of olivine only. However, the most common magma type is depleted in alumina and has very low Al_2O_3/TiO_2 (commonly about 10, but some may approach 5). As suggested by many others, this magma type requires significant fractionation of majoritic garnet during very high pressure melting. The complement to these Al-depleted komatiitic melts, those formed by later melting of a source enriched in majoritic garnet, is the other common magma type found in the Mendon Formation and includes Al-enriched komatiites, which may have Al_2O_3/TiO_2 ratios that approach 100.

This association of petrogenetic types is most consistent with magma generation at varying depths within a mantle plume or hot spot.

ACKNOWLEDGMENTS

This research was supported by grants NSF EAR79-19907 to Byerly and Lowe, NSF EAR90-18163 to Byerly, and NASA NAGT9-136 to Lowe and Byerly. Additional research funding came from an ARCO Foundation Junior Faculty Grant. Sabbatical leave research was conducted at, and supported by, the Department of Geochemistry, University of Cape Town, and the Department of Earth, Atmospheric, and Planetary Sciences, Massachusetts Institute of Technology. The following provided much-needed field support: University of the Witwatersrand, Anglo-American Mining, Anglo-Vaal Mining, and Dr. Gerhard van der Westhuizen. Maud Walsh reviewed an early version of the manuscript. Final reviews were made by Nicholas Arndt and Richard Williams. I thank my long-time colleague Don Lowe, who first introduced me to the geology of the Barberton Greenstone Belt, for careful review and editing of the final version of this manuscript.

REFERENCES CITED

Anders, E., and Ebihara, M., 1982, Solar-system abundances of the elements: Geochimica et Cosmochimica Acta, v. 46, p. 2363–2380.

Anhaeusser, C. R., 1972, The geology of the Jamestown Hills area of the Barberton Mountainland, South Africa: Transactions of the Geological Society of South Africa, v. 75, p. 225–263.

Anhaeusser, C. R., 1983, The geology of the Schapenburg Greenstone remnant and surrounding Archaean granitic terrane south of Badplaas, eastern Transvaal: Geological Society of South Africa Special Publication 9, p. 31–44.

Anhaeusser, C. R., 1985, Archean layered ultramafic complexes in the Barberton Mountainland, South Africa, *in* Ayres, L. D., Thurston, P. C., Card, K. D., and Weber, W., eds., Evolution of Archean supracrustal sequences: Geological Association of Canada Special Paper 28, p. 281–301.

Anhaeusser, C. R., Robb, L. J., and Viljoen, M. J., 1981, Provisional geological map of the Barberton Greenstone Belt and surrounding granitic terrane, eastern Transvaal and Swaziland: Geological Society of South Africa, scale 1:250,000.

Armstrong, R. A., Compston, W., de Wit, M. J., and Williams, I. S., 1990, The stratigraphy of the 3.5–3.2 Ga Barberton Greenstone Belt revisited: a single zircon ion microprobe study: Earth and Planetary Science Letters, v. 101, p. 90–106.

Arndt, N. T., 1986, Differentiation of komatiite flows: Journal of Petrology, v. 27, p. 279–302.

Arndt, N. T., 1994, Archean komatiites, *in* Condie, K. C., ed., Archean crustal evolution: Amsterdam, Elsevier, p. 11–44.

Arndt, N. T., and Jenner, G. A., 1986, Crustally contaminated komatiites and basalts from Kambalda, Western Australia: Chemical Geology, v. 56, p. 229–255.

Arndt, N. T., Naldrett, A. J., and Pyke, D. R., 1977, Komatiitic and iron-rich tholeiitic lavas of Munro Township, northeast Ontario: Journal of Petrology, v. 18, p. 319–369.

Arndt, N. T., Teixeira, N. A., and White, W. M., 1989, Bizarre geochemistry of komatiites from the Crixas Greenstone Belt, Brazil: Contributions to Mineralogy and Petrology, v. 101, p. 187–197.

Arndt, N. T., Kerr, A. C., and Tarney, J., 1996, Dynamic melting in plume heads: the formation of Gorgona komatiites and basalts: Earth and Planetary Science Letters, v. 146, p. 289–301.

Arndt, N. T., Albarede, F., and Nisbet, E. G., 1997, Mafic and ultramafic magmatism, *in* de Wit, M. J., and Ashwal, L. D., eds., Greenstone belts: London, Oxford University Press, p. 233–254.

Barley, M. E., 1986, Incompatible element enrichment in Archean basalts: a consequence of contamination by older sialic crust rather than mantle heterogeneity: Geology, v. 14, p. 947–950.

Byerly, G. R., and Lowe, D. R., 1985, Late-stage komatiitic and dacitic volcanism in the early Archean Barberton Greenstone Belt: Lunar and Planetary Science Conference, XVI, p. 101–102.

Byerly, G. R., Lowe, D. R., and Walsh, M. M., 1986, Stromatolites from the 3,300–3,500 Myr Swaziland Supergroup, Barberton Mountain Land, South Africa: Nature, v. 319, p. 489–491.

Byerly, G. R., Kröner, A., Lowe, D. R., Todt, W., and Walsh, M. M., 1996, Prolonged magmatism and time constraints for sediment deposition in the early Archean Barberton greenstone belt: Evidence from the upper Onverwacht and Fig Tree Groups: Precambrian Research, v. 78, p. 125–138.

Cameron, W. E., and Nisbet, E. G., 1982, Phanerozoic analogues of komatiitic basalts, *in* Arndt, N. T., and Nisbet, E. G., eds., Komatiites: London, Allen and Unwin, p. 347–397.

Cattell, A., Krogh, T. E., and Arndt, N. T., 1984, Conflicting Sm-Nd and U-Pb zircon ages for Archean lavas from Newton Township, Abitibi Belt, Ontario: Earth and Planetary Science Letters, v. 70, p. 280–290.

Chauvel, C., Arndt, N. T., Gruau, G., and Hofmann, A. W., 1987, Composition of the Archean mantle: evidence from Nd isotopes: TERRA Cognita,

v. 7, p. 272.
de Ronde, C. E. J., and de Wit, M. J., 1994, Tectonic history of the Barberton greenstone belt, South Africa: 490 million years of Archean crustal evolution: Tectonics, v. 13, p. 983–1005.
de Wit, M. J., 1982, Gliding and overthrust nappe tectonics in the Barberton Greenstone Belt: Journal of Structural Geology, v. 4, p. 117–136.
de Wit, M. J., Hart, R., Martin, A., and Abbott, P., 1982, Archean abiogenic and probable biogenic structures associated with mineralized hydrothermal vent systems and regional metasomatism, with implications for greenstone belt studies: Economic Geology, v. 77, p. 1783–1801.
de Wit, M. J., Hart, R. A., and Hart, R. J., 1987, The Jamestown Ophiolite Complex, Barberton mountain belt: A section through 3.5 Ga oceanic crust: Journal of African Earth Science, v. 9, p. 681–730.
Dick, H. J. B., and Bullen, T., 1984, Chromian spinel as a petrogenetic indicator in abyssal and alpine-type peridotites and spatially associated lavas: Contributions to Mineralogy and Petrology, v. 86, p. 54–76.
Duchac, K., and Hanor, J. S., 1987, Origin and timing of the metasomatic silicification of an Early Archean komatiite sequence, Barberton Mountain Land, South Africa: Precambrian Research, v. 37, p. 125–146.
Echeverria, L. M., 1982, Komatiites from Gorgona Island, Columbia, *in* Arndt, N. T., and Nisbet, E. G., eds., Komatiites: London, Allen and Unwin, p. 199–209.
Echeverria, L. M., and Aitken, B. G., 1986, Pyroclastic rocks: another manifestation of ultramafic volcanism on Gorgonia Island, Columbia: Contributions to Mineralogy and Petrology, v. 92, p. 428–436.
Gruau, G., Chauvel, C., Arndt, N. T., and Cornichet, J., 1990a, Al-depletion in komatiites and garnet fractionation in the early Archean mantle: Hf isotope constraints: Geochimica et Cosmochimica Acta, v. 54, p. 3095–3101.
Gruau, G., Chauvel, C., and Jahn, B. M., 1990b, Anomalous Sm-Nd ages for the Early Archean Onverwacht Group volcanics: Contributions to Mineralogy and Petrology, v. 104, p. 27–34.
Hamilton, P. J., Evenson, N. M., O'Nions, R. K., Smith, H. S., and Erlank, A. J., 1979, Sm-Nd dating of Onverwacht Group volcanics, southern Africa: Nature, v. 279, p. 298–300.
Hanor, J. S., and Duchac, K., 1990, Isovolumetric silicification of Early Archean komatiites: geochemical mass balances and constraints on origin: Journal of Geology, v. 98, p. 863–877.
Herzberg, C., 1992, Depth and degree of melting of komatiites: Journal of Geophysical Research, v. 97, p. 4521–4540.
Hickey, R. L., and Frey, F. A., 1982, Geochemical characteristics of boninite series volcanics: implications for their source: Geochimica et Cosmochimica Acta, v. 46, p. 2099–2115.
Huppert, H. E., Sparks, R. S. J., Turner, J. S., and Arndt, N. T., 1984, Emplacement and cooling of komatiite flows: Nature, v. 309, p. 19–22.
Irvine, T. N., 1967, Chromian spinel as a petrogenetic indicator: Part 2. Petrologic applications: Canadian Journal of Earth Sciences, v. 4, p. 71–103.
Jahn, B.-M., Gruau, G., and Glikson, A. Y., 1982, Komatiites of the Onverwacht Group, South Africa: REE geochemistry, Sm/Nd age and mantle evolution: Contributions to Mineralogy and Petrology, v. 80, p. 25–40.
Kamo, S. L., and Davis, D. W., 1994, Reassessment of Archean crustal development in the Barberton Mountain Land, South Africa, based on U-Pb dating: Tectonics, v. 13, p. 167–192.
Kinzler, R. J., and Grove, T. L., 1985, Crystallization and differentiation of Archean komatiite lavas from northeast Ontario: phase equilibrium and kinetic studies: American Mineralogist, v. 70, p. 40–51.
Kröner, A., Byerly, G. R., and Lowe, D. R., 1991, Chronology of early Archaean granite-greenstone evolution in the Barberton Mountain Land, South Africa, based on precise dating by single zircon evaporation: Earth and Planetary Science Letters, v. 103, p. 41–54.
Kröner, A., Hegner, E., Wendt, J. I., and Byerly, G. R., 1996, The oldest part of the Barberton granitoid-greenstone terrain, South Africa: evidence for crust formation between 3.5 and 3.7 Ga: Precambrian Research, v. 78, p. 105–124.
Lahaye, Y., Arndt, N., Byerly, G., Chauvel, C., Fourcade, S., and Gruau, G., 1995, The influence of alteration on the trace-element and Nd isotopic compositions of komatiites: Chemical Geology, v. 126, p. 43–64.
López-Martínez, M., York, D., Hall, C. M., and Hanes, J. A., 1984, Oldest reliable $^{40}Ar/^{39}Ar$ ages for terrestrial rocks: Barberton Mountain komatiites: Nature, v. 307, p. 352–354.
Lowe, D. R., 1994a, The abiological origin of described stromatolites older than 3.2 Ga: Geology, v. 22, p. 387–390.
Lowe, D. R., 1994b, Accretionary history of the Archean Barberton Greenstone Belt (3.55–3.22 Ga), southern Africa: Geology, v. 22, p. 1099–1102.
Lowe, D. R., and Byerly, G. R., 1986, Archaean flow-top alteration zones formed initially in a low-temperature sulphate-rich environment: Nature, v. 324, p. 245–248.
Lowe, D. R., and Knauth, L. P., 1977, Sedimentology of the Onverwacht Group (3.4 billion years), Transvaal, South Africa, and its bearing on the characteristics and evolution of the early Earth: Journal of Geology, v. 85, p. 699–723.
Lowe, D. R., and Knauth, P., 1978, The oldest marine carbonate ooids reinterpreted as volcanic accretionary lapilli, Onverwacht Group, South Africa: Journal of Sedimentary Petrology, v. 48, p. 709–722.
Ohtani, E., Kawabe, I., Moriyama, J., and Nagata, Y., 1989, Partitioning of elements between majorite garnet and melt and implications for petrogenesis of komatiite: Contributions to Mineralogy and Petrology, v. 103, p. 263–269.
Paris, I., Stanistreet, I. G., and Hughes, M. J., 1985, Cherts of the Barberton Greenstone Belt interpreted as products of submarine exhalative activity: Journal of Geology, v. 93, p. 111–129.
Sigurdsson, H., and Schilling, J. G., 1976, Spinels in the Mid-Atlantic Ridge basalts: chemistry and occurrence: Earth and Planetary Science Letters, v. 29, p. 7–20.
Smith, H. S., and Erlank, A. J., 1982, Geochemistry and petrogenesis of komatiites from the Barberton Greenstone Belt, South Africa, *in* Arndt, N. T., and Nisbet, E. G., eds., Komatiites: London, Allen and Unwin, p. 347–397.
Smith, H. S., Erlank, A. J., and Duncan, A. R., 1980, Geochemistry of some ultramafic komatiite lava flows from the Barberton Mountain Land, South Africa: Precambrian Research, v. 11, p. 399–415.
Smith, H. S., O'Neal, J. R., and Erlank, A. J., 1984, Oxygen isotope compositions of minerals and rocks and chemical alteration patterns in pillow lavas from Barberton, *in* Kröner, A., Hanson, G. N., and Goodwin, A. M., eds., Archean geochemistry: New York, Springer, p. 115–137.
Stanistreet, I. G., de Wit, M. J., and Fripp, R. E. P., 1981, Do graded units of accretionary spheroids in the Barberton Greenstone Belt indicate Archaean deep water environment?: Nature, v. 293, p. 280–284.
Storey, M., Mahoney, J. J., Kroenke, L. W., and Saunders, A. D., 1991, Are oceanic plateaus sites of komatiite formation?: Geology, v. 19, p. 376–379.
Sun, S.-S., 1984, Geochemical characteristics of Archean ultramafic and mafic volcanic rocks: Implications for mantle composition and evolution, *in* Kröner, A., Hanson, G. N., and Goodwin, A. M., eds., Archean geochemistry: New York, Springer, p. 25–47.
Sun, S.-S., and Nesbitt, R. W., 1978, Geochemical regularities and genetic significance of ophiolitic basalts: Geology, v. 6, p. 689–693.
Sun, S.-S., Nesbitt, R. W., and McCulloch, M. T., 1989, Geochemistry and petrogenesis of Archaean and Early Proterozoic siliceous high magnesian basalts, *in* Crawford, A. J., ed., Boninites and related rocks: London, Allen and Unwin, p. 148–173.
Taylor, R. N., and Nesbitt, R. W., 1988, Light rare-earth enrichment of supra subduction-zone mantle: evidence from the Troodos ophiolite, Cyprus: Geology, v. 16, p. 448–451.
Viljoen, M. J., and Viljoen, R. P., 1969a, Evidence for the existence of a mobile extrusive peridotitic magma from the Komati Formation of the Onverwacht Group: Geological Society of South Africa Special Publication 2, p. 87–112.
Viljoen, M. J., and Viljoen, R. P., 1969b, The geology and geochemistry of the lower ultramafic unit of the Onverwacht Group and a proposed new class of igneous rocks: Geological Society of South Africa Special Pub-

lication 2, p. 55–86.
Viljoen, R. P., and Viljoen, M. J., 1969, The geological and geochemical significance of the upper formations of the Onverwacht Group: Geological Society of South Africa Special Publication 2, p. 113–152.
Williams, D. A. C., and Furnell, R. G., 1979, Reassessment of part of the Barberton type area, South Africa: Precambrian Research, v. 9, p. 325–347.
Xie, Q., and Kerrich, R., 1994, Silicicate-perovskite and majorite signature komatiites from the Archean Abitibi greenstone belt: implications for early mantle differentiation and stratification: Journal of Geophysical Research, v. 99, p. 15799–15812.
Xie, Q., Kerrich, R., and Fan, J., 1993, HFSE/REE fractionations recorded in three komatiite-basalt sequences, Archean Abitibi greenstone belt: implications for multiple plume sources and depths: Geochimica et Cosmochimica Acta, v. 57, p. 4111–4118.
Xie, X., Byerly, G. R., and Ferrell, R., 1997, IIb trioctahedral chlorite from the Barberton Greenstone Belt: crystal structure and rock composition constraints with implications for geothermometry: Contributions to Mineralogy and Petrology, v. 126, p. 275–291.

MANUSCRIPT ACCEPTED BY THE SOCIETY MARCH 26, 1998

Printed in U.S.A.

Geological Society of America
Special Paper 329
1999

Shallow-water sedimentation of accretionary lapilli-bearing strata of the Msauli Chert: Evidence of explosive hydromagmatic komatiitic volcanism

Donald R. Lowe
Department of Geological and Environmental Sciences, Stanford University, Stanford, California 94305

ABSTRACT

The Msauli Chert is a 20- to 30-m-thick unit of silicified and metasomatically altered volcaniclastic and carbonaceous sediments interbedded with komatiitic volcanic rocks in the Mendon Formation, uppermost formation of the Onverwacht Group in the southern part of the Barberton Greenstone Belt, South Africa. It includes two principal lithofacies: I, graded beds of accretionary lapilli and ash; and II, thin beds of current-deposited volcaniclastic sandstone and black carbonaceous chert. The volcaniclastic sediments consisted mainly of blocky, vitric ash and dust formed during hydromagmatic eruptions. Distribution, mineralogy, and trace element composition indicate that the original debris was komatiitic, not felsic, in composition.

Accretionary lapilli and ash beds (AA beds) of lithofacies I commonly show well-developed normal size grading and a succession of sedimentary structures resembling the Bouma sequence in turbidites. AA beds have been interpreted to represent both deep-water turbidites and shallow-water, current-worked pyroclastic fall deposits. Because the Bouma sequence can form in response to a declining rate of sediment fallout from suspension, as might occur beneath pyroclastic clouds, as well as to decreasing flow velocity, as marks sedimentation from turbidity currents, its presence in pyroclastic units does not provide an unambiguous means of distinguishing these modes of sedimentation. However, many properties of AA beds are inconsistent with deposition from turbidity currents including (1) the distinctiveness of accretionary lapilli within individual sedimentation units, (2) the absence of debris derived by erosion of underlying layers, (3) the paucity of broken or abraded lapilli in the massive (T_a) divisions, and (4) the draping of delicate rippleforms by coarse accretionary lapilli of the massive (T_a) divisions of overlying beds. It is suggested that the current-structured AA beds were deposited by the fall of pyroclastic ash and lapilli into flowing water. Bouma sequences formed as a result of the decreasing rate of pyroclastic fall and consequent increasing role of bed-load transport during sedimentation. Other graded AA units lacking current structures formed when ash and lapilli from pyroclastic clouds fell into quiet, standing water. Intervening beds of lithofacies II were deposited under alternating current-active and quiet-water conditions, reflected by the alternation of thin beds of cross-bedded volcaniclastic sandstone and fine-grained, black, carbonaceous chert, respectively. The overall depositional setting closely resembled that of modern shelf, shallow subtidal, and intertidal environments.

Lowe, D. R., 1999, Shallow-water sedimentation of accretionary lapilli-bearing strata of the Msauli Chert: Evidence of explosive hydromagmatic komatiitic volcanism, *in* Lowe, D. R., and Byerly, G. R., eds., Geologic Evolution of the Barberton Greenstone Belt, South Africa: Boulder, Colorado, Geological Society of America Special Paper 329.

The komatiitic composition of the pyroclastic debris and the presence of similar silicified pyroclastic units above komatiitic flow sequences throughout the Onverwacht Group suggest that major komatiite eruptions commonly built the volcanic surface up into shallow-water or subaerial environments and were characteristically terminated by explosive hydromagmatic activity, probably related to vent flooding. The accretionary lapilli formed within widely dispersed eruption clouds as a result of the condensation of water that was vaporized and dispersed along with pyroclastic debris during the explosive eruptions.

INTRODUCTION

The Msauli Chert (Stanistreet et al., 1981), also termed the Umsoli Chert (Heinrichs, 1984), is a 20- to 30-m-thick unit of silicified volcaniclastic and biogenic sediments near the top of the Onverwacht Group in the southern part of the Barberton Greenstone Belt, South Africa (Figs. 1 and 2). It serves as a regional stratigraphic marker because of the presence of numerous, individually distinctive layers of volcanic dust, ash, and accretionary particles that can be correlated among structurally isolated blocks across much of the southern part of the greenstone belt (Fig. 2). Here and throughout this report, the term "volcaniclastic" is used in the sense of Fisher and Schmincke (1994) to refer to all types of particles with a volcanic composition, irrespective whether they have originated directly during volcanic eruptions or by the erosion of older volcanic rocks.

Previous workers have regarded the Msauli Chert as the basal unit of the Fig Tree Group (Reimer, 1983a; Stanistreet et al., 1981; Heinrichs, 1984). However, Lowe and Byerly (this volume, Chapter 1) demonstrate that the Msauli Chert lies within a thick, cyclic sequence of komatiitic volcanic rocks and chert, the Mendon Formation, at the top of the Onverwacht Group (Fig. 1). In the southernmost part of the belt, the Mendon Formation is represented by only the lowest volcanic-sedimentary cycle, M1, that includes a 300-m-thick komatiitic extrusive unit (M1v), the overlying Msauli Chert (M1c), and, at the top, 20–40 m of black chert overlain by sedimentary rocks of the Fig Tree Group. In more northern structural belts, the Msauli Chert is separated from the Fig Tree Group by as much as 700 m of komatiitic volcanic rocks and chert of higher cycles (Fig. 2).

Throughout its outcrop (Fig. 1), the Msauli Chert rests directly on heavily altered komatiitic flow rocks at the top of M1v. The alteration zone, which reaches as much as 50 m thick, is marked by intense silica, potash, and, locally, carbonate metasomatism and Mg and Fe depletion. It has been interpreted to have formed through the combined effects of early subaerial and/or submarine rock-water interaction and later hydrothermal alteration (Lowe et al., 1985; Lowe and Byerly, 1986; Lowe et al., this volume, Chapter 2).

Early alteration has also profoundly affected the Msauli Chert. All primary minerals except chrome-rich spinels have been completely replaced by alteration assemblages composed largely of microcrystalline silica (chert), microcrystalline phyllosilicate minerals (sericite and chlorite), ferroan dolomite, epidote, fine opaque oxide grains, rutile, and other trace minerals. Because much silicification was early, compaction effects in many detrital units are negligible and shearing and cleavage absent. Although few primary compositional elements remain, textural features as small as 0.05 mm across are commonly exquisitely preserved.

Prominent within the Msauli Chert are graded volcaniclastic beds ranging from a few centimeters to more than 1 m thick. The basal portions of these units are composed of spherical accretionary particles 0.1–1 cm in diameter that grade upward into coarse- to fine-grained volcanic ash and dust. Although the accretionary particles have been variously interpreted as altered carbonate ooliths (Visser, 1956; Reimer, 1975), volcanic accretionary lapilli (Lowe and Knauth, 1977, 1978; Heinrichs, 1984), and accretionary "spheroids" of unspecified origin (Stanistreet et al., 1981), their composition and structuring indicate unambiguously that they formed as volcanic accretionary lapilli (Lowe and Knauth, 1977, 1978; Reimer, 1983b, c; Heinrichs, 1984).

The Msauli Chert has been the focus of a sedimentological controversy that bears significantly on interpretation of the depositional setting of the entire Onverwacht Group. Lowe and Knauth (1977, 1978) suggested that the accretionary lapilli and ash (AA) beds were deposited in relatively shallow water during pyroclastic falls of lapilli, ash, and dust. Much of the debris was subsequently reworked locally by currents. Stanistreet et al. (1981) and Heinrichs (1984) described an association of current-produced sedimentary structures in AA units resembling that in the Bouma sequence and concluded that the layers were deposited by turbidity currents, possibly at water depths in excess of 1,500 m (Stanistreet et al., 1981).

Resolution of the sedimentology of the Msauli Chert is important to clarifying the depositional setting of the entire Onverwacht Group. Similar thin chert layers representing silicified volcaniclastic and biogenic sediments overlie komatiitic volcanic units throughout the group (Lowe, this volume, Chapter 3). All contain graded beds of accretionary lapilli and ash similar to those in the Msauli Chert and appear to represent a depositional style and setting that characteristically closed major komatiitic eruption cycles (Lowe, this volume, Chapter 3).

This discussion will develop more fully the thesis that the Msauli Chert was deposited by a combination of pyroclastic and nonturbiditic sedimentary processes in a low- to moderate-energy, generally shallow-water environment of deposition.

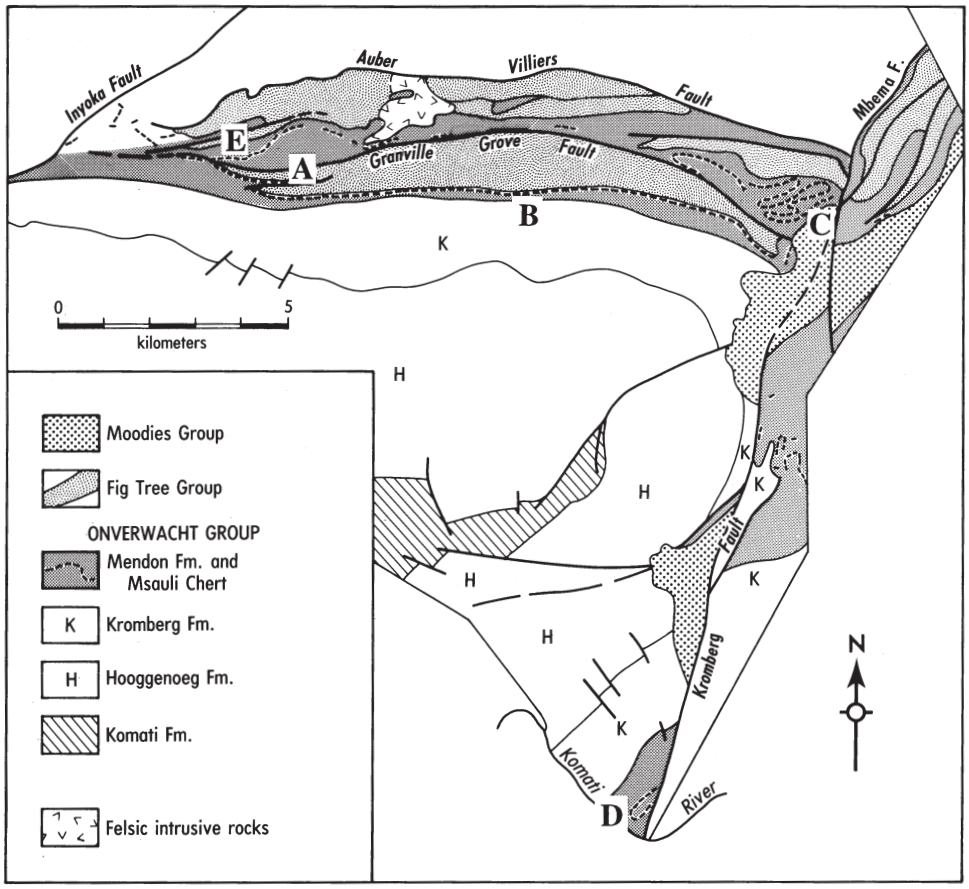


Figure 1. Outcrop map of the Msauli Chert. Sections of the Msauli Chert discussed in text include: A, the type section, SAF-127; B, SAF-191; C, SAF-114 in the hinge of the Onverwacht anticline; D, SAF-138 immediately north of the Komati River near the hinge of the Kromberg syncline; and E, between the Granville Grove and Auber Villiers faults.

STRATIGRAPHY AND LITHOFACIES

The type section of the Msauli Chert is located along the Msauli River (Figs. 1 and 3) on Farm Granville Grove 720JT (Stanistreet et al., 1981). The unit is well exposed and accessible at this locality, but many small-scale primary textural features that are well preserved in other areas have been obliterated here because the section is close to a large felsic intrusive body. Regionally, the Msauli Chert ranges from 20 to slightly over 30 m thick (Fig. 4). It rests with a sharp, low-relief depositional contact on silicified and carbonated komatiitic volcanic rocks at the top of M1v.

In most sections, the basal strata of the Msauli Chert consist of fine- to medium-grained current-worked volcaniclastic sandstone containing dispersed granules and pebbles of eroded komatiitic rock and rare detrital chrome spinels. In one outcrop, the contact is marked by a 30-cm-thick bed of cross-stratified, coarse-grained sandstone composed entirely of debris eroded from the immediately underlying volcanic rocks prior to silicification (Fig. 5). This contact appears to mark a minor regional unconformity. Rapid komatiitic volcanism during deposition of M1v probably built the depositional surface to an elevation above sea level. During post-volcanism subsidence, the surface was smoothed by weathering and erosion in subaerial and shallow-water systems. Although largely removed during later submergence, a thin cover of alluvial or energetic shallow-water sediments may have been widespread initially.

The uppermost volcaniclastic strata of the Msauli Chert are overlain by 2 to 20 m of black chert and banded black-and-white chert. A thin basal zone of sandstone, conglomerate, and breccia, generally less than 1 m thick, commonly marks the contact, and the uppermost 50 cm to 1 m of the Msauli Chert locally show in situ brecciation (Fig. 6). Fractures extend from the top of the volcaniclastic sequence downward into the chert and are filled with carbonaceous grains and debris from the overlying conglomeratic unit. This contact represents an abrupt change in sedimentation style and may mark an unconformity. However, there no evidence for significant erosion of the top of the Msauli Chert, and the same sequence of thin graded accretionary lapilli beds is present in the upper 3 to 6 m of the Msauli Chert in most sections (Fig. 7).

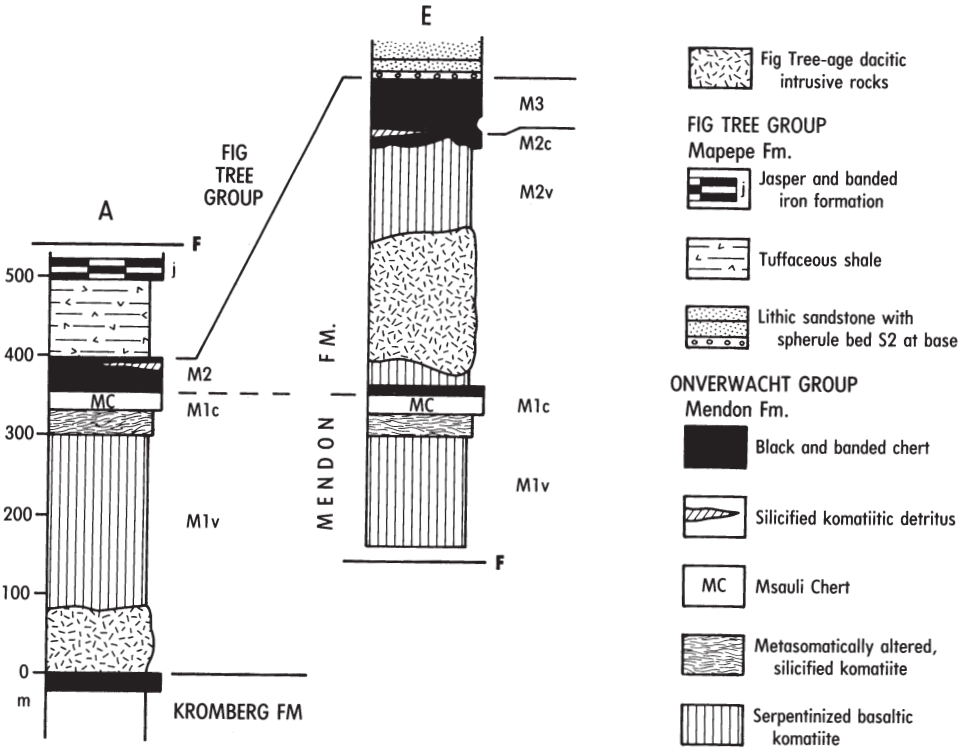


Figure 2. Stratigraphy of the upper part of the Onverwacht and lower Fig Tree Groups in the southern part of the Barberton Greenstone Belt showing the stratigraphic setting of the Msauli Chert. A, a generalized stratigraphic column for the northern part of the Southern Domain, west limb of the Onverwacht anticline, immediately south of the Granville Grove fault (Fig. 1). South of the Granville Grove fault, the Mendon Formation consists of a single volcanic-sedimentary cycle, M1, that includes M1v, a komatiitic volcanic unit, and M1c, the Msauli Chert, succeeded by about 50 m of black and banded chert that is probably in part the facies equivalent of higher volcanic-sedimentary cycles north of the fault. E, shows the stratigraphy of the southern part of the West-Central Domain, between the Granville Grove and Auber Villiers faults (Fig. 1). The Msauli Chert is overlain by a sequence of komatiitic volcanic rocks, M2v, that is capped by cherts representing M2c and higher cycles.

The Msauli Chert included two main types of sediment: (1) volcaniclastic ash and dust, and (2) carbonaceous matter. These comprise two principal lithofacies: lithofacies I, composed of beds, commonly normally graded, of accretionary lapilli and ash (AA beds) variously interpreted as turbidity current or pyroclastic fall deposits (Fig. 8); and lithofacies II, composed of sediments deposited between turbidity-current or fall events (Fig. 9).

AA beds (Fig. 8) consist of pale greenish, greenish gray, and light to medium gray beds of silicified accretionary lapilli and ash and range from less than 1 cm to more than 1.5 m thick. The basal portion of most beds is composed of essentially ash-free accretionary lapilli (Fig. 8A, B). The size of the lapilli varies from unit to unit, but the overall range throughout the Msauli Chert is from about 0.5 mm to about 13 mm in diameter with lapilli in most beds averaging 2–4 mm. Upward within individual sedimentation units, the lapilli are mixed with medium- to fine-grained ash that fines into fine- to very fine grained lapilli-free ash, which makes up the bulk of most units. The tops of the graded layers commonly consist of heavily silicified volcanic dust that may contain thin cross-laminated zones or isolated form-sets of hydraulically concentrated, slightly coarser, sand-sized ash (Fig. 8C). Some AA beds show mixed accretionary lapilli and ash throughout (Fig. 8D).

Most AA beds are normally size graded. Many are otherwise massive (Fig. 8B) whereas others also show a succession of sedimentary structures resembling that in the Bouma sequence (Bouma, 1962; Walker, 1965) including (1) a basal graded but otherwise structureless division of accretionary lapilli and ash (T_a), (2) an overlying division of flat-laminated ash with sparse lapilli (T_b), and (3) a division of cross-laminated and cross-stratified ash (T_c) that is commonly capped by or interbedded with divisions of finely flat laminated (T_d) or massive (T_e) volcanic dust.

Lithofacies II is interstratified with the graded AA beds of lithofacies I (Fig. 9). The basal 4–5 m of the Msauli Chert consist exclusively of lithofacies II in all sections studied (Fig. 9A), and thinner layers are present throughout the unit (Fig. 9B). The rock is composed of thin, interlaminated and intertonguing units of pale green to greenish gray, coarse- to fine-grained volcaniclastic sandstone and black carbonaceous chert. The sandstone is pre-

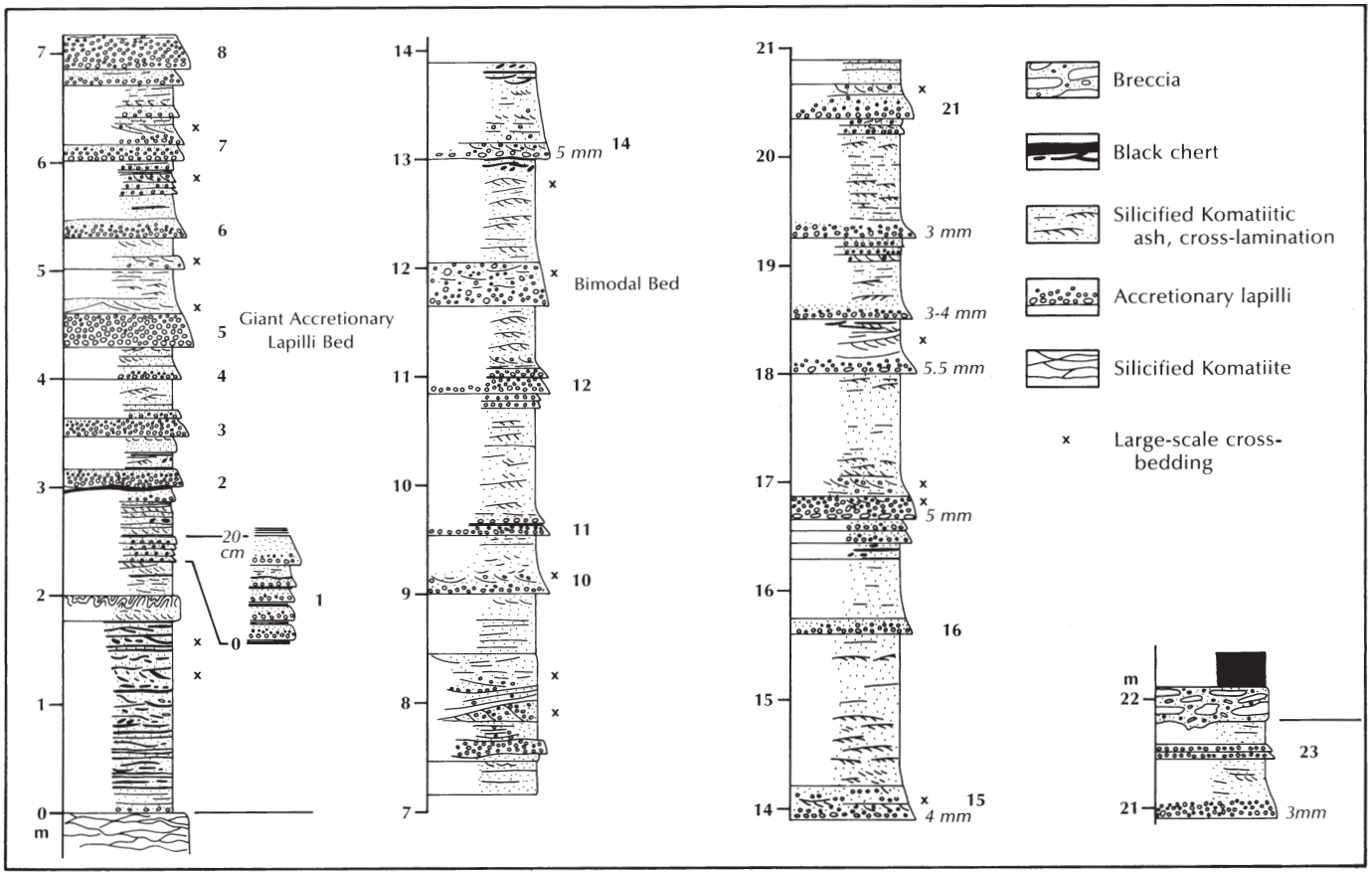


Figure 3. Detailed stratigraphy of the type section of the Msauli Chert (locality A in Fig. 1) along the Msauli River. The principal accretionary lapilli and ash units are numbered, 1 through 23.

dominantly medium-grained and occurs in cross-stratified and cross-laminated beds and lenses as much as 30 cm thick but averaging less than 15 cm. Black chert occurs as more-or-less continuous layers as much as 3 cm thick within the cross-bedded volcaniclastic sandstone, as lenticular units, as fine laminations, drapes, and flazers between and within cross-sets, and as ripped-up intraclasts within the volcaniclastic sandstone. It was deposited as nearly pure biogenic matter, mainly as loose, fluffy detrital grains that were hydraulically equivalent to very fine-grained volcaniclastic sand and silt but locally as flat bacterial mats during quiet-water intervals separating periods of current activity. Carbonaceous rocks that were probably collected from outcrops of the Msauli Chert have yielded a variety of microspheres interpreted as early prokaryotic cells (Muir and Hall, 1974; Knoll and Barghoorn, 1977).

PETROGRAPHY AND PETROLOGY

Ash and dust

More than 80% of the primary sediment in the Msauli Chert was sand- and silt-sized pyroclastic ash and dust and accretionary lapilli constructed of ash and dust. With the exception of the southeasternmost sections near SAF-138 (Figs. 2 and 4), most ash was fine- to medium-grained in size and the largest non-accretionary volcaniclastic grains were everywhere less than 2 mm in diameter. In SAF-138, several layers of coarse- to very coarse-grained and granule-sized, cross-stratified ash are present.

Ash grains, both within and outside of the accretionary lapilli, were remarkably consistent in character. From 70 to 80% of the sand-sized particles were equant, blocky, angular grains (Fig. 10A). Their boundaries were straight, irregular, or conchoidal fractures rather than crystal faces or bubble walls and commonly transected any vesicles present (Heinrichs, 1984). Most represent Type I pyroclasts of Wohletz (1983). Another 15–25% of the grains were cuspate shards (terminology of Fisher and Schmincke, 1984, p. 96) with smoothly curving surfaces and rather thick bubble walls (Fig. 10B). Original grain boundaries are defined by faint brownish "dust" rims around the outer edges of the grains, by axiolitic structure within the grains (Heinrichs, 1984), and by contrasts in the contents of opaque and phyllosilicate minerals between the grains and surrounding pore-filling materials (Fig. 10).

In thin section, the originally glassy grains are now composed largely of microquartz containing less than 15% sericite. Epidote, chlorite, and carbonate are common but irregularly dis-

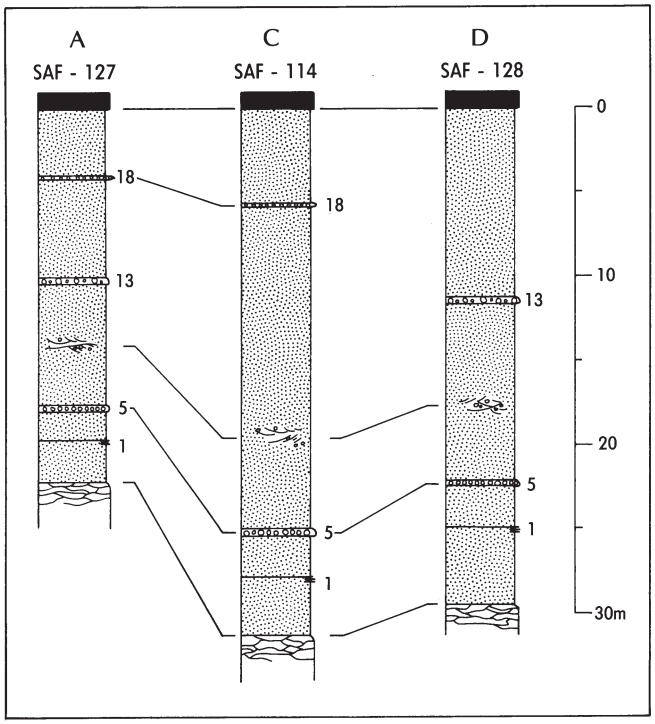


Figure 4. Generalized stratigraphy and correlation of the Msauli Chert around the Onverwacht anticline. Location of sections shown in Figure 1. Numbered sedimentation units refer to main accretionary lapilli and ash units identified in the type section (Fig. 3).

tributed constituents and clearly formed following silicification since all tend to destroy fine structures that are well preserved in silicified materials. The textural and mineralogical uniformity of the sand-sized detritus suggests that it represented a single, texturally and probably compositionally homogeneous population of vitric particles (Heinrichs, 1984).

Layers representing pyroclastic dust consist of a fine-grained micromosaic of chert (generally greater than 85%) and sericite. Original grains are not resolvable, but the absence of cross-lamination, the predominance of fine, flat lamination, and the common occurrence of this material at the tops of graded AA beds suggest that the original sediment was volcanic dust.

Accretionary lapilli

The most distinctive particles in the Msauli Chert are altered and silicified accretionary lapilli. Their properties have been discussed by Reimer (1975, 1983a, c), Lowe and Knauth (1977, 1978), Heinrichs (1980, 1984), and Stanistreet et al. (1981). Two main types can be recognized: (a) large, light colored, generally poorly structured lapilli composed almost entirely of recrystallized and altered fine-grained volcanic dust (Fig. 11); and (b) smaller, generally darker colored lapilli that are highly varied in composition. Some are fine grained throughout (Fig. 11) but many are coarse grained (Fig. 12) and others include coarse-grained interiors and fine-grained outer rims (Fig. 11). The last have been termed coated accretionary lapilli by Reimer (1983c). Both "rim-type" lapilli, characterized by a fine-grained rim and coarser interior, and "core-type" lapilli, lacking a fine-grained rim (Schumacher and Schmincke, 1991) are present (Figs. 11 and 12).

The largest accretionary lapilli are composed of very fine-grained ash and dust, range from about 5 to 13 mm in diameter, and are commonly light gray in color (Fig. 11). Many are highly spherical but others are slightly flattened. Internally, most large accretionary lapilli are massive or only crudely layered, but some show internal or outer zones containing slighter coarser grains (Fig. 11). They make up a distinctive, 10- to 30-cm-thick graded unit of "giant lapilli" about 8 m above the base of the Msauli Chert (Fig. 3, bed 5), form a conspicuously coarser modal size of lapilli in the bimodal bed (Fig. 3, unit 13; Figs. 8A and 11), and mark the bases of three widespread units near the top of the Msauli Chert (Fig. 3, units 14, 17, and 18).

Smaller accretionary lapilli range from less than 0.1 mm to about 5 mm in diameter (Figs. 11, 12, and 13). Most are highly spherical, although elongate forms are common and compound and irregular grains occur. They vary widely in internal texture, even within single sedimentation units. Some were composed exclusively of fine-grained dust, either completely massive or showing weak concentric layering defined by zones of finer grained ash and dust (Fig. 11). Others are composed of coarser ash, including blocky vitric grains (Fig. 10A) and shards (Fig. 10B), that can exceed the lapilli radii in size. The lapilli can be massive (Fig. 11) or show well-developed concentric alignment of elongate grains or textural layering defined by concentric variations in the grain size of the ash. Less than half of the lapilli possess a fine-grained outer rim (Fig. 11), as described from Phanerozoic accretionary lapilli by Moore and Peck (1962) and termed rim-type lapilli by Schumacher and Schmincke (1991). Less than 10% of the lapilli contain distinct nuclei, although more than 30% of the lapilli in the bimodal bed contain nuclei (Figs. 11 and 13).

Lithic grains

A small proportion of the noncarbonaceous particles in the Msauli Chert are not obviously of volcanic origin. Discrimination between vitric volcaniclastic and lithic grains can be difficult or impossible in such heavily altered rocks (Heinrichs, 1984). However, some beds in the Msauli Chert contain angular particles and that appear to represent lithic debris (Fig. 13). Lithic grains occur both as loose particles and as nuclei to accretionary lapilli. Most are micromosaics of tightly intergrown sericite and microquartz in subequal proportions and are more sericite rich than associated vitric ash and dust (Fig. 13B). They lack recognizable vesicles and are not shaped like shards. Most are massive but a few show truncated lamination (Fig. 13A). All are thoroughly recrystallized and lack unaltered primary constituents. Lithic grains range to as large as about 2 mm in diameter, although, as for the vitric particles, most are less than 1 mm in diameter. The original composi-

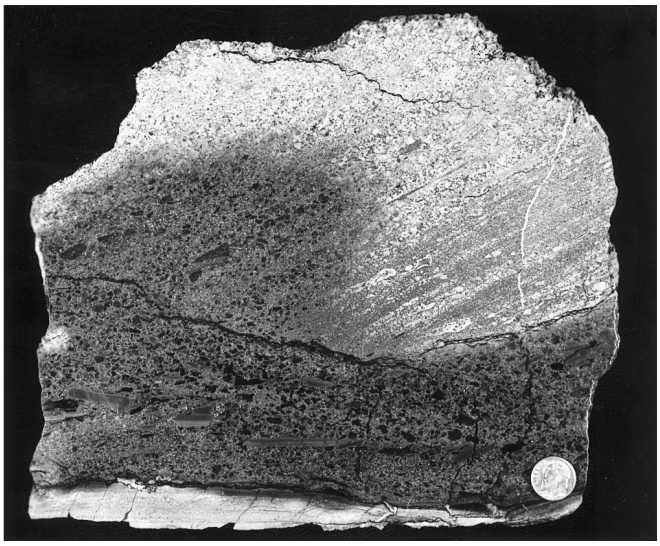


Figure 5. Cross-stratified sandstone and granule conglomerate preserved locally at the base of the Msauli Chert and composed exclusively of komatiitic debris. This locally preserved layer is probably a remnant of a more extensive alluvial and regolithic unit that was largely eroded before deposition of the Msauli Chert.

tion of these particles is unknown, although their high sericite contents suggest that they were more alumina-rich than the associated pyroclastic grains.

COMPOSITION

All volcaniclastic rocks in the Msauli Chert have bulk compositions dominated by silica, alumina, and potash (Lowe, this volume, Chapter 3, Tables 1 and 2). Previous investigators have concluded that silicified volcaniclastic sediments throughout the Onverwacht Group were originally dacitic to rhyolitic in composition based mainly on their light color and bulk compositions (Viljoen, M. J., and Viljoen, 1969; Viljoen, R. P., and Viljoen, 1969; Anhaeusser, 1973; Lowe and Knauth, 1977, 1978; Stanistreet et al., 1981; Heinrichs, 1984). Heinrichs (1984) additionally argued that the shapes of the pyroclasts making up the Msauli Chert most resemble those in younger silicic volcaniclastic deposits.

Based on trace element and rare earth compositions, Lowe (this volume, Chapter 3) has argued that silicified volcaniclastic sediments overlying komatiitic volcanic rocks throughout the Onverwacht Group, including accretionary lapilli and ash units in the Msauli Chert, were composed mainly of fine-grained komatiitic pyroclastic debris. Not only do these deposits lack primary quartz and feldspar phenocrysts and phenocryst pseudomorphs, which are abundant in well-documented felsic units in the Hooggenoeg Formation and Fig Tree Group (Lowe, this volume, Chapter 3; Lowe and Nocita, this volume, Chapter 10; Lowe and Fisher Worrell, this volume, Chapter 7), but they show immobile element and oxide ratios, principally of Al_2O_3, TiO_2, Zr, and Cr, that closely resemble those in associated komatiitic flow units but are unlike those of felsic volcanic rocks (Lowe, this volume, Chapter 3, Figs. 7 and 8).



Figure 6. Breccia developed by in situ brittle fracture of the uppermost volcaniclastic layers of the Msauli Chert (light) overlain by detrital unit (dark) composed of black chert clasts, accretionary lapilli, and volcaniclastic particles. Fractures in the Msauli Chert are filled by loose detrital material that has fallen into the fractures from above and by cavity-fill quartz (white).

SEDIMENTOLOGY OF ACCRETIONARY LAPILLI AND ASH LAYERS

Previous studies of the Msauli Chert (Lowe and Knauth, 1977, 1978; Stanistreet et al., 1981; Heinrichs, 1984) have focused on the sedimentology of the layers of graded accretionary lapilli and ash. The contrasting interpretations of these layers as current-worked pyroclastic fall deposits (Lowe and Knauth, 1977, 1978) and turbidites (Stanistreet et al., 1981; Heinrichs, 1984) have led to the conflicting interpretations of deposition in shallow and deep water, respectively. A clear understanding of Onverwacht sedimentology in general and of the environment of deposition of the Msauli Chert in particular depend on resolving the origin of these units.

Interpretation of the graded beds of accretionary lapilli and ash as turbidites rests largely on the common presence of a suc-

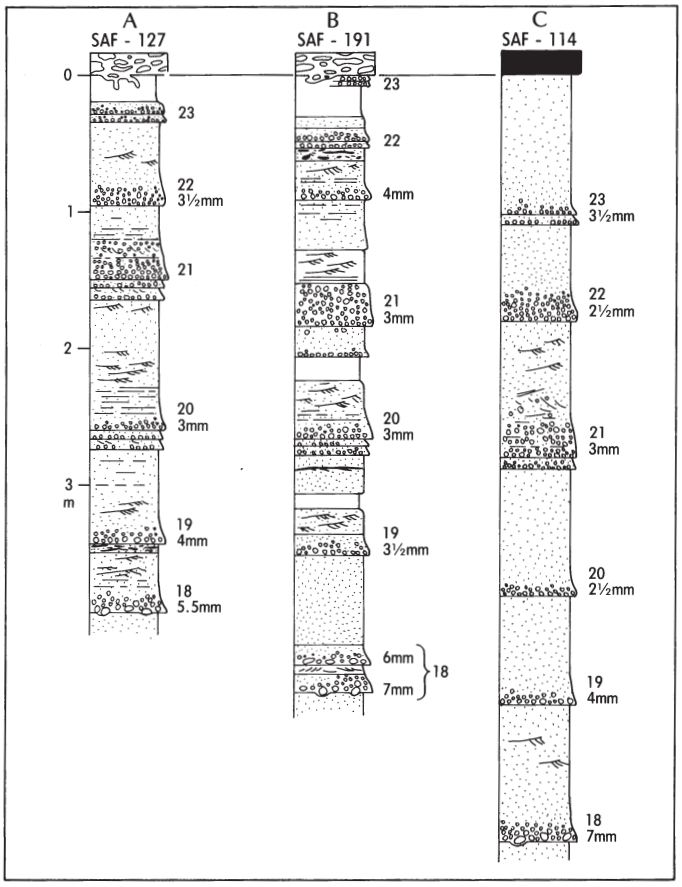


Figure 7. Correlation of accretionary lapilli units in the upper part of the Msauli Chert (see Fig. 1 for locations of sections). Each "unit" commonly includes a number of graded layers as well as zones showing current structures. The accretionary lapilli in all layers of each numbered unit are commonly petrographically and texturally distinctive from those in underlying and overlying units. The presence of the same distinctive pair of accretionary lapilli layers, comprising unit 23, in all sections indicates that little or no erosion preceded deposition of the overlying detrital layers.

cession of structural divisions resembling those of the Bouma sequence in turbidites (Bouma, 1962). The succession of bedforms developed on sand beds in response to changing flow conditions (Harms and Fahnestock, 1965; Simons et al., 1965) and the related Bouma sequence of sedimentary structures in turbidites (Walker, 1965) form largely in response to the changing structure of near-bed flow that is, in turn, controlled largely by the concentration of sediment within the bed-load layer (Simons et al., 1965; Allen and Leeder, 1980). In most terrestrial and shallow-water sedimentary environments, bed-load sediment is derived by erosion of the beds over which fluids are moving. In some flows, such as turbidity currents, however, bed-load sediment is derived largely by fallout from the suspended load, and bed-load sediment concentration is controlled largely by the suspended sediment fallout rate (Lowe, 1988). Because the bed-load layer responds to the overall rate of sediment fallout from suspension but not specifically to suspension mechanics (Lowe, 1988), the same sequence of bedforms and structures can develop in response to sediment fallout from airborne pyroclastic clouds that forms due to fallout from immediately overlying water-borne suspensions. Hence, the presence of Bouma sequences in volcaniclastic deposits is consistent with deposition from both waning pyroclastic falls into flowing water and decelerating turbidity currents and does not provide a unique solution to the origin of the AA units in the Msauli Chert.

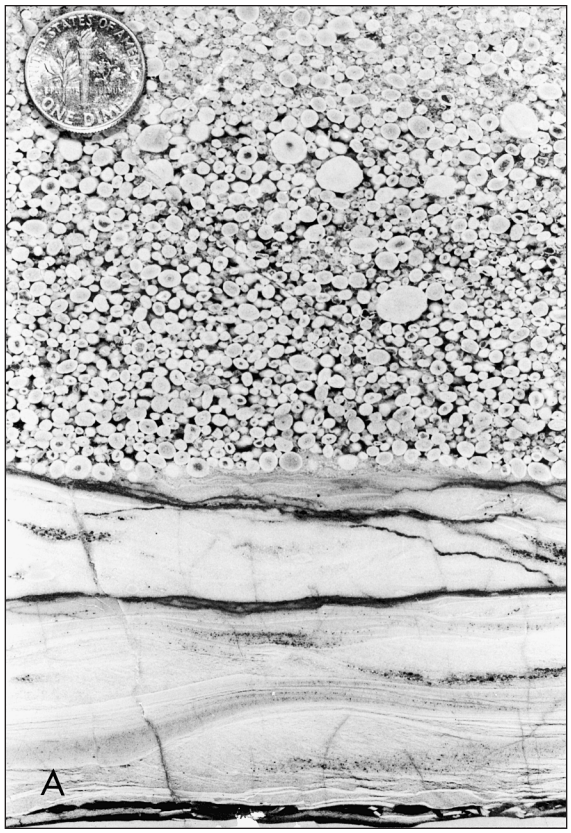
The textures and structuring of the AA beds indicate, however, that they were deposited by the fall of pyroclastic debris, not by turbidity currents.

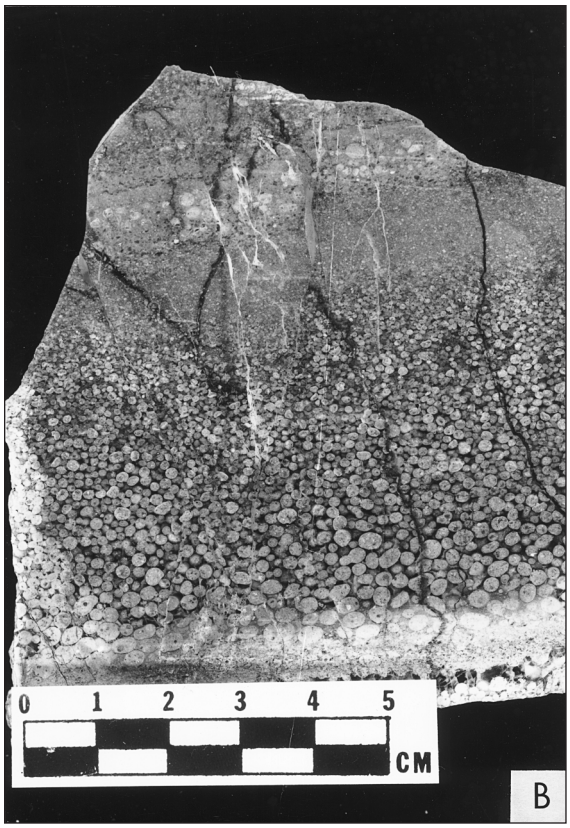
Compositional distinctiveness of individual lapilli-ash beds

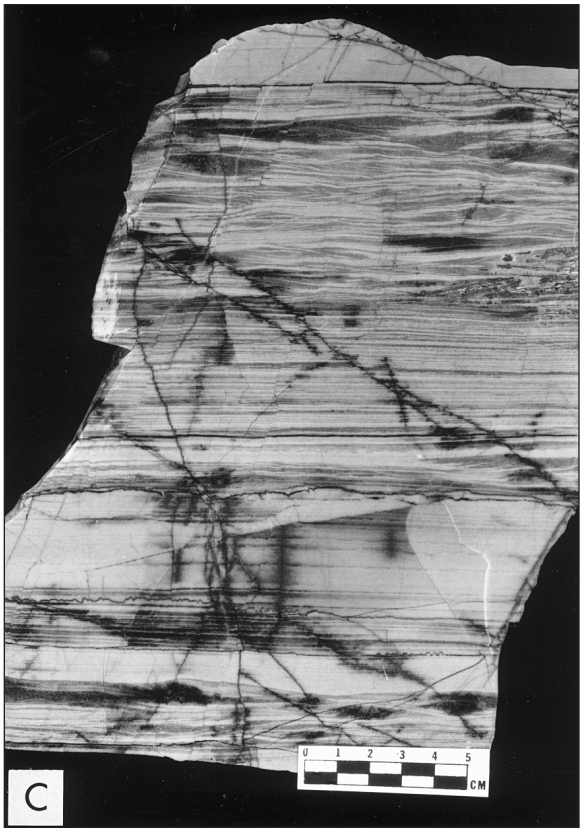
Turbidites and debris-flow deposits formed by the redeposition of loose debris on the sides of volcanic slopes are common in Phanerozoic volcanic sequences as well as in Archean greenstone belts, including the Hooggenoeg Formation of the Onverwacht Group (Lowe and Knauth, 1977). Such units are typically coarse-grained, poorly sorted, heterogeneous mixtures representing the spectrum of volcanic rocks and volcaniclastic debris making up the vent cones. They commonly include abundant pyroclasts, lithic debris eroded from older flow and fragmental units, and reworked epiclastic grains derived from alluvial, shallow-water, and submarine deposits over which the flows pass. The processes of slope failure, erosion, and downslope flowage tend to promote mixing and homogenization of the entire spectrum of materials available within the source and drainage areas.

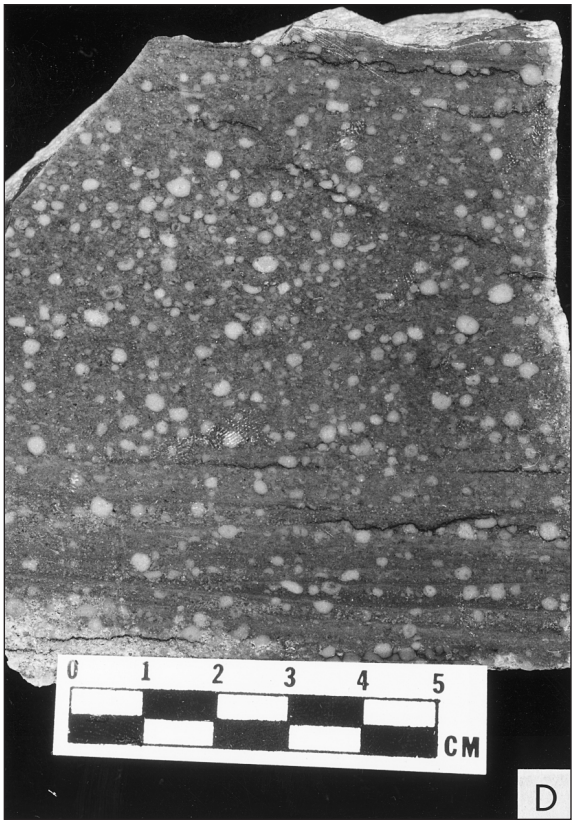
Graded lapilli-ash beds in the Msauli Chert were composed of fresh, juvenile pyroclastic particles, a small proportion of lithic grains, and accretionary lapilli constructed from these same materials. Although containing a restricted population of grain types, individual beds or groups of beds are distinctive, both texturally and compositionally, and can be recognized and correlated throughout the outcrop of the Msauli Chert (Figs. 8 and 14). Most distinctive are the composition and structuring of the accretionary

Figure 8. Lithofacies 1, accretionary lapilli and ash (AA) beds. A, Basal part of the bimodal bed (Fig. 3, unit 13) composed of small, commonly nucleated accretionary lapilli mixed with sparse, large, fine-grained lapilli. The lowest 10 cm consist of ash-free accretionary lapilli cemented by translucent chert after chalcedony. The overlying material is a mixture of accretionary lapilli and ash. Sediments below the bimodal bed represent the top of the underlying event bed and consist of fine-grained ash in ripples draped by fine dust. Cross-laminations immediately below the bimodal bed contain fine, black carbonaceous particles. B, A graded but otherwise massive AA unit. The lower part of the bed is composed of ash-free accretionary lapilli cemented by translucent chert. C, Slab from the upper part of unit 15 in the type section (Fig. 3). Irregular dark patches are post-depositional manganese and iron oxide stains. The tops of the graded AA beds commonly consist of layers of very fine-grained, flat-laminated and cross-laminated ash and dust like that shown here. D, Unit of accretionary lapilli and ash showing accretionary lapilli mixed with fine- to medium-grained ash. Faint flat laminations in the lower part of the slab and the abundance of broken lapilli suggest that the sediment was deposited by currents.


A


0 1 2 3 4 5
CM
B


C


0 1 2 3 4 5
CM
D

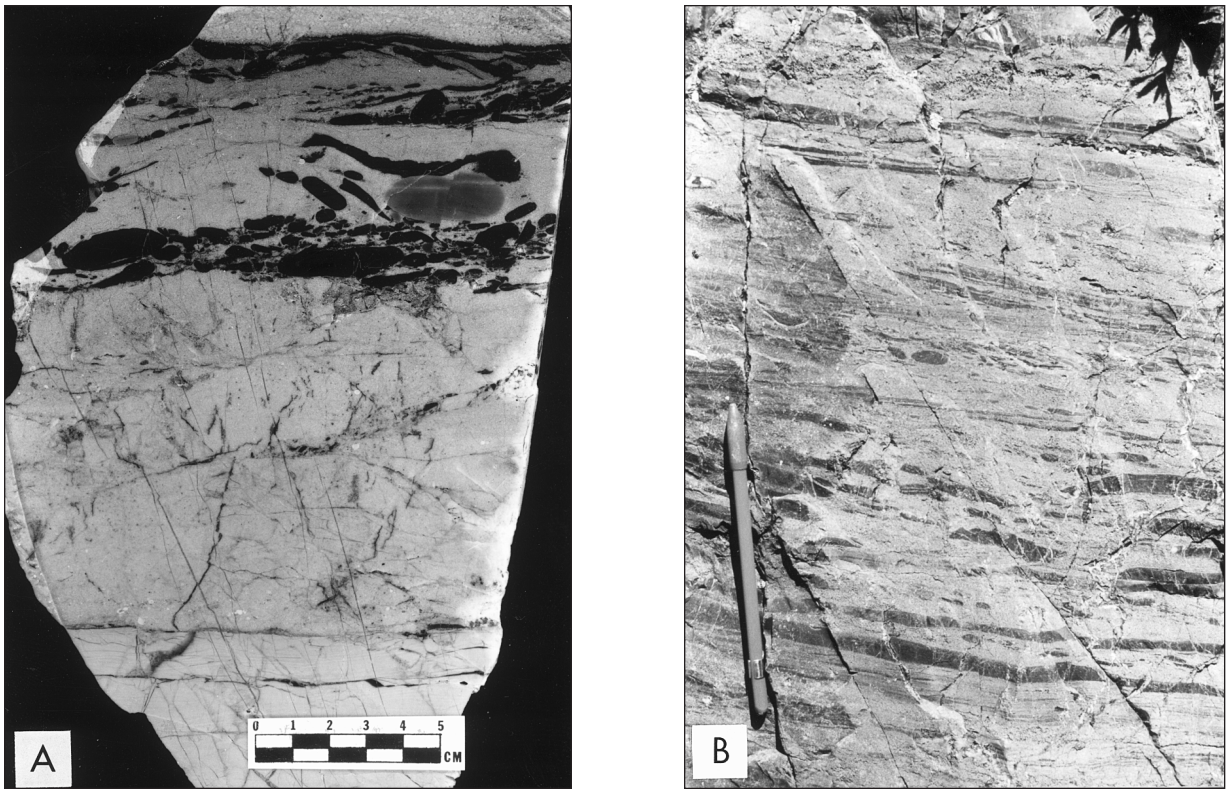


Figure 9. Lithofacies II. A, Current-deposited ash containing lenses and rip-up clasts of black carbonaceous chert from lowest 2 m of the Msauli Chert. B, Interevent unit composed of cross-laminated, fine- to medium-grained ash interlaminated with and containing rip-up clasts of black carbonaceous chert.

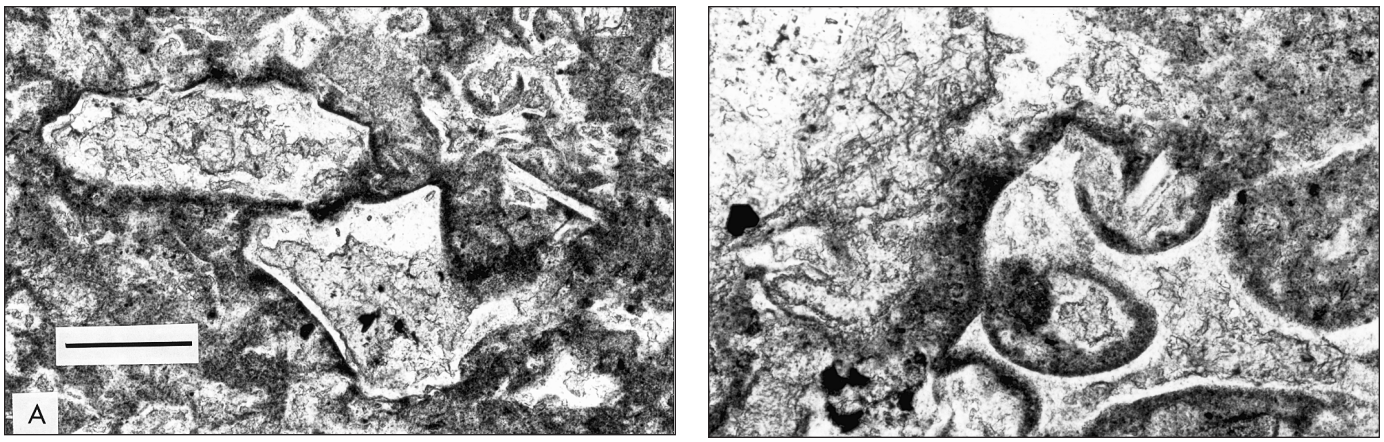


Figure 10. Pyroclasts from the Msauli Chert. A, Blocky pyroclasts lacking bubble cavities, thought to represent debris produced by thermal shock. B, Cuspate shards. Scale in both photographs is 0.2 mm.

lapilli. Unit 5 in Figure 3, for instance, is composed entirely of large accretionary lapilli, 4–10 mm in diameter, made up of extremely fine-grained volcaniclastic dust, whereas overlying and underlying accretionary lapilli layers include only small lapilli, less than 4 mm in diameter, containing abundant coarser sand-sized shards and blocky vitric grains. Although these layers are within 1 m of one another stratigraphically over the entire outcrop area of the Msauli Chert, no small, coarse-grained lapilli from bed 4 were eroded and mixed with the large, fine-grained lapilli of bed 5, and no large lapilli were reworked and mixed with smaller lapilli in immediately overlying units.

Figure 15 illustrates the makeup of accretionary lapilli

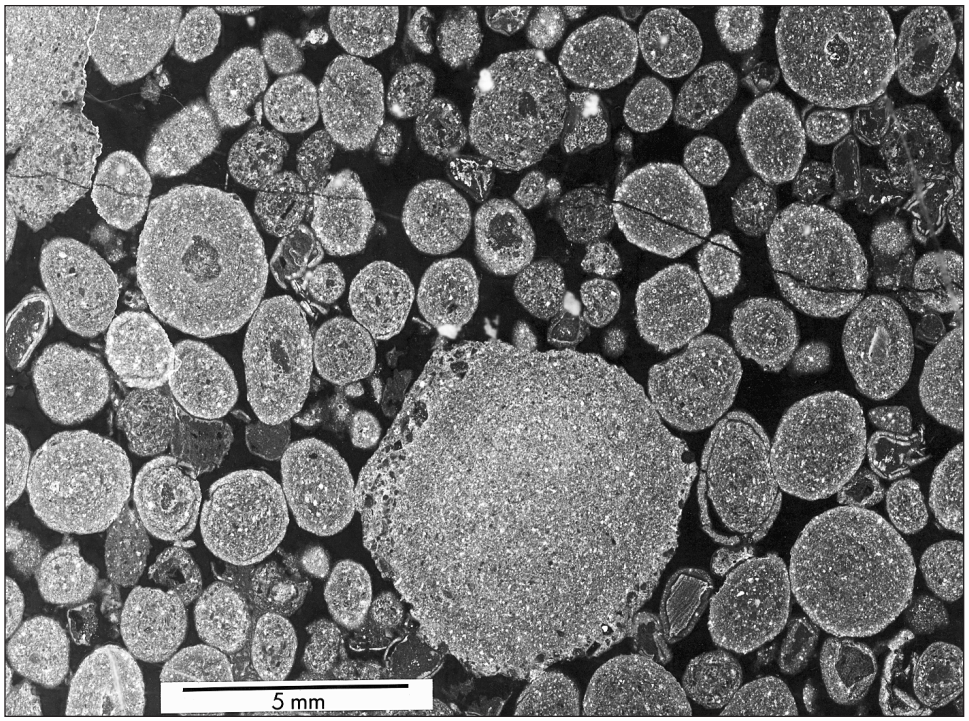


Figure 11. Negative print of a thin section from the basal, ash-free portion of the bimodal bed (unit 13, Fig. 3). The accretionary lapilli are composed largely of very fine-grained ash and dust and include both large and small lapilli types. The large lapilli are generally poorly structured, although one shows a partial outer layer of coarser material. The smaller lapilli commonly show concentric layering and finer grained outer rims, and many have nuclei.

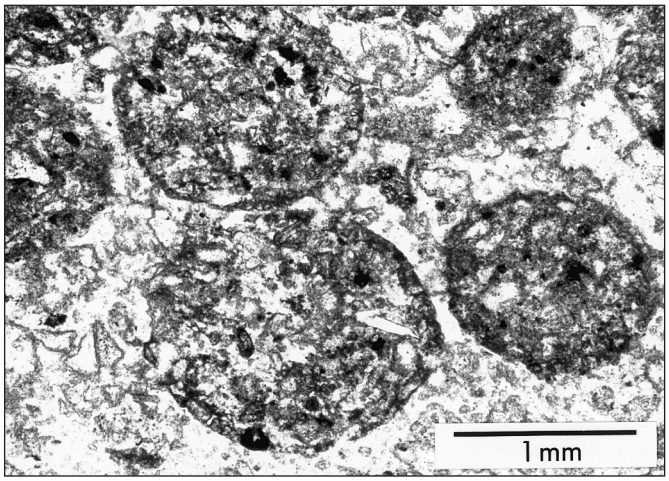


Figure 12. Structureless core-type accretionary lapilli (Schumacher and Schmincke, 1991) composed of relatively coarse volcaniclastic particles (unit 19, Fig. 3).

within the T_a divisions of individual AA units in the upper part of the Msauli Chert. Every bed or cluster of beds can be distinguished from those adjacent on the basis of accretionary lapilli structure, texture, and/or composition. These differences are not simply differences in the proportions of otherwise similar lapilli, but reflect basic differences in the structure and ash texture of accretionary lapilli in adjacent units. Nowhere is it clear that lapilli have been reworked upsection through erosion.

Such fine, regionally persistent differences among thin, closely interstratified sedimentation units are difficult to explain if the beds are turbidites originating by slope failure of debris on the sides of volcanic vents followed by transport within turbulent flows for kilometers across the sea floor. It would require not only that each triggering slope failure originated in compositionally distinctive debris but also that the ensuing debris flows and turbidity currents moved long distances without eroding older flow units. The uniqueness of accretionary lapilli within each sedimentation unit is consistent only with their deposition by fall from individual pyroclastic eruptions.

Absence of intraclasts in graded lapilli-ash beds

Mudstone intraclasts derived by erosion of channel walls or the bottom over which turbidity currents pass are common in most turbidites, especially as floating mudstone clasts within Bouma T_a divisions (Bouma, 1962). In the Msauli Chert, lithofacies II, consisting of thinly bedded volcaniclastic sandstone and silicified carbonaceous mudstone deposited between major sedimentation events, contains abundant intraclasts of carbonaceous mudstone (Fig. 9), indicating that the carbonaceous sediments were easily eroded by even weak currents. However, lithofacies I

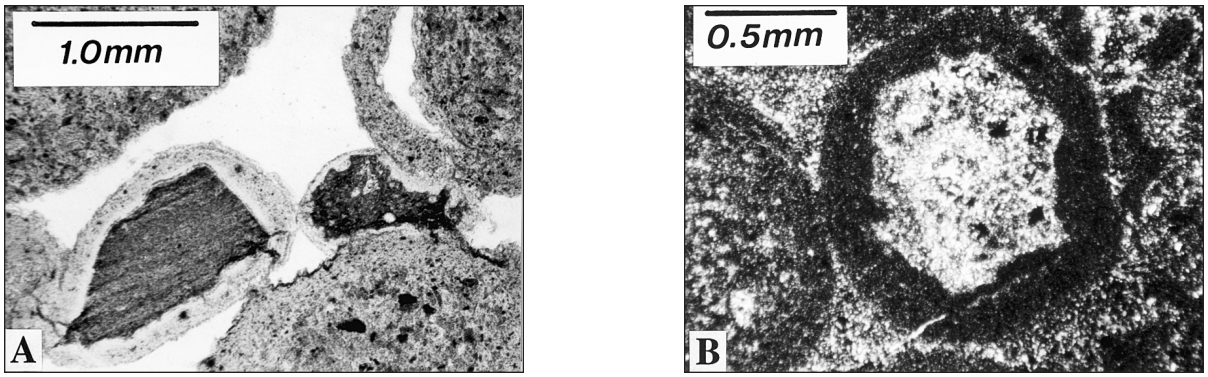


Figure 13. Lithic grains forming the nuclei of accretionary lapilli in the bimodal bed (unit 13, Fig. 3). A, very fine-grained laminated lithic grain; B, hexagonal, massive grain composed of intergrown sericite and microquartz. The grain could represent a phenocryst or lithic fragment.

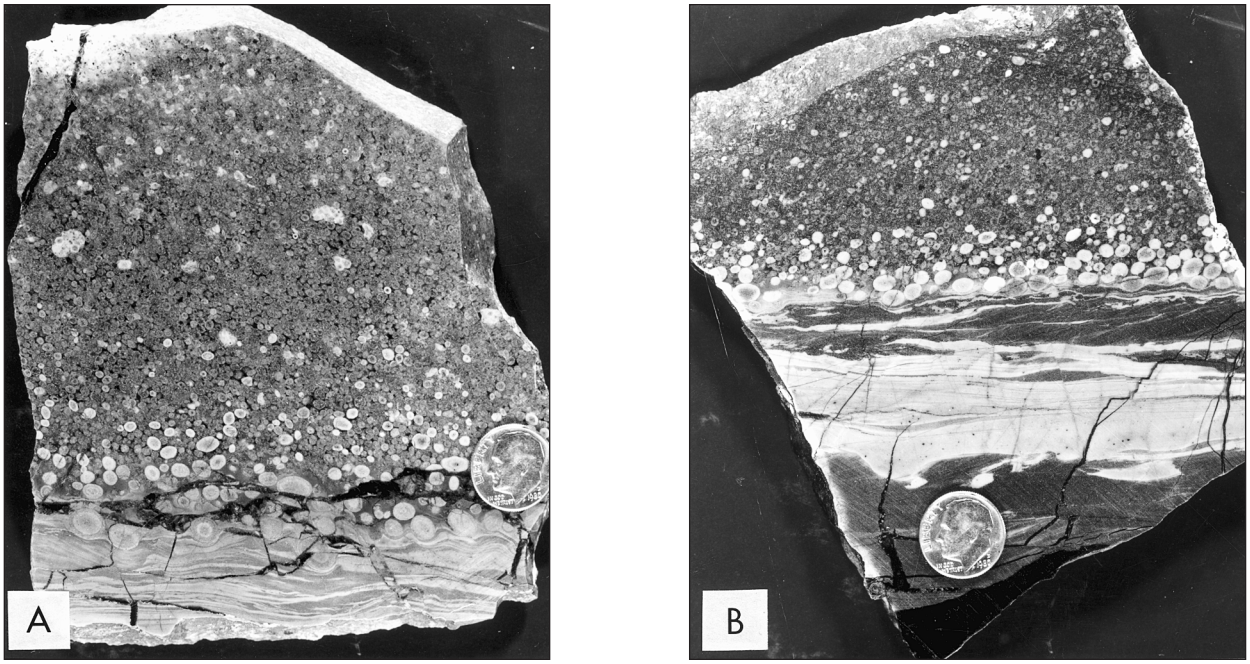


Figure 14. Unit 18 (Fig. 3) in sections SAF-138 (A) and the type section (B) showing the regional distinctiveness of lapilli types and internal structuring characterizing individual AA beds in the Msauli Chert. This bed everywhere shows large, light-colored, poorly structured lapilli at the base that have sunk into soft underlying sediments. Figure 18 shows the fine compositional layering present in the base of bed 18.

completely lacks intraclasts of carbonaceous mudstone, even where the graded layers rest directly on carbonaceous chert. If the AA beds were deposited by turbulent turbidity currents, some should have incorporated rip-up clasts of underlying, erodible carbonaceous mudstone. Fall deposits of accretionary lapilli and ash would not contain mudstone clasts.

Structuring of thick and thin lapilli-ash beds

In most turbidite sequences, thick, coarse-grained turbidites are composed largely of high-energy Bouma T_a and T_b divisions whereas associated thin-bedded, fine-grained units consist mainly of T_c, T_d, and T_e divisions (Mutti and Richi Lucci, 1972). In the Msauli Chert and related units throughout the Onverwacht Group, AA beds show an unusual reversal of these relationships (Figs. 16 and 17). Although a few of the thicker graded AA beds lack current structures altogether and may be regarded as single T_a divisions, most show complete or partial Bouma sequences in which T_a represents less than half of the bed thickness (Fig. 16). In contrast, most interbedded, thin, fine-grained lapilli-ash beds, less than 20 and many less than 3 cm thick, consist entirely of graded T_a divisions (Fig.

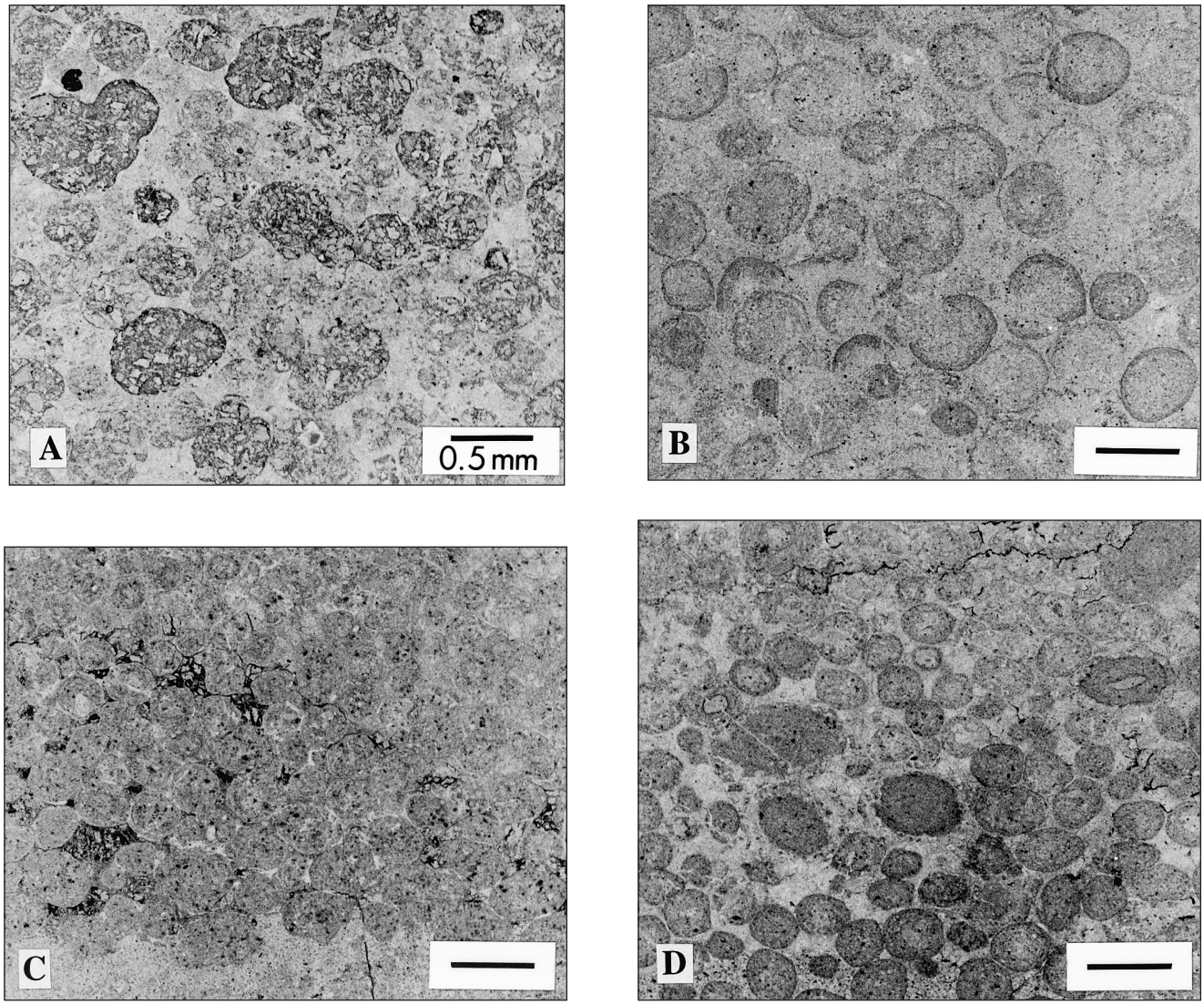


Figure 15. Photomicrographs of accretionary lapilli from successive AA units near the top of the Msauli Chert at SAF-191 (Loc. B, Fig. 3; section B, Fig. 7) showing the distinctiveness of lapilli in each layer. A, Unit 19 (Fig. 7) composed of dark-stained, irregular accretionary lapilli made up of very coarse debris that are mixed with ash and more spherical, smaller, fine-grained accretionary lapilli that are indistinct because of a lack of structuring and squashing. B, Unit 20 composed of spherical, fine-grained lapilli showing distinct fine rims. C, Part of graded accretionary lapilli layer at base of unit 21 composed of small, tightly packed relatively coarse lapilli (plane light) that have lost much of their individuality because of compaction. This bed is widely cemented by iron-rich dolomite (black material between lapilli). D, Upper part of unit 21. Lapilli in photos C and D are from separate graded beds within the general layer of accretionary lapilli termed unit 21. The lapilli in both beds are nearly identical. Both are composed of relatively coarse-grained detritus, visible mainly in plane light; most show crude concentric structure, commonly emphasized by an outer rim of fine-grained material; and many possess a small nucleus that was probably a lithic grain. In crossed nicols, the lapilli are composed of extremely fine-grained, homogeneous chert with dispersed impurities.

17). Current structures are rarely present in these thinner beds and, if they do occur, include only thin veneers of cross-laminated carbonaceous sediments at the tops of the beds, probably representing lithofacies II. In other words, thin, fine-grained, presumably lower-energy facies consist largely of the highest-energy Bouma division whereas the thick, coarse-grained presumably higher-energy beds include proportionally greater thicknesses of the low-energy divisions.

These relationships are difficult to explain in terms of the downslope evolution of turbidity currents. They are entirely consistent, however, if AA layers represent individual pyroclastic falls. Thin fall units, representing dilute, low-volume falls, would

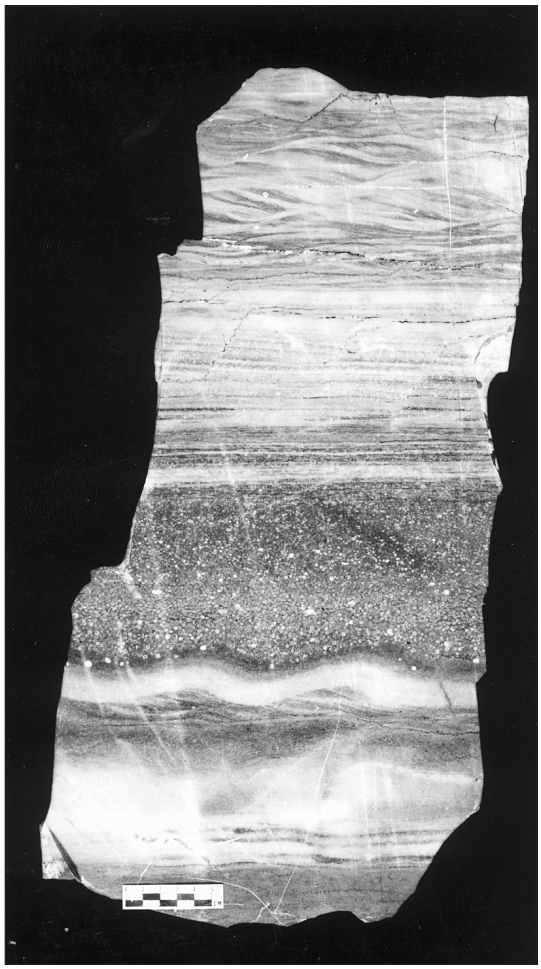
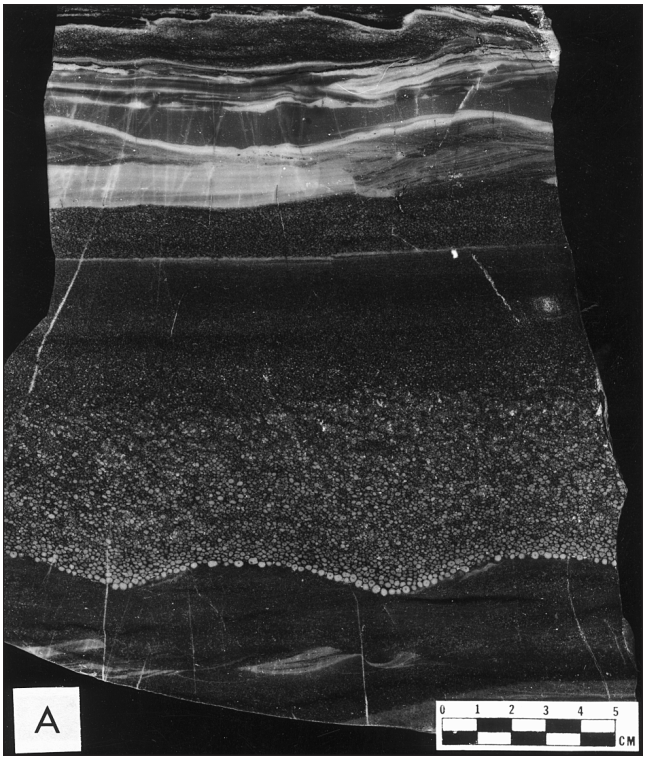


Figure 16. Thick graded AA layer from SAF-138 (loc. D, Fig. 1) showing well-developed Bouma sequence including a basal graded T_a division of lapilli and ash, an overlying flat-laminated T_b division of medium-grained ash, and an upper T_c division of climbing-ripple cross-lamination. Below the AA bed, a layer of ripples is draped by a 2-cm-thick graded but otherwise structureless ash bed that preserves the ripple morphology. The T_a division drapes the ripple-shaped surface of the fall-deposited ash without erosion. This type of delicate draping without erosion suggests that the T_a divisions represent fall-deposited layers rather than current deposits.



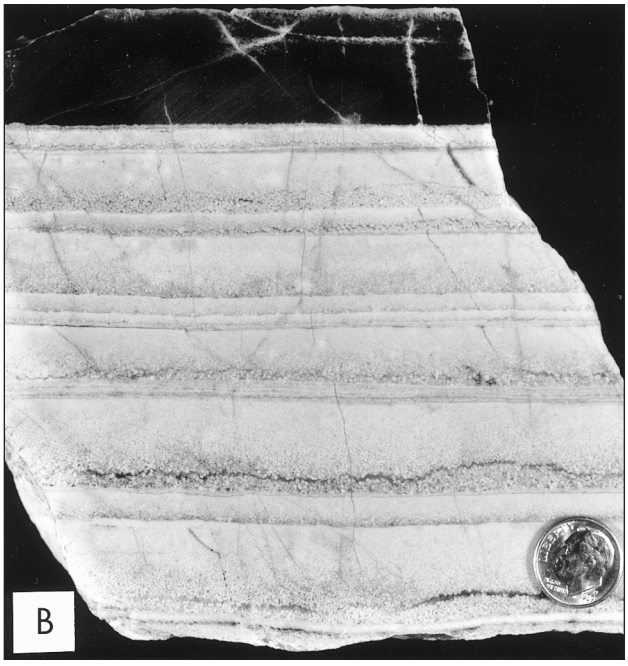


Figure 17. A, AA bed in section SAF-138 that grades from 1-mm-diameter accretionary lapilli at the base to fine ash and dust at the top but lacks current structures. The bed is a single T_a division. Overlying ash unit shows cross-lamination and soft-sediment deformation. B, Thin, graded AA units from unit 1 (Fig. 3) that represent individual, thin T_a divisions without associated current-structured T_b and T_c divisions.

have been preserved only where deposited in quiet, standing water. They accumulated under such conditions as simple graded fall layers resembling T_a divisions. Debris from similar dilute falls entering moving water would have been reworked to form units of lithofacies II. More massive falls into quiet water would also have deposited graded T_a units lacking current structures. When falling into flowing water, however, more voluminous ash falls might have initially greatly exceeded the capacity of the flowing water to transport and work the infalling ash as bed-load material. Most of the ash would have been deposited as massive T_a divisions by direct suspension sedimentation. As the falls declined in intensity, a point would have been reached when the infalling debris would have been incorporated into the bed-load

layers of the currents for a sufficient time to develop organized bedforms and produce deposits containing current-structures. The vertical sequence of current-structured divisions formed with continued decline in ash fall-out rate commonly includes flat lamination, cross-stratification, and cross-lamination and closely resembles the Bouma sequence. Details of this process have been outlined by Lowe (1988). Hence, thin deposits of dilute low-volume falls were preserved only where they accumulated in standing, quiet water and form T_a units whereas thicker deposits of more voluminous falls were preserved both where they entered quiet water to form T_a-dominated units and where they were deposited in flowing water as more complete T_{abcd} sequences.

Paucity of broken accretionary lapilli in T_a divisions

Moore and Peck (1962) concluded that accretionary lapilli were fragile particles and probably could not survive current transport. Lowe and Knauth (1977, 1978) suggested that lapilli in the Msauli Chert withstood at least some current working after fall and before deposition, and Boulter (1987) demonstrated that accretionary lapilli in the Late Archean Fortescue Group in Western Australia survived transport within an energetic alluvial environment. Ayres et al. (1991) likewise describe accretionary lapilli in energetic shallow-water sediments of Early Proterozoic age.

If graded AA units in the Msauli Chert are turbidites, the debris was transported by highly turbulent flows for kilometers to the sites of deposition. Transport-related modification of the grains should characterize particles throughout individual sedimentation units. However accretionary lapilli in the T_a divisions show little or no evidence of breakage or abrasion (Figs. 8, 11, and 15). Virtually all are whole and spherical or subspherical in shape. In contrast, from 20 to over 50% of the accretionary lapilli in the immediately overlying T_b and T_c divisions are fragments of originally spherical grains, and the surrounding coarse sandy detritus contains a high proportion of angular lapilli pieces, especially fine-grained, curved lapilli rim segments. Current transport was clearly responsible for considerable lapilli breakage. The nearly complete absence of broken lapilli in T_a divisions is inconsistent with their having also been deposited by currents. This distribution of broken and unbroken lapilli is consistent, however, if the T_a divisions represent pyroclastic fall deposits and the overlying current-structured divisions their current-worked tops.

Texture of the T_a divisions

The origin of the T_a division in turbidites has been discussed by numerous investigators (Walker, 1967; Middleton, 1966, 1967; Lowe, 1982b, 1988; and many others). Massive and graded T_a divisions form when the suspended-load fallout from turbidity currents exceeds the ability of the bed-load layers to move the settling grains. Sediment then accumulates directly with little or no traction movement, commonly forming a loosely packed or "quick" bed (Middleton, 1967). Because of the high rates of deposition, there is little tendency toward size fractionation within the settling sediment. Turbidite T_a divisions commonly show normal size grading but are characteristically poorly sorted. For similar reasons, the deposits of subaerial pyroclastic flows formed during eruptions and lahars formed by the failure of loose deposits on the sides of volcanic vents are characteristically poorly sorted (Fisher and Schmincke, 1984).

In the Msauli Chert, T_a divisions in AA beds vary considerably in texture and size properties, but in all, the only grains coarser than about 2 mm in diameter are accretionary lapilli. In one unit, the lapilli "float" in a matrix of fine ash; in a few others, lapilli are in grain-to-grain contact but contain ash matrix. In most, however, including those showing current structures and Bouma sequences, the T_a divisions are composed of extremely well sorted, largely ash-free accretionary lapilli (Figs. 8, 11, and 15). Of the 23 numbered beds or groups of beds in Figure 3, 15 and possibly more show basal lapilli zones that are completely or largely ash free. Again, because the type section has been strongly affected by contact metamorphism, textural and compositional features such as the presence or absence of ash matrix to the accretionary lapilli are poorly preserved. The pore space between lapilli is filled with precipitative cement, mainly chert, commonly recrystallized after fibrous chalcedony (Heinrichs, 1984). Other cements include phyllosilicates and, less commonly, carbonate. Ash appears in either the upper part of the T_a division (Fig. 8A) or in overlying divisions.

Such nearly perfect size fractionation is virtually unknown from the T_a divisions of turbidites, reflecting their rapid deposition. However, well-developed size fractionation of pyroclastic debris can result from the differential fall of grains of different sizes through either the atmosphere or standing water (Lowe and Knauth, 1978; Fisher and Schmincke, 1984). Although the initial ash clouds may be thoroughly mixed, the bases of the clouds do not rest directly upon the surfaces of accumulation, allowing differential settling to size segregate the falling debris prior to deposition. Size segregation and improved sorting will be particularly pronounced in units formed subaqueously because of the large differences in particle fall velocities in water as a function of size. Hence, although the deposit as a whole may contain a wide range of grain sizes, individual samples tend to be moderately to well sorted (Walker, 1980; Wright et al., 1980; Fisher and Schmincke, 1984), and in most fall deposits, the degree of sorting tends to increase toward the distal, finer grained portions of the ash sheets (e.g., Walker, 1980).

Fine-scale compositional layering in T_a divisions

The T_a divisions of turbidites typically lack lamination. In the Msauli Chert, however, it is not uncommon for the T_a divisions to show extremely fine vertical changes in the composition and/or texture of the accretionary lapilli, especially near their bases (Fig. 18). It would be difficult to explain the virtually complete fractionation of lapilli of differing only slightly, or in some cases not at all, in size and probably little or not at all in density during rapid sedimentation from a turbulent high-density tur-

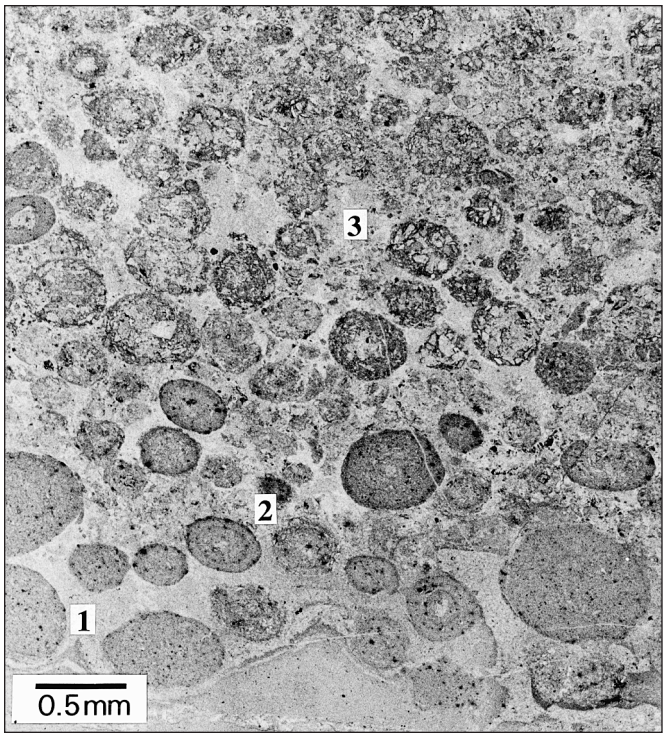


Figure 18. Photomicrograph of the basal part of bed 18 (Fig. 3) in the Msauli Chert showing the well-developed vertical changes in accretionary-lapilli type that characterize many AA beds. The basal part of the bed consists of large, fine-grained, rim-type lapilli (1), many of which have sunk into the underlying soft ash at the bottom of the photograph. Mixed with the large lapilli are many smaller oblong fine-grained lapilli containing multiple internal fine-grained layers (2). The bulk of the overlying bed consists of small, coarser grained, core-type lapilli (3).

bidity current. Fine compositional and textural layering is more consistent with the fallout of lapilli produced at different times or in different parts of pyroclastic clouds.

Grain size of pyroclastic debris within the Msauli chert

Size studies of the AA beds (Heinrichs, 1984) demonstrate that they are texturally bimodal with the accretionary lapilli forming a coarse size fraction distinct from the finer ash. In most sections, the largest nonaccretionary pyroclastic grains are between 0.75 and 1.5 mm in diameter. Accretionary lapilli are locally less than 1 mm in size, but most range between 2.0 and 4.0 mm and in a few beds large fine-grained lapilli reach 13 mm in diameter. They were everywhere composed of ash and dust less than 2 mm in diameter and altered lithic fragments as much as about 2 mm across.

If the volcaniclastic debris were transported by turbidity currents, the flows were capable of transporting grains at least a centimeter in diameter, the size of the largest accretionary lapilli. If these turbidity currents were related directly to phreatomagmatic or hydromagmatic eruptions, either by the transformation of collapsing eruption columns or pyroclastic flows into subaqueous flows or through slope failures on the sides of tuff cones (Heinrichs, 1984), we would be forced to conclude that the eruptions produced no particles coarser than 2 mm in diameter. Although some phreatoplinian eruptions produce enormous quantities of debris less than 1 mm in diameter (Self and Sparks, 1978; Walker, 1981), their proximal deposits always include larger components (Self and Sparks, 1978; Walker, 1981). Moreover, known phreatoplinian eruptions are short phases in the much longer magmatic histories of individual vents. They are preceded and followed by plinian and other eruptions that produce large amounts of coarse debris. Although thin pyroclastic layers composed largely of fine-grained ash may occur within the volcanic stratigraphies of these vents, thick near-vent sequences constructed solely of fine-grained ash are unknown. If graded layers in the Msauli Chert were deposited by turbidity currents originating on the sides of one or more volcanic cones, they should contain some coarser debris derived from the proximal volcanic sequence.

Accretionary lapilli formed within base surges and eruption columns are generally mixed with similarly sized vitric and lithic nonaccretionary grains (e.g., Fisher and Waters, 1970, Pl. 9 and 10). Turbidites derived from such materials should also contain a mixture of hydraulically equivalent accretionary and nonaccretionary particles. The absence of nonaccretionary grains in the Msauli Chert that are hydraulically equivalent to the accretionary lapilli suggests that the original debris was fine airborne ash, that the large lapilli formed through ash accretion, and that the beds formed through ash and accretionary lapilli fall, not through the reworking and resedimentation of complex pyroclastic deposits. Self and Sparks (1978) describe remarkably similar graded beds of fine ash and coarse accretionary lapilli deposited in a lake by fallout from a phreatoplinian eruption cloud.

Draping of lapilli-ash beds over underlying bed irregularities

Although Stanistreet et al. (1981) report scoured bases to some graded AA beds in the Msauli Chert, during the present study scour was observed only where cross-stratified divisions eroded through the T_a and T_b divisions to rest directly against underlying deposits. The T_a divisions not only lack erosive bases, they commonly delicately drape ripples on the underlying beds (Figs. 16 and 17). The draping of small-scale, easily erodible, low-energy bedforms composed of loose, sand-sized grains by high-energy turbidite T_a divisions is unlikely because the passage of the turbulent turbidity current head is always associated with active bed scour or at least the smoothing of preexisting bed irregularities. However, pyroclastic fall deposits commonly drape preexisting bed irregularities (Wright et al., 1980), and direct ash fall from pyroclastic clouds provides the most reasonable explanation for the preservation of unmodified ripples beneath graded accretionary lapilli and ash beds in the Msauli Chert.

Collectively, the textures, structures, and composition of the graded accretionary lapilli and ash beds in the Msauli Chert argue

persuasively that these beds formed by the fall of pyroclastic debris into both standing and running water in areas far removed from the volcanic vent. The Bouma sequence of structures in current-worked AA beds formed in response to the declining rate of lapilli, ash, and dust fallout from pyroclastic clouds (Lowe, 1988) rather than by declining suspended-load sedimentation from turbidity currents.

DISCUSSION

Depositional setting

The abundance of accretionary lapilli in the Msauli Chert clearly indicates that the eruptions from which they formed were subaerial. Arguments developed in the preceding section indicate that the accretionary lapilli and ash fell directly into surrounding water bodies, and Lowe and Knauth (1978) have calculated that, under those conditions, sedimentation of the bimodal bed occurred in water that was only a few meters deep.

The lower 5 m of the Msauli Chert consists of lithofacies II that includes current-structured detrital layers from less than 1 to about 15 cm thick interbedded with thin carbonaceous layers reaching a maximum thickness of about 4 cm. These layers record the deposition of pyroclastic and carbonaceous sediments under alternating current-active and quiet-water conditions, respectively. Few volcaniclastic units exceed 1 or 2 cross-sets in thickness. The thinness and close interlayering and interfingering of current-deposited volcaniclastic and quiet-water carbonaceous layers throughout lithofacies II suggests that the time represented by each layer was relatively short.

In the upper part of the Msauli Chert, all fall-deposited AA beds greater than 50 cm thick contain current-structured divisions, suggesting that the duration of the larger ash falls exceeded the length of the quiet-water intervals. However, most interbedded AA units less than 20 cm thick lack current structures, indicating fall periods shorter than the lengths of the quiet-water intervals. These arguments, although qualitative, suggest that individual current-active and quiet-water periods were short, perhaps a few hours to a few days in length.

These short, regular, alternating current-active and quiet-water cycles resemble tidal cycles in younger deposits. Mud drapes, mud flazers, and mudstone rip-up clasts within the rippled sand units of lithofacies II are also common in muddy tidal flat and shallow subtidal deposits, and one small-scale cross-set was discovered containing well-developed reactivation surfaces (Fig. 19). However, mudcracks, cyclic tidalites, tidal bundles, bipolar or bimodal current directions, and other common tidal features were not seen. The dominance of pyroclastic sedimentation, however, would have strongly modified the tidal lithofacies and could have completely prevented the development of progradational tidal cycles and long-lived, complex sand waves. Cross-sets thicker than 10–15 cm are also uncommon in the Msauli Chert, although coarse-grained units in southeastern sections do show cross-stratification as much as 60 cm high. Overall, sedimentary features suggest deposition under alternating current-active and quiet-water conditions like those characterizing shallow subtidal to protected intertidal environments today.

Paleocurrent patterns from cross-laminations and cross-stratification in the Msauli Chert are regionally consistent, trending generally from west to east. They suggest flow across a tidally dominated shelf rather than into and out of a tidal basin or onto and off of tidal flats. If the Onverwacht Group accumulated as a large, low-relief, mainly shallow-water volcanic platform (Lowe, 1982a) surrounded by open ocean, the surface of this platform may have been swept, when submerged, by tidal currents showing relatively unimodal flow directions.

Origin of the accretionary lapilli

Accretionary lapilli occur in most AA units in the Msauli Chert. They may have been even more abundant at the time of deposition, but softer, less resistant varieties were probably disaggregated upon impact (e.g., Walker, 1981) and during later reworking. The wide areal distribution of individual layers, the absence of hydraulically equivalent nonaccretionary volcaniclastic debris, and the lack of regional coarsening or fining trends in lapilli size suggest that the accretionary lapilli are not ballistic particles. They were probably formed within already dispersed fine-grained aerosol clouds, similar to accretionary particles distributed tens and hundreds of kilometers downwind from Mount St. Helens (Carey and Sigurdsson, 1982) and have been described from ash-fall layers elsewhere (Schumacher and Schmincke, 1991).

Accretionary lapilli form when ash particles collide and the binding forces, mainly capillary forces in moist ash clouds

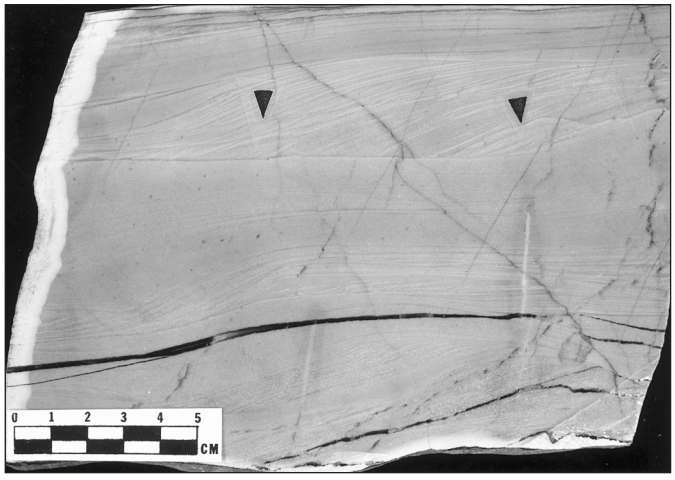


Figure 19. Cross-laminated ash from the Msauli Chert. Individual cross-sets show internal reactivation surfaces (arrows), indicating that the original ripples were partially eroded between episodes of active current flow and ripple migration from right to left. Erosion may mark intervals of slack water (no flow) or intervals when flow was reversed and flowing in the opposite direction.

(Gilbert and Lane, 1994) and electrostatic forces in dry clouds (Reimer, 1983b), exceed dispersive forces (Schumacher and Schmincke, 1991, 1995). Both rim and core types of accretionary lapilli (Schumacher and Schmincke, 1991) are present in the Msauli Chert, often within the same bed. Rim-type lapilli dominate in the bimodal bed (Figs. 11 and 13). Some beds in the upper part of the Masuli Chert have large rim-type lapilli at their bases and smaller, core types higher in the same units (Fig. 14). Beds dominated by rim type and core type directly succeed one another in some parts of the section (units 19 and 20, Fig. 15). Schumacher and Schmincke (1991, 1995) suggest that coarser, core-type lapilli form mainly in response to capillary forces in relatively wet clouds whereas fine-grained rims in rim-type lapilli form due to electrostatic forces in somewhat drier clouds. The intimate association of core and rim types within the Msauli Chert may suggest that the pyroclastic clouds from which they formed were characterized by spatial and perhaps temporal variations in ash concentration and moisture content. Core-type particles forming initially through capillary forces in wetter parts of clouds may have accreted finer rims during subsequent fall through the lower, less concentrated, drier parts of these same clouds. The immense areal distribution of both rim and core types within individual accretionary lapilli units in the Msauli Chert suggest that rim types were not restricted to a proximal settings within a few kilometers of the vent(s), as they are in the Laacher Sea volcano (Schumacher and Schmincke, 1991). We have found no evidence in any of these layers for the presence of ballistic ejecta, coarse-grained near-vent material, or surge deposits. The accretionary lapilli in these units appear to have formed entirely within dispersed ash clouds, rather than in surges or eruption columns (Schumacher and Schmincke, 1995).

Accretion was probably triggered by the condensation of water vapor ejected along with the pyroclastic debris during the eruptions. If so, the abundance of accretionary lapilli may reflect the wet character of explosive late-stage komatiitic hydrovolcanic eruptions rather than the presence of abundant water vapor in the early Archean atmosphere, as suggested by Lowe and Knauth (1978).

Volcanism

The Msauli Chert, member M1c of the Mendon Formation (Lowe and Byerly, this volume, Chapter 1), is the "type" example of a class of volcaniclastic units in the Onverwacht Group that occur as caps on predominantly komatiitic volcanic sequences. Other examples include H1 (the Middle Marker), H3c and H4c in the Hooggenoeg Formation, K2c in the Kromberg Formation, and M2c in the Mendon Formation. Similar accretionary lapilli-bearing pyroclastic units are not known from thick felsic pyroclastic and epiclastic units in H6 or the Fig Tree Group. Trace element analysis, moreover, suggests that the pyroclastic debris making up these Onverwacht pyroclastic units was also komatiitic in composition (Lowe, this volume, Chapter 3).

Basaltic and komatiitic magmatism is generally not associated with large pyroclastic eruptions because low viscosity mafic magmas degas rapidly prior to solidification (Fisher and Schmincke, 1984). Most reported komatiitic pyroclastic deposits from Archean greenstone belts are local accumulations of lapilli, probably formed mainly by hydrovolcanic explosions (Saverikko, 1985; Schaefer and Morton, 1991; Ransom et al., this volume, Chapter 6). Similarly, the shapes and low vesicularity of most debris making up the Msauli Chert and similar layers throughout the Onverwacht Group suggest that it was not formed by gas evasion. The pyroclastic events were more likely hydromagmatic eruptions than plinian or strombolian events (Heinrichs, 1984).

Every major komatiitic volcanic unit in the shallow-water facies of the Onverwacht Group is capped by silicified late-stage komatiitic volcaniclastic sediments that do not occur between flow units within the komatiitic sequences. These relations suggest that the closing stages of major episodes of komatiitic volcanism in the Onverwacht Group involved violent hydromagmatic explosions. Lowe (this volume, Chapter 3) has suggested that the rapid buildup of komatiitic volcanic sequences into shallow water may have resulted in the tops of the broad, low-relief shield volcanoes becoming subaerial. During the waning stages of volcanism, conduit collapse may have allowed sea water access to the vents resulting in direct water-magma interaction and explosive "mixing eruptions" (Mastin, 1995). The most likely mechanism for the complete fragmentation of a magma to form Type 1 pyroclasts of Wohletz (1983) is contact-surface steam explosivity (Kokelaar, 1986) or fuel-coolant interactions (Sheridan and Wohletz, 1983). In magmatic fuel-coolant interactions, fragmentation results from shocks produced as steam films and bubbles form, grow, and collapse along the magma/water interface.

The optimal water:melt mixing ratio for highly explosive fuel-coolant interactions involving basaltic magmas is in the range of 0.1–0.3, and the explosion products in experimental systems near this optimum mixture are always fine, less than 50 microns (Sheridan and Wohletz, 1983). Schumacher and Schmincke (1995) also note that accretionary lapilli are most likely to form in clouds of wet tephra containing 10–25% condensed moisture. The fine grain size and abundance of accretionary lapilli in the Msauli Chert and similar silicified komatiitic ash and dust deposits that cap komatiitic flow sequences throughout the Onverwacht Group suggest that pyroclast formation was mainly through extremely violent hydrovolcanic explosions that ejected large volumes of fine ash, dust, and water vapor into the Archean atmosphere.

CONCLUSIONS

The Msauli Chert represents a class of sedimentary units in the Onverwacht Group composed largely of metasomatically altered and silicified komatiitic tuff and silicified fine-grained carbonaceous mudstone. These units occur as thin, regionally continuous chert layers capping sequences of komatiitic lavas

and include the Middle Marker (Lanier and Lowe, 1982), members H3c and H4c of the Hooggenoeg Formation, member K2c of the Kromberg Formation, and members M1c (the Msauli Chert) and M2c of the Mendon Formation (Lowe and Byerly, this volume, Chapter 1).

The sedimentology of these units has been discussed by Lowe (this volume, Chapter 3), Ransom et al. (this volume, Chapter 6), and previously by Lowe and Knauth (1977, 1978) and Lanier and Lowe (1982). All are composed principally of nearly pure volcaniclastic layers thought to represent pyroclastic fall and locally reworked fall deposits; relatively pure carbonaceous chert, representing fine-grained interfall deposition of organic-rich mud; and current-deposited volcaniclastic and carbonaceous debris eroded from the fall and interfall deposits, respectively. Especially characteristic of these chert beds are graded layers of accretionary lapilli and ash, many showing complete or partial Bouma sequences. The sedimentology of these layers has been interpreted in terms of both deep-water turbidity currents (Stanistreet et al., 1981; Heinrichs, 1984) and pyroclastic falls into shallow water (Lowe and Knauth, 1978, 1979).

Many of these beds consist solely of graded T_a divisions of accretionary lapilli and ash from a few centimeters to more than 30 cm thick, but in others the T_a divisions are overlain by current-structured T_b, T_c, and T_d ash divisions. However, the undiluted and unmixed character of the volcaniclastic debris making up these beds, the absence of current-produced textures within the T_a divisions, the delicate draping by coarse-grained T_a divisions of unmodified ripple forms on underlying ash layers, and a variety of other features suggest that these units were deposited by pyroclastic falls rather than turbidity currents. The formation of Bouma sequences in these beds reflects the declining rate of pyroclastic fall into flowing water rather than declining velocities of turbidity currents (Lowe, 1988). Tidal currents sweeping across the shallow but probably largely subaqueous, low-relief volcanic platform reworked much of the volcaniclastic sediment, both during and between pyroclastic falls. Alternating quiet-water intervals were associated with the passive accumulation of graded but non-current-structured fall-deposited ash beds and, between falls, fine-grained carbonaceous mud.

The small size of pyroclasts making up the deposits, the regional continuity and uniformity of individual sedimentation units, and the absence of ballistic ejecta hydraulically equivalent to the accretionary lapilli suggest that the present exposures represent distal settings, many kilometers from the vents. It is also probable, however, that these were extremely violent eruptions and that the bulk of the debris formed was very fine grained (Sheridan and Wohletz, 1993). The accretionary lapilli, distinctive in many individual fall units, probably formed by accretion of loose volcaniclastic particles within widely dispersed eruption clouds.

The Msauli Chert and related chert units in the Onverwacht Group represent komatiitic, not felsic pyroclastic detritus. The extremely low viscosities and low volatile contents of komatiitic lavas argue against plinian eruptions driven by exolving magmatic volatiles. The consistent stratigraphic position of these volcaniclastic units at the tops of thick komatiitic flow sequences, the great abundance of fine-grained pyroclastic detritus, and the predominance of blocky hyaloclastic grains suggest that the layers represent debris produced by violent hydromagmatic eruptions that marked the terminal stage of large-scale komatiitic effusive events. These hydromagmatic eruptions were probably triggered by large-scale flooding of the vents during conduit collapse.

REFERENCES CITED

Allen, J. R. L., and Leeder, M. R., 1980, Criteria for the instability of upper-stage plane beds: Sedimentology, v. 27, p. 209–217.

Anhaeusser, C. R., 1973, The evolution of the early Precambrian crust of southern Africa: Royal Society of London Philosophical Transactions, ser. A, v. 273, p. 359–388.

Ayres, L. D., van Wagoner, N. A., and Ferreira, W. S., 1991, Voluminous shallow-water to emergent phreatomagmatic basaltic volcaniclastic rocks, Proterozoic (~1886 MA) Amisk Lake composite volcano, Flin Flon Greenstone Belt, Canada, *in* Fisher, R. V., and Smith, G. A., eds., Sedimentation in volcanic settings: Society of Economic Paleontologists and Mineralogists Special Publication no. 45, p. 175–187.

Boulter, C. A., 1987, Subaqueous deposition of accretionary lapilli: significance for palaeoenvironmental interpretations in Archaean greenstone belts: Precambrian Research, v. 34, p. 231–246.

Bouma, A. H., 1962, Sedimentology of some flysch deposits: Amsterdam, Elsevier, 168 p.

Carey, S. N., and Sigurdsson, H., 1982, Influence of particle aggregation on deposition of distal tephra from the May 18, 1980, eruption of Mount St. Helena volcano: Journal of Geophysical Research, v. 87, p. 7061–7072.

Fisher, R. V., and Schmincke, H. -U., 1984, Pyroclastic rocks: Berlin, Springer-Verlag, 472 p.

Fisher, R. V., and Schmincke, H. -U., 1994, Volcaniclastic sediment transport and deposition, *in* Pye, K., ed., Sediment transport and depositional processes: London, Blackwell Scientific Publications, p. 351–388.

Fisher, R. V., and Waters, A. C., 1970, Base surge bed forms in maar volcanoes: American Journal of Science, v. 268, p. 157–180.

Gilbert, J. S., and Lane, S. J., 1994, The origin of accretionary lapilli: Bulletin of Volcanology, v. 56, p. 398–411.

Harms, J. C., and Fahnestock, R. K., 1965, Stratification, bed forms, and flow phenomena (with an example from the Rio Grande), *in* Middleton, G. V., ed., Primary sedimentary structures and their hydrodynamic interpretation: Society of Economic Paleontologists and Mineralogists Special Publication 12, p. 84–115.

Heinrichs, T. K., 1980, Lithostratigraphische Untersuchungen in der Fig Tree Gruppe des Barberton Greenstone Belt zwischen Umsoli und Lomati (Sudafrika) (Lithostratigraphic studies in the Fig Tree Group of the Barberton Greenstone Belt between Umsoli and Lomati (South Africa)): Gottinger Arbeiten zur Geologie und Palaontologie, v. 22, 118 p.

Heinrichs, T. K., 1984, The Umsoli Chert, turbidite testament for a major phreatoplinian event at the Onverwacht/Fig Tree transition (Swaziland Supergroup, Archaean, South Africa): Precambrian Research, v. 24, p. 237–283.

Knoll, A. H., and Barghoorn, E. S., 1977, Archean microfossils showing cell division from the Swaziland System of South Africa: Science, v. 198, p. 396–398.

Kokelaar, P., 1986, Magma-water interactions in subaqueous and emergent basaltic volcanism: Bulletin of Volcanology, v. 48, p. 275–289.

Lanier, W. P., and Lowe, D. R., 1982, Sedimentology of the Middle Marker (3.4 Ga), Onverwacht Group, Transvaal, South Africa: Precambrian Research, v. 18, p. 237–260.

Lowe, D. R., 1982a, Comparative sedimentology of the principal volcanic

sequences of Archean greenstone belts in South Africa, Western Australia, and Canada: implications for crustal evolution: Precambrian Research, v. 17, p. 1–29.

Lowe, D. R., 1982b, Sediment gravity flows: II. Depositional models with special reference to the deposits of high-density turbidity currents: Journal of Sedimentary Petrology, v. 52, p. 279–297.

Lowe, D. R., 1988, Suspended-load fallout rate as an independent variable in the analysis of current structures: Sedimentology, v. 35, p. 765–776.

Lowe, D. R., and Byerly, G. R., 1986, Archean flow-top alteration zones formed initially in a low-temperature sulphate-rich environment: Nature, 324, p. 245–248.

Lowe, D. R., and Knauth, L. P., 1977, Sedimentology of the Onverwacht Group (3.4 billion years), Transvaal, South Africa, and its bearing on the characteristics and evolution of the early Earth: Journal of Geology, v. 85, p. 699–723.

Lowe, D. R., and Knauth, L. P., 1978, The oldest marine carbonate ooids reinterpreted as volcanic accretionary lapilli, Onverwacht Group, South Africa: Journal of Sedimentary Petrology, v. 48, p. 709–722.

Lowe, D. R., Byerly, G. R., Ransom, B. L., and Nocita, B. R., 1985, Stratigraphic and sedimentological evidence bearing on structural repetition in Early Archean rocks of the Barberton Greenstone Belt, South Africa: Precambrian Research, v. 27, p. 165–186.

Mastin, L. G., 1995, Thermodynamics of gas and steam-blast eruptions: Bulletin of Volcanology, v. 57, p. 85–98.

Middleton, G. V., 1966, Experiments on density and turbidity currents: I. Motion of the head: Canadian Journal of Earth Sciences, v. 4, p. 523–546.

Middleton, G. V., 1967, Experiments on density and turbidity currents: III. Deposition of sediment: Canadian Journal of Earth Sciences, v. 4, p. 475–505.

Moore, J. G., and Peck, D. L., 1962, Accretionary lapilli in volcanic rocks of the western continental United States: Journal of Geology, v. 70, p. 182–193.

Muir, M. D., and Hall, D. O., 1974, Diverse microfossils in Precambrian Onverwacht Group rocks of South Africa: Nature, v. 252, p. 376–378.

Mutti, E., and Ricci-Lucchi, F., 1972, Le torbiditi dell'Appennino settentrionale: introduzione all'analisi di facies: Società Geologica Italiana Memoirs, v. 11, p. 161–199.

Reimer, T. O., 1975, Paleogeographic significance of the oldest known oolite pebbles in the Archaean Swaziland Supergroup (South Africa): Sedimentary Geology, v. 14, p. 123–133.

Reimer, T. O., 1983a, Pseudo-oolites in rocks of the Ulundi Formation, lower part of the Archaean Fig Tree Group (South Africa): Precambrian Research, v. 20, p. 375–390.

Reimer, T. O., 1983b, Accretionary lapilli in volcanic ash falls: Physical factors governing their formation, *in* Peryt, T., ed., Coated grains: Berlin, Springer Verlag, p. 56–68.

Reimer, T. O., 1983c, Accretionary lapilli and other spheroidal rocks from the Swaziland Supergroup of the Barberton Mountain Land, South Africa, *in* Peryt, T., ed., Coated grains: Berlin, Springer Verlag, p. 619–634.

Saverikko, M., 1985, The pyroclastic komatiite complex at Sattasvaara in northern Finland: Geological Society of Finland Bulletin, v. 57, p. 55–87.

Schaefer, S. J., and Morton, P., 1991, Two komatiitic pyroclastic units, Superior Province, northwestern Ontario: their geology, petrography, and correlation: Canadian Journal of Earth Sciences, v. 28, p. 1455–1470.

Schumacher, R., and Schmincke, H. -U., 1991, Internal structure and occurrence of accretionary lapilli—a case study at Laacher See Volcano: Bulletin of Volcanology, v. 53, p. 612–634.

Schumacher, R., and Schmincke, H. -U., 1995, Models for the origin of accretionary lapilli: Bulletin of Volcanology, v. 56, p. 626–639.

Self, S., and Sparks, R. S. J., 1978, Characteristics of widespread pyroclastic deposits formed by the interaction of silicic magma and water: Bulletin Volcanologique, v. 41, no. 3, p. 196–212.

Sheridan, M. F., and Wohletz, K. H., 1983, Hydrovolcanism: basic considerations and review: Journal of Volcanology and Geothermal Research, v. 17, p. 1–29.

Simons, D. B., Richardson, E. V., and Nardin, C. F., 1965, Sedimentary structures generated by flow in alluvial channels, *in* Middleton, G. V., ed., Primary sedimentary structures and their hydrodynamic interpretation: Society of Economic Paleontologists and Mineralogists Special Publication 12, p. 34–52.

Stanistreet, I. G., de Wit, M. J., and Fripp, R. E. P., 1981, Do graded units of accretionary spheroids in the Barberton Greenstone Belt indicate Archaean deep water environment?: Nature, v. 293, p. 280–284.

Viljoen, M. J., and Viljoen, R. P., 1969, An introduction to the geology of the Barberton granite-greenstone terrain: Geological Society of South Africa Special Publication 2, p. 9–28.

Viljoen, R. P., and Viljoen, M. J., 1969, The geological and geochemical significance of the upper formations of the Onverwacht Group: Geological Society of South Africa Special Publication 2, p. 113–152.

Visser, D. J. L., 1956, The geology of the Barberton area: Geological Survey of South Africa Special Publication 15, 254 p.

Walker, G. P. L., 1980, The Taupo Pumice: product of the most powerful known (ultraplinian) eruption: Journal of Volcanology and Geothermal Research, v. 8, p. 69–94.

Walker, G. P. L., 1981, Characteristics of two phreatoplinian ashes, and their water-flushed origin: Journal of Volcanology and Geothermal Research, v. 9, p. 395–407.

Walker, R. G., 1965, The origin and significance of the internal sedimentary structures of turbidites: Yorkshire Geological Society Proceedings, v. 35, p. 1–31

Walker, R. G., 1967, Turbidite sedimentary structures and their relationship to proximal and distal depositional environments: Journal of Sedimentary Petrology, v. 37, p. 23–43.

Wohletz, K. H., 1983, Mechanisms of hydrovolcanic pyroclast formation: grain-size, scanning electron microscopy, and experimental studies: Journal of Volcanology and Geothermal Research, v. 17, p. 31–63.

Wright, J. V., Smith, A. L., and Self, S., 1980, A working terminology of pyroclastic deposits: Journal of Volcanology and Geothermal Research, v. 8, p. 315–336.

-Manuscript Accepted by the Society March 26, 1998

Geological Society of America
Special Paper 329
1999

Foreland basin sedimentation in the Mapepe Formation, southern-facies Fig Tree Group

Donald R. Lowe
Department of Geological and Environmental Sciences, Stanford University, Stanford, California 94305
Bruce W. Nocita*
Department of Geology and Geophysics, Louisiana State University, Baton Rouge, Louisiana 70803

ABSTRACT

The Mapepe Formation of the Fig Tree Group in the southern part of the Barberton Greenstone Belt (BGB) includes three major petrologic suites: (1) volcaniclastic rocks, (2) terrigenous rocks, and (3) chemical or precipitative deposits. These comprise three lithofacies associations reflecting the main elements of the Mapepe deposystem: (a) a basinal association, composed of fine tuff, mud, and, locally, banded ferruginous chert, jasper, and iron formation, that accumulated under quiet subaqueous conditions; (b) a fan-delta association composed of sandstone and conglomerate deposited adjacent to uplifts; and (c) a shallow-water association, including chert, jasper, bedded barite, and terrigenous and volcaniclastic units. Terrigenous sediments in the Mapepe Formation were eroded from underlying Onverwacht Group and penecontemporaneous felsic volcanic rocks. The composition of the detritus changes up section. The lowest conglomerates lack clasts of felsic volcanic rock and vary in composition from outcrop to outcrop, reflecting derivation from local, immediately underlying greenstone sources. Higher units are regionally more uniform in composition and contain clasts representing both deeper levels of erosion and felsic volcanic sources. The absence of sediment eroded from metamorphic rocks or plutonic rocks and the uniformly low detrital quartz content of Mapepe sandstones suggest that tonalitic plutons were not widely exposed in Mapepe time.

The earliest Mapepe deposystem consisted of a single large basin in southeastern parts of the BGB that accumulated iron formation and ferruginous sediments. During middle Mapepe time, this basin was divided by the nascent Onverwacht anticline. Middle and late Mapepe sedimentation occurred within paired foreland basins lying along the northwestern and southeastern margins of the BGB and separated by a structural and topographic high marking the Onverwacht anticline, which may have developed as a shared forebulge. These basins were flanked to the northwest and southeast, respectively, by uplifts, probably fold-and-thrust belts. In the southeastern basin, the lower sequence of shale, iron-formation, and jasper, deposited under quiet, deep-water conditions, is overlain by shale interbedded with coarse clastic detritus derived from uplifts to the southeast. In the northwestern basin, the lowest Mapepe strata include a basal 5- to 10-m-thick shallow-water sequence of felsic tuff, chert, jasper, and barite succeeded by 100–200 m of fine deep-water felsic tuff. The overlying 200–300 m consists of basinal

*Present address: 22849 Cypress Trail Drive, Lutz, Florida 33549.

Lowe, D. R., and Nocita, B. W., 1999, Foreland basin sedimentation in the Mapepe Formation, southern-facies Fig Tree Group, *in* Lowe, D. R., and Byerly, G. R., eds., Geologic Evolution of the Barberton Greenstone Belt, South Africa: Boulder, Colorado, Geological Society of America Special Paper 329.

tuff interbedded with coarse terrigenous sediments deposited on fan-deltas sourced to the north and northwest. Middle and upper Mapepe deposits in the southern part of the northwestern basin include thin, lenticular clastic units made up of debris eroded from small, local uplifts, possibly formed by flexural extension along the forebulge (Onverwacht anticline). These uplifts were flanked by small fan deltas extending north and west. Mapepe sedimentation in the northwestern basin closed with southward-progradation of the adjacent fold-and-thrust belt, uplift, and erosion.

Northward increase in abundance of dacitic volcaniclastic debris suggests that the northern orogen was a back-arc fold-and-thrust belt. The small amount of volcaniclastic debris in the southeastern basin suggests that shortening there was not associated with volcanic activity. These basins appear to have been smaller than large, complex Phanerozoic continental foreland basins, such as the Mesozoic-Cenozoic Andean and Cordilleran basins, but are comparable to smaller subbasins within these larger basins. The dominance of debris derived from underlying mafic and ultramafic rocks of the Onverwacht Group, the absence of deep crustal debris, such as plutonic detritus, and the small size and facing character of the basins suggest that they formed during the amalgamation of small immature crustal blocks or microplates.

INTRODUCTION

The volcanic and sedimentary sequence in the Barberton Greenstone Belt (BGB) includes a lower, predominantly mafic and ultramafic volcanic sequence, the Onverwacht Group, and an upper, largely sedimentary sequence, the Fig Tree and Moodies Groups. Both exhibit major lithologic and sedimentological changes across the belt and can be divided into distinctive northern and southern facies separated by the Inyoka fault (Heinrichs, 1969, 1980; Reimer, 1975; Heinrichs and Reimer, 1977; Eriksson, 1980 a, b; Lowe and Byerly, this volume, Chapter 1; de Ronde and de Wit, 1994).

The Fig Tree Group has been studied mainly in the northern BGB (Anhaeusser, 1969, 1973; Reimer, 1967, 1975; Condie et al., 1970; Eriksson, 1980a, b) whereas southern-facies Fig Tree rocks (Fig. 1) remain poorly known (Visser, 1956; Heinrichs and Reimer, 1977; Heinrichs, 1980). Within the study area (Fig. 1), most southern-facies Fig Tree rocks belong to the Mapepe Formation (Heinrichs, 1980; Lowe and Byerly, this volume, Chapter 1), a unit of interbedded terrigenous, volcaniclastic, and precipitative deposits. It is structurally overlain across the 24-Hour Camp fault by dacitic volcaniclastic rocks of the Auber Villiers Formation (Fig. 1; Lowe and Byerly, this volume, Chapter 1). The present report deals with the petrology and sedimentology of the Mapepe Formation.

LITHOFACIES

The Mapepe Formation comprises three major petrologic suites: (1) volcaniclastic rocks (V), (2) terrigenous clastic units (T), and (3) orthochemical precipitative deposits (O). Each petrologic suite can be further divided into individual rock types or lithofacies (Table 1 and Figs. 2 and 3).

Rocks of the Mapepe Formation have been widely affected by low-grade metamorphic and metasomatic alteration. Silicification of some fine-grained volcaniclastic units has locally converted them to impure cherts (Fig. 4), and carbonate replacement is common in many coarser grained terrigenous and volcaniclastic beds. Most primary silicate minerals except quartz (Fig. 4) and zircons have been replaced or recrystallized. Nonsilicate primary constituents, such as detrital spinels, barite, pyrite, and carbonaceous matter, are commonly well preserved. Feldspars and dacitic volcaniclastic rocks are now recrystallized micromosaics of micas, mainly sericite, fine-grained quartz, and minor opaque oxides (Fig. 4). Shear fabrics are not widely developed.

Volcaniclastic deposits (V)

Although the Onverwacht–Fig Tree contact is traditionally regarded as marking the transition from volcanic to sedimentary stages of greenstone belt evolution, perhaps 50% of the Mapepe Formation is composed of altered dacitic tuff (Vt). Most tuffaceous units consist mainly of fine-grained, light gray, tan or buff weathering, porous, earthy rock. The presence of quartz and altered plagioclase phenocrysts (Fig. 4), the extreme homogeneity of the debris, and trace element and rare earth element (REE) patterns (Lowe, this volume, Chapter 3) indicate that these represent dacitic volcaniclastic rocks. Shards are rarely preserved. Locally, dacitic tuffs have been silicified and now consist of medium bluish to greenish gray chert. Many tuffaceous rocks show both silicification and carbonation and consist of medium to light gray, brownish- to light gray–weathering, punky, chert-carbonate rock.

Two lithofacies can be distinguished: fall (Vtf) and current (Vta and Vtb) deposits.

Fall deposits (Vtf). Fall-deposited tuff ranges from massive or thickly bedded to finely laminated (Fig. 5A). Massive deposits lack structures, grading, and well-defined sedimentation units. Crude stratification, defined by vague flat parting

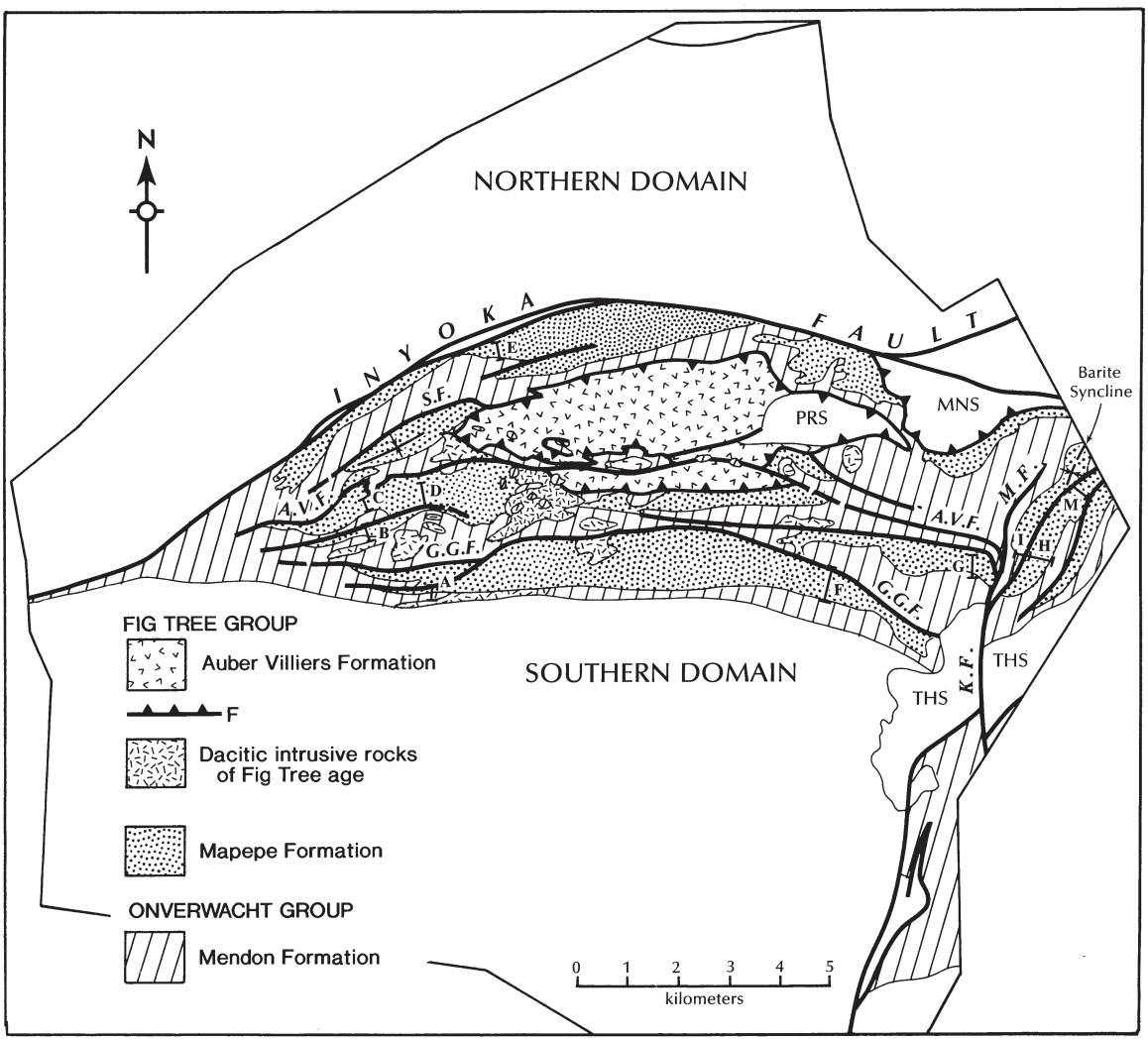


Figure 1. Geology of the central part of the study area showing the distribution of rocks of the Mendon Formation (Onverwacht Group) and Mapepe and Auber Villiers Formations (southern facies of the Fig Tree Group). Heavy lines designate major faults. The Mapepe Formation crops out along the northern edge of the Southern Domain, bounded on the north by the Granville Grove fault (G.G.F.) and the east by the Kromberg fault (K.F.); the West-Central Domain, between the Granville Grove and Mbema (M.F.) faults on the south and the Inyoka fault on the north; and the East-Central Domain, lying east of the Kromberg and Mbema faults. Faults discussed in text within the West-Central Domain include the Schultzenhorst fault (S.F.) and the Auber Villiers fault (A.V.F.). Main areas of outcropping younger Moodies Group include the Powerline Road syncline (P.R.S.), Main-of-the-Mists syncline (M.N.S.), and The Heights Syncline (T.H.S.). Letters A through I and M show location of measured sections shown in Figures 2, 3, and 15.

planes, is common. Quartz and feldspar phenocrysts, where present, are more-or-less uniformly dispersed in a matrix of altered ash (Fig. 4). Laminated fall deposits show flat, millimeter- to centimeter-thick laminations that are commonly, but not always, normally graded (Fig. 5A). The abundance of normal grading and paucity of current structures suggest that these represent fall layers. Sparse cross-sets are made up of hydraulically concentrated coarser grains lacking finer ash. Fall units make up an estimated 30–60% of the Mapepe Formation.

Current-worked volcaniclastic deposits (Vta and Vtb). Much of the pyroclastic debris falling into the Mapepe sea was reworked by currents (Fig. 5B). Current-deposited tuff ranges from isolated form sets and thin current-laminated zones within fall deposits to thick sequences of current-structured tuff. Because of the homogeneity of the tuff, field discrimination of fall and current deposits is difficult. Obvious current features, such as scour, cross-stratification, admixed detrital chert grains, and ash-clast conglomerate, are only locally present. Hydraulic segregation of coarser and finer ash into discrete laminations provides the most consistent criterion for recognizing current-deposited layers.

Distinguishable subfacies include rhythmically layered tuff

TABLE 1. MAJOR PETROLOGIC GROUPS AND LITHOFACIES OF THE MAPEPE FORMATION

Petrologic Group (Symbol)	Lithofacies Symbol	Lithofacies Description and Deposition
Volcaniclastic Deposits (V)		
	Vtf	Fall deposited tuff
	Vta	Rhythmically layered tuff deposited by turbidity currents
	Vtb	Current-structured tuff deposited in shallow water
Terrigenous Deposits (T)		
	Tm	Shale and mudstone
	Ts	Sandstone
	Tsa	Rhythmically layered sandstone deposited by turbidity currents; includes thin-bedded, more distal units interbedded with mudstone or tuff (Tsa_1) and thick-bedded, more proximal deposits (Tsa_2)
	Tsb	Non-turbiditic, current-structured sandstones; deposited in shallow water
	Tg	Conglomerate
	Tga	Conglomerate deposited subaqueously by sediment flows
	Tgb	Conglomerate deposited subaerially by fluid and sediment flows
Orthochemical Deposits (O)		
	Ob	Barite
	Ocj	Jasper and iron formation
	Oc	Chert
	Ocf	Banded ferruginous chert. commonly sideritic
	Od	Carbonate
	Ocd	Silicified carbonate
	Oct	Colorless translucent chert

deposited by surges, interpreted as turbidity currents (Vta), and non-rhythmically layered, current-structured tuff (Vtb). Rhythmically layered tuff (Vta) shows thin, rhythmic sedimentation units reflecting deposition from declining surges, interpreted to have been turbidity currents. Sedimentation units, averaging 1 to over 15 cm thick, are made up largely of Bouma T_b, T_c, and T_d divisions (Fig. 5b). Current-structured, non-rhythmically layered tuff (Vtb) is a minor lithofacies in the Mapepe Formation (Fig. 3, top section F). This lithofacies consists of fine- to medium-grained, moderately- to well-sorted tuff showing upper-stage flat lamination, cross-lamination, and large-scale cross-stratification up to 2.5 m high. Organized sedimentation units indicating deposition by currents of declining velocity are lacking.

Terrigenous Clastic Sediments (T)

Mudstone and Shale (Tm). Mudrocks occur throughout the Mapepe Formation but only locally form units more than a few meters thick. A basal unit of shale and hematitic shale as much as 100 m thick is present at the base of the formation below the Manzimnyama Jaspillite Member (Heinrichs, 1980) in the southernmost outcrop belt on the west limb of the Onverwacht anticline (Figs. 2 and 3). Thinner units of mudstone, from 1 to 20 m thick, occur interbedded with sandstone and fine-grained ash in the upper part of the formation.

Sandstone (Ts). Sandstone derived by the weathering and erosion of older rocks is present in lenticular units throughout the Mapepe Formation, but is most abundant in the upper part. Two subfacies are recognized: Tsa, rhythmically bedded sandstone deposited by turbidity currents, and Tsb, current-structured sandstone deposited by nonsurging currents.

Rhythmically layered sandstone interbedded with mudstone or tuffaceous units is a major rock type within the Mapepe Formation. It includes (Tsa_1), thin-bedded sandstone interbedded with tuff or mudstone, and (Tsa_2), thick-bedded, medium- to very coarse-grained, locally conglomeratic sandstone. Thin,

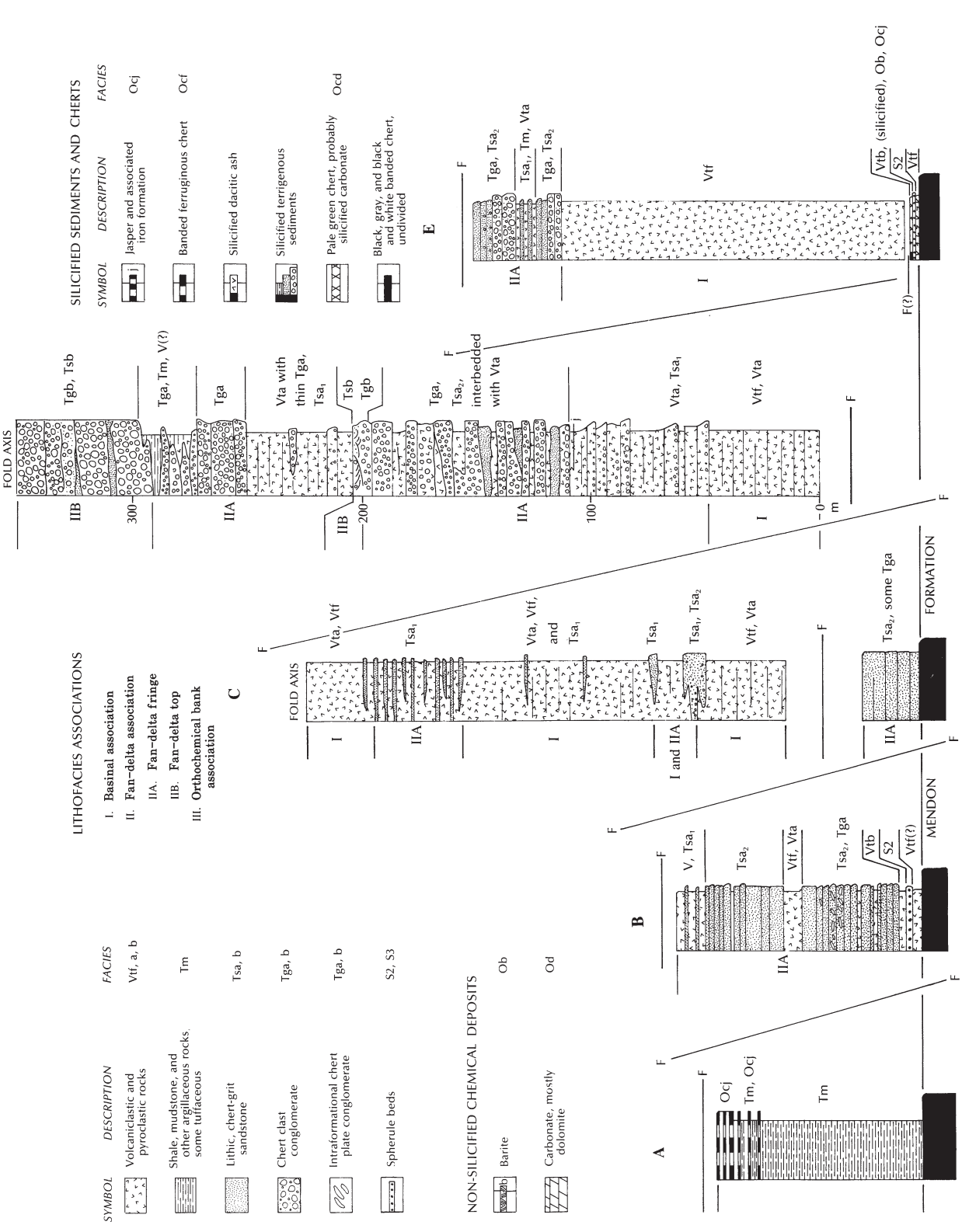


Figure 2. Stratigraphic sections of the Mapepe Formation in the western part of the study area. Sections are arranged from south (left) to north (right) and are located on Figure 1. Most are separated by major faults, indicated by lines labeled "F" between columns. Scale same for all columns. See Table 1 for full explanation of facies symbols.

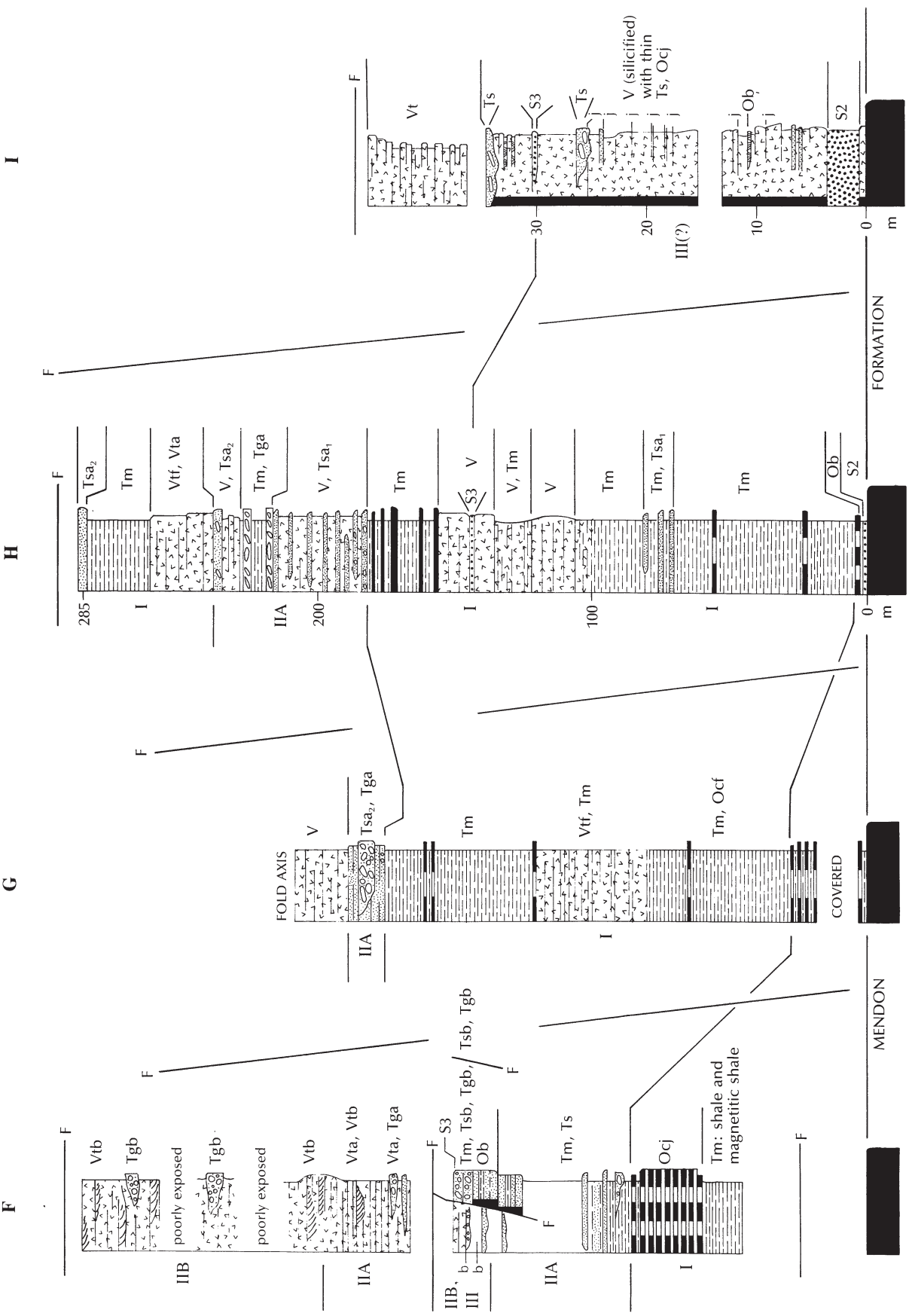


Figure 3. Stratigraphic columns of the Mapepe Formation in the eastern part of the study area. Scale same for columns F, G, and H. Black shading along left side of columns F (center) and I designates units silicified to form chert. Most columns are separated by major faults, indicated by lines labeled "F" between columns. See Figure 2 and Table 1 for full explanation of facies symbols.

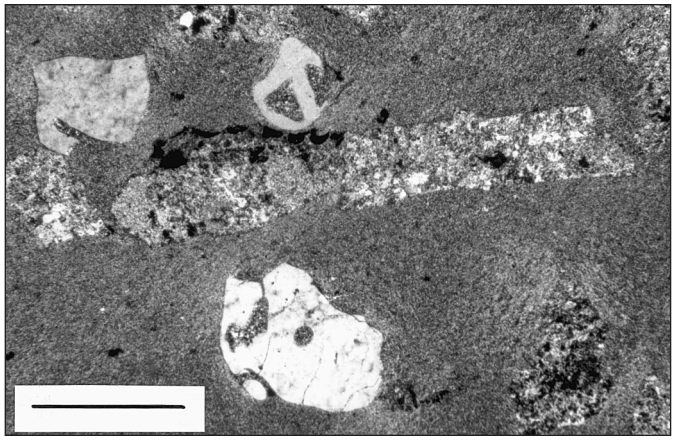


Figure 4. Photomicrograph of fall-deposited dacitic tuff (lithofacies Vtf) in Mapepe Formation. Phenocrysts include quartz (white) and lath-shaped plagioclase, which has been entirely replaced by micromosaic of quartz and phyllosilicate minerals. Groundmass is recrystallized ash and dust, now composed of intergrown microquartz and sericite. Scale bar is 1.0 mm.

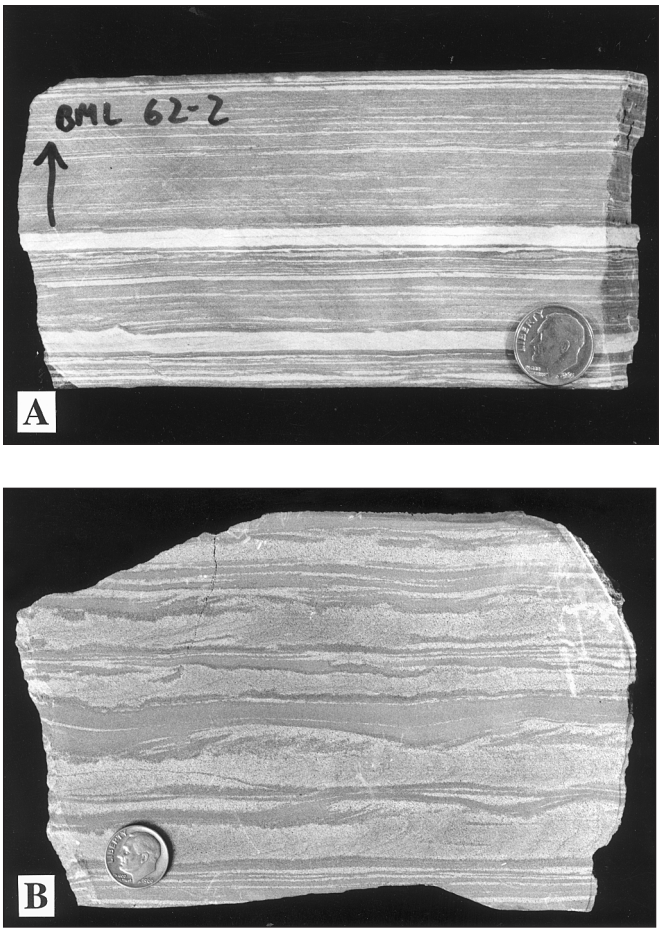


Figure 5. Tuffaceous lithofacies (Vt) in the Mapepe Formation. A, Finely laminated, probably fall-deposited dacitic tuff (lithofacies Vtf). Finer grained layers show iron-oxide staining (darker gray). Sparse, thin, lenticular white streaks in upper half of slab are hydraulically segregated coarser grained zones. B, Current-structured dacitic tuff (Vta) showing climbing-ripple cross-laminated layers (Bouma T_c divisions) draped by finer grained laminated units representing Bouma T_d divisions (dark). These cyclic T_{cd} sedimentation units appear to record low-energy surging currents, probably turbidity currents. Scale coin in both photos is 1.75 cm in diameter.

graded beds of fine- to medium-grained sandstone (Tsa_1) within thicker units of mudstone and shale (Fig. 3, section H), commonly showing Bouma T_a, T_b, and T_c divisions, are interpreted to have been deposited by turbidity currents. Many sections include graded sedimentation units composed of terrigenous sandstone and dacitic tuff (Fig. 2, section C; Fig. 3, section H, 180–220 m) from 1 to more than 50 cm thick (Nocita and Lowe, 1990, Fig. 5). Most beds greater than 20 cm thick show coarse- to medium-grained T_a and T_b divisions of chert-grit sandstone overlain by medium- to fine-grained, light gray, tuffaceous T_b, T_c and T_d divisions (Nocita and Lowe, 1990, Fig. 5a). These beds were deposited by turbidity currents containing mixed but hydraulically contrasting populations of coarse, dense cherty terrigenous debris and fine, lower-density ash and dust. Interflow units are composed largely of ash, suggesting that the currents may have initially carried only terrigenous sediment and eroded the ash en route.

Thick-bedded units of rhythmically bedded sandstone (Tsa_2) include (a) a near-basal unit 100 m thick in the western part of the study area (Fig. 2, section B), and (b) sandstones associated with conglomerates in the middle and upper parts of the formation throughout the study area, including the Gelagela Grit in the East-Central Domain (Heinrichs, 1980; Fig. 2, sections D and E). Individual beds are generally 20 cm to 1 m thick and composed largely of massive or normally graded, medium- to coarse-grained, poorly sorted, subangular, lithic sandstone (Nocita and Lowe, 1990, Fig. 10). Interbedded chert-clast conglomerate (Tga) is common. Current structures are absent in most beds (Nocita and Lowe, 1990, Fig. 10), but a few show flat laminations at the tops. Interbedded sequences of mudstone or tuffaceous rock commonly contain thin current-deposited layers made up of Bouma T_{bcd} divisions. Scour marks are present on the bases of some beds. The abundance of massive to normally graded sandstone layers, rare sole marks, lack of traction structures, and association with thin-bedded turbidites suggests that these beds are made up of T_a and T_{ab} divisions deposited by high-density turbidity currents.

Non turbiditic sandstones (Tsb) are only sporadically developed in the Mapepe Formation. Most are 2–20 m thick and consist of medium- to very coarse-grained, poorly sorted, commonly conglomeratic lithic sandstone showing cross-stratification, flat lamination, and other evidence of deposition from energetic, non-surging currents. These sands are lenticular, generally lack well-defined sedimentation units, and show abundant scour features. Lithofacies Tsb is commonly interbedded with conglomerates of facies Tgb.

Conglomerate (Tg). Although thin conglomeratic units occur throughout the Mapepe Formation, thick conglomerates

are best developed toward its top (Figs. 2 and 3), where they have been interpreted as fan-delta deposits (Nocita and Lowe, 1990). Two conglomerate subfacies are recognized: Tga, well-stratified; generally well sorted; massive, normally graded, or inversely graded polymictic conglomerate deposited by surging sediment gravity flows; and Tgb, massive to poorly stratified conglomerate deposited by nonsurging flows.

Tga units range from less than a meter to more than 30 m thick and generally include both coarse, well-stratified pebble to cobble conglomerate and interbedded lenses of granule conglomerate and coarse-grained, massive to normally graded sandstone (Fig. 6A). Pebble to cobble conglomerate beds range from 20 cm to more than 1 m thick, consist of well-rounded, highly spherical chert clasts as much as 20 cm in diameter, and can be massive, normally graded (Fig. 6A), or inversely graded (Nocita and Lowe, 1990, Fig. 7). Most are clast supported but a few consist of massive sandstone containing dispersed chert clasts. The common presence of inverse and/or normal grading and absence of current structures in both the conglomerates and interbedded sandstones suggest that these units were emplaced by sediment flows (Nocita and Lowe, 1990).

Another common variety of Tga conglomerate is composed of platy clasts of translucent or white-weathering chert in a sandstone. Such chert-plate conglomerates (Lowe, this volume, Chapter 3, Fig. 15B) are most common in sequences of Tsa-type turbiditic sandstones. Because some of the chert clasts were apparently soft and deformed during transport, they may represent intraclasts derived by local erosion within the depositional system.

Tgb includes a variety of massive to crudely stratified conglomerate composed of clast-supported, well-rounded pebbles and cobbles of chert (Fig. 6B). The matrix in most is poorly sorted lithic, commonly tuffaceous sandstone. These rocks have been described in detail by Nocita and Lowe (1990). Normally graded compound units with scoured bases, representing channels, occur but are greatly subordinate to massive, structureless conglomerate. Inversely graded beds are rare. Sedimentation units are not well defined and individual beds are lenticular and characterized by rapid lateral variations in thickness and texture. Associated sandstone beds show abundant cross-stratification. The rocks most closely resemble conglomerate deposited by stream flow and sheetflow (sheetfloods) in braided alluvial systems (Nemec and Steel, 1984; Hein, 1984).

Distinctive lenticular conglomerates associated with barite deposits in the eastern part of the study area are composed of well rounded, well-sorted polymictic chert clasts. Most had no interstitial matrix and are now cemented by authigenic microquartz but some show a matrix of fine-grained, greenish carbonate and chert, apparently representing silicified carbonate (Lowe and Knauth, 1977, Fig. 18B). Evidence for scoured basal contacts and lenticular geometry indicate that these conglomerates were deposited in channels. The sorting, lack of a sandy matrix, presence of a local carbonate matrix, and association with shallow-water orthochemical units suggest that the channels may have been tidal channels crossing low-energy intertidal or shallow subtidal flats.

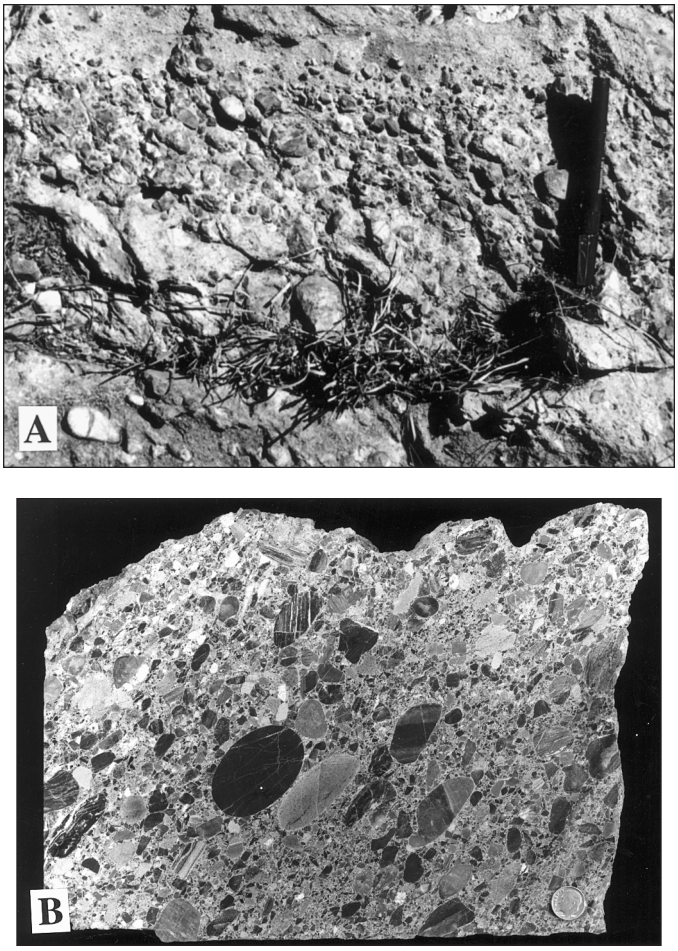


Figure 6. Conglomerate lithofacies Tg. A, Normally graded conglomerate (Tga) deposited by submarine sediment flows on fan-delta front. B, Slab of poorly sorted conglomerate of lithofacies Tgb composed of clasts of black chert, dacitic volcaniclastic rock (large light gray clast near center), and various layered and banded chert types. Elongate clasts are parallel to bedding, which runs from lower left to upper right.

Orthochemical deposits (O)

Bedded barite (Ob). Barite deposits in southern-facies Fig Tree rocks have been discussed by Visser (1956), Perry et al. (1971), Vinogradov et al. (1976), Heinrichs and Reimer (1977), Lowe and Knauth (1977), Dunlop and Groves (1978), and Reimer (1980, 1982). Regionally, two main barite zones can be identified (Figs. 2 and 3): (1) in western areas, a thin zone of barite at the base of the formation, 0.5–2 m above cherts at the top of the Onverwacht Group, and (2) in eastern areas, one or more barite zones near the middle of the formation (Fig. 3, sections F and I). The latter unit was named the Heemstede Barite Member by Heinrichs (1980). Other thin barite units occur locally (Fig. 3, section I).

Barite is present discontinuously near the base of the Mapepe Formation in both the West-Central (WCD) and western East-Central (ECD) Domains (Lowe et al., this volume, Chapter

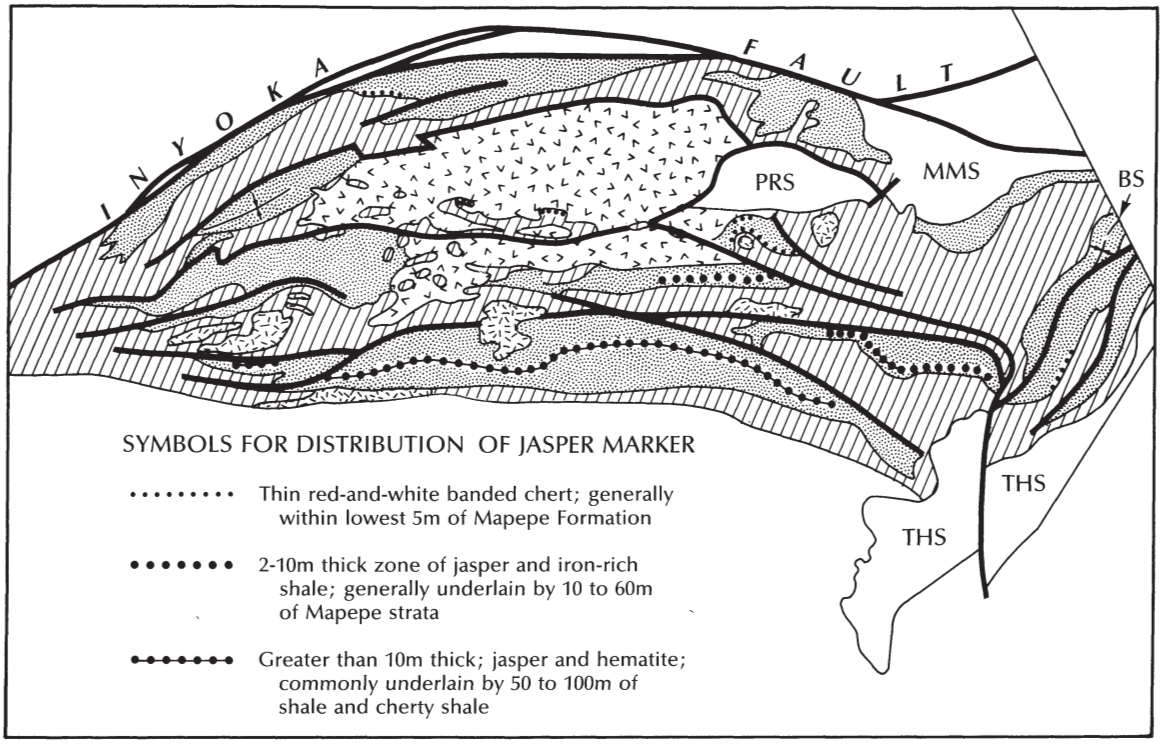


Figure 7. Map showing the distribution and facies of the Manzimnyama Jaspillite (Heinrichs, 1980) and related units on the west limb of the Onverwacht anticline. Symbols as in Figure 1.

2) in sections where the Manzimnyama Jaspillite is absent. It occurs in units less than 50 cm thick made up of beds of bladed barite and barite sand, 2–10 cm thick. This barite is interbedded with silicified volcaniclastic units and closely overlies spherule bed S2 (Lowe and Byerly, 1986; Lowe et al., 1989). The lack of muddy layers, the common presence of cross-lamination in interbedded units of silicified ash and barite sand, and absence of turbiditic layers suggest deposition in a shallow, current-active environment, similar to those characterizing sedimentation throughout much of the Onverwacht Group (Lowe, this volume, Chapter 3).

The higher barite unit occurs only in the easternmost part of the WCD (section F, Fig. 3) and in the ECD, including the Barite syncline. It marks a complex zone of unusual rock types, rapid facies changes, and local uplift and erosion termed the Proto-Inyoka Zone (Heinrichs and Reimer, 1977; Reimer, 1980, 1982) and interpreted as marking uplift on the nascent Onverwacht anticline (Lowe et al., this volume, Chapter 2). Barite is present as detrital barite sand, secondary barite blades, and clusters of upward-diverging barite blades termed "cauliflowers" (Heinrichs and Reimer, 1977). Both the detrital and cauliflower barite have been interpreted as primary sediments deposited in shallow water around and upon local uplifts (Heinrichs and Reimer, 1977; Reimer, 1980, 1982). Dunlop and Groves (1978) suggested that the cauliflower barite may represent replaced gypsum.

Jasper and iron formation (Ocj). A zone of iron-rich sediments, including jasper, hematitic shale, and oxide-facies iron formation (Beukes, 1973), named the Manzimnyama Jaspillite Member (MJM) by Heinrichs (1980), is present near the base of the Mapepe Formation in many southern sections (Figs. 2, 3, and 7) and has been mined for iron ore in adjacent Swaziland. Where thickest, the MJM is made up of centimeter-scale banded hematite and jasper (Lowe, this volume, Chapter 3, Fig. 17). The MJM reaches 20 m thick in the Southern Domain (SD) on the west limb of the Onverwacht anticline, where it is underlain by as much as 100 m of fine-grained sediments, mostly shale (Fig. 2, section A). To the north and northeast, the unit becomes thinner and less ferruginous and consists of thin jasper layers interbedded with shale. Sand-sized and coarser detritus and current structures are absent in the MJM. It was deposited under quiet, deep-water conditions.

Layers of jasper 10–30 cm thick occur elsewhere in the Mapepe Formation. A distinctive zone of barite, jasper, chert, and tuff marks the base of the formation in northwestern sections where the MJM is absent. Other thin jasper beds are commonly associated with barite and carbonate, especially in the Barite syncline, and jasper clasts are locally abundant in fan-delta conglomerates in the lower half of the formation.

Banded ferruginous chert (Ocf). Thin beds of banded, iron-rich chert, generally less than 0.5 m thick, are interbedded with shale in the lower part of the formation in southern areas (Figs. 2 and 3). The rock consists of alternating bands, 0.5–2 cm thick, of milky-weathering chert and siliceous, rusty red to tan weathering, commonly finely laminated rock. Fresh outcrops were not

seen but similar rocks in the Mendon Formation and northern-facies Fig Tree Group consist of alternating chert and cherty carbonaceous siderite bands (Lowe, this volume, Chapter 3, Fig. 16). They lack visible detrital particles and current structures and accumulated in quiet, probably relatively deep-water areas removed from major sources of clastic debris.

Carbonate (Od) and silicified carbonate (Ocd). Beds of pale to bright green and gray cherty limestone, dolomite, and calcareous chert are associated with barite and jasper in the middle part of the Mapepe Formation in the Barite syncline and along strike to the northeast. The abundance of preserved carbonate and the paucity of terrigenous and volcaniclastic materials suggest that these rocks represent primary carbonate and silicified carbonate deposits. Veizer et al. (1982) and Veizer (1983) have suggested that they include some of the least altered carbonates of early Archean age.

Primary textures and structures are well preserved, especially in the more siliceous and coarser-grained sediments. The original sediments ranged from fine mud to coarse-grained sandstone and from nearly pure carbonate to complex mixtures of carbonate and siliceous detritus. Fine-grained layers consist of finely laminated to massive chert containing variable amounts of intergrown dolomite. Many fine- to medium-grained carbonate sands include detrital chrome-rich spinels surrounded by bright green alteration halos, accounting for the common green color of the rock, and only trace amounts of coarse quartz and lithic detritus. Coarse-grained, generally well sorted sandstones are composed of carbonate mixed with coarser, angular, locally derived grains of translucent chert (Oct), minor amounts of jasper, and as much as 5% angular coarse monocrystalline quartz. A few beds contain coarse detrital muscovite.

Many carbonate layers are conglomeratic, consisting of clasts of translucent chert (Oct) set in a well-sorted, fine-grained carbonate and silicified carbonate sand matrix (Lowe, this volume, Chapter 3, Fig. 15A). Current structures are abundant, including cross-lamination, large-scale cross-stratification, and scoured bed bases. Sand deposition took place in shallow water under the influence of strong, commonly erosive currents.

Colorless translucent chert (Oct). Carbonate, silicified carbonate, and barite in the Barite syncline include thin layers of colorless, fine-grained, translucent chert. These layers have been eroded to form units of chert-clast conglomerate (Lowe, this volume, Chapter 3, Fig. 15A). The chert, except for dispersed carbonate rhombs, black carbonaceous (?) matter, and fine pyrite grains in some layers, is essentially pure silica. Textural evidence for detrital precursors is absent.

These chert layers cannot be directly correlated with any of the recognizable volcaniclastic, terrigenous, or other orthochemical deposits in the Mapepe Formation. They could represent primary siliceous deposits.

FACIES ASSOCIATIONS

Rocks in the Mapepe Formation comprise three main facies associations that can be identified with major depositional settings: (1) a basinal association, (2) a fan-delta association, and (3) a shallow-water association (Figs. 2 and 3).

Basinal Association

The basinal association includes sediments deposited under quiet subaqueous conditions in areas removed from sources of coarse terrigenous debris. It is composed largely of mudstone and shale (Tm), fall-deposited tuff (Vtf), and, locally, jasper and iron formation (Ocj) and banded ferruginous chert (Ocf). This association dominates in the lower parts of the Mapepe Formation, although lithofacies vary from place to place. In general, terrigenous and precipitative lithofacies predominate in sections in the ECD and southernmost WCD and volcaniclastic lithofacies dominate to the northwest. Basinal units, mainly volcaniclastic sediments, separate and surround fan-delta and local bank sequences in the middle and upper parts of the formation. Basinal deposits probably make up 60–70% of the Mapepe Formation.

Fan-delta association

The Mapepe sea included land areas that served as sources of detrital sediment and sites of alluvial and shallow-water sedimentation. Throughout the middle and upper parts of the formation, units of coarse terrigenous chert-grit sandstone and chert-clast conglomerate record the formation and erosion of these sources. These units make up the fan-delta association. This association includes fan-delta front and fan-delta top subfacies.

Fan-delta front. Most fan-delta sequences in the Mapepe Formation are made up largely of coarse-grained sediment gravity flow deposits of facies Tsa and Tga (Nocita and Lowe, 1990). These constitute the fan-delta front. Distal parts of the fan-delta front consist of thin, mixed terrigenous and tuffaceous turbidites of facies Tsa_1 interbedded with fine tuffaceous basinal deposits (Vtf). Shale units are rare. In thick conglomeratic fan-delta units south of the Auber Villiers fault (Nocita and Lowe, 1990, Fig. 3), distal turbidites (Tsa_1) can commonly be traced into coarser grained, more proximal fan-delta front units of coarse sandstone (Tsa_2) and conglomerate (Tga) from a few meters to 50 m thick. This transition can be seen by comparison of section C and the middle part of section D (Fig. 2).

Individual conglomeratic sedimentation units in the proximal fan-delta front are generally 20–70 cm thick and commonly inversely or normally graded (Fig. 6A). Most thick, compound, proximal fan-delta front units, 5–50 m thick, however, lack regular grading. A few coarsen upward, whereas others coarsen upward to the middle of the unit, then fine to the top. At their tops, most fine over a stratigraphic interval of 1–2 m into overlying fine-grained sections. Few, if any, fine upward throughout. Most appear to represent coarse, subaqueous fan-delta channels or gravel lobes. The thickest sequences consist of numerous lenticular sandstone and conglomerate channel/lobe units separated by fine-grained, thin bedded turbiditic sandstone, shale, and tuff (Fig. 2, section D).

Immediately south of the Inyoka fault (Fig. 1), tuffaceous strata and fan-delta conglomerates form a coarsening-upward section that exceeds 300 m thick (Fig. 3, section E). The section includes a basal unit, more than 100 m thick, of fine-grained, fall-deposited water-laid felsic tuff (Vtf) overlain by 50–100 m of sediment-flow deposited pebble and small-cobble conglomerate (Tga) and turbiditic sandstone (Tsa_2) capped by more than 100 m of thickly bedded, coarse-pebble to coarse-cobble conglomerate (Tga) with interbedded finer grained tuffaceous and sandy intervals. The lowest conglomerates in this sequence provide a representative section of subaqueous fan-delta front deposits (Fig. 8). The section is an overall normally graded unit about 9 m thick. The lower 6.5 m consists largely of conglomerate (Tga). Clasts, as much as 22 cm in diameter, are composed of chert representing a variety of silicified sedimentary and igneous rock types. Silicified mafic and ultramafic volcanic rocks were not seen; silicified dacitic debris makes up less than 5% of the clasts. Inversely graded conglomerate beds, 10–40 cm thick, predominate in the lower 2 m and massive, ungraded beds from 2–6.5 m. The few conglomerate units above 6.5 m are normally graded. This sequence reflects deposition from coarse, high-density turbidity currents. Sandstone beds (Tsa_2), abundant above 6.5 m, are coarse- to very coarse-grained and commonly pebbly from 6.5 to 9 m, and there are more-or-less equal amounts of normally graded and massive beds. Faint flat current laminations occur near the tops of some beds. Interlayered fine-grained sediments are mostly thin, argillaceous units. These sands record deposition of coarse sediment by rapid fallout from suspension from dense, sandy turbidity flows. Finer grained sand and silt largely bypassed this area at this time. Above 9 m, the section consists of thin, 5- to 15-cm-thick turbidites showing well-developed Bouma sequences and documenting the continuing decline in local current activity.

Higher in this sequence, similar subaqueous sediment-flow dominated facies are developed that pass upward into thick, alluvial conglomerates and sandstones. This sequence appears to have been deposited along the front and base of a fan-delta during an interval of progradation (coarsening-upward base) and subsequent retrogradation (fining-upward top).

Fan-delta platform. The sediment-gravity-flow-dominated fan-delta front sequences are commonly overlain or grade laterally into shallow-water or subaerial fan-delta top or platform deposits consisting mainly of coarse Tgb-type conglomerate and current-worked Tsb sandstone. One of the thickest conglomeratic sequences in the Mapepe Formation occurs on farm Auber Villiers 719 JT in the west-central part of the study area (Fig. 2, section D). This section has also been discussed by Nocita and Lowe (1990, Figs. 9 and 12). Nearly 350 m of strata are exposed in a structurally complex syncline that is sheared and disarticulated along its northern margin and cut by large faults on the south. These rocks have been studied by Nocita (1986), who concluded that they formed as one or more fan deltas. Underlying and laterally equivalent to the coarse fan-delta deposits are tuffaceous basinal sediments of facies Vtf and Vta (Fig. 2, section D). The

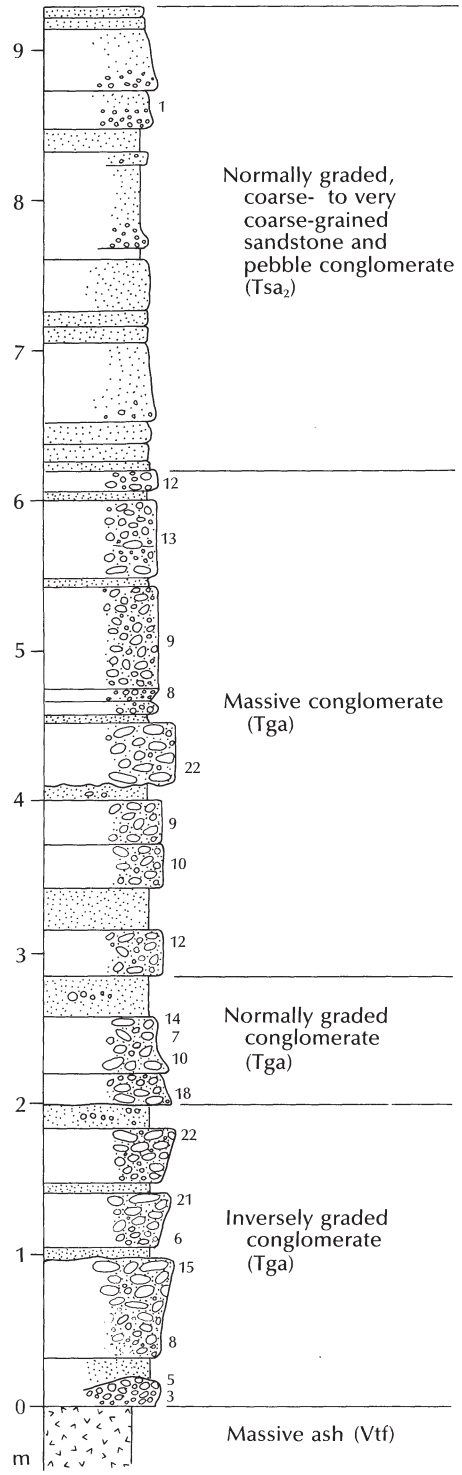


Figure 8. Section of conglomeratic sediment flow deposits developed on subaqueous fan-delta front (Fig. 2, section E, top), including conglomerate (Tga) and sandstone (Tsa). Lower conglomerate beds show well-developed inverse grading and upper conglomerate and sandstone are massive to normally graded. Numbers next to beds indicate maximum clast diameter (in cm) at that point.

thick fan-delta front sequence includes distal ash-rich (Vta) and mixed terrigenous-ash (Tsa_1) turbidites, proximal thick-bedded sandstone (Tsa_2), and conglomerate (Tga). Near the middle (200 m, section D, Fig. 2) and at the top of the section, coarse fan-delta-front sediment flow deposits grade upward into fan-delta platform sandstone (Tsb) and conglomerate (Tgb) deposited by energetic, nonsurging currents. These fan-delta platform deposits include both alluvial deposits and well-sorted, shallow-water, current-worked sands.

This sequence documents the build-up of an alluvial and fan-delta system draining a complex orogenic and volcanic source. The lower half of the section records the construction and abandonment of a series of large subaqueous fan-delta-front sand and gravel lobes and/or channels. The cross-stratified fan-delta-platform sandstone and conglomerate near the middle of the sequence record an interval of progradation and/or shoaling and exposure of the uppermost parts of the fan delta. Following deposition of another predominantly fine-grained basinal section, perhaps during regional submergence, renewed coarse sedimentation resulted in the buildup of the fan-delta front capped above 290 m (Fig. 2, section D) by massive conglomerate recording the progradation of an alluvial system over the underlying fan-delta front succession.

Another largely volcaniclastic fan-delta unit occurs near the top of the Mapepe Formation in the northernmost SD on the west limb of the Onverwacht anticline (Fig. 2, top of section F). The lower part of the section (Fig. 9) consists of terrigenous coarse-grained sandstone and granule and pebble conglomerate interbedded with finely laminated tuffaceous sediments. The coarse terrigenous layers are massive and commonly contain floating clasts of chert. Both terrigenous and ash layers lack obvious current structures. This part of the section appears to reflect turbidity-current and debris-flow deposition of coarse terrigenous debris alternating with the deposition of fine ash by either fall or extremely low energy turbidity currents.

Above 5.2 m, the section is dominated by rhythmically layered ash showing tan and maroon color banding highlighting regular sedimentation units 1 to about 5 cm thick (Fig. 5B). Each sedimentation unit includes a massive or flat-laminated, fine-grained base overlain by a thinner zone of iron-stained, fine-grained, commonly cross-laminated sandstone and siltstone (Fig. 5B). Some units show load structures along their bases. Most appear to represent turbidites. Interbedded with these deposits are lenticular, deeply scoured channel fill units, 20–50 cm thick, composed of coarse-grained terrigenous sandstone containing rip-up clasts of the associated volcaniclastic sequence. The channel sandstones show pervasive large-scale cross-stratification.

Conglomerate makes up much of the section from 18.5 m to 22.0 m (Fig. 9). It is composed largely of intraformational clasts of volcaniclastic sediment, including many thin layers of imbricate, flat-pebble conglomerate of iron-stained siltstone and mudstone fragments eroded from the associated turbidite tops. Other clasts include black chert, probably representing silicified carbonaceous mudstone. These conglomerates are interbedded with largely flat laminated, rhythmically layered tuffaceous units. Above 22.0 m are 10+ m of tuffaceous strata showing interbedded rhythmically flat layered units and beds containing large-scale trough cross-stratification that locally reaches 2.5 m high.

This section represents a shoaling-upward sequence, possibly a fan-delta sequence composed largely of reworked volcaniclastic debris. The lowest strata were derived from both volcanic and terrigenous sources and were deposited mainly by turbidity currents. Higher in the section, channels are prominent. Currents were effective in moving and eroding debris within the channels and may have been responsible for depositing the finer grained, rhythmically layered turbidites outside of the channels as overbank units. There is no evidence for exposure, although the paucity of mud might result in an absence of desiccation cracks and mudchip conglomerates. Near the top of the section, conglomerates, including mudchip units, are present and are succeeded by tuffaceous beds showing abundant large-scale cross-stratification. These deposits clearly reflect deposition under the influence of strong currents, probably in relatively shallow water.

Shallow-water association

Shallow-water deposits not obviously associated with fan deltas occur at several localities within the Mapepe Formation. They apparently record shallow-water settings developed near to and upon local structural highs. A lenticular shallow-water unit of conglomerate (Tgb) and sandstone and siltstone (Tsb), 20+ m thick, is present in the middle Mapepe Formation in the northernmost SD on the west limb of the Onverwacht anticline (Fig. 3, section F, and Fig. 10). The base of the sequence is a distinctive layer of jasper and black chert about 30 cm thick formed by the silicification of very fine carbonaceous and probably sideritic ooze. A lenticular unit of coarse-grained sandstone and massive conglomerate (Tgb) about 4 m thick fills a channel eroded through the basal jasper in the western part of the outcrop (Fig. 10). The clasts are composed of laminated, translucent, white-weathering chert and jasper. The uppermost conglomerate is overlain by and interfingers with silicified siltstone and fine-grained sandstone in beds as much as 50 cm thick. Siltstone and sandstone units that interfinger with and immediately overlie the channel-fill conglomerate are well defined, alternate with thinner mudstone layers, and are commonly massive or have massive zones overlain by flat- and cross-laminated divisions. They appear to represent the deposits of surging currents, perhaps related to floods within the channel. Away from the channels, sandstone and mudstone layers are less separable. Muddy beds and laminations contain abundant coarser material, and both sandy and muddy beds show pervasive finely developed sedimentary structures (Figs. 11 and 12). Small-scale cross-lamination and flat current lamination are most abundant (Figs. 11A, B and 12A). Much of the cross-lamination represents oscillation ripples (Fig. 11A). Cyclic surge units are absent, but the fine interlayering of sand and muddy sediments indicates frequent fluctuations in current or

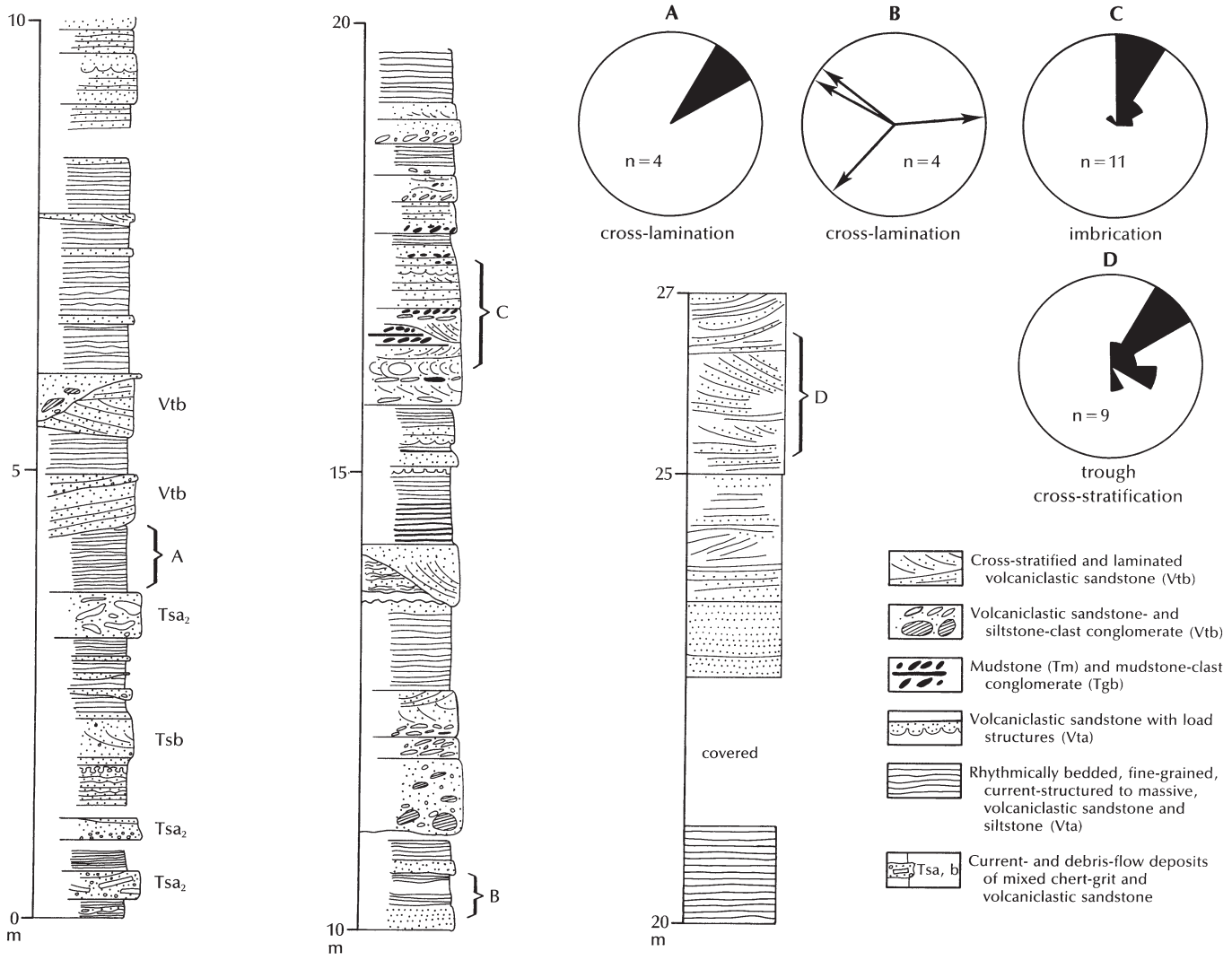


Figure 9. Detailed section of prograding, predominantly tuffaceous fan-delta sequence in upper half of section F, Figure 3. See Figure 2 and text for explanation of lithofacies symbols and abbreviations. Letters A–D adjacent to columns indicate those parts of section from which paleocurrent information shown in rose diagrams A–D was collected. Specific paleocurrent indicators used are given below the rose diagrams and the number of individual readings at each point in section by "n."

wave energy (Figs. 11A, B and 12B). Fluctuating energy levels are also shown by the presence of abundant thin, wispy mud flasers draping rippleforms within the sandstone layers (Fig. 12A) and thin sandstone laminations and lenticular form sets within muddy units. Large-scale cross bedding occurs locally, reaching 15 cm high (Fig. 12A). Many beds show load structures and convolute lamination (Fig. 11B).

The top of the fine-grained section is transitional into the overlying, coarse-grained units (Fig. 13). The uppermost 0.7 m of fine-grained strata are predominantly muddy, but include fine laminations of sandstone, most less than 1 cm thick. There are many thin sand lenses in this transition zone and, locally, sand-filled cracks (Fig. 12B), possibly mudcracks. This unit is overlain by series of cyclic, fining-upward units from 40 to 70 cm thick (0.9–2.5 m in Fig. 13). These layers grade from medium-grained, current-structured sandstone at the base through a middle zone of cross-laminated fine-grained sandstone to tops of finely interlaminated fine-grained sandstone and mudstone. Cross-bedding in the lower parts of the beds is as much as 15 cm high and the frequency of low-angle cross-sets suggests that the actual bedforms were still larger. One 15-cm-high cross-set showed well-developed reactivation surfaces.

The upper 6.5 m of section (2.5–9.0 in Fig. 13) forms a coarsening-upward sequence from medium-grained sandstone at the base to coarse, pebble and cobble conglomerate at the top. The lower meter consists mainly of medium-grained sandstone. Most beds are massive but some show flat laminations and large-scale cross-stratification. Dispersed clasts and conglomerate

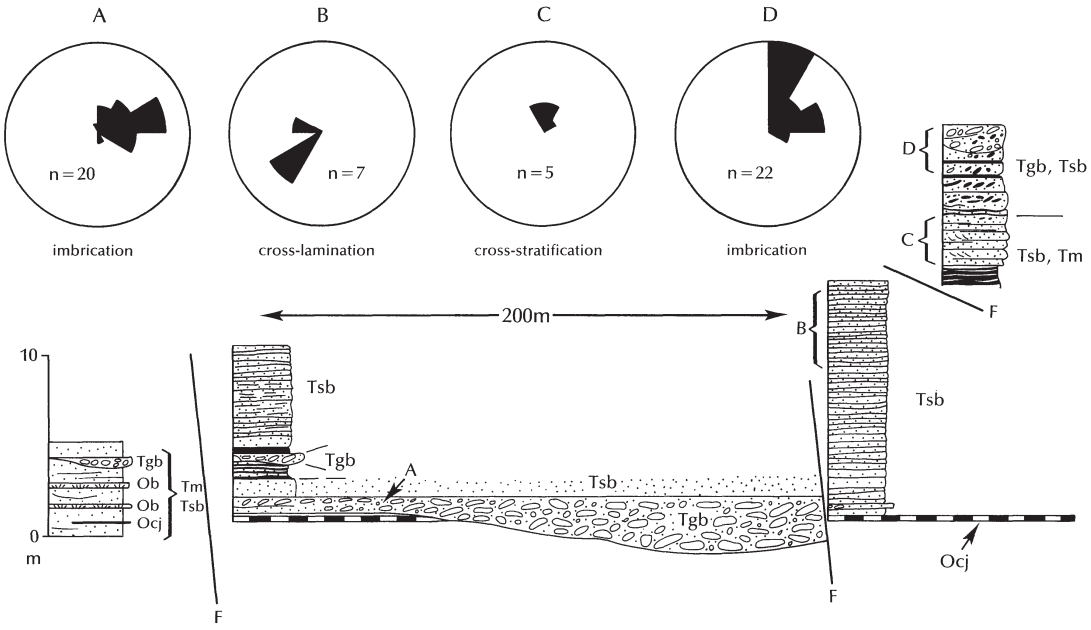


Figure 10. Generalized sections and local lithofacies of shallow-water and alluvial sequence at 120–140 m, section F, Figure 3. The outcrop is divided by a small fault, shown by line labeled "F" (far left), into a thick, clastic section east of the fault and a thin sequence west of the fault composed of volcaniclastic and terrigenous clastic units interbedded with bedded barite sand (Ob) and carbonate-matrix chert-pebble conglomerate. Letters A–D adjacent to columns indicate those parts of sections from which paleocurrent information shown in rose diagrams A–D was collected. Specific paleocurrent indicators used are given below the rose diagrams and the number of individual readings at each point in section by "n." Scale at left is the same for all sections. Details of the uppermost section at the right are shown in Figure 13.

lenses increase in thickness, proportion, and clast size upward (Fig. 13). Conglomeratic units show abundant evidence of current activity and scour. Deposition appears to have been by surging, poorly organized flows, sheetflows, and currents that were followed by intervals during which black, carbonaceous mud layers accumulated. There is little evidence for long-lived channels.

The sedimentology of this unit (Fig. 14) can be divided into four stages: (1) jasper and black chert, (2) interbedded mudstone, siltstone, fine-grained sandstone, and local conglomerate, (3) transitional units, and (4) upper coarse-grained conglomeratic sandstone.

The jasper and black chert unit represents fine-grained carbonaceous and ferruginous sediments that accumulated under quiet, probably subaqueous conditions with little or no coarse sediment influx. Most of the sediment probably settled as hemipelagic debris out of the water column. Overlying finely interlaminated siltstone, fine-grained sandstone, and mudstone shows abundant evidence of weak current and wave activity alternating with periods of mud deposition. This low-energy deposystem was crossed by channels filled with coarse, cherty conglomeratic debris. Sandy layers near conglomerate-filled channels originated through channel overbanking. Intervening areas were subject to fluctuating wave and current activity that reworked the predominantly fine-grained sediment, much of which may also have been introduced through the associated channels. The absence of mudcracks, mud-chip conglomerates, and other features indicative of exposure suggests that the environment was largely subaqueous. The presence of thick units of flat- and cross-laminated sands showing abundant wave structures, fluctuating current levels, and mud drapes and flasers suggests a very shallow-water site of deposition dominated by low-level wave and possibly tidal activity. Paleocurrents oriented at nearly 90° to those in underlying conglomeratic channel deposits and in overlying alluvial units support the inference that sediment movement was mainly in response to waves and tides.

The transitional units record the change from a low-energy, subaqueous regime to high energy, possibly subaerial deposition. The thick, predominantly mud unit with desiccation cracks at the top of the fine-grained section appears to mark the emergence of the depositional surface. The fining-upward cycles immediately above this layer could represent either small, low-gradient channels or tidalites, although none were seen to include mudcracks.

The capping sequence of coarse-grained sandstone and conglomerate reflects progradation of an alluvial sequence composed of debris derived from the immediately underlying Fig Tree sequence. Uplift had begun earlier, as indicated by the conglomerate and terrigenous sandstone units lower in the section, but had evidently stalled locally, permitting deposition of the intervening fine-grained sequence. The order of appearance of clasts in the capping coarse-grained section reflects progressively deeper erosion, first of immediately associated mudstone, then of jasper at the base of the fine-grained section, subsequently of deeper silicified sandstone units, and finally of the MJM, representing about 20–40 m of downcutting. Deposition was mainly by sheet or debris flow, although local current structures indicate





Figure 11. A, Finely structured interlaminated fine- to very fine-grained sandstone, siltstone, and mudstone. Sandy layers show abundant wave- and current-ripples draped by thin mud flasers. Load structures are developed along the bases of some sandy units. B, Load structures and convolute lamination in wave- and current-structured Tsb sandstone layers in shallow-water sequence.





Figure 12. A, Cross-stratified sandstone with muddy laminations (dark) in bottom sets. Set near center of photo is 6 cm high. B, Finely laminated sandstone and mudstone with sand-filled crack, probably a subaerial mudcrack.

more fluid flows. Interstratified mudstone and thinly bedded sandstone layers probably represent late-stage, slack-water events and perhaps interflood depositional processes.

In the eastern part of the study area on both the east and west limbs of the Barite syncline (Fig. 1) and along strike to the northeast, the middle part of the Mapepe Formation contains a distinctive suite of precipitative deposits, including bedded barite (Ob), carbonate (Od), and a variety of chert such as jasper (Ocj), silicified carbonate (Ocd), and translucent chert (Oct). Associated rocks include fine-grained, silicified, highly pyritic shale (Tm); intraformational, oligomictic, translucent-chert-clast and carbonate-clast conglomerate; silicified chert-clast conglomerate (Tgb) containing a matrix of silicified carbonate; silicified and carbonated dacitic ash (Vtf, Vta, and Vtb); and, locally, coarse, terrigenous chert-grit sandstone (Tsb). These lithofacies constitute the shallow-water bank association. It is well developed in the Barite syncline (Heinrichs and Reimer, 1977; Reimer, 1982). A similar but more restricted lithologic suite, including barite, jasper, and silicified and carbonated ash, marks the base of the Mapepe Formation over wide areas.

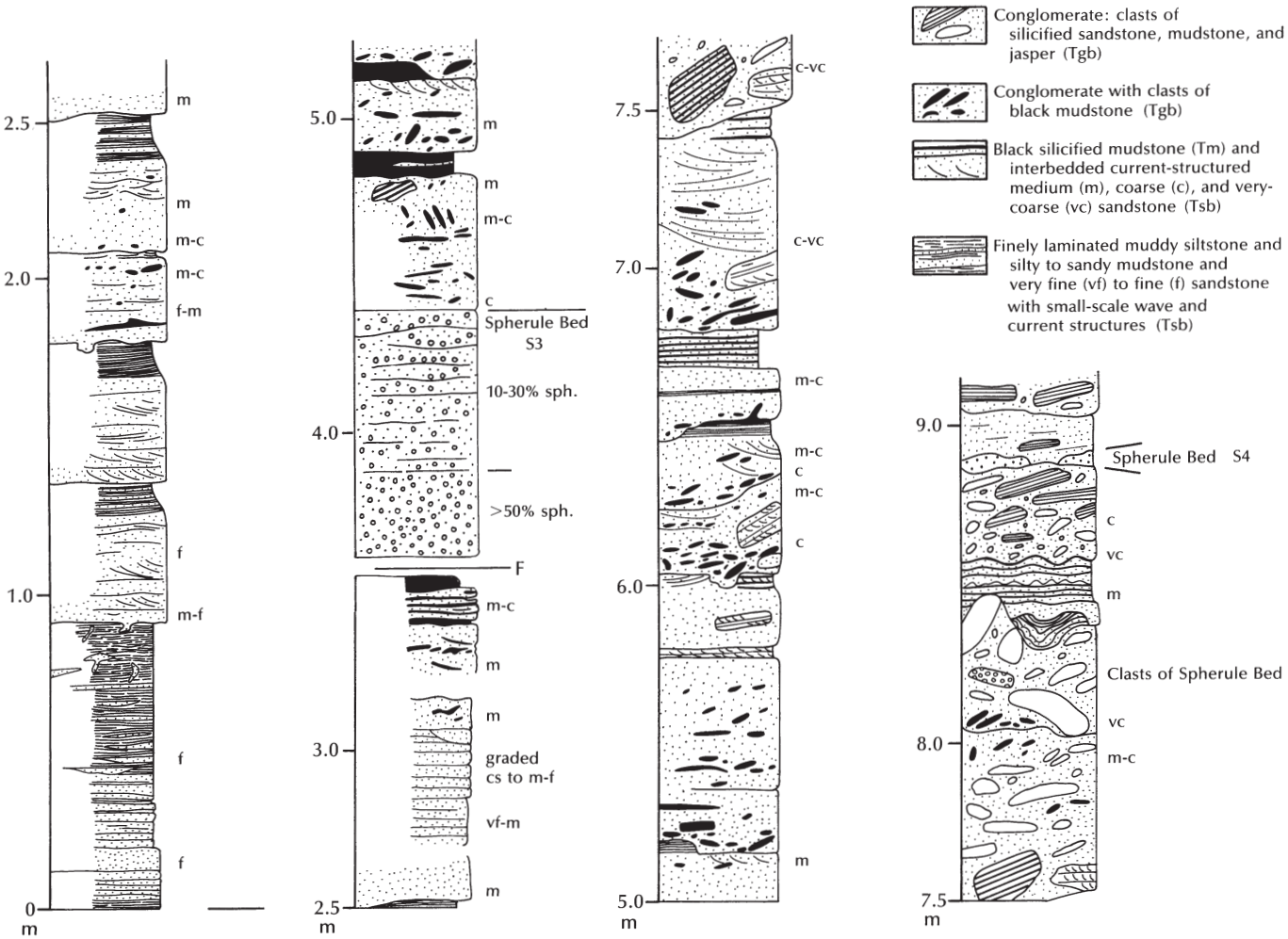


Figure 13. Detailed sections of the upper, conglomeratic part of the shallow-water and alluvial sequence shown at top right in Figure 10. Mudcracked and wave-rippled, very fine-grained sandstone and mudstone at the base of the section are replaced upward by alluvial intraformational mudstone-clast conglomerate and eventually by conglomerates containing debris derived by erosion of deeper levels of the Mapepe Formation.

The most completely exposed bank deposits are present in and north of the reference section of the Mapepe Formation (Figs. 1 and 15). The sharpness of the basal contact ("0" in sections, Fig. 15; 155 m in the reference section, Fig. 3, column H) and the lithologic diversity of immediately overlying rocks suggest the existence of a local unconformity at this point in the sequence. The lowest 20–30 m of strata above the inferred break include what may be the southern edge of a bank developed north of the sections shown. The overlying section includes a 20- to 40-m-thick sequence of sandy fan-delta deposits capped by a 20- to 35-m-thick largely precipitative bank sequence. Sections in Figure 15 provide a nearly complete bank cross-section. Less than 1 km north of section M, bank lithologies lens out into basinal deposits. The northernmost bank (Fig. 15, section M) includes two main types of deposits: (1) interbedded carbonate- and translucent-chert-clast conglomerate (Lowe, this volume, Chapter 3, Fig. 15A), cross-stratified carbonate sandstone, and silicified carbonate; and (2) fine, laminated carbonate mud, thin carbonate turbidites, carbonate channel conglomerate, and terrigenous shale. The first shows pervasive evidence of current activity. Many conglomerates show tight clast packing, well-developed imbrication, and excellent sorting of the fine- to medium-grained sandy matrix. These units are mainly current, not debris-flow deposits. Imbrication indicates paleoflow from east to west. Interbedded carbonate sandstones show abundant current structures, including low-angle cross-stratification. The second deposit type includes thin carbonate turbidites, carbonate- and chert-clast debris-flow deposits, and finely laminated carbonate and shale cut locally by small conglomerate-filled channels. These facies are interpreted to represent interbedded bank margin and upper bank slope deposits (Fig. 16).

The bank margin sequence passes southwest into bank-top

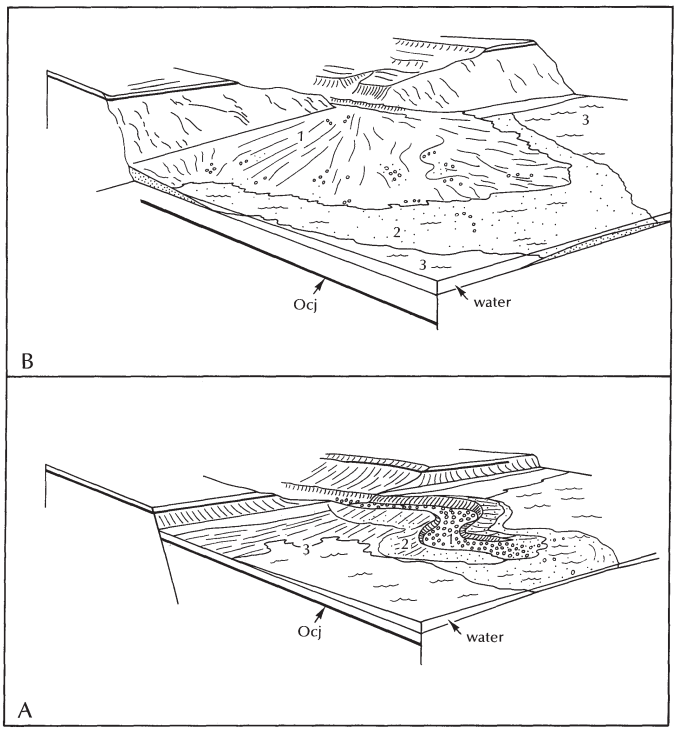


Figure 14. Schematic reconstruction of inferred depositional environment of the shallow-water and alluvial deposits shown in Figures 10 and 13. A, Local uplift initiates deposition of lower channelized conglomerate (central part of Fig. 10) containing clasts derived by erosion of the upper 5 m of underlying strata. The uplift is shown diagrammatically as a block fault but could have been an topographic fold crest or thrust block. Facies include (1) channel conglomerate, (2) fine sandstone and siltstone deposited adjacent to the channel as levee and overbank units, and (3) fine sandstone, siltstone, and mudstone deposited away from channel by waves and tidal currents in shallow-water deposystem. B, With further uplift, a small alluvial fan progrades as erosion reaches deeper into the underlying strata. Principal depositional facies include (1) coarser-grained alluvial sandstone and conglomerate units (Tgb and Tsb) deposited on subaerial or shallowest subaqueous parts of fan, (2) fringing fine- to coarse-grained, sandy and muddy sections representing shallow subaqueous and intertidal settings fed by the fan, and (3) fine-grained sandstone, siltstone, mudstone, volcaniclastic units, and barite deposited in shallow-water and intertidal areas away from the fan-dominated parts of the system. Ocj is the thin jasper unit at the base of the fan-delta section.

deposits including fine-grained, laminated carbonate capped by 5–6 m of silicified carbonate, jasper, and bedded barite. These mainly low energy bank-top deposits interfinger with units of coarse-grained, cross-stratified lithic sandstone (Tsb), indicating that deposition of terrigenous debris continued locally on the bank throughout its existence and that the orthochemical sediments accumulated on inactive parts of a fan-delta platform. Still farther to the southwest, fine-grained bank top silicified carbonate and terrigenous sediments interfinger with bank slope translucent-chert-clast conglomerate interbedded with shale and finally into thick shale and volcaniclastic basinal deposits (Fig. 17). The bank was asymmetric within the plane of exposure, having an energetic, coarse-grained, wave- and current-worked northeastern margin and a low-energy mud-dominated southwestern margin.

Heinrichs and Reimer (1977, Fig. 3, section H) illustrate another 20-m-thick middle Mapepe bank sequence developed over an erosional unconformity in the Barite syncline. The basal unit includes 10 m of dolomitic chert-grit sandstone and conglomerate resting with erosional contact on black cherts of the Mendon Formation. Overlying units include carbonate, silicified carbonate, altered dacitic ash, shale, chert, jasper, and barite. Coarser clastic carbonate, silicified carbonate, and barite sandstone layers contain detrital chrome-rich spinels derived by erosion of komatiites of the Onverwacht Group. To the southwest, along the west limb of the syncline, the unconformity disappears and the Mapepe Formation is represented by a complete but condensed section of silicified ash, silicified carbonate, jasper, barite, and thin clastic units, including both spherule beds, S2 and S3 (Fig. 3, section I; Heinrichs and Reimer, 1977, Fig. 3, section E).

Most sediments of the shallow-water bank association in the Barite syncline and along strike were fine-grained precipitative and pyroclastic deposits. Underlying and interfingering coarser grained terrigenous sediments represent fan-delta deposits and channels crossing the low-energy orthochemical banks. Coarser deposits composed of reworked chemical/precipitative detritus represent wave- and current-active bank margins and subaqueous bank slopes. Deposition of bank sequences was controlled by the emergence and erosion of shallow-water highs during middle Mapepe time (Heinrichs and Reimer, 1977). The condensed section of strata on the west limb of the Barite syncline marks a structural and topographic high termed the Proto-Inyoka zone by Heinrichs and Reimer (1977). During middle Mapepe time, this high was uplifted locally, exposed, and eroded down into ultramafic volcanic rocks of the Mendon Formation, the probable source of detrital chrome-rich spinels that are abundant in bank sandstones. Fan-deltas developed adjacent to the emergent high and the high itself served as a site of shallow-water chemical sedimentation during times of reduced clastic influx.

PETROLOGY OF THE TERRIGENOUS ROCKS

The petrology of the Fig Tree Group in southern areas has been discussed by Heinrichs (1980) and Nocita (1989). The Mapepe Formation includes both terrigenous clastic and dacitic volcaniclastic petrofacies. The abundance of fine dacitic tuff reflects the presence of active subaerial volcanoes, although the absence of coarse detritus indicates that the sites of volcanism were distant. The following discussion will focus on the types and sources of terrigenous sediment.

Shale and mudstone

Shale and mudstone occur mainly in the lower parts of Mapepe sections along the southern edge of the SD and in the ECD. Samples of mudstone and muddy siltstone were analyzed by Nocita (1986). His results indicate that these rocks are

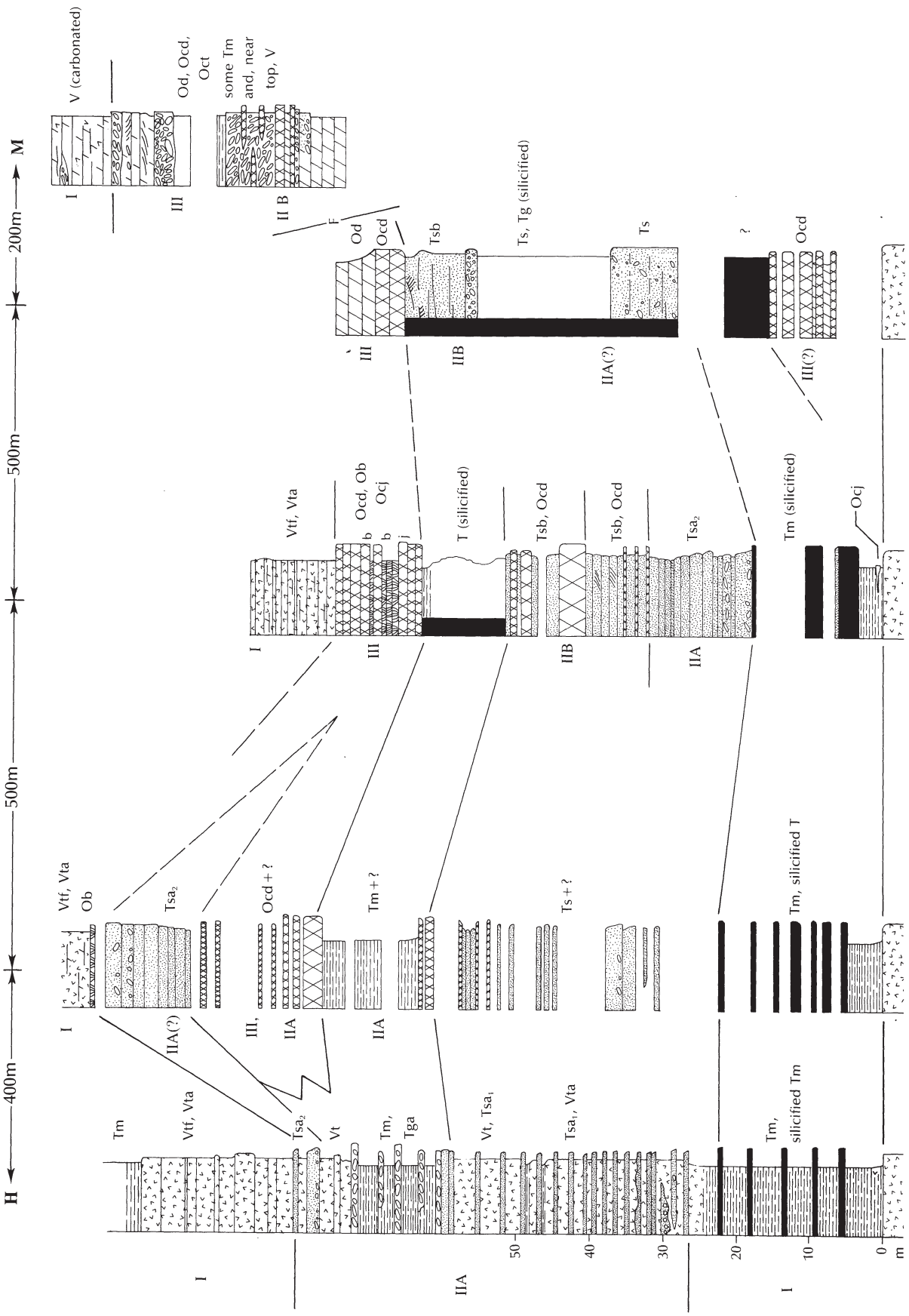


Figure 15. Stratigraphic sections through shallow-water bank deposits in the middle Mapepe Formation on the east limb of the Barite syncline. Sections H and M located in Figure 1. See Figure 2 and Table 1 for explanation of lithofacies symbols and abbreviations.

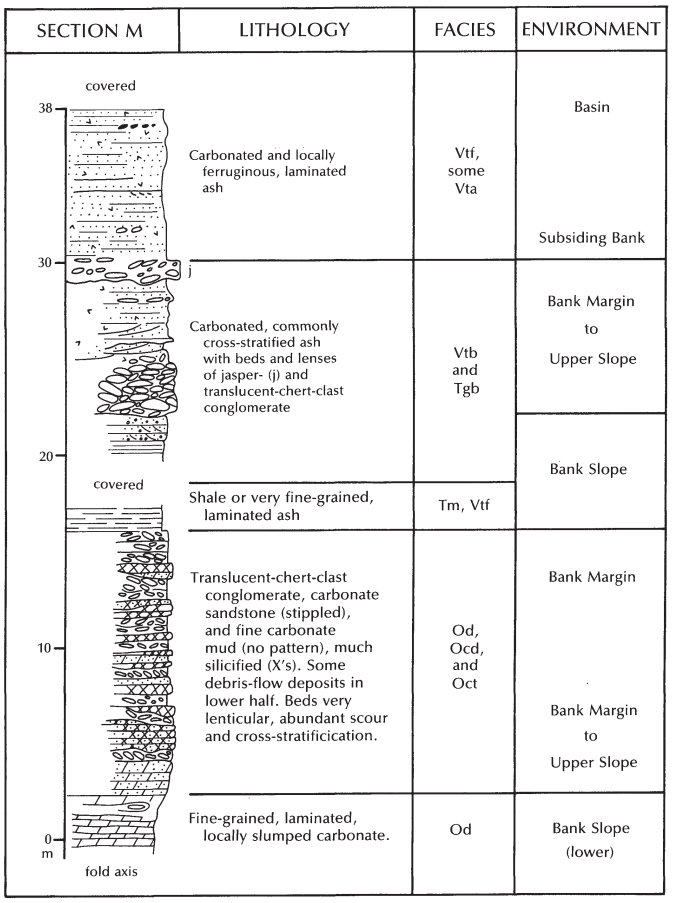


Figure 16. Stratigraphic section (section M, Figs. 1 and 15) of chert-clast, carbonate-matrix breccias and carbonate units deposited along northeastern margin of shallow-water bank in middle Mapepe Formation on east limb of Barite syncline. See Figure 2 and Table 1 for explanation of lithofacies symbols and abbreviations.

enriched in Cr and, to a lesser extent, Ni relative to associated terrigenous sandstone and volcaniclastic tuff. These results reinforce previous observations (Danchin, 1967; McLennan and Taylor, 1983) of Cr and Ni enrichment in Fig Tree shales from northern parts of the belt, and suggest, along with rare earth element data (McLennan and Taylor, 1983), that these early clastic sediments were derived in part by weathering of komatiitic igneous rocks like those in the underlying Onverwacht Group.

Sandstone

Quantitative petrography (Dickinson, 1970; Dickinson and Suczek, 1979; and many others) cannot be applied reliably to Mapepe sandstones because of pervasive metasomatic alteration that has affected both the parent rocks prior to erosion and the Mapepe sands themselves after deposition (Nocita, 1989). Gross modal petrology of Mapepe sandstones (Nocita, 1989, Fig. 3) shows that they consisted largely of lithic debris and quartz. In thin section, most Mapepe sandstones are moderately to poorly sorted mixtures of angular to subangular grains of quartz, generally making up less than 10% of the rock, and chert in a matrix of microcrystalline phyllosilicates, authigenic chert, and iron oxides representing altered lithic detritus.

Monocrystalline and polycrystalline, mainly angular to subangular quartz makes up from less than 2 to 10% of most sandstones in the Mapepe Formation. Medium- to coarse-grained beds in the lower part of the formation usually contain less than 5% quartz; those associated with conglomerates in the upper half commonly contain 5–10% quartz, although individual beds with as much as 30% quartz occur, mainly in the fan-delta platform facies in the upper part of the sequence. Grains with straight crystal faces, euhedral shapes, and embayments, indicating a volcanic origin, are abundant. Polycrystalline quartz, present in all samples, consists mainly of comb-structured or layered aggregates derived from quartz veins and cavity fill. Polycrystalline grains showing deformed, elongated crystals and extreme undulose extinction (e.g., Young, 1976) were not seen. Identifiable grains of coarse quartz appear to have been derived from felsic volcanic rocks and vein and cavity fill and do not require plutonic or higher grade metamorphic sources.

Feldspar is rarely preserved in Mapepe sandstones. A few incompletely altered grains occur in the upper part of the formation. In many sandstones, however, relict outlines of blocky, lath-shaped grains, now fully replaced by chert, appear to represent primary detrital plagioclase. Heinrichs (1980) reports the presence of rock fragments containing potash feldspar showing crude quadrille twinning intergrown with quartz and/or plagioclase.

More than 90% of the detrital grains in most Mapepe sandstones represent lithic grains (Nocita, 1989) now composed of chert or impure chert. Most are composed of relatively pure microquartz or microquartz with phyllosilicate, carbonaceous, carbonate, or opaque impurities. Probably 30–60% of the grains cannot be correlated with any specific source rock type, but, by comparison with pebbles or units in underlying formations, could represent a wide variety of silicified sedimentary and volcanic rock types. Some contain carbonaceous matter and were apparently derived from black and banded carbonaceous cherts in the Onverwacht Group. In many units, particularly in the upper half of the formation, grains containing altered plagioclase phenocrysts or microphenocrysts and apparently representing altered dacitic detritus are common. Trace amounts (< 5%) of chlorite-rich and sericite-poor grains may represent thoroughly altered mafic and ultramafic volcanic rocks.

Conglomerate

Conglomerates throughout the Mapepe Formation are made up of two main clast types: chert and felsic volcanic and volcaniclastic rock. Conglomerates in the lower half of the formation are composed entirely of chert clasts. Those in the upper half contain from a few percent to as much as 50% clasts of unsilicified, fine-grained felsic volcanic and volcaniclastic rock. The principal chert clast types are a variety of massive to laminated gray, black,

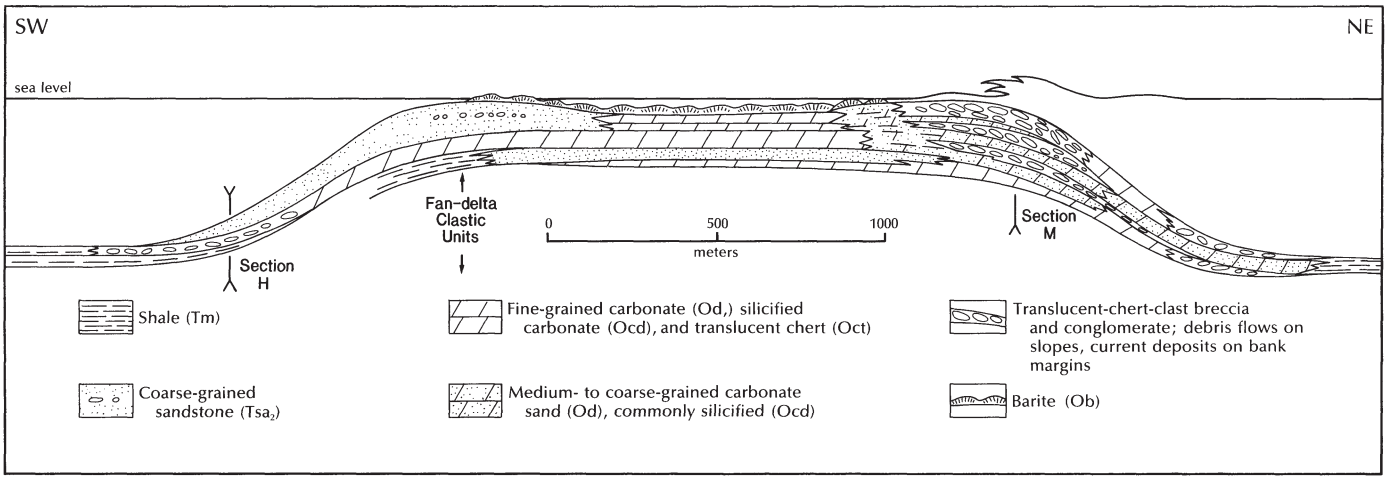


Figure 17. Reconstructed cross-section of shallow-water bank in the middle Mapepe Formation (sections in Fig. 15), east limb of Barite syncline. The wave-active northeastern bank margin shows coarse siliceous and carbonate facies that are absent on the southwestern margin. The bank appears to represent an inactive fan-delta platform.

and white chert, most representing carbonaceous black and banded black and white cherts in the underlying Onverwacht Group. These clasts have generally been bleached and weathered relative to their parent rocks. Subordinate but common chert types include banded ferruginous chert (generally less than 15%), cavity fill chert and coarse quartz (as much as 10%), and, locally, silicified intraformational siltstone and sandstone (as much as 10%). Accessory types (generally less than 1%) include jasper, carbonate, green silicified ultramafic rock, silicified accretionary lapilli, and silicified mafic and komatiitic tuff. Some locally derived conglomerates contain as much as 80% clasts of jasper and banded ferruginous chert, silicified carbonate, and translucent chert possibly representing primary silica precipitate.

Provenance

Shale geochemistry, sandstone petrology, and conglomerate clast composition all indicate that the terrigenous debris in the Mapepe Formation was derived by uplift, weathering, and erosion of the underlying parts of the Swaziland Supergroup. During the deposition of the upper part of the formation, this detritus was widely mixed with penecontemporaneously erupted ash and volcaniclastic detritus. There appears to be an upsection decrease in the areal diversity of conglomeratic units. The lowest, such as those in sections F and G (Fig. 3), exhibit significant lithologic differences from bed to bed. These units also include a high proportion of locally derived debris, such as jasper and interbedded sedimentary rocks, and lack deeper level materials, such as silicified komatiitic pyroclastic rocks. They were evidently derived from local sources that varied considerably in makeup. Higher conglomerates contain a regionally more uniform assemblage representing erosion well down into the Onverwacht Group as well as of syndepositional felsic volcanic and volcaniclastic units.

Although Heinrichs (1980) and others have reported clasts of plutonic rock from the Mapepe Formation or its equivalents, we have not identified any unambiguous plutonic debris, and a number of observations suggest either that erosion did not breach the supracrustal sequence during Mapepe time or that exposures of deeper seated rocks were extremely localized. Not only have we not observed clasts of plutonic rock, we have not seen clasts of recrystallized chert, deformed and strained polycrystalline quartz, foliated metamorphic rocks, or other lithic grains derived from strongly recrystallized or strained rocks that are abundant in the Ancient Gneiss Complex (Hunter, 1970) or in metamorphic aureoles surrounding tonalitic plutons adjacent to the Barberton Belt. There is also a lack of detrital metamorphic minerals, such as garnet and epidote, which are common in metamorphosed greenstone belt rocks adjacent to surrounding plutons and would indicate exposure of higher grade metamorphic units. Coarse quartz, abundant in both the Ancient Gneiss Complex and recrystallized cherts in metamorphic aureoles, and which would be selectively concentrated during weathering and erosion, is a minor component of Mapepe sandstones within the study area.

Micrographic, perthitic, and granophyric quartz-feldspar intergrowths reported by Heinrichs (1980) and others from Fig Tree sandstones and interpreted to represent detritus of plutonic origin are, in fact, ambiguous, especially in small, sand-sized grains. Similar intergrowths occur abundantly in metasomatically altered felsic volcanic units in the Swaziland Supergroup and, locally, in the quenched margins of mafic intrusive units. Biotite is a common accessory mineral in dacitic volcanic rocks in the Fig Tree Group and need not be of plutonic or metamorphic origin.

It is clear that considerable care must be exercised in attempting to identify the point where detritus of plutonic or high-grade metamorphic origin first appears in the Swaziland Supergroup. Many “plutonic” compositions and textures seen in

small detrital grains are abundantly developed in volcanic and metasomatically altered rocks within the supracrustal sequence. Although the presence of debris derived from such deep-level sources would not be unexpected in southern-facies Fig Tree sediments, we have no evidence yet that it is present in the Mapepe Formation within the study area.

TECTONICS AND SEDIMENTATION

Evolution of the Mapepe depositional system

The base of the Mapepe Formation marks a major sedimentological, petrologic, and tectonic transition in the evolution of the Barberton Greenstone Belt. Although volcanism continued throughout deposition of the Fig Tree Group, mafic and komatiitic magmatism ceased regionally before the close of Onverwacht time. In many if not all areas, an interval of volcanic quiescence, represented by black and banded cherts at the top of the Mendon Formation, preceded Fig Tree sedimentation. Lowest Mapepe strata also mark the beginning of tectonism and associated terrigenous sedimentation that persisted throughout later stages of greenstone belt evolution.

The depositional and tectonic evolution of the Mapepe Formation can be divided into three stages: (1) an early stage during which the MJM and related shales and iron-rich units in the lower part of the Mapepe Formation were deposited, (2) a middle stage of basin reorganization, and (3) a late stage of fan-delta sedimentation in one or more foreland basins.

Stage 1: Early Mapepe sedimentation. During early Mapepe time (Fig. 18A), iron-rich sediments were deposited throughout the southern and eastern parts of the BGB (Visser, 1956; Heinrichs, 1980; Lamb, 1984a, b; Paris, 1985; Lamb and Paris, 1988). Iron-rich units reach more than 150 m thick in Swaziland and central parts of the ECD, where they are underlain by a thin shale unit and overlain by thick sequences of shale and ferruginous shale (Davies and Urie, 1957). In the SD on the west limb of the Onverwacht anticline, immediately south of the Granville Grove fault (Fig. 3, section F) near the northwestern limit of the MJM, the MJM averages 10–20 m thick and includes banded jasper-hematite BIF overlying 75–100 m of black shale. In the southernmost structural belt in the WCD, north of the Granville Grove fault, the MJM is sporadically developed, thin, and contains few discrete hematite layers. In many sections, jaspers are interbedded with and grade laterally into thin chert bands interbedded with shale. Farther northwest, the lowest 100 m of the Mapepe Formation consists of shale interbedded with fine, distal felsic ash. The lower 100–200 m of northernmost sections in the WCD (Fig. 2, section E) consist almost entirely of fine, massive, probably deep water felsic ash with a thin, 1- to 5-m-thick zone of fall- and current-deposited ash, silicified ash, barite, and jasper at the base.

Radiometric dating suggests that Fig Tree sedimentation began earlier in southeastern areas than in the northwest. A tuff immediately below the MJM in the southernmost WCD has yielded an age of 3,258 ± 3 Ma (Byerly et al., 1996) by the single-crystal evaporation method (Kober, 1986, 1987). A dacitic tuff at the base of the formation immediately south of the Inyoka fault (Fig. 2, section E) has yielded an age of 3,243 ± 4 (Kröner et al., 1991, sample SA 326).

Jackson, et al. (1987) suggested that the MJM was deposited in a foredeep developed in front of a northwest-prograding orogenic belt. Nowhere have we seen lithic sandstones or conglomerates interbedded with the iron-rich sediments, and it appears that, if an orogenic belt existed in earliest Fig Tree time, it was far enough to the southeast that it did not provide coarse detritus to the early Mapepe basin within the study area. Fig Tree shale and iron-formation sedimentation probably began by 3,260 Ma in the SD, ECD, and southern WCD. Mafic and ultramafic volcanism may have continued to as late as 3,243 Ma in the northern WCD. Earliest Fig Tree sedimentation in the northern WCD (section E, Fig. 2) was marked by short-lived relatively shallow-water conditions followed by subsidence into deeper water and fine-grained felsic tuff sedimentation.

Stage 2: Middle Mapepe basin reorganization. In the Barite syncline and along strike to the northeast, the middle part of the Mapepe Formation includes facies reflecting local uplift and erosion of rocks as old as the Onverwacht Group and deposition of shallow-water orthochemical deposits on fan-delta surfaces and above local erosional unconformities. These facies and stratigraphic complexities are absent in Mapepe sections to the northwest and southeast, and they appear to mark the existence of an elongate, northeast-trending zone of uplift and erosion, termed the Proto-Inyoka Zone by Heinrichs and Reimer (1977). This zone could mark a locus of early faulting within the greenstone belt, but it lies along strike from the axial trace of the Onverwacht anticline, which also shows evidence of having developed initially in middle to late Mapepe time (Lowe et al., this volume, Chapter 2). We suggest that in middle Mapepe time, the early Fig Tree basin was divided into separate southeastern and northwestern basins by early folding and/or faulting along the trend of the Onverwacht anticline (Fig. 18B).

Stage 3: Middle and late Mapepe foreland basin sedimentation. In the southeastern Mapepe basin formed by growth of the Onverwacht anticline (Fig. 18B), the MJM is overlain by several hundred meters of fine, argillaceous and commonly slightly ferruginous sediments, sparse layers of very fine-grained felsic tuff, and interbedded sandstone units, including the Gelagela Grit (Heinrich, 1980), derived by erosion of rocks lying southeast of the basin. Except in the Barite syncline, these units were not studied in detail.

The northwestern Mapepe basin is represented by the middle and upper parts of the Mapepe Formation in the SD on the west limb of the Onverwacht anticline and throughout the WCD, which provide a reasonable cross section of the basin. Middle Mapepe sections in the southeastern part of the basin, in the SD and southernmost WCD, consist of subaqueously deposited fall- and current-deposited basinal tuff containing thin, lenticular units

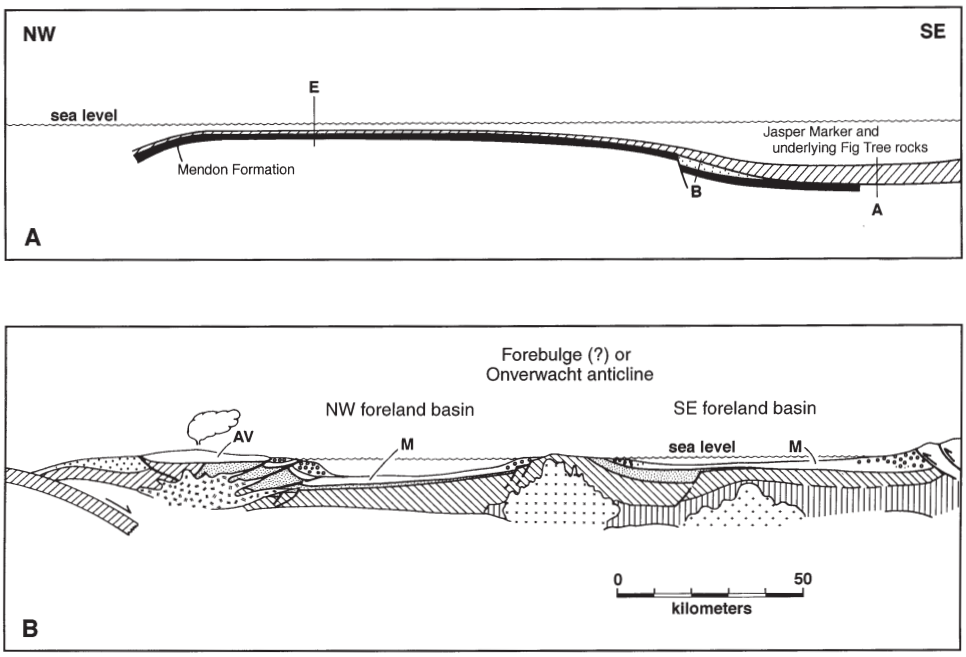


Figure 18. Schematic cross-sections of the Fig Tree depositional system in the southern part of the Barberton Greenstone Belt during deposition of the Mapepe Formation. A, Facies and depositional setting during accumulation of the Manzimnyama Jaspillite Member near the base of the Mapepe Formation. Letters indicate locations of measured sections (Fig. 1). A deep-water basin in the southeast passed northwestward into a quiet, clastic-starved subaqueous shelf. Komatiitic volcanism may have continued in this shelfal area during deposition of the MJM. B, Tectonic and depositional setting during accumulation of the middle and upper Mapepe Formation. Facing foreland basins have developed with an intervening high, the Onverwacht anticline, possibly representing a shared forebulge. The abundance of dacitic volcaniclastic debris and influx of coarse terrigenous detritus from the northwest suggest a retroarc setting for sedimentation within the northwestern basin. Southeastern basin lacks evidence of nearby volcanism and may have formed during shortening between already closely juxtaposed blocks. Symbols: Komati Formation (vertical lines), younger Onverwacht Group (diagonal lines), Mendon Formation (shaded), Mapepe Formation (unpatterned with "M" or conglomerate pattern); Auber Villiers Formation (AV); plutonic rocks (+, x, and double hatches). Scale and orientation same for both diagrams.

of fan-delta conglomerate, sandstone, and siltstone. These fan-delta units are generally less than 50 m thick and commonly include shallow-water fan-delta platform sequences, suggesting that regional water depths were not great. These facies reflect volcaniclastic sedimentation in a shallow sea punctuated by the progradation and buildup of small fan deltas flanking uplifts of immediately underlying portions of the Fig Tree and Onverwacht Groups. Sparse paleocurrent data (Fig. 10) suggest that the uplifts lay south of present exposures. The development of these small, north- to northwest-prograding fan deltas was coincident with initial folding along the Onverwacht anticline and approximately coincident with the initial influx of coarse detritus along the northwestern margin of the basin. They may represent uplift and erosion along the anticline itself or faulting associated with flexural extension (Bradley and Kidd, 1991) along the northwestern flank of the Onverwacht anticline/flexural forebulge.

Fan-delta sequences in the upper part of the Mapepe Formation throughout the WCD are commonly 100–200 m thick and include fan-delta front conglomerates and sandstones and fan-delta platform conglomerates. Especially coarse-grained fan-delta units occur in the upper 300–500 m of the Mapepe Formation immediately south of the Inyoka fault in the vicinity of section E (Fig. 2). The thickness and coarseness of these units, which include chert clasts as much as 1 m across, suggest a source to the northwest. Most coarse clastic units in the upper Mapepe Formation are lenticular along strike. Lowe et al. (this volume, Chapter 2) have argued that the major faults in the WCD, including the Inyoka, Schultzenhorst, Auber Villiers, and Granville Grove faults, formed initially as south- to southeast-directed thrust faults in late Mapepe to post-Mapepe, pre-Moodies time. It is probable that the upper Mapepe fan-deltas were diachronous across the structural belts in the WCD and were deposited on the southern, downdropped structural blocks during thrusting along the immediately adjacent faults.

Regional relationships thus suggest that middle and late Mapepe sedimentation occurred within two northeast-trending foreland basins separated by a zone of folding and uplift marking the early Onverwacht anticline. This structure may have been initiated as a common forebulge, shared by both basins. It is possible that the basins merged into a single basin to the northeast,

outside of the study area, by disappearance of the Onverwacht anticline. Each basin was flanked toward the margins of the present BGB by uplifts, interpreted to have been fold-and-thrust belts, that supplied clastic debris to the basins (Fig. 18B). Coarse clastic units at the top of the formation probably reflect thrusting on individual faults in the WCD as the northwestern fold-and-thrust belt prograded to the southeast and the northwestern Mapepe basin collapsed. No evidence has been identified to suggest syn-Mapepe deformation within the southeastern basin. It is not known whether the Mapepe basins were piggy-back basins in the sense of Ori and Friend (1984). The paucity of coarse detrital quartz and absence of clasts of plutonic rock indicates that the sources for Mapepe sediments within the study area did not include deep-seated igneous or metamorphic rocks.

Much sediment in the middle and upper parts of the Mapepe Formation is altered dacitic ash. The absence of proximal volcanic facies in the Mapepe indicates that the eruption centers lay outside of the basin of sedimentation represented by the present outcrops, and regional facies patterns, including the near absence of tuff units in the southeastern basin, suggest that the sources lay to the northwest (Fig. 18B; Lowe and Byerly, this volume, Chapter 1).

Comparison of the Mapepe and Phanerozoic foreland basins

The results of the present study support conclusions (Jackson et al., 1987; Nocita and Lowe, 1990) that middle and late Mapepe sedimentation occurred within one or more foreland basins produced by flexural loading of the crust adjacent to fold-and-thrust belts. This inference is based on the following.

1. The basins were developed adjacent to uplifts and were strongly asymmetric, with clastic debris generally entering from one side, spreading across the basins, and showing coarse proximal and distal fine depositional facies.

2. Sedimentation was associated with dacitic magmatism, but the primary sediments include both uplifted underlying volcanic and sedimentary rocks and the penecontemporaneous volcanic rocks. The dacitic magmatic centers were located outside of the basin of deposition and, based on the abundance of cherty sedimentary debris and the paucity of coarse dacitic volcaniclastic debris in the lower conglomerates, located beyond the uplifts of underlying Onverwacht rocks.

3. Felsic volcanism during Mapepe sedimentation probably occurred within a subduction-related magmatic arc (de Ronde and de Wit, 1994; Lowe, 1994, this volume, Chapter 12) located northwest of the present WCD. The close relationship between subduction-related felsic volcanism, thrust faulting verging away from the arc (toward the southeast), and basinal sedimentation southeast of the thrust zone suggest that Mapepe sedimentation in the northwestern basin occurred in a retroarc or backarc foreland basin adjacent to a backarc fold-and-thrust belt.

4. There was no attendant mafic volcanism or intrusive activity, as might have been expected if the Mapepe basins were extensional or transtensional basins.

5. Early deformation along the southeastern margin of the southeastern basin appears to have involved northwest-verging thrust faulting (Lamb, 1984a, b). Late Mapepe to early post-Mapepe, pre-Moodies deformation along large faults in the WCD appears to have involved south- to southeast-verging thrusting (Lowe et al., 1985; Lowe et al., this volume, Chapter 2).

6. The influx of coarse detritus in both northwestern and southeastern basins coincided with uplift along the central Proto-Inyoka Zone. This coincidence is consistent with the Proto-Inyoka Zone marking the northeast continuation of the Onverwacht anticline and with both forming as a northeast-trending forebulge between the two basins.

Reconstruction of the Mapepe depositional system and estimation of the amount of shortening across the BGB are still extremely qualitative. The tight, isoclinal folds and collapsed anticlinal hinges characterizing the BGB (Heubeck, 1993; Heubeck and Lowe, 1994a, b; Lowe et al., this volume, Chapter 2) make estimations of actual fold geometry and the construction of balanced cross sections impossible at this point. However, preliminary strain analysis suggests that post-Moodies shortening has reduced the preserved width of the BGB to less than one-third of its original width (Heubeck and Lowe, 1994b). Total shortening has probably reduced the widths of the Mapepe foreland basins by factors of between 4 and 10. The present outcrop belts of the Mapepe basins, representing only parts of the basins, are 5–10 km wide, suggesting original basin widths between 20 and 100 km with total fill thicknesses of 500–1500 meters.

These qualitative results suggest that the Mapepe foreland basins were probably small and accumulated relatively thin clastic sequences compared to long-lived retroarc basins developed along the Mesozoic and Cenozoic eastern Andes and the late Mesozoic and Tertiary Cordillera in Utah and Wyoming. These basins total several hundreds of kilometers across (Jordan, 1981), although much of this width reflects the progradational nature of the basin fill. Individual short-lived foreland depocenters within these larger foreland zones, such as the modern Bermejo Valley in Argentina (Johnson et al., 1986), the Maastrichtian and Danian fill of the Magallanes Basin of southern Argentina and Chile (Biddle et al., 1986), individual foreland sediment packages within the Mesozoic Cordilleran foreland (Jordan, 1981), and the modern western Taiwan foreland basin (Covey, 1986), are commonly 50–100 km in width and more comparable in scale to the Mapepe foreland basins.

Detritus derived by weathering and erosion of extrabasinal rocks makes up a relatively small part, about 40–50%, of the fill of the Mapepe basins. The overall thinness of this fill and the small amount of terrigenous detritus may reflect the dominance of extremely labile komatiites and basalts in the uplifted source terranes. Intense weathering would have removed more than 80% of Onverwacht source rocks as dissolved species or clays. The main components of the Mapepe deposystem are felsic ash, introduced with little weathering, and chert-clast conglomerate and chert-grit sandstone, representing the silicified components of the Onverwacht Group. Sands, however, are

rare, reflecting the existence of relatively few source rocks composed of sand-sized quartz and feldspar. In contrast, major Phanerozoic foreland belts derive their sediments directly or indirectly from quartz-rich cratonic sources. Many, such as Mesozoic Cordilleran and eastern Andean basins, were sourced in thick, quartz-rich passive margin sedimentary sequences. Others, such as the Laramide foreland basins, were sourced by craton-cover sediments and by continental crust. Both sources yield a comparatively high proportion of sand-sized quartz and feldspar compared to the Onverwacht sources for the Mapepe basins. Deposition of the Moodies Group during the final stage of BGB evolution is also thought to have occurred within one or more foreland basins (Jackson et al., 1987; Heubeck and Lowe, this volume, Chapter 11). TTG plutons surrounding the belt served as the primary sediment sources for the Moodies Group and the resulting basinal sequence along the northern margin of the BGB consists of more than 3,500 m of quartzose to arkosic sandstone and chert-clast conglomerate. If the sand-sized quartz and feldspar were factored out of the Moodies Group, the remaining chert-clast conglomerates would have the same general compositions and aggregate thickness as those of the Mapepe Formation.

The Mapepe foreland-basin fill was deposited on an older crust composed of rocks of the Onverwacht Group ranging from approximately 3.55 to 3.26 billion years in age intruded by tonalitic plutons from about 3.52 to 3.45 billion years in age (Armstrong et al., 1990; Kröner et al., 1991, 1996; Kamo and Davis, 1994; Byerly et al., 1996). The dominance of detritus derived from the Onverwacht Group in the terrigenous sediments making up the Mapepe Formation; the absence of polycyclic sedimentary and metasedimentary debris, such as quartz, feldspar, and lithic fragments derived by the erosion of uplifted older sandstones and mudrocks; the paucity or absence of detritus from the deeper level plutons or other plutonic or high-grade metamorphic crust; and the small size of the Mapepe foreland basins suggest that they probably formed on small, immature, crustal blocks that lacked large flanking sedimentary aprons. The northwestern basin probably formed as a retroarc basin behind a subduction-related volcanic belt along the margin of the older basement block. The southeastern basin, which lacks evidence of volcanic activity, may have formed by shortening between already closely situated microplates, such as the Onverwacht Group and intruded tonalitic plutons underlying the BGB and the Ancient Gneiss block of Swaziland.

The unusual paired character inferred for the northwestern and southeastern Mapepe basins may reflect the small size of the crustal blocks involved in deformation. The late Paleozoic orogenic belts of North America involved the formation of “paired” facing Appalachian and Cordilleran foreland basins, but these were separated by the expanse of the North American continent. If a similar tectonic situation developed around a microplate, the facing basins would be much closer and perhaps merge into one another as inferred for the Mapepe basins.

CONCLUSIONS

The Mapepe Formation provides a unique cross section of some of the world’s oldest foreland basins. It includes three distinctive petrologic groups of strata that record the interaction of three contrasting sources and styles of sedimentation: (1) thick sections of fine-grained airfall pyroclastic debris originating at volcanic centers that probably lay north and west of the study area; (2) terrigenous sediments deposited as fan deltas constructed adjacent to and deriving debris from uplifts of underlying parts of the greenstone belt sequence; and (3) orthochemical deposits, including deep-water iron formation and jasper and shallow-water barite, chert, and carbonates that accumulated locally on uplifts and inactive fan-delta platforms.

Early Mapepe time was marked by a single deep basin that accumulated iron-rich sediments in the southeastern BGB and adjacent Swaziland. The beginning of clastic sedimentation was evidently diachronous, about 3,260 Ma in the southeast and 3,245 Ma in the north and northwest. In middle Mapepe time, deformation along the northwestern margin of the Mapepe Formation basin resulted in the formation of a second basin. The older southeastern and younger northwestern basins were divided by a northeast-trending zone of uplift and erosion, probably marking initial deformation along the Onverwacht anticline, which may have represented a shared forebulge.

During late Mapepe time, iron sedimentation in the southeastern basin was followed by an influx of terrigenous sediments from uplifts farther to the southeast. In the northwestern basin, middle and upper Mapepe volcaniclastic and terrigenous rocks can be subdivided regionally into two facies. In southern areas, these rocks reflect basinal deposition punctuated by floods of terrigenous sediments across small alluvial and fan-delta systems. The debris was derived mainly from the south and southeast, probably from uplifts related to formation of the Onverwacht anticline and flexural extension along the flanks of the fold. Water depths in the southern part of this basin were not great, but the depositional surface over large areas was below wave base.

To the north, coarse clastic units occur mainly in the upper part of the formation and appear to reflect major uplift along the northwestern margin of the basin. If upper Mapepe conglomerates in this area are diachronous, they may have been deposited in a succession of basins developed immediately adjacent to major thrust faults as the northwestern fold-and-thrust belt prograded to the southeast across the foreland basin. Terrigenous detritus in the Mapepe Formation was derived largely from underlying parts of the greenstone belt sequence and from penecontemporaneous dacitic volcanic units. Major plutonic sources were apparently not unroofed until Moodies time. Following deposition of the uppermost Mapepe Formation, the northwestern foreland region was enveloped within the southwest-prograding fold-and-thrust belt. The southeastern basin may not have been deformed until post-Moodies time.

The composition and abundance of terrigenous sediment supplied to the Mapepe basins was controlled by the nature of

available source rocks. Phanerozoic foreland basins developed on or adjacent to older continental crust are typically filled by abundant recycled quartzose and feldspathic continent-derived detritus with lesser amounts of subduction-related volcaniclastic material. Older tonalitic crust in the Barberton region, ranging from pre–3,500 Ma to about 3,445 Ma (Armstrong et al., 1990; Kröner et al., 1991, 1996; Kamo and Davis, 1994; Byerly et al., 1996), which underlies the Mapepe basins, was not exposed or only locally exposed during Mapepe sedimentation. Mapepe sediments were derived mainly from uplifted rocks of the Onverwacht Group and penecontemporaneous dacitic volcanic rocks. Because the Onverwacht Group consists largely of mafic and ultramafic rocks, its weathering and erosion probably yielded largely clays and dissolved species, which are poorly represented in the Mapepe basins, but only a small amount coarse material, including chert-rich gravel and sand containing little coarse quartz. Although reconstructions are difficult because of structural style and complexity, the Mapepe basins appear to have been comparable in size to small Phanerozoic foreland basins. They probably developed during the amalgamation of small, immature crustal blocks or microplates.

REFERENCES CITED

Anhaeusser, C. R., 1969, The stratigraphy, structure, and gold mineralisation of the Jamestown and Sheba Hills areas of the Barberton Mountain Land [Ph.D. thesis]: Johannesburg, University of the Witwatersrand, 332 p.

Anhaeusser, C. R., 1973, The evolution of the early Precambrian crust of southern Africa: Royal Society of London Philosophical Transactions, ser. A, v. 273, p. 359–388.

Armstrong, R. A., Compston, W., de Wit, M. J., and Williams, I. S., 1990, The stratigraphy of the 3.5–3.2 Ga Barberton Greenstone Belt revisited: a single zircon ion microprobe study: Earth and Planetary Science Letters, v. 101, p. 90–106.

Beukes, N. J., 1973, Precambrian iron-formations of southern Africa: Economic Geology, v. 68, p. 960–1004.

Biddle, K. T., Uliana, M. A., Mitchum, R. M., Jr., Fitzgerald, M. G., and Wright, R. C., 1986, The stratigraphic and structural evolution of the central and eastern Magallanes Basin, southern South America, *in* Allen, P. A., and Homewood, P., eds., Foreland basins: International Association of Sedimentologists Special Publication 8, p. 41–61.

Bradley, D. C., and Kidd, W. S. F., 1991, Flexural extension of the upper continental crust in collisional foredeeps: Geological Society of America Bulletin, v. 103, p. 1416–1438.

Byerly, G. R., Kröner, A., Lowe, D. R., Todt, W., and Walsh, M. M., 1996, Prolonged magmatism and time constraints for sediment deposition in the early Archean Barberton greenstone belt: evidence from the Upper Onverwacht and Fig Tree Groups: Precambrian Research, v. 78, p. 125–138.

Condie, K. C., Macke, J. E., and Reimer, T. O., 1970, Petrology and geochemistry of early Precambrian graywackes from the Fig Tree Group, South Africa: Geological Society of America Bulletin, v. 81, p. 2759–2776.

Covey, M., 1986, The evolution of foreland basins to steady state: evidence from the western Taiwan foreland basin, *in* Allen, P. A., and Homewood, P., eds., Foreland basins: International Association of Sedimentologists Special Publication 8, p. 77–90.

Danchin, R. V., 1967, Chromium and nickel in the Fig Tree Shale from South Africa: Science, v. 158, p. 261–262.

Davies, D. N., and Urie, J. G., 1957, The Bomvu Ridge haematite deposits: Swaziland Geological Survey Department Special Report 3, 24 p.

de Ronde, C. E. J., and de Wit, M. J., 1994, Tectonic history of the Barberton greenstone belt, South Africa: 490 million years of Archean crustal evolution: Tectonics, v. 13, p. 983–1005.

Dickinson, W. R., 1970, Interpreting detrital modes of graywacke and arkose: Journal of Sedimentary Petrology, v. 40, p. 695–707.

Dickinson, W. R., and Suczek, C. A., 1979, Plate tectonics and sandstone compositions: American Association of Petroleum Geologists Bulletin, v. 63, p. 2164–2182.

Dunlop, J. S. R., and Groves, D. I., 1978, Sedimentary barite of the Barberton Mountain Land: a review, *in* Glover, J. E., and Groves, D. I., eds., Archaean cherty metasediments: Their sedimentology, micropalaeontology, biogeochemistry, and significance to mineralization: University of Western Australia Geology Department and Extension Service, p. 39–44.

Eriksson, K. A., 1980a, Hydrodynamic and paleogeographic interpretation of turbidite deposits from the Archean Fig Tree Group of the Barberton Mountain Land, South Africa: Geological Society of America Bulletin, v. 91, p. 21–26.

Eriksson, K. A., 1980b, Transitional sedimentation styles in the Moodies and Fig Tree Groups, Barberton Mountain Land, South Africa: evidence favouring an Archaean continental margin: Precambrian Research, v. 12, p. 141–160.

Hein, F. J., 1984, Deep-sea and fluvial braided channel conglomerates: a comparison of two case studies, *in* Koster, E. H., and Steel, R. J., eds., Sedimentology of gravels and conglomerates: Canadian Society of Petroleum Geologists Memoir 10, p. 33–49.

Heinrichs, T. K., 1969, Report on mapping carried out in search of chrysotile asbestos: Barberton, Unpublished report to Eastern Transvaal Consolidated Mines, Ltd., 5 p., map.

Heinrichs, T. K., 1980, Lithostratigraphische Untersuchungen in der Fig Tree Gruppe des Barberton Greenstone Belt zwischen Umsoli und Lomati (Sudafrika) (Lithostratigraphic study in the Fig Tree Group of the Barberton Greenstone Belt between Umsoli and Lomati (South Africa)): Gottinger Arbeiten zur Geologie und Palaontologie, v.22, 118 p.

Heinrichs, T. K., and Reimer, T. O., 1977, A sedimentary barite deposit from the Archean Fig Tree Group of the Barberton Mountain Land (South Africa): Economic Geology, v. 72, p. 1426–1441.

Heubeck, C. E., 1993, Geology of the Archean Moodies Group, central Barberton Greenstone Belt, South Africa [Ph.D. thesis]: Palo Alto, California, Stanford University, 413 p.

Heubeck, C. E., and Lowe, D. R., 1994a, Depositional and tectonic setting of the Archean Moodies Group, Barberton Greenstone Belt, South Africa: Precambrian Research, v. 68, p. 257–290.

Heubeck, C., and Lowe, D. R., 1994b, Late syndepositional deformation and detachment tectonics in the Barberton Greenstone Belt, South Africa: Tectonics, v. 13, p. 1514–1536.

Hunter, D. R., 1970, The Ancient Gneiss Complex in Swaziland: Geological Society of South Africa Transactions, v. 73, p. 107–150.

Jackson, M. P. A., Eriksson, K. A., and Harris, C. W., 1987, Early Archean foredeep sedimentation related to crustal shortening: a reinterpretation of the Barberton Sequence, southern Africa: Tectonophysics, v. 136, p. 197–221.

Johnson, N. M., Jordan, T. E., Johnsson, P. A., and Naeser, C. W., 1986, Magnetic polarity stratigraphy, age and tectonic setting of fluvial sediments in an eastern Andean foreland basin, San Juan Province, Argentina, *in* Allen, P. A., and Homewood, P., eds., Foreland basins: International Association of Sedimentologists Special Publication 8, p. 63–75.

Jordan, T. E., 1981, Thrust loads and foreland basin evolution, Cretaceous, western United States: American Association of Petroleum Geologists Bulletin, v. 65, p. 2506–2520.

Kamo, S. L., and Davis, D. W., 1994, Reassessment of Archean crustal development in the Barberton Mountain Land, South Africa, based on U-Pb dating: Tectonics, v. 13, p. 167–192.

Kober, B., 1986, Whole-grain evaporation for $^{207}Pb/^{206}Pb$-age-investigations on single zircons using a double-filament thermal ion source: Contributions to Mineralogy and Petrology, v. 93, p. 482–490.

Kober, B., 1987, Single-zircon evaporation combined with Pb^{+} emitter-bedding

for $^{207}Pb/^{206}Pb$-age investigation using thermal ion mass spectrometry, and implications to zirconology: Contributions to Mineralogy and Petrology, v. 96, p. 63–71.

Kröner, A., Byerly, G. R., and Lowe, D. R., 1991, Chronology of early Archaean granite-greenstone evolution in the Barberton Mountain Land, South Africa, based on precise dating by single zircon evaporation: Earth and Planetary Science Letters, v. 103, p. 41–54.

Kröner, A., Hegner, E., Wendt, J. I., and Byerly, G. R., 1996, The oldest part of the Barberton granitoid-greenstone terrain, South Africa: evidence for crust formation between 3.5 and 3.7 Ga: Precambrian Research, v. 78, p. 105–124.

Lamb, S. H., 1984a, Geology of part of the Archaean Barberton Greenstone Belt, Swaziland [Ph.D. dissertation]: Cambridge, Cambridge University, 250 p.

Lamb, S. H., 1984b, Structures on the eastern margin of the Archaean Barberton greenstone belt, northwest Swaziland, *in* Kröner, A., and Greiling, A., eds., Precambrian tectonics illustrated: Stuttgart, E. Schweizerbart'sche Verlagsbuchhandlung, p. 19–39.

Lamb, S. H., and Paris, I., 1988, Post-Onverwacht Group stratigraphy in the SE part of the Archaean Barberton greenstone belt: Journal of African Earth Sciences, v. 7, p. 285–306.

Lowe, D. R., 1994, Accretionary history of the Archean Barberton Greenstone Belt (3.55–3.22 Ga), southern Africa: Geology, v. 22, p. 1099–1102.

Lowe, D. R., and Byerly, G. R., 1986, Early Archean silicate spherules of probable impact origin, South Africa and Western Australia: Geology, v. 14, p. 83–86.

Lowe, D. R., and Knauth, L. P., 1977, Sedimentology of the Onverwacht Group (3.4 billion years), Transvaal, South Africa, and its bearing on the characteristics and evolution of the early Earth: Journal of Geology, v. 85, p. 699–723.

Lowe, D. R., Byerly, G. R., Ransom, B. L., and Nocita, B. R., 1985, Stratigraphic and sedimentological evidence bearing on structural repetition in Early Archean rocks of the Barberton Greenstone Belt, South Africa: Precambrian Research, v. 27, p. 165–186.

Lowe, D. R., Byerly, G. R., Asaro, F., and Kyte, F., 1989, Geological and geochemical record of 3400-million-year-old terrestrial meteorite impacts: Science, v. 245, p. 959–962.

McLennan, S. M., and Taylor, S. R., 1983, Geochemical evolution of Archean shales from South Africa. I. The Swaziland and Pongola Supergroups: Precambrian Research, v. 22, p. 93–124.

Nemec, W., and Steel, R. J., 1984, Alluvial and coastal conglomerates: Their significant features and some comments on gravelly mass-flow deposits, *in* Koster, E. H., and Steel, R. J., eds., Sedimentology of gravels and conglomerates: Canadian Society of Petroleum Geologists Memoir 10, p. 1–31.

Nocita, B. R., 1986, Sedimentology and stratigraphy of the Fig Tree Group, west limb of the Onverwacht anticline, Barberton Greenstone Belt, South Africa: [Ph.D. dissertation]: Baton Rouge, Louisiana State University, 168 p.

Nocita, B. R., 1989, Sandstone petrology of the Archean Fig Tree Group, Barberton Greenstone Belt, South Africa: Tectonic implications: Geology, v. 17, p. 953–956.

Nocita, B. R., and Lowe, D. R., 1990, Fan-delta sequence in the Archean Fig Tree Group, Barberton Greenstone Belt, South Africa: Precambrian Research, v. 48, p. 375–393.

Ori, G. G., and Friend, P. F., 1984, Sedimentary basins formed and carried piggyback on active thrust sheets: Geology, v. 12, p. 475–478.

Paris, I. A., 1985, The geology of the farms Josefdal, Dunbar and part of Diepgezet in the Barberton greenstone belt [Ph.D. thesis]: Johannesburg, University of the Witwatersrand, 239 p.

Perry, E. C., Monster, J., and Reimer, T. O., 1971, Sulfur isotopes in Swaziland System barites and the evolution of the Earth's atmosphere: Science, v. 171, p. 1015–1016.

Reimer, T. O., 1967, Die Geologie der Stolzburg Synklinale im Barberton Bergland (Transvaal Sudafrika) (The geology of the Stolzburg syncline in the Barberton Mountain Land (Transvaal, South Africa)) [MSc. thesis]: Frankfurt, Goethe Universitat, 103 p.

Reimer, T. O., 1975, Untersuchungen uber Abtragung, Sedimentation und Diagenese im fruhen Prakambrium am Beispiel der Sheba-Formation (Sudafrika) (Studies of denudation, sedimentation, and diagenesis in the early Precambrian with an example from the Sheba Formation (South Africa)): Geologisches Jahrbuch, Reihe B, v. 17, 108 p.

Reimer, T. O., 1980, Archean sedimentary baryte deposits of the Swaziland Supergroup (Barberton Mountain Land, South Africa): Precambrian Research, v. 12, p. 393–410.

Reimer, T. O., 1982, Sulfur isotopes and the derivation of detrital barytes of the Archaean Fig Tree Group (South Africa), *in* Sidorenko, A. V., ed., Sedimentary geology of highly metamorphosed Precambrian complexes: Moscow, Nauka Publishing House, p. 63–74.

Veizer, J., 1983, Geologic evolution of the Archean–Early Proterozoic Earth, *in* Schopf, J. W., ed., Earth's earliest biosphere: Princeton, New Jersey, Princeton University Press, p. 240–259.

Veizer, J., Compston, W., Hoefs, J., and Nielsen, H., 1982, Mantle buffering of the early ocean: Naturwissenschaften, v. 69, p. 173–180.

Vinogradov, V. I., Reimer, T. O., Leites, A. M., and Smelov, S. B., 1976, The oldest sulfates in Archaean formations of the South African and Aldan Shields and the evolution of the Earth's oxygenic atmosphere: Lithology and Mineral Resources, v. 11, p. 407–420.

Visser, D. J. L., 1956, The geology of the Barberton area: Geological Survey of South Africa Special Publication 15, 254 p.

Young, S. W., 1976, Petrographic textures of detrital polycrystalline quartz as an aid to interpreting crystalline source rocks: Journal of Sedimentary Petrology, v. 46, p. 595–603.

MANUSCRIPT ACCEPTED BY THE SOCIETY MARCH 26, 1998

Geological Society of America
Special Paper 329
1999

Sedimentary petrography and provenance of the Archean Moodies Group, Barberton Greenstone Belt

Christoph Heubeck* and Donald R. Lowe
Department of Geological and Environmental Sciences, Stanford University, Stanford, California 94305

ABSTRACT

The Archean Moodies Group (3.23–3.08 Ga), Barberton Greenstone Belt, South Africa, is the oldest known, well-preserved, quartz-rich sedimentary sequence on Earth. The Moodies Group is composed mainly of arkosic, lithic, and quartzose sandstones deposited in a range of terrestrial, marginal marine, and shallow-marine settings. Moodies strata are divided regionally into contrasting petrologic sequences by the Inyoka fault. North of the fault, Moodies strata include two petrofacies: the Oosterbeek and Elephant's Head petrofacies. The Oosterbeek petrofacies, making up the lower two-thirds of the group, is characterized by a low proportion of unstable lithic grains and chert, common K-feldspar, a high proportion of monocrystalline quartz, and high percentage of framework grains. This petrofacies corresponds stratigraphically to an upward-fining and -deepening sequence representing strata deposited in alluvial to open-shelf facies. The overlying Elephant's Head petrofacies is characterized by a variable but high proportion of chert, the near absence of feldspar, and a low abundance of matrix, monocrystalline quartz, and unstable lithic grains. This petrofacies corresponds to an overall upward-coarsening trend representing increasing uplift in the source area and southward progradation of syndeformational alluvial fans. All preserved Moodies strata south of the Inyoka fault are assigned to the Angle Station petrofacies, which is characterized by a lack of preserved feldspar. These southern strata were probably deposited in one or more basins that were separate from those to the north.

Interpretation of sandstone provenance based on modal analysis is aided by studies of conglomerate-clast compositions, paleocurrents, shale geochemistry, and detailed stratigraphic and structural mapping. Monocrystalline quartz and K-feldspar were derived from intermediate and silicic plutonic rocks, probably located north or northwest of the present outcrops. All remaining grain types can be accounted for by rocks within the greenstone belt. Metamorphic source areas, such as the Ancient Gneiss Complex in Swaziland, probably did not contribute significantly to the Moodies Group.

The petrofacies in the Moodies Group north of the Inyoka fault correspond to two distinct tectonic stages. The Oosterbeek petrofacies may have been related to subsidence and extension following orogeny during and immediately following deposition of the underlying Fig Tree Group. The Elephant's Head petrofacies records uplift of source areas to the north, erosion, and southward transport of debris in late Moodies time. Late Moodies sedimentation occurred mainly within a foreland basin. South-facing alluvial fans near the top of the sequence record south- or southeastward-directed shortening and the start of the last major phase of greenstone belt deformation.

*Present address: BP Amoco, P.O. Box 3092, Houston, Texas 77253.

Heubeck, C., and Lowe, D. R., 1999, Sedimentary petrography and provenance of the Archean Moodies Group, Barberton Greenstone Belt, *in* Lowe, D. R., and Byerly, G. R., eds., Geologic Evolution of the Barberton Greenstone Belt, South Africa: Boulder, Colorado, Geological Society of America Special Paper 329.

INTRODUCTION

The preserved record of Archean clastic sedimentation includes abundant immature sandstones eroded from volcanic and volcaniclastic source terranes and deposited during periods of tectonic instability and active deformation. In contrast, quartz-dominated sedimentary rocks, indicating the uplift and exposure of felsic plutonic or quartzose metamorphic rocks, are comparatively rare. Where they do occur, however, they are of particular interest to studies of early crustal evolution because they suggest the local existence of differentiated, buoyant continental crust and provide clues regarding its origin and tectonics. Some of these early continental blocks have been obliterated by crustal recycling so that the sedimentary products derived from them are the only remaining evidence of their former existence.

The Archean Moodies Group of the Barberton Greenstone Belt (BGB), South Africa, is the oldest known well-preserved quartz-rich sandstone sequence (Hall, 1918; Visser, 1956; Anhaeusser, 1968, 1969; Eriksson, 1978, 1979, 1980) and has been interpreted as the sedimentary record of the earliest continental crust in southern Africa (e.g., Krupicka, 1975; Eriksson, 1978, 1979, 1980; McLennan et al., 1983; Reimer et al., 1985), thought by many to be represented by metamorphic and plutonic rocks of the Ancient Gneiss Complex in Swaziland (Condie et al., 1970; Reimer et al., 1985; Tegtmeyer and Kröner, 1987). Deposition has been suggested to have occurred in passive-margin (Eriksson, 1980) or foreland-basin (Jackson et al., 1987) settings.

Because all rocks in the BGB have been affected by low-grade alteration and recrystallization and original stratigraphic and depositional relationships severely modified by later tectonism, it has been difficult to reconstruct the original Moodies basin(s) of deposition and to interpret sediment provenance with any degree of confidence. This study uses sandstone petrography, conglomerate clast compositions, paleocurrent patterns, and stratigraphic analysis to better constrain the provenance and tectonic setting of the Moodies Group in the central BGB.

GEOLOGIC SETTING

Regional geology

The Barberton Greenstone Belt (BGB) in the eastern Kaapvaal Craton is one of the best-preserved pre-3.0-Ga Archean greenstone belts. Supracrustal rocks in the BGB have been assigned to the Swaziland Supergroup (Anhaeusser, 1976) or the Barberton Sequence (SACS, 1980) and include three major stratigraphic units. The Onverwacht Group consists of from 1 to 10 km of mafic and ultramafic volcanic rocks with thin interbedded cherts and minor felsic volcanic units (Viljoen and Viljoen, 1969; Lowe and Byerly, this volume, Chapter 2). The overlying Fig Tree Group is a lithologically diverse association of mudstone, chert-grit, graywacke, chert-clast conglomerate, dacitic volcanic and volcaniclastic rocks, and banded iron formation. Deposition took place in synorogenic basins containing alluvial, fan-delta, and shallow- to deep-water environments (Reimer, 1967, 1975; Heinrichs and Reimer, 1977; Heinrichs, 1980; Nocita, 1989; Nocita and Lowe, 1990; Lowe and Nocita, this volume, Chapter 10). The uppermost part of the Fig Tree Group is a sequence of relatively fresh felsic volcaniclastic rocks assigned to the Schoongezicht Formation north of the Inyoka fault (Condie et al., 1970) and to Mapepe and Auber Villiers Formations south of the Inyoka fault (Heinrichs, 1980; Lowe, 1991; Lowe and Byerly, this volume, Chapter 1). Zircons from felsic tuffs of the Fig Tree Group have yielded ages ranging from about 3,259 to 3,225 Ma (Armstrong et al., 1990; Kröner et al., 1991; Kamo and Davis, 1994).

The BGB is surrounded by tonalitic, trondhjemitic, and granodioritic (TTG) plutons representing several generations of igneous activity. Most are coeval and comagmatic with the felsic volcanic units in the supracrustal succession (Hunter, 1973; Anhaeusser and Robb, 1981; Robb and Anhaeusser, 1983). The intrusive contacts have been strongly modified by later deformation and alteration. Late granitic plutons pierce some of the tonalitic batholiths, but rarely the supracrustal succession of the greenstone belt. They generally postdate both greenstone-belt sedimentation and deformation, and were associated with late stabilization of the Kaapvaal Craton (Anhaeusser et al., 1969; Viljoen and Viljoen, 1969; Anhaeusser, 1984; Tomkinson and Lombard, 1990; Kamo and Davis, 1994).

The 3.64- to 3.2-Ga Ancient Gneiss Complex (AGC) south of the BGB consists of several generations of quartzofeldspathic gneisses, intermediate and felsic plutonic rocks, and metamorphosed remnants of volcano-sedimentary (greenstone belt) sequences (Hunter, 1970, 1991; Kröner et al., 1991). The more complex structural style of the AGC compared to that of the BGB (Jackson, 1984) and the great age of some of its components have been used to interpret the AGC as the source of much of the sediment of the Moodies Group (Jackson et al., 1987). The contact between the AGC and the BGB, however, has largely been obscured by post-Moodies plutonism. Where exposed locally, it is a fault.

Moodies Group

The Moodies Group is preserved in large northeast-trending, tight to isoclinal, upright and northward overturned synclines and fault-bounded homoclines (Fig. 1) that define the structural grain of the BGB (Ramsay, 1963; Anhaeusser et al., 1981). In spite of the tight folding, angular relationships between foresets and bedding planes are preserved unmodified, conglomerate clasts are nearly undeformed, and structural fabric in the thick-bedded, competent quartzose sandstones is absent except in fold hinges and adjacent to major faults. Very fine grained sandstones and mudstones show a weak spaced cleavage. Near the margin of the BGB, many of the original contacts with the surrounding tonalitic plutons have been severely altered by metasomatic alteration, ductile shear, and brittle faulting (Anhaeusser, 1969, 1984; Fripp

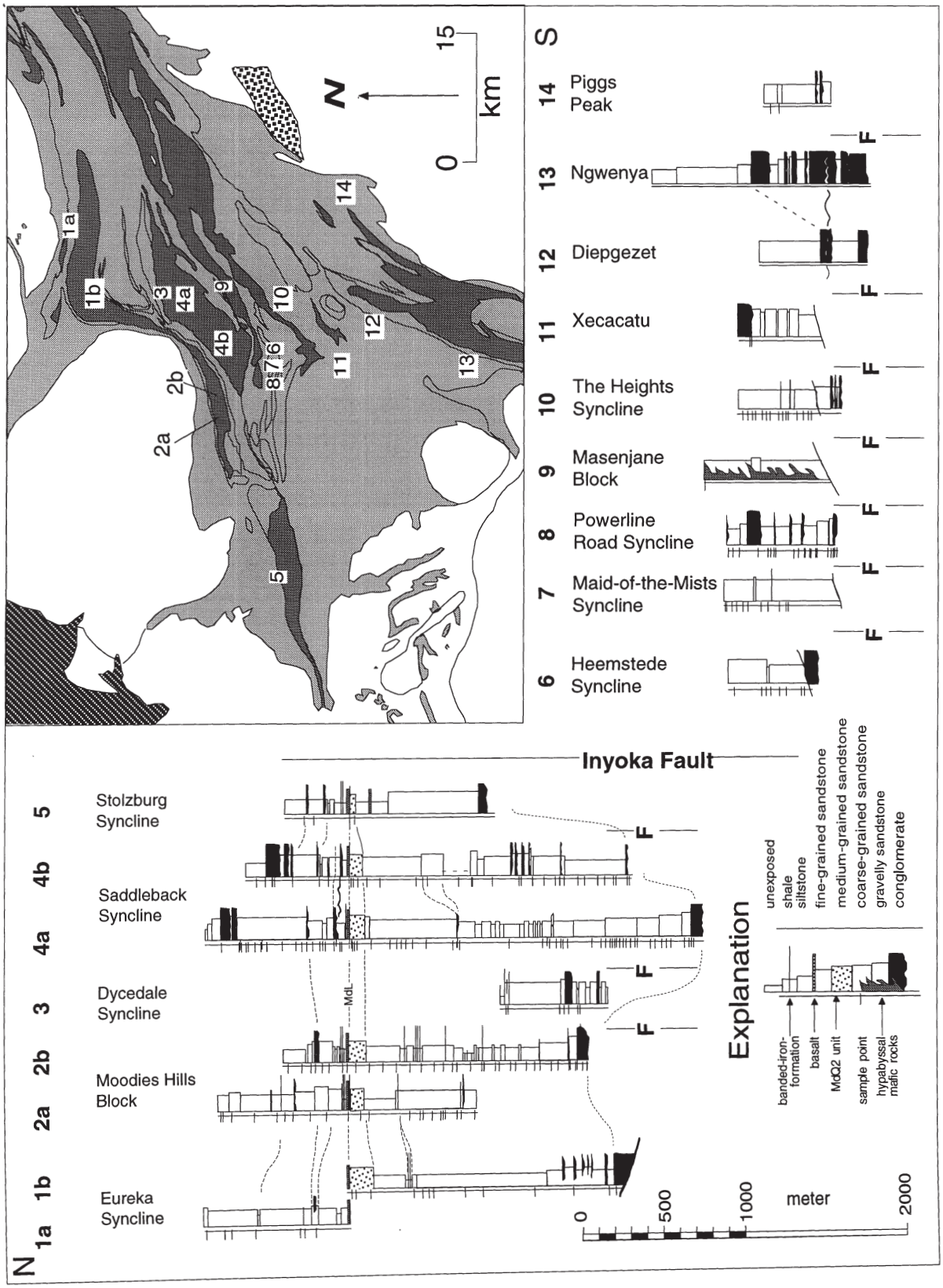


Figure 1. Stratigraphic columns of the Moodies Group in the central Barberton Greenstone Belt. Inset map shows approximate location of measured sections and main structural belts. Columns 2a, 2b, and 4b are redrafted from Hose (1990), column 5 is redrafted from Reimer (1967), and columns 11, 12, and 13 are redrafted from Lamb (1984).

et al., 1980; Faure and Harris, 1991; Tomkinson and King, 1991).

The Moodies Group in its type areas in the Moodies Hills and in the Eureka syncline (Fig. 1) consists of a structurally uninterrupted sequence more than 3500 m thick of subgraywacke, quartzose and feldspathic sandstone, and siltstone with minor banded-iron formation (BIF), shale, and conglomerate (Hall, 1918; Visser, 1956; Anhaeusser, 1968, 1969; Eriksson, 1978, 1979, 1980). Its stratigraphic base is commonly marked by a prominent basal conglomerate overlying dacitic tuff and volcaniclastic rocks of the Fig Tree Group (Fig. 1). Over wide areas north and south of the Inyoka fault, the Moodies Group and the immediately underlying felsic volcanic rocks of the Fig Tree Group have been interpreted to have been thrust above older, structurally underlying and deformed rocks of the Fig Tree and Onverwacht Groups (Lowe et al., this volume, Chapter 2). A basaltic volcanic unit (Visser, 1956) in the upper part of the Moodies Group facilitates stratigraphic correlation between the Saddleback syncline, Eureka syncline, Stolzburg syncline, and the Moodies Hills block (Hall, 1918; Visser, 1956; Reimer, 1967). The sedimentary strata of the Moodies Group were deposited in subaerial and shallow subaqueous settings, including alluvial-fan, braided-stream, tide-dominated delta, and open-shelf systems (Eriksson, 1978, 1979, 1980).

The Moodies Group was subdivided into three upward-fining cycles by Anhaeusser (1968): the basal Clutha, Joe's Luck, and uppermost Baviaanskloof Formations. Eriksson (1978) defined five stratigraphic cycles (MD1–MD5). Hose (1990) did not recognize well-defined cycles in the Moodies Group in a study area southwest of Barberton.

TECHNIQUES

Fresh sandstone samples were collected along traverses perpendicular to strike across well-exposed sections of the Moodies Group southwest of Barberton (Fig. 1). Where outcrop allowed, samples were collected at an even spacing through the sections, and multiple specimens were collected in laterally traceable units to check for lateral compositional variability. Samples collected from sections in working mines in the Barberton area and from a water tunnel through part of the Saddleback syncline were compared with correlative fresh surface samples to check the effects of modern weathering. A total of 215 thin sections of predominantly medium grained Moodies sandstone were examined for this study.

Each thin section was stained for K-feldspar, and a minimum of 300 framework grains was counted per section. Due to the variable amounts of matrix, cement, secondary carbonate, and holes, the actual number of points counted was as high as 490 and as low as 302. The average grain size ranges between 0.20 and 0.35 mm. Table 1 shows the definition of the grain-type categories used in point counting. Point counting followed the procedures outlined by Dickinson (1970), Dickinson and Suczek (1979), and Ingersoll et al. (1984) to minimize the effects of grain size and to ensure the least interpretive approach in categorizing individual grains. However, the composition of individual rock fragments was noted where identifiable. A complete tabulation of the point-count data is given in Heubeck (1993).

Thin sections of the gneisses and granodiorites of the AGC in Swaziland, the Kaap Valley tonalite, and greenstone belt units, including ultramafic, mafic, and felsic igneous rocks and cherts of the Onverwacht Group, and graywacke, banded-iron formation, chert, and felsic porphyries of the Fig Tree Group, were examined as potential source rocks and for comparison with recrystallized lithic detritus in the Moodies Group. Additional petrographic data were collected from the smaller, tectonically more disrupted Moodies sections south of the Inyoka fault, including several blocks adjacent to the Inyoka fault, from the The Heights syncline in the central BGB, and from Moodies slivers in the Swaziland part of the BGB (Fig. 1).

Estimates of conglomerate clast composition were taken at 43 sites in the Moodies Group and at 19 sites in the Fig Tree Group. Visual inspection of the conglomerates along strike showed that clast composition varies significantly over short distances. Emphasis was, therefore, placed on collecting a large number of compositional estimates from numerous sites rather than a smaller number of compositions under strictly controlled conditions. Thirteen representative block-sized samples from Moodies conglomerates and 4 samples of Fig Tree conglomerate were collected for slabbing. Populations of conglomerate clasts (20 clasts minimum) were collected from 6 sites to supplement clast-type identification. A complete breakdown of the locations, procedures, and results of conglomerate sampling is given in Heubeck (1993).

ALTERATION AND METAMORPHISM

Metamorphic grade

Rocks in the Moodies Group have been strongly affected by diagenesis, regional metamorphism, metasomatic alteration, and, locally, contact metamorphism. The regional metamorphic grade of the BGB has been best documented for the rocks of the Komati Formation in the southern part of the belt, for which Cloete (1991) suggests maximum temperatures and pressures of 550°C and 3–4 kb, respectively. The position of the Komati Formation close to the stratigraphic base of the more than 10-km-thick sequence is consistent with his interpretation that the Komati Formation has been altered by burial metamorphism in a region of high heat flow. Metamorphic grade in the stratigraphically higher Fig Tree and Moodies Groups is lower greenschist facies, and p-T conditions are likely to have been correspondingly lower. In the graywackes and volcaniclastic rocks of the Fig Tree Group in the central BGB, Heinrichs (1980) describes the common paragenetic assemblage of chlorite-quartz-phengite-albite ($An_{0–5}$) ± K-feldspar ± dolomite ± epidote and rare postkinematic chloritoid. Zoisite occurs locally in Moodies sandstones. Along the margins of the greenstone belt, rocks of the Swaziland Supergroup have been severely altered by contact

TABLE 1. PETROGRAPHIC GRAIN, CEMENT, AND MATRIX TYPES RECOGNIZED DURING POINT COUNTING

Grains

- Q_t = total quartz
  - Q_m = monocrystalline quartz (> 90% of grain made up of single crystal)
    - Q_{mu} = undulose extinction (> 5°)
    - Q_{mv} = recognizable volcanic quartz (euhedral, embayed)
  - Q_p = polycrystalline quartz (no single crystal makes up more than 90 % of grain)
    - $Q_{p2\text{-}3}$ = 2 or 3 crystals per grain
    - $Q_{p>3f}$ = more than 3 subgrains; foliated/stretched
    - Q_{pc} = chert (> 90% of grain is granular microcrystalline quartz)
      - Q_{pcc} = carbonaceous chert
      - Q_{pchem} = hematitic chert
      - Q_{pcca} = calcareous chert
      - Q_{pcevap} = radial, fan-like extinction; possibly silicified evaporite
- F_t = total feldspar (monocrystalline and polycrystalline forms)
  - F_k = potassium feldspar except microcline
  - F_m = microcline
  - F_p = plagioclase feldspar (twinned and untwinned)
- L_t = total lithic fragments
  - L_s = sedimentary rock fragments
    - L_{smud} = mudstone or shale fragment (detrital subgrains not resolvable)
    - L_{ssist} = siltstone fragment (detrital subgrains resolvable but not identifiable; commonly ferruginous)
    - L_{soth} = other sedimentary rock fragments
  - L_v = volcanic rock fragment
    - Lvser = massive sericite grains (mostly from feldspars?)
    - Lvpp = plagioclase porphyry (dacitic) rock fragment
    - Lvt = tuffaceous rock fragment (distinguishable from Lssist)
    - Lvum = ultramafic rock fragment (commonly silicified)
    - Lvoth = other volcanic rock fragment
  - L_m = metamorphic rock fragments (not metasedimentary nor metavolcanic; usually foliated and of higher grade than surrounding matrix)
- QS = fine-grained quartz-sericite mosaic grains
  - $QS_{5\text{-}30}$ = 5 - 30 % sericite in random orientation
  - $QS_{30\text{-}70}$ = 30 - 70 % sericite in random orientation
  - $QS_{70\text{-}95}$ = 70 - 95 % sericite in random orientation
  - QS_o = fine-grained quartz-sericite mosaic with oriented sericite laths

Matrix

- M_{qsc} = fine-grained quartz / sericite / carbonate

Cement

- C_{qtz} = quartz cement
- C_{ser} = sericite cement

Note: Accessory minerals tallied separately, including opaque grains, muscovite, biotite, zircon, chlorite, and other.

metamorphism, locally to amphibolite grade; shearing; recrystallization; and metasomatism (Anhaeusser, 1969, 1984; Faure and Harris, 1991).

Metasomatic alteration

Despite their low grade of metamorphism, all BGB rock types, including Moodies sandstones, have been pervasively affected by low-temperature alteration. Metasomatic alteration, including steatization, silicification, potash metasomatism, and iron alteration, has been especially well documented in rocks of the Onverwacht Group (Condie et al., 1977; Paris et al., 1985; Lowe and Byerly, 1986; Duchac and Hanor, 1987; Hanor and Duchac, 1990; de Ronde et al., 1994). The tops of ultramafic flow units and associated fine-grained tuffaceous sediments have been widely altered to impure cherts, now composed largely of silica, sericite, and trace amounts of oxides (Duchac and Hanor, 1987; Hanor and Duchac, 1990; Lowe, this volume, Chapter 3). Coarser grained mafic and ultramafic pyroclastic rocks and flow units commonly show extensive carbonate replacement (Ransom et al., this volume, Chapter 6). Silicification and potash metasomatism also locally affected rocks of the Fig Tree Group (Lowe, this volume, Chapter 3), and Toulkeridis et al. (1996) noted upward increases in the K and SiO_2 contents of illites from the Fig Tree to the Moodies Group, which they related to changes in provenance and possibly to recrystallization processes.

In the course of the present study, we have found no evidence of pervasive regional silicification, potash metasomatism,

or carbonation in rocks of the Moodies Group. Coarsely crystalline calcite, dolomite, and ankerite replacing feldspar and quartz-sericite grains and matrix are spottily developed in the interiors of major tectonic blocks but are more abundant near major fault zones and the margins of the greenstone belt (Anhaeusser, 1969; Viljoen and Viljoen, 1969; Faure and Harris, 1991). Carbonated rocks cannot readily be used for provenance analysis. Partial silicification is common in Moodies sandstones. The degree of silicification is controlled by grain size, composition, porosity, and degree of deformation; it affects matrix-rich sandstones the least whereas quartz-rich sandstones commonly show syntaxial quartz overgrowth. However, these quartz overgrowths probably reflect early silica diagenesis and cementation rather than significant silica metasomatism. The widely differing relative abundance of silica and sericite in thin section argues against pervasive regional silica or potash metasomatism. Present mineralogy and chemical composition suggest that the overall compositions of Moodies sandstones have not changed substantially during post-depositional alteration.

Quartz-sericite grains and quartz-sericite matrix

Recrystallization of unstable and fine-grained lithic grains, feldspar, and matrix material to a micromosaic of intergrown quartz and sericite is widespread in Moodies rocks. This process has strongly altered the texture of many rocks. In some, grains of quartz, chert, and preserved feldspar now appear to float in a quartz-sericite matrix. Alteration of primary components to quartz-sericite mosaic may have affected the composition in some areas. Because quartz-sericite mosaics of very similar appearance under the petrographic microscope may have widely differing origins, our point count scheme considered all polycrystalline quartz grains containing between 5 and 95% sericite as quartz-sericite (QS) grains (Table 1).

The proportions of quartz and sericite in QS grains can vary widely. In most cases, small, generally randomly oriented sericite blades and sparse finely disseminated opaque minerals are included in a mosaic of microcrystalline quartz grains (Fig. 2A). Weak alignment of sericite blades may reflect remnant crystal structure, outlining the cleavage of feldspar or mafic grains. In QS grains containing more sericite than quartz, small quartz grains float evenly or in small clusters in a matrix of randomly oriented sericite blades of variable grain size. Because sericite grains with little or no quartz are very fragile but locally show blade alignments reminiscent of crystal structure, at least some if not all of the alteration must have occurred after deposition.

Timing of alteration

The timing of alteration in the BGB and the maximum temperature attained have been the subjects of several recent studies. De Ronde (1991) demonstrated that elevated geothermal gradients exceeded the $^{40}Ar/^{39}Ar$ blocking temperature of sericite (thought to be at approximately 200°C) at 2,670–2,680 Ma in the BGB. Toulkeridis (1992) documented the resetting of the Rb-Sr, Pb-Pb, and Sm-Nd systems in carbonates from the Onverwacht and the Fig Tree Groups at about 2,700 Ma. López-Martínez et al. (1984) described severely disturbed $^{40}Ar/^{39}Ar$ age spectra of biotites from the circa 3,445-Ma Stolzburg pluton that yield ages of approximately 2,600 Ma, suggesting that temperatures approached or exceeded the blocking temperature of biotite (~300°C) several hundred million years after greenstone belt formation. $^{40}Ar/^{39}Ar$ age spectra extracted from amphiboles and serpentinites of the Onverwacht Group have yielded much older plateau ages, which approach their formation ages, presumably due to the much higher blocking temperature for these minerals (~650°C) (López-Martínez et al., 1984). Oxygen-isotope data from a jaspilite in the lower Fig Tree Group of the southern facies in the BGB indicate that the rock was subjected to temperatures of 320–360°C (Perry and Tan, 1972). De Ronde (1991) concluded that rocks of the BGB have not been exposed to temperatures exceeding 650°C since their formation but must have been overprinted by temperatures above 200°C. Most recently, de Ronde and de Wit (1994) suggested that the hydrothermal gold deposits along the northern margin of the greenstone belt were formed between 3,126 and 3,084 Ma. This age range coincides generally with the emplacement of large granitoid plutons north of the Barberton Greenstone Belt and with a change in tectonic regime (de Ronde and de Wit, 1994). The migration of hydrothermal fluids at that time may have contributed significantly to the pervasive alteration of Moodies sandstones.

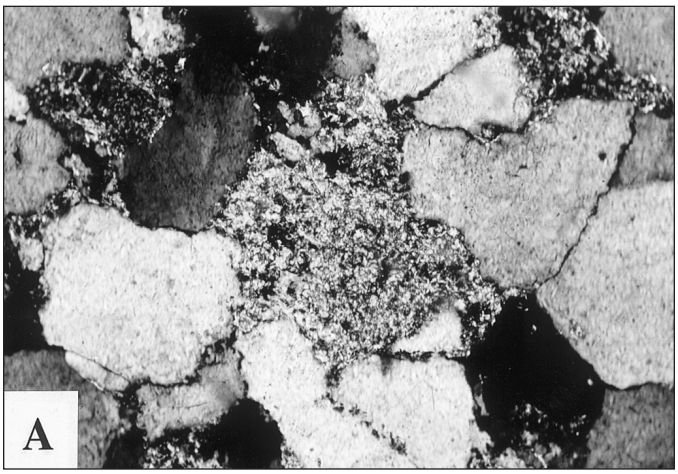
In addition to the 2,700-Ma thermal event widespread in the BGB, de Ronde (1991) found evidence for thermal overprints at 2,400 Ma and 2,090–2,025 Ma. The 2.7-Ga event is widely thought to have been related to the Limpopo orogeny approximately 250 km to the north of the BGB. The later events are probably related to the formation of the Transvaal basin and the emplacement of the Bushveld Complex, respectively (de Ronde, 1991; Toulkeridis, 1992).

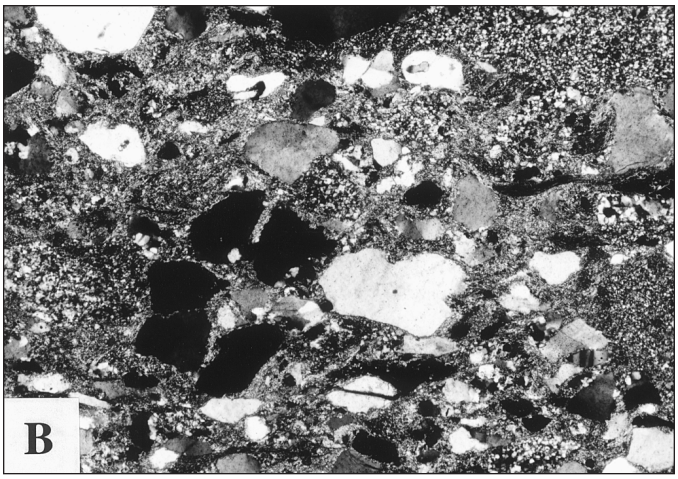
Although these studies place minimum ages on the timing of alteration of BGB rocks, they mostly record disturbances due to the last major thermal event that affected the study area. They do not exclude the possibility that temperatures may have reached the same levels at some time or for a significant period of time before the last major thermal perturbation (de Ronde, 1991). It is also possible that many changes occurred immediately after burial during diagenesis and burial metamorphism, as suggested by Reimer (1972) for graywackes of the northern facies of the Fig Tree Group.

MODAL ANALYSIS OF SANDSTONES OF THE MOODIES GROUP

Grain types

Monocrystalline and polycrystalline quartz are the principal framework components of Moodies Group sandstones. Nearly all monocrystalline quartz grains are moderately strained with





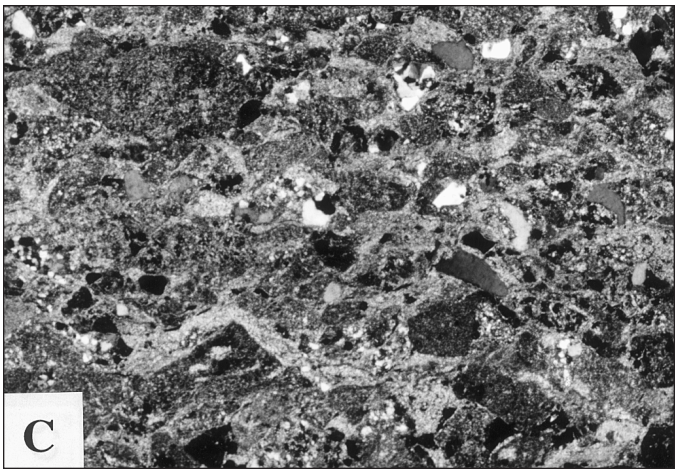


Figure 2 (above and to the right). Photomicrographs of Moodies sandstones. A, Massive sericite grain (center), probably an altered feldspar or volcanic lithic grain, surrounded by monocrystalline quartz grains. Photograph is 1.0 mm wide. Crossed nicols. The Heights syncline. Sample 3616. B, Litharenite rich in quartz-sericite grains, probably representing altered lithic fragments, and sericitic matrix that may in part be pseudomatrix representing altered lithic grains. Slight strain obscures the subtle distinction between quartz-sericite (QS) grains, represented by larger patches similar in size to quartz grains, and sericitic matrix. Photograph is 1.5 mm wide. Crossed nicols. Saddleback syncline. Sample 2190. C, Moderately strained Moodies litharenite rich in quartz-sericite (QS) grains that probably represent altered lithic fragments and sericitic matrix. Moderate strain, not visible in handsample, obscures the distinction between QS grains and QS matrix. Photograph is 2.0 mm wide. The Heights syncline. Sample 3635. Crossed nicols.

extinction over an angular rotation of 5°–20°. Strain appears to be greater in the more quartzose and silica-cemented units and less in units in which quartz grains are embedded in a fine-grained QS mosaic matrix, suggesting that strain in the quartz grains was induced after deposition and is not reflective of sand provenance. Compaction has severely affected quartz-rich units; many quartz grains display sutured grain contacts.

Monocrystalline quartz (Q_m) is the dominant quartz type. Most Q_m grains are subequant and clear, or show minor inclusions of sericite, chlorite, or opaque minerals. Water-clear grains free of inclusions, with partial resorption embayments or remnants of beta-quartz morphologies and nonundulatory extinction are interpreted to be of volcanic origin. Quartz grains with abundant inclusions, mostly of sericite, or showing "cockscomb" structure were probably derived from quartz veins and hydrothermally altered rocks and are most common in the lower third of the Moodies Group.

Four types of polycrystalline quartz were distinguished (Table 1): (1) subequant grains consisting of 2–3 domains of monocrystalline quartz, lacking preferred crystallographic or morphological orientation, and displaying undulose or straight domain boundaries; (2) grains showing preferred orientation of elongated domains and sutured contacts, reminiscent of foliation; (3) grains consisting of polygonized subequant quartz domains, typically >40 microns in size, and showing well-defined straight domain boundaries; and (4) chert, consisting of subequant domains typically <40 microns in size, with poorly defined domain boundaries.

Cherts in the BGB formed by silicification of virtually every primary volcanic and sedimentary rock type and possibly through primary precipitation in sedimentary or hydrothermal systems (Lowe and Knauth, 1977; Paris, 1985; Lowe, this volume, Chapter 3). During point counting, textural and compositional features suggestive of the origin of chert grains were noted, such as textural preservation of spinifex blades, euhedral feldspar, beta-quartz phenocrysts, carbonaceous matter, shard textures, and accretionary lapilli. Most detrital chert grains, however, are composed of structureless, translucent, microcrystalline quartz or have ambiguous internal structures. The virtually identical chemical composition of these chert varieties has been shown by Lamb (1984) and Lowe (this volume, Chapter 3) for cherts from the Fig Tree and Onverwacht Group. In most cases,

we found it impossible to assign the chert grains reliably to one of the designated subcategories. Chert grains without clearly identifiable textures were lumped into the general "chert" category (Q_{pc}). The difference between chert and QS grains was drawn at 5% sericite content.

Both K-feldspar and plagioclase are present in the Moodies Group. K-feldspar includes untwinned orthoclase, identified by staining, cloudy appearance, and cleavage planes, and polysynthetically twinned microcline in a ratio of approximately 3:1. K-feldspar grains are commonly fresh or only slightly sericitized. The degree of sericitation is least in silica-cemented samples. Hose (1990) distinguished two populations of K-feldspar, based on their differing degree of alteration, and suggested different sources for each. Plagioclase, which is unzoned, is only moderately affected by sericitization north of the Inyoka fault and readily identifiable by polysynthetic twinning. Albitization has altered its composition to $An_{0–10}$. South of the Inyoka fault, plagioclase has been altered to various degrees to QS grains. Where an altered plagioclase grain was recognizable by aligned sericite blades or by remnant polysynthetic twinning, it was counted as plagioclase. Otherwise, it was counted as QS.

Lithic fragments include volcanic, sedimentary, and metamorphic fragments. Only rarely are grains in Moodies Group sandstones sufficiently unaltered that they can be classified unambiguously as tuffaceous or ultramafic lithic fragments. Mudstone fragments are distinguished by their fine grain size and homogenous composition. Criteria identifying metamorphic rock fragments include mineral foliation or the presence of high- or medium-grade metamorphic minerals.

Quartz-sericite (QS) grains were divided into four groups on the basis of their sericite percentage: 5–30%, 30–70%, 70–95%, and massive sericite grains. Where they showed remnants of primary features that indicated their derivation from other grain types, such as microphenocrysts in altered tuffs or relict twinning in plagioclase feldspar, they were counted as the unaltered grain type.

Grains of intrabasinal provenance were rarely observed. Clay drapes and rip-up clasts, common in some outcrops, are represented in thin sections by massive detrital chlorite fragments and crushed sericite-chlorite aggregates.

Accessory detrital minerals include common biotite, muscovite, chlorite, and chlorite aggregates. Heavy minerals include common zircon, rare apatite and epidote, and both detrital and diagenetic pyrite, hematite, and other opaque minerals.

Any original detrital or authigenic matrix in Moodies Group sandstones has been recrystallized to a mosaic of fine-grained, randomly oriented sericite and fine-grained polycrystalline quartz with accessory Fe-oxide grains and finely disseminated chlorite, strongly resembling QS grains in thin section. The distinction between QS grains and QS matrix during point counting is based on the common presence of fine-grained iron-oxide stain defining remnant grain outlines, well-defined changes in the quartz/sericite ratio or in quartz-sericite grain size from matrix to grain, and oversized spaces filled by QS in a tightly packed framework (Fig. 2B). These features, however, can be easily destroyed by strain that may not be apparent in hand sample (Fig. 2C). It is, therefore, likely that at least some of the material classified as QS matrix represents crushed and deformed QS grains which should be properly counted as pseudomatrix. Where an unambiguous assignment to either the grain or the matrix category was not possible, the QS material was considered matrix, therefore contributing to a potential overestimation of matrix in the modal analysis.

A distinction between epi-, ortho-, and pseudomatrix in Moodies Group sandstones is not possible. All matrix was therefore lumped into one category. The inability to distinguish between pseudomatrix, which should be assigned to a detrital category, and epi- and orthomatrix, which should be assigned to matrix, introduces an additional uncertainty in the modal analysis. Based on visual comparison of strained samples, as in Figure 2C, with the least-strained Moodies sandstone samples, we estimate that between 5 and 15% of the total points counted in average Moodies sandstone samples actually may be pseudomatrix. Due to the inability to distinguish between pseudomatrix (or matrix in general) and QS grains, the framework percentage is therefore probably a low estimate and may be 5–15% higher.

Moodies sandstones are generally quartz or carbonate cemented. Because the sandstones are highly altered and recrystallized to various degrees, original cement textures are rarely visible in thin sections. The presence of syntaxial quartz overgrowths, recognizable by the presence of a "dust rim" on quartz-overgrown quartz grains, is common in the Q_m+Q_p-rich sandstones of the middle and upper parts of the Moodies Group. Carbonate cement occurs as patchy specks in thin section, mostly in the middle Moodies Group north of the Inyoka fault, and may be partly related to hydrothermal alteration.

Vertical variations in sandstone petrology

The south limb of the Saddleback syncline exposes the thickest section of Moodies rocks known in the BGB (Fig. 3), more than 3.5 km thick. This section serves as a "type" section for the present petrographic study with which other sections can be compared. Figure 4A and B shows variations of grain types with stratigraphic height for seven measured sections within five fault-separated tectonic blocks north of the Inyoka fault. Compositional parameters plotted include the abundance of monocrystalline quartz (Q_m), total lithic fragments including matrix (L+Q_p+M), feldspar (F), chert (Q_{pch}), total quartz (Q_m+Q_p), lithic fragments (L), and lithic fragments including matrix (L+M). In addition, the framework percentage, defined as the number of grain counts divided by the number of total counts, is plotted. For some grain types, petrographic variations are systematic and correlatable from section to section. Most trends, except framework percentage, change at or near the basaltic unit ("MdL" of Visser, 1956) in the upper Moodies Group, which is also the stratigraphic datum, suggesting a two-

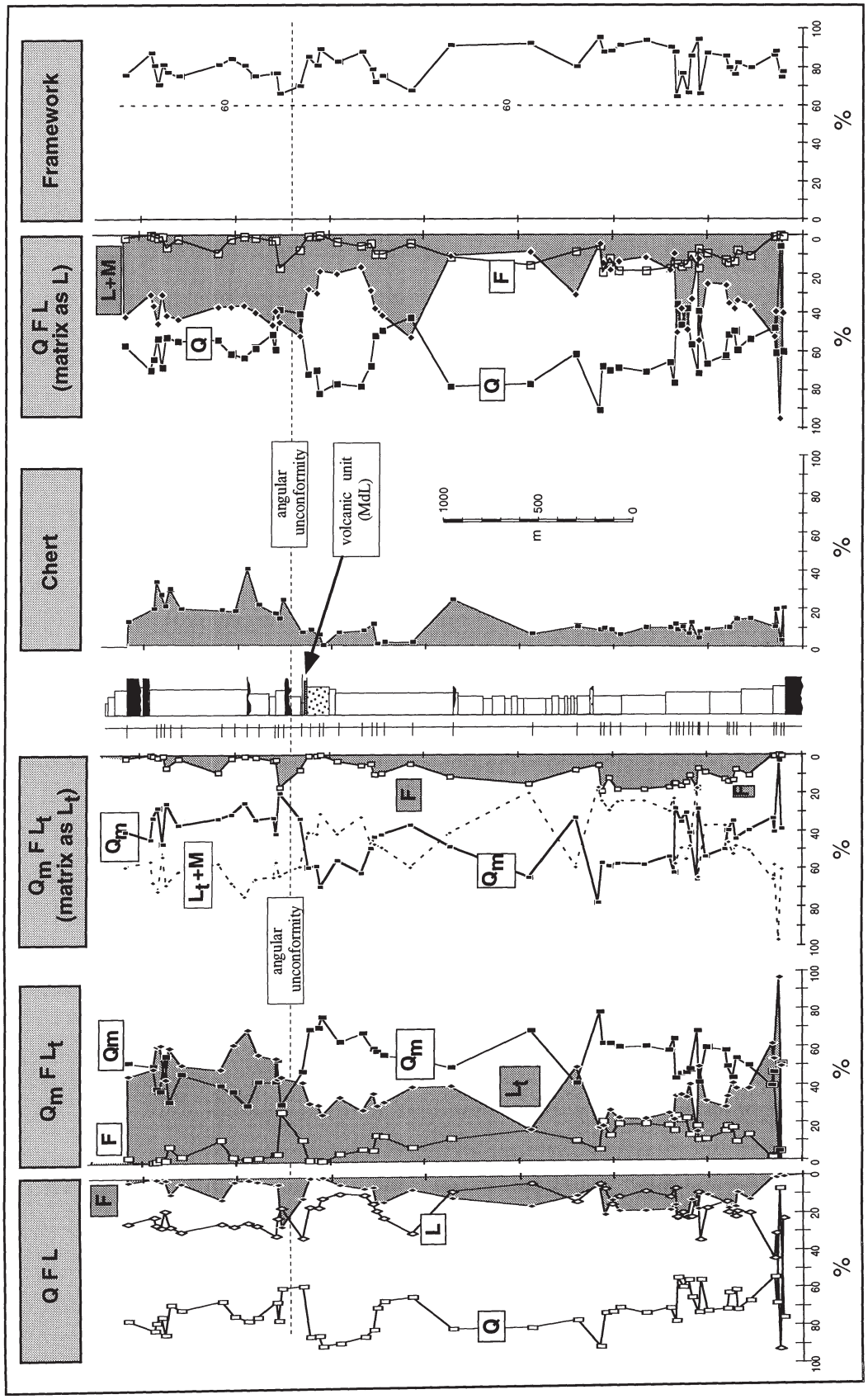


Figure 3. Petrographic variations with stratigraphic position in the Moodies Group, eastern Saddleback syncline (column 4a, Fig. 1). This area exposes the thickest section of the Moodies Group and was sampled in greatest detail. The stratigraphic column in the center shows the position of petrographic samples. QS (quartz-sericite) grains are grouped with lithic grains. Q, quartz; F, feldspar; L, lithic; Q_m, monocrystalline; L_t, total lithics.

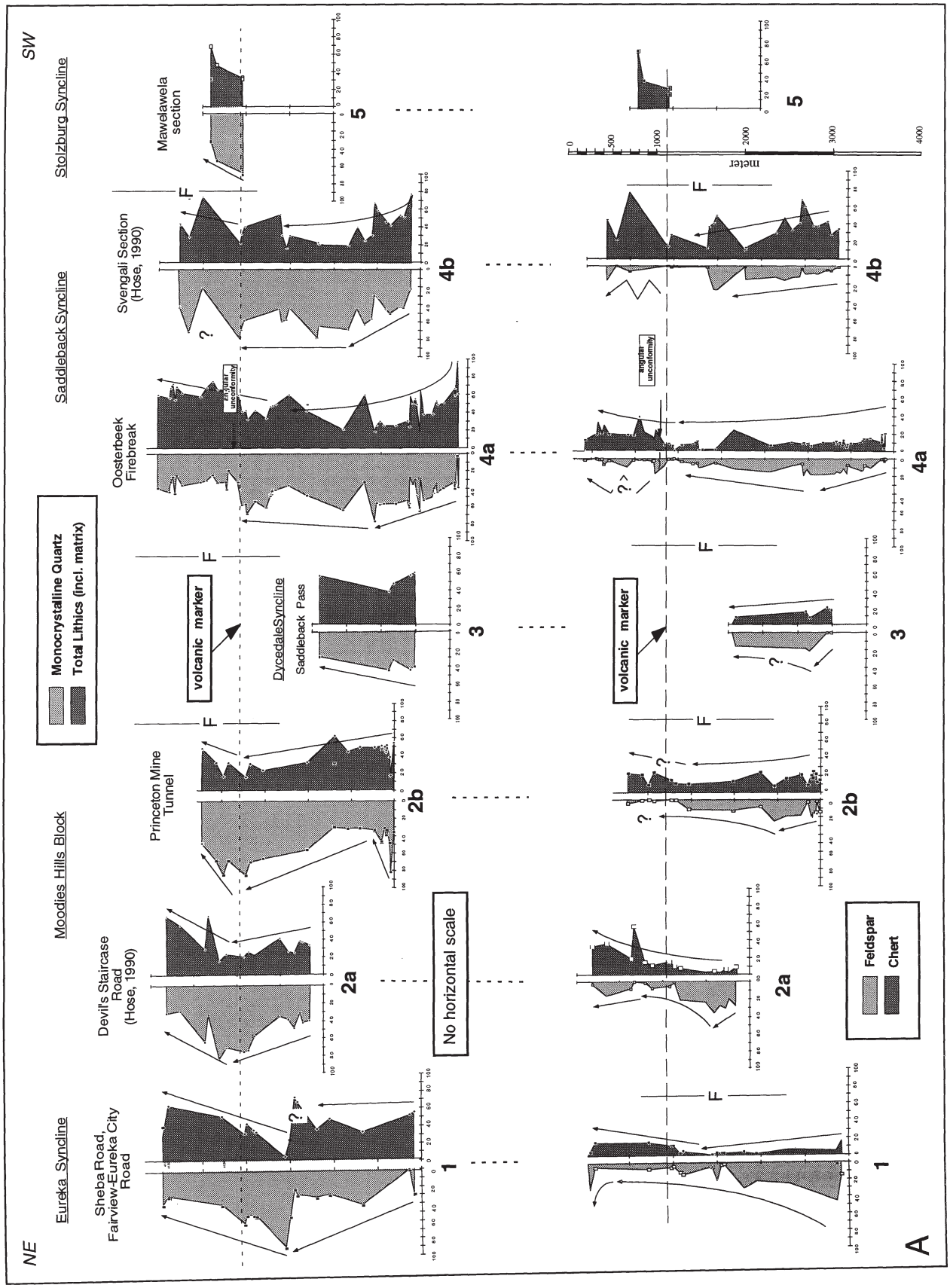
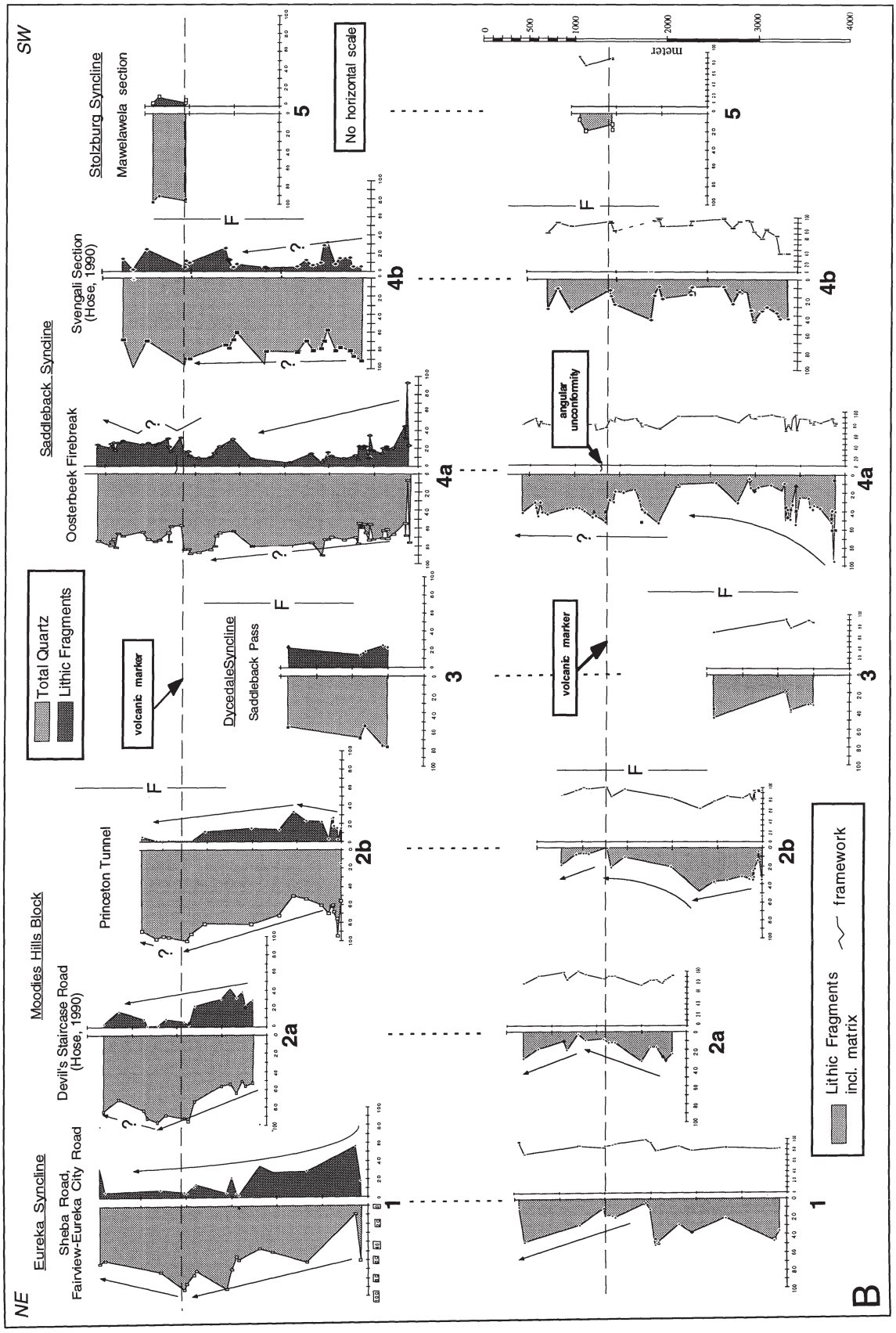


Figure 4 (this and facing page). Changes in percentage of selected compositional components with stratigraphic position for sections of the Moodies Group north of the Inyoka fault. Note distinct changes in compositional trends near the volcanic unit or near the stratigraphic level of the angular unconformity in the Saddleback syncline. A, Variations in monocrystalline quartz, total lithic rock fragments (including matrix), feldspar, and chert. Column numbers correspond to those shown in Figure 1. B, Variations in monocrystalline quartz, lithic fragments, lithic fragments (including matrix), and percentage of framework grains.


NE
SW
B
Eureka Syncline
Sheba Road, Fairview-Eureka City Road
Moodies Hills Block
Devil's Staircase Road (Hose, 1990)
Princeton Tunnel
DycedaleSyncline
Saddleback Pass
Saddleback Syncline
Oosterbeek Firebreak
Svengali Section (Hose, 1990)
Stolzburg Syncline
Mawelawela section
Total Quartz
Lithic Fragments
volcanic marker
angular unconformity
No horizontal scale
meter
0
500
1000
2000
3000
4000
1
2a
2b
3
4a
4b
5
F
Lithic Fragments incl. matrix
framework

fold subdivision of the Moodies Group based on sandstone petrography into lower and upper divisions (Fig. 4).

Monocrystalline quartz forms the major constituent of all thin sections. Its abundance generally increases upward toward the volcanic marker unit and then generally decreases above it. The narrow definition of chert (Q_{pch}; see Table 1) in this study makes this grain type a comparatively minor contributor to the Moodies Group. Its abundance is constant and low below the volcanic marker horizon but fluctuates widely above it. Foliated polycrystalline quartz grains ($Q_{p>3f}$), suggestive of a low-grade metamorphic origin, are exceedingly rare and remain below 1% of framework components in all thin sections.

Feldspar increases slightly from a nearly feldspar-free basal unit to a maximum about 1 km above the base of the section, then declines gradually upsection and disappears completely near the volcanic marker unit. Toward the top of the group, feldspar-bearing units appear again as distinctive pulses in otherwise feldspar-free sandstones. It is noticeable that all conglomeratic sections are feldspar free, and no conglomerates occur in feldspar-bearing sections.

The sum of total lithic grains, QS grains, and matrix ($L+Q_p+QS+M$) decreases upsection to the volcanic marker unit, above which it increases or shows no systematic variation.

The most significant variation in sandstone composition with stratigraphic height in the Moodies Group sandstones is the near-perfect co-variation of monocrystalline quartz and total lithic fragments plus QS grains plus matrix (Fig. 4A). The former increases in abundance to an intraformational angular unconformity approximately 2,800 m above the base of the Saddleback syncline section and then decreases to the top. The latter shows the opposite trend. Aberration from perfect co-variation in this plot is caused by not considering the feldspar component. Vertical changes in sandstone composition are also displayed using ternary diagrams (Heubeck, 1993). Ternary diagrams for the eastern Saddleback syncline (Fig. 5) show increasing quartz and monocrystalline quartz to the unconformity, followed by a decrease in quartz.

Moodies rocks in the Dycedale syncline lack distinct stratigraphic marker units that would allow a correlation to either the Moodies Hills block or the Saddleback syncline (Fig. 1). However, the high feldspar content, moderate abundance of monocrystalline quartz, and stable low abundance of chert indicate that the section is probably correlative with the lower Moodies Group. This petrographic correlation is also consistent with the similarity of its tidal-dominated facies assemblage with tidal units in the lower part of the Moodies Group in the adjacent Saddleback syncline (Heubeck and Lowe, 1994a).

Regional variations in sandstone composition

The compositional variability of individual units along strike was examined in detail only for the unit MdQ2 (Fig. 6), which shows a distinct northeast-to-southwest decrease in the abundance in feldspar that appears to be compensated by an increase in monocrystalline quartz. This decrease in feldspar toward the southeast is also apparent in the Moodies Group as a whole north of the Inyoka fault (Fig. 4A and B).

Moodies rocks south of the Inyoka fault are compositionally distinct from those north of the fault. Those north of the Inyoka fault plot over a wide range of compositions within the upper half of a QFL diagram (Fig. 7). Sandstones south of the Inyoka fault, in contrast, contain no detrital feldspar (Hose, 1990) and are therefore restricted to a narrow band along the Q-L side of the ternary diagram, plotting mostly in the sublitharenite field (Fig. 8). Monocrystalline quartz, QS grains (counted as L), and chert are the principal components of these sandstones. No evidence was found for post-depositional feldspar removal, such as skeletal feldspar remnants, oversized infilled pores, or signs of alteration conditions different from those north of the Inyoka fault. Some massive sericite grains and QS grains displaying aligned sericite blades may be remnants of completely altered plagioclase grains but these grain types combined do not exceed 3% of the total framework grains. In strong contrast to Moodies Group rocks north of the Inyoka fault, petrographic changes among blocks and with stratigraphic position within blocks south of the Inyoka fault appear to be either irregular or not apparent due to the small stratigraphic thicknesses of the exposed sections (Figs. 1 and 8).

Two occurrences of K-feldspar south of the Inyoka fault are exceptions to the general absence of feldspar in this area. One is a K-feldspar-bearing quartzose chert arenite unit in the Mapepe Formation of the lower Fig Tree Group in Paulus' syncline (location shown in Fig. 9). The other is a fault sliver of Moodies rocks located about 400 m south of the Inyoka fault in the Heemstede syncline (Fig. 1). This sliver probably originated north of the Inyoka fault and was transferred to the southern block due to a northward shift in the location of the fault trace.

Moodies strata across the Inyoka fault also differ strongly in depositional facies. Quartz-rich Moodies sandstones south of the Inyoka fault were deposited largely in lower-alluvial-fan and braided-stream environments (Heubeck and Lowe, 1994a). A thick but discontinuous and locally derived basal Moodies conglomerate overlies folded and faulted Fig Tree and Onverwacht rocks in the The Heights syncline with angular unconformity (Fig. 1; and Heubeck and Lowe, 1994a). Clay-draped ripple marks, clast- and matrix-supported conglomerate lenses, small- and medium-scale foresets with pebbles on the foresets, single-clast-thick gravel stringers, and small-scale fluid escape structures in the overlying sandstones are common. Some foresets attain vertical heights of as much as 4 m and have been tentatively interpreted to be eolian (Ascher, 1992; Lowe and Byerly, this volume, Chapter 1). However, evidence for extensive deltaic, nearshore, or offshore sedimentation common in Moodies rocks north of the Inyoka fault is absent.

The stratigraphic and petrographic contrasts between Moodies sandstones across the Inyoka fault indicate that it separates Moodies sections having different source areas, different basins of sedimentation, and/or different diagenetic histories. The

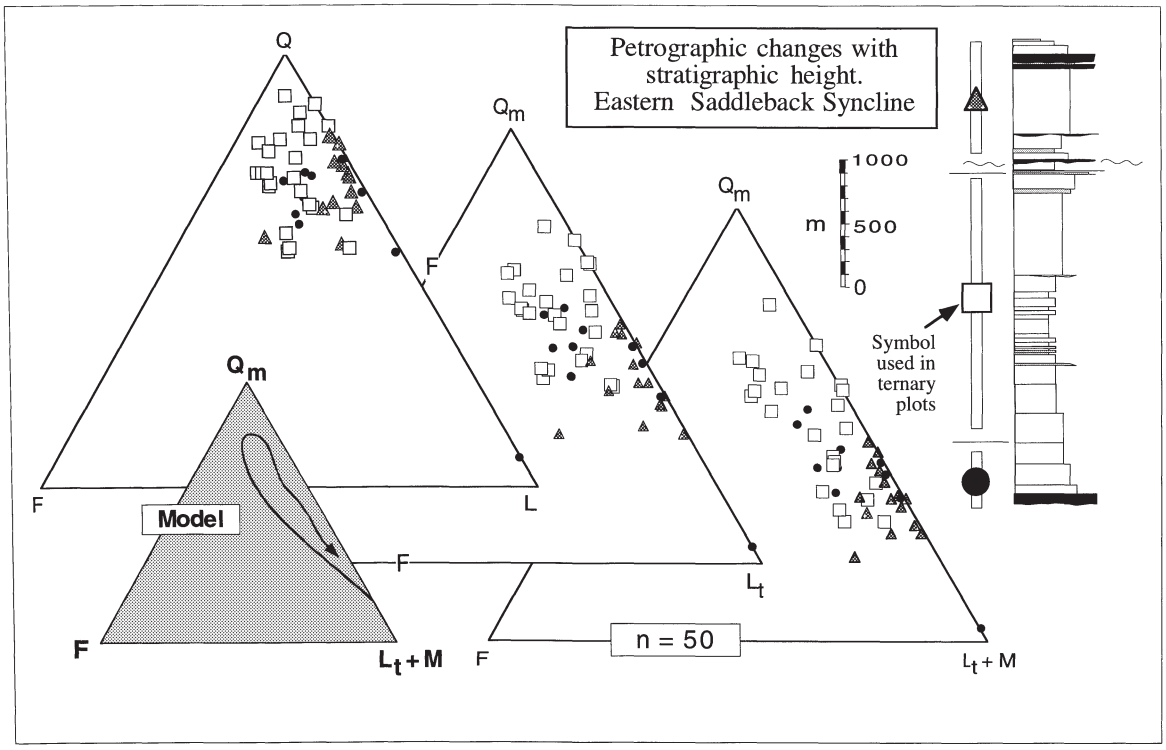


Figure 5. Ternary diagrams showing changes in sandstone composition with stratigraphic position in the Moodies Group, eastern Saddleback syncline (column 4, Fig. 1). Circles and squares represent lower and upper sections of the Oosterbeek petrofacies, respectively. Triangles represent samples from the Elephant's Head petrofacies. The best separation between the overlapping fields is shown in the Q_mFL_t diagram, where L_t includes QS grains and matrix. The model generalizes the sandstone evolution and shows an abrupt reversal of a maturation trend. For definition of grain types, see Table 1.

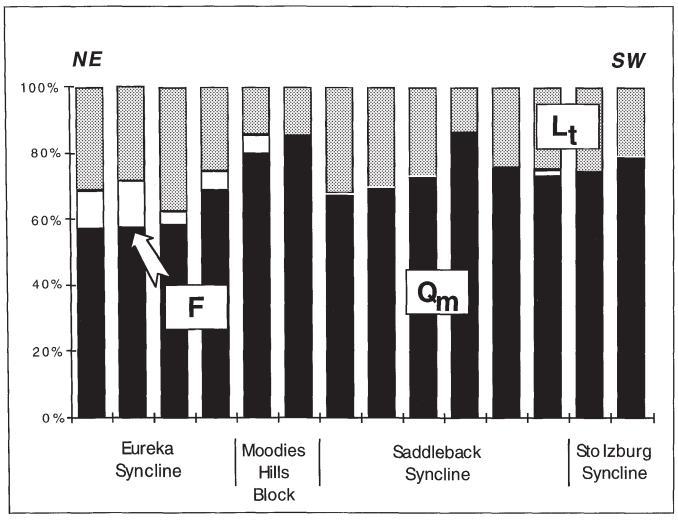


Figure 6. Lateral variations in the composition of sandstone unit MdQ2 (see Fig. 1 for stratigraphic position of MdQ2). Note that feldspar, mostly K-feldspar, decreases from northeast to southwest.

Inyoka fault is the longest identifiable fault in the BGB and can be traced continuously for more than 50 km from the western end of the belt, where it may continue westward into the poorly exposed tonalitic plutons, through the central BGB, and into the incompletely mapped northeastern region (Fig. 1). It has played an important role as a terrane boundary within the greenstone belt, separating area with differing styles of deformation (de Ronde and de Wit, 1994; Heubeck and Lowe, 1994b; Lowe et al., this volume, Chapter 2; Lowe, this volume, Chapter 3). Several phases of movement, including reverse and left-lateral strike-slip, have been documented from its central segment (Hose, 1990). Its significance as a stratigraphic divide between northern and southern Fig Tree facies was noted by Heinrichs and Reimer (1977) and Reimer (1980).

One of the largest outcrop belts of coarse clastic sedimentary rocks in the south-central BGB, the Sibubule-Emlembe belt that straddles the South African–Swaziland border and includes the Josefskop and Border Post synclines (Fig. 9), includes conglomerate units as much as 1,000 m thick that appear to represent alluvial fans. These rocks have previously been assigned to the Moodies Group (Visser, 1956; Eriksson, 1979; Heinrichs, 1980; Jackson et al., 1987), but our studies suggest that they belong to the Fig Tree Group and cannot be used to constrain

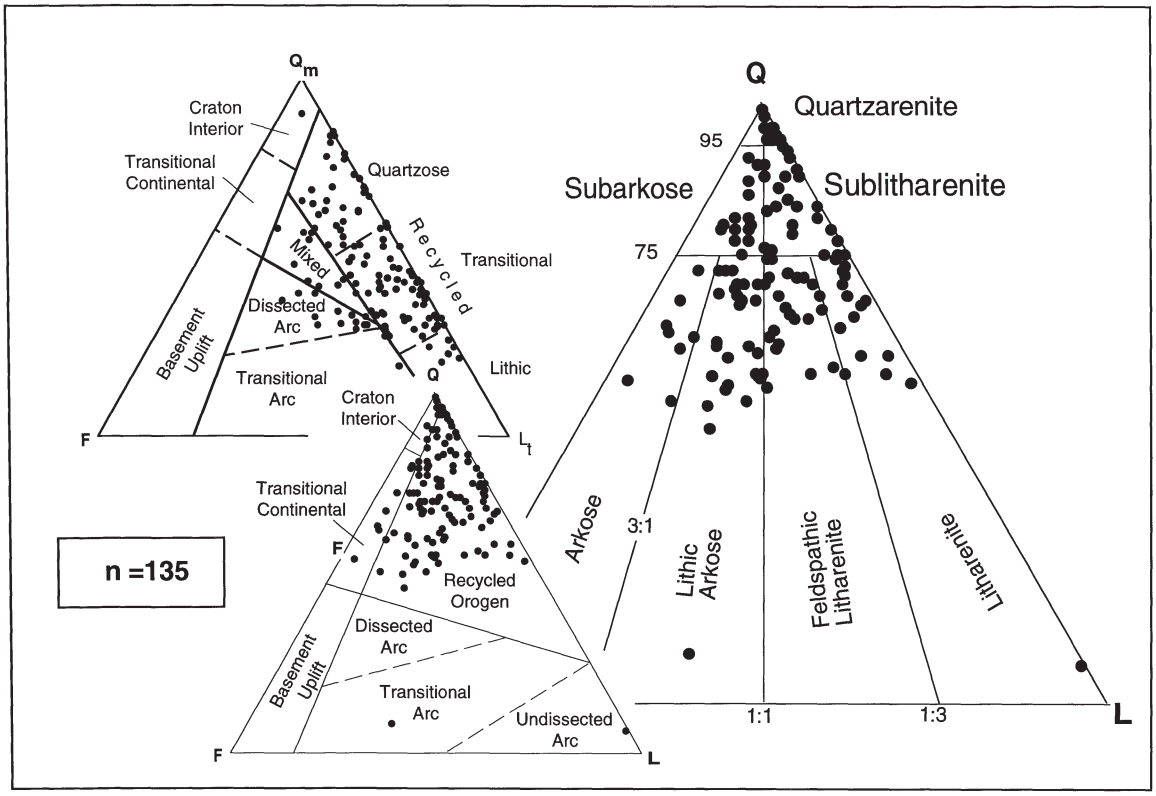


Figure 7. Composition and classification of Moodies sandstones north of the Inyoka fault (right). Fields after Folk (1968). Small ternary diagrams (left) show tectonic setting after Dickinson et al. (1983). Moodies rocks plot largely in the recycled orogen field. For definition of grain types, see Table 1.

Moodies provenance. The conglomerate conformably and gradationally overlies banded ferruginous chert, jasper, and ferruginous shale of the lower Fig Tree Group (Heinrichs, 1980; Paris, 1985). Sandstone lenses in the conglomerate are petrologically identical to unambiguous Fig Tree chert arenite in the Mapepe Formation. Like chert arenites in the Mapepe Formation (Fig. 10), the sandstone contains less than 10% monocrystalline quartz and consists almost entirely of grains of chert and minor silicified mafic and ultramafic volcanic rocks of the Onverwacht Group. It is petrologically distinct from Moodies sandstone north and south of the Inyoka fault (Fig. 10). The conglomerate is a monomict chert-clast conglomerate (Fig. 9) and dissimilar to any Moodies conglomerate examined. We suggest that the Sibubule-Emlembe belt is made up of Fig Tree conglomerate and sandstone and cannot be used in provenance or stratigraphic studies of the Moodies Group.

PETROLOGY OF CONGLOMERATES IN THE MOODIES GROUP

Moodies conglomerates are typically clast-supported and polymictic. Common clast types include chert of several varieties, mafic and ultramafic volcanic rock, jaspilite, and felsic volcanic rock. Less common components include graywacke, shale, vein quartz, quartzose sandstone, and, rarely, plutonic rock. The proportions of the clast types vary rapidly along strike, vertically, and from outcrop belt to outcrop belt. Figure 11 shows the composition of the basal Moodies conglomerate in the Saddleback syncline. The basal conglomerate is polymict and shows rapid variations in clast composition over most of the area. In contrast, in the The Heights syncline, south of the Inyoka fault, the basal conglomerate shows a relatively constant clast composition in which felsic volcanic clasts make up about 75% of the total clast population (Fig. 11). None of the Moodies or Fig Tree conglomerates examined contains clasts of metamorphic or crystalline rocks that might indicate derivation from a high-grade metamorphic terrane, such as the Ancient Gneiss Complex.

The thickest conglomerates in the Moodies Group occur near the top of the sequence in the Saddleback syncline, where two units of alluvial conglomerate occur, one overlying a south-facing intraformational angular unconformity (Heubeck and Lowe, 1994a). These conglomerates are polymict, clast supported, and dominated by chert clasts.

Conglomerate and sandstone compositions generally correlate well. The basal conglomerate in the Saddleback syncline, polymict but free of feldspar-bearing clasts, has as a matrix and is overlain by feldspar-free, quartzose, lithic-rich sandstone. Similarly, the wedges of chert-clast conglomerate higher up in the section are interbedded with chert-rich sandstone (Fig. 3), and the basal conglomerate in

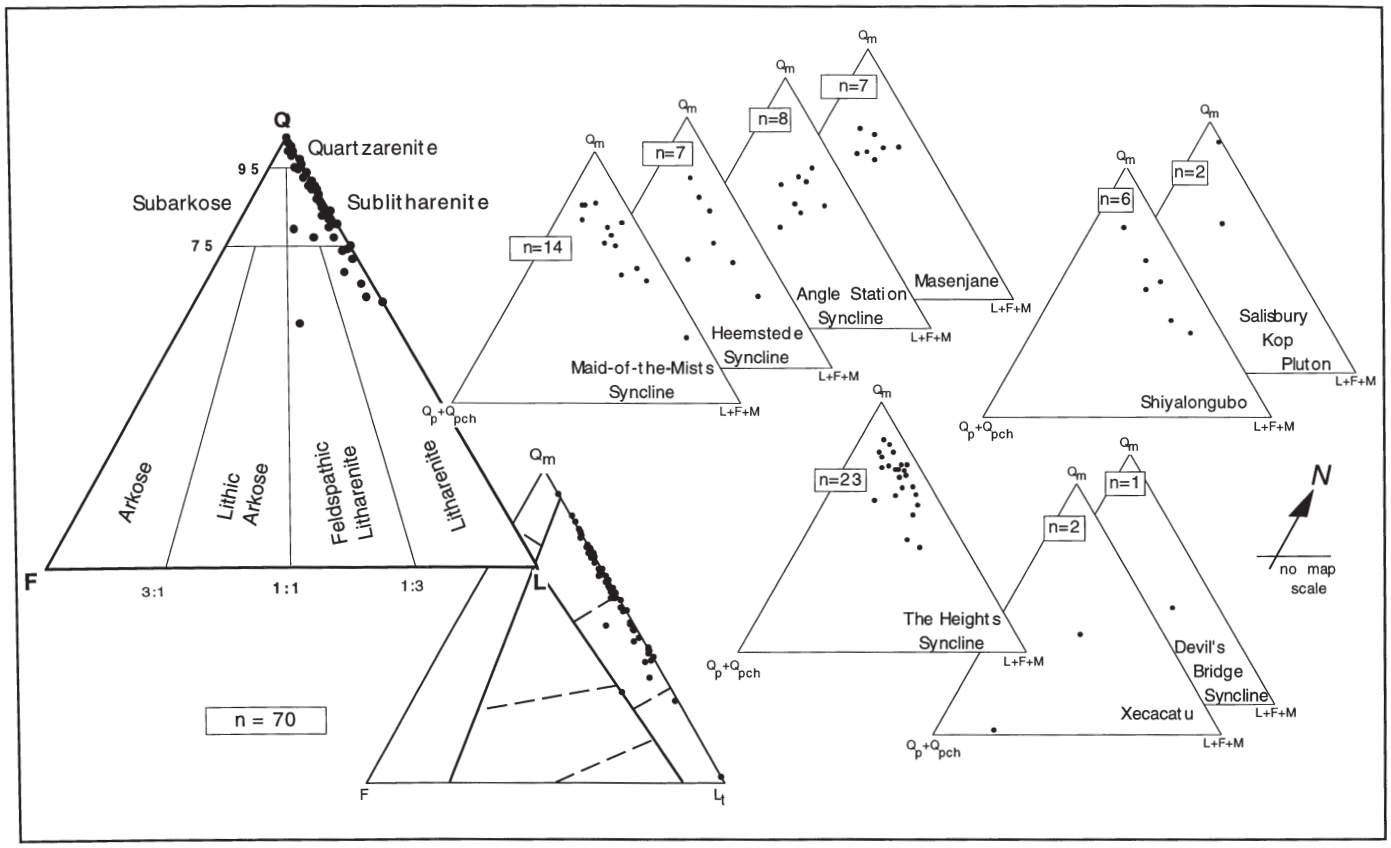


Figure 8. Composition and classification of Moodies sandstones south of the Inyoka fault (fields after Folk, 1968). Due to the paucity of feldspar, samples are spread out along the Q-L line and difficult to interpret. Therefore, the compositional data for each structural block are also shown in nonstandard ternary diagrams plotting monocrystalline quartz (Q_m), polycrystalline quartz including chert (Q_p+Qp_{ch}), and all other framework components including matrix (L+M). QS (quartz-sericite) grains are grouped with L. Small ternary diagrams are arranged according to their approximate positions on the geologic map (Fig. 1). The Xecacatu block and the Devil's Bridge syncline may include rocks of Fig Tree Group or of transitional character. For definition of grain types, see Table 1.

the The Heights syncline, dominated by clasts of dacitic rock, is interbedded with quartzose sandstone containing a high percentage of altered felsic volcanic grains (Figs. 8 and 11).

In order to better characterize the contrast between Fig Tree and Moodies conglomerates in the BGB, data on clast composition were also collected from 14 outcrops of Fig Tree conglomerate (Heubeck, 1993). In contrast to Moodies conglomerates, Fig Tree conglomerates are oligomict, consisting largely of Onverwacht black, gray, and banded chert clasts with minor components of Fig Tree and other Onverwacht rock types (Fig. 9). Altered ultramafic and high-quartz sandstone clasts, typical of Moodies conglomerate, are absent, and feldspar porphyry clasts are rare. The matrix of Fig Tree conglomerate is a chert arenite containing a variable proportion of QS grains and less than 20% monocrystalline quartz grains. The low-quartz Fig Tree conglomerates matrix contrasts strongly with the quartzose matrix of Moodies conglomerates.

PALEOCURRENTS

Several thousand paleocurrent readings from several hundred sites in all tectonic blocks in the central BGB were collected during the present study (Heubeck and Lowe, 1994a). Paleocurrents are reviewed here only in the context of provenance analysis. Most paleocurrents were taken from planar and trough cross-stratification. All data were corrected for fold axis plunge and tilt of bedding.

Paleocurrents associated with conglomeratic units represent deposition mainly in alluvial or braided fluvial facies and consistently indicate a southerly transport direction (Heubeck and Lowe, 1994a, Fig. 15). Paleocurrents in sandstone not associated with conglomerate and deposited in deltaic, tidal, and marginal marine environments indicate a northerly, southerly, or bidirectional transport direction. These paleocurrents are mostly subparallel to the strike of the orogen, perpendicular to the direction of late Moodies shortening, and also perpendicular to the direction of conglomerate clast transport. Paleocurrent directions vary rapidly

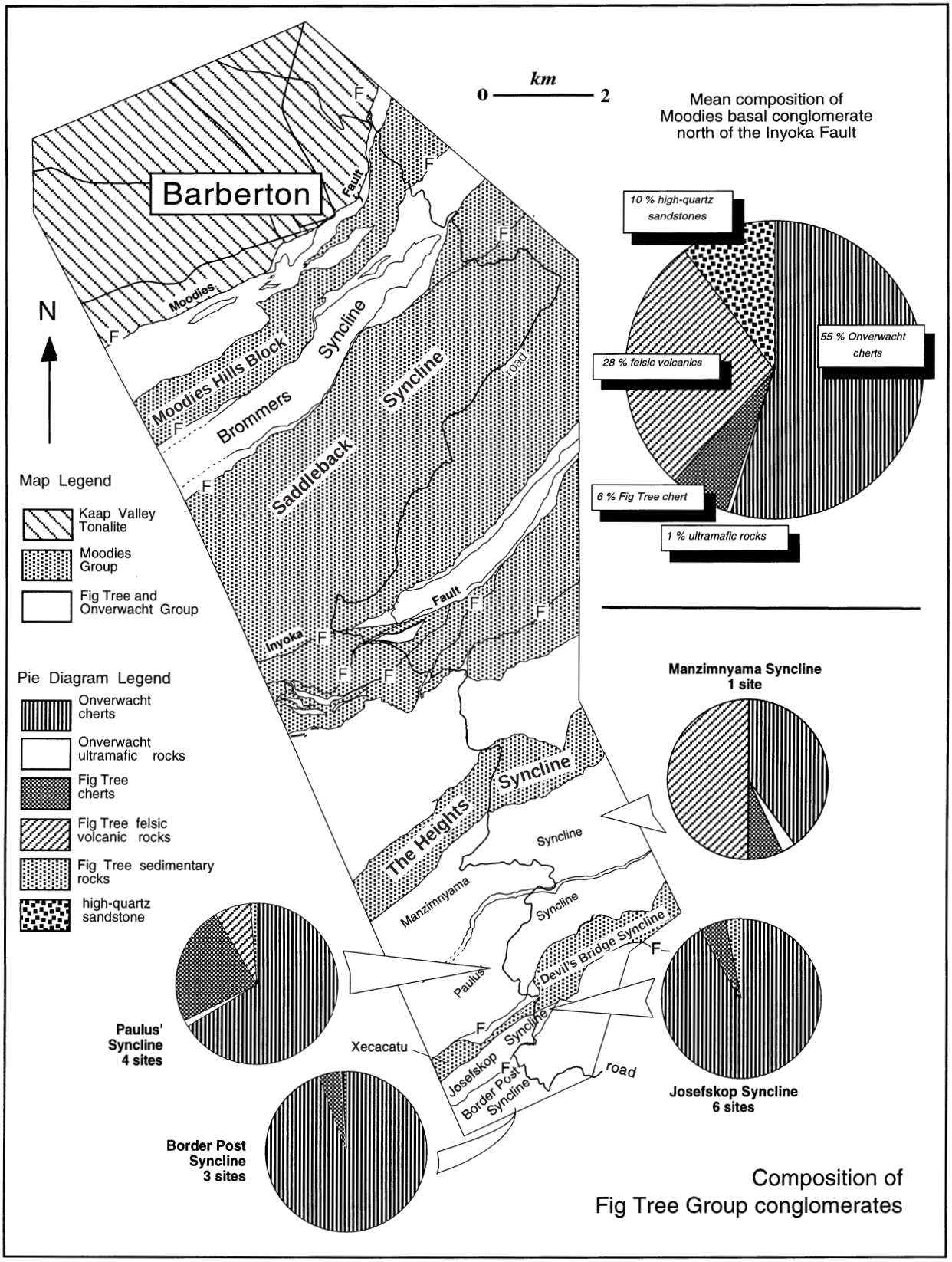


Figure 9. Composition of Fig Tree conglomerates from four structurally separated outcrop belts in the south-central Barberton Greenstone Belt. The mean composition of the Moodies basal conglomerate is given for comparison. Note the nearly monomict character of three Fig Tree chert-clast conglomerates contrasting with the polymict and quartz-sandstone–bearing composition of Moodies conglomerates.

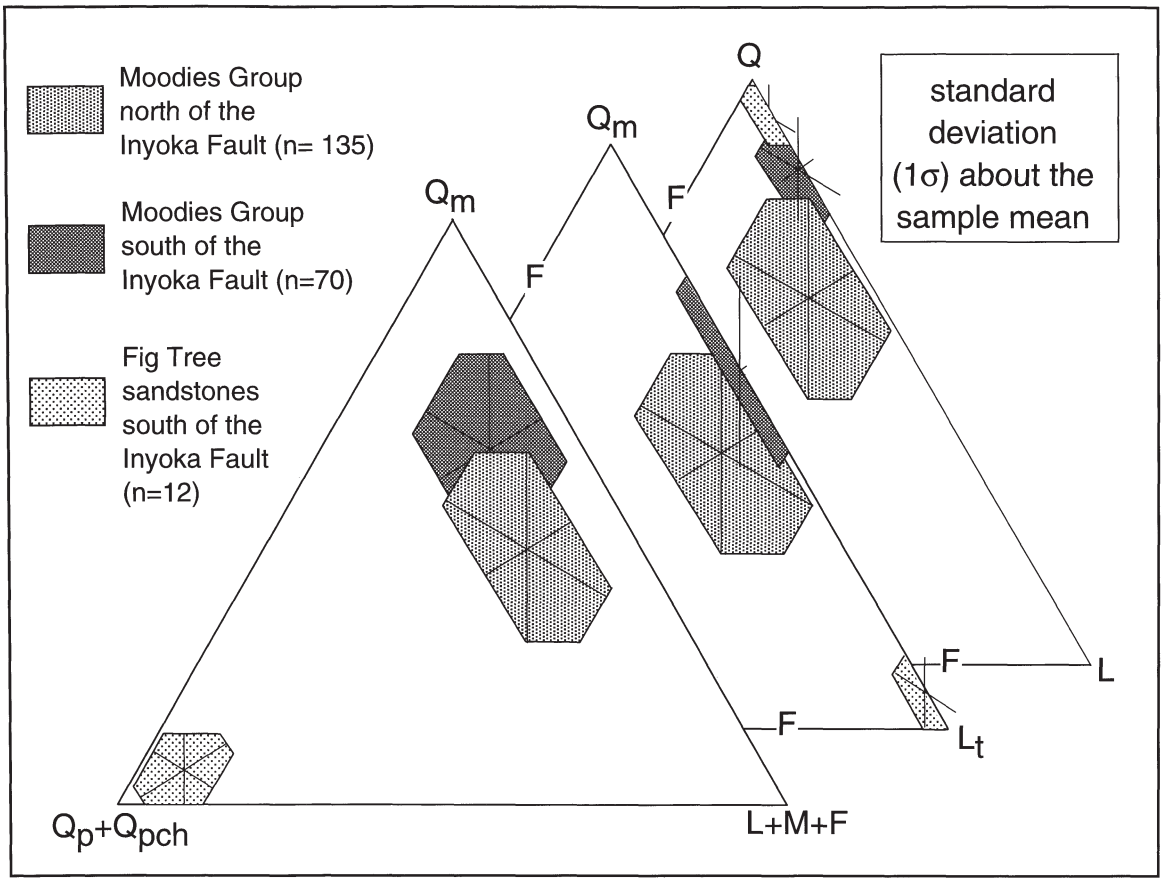


Figure 10. Ternary diagrams showing mean compositions of Moodies sandstones north of the Inyoka fault, Moodies sandstones south of the Inyoka fault, and Fig Tree sandstones south of the Inyoka fault. Note the clear differentiation of the sandstones in three characteristic fields: the chert-rich character of Fig Tree samples, the nearly feldspar-free composition of the Moodies Group south of the Inyoka fault, and the polymict, heterogeneous composition of Moodies sandstones north of the Inyoka fault. For definition of grain types, see Table 1.

laterally and with stratigraphic position, suggesting that dispersal patterns were sensitive to subtle changes in depositional parameters, such as depositional environment, shoreline position, direction and magnitude of sediment supply, and water depth.

Paleocurrent patterns suggest that most clastic material comprising the Moodies Group on both sides of the Inyoka fault in the central BGB was sourced to the north or northwest of present outcrops but was subject to intensive reworking along the basin axis in mostly marginal marine environments.

DISCUSSION

Origin of QS grains

The origin of sand-sized quartz-sericite (QS) grains can be constrained by comparison with appropriate greenstone belt lithologies and by comparison with thin sections of conglomerate clasts. Dacitic volcaniclastic, volcanic, and hypabyssal feldspar-porphyry intrusive rocks of the underlying Fig Tree Group are a major clast type in the basal Moodies conglomerate (Heinrichs, 1980; Büttner et al., 1983). Both the clasts and their in-situ parent rocks show a gradation from those with unaltered igneous textures into those having the same QS-mosaic texture that is observed in detrital grains and matrix in Moodies Group sandstones. In outcrop, fresh feldspar porphyries are composed of an extremely fine-grained, homogenous matrix of sericite, chlorite, and very fine-grained quartz containing poorly preserved phenocrysts of feldspar and quartz (Fig. 12A). Most of the feldspar phenocrysts have been altered to micromosaics of fine-grained white mica, carbonate, and common, finely disseminated iron oxides, and the matrix has been altered to coarse-grained sericite and quartz (Fig. 12B). The relative abundance of QS grains in the sandstones correlates well with the relative abundance of cobbles of felsic volcanic and volcaniclastic rocks in the Moodies Group and supports a common provenance from corresponding rocks of the Fig Tree Group. The increased proportion of QS grains in Moodies sandstones overlying subvolcanic porphyritic rocks of the Fig Tree Group in the The Heights

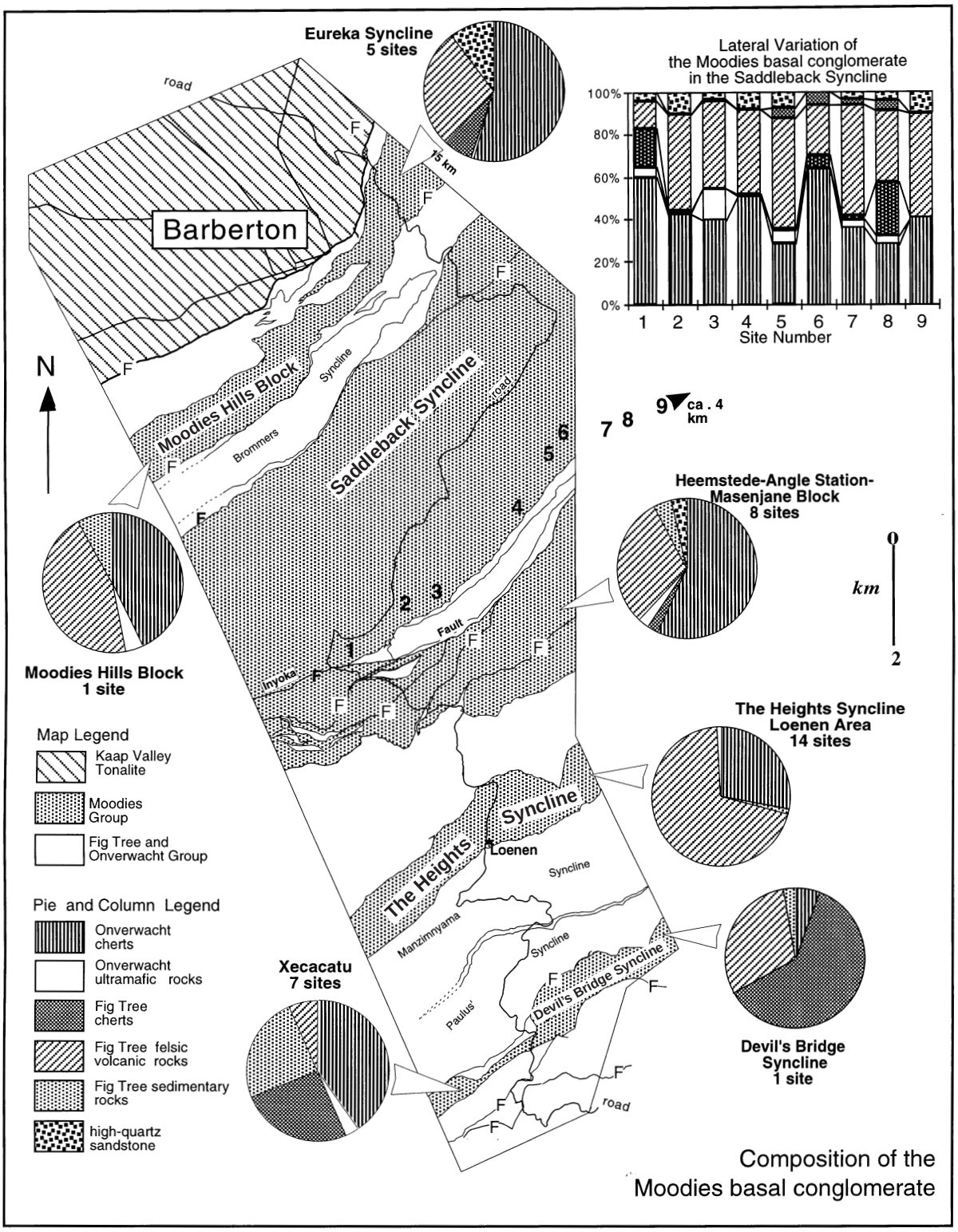


Figure 11. Composition of the Moodies basal conglomerate in various structurally separated blocks and along strike within the Saddleback syncline. The wide variation in composition and rapid lateral changes (see bar diagram in upper right) suggest that the composition of the conglomerate reflects local sources. The Heights syncline is distinguished throughout its strike length by the dominance of clasts of felsic volcanic rock in the basal Moodies conglomerate.

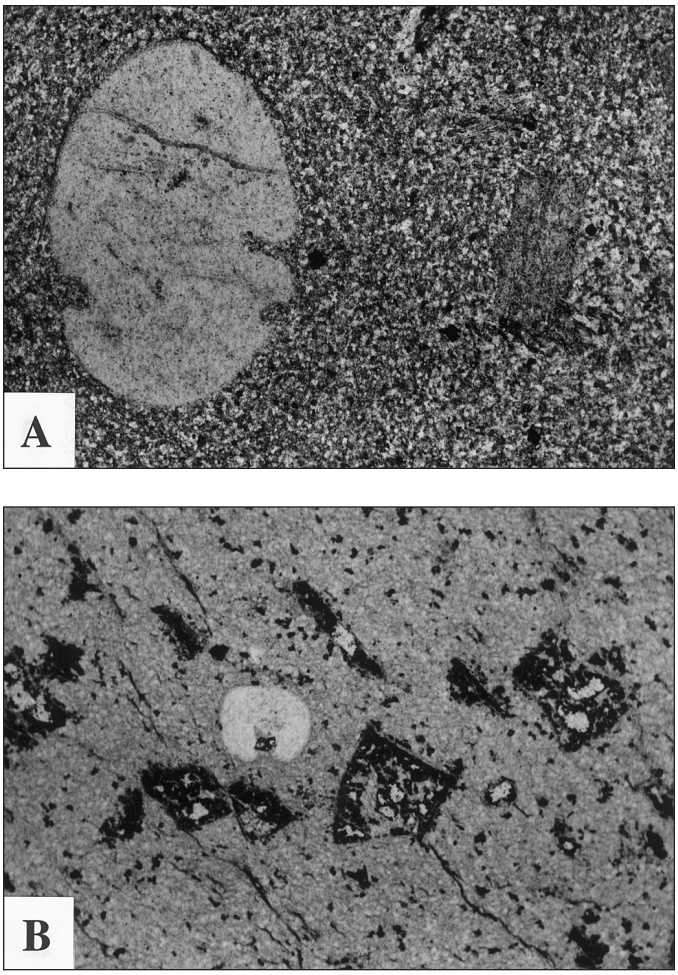


Figure 12. Photomicrographs of Fig Tree volcanic rocks. A, Fresh feldspar porphyry. Volcanic quartz, partially resorbed and showing embayments (left) and ghost of feldspar phenocryst (right) in fine-grained sericitic matrix. Quartz grain is 0.55 mm in diameter. Crossed nicols. The Heights syncline. Sample 3393. B, Altered and recrystallized feldspar porphyry showing quartz and plagioclase phenocrysts in fine-grained quartz-sericite matrix. Quartz is volcanic and partially resorbed. Plagioclase phenocrysts are completely replaced by Fe-oxides. Quartz grain is 0.30 mm in diameter. Plane light. The Heights syncline. Sample 3577.

syncline suggests significant local sources of felsic volcaniclastic debris and a rapid breakdown of the grains.

Massive sericite grains may represent thoroughly altered volcanic rock fragments or plagioclase grains. Wilson and Pittman (1977), however, demonstrated that completely altered plagioclase in an example from the Jurassic of the Gulf Coast are represented by grains of illite. By analogy, the possibility that an unknown percentage of QS grains was derived from the in-situ alteration of Ca-rich plagioclase cannot be excluded. This hypothesis is supported by rare parallel alignment of sericite blades in some QS grains, and by the variable degree of preservation of plagioclase in Moodies sandstones north of the Inyoka fault. In addition, metasomatically altered komatiites and basalts of the Onverwacht Group are also known to form QS mosaics (Lowe and Byerly, 1986; Hanor and Duchac, 1990). The strongest verifiable link of QS grain abundance observed in this study, however, is with Fig Tree felsic volcanic and volcaniclastic rocks and their proximal conglomerates and therefore justifies grouping QS grains with the lithic fragments in modal analysis. The available evidence suggests that mafic and ultramafic rocks of the Onverwacht Group and plagioclase-rich plutonic rocks were probably minor sources of QS grains and their precursors in the Moodies Group.

Origin of QS matrix

Much of the quartz-sericite-mosaic matrix, which is particularly common in the lower Moodies Group north of the Inyoka fault and widespread in Moodies sandstones south of the Inyoka fault, probably originated by in-situ alteration of fine-grained vitric volcanic fragments and weathered Fig Tree porphyries. Compaction and recrystallization have obscured the distinction between altered QS grains and matrix in many cases. Similar pervasive "argillation" of volcanogenic sandstones has been described by Carrigy and Mellon (1964) and McBride (1984).

Because part of the fine-grained QS matrix is likely to represent deformed and recrystallized QS framework grains and should properly be assigned to pseudomatrix, the calculated framework percentage shown in Figure 4A and B is likely to be low. Framework percentage ranges between 65 and 95% throughout most of the Moodies Group, averaging approximately 80% (Figs. 3 and 4).

In modal analysis of most Phanerozoic sandstones, a framework percentage of about 80% is considered the lower limit of usefulness for quantitative modal analysis (Dickinson, 1970; Dickinson and Suczek, 1979). While many Moodies sandstones contain less than 80% framework grains, we feel that conventional modal analysis is still useful as long as the limitations due to alteration, especially the potential origins of the QS matrix material, are recognized and kept in mind. It would be unfortunate to discard sandstone composition as a means of interpreting rocks as significant as those of the Moodies Group. In addition, a wealth of information from other sources, including conglomerate clast composition, paleocurrent analysis, and rare earth element (REE) geochemistry, is available for the Moodies Group to aid in constraining provenance interpretations.

Petrologic subdivisions of the Moodies Group

Based on modal abundances, the Moodies Group can be subdivided into two petrofacies north of the Inyoka fault and one petrofacies south of this fault (Fig. 13).

1. The *Oosterbeek petrofacies*, lower petrofacies of the Moodies Group north of the Inyoka fault, is characterized by a low relative abundance of unstable lithic grains (20%) and chert (10%), common K-feldspar (5–15%), and a high relative abundance of monocrystalline quartz (50–60%). The basal 400 m

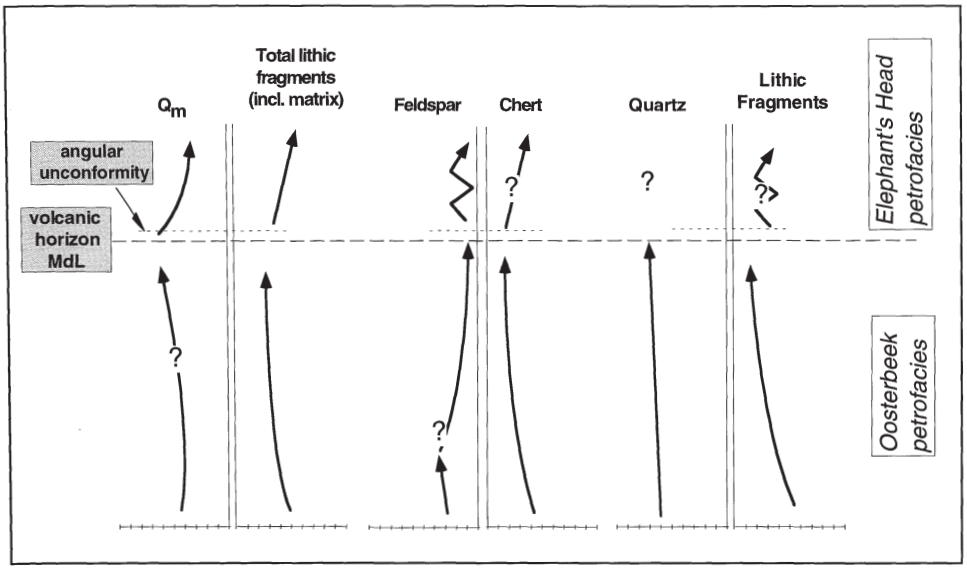


Figure 13. Characteristics of the two sandstone petrofacies in the Moodies Group north of the Inyoka fault. Trends within the Oosterbeek petrofacies are consistent with gradual maturation and contributions from a plutonic source external to the Barberton Greenstone Belt. Trends within the Elephant's Head petrofacies suggest an increasing influx of greenstone belt material and a diminishing importance of the plutonic source terrain with time. Q_m, monocrystalline quartz; MdL, Moodies basalt.

shows several vertical compositional trends: (a) a rapid upward decrease in the percentage of unstable lithic fragments, from about 90 to about 15%; (b) an upward decrease in chert (20–10%); and (c) a significant increase of potassium feldspar (0–30%) and quartz (50–75%; Figs. 3 and 4). The Oosterbeek petrofacies corresponds stratigraphically to MD1–MD3 of Eriksson (1980) and to MdbC–MdQ2 of Visser (1956). It comprises an overall upward-fining sequence from the basal alluvial conglomerate through coarse- and medium-grained fluvial sandstone into a thick package of fine-grained deltaic and marginal marine sandstone, siltstone, and shale, capped by the Moodies basalt (Figs. 1, 3, 4, and 13). Paleocurrents are predominantly unimodal toward the northeast or southwest, or bidirectional (Heubeck and Lowe, 1994a, Fig. 7).

2. The *Elephant's Head petrofacies*, also north of the Inyoka fault, overlies the Oosterbeek petrofacies. It is characterized by fluctuating but generally high proportions of lithic rock fragments (60%), particularly chert (20%), fluctuating but generally low abundances of monocrystalline quartz (30%), the near-absence of K-feldspar (0–5%), and a low abundance of unstable lithic grains (20%; Figs. 3, 4, and 13). This petrofacies, equivalent to MD4 of Eriksson (1980) and to MdS2–MdS3 of Visser (1956), corresponds stratigraphically to largely medium grained to gravelly fluvial and tidal sandstone and south-facing fan-delta conglomerate wedges in the Saddleback syncline but to marine fine-grained sandstone and siltstone in the Eureka syncline. Paleocurrents in the sandstone are irregular but conglomerate units are dominated by south- and southeastward transport (Heubeck and Lowe, 1994a, Fig. 7).

3. The *Angle Station petrofacies* occurs south of the Inyoka fault (Fig. 9). Its stratigraphic position relative to the petrofacies north of the Inyoka fault is unclear. The nearly complete absence of feldspar (0–2%) makes the Angle Station petrofacies compositionally restricted in conventional QFL or Q_mFL_t ternary diagrams (Fig. 8). In addition to the general absence of feldspar, this petrofacies is characterized by low chert (20%), high monocrystalline quartz (75%), variable lithic fragments (10–40%), and a high framework percentage (Figs. 8 and 10). This petrofacies corresponds stratigraphically to coarse- and medium-grained alluvial and fluvial sandstone overlying a discontinuous basal conglomerate (Fig. 1). Paleocurrents in the conglomerate are dominantly south-directed (Heubeck and Lowe, 1994a, Fig. 7).

Provenance

The low lateral variability of sandstone in the Oosterbeek petrofacies suggests that the early Moodies sedimentary basin north of the Inyoka fault was not constrained by the present tectonic boundaries between the Eureka, Dycedale, Saddleback, and Stolzburg synclines, which span a distance of more than 60 km (Fig. 1). It also suggests that the drainage system extended far beyond the present-day boundaries of the greenstone belt and that the depositional systems were either efficient mixers of source material or drained a homogenous source area.

In the following sections, we will discuss the provenance indicators and constraints on possible source terranes from sandstone petrology, conglomerate clast analysis, and shale geochemistry.

Sandstone petrology. Potential sources of common

monocrystalline quartz include metamorphic, silicic plutonic, and older sedimentary rocks. Volcanic rocks alone were probably not capable of providing the large amount of monocrystalline quartz present in the Moodies Group. The upsection decrease in monocrystalline volcanic quartz in Moodies sandstones may be a function of diminished availability, of mechanical abrasion due to increased transport or recycling, or of dilution by other detrital framework components. Its decrease in abundance parallels the decrease of matrix, which may have preserved the characteristic embayments and phenocrystic shape of volcanic quartz grains against abrasion. The enormous volume of the Moodies Group sandstone also rules out hydrothermal quartz as a major contributor. The rarity of evidence for sedimentary recycling in the Moodies Group, such as well-rounded quartz grains, supermaturity of sandstones, and inherited quartz overgrowths, and the absence of evidence for older quartz-rich sedimentary rocks make significant quartzose sedimentary sources unlikely. Intra–greenstone belt recycling, however, may have been substantial, as indicated by the presence of clasts of quartzose Moodies sandstone and Onverwacht- and Fig Tree–sourced chert grains in the Moodies Group, and by the similarity between clasts in the basal conglomerate and underlying greenstone belt rocks. Either high-grade metamorphic or plutonic sources probably contributed the bulk of monocrystalline quartz to the Moodies Group. Their relative contribution cannot be estimated easily on the basis of quartz grain texture alone but must be assessed within the context of other framework components.

Polycrystalline quartz grains with 2–3 domains per grain have many potential sources, including plutonic, metasedimentary, high-grade metamorphic, vein, or hydrothermal rocks. It is difficult to assign this grain type to any specific source(s) because it lacks distinguishing features. However, this grain type is overall a volumetrically minor component of the Moodies sandstones, which supports the inference that older, coarse, quartz-rich sandstone units did not contribute significantly to Moodies sediments.

Chert and its recrystallized equivalent are major constituents of Moodies sandstones and are the dominant grain types in Moodies chert arenite. Cherty sedimentary layers are common in the Onverwacht and Fig Tree Groups (Lowe, this volume, Chapter 3), and chert arenite is an important rock type in the Fig Tree Group (Reimer, 1975; Heinrichs, 1980). The texture of some chert grain types in Moodies sandstones can be linked unambiguously to specific rock types of the Fig Tree and Onverwacht Group. It is reasonable to assume that most chert in the Moodies Group was derived from pre-Moodies greenstone belt rocks of the Fig Tree and Onverwacht Groups.

Polycrystalline quartz grains showing a preferred orientation of elongated domains and sutured contacts are nearly absent in the Moodies Group. Their low abundance corresponds to an equally pronounced lack of detrital metamorphic minerals (garnet, staurolite, epidote, etc.), metamorphic rock fragments, and metamorphic clasts in the conglomerates. This lack is apparent even in Moodies samples collected in Swaziland, closest to the Ancient Gneiss Complex (AGC), and suggests that the AGC or similar metamorphic terranes were not major contributors to the Moodies basin, even when the high destruction rates of such clasts is considered (Suttner et al., 1981).

Potential sources for potassium feldspars are problematic. Detrital K-feldspars also occur as framework grains in the Sheba and Belvue Road Formations of the Fig Tree Group north of the Inyoka fault (Condie et al., 1970). Microcline ranges from 0.1 to 12% in the Sheba Formation and from 0.1 to 25% in the overlying Belvue Road Formation, suggesting that K-feldspar–bearing plutonic sources became more abundant with time (Condie et al., 1970; Reimer, 1972). K-feldspar is also present in a single sandstone unit of the Mapepe Formation in Paulus' syncline in the south-central BGB (Fig. 9). Based on the composition of Sheba graywacke, Reimer (1975) estimated that approximately 30% of its source area was underlain by granitic and felsic metamorphic rocks. The existence of granitic rocks exposed close to the northern margin of the BGB is also indicated by the presence of common granitic cobbles and boulders in the basal Moodies conglomerate in the Eureka syncline (Fig. 1), discussed in more detail below.

A variety of local sources could have contributed potassic feldspar to the Moodies Group, including (1) TTG plutons surrounding the greenstone belt (Robb and Anhaeusser, 1983); (2) felsic porphyries, enriched in K-feldspar in the hoods of those plutons; or (3) recycling of the K-feldspars of the Fig Tree Group. However, none of these sources alone or in combination appears sufficient to supply the amounts of K-feldspar present in the lower Moodies Group. A source outside of the greenstone belt was therefore the most likely source of the bulk of the potassic feldspar grains in Fig Tree and Moodies rocks. The northeast-to-southwest decrease of feldspar in the MdQ2 unit (Fig. 6) and the general north-to-south decrease in feldspar modal abundance in Moodies rocks north of the Inyoka fault may be due to mechanical abrasion possibly aided by intense Archean weathering, dilution with increasing distance from the K-feldspar source, or other factors (Suttner et al., 1981; Helmold, 1985) but suggests a generally north to northeastern provenance. Paleocurrent patterns in the MdQ2 unit and in most Moodies conglomerates also support an overall northeast-to-southwest transport direction (Heubeck and Lowe, 1994a).

Plagioclase grains are common in the Fig Tree Group but are distinctly subordinate to K-feldspar in the Moodies Group, which may be a function of their greater susceptibility to weathering and alteration (Basu, 1981; Suttner et al., 1981) in the largely alluvial-fluvial-deltaic systems of the Moodies Group. The source of plagioclase grains in the Moodies Group are probably dacitic volcanic rocks of the Fig Tree Group and TTG plutons surrounding the greenstone belt (Jackson et al., 1987).

Condie et al. (1970) argued that the upsection increase of K-feldspar from 6 to 15% in sandstone of the Fig Tree Group reflects the progressive unroofing of a granitic source. If this interpretation is correct, then it seems unusual that there is little accompanying upsection increase in quartz in the mostly lithic

Fig Tree Group sandstone. Total quartz makes up 15–30% of Sheba Formation graywackes and 24–35% of graywackes of the overlying Belvue Road Formation, both those with and without microcline. In contrast, the Moodies Group north of the Inyoka fault is dominated by quartz (54% Q_m) although it has a K-feldspar content (11%) comparable to that of Fig Tree sandstone. If the same granitic source is assumed to have provided K-feldspar to both the Fig Tree and Moodies Groups, then similar proportions of quartz to K-feldspar might be expected. The much higher quartz content of the Moodies Group suggests therefore that most of its quartz grains had other sources, probably uplifted TTG rocks around the BGB.

A high proportion of Moodies Group sandstone north of the Inyoka fault and virtually all sandstones south of the fault plot in the "recycled orogen" province of QFL and Q_mFL_t space (Figs. 7 and 8) of Dickinson et al. (1983). Phanerozoic "recycled orogen" sandstones typically derive from uplifted, deformed, and metamorphosed continental passive margin sequences and are dominated by sedimentary and metasedimentary lithic grains eroded from fine-grained quartzose sandstones, siltstones, shales and their low-grade metamorphic equivalents (Dickinson, 1970; Dickinson and Suczek, 1979; Dickinson et al., 1983). However, the Moodies Group contains little debris derived from these types of sedimentary and metasedimentary rocks. Virtually all of its lithic grain types derive from volcanic and volcaniclastic rocks and cherty sedimentary and metasedimentary rocks within the underlying greenstone belt volcanic sequence. Extra–greenstone belt sources are exclusively plutonic, and stratigraphic and structural studies in the Fig Tree and Onverwacht Groups indicate that these plutons formed in subduction-related arc settings (Robb et al., 1986; de Ronde and de Wit, 1994; Lowe, this volume, Chapter 12). Plutonic sources probably contributed most of the K-feldspar and much of the plagioclase to the Moodies Group, while the greenstone belt contributed lithic fragments and some plagioclase. Both sources, however, are represented in the first-cycle Moodies Group largely by their most resistant components: monocrystalline quartz, microcline, and chert. We therefore suggest that the compositional maturity of the Moodies Group is due to a combination of four factors: (1) the paucity of plagioclase in the mafic and ultramafic greenstone belt volcanic rocks; (2) the high-energy depositional systems in the Moodies Group, which quickly reduced the proportion of unstable grains through physical abrasion and breakage and winnowed out fine-grained material; (3) intense weathering, which may have altered and removed unstable grains, especially plagioclase, with an efficiency usually achieved only after multiple weathering cycles in the Phanerozoic; and (4) possible diagenetic removal or alteration of plagioclase grains, in particular in Moodies strata south of the Inyoka fault. All these factors probably contributed to the low proportions of feldspar and lithic fragments in the sandstone of the Moodies Group and resulted in its "pseudo-recycled orogen" character.

Although the large majority of QS grains in Moodies sandstones appear to be derived from altered volcanic rocks, in particular from intermediate porphyritic and volcaniclastic rocks of the Fig Tree Group, it seems plausible that some of the QS grains may be extensively altered plagioclase, especially if tonalites were major source rocks of Moodies sandstones. Feldspar alteration in sandstones can be extremely selective, with mid- to high-Ca plagioclase altered and obliterated and low-Ca plagioclase relatively unaffected. If all QS grains were counted as feldspars, Moodies sandstones would plot in a mature- or intermediate-arc field in a standard QFL ternary diagram (Fig. 7).

Because quantitative data on the effects of climate, relief, transport, duration and intensity of weathering, sedimentation rate, and depositional system on sand composition are sparse and conflicting even for recent settings (e.g., Blatt, 1967; Suttner et al., 1981; Johnsson, 1992, 1993), it is difficult to estimate the significance of these processes in controlling the composition of Archean sandstones and to constrain the distance of their source(s). Factors such as elevated surface temperatures in the Archean (Knauth and Epstein, 1976; Knauth and Lowe, 1978) and rapid CO_2-weathering (Kasting, 1986) may have significantly accelerated weathering and the compositional maturation of clastic sediments. The rapid lateral facies changes in the Moodies Group, granitic boulders in the basal Moodies conglomerate of the Eureka syncline, and well-preserved detrital muscovite fragments in the sandstone suggest that plutonic source rocks were exposed close to the margins of the BGB and underwent rapid disaggregation to produce sand-sized fragments. Resulting first-cycle debris was probably greatly enriched in quartz and not transported far before deposition.

Conglomerate clast composition. The polymict Moodies basal conglomerate varies rapidly in composition from place to place, suggesting that the clasts were derived from local sources. With the exception of clasts of plutonic rocks discussed below, these sources were rocks of the greenstone belt sequence. The high percentage of quartzose sandstone and chert clasts in the Elephant's Head petrofacies indicates that older Moodies and Fig Tree strata were sources of debris during late Moodies time.

None of the 52 conglomerate outcrops examined in the central part of the belt was found to contain unambiguous clasts of extra–greenstone belt provenance. However, the Moodies basal conglomerate at Ezzie's Pass in the Eureka syncline (Fig. 1), outside the study area, contains orthoclase- and microcline-bearing cobbles and boulders (Visser, 1956; Reimer et al., 1985; Tegtmeyer and Kröner, 1987; Kröner and Compston, 1988). Thin sections of these clasts show abundant monocrystalline, strongly strained quartz; common K-feldspar, including untwinned K-feldspar and microcline; plagioclase; and minor chloritized biotite. Perthite is abundant. A detailed account of the petrography and geochemistry of a large sample population of these unique clasts has been given by Reimer et al. (1985). No clasts of similar composition were found in conglomerates examined in this study in the central part of the belt, although Bell (1967), Gay (1969), Anhaeusser (1972), Krupicka (1975), and Van Niekerk and Burger (1978) report rare occurrences in the central mountain land and in the Stolzburg syncline (Reimer, 1967), and Heinrichs

(1980) describes a granitic cobble from a conglomerate in the lower Fig Tree Group south of the Inyoka fault.

The high concentration and large size of the K-feldspar–bearing clasts at the Ezzie's Pass outcrop points to a local source. A regional decrease in the thickness of the Moodies basal conglomerate and south-directed paleocurrent patterns in overlying fluvial sandstone (Heubeck and Lowe, 1994a) indicate a northerly provenance for the conglomerate. The lack of granitic clasts higher in the Eureka syncline section correlates with a corresponding decrease in total feldspar and K-feldspar (Fig. 4A) and suggests that the abundance of K-feldspar reflects the availability of nearby K-feldspar–bearing plutonic sources. In contrast, quartz shows no correlation with the decrease in feldspar (Fig. 4A). Its abundance appears to be controlled at least in part by a K-feldspar–free quartzose source. This inference is consistent with our interpretation that the bulk of the monocrystalline quartz in Moodies sandstones was derived from tonalitic plutonic rocks.

Trace-element geochemistry. Analysis of the trace-element geochemistry of rocks of the Moodies Group is limited to five shale samples of unspecified stratigraphic position (McLennan et al., 1983), one shale sample from an unspecified location (Condie and Wronkiewicz, 1990a), and clasts of plutonic rock in the basal Moodies conglomerate at Ezzie's Pass (Reimer et al., 1985). Compared to the REE pattern of the underlying Fig Tree Group, shale of the Moodies Group is characterized by more fractionated REE due to light rare earth element (LREE) enrichment, a possibly higher total REE content, and a depletion in elements associated with ferromagnesian minerals such as Cr, V, Ni, and Co (McLennan et al., 1983). Condie and Wronkiewicz (1990a) also noted a lower Cr/Th ratio compared with Fig Tree samples. Shales from the Moodies Group analyzed by McLennan et al. (1983) show a negligible Eu anomaly ($Eu/Eu^* = 0.92 \pm 0.02$). These data suggest that the Archean upper crust during Moodies time was significantly less fractionated than post-Archean upper crust and that shallow intracrustal melting, resulting in the production of igneous rocks characterized by a significant negative Eu anomaly, was still insignificant. Both findings are in strong contrast to REE data from the younger Late Archean Pongola and Witwatersrand Supergroups, which show REE patterns representative of typical Proterozoic and Phanerozoic rocks (McLennan et al., 1983; McLennan and Taylor, 1984). This change has been interpreted to reflect a fundamental change in the provenance of the sediments and, indirectly, to be the result of major changes in the composition of the exposed crust at that time (Condie and Wronkiewicz, 1990b).

In modeling the REE patterns of the Fig Tree and Moodies Groups, McLennan et al. (1983) found that the REE patterns and trace-element abundances of the two groups could be best explained by composite sources and sediment mixing. Their calculations suggest that the Fig Tree Group could have been derived from a source area or source areas composed of Archean mafic volcanic and Na-rich granitic rocks (or their volcanic equivalents) in an approximate ratio of 1:1 while the composition of the Moodies shales required 2–3 times the amount of felsic source rock.

The lack of a well-developed Eu anomaly in Moodies shales is puzzling in view of the common presence of K-feldspar and the mature character of the Moodies Group (Condie and Wronkiewicz, 1990a). In contrast, the single shale sample analyzed by Condie and Wronkiewicz (1990a) showed a pronounced negative Eu anomaly ($Eu/Eu^* = 0.67$). REE patterns from the granitic clasts in the basal conglomerate of the Moodies Group at Ezzie's Pass are also enriched in LREE and display a well-developed negative Eu anomaly (Reimer et al., 1985).

In the absence of conclusive geochemical and trace-element data on the Moodies Group and of stratigraphically well controlled samples, the provenance of the Moodies Group cannot be adequately addressed by the available geochemical data. In particular, it is not possible based on available geochemical data to assess quantitatively the role of the voluminous TTG plutons surrounding the greenstone belt as sources of Moodies detritus.

Tectonic setting of the Moodies Group

Previous models. Several tectonic settings have been suggested for the Moodies Group, including passive margin, rift, backarc, and foreland basin. None of these models have been examined using stratigraphically controlled petrographic data. Eriksson (1980, 1982) suggested that the Moodies Group was deposited along a north-facing passive continental margin of a "shelf rise type" (Curray, 1969). He interpreted the transition from the Fig Tree to the Moodies Group as the transition from rift to continental shelf setting and explained the variable styles of sedimentation in the Moodies Group, including alluvial, fluvial, deltaic, shoreline, and offshore facies, to be due to sea-level changes. Alternatively, Eriksson (1980) also envisioned a backarc or marginal-basin origin to account for the vertical distribution of sediments and their apparently asymmetrical arrangement. Sedimentation was thought to have been terminated by closure of the ocean north of the shelf followed by the accumulation of the Late Archean Pongola Supergroup (Watchorn, 1980) in a late-orogenic setting. A rift-related setting of the BGB has been proposed by Anhaeusser et al. (1969), Anhaeusser (1971), and Condie and Hunter (1976). According to this model, erosion of the rift flanks, composed of greenstone belt material and granitic rocks, resulted in deposition of the shallow-water sediments of the Moodies Group.

To date, however, it has not been possible to identify the continental basement associated with the "rift-facies" Fig Tree Group or the "shelf facies" Moodies Group. While the Oosterbeek petrofacies may have been deposited in an extensional setting, sedimentation of the Elephant's Head petrofacies occurred while the basin was undergoing shortening as part of a fold-and-thrust belt (Heubeck and Lowe, 1994a). Syndeformational deposition has also been reported from areas in the southern BGB (Lamb, 1984). The geochemistry and composition of the Fig Tree Group is more consistent with volcanism and sedi-

mentation along a convergent plate margin rather than within a rift (Anhaeusser, 1973). In addition, there is no evidence of a conjugate rift shoulder north of the BGB. The Moodies Group terminates with a distinct coarsening-upward upper petrofacies atypical of upward-fining sequences common along rift-related or passive margins (Falvey, 1974; Galloway and Hobday, 1983). While the Moodies Group shows a clearly continental provenance, its petrographic evolution is at variance with models of rift- and passive-margin sequences, which ideally evolve from immature basal arkosic sandstones towards supermature quartzarenites.

Jackson et al. (1987) suggested that the Fig Tree and Moodies Groups were deposited in a foreland basin that developed in response to thrust loading of the Onverwacht crust by the uplift and northward transport of the AGC. They proposed that the composition, paleocurrent patterns, and facies of the Fig Tree and Moodies Groups are characteristic of a synorogenic accumulation having a southern provenance that included the AGC and Onverwacht Group. Subsequent deformation into north-vergent synclines and intervening, steeply dipping fault zones resulted from continued north- and northwest-directed shortening and the diapiric rise of the Kaap Valley tonalite (Jackson et al., 1987). Lamb (1984) mapped as much as 1,800 m of coarse clastic quartzose sedimentary rocks in the southern BGB in Swaziland associated with intraformational unconformities overlying strata similar to the Fig Tree Group. However, neither sufficient paleocurrent nor petrographic data are available from this area, and the stratigraphic position of this sequence relative to the Moodies rocks north of the Inyoka fault remains uncertain (Lamb and Paris, 1988).

Although the AGC provides an attractive source for Moodies detritus, the Moodies Group in the central BGB appears to contain little southerly derived sediment. Petrographic data presented here, unit-by-unit paleocurrent measurements, and thickness variation of Moodies conglomerates in the central BGB suggest that little or no sediment was derived from southerly sources (Heubeck and Lowe, 1994a). The Moodies Basin appears to be characterized by southwest–northeast, largely strike-parallel transport of sand and by conglomerate input from the north and northwest. In addition, the different composition of the Moodies Group sandstones north and south of the Inyoka fault argues against the existence of a large throughgoing sediment transport system as suggested by Eriksson (1979).

Present study. The results of the present study suggest a two-stage tectonic evolution for the Moodies basin in the central BGB, north of the Inyoka fault, corresponding to the Oosterbeek and Elephant's Head petrofacies. Rocks of the Oosterbeek petrofacies, overlying the basal alluvial conglomerate, fine gradually upward through approximately 1,000 m of fluvial-deltaic sandstones into tidal and deltaic facies (MdQ1 of Anhaeusser, 1969; MD1 and MD2 of Eriksson, 1980). In the Saddleback syncline, Eureka syncline, and the Moodies Hills block, these rocks are overlain by approximately 1,000 m of generally poorly exposed fine-grained sandstone, siltstone, and subordinate banded-iron-formation deposited mainly in shelf and marginal marine environments (MdS1 of Anhaeusser, 1969; MD3 of Eriksson, 1980). The gradual upsection-deepening and -fining trends within the Oosterbeek petrofacies suggest that subsidence outstripped sediment supply (Eriksson, 1980). This subsidence may have been related to extensional unroofing of an orogen produced during late Fig Tree, pre-Moodies deformation (Lowe and Heubeck, 1994b).

The petrology of the Elephant's Head petrofacies, upper Moodies Group stratigraphy, and the structure of the central BGB suggest that late Moodies sedimentation north of the Inyoka fault occurred within a foreland basin developed adjacent to an orogenic front to the north or northwest (Heubeck and Lowe 1994a, b; Lowe, this volume, Chapter 12). Visser (1956), Fripp et al. (1980), and others recognized that the northern margin of the central BGB is defined by numerous closely spaced and subparallel vertical faults, including the regionally traceable Moodies, Sheba, Haki, and Saddleback faults (Lowe and Byerly, this volume, Chapter 1) as well as faults of shorter length. Within the supracrustal sequence, fault spacing decreases towards the contact with the Kaap Valley pluton. Ductile strain is of a flattening type, maximum shortening strain is oriented subhorizontally, and lineations are subvertical (Ramsay, 1963; Anhaeusser, 1969; Heubeck and Lowe, 1994b). Strain also increases towards the Kaap Valley pluton (Gay, 1969). Structures along this margin suggest major vertical displacement and nearly complete elimination of the contact aureole of the Kaap Valley pluton. In addition, displacements across the major faults within the greenstone belt suggest consistent up-to-the-north sense of faulting (Daneel, 1987; Lowe et al., this volume, Chapter 2). This sense of displacement agrees with the truncation, structural attenuation, or even complete elimination of the northern limbs of the Eureka, Dycedale, Saddleback, and Maid-of-the-Mists synclines and of the Moodies Hills block (Fig. 1). The southern limbs of these structural units, in contrast, are well preserved and include complete stratigraphic sections commonly extending below the Moodies basal conglomerate into the Fig Tree Group. The resulting cross-sectional geometry of the central belt, showing a synclinal fold train with heavily faulted intervening anticlines, closely resembles that of highly shortened foreland fold belts (Ganss and Schmidt-Thomé, 1953; Julivert, 1971; Laubscher, 1977; Mountjoy, 1992; Heubeck and Lowe, 1994b).

Stratigraphic arguments also favor the presence of an orogenic front along the northern margin of the central BGB in late Moodies time. The presence of at least one intraformational angular unconformity, which truncates Moodies strata upturned along the Saddleback fault, is a strong indication of the onset of synsedimentary shortening in late Moodies time (Heubeck and Lowe, 1994a). This unconformity is overlain by a southward-facing conglomerate wedge that can be traced southward into thinner gravelly sandstones.

We suggest that a foreland basin formed in the central BGB in late Moodies time in response to loading by the uplift and

south- or southeastward displacement of the terrain to the north. This terrain possibly included the Kaap Valley tonalite, its hypabyssal equivalents, and its supracrustal cover sequence. South- and southeast-directed shortening along thrust faults, concentrated at the northern margin of the belt and within the greenstone belt, resulted in increased sedimentation rates, widespread erosion of the uplifted block, deposition of south-facing alluvial fans interfingering with fluvial and deltaic facies, and syndepositional deformation.

The Angle Station petrofacies, representing the Moodies strata of the central BGB south of the Inyoka fault, is sedimentologically, stratigraphically, and petrologically similar to lower Moodies strata north of the fault (Fig. 10). Both sequences unconformably or structurally overlie folded and faulted strata of the Fig Tree and Onverwacht Groups above a basal, polymict but largely locally derived conglomerate, are quartzose and rich in altered volcanic grains, and show depositional structures characteristic of alluvial and fluvial environments (Eriksson, 1980; Heubeck and Lowe, 1994a). These features have prompted previous workers (Visser, 1956) to address the quartzose sandstones south of the Inyoka fault as lower Moodies Group. However, these strata lack unequivocal detrital feldspar grains, preserved thicknesses are only several hundred meters, and no regionally traceable units have been identified (Heubeck and Lowe, 1994a). We suggest that the Moodies Group south of the Inyoka fault may have formed in response to the same tectonic pulse that initiated Moodies sedimentation in the north and received large proportions of its monocrystalline quartz from TTG plutons but was deposited in one or more basins separate from those to the north.

CONCLUSIONS

Sandstone petrography, conglomerate clast composition, and sedimentology of clastic rocks of the Moodies Group, uppermost rocks of the Swaziland Supergroup, provide a number of significant constraints on interpretations of late-stage sediment provenance and tectonic development of the Barberton Greenstone Belt.

1. Exposed TTG plutons contributed most of the quartz to the Moodies Group in the central BGB while K-feldspar and remaining quartz had their sources in granitic rocks that are apparently no longer preserved. North of the Inyoka fault, these plutonic source rocks were located north of and probably close to the present greenstone belt. Intra–greenstone belt sources were important sources of detritus especially during earliest and latest Moodies deposition. The Moodies Group probably did not receive major input from metamorphic rocks, including metamorphic rocks of the Ancient Gneiss Complex in Swaziland. Quartz-sericite grains and matrix, formed through post-depositional metasomatism, make up a significant part of Moodies sandstone. They are probably altered lithic grains but derivation of some from calcic plagioclase cannot be excluded.

2. North of the Inyoka fault, the Moodies Group can be subdivided into two petrofacies. (A) The Oosterbeek petrofacies, comprising the lower two-thirds of the Moodies Group, records the uplift and proximity of plutonic source rocks next to the subsiding Moodies basin. Relative abundances of monocrystalline quartz and K-feldspar from plutonic sources outside the greenstone belt increase and reach a maximum in shallow-marine and shoreline systems as the proportion of intra–greenstone belt material decreases. (B) The overlying Elephant's Head petrofacies marks the onset of syndepositional deformation within the Moodies basin. Uplift of rocks within the greenstone belt is expressed petrographically by pulses of chert-rich sandstone and chert-clast conglomerate and stratigraphically by southward-shed wedges of conglomerate overlying at least one intraformational angular unconformity. The proportion of material derived from TTG and granitic sources decreases relative to intra–greenstone belt material.

3. The composition and depositional setting of the Oosterbeek petrofacies are consistent with deposition in an extensional basin following late Fig Tree orogenesis. Lowe et al. (this volume, Chapter 2) and Lowe (this volume, Chapter 12) have suggested that this basin may have been a back-arc basin developed between the offshore Kaap Valley magmatic arc and a block made up of deformed Fig Tree and Onverwacht rocks and their plutonic roots. Composition, structure, and stratigraphy of the Elephant's Head petrofacies suggest deposition in a foreland basin in front of a south-or-southeast-advancing orogenic front.

4. Moodies strata south of the Inyoka fault, assigned here to the Angle Station petrofacies, can be correlated best with the lower Moodies Group north of the fault. It is likely, however, that these strata formed in one or more separate basins that evolved adjacent to or upon the block of older Fig Tree and Onverwacht rocks (Lowe et al., this volume, Chapter 2; Lowe, this volume, Chapter 12).

ACKNOWLEDGMENTS

This publication forms part of a Ph.D. dissertation by the first author under the direction of DRL at Stanford University. Research was supported by NSF-grant EAR 89-04830 and NASA-grant NCA2-232 from the Exobiology Program to DRL. CEH acknowledges support by McGee grants from the School of Earth Sciences, Stanford University, a GSA Penrose Grant, and a Jahns Memorial Fellowship in Field Geology. CEH also thanks his field assistants Daniel Sigman, James Cramton, and Kevin Ascher. We are grateful to Anglo-American Prospecting Services for logistical support, to Dr. Gerhard v.d. Westhuizen and Frans v.d. Merwe for their hospitality, and to Lomati Bosbou Ltd., Piggs Peak Plantations, and Peter Hitchins of the Songimvelo Game Reserve for permission to access their land. We thank Sandra Kamo for unpublished material. Helpful reviews by Ray Ingersoll and Ken Eriksson clarified our interpretations. We have benefited greatly from discussions with C. R. Anhaeusser, G. Byerly, C. de Ronde, A. Kröner, S. Lamb, D. Marcini, H. Philpots, L. Robb, and M. Tomkinson.

REFERENCES CITED

Anhaeusser, C. R., 1968, The geology of the Lily syncline and portion of the Eureka syncline between Sheba Siding and Louw's Creek Station, Barberton Mountain Land [M.Sc. thesis]: Johannesburg, University of the Witwatersrand, 150 p.

Anhaeusser, C. R., 1969, A comparison of pebble and fold deformation in the Nelspruit granite contact aureole, Barberton Mountain Land: Geological Society of South Africa Transactions, v. 72, p. 49–60.

Anhaeusser, C. R., 1971, The Barberton Mountain Land, South Africa—a guide to the understanding of the Archean geology of western Australia: Geological Society of Australia Special Publication 3, p. 57–70.

Anhaeusser, C. R., 1972, The geology of the Jamestown Hills area of the Barberton Mountain Land, South Africa: Geological Society of South Africa Transactions, v. 75, p. 225–263.

Anhaeusser, C. R., 1973, The evolution of the early Precambrian crust of southern Africa: Royal Society of London Philosophical Transactions, ser. A, v. 273, p. 359–388.

Anhaeusser, C. R., 1976, The geology of the Sheba Hills area of the Barberton Mountain Land, South Africa, with particular reference to the Eureka syncline: Geological Society of South Africa Transactions, v. 79, p. 253–280.

Anhaeusser, C. R., 1984, Structural elements of Archean granite-greenstone terrains as exemplified by the Barberton Mountain Land, southern Africa, *in* Kröner, A., and Greiling, R., eds., Precambrian tectonics illustrated: Stuttgart, Schweizerbart, p. 57–87.

Anhaeusser, C. R., and Robb, L. J., 1981, Magmatic cycles and the evolution of the Archean granitic crust in the Eastern Transvaal and Swaziland: Geological Society of Australia Special Publication 7, p. 457–467.

Anhaeusser, C. R., Mason, R., Viljoen, M. J., and Viljoen, R. P., 1969, A reappraisal of some aspects of Precambrian Shield geology: Geological Society of America Bulletin, v. 80, p. 2175–2200.

Anhaeusser, C. R., Robb, L. J., and Viljoen, M. J., 1981, Provisional geologic map of the Barberton Greenstone Belt and surrounding granitic terrane, Eastern Transvaal and Swaziland: Geological Society of South Africa, scale 1:250,000.

Armstrong, R. A., Compston, W., de Wit, M. J., and Williams, I. S., 1990, The stratigraphy of the 3.5–3.2 Ga Barberton Greenstone Belt revisited: a single zircon ion microprobe study: Earth and Planetary Science Letters, v. 101, p. 90–106.

Ascher, K., 1992, Stratigraphic and structural study of part of the Early Archean Moodies Group, Maid-of-the-Mist syncline, Barberton Greenstone Belt, South Africa [B.Sc. thesis]: Stanford, California, Stanford University, 25 p.

Basu, A., 1981, Weathering before the advent of land plants: evidence from unaltered detrital K-feldspars in Cambrian-Ordovician arenites: Geology, v. 9, p. 132–133.

Bell, C. M., 1967, The geology of the farm Heemsteede 33 and portions of the farms Schultzenhorst 31 and Mendon 32 in the Barberton Mountainland [M.Sc. thesis]: Durban, University of Natal, 115 p.

Blatt, H., 1967, Provenance determinations and recycling of sediments: Journal of Sedimentary Petrology, v. 37, p. 1031–1044.

Büttner, W., Barton, J. M., and Saager, R., 1983, Geochemistry, age and origin of some porphyry intrusions in the Onverwacht Group, Barberton Greenstone Belt: Geological Society of South Africa Transactions, v. 86, p. 1–10.

Carrigy, M. A., and Mellon, G. B., 1964, Authigenic clay mineral cements in Cretaceous and Tertiary sandstones of Alberta: Journal of Sedimentary Petrology, v. 34, p. 461–467.

Cloete, M., 1991, An overview of metamorphism in the Barberton Greenstone Belt, *in* Ashwal, L. D., ed., Two cratons and an orogen—Excursion guidebook and review articles for a field workshop through selected Archean terranes of Swaziland, South Africa and Zimbabwe: IGCP Project 280 and Johannesburg, University of the Witwatersrand, Department of Geology, p. 84–98.

Condie, K. C., and Hunter, D. R., 1976, Trace element geochemistry of Archaean granitic rocks from the Barberton region, South Africa: Earth and Planetary Science Letters, v. 29, p. 389–400.

Condie, K. C., and Wronkiewicz, D. J., 1990a, The Cr/Th ratio in Precambrian pelites from the Kaapvaal Craton as an index of craton evolution: Earth and Planetary Science Letters, v. 97, p. 256–267.

Condie, K. C., and Wronkiewicz, D. J., 1990b, A new look at the Archean-Proterozoic boundary: Sediments and the tectonic setting constraint, *in* Naqvi, S. M., ed., Precambrian continental crust and its economic resources: Amsterdam, Elsevier, p. 61–84.

Condie, K. C., Macke, J. E., and Reimer, T. O., 1970, Petrology and geochemistry of early Precambrian greywacke from the Fig Tree Group, South Africa: Geological Society of America Bulletin, v. 81, p. 2759–2776.

Condie, K. C., Viljoen, M. C., and Kable, E. J. D., 1977, Effects of alteration of element distributions in Archean tholeiites from the Barberton Greenstone Belt, South Africa: Contributions to Mineralogy and Petrology, v. 64, p. 75–89.

Curray, J. R., 1969, Shallow structures of the continental margin, *in* Stanley, D. J., ed., The new concepts of continental margin sedimentation: Society of Economic Paleontologists and Mineralogists Special Publication 19, p. 304–310.

Daneel, G. J., 1987, The structural controls of gold mineralization in the Moodies Hills which surround the Agnes Gold Mine, Barberton Greenstone Belt [M.Sc. thesis]: Durban, University of Natal, 128 p.

de Ronde, C. E. J., 1991, Structural and geochronological relationships and fluid-rock interaction in the central part of the ~3.2–3.5 Ga Barberton Greenstone Belt, South Africa [Ph.D. thesis]: Toronto, University of Toronto, 370 p.

de Ronde, C. E., and de Wit, M. J., 1994, Tectonic history of the Barberton Greenstone Belt, South Africa: 490 million years of Archean crustal evolution: Tectonics, v. 13, p. 983–1005.

de Ronde, C. E. J., de Wit, M. J., and Spooner, E. T. C., 1994, Early Archean (>3.2 Ga) Fe-oxide-rich, hydrothermal discharge vents in the Barberton Greenstone Belt, South Africa: Geological Society of America Bulletin, v. 106, p. 86–104.

Dickinson, W. R., 1970, Interpreting detrital modes of graywacke and arkose: Journal of Sedimentary Petrology, v. 40, p. 695–707.

Dickinson, W. R., and Suczek, C. A., 1979, Plate tectonics and sandstone compositions: American Association of Petroleum Geologists Bulletin, v. 63, p. 2164–2187.

Dickinson, W. R., Beard, L. S., Brakenridge, G. R., Erjavec, J. L., Fergusson, R. C., Inman, K. F., Knepp, R. A., Lindberg, F. A., and Ryberg, P. T., 1983, Provenance of North American Phanerozoic sandstones in relation to tectonic setting: Geological Society of America Bulletin, v. 94, p. 222–235.

Duchac, K. C., and Hanor, J. S., 1987, Origin and timing of metasomatic silicification of an Early Archean komatiite sequence, Barberton Mountain Land, South Africa: Precambrian Research, v. 37, p. 125–146.

Eriksson, K., 1978, Alluvial and destructive beach facies from the Archean Moodies Group, Barberton Mountain Land, South Africa and Swaziland, *in* Miall, A. D., ed., Fluvial sedimentology: Canadian Society of Petroleum Geologists Memoir 5, p. 287–311.

Eriksson, K., 1979, Marginal marine depositional processes from the Archean Moodies Group, Barberton Mountain Land, South Africa: Evidence and significance: Precambrian Research, v. 8, p. 153–182.

Eriksson, K., 1980, Transitional sedimentation styles in the Moodies and Fig Tree Groups, Barberton Mountain Land, South Africa: evidence favouring an Archean continental margin: Precambrian Research, v. 12, p. 141–160.

Eriksson, K., 1982, Sedimentation patterns in the Barberton Mountain Land, South Africa, and the Pilbara Block, Australia: evidence for Archean rifted continental margins: Tectonophysics, v. 81, p. 179–193.

Falvey, D. A., 1974, The development of continental margins in plate tectonic theory: Journal of the Australian Petroleum Exploration Association, v. 14, p. 95–106.

Faure, K., and Harris, C., 1991, Oxygen and carbon isotope geochemistry of the 3.2-Ga Kaap Valley tonalite, Barberton Greenstone Belt, South Africa:

Precambrian Research, v. 52, p. 301–319.
Folk, R. L., 1968, Petrology of sedimentary rocks: Austin, Texas, Hemphill's Bookstore, 182 p.
Fripp, R. E. P., Van Nierop, D. A., Callow, M. J., Lilly, P. A., and DuPlessis, L. U., 1980, Deformation in part of the Archean Kaapvaal craton, South Africa: Precambrian Research, v. 13, p. 241–251.
Galloway, W. E., and Hobday, D. K., 1983, Terrigenous clastic depositional systems: New York, Springer, 423 p.
Ganss, O., and Schmidt-Thomé, P., 1953, Die gefaltete Molasse am Alpenrand zwischén Bodensee und Salzach (Folded molasse along the alpine margin between Lake Constance and Salzach): Zeitschrift der Deutschen Geologischen Gesellschaft, v. 105, p. 402–495.
Gay, N. C., 1969, The analysis of strain in the Barberton Mountain Land, eastern Transvaal, using deformed pebbles: Journal of Geology, v. 77, p. 377–396.
Hall, A. L., 1918, The geology of the Barberton gold mining district: Geological Survey of South Africa Memoir 9, 347 p.
Hanor, J. S., and Duchac, K., 1990, Isovolumetric silicification of Early Archean komatiites: geochemical mass balances and constraints on origin: Journal of Geology, v. 98, p. 863–877.
Heinrichs, T. K., 1980, Lithostratigraphische Untersuchungen in der Fig Tree Gruppe des Barberton Greenstone Belt zwischen Umsoli and Lomati, Südafrika (Lithostratigraphic investigations in the Fig Tree Group of the Barberton Greenstone Belt between Umsoli and Lomati, South Africa): Göttinger Arbeiten zur Geologie und Paläontologie, v. 22, 118 p.
Heinrichs, T. K., and Reimer, T. O., 1977, A sedimentary barite deposit from the Archean Fig Tree Group of the Barberton Mountain Land (South Africa): Economic Geology, v. 72, p. 1426–1441.
Helmold, K. P., 1985, Provenance of feldspathic sandstones: the effect of diagenesis on provenance interpretations: a review, *in* Zuffa, G. G., ed., Provenance of arenites: NATO Advanced Studies Series, C, v. 148, p. 139–163.
Heubeck, C., 1993, Geology of the Archean Moodies Group, Barberton Greenstone Belt, South Africa [Ph.D. thesis]: Stanford, California, Stanford University, 413 p.
Heubeck, C., and Lowe, D. R., 1994a, Depositional and tectonic setting of the Archean Moodies Group, Barberton Greenstone Belt, South Africa: Precambrian Research, v. 68, p. 257–290.
Heubeck, C., and Lowe, D. R., 1994b, Late syndepositional deformation and detachment tectonics in the Barberton Greenstone Belt, South Africa: Tectonics, v. 13, p. 1514–1536.
Hose, L. D., 1990, The geology and stratigraphic evolution of the north-central part of the Early Archean Barberton Greenstone Belt, South Africa [Ph.D. thesis]: Baton Rouge, Louisiana, Louisiana State University, 327 p.
Hunter, D. R., 1970, The Ancient Gneiss Complex in Swaziland: Geological Society of South Africa Transactions, v. 73, p. 107–150.
Hunter, D. R., 1973, The granitic rocks of the Precambrian in Swaziland: Geological Society of South Africa Special Publication 3, p. 131–145
Hunter, D. R., 1991, An overview of the pre-3.1 Ga-old Gneiss terrane, Swaziland, *in* Ashwal, L. D., ed., Two cratons and an orogen—Excursion guidebook and review articles for a field workshop through selected Archean terranes of Swaziland, South Africa and Zimbabwe: IGCP Project 280 and Johannesburg, University of the Witwatersrand, Department of Geology, p. 1–7.
Ingersoll, R. V., Bullard, T. F., Ford, R. L., Grimm, J. P., Pickle, J. D., and Sares, S. W., 1984, The effect of grain size on detrital modes: a test of the Gazzi-Dickinson point-counting method: Journal of Sedimentary Petrology, v. 54, p. 103–116.
Jackson, M. P. A., 1984, Archean structural styles in the Ancient Gneiss Complex of Swaziland, Southern Africa, *in* Kröner, A., and Greiling, R., eds., Precambrian tectonics illustrated: Stuttgart, Schweizerbart, p. 1–18.
Jackson, M. P. A., Eriksson, K. A., and Harris, C. W., 1987, Early Archean foredeep sedimentation related to crustal shortening: A reinterpretation of the Barberton sequence, southern Africa: Tectonophysics, v. 136, p. 197–221.
Johnsson, M. J., 1992, Chemical weathering controls on sand composition, *in* Nierenber, W. A., ed., Encyclopedia of Earth systems science: Orlando, Florida, Academic Press, v. 1, p. 455–466.
Johnsson, M. J., 1993, The system controlling the composition of clastic sediment, *in* Johnsson, M. J., and Basu, A., eds., Processes controlling the composition of clastic sediments: Geological Society of America Special Paper 284, p. 1–20.
Julivert, M., 1971, Decollement tectonics in the Hercynian cordillera of northwest Spain: American Journal of Science, v. 270, p. 1–29.
Kamo, S. L., and Davis, D. W., 1994, Reassessment of Archean crustal development in the Barberton Mountain Land, South Africa, based on U-Pb dating: Tectonics, v. 13, p. 167–192.
Kasting, J. F., 1986, Theoretical constraints on oxygen and carbon dioxide concentrations in the Precambrian atmosphere: Precambrian Research, v. 34, p. 205–229.
Knauth, L. P., and Epstein, S., 1976, Hydrogen and oxygen isotope ratios in nodular and bedded cherts: Geochimica et Cosmochimica Acta, v. 40, p. 1095–1108.
Knauth, L. P., and Lowe, D. R., 1978, Oxygen isotope geochemistry of cherts from the Onverwacht Group (3.4 billion years), Transvaal, South Africa, with implications for secular variations in the isotopic composition of cherts: Earth and Planetary Science Letters, v. 41, p. 209–222.
Kröner, A., and Compston, W., 1988, Ion microprobe ages of zircons from Early Archean pebbles and greywacke, Barberton Greenstone Belt, southern Africa: Precambrian Research, v. 38, p. 367–380.
Kröner, A., Byerly, G. R., and Lowe, D. R., 1991, Chronology of Early Archean granite-greenstone evolution in the Barberton Mountain Land, South Africa, based on precise dating by single zircon evaporation: Earth and Planetary Science Letters, v. 103, p. 41–54.
Krupicka, J., 1975, Early Precambrian rocks of granitic composition: Canadian Journal of Earth Sciences, v. 12, p. 1307–1315.
Lamb, S. H., 1984, Structures on the eastern margin of the Archean Barberton Greenstone Belt, northwest Swaziland, *in* Kröner, A., and Greiling, R., eds., Precambrian tectonics illustrated: Stuttgart, Schweizerbart, p. 19–39.
Lamb, S. H., and Paris, I., 1988, Post–Onverwacht Group stratigraphy in the southeastern part of the Archean Barberton Greenstone Belt: Journal of African Earth Sciences, v. 7, p. 285–306.
Laubscher, H. P., 1977, Fold development in the Jura: Tectonophysics, v. 37, p. 337–362.
López-Martínez, M., York, D., Hall, C. M., and Hanes, J. A., 1984, Oldest reliable $^{40}Ar/^{39}Ar$-ages for terrestrial rocks: Barberton Mountain Land komatiites: Nature, v. 307, p. 352–355.
Lowe, D. R., 1991, Geology of the Barberton Greenstone Belt: an overview, *in* Ashwal, L. D., ed., Two cratons and an orogen—Excursion guidebook and review articles for a field workshop through selected Archean terranes of Swaziland, South Africa and Zimbabwe: IGCP Project 280 and Johannesburg, University of the Witwatersrand, Department of Geology, p. 47–58.
Lowe, D. R., and Byerly, G. R., 1986, Archean flow-top alteration zones formed initially in a low-temperature sulphate-rich environment: Nature, v. 324, p. 245–248.
Lowe, D. R., and Knauth, L. P., 1977, Sedimentology of the Onverwacht Group (3.4 billion years), Transvaal, South Africa, and its bearing on the characteristics and evolution of the early Earth: Journal of Geology, v. 85, p. 699–723.
McBride, E. F., 1984, Diagenetic effects that affect provenance determinations in sandstone, *in* Zuffa, G. G., ed., Provenance of arenites: NATO Advanced Studies Institute Series C, v. 148, p. 95–113.
McLennan, S. M., and Taylor, S. R., 1984, Archaean sedimentary rocks and their relation to the composition of the Archaean continental crust, *in* Kröner, A., Hanson, G. N., and Goodwin, A. M., eds., Archean geochemistry: New York, Springer, p. 49–72.
McLennan, S. M., Taylor, S. R., and Kröner, A., 1983, Geochemical evolution of Archean shales from South Africa. I. The Swaziland and Pongola Supergroups: Precambrian Research, v. 22, p. 93–124.
Mountjoy, E. W., 1992, Significance of rotated folds and thrust faults, Alberta Rocky Mountains, *in* Mitra, S., and Fisher, G. W., eds., Structural geology of fold and thrust belts: Baltimore, Maryland, Johns Hopkins University

Press, p. 207–223.
Nocita, B. W., 1989, Sandstone petrology of the Archean Fig Tree Group, Barberton Greenstone Belt, South Africa: Tectonic implications: Geology, v. 17, p. 953–956.
Nocita, B. W., and Lowe, D. R., 1990, Fan-delta sequence in the Archean Fig Tree Group, Barberton Greenstone Belt, South Africa: Precambrian Research, v. 48, p. 375–393.
Paris, I. A., 1985, The geology of the farms Josefsdal, Dunbar, and part of Diepgezet in the Barberton Greenstone Belt [Ph.D. thesis]: Johannesburg, University of the Witwatersrand, 239 p.
Paris, I. A., Stanistreet, I. G., and Huges, M. J., 1985, Cherts of the Barberton Greenstone Belt interpreted as products of submarine exhalative activity: Journal of Geology, v. 93, p. 111–130.
Perry, E. C., and Tan, F. C., 1972, Oxygen and carbon isotope determinations in early Precambrian metasediments of the southern African Shield: Geological Society of America Bulletin, v. 83, p. 647–664.
Ramsay, J. G., 1963, Structural investigations in the Barberton Mountain Land, eastern Transvaal: Geological Society of South Africa Transactions, v. 66, p. 352–398.
Reimer, T. O., 1967, Die Geologie der Stolzburg-Synklinale im Barberton Bergland (Transvaal, Südafrika) [Diplomarbeit] (Geology of the Stolzburg Syncline in the Barberton Mountain Land (Transvaal, South Africa): Frankfurt, Germany, Geologisch-Paläontologisches Institut, Universität Frankfurt, 121 p.
Reimer, T. O., 1972, Diagenetic reactions in early Precambrian graywackes of the Barberton Mountain Land (South Africa): Sedimentary Geology, v. 7, p. 263–282.
Reimer, T. O., 1975, Untersuchungen über Abtragung, Sedimentation und Diagenese im frühen Präkambrium am Beispiel der Sheba-Formation (Südafrika): Geologisches Jahrbuch, Reihe B, v. 17, 108 p.
Reimer, T. O., 1980, Archaean sedimentary barite deposits of the Swaziland Supergroup (Barberton Mountain Land, South Africa): Precambrian Research, v. 12, p. 393–410.
Reimer, T. O., Condie, K. C., Schneider, G., and Georgi., A., 1985, Petrography and geochemistry of granitoid and metamorphic pebbles from the Early Archean Moodies Group, Barberton Mountain Land, South Africa: Precambrian Research, v. 29, p. 383–404.
Robb, L. J., and Anhaeusser, C. R., 1983, Chemical and petrogenetic characteristics of Archean tonalite-trondhjemite gneiss plutons in the Barberton Mountain Land, *in* Anhaeusser, C. R., ed., Contributions to the geology of the Barberton Mountain Land: Geological Society South Africa Special Publication 9, p. 103–116.
Robb, L. J., Barton, J. M., Kable, E. J. D., and Wallace, R. C., 1986, Geology, geochemistry and isotopic characteristics of the Archean Kaap Valley Pluton, Barberton Mountain Land, South Africa: Precambrian Research, v. 31, p. 1–36.
SACS (South African Committee on Stratigraphy), 1980, Stratigraphy of South Africa, Part 1. Lithostratigraphy of the Republic of South Africa, South West Africa/Namibia, and the Republics of Bophuthswana, Transkei and Venda: Geological Survey of South Africa Handbook 8, 690 p.
Suttner, L. J., Basu, A., and Mack, G., 1981, Climate and the origin of quartzarenites: Journal of Sedimentary Petrology, v. 51, p. 1235–1246.
Tegtmeyer, A. R., and Kröner, A., 1987, U-Pb zircon ages bearing on the nature of Early Archean greenstone belt evolution, Barberton Mountain Land, southern Africa: Precambrian Research, v. 36, p. 1–20.
Tomkinson, M. J., and King, V. J., 1991, The tectonics of the Barberton Greenstone Belt—an overview, *in* Ashwal, L. D., ed., Two cratons and an orogen—Excursion guidebook and review articles for a field workshop through selected Archean terranes of Swaziland, South Africa and Zimbabwe: IGCP Project 280 and Johannesburg, University of the Witwatersrand, Department of Geology, p. 69–83.
Tomkinson, M. J., and Lombard, A., 1990, Structure, metamorphism, and mineralization in the New Consort Gold Mines, Barberton Greenstone Belt, South Africa, *in* Glover, J. E., and Ho, S. E., compilers, Extended abstracts volume: Third International Archean Symposium, Perth, p. 377–380.
Toulkeridis, T., 1992, Stratigraphische, geochemische, isotopische und geochronologische Untersuchungen an Karbonatgesteinen aus dem Barberton Grünsteingürtel, östliches Transvaal, Südafrika [Diplomarbeit] (Stratigraphic, geochemical, isotope and geochronologic investigations of carbonates of the Barberton Greenstone Belt, eastern Transvaal, South Africa): Mainz, Germany, Fachbereich Geowissenschaften, Universität Mainz, 162 p.
Toulkeridis, T., Clauer, N., and Kröner, A., 1996, Chemical variations in clay minerals of the Archaean Barberton Greenstone Belt (South Africa): Precambrian Research, v. 79, p. 195–207.
Van Niekerk, C. B., and Burger, A. J., 1978, The age of the Moodies conglomerate boulders: Geological Society of South Africa Special Publication 4, p. 99–106.
Viljoen, M. J., and Viljoen, R. P., 1969, An introduction to the geology of the Barberton granite-greenstone terrain: Geological Society of South Africa Special Publication 2, p. 9–27.
Visser, D. J. L., 1956, The geology of the Barberton area: Geological Society of South Africa Special Publication 15, 254 p.
Watchorn, M. B., 1980, Fluvial and tidal sedimentation in the 3000 Ma old Mozaan basin, South Africa: Precambrian Research, v. 13, p. 27–42.
Wilson, M. D., and Pittman, E. D., 1977, Authigenic clays in sandstones: Recognition and influence on reservoir properties and paleoenvironmental analysis: Journal of Sedimentary Petrology, v. 47, p. 3–31.

MANUSCRIPT ACCEPTED BY THE SOCIETY MARCH 26, 1998

Geological Society of America
Special Paper 329
1999

Geologic evolution of the Barberton Greenstone Belt and vicinity

Donald R. Lowe
Department of Geological and Environmental Sciences, Stanford University, Stanford, California 94305

ABSTRACT

The Kaapvaal Craton in the vicinity of the Barberton Greenstone Belt (BGB) is here divided into five major blocks: (1) the Ancient Gneiss Complex Block in Swaziland; (2) the Steynsdorp Block, which includes the southeasternmost portion of the BGB, and the 3,509-Ma Steynsdorp pluton; (3) the Songimvelo Block, which includes much of the south-central part of the BGB and the adjacent 3,445-Ma tonalite-trondhjemite-granodiorite (TTG) intrusive suite; (4) the Umuduha Block, occupying the central part of the BGB; and (5) the Kaap Valley Block, which includes the BGB north of the Inyoka fault and the 3,227-Ma TTG plutonic suite. The Steynsdorp, Songimvelo, Umuduha, and Kaap Valley Blocks each formed through early magmatic and late deformation periods. The magmatic period can be divided into (1) an ultramafic and mafic volcanic stage, involving the eruption of a thick, predominantly komatiitic volcanic sequence; and (2) a felsic magmatic stage during which the mafic and ultramafic sequence was intruded by TTG plutons and covered by comagmatic dacitic to rhyolitic volcanic rocks. The stratigraphic relationships, structural styles, and petrologic aspects of these magmatic stages suggest that early komatiitic volcanism occurred along rifts and/or on oceanic islands or plateaus, and that late TTG-felsic magmatism marked the development of subduction-related magmatic arcs. The products of the magmatic stage of greenstone belt evolution were small, thickened, buoyant masses of crust composed of the volcanic sequences and their underlying intrusive complexes. These are here termed protocontinents. The widespread deposition of younger ultramafic and mafic and felsic sequences on older protocontinental blocks and the presence in younger felsic magmatic units of xenocrystic zircons representing older periods of felsic magmatism indicate that most protocontinental blocks in the BGB and vicinity formed upon and along the margins of older protocontinental blocks.

Early deformation in each block probably accompanied late felsic magmatism. In the Songimvelo Block, this deformation at about 3,445 Ma is termed D_1. Later deformation was related to regional shortening of the largely unmetamorphosed volcanic and sedimentary sequences between the more competent, thickened nuclei of the protocontinental blocks. In the Songimvelo, Umuduha, and Kaap Valley Blocks, major shortening, D_2, occurred between about 3,240 and 3,230 Ma and is represented by sediments of the Fig Tree Group. D_2 shortening involved the formation of inward-facing fold-and-thrust belts along the northwestern and southeastern margins of the exposed BGB and culminated in southward and southeastward thrusting of the Umuduha and marginal Songimvelo volcanic successions onto the central part of the Songimvelo Block along the Komati fault.

Subsequent late Fig Tree arc-related magmatism and deformation jumped to the

Lowe, D. R., 1999, Geologic evolution of the Barberton Greenstone Belt and vicinity, *in* Lowe, D. R., and Byerly, G. R., eds., Geologic Evolution of the Barberton Greenstone Belt, South Africa: Boulder, Colorado, Geological Society of America Special Paper 329.

northwest, isolating a basin, possibly a back-arc basin, in which 3,225-Ma tuffs of the Schoongezicht Formation, derived from the Kaap Valley arc, were deposited directly on ultramafic volcanic rocks and cherts of the Weltevreden Formation at the top of the Onverwacht Group. The Moodies Group was deposited in this back-arc basin and in basins developed through D_3 extension within the older D_2 orogen. Late to post-Moodies deformation (D_4) involved closure of the Moodies basins and southeast-verging thrusting of the basinal sequences onto the surrounding older Onverwacht and Fig Tree rocks deformed during D_2. D_4 was followed by formation of a regional northwest-verging fold-and-thrust belt, rotation of bedding and other planar structures to the vertical, and heterogeneous shortening of the supracrustal succession during convergence and suturing of the protocontinental blocks (D_5).

The Kaapvaal Craton in the vicinity of the BGB is a compound crustal block made up of amalgamated protocontinental blocks formed over at least 330 m.y. between 3.55 and 3.22 Ga. The Steynsdorp, Songimvelo, and Umuduha Blocks were amalgamated magmatically at the time of their formation because younger blocks typically formed adjacent to and on top of older blocks and tectonically during late-stage regional shortening. These blocks and the AGC and Kaap Valley Blocks were amalgamated tectonically by subduction and shortening of the intervening volcanic sequences/crust and suturing of the TTG nuclei. This collage of protocontinental blocks did not form simply as an accretionary prism in which unrelated, far-removed blocks were tectonically amalgamated above one or more long-lived subduction zones. Rather, it formed through multiple, complex cycles of rifting, mafic and ultramafic magmatism, volcanic quiescence, and subduction-related magmatism. Although the growing accretionary tract was not thickened or stabilized to form a large, buoyant cratonic block until about 3,100 Ma, this and similar loose collections of protocontinental blocks may have served as the first continentlike domains on the pre-3.0-Ga Earth. Their assembly began as the Earth cooled and tectonic recycling systems decreased in efficiency, allowing the most buoyant crustal blocks to resist subduction and serve as the nuclei for long-term accretion and large-scale continent growth.

INTRODUCTION

Preceding papers in this volume have outlined the stratigraphy, petrology, and sedimentology of the Barberton Greenstone Belt (BGB). Structural analysis of the main body of the belt is still lacking, although geologic mapping and stratigraphic studies have provided a general picture of the structural framework and evolution of southern and western areas (de Wit, 1982; de Wit et al., 1983, 1987a, b, 1992; Paris, 1985; Lowe et al., 1985; de Ronde and de Wit, 1994; Heubeck and Lowe, 1994a, b; Lowe et al., this volume, Chapter 2), and a number of studies have outlined structural styles and histories along the margins of the belt (Ramsay, 1963; Gay, 1969; Anhaeusser, 1976, 1984; Lamb, 1984a, b; Jackson et al., 1987).

Recent scenarios suggest that the BGB formed through the assembly of discrete terranes or tectonic and stratigraphic blocks (Lowe et al., 1989; de Wit et al., 1992; Kröner et al., 1992; de Ronde and de Wit, 1994; Lowe, 1994). Lowe (1994) identified five major tectono-stratigraphic blocks in the southern part of the BGB and vicinity (Fig. 1): (1) the *Ancient Gneiss Complex (AGC) Block* in Swaziland; (2) the *Steynsdorp Block*, including the southeastern part of the BGB in the Steynsdorp anticline and the pre-3.5-Ga Steynsdorp pluton; (3) the *Songimvelo Block*, comprising the Southern Domain of Lowe et al. (this volume, Chapter 2) and 3,445-Ma intrusive rocks along the southern margin of the BGB; (4) the *Umuduha Block*, occupying the central part of the BGB south of the Inyoka fault and lacking exposed tonalite-trondhjemite-grandiorite (TTG) units; and (5) the *Kaap Valley Block*, including the Northern Domain and areas north of the Inyoka fault, which formed as a volcanic sequence that was intruded by TTG magmas between 3,229 and about 3,212 Ma. The stratigraphic relationships within and among these blocks are shown in Figure 2, a general cross section of the BGB is shown in Figure 3, and the schematic relationships among the blocks is shown in Figure 4. Available high-precision geochronological data for the BGB and vicinity are given in Table 1. After a brief discussion of Archean plate tectonics, this report will summarize the development of the individual blocks in the BGB and vicinity.

ARCHEAN PLATE TECTONICS

Although considerable controversy has surrounded the nature of Archean geodynamics, theoretical and actualistic models point strongly to an Archean tectonic regime not fundamentally different from that of today. Windley (1976), Condie (1981),

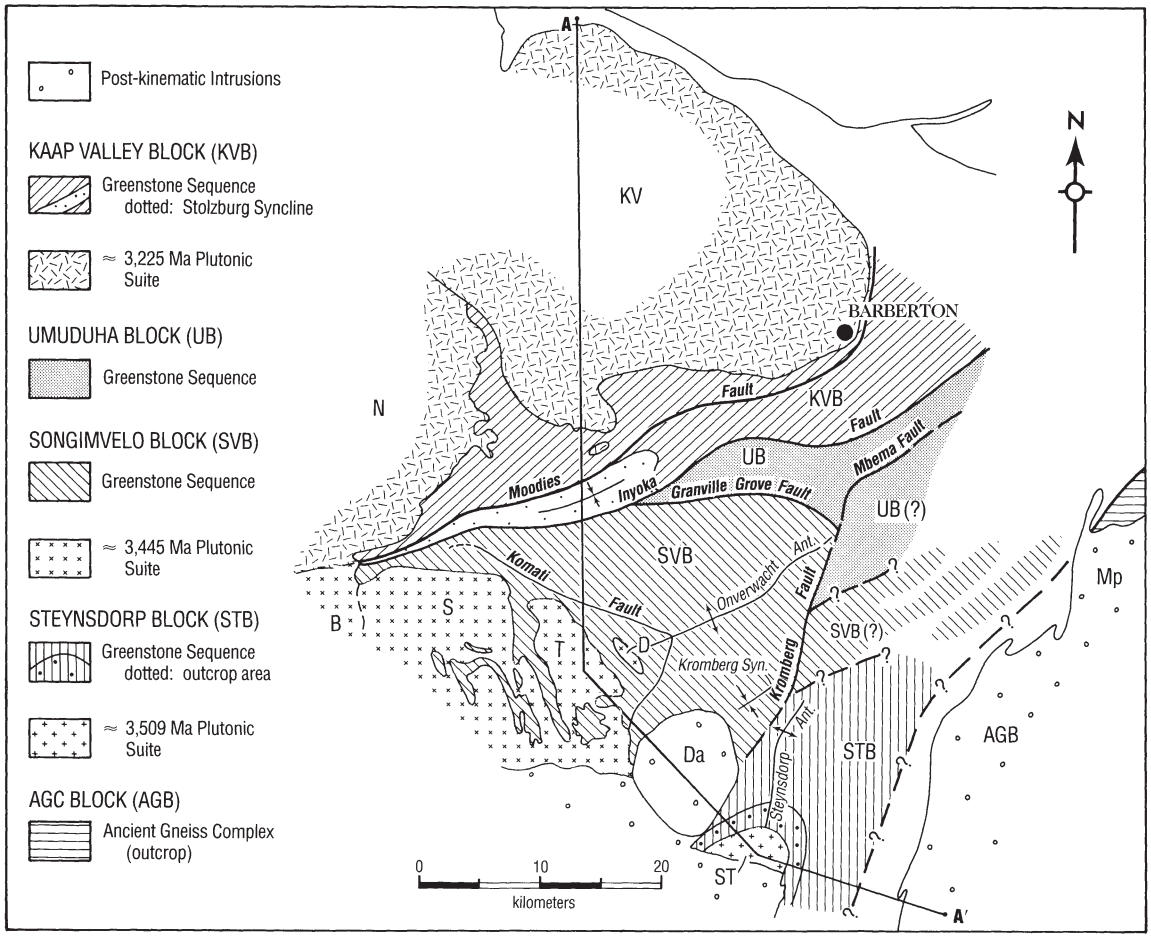


Figure 1. Generalized map of the southwestern part of the Barberton Greenstone Belt showing the locations and boundaries of the major tectono-stratigraphic blocks that comprise the basement in this part of the eastern Kaapvaal Craton. A–A′ shows the line of the cross section in Figures 5, 6, and 7. Abbreviations: KV, Kaap Valley pluton; N, Nelshoogte pluton; B, Badplaas pluton; S, Stolzburg pluton; T, Theespruit pluton; D, Doornhoek pluton; Da, Dalmein pluton; ST, Steynsdorp pluton; Mp, Mpuluzi pluton.

Bickle (1978, 1986), Burke and Kidd (1978), and many others have reasoned that the higher heat flow in the Archean would have necessitated an efficient system of heat dissipation best accomplished through the rapid creation, cooling, and recycling of oceanic crust. Hoffman (1988, 1989) and Card (1990) have summarized geologic evidence that subduction-related magmatism, the assembly of accretionary complexes at convergent plate boundaries, and horizontal plate movements accounted for crustal evolution throughout much of the Precambrian (Lowe and Ernst, 1992).

A number of aspects of BGB evolution provide strong supporting evidence for Archean plate tectonics. (1) The geochemistry of the felsic volcanic and TTG intrusive suites in and around the BGB are most comparable to those of modern subduction-related magmatic arcs (de Wit et al., 1987b, 1992; de Ronde and de Wit, 1994). Although the general geochemistry of Archean felsic magmatic rocks differs in many respects from their apparent modern magmatic-arc counterparts (summary in Arkani-Hamed and Jolly, 1989), these differences appear to provide important details about the nature of Archean subduction processes rather than indicating the existence of fundamentally different tectonic settings of magmatism. The bimodality of BGB volcanism and greenstone magmatism in general has been regarded as suggestive of continental rift-related volcanism (Condie and Hunter, 1976; Thurston et al., 1985), but other studies have shown that bimodal basaltic-felsic volcanism may characterize magmatic arcs associated with the subduction of young, hot oceanic lithosphere (Abbott and Hoffman, 1984; Defant and Drummond, 1990). If the Archean oceanic lithosphere was generally hotter and younger than modern oceanic lithosphere, as might be supposed with the requirement for a significantly higher Archean rate of heat dissipation, more mafic and more strongly bimodal volcanic units, like those in the BGB, might be expected (Abbott and Hoffman, 1984). Other compositional differences may reflect Archean magma genesis within the subducting rather than the overriding plate

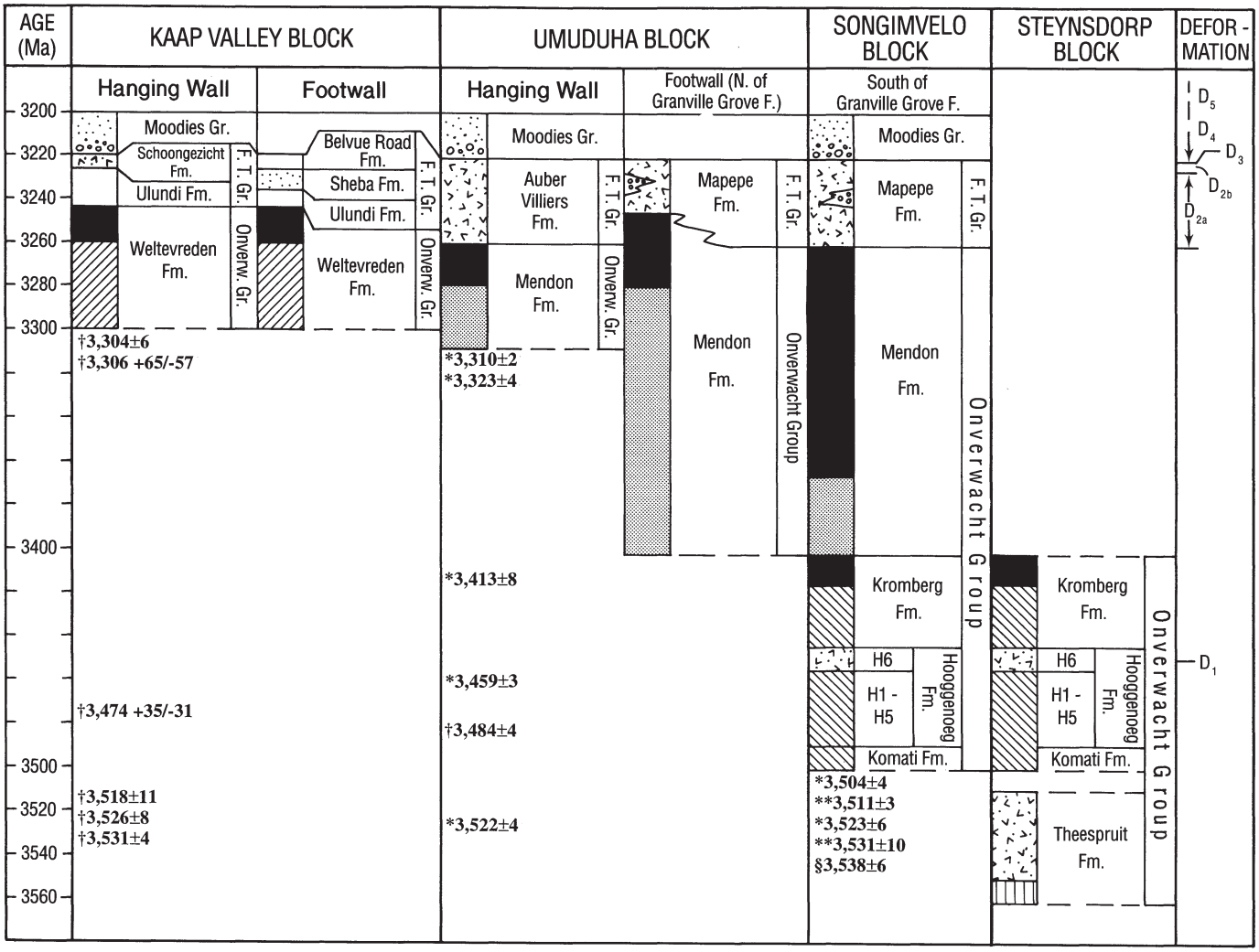


Figure 2. Generalized stratigraphy and deformational events of the major tectono-stratigraphic blocks in the BGB and vicinity. Black units are cherts marking probable condensed sections deposited following major magmatic cycles. Symbols for principal mafic volcanic sequences as in Figure 1. Ages with asterisks (*) below stratigraphic columns indicate the ages of xenocrysts within the magmatic rocks on that block. Ages with daggers (†) indicate detrital grains and rock fragments within sedimentary units. Age with section marks (§) is from gneiss block within shear zone on Songimvelo Block south of Komati fault. Ages with double asterisks (**) are from volcanic and volcaniclastic rocks of the Theespruit Formation on the Songimvelo Block south of the Komati fault.

(Arkani-Hamed and Jolly, 1989), the composition of source rocks, and the degree of partial melting.

(2) Perhaps the most persuasive evidence for Archean plate tectonics during formation of the BGB is the dominance of horizontal shortening during deformation. Both the initial stage of deformation in late Fig Tree time, D_2 of Lowe et al. (this volume, Chapter 2), and later culminating stages of deformation in late and post-Moodies time, D_4 and D_5, involved the formation of fold-and-thrust belts and the tectonic stacking and duplication of the greenstone sequence (de Wit, 1982; de Ronde and de Wit, 1994; Heubeck and Lowe, 1994a, b; Lowe et al., this volume, Chapter 2). The latest deformation included extreme regional shortening of the supracrustal sequence and intense rotation of virtually all bedding and early fault planes to the vertical accompanying suturing of the intrusive complexes. This style of deformation has characterized the growth not only of Archean but Proterozoic continents (Hoffman, 1989) and is most consistent with well-documented Phanerozoic scenarios of continental growth and plate interactions.

(3) Late-stage strike-slip accommodation faulting during heterogeneous shortening and the lateral escape of supracrustal blocks from between converging rigid TTG intrusive complexes during D_5 (Ramsay, 1963; Lowe et al., this volume, Chapter 2) also implies large relative horizontal movements of major segments of the Archean crust.

The following discussion of the tectonic development of the

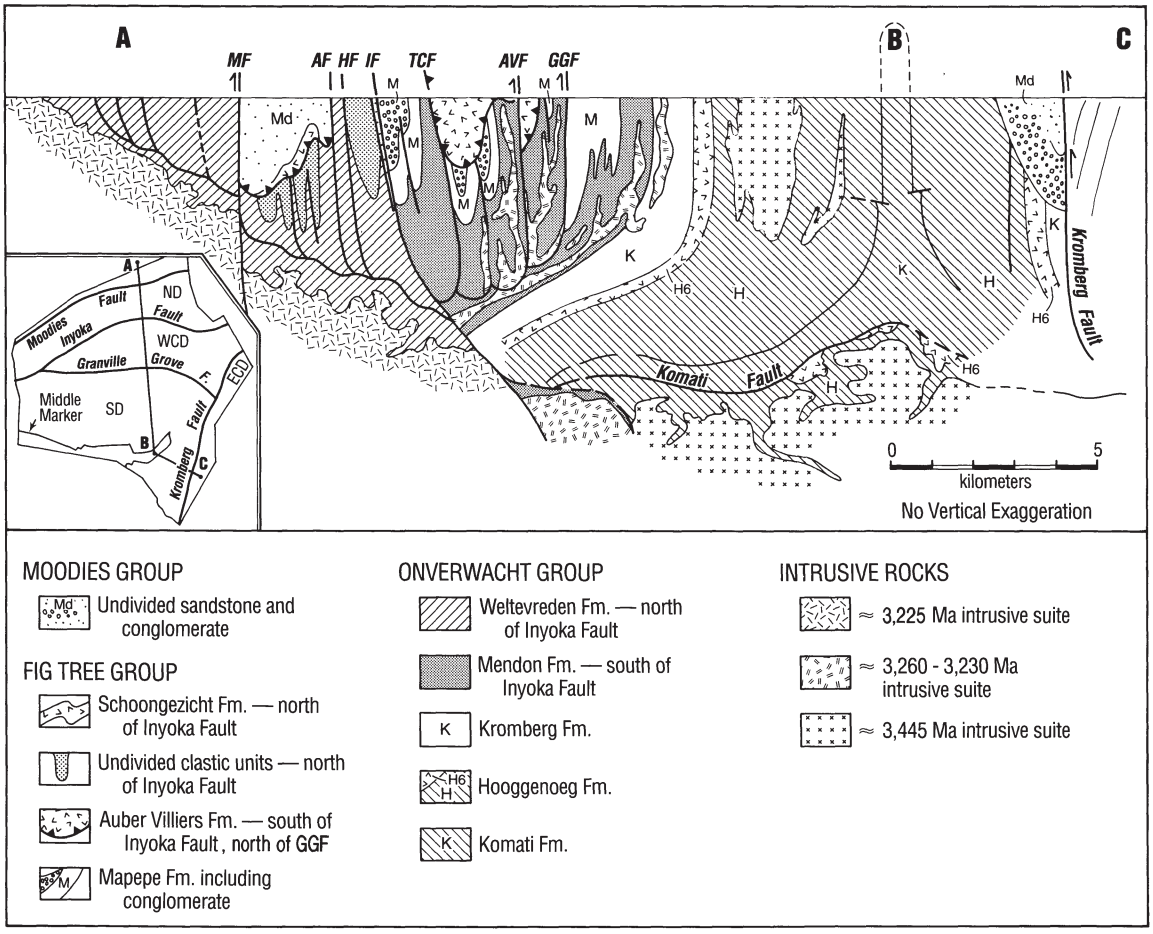


Figure 3. Cross section of the Barberton Greenstone Belt. Inset shows the line of the section and the structural domains of Lowe et al. (this volume, Chapter 2).

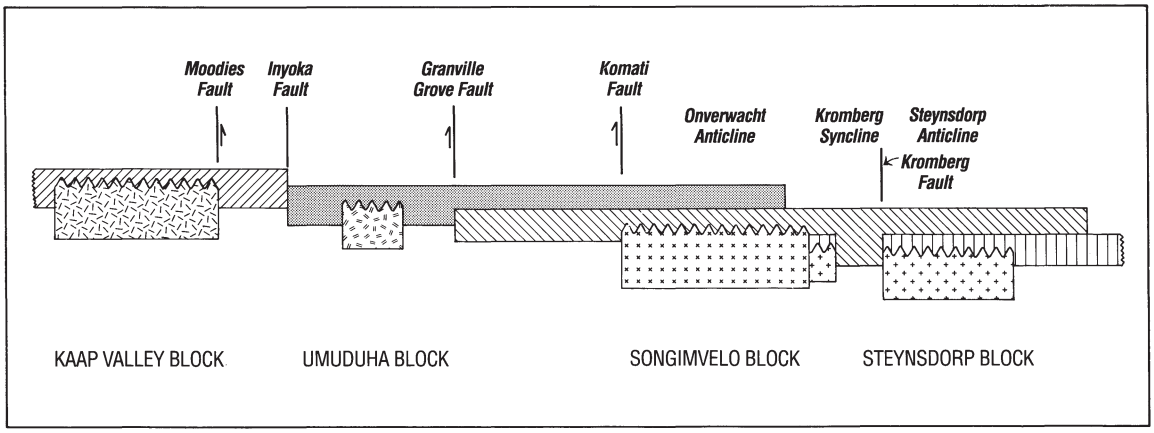


Figure 4. Schematic relationships of the volcanic and intrusive TTG suites comprising the major blocks in the Barberton Greenstone Belt. Patterns as in Figures 1 and 3.

TABLE 1. U-PB AND PB-PB ZIRCON AGES FOR ROCKS OF THE BARBERTON GREENSTONE BELT AND VICINITY, EASTERN KAAPVAAL CRATON, SOUTH AFRICA AND SWAZILAND

Unit	Rock Type	Age (Ma)	Method*	Interpretation†	Ref.§
ANCIENT GNEISS BLOCK (AGB)					
Ngwane Gneiss (NG)					
NG	tonalitic gneiss NE Swaziland	3,644±4	b	Oldest date from AGC. [*Xenocryst or metagreenstone remanent in younger orthogneiss*]	16
NG	tonalitic gneiss NE Swaziland	3,586±6	b	Age of emplacement/crystallization	5
NG	tonalitic orthogn.	3,563±3	b	Age of emplacement/crystallization	5
NG	TTG orthogneiss	3,505±24	b	Age of emplacement/crystallization	5
NG	TTG orthogneiss	3,214±20	b	Age of emplacement/crystallization	5
Dwalile Supracrustal Suite (DSS)					
DSS	metagraywacke	3,566±33	c	Oldest dated detrital zircon in DSS	10
DDS	metagraywacke	3,523±22 to 3,566±33 (20 dated zircons)	b	Detrital zircons in DSS eroded from igneous rocks representing ~3,547-3,510 Steynsdorp-age felsic magmatic events	10
DDS	metagraywacke	3,497±50 to 3,408±29 (23 dated zircons)	b,c	Detrital zircons in DSS eroded from igneous rocks representing 3,445-Ma felsic magmatic event	10
DDS	metagraywacke	3,423±30	c	Youngest concordant detrital zircon	10
Tsawela Gneiss (TG)					
TG	tonalitic gneiss	3,458±3	c	Age of emplacement/crystallization	5
TG	tonalitic gneiss	3,490±3	b	Age of emplacement/crystallization	10
TG	foliated tonalite	3,458±6	c	Age of emplacement/crystallization	5
TG	foliated tonalite	3,455±4 to 3,456±3	b	Age of emplacement/crystallization	10
TG	foliated tonalite	3,436±5	b	Age of emplacement/crystallization	
Onverwacht Group (OG): Theespruit Formation (TF)					
TF	felsic schist	3,547±3	c	Age of felsic volcanism	11
Steynsdorp Pluton (SP					
SP	tonalitic gneiss	3,531±3	c	Xenocryst	7
SP	tonalitic gneiss	3,553±4	c	Xenocryst	11
SP	trondhjemitic gneiss	3,509 +8/-7	a	Age of emplacement/crystallization	9
Fig Tree Group (FTG): Sedimentary units (Lamb, 1984a,b) near boundary of Steynsdorp and Ancient Gneiss Blocks.					
FTG	graywacke	3,461±16	b	Detrital grains; age of source rocks of Fig Tree sandstones; [*3,445 Ma magmatic suite*]	2
SONGIMVELO BLOCK					
Onverwacht Group (OG): Theespruit Formation (TF)					
TF	tectonic block of tonalitic gneiss	3,538±6	b	Age of crystallization	6
	same	3,538 +4/-2	a	Age of crystallization	9
TF	volcaniclastic diamictite	3,531±10	b	Age of volcanism [*Possibly a tectonic breccia developed along a fault*]	6
	same	3,453±6	b	Age of volcanism [*same*]	6
TF	volcanic unit	3,511±3	c	Age of volcanism	11
Onverwacht Group: Komati Formation (KF)					
KF	metagabbro dike	3,523±6	b	Xenocryst	6
	same	3,482±5	b	Age of gabbro emplacement/crystallization [*Xenocrysts from 3,445-Ma magmatic suite*]	6
	same	3,351±6	b	Metamorphic zircons or contaminants	6
	same	3,352±6	a	Age of gabbro emplacement/crystallization	9
KF	quartz-feldspar porphyry dike	3,470 +39/-9	a	Age of dike emplacement/crystallization; Minimum age of Komati Formation	9
KF	komatiitic metabasalt	3,486±8	d	Age of metamorphism	12
KF	clastic unit	ca. 3,472	b	Age of volcanism	6
Onverwacht Group: Hooggenoeg Formation (H)					
H1 (Middle Marker)	felsic tuff	3,472±5	d	Age of Middle Marker deposition, base of Kromberg Fm., upper limit on Komati Fm. volcanism	6
H6	felsic tuff	3,504±4	c	Xenocryst	7
H6	felsic hyp. intrusion	3,445±8	b	Age of emplacement/crystallization	6
H6	dacitic tuff	3,445±3	c	Age of volcanism	7
H6	felsic flow	3,438±6	c	Age of volcanism	3
H6	metaquartzite	3,457±15	c	Age of felsic magmatism represented by detrital zircons in banded metaquartzite [*banded metaquartzite: probably represents metamorphosed Buck Reef Chert; zircons derived from 3,445-Ma magmatic suite*]	3

TABLE 1. U-PB AND PB-PB ZIRCON AGES FOR ROCKS OF THE BARBERTON GREENSTONE BELT AND VICINITY, (CONTINUED, p. 2)

SONGIMVELO BLOCK (cont.)					
Hooggenoeg-Age, 3,445-Ma TTG Intrusive Suite					
Stolzburg pluton	trondhjemitic gneiss	3,445±3	c	Age of emplacement/crystallization	7
Stolzburg plu. (older phase)	trondhjemitic gneiss	3,460 +5/-4	a	Age of emplacement/crystallization	9
Theespruit plu.	trondhjemite	3,437±6	b	Age of emplacement/crystallization	6
Theespruit plu.	tonalitic gneiss	3,440±5	c	Age of emplacement/crystallization	7
Theespruit plu.	trondhjemite	3,443 +4/-3		Age of emplacement/crystallization	9
Doornhoek plu.	trondhjemite	3,448±4	a	Age of emplacement/crystallization	9
Onverwacht Group: Kromberg Formation (K)					
K1 (Buck Reef Chert)	tuff	3,416±5	c	Age volcanism and of basal part of Kromberg Formation [*Incorrectly assigned to the Hoog. Fm. by Kröner et al., 1991a*]	7
K3c Footbridge Chert)	felsic tuff	3,334±3	c	Age of uppermost Kromberg Fm.	8
Onverwacht Group: Mendon Formation: No dates available from Songimvelo Block					
Fig Tree Group: Mapepe Formation: No dates available in Songimvelo Block					
Fig Tree-Age Felsic Hypabyssal Intrusions:					
Hypabyssal felsic porphyry in Kromberg Fm.		3,241±6	c	Age of emplacement/crystallization	7
Moodies Group: No dates available					
Post-Moodies Plutonic Suites					
Dalmein Pluton (post-kinematic pluton)	quartz monzonite	3,216 +2/-1	a	Age of emplacement/crystallization: Minimum age of deformation; minimum age of Moodies Group in Southern Domain	9
Boesmankop plu.	syenite	3,107±2	a	Age of emplacement/crystallization	9
Mpuluzi batholith	granodiorite	3,107 +4/-2	a	Age of emplacement/crystallization	9
Felsic dike in Komati Formation		3,457±3	a	[*Xenocrysts from 3,445-Ma mag. event*]	9
		3,080±3	a	Age of emplacement/crystallization	9
UMUDUHA BLOCK					
Onverwacht Group: Mendon Formation (M)					
M2c or M3c	felsic tuff	3,298±3	c	Age of volcanism	8
	same	3,310±2		Xenocryst	8
Mendon Fm.	komatiites	3,317±326	e	Age of volcanism	17
Fig Tree Group: Mapepe Formation (MF)					
MF, upper, post-D_2	dacitic tuff	3,484±4	c	Xenocrysts from 3,445-Ma magmatic	7
		3,476±3	c	suite	
	same	3,227±4	c	Age of volcanism; [*upper limit on D_2*]	7
MF, basal, north	dacitic tuff	3,243±4	c	Age of basal Mapepe Fm. [*in northern part of Umuduha Block*]	7
MF, basal, south	dacitic tuff	3,258±3	c	Age of basal Mapepe Fm. in southern Umuduha Block	8
Fig Tree Group: Auber Villiers Formation (AVF)					
AVF	dacitic breccia	3,522±4	c	Xenocryst	7
	same	3,459±3 to	c	Xenocrysts [*3,445 Ma and early Kromberg*	
		3,413±8	c	*magmatic events*]	7
	same	3,323±4	c	Xenocrysts [*Mendon-age felsic magmatism*]	7
	same	3,256±4	c	Age of volcanism in AVF	7
	tuffaceous sandstone	3,253±3	c	Age of volcanism	8
	same	3,310±3	c	Xenocryst [*Mendon-age felsic magmatism*]	8
Fig Tree Group-Age Felsic Hypabyssal Intrusions					
Feldspar-quartz porphyry		3,229 +4/-3	a	Age of emplacement	9
Feldspar-quartz porphyries		circa 3,230	a	Age of emplacement/crystallization: minimum age of Mapepe Formation	15
Moodies Group: No dates available					
Post-Moodies Intrusions:					
Hypabyssal felsic dike into into lower Moodies Gr.		3,207±2	c	Age of emplacement/crystallization; minimum age of basal Moodies Gr.	14
KAAP VALLEY BLOCK					
OG: Weltevreden Formation (WF):					
WF	komatiites	3,286±29	e	Age of volcanism	18
FTG: Ulundi Formation: No dates available					
FTG: Sheba Formation: No dates available					

TABLE 1. U-PB AND PB-PB ZIRCON AGES FOR ROCKS OF THE BARBERTON GREENSTONE BELT AND VICINITY (CONTINUED, p. 3)

KAAP VALLEY BLOCK (cont.)					
FTG: Belvue Road Formation: No dates available					
FTG: Schoongezicht Formation (SF):					
SF (?)	felsic tuff	3,259±5	c	Age of volcanism [*Although north of Inyoka Fault, this sample is from NE part of BGB*]	
(All samples below from rocks mapped as Schoongezicht Formation in Stolzburg Syncline)					
SF	clasts in fresh, dacitic congl.	3,225±3	c	Age of volcanism	7
SF	cross-bedded ash	3,226±1	a	Age of volcanism	9
SF	felsic porphyry intrusion in SF	3,222 +10/-4	a	Age of emplacement; minimum age of Schoongezicht volcanism	9
SF	felsic volcanics-volcaniclastics	3,526±8	a	Xenocrysts [*May be detrital grains*]	6
		3,164±12	a	Age of volcanism; maximum age of Moodies Group in Stolzburg Syncline	6
Fig Tree Group-Age, 3,227-Ma Plutonic Suite					
Kaap Valley pluton					
marginal phase	tonalite	3,227±1	a	Age of emplacement/crystallization	9
marginal phase	tonalite	3,226±5	c	Age of emplacement/crystallization	4
marginal phase	tonalite	3,229±5	a	Age of emplacement/crystallization	1
Kaap Valley pluton					
interior phase	tonalite	3,228 +2/-1	a	Age of emplacement/crystallization	9
interior phase	tonalite	3,226±14	b	Age of emplacement/crystallization	6
interior phase	tonalite	3,223±4	c	Age of emplacement/crystallization	4
Moodies Group (MG):					
MG	granitic gneiss boulder	3,531±4	b	Age of crystallization of source rock	2
MG	granite boulder	3,518±11	b	Age of crystallization of source rock	2
MG	granite pebble	3,474 +35/-31	a	Age of crystallization of source rock *[3,445-Ma magmatic suite]*	1
MG	granite pebble	3,234±1 to 3,339±2	a	Minimum age range for crystallization of source rock	1
MG	granite pebble	3,306 +65/-57	a	Age of crystallization of source rock	1
MG	granite pebble	3,224±6	a	Youngest near-concordant age of clasts in Moodies Group: age of crystallization of source rock: maximum age of Moodies Group	1
Late Intrusive Rocks:					
Felds.-Qtz. Porphyry		3,216±21	a	Maximum age of crystallization; max. age of gold mineralization	15
Salisbury Kop pluton	undeformed granodiorite	3,109 +10/-8	a	Age of emplacement/crystallization: Minimum age of Moodies Group	9
Salisbury Kop pluton	undeformed granodiorite	3,079±6	c	Age of emplacement/crystallization: Minimum age of Moodies Group	13
Stentor pluton	granodiorite	3,107±5	a	Age of emplacement/crystallization	9
Nelspruit bath.	gneissic tonalite xenolith	3,304±6	a	Xenolith: Age of crystallization of source rock	9
	porphyritic phase	3,106 +3/-4	a	Age of emplacement/crystallization	9
Hebron pluton	granodiorite	3,104 +3/-2	a	Age of emplacement/crystallization	9

* Methods of analysis: (a) conventional U-Pb isotope dilution; (b) U-Pb high-resolution ion microprobe; (c) Pb-Pb evaportaion; (d) $^{40}Ar/^{39}Ar$ step-wise heating; (e) Sm-Nd or Nd isotope.

† Notes in italics by present author.

§ References: (1) Tegtmeyer and Kröner, 1987; (2) Kröner and Compston, 1988; (3) Kröner and Todt, 1988; (4) Layer et al., 1992; (5) Kröner et al., 1989; (6) Armstrong et al., 1990; (7) Kröner et al., 1991a; (8) Byerly et al., 1993, 1996; (9) Kamo and Davis, 1991, 1994; (10) Kröner and Tegtmeyer, 1994; (11) Kröner et al., 1992, 1996; (12) López-Martínez et al., 1992; (13) Heubeck et al., 1993; (14) Heubeck and Lowe, 1994a; (15) de Ronde et al., 1991; (16) Compston and Kröner, 1988; (17) Chauvel et al., 1987; (18) Lahaye et al., 1995.

Kaapvaal Craton in the vicinity of the Barberton Greenstone Belt is based, therefore, on a plate-tectonic geodynamic system.

EVOLUTION OF THE ANCIENT GNEISS COMPLEX BLOCK

The Ancient Gneiss Complex (AGC) borders the BGB to the east and southeast, although the contact has been obscured in most areas by the circa 3.1-Ga Mpuluzi batholith (Fig. 1). Locally, in northern Swaziland, the contact is a fault (Fig. 1). The AGC has been widely regarded as a possible basement to the BGB (e.g., Hunter, 1974; Kröner and Todt, 1988) or as a pre-BGB basement block that rifted to create the basin in which the BGB supracrustal sequence was deposited (Condie and Hunter, 1976). It was examined only briefly during the present study.

Regionally, the AGC includes four main rock suites: the Ngwane Gneiss, the Dwalile Supracrustal Suite, the Tsawela Gneiss, and the Usutu Suite (Hunter, 1991; Kröner et al., 1991b; Kröner and Tegtmeyer, 1994). The Ngwane Gneiss (NG), also called the Bimodal Suite, crops out widely in Swaziland and is composed of tonalitic and trondhjemitic orthogneiss containing interlayered amphibolite. It is clearly polygenetic and contains zircons ranging in age from 3,644 ± 4 Ma to 2.7 Ga (Compston and Kröner, 1988; Kröner et al., 1989, 1991b). The high degree of metamorphism of the NG coupled with pre-3.6-Ga ages provide the rationale for suggesting that the AGC may include part of a pre-BGB basement. However, the pre-3.6-Ga ages are not representative of widespread rock units but come from a banded gneiss from a roadside outcrop in northeastern Swaziland (Compston and Kröner, 1988; Kröner et al., 1989). This same outcrop also yields whole zircons and overgrowths with ages of about 3,580, 3,500, 3,430, 3,200, 2,990, and 2,870 Ma (Kröner et al., 1989). The presence of pre-3.6-Ga zircons in gneisses containing hornblende- and biotite-rich amphibolitic bands suggests that they may in part represent greenstone enclaves within a younger plutonic terrane. They bear little on the question of a pre-BGB basement but do indicate the existence of rocks and/or zircons older than any yet recovered from supracrustal rocks in the BGB. The age span of the NG overlaps that of the entire AGC and that of the entire BGB and the adjacent plutonic suites.

The Dwalile Suite comprises metagreenstone and metasedimentary rocks, including "quartzites" that have yielded detrital zircons between 3,423 ± 30 and 3,566 ± 33 Ma (Kröner et al., 1991b; Kröner and Tegtmeyer, 1994). These "quartzites" are extremely dirty metasedimentary units and probably represent immature clastic rocks, such as graywackes or siliceous volcaniclastic rocks. The geochemistry of the Dwalile mafic and komatiitic volcanic rocks closely resembles that of volcanic units in the Onverwacht Group in the BGB (Kröner et al., 1991b; Kröner and Tegtmeyer, 1994) and their geochronological similarity suggests a general correlation of these major sequences (Jackson et al., 1987; Kröner and Tegtmeyer, 1994). Detrital zircons in the Dwalile Suite analyzed to date are no younger than 3,423 ± 30 Ma (Kröner and Tegtmeyer, 1994) and tonalitic gneisses of the Tsawela Gneiss, intrusive into the Dwalile Suite, yield youngest ages of 3,436 ± 5 Ma. The Dwalile volcaniclastic units and associated Tsawela tonalitic gneisses are probably correlative with and perhaps genetically related to the 3,445-Ma magmatic units in and around the BGB (Kröner and Tegtmeyer, 1994), including member H6 of the Hooggenoeg Formation (Lowe and Byerly, this volume, Chapter 1).

The Tsawela Gneiss is a coarse-grained, well-foliated hornblende-biotite tonalite. Single-grain zircon ages indicate emplacement from 3,490 ± 3 to 3,436 ± 5 Ma (Kröner and Tegtmeyer, 1994). However, a second area of gneiss yields an age of 3.36 Ga, suggesting that more than one intrusive episode may be represented (Kröner et al., 1991b). The Usutu Granodiorite is a heterogeneous intrusive suite ranging from hornblende gabbro to trondhjemite. It is relatively undeformed and yields zircon ages from 3,306 ± 4 to 3,220 ± 8 Ma (Kröner et al., 1991b).

The lithological, petrological, and geochronological evolution of the AGC corresponds closely to that of the BGB and surrounding plutonic units. The main difference lies in the higher metamorphic grade of many AGC rocks. The AGC appears to have evolved as a separate block that has been juxtaposed structurally against blocks to the west, probably during Fig Tree and post-Moodies deformation between 3.26 and 3.20 Ga.

EVOLUTION OF THE STEYNSDORP BLOCK

Exposed parts of the Steynsdorp Block include the 3,509+8/–7 Ma TTG Steynsdorp pluton (Kamo and Davis, 1991, 1994) and surrounding rocks of the Theespruit Formation in the Steynsdorp anticline (Fig. 1). Parts of the Steynsdorp Block volcanic succession are also exposed in the Onverwacht anticline south and west of the Komati fault, based on age dates on felsic volcanic rocks of the Theespruit Formation in this area of 3,531 ± 10 Ma (Armstrong et al., 1990) and 3,511 ± 3 Ma (Kröner et al., 1992). TTG blocks with crystallization ages of 3,538 ± 6 Ma (Armstrong et al., 1990) and 3,538 +4/–2 Ma (Kamo and Davis, 1991, 1994) have additionally been brought up along faults south of the Komati fault, suggesting that Steynsdorp-age plutonic equivalents are present at depth. This area has not been distinguished as a separate exposure of the Steynsdorp Block (Fig. 1) because it apparently contains substantially younger units, including felsic volcanic rocks dated 3,453 ± 6 Ma (Armstrong et al., 1990) and possible equivalents of the Msauli Chert of the Mendon Formation (de Wit et al., 1983).

Outcrops of the Theespruit Formation in both the Steynsdorp and Onverwacht anticlines were examined but not studied in detail during the present investigation. Relationships between the Steynsdorp pluton and surrounding greenstone units in the Steynsdorp anticline are dominated by late shearing. The Onverwacht Group in the Steynsdorp anticline includes recognizable lithologic and stratigraphic equivalents of the post-3.5-Ga Hooggenoeg and Komati Formations in the Songimvelo Block (Viljoen, M. J., and Viljoen, 1969). Below heavily sheared and altered ultramafic rocks of the Komati Formation in the Steynsdorp Block is a thick sequence of mafic and felsic schists, representing altered mafic and felsic volcanic rocks, respectively, and thin interlayered metaquartzites, representing metamorphosed cherts. These metamorphic units were assigned to the Theespruit Formation by Viljoen, M. J., and Viljoen (1969). Felsic volcanic units in the Theespruit Formation in the Steynsdorp anticline have been dated at 3,547 ± 3 Ma (Kröner et al., 1992). The Steynsdorp pluton also contains zircon xenocrysts as old as 3,553 ± 4 Ma (Kröner et al., 1992). Formation of the Steynsdorp Block was probably initiated prior to 3,553 Ma by komatiitic and mafic volcanism. This mafic volcanic sequence was intruded by TTG magmas and probably concurrently mantled by felsic

volcanic units of the Theespruit Formation between at least 3,547 ± 3 and 3,509 +8/–7 Ma (Fig. 5A).

Metamorphism and strain have obscured the original relationships between the Theespruit Formation and the overlying Komati Formation in the Steynsdorp anticline. It is possible that the Theespruit Formation was covered more-or-less conformably by younger ultramafic volcanic flows of the Komati Formation during the initial stage of formation of the Songimvelo volcanic suite (Fig. 5B). However, it is also possible that either an unconformity or structural break

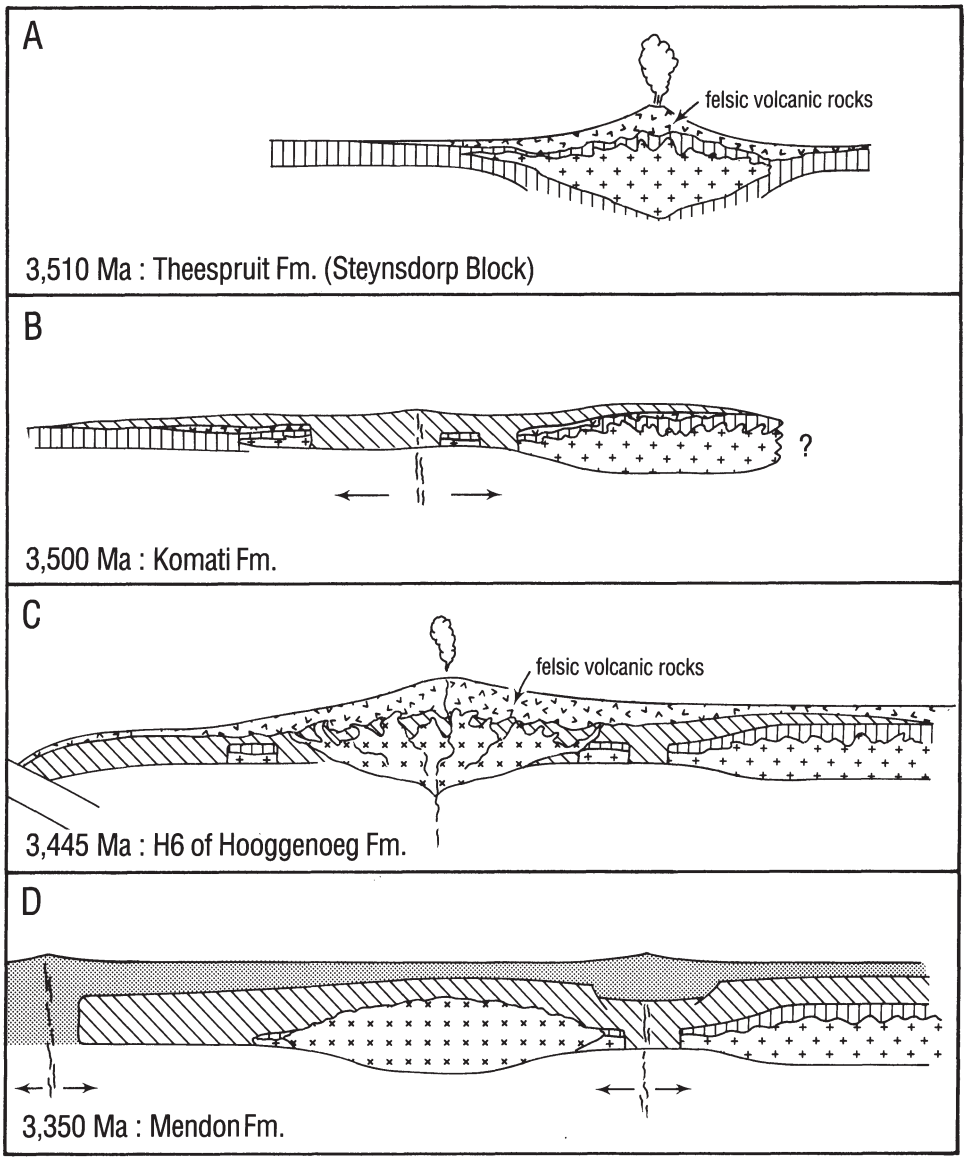


Figure 5. Geologic evolution of the Steynsdorp (A) and the Songimvelo Blocks (B–D) in the southern part of the Barberton Greenstone Belt. Patterns as in Figure 3. A, Subduction-related felsic volcanism and intrusion of the Steynsdorp pluton into an older to coeval mafic volcanic sequence forms a thickened, relatively buoyant block of differentiated crust, the Steynsdorp Block. B, Rifting of the Steynsdorp Block is accompanied by komatiitic volcanism during the early stages of deposition of the Komati Formation, oldest unit on the Songimvelo Block. Metamorphosed portions of the older Steynsdorp Block widely underlie mafic volcanic rocks of the Komati Formation. C, Felsic magmatism represented by member H6 of the Hooggenoeg Formation and the 3,445-Ma TTG suite occurred along a magmatic arc developed at a convergent plate boundary during late-stage evolution of the Songimvelo Block. D, The older Songimvelo volcanic sequence (Komati through Kromberg Formations, shown in cross hatching) were buried beneath komatiites of the Mendon Formation during rifting along the northwestern margin of the Songimvelo Block. Volcanic rocks of the Mendon Formation comprise the oldest rocks of the Umuduha Block.

lies at the base of the Komati Formation in the Steynsdorp Block.

The northern extent of the pre-3.5-Ga intrusive and extrusive Steynsdorp suite beneath the younger Komati and post-Komati Formation Songimvelo sequence is unknown, although similar-aged intrusive units are recorded from the AGC in northeastern Swaziland (Kröner et al., 1991b). To the west, the pre-3.5-Ga Steynsdorp suite is largely covered by post-3.5-Ga rocks of the Songimvelo Block.

EVOLUTION OF THE SONGIMVELO BLOCK

Lowe et al. (this volume, Chapter 2) divide the BGB into four domains characterized by contrasting stratigraphic and structural histories (Fig. 3, inset): (1) the Southern Domain (SD), (2) the West-Central Domain (WCD), (3) the East-Central Domain (ECD), and (4) the Northern Domain (ND). The SD, WCD, and ND represent the greenstone portions of the Songimvelo, Umuduha, and Kaap Valley Blocks, respectively. The ECD is dominated by outcrops of relatively young Fig Tree and Moodies rocks and may include portions of the Umuduha, Songimvelo, and Steynsdorp Blocks (Fig. 1).

The Songimvelo Block includes a large area within and south of the BGB (Fig. 1). It is made up of the Moodies, Fig Tree, and Onverwacht Groups south of the Granville Grove fault and west and possibly east of the Kromberg fault and includes the Badplaas, Stolzburg, Theespruit, Doornhoek, and smaller plutons (Fig. 1) intruded from about 3,460 +5/–4 to 3,437 ± 6 Ma (Armstrong et al., 1990; Kröner et al., 1991a; Kamo and Davis, 1994). These intrusive rocks and their associated felsic volcanic units are here referred to as the 3,445-Ma magmatic suite. The northeastern extent of the 3,445-Ma TTG intrusive suite and the 3,500- to 3,445-Ma komatiitic and mafic volcanic suite beneath younger volcanic and sedimentary units is uncertain. To the south, TTG and metagreenstone rocks of the Songimvelo Block are covered by the sill-like Mpuluzi batholith dated at 3,107 +4/–2 Ma (Kamo and Davis, 1994).

The evolution of the Songimvelo Block included (I) an early volcanic period, and (II) a late orogenic period. These periods can be divided into nine evolutionary stages. Initial growth of the block during the volcanic period included: (Ia) a early ultramafic to mafic volcanic stage (Komati Formation and Hooggenoeg Formation members H1–H5) from about 3,480 to 3,460 Ma, and (Ib) a felsic volcanic and intrusive stage (Hooggenoeg Formation member H6) at about 3,460–3,435 Ma. (Ic) A late mafic volcanic stage, represented by rocks of the Kromberg Formation, extended from about 3,416 ± 5 to 3,334 ± 3 Ma (Byerly et al., 1993, 1996). (Id) Initial ultramafic volcanism to form the Umuduha Block overlapped onto the Songimvelo Block with deposition of peridotitic and basaltic komatiites of the Mendon Formation from about 3,334 ± 3 Ma to about 3,260 Ma. (IIa) The orogenic period involved initial deformation (D_{2a}) and felsic volcanism along the northwestern margin of the Songimvelo Block from 3,260 to 3,230 Ma, reflected in early clastic foreland sedimentary deposits of the Mapepe and Auber Villiers Formations of the Fig Tree Group. (IIb) This deformation culminated in intense folding and faulting, D_{2b}, in post-Mapepe, pre-Moodies time. (IIc) Deformation was followed by deposition of fine-grained felsic volcaniclastic debris of the Schoongezicht Formation derived from volcanoes located on the Kaap Valley Block at about 3,225 Ma. The final events in the evolution of the Songimvelo Block included a late basinal stage represented by clastic rocks of the Moodies Group (IId), probably about 3,220 Ma, and (IIe) late to post-Moodies stages of deformation, $D_{4–5}$.

Early volcanic period

Early ultramafic and mafic volcanic stage. The stratigraphically intact section of the Onverwacht Group in the Songimvelo Block totals 8–10 km thick (Lowe and Byerly, this volume, Chapter 1) but is truncated by the Komati fault at its base. Age data suggest that exposed rocks of the Komati Formation are less than 3.5 Ga (Armstrong et al., 1990; Kröner et al., 1991a; Kamo and Davis, 1991, 1994; López-Martínez et al., 1984, 1992). More highly metamorphosed, tectonically disarticulated, and intruded rocks of the Theespruit and Sandspruit Formations south of the fault in the Onverwacht anticline are at least partially age equivalent to the intact sequence north and east of the fault (de Wit et al., 1983; Armstrong et al., 1990) but also include felsic volcanic units older than 3.5 Ga (Kröner et al., 1992; Armstrong et al., 1990). Onverwacht units south of the Komati fault were intruded and metamorphosed during emplacement of the 3,445-Ma TTG intrusive suite. Rocks north of the Komati fault represent parts of the ultramafic and mafic volcanic sequence that lay farther from the TTG intrusive centers, and, hence, escaped large-scale intrusion and metamorphism during the 3,445-Ma event.

No depositional base to the Onverwacht Group has been identified in the Songimvelo Block, and it may not exist over large areas. The presence of older Steynsdorp-age rocks in the Onverwacht anticline and of the Komati and Hooggenoeg Formations overlying rocks of the Theespruit Formation in the Steynsdorp anticline indicate that, over large areas, the post-3.5-Ga Songimvelo volcanic sequence was deposited on top of the pre-3.5-Ga Steynsdorp Block.

Vertical to subvertical volcanic and sedimentary rocks of the Komati and Hooggenoeg Formations crop out in a series of large, vertically plunging folds along the southern margin of the BGB, including the Onverwacht anticline and Kromberg syncline (Fig. 1). Sedimentological studies (Lowe and Knauth, 1977; Lowe, 1980, 1982; Lanier and Lowe, 1982; Lowe, this volume, Chapters 3 and 9) have shown that during their accumulation these mafic and ultramafic flows formed a broad, low-relief volcanic surface (Fig. 5B, C). Volcanism was locally, and probably regionally, episodic. Periods of rapid effusion produced thick flow sequences lacking or containing very few interflow sedimentary layers and weathering zones, such as the Komati Formation. Where volcanism was less continuous, periods of volcanic quiescence were marked by the deposition of

fine pyroclastic, biogenic, and orthochemical sediments, represented by thin cherty sedimentary units, such as the Middle Marker (H1), and the development of weathering and alteration zones on exposed flow surfaces.

During ultramafic and mafic volcanism, there was a close relationship among magma composition, eruption style, and sedimentation patterns (Lowe, this volume, Chapter 3). Komatiitic lavas were erupted rapidly, forming low-relief volcanic surfaces that commonly aggraded into shallow-water or even subaerial settings. Individual komatiitic eruptive cycles were usually closed by explosive phreatomagmatic volcanism that formed thin komatiitic ash beds capping the flow sequences (Lowe, this volume, Chapter 3). Postvolcanism subsidence submerged the volcanic surfaces and thin, regional sheets of carbonaceous and orthochemical sediments accumulated, mainly under shallow-water conditions. Early, low-temperature sea-floor and hydrothermal alteration resulted in widespread silicification of the tops of the komatiite flow sequences (Lowe and Byerly, 1986; Duchac and Hanor, 1987; Hanor and Duchac, 1990).

During basaltic eruptions, subsidence largely kept pace with or exceeded the rate of volcanic aggradation, and major basaltic sequences were deposited in predominantly subaqueous settings. Pillows are abundant. Thin interflow sedimentary layers are more common than in komatiitic sequences and show evidence of deposition under quiet, relatively deeper-water conditions (Lowe, this volume, Chapter 3). Little explosive pyroclastic activity accompanied volcanism.

Onverwacht volcanism was markedly bimodal, with an abundance of komatiitic (including peridotitic and basaltic varieties) and tholeiitic volcanic rocks and local development of thick dacitic to rhyolitic sequences. Andesites are sparse to absent in the Songimvelo Block and in the Swaziland Supergroup as a whole. Although previous workers have emphasized the existence of mafic to felsic volcanic cycles in the Onverwacht Group, especially within the Hooggenoeg Formation (Viljoen, R. P., and Viljoen, 1969; Anhaeusser, 1973), detailed petrologic and geochemical studies indicate that the "felsic" cycle tops are actually the metasomatically altered and silicified tops of basaltic and komatiitic volcanic units (Byerly et al., 1983; Smith et al., 1984; Duchac and Hanor, 1987; Hanor and Duchac, 1990). No evidence of small-scale volcanic cyclicity was found during the present study.

Sedimentation during accumulation of the Onverwacht Group was dominated by pyroclastic, biological, and orthochemical processes. Little sediment was derived by erosion of the volcanic sequence itself or of older rocks. Shales are virtually absent, suggesting that, locally and regionally, little rock was exposed to chemical weathering. Clastic units in the Onverwacht Group were originally made up largely of fresh pyroclastic and locally derived volcaniclastic materials. Relief, where present, developed through either volcanism or magmatically controlled subsidence and uplift (Lowe and Knauth, 1977; Lowe, 1980, 1982).

The boundaries of this early Onverwacht volcanic sequence have been obliterated by later tectonism. Evidence of long-lived shallow-to-deep-water facies transitions occur along both the west and east limbs of the Onverwacht anticline. Along the west limb, volcanic units in the Komati and Hooggenoeg Formations, north of the Komati fault, thin progressively from east to west (Viljoen, M. J., and Viljoen, 1969; Viljoen, R. P., and Viljoen, 1969). This thinning has been attributed to both primary depositional thinning (Viljoen, M. J., and Viljoen, 1969; Viljoen, R. P., and Viljoen, 1969) and tectonic attenuation of the western parts of the sequence (Williams and Furnell, 1979). However, facies changes in Hooggenoeg and Kromberg sedimentary units along the west limb indicate that western sections were deposited at greater water depths and in more distal settings relative to volcanic centers than those farther east: (1) The Middle Marker thins and loses coarse, current-deposited volcaniclastic units and shallow-water facies to the west (Lanier and Lowe, 1982). (2) Coarse proximal breccias of H6, more than 1,500 m thick adjacent to the intrusive complex on the central part of the west limb (Lowe et al., this volume, Chapter 2), thin and fine to less than 100 m of massive, fine-grained, silicified ash in westernmost exposures. (3) Cherts at the base of the Kromberg Formation lose shallow-water evaporite layers to the west and are composed mainly of fine-grained, subaqueously deposited black carbonaceous chert along the western half of the west limb (Lowe and Fisher Worrell, this volume, Chapter 7). (4) The thickest sections of the Buck Reef Chert (K1) occur in the hinge zone and along the eastern part of the west limb of the Onverwacht anticline. The unit thins progressively to the west and is probably less than 100 m thick in its westernmost outcrops. (5) A unit of highly carbonaceous, laminated, tuffaceous shale, K2v-a of Ransom et al. (this volume, Chapter 6), deposited under quiet-water conditions, appears at the base of the middle member of the Kromberg Formation (K2v) in the central part of the west limb and thickens progressively to the west (Ransom, 1987). Collectively, these features suggest that sections of the Komati, Hooggenoeg, and Kromberg Formations along the eastern and central parts west limb of the Onverwacht anticline accumulated under mainly shallow-water conditions whereas more western sections were deposited in deeper and quieter water, and point to a long-lived on- to off-platform transition in this area.

There is also evidence for deeper water conditions along the southern part of the east limb of the Onverwacht anticline: (1) Volcaniclastic units in H6 thin and fine and pass from alluvial and fan-delta into turbiditic units from north to south along the east limb. (2) Paleoflow directions of slope-controlled turbidity currents in H6 suggest general north-to-south transport. (3) Evaporites at the base of the Buck Reef Chert are absent along the east limb of the Onverwacht anticline. (4) The Buck Reef Chert consists largely of black-and-white banded chert along the central part of the west limb of the Onverwacht anticline, but thins to the south on the east limb and includes an increasing amount of banded ferruginous chert, reflecting deeper, quieter water conditions (Lowe, this volume, Chapter 3), and interbedded mafic volcanic rock.

These facies patterns suggest that the Onverwacht volcanic sequence represented by the Komati, Hooggenoeg, and Kromberg Formations was characterized by a long-lived, high-

standing, predominantly shallow-water central area that passed to the west and southeast into more fully subaqueous, deeper water settings.

Felsic volcanic and TTG intrusive stage. Felsic volcanism and shallow intrusion, represented by H6 at the top of the Hooggenoeg Formation (Fig. 5C), was directly related to deeper level TTG plutonism (de Wit et al., 1987a, b; de Ronde et al., 1991). Deformation associated with 3,445-Ma volcanism and intrusion has been termed D_1 by Lowe et al. (this volume, Chapter 2). Sections of H6 around the Onverwacht anticline and Kromberg syncline record the presence of extrusive and local high-level intrusive units that served as sources of voluminous volcaniclastic debris for large, coarse flanking sedimentary aprons. The surrounding deposits grade from proximal alluvial and fan-delta units into distal subaqueous debris-flow deposits and turbidites. The principal volcanic vents probably lay above present-day TTG units south of present outcrops of H6 on the west limb of the Onverwacht anticline.

Following volcanism, the high-standing felsic volcanoes were eroded and capped by a sequence of coarse, alluvial to shallow-water, felsic volcaniclastic sandstone and conglomerate. This sequence is well developed on the west limb of the Onverwacht anticline. Off the high-standing central part of the edifice, eroded felsic debris accumulated as a series of coarse rubbly debris-flow deposits grading upward into thick, sandy, high-density turbidity-current deposits capped by a thin unit of low-density turbidity-current units. These have been described and illustrated by Viljoen, R. P., and Viljoen (1969) and Lowe and Knauth (1977) from outcrops of H6 along the Komati River on the east limb of the anticline.

Late ultramafic and mafic stage: Kromberg Formation. Following erosion and subsidence of the felsic complex, the higher standing remnants were covered by shallow-marine waters. A local evaporitic unit at the base of the formation on the west limb of the Onverwacht anticline (Lowe and Fisher Worrell, this volume, Chapter 7) is succeeded by from 200 to 400 m of black-and-white banded and ferruginous cherts of the Buck Reef Chert. On the east limb of the Onverwacht anticline, this thick chert succession is represented by three thin, 10- to 30-m-thick units of banded chert separated by basalt. Evidently the higher standing parts of the older felsic eruptive center accumulated fine biogenic and orthochemical sediments during early Kromberg time whereas surrounding, lower areas were commonly inundated by coeval basalt flows. Middle Kromberg volcanism (K2v) is represented by more than 1,000 m of mafic lapillistone on the west limb of the Onverwacht anticline, where its eruption was associated with removal of as much as 300 m of the underlying Buck Reef Chert (Ransom et al., this volume, Chapter 6; Lowe and Byerly, this volume, Chapter 1). The corresponding interval on the east limb is represented by a complexly interbedded sequence of tholeiitic basalts, basaltic komatiite, and mafic lapillistone units. The upper third of the formation (K3v) in both areas is a thick succession of basaltic flows, pillow breccias, and minor lapillistones and tuffs. Basaltic and komatiitic volcanic rocks in the Kromberg Formation have been studied by Viljoen, R. P., and Viljoen (1969) and Vennemann and Smith (this volume, Chapter 5).

The Kromberg Formation represents a late, ultramafic and mafic volcanic sequence erupted over the Songimvelo Block. The significance and setting of Kromberg volcanism are unclear. Kromberg volcanic units may represent the distal part of a volcanic sequence erupted from a volcanic center located off of the Songimvelo Block. However, there is evidence for an eruptive center located on the west limb of the Onverwacht anticline during deposition of the middle Kromberg mafic lapillistone unit (K2) (Ransom et al., this volume, Chapter 6; Lowe and Byerly, this volume, Chapter 1). The presence of thick, varied Kromberg basalt units in the southernmost East-Central Domain and on the east limb of the Onverwacht anticline also suggests the existence of one or more additional volcanic centers in these areas. Because Kromberg volcanism and sedimentation have yet to be investigated in detail, it is impossible at present to constrain the setting of volcanism. I would suggest that it was related to extension within and around the Songimvelo Block.

The Footbridge Chert at the top of the Kromberg Formation is a regional unit representing quiet, subaqueous sedimentation of fine-grained biogenic, orthochemical, and tuffaceous sediments. It marks a regional cessation of volcanic activity and probably represents a condensed section deposited over a considerable interval of time characterized by volcanic quiescence and slow sedimentation. The age of the Kromberg Formation is constrained by zircon ages of 3,416 ± 5 Ma on a thin felsic tuff near its base (Kröner et al., 1991a, Table 2, sample MW-64; Byerly et al., 1993, 1996) and 3,334 ± 3 Ma on a tuff in the Footbridge Chert (Byerly et al., 1993, 1996).

Late ultramafic overlap stage: Mendon Formation. Mafic volcanism in the Songimvelo Block ended with eruption of a second major succession of komatiitic lavas (Figs. 5D and 6A), named the Mendon Formation by Lowe and Byerly (this volume, Chapter 1). In the Songimvelo Block itself, the Mendon Formation is represented by a single unit, 100–300 m thick, of altered peridotitic and basaltic komatiitic volcanic rocks capped by the Msauli Chert, which is overlain by the Fig Tree Group. This komatiitic sequence marks the initiation of volcanism associated with formation of the Umuduha Block. Age constraints on this stage of volcanism are provided by a 3,334 ± 3-Ma age on a thin tuff in cherts at the top of the Kromberg Formation, an age of 3,298 ± 3 Ma on a thin felsic tuff in higher parts of the Mendon Formation on the Umuduha Block, and an oldest age of 3,259 ± 5 Ma on rocks of the Fig Tree Group (Kröner et al., 1991a; Byerly et al., 1996).

The close of Onverwacht volcanism in the Songimvelo Block was marked regionally by volcanic quiescence and the deposition of extremely fine-grained, organic-rich, tuffaceous and argillaceous oozes, now represented by black and banded cherts at the top of the Mendon Formation. These cherts also

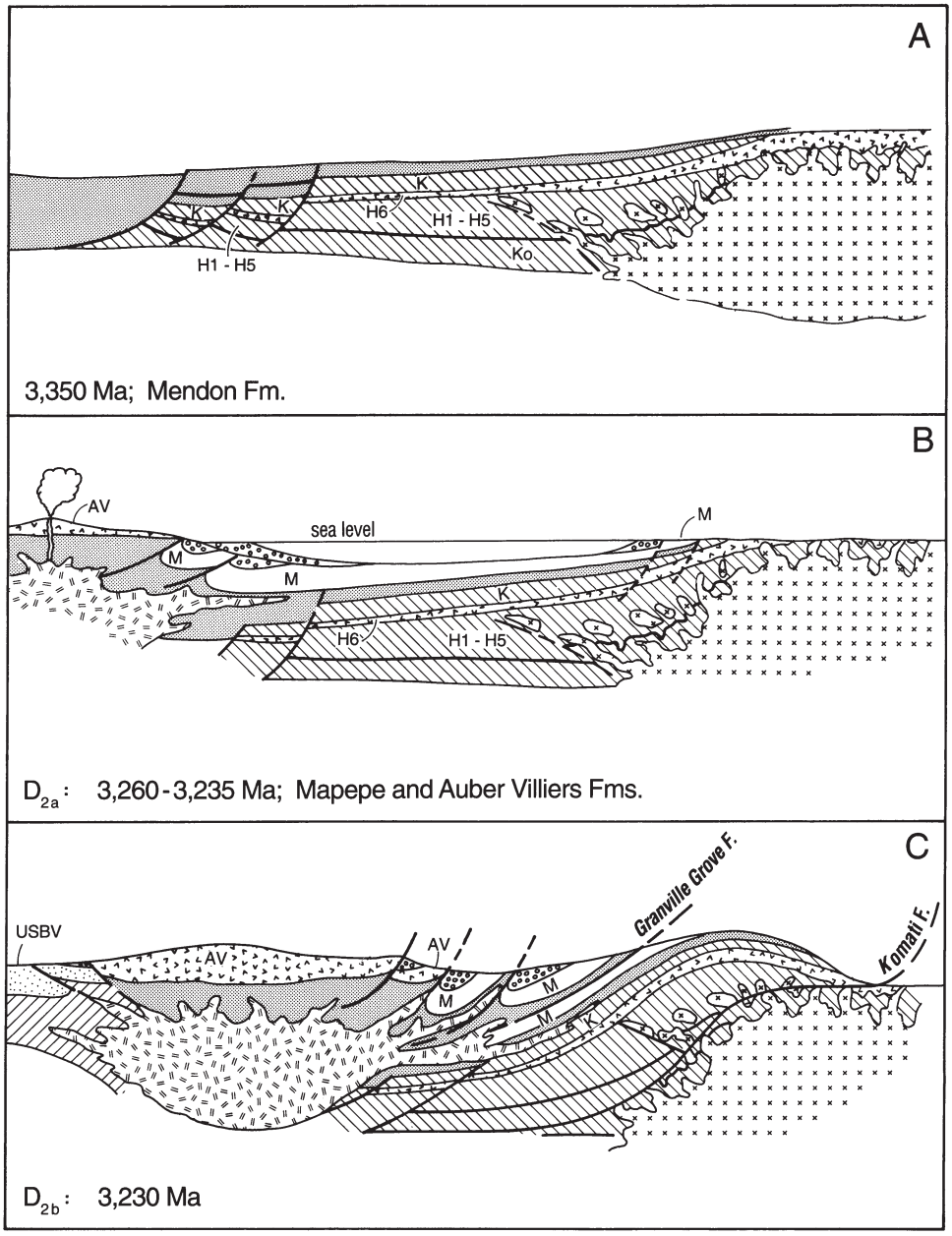


Figure 6. Geologic evolution of the northwestern edge of the Songimvelo Block and southeastern margin of the Umuduha Block during late Onverwacht and early Fig Tree time. Patterns as in Figure 3. A, Deposition of the Mendon Formation as a rift sequence along the northwestern margin of the Songimvelo Block. The earliest stage of Mendon volcanism, represented by member M1 of Lowe and Byerly (this volume, Chapter 1), covered much of the Songimvelo Block. B, Deposition of the Mapepe (M) and Auber Villiers (AV) Formations as proximal and distal units within a back-arc foreland basin. C, Collapse of the foreland basin in late Fig Tree time involved tectonic stacking of the foreland basin sequence and thrusting of the succession onto the central part of the Songimvelo Block along the Komati fault.

appear to represent a condensed section marking a prolonged interval of quiet, probably largely deep-water sedimentation. On the Songimvelo Block, these cherts are 30–80 m thick and separate the Msauli Chert from overlying rocks of the Fig Tree Group.

Orogenic period

Early foreland stage (Mapepe Formation). The orogenic period in the Songimvelo Block began with deposition of Fig Tree clastic and volcaniclastic units at about 3,260 Ma. The lowest

10–150 m of Fig Tree strata in the Songimvelo Block are fine-grained carbonaceous shale, jaspillite, and iron formation on the west limb of the Onverwacht anticline. These strata were deposited under deep, quiet-water conditions (Beukes, 1973; Heinrichs, 1980; Lowe and Byerly, this volume, Chapter 1; Lowe and Nocita, this volume, Chapter 10). Similar lower Fig Tree strata are widely developed in the southern and eastern parts of the BGB (Heinrichs, 1980; Lowe and Nocita, this volume, Chapter 10). They represent an early Fig Tree basin that developed largely in areas underlain by the 3,445-Ma Songimvelo and/or Steynsdorp basements.

Subsequent Fig Tree sediments on and adjacent to the Songimvelo Block relate to concurrent D_{2a} uplift and felsic pyroclastic volcanism. The southern iron-formation basin shoaled and became the site of mixed terrigenous and volcaniclastic sedimentation, probably as part of a foreland basin (Jackson et al., 1987; Nocita, 1989; Nocita and Lowe, 1990; Lowe and Nocita, this volume, Chapter 10). Middle and upper Mapepe facies in the East-Central Domain show a southeast-to-northwest decrease in the number, thickness, and grain size of chert-clast conglomerate and lithic sandstone units, suggesting that clastic detritus was sourced in uplifts of greenstone rocks to the southeast. On the west limb of the Onverwacht anticline, middle and upper Mapepe strata along the northern edge of the Southern Domain contain thin units of chert-grit sandstone and chert-clast conglomerate derived from local uplifts to the south. Faults associated with these uplifts may have developed as normal faults along the southern, exterior side of the foreland basin represented by Mapepe and Auber Villiers strata in the West-Central Domain (Lowe and Nocita, this volume, Chapter 10).

Early Orogenic stage (D_2). In the hinge of the Onverwacht anticline, deformed Mapepe strata are overlain with angular unconformity by rocks of the Moodies Group at the southern end of The Heights syncline. Deformation during and following early Mapepe sedimentation and preceding deposition of the Moodies Group has been termed D_2 by Lowe et al. (this volume, Chapter 2). The principal effects of D_2 in the Songimvelo Block, in addition to elevating sources of early clastic detritus in areas outside the presently preserved depositional basins, included early D_{2a} folding along the Onverwacht anticline, southward-directed thrusting along the Komati fault during D_{2b}, and late tightening and collapse of the Onverwacht anticline (Lowe et al., this volume, Chapter 2). The effects of this deformation are discussed more fully in the following section on the Umuduha Block.

Late basinal stage (Moodies Group) (D_3). Moodies strata are sparsely developed on the Songimvelo Block. The facies and petrology of Moodies strata in the Baviaanskloof block on the east limb of the Onverwacht anticline, The Heights syncline, and in the West-Central Domain suggest that the Songimvelo Block was elevated during D_3 and served as a source of detritus throughout much of Moodies time. The effects of this uplift are most evident in areas surrounding the Songimvelo Block, which were sites of Moodies sedimentation.

Post-Moodies deformation (D_4 and D_5). The Songimvelo Block was involved in late BGB deformation, in large part serving as a rigid block between which supracrustal sequences were shortened. The effects of this deformation are better displayed in the Umuduha and Kaap Valley Blocks.

EVOLUTION OF THE UMUDUHA BLOCK

Although there are similarities in the geologies of the Southern Domain (SD), West-Central Domain (WCD), and Northern Domain (ND), contrasts in Onverwacht, Fig Tree, and Moodies Group stratigraphy, petrology, and evolution (Lowe and Byerly, this volume, Chapter 1; Lowe et al., this volume, Chapter 2) suggest that they represent portions of separate tectonic and stratigraphic blocks (Lowe, 1994). The Umuduha Block was constructed upon and along the northwestern margin of the Songimvelo Block, beginning with extrusion of komatiites of the Mendon Formation after 3,334 ± 3 Ma and concluding with felsic volcanism and TTG intrusion from about 3,260 to 3,230 Ma. Unlike other tectono-stratigraphic blocks in and around the BGB, the TTG suite in the Umuduha Block, if present, is not exposed in the study area.

Volcanic period

Ultramafic and mafic stage (Mendon Formation). Initial ultramafic and mafic volcanism in the Umuduha Block is represented by komatiites of the Mendon Formation. In the WCD, the Mendon Formation includes at least five cycles of predominantly komatiitic volcanism separated by thin cherty units marking pauses in eruptive activity (Lowe and Byerly, this volume, Chapter 1; Byerly, this volume, Chapter 8). Only the lowest cycle, M1, overlaps onto the Songimvelo Block. In the Umuduha Block, younger cycles appear progressively to the north as the formation is traced across faults in the WCD, where pre-Mendon rocks are absent or not exposed (Lowe and Byerly, this volume, Chapter 1). Mendon cherts show a corresponding transition from mainly shallow water and shelfal sedimentation in Mendon cycles M1c, M2c, and M3c, exposed in the SD and the southern part of the WCD, to deeper water deposition in stratigraphically higher units, M4c and M5c, exposed in the northern part of the WCD. In the northern part of the WCD, the oldest outcropping rocks are komatiites of M3 and higher members of the Mendon Formation. These facies relationships suggest that the locus of Mendon volcanism migrated progressively northward, off the Songimvelo Block, and are consistent with the interpretation that the formation was deposited during rifting along the northern and northwestern margins of the Songimvelo Block (Figs. 5D and 6A). M1, with the Msauli Chert at its top, was deposited largely as an overlap sequence upon older rocks of the Songimvelo block during the earliest phase of rifting, but younger members were largely confined within the developing rift. The presence of a thick sequence of Mendon komatiites and ultramafic intrusive rocks in the southern ECD, immediately east of the Kromberg fault, suggests that extension and komatiitic volcanism may have affected eastern parts of the Songimvelo and Steynsdorp Blocks as well.

Felsic volcanic and TTG intrusive stage (lower Mapepe and Auber Villiers Formations). The Mapepe Formation in the Songimvelo Block includes a thick sequence of quartz-phyric tuff and reworked ash reflecting felsic volcanism between about 3,260 and 3,230 Ma. In the SD and WCD, ash accumulated both as fall-deposited sediment and, in the middle and upper parts of the formation, as current-deposited detritus in alluvial and fan-delta units. Mapepe tuffs in the ECD are finer grained, less abundant, and interbedded with iron-rich sediments. The Auber Villiers Formation, which is inferred to have been structurally transported from the northwest to the southeast (Lowe et al., this volume, Chapter 2), contains the coarsest Fig Tree dacitic materials south of the Inyoka fault. These relationships suggest that the locus of volcanism represented by Fig Tree rocks in the SD, ECD, and WCD lay northwest of the present outcrops (Figs. 6B and 7A).

This volcanism is not represented by known felsic volcanic sequences in the western BGB. However, on farm Bien Venue, 10 km east-northeast of the eastern end of the Eureka syncline, a felsic volcanic sequence dated at 3,259 ± 5 Ma (Kröner et al., 1991a, sample SA 259, Table 2) includes more than 1,000 m of coarse quartz-bearing volcanic rock and ash-flow tuff. These rocks have not been studied in detail, but appear be proximal Auber Villiers–age volcanic units. It seems likely that this volcanism was associated with TTG plutonism at depth. This volcanism continued into the following orogenic period of block development.

Orogenic period

Early foreland stage (Mapepe Formation). The middle and upper parts of both the Mapepe and Auber Villiers Formations in the WCD contain thick units of chert-grit sandstone and chert-clast conglomerate interbedded with felsic volcaniclastic strata. These units reflect concurrent felsic volcanism and the uplift of older greenstone rocks. Thickness and/or coarsening trends in both types of units suggest that volcanism and uplift were centered northwest of the basin of sedimentation. The Mapepe Formation in the WCD has been interpreted to represent the fill of a foreland basin (Jackson et al., 1987; Nocita and Lowe, 1990; Lowe and Nocita, this volume, Chapter 10) developed along a southeast-verging backarc D_{2a} fold-and-thrust belt (Lowe et al., this volume, Chapter 2). Regionally across the Umuduha and Songimvelo Blocks, D_{2a} appears to have involved the formation of paired foreland basins adjacent to inward-facing fold-and-thrust belts southeast and northwest of the present BGB (Lowe and Nocita, this volume, Chapter 10). These basins were filled by Mapepe sediments and were separated, in the southwest, by the 3,445-Ma TTG block and, to the northeast, by the Onverwacht anticline, which may have formed in middle Mapepe time as a shared forebulge to both basins (Figs. 6B and 7A).

Late Orogenic stage (D_{2b}). During D_{2b}, southward and eastward progradation of the northern D_{2a} fold-and-thrust belt resulted in collapse of the Mapepe foreland basin west of the Onverwacht anticline, and thrusting of the basinal sequence onto the Songimvelo block along the Granville Grove fault. This shortening culminated when the marginal part of the Songimvelo sequence (Onverwacht Group) and structurally overlying foreland basin sequence (Fig Tree Group) were thrust southward onto the 3,445-Ma Songimvelo intrusive and metamorphic complex (Figs. 6C and 7B) along the Komati fault (Lowe et al., this volume, Chapter 2).

The location of the center of Fig Tree felsic volcanism and the location and kinematics of D_2 deformation seem most consistent with the interpretation that Fig Tree rocks in the Umuduha Block were deposited in a foreland basin lying south and southeast of a backarc fold-and-thrust belt (Figs. 6B and 7A). Arc magmatism is represented by distal Mapepe tuffs, proximal Auber Villiers units, and co-magmatic hypabyssal intrusions into the greenstone sequence along the west limb of the Onverwacht anticline. It appears that back-arc thrusting during D_{2a} and D_{2b} in late Mapepe and post-Mapepe time (about 3,240–3,230 Ma) accompanied intrusion and culminated in collapse of the foreland basin and obduction of the flanking supracrustal succession onto the older Songimvelo Block (Figs. 6C and 7B).

Late felsic overlap stage. The Auber Villiers and Mapepe Formations south of the Inyoka fault include volcaniclastic units from 3,256 ± 4 Ma to about 3,230 Ma in age. These units are at least in part older than dated felsic volcaniclastic rocks in the Schoongezicht Formation north of the fault, which appears to represent volcanism at about 3,226 ± 1 to 3,225 ± 3 Ma (Kröner et al., 1991a; Kamo and Davis, 1994). However, fine-grained, post-D_2 tuffs near the top of the Mapepe Formation in the reference section in the ECD (Lowe and Byerly, this volume, Chapter 1, Fig. 14) have been dated at 3,226 ± 3 Ma (Kröner et al., 1991a, Table 2, sample LH-842) and felsic tuffs near the top of the Auber Villiers Formation in the type section (Lowe and Byerly, this volume, Chapter 1, Fig. 17), which overlie coarse D_2 clastic units, may also represent post-D_2 volcanism. These youngest fine-grained felsic tuffs south of the Inyoka fault are probably composed of distal airborne pyroclastic debris from Schoongezicht volcanism on the Kaap Valley Block that was deposited on the Umuduha Block.

Late basinal stage (Moodies Group). Moodies strata in the Umuduha Block are less than 1,000 m thick, nowhere attaining the enormous thicknesses found north of the Inyoka fault (Reimer, 1967; Anhaeusser, 1973; Eriksson, 1977a, b, 1978; Hose, 1990; Heubeck and Lowe, 1994a, b) or adjacent to the southeastern margin of the belt in Swaziland (Lamb, 1984a, b). Basal Moodies conglomerates paraconformably overlie rocks of the Auber Villiers Formation or rest with angular unconformity or structural contact against Mapepe and Onverwacht units. Nowhere do Moodies strata appear to overlie intrusive TTG rocks, but southward toward present TTG exposures in the Songimvelo Block, they overlap unconformably onto increasingly older parts of the Onverwacht Group reflecting pre-Moodies D_2 deformation and uplift of the central part of the Songimvelo Block.

These stratigraphic relationships and the enormous flood of quartz-rich terrigenous detritus represented by the Moodies Group reflect regional uplift and erosion of TTG plutons during Moodies

sedimentation (Jackson et al., 1987; Heubeck and Lowe, this volume, Chapter 11). Previous investigators (Eriksson, 1977a, b, 1978; Jackson et al., 1987) have concluded that Moodies strata throughout the BGB were derived from sources east and south of the belt, mainly the AGC, and distributed to the north and west within a large alluvial, fluvial, deltaic, and shallow-marine deposystem. However, contrasting conglomerate and sandstone compositions in individual Moodies belts in the ND, WCD, and ECD suggest that Moodies strata were deposited within a number of different basins (Hose, 1990; Lowe and Byerly, this volume, Chapter 1; Heubeck and Lowe, 1994a, this volume, Chapter 11). Uplift of the TTG basement blocks during D_3 was accompanied by the formation of basins within which sediments of the Moodies Group were deposited. The lack of continuous stratigraphic sections containing both older, footwall Onverwacht and Fig Tree units and younger, hanging-wall Fig Tree and Moodies sequences in the WCD and the post-Moodies thrusting of predominantly younger hanging-wall over largely older footwall sequences suggest that the basins in which Moodies sediments were deposited were not underlain by thick sequences of older Fig Tree rocks. The presence of komatiites of the Weltevreden Formation beneath Schoongezicht and overlying Moodies strata at the eastern end of the Stolzburg syncline (Lowe and Byerly, this volume, Chapter 1) suggests that the Moodies basins may have been floored, at least in part, by mafic and ultramafic volcanic rocks overlain by a thin veneer of Fig Tree felsic volcanic or volcaniclastic rocks. The nature of D_3 tectonism, which formed the Moodies basins, remains unclear. Lamb (1984a, b) and Lamb and Paris (1988) report thrust faulting concurrent with late Fig Tree or Moodies sedimentation in western Swaziland. However, it is also likely that Moodies basins developed through extension following D_2 shortening.

Post-Moodies deformation (D_4 and D_5). Late Moodies and early post-Moodies deformation, D_4, in the Umuduha Block involved folding and southeastward thrusting (Fig. 7E). The 24-Hour Camp fault in the WCD formed at this time through collapse of a D_3 basin lying farther to the north and west. The displacement along the 24-Hour Camp fault is unknown.

D_5 involved formation of a regional northwest-verging fold-and-thrust belt (D_{5a}) and rotation of virtually all bedding, faults, and axial planes of folds to vertical or subvertical dips and the formation of axial plane cleavage (D_{5b}). These events reflect convergence of the buoyant central TTG blocks and shortening of the intervening supracrustal sequences. Evidence for major strike-slip faulting during D_{5c} is less well developed in the Umuduha Block than in areas north of the Inyoka fault.

EVOLUTION OF THE KAAP VALLEY BLOCK

The geology and geologic development of the Kaap Valley Block are less well resolved than those of the Songimvelo and Umuduha Blocks: (1) the Onverwacht Group north of the Inyoka fault has been little studied (Wuth, 1980; Anhaeusser, 1985) and its stratigraphy, petrology, and age remain unclear; (2) although local details of Fig Tree stratigraphy and sedimentology north of the Inyoka fault are available (Reimer, 1967, 1975; Condie et al., 1970) regional sedimentation patterns and geochronology remain unresolved; and (3) the ND is cut by numerous large, late strike- or oblique-slip faults (Ramsay, 1963; Lowe et al., this volume, Chapter 2). The offsets and net effect of these faults remain uncertain.

North of the Inyoka fault and south of the frontal Moodies fault, the Swaziland Supergroup can be divided into footwall and hanging wall sequences by a regional thrust fault (Lowe et al., this volume, Chapter 2). Virtually all Onverwacht rocks occur in the footwall sequence; Fig Tree units are distributed in both sequences; Moodies rocks are confined to the hanging wall.

Volcanic period

The Weltevreden Formation of the Onverwacht Group accumulated as a thick succession of predominantly peridotitic and basaltic komatiitic volcanic rocks, komatiitic tuff, and ultramafic intrusions. Interbedded nontuffaceous sedimentary units are rare, although a number of thin carbonaceous shales occur north of the Moodies fault and a prominent black and black-and-white banded chert unit is present within the upper 200 m of the formation. Facies relationships in the uppermost Weltevreden Formation and conformably overlying Ulundi Formation of the Fig Tree Group record a southwest-to-northeast shallow-to-deep-water transition along the northern BGB front. There is no evidence of tectonism or deformation during Weltevreden deposition, but details of the stratigraphy, facies, and structure of rocks north of the Moodies fault remain poorly resolved. The age of the Weltevreden Formation is constrained by Nd isotopic data at 3,286 ± 29 Ma (Lahaye et al., 1995), and the Onverwacht–Fig Tree transition in the Kaap Valley Block probably occurred at or after 3,243 ± 4 Ma, the age of a felsic tuff at the base of the Fig Tree Group immediately south of the Inyoka fault (Kröner et al., 1991a).

Orogenic Period

Early basinal stage (Ulundi and Sheba Formations). The Ulundi Formation represents an interval of slow sedimentation following the end of Weltevreden komatiitic volcanism. Iron-rich facies accumulated in deeper water while somewhat shallower areas were covered by a thin sequence of carbonaceous shale, silicified shale, and black and jasper-bearing cherts. The unit probably marks a condensed section.

Massive quartz-poor turbiditic graywackes of the overlying Sheba Formation reflect erosion mainly of greenstone belt rocks. Although regional facies trends are consistent with the Mapepe and Sheba Formations representing proximal, southern, shallow-water and distal, northern, deep-water portions, respectively, of the same basinal sequence, the absence of microcline and abundance of dacitic volcaniclastic debris in the Mapepe Formation and presence of microcline and paucity of fresh volcaniclastic debris in the Sheba Formation argue against this interpretation. The presence of microcline in Sheba graywackes indicates that uplifts sourcing post-Onverwacht clastic units in the Kaap Valley

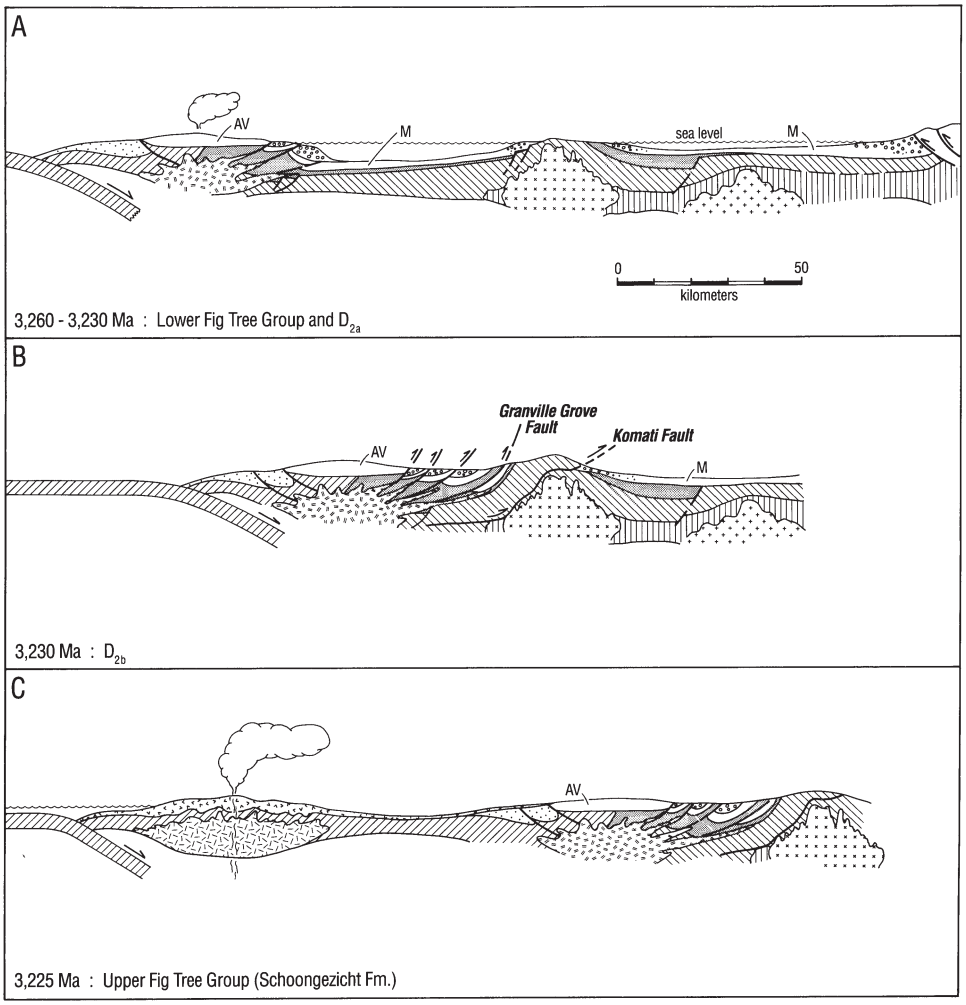
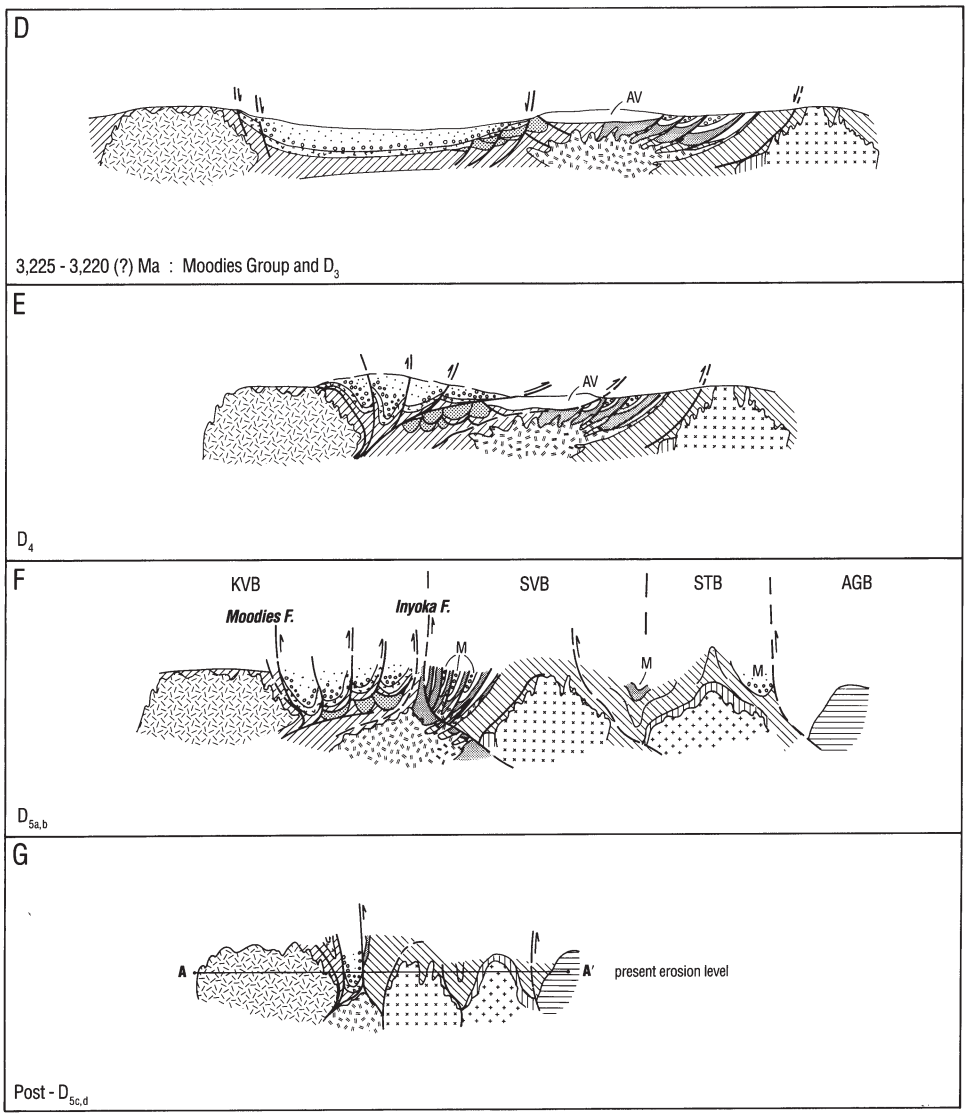


Figure 7 (this and facing page). Late geologic evolution of the southern part of the Barberton Greenstone Belt (BGB). Location of line of sections in Figure 1. Patterns as in Figure 3. A, Deposition of the Mapepe Formation in paired foreland basins separated by the Onverwacht anticline and bounded by fold-and-thrust belts to the southeast and northwest. Northern-facies Fig Tree units, north of the Inyoka fault, are shown by stippled pattern in forearc setting along the northwestern margin of the Auber Villiers (Umuduha) volcanic arc. B, Collapse of the northwestern foreland basin during D_{2b}. C, A jump in the location of subduction zone and arc magmatism in late Fig Tree time resulted in formation of a marginal sea between the older, inactive Umuduha magmatic arc and the newly active Kaap Valley arc from which felsic materials of the Schoongezicht Formation were erupted. D, Deposition of the Moodies Group in the back-arc basin between the uplifted Kaap Valley arc and pluton and the Umuduha Block, probably accompanied by extension, D_3. E, Late Moodies and early post-Moodies D_4 collapse and shortening of the back-arc basin was accompanied by southeast-vergent thrusting of the back-arc basinal sequence. F, Initial $D_{5a,b}$ convergence of protocontinental blocks and formation of regional, northwest-vergent fold-and-thrust belt. G, Present schematic cross section of BGB at same scale as sections in A–F.

Block included exposures of potassium-feldspar–bearing plutonic rocks as early as lower Fig Tree time. The source(s) of this debris have yet to be identified and may not be preserved, but the coarseness and abundance of K-spar–bearing clasts in the basal Moodies conglomerate in the Eureka syncline and the absence of K-spar in Fig Tree and Moodies units south of the Inyoka fault suggest a northerly or westerly source (Anhaeusser, 1969).

It is presently impossible to resolve the paleogeographic and paleotectonic setting of the northern-facies Fig Tree formations with any degree of confidence. In Figures 6C and 7A the Sheba Formation is shown as occupying a forearc or trench setting relative to the 3,260–3,230 magmatic arc, but more detailed studies of the geochronology, stratigraphy, and sedimentology of the northern-facies Fig Tree units are required to resolve their depositional setting.

Early Orogenic stage (D_2). Available evidence suggests that Onverwacht Group and overlying Ulundi, Sheba, and possibly



the Belvue Road Formations of the Fig Tree Group, the footwall assemblage, were deformed before deposition/emplacement of hanging-wall Schoongezicht and Moodies strata (Lowe et al., this volume, Chapter 2). Although pre-Moodies structures in the Kaap Valley Block have been strongly overprinted by younger tectonic events, it appears that post-Sheba, pre-Schoongezicht deformation involved shortening of the footwall sequence, possibly within a fold-and-thrust belt. The amount and age of deformation are poorly constrained. If the Sheba and lower Belvue Road Formations, the main clastic units in the northern facies, are rough time equivalents of clastic units in the Mapepe Formation south of the Inyoka fault, D_2 in the Kaap Valley, Umuduha, and Songimvelo Blocks was probably generally synchronous between about 3,250 and 3,230 Ma.

Felsic volcanic and intrusive stage (Belvue Road and Schoongezicht Formations). Sheba graywackes fine abruptly into overlying shale and tuff of the Belvue Road Formation. Thin tuff beds occur in the lowest few meters of the Belvue Road Formation and are interbedded with shale and thin, fine-grained turbiditic sandstone beds throughout the unit. Layers of massive, coarse-grained dacitic tuff as much as several meters thick occur in the top 50 m of the formation in the Stolzburg syncline. This predominantly fine grained unit records continuing deep-water sedimentation in areas far removed from the centers of both volcanism and uplift until latest Belvue Road time.

The age of the Belvue Road Formation is unclear. It could range anywhere between about 3,260 and 3,225 Ma, representing the distal equivalent of either the Schoongezicht Formation, in which case it is less than 3,230 Ma, or the lower Auber Villiers and lower Mapepe Formations, implying that it is between 3,260 and 3,230 Ma in age.

Schoongezicht rocks in the study area crop out around the east end of the Stolzburg syncline and at the west end of the Moodies Hills. The type section at the east end of the Stolzburg syncline records a facies transition from coarse, massive, proximal high-density turbidity-current deposits in the lower half of the

unit upward into shallow-water or alluvial conglomerates and breccias at the top (Lowe and Byerly, this volume, Chapter 1). Several kilometers to the northwest, the Schoongezicht consists of more distal, thinly bedded volcaniclastic turbiditic sandstones and mudstones. Schoongezicht rocks in the Moodies Hills consist of fine clay shales grading upward into coarse, plagioclase-rich sandstones and at the top, coarse volcaniclastic debris-flow deposits and conglomerate (Lowe and Byerly, this volume, Chapter 1).

Stratigraphic and structural relationships between the hanging-wall Schoongezicht Formation and the footwall formations of the Fig Tree Group in the Kaap Valley Block remain ambiguous. It seems clear that the Schoongezicht Formation records felsic volcanism that was coeval and comagmatic with intrusion of the Kaap Valley tonalite at about 3,226 Ma. If the Schoongezicht is the uppermost formation in a continuous stratigraphic sequence that includes the other northern formations of the Fig Tree Group (Condie et al., 1970), then northern-facies Fig Tree rocks represent deposition within a single basin on the Kaap Valley Block. If, however, as seems likely, the Schoongezicht is part of an allochthonous hanging-wall succession that includes conformably underlying Onverwacht cherts and komatiites and paraconformably overlying Moodies strata and is everywhere in structural contact with underlying footwall Fig Tree and Onverwacht units, it represents sedimentation in one or more separate basins (Fig. 7C).

Based on age, petrologic, and stratigraphic relationships, it seems likely that the inception of Schoongezicht volcanism and Kaap Valley TTG plutonism at about 3,226 Ma involved a northwestward jump in the locus of subduction and arc-magmatism (Fig. 7C). This jump resulted in the isolation of a piece of pre-3,225-Ma Onverwacht crust within a back-arc basin between the new Kaap Valley magmatic arc and the older, remnant Umuduha magmatic arc (Fig. 7C). Felsic volcaniclastic debris produced by magmatism along the Kaap Valley arc was deposited as the Schoongezicht Formation in the back-arc basin, directly on deep-water sediments of the Ulundi Formation that overlay rocks of the Onverwacht Group (Fig. 7C). Fine-grained, distal Belvue Road Formation tuffs may represent the eastern basinal equivalents of the more proximal Schoongezicht felsic volcaniclastic strata.

Late basinal stage (Moodies Group). The Moodies Group in the Kaap Valley Block includes 2,000–3,700 m of feldspathic and quartzose sandstone. Microcline is a widespread minor but erratically distributed constituent and microcline-bearing plutonic clasts characterize the basal conglomerate in some sections. The source of this granitic detritus is unknown. The upper, commonly medium- to fine-grained sandstones and siltstones of the Joes Luck and Baviaanskop Formations of Anhaeusser (1969) appear to be restricted to the Kaap Valley Block. The enormous thickness of Moodies strata indicates uplift and deep erosion of surrounding quartz-bearing TTG rocks, probably including the Kaap Valley tonalite but also microcline-bearing plutonic rocks as old as 3,531 ± 4 Ma (Kröner and Compston, 1988).

The Moodies Group has been interpreted as foreland-basin fill (Jackson et al., 1987; Hose, 1990). However, the presence of basaltic agglomerate in the basal Moodies strata at the west end of the Moodies Hills and of syn-Moodies basaltic volcanism higher in the group suggest that early Moodies sedimentation on the Kaap Valley Block may have taken place within an extensional setting (Fig. 7D). The present author suggests that Moodies rocks north of the Inyoka fault were deposited in the back-arc basin formed at about 3,225 Ma and bounded during Moodies time by an uplifted greenstone belt and tonalitic rocks to the southeast and the uplifted Kaap Valley pluton and its roof rocks to the northwest. Back-arc thrusting may have contributed to uplift and sedimentation in the northern part of this basin throughout Moodies time.

Late- to post-Moodies deformation (D_4 and D_5). D_4 in the Kaap Valley Block involved the formation of a southeast-verging fold-and-thrust belt across the present Northern Domain (Lowe et al., this volume, Chapter 2; Heubeck and Lowe, 1994a, b). Details of this deformation are poorly constrained, but it apparently involved shortening and collapse of the back-arc basin containing the hanging-wall sequence during convergence of the Kaap Valley and remnant Umuduha magmatic-arcs (Fig. 7E). Collapse was accompanied by obduction of the back-arc-basin sequence onto the older footwall units to the southeast along the thrust fault that now separates hanging-wall and footwall sequences in the ND.

D_5 involved final convergence and suturing of the Kaap Valley and Umuduha Blocks (Figs. 7F and G). Because of the extremely irregular shape of the large, undeformed Kaap Valley and Nelshoogte plutons, late-stage deformation involved heterogeneous shortening of the intervening supracrustal sequences (D_{5c}) and a final stage during which the supracrustal rocks were molded around the margins of these TTG units (D_{5d}). Strike-slip faulting may have played a major role in this deformation.

DISCUSSION

The BGB is a compound terrane formed through long-term magmatic activity and late-stage tectonic accretion (Lowe et al., 1989; de Wit et al., 1992; Kröner et al., 1992; de Ronde and de Wit, 1994; Lowe, 1994). Its formation involved at least four discrete magmatic cycles: (1) a 3.55- to 3.50-Ga pre-Komati Formation magmatic cycle during which the Theespruit Formation and related volcanic units exposed in the Steynsdorp and Onverwacht anticlines were deposited and subsequently intruded by TTG magmas at about 3,509 Ma; (2) a cycle extending from about 3.50 to about 3.43 Ga during which rocks of the Komati and Hooggenoeg Formations were erupted and intruded by 3,445-Ma-event TTG plutons; (3) a 3,335- to 3,230-Ma cycle during which volcanic rocks of the Mendon Formation of the Onverwacht Group and felsic Mapepe and Auber Villiers volcaniclastic and epiclastic formations of the Fig Tree Group were deposited and probably intruded by as-yet-unseen 3,260- to 3,230-Ma TTG plutons; and (4) a young, 3,300(?)- to 3,212(?)-Ma cycle during which komatiites of the Weltevreden Formation were deposited and subsequently covered by felsic volcanic rocks of the Schoongezicht Formation and intruded by the Kaap

Valley and Nelshoogte TTG plutons. These cycles are termed the Steynsdorp, Songimvelo, Umuduha, and Kaap Valley cycles corresponding to the formation of the basement blocks of the same names. We presently lack precise age constraints on the beginning of most cycles because of poor exposure and poor dating of the mafic volcanic units marking their bases. The significance of the Kromberg Formation within the cycle history is uncertain. It may represent a separate 3,416- to 3,334-Ma cycle that is not represented by outcropping TTG plutonic or felsic volcanic units in the vicinity of the BGB or to localized magmatism, perhaps related to extension, on and around the Songimvelo Block.

The formation of the continental crust in the eastern Kaapvaal Craton can be described in terms of three generalized evolutionary stages. (1) The first stage involved the formation of small, buoyant blocks representing individual volcanic-intrusive complexes. These will here be termed protocontinental blocks because, although including differentiated and fractionated "continental" TTG crust, they were thin, small, and not of continental proportions or stability. Each block formed through an initial period of (1a) ultramafic and mafic volcanism, followed by (1b) thickening of the ultramafic and mafic volcanic sequence by the intrusion of TTG magmas into the base of the volcanic sequence and eruption of comagmatic felsic volcanic units at the surface. Volcanism was followed by (2) amalgamation and suturing of the protocontinental blocks to form a larger quasi-continental block. The final stage of continent formation, which is not the subject of this paper, involved (3) underplating, late intracrustal melting, and post-kinematic potassic plutonism forming a large, thick, stabilized, buoyant continental (cratonic) block.

Ultramafic and mafic volcanic stage

The oldest component of each tectonic and stratigraphic block in the BGB and vicinity is a thick sequence of mafic and ultramafic volcanic rocks of the Onverwacht Group composed largely of peridotitic and basaltic komatiites and high-magnesium basalts; their pyroclastic equivalents; and, in some areas, mafic and ultramafic intrusions. With the exception of the youngest Umuduha and Kaap Valley Blocks, within which the ultramafic and mafic sequences may be partial age equivalents, these sequences represent temporally discrete eruptive episodes.

The tectonic settings of ultramafic and mafic volcanism in Archean greenstone belts were probably as varied as those of mafic volcanism on the modern Earth. Proposed settings for preserved Archean greenstone sequences include intracratonic rifts (Condie and Hunter, 1976; Nisbet, 1982), oceanic spreading centers (de Wit et al., 1987a), subduction-related volcanic arcs (Langford and Morin, 1976; Hoffman, 1989; Arkani-Hamed and Jolly, 1989; Card, 1990; de Ronde et al., 1991; de Ronde and de Wit, 1994), back-arc spreading centers (Tarney et al., 1976; Sawkins, 1990), and oceanic islands and plateaus (Campbell et al., 1989; Storey et al., 1991; Kusky and Kidd, 1992; Kröner and Layer, 1992; Abbott, 1996; Kent et al., 1996).

The komatiite-dominated Mendon Formation appears to have been erupted during rifting of the Songimvelo Block. The oldest lavas erupted during the initial stages of rifting, represented by cycle M1 of the Mendon Formation (Lowe and Byerly, this volume, Chapter 1), spread out over the surface of the older Songimvelo block. Younger lavas of M2, M3, M4, and M5 were confined to the growing rift and the age of the oldest units at each point decreases progressively, across a series of intervening faults, away from the older Songimvelo Block. This style of volcanism is consistent with that occurring today along both mid-ocean and back-arc spreading centers and ridge-centered or near-ridge oceanic islands. In all of these settings, a fixed depositional site is displaced progressively away from the volcanic center.

Age and stratigraphic constraints on the Komati Formation are insufficient to determine whether it displays similar progressive age or stratigraphic changes. It appears to have been deposited over a relatively continuous or fragmented basement of pre-3.5-Ga, Steynsdorp-age volcanic and plutonic units, suggesting a rift or extensional setting. However, the enormous thickness of volcanic units in the Hooggenoeg Formation, the presence of numerous breaks in volcanism represented by thin chert units, and the apparent absence of systematic trends in age, thickness, or composition of volcanic rocks suggest that the Hooggenoeg Formation was not erupted along a spreading center. The striking change from komatiitic to basaltic volcanism and from enormously high eruption rates to more modest rates represented by the transition from the Komati to the Hooggenoeg Formation may reflect a change in tectonic setting. If the Komati Formation was related to extension on the western edge of the Steynsdorp Block, the Hooggenoeg Formation may mark the initiation of arc-related magmatism that culminated in H6 and the intrusion of the 3,445-Ma TTG suite.

Every major magmatic cycle/belt in the BGB, with the possible exception of the Steynsdorp Block, where appropriate-aged rocks are heavily altered and sheared, was initiated by both a shift in the locus of magmatism and an initial interval of komatiitic volcanism. Although these mafic units locally overlap onto adjacent, older crustal blocks, each also marks the formative stage of a new crustal unit. Because the geometry of these komatiitic sequences has not been resolved, it is not clear whether they represent local, high-standing volcanic islands, such as oceanic islands developed over hot spots, broad oceanic plateaus developed over mantle plumes, or tabular sheets, similar to oceanic crust produced along spreading centers. Compositional contrasts between komatiitic sequences in the BGB (Viljoen, M. J., and Viljoen, 1969) may indicate that more than one of these magmatic settings is represented in the preserved greenstone sequence. The inference that the Komati and Hooggenoeg Formations may have formed a high-standing, predominantly shallow-water to subaerial platform that was surrounded by deeper water settings may indicate that it existed as a plateau or island, similar to oceanic plateaus or Hawaiian-type oceanic islands formed over hotspots.

Arndt (1994) argued that spinifex-bearing komatiites themselves indicate deep mantle sources most likely associated with

mantle plumes or hot spots. The regular eruption of komatiites as the initial stage in the formation of individual blocks in the BGB area would thus suggest that rifting of older crust or protocontinental blocks above hotspots or mantle plumes initiated each cycle of crustal growth. The resulting ultramafic and mafic volcanic sequences would have formed oceanic islands or a broad oceanic plateaus, respectively. Many Archean hotspots may have been situated upon or near oceanic spreading centers (Abbott, 1996), and the resulting volcanic sequences may have been influenced by both deep-mantle hotspot and shallow spreading-center melting. Although the komatiitic sequences may represent or contain segments of Archean oceanic crust, we have seen no evidence that any preserve sheeted dike complexes as suggested by de Wit et al. (1987a). These are not simply Phanerozoic-style ophiolites of Archean age. The results of this study suggest that Archean ocean-floor magmatism, along spreading centers and possibly over mantle plumes or hot spots located near or beneath spreading centers, was characterized by komatiitic volcanism and that preserved komatiitic sequences may locally include pieces of Archean oceanic crust and oceanic island and plateaus sequences that have been preserved by later thickening and increased buoyancy through the intrusion of large bodies of TTG magma.

In view of the compound nature of the Barberton Greenstone Belt, there is no reason to suppose that all of the ultramafic and mafic volcanic sequences originated in the same tectonic setting. The Komati Formation may have originated largely as an eruptive sheet, resembling plateau or flood basalts, perhaps with only minor extension of the underlying Steynsdorp basement. In contrast to the Komati Formation, ultramafic and mafic sequences in both the Umuduha and Kaap Valley Block include numerous thick, layered ultramafic intrusions and the interbedded sediments suggest fully subaqueous, often deep-water settings of volcanism and sedimentation. The early ultramafic and mafic sequence in the Umuduha block was clearly associated with rifting, and spreading centers may have been involved in the initial stages of formation of both of these crustal blocks.

Felsic volcanic-TTG intrusive stage

In each of the blocks, initial mafic volcanism was followed by comagmatic felsic volcanism, shallow hypabyssal intrusion, and deep-seated TTG intrusion. Although dating is imprecise, individual episodes of felsic magmatism appear to have lasted about 25–35 m.y. TTG-felsic magmatism in Archean greenstone belts has been widely related petrologically to subduction-related arc magmatism (Langford and Morin, 1976; Hoffman, 1989; Arkani-Hamed and Jolly, 1989; Card, 1990; de Ronde et al., 1991; de Ronde and de Wit, 1994).

In the Songimvelo Block, felsic magmatism closely followed deposition of a thick succession of basalts (Hooggenoeg Formation members H1–5), with no evidence for a long intervening period of magmatic quiescence. In the Kaap Valley block, basalts are essentially absent in the Weltevreden Formation (Onverwacht Group) and felsic magmatism followed an interval of magmatic quiescence represented by the Ulundi Formation (Fig Tree Group). It seems likely that Songimvelo felsic magmatism occurred within a long-lived magmatic arc, possibly characterized throughout much of its history by basaltic volcanism (Hooggenoeg Formation), whereas Kaap Valley felsic magmatism followed immediately after arc magmatism jumped abruptly to a previously intraplate setting. As a result, Kaap Valley felsic volcanic units (Schoongezicht Formation) were deposited directly on deep-water oceanic sediments (hanging-wall Ulundi Formation) overlying komatiites produced at a spreading center or oceanic island (hanging-wall Weltevreden Formation).

TTG magmatism injected the ultramafic and mafic sequences with enormous volumes of buoyant, leucocratic, quartz-bearing intrusive rocks. Comagmatic felsic volcanism mantled the ultramafic and mafic sequences with sheets of low-density, quartz-bearing dacitic to rhyolitic volcanic rock. The product of the combined high-volume mafic-komatiitic volcanism followed by TTG-felsic magmatism was a small, thickened, block or belt of crust that was considerably less dense and more buoyant than either the mafic and komatiitic sequence from which it formed or the surrounding oceanic(?) crust. These blocks have been here informally termed protocontinents. Each protocontinent consisted of (1) a core made up of TTG intrusive units and overlying, deformed and metamorphosed supracrustal roof rocks; and (2) a flanking assemblage of komatiitic and felsic volcanic rocks correlative with roof rocks of the central complex but less metamorphosed and deformed and lacking large TTG intrusions.

Protocontinent amalgamation

The growth of larger, quasi-continental blocks in the BGB region occurred through accretion of protocontinental blocks. Accretion occurred in two ways. There is considerable evidence that the Songimvelo Block formed along and upon the older Steynsdorp Block, forming a larger, compound buoyant block through magmatic accretion. In contrast, the Kaap Valley Block formed as a separate unit, perhaps separated from the Songimvelo and Umuduha Blocks by a back-arc basin. Subsequently, this basin collapsed and the Kaap Valley Block was sutured to the older TTG complex through tectonic accretion.

In the BGB region, late-stage amalgamation of protocontinental blocks involved (a) thrusting of the marginal, unmetamorphosed portions of the mafic volcanic sequences onto adjacent central TTG complexes or over deformed older orogenic greenstone sequences, (b) uplift of the central TTG complexes and their emplacement against higher level, less metamorphosed portions of the overlying supracrustal sequences; and (c) extreme shortening and thickening of the supracrustal sequences between the high-standing, converging TTG blocks.

D_{4-5} appear to reflect more-or-less complete, regional amalgamation of the protocontinent TTG nuclei. The southeastern portions of the BGB were deformed during extreme shortening resulting from the amalgamation of the Steynsdorp and possibly Songimvelo Blocks and the Ancient Gneiss Complex. D_5 resulted

in development of a northwest-verging fold-and-thrust belt across the southeastern and central portions of the BGB. At the same time, Onverwacht, Fig Tree, and Moodies rocks between and upon the margins of the Songimvelo, Umuduha, and Kaap Valley Blocks were shortened between the converging TTG nuclei. The extremely massive character of Moodies sandstones and the extreme ductility of Onverwacht serpentinites and Fig Tree shales and tuffs resulted in the growth of large Moodies synclines separated by thin, attenuated serpentinite-cored anticlines commonly marked by thrust faults.

The post-Moodies, post-D_5 product of this activity was a much larger and thicker block of crust representing an amalgamation of smaller protocontinental blocks and intervening supracrustal sequences. The final stages of this activity may have been completed at about 3.1 Ga, the time of large-scale potassic plutonism across all of the blocks in the BGB and vicinity and of gold mineralization in the northern BGB.

Crustal thickening

The final stage of craton formation in the BGB and vicinity involved post-D_5 underplating and melting of the roots of the amalgamated and thickened quasi-continental collage to form late-stage potassic intrusions, such as the 3,107 +4/–2 Ma-Mpuluzi Batholith, the 3,079 ± 6-Ma Salisbury Kop pluton, and the 3.1-Ga Nelspruit and Hebron batholiths. The overall construction and stabilization of this part of the eastern Kaapvaal Craton was completed by about 3,050 Ma.

CONCLUSIONS

The eastern Kaapvaal Craton in and around the Barberton Greenstone Belt comprises a number of crustal blocks, each of which developed through a generally similar sequence of events, commonly over intervals of 50–80 m.y. The evolution of each block began with the eruption of a thick sequence of predominantly komatiitic lavas. Although these lavas commonly overlapped onto and covered large parts of older blocks, over large areas, they appear to form the oldest supracrustal rocks present, commonly reaching 2–3 km thick without an exposed base. In the Songimvelo Block, these volcanic rocks belong to the Komati Formation and formed a broad, high-standing komatiitic platform, along and upon the older Steynsdorp Block, that served as the nucleus for later sedimentation and magmatism. Komatiitic magmatism represented by the Komati Formation may have may have accompanied rifting of the older Steynsdorp basement. Progressive migration of the locus of volcanism during eruption of the Mendon Formation on the Umuduha Block is most consistent with eruption during rifting and spreading within the Songimvelo Block. It seems likely that these early komatiitic volcanic sequences record oceanic magmatism associated with hotspots or hotspots associated with mid-ocean or back-arc spreading centers.

The mafic volcanic sequences were commonly capped by carbonaceous and cherty sediments, such as the Middle Marker in the Songimvelo Block, the capping cherts of the Mendon Formation in the Umuduha Block, and the Ulundi Formation in the Kaap Valley Block. These units probably represent condensed sections, marking rather long, magmatically quiescent intervals during which the newly formed ultramafic and mafic sequences cooled and subsided within a magmatically quiescent, oceanic, intraplate setting. Subsequently, those parts of the mafic sequences now preserved within the BGB were thickened by comagmatic TTG intrusion and felsic eruption representing subduction-related magmatism along convergent plate boundaries. The volcanic histories of individual blocks thus record their initial formation along oceanic spreading centers or over hot spots or mantle plumes, a succeeding stage of magmatic quiescence within an intraplate setting, and a final episode of crustal thickening to form buoyant protocontinental blocks along a magmatic arc at a convergent plate boundary.

Late-stage tectonism involved all of the blocks that had developed over the preceding 300 m.y. and reflects the amalgamation and suturing of protocontinental blocks followed by post-greenstone underplating, intracrustal melting, and crustal thickening. This pre-3.0-Ga Archean tectonic cycle closely resembles the Phanerozoic tectonic cycle except that it does not involve the participation of large, craton-scale continental blocks. It represents a plate-tectonic cycle of crustal evolution on an Earth with few or no large continental crustal blocks.

Accumulation of rocks making up the Barberton Greenstone Belt began before 3,550 Ma and culminated with deposition and deformation of the Moodies Group after 3,225 Ma, a span exceeding 325 m.y. Unlike the Abitibi Greenstone Belt of eastern Canada, which formed during a single major cycle of volcanism, intrusion, and tectonism lasting about 60 m.y. (Corfu and Davis, 1992), the Barberton Belt evolved over a prolonged interval through a number of discrete magmatic cycles, each involving a succession of stages marked by contrasts in magmatism, tectonic style, and sedimentation, and each lasting about as long as the Abitibi cycle. The belt is not a simple prograding accretionary prism developed adjacent to a long-lived subduction zone but an accretionary tract that developed through multiple cycles of rifting, magmatic accretion, and subduction-related crustal thickening.

Magmatism in similar tectonic settings probably characterized the Earth well before 3.55 Ga. The oldest known rocks are 3.96-Ga TTG gneisses containing metagreenstone xenoliths in Canada (Bowring et al., 1989) that probably represent protocontinental remnants like those in the eastern Kaapvaal Craton. The critical step leading to the evolution of continental crust during the Archean was the first preservation, not formation, of differentiated continental crust and protocontinental blocks. The declining rate of heat loss on the early Earth would have been accompanied by a decrease in the efficiency of early crustal recycling systems. Eventually a time was reached when the most buoyant blocks, either large oceanic plateaus or pieces of oceanic plateau or oceanic islands thickened by subsequent TTG magmatism, resisted recycling. As soon as these buoyant protocontinental units were preserved instead of recycled, they became building blocks for the

evolution of still larger compound, magmatically more evolved continental terranes.

The evolutionary scenario suggested for the eastern Kaapvaal Craton also helps explain the apparent existence and influence of differentiated or "continental" crust on the evolution of belts such as the BGB and eastern Pilbara greenstone belts of Western Australia (Kröner and Tegtmeyer, 1994; Bickle et al., 1994), which show little or no structural, sedimentological, or petrologic evidence that they were deposited on or adjacent to large, stabilized continental blocks or cratons (Lowe and Knauth, 1977; Lowe, 1980, 1982). Protocontinental blocks represent differentiated and fractionated magmas and crustal units and provide sources of geochronological and isotopic contamination to younger magmas erupted upon or around them. Throughout the BGB region, older protocontinental blocks commonly served as basement through which younger magmas moved and upon which they were erupted during the formation of younger blocks through rifting and magmatic accretion. Widespread xenocrystic zircons in younger magmatic sequences indicate extensive contamination by older TTG intrusive or volcanic suites. However, protocontinental blocks were not continents or continental blocks in the sense of being large, thick, stable, buoyant, craton-scale platforms. They were apparently not thick enough to serve as long-term, high-standing sources of clastic detritus, and there is no evidence that their plutonic nuclei were uplifted and exposed to erosion until late-stage shortening greatly thickened the supracrustal sequences and uplifted the TTG-supracrustal blocks. Even then, high-level emplacement and eventual exposure of the buoyant TTG nuclei may have occurred mainly because they were tectonically buried beneath overthrust, dense, marginal portions of the protocontinental volcanic sequences.

Thus, during the early Archean, the formation of large stable cratons, such as the Kaapvaal Craton, appears to have involved several hundred million years of precratonic crustal evolution. This was an interval that produced numerous small, buoyant protocontinental blocks that were only later tectonically amalgamated, shortened, and thickened to form the first preserved large stable continental blocks or cratons.

REFERENCES CITED

Abbott, D. H., 1996, Plumes and hotspots as sources of greenstone belts: Lithos, v. 37, p. 113–127.

Abbott, D. H., and Hoffman, S. E., 1984, Archaean plate tectonics revisited 1. Heat flow, spreading rate, and the age of subducting oceanic lithosphere and their effects on the origin and evolution of continents: Tectonics, v. 3, p. 429–448.

Anhaeusser, C. R., 1969, The stratigraphy, structure, and gold mineralisation of the Jamestown and Sheba Hills areas of the Barberton Mountain Land [Ph.D. thesis]: Johannesburg, University of the Witwatersrand, 332 p.

Anhaeusser, C. R., 1973, The evolution of the early Precambrian crust of southern Africa: Royal Society of London Philosophical Transactions, ser. A, v. 273, p. 359–388.

Anhaeusser, C. R., 1976, The geology of the Sheba Hills area of the Barberton Mountain Land, South Africa, with particular reference to the Eureka syncline: Geological Society of South Africa Transactions, v. 79, p. 253–280.

Anhaeusser, C. R., 1984, Structural elements of Archaean granite-greenstone terranes as exemplified by the Barberton Mountain Land, southern Africa, *in* Kröner, A., and Greiling, A., eds., Precambrian tectonics illustrated: Stuttgart, E. Schweizerbart'sche Verlagsbuchhandlung, p. 57–78.

Anhaeusser, C. R., 1985, Archean layered ultramafic complexes in the Barberton Mountain Land, South Africa, *in* Ayres, L. D., Thurston, P. C., Card, K. D., and Weber, W., eds., Evolution of Archean supracrustal sequences: Geological Association of Canada Special Paper 28, p. 281–302.

Arkani-Hamed, J., and Jolly, W. T., 1989, Generation of Archean tonalites: Geology, v. 17, p. 307–310.

Armstrong, R. A., Compston, W., de Wit, M. J., and Williams, I. S., 1990, The stratigraphy of the 3.5–3.2 Ga Barberton Greenstone Belt revisited: a single zircon ion microprobe study: Earth and Planetary Science Letters, v. 101, p. 90–106.

Arndt, N. T., 1994, Archean komatiites, *in* Condie, K. C., ed., Archean crustal evolution: Amsterdam, Elsevier, p. 11–44.

Beukes, N. J., 1973, Precambrian iron-formations of southern Africa: Economic Geology, v. 68, p. 960–1004.

Bickle, M. J., 1978, Heat loss from the Earth: a constraint on Archaean tectonics from the relation between geothermal gradients and the rate of plate production: Earth and Planetary Science Letters, v. 40, p. 301–315.

Bickle, M. J., 1986, Implications of melting for stabilization of the lithosphere and heat loss in the Archaean: Earth and Planetary Science Letters, v. 80, p. 314–324.

Bickle, M. J., Nisbet, E. G., and Martin, A., 1994, Archean greenstone belts are not oceanic crust: Journal of Geology, v. 102, p. 121–138.

Bowring, S. A., Williams, I. S., and Compston, W., 1989, 3.96 Ga gneisses from the Slave province, Northwest Territories, Canada: Geology, v. 17, p. 971–975.

Burke, K., and Kidd, W. S. F., 1978, Were Archaean continental geothermal gradients much steeper than those of today? Nature, v. 272, p. 240–241.

Byerly, G. R., Lowe, D. R., Nocita, B. W., and Ransom, B. L., 1983, Apparent volcanic cycles in the Archean Swaziland Supergroup, Barberton Mountain Land, South Africa: a result of non-magmatic processes: Lunar and Planetary Science Conference, 14th, Houston, Abstracts, pt. 1, p. 84–85.

Byerly, G. R., Kröner, A., Lowe, D. R., and Walsh, M. M., 1993, Sequential magmatic evolution of the early Archean Onverwacht Group: evidence from the upper formations: Eos (Transactions, American Geophysical Union), v. 74, p. 660.

Byerly, G. R., Kröner, A., Lowe, D. R., Todt, W., and Walsh, M. M., 1996, Prolonged magmatism and time constraints for sediment deposition in the early Archean Barberton greenstone belt: evidence from the Upper Onverwacht and Fig Tree Groups: Precambrian Research, v. 78, p. 125–138.

Campbell, I. H., Griffiths, R. W., and Hill, R. I., 1989, Melting in an Archaean mantle plume: heads it's basal, tails it's komatiites: Nature, v. 339, p. 697–699.

Card, K. D., 1990, A review of the Superior Province of the Canadian Shield, a product of Archean accretion: Precambrian Research, v. 48, p. 99–156.

Chauvel, C., Arndt, N. T., Gruau, G., and Hofmann, A. W., 1987, Composition of the Archean mantle: evidence from Nd isotopes: TERRA Cognita, v. 7, p. 272.

Corfu, F., and Davis, D. W., 1992, A U-Pb geochronological framework for the western Superior Province, Ontario, *in* Thurston, P. C., Williams, H. R., Sutcliffe, R. H., and Stott, G. M. eds., The geology of Ontario: Ontario Geological Survey Special Volume 4, part 2, p. 1335–1346.

Compston, W., and Kröner, A., 1988, Multiple zircon growth within early Archaean tonalitic gneiss from the Ancient Gneiss Complex, Swaziland: Earth and Planetary Letters, v. 87, p. 13–28.

Condie, K. C., 1981, Archean greenstone belts: Amsterdam, Elsevier, 434 p.

Condie, K. C., and Hunter, D. R., 1976, Trace element geochemistry of Archaean granitic rocks from the Barberton region, South Africa: Earth and Planetary Science Letters, v. 29, p. 389–400.

Condie, K. C., Macke, J. E., and Reimer, T. O., 1970, Petrology and geochemistry of early Precambrian graywackes from the Fig Tree Group, South Africa: Geological Society of America Bulletin, v. 81, p. 2759–2776.

Defant, M. J., and Drummond, M. S., 1990, Derivation of some modern arc magmas by melting of young subducted lithosphere: Nature, v. 347, p. 662–665.

de Ronde, C. E. J., and de Wit, M. J., 1994, Tectonic history of the Barberton greenstone belt, South Africa: 490 million years of Archean crustal evolution: Tectonics, v. 13, p. 983–1005.

de Ronde, C. E. J., Kamo, S., Davis, D. W., de Wit, M. J., and Spooner, E. T. C., 1991, Field, geochemical and U-Pb isotopic constraints from hypabyssal felsic intrusions within the Barberton greenstone belt, South Africa: Implications for tectonics and the timing of gold mineralization: Precambrian Research, v. 49, p. 261–280.

de Wit, M. J., 1982, Gliding and overthrust nappe tectonics in the Barberton Greenstone Belt: Journal of Structural Geology, v. 4, p. 117–136.

de Wit, M. J., Fripp, R. E. P., and Stanistreet, I. G., 1983, Tectonic and stratigraphic implications of new field observations along the southern part of the Barberton Greenstone Belt, *in* Anhaeusser, C. R., ed., Contributions to the geology of the Barberton Mountain Land: Geological Society of South Africa Special Publication 9, p. 21–29.

de Wit, M. J., Hart, R. A., and Hart, R. J., 1987a, The Jamestown Ophiolite Complex, Barberton mountain belt: a section through 3.5 Ga oceanic crust: Journal of African Earth Sciences, v. 6, p. 681–730.

de Wit, M. J., Armstrong, R. J., Hart, R. J., and Wilson, A. H., 1987b, Felsic igneous rocks within the 3.3 to 3.5 Ga Barberton Greenstone Belt: high crustal-level equivalents of the surrounding tonalite-trondhjemite terrain, emplaced during thrusting: Tectonics, v. 6, p. 529–549.

de Wit, M. J., Roering, C., Hart, R. J., Armstrong, R. A., de Ronde, C. E. J., Green, R. W. E., Tredoux, M., Peberdy, E., and Hart, R. A., 1992, Formation of an Archaean continent: Nature, v. 357, p. 553–562.

Duchac, K. C., and Hanor, J. S., 1987, Origin and timing of the metasomatic silicification of an Early Archean komatiite sequence, Barberton Mountain Land, South Africa: Precambrian Research, v. 37, p. 125–146.

Eriksson, K. A., 1977a, A paleoenvironmental analysis of the Archaean Moodies Group, Barberton Mountain Land, South Africa [Ph.D. thesis]: Johannesburg, University of the Witwatersrand, 155 p.

Eriksson, K. A., 1977b, Tidal deposits from the Archaean Moodies Group, Barberton Mountain Land, South Africa: Sedimentary Geology, v. 18, p. 257–281.

Eriksson, K. A., 1978, Alluvial and destructive beach facies from the Archaean Moodies Group, Barberton Mountain Land, South Africa and Swaziland, *in* Miall, A. D., ed., Fluvial sedimentology: Canadian Society of Petroleum Geologists Memoir 5, p. 287–311.

Gay, N. C., 1969, The analysis of strain in the Barberton Mountain Land, eastern Transvaal, using deformed pebbles: Journal of Geology, v. 77, p. 377–396.

Hanor, J. S., and Duchac, K., 1990, Isovolumetric silicification of Early Archean komatiites: geochemical mass balances and constraints on origin: Journal of Geology, v. 98, p. 863–877.

Heinrichs, T. K., 1980, Lithostratigraphische Untersuchungen in der Fig Tree Gruppe des Barberton Greenstone Belt zwischen Umsoli und Lomati (Sudafrika) (Lithostratigraphic study in the Fig Tree Group of the Barberton Greenstone Belt between Umsoli and Lomati (South Africa)): Gottinger Arbeiten zur Geologie und Palaontologie, v. 22, 118 p.

Heubeck, C., and Lowe, D. R., 1994a, Depositional and tectonic setting of the Archean Moodies Group, Barberton Greenstone Belt, South Africa: Precambrian Research, v. 68, p. 257–290.

Heubeck, C., and Lowe, D. R., 1994b, Late syndepositional deformation and detachment tectonics in the Barberton Greenstone Belt, South Africa: Tectonics, v. 13, p. 1514–1536.

Heubeck, C., Wendt, J. I., Toulkeridis, T., Kröner, A., and Lowe, D. R., 1993, Timing of deformation of the Archaean Barberton Greenstone Belt, South Africa: constraints from zircon dating of the Salisbury Kop pluton: South African Journal of Geology, v. 96, p. 1–8.

Hoffman, P. F., 1988, United plates of America, the birth of a craton: Early Proterozoic assembly and growth of Laurentia: Annual Review of Earth and Planetary Sciences, v. 16, p. 543–603.

Hoffman, P. F., 1989, Precambrian geology and tectonic history of North America, in Bally, A. W., and Palmer, A. R., eds., The geology of North America—An overview: Boulder, Colorado, Geological Society of America, The Geology of North America, v. A, p. 447–512.

Hose, L. D., 1990, The geology and stratigraphic evolution of the north-central part of the Early Archean Barberton Greenstone Belt, South Africa [Ph.D. dissertation]: Baton Rouge, Louisiana State University, 381 p.

Hunter, D. R., 1974, Crustal development in the Kaapvaal craton, I. The Archaean: Precambrian Research, v. 1, p. 259–294.

Hunter, D. R., 1991, An overview of the pre-3.1 Ga-old gneiss terrane, Swaziland, *in* Ashwal, L. D., ed., Two cratons and an orogen: Excursion guidebook and review articles for a field workshop through selected Archaean terranes of Swaziland, South Africa, and Zimbabwe: IGCP Project 280, and Johannesburg, University of the Witwatersrand, Department of Geology, p. 1–7.

Jackson, M. P. A., Eriksson, K. A., and Harris, C. W., 1987, Early Archean foredeep sedimentation related to crustal shortening: a reinterpretation of the Barberton Sequence, southern Africa: Tectonophysics, v. 136, p. 197–221.

Kamo, S. L., and Davis, D. W., 1991, A review of geochronology from the Barberton Mountain Land, in Ashwal, L. D., ed., Two cratons and an orogen: Excursion guidebook and review articles for a field workshop through selected Archaean terranes of Swaziland, South Africa, and Zimbabwe: IGCP Project 280, and Johannesburg, University of the Witwatersrand, Department of Geology, p. 59–68.

Kamo, S. L., and Davis, D. W., 1994, Reassessment of Archean crustal development in the Barberton Mountain Land, South Africa, based on U-Pb dating: Tectonics, v. 13, p. 167–192.

Kent, R. W., Hardarson, B. S., Saunders, A. D., and Storey, M., 1996, Plateaux ancient and modern: Geochemical and sedimentological perspectives on Archaean oceanic magmatism: Lithos, v. 37, p. 129–142.

Kröner, A., and Compston, W., 1988, Ion microprobe ages of zircons from early Archaean granite pebbles and greywacke, Barberton greenstone belt, southern Africa: Precambrian Research, v. 38, p. 367–380.

Kröner, A., and Layer, P. W., 1992, Crust formation and plate motion in the Early Archean: Science, v. 256, p. 1405–1411.

Kröner, A., and Tegtmeyer, A., 1994, Gneiss-greenstone relationships in the Ancient Gneiss Complex of southwestern Swaziland, southern Africa, and implications for crustal evolution: Precambrian Research, v. 67, p. 109–139.

Kröner, A., and Todt, W., 1988, Single zircon dating constraining the maximum age of the Barberton Greenstone Belt, southern Africa: Journal of Geophysical Research, v. 93, p. 15329–15337.

Kröner, A., Compston, W., and Williams, I. S., 1989, Growth of early Archaean crust in the Ancient Gneiss Complex of Swaziland as revealed by single zircon dating: Tectonophysics, v. 161, p. 271–298.

Kröner, A., Byerly, G. R., and Lowe, D. R., 1991a, Chronology of early Archaean granite-greenstone evolution in the Barberton Mountain land, South Africa, based on precise dating by single zircon evaporation: Earth and Planetary Science Letters, v. 103, p. 41–54.

Kröner, A., Wendt, J. I., Tegtmeyer, A. R., Milisenda, C., and Compston, W., 1991b, Geochronology of the Ancient Gneiss Complex, Swaziland, and implications for crustal evolution, *in* Ashwal, L. D., ed., Two cratons and an orogen: Excursion guidebook and review articles for a field workshop through selected Archaean terranes of Swaziland, South Africa, and Zimbabwe: IGCP Project 280, and Johannesburg, University of the Witwatersrand, Department of Geology, p. 8–31.

Kröner, A., Hegner, E., Byerly, G. R., and Lowe, D. R., 1992, Possible terrane identification in the early Archean Barberton Greenstone Belt, South Africa, using single zircon geochronology: Eos (Transactions, American Geophysical Union), v. 73, p. 616.

Kröner, A., Hegner, E., Wendt, J. I., and Byerly, G. R., 1996, The oldest part of the Barberton granitoid-greenstone terrain, South Africa: evidence for crust formation between 3.5 and 3.7 Ga: Precambrian Research, v. 78, p. 105–124.

Kusky, T. M., and Kidd, W. S. F., 1992, Remnants of an Archean oceanic plateau, Belingwe greenstone belt, Zimbabwe: Geology, v. 20, p. 43–46.

Lahaye, Y., Arndt, N., Byerly, G. R., Chauvel, C., Fourcade, S., and Gruau, G., 1995, The influence of alteration on the trace-element and Nd isotopic compositions of komatiites: Chemical Geology, v. 126, p. 43–64.

Lamb, S. H., 1984a, Geology of part of the Archaean Barberton Greenstone Belt,

Swaziland [Ph.D. dissertation]: Cambridge, Cambridge University, 250 p.
Lamb, S. H., 1984b, Structures on the eastern margin of the Archaean Barberton Greenstone Belt, northwest Swaziland, *in* Kröner, A., and Greiling, A., eds., Precambrian tectonics illustrated: Stuttgart, E. Schweizerbart'sche Verlagsbuchhandlung, p. 19–39.
Lamb, S. H., and Paris, I., 1988, Post-Onverwacht Group stratigraphy in the SE part of Archaean Barberton greenstone belt: Journal of African Earth Sciences, v. 7, p. 285–306.
Langford, W. P., and Morin, J. A., 1976, The development of the Superior Province of northwestern Ontario by merging island arcs: American Journal of Science, v. 276, p. 1023–1034.
Lanier, W. P., and Lowe, D. R., 1982, Sedimentology of the Middle Marker (3.4 Ga), Onverwacht Group, Transvaal, South Africa: Precambrian Research, v. 18, p. 237–260.
Layer, P. W., Kröner, A., and York, D., 1992, Pre-3000-Ma thermal history of the Archean Kaap Valley pluton, South Africa: Geology, v. 20, p. 717–720.
López-Martínez, M., York, D., Hall, C. M., and Hanes, J. A., 1984, Oldest reliable $^{40}Ar/^{39}Ar$ ages for terrestrial rocks: Barberton Mountain komatiites: Nature, v. 307, p. 352–354.
López-Martínez, M., York, D., and Hanes, J. A., 1992, A $^{40}Ar/^{39}Ar$ geochronological study of komatiites and komatiitic basalts from the Lower Onverwacht Volcanics: Barberton Mountain Land, South Africa: Precambrian Research, v. 57, p. 91–119.
Lowe, D. R., 1980, Archean sedimentation: Annual Review of the Earth and Planetary Sciences, v. 8, p. 145–167.
Lowe, D. R., 1982, Comparative sedimentology of the principal volcanic sequences of Archean greenstone belts in South Africa, Western Australia and Canada: implications for crustal evolution: Precambrian Research, v. 17, p. 1–29.
Lowe, D. R., 1994, Accretionary history of the Archean Barberton Greenstone Belt (3.55–3.22 Ga), southern Africa: Geology, v. 22, p. 1099–1102.
Lowe, D. R., and Byerly, G. R., 1986, Archean flow-top alteration zones formed initially in a low-temperature sulphate-rich environment: Nature, v. 324, p. 245–248.
Lowe, D. R., and Ernst, W. G., 1992, The Archean geologic record, *in* Schopf, J. W., and Klein, C., eds., The Proterozoic biosphere: Cambridge, Cambridge University Press, p. 13–20.
Lowe, D. R., and Knauth, L. P., 1977, Sedimentology of the Onverwacht Group (3.4 billion years), Transvaal, South Africa, and its bearing on the characteristics and evolution of the early Earth: Journal of Geology, v. 85, p. 699–723.
Lowe, D. R., Byerly, G. R., Ransom, B. L., and Nocita, B. R., 1985, Stratigraphic and sedimentological evidence bearing on structural repetition in early Archean rocks of the Barberton Greenstone Belt, South Africa: Precambrian Research, v. 27, p. 165–186.
Lowe, D. R., Byerly, G. R., and Kröner, A., 1989, Relationship between episodic dacitic volcanism and tonalitic plutonism in the Archean Barberton Greenstone Belt (BGB), South Africa: Eos (Transactions, American Geophysical Union), v. 70, p. 1391.
Nisbet, E. G., 1982, The tectonic setting and petrogenesis of komatiites, in Arndt, N. T., and Nisbet, E. G., eds., Komatiites: London, Allen & Unwin, p. 501–526.
Nocita, B. R., 1989, Sandstone petrology of the Archean Fig Tree Group, Barberton Greenstone Belt, South Africa: Tectonic implications: Geology, v. 17, p. 953–956.
Nocita, B. R., and Lowe, D. R., 1990, Fan-delta sequence in the Archean Fig Tree Group, Barberton Greenstone Belt, South Africa: Precambrian Research, v. 48, p. 375–393.
Paris, I. A., 1985, The geology of the farms Josefsdal, Dunbar and part of Diepgezet in the Barberton greenstone belt: [Ph.D. thesis]: Johannesburg, University of the Witwatersrand, 239 p.
Ramsay, J. G., 1963, Structural investigations in the Barberton Mountain Land, eastern Transvaal: Geological Society of South Africa Transactions, v. 66, p. 353–401.
Ransom, B. L., 1987, The paleoenvironmental, magmatic, and geologic history of the 3,500-Myr Kromberg Formation, west limb of the Onverwacht anticline, Barberton Greenstone Belt, South Africa [Masters thesis]: Baton Rouge, Louisiana State University, 103 p.
Reimer, T. O., 1967, Die Geologie der Stolzburg Synklinale im Barberton Bergland (Transvaal-Sudafrika) (The geology of the Stolzburg syncline in the Barberton Mountain Land (Transvaal, South Africa)) [M.Sc. thesis]: Frankfurt, Goethe Universitat, 103 p.
Reimer, T. O., 1975, Untersuchungen uber Abtragung, Sedimentation und Diagenese im fruhen Prakambrium am Beispiel der Sheba-Formation (Sudafrika) (Studies of denudation, sedimentation and diagenesis in the early Precambrian, an example from the Sheba Formation (South Africa)): Geologisches Jahrbuch, Reihe B, v. 17, 108 p.
Sawkins, F. J., 1990, Integrated tectonic-genetic model for volcanic-hosted massive sulfide deposits: Geology, v. 18, p. 1061–1064.
Smith, H. S., O'Neill, J. R., and Erlank, A. J., 1984, Oxygen isotope compositions of minerals and rocks and chemical alteration patterns in pillow lavas from Barberton, *in* Kröner, A., ed., Archean geochemistry: New York, Springer, p. 115–137.
Storey, M., Mahoney, J. J., Kroenke, L. W., and Saunders, A. D., 1991, Are oceanic plateaus sites of komatiite formation?: Geology, v. 19, p. 376–379.
Tarney, J., Dalziel, I. W. D., and de Wit, M. J., 1976, Marginal basin 'Rocas Verdes' Complex from S. Chile: A model for Archaean greenstone belt formation, *in* Windley, B. F., ed., The early history of the Earth: London, John Wiley & Sons, p. 131–146.
Tegtmeyer, A. R., and Kröner, A., 1987, U-Pb zircon ages bearing on the nature of early Archaean greenstone belt evolution, Barberton Mountainland, southern Africa: Precambrian Research, v. 36, p. 1–20.
Thurston, P. C., Ayres, L. D., Edwards, G. R., Gelinas, L., Ludden, J. N., and Verpaelst, P., 1985, Archean bimodal volcanism, *in* Ayres, L. D., Thurston, P. C., Card, K. D., and Weber, W., eds., Evolution of Archean supracrustal sequences: Geological Association of Canada Special Paper 28, p. 7–22.
Viljoen, M. J., and Viljoen, R. P., 1969, The geology and geochemistry of the lower ultramafic unit of the Onverwacht Group and a proposed new class of igneous rocks: Geological Society of South Africa Special Publication 2, p. 55–86.
Viljoen, R. P., and Viljoen, M. J., 1969, The geological and geochemical significance of the upper formations of the Onverwacht Group: Geological Society of South Africa Special Publication 2, p. 113–152.
Williams, D. A. C., and Furnell, R. G., 1979, A reassessment of part of the Barberton type area: Precambrian Research, v. 9, p. 325–347.
Windley, B. F., 1976, Crustal evolution in the Archaean, *in* Windley, B. F., ed., The evolving continents: London, John Wiley & Sons, p. 45–64.
Wuth, M., 1980, The geology and mineralization potential of the Oorschot-Weltevreden schist belt south-west of Barberton–Eastern Transvaal [M.Sc. thesis]: Johannesburg, University of the Witwatersrand, 185 p.

MANUSCRIPT ACCEPTED BY THE SOCIETY MARCH 26, 1998

Geologic Evolution of the Barberton Greenstone Belt, South Africa

Edited by Donald R. Lowe and Gary R. Byerly

Foreword v

1. *Stratigraphy of the west-central part of the Barberton Greenstone Belt, South Africa* 1
   Donald R. Lowe and Gary R. Byerly
2. *Structural divisions and development of the west-central part of the Barberton Greenstone Belt* 37
   Donald R. Lowe, Gary R. Byerly, and Christoph Heubeck
3. *Petrology and sedimentology of cherts and related silicified sedimentary rocks in the Swaziland Supergroup* 83
   Donald R. Lowe
4. *Modes of accumulation of carbonaceous matter in the Early Archean: A petrographic and geochemical study of the carbonaceous cherts of the Swaziland Supergroup* 115
   Maud M. Walsh and Donald R. Lowe
5. *Geochemistry of mafic and ultramafic rocks in the Kromberg Formation in its type section, Barberton Greenstone Belt, South Africa* 133
   T. W. Vennemann and H. S. Smith
6. *Subaqueous to subaerial Archean ultramafic phreatomagmatic volcanism, Kromberg Formation, Barberton Greenstone Belt, South Africa* 151
   Barbara Ransom, Gary R. Byerly, and Donald R. Lowe
7. *Sedimentology, mineralogy, and implications of silicified evaporites in the Kromberg Formation, Barberton Greenstone Belt, South Africa* 167
   Donald R. Lowe and Gail Fisher Worrell
8. *Komatiites of the Mendon Formation: Late-stage ultramafic volcanism in the Barberton Greenstone Belt* 189
   Gary R. Byerly
9. *Shallow-water sedimentation of accretionary lapilli-bearing strata of the Msauli Chert: Evidence of explosive hydromagmatic komatiitic volcanism* 213
   Donald R. Lowe
10. *Foreland basin sedimentation in the Mapepe Formation, southern-facies Fig Tree Group* 233
    Donald R. Lowe and Bruce W. Nocita
11. *Sedimentary petrography and provenance of the Archean Moodies Group, Barberton Greenstone Belt* 259
    Christoph Heubeck and Donald R. Lowe
12. *Geologic evolution of the Barberton Greenstone Belt and vicinity* 287
    Donald R. Lowe

Index 313

ISBN 0-8137-2329-9

9 780813 723297

The Geological Society of America

3300 Penrose Place • P.O. Box 9140 • Boulder, CO 80301-9140

Urheberrechtlich geschütztes Material